


Scientific Sessions

Session numbers are prefixed by SS.
Presentation numbers are prefixed by
the letter B.

Sessions and abstracts are listed by
days.

Presentations for which the author(s)
have submitted additional material and
images to EPOS™ are marked with
the  icon.

Thursday	139
Friday	199
Saturday	249
Sunday	275
Monday	305

Thursday, March 1

10:30 - 12:00

Room B

Neuro

SS 111a

Neurovascular - MRI

Moderators:

G. Guarnieri; Naples/IT

Z. Merhemic; Sarajevo/BA

B-0001 10:30

Non-invasive CVR assessment using ASL and BOLD

A. Portelo, I. Sousa, P. Vilela, P. Figueiredo; Lisbon/PT (ferrovilela@sapo.pt)

Purpose: We aimed to develop a reproducible protocol for non-invasive assessment of cerebrovascular reactivity (CVR) combining a breath hold (BH) challenge with CBF measurements using ASL, in comparison with a matching BOLD protocol.

Methods and Materials: A group of 10 healthy subjects was studied over 2 sessions on a 3 T MRI. BOLD images were obtained using GE-EPI sequence and ASL images were obtained using Q2TIPS-PICORE sequence from 9 contiguous slices. The BH protocol consisted on 3 (BOLD)/8 (ASL) cycles of 20s BH alternated with normal breathing. The data were analysed using FSL, including standard pre-processing steps and general linear model statistical analysis. Both BOLD and CBF maps of CVR were obtained for each subject and session, showing significant responses to BH, especially in grey matter. CVR measurements were obtained as percent signal changes averaged across the activation maps associated with the BOLD and CBF responses. Intra and intersubject variability was measured in terms of the respective coefficients of variation (CV).

Results: The mean percent signal change averaged across the CVR maps was $1.0 \pm 0.2\%$ and $1.6 \pm 0.2\%$ for BOLD sessions 1 and 2, $0.6 \pm 0.1\%$ and $0.7 \pm 0.1\%$ for BOLDASL sessions 1 and 2, and $74 \pm 7\%$ and $73 \pm 9\%$ for CBF sessions 1 and 2. The intra and intersubject variability was: $CV_{intra}=12\%$ and $CV_{inter}=36\%$ for BOLD, $CV_{intra}=17\%$ and $CV_{inter}=25\%$ for BOLDASL, and $CV_{intra}=31\%$ and $CV_{inter}=36\%$ for CBF.

Conclusion: Non-invasive CVR assessed by fMRI by measuring the BOLD and CBF responses to breath hold (BH) challenges is a reproducible method.

B-0002 10:39

Acute-onset migrainous aura mimicking acute stroke: MR perfusion imaging features

D. Floery¹, M.R. Vosko¹, F.A. Fellner¹, F. Gruber¹, C. Ginthoer¹, G. Ransmayr¹, M. Uder², W.G. Bradley³, C. Fellner⁴; ¹Linz/AT, ²Erlangen/DE, ³San Diego, CA/US, ⁴Regensburg/DE (daniel.floery@akh.linz.at)

Purpose: In a very limited number of cases, acute migrainous aura may present clinically as acute brain infarction. Since these patients increasingly undergo stroke MR, the aim of this study was to evaluate patterns of MR perfusion abnormalities in acute migrainous aura.

Methods and Materials: In a retrospective analysis, 1850 MR studies performed for the suspicion of acute brain infarction were analysed for patients suffering from acute migrainous aura and not from stroke (clinically and imaging based). All patients were examined clinically by two neurologists and underwent a stroke MR protocol including perfusion-weighted imaging. Two radiologists reviewed perfusion maps visually and quantitative for presence, vascular territory and grade of perfusion abnormality.

Results: Among 1850 MR studies, 20 (1.08%) patients were found who received acute migrainous aura as the final diagnosis after complete clinical and imaging workup. Hypoperfusion was found in 14 of 20 patients (70%) with delayed rMTT and TTP and decreased rCBV and rCBF, not confined to a single vascular territory. Bilateral hypoperfusion was seen in 3/14 cases, in 11/14 cases hypoperfusion with a posterior predominance was found. TTP and rMTT were the best maps to depict perfusion changes at visual assessment, but also rCBF maps demonstrated significant hypoperfusion at quantitative analysis. In all patients, clinical and imaging follow-up was negative for stroke.

Conclusion: Acute migrainous aura is a rare, but important differential diagnosis among patients referred for MR under the suspicion of acute brain infarction. Characteristic perfusion abnormalities can be seen in the majority of cases.

B-0003 10:48

Remission of diffusion lesions in acute stroke MR imaging: a follow-up study with 176 consecutive patients

D. Floery, C. Ginthoer, R. Wunn, F.A. Fellner; Linz/AT (daniel.floery@akh.linz.at)

Purpose: The mismatch concept in stroke MR is based on the assumption that diffusion-weighted imaging indicates infarct core representing irreversibly damaged tissue. However, this thesis has not yet been proven in a large patient cohort with adequate MR follow-up. Thus, the aim of this study was to analyse temporal evolution of restricted diffusion at follow-up MR within 24 hours.

Methods and Materials: 176 consecutive stroke patients (within 12 months) demonstrating restricted diffusion at initial MR examination were evaluated. Extension of diffusion restriction was judged both on initial MR as well as on follow-up after 24 hours. Changes in lesion extension were assessed by two radiologists independently, as well as overall image quality (4-tier scale).

Results: Extension of lesions with restricted diffusion at follow-up MR was identical to the initial scan in 105/176 (59.7%) and increased in 67/176 (38.1%). The lesions were decreased (meaning partial involution of the lesion) in 3/176 (1.7%) and completely resolved in 1/176 (0.5%). Mean rating of image quality was 2.1 for initial MRI and 2.3 for follow-up. That means, in 97.8% the initial lesion with restricted diffusion proved to be the infarction core indeed, whereas in 1.7% partial resolution was seen. Only in 0.5% of all patients the initial lesion did not result in complete infarction.

Conclusion: Our findings prove the existing assumption that diffusion restriction represents infarct core, which may remain unchanged or increase in volume over time, indicating an accuracy of almost 98%. Partial or complete resolution of diffusion-restriction is extremely rare.

B-0004 10:57

Arterial hypertension is associated with rostral ventrolateral medulla neurovascular compression

M. Hartel¹, M. Wójcik², M. Rudzińska², A. Szczudlik², E. Kluczevska³; ¹Zabrze/PL, ²Kraków/PL, ³Katowice/PL (hartel@voxel.pl)

Purpose: Ventrolateral medulla (VLM) is the vasomotor centre comprising neurons which control blood pressure through efferent parasympathetic connections. Previous studies suggest that hypertension in hemifacial spasm (HFS) patients is caused by VLM vascular compression.

Methods and Materials: 89 HFS patients and 59 controls (matched according to age and sex) were scanned with MRI. Hypertension was confirmed according to WHO criteria. The compression was graded from 0 to 3 (0-lack of vessel contact with brain stem, 1-vessel contact with no stem compression, 2-vessel contact with moderate stem compression, 3- vessel contact with marked brain stem compression and its deformation/displacement). Statistical analysis was carried out using Chi-squared test.

Results: VLM vascular compression was significantly more frequent among participants with vs. without hypertension in HFS (53.7% vs 31.4%, $\chi^2=,26$, $p=0.04$) as well as in control group (70.4% vs 40.6%, $\chi^2=,2$, $p=0.02$). The occurrence of VLM compression was not related to the body side. Marked compression graded as 2 and 3 correlated with arterial hypertension in HFS patients.

Conclusion: Hypertension in both groups - with and without HFS is present significantly often in patients with VLM compression on the right or the left side (without lateralization). Hypertension is present more often with 2nd and 3rd grade VLM vascular compression comparing to grade 0 and 1. The study confirmed correlation between occurrence of hypertension and VLM vascular compression not only in HFS but also in patients referred for MRI due to other diseases. The central mechanism of hypertension should be further evaluated.

B-0005 11:06

Carotid atherosclerotic plaque morphology and ischaemic vascular brain disease on MRI

Q.J.A. van den Bouwhuisen, M.W. Vernooij, G.P. Krestin, W.J. Niessen, M.A. Ikram, A. Hofman, J.C.M. Witteman, A. van der Lugt; Rotterdam/NL (q.vandenbouwhuisen@erasmusmc.nl)

Purpose: Vulnerable plaque components in carotid arteries can be detected non-invasively with magnetic resonance imaging (MRI). In asymptomatic persons, the relation between carotid plaque composition and vascular brain disease is not well studied. We studied the association between carotid atherosclerotic plaque characteristics and ischaemic brain disease on MRI.

Methods and Materials: From the population-based Rotterdam Study, 952 participants with carotid wall thickening on ultrasound > 2.5 mm underwent both carotid MRI and brain MRI. Maximum carotid wall thickening, degree of stenosis and

presence of intraplaque haemorrhage, lipid core and calcification were assessed in both carotid arteries. Associations between plaque characteristics and white matter lesions (WMLs), lacunar and cortical infarcts were investigated per participant and additionally per carotid artery. Analysis were adjusted for cardiovascular risk-factors. **Results:** Carotid stenosis (OR per 10% stenosis increase 1.2), 95% confidence interval (1.0-1.4), maximum carotid wall thickness (per mm increase 1.3.1.1-1.6) in the presence of intraplaque haemorrhage (1.9.1.1-3.3) were all found to be significantly associated with the presence of cortical infarcts, both in the participant-based analysis and in the carotid artery-based analysis. There were no associations between any plaque characteristics and presence of lacunar infarcts. In the subject-based analysis, maximum plaque thickness, presence of intraplaque haemorrhage and calcification were associated with WML-volume. In the artery-based analysis only the association for calcifications remained.

Conclusion: Presence of carotid intraplaque haemorrhage and measures of carotid plaque size are independently associated with cortical infarcts, but not with lacunar infarcts. Plaque calcification, but not vulnerable plaque components, is related to WML-volume.

B-0007 11:15

Progression of the multiple hypointense vessel sign on the susceptibility weighted images after recanalisation in patients with hyperacute ischaemic stroke

Y.-W. Kim, S. Baik, J.-Y. Jang, S. Ahn; *Yongsan/KR (vimgs@hanmail.net)*

Purpose: The multiple hypointense vessel sign (MHVS) on the SWI has been reported to identify the ischaemic territory in pts with hyperacute ischaemic stroke. We evaluated the progression of this MHVS on the immediate SWI after recanalisation and its clinical implications.

Methods and Materials: 11 hyperacute ischaemic stroke pts who were treated with intraarterial or intravenous thrombolysis within 6 hours of Sx. onset and who underwent immediate MRI after recanalisation were enrolled in this study. The recanalisation status was evaluated in cerebral infarction (TICI) score before and after thrombolysis. The SWIs were evaluated for the presence of MHVS in the ischaemic territory. The veins in the ischaemic territory were classified into 3 grades.

Results: The initial TICI grades were 0 in 9 cases and 2b in 2 cases. After thrombolysis, the TICI grades were 3 in all cases. The SWIs showed the MHVS over the affected side in all 5 pts before recanalisation (5/5). After recanalisation, all 11 pts did not show the MHVS on SWI. The observed veins in the affected area were equal in 6 pts, less in 4 pts and equal and less together in one pt.

Conclusion: The MHVS on SWI can be indicative of acute thromboembolic occlusion and its change immediately after recanalisation can be used to predict the status of the final infarction. After recanalisation, the appearance of the equal cortical vessel sign (return to normal) on SWI was associated with a favourable clinical outcome and escaped infarction in our small series study.

B-0008 11:24

Utility of susceptibility-weighted imaging for detection of carotid cavernous fistula: a case control study

H.J. Kamble, R.J. Basti, C.J. Kesavadas, B.J. Thomas; *Thiruvananthapuram/IN*

Purpose: To determine the utility and accuracy of susceptibility-weighted MRI (SWI) for the detection of carotid cavernous fistula.

Methods and Materials: We retrospectively identified 9 patients (group 1) of DSA proved carotid cavernous fistula (CCF) [case group], 19 patients (group 2) DSA negative for CCF [control group] and 2 patients of cavernous sinus thrombosis with prominent SOV (group 3). For all patients SWI sequence was available. Using uniform region-of-interest (ROI), signal intensity within superior ophthalmic vein (SOV) and superior sagittal sinus (SSS) were measured in magnitude image. SOV/SSS signal intensity ratio was calculated in each patient; mean values of the three groups were compared for accuracy.

Results: 11 SOV/SSS signal intensity ratios in group 1, 38 in group 2 and 4 in group 3 were included. Mean \pm standard deviation of SOV/SSS ratios for group 1, group 2, group 3, indirect type and direct type were 0.93 ± 0.29 , 0.40 ± 0.11 , 0.35 ± 0.10 , 0.84 ± 0.14 and 1.34 ± 0.19 , respectively. Mann-Whitney (2 tailed) test between group 1 and 2 and group 1 and 3 was statistically significant with $P < 0.0001$ ($P < 0.05$ significant). All cases and controls were reliably distinguished with SOV/SSS signal intensity ratio of 0.64 as cut off. This increased signal intensity ratio was because of arterIALIZED flow in SOV secondary to CCF.

Conclusion: SWI is feasible as well as accurate for detection of both direct and indirect carotid cavernous fistula and non-invasive follow-up of treated patients.

B-0009 11:33

Preserved regulation of intracranial pressure in patients with cerebral arteriovenous malformations

F.G. Meinel¹, J. Fischer¹, N. Woehrle¹, I. Koerte¹, D. Steffinger¹, R.P. Laubender¹, M.F. Reiser¹, N. Alperin², B. Ertl-Wagner¹; ¹Munich/DE, ²Miami, FL/US (felix.meinel@med.uni-muenchen.de)

Purpose: Cerebral arteriovenous malformations (cAVMs) may lead to a significant mass effect. To identify patients at risk, we non-invasively evaluated intracranial pressure (ICP) in patients with cAVMs and correlated it with nidus volume.

Methods and Materials: 30 consecutive cAVM patients and 30 controls matched for age and gender were investigated with a 3.0 Tesla MRI scanner. Nidus volume was quantified by MR angiography. Total arterial cerebral blood flow (tCBF), venous outflow and aqueductal and craniospinal CSF stroke volumes were obtained using velocity-encoded cine-phase contrast MRI. ICP was derived from systolic intracranial volume change (ICVC) and pulse pressure gradient.

Results: tCBF was found to be significantly higher in cAVM patients (median nidus volume 1.0 cm³, range 0.0 - 51.5 cm³) as compared to controls (median 802 vs. 688 mL/min, $p < 0.001$). The major proportion of increased venous outflow was found in the ipsilateral internal jugular vein (IJV, 318 vs. 225 mL/min, $p=0.03$), while there was no significant increase in secondary venous outflow (epidural, vertebral and deep cervical veins; 22 vs. 36 mL/min, $p=0.07$). There was no significant difference in median ICP between cAVM patients and healthy subjects (7.6 vs. 8.3 mmHg, $p=0.68$) and ICP did not correlate with nidus volume in cAVM patients (Spearman's $\rho=0.08$). We did not observe significant differences between patients and controls regarding ICVC, craniospinal or aqueductal stroke volume.

Conclusion: ICP is kept within normal limits even in patients with large cAVMs (nidus volume up to 51.5 cm³). Elevated venous outflow is mostly found in the ipsilateral jugular veins.

B-0010 11:42

Intracranial pressure across the life-span: a study with phase-contrast imaging

I. Koerte¹, A. Pomschar¹, R.P. Laubender¹, D. Steffinger¹, F. Heinen¹, M. Reiser¹, N. Alperin², B. Ertl-Wagner¹; ¹Munich/DE, ²Miami, FL/US

Purpose: Intracranial pressure (ICP) is an important clinical parameter for diagnostic and therapeutic decision making and follow-up, for example, in hydrocephalus, traumatic brain injury, normal pressure hydrocephalus (NPH), or idiopathic intracranial hypertension (IIH). However, normative data across the lifespan are not available until present. We aimed to non-invasively assess the intracranial pressure in healthy subjects across the life-span using MRI.

Methods and Materials: After informed consent, 147 healthy subjects (66 males, 81 females, age 3 to 69 years) were investigated on a 3 T MRI. Cine-phase contrast sequences were performed to quantify arterial inflow, venous outflow and craniospinal CSF flow, to derive an MR-estimate of intracranial compliance from the ratio of the maximal volume and pressure changes that occur during the cardiac cycle. Intracranial pressure (MR-ICP) was estimated based on the inverse relationship between compliance and pressure. Data were analysed using linear regression.

Results: An increase of age by one year predicted a decline by -0.021 units of square rooted MR-ICP ($p < 0.001$) holding gender constant. Women showed a 0.27 mmHg (95% confidence interval: 0.09, 0.46; $p=0.004$) higher MR-ICP when compared to men holding age constant.

Conclusion: Non-invasively measured MR-ICP decreases with age, with a gender-dependence. These age- and gender-related changes need to be taken into consideration when patients with suspected pathology are evaluated.



10:30 - 12:00

Room C

Oncologic Imaging

SS 116

Tumour biology, response and prognosis

Moderators:

G. Brown; Sutton/UK

N. Power; Waterford/IE

B-0011 10:30

Diffusion-weighted imaging: an imperfect biomarker for the malignancy of breast tumours

H. Bickel, K. Pinker-Domenig, W. Bogner, S. Gruber, M. Weber, T. Helbich; Vienna/AT (hubert.bickel@meduniwien.ac.at)

Purpose: To evaluate differences in apparent diffusion coefficient (ADC) values of different types and grades of malignant breast tumours and the influence of these differences on the diagnostic accuracy of diffusion-weighted (DWI) MRI at 3 T.

Methods and Materials: 233 patients with 279 pre-detected focal breast lesions were included. All scans were performed on a 3 T MR imager, before the application of any therapy. A T2-weighted sequence, a diffusion-weighted single-shot echo planar imaging diffusion-weighted sequence with (b-values: 0/850 sec/m²) and a dynamic, contrast-enhanced (DCE)-T1 sequence were applied. Lesions were identified on the DCE-sequence and ADC was measured in the corresponding ADC-maps, using 2-dimensional regions of interest. An ADC-threshold of 1.25 x 10⁻³ mm²/s was used to differentiate benign from malignant lesions. All lesions were biopsied and histopathologically classified using the TNM-system.

Results: While ADC-values were significantly lower in all subtypes of malignant tumours, than in benign lesions, ADC-values of non-invasive lesions were significantly higher than those of invasive ones. Tumour grades inversely correlated with ADC values, but the difference was only significant between grade I and grade III lesions. While the overall sensitivity (89.9%) and specificity (90.0%) of DWI were good, analysis of the different tumour subtypes revealed a sensitivity of only 60.9% for non-invasive tumours, while for invasive tumours, 98.5% (invasive ductal) and 92% (invasive lobular) could be obtained.

Conclusion: Non-invasive breast tumours may present significantly higher ADC values than invasive ones. This may lead to many false negative results, which has to be considered when using DWI as a diagnostic tool.

B-0012 10:39

A new diffusion-weighted MR imaging approach for evaluating response to sorafenib treatment in advanced hepatocellular carcinoma

M. Lewin¹, L. Fartoux², A. Vignaud³, L. Arrive², Y. Menu², O. Rosmorduc²; ¹Villejuif/FR, ²Paris/FR, ³Saint-Denis/FR (maite.lewin@pbr.aphp.fr)

Purpose: To prospectively evaluate the apparent diffusion coefficient (ADC), the pure diffusion coefficient (D) and the perfusion fraction (f) in advanced hepatocellular carcinoma (HCC) patients receiving sorafenib.

Methods and Materials: Diffusion-weighted imaging (DWI) was performed in 12 patients using b values of 0, 200, 400 and 800 s/mm². Two tumours were analysed in each patient at baseline, 2-weeks and 2-months treatment. ADC, D and f were calculated by statistical regression.

Results: The means of lesion size, ADC and D values did not change under treatment (respectively, 47.8 ± 31 mm; 1.34 ± 0.14 x 10⁻³ mm²/s and 1.18 ± 0.22 x 10⁻³ mm²/s). However, at 2 weeks and 2 months, in seven responder patients, f values significantly increased (+38.39%; P=0.005 and +50.94%, P=0.005, respectively) whereas in five non-responder patients f values decreased (-41.93%, P=0.008 and -23.46%, P=0.108, respectively). Furthermore, f values were inversely correlated with αFP levels (P=0.032) and responder patients showed a higher overall survival (OS) than non-responder patients (12.29 ± 4.46 vs 7.8 ± 4.97 months). The relative variation of f over baseline at 2-month treatment was highly correlated with OS (P = 0.038) and symptomatic time to progression (P=0.022).

Conclusion: In contrast to ADC and D, the perfusion fraction f is significantly affected by sorafenib and could be a potential marker of early response to treatment.

B-0013 10:48

Multi-zone tumour model exposed by multiparametric, dynamic contrast-enhanced and diffusion-weighted MR imaging

K. Holzapfel, C. Ganter, M. Settles, S. Lorenzen, A.J. Beer, E.J. Rummeny, S. Metz; Munich/DE (holzapfel@roe.med.tum.de)

Purpose: To correlate kinetic parameters derived from dynamic contrast-enhanced MR imaging (DCE-MRI) with apparent diffusion coefficient (ADC) values determined by diffusion-weighted MR imaging (DWI) in a spatially resolved, multiparametric imaging approach for phenotyping of tumour biology in living organisms.

Methods and Materials: In 16 chemo-naïve patients with histologically proven adenocarcinomas of the lung or the gastrointestinal tract 49 lesions were imaged (DWI, DCE-MRI). Transfer constant K_{trans}, rate constant k_{ep}, and fractional extravascular extracellular space v_e were calculated for each pixel (Tissue 4D software, Siemens) and correlated with ADC values. Whole tumour regions of interest (ROIs) were compared using the Spearman's rank correlation coefficient. Additionally, parameters were correlated on a pixel-by-pixel basis and, to reflect spatial heterogeneity, all tumour sections were divided into pixel rings (periphery to centre).

Results: For whole tumour ROIs no significant correlation between ADC values and kinetic parameters could be demonstrated. However, pixelwise analysis of ADC and kinetic parameters revealed a distinct pattern in spatial distribution of the parameters: restricted ADC, highest K_{trans} and v_e values in the tumour rim; very high ADC values and break down in perfusion in the centre; increasing ADC values, constant K_{trans}, and increasing k_{ep} in a transitional zone when approaching from peripherally to centrally.

Conclusion: Non-invasive multiparametric assessment of the spatial heterogeneity of tumour biology is feasible using DCE-MRI and DWI. Combining both functional imaging methods identifies tumour regions with different biological characteristics exposing a multi-zone tumour model.

B-0014 10:57

Perfusion CT sub-classifies FDG-PET metabolic responders in oesophagogastric adenocarcinoma

T.S. Ahearn, R. Petty, G. Bain, A. Denison, A. Welsch, V. Cunningham, L. Schweiger, F. Gilbert; Aberdeen/UK (f.gilbert@abdn.ac.uk)

Purpose: Identifying predictive biomarkers to optimise treatment selection in oesophagogastric adenocarcinoma (OGC) and to avoid ineffective treatment is important. Around 50% of oesophageal cancer patients that have a metabolic response (MR) to chemotherapy with FDG-PET at 14 days go on to respond to the full course of treatment. As part of a larger study, we investigated the predictive accuracy of combining perfusion CT (PCT) with FDG-PET for chemotherapy response.

Methods and Materials: Locally advanced/metastatic OGC patients were recruited into the PCT arm of the study (n=20). Imaging was performed on days 0 and 14 after chemotherapy (FDG-PET and PCT). Patients were classified MR if standard uptake values (SUV) decrease was > 35%. PCT was performed with 52 frames (100kVp, 120 mAs). 50 ml of Omnipaque350 was infused at frame 3. Images were analysed offline using in house software. Perfusion and blood volume were calculated using the maximum slope model. 15 PCT patients have been analysed. Radiological response (RR) was assessed by RECISTv1.1. (assessments were based on assessment of the primary tumour).

Results: 10/15 patients were classified as metabolic responders, 3/10 were also radiologic responders. Tumour perfusion was significantly increased (p=0.016) in FDG-PET MRs (mean increase 39%) that do go on to have a RR as compared to those that do not have a RR (mean increase 7%).

Conclusion: PCT potentially sub-classifies FDG-PET metabolic responders into patients that will and will not go onto to have a radiological response. PCT may have clinical utility in combination with FDG-PET as a predictive biomarker to optimise treatment selection in OGC.

B-0015 11:06

Intravoxel incoherent motion (IVIM) analysis of breast carcinomas: a pilot study

A.M. Chow, V. Ai, P.S.Y. Cheung, K.M. Chan, S.K. Yu, G.G. Lo; Happy Valley/HK (aprilcmk@gmail.com)

Purpose: To characterise changes in diffusion and perfusion effects in breast carcinomas using intravoxel incoherent motion (IVIM) analysis.

Methods and Materials: 24 female patients with biopsy-proven breast carcinomas were prospectively evaluated. All MRI examinations were performed on a 3 T MRI scanner (MAGNETOM Trio, Siemens) using a dedicated 4-channel phased array coil. A single-shot echo-planar imaging DWI protocol was performed to obtain

also
EPOS

images axially with 8 b-values (0.50, 100, 150, 200, 400, 600, 1000 s/mm²). A circular ROI was defined in the DW images over the breast carcinomas and normal fibroglandular tissue for IVIM measurements. True diffusion coefficient (Dtrue), pseudodiffusion coefficient (Dpseudo), and perfusion fraction (Pfraction) were estimated by fitting the DW signal decay in the ROI to the IVIM bi-compartmental model: $SI/SI_0 = (1 - Pfraction) \times \exp(-bDtrue) + Pfraction \times \exp(-bDpseudo)$.

Results: Dtrue of breast carcinomas ($0.65 \pm 0.22 \times 10^{-3}$ mm²/s) was significantly lower ($p < 0.001$, two-tailed Wilcoxon matched pairs test) than that of fibroglandular tissue ($1.29 \pm 0.48 \times 10^{-3}$ mm²/s). Moreover, significant difference ($p < 0.05$) in Pfraction was observed in breast carcinomas (0.20 ± 0.10) and fibroglandular tissue (0.31 ± 0.22), while similar Dpseudo in breast carcinomas ($26.02 \pm 4.82 \times 10^{-3}$ mm²/s) and fibroglandular tissue ($20.86 \pm 4.06 \times 10^{-3}$ mm²/s) were observed.

Conclusion: IVIM analysis revealed decreased Dtrue and Pfraction in breast carcinomas, showing that alterations in both cellularity and perfusion effects contribute to the changes in apparent diffusion using DWI. IVIM analysis may be valuable for characterising breast carcinomas and monitoring its progression non-invasively.

B-0016 11:15

Early assessment of tumour response to sorafenib in uveal melanoma with liver metastases using semi-quantitative DCE-MRI

F. Nensa¹, J. Statta¹, B. Nokay¹, B. Thiering², H.-G. Lipinski², M. Forsting¹, M. Scheulen¹, J. Kalkmann¹; ¹Essen/DE, ²Dortmund/DE (felix.nensa@gmail.com)

Purpose: Evaluation of semi-quantitative dynamic contrast-enhanced MRI (DCE-MRI) to assess therapy response in patients with liver metastases of uveal melanoma (UM) treated with Sorafenib.

Methods and Materials: This study was approved by our local institutional review board. Seventeen patients with liver metastases of UM were treated with Sorafenib and examined by DCE-MRI (1.5 T Avanto, Siemens) at baseline and for follow-up scans every 6 weeks. The lesion with the longest diameter was selected as target. Measurements were performed paracoronally for 300sec using a T1-Flash sequence (7 mm slice-thickness, temporal resolution 1sec) and Gadobutrol (0.1 mmol/kg, flow 3 ml/sec). Automated respiratory motion correction was applied to the image series, thereafter the target lesion was manually delineated by a region of interest. Contrast-enhancement time curves were fitted using smoothing spline interpolation and semi-quantitative parameters were calculated: maximum slope during initial contrast agent uptake (iSlopemax) and initial area under the curve to 60 (iAUC60) and 90 seconds (iAUC90) after the onset time. Therapy response was assessed according to response evaluation criteria in solid tumors (RECIST) with a mean time-to-progression of 390 days.

Results: After 6 weeks iSlopemax, iAUC60 and iAUC90 showed a statistically significant mean decrease of 41.71% ($\pm 23.44\%$), 29.00% ($\pm 20.09\%$) and 26.97% ($\pm 18.48\%$), respectively (each $p < 0.01$), before subsequently entering steady state. A decrease in DCE-MRI parameters was not associated with therapy response or time-to-progression.

Conclusion: Respiratory motion corrected semi-quantitative DCE-MRI shows a rapid and significant decrease in liver metastases of UM under treatment with sorafenib, but a correlation to clinical outcome could not be observed.

B-0017 11:24

Combined qualitative and quantitative analysis of DWI in early assessment of poor responders after chemoradiation therapy: preliminary results in locally advanced rectal cancer

L. Monguzzi¹, D. Ippolito, C. Capraro, C. Talei Franzesi, S. Galimberti, S. Sironi; Monza/IT (letizia.monguzzi@gmail.com)

Purpose: To evaluate the potential role of DWIBS and ADC map in identifying poor responders to neoadjuvant chemoradiation treatment (CRT) for LARC.

Methods and Materials: 40 patients (mean age 60) with biopsy-proven diagnosis of rectal cancer were prospectively enrolled in our study. MR examinations were performed prior to therapy (T3-T4 or N+ stage) and after CRT (6 weeks after the completion of treatment) on a 1.5 Tesla (Achieva, Philips) scanner with a pelvic phased array multi-coil; multiplanar T1 and T2TSE and DWIBS sequences (b factor: 0 and 1000 mm²/sec) were acquired. For quantitative analysis, mean ADC values of the tumour regions were measured by 2 radiologists, by manually drawing ROI (covering entire tumour regions on ADC maps). Mean pre- and post-CRT ADC values were compared between responders and non-responders, being the histopathologic response (according to Mandard's criteria) as the reference standard.

Results: After surgical resection, imaging findings were compared with pathological results. Twenty-seven patients (68%) showed complete (TRG1) or subtotal regression (TRG2) and were considered as responders; while 13 (32%) were classified as poor responders (TRG3-5). The mean post-CRT ADC value of poor responders

($1.19 \pm 0.25 \times 10^{-3}$ mm²/sec) was significantly ($p < 0.001$) lower than that of responder group ($1.40 \pm 0.22 \times 10^{-3}$ mm²/sec). The best cut-off ADC value in distinguishing responders from non-responders was 1.28×10^{-3} mm²/s on the basis of post-CRT ADC yielded a good specificity (87%); combining qualitative analysis of DWI to morphological findings we could lead to more accurate results.

Conclusion: DWMRI represents a powerful and effective tool to monitor therapeutic response in LARC, being able to detect cellular changes in treated tumours.

B-0018 11:33

Assessment of tumor heterogeneity: CT texture as a biomarker of overall survival in primary colorectal cancer

F.K.H. Ng¹, B. Ganeshan², R. Kozarski³, K. Miles², V. Goh⁴; ¹Northwood/UK, ²Brighton/UK, ³Hertfordshire/UK, ⁴London/UK

Purpose: To determine if CT texture is related to overall survival in primary colorectal cancer.

Methods and Materials: Following IRB approval 57 patients (26 males, 31 females, mean 67.8years) underwent staging contrast-enhanced CT (120 kV, 280 mA, 0.6s rotation time, 5 mm slice collimation; 100 mL 340 mg/ml iodinated contrast at 5 mL/s, 75 second delay). The entire colorectal tumour texture features were assessed using proprietary image texture analysis software (TexRAD) deriving entropy (E), uniformity (U), kurtosis (K), skewness (S) and standard deviation (SD) from the CT images without filtration and with filter values corresponding to fine (1.0), medium (1.5, 2.0), and coarse (2.5) textures. Patients were followed up till death, or censored at 5 years if alive. ROC and Kaplan-Meier analysis was performed to determine the relationship, if any, between CT texture and 5-yr overall survival.

Results: Data were available from 55 patients. There were 8 stage I, 19 stage II, 17 stage III and 11 stage IV cancers. Fine texture Kaplan Meier survival plots for E, U, K, S and SD were significantly different ($p=0.002$, $p=0.018$, $p=0.032$, $p=0.008$ and $p=0.002$, respectively) for thresholds of ≤ 7.89 (E), > 0.01 (U), ≤ 2.48 (K), > -0.38 (S) and ≤ 61.83 (SD), respectively. Cox regression analysis showed these parameters were independent predictors of overall survival with stage.

Conclusion: Lower entropy, kurtosis and SD, and higher uniformity and skewness at fine textures are predictors of poorer 5-year overall survival in colorectal cancer.

B-0019 11:42

Evaluation of radiological prognostic factors of hepatic metastases in patients with pancreatic neuroendocrine neoplasms

C. Ihm, A. Baur, I.G. Steffen, E.B. Tischer, M. Pavel, T. Denecke; Berlin/DE (alexander.baur@charite.de)

Purpose: Pancreatic neuroendocrine neoplasms (pNEN) are rare tumours and often diagnosed at an advanced stage of disease. The liver is the most frequent site of metastases and progression of hepatic metastases often determines prognosis. This study aimed to evaluate the characteristics of liver metastases of pNEN in multiphasic contrast-enhanced CT or MRI determining risk factors for progression.

Methods and Materials: We retrospectively analysed the CT and MRI appearance of liver metastases in 44 patients with histologically proven well-differentiated (G1/2) pNEN for contrast enhancement, necrosis, vascular infiltration as well as the number of metastases and tumour burden. Progression of liver metastases was judged according to the RECIST criteria.

Results: During surveillance 14 patients received biotherapy (octreotide LAR) and 30 patients obtained no antitumoral therapy. Median time to progression of patients with biotherapy and patients without therapy was 12.1 and 6.0 months, respectively (HR, 3.0; 95%-CI, 1.3-6.9; $p=0.009$). The only significant radiological factor shown to have a less favourable independent prognostic significance is the hypovascularisation (defined as hypoenhancement during the early arterial and portal venous phases) of hepatic metastases (HR, 2.6; 95%-CI, 1.0-6.7; $p=0.042$). This significantly predicted early progression in the subgroup without octreotide therapy (1-year progression rate with hypervascularisation, 38.3%; hypovascularisation 100% (8/8); $p=0.034$), while biotherapy masked this predictor (all patients, $p=0.506$).

Conclusion: Patients treated with octreotide LAR had a significantly longer time to tumour progression. Hypovascularised metastases might be an easy accessible risk factor for tumour progression and therefore important to take into account when deciding on therapeutic approach.

B-0020 11:51

CT-based response assessment of advanced gastrointestinal stromal tumour: is dual energy CT a more predictive imaging biomarker of response than RECIST or Choi criteria?

M. Meyer, P. Apfaltrer, T. Henzler, D.J. Dinter, P. Hohenberger, S.O. Schönberg, C. Fink; Mannheim/DE (mr.meyer.mathias@gmail.com)

Purpose: Dual energy CT (DECT) allows the assessment of iodine distribution in tumours. This may be considered as a surrogate marker for perfusion and tumour vascularity. This study evaluated whether DECT allows a better prediction of survival than established response criteria (RECIST and Choi criteria).

Methods and Materials: Seven-teen patients with advanced GIST treated with tyrosin-kinase inhibitors were assessed by contrast-enhanced DECT after 2 and 6 months follow-up. Response was rated according to RECIST, Choi criteria and DECT analysis of iodine related attenuation. Progressive disease was defined as a 20% increase of tumour size (RECIST) and tumour density (Choi) or either an increase greater than 50% of tumour size or iodine-related attenuation on DECT. Progression-free survival (PFS) and overall survival (OS) were calculated by Kaplan-Meier analysis.

Results: Independent from the used response criteria patients with partial response or stable disease had a significantly longer median PFS than patients with progressive disease (median: 9-29 months vs. 2-6 months; $p < 0.0228$). Only DECT at 6 months allowed a valid discrimination of patients with good or poor OS (median: 32 vs. 18 months; $p < 0.0496$).

Conclusion: This study indicates that DECT is a promising predictive imaging biomarker of response if compared to established response criteria as it allowed the best prediction of survival.

10:30 - 12:00

Room D1

Chest

SS 104

Neoplasms: staging, risk and surgery

Moderators:

S. Ley; Toronto, ON/CA
K. Malagari; Athens/GR

B-0021 10:30

The presurgical T staging of non-small cell lung cancer: efficacy comparison of 64-MSCT versus 3.0 T MR imaging

T.W. Tang, W.N. Wu, O.H. Ouyang, H.Y. Huang, L.L. Liu, L.M. Li, W.Y. Wang, X.X. Xu; Beijing/CN (nicky⁸⁸⁴⁶⁵@hotmail.com)

Purpose: To compare prospectively the diagnostic efficacies of 64-MDCT and 3.0 T MRI for determining T staging in NSCLC.

Methods and Materials: Institutional review board approval and informed consent were obtained. 40 patients with NSCLC proved by pathology were enrolled in the study. Totally 40 patients underwent non-enhanced MRI, enhanced MRI, and enhanced MDCT. T staging were preliminarily evaluated according to these imaging manifestations and correlated with that of pathology using the Kappa test. Diagnostic efficacies for T staging of NSCLC on non-enhanced MRI, enhanced MRI and enhanced CT imaging were compared using the McNemar test, respectively.

Results: Diagnostic efficacy for T staging of NSCLC was 85% on non-enhanced MRI, 87.5% on enhanced MRI, and that on enhanced CT was 80%, respectively. There was no significant difference among these 3 different protocols on the diagnostic efficacy for T staging of NSCLC ($P > 0.05$). Although there were no significant differences, for the NSCLC with T1~2 staging, diagnostic efficacy of enhanced CT was slightly superior to that of non-enhanced MRI and enhanced MRI, for the NSCLC with T3~4 staging, diagnostic efficacy of enhanced MRI was slightly superior to that of enhanced CT and non-enhanced MRI.

Conclusion: Compared to MDCT, non-enhanced MRI and enhanced MRI provided slightly superior diagnostic efficacy for the presurgical T staging of NSCLC, especially for the T3~4 tumour. For patients who cannot stand with enhanced MDCT scan, 3.0 T MRI would be a substituted examination for the presurgical T staging of NSCLC.

B-0022 10:39

Single source dual energy CT improving differentiation between atelectasis and tumour in central lung cancer: clinical practice of a novel technique

Y. Chen, L. Tang, X.-T. Li, L.-P. Qi, Y.-L. Li, X.-Y. Zhang, Y. Cui, Y.-S. Sun, X.-P. Zhang; Beijing/CN (tanglei@bjcancer.org)

Purpose: To evaluate the performance of single source dual energy CT for differentiation between atelectasis and tumour in central lung cancer.

Methods and Materials: The study comprises 27 consecutive patients with confirmed central lung cancer associated with atelectasis on single source dual energy CT. The optimised mono-chromatic images were obtained by selecting the best CNR, and the iodine-based material decomposed images were obtained with iodine concentration measured. Images were assessed by two radiologists working in consensus for the display of tumour-atelectasis interface. The iodine concentrations between tumour and atelectasis was compared by paired t test with SPSS.

Results: The optimal energy level was in the range of 40-68 keV (median 52 keV) for displaying tumour-atelectasis interface at 30s delayed scanning phase and in the range of 40-70 keV (median 50 keV) at 90s delayed scanning phase. Tumour-atelectasis interface could be defined in 16 (59.3%) and 26 (96.3%) patients using combination of the optimised mono-chromatic images with iodine-based material decomposed images at 30s and 90s delayed phase, respectively, more than 9 (33.3%) and 16 (59.3%) using the optimised mono-chromatic images alone, with $p=0.056$ and $p=0.001$, respectively. The iodine concentrations of atelectasis was much higher than tumour, $p < 0.001$, and the iodine-based material decomposed images enabled differentiation between atelectasis and tumour in 4 more patients.

Conclusion: The single source dual energy CT could improve differentiation between atelectasis and tumour in central lung cancer with the optimised CNR technique and material decomposition technique. This modality manifested as a potentially useful radiologic tool for routine clinical diagnosis.

B-0023 10:48

Predictive features of FDG-PET/CT and CT in diagnosing nodal metastasis of T1 non-small cell lung cancers manifesting as part-solid nodules

H. Kim, C.M. Park, S.M. Lee, J.C. Paeng, J.M. Goo, H.J. Lee; Seoul/KR (khj.snuh@gmail.com)

Purpose: To retrospectively investigate the predictive factors of FDG-PET/CT and CT for LN metastasis in T1 NSCLCs manifesting as part-solid nodules (PSNs).

Methods and Materials: The institutional review board approved this study and waived informed consent. From January 2005 to May 2011, 144 patients with pathologically proven T1 NSCLCs manifesting as PSNs with LN staging were included in this study. SUVmax and CT features of primary tumours were evaluated to investigate predictive factors for LN metastasis. In addition, optimal cut-off values for each predictor were determined and the diagnostic performance of the prediction model using the predictors was evaluated using a receiver-operating characteristic (ROC) analysis.

Results: LN metastases were found in 9 of 144 patients (6.25%). No LN metastasis was present in patients with solid proportion $< 77\%$. There were significant differences in SUVmax, solid proportion, and lesion location of the primary tumour between patients with and without LN metastasis ($P < 0.05$). Multivariate analysis revealed that higher SUVmax [odds ratio (OR), 1.823; $P=0.030$], larger solid proportion [OR, 1.150; $P=0.027$] and central location [OR, 17.902; $P=0.011$] were independent predictors for LN metastasis. The optimal cut-off values of SUVmax and solid proportion were 2.98 and 77.273, respectively. The area under the ROC curve of the predictive model using all three variables was 0.951.

Conclusion: Higher SUVmax, larger solid proportion and central location of the primary tumour are significant independent predictors for LN metastasis in T1 NSCLCs manifesting as PSNs, which can enable a very accurate preoperative prediction of LN status in these cancers.

B-0024 10:57

Prevalence, clinical significance and diagnostic value of extrapleural and cardio-phrenic lymph nodes

C. Mantini, B. Feragalli, N. Civitareale, R. Polverosi, A. Tartaro, A. Cotroneo; Chieti/IT

Purpose: To evaluate the prevalence, clinical meaning and diagnostic value of extrapleural and cardio-phrenic nodes occasionally observed on CT scans of the chest. To define a CT dimensional cut-off value for extrapleural and cardio-phrenic

nodes. To evaluate the frequency of these nodes in different diseases, particularly in primary or secondary malignant pleural diseases.

Methods and Materials: We included 750 consecutive patients, who underwent MDCT of the chest for different clinical purposes (370 non-neoplastic patients, 250 with extrathoracic neoplasm, 100 with intrathoracic neoplasm and 30 with pleural metastasis) and 91 patients with histologically proven malignant pleural mesothelioma (MPM). For each group of patients we analysed the presence of extrapleural and cardio-phrenic nodes, their number (single or multiple) and their size (≤ 5 mm, between 6 and 10 mm and > 10 mm).

Results: The prevalence of extrapleural nodes, independently from their size, resulted less than 1% in all groups of patients, except for patients with MPM (62/91 - 68%). The prevalence of cardio-phrenic nodes > 5 mm was 66% (60/91) in patients with MPM, 53% (16/30) in patients with pleural metastasis and less than 2% in all other groups of patients. No significant differences in the prevalence of cardio-phrenic nodes ≤ 5 mm in all groups of patients ($p > 0.05$) were found.

Conclusion: The presence of extrapleural nodes of any size and cardio-phrenic nodes greater than 5 mm have a significant diagnostic value in malignant pleural disease, either primary or secondary, while they are extremely rare in other diseases, neoplastic or not.

B-0025 11:06

Diffusion-weighted imaging add diagnostic value to MRI in differentiating thoraco-mediastinic lesions: comparison with PET-CT

F. Bue^{mi}, F. Tondo, G. Strangio, A. Stecco, A. Carriero; *Novara/IT (franbuemi@virgilio.it)*

Purpose: The aim of this study was to assess the diagnostic accuracy of diffusion-weighted MRI sequences versus PET-CT in the detection and characterisation of thoraco-mediastinal district lesions, using the histopathological findings as gold standard.

Methods and Materials: 34 patients with thoracic-mediastinal lesions underwent PET-CT and MRI; standard and diffusion-weighted sequences were performed and ADC maps were generated. To optimise the comparison between PET-CT and MRI in discriminating benign from malignant lesions, an ADC cut-off value was stated (1.5×10^{-3} mm²/s). Considering the findings of histopathological lesions as "gold standard" reference, values of sensitivity, specificity, diagnostic accuracy, positive predictive value (PPV) and negative predictive value (NPV) of MRI and CT-PET were calculated.

Results: The obtained values showed diffusion-weighted MRI having a sensitivity comparable to CT-PET (90% vs 87%) and greater specificity (100% vs 33%). Overall, the diagnostic accuracy of diffusion-weighted MRI returned a value of 91%, compared to 85% of PET-CT. The PPV obtained with diffusion-weighted sequences was similar to the one obtained with PET-CT (100% vs 96%), with diffusion-weighted NPV sequences being more accurate than PET-CT (57% vs 33%). No statistically relevant differences among the sensitivity and specificity values of the two methods were found after a comparison with the McNemar's test.

Conclusion: Calculation of the ADC with diffusion-weighted MRI has proved to be extremely sensitive in the thoraco-mediastinal masses discrimination, and it may be an important technical feature to complete basic MRI sequences with or without contrast media.

B-0026 11:15

Do pleural plaques carry an excess of risk of lung cancer in asbestos-exposed workers?

R. Barbot¹, C. Le Marquand², J.-C. Pairon³, C. Paris⁴, P. Brochard⁵, F. Laurent⁶; ¹Villenave d'Ornon/FR, ²Clamart/FR, ³Creteil/FR, ⁴Vandoeuvre-les-Nancy/FR, ⁵Bordeaux/FR, ⁶Pessac/FR (remibarbot@free.fr)

Purpose: Most studies evaluating relationships between pleural plaques and lung cancer have been based on chest radiographs and due to the low sensitivity and specificity of chest radiograph to identify pleural plaques, their results are still controversial. The aim of this study was to evaluate whether the presence of pleural plaques detected using low-dose chest CT leads to an additional risk of lung cancer to that provided by asbestos exposure without presence of plaques.

Methods and Materials: A large screening programme for formerly asbestos-exposed workers was organised in France from 2003 to 2005, including exposure assessment measured by a cumulative exposure index and detection of pleural and lung abnormalities by low dose computed tomography. Reading was performed blindly independently by 2 readers. Cases of incident lung cancer in this population were counted up to January 2011. Relationship between presence of pleural plaques and occurrence of lung cancer was assessed by adjusted odds ratios (OR) for age, sex, smoking status and asbestos exposure.

Results: The study population included 5825 subjects. The mean duration of follow-up was 6.29 years. Data regarding the presence of pleural plaques were available in 73 subjects among the 75 cases of lung cancer identified. Adjusted OR estimating the risk of lung cancer associated with pleural plaques was 1.14 (95% confidence interval, 0.65 to 2.00).

Conclusion: Among a population of formerly asbestos-exposed workers, the presence of pleural plaques does not lead to an excess risk of lung cancer.

B-0027 11:24

Incidental findings in a study screening asbestos exposed workers for lung cancer and mesothelioma using low-dose computed tomography (LDCT): what you can find when you are not looking

E. Tarulli¹, H. Roberts², M. de Perrot², B. O'Sullivan², G. Dong², N.S. Paul², D. Patsios²; ¹Kingston, ON/CA, ²Toronto, ON/CA (eat@queensu.ca)

Purpose: The purpose of our study is to assess the frequency of incidental findings (IFs) and their potential impact in an asbestos-exposed population screened for lung cancer and mesothelioma using LDCT.

Methods and Materials: 1111 patients (98.4% men) screened between March 2005 and 2011 using LDCT. IFs were considered any findings not related to the primary purpose of the screening study in detecting pulmonary and pleural focal and diffuse abnormalities secondary to asbestos exposure categorised anatomically. Necessity for follow-up was decided based on the findings by the reading radiologist. The costs of the associated follow-up were calculated based on the Schedule of Benefits published by the Ministry of Health and Long Term Care of the province of Ontario/CA.

Results: The average age was 61±10 years. 179 participants were current smokers, 619 former smokers, and 313 non-smokers. The average number of pack-years in the smoking population was 23 and asbestos exposure was 27 in the entire screened population. Clinically significant IFs requiring follow-up were found in 394 of 1111 (35%) of baseline screening studies. The most common incidental findings were cardiac (53%), hepatic (13%), hiatal hernias (11%), biliary (6%), renal (6%), splenic (3%) and those related to the thyroid (2%). The total cost of investigating IFs was estimated at approximately \$44,000 CAN whereas the total cost of the baseline screening studies is estimated at \$74,000 CAN.

Conclusion: IFs in screening studies are both clinically and financially significant. Their impact should be considered when determining the implementation and validation of new screening tests.

B-0028 11:33

Lung cancer screening by morphological MRI in comparison to low-dose CT

J. Tremper, M. Puderbach, B. Stieltjes, M. Eichinger, H.-P. Schlemmer, S. Delorme; *Heidelberg/DE (j.tremper@dkfz.de)*

Purpose: Lung cancer screening with CT applies ionising radiation. This is problematic in long-term follow-up with accumulating doses. The aim of this study was to examine the potential of magnetic resonance imaging (MRI) for the detection of suspected lung lesions in comparison to low-dose CT.

Methods and Materials: 37 participants of the Heidelberg lung cancer screening trial (LUSI) showing a suspicious lung lesion in CT because of size (> 10 mm) or significant growth (< 400 days doubling time) that requires immediate workup (invasive procedures or short-term follow-up) received a non-contrast lung MRI (HASTE, VIBE, TruFisp in coronal and transversal orientation). The study time was approx. 7 minutes. The MR data were checked for suspicious lesions. The results were compared to CT.

Results: 33 of the 37 suspicious lesions could be identified by MRI comparable to CT. 4 lung lesions could not be identified in MRI (2 of them being smaller than 8 mm; 2 lesions had probably already resolved by the time the MRI was performed, f.e. small infiltrates or atelectases). In Fisher's exact test independence can be rejected ($p = 0.11$), proving MRI being as accurate as CT in detecting relevant lung lesions.

Conclusion: These results show that suspicious lung lesions on low-dose CT are depicted in 89% also on morphological MRI of the lung.



Thursday



B-0029 11:42



Lung volume in patients with pectus excavatum: quantifying the pulmonary involvement?

J. Vallejos¹, C. Capunay¹, P. Carrascosa¹, M. Martinez Ferro², J. Carrascosa¹;
¹Vicente Lopez/AR, ²Buenos Aires/AR (javss⁹⁹@yahoo.com.ar)

Purpose: To quantify the lung volume of pectus excavatum (PE) patients using chest multi-slice computed tomography (MDCT), and to compare these with a control group.

Methods and Materials: Thirty-six patients (mean age: 17.2 year-old) with PE and 12 controls underwent low dose chest MDCT. The volume of lung parenchyma in each examination was determined by performing a three-dimensional reconstruction. We determined values for the volume of the right lung, left lung, and the pulmonary volume index (PVI: right/left). Severity indices of the deformity using the standard Haller index (HI), chest wall asymmetry index (CWA), cardiac compression index (CCI), cardiac asymmetry index (CAI) and sternal tilt angle were also calculated from CT scans. Statistical differences of measurements were calculated using the Student-t and Kruskal-Wallis tests.

Results: We found evidence ($p=0.01$) of a lower PVI in PE patients (1.21 ± 0.17) in comparison with control patients (1.09 ± 0.4). The PVI was directly correlated with the HI ($r=0.33$, $p=0.04$) and with the CCI ($r=0.44$, $p < 0.01$).

Conclusion: This preliminary study showed differences in lung volumes between PE patients and control group. Therefore PVI correlated with severity indices. These findings suggest that lung volume quantification may be a severity index of pulmonary involvement.

B-0030 11:51

Prediction of postoperative pulmonary function by single-breath dual energy xenon CT: a preliminary report

H. Yanagita, W. Watanabe, Y. Shimizu, T. Okada, H. Ohno, H. Osada, N. Honda, M. Nakayama; Kawagoe Saitama/JP (hyanagit@saitama-med.ac.jp)

Purpose: Chronic obstructive pulmonary disease (COPD) is common and lung cancer is still one of the leading causes of death worldwide. So it is important to ascertain operability of patients having both COPD and lung cancer. The purpose was to assess the ability of xenon dual energy CT to predict postoperative pulmonary function.

Methods and Materials: Eight patients with lung cancer planned for resection were enrolled in this study. Institutional review board approved this study and written informed consent was obtained from all patients. They were scanned with a dual source CT scanner in dual energy mode (80 kV/Sn 140 kV) during a breath-hold after single vital-capacity breath of a mixture of xenon and oxygen in the ratio of 35:65 (35%-xenon). Xenon images (Xe-images) were calculated by three-material decomposition. The sum of the pixel values of the Xe-images within the part of the lung to be remained after resection (A) and that of the whole lung (B) were enumerated. We multiplied A/B and pre-operative forced expiratory volume in one second (FEV1) or forced vital capacity (FVC) to predict postoperative FEV1 or FVC. Predicted FEV1 and FVC were compared with measured postoperative FEV1 and FVC, and regression was tested by t-statistics.

Results: The predicted values of FEV1 and FVC from Xe-images correlated to the postoperative measurements ($R = 0.66, 0.72$), and the regression was significant for FVC ($p = 0.07, 0.04$).

Conclusion: Predicted postoperative FEV1 and FVC with the Xe-images correlated to the postoperative FEV1 and FVC.

10:30 - 12:00

Room D2

Interventional Radiology

SS 109

Genitourinary, gastrointestinal and biliary interventions

Moderators:
 M. Given; Dublin/IE
 T. Jargiello; Lublin/PL

B-0031 10:30

Uterine artery embolisation: pre-interventional prediction of the best tube angle obliquity for visualisation of the uterine artery origin using 3D reconstructed contrast-enhanced MR angiography

N.N.N. Naguib, N.-E.A. Nour-Eldin, B. Schell, T. Gruber-Rouh, T. Lehnert, T.J. Vogl; Frankfurt a. Main/DE (nagynnn@yahoo.com)

Purpose: To test the accuracy of 3D-reconstructed contrast-enhanced MR angiography (3D-CE-MRA) in predicting the best tube angle obliquity to visualise the uterine artery origin (UAO) before uterine artery embolisation (UAE).

Methods and Materials: The prospective study included 40 females (mean age: 45.4 years) to whom UAE was performed. CE-MRA was performed before UAE and 3D-images were reconstructed using Inspace-application. The 3D-figure was rotated in all directions to determine the best angle for visualising the UAO by two radiologists in consensus. The suggested angle was provided to the interventionist for optional usage. After UAE the actual angle used for visualisation was recorded and compared with the suggested angle. Correlation between the suggested angle and actual angle was tested using Spearman's correlation test.

Results: For visualising the left UA the suggested-angle in the side-to-side direction showed a mean of 8.38° right $\pm 28.6^\circ$, the actual-angle was 7.3° right $\pm 28.7^\circ$. In the cephalo-caudal direction the suggested-angle was 2.53° caudal $\pm 6.52^\circ$, the actual-angle was 2.53° caudal $\pm 6.52^\circ$. A statistically significant strong positive correlation was detected between the suggested and actual angles in the side-to-side ($\rho=0.981$, $p < 0.0001$) and cephalo-caudal directions ($\rho=1$, $p < 0.0001$). For the right UA the suggested-angle in the side-to-side direction was 9.95° left $\pm 27.5^\circ$, the actual-angle was 7.98° left $\pm 29.1^\circ$. In the cephalo-caudal direction the suggested-angle was 0.38° caudal $\pm 8.67^\circ$, the actual-angle was 0.38° caudal $\pm 8.67^\circ$. A statistically significant strong positive correlation was detected in the side-to-side ($\rho=0.865$, $p < 0.0001$) and cephalo-caudal directions ($\rho=1$, $p < 0.0001$).

Conclusion: Pre-interventional 3D CE-MRA can accurately predict the best tube angle obliquity for visualisation of the uterine artery origin before UAE.

B-0032 10:39

Advantages of the brachial approach in uterine arteries embolisation

P.R. Nechifor, B. Dorobat; Bucharest/RO (office@drnechifor.ro)

Purpose: Description of advantages of the brachial approach in uterine arteries embolisation.

Methods and Materials: 4020 consecutive cases of uterine fibroids embolisation using brachial approach. Some parameters that permit the estimation of this technique's results, the complications and the postprocedure quality of life were followed.

Results: The catheterisation of bilateral uterine arteries was possible in 99.95% of cases. The mean time of the intervention was 42 min (SD ± 11 min). Radioscopy time ranged between 2.8 minutes and 18.2 minutes with a mean time of 3.6 minutes (SD ± 2.4 minutes). The complications at the puncture site were: brachial artery spasm in 3.75% of cases, local haematoma in 1.56% of cases, brachial artery thrombosis in 0.12% of cases and 1 case of tegument adherence to the deeper layers. Readmission for complications was necessary in 3 cases. The postembolisation pain was perceived less intense (mean 4 on a scale 0-10), 100% of the patients appreciated the absence of any constraint to rest as an important advantage.

Conclusion: The brachial approach is a successful technique, superior to femoral approach, that permits a significant reduction in radioscopy time and radiation dose. Complications at the puncture site are very rares, in direct relation with operator's experience. The patient's comfort during first 24 hours after intervention is significantly increased. The postembolisation pain is less intense. Microcatheters were not necessary as diagnostic catheters were used in all the interventions, thus leading to cost reductions.

B-0033 10:48

Arterial embolisation for cervical leiomyoma: should we treat it as adenomyosis?

J. Koh, M. Kim, M. Lee, D. Jung, S. Park, M. Lee, J. Won, D. Lee, K. Lee; Seoul/KR (qhs02@yuhs.ac)

Purpose: The aim of this study is to compare the effectiveness of uterine artery embolisation (UAE) in treating symptomatic fibroids in the uterine cervix to that in the uterine body or fundus.

Methods and Materials: From the data for 537 patients who underwent UAE between 2007 and 2010, we retrospectively analysed the data for 10 patients with fibroids located in the uterine cervix. Seven of the 10 patients presented a total of 10 fibroids in the uterine body or fundus as well as in the uterine cervix. The effects of UAE and vascularities on angiographic findings were compared between fibroids in the cervix and fibroids in the uterine body or fundus. Necrosis of fibroids was assessed by MRI 3 months after UAE. Statistical analysis was performed using the Mann-Whitney test and Fisher's exact test.

Results: Complete necrosis of leiomyomas in the uterine cervix was seen in only 2 patients of the 10, while all fibroids in the uterine body or fundus were completely infarcted ($p < 0.05$). Partial necrosis was seen in 6, and no necrosis in 2. One patient underwent hysteroscopic resection for removal of incompletely infarcted fibroid. Poor vascularities were noted in 5 of 9 patients (55.6%) with cervical fibroids but in none of the patients with fibroids in the uterine body or fundus ($p < 0.05$).

Conclusion: Poor vascularities were frequent finding in cervical leiomyomas and outcomes of UAE for cervical leiomyomas were disappointing and indicate caution in selecting and counselling patients for this treatment.

B-0034 10:57

Transcatheter pelvic arterial embolisation for control of obstetric haemorrhage

M. Ferrer-Puchol¹, C. Lanciego², E. Esteban¹, J. Ciampi², M. Edo¹, S.E. Gonzalez¹, S.E. Gonzalez²; ¹Alzira/ES, ²Toledo/ES (lolesferrer@ono.com)



Purpose: Excessive blood loss is considered to be greater than 500 ml in vaginal delivery or 1000 ml after caesarean section. The purpose of this work is to present our experience in emergency selective arterial embolisation in two hospitals.

Methods and Materials: We present 27 women who underwent intractable obstetric bleeding. Mean patient age was 26 years \pm 7. In both hospitals there was a trained team on call for interventional procedures. Indication for selective arterial embolisation was made by gynaecologists and anaesthetists. Non-selective pelvic arteriography was performed via transfemoral approach to demonstrate the anatomy and points of bleeding. We performed intraarterial embolisation using gelatine sponge, particles or coils depending on bleeding source.

Results: 24/27 were primary haemorrhages and 2/27 were secondary. Causes were: 20 after vaginal deliveries: 1 placenta accreta, 1 cervical tear and 18 uterine atony. 5 after caesarean section: 2 arterial tears, 2 uterine atony and 1 pseudoaneurysm. 1 after abortion: pseudoaneurysm. 1 after ectopic cervical pregnancy. The two secondary haemorrhages were due to pseudoaneurysms. Catheterisation of both uterine arteries was performed in 25 patients. Embolisation material: 17/27 we employed gelatine sponge, 9/27 using PVA particles and 1 patient with coils. We had not complications related to procedure. The result was satisfactory in 24 patients with complete cessation of bleeding, but two cases presented some hours later embolisation an episode of rebleeding that underwent emergent hysterectomy.

Conclusion: Intraarterial embolisation is an alternative to surgical measures, offers good results, is safe and preserves fertility of women.

B-0035 11:06

A novel technique of percutaneous closure of enterocutaneous fistula

B. Sekovski, L. Cambj Sapunar; Split/HR (budimir9008@yahoo.com)

Purpose: Patients with a postoperative enterocutaneous fistula have significantly reduced quality of life. Recently, several minimally invasive methods were developed as an alternative to surgical therapy for this condition. We present our technique of percutaneous closure of enterocutaneous fistula under fluoroscopy guidance.

Methods and Materials: Five patients who have developed low-output enterocutaneous fistula since March 2010 were included in this study. Enterocutaneous fistula occurred as a postoperative complication of colorectal carcinoma in four patients and in one patient fistula was a post-surgery complication of a perforated diverticulitis. N-butyl cyanoacrilic glue mixed with lipiodol as an embolisation material was deployed in a fistula through 4 F hydrophilic catheter under fluoroscopy guidance. Procedure takes less than 10 minutes and requires approximately 30 seconds of fluoroscopy.

Results: In all five patients fistula was immediately closed and there were no complications considering our procedure. In one patient local cancer recurrence occurred 4 months after the intervention and in the patient with diverticulosis 15 months later the new episode of diverticulitis caused abscess formation.

Conclusion: Percutaneous closure of low-output enterocutaneous fistulas with cyanoacrilic glue under fluoroscopy guidance is a simple and effective method that represents a good alternative to surgical therapy. Advantage of this method is that the gluing of the fistula could be easily detected under fluoroscopy since lipiodol makes the glue visible. Short-term results of this novel technique are excellent but further evaluation of long-term results is required.

B-0036 11:15

Fluoroscopically guided dilations of oesophageal strictures due to epidermolysis bullosa dystrophica: long-term results from a single centre study

S.C. Spiliopoulos, R. Inchingolo, M. Krokidis, P. Gkoutzios, A. McGarth, I. Ahmed, N. Karunanithy, R. Salter, T. Sabharwal; London/UK

Purpose: To investigate the immediate and long-term results following the fluoroscopically guided oesophageal balloon dilations for the management of dysphagia, in a series of patients suffering from epidermolysis bullosa dystrophica (DEB).

Methods and Materials: The medical records of all patients treated with fluoroscopically guided balloon dilatation of oesophageal strictures and DEB between 2005 and 2011 were included in the study and retrospectively analysed. The indication for the treatment was dysphagia attributed to at least one radiologically verified oesophageal stricture. The study's primary endpoints included procedural technical success, clinical improvement assessed by a 0 to 4 dysphagia score and major complications rate. Secondary endpoints included patient survival and re-intervention rates.

Results: In total, 19 consecutive DEB patients (mean age 30 \pm 12.2, range: 10-51 years) suffering from dysphagia due to oesophageal strictures were treated with fluoroscopically guided balloon dilations. In total 90 procedures and 121 dilations in 28 lesions were performed. The balloon diameters ranged from 8 to 18 mm. Mean time follow-up was 47.51 \pm 16.64, range 17-73 months. Technical success rate was 97.6% (87/90 procedures). There were no major complications. Mean re-intervention free interval rate was 10 months, while post-procedural dysphagia score was significantly lower compared to baseline (0.72, 95%CI 0.56-0.87 vs. 2.50, 95%CI 2.35-2.65, respectively; $p < 0001$).

Conclusion: Fluoroscopically guided balloon dilatation for the management of dysphagia caused by oesophageal strictures owing to DEB is safe and effective. The specific method demonstrated a significant clinical improvement of dysphagia and long-term satisfactory re-intervention rates, while no major complications were noted.

B-0037 11:24

Effectiveness of percutaneous biliary stone removal as primary treatment compared with endoscopic retrograde technique: in cases of IHBD stones, ≥ 15 mm bile duct stones, history of GI bypass surgery

S. Choi, Y. Han, S. Lee, H. Yu; Jeonju-si/KR (maumzoa@gmail.com)

Purpose: To evaluate the effectiveness of percutaneous biliary stone removal as primary treatment compared with endoscopic retrograde technique, in cases of IHBD stones, ≥ 15 mm bile duct stones, history of GI bypass surgery.

Methods and Materials: From March 2004 to May 2011, a total of 122 consecutive patients with biliary stones underwent percutaneous biliary stone removal as primary treatment (group I, n=40) or secondary treatment after endoscopic retrograde techniques had failed (group II, n=82). In two groups, the ones who satisfied the inclusion criteria were 17 (group I', M:F=14:3, Mean age; 72 years) and 33 (group II', M:F=21:12, Mean age; 78 years), respectively. The inclusion criteria were as follows: patients who i) had IHBD stones, ii) had ≥ 15 mm bile duct stones, iii) had history of previous GI bypass surgery (e.g. subtotal gastrectomy with Billroth II op, total gastrectomy, pylorus preserving pancreaticoduodenectomy; PPPD, R en Y choledochojunostomy). We analysed success rates and length of postprocedural hospital stay of the two groups.

Results: There was no significant difference in success rate between the two groups, 94.1%(16/17) in group I' and 97.1% (32/33) in group II'. (P=0.63) And the length of postprocedural hospital stay was significantly increased in group II' (mean 17 days, group I': mean 13 days, P=0.02). Amylase and lipase level between pre- and post-procedure was not significantly different (P=0.27 and 0.47, respectively) There was no procedural complication.

Conclusion: Therefore, in cases of above-mentioned patients, primary percutaneous biliary stone removal can be more efficient.

B-0038 11:33

The comparison of visualisation among balloon-occluded retrograde transvenous venography using iodine contrast and carbon dioxide gas, and the subsequent obliteration by foam sclerosants for gastric varices under DSA

J. Koizumi, T. Hashimoto, K. Myojin, C. Itou, T. Hara, T. Sekiguchi, T. Ichikawa, T. Kagawa, N. Watanabe; *Isehara/JP (jkoizumi@is.icc.u-tokai.ac.jp)*

Purpose: Previously we applied carbon dioxide gas DSA for balloon-occluded retrograde transvenous venography (BRTV) prior to obliteration (BRTO) using foam sclerosants, and clarified CO2 demonstrated gastric varices (GV) more clearly than iodine contrast. However, the physiological properties of CO2 and foam are different. Thus, we compared the visualisation of them under DSA.

Methods and Materials: For fifteen patients with GV, BRTV using iodine contrast was performed first and then CO2 second. These BRTV were repeated after changing patient's habitus, the catheter positions or downgradings. When GV were opacified on CO2-BRTV, foam sclerosants were injected. Each visualisation grade of GV (grade 1; GV only, 2; GV>collaterals, 3; GV<collaterals, 4; collaterals only) was determined by two observers. C-arm CT was performed to confirm the reach of air into GV.

Results: Thirty-four pairs of BRTV were performed for fifteen patients. The grades on CO2-BRTV (1.8±0.8) were significantly ($p < 0.01$) smaller than the grades on iodine-BRTV (3.3±0.9). On the other hands, the grades on foam-BRTO (1.1±0.4) are similar to the last grades on CO2-BRTV (1.1±0.4), while significantly ($p < 0.01$) different from the last grades on iodine-BRTV (3.1±1.0). In all patients GV were opacified by foam on C-arm CT and complete thrombosis of GV was obtained without any complication.

Conclusion: CO2-BRTV visualised GV better than iodine-BRTV and provided a good simulation of BRTO using foam sclerosants leading successful thrombosis of GV.

B-0039 11:42

Retrievable covered stent in the treatment of benign biliary strictures: intermediate-term outcomes

C. Kim, D. Gwon, G.-Y. Ko, K.-B. Sung, H.-K. Yoon, J. Shin, J. Kim, H.-Y. Song; *Seoul/KR (cherrykim73@dreamwiz.com)*

Purpose: To investigate the intermediate-term outcomes of a retrievable covered stent in the treatment of benign biliary strictures.

Methods and Materials: From April 2007 to February 2010, 33 patients with benign biliary strictures were enrolled in this study. Seventeen patients had not previously undergone interventional treatment. Sixteen patients had recurrent or refractory strictures despite prolonged catheter interposition after balloon dilation procedures. The retrievable stent was fully PTFE (polytetrafluoroethylene)-covered, self-expandable nitinol stent. Technical success, clinical success (drainage catheter removal after percutaneous treatment using a retrievable stent), and primary patency rate were evaluated.

Results: A total of 49 retrievable covered stents were placed due to stent migration (n=5, 15%) or persistent stricture (n=7, 21%) after 1-3 sessions of stent removal procedures. The stents were successfully placed and removed in all cases. The mean stent indwelling period was 2.8 months (range, 1-6 months). Clinical success was achieved in 30 patients (91%). During the mean follow-up of 27.5 months (range, 13.3-48 months), three of 30 patients had recurrence of clinically significant strictures. The primary patency rates at 1, 2, and 3 years were 87%, 83%, and 63%, respectively.

Conclusion: Intermediate-term outcomes indicate that percutaneous treatment of benign biliary strictures using a retrievable covered stent appears to be feasible and clinically effective method.

B-0040 11:51

Percutaneous Y-configured covered stent placement for malignant hilar biliary obstruction: a prospective pilot study

N. Seo, D. Gwon, G.-Y. Ko, K.-B. Sung, H.-K. Yoon, J. Shin, J. Kim, H.-Y. Song; *Seoul/KR (sldmsdl@hanmail.net)*

Purpose: To investigate the technical and clinical safety and efficacy of percutaneous Y-configured covered stent placement in patients with malignant hilar biliary obstruction.

Methods and Materials: This is a prospective, pilot study that enrolled 20 consecutive patients with malignant hilar biliary obstructions from October 2009 to December 2010. This study was approved by the Institutional Review Board of our Institution and informed consent was obtained from each patient. All patients were

treated with percutaneous transhepatic placement of partially ePTFE (expanded polytetrafluoroethylene)-covered stents in a Y configuration.

Results: Bilateral Y-configured covered stent deployment was technically successful in all patients. Minor complications including procedure-related complications (self-limiting haemobilia [n=1] and rapidly resolving cholangitis [n=3]) occurred in four patients (20%). Bilirubin level decreased significantly following stent placement ($p < 0.001$). Median patient survival and stent patency times were 218 days (95% confidence interval [CI], 112-324 days) and 375 days (95% CI, 55-695 days), respectively. Seven patients (35%) presented with stent occlusion due to sludge incrustation (n=6) and tumour overgrowth (n=1), and required repeated PTBD. Tumour ingrowth, acute cholecystitis or stent migration was not observed in any of these patients.

Conclusion: The preliminary results of percutaneous palliative treatment of malignant hilar biliary obstruction with Y-configured covered stents suggest that they are safe and clinically effective.

10:30 - 12:00

Room E1

Musculoskeletal

SS 110

Osteoporosis and bone marrow

Moderators:

J.E. Adams; *Manchester/UK*
M. Vlychou; *Larissa/GR*

B-0041 10:30

Impact of exercise on bone mineral density

I. Abbas, H. Elghawabi, W. Younan, A. Sabour, M. Gobrial; *Cairo/EG (imanabbas65@yahoo.com)*

Purpose: To assess the impact of caloric restriction diet versus caloric restriction diet in addition to aerobic exercises on bone mineral density in obese women.

Methods and Materials: Forty obese women were classified randomly into two groups of equal in number. The first group received caloric restriction diet, while the second received caloric restriction diet in addition to a program of aerobic exercises, over 3 months. The variables measured included body mass index, fat weight, lean mass, basal metabolic rate, and bone mineral density.

Results: Comparison between both groups showed significantly higher post-treatment lean mass, basal metabolic rate, and bone mineral density in weight-bearing bones (lumbar spine and hip) in the second group compared to the first one. On the other hand, the bone mineral density of the radius showed significant decrease between the pre- and post-treatment results in both groups with no significant differences between the two groups.

Conclusion: Significant increase in the bone mineral density of the weight-bearing bones was noted in obese women undergoing caloric restriction in addition to aerobic exercises than in those not undergoing exercises. Aerobic exercises should be added to weight loss programs for obese women to reduce the adverse effects of caloric restriction diet on bone mineral density.

B-0042 10:39

Quantitative ultrasound at the phalanges in a cohort of twins of different ages

G. Guglielmi¹, F. De Terlizzi², A. Carini², L. Sinibaldi³, R. Mingarelli³, F. Brancati³; ¹Foggia/IT, ²Carpi/IT, ³Rome/IT (g.guglielmi@unifg.it)

Purpose: Preliminary study of bone tissue quality by quantitative ultrasound (QUS) at the phalanges in twin children and adults.

Methods and Materials: 129 twin couples of healthy children under 18 years of age (N=42) and of adults (N=87) in the age range 19-71 years were recruited for QUS measurement at the phalanges. Anthropometric data (sex, age, height, and weight) were recorded, together with amplitude-dependent speed of sound (AD-SoS) and bone transmission time (BTT).

Results: Mean age in children group was 11.6±5.2 yrs, height 143±29 cm, weight 41±19 kg. Mean age in adult group was 31.2±12.2 yrs, height 170±9 cm, weight 62±12 kg. In children, AD-SoS and BTT were positively correlated with age (r=0.91, r=0.91), height (r=0.88, r=0.90) and weight (r=0.81, r=0.87); in adults AD-SoS was negatively related to age (r=-0.36), AD-SoS and BTT were positively related to height (r=0.37, r=0.58). Correlation coefficients for AD-SoS and UBPI between coupled of twins are significantly higher for children (r=0.985 for AD-SoS and r=0.987 for BTT) than for adults (r=0.882 for AD-SoS and r=0.920 for BTT). The absolute value of the differences between twins for AD-SoS and BTT is significantly higher in adult twins

than in children: AD-SoS diff - children:14.5±12.4, adults:25.9±21.9, t-test:0.0003; BTT diff - children:0.05±0.04, adults:0.08±0.08, t-test: 0.0039. Absolute difference between twins increases significantly with age (r=0.374, p < 0.0001 for AD-SoS and r=0.400, p < 0.0001 for BTT).

Conclusion: Differentiation in bone tissue quality in twins is increasing with age among twins couples, and this probably reflects differentiation in lifestyle, life habits and diet.

B-0043 10:48

Bariatric surgery and radiologists: besides complications, an important role in the evaluation of treatment efficacy and effects

D. Diano¹, F. Ponti¹, C. Sassi¹, G. Garzillo¹, G. Guglielmi², E. Salizzoni¹, G. Battista¹, A. Bazzocchi¹; ¹Bologna/IT, ²San Giovanni Rotondo, Foggia/IT (dan¹@libero.it)

Purpose: Bariatric surgery is the most effective way of controlling severe obesity and its medical comorbidities. Our aim was to investigate the impact of bariatric treatment on body composition (BC) and bone metabolism over a period of 24 months following the surgical intervention and to determine the role of dual energy x-ray absorptiometry (DXA) in the management of obesity.

Methods and Materials: We prospectively enrolled 22 female patients (46.5±8.0 year-old; 42.7±7.1Kg/m²) directed to bariatric surgery (Roux-en-Y gastric bypass on vertical banded gastroplasty). All patients underwent whole body and lumbar spine DXA scans before treatment and after 3-6-12 and 24 months. BC parameters were assessed (fat mass-FM; non-bone lean mass-LM; bone mineral content, and density-BMD) on whole body and regional-basis. Thus, differential rates of mass and BMD changes were calculated to define the trend in the overall weight loss.

Results: Body mass index decreased in the first 12 months and grew steady between 12 and 24 months (p < 0.05). A decrease of FM/LM ratio was observed in both total and android region at 12 months (FM/MLMD), while slightly increased between 12 and 24 months (FM/MLMD). Similar trend was observed for central and peripheral fat distribution ratio (Δ=-30.4%±31.0% and Δ=-6.9%±13.4%, respectively; p < 0.05). A reduction of total and lumbar BMD was observed at 12 months, even stronger at 24 months compared to pre-treatment values (Δ=-3.9%±1.7% and Δ=-6.1%±3.3%, respectively; p < 0.05).

Conclusion: BC and bone metabolism are significantly modified after bariatric surgery. DXA is fundamental in the investigation of patients submitted to surgical treatment for morbid obesity and in their clinical management.

B-0044 10:57

Fat fraction and T2* values of vertebral bone marrow utilising a new fat separation MR technique in peri-menopausal women: comparison with bone mineral densitometry

F.B. Ergen¹, G. Yildirim², A. Celik², A.E. Yildiz¹, J. Karakaya¹, U. Aydingoz¹; ¹Ankara/TR, ²Istanbul/TR (aelcindr@gmail.com)

Purpose: To use fat fraction and T2* values to investigate bone mineralisation level using a new MR technique called "iterative decomposition of water and fat with echo asymmetry and least squares estimation quantification" in peri-menopausal women.

Methods and Materials: Between October and December 2010, 45 (mean age, 40.4 years, max, 64; min, 28) consecutive patients who agreed to undergo MRI and who had a spinal dual energy x-ray absorptiometry (DEXA) examination constituted the study population. 3D fast gradient recalled echo (FGRE) pulse sequence with six asymmetric echoes was used. Fat fraction and T2* values were measured from L1-L4 vertebrae by placing ROIs. Depending on t-scores derived from BMD, vertebrae were classified into 3 groups (1, normal; 2, osteopaenia; 3, osteoporosis). One-way ANOVA or Welch ANOVA was performed to compare the differences among groups. The ability of fat fraction for the prediction of osteoporosis/osteopaenia was evaluated by ROC analysis.

Results: For fat fraction, the mean values were found to be different in three groups (P < 0.001). Group 1 vertebrae were different from groups 2 and 3 (P < 0.001). The area under ROC curve for fat fraction was 0.80 (95% CI, 0.72-0.86). The optimal cut-off point was obtained as 39%. For this, sensitivity and specificity of fat fraction were 80% and 66%, respectively. For T2* there was no statistically significant difference between the groups (P=0.155).

Conclusion: It is possible to estimate the level of bone mineralisation by quantification of the fat fraction with the new MR technique with an acceptable sensitivity and specificity levels.

B-0045 11:06

Scaling relations between trabecular bone mass and 3D microstructure in two locations of the human femur

T. Baum¹, J.S. Bauer¹, I. Sidorenko², R. Monetti², F. Eckstein³, M. Matsuura¹, E.-M. Lochmueller³, P.K. Zysset⁴, C. Raeth²; ¹Munich/DE, ²Garching/DE, ³Salzburg/AT, ⁴Vienna/AT (thbaum@gmx.de)

Purpose: To investigate possible site-differences of bone mass-microstructure scaling relations that may be related to different loading conditions according to Wolff's law of bone remodelling.

Methods and Materials: Cylindrical bone specimens with a diameter of 8 mm were harvested from human femora. Eighty-eight specimens were taken from the femoral neck and 126 specimens from the greater trochanter. 3D micro-CT images with isotropic spatial resolution of 26 micrometre were obtained. Bone mass (BV/TV) of each specimen was calculated. To determine the local structure of the trabecular network as well as its alignment with the direction of the external force acting on the bone, isotropic (alpha) and anisotropic scaling indices (alpha-z) were computed. Then the moments of the distribution (mean: []; variance: var) of the isotropic and anisotropic scaling indices were calculated. Scaling exponents were determined as the slope of a linear fit in the double-logarithmic representation of the correlations of BV/TV against the moments of the distribution of the scaling indices.

Results: All correlations obeyed very accurately power laws with scaling exponents of 0.48 and 0.45 ([alpha]), -1.45 and -1.59 (var (alpha)), 0.50 and 0.44 ([alpha-z]), and -1.47 and -1.32 (var (alpha-z)) (neck and trochanter, respectively). Thus, bone mass-microstructure scaling relations of the bone probes taken from two different sites of the femur showed surprisingly small variations.

Conclusion: In the femur, trabecular bone mass-microstructure scaling relations may have a rather universal character and do not depend so much on the type of external mechanical forces.

B-0047 11:15

Quantitative analysis of perfusion parameters in osteoporotic patients with acute vertebral fracture using dynamic contrast-enhanced MRI

G.P. Schmidt¹, A. Biffar¹, O. Dietrich¹, S. Sourbron², M. D'Anastasi¹, K. Nikolaou¹, M.F. Reiser¹, A. Baur-Melnyk¹; ¹Munich/DE, ²Leeds/UK (gerwin.schmidt@med.uni-muenchen.de)

Purpose: To evaluate the potential of quantitative dynamic contrast-enhanced MRI (DCE-MRI) in vertebral bone marrow (vBM) of patients with osteoporosis and acute vertebral compression fractures.

Methods and Materials: 26 patients with acute fractures (16 females, 10 males, median age 72, range 48-89) and 10 subjects without known history of osteoporosis (6 females, 4 males, median 65, 31-77) were examined using two-dimensional DCE-MRI. ROI-Data in fractured (n=26) and normal appearing vertebrae (n=271) were analysed with a two compartment tracer-kinetic-model, providing estimates of at least 3 independent parameters: plasma flow (PF), plasma volume (PV) and extraction flow (EF). Parameters were correlated with dual x-ray absorptiometry (DXA) (n=15) and quantitative computed tomography (QCT)-densitometry (n=10).

Results: Mean PF was significantly higher in fractures than in normal appearing vertebrae (69.37 vs 11.72 mL/100 mL/min, p < 0.001). Similarly, mean PV and EF differed significantly (24.29 vs. 4.49 mL/100 mL and 10.42 vs. 0.06 mL/100 mL/min). Mean PF was significantly decreased in normal appearing vBM of osteoporotic patients compared to the control group (11.72 vs. 17.55 mL/100 mL/min, p = 0.008). Mean values of PF and PV were significantly decreased in lumbar compared to thoracic vertebrae (p=0.002). PV showed a significant correlation with QCT (p = 0.002).

Conclusion: DCE-MRI is useful to differentiate normal appearing vBM in osteoporotic patients from healthy subjects, as well as acute compression fracture. Furthermore, it may serve as a tool to grade osteoporosis.

B-0048 11:24

Role of diffusion-weighted whole body MRI with background body signal suppression (DWIBS) for disease detection in patients with multiple myeloma: preliminary results

P.A. Bonaffini, D. Ippolito, I. Macchi, F. Rossini, A. Di Lelio, S. Sironi; Monza/IT (pa.bonaffini@gmail.com)

Purpose: To assess the overall diagnostic capability of whole body MRI, with DWIBS technique, combined with standard T1 and STIR T2 sequences, for detection of bone marrow lesions in patients with multiple myeloma (MM).

Methods and Materials: 45 patients with MM underwent 1.5 T (Achieva, Philips) WB-MRI study from skull vertex to feet, using a built-in-body coil and stepping

table technique. The protocol consisted of coronal and sagittal short tau inversion recovery (STIR) T2, T1 TSE and axial DWIBS sequences, in order to characterise bone involvement in terms of pattern, size and distribution. DWIBS images were compared with T1 and STIR images in five districts (skull; spine; sternum and ribs; pelvis; upper and lower limbs), in patients with focal (23), diffuse (16) or combined (8) disease. All patients were clinically staged according to Durie and Salomon System. **Results:** In focal and combined disease, 165 focal bone lesions were detected: 159 (98%) were correctly identified with T1/T2 sequences and 150 (95%) with DWIBS alone. In patients with diffuse disease DWIBS always showed homogeneous increased signal intensity within the bones involved, with greater sensitivity in demonstrating widespread involvement of bone marrow than T1/T2 sequences, due to their inhomogeneous alteration of intensity signal. 7 patients were correctly staged as diffuse disease with DWIBS, while T1 and T2 sequences showed focal or combined disease.

Conclusion: WB-MRI with DWIBS sequences in patients with MM appears to be technically feasible and a promising, non-invasive tool for early detection and characterisation of bone marrow lesions, particularly in widespread form.

B-0049 11:33

Diagnostic value of whole body low-dose computed tomography (WBLDCT) in the staging of patients with multiple myeloma

V. Besostri¹, D. Ippolito¹, M. Crivellaro¹, E.M. Pogliani¹, A. Di Lelio², S. Sironi¹; ¹Milan/IT, ²Monza/IT (valeribesostri@gmail.com)

Purpose: To assess the role of whole body low-dose computed tomography (WBLDCT) in the diagnosis and staging of patients with suspicion of multiple myeloma (MM).

Methods and Materials: A total of 138 patients, with early multiple myeloma, underwent unenhanced whole body low-dose CT protocol study, performed on 16-slice scanner (Philips, Brilliance, 16P): tube voltage 120 KV; tube current time product 40 mAs; collimation 16 x 0.75. All the patients were clinically staged according to Durie and Salmon System. Diagnosis of osteolytic lesions was performed on the basis of axial and multiplanar reformatted images, whereas the assessment of spinal misalignment and fracture was done using multiplanar reformatted images.

Results: In all 138 patients, image resolution was diagnostic, enabling correct classification of multiple myeloma patients. WBLDCT showed a total of 328 pathologic bone findings in 81 patients. CT scanning resulted in complete evaluation of the bone lesions in these areas of the skeleton: skull (42), humerus (15), femur (20), ribs (7), scapulae (13), pelvis (35), clavicle (13), sternum (10), cervical (39), dorsal (65), lumbar (48) and sacral rachis (21). In 40 patients the CT detection of bone involvement was the only criterion for the treatment. Furthermore, in 19 patients WBLDCT scanning demonstrated pulmonary or pleural lesions (11 cases due to infective source and 7 cases due to multiple myeloma localisations) and 1 case of renal neoplasia as a related pathology. The overall dose delivered to each patient was 3.2 mSv.

Conclusion: Whole body low-dose CT investigational protocol is a reliable imaging-based method for the direct management of patients with multiple myeloma. WBLDCT has a superior reproducibility and it is faster than conventional radiography, being, furthermore, able to demonstrate extraosseous findings.

B-0050 11:42

Quantitative assessment of perfusion and permeability in osteochondritis dissecans lesions: feasibility and initial results

A.P. Arnoldi, M. Ingrisch, S. Utzschneider, M.F. Reiser, S. Weckbach; Munich/DE (andreas.arnoldi@med.uni-muenchen.de)

Purpose: While the exact pathophysiology of osteochondritis dissecans (OCD) has not yet been clearly understood, determination of the best management of the condition still remains continuously discussed [O'Loughlin 2010] [Kocher 2006]. Purpose of this study was to evaluate the feasibility of I) detection II) quantitative assessment III) monitoring of perfusion and permeability in OCD lesions by 3D DCE-MRI.

Methods and Materials: 14 (mean age 15y) patients with OCD of the medial femoral condyle/the medial talar dome (n=6/8) underwent DCE-MRI at 3 T (Magnetom-Verio-Siemens-Medical-Solutions-Germany) using a view-sharing 3D-GE-sequence (TE/TR=2.46/4.78 ms, flip angle=18°, spatial resolution=0.6x0.6x4.0 mm³, matrix size=256*220*16, temporal resolution=3.0s) after bolus injection of 0.2 mmol/kg Gd-DTPA. 3 patients obtained follow-up scan after an average of 4.5 months. The AIF was measured in the popliteal artery (knee)/in the anterior tibial artery (ankle). ROIs in OCD lesions were drawn on AUC-maps; haemodynamic parameters in these regions were determined using a 2-compartment-exchange-model, yielding estimates of plasma flow (PF), plasma volume (PV), permeability surface product (PS) and interstitial volume (VEE) [Sourbron 2009].

Results: In all patients, OCD lesions were clearly visible on the AUC-maps and showed strongly elevated perfusion and permeability. Mean values (SD) were: PF=68 (54)ml/100 ml/min, PV=15.2 (8.4)%, PS=11.4 (6.4)ml/100 ml/min and VEE=16.0 (8.5)%. The 3 follow-up-scans indicated a decrease of the median PV from 15% to 8%.

Conclusion: Our study shows the feasibility of DCE-MRI to I) detect OCD lesions, II) quantify perfusion and permeability using a 2-compartment model and III) reveal changes of PV in different disease stages. This quantitative approach provides additional information on the pathophysiology of the condition, might influence disease management and could offer a non-invasive means of therapy monitoring.

10:30 - 12:00

Room E2

GI Tract

SS 101a

Crohn's disease and intestinal inflammation

Moderators:

A. Gupta; London/UK
S. Romano; Naples/IT

B-0051 10:30

MR perfusion of normal small bowel

J.H. Yacoub, C. Zini, X. Fan, A. Yousuf, D.T. Rubin, A. Oto; Chicago, IL/US (zini.chiara@gmail.com)

Purpose: To determine the feasibility of quantitative analysis of small bowel perfusion using dynamic contrast-enhanced MRI (DCE-MRI) and compare perfusion patterns of jejunum and ileum.

Methods and Materials: Six normal subjects were prospectively enrolled to undergo MR-enterography. Regions of interest were drawn over the jejunum, ileum and terminal ileum (TI) to calculate the volume transfer constant (K-trans) and extravascular extracellular space (Ve). The difference between the small bowel regions was assessed using paired t-test.

Results: The jejunum demonstrates earlier and more intense enhancement compared to the ileum and TI. The mean K-trans (min⁻¹) at the jejunum, ileum and TI, respectively, were 0.97±0.23, 0.34±0.14, and 0.41±0.11. The mean Ve (%) at the jejunum, ileum and TI, respectively, were 0.23±0.08, 0.13±0.04, and 0.15±0.05. The K-trans was significantly higher in the jejunum compared to the ileum (P < 0.005) and TI (P < 0.007). The Ve was significantly higher in the jejunum compared to the ileum (P < 0.005) and TI (P < 0.03). There was no significant difference between the ileum and TI in K-trans and Ve (P=0.3 and 0.6, respectively).

Conclusion: DCE-MRI is a feasible method for quantitative analysis of small bowel perfusion. The jejunum demonstrates earlier and more intense enhancement compared to the ileum. Better understanding of small bowel perfusion is important for accurate identification of diseased segments.

B-0052 10:39

Dark lumen MR in patients with Crohn's disease: two-step whole intestinal preparation with polietilenglicol

I. Sansoni, C.L. Piccolo, F. Pitocco, R. Del Vecovo, M. Cicala, B. Beomonte Zobel; Rome/IT

Purpose: The dark lumen technique (MRE and MRC) is an excellent modality for small bowel assessment in patients with IBD, but it can cause discomfort for patients. We propose an alternative method to distend and evaluate both small and large bowel by applying the dark lumen technique: 2 time polietilenglicole (PEG) administrations.

Methods and Materials: 158 patients with known CD were asked to drink twice 1.5 L of PEG solution: 2-4 hours and during 45 minutes before MR examination. A biphasic-lumen MR (1.5 T scanner) examination was performed: on axial and coronal planes we obtained T2-w and True-FISP sequences and T1-w fat-sat sequences, before and after i.v. dynamic administration of gadolinium. Scanner Time was ~23 min (range: 21-28 min). Grading of bowel distension, cleansing and parietal inflammation (active, inactive, none) was evaluated using conventional colonoscopy (CC) and post-biopsy histopathological results as gold standard in all patients.

Results: With respect to CC (achieved in 125/158 pts), in 169 sick segments MR showed a complete correlation of the presence and localisation of flogosis, and good correlation of flogosis grading (PPV 95.8%, NVP 92.3%). Only 5% of colonic segments were hindered by faeces, making an adequate intraluminal diagnosis impracticable.

Conclusion: The combination of MRE and MRC allows a complete assessment of inflammation in small and large bowel in patients with CD, requiring minimal effort to patient. So whole bowel assessment with "2 steps" distension is feasible, satisfying, does not require any particular preparation or retrograde manual colon distension and it lacks of ionising radiation.

B-0053 10:48

Diffusion-weighted MR imaging of acute appendicitis in paediatric patients: comparison with conventional MRI and surgical findings
U. Bayraktutan, M. Kantarci; *Erzurum/TR (akkanrad@hotmail.com)*

Purpose: The aim of this study is to determine the value of diffusion-weighted magnetic resonance imaging for the diagnosis of acute appendicitis in paediatric patients.

Methods and Materials: Forty-five consecutive patients with a clinical diagnosis of acute appendicitis underwent abdominal MRI; 36 were operated on for acute appendicitis. First, the DWI alone was reviewed, followed by conventional MRI alone, and then conventional MRI and DWI were reviewed by two observers. The surgical findings were compared with the MRI results. Sensitivity, specificity, and accuracy were calculated for DWI, conventional MRI, and combined DWI and conventional MRI for the depiction of acute appendicitis.

Results: A combination of DWI and conventional MRI was the most sensitive and the most accurate, with corresponding sensitivity and accuracy for observers 1 and 2 (sensitivity of 0.91 and 0.88, respectively; accuracy of 0.92, 0.87, respectively). Using DWI alone the sensitivity was found to be 0.86 and 0.83, and accuracy of 0.84 and 0.82, for observers 1 and 2, respectively. Using conventional MRI alone, sensitivity of 0.80 for both, and accuracy of 0.84 and 0.82, was found, respectively, for the two observers. The accuracy of the depiction of acute appendicitis was superior using the combination of DWI and conventional MRI for both observers (accuracy of 0.92 and 0.87, respectively).

Conclusion: The use of combination of DWI and conventional MRI is a valuable technique in the diagnosis of acute appendicitis, especially in children after sub-optimal or nondiagnostic sonography.

B-0054 10:57

MRI-derived small bowel motility as a marker of disease activity in Crohn's disease using a histopathological standard of reference
A. Menys, D. Atkinson, S. Punwani, I. Proctor, M. Novelli, M. Rodriguez-Justo, D. Hawkes, S. Halligan, S. Taylor; *London/UK (alex.menys.09@ucl.ac.uk)*

Purpose: To investigate the relationship between software-derived small bowel motility index and histopathological grading of Crohn's disease activity.

Methods and Materials: A software solution designed to quantify bowel wall motion was applied to coronal breath hold cine FISP sequence (20 second breath hold, TR 4 ms, TE 1.7 ms, slice thickness 10 mm, 1 slice/0.8sec) through the terminal ileum (TI) in 27 Crohn's disease patients (13 females, mean age 33) undergoing standard MR enterography. The previously validated software uses non-rigid registration to track intensity changes over time using a manually placed linear region of interest within the bowel, providing automated estimation of bowel wall displacement, expressed as the standard deviation of jacobian determinant (motility index). All patients underwent subsequent colonoscopy and TI biopsy within a mean of 7 days. Histopathological grading of TI activity was undertaken by two experienced pathologists who derived a endoscopic acute inflammatory score (eAIS), based on the presence of ulceration, neutrophils in the lamina propria, cryptitis, crypt abscess formation, inflammatory exudates and granulomas (1-present, 0-absent). The MRI motility index was correlated with the eAIS using Kendall's rank correlation.

Results: The mean motility index and pathology score was 0.29 (range 0.07-0.56), and 2 (range 0-5), respectively. There was a statistically significant negative correlation between the motility index and activity score (Kendall tau -0.32, p=0.03)

Conclusion: Quantified small bowel motility is negatively correlated with histopathological markers of disease activity suggesting it may be used as a quantitative marker of inflammation.

B-0055 11:06

Proposal of a qualitative MRI activity index for Crohn's disease
F. Maccioni, V. Buonocore, I. Staltari, A. Pino, G. Bella, V. De Marco, M. Marini; *Rome/IT (francesca.maccioni@uniroma1.it)*

Purpose: To propose a MRI activity index for Crohn's disease (CD).

Methods and Materials: 50 patients with CD underwent ileocolonoscopy (gold standard) and MR Enterography. Endoscopic (CDEIS), biological (BA) and clinical activity (CDAI) were assessed and scored 0-3 (absent, low, definitely present, marked activity). Three activity MRI parameters were qualitatively scored 0-3:

wall oedema (a) mesenteric oedema (b) on T2-w images; Gd-enhancement on T1-weighted images (c). Two quantitative parameters were assessed: presence and number (0, 1-3, < 3) of lymph nodes (d), wall thickening (4-6 mm, 7-10 mm, > 10 mm) (e). These 5 parameters produced a basic activity score ranging between 0 and 15: 0-2 suggesting inactivity; 3-5 low activity; 6-12 activity, 13-15 high activity. This score was correlated with CDEIS, BA and CDAI. It was further multiplied for a factor 1.5 or 2 according to the length of the affected segment (length > 30 cm or > 50 cm), obtaining a length-activity score (B); then for a factor 1.5 to 2 in the presence of fistulas, abscesses or perianal disease, in relation to their extent and severity, providing a complication-activity score (C). A final integrated MRI score (D) ranged 0-60.

Results: Significant correlation between basic score and CDAI (r=0.75), CDEIS (r= 0.87) and BA (r=0.74) p < 0.0001 was obtained. High correlation (r=0.89) was obtained between complication-activity score and B, good correlation between length-activity score and CDEIS (r=0.80).

Conclusion: The basic MRI activity index correlated with clinical and endoscopic activity. Integrated scores (B, C, D) correlated with BA or endoscopy.

B-0056 11:15

MR activity assessment in Crohn's disease of the terminal ileum: free-breathing diffusion-weighted imaging (DWI) and dynamic motility evaluation as a possible alternative to MR with intravenous contrast agent

I. Sansoni, C.L. Piccolo, F. Pitocco, R. Del Vecovo, M. Cicala, B. Beomonte Zobel; *Rome/IT*

Purpose: Contrast-enhanced dynamic MR-enterography (D-CE-MRE) is an accepted method to assess Crohn's disease (CD) activity; it needs for gadolinium contrast materials. Recently, diffusion-weighted MR imaging (DWI) and its related ADC map have been used in multiple clinical condition including bowel study and Crohn's disease activity. Our aim is to investigate the value of free-breathing DWI MR imaging in the assessment of small bowel CD activity.

Methods and Materials: 77 patients with terminal ileum CD underwent MR examination after bowel oral distension with polyethyleneglycol solution. We based MR-assessment of disease activity on morphology and motility of small bowel and perivisceral structures (true-FISP, cine-true-FISP, HASTE T2W sequences), parietal signal intensity in DWI and dynamic assessment of parietal contrast enhancement (FLASH T1W-sequence). Patients were divided into three categories (negative, inactive, active disease), basing on endoscopic biopsy as the standard reference (38 cases), whole of clinical findings and MR sequences (24 cases).

Results: On DWI, Inflammatory bowel tracts showed higher signal compared to normal segments (accuracy: 89.1%, sensitivity: 89.7%, specificity: 88.2%, PPV: 92.9%, NPV: 83.3). ADC value in active disease was lower than in inactive disease (negative: $1.9 \times 10^{-3} \pm 0.3 \times 10^{-3}$ mm²/s, inactive: $1.38 \times 10^{-3} \pm 0.26 \times 10^{-3}$ mm²/s, active: $1.08 \times 10^{-3} \pm 0.22 \times 10^{-3}$ mm²/s). In all patients a complete MR examination allowed to perform a detailed and panoramic evaluation of small bowel.

Conclusion: Cine-MR mode adds suitable functional information about motility of affected loops and condition of proximal loops. Free-breathing-DWI is useful in visual assessment of CD activity; ADC values may facilitate quantitative analysis of disease activity, decreasing in inflamed bowel segments, because of restricted diffusion.

B-0057 11:24

Non-invasive assessment of bowel wall fibrosis in Crohn's disease: role of the qualitative elastographic imaging (IE) and correlation with baseline (US), colour Doppler (CD-US) and contrast-enhanced ultrasound (CE-US) patterns

V. Migaleddu, G. Virgilio, A. Scanu, M. Dore, A. Porcu, M. Marzo, D. Sirigu, D. Scanu; *Sassari/IT (migaleddu@smirg.org)*

Purpose: To correlate the ultrasonographic scores for morphologic (US), vascular (CD-US) and perfusion (CE-US) patterns with a new qualitative elastographic evaluation (EI), for defining fibrostenotic versus inflammatory bowel wall involvement.

Methods and Materials: 27 CD patients (17 females, 10 males) were included in the study, 16 patients had inflammatory, 6 stricturing and 5 penetrating disease, (18 ileal, 6 colonic and 3 ileo-colonic). We performed 27 trans-abdominal ultrasound examinations, including baseline US, CD-US, CE-US after endovascular contrast administration (SonoVue), with Siemens-Acuson Sequoia 512 (8-14 MHz linear probe) and Siemens-Acuson S2000 (9-18 MHz linear probe). The last one was used for qualitative elastographic evaluation, through a recent EI software; the quantification of contrast-enhanced sonographic perfusion was obtained using Qontrast software (Bracco). The following parameters, PEAK%, time to peak (TTP), regional blood volume (RBV), were considered. US, CD-US and CE-US



scores to assess layer (1 - 5), vascularisation (1 - 4), intraparietal or transparietal enhancement (1 - 4), characteristics, respectively, were used. We defined a new score of fibrosis comparing abdominal and bowel wall stiffness (1- 4). Correlation between EI score and US, CD-US, CE-US scores were evaluated with the non-parametric Spearman rank test.

Results: Elastographic score was significantly correlated with US score ($p=0.0001$) and qualitative CE-US score ($p < 0.0001$). Significant correlation neither with CD-US nor with PEAK, TTP and RBV were obtained with Qontrast.

Conclusion: The introduction of dedicated US software for elastographic assessment of fibrosis can improve the US diagnosis in the assessment of fibrotic versus inflammatory involvement in CD.

B-0058 11:33



Magnetic resonance imaging is correlated with faecal calprotectin level in the evaluation of small bowel and colonic Crohn's disease

J. Makanyanga, D. Pendse, E. Atkins, M. Steward, S. Bloom, S. McCartney, S. Punwani, S. Halligan, S. Taylor; London/UK (cmakanyanga@yahoo.com)

Purpose: Therapeutic strategy in Crohn's disease requires knowledge of the overall disease burden. A new MRI score of activity was tested against validated clinical reference standards reflecting global activity - Harvey Bradshaw index (HBI) and faecal calprotectin.

Methods and Materials: 27 patients (13 males) median age 33 (range 20-78) with known or suspected Crohn's disease underwent standard 1.5 T MR enterography (axial and coronal HASTE, TrueFisp and post-gadolinium coronal VIBE), completed a HBI questionnaire and provided a stool sample for faecal calprotectin. Two observers qualitatively graded bowel wall thickness, mural T2 signal, mesenteric oedema, T1 enhancement, haustral loss (colon) from 0 (normal) to 3 (most abnormal) for jejunum, proximal ileum, terminal ileum and colon (divided into 6 segments). The length of disease in each segment was measured and the individual segmental score multiplied as follows: 0-5 cm x1, 6-15 cm x1.5, and ≥ 16 cm x2. A score of 5 was added for each of the following if present: lymphadenopathy, comb sign, abscesses and fistulae. Kendall's rank correlation was used to evaluate the relationship between MRI score, faecal calprotectin and HBI.

Results: The mean MRI activity score was 13 (range 0-49). A positive correlation was found between the MRI score and calprotectin, Kendall's tau $b=0.37$ (95% CI 0.1 to 0.6) $p=0.01$. No correlation was found between MRI and HBI, Kendall's tau $b=0.01$, $p=0.9$.

Conclusion: Global Crohn's disease activity measured using a simple clinical MRI score is correlated with the faecal calprotectin level. MRI is useful for the global assessment of disease activity in Crohn's disease.

B-0059 11:42



The diagnostic value of small bowel wall vascularity after sulphur hexafluoride-filled microbubble injection in the differentiation of inflammatory and fibrotic stenoses in patients with Crohn's disease

E. Quaia, L. De Paoli, B. Cabibbo, F. Degrassi, M. Cova; Trieste/IT (quaia@units.it)

Purpose: To assess the value of small bowel wall vascularity after microbubble contrast agent injection to differentiate inflammatory from fibrotic stenoses in patients with Crohn's disease.

Methods and Materials: Fifteen patients (7 males and 8 females; mean age \pm SD, 40 years \pm 6) with a biopsy-proven diagnosis of Crohn's disease - Crohn's disease activity index (CDAI) > 150 ($n=12$ patients) or < 150 ($n=3$) - involving at least one ileal loop (wall thickness measured by unenhanced US, > 5 mm) were included. In each patient the terminal loop was scanned by contrast-enhanced ultrasound (CEUS) after sulphur hexafluoride-filled microbubble injection, and digital cine-clips (30 seconds) were stored in DICOM format. The vascularity of the terminal loop was quantified in grey-scale levels (0-255) by a manually drawn ROI encompassing the thickened bowel wall and it was correlated with CDAI. The percentage of enhancement compared to baseline, the time to peak enhancement, and the area under curve were calculated.

Results: All patients revealed diffuse transparietal contrast enhancement after microbubble injection, except for 3 patients with fibrotic stenosis who revealed contrast enhancement limited to the submucosa. Inflammatory vs fibrotic stenoses did not differ in the percentage of enhancement (46.45 ± 8.13 vs $48.25 \pm 25.24\%$) and in the time to peak enhancement (16.58 ± 4.76 vs 11.55 ± 4.1 secs; $P > .05$), while difference in the area under the enhancement curve was found (1684 ± 651.76 vs 778.15 ± 309.2 ; $P < .05$) with a significant correlation with the CDAI score ($\rho = .85$, $P < .05$).

Conclusion: The quantitative analysis of bowel wall hypervascularity on CEUS may differentiate inflammatory from fibrotic stenoses in patients with Crohn's disease.

B-0060 11:51

Low-dose CT in initial evaluation of Crohn's disease in the emergency setting? Toward replacing the PFA

S.B. O' Neill, F. O' Neill, A. McGarrigle, F. Shanahan, M.M. Maher; Cork/IE (siobhanxx@gmail.com)

Purpose: Crohn's disease (CD) patients are "at risk" for exposure to significant cumulative effective doses of radiation from diagnostic imaging studies. The purpose of this study is to compare the diagnostic yield of low dose CT (LDCT) with iterative reconstruction to that of conventional plain film of abdomen (PFA).

Methods and Materials: Following ethical approval, 50 patients with CD referred for clinically indicated CT abdomen/pelvis (CTAP) were prospectively recruited to undergo additional LDCT at time of CTAP. Of these, 34 patients had a contemporaneous PFA (within 24 hrs of CT) (male:female, 13:21; mean age, 37 years, range 19-39; mean BMI 24.6 kg/m², range 17.4-35.5). The effective dose (ED) in mSv for each LDCT was calculated. 2 radiologists, in consensus, reviewed the LDCT images and the PFAs (9 months later) with a validated Crohn's-specific coding system.

Results: The mean ED for LDCT was 1.21 ± 0.7 mSv (range, 0.46-3.2 mSv) ($p < 0.001$), a mean dose reduction of 74% from conventional CT, without loss of diagnostic utility. The mean ED for BMI < 25 kg/m² was 8.8 ± 0.2 mSv and for BMI > 25 kg/m² was 1.8 ± 0.7 mSv. The approximate mean ED of a PFA is 0.7 mSv. There was agreement between PFA and LDCT in 4 patients only (no abnormal findings). Findings on LDCT missed on PFA included abscesses ($n=3$), obstruction ($n=5$), colitis ($n=13$) and enteritis ($n=18$). LDCT detected more clinically significant incidental findings.

Conclusion: LDCT with iterative reconstruction yielded far superior diagnostic information than PFA at an ED that approximates to 1-2 PFAs. LDCT may represent a feasible replacement for initial PFA, imparting very little additional radiation exposure.

10:30 - 12:00

Room F1

Genitourinary

SS 107

Prostate MR imaging

Moderators:

J.J. Fütterer; Nijmegen/NL
J. Richenberg; Brighton/UK

B-0061 10:30

Functional prostate MRI: evaluation of a scoring system

S. Roehlen, C. Arsov, D. Blondin, J. Klasen, R. Lanzman, G. Antoch, P. Albers, M. Quentin; Düsseldorf/DE (michael.quentin@med.uni-duesseldorf.de)

Purpose: Functional prostate MRI is performed in varying combinations of T2-weighted images with diffusion-weighted imaging (DWI), dynamic contrast-enhanced MRI (DCE-MRI) and spectroscopic imaging (MRSI). Recently, a European consensus meeting proposed the use of a simple 5-point scale for estimating the probability of a lesion to be malignant. This recommendation has not been validated so far, which is the aim of the present study.

Methods and Materials: The appearance of 108 predefined lesions in three different MR sequences (T2-weighted images, DWI, and DCE-MRI) in 50 functional prostate MRI examinations have been retrospectively scored by three blinded radiologists using the 5-point scale for each MR sequence. After scoring T2/DWI and T2/DWI/DCE-MRI every lesion was graded based on its probability for malignancy. Inter-observer reliability was evaluated using Kappa statistics (k).

Results: With respect to T2-weighted images, DWI and DCE-MRI k were 0.5, 0.96, and 0.78, respectively. Combined scoring of T2-weighted images and DWI demonstrated correct tumour diagnosis (true positive) in 71%-88% (depending on reader) of cases ($k=0.81$). The accuracy was further improved to 88%-96% after scoring all three MR sequences including DCE-MRI ($k=0.91$).

Conclusion: The use of a simple 5-point scoring system for T2-weighted images, DWI, and DCE-MRI is feasible in functional prostate MRI and comes along with a high inter-observer reliability.

B-0062 10:39

Prostate cancer screening: the role of pre-biopsy MRI of the prostate in ruling out prostate cancer

T. Franiel¹, H.A. Vargas², Y. Mazaheri², S. Boehmer¹, H. Hricak², O. Akin², D. Beyersdorff¹; ¹Berlin/DE, ²New York, NY/US (tobias.franiel@charite.de)

Purpose: To evaluate the role of prostate magnetic resonance imaging (MRI) in patients with suspected prostate cancer.

Methods and Materials: Ethics board approval was received for this retrospective analysis of prospectively acquired data. Ninety men (median age 66 years; median PSA 4.8 ng/ml) underwent combined endorectal/body phased-array coil 1.5-Tesla MRI before their first systematic 12-core biopsy with transrectal ultrasound (TRUS) guidance. MR images were analysed independently by three radiologists. The radiologists divided the prostate into 12 regions corresponding to the biopsy scheme and evaluated each region for the presence of cancer in a standardised manner using a 5-point scale. At statistical analysis, scores were dichotomised as benign (0.1) vs. malignant (2,3,4). Results were analysed by sextant. Receiver operating characteristic (ROC) analysis was done and descriptive statistics were calculated. **Results:** Systematic TRUS-guided 12-core biopsy found cancer in 48/90 patients (26 low-grade cancer (Gleason score = 3+3), 22 high-grade cancer (Gleason score \geq 3+4)), and 185/1080 cores (76 low-grade cancer, 109 high-grade cancer). Areas under ROC curves were for the three readers by sextants 0.61-0.65 for overall prostate cancer detection and 0.64-0.72 for detection of high-grade cancer. Descriptive statistics for detection of all cancers/high-grade cancers by sextant were as follows: negative predictive value, 81.7%-83.0%/ 91.9%-92.4%; specificity, 73.2%-80.2%/ 73.1%-80.1%; sensitivity, 44.0%-50.8%/ 58.6%-64.3%; and positive predictive value, 35.7%-40.4%/ 28.8%-33.3%.

Conclusion: In patients with suspected prostate cancer, negative MRI findings rule out high-grade prostate cancer on subsequent TRUS-guided 12-core biopsy with a high probability. However, sensitivity is low, and patients should undergo close follow-up.

B-0063 10:48

Prostate cancer: role of pretreatment multiparametric MRI in predicting biochemical recurrence following radical prostatectomy

J. Park, C. Kim, B. Park, H. Lee, S. Jeon, S. Seo, H. Choi; Seoul/KR (jungjaesmc.park@samsung.com)

Purpose: To retrospectively determine whether pretreatment multiparametric MRI findings can predict biochemical recurrence (BCR) in patients who undergo radical prostatectomy (RP) for prostate cancer.

Methods and Materials: 282 patients (median age, 64 years; age range, 38-88 years) with biopsy-proven prostate cancer who received RP underwent pretreatment multiparametric MRI at 3 T, including T2-weighted (T2WI), diffusion-weighted (DWI) and dynamic contrast-enhanced imaging (DCEI). MRI variables, derived from retrospective consensus assessments by two readers, included apparent tumour presence at T2WI + DWI, T2WI + DCEI, and T2WI + DWI + DCEI, extracapsular extension, seminal vesicle invasion and tumour size at DWI or DCEI. Clinical variables included pretreatment prostate-specific antigen (PSA), clinical T stage and Gleason score. Univariate and multivariate Cox regression analyses investigated the relationship between clinical and imaging variables and BCR.

Results: After a median follow-up of 26 months, BCR developed in 61 patients (22%). Univariate analysis revealed that MRI and clinical variables were all significantly related to BCR ($P < 0.01$). Multivariate analysis revealed that pretreatment PSA [hazard ratio (HR) 1.05; $P = 0.002$] and Gleason score (HR 1.36; $P = 0.017$) were the only significant independent predictors for BCR. Apparent tumour presence at T2WI+DWI+DCEI was an independent predictor of borderline significance for BCR on multivariate analysis (HR 2.37; $P = 0.069$).

Conclusion: Apparent tumour presence at combined T2WI, DWI and DCEI appears to be an independent predictor of borderline significance for BCR following RP, and pretreatment PSA and Gleason score are significant independent predictors for this endpoint.

B-0064 10:57

Assessment of aggressiveness and tumour volume of prostate cancer: correlation of ADC with histologic grade and pathological tumour volume

G. Khoury, D. Eiss, F. Beuvon, N.B. Delongchamps, F. Cornud; Paris/FR (khoury.gab@gmail.com)

Purpose: To correlate apparent diffusion coefficient (ADC) values, tumour volume (TV) with Gleason score (GS) and pathological volume of prostate cancer (PCa) on whole mount radical prostatectomy (RP) specimens.

Methods and Materials: 144 PCa, 97 in the PZ and 47 in the TZ were evaluated in 84 patients by endorectal prostate MRI at 1.5 T, including T2-weighted and diffusion-weighted MRI, before RP. MRI-tumour volume was compared to pathological findings of digitised slides of whole mount RP. Correlation between ADC values and GS was performed in the PZ and the TZ for tumours with no high Gleason grade (group1) versus tumours with 0-20 (group2), 30-50 (group3), and more than 50% of high Gleason grades (group4). TV were compared by the Bland-Altman test.

Results: ADC values were not significantly different between groups 1 and 2 and between groups 3 and 4. When groups 1+2 versus groups 3+4 were compared, ADC values were significantly lower in group 3+4 (866 ± 272 vs 1378 ± 370 , in the PZ and 828 ± 251 vs 1155 ± 52 , $p < 0.0001$). Distinction between these two groups was achieved with a sensitivity of 78 and 84% and a specificity of 81% and 71%, respectively. Comparison of pathological with T2W-MRI and DW-MRI tumour volume showed a mean difference of 15% (range-128/+157) and of 25% (range-91/+141), respectively. When both sequences predicted a TV < 0.5 cc, concordance with the pathological volume was observed in 86% cases.

Conclusion: Tumours with more than 20% of high Gleason grades can be predicted by measurement of the ADC value. Concordance between TV on MRI and pathological volume was high for tumours < 0.5 cc.

B-0065 11:06

Multi-parametric MR imaging for detection and localisation of transition zone prostate cancer

C.M.A. Hoeks, T. Hambrock, D. Yakar, C. Hulsbergen-vande Kaa, A.J. Witjes, J.J. Futterer, J.O. Barentsz; Nijmegen/NL (C.Hoeks@rad.umcn.nl)

Purpose: To retrospectively determine detection and localisation accuracy for Gleason grade (GG) 2-3 and GG 4-5 transition zone (TZ) cancer of T2-weighted (T2WI) MR imaging (MRI) versus multi-parametric MR imaging (MP-MRI) using radical prostatectomy specimens (RP) as gold standard.

Methods and Materials: Inclusion criteria were TZ cancer > 0.5 cm³ upon RP and 3 T endorectal MP-MRI (T2WI, diffusion weighted MRI + apparent diffusion coefficient maps (ADC) and dynamic contrast-enhanced MRI (DCE-MRI)). From 98 RP, 20 patients with TZ cancers were included. Twenty-two patients without TZ- with peripheral zone (PZ) cancer were randomly selected as control-group. Four radiologists randomly scored T2WI, T2WI+ADC, T2WI+DCE-MRI and T2WI+ADC+DCE-MRI with a two-week interval. TZ cancer suspicion was rated on a 5-point scale in 6 TZ regions of interest (ROI). A 4-5 score was a positive detection accuracy result. Localisation accuracy was analysed using ROI-ROC with generalised estimation equations.

Results: Significantly more GG 4-5 (86-91%) versus GG 2-3 (28-47%) TZ cancers were detected ($p < 0.001$). Only for GG 2-3 TZ cancers detection accuracy was significantly improved by MP-MRI compared to T2WI (61% versus 44%, $p = 0.02$). Using MP-MRI localisation accuracy was improved for GG 4-5 TZ cancers only (AUC: 0.94 for MP-MRI versus 0.91 for T2WI, $p = 0.02$).

Conclusion: Detection rates of GG 4-5 TZ cancers are significantly higher than those of GG 2-3 TZ cancers. MP-MRI compared to T2WI improves detection accuracy for GG 2-3 TZ cancers only. MP-MRI slightly improves TZ cancer localisation accuracy compared to T2WI.

B-0066 11:15

Retrospective correlation between pathological specimens and multiparametric MRI for detection of prostate cancer

F. Russo¹, E. Armando¹, S. Mazzetti¹, I. Bertotto¹, E. Bollito², F. Porpiglia², D. Regge¹; ¹Candiolo/IT, ²Orbassano/IT (filippo.russo@ircc.it)

Purpose: To understand causes of failure to identify cancer lesions.

Methods and Materials: 42 patients with bioptic diagnosis of prostate cancer (PCa) underwent MRI examination at 1.5 T. T2, DWI and DCE-MRI images were analysed for the identification of PCa. On the basis of pathologic examination after surgery, MRI findings were reanalysed by an expert radiologist to evaluate MRI features of PCa missed at the first analysis.

Results: Pathologic analysis found 87 PCa; 60 had a pathological volume > 0.2 ml. Before prostatectomy MRI detected 45/60 lesions > 0.2 ml (sens.75%), 40/48 (sens.83%, mean ADC:0.82) in the peripheral zone (PZ) and 5/12 (sens.42%, mean ADC:0.69) in the transitional zone (TZ). Pathology-based MRI reanalysis allowed to recognise 54/60 PCa, 45/48 in PZ and 9/12 in TZ. The 5 missed lesions in PZ had smaller volumes (0.68±0.23 vs 1.7±1.59 ml). Among 9 missed lesions only one, localised in PZ, had an ADC > 1.1. 7/9 had ADC values < 1 and 1/9 an ADC of 1.07. A mild hypointense lesion, interpreted as prostatitis, had a type1 T/I curve and an ADC of 0.93. 2 lesions of PZ and TZ were hypovascularised (ADC:

0.66 and 0.6, respectively). A PZ lesion was missed for its linear shape ($ADC < 1$). 3/4 TZ lesions with low ADCs (mean:0.73) were interpreted as stromal adenomas.
Conclusion: We found many causes of diagnostic failure: hypovascularised lesions in PZ and TZ, thin lesions in PZ, gland inhomogeneity especially in TZ, lesions size, intermediate ADC values. MRI reanalysis identifies in ADC values the most accurate method to identify prostate cancer.

B-0067 11:24

Is it possible to model the risk of malignancy of focal abnormalities found at prostate multiparametric MRI?

O. Rouviere, M. Papillard, N. Girouin, R. Boutier, M. Rabilloud, B. Riche, F. Mege-Lechevallier, M. Colombel, A. Gelet; *Lyon/FR* (*olivier.rouviere@chu-lyon.fr*)

Purpose: To evaluate whether focal abnormalities (FAs) depicted by prostate MRI could be characterised using simple semiological features.

Methods and Materials: 134 patients who underwent T2-weighted, diffusion-weighted and dynamic contrast-enhanced MRI at 1.5 T before prostate biopsy were prospectively included. FAs visible at MRI were characterised by experienced uro-radiologists using their shape, the degree of signal abnormality (0=normal to 3=markedly abnormal) on individual MR sequences, and a subjective score (SS1=probably benign to SS3=probably malignant). FAs were then biopsied under US guidance.

Results: 56/233 FAs were positive at biopsy. The subjective score significantly predicted biopsy results ($p < 0.01$). As compared to SS1 FAs, the odds ratios (OR) of malignancy of SS2 and SS3 FAs were 9.9 (1.8-55.9) and 163.8 (11.5-2331). The shape of FAs was not a significant predictor of biopsy results in the peripheral zone (PZ); its predictive value was not tested in the transition zone due to the small number of cases. In contrast, a simple combination of MR signal abnormalities (into "low-risk", "intermediate" and "high-risk" groups) significantly predicted biopsy results ($p < 0.008$). As compared to "low risk" FAs, the OR of malignancy of "intermediate" and "high-risk" FAs were 4.5 (1.1-18.4) and 52.7 (6.8-407) in the overall population and 5.4 (1.1-27.2) and 118.2 (6.1-2301) in PZ.

Conclusion: A simple combination of signal abnormalities of individual MR sequences can significantly stratify the risk of malignancy of FAs and give similar results to a subjective score assigned by expert uro-radiologists. This holds promise of a more standardised interpretation of MRI by readers with varying experience.

B-0068 11:33

Accuracy of ultrahigh b values (b2000) to differentiate benign from malignant prostatic nodules on endorectal diffusion-weighted imaging

Q. Monzani, A. Schull, N.B. Delongschamps, F. Beuvon, P. Legmann, F. Cornud; *Paris/FR* (*qmonzani@yahoo.com*)

Purpose: To assess the accuracy of endorectal diffusion-weighted MRI (erDWI-MRI) at 1.5 Tesla with ultrahigh b values to differentiate benign from malignant prostatic nodules.

Methods and Materials: 67 consecutive patients with no previous biopsy, a normal digital rectal examination and a PSA level of 4-10n g/ml were referred underwent erMRI T2-weighted and DWI-MRI (10b-value apparent-diffusion-coefficient (ADC) mapping and b2000 images) was performed before sextant and TRUS-MRI image fusion-guided biopsies. On b2000-DWI, signal intensity (SI) was prospectively measured on hyperintense nodules originating in the peripheral and transition zone (PZ and TZ) and on the remaining surface on the same slice. SI of the corresponding areas on ADC and b1000 images was measured. Nodule/prostate SI ratios were calculated for b1000 and b2000 and b2000ratio/b1000ratio was then calculated. Areas under the curves (AUC) of ADC mapping and b2000ratio/b1000ratio were compared to biopsy results.

Results: MRI examination showed 58 nodules in 41 patients (26 in the PZ and 32 in the TZ). Twenty-nine nodules were malignant (29/58.50%). b2000ratio/b1000ratio value was significantly higher in malignant nodules than in benign nodules ($p=0.0001$). AUC value of the b2000ratio/b1000 ratio was not significantly higher than that of ADC (0.82vs0.71, $p=0.052$). Sensitivity and specificity were 93 vs 62% and 76 vs 72%, respectively.

Conclusion: b2000ratio/b1000ratio SI value helps to differentiate benign from malignant prostatic nodules in both PZ and TZ. Although performance was better than that of ADC mapping, the difference only approached significance.

B-0069 11:42

Feasibility and reliability of MR-guided biopsy of the prostate gland: comparison to histopathological outcome

A. Malich, A. Kott, A. Ulrich, J. Feger, R. Chelaru; *Nordhausen/DE* (*chelaru_robert²⁰⁰⁷@yahoo.com*)



Purpose: A relevant number of patients suffering from prostate cancer remain undetected after ultrasound guided biopsy. Prostate-MRI and MR-guided biopsy might overcome this diagnostic gap.

Methods and Materials: As a result of a diagnostic prostate MRI (Philips Intera-Achieva; 1.5 T), performed at patients who underwent ultrasound-based biopsy of the prostate gland with a negative result, 68 lesions were detected to be suspicious due to pathological contrast uptake ($> 200\%$ initial uptake, dynamic series 14s, 11 series) and suspicious diffusion coefficient. These lesions were biopsied MR-guided using CAD-calculation for access (DynaCAD for prostate Invivo-Philips, NL) and related hardware (DynaTRIM). Intervention was performed with a 18G biopsy needle.

Results: 26/68 histologically verified lesions were proven to be malignant/premalignant (38.2%), in 11/194 samples no prostatic tissue was found (5.7%). Among the 21 verified invasive malignant lesions, 4 were summarised as high grade, 7 intermediate and 9 low grade. 4 malignant lesions were histologically confirmed as T1, 9 as 2a and 8 as 2b. Mean Gleason-score was 6.2. 5 lesions were verified as high risk ASAP-lesions, 4 were of other benign histology. Among the benign entities prostatitis was commonly observed in 21 cases, hyperplasia in further 8 cases and atrophic glandular tissue in 9 cases (13.6%). Only 2 malignant lesions were located in the peripheral zone, 4 in the central zone exclusively.

Conclusion: MR-guided prostate biopsy is a precise technology with a high detection rate of prostate cancer to be recommended as the method of choice after a negative sonographical biopsy with suspicious diagnostic prostate-MRI.

B-0070 11:51

MRI and ultrasound-guided prostate biopsy using real time soft image fusion (Koelis®): a pilot study

E. Rud, E. Baco, D. Klotz, A. Svindland, H.B. Eggesbo; *Oslo/NO* (*p.e.rud@medisin.uio.no*)



Purpose: Transrectal ultrasound (TRUS)-guided biopsies are the gold standard when diagnosing prostate cancer. However, exact biopsy locations cannot be verified, and there is a high rate of false negative biopsies. Magnetic resonance imaging (MRI) can identify tumours, but it is still not possible to document biopsy positions using TRUS. A new 3D-guided TRUS biopsy method (Koelis®), can document exact biopsy locations, and with real time soft image MRI fusion, targeted biopsies can be performed. The aim of the study was to evaluate Koelis® 3D ultrasound and MRI fusion-guided biopsy technique.

Methods and Materials: Ninety patients (50-80 yrs, mean 64 yrs, mean PSA 7 ng/ml) underwent MRI prior to prostate biopsies. Subgroups: primary biopsy: 11 pts, 1st-5th rebiopsies: 62 pts, and biochemical recurrence (BCR) after radiotherapy: 17 pts. MRI: 1.5T Avanto (Siemens, Erlangen) and body array coil. Sequences: ax 3D T2 and DWI. Post-imaging processing: Nordic ICE®. Tumours were highlighted on axial T2 images and classified as high-, moderate- or low degree of suspicion. Biopsies: 3D AccuvixV10 (Medison® Korea), navigation system: Koelis® Grenoble, France.

Results: 121 nodules were biopsied. Positive biopsies according to degree of suspicion; high 47/52 (90%), medium 6/22 (27%) and low 4/47 (9%). Random biopsies were and positive in 6/47 (13%). Biopsy positive subgroups: primary biopsy positive 9/11 (81%), 1st-5th rebiopsy 32/62 (51%), BCR after radiotherapy: 13/17 (76%).

Conclusion: The Koelis® method is feasible and allows accurate targeted biopsies. Hence, false negative biopsies and the use of random biopsies can be reduced.

10:30 - 12:00

Room F2

Breast

SS 102

MRI: 3 T, unenhanced and more

Moderators:

A. Linda; Udine/IT

C. Loo; Amsterdam/NL

B-0071 10:30

The influence of hormonal fluctuations on quantitative diffusion-weighted magnetic resonance imaging (DW-MRI) of the glandular breast tissue in healthy premenopausal participants at 3 T

N.M.M.R. AlRashidi, G. Waite, T. Ahearn, F.J. Gilbert, T.W. Redpath; Aberdeen/UK (n.alrashidi.07@aberdeen.ac.uk)

Purpose: To determine whether the cyclical changes in the hormonal levels affect quantitative values of apparent diffusion coefficient (ADC) and transverse relaxation time (T2) for glandular tissues in healthy premenopausal women.

Methods and Materials: The study was performed using a 3 T MRI Philips Scanner and a dedicated bilateral 16 channel phased array breast coil. Participants were scanned four times during the menstrual cycle. ADC map was generated from a diffusion-weighted imaging (DWI) pulse sequence with four b values (0, 50, 150, and 800 s/mm²). T2 map was generated from a multiple spin echo (SE) pulse sequence with four echo times (TE) (20, 40, 60, and 80 ms). Regions of interest (ROI) were placed in the glandular tissue at the each of the four different phases of the menstrual cycle in each breast.

Results: Quantitative measurements were obtained in 20 healthy participants (22-50 years old) with regular menstrual cycle. The results of the ADC ($\times 10^{-3}$ mm²/s) during 1st, 2nd, 3rd, and 4th week were (1.74 \pm 0.3, 1.7 \pm 0.3, 1.73 \pm 0.3, and 1.75 \pm 0.2, respectively) and T2 values (ms) were (61.8 \pm 7.7, 61 \pm 8, 61.7 \pm 7.6, and 62 \pm 7 respectively). ANOVA test shows that there was no statistically significant influence of menstrual cycle on mean ADC or T2 values. However, there was a significant age by week of cycle interaction.

Conclusion: There was no significant difference in mean ADC and T2 values across the weeks of the menstrual cycle. However, age can be considered as influencing factor.

B-0072 10:39

Effects of inhomogeneous radiofrequency power deposition on the apparent diffusion coefficient of the normal breast at 3.0 T

R. Girometti, M. Maieron, M. Bazzocchi, R. Padovani, C. Zuiani; Udine/IT (rgirometti@sirm.org)

Purpose: To investigate whether the apparent diffusion coefficient (ADC) quantification in the breast is affected by the inhomogeneity of radiofrequency power deposition (RPD) inherent to 3.0 T systems.

Methods and Materials: We enrolled 21 patients without evidence of breast lesions at bilateral breast magnetic resonance imaging performed on a 3.0 T magnet. Before contrast administration, two sequences were consecutively acquired: a) a transmit magnetic field (B1)-mapping sequence generating a B1-map; b) a diffusion-weighted echo-planar sequence generating b=0, 500 and 1000 sec/mm² images together with an ADC-map. In each patient, breasts were divided into four per-side symmetrical regions (I-IV) on the axial slice passing through the nipples, in order to calculate - on a per region basis: a) the percent of RPD flip-angle from B1-map; b) the apparent diffusion coefficient (ADC) of fibroglandular tissue (FIT). Analysis was performed with a Kruskal Wallis test and the u-Mann-Whitney test.

Results: RPD was significantly higher in left breast regions as compared to the right ones (p < 0.0001). Lowest RPD was found in the right internal region (rIII) (41.14 \pm 5.60%). The same trend was observed for the FIT-ADC value, although differences were not statistically significant (average ADC of 0.88 \pm 0.53 $\times 10^{-3}$ mm²/sec at the region rIII).

Conclusion: Inhomogeneity in RPD at 3.0 T affected the right breast. Although not statistically significant, related difference between right and left breast FIT-ADC suggests that ADC quantification is potentially unreliable at 3.0 T unless systems to homogenise RPD are used.

B-0073 10:48

Accuracy of 3 T magnetic resonance imaging with a high-relaxivity contrast agent in assessing treatment response in patients undergoing neoadjuvant chemotherapy

M. Telesca, F. Pediconi, M. Luciani, F. Vasselli, V. Casali, E. Miglio, C. Catalano; Rome/IT (mariannatelesca@yahoo.it)

Purpose: To assess the accuracy of magnetic resonance imaging at 3 T (3 T MRI) in evaluating residual disease after neoadjuvant chemotherapy (NAC) in patients with advanced breast cancer.

Methods and Materials: Between March 2010 and July 2011, 17 women with advanced breast cancers underwent dynamic 3 T MRI before and after NAC. The MRI protocol comprised precontrast FSE T2w IDEAL sequence and VIBRANT 3D T1w sequence acquired before and after administration of gadobenate dimeglumine (MultiHance) at 0.1 mmol/kg body weight. A dedicated bilateral breast coil was used. For each patient tumour size was determined before and after NAC. If bilateral, multifocal or multicentric disease was present, only the major lesion was considered. The MRI evaluation of treatment response was classified based on RECIST criteria. Residual tumour sizes obtained using MRI were compared with pathological findings.

Results: A total number of 20 lesions were evaluated. The sensitivity, specificity and accuracy of MRI in detecting residual disease was 100%, 78%, and 90%, respectively (area under ROC curve: 0.941). MRI overestimated the presence of residual tumour in 2 cases. The mean of the largest diameters measured at baseline MRI, post-treatment MRI and histology were 32.4, 9.25 and 5.45 mm, respectively. The tumour size difference between MRI and histology was not statistically significant (P value=0.19). We found a statistically significant correlation between MRI and pathology measurements (Spearman r = 0.6114; P value=0.0042).

Conclusion: The presence and size of residual disease in breast patients treated with NAC could be accurately evaluated using 3 T MRI and high-relaxivity contrast agent.

B-0074 10:57

MR-mammography at 3 T in clinical practice: prospective single centre experience

P.A.T. Baltzer, W.A. Kaiser, H.P. Burmeister, M. Dietzel; Jena/DE (pascal.baltzer@med.uni-jena.de)

Purpose: Higher magnetic field strength leads to higher signal-to-noise ratio, which may be invested in higher spatial or temporal resolution for breast imaging. While stronger chemical shift between fat and water may be useful in fat saturated 3D gradient echo imaging, B0 and B1 inhomogeneities may negatively affect imaging. We report on our prospective experience using 3 T MR-mammography (MRM) in clinical practice.

Methods and Materials: Consecutive patients underwent MRM (3 T, Rapid 16-channel breast coil) according to European recommendations (dynamic T1w fat saturated 3D-VIBE, 0.1 mmol/kg Omniscan, T2w-TSE, STIR, acquisition time 15 min). Reference standard was histopathology or follow-up \geq 12 months. Results from double reading by two experienced radiologists in clinical practice were recorded prospectively. Results per breast were compared with the reference standard using contingency tables. Sensitivity, specificity, positive and negative likelihood ratio (LR+, LR-) were calculated.

Results: 224 breasts in 112 patients were included. Indications for MRM were unclear (n=42) or suspicious (n=54) results in conventional imaging, aftercare (n=24), clinical findings (n=6), follow-up of benign lesions (n=22) and contralateral findings (n=76). Sensitivity, specificity, LR+ und LR- of 98.0%, 90.8%, 10.7 und 0.02 were observed. Regularly, inhomogeneous fat saturation due to B0 inhomogeneities was observed which did not have a detrimental influence on diagnostic accuracy. All false positive findings presented as non-mass enhancements.

Conclusion: MRM at 3 tesla showed excellent diagnostic accuracy. Similar to MRM at 1.5 T, non-mass like enhancements were diagnostically challenging. 3 T typical artefacts did not have a detrimental effect on diagnostic performance.

B-0075 11:06

Back to the future: non-contrast breast MRI (nc-BMRI) using a combination of T1-weighted, diffusion-weighted and STIR imaging

R.M. Trimboli¹, N. Verardi¹, L.A. Carbonaro¹, F. Cartia¹, G. Di Leo², F. Sardanelli¹; ¹San Donato Milanese/IT, ²Corunna/IT

Purpose: Our aim was to assess per-breast sensitivity and specificity of nc-BMRI.

Methods and Materials: A consecutive series of women who underwent breast MRI at our institution from November 2009 to December 2010 was included in this retrospective study. Two blinded readers with 3- (R1) and 1-year (R2) of

Thursday

BMRI experience evaluated nc-BMRI studies performed using gradient-echo T1-weighted, T2-weighted STIR, and diffusion-weighted imaging ($b=0$ and 750-1,000 s/mm^2) assigning a BI-RADS 1-5 score for each breast. Readers were blinded to contrast-enhanced (CE) BMRI and final diagnosis. Breasts assigned BIRADS 1-3 were considered as negatives and those assigned BIRADS 4-5 as positives. Sensitivity, specificity, and accuracy were estimated. A combination of mammography, ultrasound, CE-BMRI (0.1 mmol/kg of gadobenate dimeglumine), and pathology was considered as a standard of reference. Interobserver agreement was estimated using Cohen kappa statistics.

Results: A total of 133 breasts in 68 patients aged 55 ± 12 years (range 24-88 years) were analysed. Per-breast cancer prevalence was 33/133 (25%): IDC ($n=24$), ILC ($n=2$), DCIS ($n=3$); cancers not otherwise specified ($n=4$). R1 had sensitivity of 26/33 (79%), specificity of 86/98 (88%), and accuracy of 112/133 (85%); R2 had sensitivity of 26/33 (79%), specificity of 90/98 (90%), and accuracy of 116/133 (87%). For R1, false negatives were four IDC, one DCIS, and one ILC, one cancers not otherwise specified. For R2, false negatives were four IDC, one DCIS, and one ILC, one cancers not otherwise specified. Interobserver agreement was almost perfect ($k=0.925$).

Conclusion: A combination of T1-weighted, diffusion-weighted, and STIR imaging allowed for a good diagnostic performance with high specificity.

B-0076 11:15

Breast MRI at 3 T: a pilot study estimating sensitivity and specificity of unenhanced MRI (DWI combined with T2 IDEAL sequence) vs CE-MRI in the assessment of response to neo-adjuvant chemotherapy

F. Pediconi, M. Telesca, M. Luciani, F. Vasselli, V. Casali, E. Miglio, C. Catalano; Rome/IT (federica.pediconi@uniroma1.it)

Purpose: To identify sensitivity and specificity of a contrast-agent-free diagnostic approach combining only DWI with T2 IDEAL images (ueMRI) and compare the results with contrast-enhanced MRI (CE-MRM) in the assessment of response to neo-adjuvant chemotherapy using a 3 T Magnet.

Methods and Materials: Consecutive patients undergoing neo-adjuvant chemotherapy for biopsy-proved breast cancer > 2 cm underwent 3 T-MR prior to chemotherapy (every two cycles) and before surgical excision. MR protocol comprised an FSE-T2-IDEAL and DWI sequences, and Vibrant 3D T1-weighted sequence acquired before and after administration of contrast media. Tumour response was classified using RECIST criteria using tumour size at MRI. Tumour response at MRI after chemotherapy was compared to histological specimen after surgery. Two blinded observers rated ueMRI and then CE-MRI for the evaluation of tumour response. Lesion size, ADC values and FSE-IDEAL descriptors were assessed.

Results: 32 patients were enrolled. Sensitivity of ueMRI was 92% (observer 1) and 84% (observer 2). Sensitivity of CE-MRI was 100% for both observers. Specificity was 82% (ueMRI) and 86% (CE-MRI) for both observers. The differences between both methods and observers were not statistically significant ($P \geq 0.09$). Lesion size measurements did not differ significantly between all sequences analysed. Tumour ADC values demonstrated significant differences between responders and non-responders after the first II cycles of treatment.

Conclusion: Combination of DWI and T2-IDEAL allow to obtain similar value of sensitivity and specificity of CE-MRI in the evaluation of tumour response to neo-adjuvant chemotherapy. ADC values could be useful for differentiating responders from non-responders earlier during the treatment.

B-0077 11:24

To contrast or not to contrast? A new approach to unenhanced MR mammography

M. Lorenzon, C. Zuiani, A. Linda, S. De Stefani, M. Maieron, R. Girometti, M. Bazzocchi; Udine/IT (michele.lorenzoni@gmail.com)

Purpose: To assess sensitivity, specificity, positive and negative predictive value (PPV, NPV) of unenhanced (UE) MR-mammography (MRM).

Methods and Materials: we enrolled all patients undergoing contrast-enhanced (CE) MRM in our institution between February and May 2010, with histological diagnosis or one-year follow-up. Patients undergoing neoadjuvant chemotherapy were excluded. Using a 1.5 T-scanner, STIR-T2W, DW and T1W images before and after Gadolinium injection were acquired. Two readers in consensus prospectively assessed ueMRM (i.e. T2W, DW and T1W images acquired before Gadolinium injection), without the knowledge of clinical, mammography, ultrasound and pathological diagnosis. Based on morphological features (asymmetry, architectural distortion or mass - for masses: shape, margins, signal features) and ADC-values (cut-off: $1.2 \cdot 10^{-3} mm^2/s$), readers reported whether they were confident in excluding an underlying malignancy or not, hypothetically addressing patients to contrast agent injection only in the second case. Clinical, mammography, ultrasound,

ceMRM, pathological findings and follow-up data were considered the reference standard (RS). Sensitivity, specificity, PPV and NPV of ueMRM were assessed. A Chi-square test was used to assess any statistically significant differences between ueMRM and the RS.

Results: 112 patients fulfilled our selection criteria. 5 were affected by 2 different lesions. 30 malignancies were diagnosed. After ueMRM, 3 of 30 malignancies were not hypothetically addressed to ceMRM and were considered as false-negative. Sensitivity, specificity, PPV and NPV of ueMRM were 90% (27/30- $p=0.24$), 51.7% (45/87- $p < 0.0001$), 39.1% (27/69- $p < 0.0001$), 93.7% (45/48), respectively.

Conclusion: Compared to the RS, ueMRM sensitivity and NPV were not statistically different. In patients who cannot receive Gadolinium injection, ueMRM could be a safe, highly informative technique.

B-0078 11:33

A comparison between FAST technique and standard breast MRI: are we ready for MR screening?

C. Caborni, C. Losio, P. Panizza, E. Venturini, F. De Cobelli, A. Del Maschio; Milan/IT

Purpose: Breast MRI offers advantages over mammography in screening breast cancer among young women, but specificity should be improved to reduce expensive follow-up. Diffusion-weighted imaging (DWI) can increase positive-predictive value of dynamic MRI. We compared the diagnostic performance of a FAST technique (including DWI) with standard examination in this setting.

Methods and Materials: We retrospectively selected 161 breast MRI (T2, DWI, dynamic study) showing enhancing lesions > 5 mm, which nature was assessed cyto-histologically or with follow-up. Two trained radiologists in consensus reviewed each examination, considering the informations derived from a "short" dynamic study (1st post-contrast subtraction only) plus DWI (FAST-MRI) separately from standard examination (T2 and 5 post-contrast subtraction), and comparing their diagnostic performance.

Results: FAST-MRI depicted 167/169 (98.8%) enhancing lesions identified with standard exam (no cancer was missed). Quantitative DWI with assessment of ADC (apparent diffusion coefficient) was possible in 161/169, showing lower ADC values in malignant lesions than benign (0.99 ± 0.37 vs 1.64 ± 0.36 , $P < 0.00001$). In standard examination, the kinetic analysis showed limited value, with only 29% of cancers exhibiting a type 3 curve, and most (63.5%) an indeterminate curve. ADC was more predictive of benign or malignant nature using a cut-off of 1.29 mm^2/s (ROC analysis). FAST-MRI accuracy was superior than standard-MRI (88.2vs78%), with a significantly better negative-predictive value (93.4vs77.6%) and contribution for BI-RADS 3-4 lesions.

Conclusion: In our experience, FAST-MRI showed a better accuracy than standard examination, due to the superiority of ADC over dynamic criteria. The higher negative-predictive value and the shorter examination time could potentially extend the application of MRI in a screening context.

B-0079 11:42

Subgroup analysis of the final results of the Austrian screening trial for familial breast cancer

C.C. Riedl, N. Luft, C.B. Bernhart, G. Heinz-Peer, K. Pinker, T.H. Helbich; Vienna/AT (christopher.riedl@meduniwien.ac.at)

Purpose: To assess the value of mammography, ultrasound, and MRI of the breast in the surveillance of various subgroups of women at high risk for breast cancer.

Methods and Materials: In a prospective trial, women at high risk for breast cancer were offered annual surveillance examinations, consisting of mammography, ultrasound, and MRI. Sensitivity, specificity, positive predictive value, negative predictive value, positive likelihood ratio and negative likelihood ratio of the three surveillance modalities were assessed for various subgroups of participants, dichotomised by mutation status, age, menopausal status and personal history of breast cancer.

Results: In 558 patients 1365 complete imaging rounds were performed. A total number of 38 cancers were detected with sensitivities for mammography, ultrasound, and MRI of 50%, 38%, and 90%, respectively ($p < 0.01$). Of 38 cancers 18 (47%) were DCIS. For these mammography, ultrasound, and MRI demonstrated sensitivities of 50%, 28% and 90%, respectively ($p < 0.01$). Mammography, ultrasound, and MRI led to 38, 41, and 147 false-positive findings, which resulted in specificities of 98%, 97%, and 92%, respectively ($p < 0.05$). Of these, 49 were atypical ductal hyperplasias. Of these premalignant lesions, mammography, ultrasound, and MRI detected 31%, 16% 94% ($p < 0.05$). Comprehensive subgroup analyses revealed a higher specificity of MRI in the subgroup of mutation carriers (94%) and postmenopausal women (97%) compared to non-mutation carriers (86%) and pre/perimenopausal women (88) (with $P < 0.001$).

Conclusion: The use of MRI improves the detection of invasive and preinvasive cancers, as well as of high risk lesions. Specificities for MRI are highest for mutation carriers and postmenopausal women.

B-0080 11:51

Treatment of invasive breast cancer: initial clinical experience using high intensity focused ultrasound therapy with 3 T magnetic resonance guidance

A. Napoli, F. Pediconi, M. Anzidei, L. Di Mare, G. Cartocci, L. Bertaccini, F. Boni, V. Noce, C. Catalano; *Rome/IT (alessandro.napoli@uniroma1.it)*

Purpose: To determine the efficacy of non-invasive high-intensity MR-guided focused ultrasound (MRgFUS) treatment for biopsy-proven invasive ductal breast cancer (IDC) (stage T1 M0 N0) scheduled to surgical resection and sentinel lymph node biopsy.

Methods and Materials: Under the IRB approval, 6 patients with unifocal biopsy-proven IDC less than 2 cm in size scheduled and consented to surgical (lumpectomy or mastectomy) resection and sentinel lymph node biopsy, and in which breast MRI confirmed an enhancing lesion in a treatable location underwent MRgFUS treatment using the ExAblate 2000 system (InSightec). Treatments were done in a single session, in an ambulatory setting. Effectiveness of the treatment was evaluated at pathology after surgery.

Results: All 6 lesions were treated. No enhancement was seen at breast MRI after treatment in all patients. In all cases pathology demonstrated the absence of residual cancer after surgical excision. We found only necrotic tissue with at least 5 mm margins of normal breast tissue around the necrosis. We obtained excellent agreement between MRI post-treatment and pathology.

Conclusion: MRgFUS is a promising noninvasive treatment modality for unifocal breast cancer.

10:30 - 12:00

Room G/H

Neuro

SS 111b

White matter diseases

Moderators:

C. Auger Acosta; *Barcelona/ES*
M.P. Wattjes; *Amsterdam/NL*

B-0081 10:30

Comparison of 1.5 T and 3 T scanners for evaluating myelination in neonatal brains

D. Tortora, V. Panara, S. Salice, P.A. Mattei, C. Briganti, A.R. Cotroneo, A. Tartaro, M. Caulo; *Chieti/IT (domenicotortora@hotmail.it)*

Purpose: MR imaging is presently the most sensitive method for the in-vivo evaluation of white matter maturation in neonatal brains. Evaluating myelination is technically conditioned by the sequence and the scanner field intensity. The objective of this study was to retrospectively compare the level of myelination of various cerebral structures in two groups of term and pre-term neonates evaluated with either a 1.5 or 3 T scanner.

Methods and Materials: Routine brain MR of 77 neonates was retrospectively evaluated: 56 preterm. After informed consent was obtained from legal guardians, all neonates were sedated and underwent MR exams at a gestational age between 38 and 44 weeks (equivalent corrected age for pre-terms). 1.5 T scanner was used in 44 (34 pre-term) and 3 T in 33 (22 pre-term) neonates. Two blinded neuroradiologists independently evaluated myelination on TSE-T2-weighted axial images in the brainstem, inferior cerebellar peduncle, inferior colliculus, cerebellar vermis, globus pallidus, ventroposterolateral thalamic nucleus, internal capsule, optic radiation, corona radiata and precentral gyrus. Statistical differences were evaluated using a Pearson's Chi-squared test: $p < 0.05$.

Results: Myelination of the cerebellar vermis ($p=0.008$), globus pallidus ($p < 0.001$), internal capsule ($p=0.04$), and optic radiation ($p < 0.001$) was identified with a higher frequency with 3 T in both the pre-term and full term neonates.

Conclusion: TSE-T2-weighted sequences obtained with a 3 T compared with a 1.5 T scanner present a higher sensitivity for myelinated brain structure in neonates. This result and the loss of contrast in T1-weighted images encourage the use of T2-weighted sequence at 3 T to evaluate the process of myelination in newborns.

B-0082 10:39

Imaging of multiple sclerosis at 3 T: increased diagnostic yield using subtraction imaging

S. Langner, R. Seipel, B. Mensel, S. Otto, A. Dressel, N. Hosten, M. Kirsch; *Greifswald/DE (soenke.langner@uni-greifswald.de)*

Purpose: The detection of contrast-enhanced (Gd+) demyelinating lesions is important for the diagnosis and treatment of multiple sclerosis. The aim of our study was to evaluate the applicability of subtraction MR images for the detection of active MS lesion at 3 Tesla using a 32-channel head coil.

Methods and Materials: We prospectively included 108 patients (82 females, mean age: 39 ± 12.83 years) with proven multiple sclerosis. MR imaging was performed at 3 Tesla using a 32 channel head coil. All patients received intravenous contrast media (Gadovist-1.0®, Bayer Schering Pharma, Berlin) with a dose of 0.1 mmol Gd/kg body weight. Follow-up MRI was performed after 3 months. In all patients we acquired axial T2w and T1w fl3d images before and 5 minutes after administration of Gadobutrol. Precontrast images were subtracted from the postcontrast. Enhancing lesions were counted on pre- and postcontrast images. Lesion count was evaluated by two independent neuroradiologists.

Results: Lesion load on T2w images was 12.91 ± 5.15 . Using unsubtracted post-contrast images 38 Gd+ lesions (mean: 2.92 ± 2.10) in 13 patients were identified. On subtraction images, 97 Gd+ lesions in 20 patients were detected. In 7 of these patients 14 Gd+ lesions were not identified on unsubtracted images. In 10 patients 31 additional Gd+ lesions were detected and in 3 patients the size of the lesions increased. There was good interreader agreement ($\kappa=0.83$).

Conclusion: Using a 32 channel head coil and contrast-enhanced 3D subtraction MR images improve the diagnostic yield of MRI at 3 Tesla for detection of active MS lesion.

B-0083 10:48

Value of DIR MR sequences in comparison to FLAIR and DP/T2 when identifying cortical and juxtacortical lesions in patients with multiple sclerosis

M. Vera Cartas, V. Schonstedt Geldres, C. Auger Acosta, R. Mitjana Penella, A. Rovira-Cañellas; *Barcelona/ES (martavera01@gmail.com)*

Purpose: The detection by MR of cortical-juxtacortical lesions in patients with the diagnostic suspicion of multiple sclerosis is of great relevance. The purpose of this work is to compare the sensibility of "double inversion recuperation" sequence (DIR) in comparison to "fluid attenuated inversion recovery" (FLAIR) and protonic density sequence (DP/T2) in identifying demyelinating cortico-juxtacortical lesions in this patients.

Methods and Materials: 46 patients were included (65% women; 38.9 middle age ± 11.0) with the diagnosis of a single neurologic syndrome or multiple sclerosis. All the studies were made in a 3 T equipment and included sequences DIR, FLAIR and DP/T2 obtained in an axial shot with contiguous images 3 mm width. One observer identified the cortical-juxtacortical lesions in each sequence independently and as a whole.

Results: Of a total of 173 lesions detected in the three sequences as a whole, FLAIR identified by itself 73.4% of them, DP/T2 77.5% and DIR 82.1%. The comparison between the DIR sequence and the FLAIR and DP/T2 shows a gain in the number of detected lesions of a 12% when comparing DIR to FLAIR and of a 6% when comparing DIR to DP/T2. When comparing FLAIR and DP/T2 as a whole to DIR sequence by itself the gain is of a 6% ($p=0.01$).

Conclusion: The DIR sequence is significantly more sensible in detecting demyelinating cortico-juxtacortical lesions than FLAIR and DP/T2. Nevertheless, the combination of the three sequences offers a higher sensibility in detecting this lesions, which is relevant to confirm the diagnosis of multiple sclerosis.

B-0084 10:57

Infratentorial lesions in multiple sclerosis: improved detection with T2 TIRM MR imaging at 1.5 T magnet

O. Kiritsis¹, K. Tsitas¹, G. Noussios¹, G. Kiritsis²; ¹Thessaloniki/GR, ²Athens/GR (kirolga@hotmail.com)

Purpose: To prospectively compare the depiction of infratentorial lesions using fluid-attenuated inversion-recovery (FLAIR), and T2-TIRM magnetic resonance (MR) imaging in patients with multiple sclerosis.

Methods and Materials: Local ethics review board approval and informed consent were obtained. Conventional FLAIR in axial plane and T2 TIRM images in sagittal plane (2.5 mm thick) were acquired in 250 patients with multiple sclerosis (162 women, 88 men) and 100 age-matched healthy control subjects (60 women, 40 men). Mean age was 36 years (range, 17-54 years) in patients and 35 years

Thursday

(range, 18-54 years) in control subjects. Only infratentorial lesions were detected and reported. The numbers of lesions were compared between techniques.

Results: Total number of lesions differ between T2 TIRM and FLAIR Sequences. T2 TIRM images depicted more infratentorial lesions (1114 lesions in 250 patients) than FLAIR (640 lesions in 250 patients) images [t Student, $p=0.001$]. On average, T2 TIRM imaging depicted 1.86 more Infratentorial lesions per patient than did FLAIR imaging. Only 20 infratentorial lesions were detected in control subjects, with T2 TIRM sequence.

Conclusion: MR imaging with T2 TIRM enables increased infratentorial lesion detection in the multiple sclerosis brain.

B-0085 11:06

Vein density in patients with multiple sclerosis at 7T: a pilot study

S. Goed, A. Dal-Bianco, G. Grabner, M. Scherthner, K. Vass, S. Trattnig; Vienna/AT (sabine.goed@meduniwien.ac.at)

Purpose: Intralesional veins and perivenous inflammation are known to be a pathohistological hallmark of multiple sclerosis (MS). Susceptibility-weighted imaging (SWI) at 7T allows the imaging of veins as small as 0.2 mm in diameter. The purpose of our study was the identification of intralesional characteristics of veins in MS patients.

Methods and Materials: 10 patients, mean aged 42 years, with relapsing-remitting MS (RRMS; $n=6$) and secondary-progressive MS (SPMS; $n=4$) with an expanded-disability-status-scale (EDSS) ≤ 6.5 were included. The MR protocol at 7T comprised a FLAIR-FSE-sequence and a SWI-sequence (TR/TE 28/15 ms, voxel size 0.3x0.3x1.2 mm³). The examination was performed at baseline and 1 year after. Data from 8 patients (RRMS, $n=5$; SPMS, $n=3$) could finally be analysed. 18 plaques and its corresponding normal appearing white matter (NAWM) were assessed for lesion-volume and vein-volume with a 3D-Software.

Results: Patients with a relapsing-remitting-course showed a mean intralesional vein-density of 13.9%, patients with secondary-progressive multiple sclerosis a mean of 7.3%. This indicates a twofold higher vein-density in RRMS-plaques (13.9%). Vein-density in NAWM constantly accounted for a mean of 3.6% in patients with RRMS and SPMS. Compared to the corresponding NAWM, RRMS-plaques show a threefold higher vein-density and SPMS-plaques a twofold-higher vein-density. We could further precisely display intralesional small veins, partially showing a straight-lined course. Additionally, we could depict three newly developed vein-associated MS-plaques within 1 year.

Conclusion: Patients with a relapsing-remitting course of multiple sclerosis represent a higher intralesional vein-density than patients with a secondary progressive course of multiple sclerosis.

B-0086 11:15

Ultra-high-field MRI detected iron accumulation in multiple sclerosis plaques: a pilot study

S. Goed, A. Dal-Bianco, G. Grabner, M. Scherthner, K. Vass, H. Lassmann, S. Trattnig; Vienna/AT (sabine.goed@meduniwien.ac.at)

Purpose: Free iron is discussed to contribute as a neurotoxic agent to neuroinflammation and neurodegeneration in multiple sclerosis (MS). The purpose of our study was to visualise and analyse focal iron-accumulations within MS plaques and perform a follow-up after one year.

Methods and Materials: 10 patients, mean aged 42 years, with relapsing-remitting MS (RRMS; $n=6$) and secondary-progressive MS (SPMS; $n=4$) with an Expanded-Disability-Status-Scale (EDSS) ≤ 6.5 were examined on a 7T MR scanner (Siemens Healthcare, Erlangen, Germany) at baseline and 1 year after. The protocol comprised a FLAIR-FSE-sequence and a SWI-sequence (TR/TE 28/15 ms, voxel size 0.3x0.3x1.2 mm³). Qualitative analysis was performed to assess iron accumulation in MS-plaques within 1 year.

Results: In 4 out of 9 patients a total of 10 iron-loaded MS-plaques were detected within 1 year. Iron-accumulations were only observed in patients with RRMS (4/6). In 2 RRMS patients iron-containing lesions dominated. 1 lesion showed increased iron-load, 1 lesion reduced iron-load and 1 lesion a changed shape. In 2 lesions initially isolated iron-deposits attained confluence and 5 further lesions showed no change of iron-accumulation. Furthermore, the size of 3 MS-plaques with increased or confluent iron-accumulation was reduced.

Conclusion: In this pilot-study iron-accumulations were detected in patients with relapsing-remitting multiple sclerosis and showed dynamics in shape and size within 1 year.

B-0087 11:24

Disrupted white matter structural networks in clinically isolated syndromes suggestive of MS

Y. Liu, N. Shu, Y. Duan, Y. He, K. Li; Beijing/CN

Purpose: To investigate the topological organisation of the white matter structural networks in patients with clinically isolated syndrome (CIS) and relapsing-remitting multiple sclerosis (RRMS) by DTI tractography and graph theoretical approaches.

Methods and Materials: Twenty-eight patients with CIS, 28 patients with RRMS and 51 healthy controls (HC) were included. All participants were scanned with a 1.5 T MRI scanner. T1 and DTI images were acquired. We constructed the white matter structural network for each participant. Based on the FN-weighted network for each subject, we calculated the network properties, including the strength, global efficiency and local efficiency at the global level, and the regional efficiency at the nodal level. A multiple linear regression analysis was performed on each network metric between any two groups, $P < 0.05$ (corrected) was regarded as significant.

Results: Small-world characteristics of the WM structural networks were identified in both the controls and the patients. Among the three groups, we found the MS patients have the lowest network efficiency. Compared with HC, the CIS patients exhibited significant decreases in the strength and global efficiency of their WM structural networks. For all the network properties, the CIS network exhibited intermediated values. Compared with HC, the CIS patients exhibited a reduction in the nodal efficiency in bilateral precentral gyrus and left postcentral gyrus, while the MS patients have widespread efficiency reduction in many brain regions.

Conclusion: Disrupted topological organisation in the white matter network is already found at the CIS. The most significant regional changes were located at the primary sensorimotor system in CIS.

B-0088 11:33

Revised McDonald's criteria for dissemination in space; accuracy in diagnosis of multiple sclerosis from Neurobehcet's disease

S. Sefidbakht, M. Babainezhad, A. Borhani Haghighi, R. Jalli, Z. Zare; Shiraz/IR (sefidehsfidbakht@yahoo.com)

Purpose: To retrospectively determine accuracy of modified Mc Donald's criteria for dissemination in space in differentiating multiple sclerosis (MS) from Neurobehcet disease (NBD) in a high prevalence area of both diseases.

Methods and Materials: Two radiologists retrospectively reviewed 76 brain MRIs belonging to 48 patients with MS and 28 patients with NBD, blinded to the clinical diagnosis. Accuracy of McDonald criteria in diagnosing MS was assessed using Poser criteria as the gold standard.

Results: Out of all McDonald criteria for dissemination in space only infratentorial lesions were not significantly more prevalent in MS. Corpus callosal lesions were the most significant discriminating factor between the two diseases (six times more prevalent in MS). Sensitivity, specificity and accuracy of McDonald criteria were 80%, 61% and 71.5%, respectively. The two findings more prevalent in NBD patients were mesodiencephalic involvement and extension of the lesion from one anatomic site to the neighbouring site. Interobserver agreement was near perfect in diagnosing MS using modified McDonalds criteria for dissemination in space (kappa of 0.82).

Conclusion: Specificity of Mc Donald's criteria as a standalone test in differentiating MS from NBD is suboptimal with a possible high rate of false positive studies. MRIs should be interpreted in the proper clinical background to avoid mislabelling patients with alternate diagnoses as MS.

B-0089 11:42

Evaluation of metabolic, perfusion and microstructural cerebral alterations in patients with systemic lupus erythematosus using MR spectroscopy, perfusion and diffusion tensor imaging

P. Szewczyk, A. Zimny, J. Bladowska, M. Szymyka-Kaczmarek, M. Sasiadek; Wroclaw/PL (abernac@wp.pl)

Purpose: The aim of the study was to evaluate metabolic, perfusion and microstructural cerebral alterations in patients with systemic lupus erythematosus (SLE) and normal appearing brain on plain MR using advanced techniques: MR spectroscopy (MRS), perfusion weighted and diffusion tensor imaging (PWI and DTI).

Methods and Materials: Forty-two SLE patients (mean age 36.9 yrs) with normal appearing brain on plain MR and 18 age-matched control subjects underwent single voxel MRS, dynamic susceptibility contrast-enhanced PWI and DTI in 25 directions on 1.5 T MR unit. Metabolite ratios (NAA/Cr, Cho/Cr, ml/Cr) were calculated from posterior cingulate cortex and left parietal white matter. Values of cerebral blood volume related to cerebellum (rCBV) were assessed from 14 regions including different cortical locations, basal ganglia and fronto-parietal white matter. Frac-

tional anisotropy (FA) values were obtained from 14 white matter tracts including projection, commissural and association fibres.

Results: Compared to controls, SLE patients showed significantly ($p < 0.05$) lower NAA/Cr ratios within both evaluated regions, lower rCBV values only within right parietal cortex and decreased values of FA in multiple white matter tracts: right middle cerebellar peduncle, genu of corpus callosum, left superior and inferior longitudinal fascicles, left inferior fronto-occipital fascicle and both cingula.

Conclusion: The results of advanced MR techniques reflect neuronal loss within grey and white matter and disintegrity within multiple white matter tracts in patients with SLE. MRS and DTI seem to be especially promising noninvasive neuroimaging biomarkers for assessing the severity of microstructural changes in patients with SLE.

B-0090 11:51

Early and progressive signs on MRI in patients with progressive multifocal leukoencephalopathy

M. Sakai, K. Nakanishi, Y. Tomita, Y. Yamashita, K. Kuriyama; *Osaka/JP* (xiaohumeixu@gmail.com)

Purpose: To illustrate early and progressive signs on MR images in patients with progressive multifocal leukoencephalopathy (PML).

Methods and Materials: MR images of seven patients with PML were reviewed. The diagnosis of PML was established by clinical, laboratory (CSF-PCR for JC-virus) and MR images in all patients. One patient was also underwent brain biopsy. All patients underwent repeated MR examinations on 1.5- or 3.0-tesla MR units for the initial diagnostic workup and treatment control.

Results: In all patients, MR images showed worsening of findings. Duration of follow-up studies was 0 to 32 months. Newer margins in spreading lesions showed heterogeneous mild hyperintense with numerous dots of severe hyperintense on T2-weighted images ("Milky way appearance"), heterogeneous mild-slight hypointensity on T1-weighted images, and hyperintense on diffusion-weighted images with mild decreased or increased diffusion. With the progress, signal intensity of these lesions gradually increased on T2-weighted images and inversely decreased on T1-weighted images with increase of diffusion, finally near CSF intensity with atrophy. These findings seemed to correspond the pathological findings of numerous foci with myelin and axon loss that merge together to be large demyelinating lesion and finally to be severe atrophy and cavity.

Conclusion: "Milky way appearance" on T2-weighted images and hyperintense areas on diffusion-weighted images may be early and progressive signs in patients with PML.

10:30 - 12:00

Room /K

Abdominal Viscera

SS 101b

Biliary tract

Moderators:

T. Denecke; *Berlin/DE*

G.G. Karmazanovsky; *Moscow/RU*

B-0091 10:30

Gadoxetic acid-enhanced T1-weighted MR cholangiography in primary sclerosing cholangitis

A. Frydrychowicz¹, A.R. Jedynek², F. Kelcz², S.K. Nagle², S.B. Reeder²; ¹Madison, WI/US, Lübeck/DE, ²Madison, WI/US (alex.frydrychowicz@uksh.de)

Purpose: To determine the value of gadoxetic acid-enhanced 3-dimensional T1-weighted MR cholangiography (T1w-MRC) in comparison with 3-dimensional T2-weighted MR cholangiopancreatography (T2w-MRCP) in patients with primary sclerosing cholangitis (PSC).

Methods and Materials: We retrospectively evaluated 34 MR exams in 29 patients (46.0±16.1years (18-81); 80.5±13.9 kg (56.7-115.2 kg); 19men/10women). Scans were performed at 1.5 T with an eight-channel phased-array torso coil. 3D-T2w-MRCP was performed with a spatial resolution of 1.1x1.1x1.8 mm³, interpolated to 0.6x0.6x0.9 mm³ through zero-filling. T1w-MRC was achieved 20-25 min after injection of 0.05 mmol/kg gadoxetic with a navigator-gated 3D spoiled gradient recalled echo (SPGR) sequence with intermittent spectrally-selective partial inversion-recovery fat suppression (LAVA). The spatial resolution of 1.4x1.3x1.8 mm³ was interpolated to 0.7x0.6x0.9 mm³. Image quality was evaluated in a blinded fashion regarding image contrast, image quality degradation due to artefacts, and visualisation quality of ducts by two abdominal radiologists. Reader preference towards and

number of orders of visualised biliary tree branches were recorded. A helpfulness scoring of gadoxetic-acid-enhanced T1w-MRC was performed in consensus.

Results: Image quality of T1w-MRC and T2w-MRCP was graded good to excellent in all cases. There were advantages for both T1w-MRC (functional information, less artefact degradation) and T2w-MRCP (higher order of visualised branches, better branch depiction). Both readers showed preference for T2w-MRCP (reader 1: 17/34, reader 2: 20/34); however, in the majority of cases (28/34 cases, 82.4%), both readers agreed that gadoxetic acid-enhanced T1w-MRC was helpful.

Conclusion: Gadoxetic acid-enhanced T1w-MRC is complementary to, but should not replace, T2w-MRCP. T1w-MRC is a useful adjunct for morphologic evaluation and provides additional diagnostic information.

B-0092 10:39

Biliary-enteric anastomoses: usefulness of Gd-EOB-DTPA-enhanced MR cholangiography

P. Boraschi, F. Donati, S. Salemi, R. Gigoni, C. Bartolozzi, F. Falaschi; *Pisa/IT* (p.boraschi@do.med.unipi.it)

Purpose: To assess the usefulness of Gd-EOB-DTPA-enhanced MR-cholangiography (MRC) in patients with biliary-enteric anastomoses.

Methods and Materials: Forty-four patients with pre-existing biliary-enteric anastomoses and clinical-echographical suspect of biliary pathology underwent MR imaging at 1.5 T-device. After acquisition of T1w/T2w images, conventional MRC was performed through thin-slab 3D FRFSE and thick-slab SSFSE T2w sequences. In each patient a 3D fat-suppressed LAVA sequence was performed before and 15,20,25,30,40 minutes after intravenous administration of 10 ml Gd-EOB-DTPA (Primovist®, Bayer HealthCare), followed by injection of isotonic saline (20 ml). T1w sequence was also obtained after 90-120 minutes in 5/44 cases. Visualisation of each segment of the biliary tree and anastomotic bowel was graded by two radiologists in conference on a four-point scale: 0, absent; 1, poor; 2, good; 3, excellent. All segments were assessed for the presence of ductal dilatation, stricture, bile leakage, intraductal filling defects and other abnormalities. MRI findings were compared to surgical findings, when scheduled, and/or a six-month-lasting clinical-radiological follow-up.

Results: Gd-EOB-DTPA-enhanced-MRC significantly out-performed conventional MRC in the visualisation of the extra-hepatic biliary system and anastomotic region and in the assessment of anastomotic strictures and pneumobilia ($p < 0.05$). The grading of visualisation and depiction of dilation of the second and third order intra-hepatic bile ducts was significantly superior on T2w MRC ($p < 0.05$). No significant difference was identified between the two techniques in the detection of biliary stones.

Conclusion: Contrast-enhanced MRC using Gd-EOB-DTPA can improve the diagnostic performance of conventional T2w MRC in the post-operative assessment of biliary-enteric anastomoses since it provides both anatomical and functional information of the biliary tract.

B-0093 10:48

Characterisation and staging of hilar cholangiocarcinoma (Klatskin Tumour): evaluation of the hepatocyte-specific contrast agent gadoxetate disodium

K.I. Ringe¹, H. Bektas¹, B.P. Ringe¹, P.J. Opherk¹, A. Reichelt¹, F. Wacker¹, J. Lotz², B.C. Meyer¹; ¹Hannover/DE, ²Göttingen/DE (ringe.kristina@mh-hannover.de)

Purpose: To assess the value of gadoxetate disodium for characterisation and staging of hilar cholangiocarcinoma (hCCC).

Methods and Materials: This prospective HIPAA-compliant study was IRB approved. 14 patients (8 males, 6 females; 36-80y) with clinical suspicion of central bile duct stenosis (CBDS) underwent preoperative MRI. Images were assessed for aetiology of CBDS. A modified Bismuth classification was applied for tumour extension. To estimate the value of hepatocyte phase images, only T2w images (T2), only post-contrast images (CM), or both image datasets were assessed in three reading sessions by 3 readers (two weeks interval). Agreement of each reading session with the intraoperative findings in terms of CBDS aetiology and tumour extension (weighted kappa statistic) was calculated.

Results: CBDS was caused by hCCC (n=9), gallbladder carcinoma (n=4) and pancreatic carcinoma (n=1). Characterisation of CBDS aetiology was correct by use of T2w images in 57%, 64% and 50%; by use of CM images in 64%, 57% and 50%; by combination of both in 71%, 64% and 64%. Agreement comparing reading sessions and intraoperative findings regarding tumour extension was fair up to moderate ($\kappa=0.21$ (T2); 0.34 (CM); 0.54 (both)) as a result of common understaging. Interobserver agreement for tumour extension was fair (κ range = 0.31-0.33).

Conclusion: By means of combined evaluation of T2w sequences and post-contrast images after injection of gadoxetate disodium, a more reliable characterisation of CBDS was possible. Even though CBDS tended to be understaged before as well as after contrast injection, assessment of exact tumour extension was improved by contrast administration.

B-0094 10:57

Relationship between biliary complications and hepatic arterial buffer response after liver transplantation, based on ultrasound data

A. Doros, E. Hartmann, A. Nemeth, V. Kozma, A.P. Deak, S. Kudrnova, J. Fazakas, L. Kobori; *Budapest/HU (dorattila@yahoo.com)*

Purpose: Biliary stricture and leakage are common complications after liver transplantations (LT). One of the main cause is arterial ischaemia. The relationship between arterial and portal vein flow (hepatic arterial buffer response) concerning late biliary complications are not frequently analysed.

Methods and Materials: 70 consecutive LTs intra-, and postoperative ultrasound examinations were retrospectively analysed and compared with the one-year follow-up clinical results focusing on biliary strictures and leakage. The ultrasound data were composed of the routine controls, arterial resistive index (RI), hepatic vein velocity curves and portal vein velocities.

Results: Altogether 22 minor (symptom free) and major (treatment required and performed) biliary complications were diagnosed. In 8 cases low RI suggesting arterial stenosis were noticed while the remaining 14 cases showed consequent high (> 50 cm/s) portal venous velocities and RI values (> 0.75). On the contrary, 25 cases were found with the same flow patterns without any signs of biliary complications.

Conclusion: The high portal velocity and high RI may only roughly represent the hepatic arterial buffer response; however, these values are measured routinely after LT. Half of our patients (55%) showed this flow combination, but only 20% developed biliary complications of any severity. The routinely measured parameters are not sufficient enough to predict late biliary complications, although medical, surgical or interventional treatment of excessively high portal flow combined with high RI arterial flow may be beneficial. The decision of potential treatment should be made individually.

B-0095 11:06

Steady state free precession sequences can add valuable diagnostic details to conventional MR cholangiography

A. Iozzelli, L. Oncini; *Macerata/IT (aiozzelli@sirm.org)*

Purpose: Adding a steady-state free precession sequence (SSFP) to the conventional 3D-T2-weighted magnetic resonance cholangiography sequence (3DC) provides additional diagnostic data.

Methods and Materials: In 130 consecutive patients that underwent MR cholangiography examination along 6 years for suspected biliary obstruction or biliary diseases received 2-3 non-breath-hold coronal oblique SSFP sequences after the conventional 3DC sequence. The SSFP sequences in all the examinations were retrospectively examined by one expert reader to confirm the 3DC sequence diagnosis and search for additional details that could contribute to the main diagnosis.

Results: In all the cases (100%) the breathing artefacts were not influencing the diagnostic quality of the sequences. In 92/130 (70.8%) cases the 3DC diagnosis was confirmed by SSFP, in the remaining 38/130 (29.2%) cases SSFP identified the correct diagnosis that was not clear with 3DC alone. In 75/130 (57.7%) cases added some details that were not visible in the 3DC.

Conclusion: SSFP is a useful sequence that can add details to the conventional 3DC sequence, due to better resolution, high extra-luminal and biliary wall details, lower sensitivity to breathing artefacts and does not add significant time to complete the examination.

B-0096 11:15

Functional imaging using Gadoxetate disodium-enhanced 3.0-T MR cholangiography versus conventional 3.0-T MR cholangiography: comparison with ERCP in patients with primary sclerotic cholangitis

R. Nolz, A. Wibmer, H. Einspieler, U. Asenbaum, S. Magnaldi, M. Peck-Radosavljevic, A. Ba-Ssalamah; *Vienna/AT (richard.nolz@meduniwien.ac.at)*

Purpose: To evaluate the diagnostic value of Gadoxetate disodium-enhanced 3.0-T MR cholangiography delayed hepatobiliary phase versus conventional 3.0-T MR cholangiography in comparison to ERCP in patients with primary sclerotic cholangitis.

Methods and Materials: 21 patients with primary sclerotic cholangitis confirmed by ERCP, clinical presentation and laboratory tests as standard of reference, who underwent Gadoxetate (Primovist, Bayer Health Care, Berlin, Germany)-enhanced

3.0-T MR cholangiography, were retrospectively evaluated. Conventional T2-weighted MR cholangiography and Gadoxetate-enhanced MR cholangiography in delayed hepatobiliary phase in coronal and axial planes were separately assessed and then compared to ERCP. The presence of peripheral and central stenosis, dilatation and contour irregularities for characterisation of PSC was evaluated using a 5-point scoring system.

Results: The study cohort consisted of 21 patients (14 females) with a mean age of 54.3 years (range 36 - 75 years). Mean time between ERCP and MR imaging was 58 days. In patients with PSC features, delayed hepatobiliary phase showed an excellent correlation with ERCP ($\kappa=1.00$, $\rho=1.00$), whereas correlation of T2-weighted MR was only moderate ($\kappa=0.694$; $\rho=0.708$). Furthermore, delayed hepatobiliary phase demonstrated a statistically significant better detection of obstructive central stenosis in comparison to conventional MRCP ($p=0.005$). The corresponding AUCs were 0.796 versus 0.607 in comparison with ERCP.

Conclusion: Delayed hepatobiliary phase of Gadoxetate-enhanced MR increases accuracy for early depiction of PSC features and provides additional functional information of bile ducts, which allows appropriate treatment of PSC associated clinically significant central stenosis.

B-0097 11:24

Role of GD-EOB-DTPA-enhanced magnetic resonance cholangiography (MRC) in the evaluation of biliary strictures after orthotopic liver transplantation (OLT): preliminary results

A. Pecchi, M. Gibertini, M. De Santis, F. Di Benedetto, P. Torricelli; *Modena/IT (anna_pecchi@libero.it)*

Purpose: To describe the role of GD-EOB-DTPA-enhanced magnetic resonance cholangiography (MRC) in the evaluation of biliary strictures in liver-transplanted patients.

Methods and Materials: Between July 2010 and September 2011, 4 liver-transplanted patients with clinical suspected biliary strictures were evaluated with GD-EOB-DTPA-enhanced MRC. Axial and coronal T1-w and T2-w sequences, radial 2D-SSFSE, coronal 3D-T2wFSE sequences were acquired in precontrastographic phase. T1-w3D GRE sequences were performed before and after injection of GD-EOB-DTPA (0.1 ml/kg), including dynamic and delayed hepatobiliary phases acquired 15, 20, 30 minutes after GD-EOB-DTPA administration. Diagnostic confirmation was obtained with hepatobiliary scintigraphy (HBS) and percutaneous transhepatic cholangiography (PTC).

Results: In all cases GD-EOB-DTPA-enhanced MRC depicted 7 biliary strictures (6 intrahepatic; one bilio-enteric anastomotic stricture). At GD-EOB-DTPA-enhanced MRC, when intrahepatic strictures were associated with areas of liver parenchyma without GD-EOB-DTPA excretion for diminished hepatobiliary function caused by biliary obstruction, strictures were considered relevant. In one case, dilatation of upstream biliary tree and lack of GD-EOB-DTPA excretion into the bilio-enteric anastomoses was associated with bilio-enteric anastomotic stricture. HBS confirmed areas of liver parenchyma with unhomogeneous and delayed uptake of radiotracer, as depicted at MRC. All intrahepatic strictures detected at GD-EOB-DTPA-enhanced MRC were confirmed at PTC. Three intrahepatic strictures associated with parenchymal areas of no GD-EOB-DTPA excretion were treated with PTC, with normalisation of biliary tree. One bilio-enteric anastomotic stricture received no confirmation at HBS.

Conclusion: GD-EOB-DTPA-enhanced MRC is a useful technique in the evaluation of biliary strictures after OLT as it allows the selection of strictures associated with abnormal parenchymal function.

B-0098 11:33

Ultrasound scoring system for preoperative evaluation of cholelithiasis: how accurate it is for preoperative prediction of difficult laparoscopic cholecystectomy

M.A. Siddiqui, I. Ahmad, S.A.A. Rizvi, E. Ullah; *Aligarh/IN (drazfarsiddiqui@gmail.com)*

Purpose: Laparoscopic cholecystectomy (LC) has become treatment of choice for cholelithiasis, but there are still some patients requiring conversion to open cholecystectomy (OC) mainly because of technical difficulty. Our aim was to develop a standardised ultrasound-based scoring system for preoperative prediction of difficult LC.

Methods and Materials: Ultrasound findings of 300 patients who underwent LC were retrospectively reviewed. Four parameters (time taken, biliary leakage, injury to duct or artery, and conversion to OC) were analysed to classify LC as easy or difficult. Ultrasound findings were analysed with emphasis on GB wall thickness, pericholecystic collection, distended GB, impacted stones, multiple stones, CBD diameter and liver size. A score of two was assigned for the presence of each finding with a total score of 14. A cut-off value of 6 was taken to predict easy and difficult

laparoscopic cholecystectomy. Sensitivity, specificity along with positive predictive values for predicting easy and difficult cases were calculated.

Results: 58 out of 67 cases of difficult LC and 208 out of 233 cases of easy LC were correctly predicted on the basis of this scoring system. A score of 6 had a sensitivity 69.6% and specificity 95.8% for correctly identifying difficult LC. Prediction came true in 89.3% for easy and 86.6% difficult cases. Ultrasound findings of GB wall thickness, distended GB, impacted stones and dilated CBD were found statistically significant.

Conclusion: This scoring system is very effective in predicting conversion risk of LC to OC. Patients having high risk may be informed and scheduled appropriately.

B-0099 11:42

Hepatobiliary excretion of gadoxetate disodium (Primovist) in patients with primary sclerosing cholangitis (PSC)

K.I. Ringe¹, J. Hinrichs¹, E.M. Merkle², F. Wacker¹, B.C. Meyer¹; ¹Hannover/DE, ²Durham, NC/US (ringe.kristina@mh-hannover.de)

Purpose: To evaluate hepatobiliary excretion of Gd-EOB-DTPA into different segments of the hepatobiliary system in patients with PSC, and to assess possible correlation with liver function tests (LFT).

Methods and Materials: This retrospective study was IRB approved. 54 patients (16 females, 38 males, mean age 42.7 years) with confirmed diagnosis of PSC who underwent contrast-enhanced hepatic MRI after injection of 0.1 mL/kg body weight were included. Delayed phase images acquired between 10 and 20 minutes after contrast injection were assessed for the presence of contrast agent in the intrahepatic bile ducts (IBD), common bile duct (CBD), gallbladder and duodenum. A Kruskal-Wallis test was performed to determine whether excretion was affected by LFT. Hepatobiliary excretion was compared with data collected in a previous study from patients without liver disease by means of a Mann-Whitney U test.

Results: 20 minutes after contrast initiation, Gd-EOB-DTPA could be detected in the IBD in 55.5%, CBD in 53.7%, gallbladder in 38.8%, duodenum in 13%, respectively. Contrast excretion into the IBD, CBD and gallbladder was significantly affected by serum bilirubin levels, but not by alkaline phosphatase, γ -glutamyltransferase, patient sex or age.

Conclusion: Contrast excretion into all hepatobiliary segments is significantly reduced in patients with PSC compared to patients without liver disease, and is further dependent on serum bilirubin level. Within 20 minutes post-contrast initiation Gd-EOB-DTPA can be expected in the IBD and CBD in only about 50% of patients. Delayed phase imaging therefore needs to be carried out significantly longer in PSC patients in order to assess functional information.

B-0100 11:51

Secretin-stimulated magnetic resonance cholangio-pancreatography: safety, reliability, and assessment of pancreatic exocrine function

P. Messner, J.P. Kuehn, T. Ittermann, B. Mensel, K. Hegenscheid, H. Voelzke, J. Mayerle, N. Hosten, R. Puls; Greifswald/DE (philseabames@yahoo.de)

Purpose: To investigate the safety, reliability of secretin-stimulated magnetic-resonance-cholangio-pancreatography (SS-MRCP), and assessment of pancreatic exocrine function (PEF) in volunteers.

Methods and Materials: The study was IRB approved. 995 volunteers (538 men, mean age 51.9±13.4years) underwent navigator-triggered T2-weighted 3D-MRCPs before and after secretin stimulation (1UE/kg/BW) using a 1.5 T MR-system (Avanto, Siemens). The mean time between intravenous secretin injection and the SS-MRCP was 11.9±2.8 min. For 2 hours after injection of secretin, adverse reactions were evaluated. Improvement of duct visualisation after secretin stimulation was observed by two readers (r1/r2) subjectively and quantitatively through measurement of duct size diameters. PEF was assessed subjectively using Matos criteria's by two readers and quantified with calibrated volumetric measurement of total excreted volume (TEV) and pancreatic flow output (PFO).

Results: Minor adverse reactions were observed in only 2 cases (0.2%), consisting of flushing, and no major reactions were observed. Subjectively, duct visualisation after secretin stimulation was improved in r1/r2: 59/60%, unchanged in r1/r2: 38/37%, and worse in r1/r2: 3/3%, (inter-rater-agreement; kappa=0.910). Duct diameters increased significantly after secretin stimulation (head: 2.0-2.2 mm; body: 1.7-1.9 mm; tail: 1.3-1.4 mm; p=0.001). PEF, evaluated using Matos criteria's, was restricted in Matos 0: r1/r2: 1/1%, Matos 1: r1/r2: 5/5%, Matos 2: r1/r2: 31/26%, and Matos 3: r1/r2: 63/68%, (kappa=0.828). The mean TEV was 110.7±48.7 ml and the mean PFO was 9.5±4.1 ml/minute. According to the time, normal values of TEV/PFO were regressed to a logarithmic function (R2TEV= 0.937; R2PFO= 0.912).

Conclusion: SS-MRCP provides an improvement in main pancreatic duct visualisation and a non-invasive quantification of PEF with negligible risk of side effects.

10:30 - 12:00

Room L/M

Molecular Imaging

SS 106

Advanced topics

Moderators:

I. Carrió; Barcelona/ES

T.D. Henning; Cologne/DE

B-0101 10:30

In vivo molecular MRI of the estrogen receptor in breast cancer using a targeted contrast agent

A. Pais¹, R. Margalit¹, I.E. Biton¹, A. Yosepovitch², H. Degani¹; ¹Rehovot/IL, ²Tel Hasomer/IL (Adi.pais@weizmann.ac.il)

Purpose: Developing in vivo molecular MRI for detecting estrogen receptor (ER) expression in a breast cancer animal model utilising a novel ER targeted contrast agent.

Methods and Materials: ER-targeted contrast agent based on pyridinium-tetraacetate-Gd (III) chelate (PTA-Gd) conjugated to 17 β -estradiol (EPTA-Gd) was synthesised and characterised in solution, and in stably transfected with ER (ER-positive) and wild type MDA-MB-231 (ER-negative) human breast cancer cells, as well as tumours implanted orthotopically in the same mouse. In vivo pharmacokinetics and DCE-MRI studies were conducted on 9.4T scanner. Image processing included model-based and model-free analyses.

Results: The affinity of EPTA-Gd to ER was found to be in the micromolar range. The T1 relaxivity in solution was 6.8 (mM⁻¹s⁻¹) and increased to 28.5 (mM⁻¹s⁻¹) in ER-positive breast cancer cells. In vivo DCE-MRI using a low dose of EPTA-Gd (0.03-0.075 mmol/kg) demonstrated high enhancement in ER-positive breast cancer tumours as compared to the enhancement in ER-negative tumours, and in normal muscle tissue. In contrast, both tumours showed similar enhancement and hence, vascular perfusion, in DCE of non-targeted diffusible contrast agent (Gd-DTPA and PTA-Gd). Furthermore, specific interaction of EPTA-Gd with ER was validated by in vivo competition DCE-MRI experiments with tamoxifen.

Conclusion: The results in the breast cancer animal model provide a proof of principle of the ability of EPTA-Gd to be targeted in vivo to ER and identify ER-positive tumours. In addition, these results provide a basis for the clinical translation as a means for detecting, localising, and monitoring ER non-invasively.

B-0102 10:39

PET imaging of therapy-induced prostate cancer cell death by targeting the internal epitope of prostate-specific membrane antigen

A. Ruggiero¹, J.P. Holland², T. Hudolin², J.S. Lewis², J. Grimm²; ¹Rotterdam/NL, ²New York, NY/US (a.ruggiero@erasmusmc.nl)

Purpose: We report the preparation and use of 89Zr-desferrioxamine B (DFO)-7E11, a novel 89Zr-labeled monoclonal antibody (mAb) construct for targeted immuno-positron emission tomography of prostate-specific membrane antigen (PSMA), a prototypical cell surface marker highly overexpressed in prostate cancer (PC). We present an approach to monitor PC therapy using the 89Zr-DFO-7E11 as a marker of response. 7E11 recognises an intracellular epitope of PSMA and thus can only bind its cognate antigenic epitope when the cell membrane is disrupted, as in dead or dying cells.

Methods and Materials: 7E11 as a marker of dying cells was studied by flow cytometry and microscopy of cells after antiandrogen-, radio- and chemotherapy treatment in LNCaP and PC3-PSMA positive cells. The in vivo behaviour of 89Zr-DFO-7E11 was characterised in mice bearing subcutaneous LNCaP (PSMA-positive) by biodistribution studies, immuno-PET and optical imaging. The potential of assessing tumour response was evaluated in vivo after radiotherapy and chemotherapy treatment.

Results: In vitro studies correlated 7E11 binding with markers of necrosis/apoptosis. In vivo biodistribution experiments revealed high, target-specific uptake of 89Zr-DFO-7E11 in LNCaP tumours after 24 h (20.35±7.50%ID/g), 48 h (22.82±3.58%ID/g), 96 h (36.94±6.27%ID/g) and 120 h (25.23±4.82%ID/g). Excellent image contrast was observed with immuno-PET. 7E11 uptake was statistically increased in treated versus control tumour as measured by immuno-PET and biodistribution studies. Blocking studies at 48 h confirmed binding specificity.

Conclusion: 89Zr-DFO-7E11 displays high tumour-to-background tissue contrast in immuno-PET and can be used as a tool to monitor the tumour response in PSMA-positive PC.

B-0103 10:48

Molecular imaging of apoptosis in the early course after myocardial infarction using hybrid fluorescence molecular tomography/x-ray computed tomography FMT-XCT targeting Annexin V

M. Wildgruber, A. Ale, K. Kosanke, E. Rummeny, V. Ntziachristos; Munich/DE (moritz.wildgruber@tum.de)

Purpose: To investigate Annexin V targeted molecular imaging of cardiomyocyte apoptosis in the early course after murine myocardial infarction.

Methods and Materials: Myocardial infarction (MI) was induced in C57BL/6J mice by 30 minutes ligation of the left anterior descending artery (LAD) with subsequent reperfusion. Mice were injected with the Annexin V targeted molecular imaging probe Annexin-Vivo750 4 hours prior to imaging. Additionally, mice were injected with a long-circulating iodine-based contrast agent (Exitron 12000) prior to imaging for better visualisation of cardiac anatomy with subsequent facilitated organ segmentation. Hybrid FMT-XCT was performed 6 hours, 24 hours and 7 days after induction of ischaemic injury. Molecular imaging signal for Annexin-Vivo750 was validated by ex-vivo immunohistochemistry and flow cytometry.

Results: Successful image acquisition of both FMT and CT angiography was achieved in all mice. Molecular imaging signal for Annexin-Vivo750 could be localised to the anterior-lateral wall of the left ventricle at the site of myocardial infarction. FMT signal for Annexin V peaked at 6 hours after myocardial infarction with subsequent decrease at 24 hours and 7 days after onset of ischaemic injury. FMT signal for Annexin V colocalised with apoptosis staining (Caspase 3) using immunohistochemistry and flow cytometry. Hybrid acquisition of x-ray computed tomography allows exact localisation of the FMT signal to the left-ventricle and facilitates organ segmentation and attenuation correction.

Conclusion: Hybrid FMT-XCT targeting Annexin V enables accurate in-vivo assessment of apoptosis in the early course after myocardial infarction in a murine ischaemia-reperfusion model.

B-0104 10:57

First parallel, specific visualisation of inflammatory activity and consecutive demyelination in experimental multiple sclerosis (MS) in-vivo using dual-channel optical molecular imaging

M. Eisenblaetter, S. Albrecht, L. Wachsmuth, W. Heindel, T. Vogl, T. Kuhlmann, C. Bremer; Münster/DE (eisenblaetter@uni-muenster.de)

Purpose: A method for continuous surveillance of central-nervous inflammatory processes and underlying pathophysiology was desired for examination of murine models of disease. Activated macrophages have been shown to play a crucial role in initialisation and maintenance of inflammation. Previous work proved expression of macrophage-related protein S100 A9 to be correlated with local disease activity and optical imaging (OI) of S100 A9 has successfully been performed. Near-infrared fluorescent 3,3'-diethylthiatricarbocyanine-iodide (DBT) has been shown to selectively bind myelin.

Methods and Materials: MS-equivalent lesions were induced in C57BL6 mice by Cuprizone-application over 35 days. Healthy mice served as control. Anti-S100 A9 or Immunoglobulin G (IgG; control for non-specific label distribution) were labelled with Cy5.5 for OI. Tracer doses per animal were 100µg anti-S100 A9-Cy5.5, 24h and 2µg DBT, 5 min prior to fluorescence-mediated tomography with excitation/emission of 680/700nm (Cy5.5) and 750/780nm (DBT). For correlation of in-vivo OI, magnetic resonance tomography (MRI) for lesion-detection and immunohistochemistry were performed. Statistical analysis: student-t-test.

Results: In Cuprizone-treated animals, injection of anti-S100 A9-Cy5.5 resulted in three-fold higher tracer accumulation than in healthy animals (3.65pmol vs. 1.2pmol; p=0.02); whereas unspecific IgG-Cy5.5 accumulated to a significantly lower scale (2.2pmol vs. 3.65pmol; p=0.03). Myelin-associated DBT-accumulation dropped from 30.7pmol (healthy) to 1.5pmol (Cuprizone), reflecting significant demyelination. For all measurements, a ROI-analysis of the corpus callosum-region was performed, where histology and MRI proved lesion location and severity as depicted by OI.

Conclusion: Anti-S100 A9-Cy5.5 in combination with DBT may serve for specific visualisation of central-nervous inflammation like MS and allows for grading according to immune-cell activity and demyelination.

B-0105 11:06

Can molecular imaging of breast tumours with high-field multiparametric MRI obviate unnecessary breast biopsies?

K. Pinker-Domenig, H. Bickel, H. Magometschnigg, B. Brueck, S. Gruber, W. Bogner, M. Scherthner, D. Berzaczy, T.H. Helbich; Vienna/AT (katja.pinker@meduniwien.ac.at)

Purpose: To evaluate if multiparametric assessment of breast lesions with proton MR spectroscopy (3D-1H-MRSI), diffusion-weighted MR imaging (DWI) and, contrast-enhanced (CE-MRI) obviates unnecessary breast biopsies.

Methods and Materials: 112 patients with breast lesions detected by mammography or ultrasound and classified as BIRADS 3-5 were included in this IRB approved prospective study. All patients were examined multiparametric MRI of the breast at 3 T. MRI protocol included: 3D-1H-MRSI before application of contrast agent to avoid contamination of spectra, a DWI, a T2-weighted sequence and a combined contrast-enhanced high temporal and spatial resolution 3D-T1-w sequence before and after application of a standard dose Gd-DOTA. MRI was assessed for lesion morphology and EH-kinetics according to the BIRADS classification, restricted diffusivity and increased Choline (Cho)-levels. An ADC threshold 1.25 x10⁻³ mm²/s and a signal-to-noise ratio of the Cho resonance peak > 2.55 were defined as a marker of malignancy. A predefined evaluation algorithm was used for assignment of a final BIRADS classification. All lesions were histopathologically verified.

Results: 3D-1H-MRSI had a sensitivity of 69% and a specificity of 81%. DWI had a sensitivity of 95% and a specificity of 95%. CE-MRI demonstrated a sensitivity of 100% and a specificity of 76%. Multiparametric MRI increased sensitivity to 100%, specificity to 89% and had a very good diagnostic accuracy of 96%. Breast biopsies could have been obviated in 89% of benign lesions.

Conclusion: Multiparametric MRI of the breast at 3 T improves differentiation between benign and malignant breast lesions obviating unnecessary breast biopsies.

B-0106 11:15

Effect of cyclopamine on 18 F-FDG-uptake of pancreatic cancer xenografts in nude mice: evaluation by clinically implemented high-resolution PET-CT

H. Kaye, P. Meyer, B. Kraenzlin, N. Gretz, C. Fink, S.O. Schönberg, M. Sadick; Mannheim/DE (hany.kayed@umm.de)

Purpose: We quantitatively analysed the effects of cyclopamine on the 18 F-FDG-uptake of pancreatic cancer xenografts (PCX) using a clinically implemented PET-CT scanner with high-resolution reconstruction.

Methods and Materials: PCX from two pancreatic cancer cell lines were induced subcutaneously in the hip and shoulder of nude mice. PCX were treated with the anti-hedgehog signalling agent cyclopamine intraperitoneally for one week. Mice were injected intravenously with 7.4 MBq 18 F-FDG and scanned with a 40-detector mCT-scanner (Siemens Healthcare Sector, Erlangen, Germany). To adapt for the small size of mice, we changed the zoom to 10 instead of 1, the scan time per bed position to 10 minutes instead of 3 minutes and we used 1 mm Gaussian Filter instead of 3 mm. The dataset was reconstructed and quantified using the TrueX and TrueD softwares.

Results: MiaPaCa-2 cells; which respond to cyclopamine, showed decreased 18 F-FDG-uptake without changes in tumour size. The hip tumours showed a reduction of the SUVmax by -24.5 ± 9.2%, the SUVavg by -33.5 ± 7.0% and SUVmin by -54.4 ± 11.5% (p < 0.05). The shoulder tumours showed reduction of the SUVmax by -14.7 ± 7.5%, SUVavg by -12.6 ± 6.3 and SUVmin by -30.3 ± 16.7% (p < 0.05). Capan-1 cells; which do not respond to cyclopamine, did not show significant SUV changes.

Conclusion: The clinically implemented PET-CT scanner with high-resolution reconstruction can detect minimal changes in response to low-dose short-term therapy of pancreatic cancer xenografts even without changes in tumour size and thus offers the potential for translational research in anti-tumour therapy.

B-0107 11:24

Impact of normal tissue uptake using 68Ga DOTATOC-PET/CT in patients with neuroendocrine tumour - a follow-up study

M. Stefanova¹, C. Kratochwil², L. Schwartz³, U. Haberkorn², F.L. Giesel²; ¹Stip/MK, ²Heidelberg/DE, ³New York, NY/US (f.giesel@dkfz.de)

Purpose: Imaging with somatostatin analogues such as 68Ga-DOTA (0)-Phe (1)-Tyr (3)-octreotide (DOTATOC) became a standard approach for staging and restaging the neuroendocrine tumours. The aim of this study is to assess the impact of the normal tissue uptake using 68Ga-DOTATOC-PET/CT in patients with neuroendocrine tumour prior and after 4-6 cycles of peptide receptor radionuclide therapy (PRRT) with 90Y-DOTATOC and 177Lu-DOTATOC.

also
EPOS

Methods and Materials: Sixteen patients with histological confirmed metastatic neuroendocrine tumours were enrolled in this study. In each patient 68Ga-DOTA-TOC PET/CT examinations prior and after 4-6 cycles of PRRT (mean administered activity: 13.8 GBq Y-90 + 9.6 Lu-177) were evaluated. The maximum standardised uptake value (SUV max) of the following normal target tissues: pituitary gland, thyroid gland, spleen, liver background, head of the pancreas, kidneys and suprarenal glands were determined prior and after therapy.

Results: SUVmax before and after PRRT were determined as: pituitary gland (5, 56±2.91/4.47 ±2.53), thyroid gland (2.05 ±1.11/ 2.49 ±2.47), spleen (24.95 ±14.20/ 20.06 ±8.53), liver parenchyma (7.13 ±3.96/6.62 ±2.63), head of the pancreas (6.96 ±1.99/6.83 ±2.00), kidneys (13.0 ±3.85/11.31 ±3.31) and suprarenal glands (9.65 ±4.20/7.10 ±2.86). Therefore, no statistical significant differences were found (p > 0.05) for all organs.

Conclusion: The uptake of 68Ga-DOTATOC in normal tissue is not significantly affected by PRRT. Despite the non-impact of neuroendocrine side-effects this might also be relevant with regard to tumour to non-tumour ratios for follow-up assessment, particularly liver parenchyma uptake demonstrated to be robust.

B-0108 11:33

Pre-clinical assessment of antiangiogenic effects on mice with mammary carcinoma using dynamic contrast-enhanced micro-CT

F. Eisa, R. Brauweiler, M. Hupfer, T. Nowak, R. Dittrich, M.W. Beckmann, W.A. Kalender; Erlangen/DE (Fabian.Eisa@imp.uni-erlangen.de)

Purpose: To evaluate the potential of in-vivo dynamic contrast-enhanced (DCE) micro-CT for the preclinical assessment of antiangiogenic drug therapy response on mice with mammary carcinoma.

Methods and Materials: Among 20 female mice with implanted MCF7 tumours in the fourth inguinal mammary gland, 10 were treated with an antiangiogenic drug and 10 served as control group. Four weeks after tumour implantation all mice underwent DCE micro-CT (65 kV, 300 µA). The scan consisted of 12 gantry rotations with a total scan time of 180 s. Overlapping 360° reconstructions with an isotropic voxel size of 81 µm were performed in 7.5 s intervals. In a 3D analysis the relative blood volume (rBV), vascular permeability (K), area under the time concentration curve (AUC) and the morphology of the tumours were compared between therapy and control group. All parameters were determined for a total, peripheral and central tumour volume of interest (VOI). Moreover, immunohistochemistry was performed to characterise the tumour vascularisation.

Results: The mean AUCs were significantly lower in therapy with p-values of 0.012, 0.007 and 0.023 for total, peripheral and central tumour VOI, respectively. K and rBV showed significant differences for the peripheral VOI (pKper=0.032, prBVper=0.029), but not for the total and central tumour VOIs (pKtotal=0.108, pKcentral=0.246, prBVtotal=0.093, prBVcentral=0.136). Mean tumour volume was significantly smaller in therapy (pin-vivo=0.001, pex-vivo=0.005). Histology revealed higher vascularisation in the control group and showed central tumour necrosis.

Conclusion: This study indicates the high potential of DCE micro-CT for early in-vivo assessment of antiangiogenic drug therapy response in mice.

B-0109 11:42

Comparison of ADC measurements and USPIO uptake into different human xenograft tumour models at 7T MRI

N. Raabe, T. Ernst, M. Heine, S.C. Salmen, M. Kaul, C. Habermann, G. Adam, H. Iltrich; Hamburg/DE (nraabe@uke.uni-hamburg.de)

Purpose: The evaluation of apparent diffusion coefficient measurements (ADC) as a diagnostic marker for the uptake of SPIO in different human xenograft tumour models in mice at 7T MRI.

Methods and Materials: Five mice, each with different human xenograft tumours (OH1-small cell lung cancer, LOX-malignant melanoma, DU4475-breast cancer) were measured on a 7T small animal MR scanner (ClinScan®, Bruker, Germany), whereas one served as control (no USPIO injected). Diffusion-weighted imaging (DWI) was performed prior to the intravenous injection of 150µg PEGylated superparamagnetic iron oxide nanoparticles (USPIO, core size 13 nm). DWI measurements were performed using six different b-factors (0, 50, 100, 500, 700 and 1000 s/mm). ADC measurements were performed three times in a homogeneous area of the tumour. Mean ADC values of tumour types were statistically compared to each other via analysis of variance. T2-weighted and T2* relaxometric sequences were performed to evaluate the uptake of SPIO in the tumours.

Results: All three tumour types differed significantly (p < 0.01) in ADC values (in 10⁻³ x mm²/s) with highest values in the LOX tumour (0.96 ± 0.04), followed by the DU4475 tumour (0.83 ± 0.03) and the OH1 tumour model (0.73 ± 0.01). An inhomogeneous signal alteration due to SPIO-uptake on T2-weighted images and relaxometric measurements could only be detected in the LOX tumour.

Conclusion: ADC measurements can help to distinguish between different tumour types and could serve as a prognostic marker for the uptake of molecules into tumours.

B-0110 11:51

Comparison of consecutive bolus tracking and flash replenishment measurements for the assessment of tissue haemodynamics using contrast-enhanced ultrasound (CEUS) in an experimental squamous cell carcinoma model

P.M. Paprottka, M. Ingrisch, P. Zengel, C.C. Cyran, K. Nikolaou, M.F. Reiser, D.A. Clevert; Munich/DE (philipp.paprottka@med.uni-muenchen.de)

Purpose: To evaluate “bolus-tracking” (BT) and “flash-replenishment” (FR) for the assessment of tissue haemodynamics by contrast-enhanced ultrasound (CEUS) in an experimental small-animal-squamous-cell-carcinoma-model. Since the underlying tissue is the same, strong correlations between parameter outcomes of both techniques are expected.

Methods and Materials: Human hypopharynx-carcinoma-cells were subcutaneously injected into the left flank of 18 female athymic-nude-rats. After 14 days of subcutaneous tumour growth, BT and FR measurements were performed in each rat after bolus-injection of SonoVue via the lateral tail vein using a high-end ultrasound system with a 15 MHz probe. Video-sequences were exported; both modalities were analysed with VueBox (Bracco-Suisse). BT yields the parameters peak enhancement (PE), area-under-the-curve (AUC), rise-time (RT), mean-transit-time (MTTb), wash-in-rate (wiRb) and perfusion-index (PIb); FR yields relative-blood-volume (rBV), MTTf, PI and wiRf.

Results: Highly significant correlations were observed between rBV and PE (r=0.609/p=0.007), rBV and AUC (r=0.799/p < 0.001), rBV and MTTb (r=0.64/p=0.004), MTTb and MTTf (r=0.560/p=0.016), PI and PE (r=0.813/p < 0.001), PI and AUC (r=0.693/p=0.001) and PI and wiRf (r=0.688/p=0.002).

Conclusion: Whereas bolus tracking can be used in a wide range of modalities including CEUS, CT and MR, FR as a technique for the assessment of tissue haemodynamics is unique to CEUS. Although BT and FR yield different parameters, the underlying tissue haemodynamics are equal. In this work, we were able to demonstrate strong correlations between different parameters of both modalities in a small-animal-tumour-model, indicating that flash-replenishment is a valid alternative to the more established bolus-tracking technique. Although the lack of absolute, quantitative parameters hinders a direct comparison of both modalities, FR and BT should both be suitable for a relative comparison, e.g. between baseline and follow-up examinations.

10:30 - 12:00

Room N/O

Vascular

SS 115

Thoracic and abdominal aorta

Moderators:

A. Mishra; New Delhi/IN
I.P. Vulev; Bratislava/SK

B-0111 10:30

Triphasic multidetector CT for the assessment of intramural haematoma of the aorta and the pulmonary artery

M. Simon, F. Drueschler, A. Kovacs, P. Hunold, K. May, J. Barkhausen, F. Vogt; Luebeck/DE (martin.simon@uk-sh.de)

Purpose: This study aimed to evaluate the diagnostic accuracy of a triphasic multidetector CT (MDCT) protocol for the detection of aortic dissections/intramural haematoma (IMH) and vascular complications in patients with suspicion of acute aortic syndrome (AAS).

Methods and Material: Within 32 months 432 patients underwent a triphasic (without contrast, arterial and venous phase) MDCT of the entire aorta. One millimeter slices of all data sets were assessed by two independent radiologists using multiplanar reformations on a dedicated workstation. The evaluation included the detection and characterisation of AAS as well as the assessment of clinically relevant concomitant vascular findings. Follow-up MDCT scans as well as intra-operative findings served as the standard of reference.

Results: MDCT confirmed the diagnosis of an acute aortic syndrome in 56 patients, classified as Type A dissection (n=25), type B dissection (n=19) and intramural haematoma (n=12). The concomitant relevant vascular findings included dissection of supraaortal vessels (n=17), dissection of abdominal visceral arteries (n=22),

pericardial effusion/haematoma (n=21) and intramural haematoma of the pulmonary arteries (n=5). The 5 IMH of the pulmonary arteries were combined with an IMH of the aorta in three and a dissection of ascending aorta in 2 cases. All intramural haematoma were detected at best on the non-contrast enhanced scans.

Conclusion: Non-enhanced CT scans are a prerequisite for the accurate detection of intramural haematoma in patients with suspicion of acute aortic syndrome. Our directed analysis of high-resolution MDCT scans showed that intramural haematoma of the pulmonary artery are more frequent than expected.

B-0112 10:39

Measuring aortic and pulmonary trunk diameters in epidemiologic research: do we need gadolinium and orthogonal slices?

B. Mensel, J.P. Kühn, S. Langner, N. Hosten, R. Puls;
Greifswald/DE (*birger.mensel@uni-greifswald.de*)

Purpose: Cardiovascular magnetic resonance imaging has become increasingly popular in population-based research. Our study evaluates the validity and reliability of measuring the diameters of the aorta and pulmonary trunk from plain axial VIBE (volume-interpolated breath-hold examination) images.

Methods and Materials: The study included 50 male subjects from the population-based Study of Health in Pomerania (SHIP). In these subjects, the thoracic and abdominal aorta and pulmonary trunk were imaged at 1.5 Tesla using a plain VIBE sequence and contrast-enhanced magnetic resonance angiography (CE-MRA). Diameters were measured at predefined anatomic sites from axial VIBE images and reformatted orthogonal CE-MRA images. The measurements were validated using Pearson correlation and Bland-Altman analysis. Reliability was assessed using the Bland-Altman method.

Results: Comparison of the diameters revealed strong correlation for the ascending and descending aorta with $r=0.95$ ($p < 0.0001$) and 0.88 ($p < 0.0001$), respectively. Moderate correlation was found for the aortic arch and pulmonary trunk with $r=0.78$ ($p < 0.0001$) and $r=0.74$ ($p < 0.0001$), respectively. The abdominal aorta showed strong correlation as well with $r=0.90$ ($p < 0.0001$) and $r=0.92$ ($p < 0.0001$) for the infradiaphragmal and suprarenal aorta and $r=0.87$ ($p < 0.0001$) and $r=0.86$ ($p < 0.0001$) for the infrarenal aorta and aortic bifurcation. Mean bias was less than or equal to 0.1 cm (7 %); 95% limits of agreement were less than 0.5 cm (20 %). Intra- and interobserver agreement was excellent.

Conclusion: Axial measurement of the diameters of the thoracoabdominal aorta and pulmonary trunk using plain VIBE images is highly valid and reliable.

B-0113 10:48

Intraobserver and interobserver variability of CT-based volumetry and diameter measurements of abdominal aortic aneurysms after endovascular aneurysm repair

W.H. Sommer, M. Haack, F. Meinel, M.F. Reiser, R. Weidenhagen;
Munich/DE (*wieland.sommer@med.uni-muenchen.de*)

Purpose: To determine the most reproducible and suitable measurements for changes of abdominal aortic aneurysms after endovascular aneurysm repair (EVAR).

Methods and Materials: 14 consecutive patients successfully treated by EVAR underwent 128-row follow-up CTA in 1.5-mm collimation. Manual diameter and volumetric measurements were performed twice by two blinded and experienced readers with at least a 4-week interval between readings. Maximum axial and orthogonal aortic diameters, as well as volumetry of the abdominal aortic aneurysm was performed using Osirix software. Intra- and interreader variabilities were determined by concordance correlation coefficients (CCC). Mean time for semiautomated volumetry of the aortic aneurysm and for diameter measurements was recorded.

Results: Interreader agreement was significantly higher for volumetry (CCC=0.996; 95%CI 0.986-0.999), than for the axial diameter (CCC=0.964; 95%CI: 0.866-0.990) and the orthogonal diameter measurement (CCC=0.943; 95%CI: 0.897-0.982) ($p < 0.01$). Both for readers 1 and 2, intrareader agreement was significantly higher for volumetry (CCC=0.999; 95%CI 0.998-0.999), compared to the orthogonal diameter (CCC=0.983; 95%CI 0.941-0.995) and the axial diameter (CCC=0.983; 95%CI 0.952-0.995). The mean time for aortic volumetry was 16.6 ± 3.6 min, while it was 1.8 ± 0.4 min and 1.3 ± 0.3 min for orthogonal and axial aortic diameter, respectively ($p < 0.0001$).

Conclusion: The reliability of aneurysmal volumetry using CTA is excellent for serial measurements by individual readers and between different readers. Although it is time-consuming, this method is the most suitable to detect small changes in aneurysmal size.

B-0114 10:57

Screening for aortic root aneurysms in patients with suspected or known Marfan syndrome: intraindividual comparison of enhanced and unenhanced MR angiography with echocardiography

P. Bannas, M. Groth, M. Rybczynski, S. Sheikhzadeh,
Y. von Kodolitsch, J. Grassner, G. Lund, G. Adam, C. Habermann;
Hamburg/DE (*p.bannas@uke.de*)

Purpose: Patients with Marfan syndrome have to be screened for initial assessment and follow-up of aortic root dilatation. Our purpose was to evaluate intraindividually the performance of unenhanced (3D SSFP-MRA) with contrast-enhanced (3D CE-MRA) magnetic resonance angiography for aortic root diameter measurements and to compare the results with routinely performed echocardiography in patients with Marfan syndrome.

Methods and Materials: Aortic roots were examined prospectively in 51 consecutive patients with suspected or known Marfan syndrome using a 3D SSFP-MRA and a 3D CE-MRA at 1.5 Tesla. Two readers independently measured aortic root diameters at the annulus, sinuses of Valsalva and sinotubular junction in both datasets and compared results with echocardiographic data. Intraclass correlation coefficient, Pearson's correlation coefficient, Bland-Altman, and two-sided t-test were used to assess agreement between observers and methods.

Results: 38 (74.5%) of the included 51 patients (mean age 37.1 ± 13.7 years) had Marfan syndrome, the remaining 13 were healthy individuals (25.5%). Both, SSFP-MRA and CE-MRA measurements of the sinuses of Valsalva revealed a strong correlation with echocardiography ($r=0.893$ and $r=0.850$, respectively). Intraclass correlation was markedly better for SSFP-MRA ($r = 0.904$) when compared to CE-MRA ($r = 0.690$). Image quality as well as intra- and interobserver agreement of measurements of the sinuses of Valsalva was significantly better for SSFP-MRA than for CE-MRA.

Conclusion: 3D SSFP-MRA measurements of the aortic root are superior to 3D CE-MRA measurements and should be used for establishing the diagnosis of aortic involvement in Marfan syndrome and monitoring the course of aortic enlargement.

B-0115 11:06

Feasibility of time-resolved MR angiography with interleaved stochastic trajectories (TWIST) for the diagnosis of thoracic outlet syndrome

T.C. Lauenstein, L. Umutlu, A. Fischer, C. Kloeters, A. Quinsten, S. Kinner;
Essen/DE (*thomas.lauenstein@uni-due.de*)

Purpose: The thoracic outlet syndrome (TOS) is defined as a positional compression of the vertebral and subclavian artery. TOS can be diagnosed by magnetic resonance angiography (MRA) in conjunction with postural manoeuvres. This technique requires high amounts of gadolinium and exact timing of contrast delays. A new time-resolved MRA technique (TWIST) combines parallel imaging with a 3D view sharing implementation. Hence, 3D datasets can be collected with only little intravenous gadolinium, but high temporal resolution. We aimed to assess whether TOS can be diagnosed with TWIST MRA.

Methods and Materials: 21 patients with suspected TOS were studied. Examinations were performed on a 1.5-T system (MAGNETOM Avanto; Siemens). A Body Matrix RF surface coil was used for signal reception of the upper thorax. Following the i.v. administration of 3 cc gadobutrol (Gadovist, Bayer) at a flow-rate of 3 cc/s, 20 consecutive coronal T1-weighted 3D datasets were acquired using a TWIST protocol (TR/TE/flip = 2.5 ms/0.9 ms/25°; matrix: 384x202; 60slices; temporal resolution: 3.0s). The acquisition was performed twice: with the arms alongside the body and after elevation. Images were analysed concerning stenotic changes of the subclavian arteries. Results of subsequent B-mode and colour duplex ultrasonography were used as standard of reference.

Results: 6 patients did not reveal a stenosis of the right or left subclavian artery. In 15 patients a compression of the subclavian artery was observed after arm elevation (unilateral n=9, bilateral n=6). Findings were confirmed by the standard of reference.

Conclusion: TWIST MRA is a fast and robust technique to identify patients with TOS.

B-0116 11:15

Quantification of microvascular vessel wall characteristics of abdominal aortic aneurysms with MRI: feasibility, reproducibility and initial experience

V.L. Nguyen¹, W.H. Backes¹, E.M. Kooi¹, M.C.J. Wishaupt¹, F.A.M.V. Helleenthal¹, M.E.H. Bosboom², R.J. Van der Geest³, G.W.H. Schurink¹, T. Leiner⁴; ¹Maastricht/NL, ²Eindhoven/NL, ³Leiden/NL, ⁴Utrecht/NL (vl.nguyen@maastrichtuniversity.nl)

Purpose: A prominent characteristic of the abdominal aortic aneurysm (AAA) vessel wall is neovascularisation, which has been linked with AAA progression and rupture. The aim of the present study was to investigate the potential of dynamic contrast-enhanced-MRI (DCE-MRI) to characterise AAA vessel wall neovascularity by quantification of the enhancement dynamics.

Methods and Materials: 30 patients underwent DCE-MRI of the abdominal aorta at 1.5 Tesla. Enhancement dynamics were quantified by calculating the transfer constant (Ktrans) using pharmacokinetic modelling and the area-under-curve (AUC). Ten patients were imaged twice on different occasions. Intraclass correlation coefficients (ICC) were determined to investigate interscan, inter- and intraobserver variability. Associations between Ktrans, AUC and maximal diameter were computed as a Pearson correlation coefficient (r).

Results: In total, 28 of the 30 MRI examinations could be included for pharmacokinetic analyses. Interscan, inter- and intraobserver variability for Ktrans and AUC measurements were excellent (ICC > 0.88). The maximal diameter (mean ± SD: 49.5 ± 5.9 mm) was significantly correlated with Ktrans (0.024 ± 0.009 min⁻¹) (r = 0.51; p = 0.006), but not with AUC measurements.

Conclusion: Quantitative analysis of enhancement dynamics of the AAA vessel wall, which may reflect the extent of neovascularisation, is feasible and reproducible. There is a moderate correlation between the aortic aneurysm wall enhancement (Ktrans) and AAA maximal diameter. This study was funded by the Dutch Heart Foundation (2008B042).

B-0117 11:24

Using engineering, mathematical models and CT 4D imaging to understand the haemodynamic after aortic prosthesis insertion

L.V. Forzenigo¹, P. Biondetti¹, M. Domanin¹, C. Vergara², B. Barberis¹; ¹Milan/IT, ²Ranica/IT (pibionde@tin.it)

Purpose: The main goal of this study is to demonstrate the possibility of mathematical modelling of the blood flow in cardiovascular pathologies such as AAA both before and after endovascular treatment (EVA), using dynamic 4D.

Methods and Materials: Since 2007 till 2011 we enrolled 19 who underwent endoprosthesis insertion because of AAA. Each patient was studied before and after intervention with Doppler Ultrasound and Double Source ECG-gated 64 Rows CT Angiography. CT DICOM data were for 3D model/geometry extraction and Mesh generation, and for mathematical modelling of aortic haemodynamic before and after prosthesis insertion. From these data maps of peak wall stress, of flow velocity profiles and of inward/outward wall displacement during one cardiac cycle were calculated.

Results: Preliminary results show that in the native AAA the systolic outward wall displacement is correlated with low velocity, high pressure and flow velocity profiles. After endoprosthesis insertion there is an increase of intra-prosthesis flow velocity, with a decrease of lateral pressure. Deformation and pulsation of the metallic stent structure happened after the first year of follow-up. The midstent location of the deformation well correlated with the location of the maximum velocity change during cardiac pulsation. The rigid prosthesis interrupts the pressure wave originated by the cardiac pulsation, with generation of backward components with possible long-term negative effects on the cardiac function.

Conclusion: Computational blood flow dynamics using 4D CT data could predict the risk of aneurysmal rupture. Late deformation of EVAR can be explained by changes in blood flow dynamics.

B-0118 11:33

Dynamic (dCTA) versus static (sCTA) computed tomography angiography after abdominal aortic endovascular aneurysm repair (EVAR): influence of enhancement patterns and optimal bolus timing on endoleak detection

C. Andres, C. Luecke, B. Foldyna, M. Grothoff, S. Nitzsche, A. Schmidt, D. Scheinert, M. Gutberlet, L. Lehmkuhl; Leipzig/DE (claudia.andres.mail@googlemail.com)

Purpose: To assess differences of aortic and endoleak enhancement in patients after EVAR using the recently introduced dCTA versus sCTA, to evaluate the

impact of enhancement patterns on the endoleak detection rate and to define the optimal scan timing.

Methods and Materials: Seventy-one patients (72±8 years) after EVAR of the abdominal aorta were retrospectively included. All patients underwent dCTA with 10 uni-directional scan phases on a second generation dual source CT (80 kV, 120Ref.-mAs, z-FOV=283 mm, temporal resolution 5sec; 80 ml [4 ml/sec] contrast [400 mg iodine/ml], bolus tracking: 90 HU, followed by a venous phase) and a preliminary biphasic sCTA. Enhancement was assessed for all scan phases by ROI measurements in aorta and detectable endoleaks. Image quality was rated by a 5-point confidence scale.

Results: In dCTA, the highest mean aortic enhancement could be achieved 12sec post-threshold (p.t.), the highest mean endoleak enhancement considerably later at 22sec p.t. Within a total of 48 endoleaks, 14 (37.8%) were newly detected not visible in preliminary sCTA. Detection rates differed significantly in-between the dCTA phases (p < 0.01). The highest detection rate (n=44) was obtained 27sec p.t., when the differences between aortic and endoleak enhancement, and therefore the contrast reached its maximum. The mean dose-length product differed by 11% (dCTA: 1344±131 mGy*cm, sCTA 1224±165 mGy*cm, p < 0.01).

Conclusion: Dynamic CTA in the post-EVAR follow-up revealed that the peak enhancement of endoleaks and aorta are significantly different and not covered sufficiently by conventional biphasic sCTA protocols. The use of dCTA is associated with a significantly increased detection rate of endoleaks.

B-0119 11:42

One year after endovascular abdominal aortic aneurysm repair (EVAR) one third of the aneurysm sac still consists of unorganised thrombus in patients with and without detectable endoleak

S.A. Cornelissen¹, E.-J. Vonken², J. Van Prehn², H.J.M. Verhagen³, F.L. Moll², L.W. Bartels²; ¹Amersfoort/NL, ²Utrecht/NL, ³Rotterdam/NL (sap.cornelissen@meandermc.nl)

Purpose: The purpose of this study was to monitor thrombus organisation during the first year after EVAR with MRI.

Methods and Materials: In this IRB-approved prospective study 30 patients underwent MRI-exams pre-operatively, < 6 weeks postoperatively, 6 months and 1 year after EVAR. Pre-contrast T1-, T2- and postcontrast T1-w images were acquired. An experienced radiologist subdivided the aneurysm sac into regions of endoleak, unorganised and organised thrombus based on the signal intensities on the differently weighted images using custom written software.

Results: The mean unorganised thrombus volume pre-operatively was 23 ml (95%CI 16-30 ml), postoperatively 51 ml (95%CI 41-61 ml), after 6 months 39 ml (95%CI 29-48 ml), and after 1 year 32 ml (23-41 ml). There was a significant increase in unorganised thrombus volume postoperatively compared with pre-operatively (paired t-test, p < 0.05) after which the unorganised thrombus volume significantly decreased after one year (paired t-test, p < 0.05). 10 patients had a type II endoleak on the postoperative CT-exam. In these patients a larger part of the aneurysm sac consisted of unorganised thrombus after 6 months than in patients without a type II endoleak (mean 48% of aneurysm sac volume, 95%CI 38-58% vs. mean 33% of aneurysm sac volume, 95%CI 25-41%, independent t-test p < 0.05).

Conclusion: Measurement of the degree of thrombus organisation of the intra-aneurysmal thrombus after EVAR is possible with MRI. After EVAR the unorganised thrombus volume decreases in time, however, both in patients with and without endoleak, one year after EVAR still one-third of the aneurysm sac consists of unorganised thrombus of unknown aetiology.

B-0120 11:51

Validation of radially undersampled 5-point-encoded 4D flow MR (PC-VIPR) in thoracic aorta and main pulmonary artery

A. Frydrychowicz¹, E. Niespodzany², S.B. Reeder², O. Wieben², K.M. Johnson², C.J. Francois²; ¹Madison, WI/US, Lübeck/DE, ²Madison, WI/US (alex.frydrychowicz@uksh.de)

Purpose: To validate radially undersampled 5-point velocity-encoded 4D-flow-MR (PC-VIPR) for quantification of aortic (AAO) and main pulmonary artery (MPA) flows in comparison to cardiac MR volumetry and 2D phase contrast imaging (2D-PC-MRI).

Methods and Materials: 14 cardiovascular healthy volunteers (39.2±16.8years (22-73); BMI 26.1±3.3 (20.6-31.4)) were scanned at 3 T with 20 elements of a 32-channel-coil. Left and right ventricular volumetry using CINE-bSSFP in contiguous short-axis slices and 2D-PC-MRI in AAO and MPA served as references. All 2D-PC-MRI exams and 8/14 PC-VIPR exams were phantom-corrected according to Chernobelsky et al. PC-VIPR was performed with venc=150 cm/s reconstructed to 20 time frames. PC VIPR data were automatically corrected for eddy currents

and Maxwell terms. Contrast-enhanced MRA using 0.03 mmol/kg gadofosveset trisodium was performed to facilitate 2D plane placement simultaneously providing constantly high signal-to-noise ratio throughout the exam. Bland-Altman analysis (average difference \pm 2SD) and correlation were applied for statistical testing.

Results: Bland Altman analysis shows a marked bias between non-corrected PC-VIPR and CINE-bSSFP (AAO: -11.9 mL (BA-window -48.0 to 24.1); MPA: -6.7 mL (-33.4 to 19.9)) and between non-corrected PC-VIPR and phantom-corrected 2D-PC-MRI (AAO: -14.3 (-44.0 to 15.4); MPA: -11.7 mL (-63.0 to 39.5)). Phantom-correction of PC-VIPR data improved the bias towards both CINE-bSSFP and 2D-PC-MRI. The best correlation was reached between phantom corrected PC-VIPR and 2D-PC-MRI ($R^2=0.62$).

Conclusion: PC-VIPR with 5-point velocity-encoding permits the measurement of blood flow in the thoracic aorta and pulmonary artery simultaneously to morphologic and haemodynamic information. This ongoing evaluation is limited by the variability of the reference methods and outliers influencing the results disproportionately.

10:30 - 12:00

Room P

Physics in Radiology

SS 113

Functional imaging

Moderators:

C. Leidecker; Forchheim/DE
M. Onu; Bucharest/RO

B-0121 10:30

Metal artefact reduction in dual source computed tomography using monoenergetic extrapolation: a systematically optimised protocol

F.G. Meinel¹, Q. Zhang², F. Bamberg¹, B. Bischoff¹, M.F. Reiser¹, T.R.C. Johnson¹; ¹Munich/DE, ²Hangzhou/CN (felix.meinel@med.uni-muenchen.de)

Purpose: Monoenergetic extrapolation is a promising strategy to reduce metal artefacts in dual source computed tomography (DSCT). We performed this study to systematically optimise image acquisition and reconstruction parameters for this approach.

Methods and Materials: A standard hip phantom was loaded with titanium and cobalt chromium models of hip prostheses and scanned on a DSCT scanner (Somatom Definition Flash, Siemens, Forchheim, Germany). Tube spectra, tube current ratio, collimation, pitch, rotation time, and extrapolated energies were optimised in a step-wise process. Artefacts and image noise were quantified by measuring the standard deviation (SD) of the CT density in a circular region of interest placed around the prosthesis and contralaterally, respectively.

Results: Sn140/100 kVp proved superior to Sn140/80 kVp and 140/100 kVp, especially for thick cobalt chromium elements (SD 339 HU vs. 434 HU). There was a benefit for increasing tube current ratio from 1:1 to 3:1 - but not beyond - in favour of the Sn140 kVp spectrum (SD 49 HU vs. 69 HU for cobalt chromium). Artefacts were less severe for a collimation of 32x0.6 as compared to 40x0.6 (SD 30 HU vs. 43 HU for cobalt chromium). A pitch of 0.5 at a rotation time of 0.5 was chosen as optimal when comparing different combinations with comparable scanning times. The optimal extrapolated photon energies were 105-110keV for titanium, and 110-135keV for cobalt chromium.

Conclusion: Sn140/100 kVp with a tube current ratio of 3:1, a collimation of 32x0.6 and extrapolated energies of 105-135keV are optimal parameters for a dedicated DSCT protocol that effectively reduces metal artefacts by monoenergetic extrapolation.

B-0122 10:39

Model-dependent differences in tumour perfusion CT

E. Klotz¹, M. Juergens¹, V. Goh², H. Alkadhi³; ¹Forchheim/DE, ²London/UK, ³Zurich/CH

Purpose: Simplified models such as maximum-slope (MS) and Patlak (PL) have the reputation to be less accurate than deconvolution (DC) approaches. Our goal was to quantify the differences and assess their relevance for clinical studies.

Methods and Materials: We generated enhancement curves from patient arterial input functions by convolution with parametric impulse-residue functions varying blood-flow (BF), blood-volume (BV), mean transit-time (MTT) and extraction-fraction (E) over the range typically found for tumours. Simulated curves were analysed with MS and PL and the results compared to the input. Dynamic data from 15 patients

with renal cell carcinoma (RCC) and known tumour microvascular density (MVD) were analysed with all models and results compared.

Results: Simulation: For injection-times shorter than tumour MTT, BF (MS) agrees perfectly with BF (input), for injection-times not longer than twice the tumour MTT, BF (MS) underestimates BF (input) by not more than 25%. BV (PL) was typically 20% lower than BV (input). As BV (input)*(1-E) agreed within 3% with BV (PL) this appears to be rather a difference in BV definition (first-pass distribution vs. capillary volume). RCC study: BF and BV from all models correlated equally well with MVD (r : 0.77 to 0.83, $p < 0.001$). As predicted (injection-time 10s, MTT: 10.0 \pm 1.9s), agreement between BF (MS) and BF (DC) was excellent (slope 1.01, $r=0.98$). BV (PL) was 24% lower than BV (DC) (slope 0.76, $r=0.95$). If corrected with (1-E) the difference reduced to 4%.

Conclusion: Simplified models can be useful alternatives if radiation exposure and/or temporal sampling need to be limited. Systematic differences can be corrected for allowing comparison with other studies.

B-0123 10:48

Reduced time CT perfusion acquisitions are sufficient to measure the permeability surface area product with a deconvolution method

M.A. Mazzei¹, E. Sani², S. Guerrini¹, N. Cioffi Squitieri¹, E. Fodera¹, C. de Mauro¹, F.G. Mazzei¹, L. Volterrani¹; ¹Siena/IT, ²Florence/IT (mmazzei@sirm.org)

Purpose: The acquisition time in CT perfusion studies significantly affects patient's dose exposure. In order to reduce the radiation dose, reduced time CT perfusion acquisitions are tested to measure PS with a deconvolution method.

Methods and Materials: PS was calculated with repeated measurements (n=259) while truncating the time density curve at different time values in 11 CT perfusion studies conducted for lung cancer (n=2), Hodgkin lymphoma (n=7) and renal cell carcinoma (n=2), using CT perfusion 4D software (GE Healthcare). The median acquisition time of CT perfusion studies was 62 sec (range 49-120 sec). To verify the accuracy of the deconvolution algorithm, a variation of the truncated PS within the error measurements was searched, i.e. within 3 standard deviations from the mean nominal error provided by the software. As a sanity check the test was performed for all the parameters measured using CT Perfusion 4D software.

Results: PS was consistent within 7% in ~10 to ~20 seconds; and within 0.9% in ~20 to ~23 seconds; PS was constant after 25 to 35 sec. A consistent result lasted for all the observed parameters (MTT, BV, BF) as expected from their analytical dependence.

Conclusion: Thirty-five seconds are enough to obtain a reliable IRF (impulse residual function). For an accurate measurement of the PS a 45 sec acquisition time should be an optimal compromise to obtain reliable PS measurements and a reasonable dose exposure. No additional information can be provided with longer perfusion acquisition times.

B-0124 10:57

Improving image quality of volumetric helical perfusion CT at 100 kV using spatiotemporal filtering: a strategy for dose reduction

A. Radhakrishnan, I. Simcock, J. Stirling, A. Khan, R. Glynne-Jones, V.J. Goh; London/UK

Purpose: To assess the change in image quality of pelvic volumetric helical perfusion CT techniques with the application of a spatiotemporal filter.

Methods and Materials: Following ethical approval and informed consent, 23 patients (11 males, 12 females) with pelvic cancers underwent a volumetric helical perfusion CT study (Somatom Definition, Siemens) using the following parameters: (100 kV, 120 mAs, 4D adaptive spiral, 1.5-3s cycle time; 11.4 cm z-axis; 50 mL 350 mg/mL Ioversol IV at 6 mL/sec). Following motion correction, images were reconstructed at 3 mm and 5 mm slice thickness with and without application of a spatiotemporal filter (4D noise reduction). Image noise was assessed by placement of a region of interest within muscle and tumour at 3.0 and 5.0 mm slice thickness, respectively. The standard deviation of the ROI, equivalent to 'noise', was recorded. The tumour contrast-to-noise ratio (CNR) was calculated by dividing tumour enhancement by noise. CNR before and after filter application were compared using paired t-testing with significance at 5%.

Results: Mean noise decreased following filter application from 25.3 to 23.4 at 3 mm and 22.6 to 21.8 at 5 mm for muscle; and from 27.5 to 26.3 at 3 mm and 23.9 to 21.8 at 5 mm for tumour. Contrast-to-noise ratio increased from 1.97 to 2.16 (+9.22%) at 3 mm ($p=0.008$) and 2.29 to 2.36 (+6.58%) at 5 mm ($p=0.39$).

Conclusion: Application of a spatiotemporal filter decreases noise and significantly increases the contrast-to-noise ratio at 3 mm. This has the effect of increasing the CNR at 3 mm to an equivalent 5 mm slice thickness.

B-0125 11:06

Functional imaging on an interventional C-arm flat detector CT system

R. Brauweiler, F. Eisa, M. Hupfer, T. Nowak, D. Kolditz, W.A. Kalender; Erlangen/DE (Robert.Brauweiler@imp.uni-erlangen.de)

Purpose: To investigate the potential of dynamic C-arm CT to assess functional parameters from a time-resolved sequence of volumetric images.

Methods and Materials: Measurements were performed on an experimental robotic C-arm flat detector CT system allowing for a scan time of 2 s/180° and for validation purpose on a clinical CT scanner. For half-scan reconstructions the resulting temporal sampling was 2 s, for full-scan reconstructions 4 s. On the clinical CT we performed scans at 1, 2, 3 and 4 s temporal sampling. We used a perfusion phantom which provides reproducible contrast curves. Three different water flow rates were utilised to simulate different functional behaviour. Scans were repeated three times and post-processed using the maximum slope method to assess the functional parameters blood volume (BV), blood flow (BF), mean transit time (MTT) and time to peak (TTP).

Results: For each sampling rate and all functional parameters, reproducibility errors did not exceed 5% for both clinical CT and C-arm CT. For 2 s temporal sampling, interventional C-arm CT and clinical CT were in agreement with deviations below 10% for BF, BV and TTP and below 15% for MTT. For lower temporal samplings of 3 s and 4 s, functional parameters deviated by up to 40% compared to the 1 s sampling case.

Conclusion: The assessment of functional parameters by C-arm CT shows promising results and may save valuable time in patient treatment, when no additional CT or MRI scan is required before or during therapeutic intervention.

B-0126 11:15

Virtual non-contrast in second-generation, dual energy computed tomography: reliability of attenuation values

M. Toepker¹, T. Moritz¹, M. Weber¹, B. Krauss², T. Mang¹, G. Euler¹, F. Wolf¹, C.J. Herold¹, H. Ringl¹; ¹Vienna/AT, ²Forchheim/DE (michael.toepker@meduniwien.ac.at)

Purpose: To evaluate the reliability of attenuation values in virtual non-contrast images (VNC) reconstructed from contrast-enhanced, dual energy scans performed on a second-generation dual energy CT, compared to single-energy, non-contrast images (TNC).

Methods and Materials: The institutional review board approved this research and waived informed consent. Sixteen phantoms containing a mixture of contrast agent and water at different attenuations (0-1400 HU) were investigated on a Definition Flash-CT scanner using a single-energy scan at 120 kV and a DE-CT protocol (100 kV/SN140 kV). For clinical assessment, 86 patients (35 females) who received a dual phase CT, containing an unenhanced single-energy scan at 120 kV and a contrast enhanced (110 ml Iomeron 400 mg/ml; 4 ml/sec) DE-CT (100 kV/SN140 kV) in an arterial (n=43) or a venous phase, were retrospectively analysed. Mean attenuation was measured within regions of interest of the phantoms and in different tissue types of the patients within the corresponding VNC and TNC images. Paired t-tests and Pearson correlation were used for statistical analysis.

Results: For all phantoms, mean attenuation in VNC was 5.3±18.4 HU. In 86 patients overall, 2637 regions were measured in TNC and VNC images, with a mean difference between TNC and VNC of -3.6± 8.3 HU. In 91.5% (n=2412) of all cases, absolute differences between TNC and VNC were under 15 HU, and, in 75.3% (n=1986), differences were under 10 HU.

Conclusion: Second-generation dual energy CT-based VNC images provide attenuation values close to those of TNC. To use VNC as an alternative to TNC in daily clinical routine, a safety margin of 10 HU should be applied.

B-0127 11:24

Characterisation of the biograph mMR

S. Fürst¹, G. Delso¹, B.W. Jakoby², R. Ladebeck³, C. Ganter¹, S.G. Nekolla¹, E.J. Rummeny¹, M. Schwaiger¹, S.I. Ziegler¹; ¹Munich/DE, ²Knoxville, TN/US, ³Erlangen/DE (sebastian.fuerst@tum.de)

Purpose: The physical performance of the first fully integrated whole body MR/PET scanner, the biograph mMR (mMR), was studied and compared to current MR and PET/CT systems, the Magnetom Verio 3 T and the biograph mCT (mCT), respectively. Simultaneous operation and its effects were also considered.

Methods and Materials: The key components of the mMR are a 3 T magnet and APD-LSO block detectors. Measurements were prepared and performed as described in the NEMA NU 2-2007 protocol (PET) and in the ACR quality control manual (MRI). PET sensitivity and spatial resolution were assessed both with and without an MRI VIBE sequence running.

Results: Based on its geometry, the mMR has an increased sensitivity of 15kcps/MBq in and 14kcps/MBq off the FOV centre (mCT: 10kcps/MBq). The average spatial resolution values of the mMR and the mCT are comparable (4.3 mm/4.4 mm near the FOV centre). These findings were unaffected by parallel MRI scans. The noise equivalent count rate of the mMR peaks at 23.1kBq/ml with 183.5kcps (mCT: 180.3kcps@28.3kBq/ml). The scatter fraction was measured to be 36.7% (mCT: 33.2%). The image contrast increases from 32.5% to 70.8%, whereas the background variability decreases from 5.3% to 3.7% with increasing diameters of active spheres (4:1 sphere:background). Measurement of B0 homogeneity (< 1 ppm in a 22 cm sphere), B1 field distribution and RF noise showed no significant differences to the reference MR system. Simultaneous PET acquisitions had no effect. **Conclusion:** Proper integration of APD-PET technology and 3 T MRI does not limit the performance of either component in comparison to state-of-the-art stand-alone instrumentation.

B-0128 11:33

Comparison of SPACE and 3D-TSE-MRCP regarding image quality and diagnostic certainty in patients in a routine clinical setting

P. Sudholt¹, C. Urigo², G. Bongartz¹, J. Hohmann¹; ¹Basle/CH, ²London/UK (sudholt@uhbs.ch)

Purpose: We compared 3D-SPACE-(sampling perfection with application optimised contrast)-MRCP with conventional 3D-TSE-MRCP in a routine clinical setting. Aim was to evaluate whether or not the 3D-SPACE-MRCP allows better image quality in patients and if this translates also to a higher level of confidence regarding the diagnosis of choledocholithiasis.

Methods and Materials: 3D-TSE and 3D-SPACE sequences were consecutively obtained from 12 patients undergoing MRCP at our institution. For evaluation, the pancreaticobiliary tree was sub-divided into 10 segments which were scored separately for visibility and diagnostic certainty on a five-point-scale each by three experienced radiologists.

Results: In total, 104 segments were reviewed in both sequences. The average image quality was rated good in both sequences but higher for SPACE-MRCP than for 3D-TSE (4.59 versus 4.14 n=104, p=0.0025). In 36 of 104 segments, image quality in 3D-SPACE was superior to 3D-TSE while image quality in 3D-TSE was better in only 11 segments (57 segments where rated as equal). Diagnostic certainty was evaluated better for 3D-SPACE than 3D-TSE in 24 of 104 segments while 3D-TSE had a higher diagnostic certainty in only 6 segments (74 segments where rated as equal).

Conclusion: 3D-SPACE-MRCP allows superior image quality and offers a higher diagnostic certainty compared to conventional 3D-TSE-MRCP. It should be used as the MRCP-sequence of choice in a clinical routine setting.

B-0129 11:42

Development of a tissue-equivalent phantom for standardisation of diffusion-weighted MRI

G. Wolf, M. Laniado, N. Abolmaali, T. Paulus; Dresden/DE

Purpose: Wide-spread application of diffusion-weighted MRI (DWMRI) in oncology is currently impaired due to limited standardisation across instruments. Therefore, we aimed to develop a phantom with tissue-equivalent MRI properties (ADC, R1, R2) for DWMRI standardisation.

Methods and Materials: The influences of individual phantom components agarose gel (concentration=0-4%), sucrose (0-40%), Gd-DTPA (0-0.4mM), SPIO (0-0.1mM) and preservative sodium azide (0.05%) on MRI properties were systematically evaluated. Based on a linear combination model of single components effects, the tissue-equivalent phantom was composed to resemble in-vivo MRI properties of various normal and neoplastic tissues according to literature values. ADC, R1 and R2 of tissue-equivalents were measured by diffusion-weighted spin-echo EPI (9 b-values=0-1000s/mm²), multi-contrast inversion-recovery TSE (9 T1-values=25-2000 ms) and multi-contrast SE (10 TE-values=10-100 ms) using a 1.5 T scanner (Avanto; Siemens). Intra- and inter-series variability was evaluated across multiple acquisitions within the same and all imaging sessions, respectively.

Results: Individual components show inverse linear scaling with concentrations for ADC and linear scaling for R1 and R2. The tissue-equivalent phantom yielded stable MRI parameters over at least 216 days at room temperature storage. Experimental and reference ADC values of tissue-equivalents were significantly correlated (r=0.996, p=0.0003). However, R1 and R2 were less adequately imitated (p> 0.05). Intra- and inter-series ADC variability was 1.4±0.7% and 3.4±1.4%, respectively.

Conclusion: The tissue-equivalent phantom permits repeated quantifications of MRI parameters in combination with easy preparation and long-time stability as well as simple handling and positioning. It may be useful in quality assurance and system standardisation procedures. DWMRI shows excellent repeatability within the same scanner.

B-0130 11:51

Towards standardisation of diffusion-weighted MRI: status survey across instruments using a tissue-equivalent phantom

G. Wolf¹, F. De Keyzer², T. Paulus¹, R. Hermans², N. Abolmaali¹; ¹Dresden/DE, ²Leuven/BE

Purpose: Wide-spread application of oncologic diffusion-weighted MRI (DWMRI) is currently impaired due to limited standardisation across instruments and imaging parameters. We therefore aimed to perform a status survey of DWMRI at different scanners using a tissue-equivalent phantom.

Methods and Materials: The phantom was prepared from agarose gel, sucrose and Gd-DTPA to resemble in vivo MRI properties (ADC, R1, R2) of various normal and neoplastic tissues according to literature values. ADC of tissue-equivalents was measured by diffusion-weighted spin-echo EPI (9 b-values=0-1000s/mm², TE=69-180 ms, TR=1000-10000 ms, parallel imaging factor (PIF)=1-4) on several scanners (1.5 T Avanto, 1.5 T Sonata and 3 T Trio; Siemens). Median intra- and inter-scanner variability was evaluated across multiple image acquisition sessions within the same and all scanners, respectively.

Results: With growing TE we observed a marked early ADC decrease for Sonata (down to 12% relative to TE=minimal) and moderate late decreases for Avanto and Trio (81% and 83%). Avanto ADC was lower than on Trio ($\Delta=160\mu\text{m}^2/\text{s}$) independent of TE, whereas it was higher than on Sonata ($\Delta=220-1640\mu\text{m}^2/\text{s}$) increasing with TE. Correspondingly, inter-scanner variability increased with TE (15-143%). At our optimal settings (TE=minimal, TR=3000 ms, PIF=3), intra-scanner variabilities were 2.8% (Avanto), 3.2% (Sonata) and 5.7% (Trio), while inter-scanner variability was 15% (10-37%).

Conclusion: ADC quantification and variability strongly depend on imaging parameters. In general, DWMRI reveals substantial variability across scanners, which largely complicates setup of multi-centre studies and comparison of results. Nevertheless, at optimal settings, DWMRI provides excellent repeatability at the same scanner. However, future efforts are needed to bring standardisation into clinical practice.

10:30 - 12:00

Room Q

Cardiac

SS 103

Acute coronary syndromes: viability

Moderators:

G. Hadjidekov; Sofia/BG
G.A. Krombach; Giessen/DE

B-0131 10:30

Sensitivity of cardiac magnetic resonance varies with clinical presentation of biopsy-proven acute myocarditis

G. Cannavale, M. Francone, I. Iampieri, B. Conti, A. Frustaci, C. Catalano; Rome/IT

Purpose: Recently T2-weighted imaging allowed depiction of myocardial oedema as a specific marker of disease in acute clinical setting. Its sensitivity, however, varies in acute and chronic manifestations. We report great sensitivity variations of MR in acute myocarditis depending on clinical presentation.

Methods and Materials: We retrospectively evaluated MR sensitivity in comparison with clinical presentation in 70 patients who had in the last two years an endomyocardial biopsy diagnosis of active myocarditis and a clinical history ≤ 3 months. All subjects underwent at time of diagnosis a cardiac MR (CMR) and invasive cardiac examination.

Results: Three types of clinical patterns of myocarditis were recognised: 1) infarct-like (fever, chest pain, ST segment deflection at ECG and serum Troponin I elevation). 2) Cardiomyopathy (left ventricular dysfunction in absence of ECG, serologic or systemic abnormalities). 3) Arrhythmic (sudden occurrence of supraventricular and/or ventricular arrhythmias in absence of systemic evidence of inflammation). Delayed enhancement at CMR suggesting a myocarditis was documented in 72% of patients (n=18/25) of pattern 1, 57% (n=15/26) of pattern 2 and 47% (n=9/19) of pattern 3. Tissue oedema was observed in 80% (n=20/25) of pattern 1.30% (n=8/26) in pattern 2 and 26% (n=5/19) in pattern 3. Early enhancement was positive in 71% (17/25) of the cases with pattern 1.66% (17/26) with pattern 2 and 52% (10/19) with pattern 3.

Conclusion: Sensitivity of cardiac MR is high for infarct-like myocarditis, low for cardiomyopathy and very low for arrhythmic pattern. A more extensive vascular involvement in pattern 1 compared with focal myocyte and conduction tissue damage of pattern 2 and 3, are the most likely explanation.

B-0132 10:39

Hybrid PET/MRI in the assessment of cardiac viability: added value compared to PET/CT

O. Rattib¹, R. Nkoulou¹, M.G. Vincenti¹, A. Quercioli¹, S. Heinzer¹, D. Didier¹, M. Stuber², T.H. Schindler¹, J.-P. Vallee¹; ¹Geneva/CH, ²Lausanne/CH (Rene.Nkoulou@hcuge.ch)

Purpose: We evaluated the potential for hybrid PET/MRI devices to provide integrated metabolic, functional and anatomic characterisation of patients with suspected coronary artery disease.

Methods and Materials: Ten patients (5 with suspected hibernating myocardium and 5 healthy volunteers) performed an imaging study using a hybrid PET/MRI (Philips). Viability assessed by 18 F-FDG was performed in diseased patients along with MRI anatomic and functional study and reassessed within 30 minutes by conventional PET/CT. Non-contrast right coronary artery (RCA) targeted and whole heart 3D coronary angio-MRI using ECG-gating and respiratory navigator was performed in healthy volunteers with reconstruction performed using MPR and volume rendering. The extent of metabolic defect (MD) using PET/MRI and PET/CT was compared in patients and coronary territories (LAD, CX, RCA). Assessability of coronary lumen was judged as good, sub-optimal or non-assessable using a 16-segments coronary model.

Results: Metabolic assessment was successful in all patients with MD being 19.2% vs 18.3% using PET/MRI and PET/CT, respectively (P=ns). The MD was 10.2%, 6%, and 3% vs 9.3%, 6% and 3% for LAD, CX and RCA territories, respectively (P= ns). Coronary angio-MRI was successful in all volunteers with 66 coronary segments visualised overall. The RCA was fully visualised in 4/5 volunteers and the left coronary arteries in 4/5 volunteers. Assessability in visualised segments was good, sub-optimal and non-assessable in 88%, 2% and 10%, respectively.

Conclusion: Hybrid PET/MRI devices may enable metabolic evaluation comparable to PET/CT with additional value owing to accurate functional and anatomical information including coronary assessment.

B-0133 10:48

Is angiographic perfusion score assessed in patients with acute myocardial infarction correlated with cardiac magnetic resonance infarct size and N-terminal pro-brain natriuretic peptide in 6-month follow-up

A.A. Brzozowska-Czarnek, A. Urbanik, T. Rakowski; Krakow/PL

Purpose: Aim of the study was to analyse the correlation between APS and CMR infarct size and LFFunction parameters in 6-month follow-up.

Methods and Materials: In a cohort of 68 patients with STEMI treated with PCI APS was calculated for infarct-related artery based on angiographic parameters and was defined as the sum of the TIMI flow grade (0-3 points) and the TIMI myocardial perfusion grade (0-3 points) before and after PCI (range of points from 0 to 12). Full perfusion was defined as APS ≥ 10 . Bare metal stents were used during primary PCI. In patients with multivessel disease PCI was performed in the infarct-related artery. CMR parameters and NT pro-BNP were assessed at 6 months.

Results: Median APS was 7.5 points. APS ≥ 10 was present in 42% of patients. The significant correlation was found between APS and: CMR infarct size ($r = -0.48$; $P = 0.0001$), CMR left ventricular (LV) ejection fraction ($r = 0.5$; $P = 0.002$), LV end-diastolic volume index ($r = -0.37$; $P = 0.004$), LV end-systolic volume index ($r = -0.41$; $P = 0.001$), NT pro-BNP ($r = -0.5$; $P = 0.02$). Patients with APS ≥ 10 had significantly lower infarct size, LV volumes, higher EF and lower NT pro-BNP.

Conclusion: APS assessed in patients with STEMI treated with PCI is a good predictor of infarct size and left ventricular function in 6-month follow-up. There was a significant correlation of APS and CMR parameters and NT pro-BNP after 6 months.

B-0134 10:57

In vivo MRI characterisation of the myocardium with a diffusion-weighted sequence in 3 T

A. Alberich-Bayarri¹, S. Uribe², J. Sanchez-Gonzalez³, R. Sanz-Requena¹, S. Costa¹, L. Marti-Bonmati¹; ¹Valencia/ES, ²Santiago de Chile/CL, ³Madrid/ES (aalberich.val@quiron.es)

Purpose: Heart motion limits the use of MR diffusion-weighted (MR-DW) sequences in routinely cardiac examination due to the time required by the pair of gradient pulses. Our objective was to define an MR sequence, which could be used to quantitatively analyse in vivo myocardium tissue diffusion in humans.

Methods and Materials: In vivo cardiac MR diffusion images were acquired in a population of 10 healthy volunteers (age 35 \pm 12 years) using a 3 T MR system (Achieva-TX, Philips Healthcare) and a surface coil with 32 channels. The pulse sequence was a spin-echo echo-planar-imaging (SE-EPI) with a TE of 43 ms, the



TR synchronised with every other ECG pulse. The selected b values were 40 and 200 s/mm². Fat was suppressed by a SPAIR configuration in combination with gradient reversal pulses. The acquisition was performed in diastole and the delay in the R-R period was calculated from a high temporal resolution sequence performed immediately before the diffusion acquisition. Slices were acquired in breath-holds of 12s. The spatial resolution was of 3x3x5 mm in 15 short-axis slices along the left ventricle. After co-registering the images to the lowest b-value, the myocardium was segmented and the ADC calculated voxel-by-voxel.

Results: The mean ADC values obtained in the myocardium of the subjects were 2.10 ± 1.27 [10-3 mm²/s]. Images presented a good SNR and absence of geometry distortion artefacts.

Conclusion: The MR-DW described technique can be performed efficiently with an accurate synchronisation of the acquisition to the R-R cycle and may help to analyse myocardial structure in different diseases.

B-0135 11:06

Acute coronary syndrome with normal coronary arteries and positive enzymes; differential diagnosis with cardiac-MRI

M. Danti, S. Sbarbati, G. Camastra, N. Alsadi, F. Marconi, S.W. Della Sala; Rome/IT (massilianodanti@hotmail.com)

Purpose: To demonstrate the role of cardiac MRI in the differential diagnosis of myocardial infarction with normal coronary arteries, and other forms of heart disease with infarct-like presentation (myocarditis, Tako-tsubo, etc). Study design: prospective study performed in a single centre on patients admitted to our UTIC.

Methods and Materials: 65 consecutive patients with chest pain, electrocardiographic changes similar in type-infarct, elevated Troponin and coronary angiography with evidence of normal coronary arteries, were performed within one week of onset of symptoms, a cardiac magnetic resonance with contrast agent (INTERA 1.5 T, Philips Medical Systems, Best, The Netherlands).

Results: Magnetic resonance imaging showed in 56 patients the presence of significant morpho-functional alterations in terms of diagnostic; in 9 patients no pathological changes were observed. In 41 patients was found late-enhancement: in 13 patients the localisation was compatible with myocardial infarction, in 28 patients with myocarditis. In 15 patients, which was not present late-enhancement, there was a severe cardiac akinesia in the apical segments average, framework compatible with Tako-tsubo syndrome.

Conclusion: The cardiac MRI may have key role in the differential diagnosis of acute coronary syndromes with normal coronary arteries and/ or other cardiomyopathies.

B-0136 11:15

Improved agreement between experienced and inexperienced observers using a standardised evaluation protocol for cardiac volumetry and infarct size measurement

G.K. Lund, K. Millerleile, M. Groth, D. Sring, T. Klinik, S. Halaj, G. Folwarski, M. Kaul, G. Adam; Hamburg/DE (glund@uke.de)

Purpose: To study the agreement between experienced and inexperienced observers before and after training using a standardised evaluation protocol for cardiac magnetic resonance imaging (CMR) measurements of left ventricular (LV) volumes, mass and infarct size.

Methods and Materials: 20 CMR studies from 19 patients with myocardial infarction were evaluated. First, 10 CMR studies were analysed by 2 experienced and 4 inexperienced observers with respect to end-diastolic volume (EDV), end-systolic volume (ESV), ejection fraction (EF), LV mass and infarct size. Planimetric measurements were performed on short axis slices (Simpson's method) using a heart analysis tool (HeAT). Subsequently, the inexperienced observers were trained using a standardised evaluation protocol. Thereafter, all observers analysed another 10 CMR studies. Agreement and variance was compared before and after training using Bland-Altman analysis.

Results: Before training the relative difference between experienced and inexperienced observers was -4.3 ±8.2% for EDV, -13.3 ±14.2% for ESV, 5.9 ±8.2% for EF, -12.2 ±10.9% for LV mass and -27.0 ±29.0% for infarct size. After training, agreement significantly improved to 0.2±8.8% for EDV (P < 0.05), -2.1±10.9 for ESV (P < 0.01), 1.5±6.9% for EF (P < 0.05), and -3.6±17.1% for infarct size (P < 0.0001). Slice-based analysis showed that inclusion of the most basal and apical slices were mainly responsible for the initial low agreement.

Conclusion: Training and adherence to the proposed evaluation protocol significantly improved the agreement between experienced and inexperienced observers for LV volumes, EF and infarct size. The proposed evaluation protocol can be used as a guideline for teaching of novel CMR examiners.

B-0137 11:24

Magnetic resonance T1-mapping in acute myocardial infarction: from core to periphery

K.U. Bauner, D. Theisen, T. Sandner, M.F. Reiser, B. Wintersperger; Munich/DE (daniel.theisen@med.uni-muenchen.de)

Purpose: To evaluate T1 characteristics of acute myocardial infarction (AMI) and to delineate AMI in pre- and postcontrast-enhanced myocardial T1-mapping.

Methods and Materials: 18 patients (mean age, 57±10; 4 females) with AMI (2-5 d) underwent cardiac MRI after acute percutaneous coronary intervention on a 1.5 T scanner (Magnetom Avanto) with 32-element coil. For T1 mapping purposes a modified Look-Locker inversion recovery (MOLL) sequence was applied pre- and 10 min post-contrast (0.15 mmol/kg Gadobutrol) at three short axis slice positions. T1 evaluation was based on 11 measurements with different T1 times clustered in 3 groups during T1 relaxation. Pre- and post-contrast T1-maps were calculated and AMI was defined having a cut-off of > 3 standard deviations (SD) as compared to T1 values of normal myocardium (MYO). ROI-based measurements of T1-values of AMI, normal myocardium (MYO) and of myocardial-vascular-obstruction (if present) in the AMI core (MVO) were performed.

Results: The comparison of T1 values of AMI and MYO revealed significant differences in pre-contrast scans (1050±10 ms vs. 818±77 ms; p < 0.001). There was no significant difference of MVO (1015±176 ms) compared to AMI or MYO. Postcontrast T1-values of AMI, MYO and MVO dropped by 72%, 49% and 57%, respectively. The differences of T1 values in AMI and MYO were significant (284±64 ms vs. 449±51 ms; p < 0.001). T1 values of MVO were significantly higher compared to AMI (434±95 ms; p=0.009); however, there was no significant difference between MVO and MYO.

Conclusion: T1 values of acute myocardial infarction are significantly different compared to normal myocardium in both, pre- and postcontrast imaging.

B-0138 11:33

Right ventricular involvement in acute left ventricular myocardial infarction: prognostic implications of cardiac MRI findings

T. Schlosser, C. Jensen, O. Bruder, K. Nassenstein; Essen/DE (thomas.schlosser@uni-due.de)

Purpose: The purpose of this study was to investigate the prevalence and prognostic importance of the cardiac MRI finding of right ventricular involvement in patients with acute ST-segment elevation myocardial infarction (MI).

Methods and Materials: Fifty patients with first-ST-segment elevation MI underwent 1.5-T cardiac MRI immediately after successful percutaneous coronary intervention. The MRI protocol included inversion recovery FLASH delayed enhancement sequences after contrast administration for the quantification of myocardial damage. The prevalence of right ventricular involvement detected with ECG and echocardiography was compared with the prevalence detected with cardiac MRI, which was the reference standard. Patients underwent follow-up for 32 ± 8 months.

Results: Right ventricular involvement was diagnosed with cardiac MRI in 27 patients (54%): 14 of 30 patients (47%) with inferior ST-segment elevation MI and 13 of 20 patients (65%) with anterior ST-segment elevation MI. Patients with right ventricular involvement in anterior ST-segment elevation MI had larger infarcts (delayed enhancement, 25.9% ± 14.5% vs 11.4% ± 10.1%; p = 0.030), lower left ventricular ejection fraction (34.3% ± 8.2% vs 45.2% ± 9.5%; p < 0.015), and lower right ventricular ejection fraction (39.8% ± 6.6% vs 54.9% ± 8.8%; p < 0.001) than those without right ventricular involvement. In a multivariate logistic regression model, right ventricular involvement was a strong independent predictor (odds ratio, 15.8; 95% CI, 4-63%) of major cardiac adverse events.

Conclusion: Right ventricular involvement in ST-segment elevation MI is detected more frequently with cardiac MRI than with ECG and echocardiography and is an independent prognostic indicator.

B-0139 11:42

Value of cardiac magnetic resonance imaging in patients with acute chest pain, elevated cardiac enzymes and a negative coronary angiogram

T. Emrich, K. Emrich, N. Abegunewardene, K. Oberholzer, T. Muenzel, C. Dueber, K.-F. Kreitner; Mainz/DE (emrich@radiologie.klinik.uni-mainz.de)

Purpose: To assess the value of cardiac MRI in patients with acute chest pain, elevated cardiac enzymes and a negative coronary angiogram and analyse factors of influence on the accuracy of the diagnosis.

Methods and Materials: In a 39-month period, 126 patients from the chest pain unit could be included in this study. The MR imaging protocol was kept as simple as possible and consisted of cine, oedema sensitive and late gadolinium enhancement imaging. Clinical follow-up and the synopsis of all clinical, laboratory and imaging

data were the basis for establishing a consensus-based diagnosis. This diagnosis served as the standard of reference.

Results: Besides the five main diagnoses (ischaemic cardiomyopathy, dilative cardiomyopathy, myocarditis, TakoTsubo cardiomyopathy and hypertensive cardiomyopathy; n=111) there were miscellaneous cardiac diagnoses (e.g. hypertrophic cardiomyopathy, cardiac amyloidosis or non-compaction cardiomyopathy n = 15). Compared with the final standard of reference diagnosis, cMRI enabled establishing the final diagnosis in 110/126 patients (87%). Only in 16 patients cMRI could not detect the final diagnosis. Further analysis showed no significant correlation between age, sex and time to cMRI examination and the correctness of the diagnosis ($p > 0.05$). The only important factor was the kind of diagnosis itself.

Conclusion: cMRI helps establishing the final diagnosis in patients with acute chest pain, elevated cardiac enzymes and a negative coronary angiogram in the vast majority of cases. Age, sex and time to examination had no influence on the accuracy of the diagnosis.

B-0140 11:51

Partition coefficient for gadolinium chelates in the normal myocardium: comparison of gadopentetate dimeglumine and gadobenate dimeglumine

N. Kawel¹, M. Nacif², F. Santini², S. Liu¹, J. Bremerich², A. Arai¹, D. Bluemke¹; ¹Bethesda, MD/US, ²Basle/CH (nadine.kawel@gmx.de)

Purpose: To evaluate the influence of contrast agents with different relaxivity on the partition coefficient (λ) and timing of equilibration using a modified look-locker inversion recovery (MOLLI) sequence in cardiac MRI.

Methods and Materials: MOLLI was acquired in healthy subjects (1.5 T) at mid-ventricular short axis pre-contrast and 5, 10, 20, 25, and 30 min after intravenous administration of a bolus of either 0.15 mmol/kg Gadobenate dimeglumine (Gd-BOPTA) (n=10) or Gadopentetate dimeglumine (Gd-DTPA) (n=10) using the following parameters: TE/TR 1.06/2.5 ms; flip angle 35°; bandwidth 1002 Hz/Px; slice thickness 8 mm. T1 times were measured in myocardium and blood pool. λ was approximated by $(1/T1\text{Myocardium pre-contrast} - 1/T1\text{Myocardium post-contrast}) / (1/T1\text{Blood pool pre-contrast} - 1/T1\text{Blood pool post-contrast})$. Values for Gd-BOPTA and Gd-DTPA were compared (t-test). Inter-observer agreement was evaluated (intraclass correlation coefficient [ICC]).

Results: Overall, 120 scans pre-contrast and at 5 time-points post-contrast administration in 20 subjects were evaluated. T1 times of myocardium and blood pool ($p < 0.001$) and λ (0.42 ± 0.03 and 0.47 ± 0.04 , respectively, $p < 0.001$; excluding 5 min for Gd-BOPTA) were significantly lower for Gd-BOPTA than Gd-DTPA. λ (Gd-DTPA) showed no significant variation between 5 and 30 min. λ (Gd-BOPTA) values were significantly lower at 5 min compared to other times (0.38 vs. 0.42; $p < 0.05$). Inter-observer agreement for λ values was excellent with Gd-BOPTA (ICC=0.818) and good for Gd-DTPA (ICC=0.631).

Conclusion: λ (Gd-BOPTA) values are significantly lower compared to λ (Gd-DTPA) at the same administered dose. Using Gd-BOPTA, the equilibrium between myocardium and blood pool is not achieved until 10 min post-contrast.

10:30 - 12:00

Room Z

Computer Applications

SS 105

Image processing (part 1)

Moderators:

P. Badura; Gliwice/PL
E. Kotter; Freiburg/DE

B-0141 10:30

Automated detection and volumetric segmentation of the spleen in CT scans of patients with malignant lymphoma

M. Hammon, R. Janka, S. Seifert, M. Kramer, M. Uder, A. Cavallaro; Erlangen/DE (matthias.hammon@uk-erlangen.de)

Purpose: We introduce an automated detection and volumetric segmentation of the spleen in spiral CT scans. Correlation analysis of automated volumetry (aV), estimated volume determination (eV) and manual volume segmentation (mV) was performed.

Methods and Materials: We retrospectively evaluated the THESEUS-MEDICO CAD-system on spiral CT scans of 15 consecutive lymphoma patients at three consecutive time points. Determination of the eV (splenic volume (cm³) = 30 cm³

+ 0.58 (W x L x Th) and mV as the gold standard were performed by an experienced radiologist.

Results: The automated volumetry (aV) could be performed in all CT scans within approximately 15 seconds. The average splenic volume measured by aV was 268.21 cm³ compared to 281.58 cm³ in manual volume segmentation (mV) and 268.93 cm³ in estimated volume determination (eV). The correlation coefficient of aV and mV was 0.99, of mV and eV 0.91 and of aV and eV 0.91. There was an almost perfect correlation of the changes in splenic volume measured with the new aV and mV (0.95), mV and eV (0.95) and aV and eV (0.86) between two time points. All values are significant ($p < 0.05$).

Conclusion: Our automated detection and volumetric segmentation software rapidly provides objective and reader-independent measurement of the splenic volume in CT scans. The automated volumetry is not as time consuming as manual volumetry. Splenic volume changes can provide evidence of the course of lymphoma.

B-0142 10:39

Assessment of a new 3D visualisation technique in CT colonography, the Funnel view, compared to standard interpretation strategies and other recent 3D rendering technologies

F. Chandelier¹, L. Stein², T. Cabrera²; ¹Granby, QC/CA, ²Montreal, QC/CA

Purpose: The study objective is to assess the performance of a new 3D rendering technique applied to CT colonography (CTC), namely the Funnel view (FV). It aims at addressing current reviewing short-comings during uni- and bi-directional standard reviews (USV & BSV) such as limited colonic surface coverage despite long reviewing-time [EurRadiol;(2007)61:388-399], and the higher degree of distortions and reduced "polyp display time" of new rendering techniques [EurRadiol;(2011)21:653-662].

Methods and Materials: We designed a unique 3D virtual lens, arranging rays transmission based on the best ray-casting strategy optimising the respective field of view. It allows for distortion-limited visualisation of areas behind folds within a traditional perspective rendering. 20 endoscopy-validated CTC datasets with good colonic distensions were involved in this retrospective study, to compare USV, BSV and FV; 3D manual fly-through was deemed reference standard by manually assessing the complete colonic surface visible. Furthermore, FV will be involved in an academic protocol (McGill University, Quebec, Canada) to prospectively investigate its contribution to CTC reviews.

Results: A single fly-through with FV rendered 100% of the visible colonic mucosa, compared to #73% and #92%, respectively, for the USV and BDV. In addition, it significantly increased the display-time closer to the display periphery, required for quality assessment of potential lesions without inducing major distortion.

Conclusion: Funnel view for CTC provides a time-efficient interpretation strategy to assess the entire colonic mucosa with a single automatic fly-through, increasing potential lesion conspicuity and display-time. It has the potential to significantly reduce reviewing time, while maintaining sensitivity and specificity.

B-0143 10:48



CT coronary angiography with 100 kV tube voltage and a low noise reconstruction filter in non-obese patients: evaluation of radiation dose and diagnostic quality of 2D and 3D image reconstructions using open source software (OsiriX)

L. Faggioni, M. Bianchi, P. Marraccini, L. D'Errico, E. Neri, D. Caramella, C. Bartolozzi; Pisa/IT (lfaggioni@sirm.org)

Purpose: To evaluate the diagnostic quality of 2D and 3D image reconstructions from CT coronary angiography (CTCA) studies performed using a tube voltage of 100 kV and a low noise reconstruction filter.

Methods and Materials: Fifty non-obese patients with comparable body-mass index (BMI) underwent CTCA using a 64-row CT scanner. Out of them, 25 were imaged using a tube voltage of 100 kV and a low noise (Soft) reconstruction filter, while in the remaining 25 patients, a tube voltage of 120 kV and a standard reconstruction kernel were selected. Maximum intensity projection (MIP), curved planar reformation (CPR), and volume rendering (VR) views were generated using open source software (OsiriX 3.9; www.osirix-viewer.com), and their diagnostic quality was assessed visually using a three-point score (poor, good, excellent).

Results: Effective dose was significantly lower with the 100 kV than with the 120 kV protocol ($9.8 \pm 3.5\text{mSv}$ vs $18.3 \pm 5.8\text{mSv}$, $p < 0.0001$). Image quality of all reconstructions was good to excellent both at 100 kV and 120 kV, with a statistical trend towards better quality of CPR views with the 100 kV, low noise filter protocol (MIP 2.83 ± 0.55 vs 2.54 ± 0.71 , $p=0.3223$; VR 2.89 ± 0.55 vs 2.40 ± 0.81 , $p=0.2165$; CPR 2.92 ± 0.25 vs 2.34 ± 0.83 , $p=0.0815$, respectively).

Conclusion: Compared with a standard tube voltage of 120 kV, usage of 100 kV and a low noise filter leads to a significant reduction of radiation dose with equivalent diagnostic quality of MIP, VR, and CPR reconstructions in non-obese patients.

B-0144 10:57

Image registration beyond PET/CT - advanced registration of x-ray - and MR-mammograms is feasible and provides morphological and functional information at a glance

M. Dietzel¹, T. Hopp², N.V. Ruiten², W.A. Kaiser¹, P.A.T. Baltzer¹; ¹Jena/DE, ²Karlsruhe/DE

Purpose: Image registration of x-ray- and MRI-mammograms (XM and MM) would allow combining morphological information of XM (e.g. microcalcification) with topographic and functional parameters of 3D MM (diffusion, perfusion, etc). Yet, the few previous research on this topic investigated solely the topographic registration of XM with MM. Accordingly, we: [1] developed a software allowing both topographic matching of breast lesion as well as fusion of the corresponding functional MRI-data and [2] evaluated overall radiological quality and accuracy of this approach.

Methods and Materials: Patients with visible mass-lesions both in XM and MM were enrolled. Based on the MM a "virtual XM" was calculated using our in-house developed software. Based on dynamic enhancement characteristics of the MM, a colour-coded overlay was calculated to characterise tumour vascularisation. This overlay was registered with the "virtual XM". Overall image quality and accuracy of the registration and further tissue parameters were assessed by two experienced readers in consensus.

Results: 11 patients were enrolled (range: 43-73years; mean: 59years). In all patients fusion was performed, successfully. Overall accuracy was defined as displacement of the centres of the lesion between XM and MM divided by the lesion size. It reached 0.82 (mean). The colour-coded overlay allowed identification and characterisation of all cases (n:11/11; 100%).

Conclusion: Clinical feasibility of advanced x-ray- and MR-mammograms registration could be demonstrated. As it allows combination of topographic, morphologic and functional data into one single image, it is a promising tool to further enhance diagnostic accuracy and clinical workflow in breast imaging.

B-0145 11:06

Trabecular direction and deformation distribution in lung transplant patients with severe osteoporosis risk

L. Fischer¹, J. Patsch², A. Valentinitzsch², C. Schueller-Weidekamm¹, B. Zweytick¹, F. Kainberger¹, G. Langs¹; ¹Vienna/AT, ²San Francisco, CA/US (lukas.a.fischer@meduniwien.ac.at)

Purpose: New onset osteoporosis or progression of a pre-existing disease with bone fractures within the first years after lung-transplantation (LuTX) is a severe but poorly understood problem. High-resolution peripheral quantitative computed tomography (HRpQCT) offers novel options for the assessment of disease progression. It provides volumetric BMD, detailed cortical bone geometry and trabecular microarchitecture. We propose and evaluate a novel optical-flow-based registration approach to capture trabecular reorganisation and observe significant differences between LuTX indications.

Methods and Materials: 13 patients (indication groups: (a) vascular diseases, (b) cystic fibrosis, (c) parenchymal diseases) were scanned with HR-pQCT at baseline and 3 months after LuTX. To capture trabecular reorganisation the volumes were rigidly registered. Subsequently trabecular deformation was measured using optical-flow. We obtained deformation-field-maps for each case and quantified the increase of trabecular thickness together with trabecular direction. Entropy was used to quantify directional dominance, Kullback-Leibler (KL) divergence between direction and change distribution to quantify the relationship of two measurements.

Results: No significant differences between LuTX indication groups were observed when comparing directional dominance at a single time point. However, when including reorganisation information by combining trabecular direction and thickness change, significant differences (p < 0.05, fdr corrected) were found between indication groups (a)(b) and (b)(c) (mean KL (a) 0.4197, (b) 0.2991, (c) 0.4964).

Conclusion: Computer-based analysis of bone microarchitecture detected significant differences in osteoporosis progression among different LuTX groups, while microarchitecture assessment at a single time point does not. Trabecular reorganisation can be measured quantitatively in HR-pQCT data, and reveals disease-specific patterns.



B-0146 11:15

Does JPEG lossy compression disguise cranial fractures?

M.F. McEntee¹, I. Nikolovski¹, R. Bourne¹, M. Pietrzyk¹, M. Evanoff², P. Brennan¹, K. Tay¹; ¹Sydney/AU, ²Tuscon, AZ/US (mark.mcentee@sydney.edu.au)

Purpose: The current study aims to establish whether detection of cranial vault fractures is affected by JPEG2000 x30 and x60 lossy compression when compared to JPEG2000 lossless compression.

Methods and Materials: 55 CT images, with three levels of JPEG 2000 compression (lossless, x30 & x60) were presented to 14 senior radiologists. 32 Images contained a single skull fracture while 23 were normal. Observers were asked to identify the presence or absence of a fracture and where a fracture was present to locate and rate their confidence in its presence. A JAFROC and ROC methodology was employed and the DBM MRMC method was used to explore differences between the lossless and lossy compressed images.

Results: The mean JAFROC FOM and ROC AUC scores with lossless JPEG2000 compression were 0.74.0.78 compared to 0.74, 0.79 for x30 lossy and 0.66, 0.71 with x60 lossy. Significant differences were seen only between JPEG2000 Lossy x30 and x60 (p < 0.01). An overall trend of decreased performance with x60 lossy compression was seen while JPEG2000 lossless and JPEG2000 Lossy x30 were seen to perform equally (p < 0.41). A significant trend of increased confidence in true and false positive scores was seen with JPEG2000 Lossy x60 compression.

Conclusion: This work demonstrates that JPEG2000 x60 lossy compression degrades the detection of skull fractures significantly while increasing the confidence with which readers rate fractures. JPEG2000 lossy compression at x30 does not significantly change performance when compared to JPEG2000 lossless compression for the detection of skull fractures in CT.

B-0147 11:24

Intra-operator variability of liver segment volumetry using vessel-based and plane-based techniques

I. Mateka¹, L. Rusko¹, Z. Varadi¹, A. Kriston¹, A. Perenyi¹, Z. Berenyi¹, V. Petrovski¹, O. Demjen¹, A. Palko¹; Szeged/HU (matekailona@yahoo.com)

Purpose: To measure the intra-operator variability of liver segment volumetry. Two approaches were compared in point of difficulty, variability and duration.

Methods and Materials: 14 patients with primary or metastatic liver tumour were selected from a public dataset (http://sliver07.org). One radiologist separated the 8 Couinaud segments on portal-venous CT scans using a research prototype. Starting from gold-standard liver contour the radiologist applied two different techniques: In the vessel-based approach portal vein (PV) was segmented from manually defined root point. Then, non-PV structures were removed, and the 8 main PV branches were labelled in 3-dimensional view, manually. Finally, the vascular territory belonging to each labelled PV branch was computed. In the plane-based approach 2-dimensional views were used to draw 5 traces along the main vein branches: left-, middle-, and right hepatic vein; right PV, and branches of left PV feeding segments II and III. Using these traces 5 smooth surfaces were computed, which were used in a hierarchical order to separate the liver. All patients were processed 3 times with both methods, the standard deviation of volume for each segment was computed (in % of the total liver), and processing time was measured.

Results: The average standard deviation in segment volumetry was 1.8% and 2.0%, while the processing time was 398 and 201 seconds for vessel- and plane-based approach, respectively.

Conclusion: The intra-operator variability of segment volumetry did not proved to be significantly different for the 2 techniques. Vessel-based approach takes significantly longer due to difficulties of labelling the right PV.

B-0148 11:33

Fast automatic computation of path proposals for CT-guided radiofrequency (RF) ablation of malignant liver tumours: initial clinical experience

D. Schmidt¹, J. Bieberstein², C. Schumann², C. Trumm³, S. Clasen⁴, C.D. Claussen⁴, P.L. Pereira⁵; ¹Zurich/CH, ²Bremen/DE, ³Munich/DE, ⁴Tübingen/DE, ⁵Heilbronn/DE (diethard.schmidt@usz.ch)

Purpose: To demonstrate feasibility and effectivity of a fast automatic physician-independent method that computes a list of path proposals for computer tomographic (CT)-guided radiofrequency ablation (RFA) of malignant liver tumours.

Methods and Materials: 26 CT datasets of patients with malignant liver tumours treated by CT-guided hepatic RFA were retrospectively evaluated. Optimal access paths were determined from three experienced interventional radiologists considering following parameters: distance tumour to skin, at risk structures (lung, epigastric

vessels, bowel), and angulation. The planning software (MeVislab, CTI prototype, FraunhoferMEVIS, Bremen) was evaluated with focus on clinical usability by marks 1-6 (1=very good; 2=good; 3=satisfactory; 4=sufficient; 5=insufficient; 6=fail) to determine the best proposal. The best proposals were compared with those of three experts by a score 1-4 (1=better; 2=the same quality; 3=less good; 4=not useful). For statistical analysis the best proposal of the automatic method was correlated with the expert proposals (non-parametric Spearman's, JMP IN, SAS Institute, Cary, USA).

Results: Automatic path proposal computation was successful in all 26 cases (100%). Image processing time was approximately 3.7 sec (± 1.4 sec). The mean mark of the automatic path proposal was 1.77 demonstrating a clinical usability. The automatic method correlated well with the three expert proposals ($r=0.79$; $r=0.81$; $r=0.80$).

Conclusion: The automatic path proposal computation for CT-guided RFA of malignant liver tumours is feasible and effective with a good correlation to expert proposals used in clinical routine work.

B-0149 11:42

Evaluation of hepatic fatty infiltration with dual energy spectral CT

P. Lv¹, X. Lin², J. Li³, J. Gao¹, M. Ke²; ¹Zhengzhou/CN, ²Shanghai/CN, ³Beijing/CN (Lvpeijie²@163.com)

Purpose: To investigate the accuracy and sensitivity of the dual energy spectral CT in the assessment and classification of fatty infiltration in liver.

Methods and Materials: This prospective study was institutional review board approved, and written informed consent was obtained from all patients. The authors examined 42 patients (13 men, 29 women) with dual energy spectral CT imaging during the plain CT scan. There were 29 hepatic patients with mild (18), moderate (6) and severe (5) fatty infiltration, respectively, as the study group; 13 normal hepatic patients as the control group. The degree of fatty infiltration was classified according to the measured liver-to-spleen attenuation ratio. Fat concentrations in the liver were derived from fat-based material-decomposition spectral CT images. The quantitative parameter between the control and study group and among the three hepatic fatty infiltration groups were compared, respectively (two-sample t test, the analysis of variance).

Results: Fat concentrations in normal hepatic patients (1041.04 mg/mL ± 7.25) differed significantly from those patients with hepatic fatty infiltrations (1024.83 ± 10.00) ($P < .001$) with the sensitivity of 92.3% and specificity of 72.4%. Significant differences were also found among the patients with mild (1029.62 mg/mL ± 5.28), moderate (1024.19 mg/mL ± 8.63) and severe (1008.38 mg/mL ± 6.80) fatty infiltrations in liver, respectively ($P \leq .001$).

Conclusion: The fat concentrations derived from the fat-based material-decomposition in the dual energy spectral CT were statistically different among patients with different degrees of fatty infiltration and may provide a quantitative method to assess and classify the hepatic fatty infiltration.

B-0150 11:51

Impact of robust image processing to reduce error in computational haemodynamics

A.J. Joao, A.M. Gambaruto, A. Sequeira; Lisbon/PT (ana.joao@ist.utl.pt)

Purpose: Cardiovascular diseases are associated with a number of factors that include biochemistry, haemodynamics and genetic predisposition. These factors are specific to each individual and it is important to accurately represent patient-specific information in order to assess patient state at diagnosis and prognosis stages. Here, we focus on the effects of uncertainty in clinically acquired medical imaging to variability in the reconstructed vessel geometry, and this error propagation to the computed haemodynamics.

Methods and Materials: The effects of filtering, contrast enhancement and segmentation of medical images are examined with relation to changes in the reconstructed geometry. The images used include MRI and CT data sets, largely focused on the cerebral vasculature. Different image processing methods are chosen and tested, and the most suitable combination of approaches is discussed. Numerical simulations of the haemodynamics are performed and the impact of variability in the vessel geometry is considered with respect to flow parameters commonly associated with disease: transport and stresses on the vessel wall. The discussion is therefore with a clinical relevance.

Results: Results indicate that image preprocessing can substantially alter the quality of the image to improve vessel extraction. This removes a certain level of uncertainty in the segmentation process. Nevertheless, care must be taken to choose appropriate and robust schemes. Results of computational haemodynamics are presented with error bars.

Conclusion: Automatic procedures for medical image processing and geometry reconstruction are important in analysing clinical data. Robust schemes are proposed, reducing the effect of errors in subsequent analysis and post-processing.

14:00 - 15:30

Room C

Oncologic Imaging

SS 216

Colorectal cancer: assessing tumour behaviour

Moderators:

R.G.H. Beets-Tan; Maastricht/NL
P.A. Bonaffini; Monza/IT

B-0151 14:00

Rectal cancer: assessment of response to neoadjuvant chemoradiation by dynamic contrast-enhanced MR imaging

K. Oberholzer, A. Lollert, T. Junginger, A. Heintz, A. Kreft, T. Hansen, C. Dueber; Mainz/DE (lollert@radiologie.klinik.uni-mainz.de)

Purpose: Pre-treatment assessment of functional and morphological tumour characteristics with magnetic resonance imaging (MRI) in locally advanced rectal carcinoma and identification of factors which influence response to neoadjuvant chemoradiation.

Methods and Materials: In a prospective study, ninety-five patients with advanced mrT3 and mrT4 carcinomas underwent dynamic contrast-enhanced MRI (DCE-MRI) before and after neoadjuvant chemoradiation (50.4 Gy). Quantitative parameters were derived from a pharmacokinetic two compartment model (contrast medium exchange rate k_{21} [min⁻¹] relates to microcirculation and amplitude A represents the interstitial space). Tumours were also characterised with regard to morphology as nonmucinous or mucinous at pre-treatment high-resolution MRI. Response to treatment was defined as down shift in the UICC stage.

Results: In nonmucinous carcinomas (74/95) contrast medium exchange rate was higher at pre-treatment MRI compared with mucinous carcinomas (21/95, $p < 0.001$). Effect of chemoradiation on dynamic MR parameters was higher in nonmucinous carcinomas than in within the mucinous subtype ($p < 0.001$). A down shift in the UICC stage was seen in 60/95 patients, a complete response in 11/95. A higher rate of response to treatment was linked with a nonmucinous morphology ($p < 0.001$). Logistic regression revealed an association between mucinous tumour morphology and poor response (odds ratio [95% confidence interval]: 0.113 [0.032-0.395], $p=0.001$) as well as an association between a high 75th percentile of the contrast medium exchange rate and a higher response rate (odds ratio: 1.043 [1.001-1.086], $p=0.045$).

Conclusion: Functional and morphological parameters of pre-treatment MRI can assess tumour characteristics which are associated with effectiveness of chemoradiation before treatment is initiated.

B-0152 14:09

Accuracy of gadofosveset-enhanced 3D T1W MRI for selection of ypT1-2 after chemoradiation for rectal cancer

M. Maas, D.M.J. Lambregts, U. Lalji, M.J. Lahaye, G.L. Beets, R.G.H. Beets-Tan; Maastricht/NL (moniquemaas@live.nl)

Purpose: Selection of ypT1-2 tumours after CRT allows for local excision after CRT. Purpose of this study was to compare diagnostic performance at gadofosveset-enhanced T1W-MRI for selecting ypT1-2 tumours with that of T2W-MRI.

Methods and Materials: 50 patients with locally advanced rectal cancer underwent 2DT2W-FSE-MRI (3 planes) and axial gadofosveset-enhanced 3DT1W-GRE-MRI before and after 6-8 weeks after CRT. Two abdominal radiologists (expert and non-expert) predicted yT-stage at T2W-MRI, at ce-T1W-MRI (after a 2-week interval). After another 2-week interval the T2W and ce-T1W images were scored simultaneously. With ceT1W reading, multiplanar reformatting was used. Patient order was randomised between each reading. Likelihood of a yT1-2 was scored using a confidence level score (0=definitely outgrowing wall to 4=definitely confined to wall). Histology was gold standard. ROC-analyses were performed to compare diagnostic performance.

Results: For the expert AUCs were 0.79 (T2W), 0.74 (ceT1W) and 0.76 (ceT1+T2W). Corresponding sensitivities and specificities were: 68 and 81% (T2W), 43 and 100% (ceT1W) and 61 and 81% (T1+T2W). For the non-expert, AUCs were 0.68 (T2W), 0.70 (ceT1W) and 0.75 (ceT1+T2W). Corresponding sensitivities and specificities were: 61 and 62% (T2W), 82 and 57% (ceT1W) and 86 and 52% for (ceT1+T2W).

Inter-observer agreement (kappa) was 0.58 (ceT1+T2W), 0.36 (ceT1W) and 0.25 (T2W).

Conclusion: The use of gadofosveset-enhanced T1W-MRI improved sensitivity in the non-expert and specificity in the expert reader for selecting ypT1-2 tumours after CRT. Interestingly, T1W-imaging alone showed equal diagnostic performance as T2W-imaging alone. Inter-observer agreement was higher when T1W-imaging was added to T2W-imaging. Gadofosveset MRI might help both expert and non-expert readers in more accurate selection of tumours confined to the rectal wall after CRT.

B-0153 14:18

Rectal cancer: dynamic contrast-enhanced MRI correlates with lymph node status, distant metastases and EGFR expression

A. Lollert¹, K. Oberholzer¹, T. Junginger¹, S. Biesterfeld², C. Schimanski¹, P. Mildnerberger¹, C. Dueber¹; ¹Mainz/DE, ²Düsseldorf/DE (lollert@radiologie.klinik.uni-mainz.de)

Purpose: To evaluate correlations between dynamic contrast-enhanced magnetic resonance imaging (DCE-MRI) and clinicopathological data as well as immunostaining of the markers of angiogenesis EGFR and CXCR4 in patients with rectal cancer.

Methods and Materials: Presurgical DCE-MRI was performed in 41 patients according to a standardised imaging protocol (1.5 T system, T1-weighted rapid turboFLASH sequence, FoV: 350 mm, matrix: 256 x 192; slice thickness 7 mm, TR/TE/TI: 7.0/3.86/120 ms, flip angle 12°, 200 Hz/px bandwidth, voxel size 1.37 x 1.37 x 7.0 mm³). Two quantitative parameters (k21, A) were derived from a pharmacokinetic two-compartment model, one semi-quantitative parameter (TTP) was assessed. Standardised surgery and histopathological examination were applied for the whole patient population. Immunostaining for EGFR and CXCR4 was performed using the avidin-biotin complex method and evaluated with a standardised scoring system.

Results: DCE-MRI parameter A correlated significantly with the N-category (p=0.048) and k21 with the occurrence of synchronous and metachronous distant metastases (p=0.029). A significant correlation between DCE-MRI data (TTP) and the expression of EGFR was found (p=0.044). A trend to a correlation between k21 and EGFR expression could be shown (p=0.107). DCE-MRI data did not correlate with CXCR4 expression.

Conclusion: DCE-MRI is a non-invasive method which can characterise angiogenesis in rectal cancer and correlates with EGFR expression. Due to the relationship between the dynamic parameters and clinicopathological data, DCE-MRI might be a prognostic indicator for lymph node status and distant metastases in patients with rectal cancer.

B-0154 14:27

High-b-value diffusion-weighted imaging with background body-signal suppression: a pivotal role for the evaluation of complete response to neoadjuvant treatments in rectal cancer

L. Monguzzi, D. Ippolito, M. Colombo, P.A. Bonaffini, S. Sironi; Monza/IT (letizia.monguzzi@gmail.com)

Purpose: To evaluate the efficacy of DWI, qualitative and quantitative tool, in combination with T2-weighted imaging in assessing tumour response to CRT, as compared to T2WI alone, by correlating histologic downstaging as the reference standard.

Methods and Materials: 35 LARC patients underwent pre- and post-CRT MRI examination (6 weeks after the completion of treatment) on a 1.5 T scanner (Achieva, Philips) with following protocol: multiplanar T2 and T1 TSE images and DWIBS sequences (b factor: 0 and 1000 mm²/sec). After total mesorectal excision, the histopathological response was classified as tumour regression grade (according to Mandard's criteria: TRG1-2 responders; 3-5 non-responders). Two readers in consensus, blinded to the results, evaluated T2WI without and with DWI to detect the presence of complete response by a four-point scale as follows (1: definitely absent; 2: probably absent; 3: probably present; 4: definitely present). Mean value of ADC of pre- and post-CRT DWI were measured and compared between responders and non-responders.

Results: On the basis of pathological features according to Mandard's criteria, 26 patients (74%) were classified as responders, showing complete or subtotal regression, and 9 (26%) were classified as non-responders. Mean ADC value in MR1 examination was 0.86±0.22 x10⁻³ mm²/sec, whereas mean values after CRT were 1.43±0.25x10⁻³ mm²/sec. On T2W images both readers correctly identified 19/26 patients with complete response (specificity 73%), while after addition of DWI, the readers correctly identified 25/26 of CR (spec 96%). Our preliminary results showed that the two readers achieved more accurate results combining the analysis of DW images with T2WI than T2W images alone.

Conclusion: The functional DW-MRI plays a crucial role in detecting the complete response in LARC patients, by adding information about changes in tumour pathophysiology useful for the assessment of viability of the tumour after CRT.

B-0155 14:36

Long-term outcome of MRI-based individualised treatment for rectal cancer: a multicentre study

M. Maas, S.M. Engelen, M. Lahaye, D. Lambregts, J.W. Leijtens, C.L. Van Berlo, H. Verkooijen, G.L. Beets, R.G.H. Beets-Tan; Maastricht/NL

Purpose: A differentiated treatment according to each individual risk profile in rectal cancer patients was introduced over the last decade. The purpose of this study was to evaluate whether MRI-based individualised treatment can improve long-term outcome of rectal cancer patients.

Methods and Materials: From 2003 until 2008 228 patients were included in a multicentre prospective cohort study with expert and non-expert rectal MRI readers. All underwent preoperative MRI using a lymph-node-specific contrast agent to predict CRM, T- and N-stage. Based on the MRI, patients were stratified in different risk groups for local recurrence: (a) early tumour (wide CRM&N0), (b) non-locally advanced tumour and (c) locally advanced tumour (close/involved CRM, N2-status, distal tumours). Group (a) underwent surgery, (b) preoperative 5x5Gy followed by immediate surgery and (c) a long-course of chemoradiation with surgery after a 6-8 week interval. Kaplan-Meier curves were used to estimate long-term outcome.

Results: After a median follow-up of 41 months the 3-year local recurrence, disease-free survival and overall survival are 2.2%, 80% and 84.5%, respectively.

Conclusion: MRI-based individualised treatment of rectal cancer leads to excellent long-term outcome, specifically regarding local control, both in expert and non-expert centres. The results compare favourably to other published reports. The results confirm that MRI is mandatory in the staging of rectal cancer and show that good local control is achieved, while now distant metastases determine overall survival. Therefore, radiologists should focus on early detection of metastases with the aim to improve overall survival.

B-0156 14:45

Diffusion-weighted MR imaging for prediction of early response of locally advanced rectal cancer to chemoradiation therapy

R. Cianci, A. Filippone, E. Pace, V. Bianco, G. Esposito, A. Tartaro, A.R. Cotroneo; Chieti/IT (r.cianci@rad.unich.it)

Purpose: To evaluate DWI for assessment of early treatment response of locally advanced rectal cancer (LARC) 2 weeks after chemoradiotherapy (CRT).

Methods and Materials: Twenty-eight patients with LARC underwent MRI prior to, 2 and 8 weeks after CRT, including T2-weighted images and echo-planar DWI with 6 b-values (0 to 1000 sec/mm²); ADC values were measured. Imaging was correlated to post-surgical histopathologic tumour regression grade, according to Mandard's classification. Two- and 8-week post-treatment ADC changes respect to baseline (%ΔADC) in the group with complete response (CR) were compared with those in the non-complete response group (non-CR). Moreover, 2- and 8-week post-treatment ADC changes were compared either in CR or in non-CR group.

Results: At 8 weeks the median %ΔADC of CR group (86.91%) was significantly higher compared to that of non-CR group (37.66%) (p=.05). Similarly, at 2 weeks the median %ΔADC of CR group (47.5%) was significantly higher than that of non-CR group (-0.84%) (p=.024). The best %ΔADC cut-off to differentiate CR from non-CR at 2 weeks was 25% (p=.0001), which yielded a sensitivity of 91%, a specificity of 77%, and an Az value of 0.88; at 8 weeks it was 29.5% (p=.0001) with a sensitivity of 83%, a specificity of 90% and an Az value 0.91. When comparing median %ΔADC obtained at 2 and 8 weeks after CRT, no significant differences were found either for CR or for non-CR group (p=.13).

Conclusion: The median %ΔADC at 2 weeks after CRT represents an early and reliable predictor of preoperative treatment outcome.

B-0157 14:54

Vascular mapping using an MRI blood pool contrast agent reveals vascular asymmetry and chemoradiotherapy-induced vascular remodelling in the mesorectum of rectal cancer patients

R. Kluzka, J.-P. Kleijnen, M. Maas, C. Jeukens, W. Backes, G. Beets, R. Beets-Tan; Maastricht/NL

Purpose: In rectal cancer patients, the tumour-surrounding mesorectum exhibits the enhanced vasculature and desmoplastic pattern. Our aim was to determine the vascular changes in the mesorectum related to the tumour growth and the influence of neoadjuvant chemoradiotherapy on the structure of mesorectal vasculature using MRI vascular mapping with a blood pool contrast agent.

Methods and Materials: The staging and restaging MRI was performed for six patients on a 1.5 T scanner using a phased-array coil. A routine imaging protocol was complemented with a dynamic T1-weighted scan (TE/TR=4.6/7.9 ms, $\alpha=30^\circ$, time resolution=8s, matrix=512x512). 0.03 mmol/kg of gadofosveset was administered during the acquisition. Maximal intensity projections were derived from the difference images, obtained by subtracting the pre-contrast baseline from 2 min post-contrast images. The number of vascular branches was determined in the tumour-neighbouring and tumour-distant mesorectum using the primary-staging data. The pre- and post-chemoradiotherapy vascular maps were compared with respect to the number of vascular branches, their length and diameter using OsiriX. **Results:** A significantly higher number of vessels was found in the tumour-neighbouring mesorectum compared to tumour-distant mesorectum ($p=0.003$). The difference was between two- and eight-fold for different patients. The comparison of pre- and post-chemoradiotherapy maps revealed a 54% lower vessel branching after treatment ($p=0.055$). Moreover, the vascular diameter of 1.8 ± 0.7 mm at the primary staging was significantly decreased to 1.3 ± 0.3 mm after the therapy ($p=0.0001$). No difference was found in the vessel length. **Conclusion:** Vascular mapping of the mesorectum of rectal cancer patients revealed the enhanced vasculature around the tumour and vascular remodelling after chemoradiotherapy.

B-0158 15:03

Assessment of preoperative radio-chemo therapy (pCRT): a novel numerical semi-quantitative DCE-MRI parameter compared with morphologic MRI (mMRI) and qualitative time intensity curves (tMRI)
M. Petrillo, R. Fusco, V. Granata, O. Catalano, M. Sansone, A. Rotondo, R. Grassi, A. Petrillo; *Naples/IT (mario.petrillo@gmail.com)*

Purpose: mMRI evaluation is considered the best available tool for LARC staging after pCRT. To compare the accuracy of a novel semi-quantitative numerical parameter based on pattern analysis (SIS) with mMRI and DCE-MRI based on qualitative tMRI in differentiating between responders (R, TRG1 or TRG2) and non responders (NR, TRG3 or TRG4) after pCRT.

Methods and Materials: 40 patients underwent DCE-MRI examination before and after pCRT. Pre and post-contrast T1w scans were acquired after Gd-DOTA injection. Regions of interest (ROI) were drawn inside the tumour, respectively, TIC evaluation and SIS analysis were computed for each ROI. mMRI, tMRI and SIS-based evaluations were performed.

Results: mMRI evaluation gave 54.2% sensitivity (SEN), 56.2% specificity (SPE), 65.0% positive predictive value (PPV) and 45% negative predictive value (NPV). Performing tMRI evaluation 79.2% SEN, 50% SPE, 73.1% PPV and 61.4% NPV were obtained whilst using a cut-off value of 11.6% in SIS change, 85.0% SEN, 83.3% SPE, 91.7% PPV and 71.4% NPV were obtained. Performing a SIS-based evaluation a relevant gain respect to mMRI alone (+30% and +14.1%) and tMRI (+7.2% and +37.2%) was obtained.

Conclusion: Standardised index of shape (SIS) basing on a numerical semi-quantitative DCE-MRI parameter, obtained through pattern analysis, results an accurate tool to predict tumour activity of pCRT in LARC patients through a well-defined cut-off (11.6%) to differentiate R by NR.

B-0159 15:12

Treatment monitoring in LARC: role of diffusion-weighted imaging and 18-FDG-PET-CT in evaluation of tumour regression grade during and after CRT
L. Monguzzi, D. Ippolito, L. Guerra, E. De Ponti, C. Messa, S. Sironi; *Monza/IT (letizia.monguzzi@gmail.com)*

Purpose: To assess the role of ADC values (DW MRI) in comparison with SUVmax values (18 FDG-PET-TC) before, during and after chemo-radiation therapy in patient with LARC, being the histologic examination as reference standard.

Methods and Materials: Three sequential 18 F-FDG PET/CT studies were performed in 35 patients with biopsy-proven primary rectal carcinoma as follows: before starting CRT (PET/CT1), during CRT (PET/CT2), and after completion of treatment (PET/CT3). MR scanning was performed before (MR1) and after CRT (MR2), on 1.5T magnet (Philips Achieva) and comprised T2TSE multiplanar sequences and DWIBS (b factor: 0 and 1000 mm²/sec). The percentage decrease of SUVmax (Δ SUV 1 and 2) and ADC (Δ ADC) values from baseline to presurgical scan were assessed and correlated with pathologic response classified as tumour regression grade (Mandard's criteria; TRG 1= complete regression, TRG5= no regression).

Results: Tumour was detected in all patients at both MR imaging and FDG PET/CT, and after CRT all patients were submitted to surgery. According to the Mandard's criteria, 26 (74%) showed complete (TRG1) or subtotal regression (TRG2) and were classified as responders; nine (26%) were classified as non-responders (TRG3, 4

and 5). In all patients the mean values of SUVmax in PET1 were higher than the mean value of SUVmax in PET2 and PET3 ($p < 0.001$), whereas the mean ADC values were lower in RM1 than RM2 ($p < 0.001$), with a significant percentage decrease of values after the treatment ($p < 0.005$). The best predictors for TRG response were SUV3 (threshold of 4.4) and ADC2 (1.28×10^{-3} mm²/sec) with sensitivity, specificity accuracy, negative predictive value, and positive predictive value of 77.3%, 88.9%, 80.7%, 61.5%, and 94.4%, respectively. A significant correlation (linear regression) between ADC values and TRG's data was also found ($p < 0.001$). **Conclusion:** DW MRI and FDG-PET/CT have a complementary diagnostic role in the follow-up of patients with LARC, by differentiating fibrosis from viable tumour tissue after CRT.

B-0160 15:21

Lymph node staging in colorectal cancer by contrast-enhanced CT: development of a new reporting model for higher diagnostic accuracy
A. Bartels, E. Oevermann, S. Hollmann, J.H. Marxsen, F.M. Vogt, A. Kovacs, P. Hunold; *Lübeck/DE (Antonia.bartels@gmx.de)*

Purpose: Lymph node (LN) staging in patients with colorectal cancer (CRC) is important for optimal treatment planning. However, it is difficult by CT based on simple criteria. Purpose of this study was to establish a reporting model to accurately distinguish histologically proven LN negative (N0) from positive (N1/2) CRC patients by CT.

Methods and Materials: This retrospective study included 97 patients with proven CRC and preoperative contrast-enhanced CT from an interdisciplinary tumour-board database. In a blinded manner, the following LN features were evaluated: different metric traits, total LN count, form, structure/density, presence of a hilum, contrast-medium-enhancement. The accuracy of those criteria in combination was examined by logistic regression. All collected parameters were correlated with postoperative histopathological findings (N0 vs. N1/2).

Results: Some parameters reached significance for predicting LN-metastases; however, only intermediate accuracies: Largest LN > 9.05 mm (sens., 66%; spec., 81%, accuracy, 74%), SD of longest LN diameters > 1.4 mm (85%, 55%, 70%), n> 6 locoregional LN> 3 mm (61%, 67%, 64%). The combination of the following criteria significantly predicted LN-metastases: Presence of amorphous LNs, SD of LN longitudinal diameters > 1.4 mm, mean of the LN cross-diameter > 5 mm, and SD of the cross-diameter/longitudinal-diameter ratio > 0.136. If ≥ 3 of these four criteria were fulfilled, LN-metastases were predictable with a slightly higher accuracy (73%, 83%, 78%). A reporting model was developed for clinical decision making on LN malignancy.

Conclusion: The developed reporting model (decision tree) might facilitate and improve LN staging by contrast-enhanced CT in CRC patients. Prospective studies have to confirm this suggestion.

14:00 - 15:30

Room D1

Chest

SS 204

Pulmonary nodules

Moderators:
M. Das; *Maastricht/NL*
B. Feragalli; *Chieti/IT*

B-0161 14:00

Iodine uptake ratio (IUR): a novel approach to differentiate between malignant and benign lung lesions
G.G. Lo¹, E. Ueno², W.H. Yeung¹, R.K.P. Wong¹, A.M. Chow¹, S.K. Yu¹;
¹Happy Valley/HK, ²Tokyo/JP (cwhy@hksh.com)

Purpose: To investigate the feasibility of iodine uptake ratio (IUR) for differentiating malignant and benign lung lesions using contrast-enhanced CT spectral imaging.

Methods and Materials: 41 patients with known biopsy-proven lesions were prospectively evaluated. All CT examinations were performed on a high definition CT scanner (Discovery CT750 HD, GE). For each imaging session, 70 mL of iodinated contrast agent (300 mgI/mL) was injected intravenously at 1.5 mL/s. After a delay time of 70 s, spectral images were acquired with dual energy at 80/140 kVp. Material decomposition iodine images were reconstructed. Circular ROI were defined in the iodine density images over the lung lesions with maximum enhancement and normal lung parenchyma for iodine concentration measurements. IUR was defined as the ratio between iodine concentration of the lesion and that of normal lung parenchyma.

Results: Pathological results showed that 30 lesions were malignant lesions, while 11 lesions were benign. IUR of malignant lesions (3.86 ± 1.94) was significantly higher ($p < 0.05$, two-tailed Mann-Whitney test) than that of benign lesions (2.47 ± 1.58). The area under receiver operating characteristic curve was 0.712, indicating the potential capability of IUR in differentiating malignant and benign lung lesions. An IUR threshold value of 2.36 was determined, allowing differentiation between malignant and benign lung lesions with sensitivity, specificity and accuracy of 90.0%, 63.6% and 82.9%, respectively.

Conclusion: IUR is first demonstrated as a novel approach to differentiate between malignant and benign lung lesions, suggesting its potential applications in monitoring disease progressions and therapeutic interventions.

B-0162 14:09

Newly developed mathematical model for perfusion CT using 320-detector row CT in patients with pulmonary nodules: comparison of diagnostic capability with previously utilised models for first-pass perfusion CT and FDG-PET/CT

Y. Ohno¹, M. Nishio¹, H. Koyama¹, D. Takenaka¹, T. Yoshikawa¹, S. Matsumoto¹, Y. Fujisawa², K. Sugimura¹; ¹Kobe/JP, ²Ohtawara/JP (yosirad@kobe-u.ac.jp)

Purpose: To compare diagnostic capabilities among newly developed and previously utilised mathematical models on first-pass perfusion 320-detector row CT and FDG-PET/CT.

Methods and Materials: 52 consecutive patients with 86 nodules underwent first-pass perfusion CT using a 320-detector row CT, PET/CT, and microbacterial and/or pathological examinations. 86 nodules were classified into two groups based on the final diagnoses: malignant (n=56) and benign nodules (n=30). From perfusion CT data in each nodule, total blood flow (TF) was calculated from pulmonary arterial flow and bronchial arterial flow by dual-input maximum slope model. In addition, blood flow within the nodule (BF), ejection fraction (EF) and distribution volume (DV) were also calculated by single input maximum slope or Patlak plot modes. On PET/CT, SUVmax within each nodule was determined by ROI measurement. To compare diagnostic capability among all indexes, ROC tests were performed. Finally, sensitivity, specificity and accuracy were compared each other using McNemar's test.

Results: Area under the curve of TF ($Az=0.83$, $p < 0.05$) was significantly larger than that of EF ($Az=0.72$), DV ($Az=0.50$, $p < 0.05$) and SUVmax ($Az=0.72$). When feasible cut-off values were adopted, specificity and accuracy of TF were significantly higher than those of BF ($p < 0.05$), EF ($p < 0.05$) and SUVmax ($p < 0.05$). In addition, sensitivity and accuracy of TF were significantly higher than those of DV ($p < 0.05$).

Conclusion: Newly developed model for first-pass perfusion CT on 320-detector row CT was more accurate than previously utilised models, and can play as more specific and accurate role for diagnosis of pulmonary nodule than PET/CT.

B-0163 14:18

Evaluation of adaptive iterative dose reduction (AIDR) for lung nodule detection in ultra-low-dose thoracic CT

N.S. Paul, H. Mehrez, M. Hashemi, S. Alhumayyd, G. Murphy, R. Cobbold; Toronto, ON/CA (narinder.paul@uhn.on.ca)

Purpose: To demonstrate the accuracy of ultra-low-dose CT (ULDCT) with AIDR image reconstruction for lung nodule detection compared to ULDC and LDCT filtered back projection (FBP) images.

Methods and Materials: Raw data from 50 LDCT: 64x0.5 mm, 120 kVp, and 25 mAs (dose~1mSv) were selected so that 25 studies contained a single lung nodule mean diameter 6.7 mm (3-18 mm), mean density -250 HU (-570 HU to +170 HU) with variable location from apices to bases. LDCT images were reconstructed with FBP (group-A) and taken as the clinical reference. Noise was applied to the raw data to generate simulated ULDC at 5 mAs (dose~0.2mSv) and reconstructed images with FBP (group-B), and AIDR (group-C) at 5/2.5 mm. Two chest fellows (R1, R2) read all images in randomised blinded study and performed a 5-point ROC analysis for lung nodule detection and a 3-point scale for image quality (IQ); 1=poor, 2=good, 3=excellent.

Results: Qualitative analysis: IQ rating for groups A, B, and C for each reader were, R1=2.06, 1.22, and 1.08 and R2=2.1, 1.5 and 1.7. Quantitative analysis: nodule detection by (R1, R2) for all image sets were: group-A: sensitivity=95.8%, 100%; specificity=95.7%, 100%; accuracy= 95.7%, 100%; AUC=0.9755, 1.000; group-B: sensitivity=95.8%,91.7%; specificity=100%, 100%; accuracy= 97.9%,95.7%; AUC=0.9964, 0.9937; group-C: sensitivity=95.8% ,95.8%; specificity=100%, 100%; accuracy=97.9%, 97.9%; AUC=0.9964, 0.9982. Results of group-C (ULDCT/AIDR) were superior to group-B (ULDC/FBP) and comparable to group-A (LDCT/FBP).

Spearman's rank correlation coefficient between groups-C and A were: R1=0.838, and R2=0.954 ($p < 0.001$).

Conclusion: Ultra-low-dose CT with AIDR has comparable clinical performance to conventional LDCT for lung nodule detection and achieves 80% dose reduction.

B-0164 14:27

Small pulmonary nodules less than 7 mm: how to distinguish malignancy and benignity?

K. Yoon, G. Jin, Y. Han, Y. Lee; Jeonju/KR (shingha@paran.com)

Purpose: We investigated radiologic-pathologic correlation of small pulmonary nodules less than 7 mm to evaluate the major differences of benign and malignant nodules on CT findings.

Methods and Materials: The study included 113 patients (66:47=M:F, mean age:59) with small pulmonary nodules less than 7 mm. Tissue diagnosis was made in all patients with surgical resection. The histologic characteristics of the nodule were correlated with radiologic findings such as shape, margin and density. We also evaluated the major differences of benign and malignant nodules less than 5 mm.

Results: Mean diameter of nodules on CT was 4.95 cm. In the 113 nodules, malignant nodules were 23 (20.4%) and benign 91 (80.5%). Major differences of benign and malignant nodules were shape, density and margin. In margin, spiculation and lobulation occurred with a significantly higher frequency among malignant nodules ($p < 0.0001$). In subsolid nodules, malignancy rates were significantly higher than solid nodules ($p < 0.0001$). In subsolid nodules, a lobulated or spiculated margin was associated with a higher risk of malignancy ($p=0.005$). Important predictive findings of fibrotic nodules and anthracotic pigmentations (44% of benign nodules) compared to malignant nodules were as follows: smooth margin and solid attenuation. Especially in nodules less than 5 mm, smooth border and solid attenuation were proved as independent morphological predictors of benignity (predictive value : 94.4%).

Conclusion: Malignant pulmonary nodules less than 7 mm show spiculated margin, GGO or mixed GGO with significantly greater frequency. Especially, smooth border and solid attenuation were independent predictors of benignity in less than 5 mm nodules.

B-0165 14:36

Differentiating subsolid and solid pulmonary nodules on CT: inter- and intraobserver agreement among experienced thoracic radiologists

A. Yildirim¹, C.A. Ridge², P.M. Boiselle², T. Franquet³, P.A. Gevenois⁴, C.M. Schaefer-Prokop⁵, D. Tack⁶, A.A. Bankier²; ¹Kayseri/TR, ²Boston, MA/US, ³Barcelona/ES, ⁴Brussels/BE, ⁵Amerfoort/NL, ⁶Baudour/BE (afra_yildirim@hotmail.com)

Purpose: The recommended CT surveillance period is longer for subsolid than for solid pulmonary nodules, due to the slower growth rate of bronchoalveolar carcinoma compared to other lung cancers. This study tests the hypothesis that inter- and intraobserver agreement whether a pulmonary nodule is subsolid is "good".

Methods and Materials: Six thoracic radiologists from five institutions with an average of 21 year's CT experience submitted images of 10 subsolid and 10 solid nodules each, to construct a database of 120 pulmonary nodules. Individual nodule selections were set as the reference standard. Twelve randomly arranged image databases were created. Each blinded radiologist read two different versions within a period of 10 days, indicating whether or not each nodule was subsolid. A correct answer was defined by the reference standard. Selections were correlated with nodule size. Inter- and intraobserver agreement was assessed using the kappa statistic (k), assuming "good" agreement lies within the kappa range of 0.61-0.8.

Results: For readings 1 and 2, 57% and 60% of pulmonary nodules were correctly identified as either subsolid or solid. There was no statistically significant correlation with nodule size ($rs=0.161$; $P=0.049$; $rs=0.250$; $P=0.005$, and $rs=0.128$; $P=0.163$; $rs=0.212$; $P=0.002$). Interobserver agreement was at the lower range of "good" for readings 1 and 2 ($k=0.619$ and $k=0.654$). Intraobserver agreement was also "good" ($k=0.793$).

Conclusion: Radiologist inter- and intraobserver agreement in the decision whether or not a pulmonary nodule is subsolid is in the lower range of "good". Nodule size is not a contributor to observer agreement.

B-0166 14:45

Which solitary ground-glass opacity pulmonary lesion necessitates invasive investigation?

R. Rozenberg, I. Kogan, M. Leiderman, A. Engel, L. Guralnik; *Haifa/IL (r_rozenberg@rambam.health.gov.il)*

Purpose: To evaluate the histological significance of solitary ground-glass opacity (GGO) in order to determine the cases in which CT-guided FNA should be the next step in evaluation.

Methods and Materials: We retrospectively reviewed 891 CT-guide FNA of pulmonary lesions as a primary diagnostic work up performed at our institution between 2007 and 2010. Our study included 56 patients that had a solitary GGO pulmonary lesion with a mean age of 66.7 years. The lesions were in the RUL in 33.9%, RML in 5.3%, RLL in 21.4%, LUL in 21.4% and LLL in 17.8% of patients. The mean diameter of the GGO lesion was 1.93 cm with a range from 0.7 to 4.7 cm. Each case was reviewed for diagnostic yield and complications.

Results: After cytological examination, malignancy was diagnosed in 73.2% of patients: in 55.4% adenocarcinoma, 8.9% NSCLC and 8.9% unspecified malignancy. A negative result was obtained in 15 patients, among them 3 cases revealed malignancy after surgical excision.

Conclusion: Most of the solitary GGO pulmonary lesions turned out to be malignant. Even though histologically most of them are slow growing adenocarcinomas, for those lesions with malignant appearance, surgical excision should follow the CT diagnostic. We recommend CT-guided FNA in cases of equivocal GGO lesions or in patients that are not able to undergo a surgical procedure and a diagnosis is mandatory for further treatment.

B-0167 14:54

Computer-aided detection of ground glass nodules in lung cancer screening: retrospective evaluation of potential benefit

C. Jacobs¹, E.T. Scholten², S.C. Saur¹, T. Twellmann¹, P.A. de Jong³, B. van Ginneken⁴; ¹Bremen/DE, ²Haarlem/NL, ³Utrecht/NL, ⁴Nijmegen/NL (*colin.jacobs@mevis.fraunhofer.de*)

Purpose: Ground glass nodules (GGNs) have a high probability of being malignant. We retrospectively investigated the usefulness of a dedicated computer-aided detection (CAD) system for GGNs in a clinical screening setting.

Methods and Materials: A set of 620 low-dose chest CT scans (16x0.75 mm, 120-140 kVp, 30 mAs) were randomly selected from a lung cancer screening trial. All scans were processed with a research prototype CAD system for GGNs (Diagnostic Image Analysis Group, Nijmegen, The Netherlands, Fraunhofer MEVIS, Bremen, Germany). Two chest radiologists inspected all CAD marks and classified them as GGN, other lesion, or false positive. Findings were compared with the annotations recorded in the screening trial database, which were obtained without the support of CAD.

Results: GGN CAD found 386 marks (0.62 per scan). Radiologist 1 classified 22 marks as GGN, 222 as other lesions and 142 as false positives. For radiologist 2 these numbers were 39, 107, and 240, respectively. Fifteen findings were considered to be GGNs by both radiologists. Of these 15, only 3 had been annotated in the screening trial. CAD marks that were classified by the radiologists as other lesions involved mainly scars and areas of inflammation. A common source of CAD false positives were hazy opacities caused by cardiac motion.

Conclusion: At less than 0.7 false positives per scan, the CAD system can substantially increase the number of GGNs identified in a lung cancer screening trial at a false positive rate that does not impose a burden on the reading process.

B-0168 15:03

New gold-standard for designing a CXR CAD algorithm for lung nodules and assessing its performance

D. Shaham, I. Leichter, A. Manevitch, N. Bogot, R. Lederman; *Jerusalem/IL (dshaham@hadassah.org.il)*

Purpose: Currently, readers are reluctant to accept low-conspicuity lung nodules detected by CAD on chest-radiographs, even when they are CT-confirmed. This study describes a new CAD algorithm designed to detect lung nodules considered reportable by expert radiologists.

Methods and Materials: The new prototype CXR CAD algorithm (Siemens) was trained on 815 digital frontal chest-radiographs from 5 vendors, culled from 13 sites, and reviewed retrospectively by 4 independent expert radiologists. To establish the new gold standard, a nodule reported by at least 2 readers was considered reportable. 195 such nodules (5-30 mm) were found. The performance of CAD using the new gold standard was tested on a different set 6043 chest-radiographs, reviewed for nodules by 6-8 independent readers. CAD sensitivity was evaluated

by the percentage of readers who concurred. CAD marks for findings reported by fewer than 2 readers were considered false.

Results: On the 6043 chest-radiographs, 649 nodules were considered reportable. CAD sensitivity for nodules with 80-100% concurrence was 71.4%, and it decreased to 52.1%, 43.4% and 27.6%, with 60-79%, 40-59% and 20-39% concurrence, respectively. The readers' percentage concurrence and CAD sensitivity were highly correlated (R=0.99). The CAD false mark rate was 0.80, while the readers' false mark rate ranged from 0.02 to 0.34 (mean of 0.11).

Conclusion: CXR CAD designed to mimic the performance of experts rather than to detect CT-confirmed nodules, should improve the usefulness of CAD in the clinical setting as it will increase the willingness of general radiologists to accept the CAD prompts on chest-radiographs.

B-0169 15:12

Computer-aided lung nodule volumetry: can MDCT be replaced by highfield MRI at 3 T?

M. Regier¹, S. Kandel², H. Bolte³, B. Hoffmann³, G. Adam¹, J. Biederer¹; ¹Hamburg/DE, ²Berlin/DE, ³Kiel/DE (*mregier@uke.de*)

Purpose: To determine the accuracy of computer-aided volumetry of artificial pulmonary nodules in highfield MRI at 3 T in an intraindividual comparison to MDCT.

Methods and Materials: By injecting 0.25-2 ml of an agarose solution 72 nodules of diameters ranging 4-16 mm were implemented into 10 porcine lungs within a dedicated chest phantom. Signal on T1-weighted images and radiopacity were adjusted by adding 0.125 mmol/l Gd-DTPA and 1.5 g/l of iodine. A T1-weighted three-dimensional gradient echo sequence (T1-3D-GRE; TR/TE 3.3/1.1 ms, slice 4 mm, FOV 375 mm, matrix 256x205, Flip-angle 10°) was applied in axial orientation, followed by MDCT (16x0.5 mm; reconstructed slice thickness 1 mm; increment 0.5 mm) which served as the reference. Computer-aided volumetry was performed using a commercially available software tool (Oncotreat, MeVis, Germany). After the experiments all specimens were harvested and true lesion size and shape were assessed for all nodules. Statistics included comparison of mean values and logistic regression analysis.

Results: Compared to the MDCT data, using MRI mean lesion volume was over-estimated by 28%. Consequently, the slope of the regression line was 0.85 for the MRI data and was subordinate to the identity line.

Conclusion: Due to the lower spatial resolution the accuracy of computer-aided volumetry was lower for the MRI-based datasets than for MDCT data. Nevertheless, a variance in volume assessment of < 30% implies that MRI can sufficiently be used to monitor the volume of small pulmonary nodules and to detect doubling of nodule volume, indicating malignancy.

B-0170 15:21

Positron emission tomography and lung nodules: prognostic value of standard uptake value

A. Bazzocchi, S. Brocchi, F. Ponti, V. Ambrosini, G. Facchini, S. Fanti; *Bologna/IT (stefano.brocchi@gmail.com)*

Purpose: Our aim was to investigate the prognostic value of standardised uptake value (SUV) in patients submitted to positron emission tomography (PET) for solitary lung nodule.

Methods and Materials: We retrospectively analysed the clinical history of 75 patients (44 males, 31 females, 70.3±11.2-year old) who underwent PET/CT for lung nodules, in a single-centre experience. The analysis included evaluation of images and physicians' reports of PET/CT exams, anamnesis of patients and subsequent diagnostic examinations in their follow-up (imaging, biopsy specimen and/or pathological analysis after surgical resection). Follow-up of all patients ended with survival control in September 2011. Receiver operating characteristic curves and Kaplan-Meier method were used.

Results: Mean follow-up was 26.1±19.3 months. Three out of 75 (4%) patients were affected by lung metastases and were excluded from further analysis. In 33/75 (44.0%) subjects a non-small cell lung cancer was diagnosed (20/33 adenocarcinomas and 13/33 squamous carcinomas); 17/33 (51.5%) patients underwent surgery. In all other patients (42/75-56%) lesions were classified as non-oncologic diseases or benign. The best combination to properly characterise the neoplastic nature of nodules found a SUVmax cut-off value of 3.1, resulting in 87.9% and 74.4%, sensitivity and specificity, respectively. Nodules with higher SUVmax value (> 3.1) were associated with lower survival rate (p=0.05), independently from surgical/non-surgical approach. For SUV > 3.1 and < 3.1 the survival rates 1 year after PET imaging were 74.2% and 90.9%, while survival expectancies after 2 years were 54.5% and 78.1%, respectively.

Conclusion: In conclusion, prognostic value of SUVmax value was proved; a cut-off value of 3.1 seems to offer good reliability and accuracy.

14:00 - 15:30

Room D2

Interventional Radiology

SS 209

Ablation

Moderators:

R.F. Dondelinger; Liège/BE

D. Filippiadis; Athens/GR

B-0171 14:00

CT: morphological change of aldosterone-producing adenoma after radiofrequency ablation

K.L. Lee, Y.S. Liu, S.C. Tong, E.K. Ng, A.T. Ahuja; Hong Kong/HK
(leekalok²⁰⁰⁹@yahoo.com.hk)

Purpose: To evaluate the morphological changes of aldosterone-producing adenoma (APA) on computed-tomography scan before and after radiofrequency ablation (RFA) and to identify factors that are important in determining successful complete ablation of these tumors.

Methods and Materials: Between August 2004 and August 2008, 24 consecutive patients with APA undergoing CT-guided percutaneous RFA were identified from our prospective database. The pre-RFA and post-RFA CT appearances of these APA were retrospectively reviewed for their three-dimensional size, tumor volume, and Hounsfield units (HU). Comparison of these parameters before and after RFA was performed.

Results: In this study, there were 23 APA that showed biochemical cure of primary aldosteronism after RFA. Comparing post-RFA to pre-RFA CT scans, there was no significant change in tumor size (anterior-posterior dimension: 11.7 mm versus 11.9 mm, $P=0.97$; medial-lateral dimension: 16.2 mm versus 16.5 mm, $P=0.97$; cranial-caudal dimension: 15.6 mm versus 15.5 mm, $P=0.56$) and tumour volume (1.27 cm³ versus 1.31 cm³, $P=0.41$) after RFA. In non-enhanced CT images, there was no significant reduction in HU from pre-RFA to post-RFA measurements (4.4 versus 7.9, $P=0.52$). In contrast-enhanced CT scans, there was a significant drop in HU after RFA (from 48.3 to 14.7, $P=0.03$). None of the included cases showed focal region of contrast enhancement to suggest residual tumour.

Conclusion: Change in tumour size, tumour volume and HU in non-enhanced CT were unreliable in defining radiological treatment success. Only change in HU in contrast-enhanced CT scan was useful in confirming positive treatment response after RFA for APA.

B-0172 14:09

Radiofrequency ablation of hepatic metastases after curative resection of extrahepatic cholangiocarcinoma

S.-Y. Park, J. Kim, H. Won, Y. Shin, P. Kim; Seoul/KR (sunypark⁸³@naver.com)

Purpose: To retrospectively evaluate local control and survival after radiofrequency ablation (RFA) in patients with liver metastases arising from extrahepatic cholangiocarcinoma (ECC) who had previously undergone curative resection.

Methods and Materials: From May 2003 to May 2009, RFA using an internally cooled electrode was performed on 29 metachronous liver metastases (1.6 tumour per patient) arising from ECC in 18 patients (mean age, 66 years). Tumour size ranged from 0.9 cm to 4.6 cm in maximum dimension (mean, 2.3 cm). As historical comparisons, we included 24 patients diagnosed with recurrent metastasis limited to the liver between February 1997 and April 2003 and who met the inclusion criteria for RFA: 16 patients received supportive therapy only, while 8 patients underwent chemoradiotherapy.

Results: Five patients had major complications (four with liver abscess and one with biliary stricture, 17% per treatment), but there were no procedure-related deaths. Complete tumour necrosis was achieved in all 29 tumours after one session of RFA. The local tumour progression rate was 38% (median time to detection, 5 months). From the first diagnosis of liver metastasis, the median overall survival was 12.4 months and the 3-year survival rate was 10%. Patient survival was significantly longer in patients who received RFA than in those who received chemoradiotherapy (median survival 5.6 months) or supportive treatment (median survival: 5.3 months) ($P < 0.001$).

Conclusion: Percutaneous RFA results in effective local tumour control and may prolong survival in patients with recurrent hepatic metastases after curative resection for ECC.

B-0173 14:18

Contrast-enhanced ultrasound (CEUS) improves real-time imaging of ablation region during radiofrequency ablation (RFA): preliminary results

P. Wiggemann, E.-M. Jung, C. Stroszczyński;
Regensburg/DE (philippwiggemann@googlemail.com)

Purpose: To assess the added value of depicting tumour microvascularisation, using contrast-enhanced ultrasound (CEUS), during RFA, as a means of achieving a complete ablation (CA) of malignant liver lesions.

Methods and Materials: 18 consecutive patients (2 females, 16 males, age range 52-79 years, mean 64.1 ± 9.9 years) with 22 histologically confirmed hepatic malignancies (HCC: n = 10, liver metastases: n = 12) underwent RFA. Before RFA, conventional US, CEUS and contrast-enhanced CT (ceCT) of the liver were performed. During the CT-guided RFA procedure, CEUS was performed to assess the ablation defect. In case of partial ablation a subsequent ablation was performed with a corrected electrode position and evaluated again using CEUS. This procedure was repeated until a CA was achieved. The number of ablations per patient was recorded. Secondary efficacy parameters assessed were lesion detectability in the different imaging modalities and contrast phases.

Results: Overall intraprocedural CEUS led to a change in therapeutic management in 59% of cases, resulting in 17 additional ablations. Lesion detectability during CT-fluoroscopy was the sole statistical significant predictor of incomplete ablations ($p=0.008$). The mean number of ablations for detectable lesions was 1.27 vs. 2.27 ablations for not detectable lesions ($p=0.002$). The combined CT and CEUS RFA procedure led to a CA for all treated lesions in follow-up 3-month post-intervention.

Conclusion: CEUS does allow a reliable, immediate assessment of therapeutic efficacy of percutaneous RFA procedures of malignant liver lesions.

B-0174 14:27

Percutaneous US-guided interstitial laser ablation of metastatic lymph nodes in the neck from papillary thyroid carcinoma following thyroidectomy and lymphadenectomy

G. Mauri¹, L. Cova², T. Ierace², T. Tondolo¹, G. Lomuscio², A. Baroli², L. Solbiati²;
¹Milan/IT, ²Busto Arsizio/IT (gio.mauri@tiscali.it)

Purpose: We report our experience with percutaneous US-guided interstitial laser ablation for metachronous cervical nodal metastases from papillary thyroid carcinoma following total thyroidectomy and central + laterocervical lymph node.

Methods and Materials: Twenty-three metachronous metastatic nodes (mean size 1.2 cm; range 0.6-2.6 cm) in 19 patients were treated. A 1,064 nm Nd:YAG laser (EchoLaser X4, Esaote, Genoa, Italy) was used. All cases were negative at 131I whole body scan, but had positive 18 F-FDG PET and elevated serum levels of thyroglobulin. Under local anaesthesia a 300-µm quartz fiberoptic guide was placed into the node through a 21G needle. Nodes were treated with one (17 cases) or two (6) fiber insertions, each one with 3 W power for 400-600 sec (total energy 1,200-1,800 joules). All cases were followed at 3 and 6 months with B-mode US, CEUS, 18 F-FDG PET and assessment of serum levels of Tg.

Results: Laser ablation was technically feasible and well tolerated in all patients, with either immediate or late complications. In 21/23 (91.3%) nodes complete ablation (lack of enhancement at CEUS, negative 18 F-FDG PET with normalisation of SUV and > 90% decrease of Tg serum levels) was achieved. In 2 cases residual uptake at 18 F-FDG PET with abnormal SUV was found and laser ablation was repeated.

Conclusion: Percutaneous US-guided interstitial laser ablation seems to be an effective, low cost and safe therapeutic tool for the treatment of metachronous nodal metastases from papillary thyroid carcinoma in the neck which would otherwise require often challenging further resections.

B-0175 14:36

The crucial role of fiducial markers on assessment of ablative margin

M. Trakymas, A. Ulys; Vilnius/LT (mantas.trakymas@vuoi.lt)

Purpose: To assess the benefit of implanted fiducial markers on exact detection of ablative margin and on local tumour progression rate.

Methods and Materials: Each of 50 metastatic liver tumours (8-71 mm, median 21.5 mm) was marked with three titanium fiducials before radiofrequency ablation. Fiducials were implanted near the tumour under ultrasound guidance. The three phase contrast-enhanced MDCT scan was performed for each patient after the implantation of fiducials. All the tumours were treated by US-guided RFA using perfused and multipolar internally cooled electrodes. The control contrast-enhanced MDCT scan was performed next day after ablation. The evaluation of ablative margin was made by fusing CT scans according to each fiducial.

Thursday



Results: RFA was technically successful in all cases. The detected minimal ablative margin ranged from 0 to > 10 mm and the accurate detection of ablative margin was possible for all the tumours. In four cases the repeated ablation was performed since the ablation margin was less than 5 mm and a larger ablation of particular region was feasible. On follow-up (3-18 months, median 11 months) only one local tumour progression was detected. In this case the ablative margin was 0 mm and the reablation was not feasible due to the proximity of the tumour to a large portal vein.

Conclusion: The use of fiducial markers for ablation treatment gives us new possibilities for radical treatment options, enables direct assessment of ablative margin and raises the ablation to a higher qualitative level.

B-0176 14:45

The significance of persistent intra-lesional enhancement of renal tumours following percutaneous cryoablation

B. Shepherd, P. Kumar, T.J.C. Bryant, D.J. Breen; *Southampton/UK* (*beth_shep@hotmail.com*)

Purpose: We evaluated the occurrence of 'thread-like' intra-tumoral enhancement on initial cross-sectional imaging in renal tumours treated by percutaneous cryoablation.

Methods and Materials: We performed a retrospective review of the post-procedural imaging of all solid renal tumours treated with percutaneous cryoablation from May 2007 to June 2011. We recorded all patients with intra-tumoral enhancement seen on the initial CT or MR performed within 2 weeks.

Results: 139 tumours in 118 patients were identified, out of the 139 tumours 15 (10.8%) showed initial 'thread-like' intra-tumoural enhancement. Of these 15 tumours none had evidence of residual or recurrent disease at a mean radiological follow-up of 13.9 months. Of the 15 tumours, 11 were confirmed renal cell carcinoma, 2 oncocytomas and 2 were indeterminate. This was proportional with the pathological distribution of the larger cohort.

Conclusion: A small but significant minority of solid renal cell tumours demonstrate, seemingly benign, intra-lesional 'thread-like' enhancement post-cryoablation. It is important to be aware of this phenomenon as to avoid the sequelae of misreporting this as residual disease.

B-0177 14:54

Microwave ablation (MWA) versus radiofrequency ablation (RFA) for small liver malignancies: rates of technical success

G. Mauri, T. Tondolo, L. Cova, T. Ierace, L. Solbiati; *Busto Arsizio/IT* (*vanni.mauri@gmail.com*)

Purpose: To compare primary technical success of MWA and RFA for the treatment of small liver tumours.

Methods and Materials: 388 liver malignancies (234 HCCs and 154 metastases) smaller than 2.5 cm in 240 patients undergone US-guided thermal ablation with MWA (n=162) or RFA (n=226) between January 2008 and June 2011 were retrospectively evaluated. A single needle insertion was preoperative planned. Primary technical success (complete coverage of the tumour after one ablation) achieved in the MWA group and in the RFA group was distinctly assessed by intraoperative contrast-enhanced US (CEUS). Further ablations were performed during the same session when CEUS showed residual lesion enhancement, until achievement of complete lack of enhancement. 24-hour CT or MRI were performed to assess the final technical success.

Results: Primary technical success was achieved in 134/162 (82.7%) tumours in the MWA group and in 153/226 (67.7%) in the RFA group (p=0.001), in 77/86 (89.5%) HCCs in the MWA group and 105/148 HCCs (70.9%) in the RFA group (p=0.001), in 57/76 metastases (75%) in the MWA group and in 48/78 metastases (61.5%) in the RFA group (p=0.084). Complete ablation at 24 hours was achieved in 376/388 tumours (96.9%): 158/162 (97.5%) tumours in the MWA group and 218/226 (96.4%) in the RFA group (p=0.767).

Conclusion: MWA provides a significantly higher primary technical success than RFA in liver tumours smaller than 2.5 cm, and particularly in HCCs. After multiple ablations technical effectiveness is similar between MWA and RFA. MWA should be considered the first choice treatment for small HCCs.

B-0178 15:03

Renal radiofrequency ablation (RFA): effect of primary thermal ablation on the medium-term survival

C. Migliorisi, F. Barbosa, C. Ticca, M. Nichelatti, D. Mazzone, R. Vercelli, M. Solcia, A. Rampoldi, G. Cornalba; *Milan/IT* (*carmelo.migliorisi@ospedaleniguarda.it*)

Purpose: To assess the effect of primary thermal ablation (complete or incomplete) on the survival. Prevalence of synchronous, metachronous lesions, relapse, metastasis, local tumour progression as well complication rates were reported.

Methods and Materials: Fifty-two patients (92 renal lesions) underwent RFA were retrospectively selected. The average follow-up time was 21.43 months (1-77months). Mean age was 71.52 years (33-90 years), 34 males/18 females. The mean tumour size of SRMs was 23.89 mm (8-52 mm). RFA were carried out under ultrasound or CT guidance. Chi-squared test, Fisher's exact test, Kaplan-Meier and Cox semiparametric regression were used.

Results: RFA was successfully performed in 88/92 (95.6%) of lesions (74 SRMs, 10 residual lesions and 4 relapse disease). Complete primary thermal ablation (PTA) of SRMs was 62%, 90% of residual lesions and 75% of relapse disease. Complications were observed in 13/88 (14%) of treated lesions: minimum ground blood (6/13), haematoma (4/13), haematoma and infection (2/13) and liver damage (1/13); non-relation between procedure complications and primary thermal ablation was observed. Synchronous lesions were present in 8/52 patients (15.38%). During follow-up, 5/52 (9%) patients developed metachronous lesions and 4/52 (7%) relapse, 10/52 (19%) presented metastatic disease, of these 7/10 (70%) already had metastasis before treatment. Local tumour progression were present in 4/52 (7.69%) patients of these 2/4 (50%) died.

Conclusion: RFA provide an feasible, safety and effective minimally invasive treatment of renal lesions in selected patients, with low rate of recurrence.

B-0179 15:12

Percutaneous microwave ablation (MWA) with a high energy antennae system of pulmonary malignancies: technical success, safety and imaging follow-up

D.Y.F. Chung, M. Little, P. Boardman, F.V. Gleeson, E.M. Anderson; *Oxford/UK*

Purpose: Evaluation of the technical success, safety and imaging follow-up of malignant pulmonary nodules treated with high energy percutaneous MWA.

Methods and Materials: From July 2010 to September 2011, 20 patients (11 females, mean age 68) with 26 pulmonary malignancies of median diameter 21 mm (range 8-57 mm) were treated with percutaneous MWA under CT guidance. A 16G microwave needle antenna (Microsulis, Portsmouth, UK) was used with power up to 180 W. Technical success of ablation was defined as > 5 mm ground glass or solid opacification margin around the ablated lesion at contrast-enhanced CT day 1 post-procedure. Local tumour recurrence was assessed at 1, 3 and 6 months post-ablation. Measurements and assessment of local tumour recurrence were undertaken by the radiologist performing the procedure and a second radiologist, not involved in the patient's care. Complications were recorded at the time of procedure and at follow-up.

Results: Median ablation time was 3 min (range 1.5-8 min). The procedure was technically successful in 23 (88%) lesions. 10 (53%) patients developed pneumothorax during the procedure, of which 3 required a chest drain. 83% of patients were discharged 1 day post-procedure. No patients died as a direct result of the procedure. At 3-month follow-up, local recurrence was identified in 2 patients.

Conclusion: MWA using a novel high power antenna of lung lesions is a safe, successful technique that allows shorter ablation times compared to radiofrequency ablation (RFA). The complication rates are comparable to RFA.

B-0180 15:21

Local control of focal hepatic malignancies treated with microwave ablation with a high-power applicator system in 151 patients

G. Mauri¹, L. Cova¹, T. Ierace¹, T. Tondolo¹, S.N. Goldberg², L. Solbiati¹; ¹Busto Arsizio/IT, ²Jerusalem/IL (*vanni.mauri@gmail.com*)

Purpose: To assess the efficacy and safety of microwave ablation for the treatment of hepatic malignancies using a high-power applicator system.

Methods and Materials: Over a 22-month period, 241 hepatic malignancies (135 HCC, 1 cholangiocarcinoma and 105 metastases) in 148 patients were percutaneously treated under US guidance using a high-power (140 Watt, 2.45 GHz) microwave system (AMICA-Probe: Hospital Service, Aprilia, Italy). One (n=207) or two (n=34) antenna insertions were performed. Power and time of application ranged from 45 to 100 Watt and from 4 to 15 min, respectively. Imaging (either contrast-enhanced MDCT or MRI) at 3-6-9-12 months was used for post-ablation

follow-up. Results were assessed after a minimum 6-month follow-up for a total of 124 malignancies (76 HCCs and 48 metastases, size range 0.5-5.5 cm, mean 2.2) in 74 patients.

Results: Immediate complete ablation was achieved in 111/124 malignancies (89.5%); 67/76 (88.1%) of HCCs and 44/48 metastases (91.7%). Local tumour progression occurred in 13/124 malignancies (10.5%); 3/57 (5.3%) with sizes ≤ 1.9 cm, 6/46 (13%) for tumours ranging 2.0-2.9 cm; and 4/21 (19%) for tumours > 3 cm. All local progression was successfully re-treated within 4 months using the same method. Minor complications occurred in 21/148 (14.2%) patients. Only one delayed major complication was noted (0.8%).

Conclusion: In our series, valuable local control of hepatic malignancies without significant complications was achieved. Even lesions bigger than 3 cm were successfully treated with few antenna insertions and in a short time.

14:00 - 15:30

Room E1

Musculoskeletal

SS 210

MRI of ligaments, tendons and muscles

Moderators:

M. Reijnierse; Leiden/NL
V. Zubler; Zurich/CH

B-0181 14:00



The use of diffusion-weighted and dynamic contrast-enhanced MRI for quantitative evaluation of the tibial tunnel after anterior cruciate ligament reconstruction with intraoperatively administered platelet-rich plasma gel

M. Ruprecht¹, M. Vogrin¹, M. Jevsek¹, I. Sersa², V. Jevtić²; ¹Maribor/SI, ²Ljubljana/SI (mitja.ruprecht@quest.arnes.si)

Purpose: To quantitatively evaluate the effect of platelet-rich plasma gel (PRPG), locally administered during the anterior cruciate ligament (ACL) reconstruction. The proximal tibial tunnel was assessed with diffusion-weighted imaging (DWI) and with dynamic contrast-enhanced imaging (DCEI).

Methods and Materials: In fifty patients, arthroscopic ACL reconstructions were performed. The patients in the PRPG group (n=25) received a local application of PRPG into the bone tunnels and into the graft itself. DWI and DCEI were utilised to examine the proximal tibial tunnel with subsequent calculation of apparent diffusion coefficient (ADC) values, as well as the contrast enhancement gradient (Genh) and enhancement factor (Fenh) values.

Results: At one month, the ADC value in the PRPG group (1.41 (10-3 mm²/s)) was significantly lower than in the control (1.50 (10-3 mm²/s)) group (p=0.033). At two and a half and at six months, the differences in the ADC values were not significant. At the first and second control, Genh was significantly higher in the PRPG (2.07 %/s and 1.64 %/s) than in the control (1.41%/s and 1.15%/s) group (p=0.019 and 0.008). At six months, there was no significant difference in Genh values. There were no significant differences in Fenh between the groups at any control examination.

Conclusion: DWI and DCEI measurements indicate a reduced extent of oedema during the first postoperative month as well as an increased vascular density and microvessel permeability in the proximal tibial tunnel at one and two and a half postoperative months as the effect of the application of PRPG.

B-0182 14:09

Dedicated 0.31 T MR vs. whole body 1.5 T MR in the diagnosis of meniscal lesions with arthroscopic correlation

D. Caramella, A. Paolicchi, F. Ruschi, S. Vitali, I. Castellini, P. Parchi, M. Lisanti; Pisa/IT (davide.caramella@med.unipi.it)

Purpose: To compare the diagnostic accuracy of a dedicated MR system (0.31 T) and a high-field whole body MR scanner (1.5 T) in the study of menisci.

Methods and Materials: Thirty-seven patients underwent two subsequent MR examinations with the dedicated MR system and the high-field traditional scanner. Inclusion criteria were: age between 18 and 60 years, clinical suspicion of meniscal lesion, no history of surgery on the affected knee. Sequences used were sagittal SE T1, FSE PD, STIR, in both scanners. On the coronal plane X BONE was used at 0.31 T and GE T2 fat sat at 1.5 T. Thirty-one patients (with positive MRI) underwent arthroscopy, while 6 (with negative MRI) were followed up clinically. Two expert radiologists performed a double-blind reading with arthroscopy as the gold standard. For each meniscus anterior and posterior horns were considered, with the

following scores: 0, absence of lesion; 1, uncertain interpretation; 2a, degenerative lesion; 2b, complete fracture and/or parameniscal cyst and/or bucket handle lesion. **Results:** Reader A: sensitivity and specificity: 84% - 92.5% (0.31 T), 84% - 97.5% (1.5 T); diagnostic accuracy: 89.5%, 92.7%, respectively. Reader B: sensitivity and specificity: 79.5% - 96.2% (0.31 T), 81.8% - 95% (1.5 T); diagnostic accuracy: 90.3% for both systems.

Conclusion: The two MR systems have similar diagnostic accuracy in detecting and classifying meniscal lesions, thus suggesting that a less expensive dedicated MR can be employed in this diagnostic domain, avoiding the inconvenience for the patient to be scanned in a whole body system.

B-0183 14:18

Sodium (23Na) MRI of Achilles tendon disease at 7 Tesla: preliminary results

V. Juras, C. Pressl, S. Zbyn, S. Apprich, P. Szomolanyi, J. Wimmer, S. Domayer, S. Trattng; Vienna/AT (vladimir.juras@meduniwien.ac.at)

Purpose: It has been reported that the glycosaminoglycan (GAG) content increases in chronic Achillotendinopathy compared to healthy Achilles tendon (AT). The aim of this study was to utilise sodium MRI at 7 Tesla to visualise and quantify biochemical composition changes within the tendon between healthy tendon and chronic Achillotendinopathy.

Methods and Materials: Twenty healthy subjects and eight patients with chronic Achillotendinopathy diagnosed on standard MRI at 3 T were included in the study. All sodium MR measurements were performed on a 7T whole body MR system using a circularly polarised 23Na transmit/receive knee coil. 3D-GRE sequence optimised for sodium imaging was used with the following parameters: TE=7.71 ms, TR=17 ms, averages=13, matrix=128x128, flip angle=30°, FOV=180x180 and slice thickness=3 mm. Signal-to-noise ratios were calculated for three different regions of segmented Achilles tendon (insertion, middle portion and tendon-muscle junction). The difference of sodium signal-to-noise ratio between healthy subjects and patients was calculated using two-sample unequal-variance T-Test.

Results: Mean bulk SNR of AT in healthy subjects was 4.94±2.14 and in patients 9.31±2.26. In respective regions (healthy->patient), the following mean SNR values were observed: (6.31±2.83 -> 12.27±4.52) in insertion, (4.81±2.24 -> 9.37±3.0) in middle portion and (3.69±1.62 -> 6.30±2.21) in tendon-muscle junction. Statistically significant differences of sodium SNR were observed in insertion (p=0.006), middle portion (p=0.0028) and tendon-muscle interface (p=0.0101).

Conclusion: The results of the study clearly demonstrated the ability of sodium MR imaging to detect and quantify changes in chronic Achilles tendinopathy. Those findings could lead to new approaches concerning early onset diagnosis and individualised treatment monitoring.

B-0184 14:27

Ankle cartilage: correlation between T2 value and ligament injury

S. Lee, Y. Yoon; Seoul/KR (odc42@gmail.com)

Purpose: To evaluate differences in T2 values in ankle cartilage at magnetic resonance (MR) imaging in patients with injury of anterior talofibular ligament (ATFL) compared with healthy subjects.

Methods and Materials: Ankle cartilage was evaluated in 51 subjects with ankle pain who were categorised as having normal ATFL (n = 23, mean age 39), partial tear (PT) (n = 21, mean age 39.7), or complete tear (CT) of ATFL (n = 8, mean age 34) using multiecho spin-echo T2-weighted sequences. Trochlear cartilage regions of the talus were divided into six compartments (anteromedial, medial centre, posteromedial, anterolateral, lateral centre, and posterolateral). Mean value of compartmental region of interest T2 measurements was obtained in three groups. Statistical analysis of variance was performed.

Results: Mean value of compartmental T2 values showed significant difference between normal, PT, and CT (P=0.0001). T2 relaxation time between three ligament groups was significantly different in the compartment of anteromedial, medial centre, anterolateral, and lateral centre cartilage (P=0.003, 0.042, 0.001, 0.001, respectively). No significant difference was found between normal and ATFL injury groups in posteromedial and posterolateral compartment. CT group had higher T2 values compared with normal in anteromedial, medial centre, anterolateral, and lateral centre. PT group had higher T2 values compared with normal in anteromedial and anterolateral compartment.

Conclusion: ATFL injury is associated with an increase in T2 value of the articular cartilage of the trochlea of the talus in ankle especially in anterior and posterior compartment.

B-0185 14:36

Rhabdomyolysis revisited: magnetic resonance (MR) imaging finding in detail

S. Cho¹, Y. Kim¹, S. Cho¹, K.-H. Lee¹, B. Kim¹, R. Kim¹, S. Cho², S. Koh², M.-K. Lim¹; ¹Incheon/KR, ²Anyang/KR (josungehn@naver.com)

Purpose: To retrospectively evaluate magnetic resonance (MR) imaging finding of rhabdomyolysis in detail.

Methods and Materials: Eighteen patients (14 males and 4 women age range, 24 - 88 years; mean age, 49.4 years) were included in this study. Signal intensity on T1- and T2-weighted images, presence of intramuscular haemorrhage, presence of stipple sign, presence of non-enhancing portion in muscle, increased volume of muscle, abnormal signal intensity in subcutaneous fat layer and deep fascia are evaluated.

Results: On T1-weighted image, 11 patients (11/18, 61.1%) showed homogeneous iso signal intensity and 7 (11/18, 38.9%) patients showed heterogeneous mixed high and iso signal intensity. On T2-weighted image, 9 (9/18, 50%) patients showed heterogeneous signal intensity combined high and low signal intensity. Ten patients (10/18, 55.6%) had T1 high or T2 dark signal intensity in muscle representing haemorrhage. Twelve patients (12/18, 66.7%) had stippled sign. Seven patients (7/18, 38.9%) had focal or diffuse non-enhancing portion in involved muscle. Fifteen patients (15/18, 83.3%) showed increased volume of muscle. Nine patients (9/18, 50%) had T2 high signal intensity oedema in subcutaneous fat layer. T2 high signal intensity in facial plane is seen in 11 patients (11/18, 61.1%).

Conclusion: Increased volume of muscle is most common imaging finding in rhabdomyolysis on MRI. Other common imaging findings were stippled sign, T2 high signal intensity in facial plane, intramuscular haemorrhage, T2 high signal intensity oedema in subcutaneous fat layer, and focal or diffuse non-enhancing portion in involved muscle.

B-0186 14:45

Magnetic resonance quantitative monitoring of muscle healing through diffusion tensor imaging (DTI) and T2-mapping assessment

A. Esposito, F. De Cobelli, A. Palmisano, T. Canu, L. Campana, G. Pezzetti, A. Manfredi, P. Rovere-Querini, A. Del Maschio; *Milan/IT* (esposito.antonio@hsr.it)

Purpose: To prospectively evaluate a multiparametric MRI protocol as a non-invasive and quantitative tool for monitoring muscle damage/healing process, obtaining dynamic information about inflammatory infiltrate and fibres regeneration.

Methods and Materials: Acute muscle injury was obtained by cardiotoxin (CTX) injection into tibialis-anterior (TA) of C57BL/6 mice. An MRI study including T2-mapping, diffusion-weighted imaging and diffusion-tensor imaging (DTI) was performed before and at 1, 3, 5, 7, 10, 15 and 30 days after injury. At each time-point 3 animals underwent MRI and were sacrificed immediately after imaging to obtain tissue's samples for histological analysis.

Results: T2 relaxation time (T2_{rt}) significantly increased after injury reaching the top at 3 days; subsequently T2_{rt} progressively decrease from 3rd to 30th day, recovering a complete normalisation. A general increase of muscle diffusivity, associated with an important loss of fractional anisotropy (FA), was observed 24 hours after injury. Afterward, FA progressively increased from day 1 to day 5, up to values above the normal level. From day 5 forward FA showed a very slow progressive decrease towards basal level. Pearson test revealed good correlations of T2_{rt} with histological damage score (r=0.89; p < 0.05) and especially with number of infiltrating leucocytes (r=0.94; p < 0.005); FA correlated with the histological count of centre-nucleated regenerating fibres (r=0.89; p < 0.005).

Conclusion: MRI with T2-mapping and DTI could be considered an effective non-invasive tool to obtain panoramic monitoring of muscle damage and repairing process with quantitative readout about leucocytes infiltration and the fibres regeneration.

B-0187 14:54

Quantitative magnetic resonance imaging of the lower limb muscles in Duchenne muscular dystrophy: a new approach for monitoring the disease progression and response to therapy

C. Godi, S. Gerevini, S. Napolitano, F. Ciceri, G. Cossu, Y. Torrente, G. Scotti, L.S. Politi; *Milan/IT* (claudia.godi@collegiodymiano.it)

Purpose: 1) To determine through magnetic resonance imaging (MRI) the pattern of lower limb involvement in Duchenne muscular dystrophy (DMD); 2) to compare quantitative MRI parameters with functional measures in DMD patients.

Methods and Materials: Twenty-six (6- to 12-year-old) DMD patients and 4 matched healthy controls underwent 3 T MRI examinations of the lower limbs

without sedation, at baseline and after nine months. Axial and coronal SE T1, multi-echo T2, STIR, FSE T2-weighted (w) and 3D THRIVE images of the legs and thighs were acquired. After threshold segmentation on T1w images, the muscle volumes (MV) were measured and normalised to the entire limb volume. Muscle signal intensity derived from T1w images was normalised to nearby fat intensity to obtain muscular signal intensity ratios (SIRs) as markers of fatty degeneration. MVs and SIRs were compared with clinical measures and tests, including North Star Score and KinCom. Six patients underwent further MRI examinations every 6 months before being treated with intra-arterial injection of mesoangioblasts.

Results: DMD patients' MV was lower than healthy subjects. Except for sartorius and gracilis, patients' SIRs were significantly higher than controls' ones. During follow-up, patients showed significant thigh-MV decrease and leg-MV increase, while SIRs were stable or increased over time. Significant Spearman correlations between SIRs, functional measures and thigh-MVs were found. In some patients with suspected bad compliance, MRI disconfirmed the poor clinical results. Follow-up after mesoangioblast transplantation is ongoing.

Conclusion: MRI could provide reliable markers of muscle degeneration which correlate to neurological/functional performances and should be employed in clinical trials as outcome measures.

B-0188 15:03

In-vivo assessment of skeletal muscle ischaemia in diabetic rats by MR angiography, MR imaging and proton MR spectroscopy

S. Delli Pizzi, R. Madonna, A. Giammarini, G.L. Romani, R. De Caterina, A. Tartaro; *Chieti/IT* (sdellipizzi@gmail.com)



Purpose: To evaluate the feasibility of using MR techniques for in-vivo investigating a rat diabetic model of hind limb ischaemia.

Methods and Materials: Experiments was approved by our Institutional Ethics Committee for animal research. Unilateral hind limb ischaemia was induced by ligation of the femoral artery in male streptozotocin (STZ)-treated (blood glucose ≥400 mg/dL) and healthy non-diabetic control rats. Four weeks after ligation, rats underwent 2D-time-of-flight (TOF) MR angiography (MRA), T1-weighted (T1-W) and short time inversion recovery (STIR) sequences and muscle proton MR spectroscopy (1H-MRS) on both hind limbs. After MR examinations, immunoblotting and immunofluorescence analysis were performed.

Results: MRA showed a signal void due to flow discontinuation distal to the ligation of common iliac-femoral artery. MRI showed the presence of tissue swelling (p=0.028 for non-diabetic; p=0.028 for diabetic rats) and signal hyperintensity in tissue affected by occlusion. 1H-MRS showed a significant reduction of total creatine/water in occluded vs non-occluded limbs (p=0.028 for non-diabetic; p=0.018 for diabetic rats). MRI and 1H-MRS changes were more pronounced in diabetic than in non-diabetic occluded limbs (p=0.032). MR findings were confirmed using histological findings.

Conclusion: Combined MR techniques can be used to demonstrate the presence of structural and metabolic changes produced in a rat diabetic model of limb ischaemia. This MR-protocol coupled with an experimental rat model of peripheral artery occlusion may be useful for evaluating in-vivo the efficacy of novel pharmacological, as well as gene- and cell-based therapies.

B-0189 15:12

Quantitative assessment of fat infiltration in the rotator cuff muscles using MRI

L. Nardo, J. Carballido-Gamio, D. Karampinos, H. Alizai, B.C. Ma, T.M. Link, R. Krug; *San Francisco, CA/US*

Purpose: To validate the established, qualitative, Goutallier's classification (GC) of fatty infiltration (FI) within the rotator cuff (RC) muscles using a novel chemical shift-based MRI technique (IDEAL) and to establish the reproducibility of IDEAL in the assessment of FI.

Methods and Materials: 31 patients with RC tear symptoms (22 males, 9 females, aged 23-64 years) was used and 6 of these patients were scanned twice. Shoulder MR examinations were performed at 3 Tesla with an 8-channel shoulder surface coil using sagittal plan PD-FSE and IDEAL (FOV=12; ST=4 mm for both). Fat fraction maps were reconstructed online with T2* correction and a multi-peak fat spectrum. FI for each of the rotator cuff muscle was scored in the proton density-weighted images using GC. Spearman's correlation coefficient compared IDEAL fat fraction values with GC for each RC muscle; reproducibility of IDEAL technique was determined using absolute precision error in the doubled-scanned patients.

Results: Spearman's coefficient between IDEAL and GC was 0.90 (p < 0.001). Using IDEAL measurements the amount of FI ranged for Goutallier grade 0 from 0 to 5.5%, for grade 1 from 4 to 7.7%, for grade 2 from 6.3 to 12.5%, from grade 3

from 15.3 to 17.5% and for grade 4 from 18.3 to 27.3%. The precision error of the IDEAL fat fraction value ranged from 0.6% to 1.0% for each RC muscle.

Conclusion: RC qualitative clinical grading of FI using the GC and quantitative fat-fraction values derived using IDEAL were strongly associated. IDEAL permitted a quantitative and well-reproducible measurement of FI.

B-0190 15:21

Lesions of the biceps pulley: diagnostic accuracy of MR arthrography of the shoulder and evaluation of new and established diagnostic criteria

C. Schaeffeler, S. Waldt, K. Holzapfel, C. Kirchhoff, P. Jungmann, P. Wolf, E.J. Rummeny, A.B. Imhoff, K. Woertler; *Munich/DE (schaeffeler@me.com)*

Purpose: To retrospectively determine the diagnostic accuracy of magnetic resonance arthrography (MR-A) of the shoulder in the evaluation of lesions of the biceps pulley and to evaluate established and new diagnostic criteria.

Methods and Materials: MR arthrograms of 80 consecutive patients (mean age: 34.2 years; male: 53, female: 27) with arthroscopically proven either intact or torn pulley systems were assessed by three radiologists. Evaluated diagnostic criteria were: displacement of the long head of the biceps tendon (LHBT) relative to the subscapularis muscle tendon on parasagittal images (displacement sign); medial (sub-)luxation of the LHBT on transverse images; discontinuity or invisibility of the superior glenohumeral ligament (SGHL); presence of tendinopathy of the LHBT on transverse or parasagittal images; rotator cuff tears adjacent to the rotator interval. Interrater and intraobserver variability was calculated.

Results: On arthroscopy, 28/80 pulley lesions were diagnosed. MR-A showed a sensitivity of 89.3%/85.7%/82.1% (reader 1/reader 2/reader 3) and a specificity of 96.2%/98.1%/86.5%. Interobserver agreement was substantial ($\kappa=0.74$). Assessment of the SGHL showed a sensitivity of 78.6%/89.3%/78.6% and a specificity of 82.7%/78.9%/75.0%. With the displacement sign sensitivity was 85.7%/82.1%/75.0%; specificity was 96.2%/98.1%/90.4%. Tendinopathy of the LHBT on parasagittal images showed a sensitivity of 92.9%/82.1%/64.3%; specificity was 80.8%/96.2%/84.6%. Subluxation of the LHBT was insensitive (35.7%/50.0%/64.3%) but specific (100.0%/98.1%/96.2%).

Conclusion: MR-A is accurate in the evaluation of the biceps pulley. The displacement sign, invisibility or discontinuity of the SGHL, and signs of tendinopathy of the LHBT on parasagittal images are the most accurate criteria in the detection of pulley lesions.

14:00 - 15:30

Room E2

GI Tract

SS 201a

GI tract: structure and function

Moderators:

S. Jackson; *Plymouth/UK*
B. Lucey; *Galway/IE*

B-0191 14:00

Dynamic MRI defecography vs. entero-colpo-cysto-defecography in the evaluation of midline pelvic floor hernias in female pelvic floor disorders

G. Di Grezia, G. Gatta, R. Lieto, F. Iacobellis, L. Urciuoli, V. Parlato, R. Grassi, A. Rotondo; *Naples/IT (graziella.digrazia@yahoo.it)*

Purpose: The aim of this study was to compare the diagnostic efficacy of dynamic MR defecography (MR-D) with entero-colpo-cysto-defecography (ECCD) in the assessment of midline pelvic floor hernias (MPH) in female pelvic floor disorders.

Methods and Materials: From August 2004 to August 2010, 3,006 female patients who required ECCD for the evaluation of pelvic floor disorders were enrolled in this study. All the 1,160 patients with ECCD findings of MPH were asked to undergo MR-D; 1,142 accepted to undergo MR-D and constituted the object of analysis. This study was approved by the Institutional Ethical Committee. All the patients gave their written informed consent to take part in the study.

Results: Overall, the prevalence of MPH at ECCD was higher if compared with that at MR-D. Concerning the hernia content, there were significantly more enteroceles and sigmoidoceles on ECCD than on MR-D, whereas in relation to the hernia development modalities, the prevalence of elythroceles, edroceles, and Douglas' hernias at ECCD was significantly higher than that at MR-D. In spite of a 100% specificity, the sensibility of MR-D in the detection of an omentocele,

sigmoidocele, and enterocele was, respectively, 95%, 82%, and 65%, showing an inferior diagnostic capacity if compared with that of ECCD.

Conclusion: MR-D shows lower sensitivity than ECCD in the detection of MPH development. The less-invasive MR-D may have a role in a better evaluation of the entire pelvic anatomy and pelvic organ interaction especially in patients with multicompartmental defects, planned for surgery.

B-0192 14:09

Improving anorectal angle measurement reproducibility by a semi-automated method

M.A. Alkubeyyer¹, B.J. Erickson², J.G. Fletcher²; ¹Riyadh/SA, ²Rochester, MN/US (*dr.metab@gmail.com*)

Purpose: Much has been written about poor reproducibility of anorectal angle (ARA) measurement in defecography. ARA is often determined by estimating a straight line along the posterior border of the rectum and the anal canal. A semi-automated method for ARA measurement is introduced to enhance reproducibility.

Methods and Materials: 30 consecutive cases of magnetic resonance defecography with variable evacuatory disorders were recruited. After adding 150 mL of ultrasound gel to the rectum, 3 mid-sagittal images of the pelvis at rest, squeeze and strain were obtained using T2-weighted steady state free precession (SSFP) sequence. Two readers MK (fellowship-trained radiologist) and ZK (MD-PhD student) have measured ARA manually and semi-automatically in two session with one week interval. Manual measurement has been done by plotting a line through the anal axis and through the posterior aspect of the lower rectum. Semi-automatic measurement has been done by clicking along the proximal and the distal end of the anal canal and the program will automatically estimate the ARA by thresholding the lower rectum then applying a convolution filter followed by oval-fitting to the largest filtered posterior segment of the rectum.

Results: Bland-Altman analysis showed high reproducibility of ARA measurements using the semi-automated method compared to manual method with bias, standard deviation, 95% limits of agreement of 0.91, 7.86, [-14.82.16.64] and -3.11, 14.08, [-31.26.25.05], respectively.

Conclusion: A semi-automated method can decrease the inter-observer variability of ARA measurement for which future defecography comparative studies become more feasible and reproducible.

B-0193 14:18

Scattered radiation doses to operators performing fluoroscopic studies on bariatric patients

M.A. Arshad, A. Sergot, D. Blunt, L. Morris; *London/UK* (*mubarik@doctors.org.uk*)



Purpose: Fluoroscopy is frequently used for assessing post-operative complications and surveillance after bariatric surgery. In this study, the amount of scattered radiation encountered was measured.

Methods and Materials: A prospective study involving 20 post-operative bariatric surgery patients and 21 controls was undertaken. The scattered radiation was measured whilst performing upper gastrointestinal fluoroscopic studies using a badge dosimeter worn over the protective lead shielding. The body mass index (BMI), screening time and dose area product (DAP) were also measured.

Results: In the bariatric group, the mean BMI was 37.4 (31.4, 48.6) (95% CI), control group of 26.6 (22, 35.5), ($p < 0.0001$). For the bariatric group, the average screening time was 1:27 and for the control 1:17 ($p=0.62$). The DAP measured 7.56 Gy cm² (0, 23.9) in the bariatric group, control group 2.64 (0.35, 7.04) ($p=0.068$). The average deep dose scatter reading for each bariatric patient was 0.009 mSv compared with 0.006 for each control and the average surface reading dose for a bariatric patient was 0.012 compared with 0.006 for non-bariatric patients.

Conclusion: The screening times were similar due to a combination of careful collimation and using last image hold in the bariatric group. There was, however, a 1.5- to 2-time increase in the amount of scattered radiation whilst screening bariatric patients. This study highlights the increased radiation exposure to operators providing bariatric fluoroscopic services. The implications of this are discussed, with reference to the increasing volume of bariatric surgical procedures and their impact on radiology departments.

B-0195 14:27

Multiple swallowing disorders of oro-oesophageal tract and gastro-oesophageal junction: role of MR-fluoroscopy with high-speed kinetic sequences

I. Sansoni, C.L. Piccolo, F. Pitocco, R.L. Alloni, R. Del Vescovo, R. Coppola, B. Beomonte Zobel; *Rome/IT*

Purpose: To define upper and lower swallowing disorders testing the feasibility of high-speed kinetic MR sequences.

Methods and Materials: 33 patients (10 male and 23 female) with oro-oesophageal and gastro-oesophageal disorders underwent MR examination on a 1.5 Tesla scanner. We acquired BH GRE unspoiled T1-w and HASTE T2-w sequences on multiple planes in order to define the anatomic details (f.e. Nissen fundoplication position above or below diaphragmatic plane). Visualisation of oesophageal bolus transit, bolus transit-time, peristalsis, gastro-oesophageal junction patency and competency during oral administration of contrasted yogurt were evaluated.

Results: MR-fluoroscopy revealed to be a reliable tool to evaluate bolus propulsion from oesophagus to stomach. MR-fluoroscopy showed swallowing abnormalities in 31/33 patients: 3 upper motility disorder, 8 achalasia, 1 megaesophagus, 2 para-oesophageal Hjalatal Hernia, 7 gastro-oesophageal reflux (2 of those with sliding Hjalatal Hernia), 12 after Nissen-fundoplication, 1 after gastrectomy. MR findings well correlated with other different instrumental examination findings.

Conclusion: In symptomatic subjects, after Nissen fundoplication, MR-fluoroscopy can detect motility alterations, providing additional information for diagnostic work-up. Finally, MR-Fluoroscopy is a radiation-free and non-invasive tool, able to evidence swallowing disorder; it is simple, non-invasive, rapid and well-tolerated for diagnosing GE reflux or motility disorders.

B-0196 14:36

MRI sinography/fistulography is a newer and less used technique for imaging patients with sinus/fistulas when compared to conventional sinography/fistulography but more helpful and accurate without radiation

H.P. Parekh, N.U. Bahri, D.P. Vasavada; *Jamnagar/IN*

Purpose: MRI sinography/fistulography is considered a newer and less used technique for imaging patients with perianal sinus/fistulas. To evaluate sterile lignocaine jelly as a contrast agent for MRI, as a cheaper alternative to gadolinium-based contrast, for lesions where no vascular communication is probable.

Methods and Materials: 20 patients are studied to date to compare the information provided by conventional imaging versus MRI. 15 patients in whom the external opening was visible, 3% sterile lignocaine jelly was injected and MRI was done. 5 patients in whom the external opening was not visible, Heavily T2WI images were taken without injecting lignocaine. All the images studied for exact location, track, openings, both internal and external and any visceral communication. Results were analysed and compared with the findings of conventional study.

Results: In the 20 patients studied, 4 patients had the same findings on both modalities. 12 patients had additional information on MRI, inter-communicating or more tracks, 4 symptomatic patients had non-conclusive conventional study, where MRI delineated detailed pathology. Sterile lignocaine jelly provided adequate contrast along with heavily T2-weighted imaging provided diagnostic information and no adverse reactions were noted.

Conclusion: MR sinography, being a newer and advanced technique, should be applied in all symptomatic patients where the conventional imaging findings are not satisfactory. In addition, symptomatic patients without visible external opening, MRI is most useful for detection and surgical guidance. Sterile lignocaine jelly is cheaper, easily available and suitable contrast material for this study with good patient compliance.

B-0197 14:45

Sandwich sign of Borrmann type 4 gastric cancer on diffusion-weighted magnetic resonance imaging

L. Tang, X.-P. Zhang, Y.-S. Sun, Z.-Y. Li, J.-F. Ji, X.-T. Li, Y.-Q. Liu, Q. Wu; *Beijing/CN (tanglei@bjcancer.org)*

Purpose: To assess the appearance of Borrmann type 4 (BT4) gastric cancer on diffusion-weighted magnetic resonance imaging (DWI) and to investigate the potential of qualitative and quantitative DW images analysis to differentiate BT4 gastric cancer from poorly distended normal stomach wall.

Methods and Materials: DWI was performed on 23 patients with BT-4 gastric cancer and 23 healthy volunteers. The signal characteristics and correlated histopathological basis of the cancers on DWI were investigated. The contrast-to-noise ratios (CNR) of cancer were compared between DWI and T1WI/ T2WI. The

thickness and apparent diffusion coefficient (ADC) of cancer and normal stomach wall were compared.

Results: All of the gastric cancers displayed hyperintensity compared to the nearby normal gastric wall on DWI. A three-layer sandwich sign that demonstrated high signals in the inner and outer layer, and low signal in the intermediate layer was observed in 69.6% of cancers on DWI. The low signal represents the muscularis propria through the comparison with pathology, and it is postulated scattering distribution of the cancer cells in this layer causes less damage and subsequently less restriction of water movement, which causes the low signal on DWI. The mean ADC value of BT-4 gastric cancer was significantly lower than the poorly distended normal stomach wall ($1.12 \pm 0.23 \times 10^{-3} \text{ mm}^2/\text{s}$ vs. $1.93 \pm 0.22 \times 10^{-3} \text{ mm}^2/\text{s}$, $P < 0.01$).

Conclusion: DWI can highlight the signals of BT-4 gastric cancer which may present a characteristic three-layer sandwich sign, and ADC values are helpful in the discrimination of gastric cancer from poorly distended stomach wall.

B-0198 14:54

Acute mesenteric ischaemia: do different findings suggest different aetiology? 7T-MRI on a rat model

D. Berritto, F. Somma, F. Iacobellis, M. Belfiore, S. Cappabianca, A. Rotondo, R. Grassi; *Naples/IT (daniela.berritto@libero.it)*

Purpose: The signs of acute mesenteric ischaemia (AMI) vary depending on the cause and underlying pathophysiology. Magnetic resonance (MR) findings, intestinal morphodynamism and histological pattern of AMI due to various primary causes are discussed.

Methods and Materials: Twelve SpragueDawley rats were divided into three groups (n=4). Two rats of each group underwent superior mesenteric artery (SMA) (groups 1 and 3) or vein (SMV) (group 2) ligation. Externalised bowel underwent macroscopic monitoring. The remaining two rats of each group had a non-occluding loop tied around SMV or SMA and three days after surgery vessels were occluded by squeezing the tips tunnelled to the posterior cervical area. Seven Tesla MR (Bruker-Biospec-70/16-US) scans were performed. All rats of groups 1 and 2 were monitored until 8 hour; in group 3 the ligation was loosen after 1 hour and reperfusion was observed until 7 hours. The bowel was removed for histological analysis at the end of observation.

Results: In all type of AMI the mesentery is the first to react. In the arterial ischaemia it appears the contraction of bowel wall followed by hypotony and a bowel wall thinning is distinctive. In case of SMV ligation the spasm is absent due to bowel wall congestion but thickening and early chromatic change of the intestinal wall, mesenteric ulcers and thumbprinting are typical. In case of reperfusion the appearance steer the course of SMV ligation.

Conclusion: This animal model detected morpho-functional alterations of ischaemic bowel and identify the specific pattern of lesions of AMI.

B-0199 15:03

Early MRI findings of small bowel obstruction: an experimental study

F. Iacobellis, D. Berritto, F. Somma, M.P. Belfiore, S. Cappabianca, A. Rotondo, R. Grassi; *Naples/IT (francesca.iacobellis@libero.it)*

Purpose: The aim of this study is to document the early 7T micro-MRI findings of small bowel obstruction and their evolution in the time, correlating them to the anatomopathological features.

Methods and Materials: Adult Sprague Dawley rats (n=8) were divided into 2 groups: in the first (n=4), rats underwent a surgical procedure of small bowel ligation followed by 8 hrs macroscopical monitoring; in the latter (n=4), 7T micro-MR scannings were performed before and after ligation. In both cases, injured bowel was processed for histological analysis.

Results: Pathological findings got evident already 30 min after small bowel ligation, when a spastic reflex ileus and a chromatic change of the injured bowel were found. 7T micro-MR imaging gave early evidence (15 min) of bowel wall hyperintensity and mural thickness associated with little amount of peritoneal free fluid. These findings got worsen and worsen till the end of the monitoring period when an increase of hyperintensity, bowel wall thickness, initial loop calibre dilation and peritoneal free fluid were found. These findings were confirmed at the anatomopathological examination.

Conclusion: This study allows to define the early MRI features of bowel occlusion and their chronological evolution, also confirmed by anatomopathological exam. Our data suggest a relevant role of MR imaging in the early diagnostic assessment and management of patients with small bowel obstruction. The chance to achieve an early detection of bowel injury and to correlate the histological pattern with imaging findings could address towards a finer and earlier diagnosis and a more effective treatment.



B-0200 15:12

Contrast-enhanced ultrasound for differential diagnosis of suspected GvHD in patients after allogeneic transplantation

L.M. Dendl, K. Landfried, E.M. Jung, N. Platz Batista da Silva, C. Friedrich, C. Stroszczynski, A.G. Schreyer; Regensburg/DE (lena_marie_dendl@yahoo.de)

Purpose: Early diagnosis of GvHD (graft versus host disease), after differentiation from other causes leading to the same symptoms, such as viral or bacterial enteritis, is important because the time needed for diagnosing GvHD is directly correlated to a worsening of the outcome. We evaluate the value of contrast-enhanced ultrasound (CEUS) for the differential diagnosis of GvHD.

Methods and Materials: We examined 23 patients presenting with the abdominal symptoms of GvHD. All patients underwent CEUS with particular attention to penetration of the intravenously applied microbubbles in the bowel lumen. In the patients having allo-SCT in their history we had histological confirmation of GvHD. The resulting examinations were documented digitally.

Results: Out of 17 patients with confirmed GvHD of the GI tract, 14 showed penetration of the intravenously applied microbubbles into the bowel lumen, leading to a sensitivity and specificity of 82% and 100% for transmural bubble penetration for GvHD of the GI-Tract, since the patients without GvHD of the GI tract showed no transmural bubble penetration. In patients with viral or bacterial infections of the GI tract, no transmural penetration of the microbubbles into the bowel lumen was observed. For microbubble penetration as a criterion for GvHD of the GI-Tract, this leads to a negative predictive value (NPV) of 67%, and a positive predictive value (PPV) of 100%.

Conclusion: Our study strengthens the hypothesis that transmural bubble penetration may be a highly specific and adequately sensitive non-invasive-diagnostic criterion for GvHD of the GI tract.

14:00 - 15:30

Room F1

Genitourinary

SS 207

Genitourinary CT

Moderators:

O. Nikolic; Novi Sad/RS
J. Stoker; Amsterdam/NL

B-0201 14:00

Impact of 4th generation iterative reconstruction techniques on image quality in low-dose computed tomography of the upper urinary tract

M. Regier, A. Laqmani, H.C. von Schultendorff, D. Hammerle, F.O. Henes, M. Groth, H.D. Nagel, G. Adam, J.H. Buhk; Hamburg/DE (mregier@uke.de)

Purpose: To intraindividually compare and evaluate the influence of the 4th generation iterative reconstruction (IR) technique iDoseTM on low-dose MDCT of the upper urinary tract with regard to anatomical delineation and artefact reduction.

Methods and Materials: In 26 consecutive patients suffering from urolithiasis the raw data of unenhanced MDCT scans (120 kV, mean CTDIvol: 5.9 mGy) were reconstructed using a prototypic reconstruction processor featuring iDose4TM software (Philips, Best, the Netherlands). iDoseTM levels varied between 0, 2, 4, 6 and 7. For each setting two different kernels were applied (standard=B; sharp=C). All images were reconstructed with a slice thickness of 1 mm. Blinded image analysis was performed by three radiologists. A 4-point grading-scale was applied regarding the depiction of anatomical details and degree of artefacts (1, worst; 4, excellent). The signal-to-noise ratio (SNR) was assessed. Statistics included kappa-analysis and Wilcoxon-test.

Results: The highest image quality was assessed applying an iDoseTM level of 4. Even at the lower iDoseTM level of 2 the ratings were superior to standard filtered-back-projection (iDoseTM level 0). If the comparison was made at almost identical image noise, there was a trend towards the superiority of filter C over B. Overall, inter-rater reliability was excellent (K> 0.8). With increasing iDoseTM levels, reduction of streak artefacts was successfully quantified by a decrease of the standard deviation at constant mean attenuation values.

Conclusion: Iterative reconstruction seems to be a powerful tool for the improvement of image quality in low-dose MDCT of the upper urinary tract. Even at relatively low iDoseTM levels higher image quality compared to filtered back-projection can be achieved.

B-0202 14:09

CT virtual hysterosalpingography: experience in 5000 cases

J. Vallejos¹, P. Carrascosa¹, C. Capunay¹, A. Vasconcelos¹, M. Baronio², S. Papier²; ¹Vicente Lopez/AR, ²Buenos Aires/AR (javss⁹@yahoo.com.ar)

Purpose: To illustrate the spectrum of findings and the differential diagnosis with other pathologies in computed tomography virtual hysterosalpingography (CT-VHSG) studies.

Methods and Materials: We retrospectively evaluated 5000 CT-VHSG studies performed in our institution for the evaluation of infertility. The exams were performed using a 64-row and 256-row CT scanners. Scans parameters were: 0.9 mm slice thickness, 0.45 mm reconstruction interval, 120 kV and 50-200 mAs. A total volume of 20 ml iodine contrast dilution (3 ml of iodine contrast and 17 ml of saline solution) were administered into the uterine cavity using a semi-rigid plastic cannula.

Results: In the cervical region CT-VHSG demonstrated: wall irregularities (23%), folds thickening (10%), cervical polyps (9%), diverticulae (6%), cervical stenosis (8%), cervical synechiaes (1%). Uterine cavity findings were: polyps (40%), submucous myomas (9%), synechiaes (11%). Uterine wall abnormalities included: intramural and subserous myomas (9%), uterine malformations (8%), adenomyosis (5%) y C-section scar (3%). Fallopian tubes findings included: unilateral hydrosalpinx (8%) and bilateral hydrosalpinx (2%), tubal obstruction (4%). The 7% of the fallopian tubes were partially visualised in the CT-VHSG studies. The scan time was 3.2 ± 1.1 sec. The effective radiation dose was 0.93 ± 0.08 mSv. The 86% of the patients referred only mild or no discomfort.

Conclusion: CT-VHSG allowed an adequate and accurate evaluation of the female internal genital organs, providing comprehensive diagnostic information in patients with infertility. This is minimally invasive low radiation dose technique, well tolerated for the vast majority of the patients.

B-0203 14:18

Detectability of small urinary stones on virtual nonenhanced images with different slice thickness, generated at pyelographic phase dual energy CT

S. Lim, Y. Lee, S. Moon, D. Kang, S. Wee, M. Kim; Iksan/KR

Purpose: To evaluate the detectabilities of small urinary stones by 1 mm, 3 mm, 5 mm slice thickness, virtual nonenhanced (VNE) images.

Methods and Materials: 45 patients who had undergone abdominopelvic CT scans, which consisted of true nonenhanced (TNE) and pyelographic-phase dual source dual energy CT scans, were enrolled. 40 patients who have urinary stones less than 5 mm in diameter were enrolled randomly, and 5 patients who have no urinary stone were enrolled for control group. Total 50 stones were enrolled. Two radiologists independently evaluated the VNE images for the presence of stone, size and location. In addition, the image quality, artefacts, associated renal abnormalities, and radiation dose were also calculated. Sensitivities were calculated for stones with diameter of 2-2.9 mm, 3-4.9 mm and overall. Specificities, accuracies and positive predictive values were also calculated. The TNE image was considered the reference standard.

Results: The mean overall sensitivities of two observers for detecting stones at 1 mm, 3 mm, 5 mm VNE images were 84%, 74%, 70%. The sensitivities for detecting 3-4.9 mm sized stones were 96.30%, 92.59%, 90.74%. The sensitivities for 2-2.9 mm sized stones were 71.74%, 52.18%, 45.66%. The overall specificities were 43.41%, 41.67%, 22.62%. Accuracies were 75.44%, 66.59%, 60.31%. PPV were 85.28%, 81.98%, 77.78%. Interobserver agreement showed good (k=0.613). 30.91% of total radiation dose could have been reduced if TNE images were not taken. Symptomatic ureteral and ureterovesical junction stones (21 of 50 stones) were detectable in 97.62%.

Conclusion: VNE image is useful even for detecting small urinary stones, and detectability of small stones can be enhanced with 1 mm slice thickness VNE image.

B-0204 14:27

CT in urolithiasis: potential of dose reduction and impact on image quality using iterative reconstruction

J. Hansmann, G.M. Schoeppler, T. Henzler, H. Haubenreisser, M. Reichert, U.I. Attenberger, S.O. Schönberg, C. Fink; Mannheim/DE (jan.hansmann@medma.uni-heidelberg.de)

Purpose: To determine the potential of dose reduction and impact on image quality using iterative reconstruction for CT of urolithiasis.

Methods and Materials: A 4.8x4.3 mm uric acid ureteral stone was placed inside an anthropomorphic Alderson phantom at the pelvic level. Measurements were performed on a 64-channel-MDCT-system using different kV (120, 100, 80 kV) and mAs (100, 70, 30, 15, 8) settings. For each kV and mAs setting 1 mm data sets were

reconstructed using standard filtered back projection and iterative reconstruction soft tissue kernels (B30 and I30). The resulting 30 scans were randomised into 6 groups and image quality was independently assessed by two blinded readers. The best two scans of each group were again randomised and pitted against each other until the best 8 scans were determined. Effective dose (ED) was estimated for each data set from dose length product and a conversion factor. Noise measurements were performed in an additional water phantom used with each scan.

Results: Low-dose images using a mAs setting of 8 were not diagnostic and could not visualise the stone. Among the 8 best data sets, 5 were based on iterative reconstructions. Image quality using iterative reconstruction at the highest dose were rated to have the best image quality (120kV, 100 mAs, ED=2.53, Noise level-12.7). Lower dose settings (120 kV, 30 mAs, ED=0.75, Noise level-25.7) allowed for diagnostic image quality with a dose savings potential of 70%.

Conclusion: Iterative reconstruction allows for a potential dose saving of up to 70% while still yielding diagnostic image quality in CT of urolithiasis.

B-0205 14:36

Dual energy split-bolus CT for the detection of urinary stone disease.

One phase acquisition: threefold information

P. Stolzmann, R. Gnannt, A. Winklehner, M. Fischer, H. Alkadhi, C. Karlo; Zurich/CH (paul.stolzmann@usz.ch)

Purpose: To prospectively assess image quality, diagnostic performance, and radiation dose of dual energy split-bolus CT for the evaluation of urinary stone disease.

Methods and Materials: Fifty consecutive patients (19 women; 45±15 yrs) referred for the evaluation of urinary stone disease and urinary tract obstruction underwent CT with a standard unenhanced and dual energy (dual source CT, 100-140 kVp/tin filter) contrast-enhanced phase. Contrast media (300 mg Iodine/ml) was administered in a split-bolus fashion (1st bolus 30 ml, 2nd bolus 50 ml after 9 min). Dual energy data were acquired 10 min after initiation of contrast injection. Virtual non-enhanced (VNC) images were reconstructed by iodine subtraction. Two blinded readers independently assessed image quality. Sensitivity, specificity and diagnostic accuracy for the detection of urinary stone disease were calculated for VNC images using standard unenhanced images as the reference.

Results: Image quality of contrast-enhanced dual energy and VNC images were rated diagnostic in all 50 patients (100%). Image noise of VNC images was low (7±1 HU, 5-11 HU). Standard unenhanced CT revealed 39 urinary stones in 25/50 patients (50%); VNC demonstrated 37 uroliths in 24/50 patients (48%). The two missed stones (2, 3 mm) were significantly ($p < 0.001$) smaller than the detected ones. Sensitivity, specificity, and diagnostic accuracy were 95%, 100%, and 97% on a per-urolith and 96%, 100%, and 98% on a per-patient basis, respectively. The effective dose of dual energy split-bolus CT was significantly ($p < .001$) lower than that of standard bi-phasic protocol (-41%).

Conclusion: Split-bolus dual energy CT allows for the evaluation of urinary stones, nephrographic and excretory phases in a single acquisition, thus, it facilitates comprehensive CT evaluation of urinary stone disease at a considerably reduced radiation dose.

B-0206 14:45

Can virtual non-contrast images of dual energy CT replace true non-contrast images in evaluation of renal pathologies

H.S. Teh, S.N. Shikhare, M.I. Othman, K.K. Yeow; Singapore/SG (cyber_xray@yahoo.com)

Purpose: To assess the efficacy of the virtual non-contrast CT (VNC) in evaluating the renal lesions compared to true non-contrast CT (TNC) and its capability to reduce the radiation dose.

Methods and Materials: 100 patients underwent triple bolus CT urography using DECT scanner. VNC images were obtained using commercial dual energy software. Two readers independently and retrospectively reviewed, rated and compared VNC images with TNC control images using mean HU value, signal-to-noise ratio (SNR), image quality, lesion detectability and radiation doses as parameters. Statistical analysis was performed.

Results: Of the 100 cases studied, 32 were normal, simple cysts (47), renal carcinoma (9), complicated cysts (2) and renal calculi (10). The mean HU values and SNR of these lesions were comparable in VNC images and corresponding TNC images. The image quality of VNC images was comparable and diagnostic. VNC images were equally efficient as TNC images in detecting solid focal lesions and cysts. However, 8 of 10 (80%) calculi were detected using VNC images, whereas all were visualised on TNC images. With this new technique, calculated radiation dose was 9.8 mGy, vs 18.2 mGy received using conventional technique.

Conclusion: Obtaining VNC images of the kidneys and the urinary tract using DECT software significantly reduces effective radiation dose without compromising

SNR, image quality and lesion detectability. This can potentially obviate the need to obtain TNC images in CT urography.

B-0207 14:54

Triple bolus technique with dual energy MDCT: a new perspective in CT urography

H.S. Teh, S.N. Shikhare, P.P.L. See, K.K. Yeow; Singapore/SG (cyber_xray@yahoo.com)

Purpose: To retrospectively evaluate and compare renal, vascular and urinary tract visualisation as well as radiation dose efficiency following triple bolus injections in a single acquisition with conventional triphasic CT urography technique.

Methods and Materials: 60 patients underwent triple bolus CT urography using dual source CT scanner. The protocol followed was: 30 mL of i.v. contrast at 2 mL/sec at 0 and 410 seconds and 40 mL at 3 mL/sec at 510 seconds, with total scanning time of 536 seconds. Virtual non-enhanced images were obtained using commercial dual energy software. Two readers independently and retrospectively reviewed and rated the images for contrast opacification of the renal parenchyma, vasculature and urinary tract distension and compared with conventional triphasic CT urography (cCTU) images.

Results: Complete opacification of the intrarenal collecting system and proximal ureter was achieved in 100% of segments, respectively (cCTU, 100% and 95%). The distal ureter and bladder was not opacified in 30% and 5% of cases, respectively (cCTU, 25% and 0%, $p > 0.05$). Image quality of renal parenchymal enhancement was excellent in 73% cases (conventional CTU, 80%, $p > 0.05$). Vascular image quality was excellent in 88% of cases (cCTU, 90%, $p > 0.05$). With this new study, calculated radiation dose was 9.8 mGy, much less than the conventional triphasic CT urography (34.2 mGy).

Conclusion: Triple-bolus CT urography technique using dual energy CT is a dose-efficient protocol permitting comprehensive study of the urinary system in a single acquisition and can be potentially used as standard protocol for CT urography.

B-0208 15:03

The diagnostic accuracy of multidetector computed tomography with multiplanar reformatted imaging and virtual cystoscopy in the early detection and evaluation of bladder carcinoma

M.F. Amin, A.A. Abd El Kafy; Elminya/EG (Mohammed_amin@yahoo.com)

Purpose: To evaluate the diagnostic accuracy of multi-detector computed tomography with multi-planar reformatted imaging and virtual cystoscopy in early detection and evaluation of bladder masses with comparison with conventional cystoscopic findings.

Methods and Materials: This prospective study included thirty-five patients with suspected bladder cancer were studied by (computed tomographic cystography (CTC) and virtual cystography (VC) in both the supine and prone positions after distending the bladder with air. The patient population was divided into three groups based on lesion size at conventional cystoscopy. Results of the CT study were compared with those of conventional cystoscopy (CC). Main outcome measures: sensitivity, specificity, positive and negative predictive value was used to study the association between VC and CC as regarding lesion detection.

Results: The size of the tumours varied from 2 mm to occupying more than three-quarters of the bladder. Of the 71 lesions detected on CC, 47 lesions were positive in histopathology, 28 were 4 mm were detected by VC and 24 of 28 < 4 mm. The locations of all were correctly described at VC when compared with CC. The overall sensitivity of VC versus CC was 94.36%, specificity 71.42%, PPV was 97.1% and NPV was 55.55.

Conclusion: Cystoscopy remains the standard of reference for the evaluation of the urinary bladder, but MDCT is indicated for examination of patients on whom conventional cystoscopy is contraindicated, difficult to perform, unsatisfactory in interpretation, and as an adjuvant tool in the evaluation of areas difficult to assess with conventional cystoscopy.

B-0209 15:12

Evaluation of diagnostic strategies for diagnosing bladder cancer using CT urography, flexible cystoscopy and voided urine cytology: results for 778 patients

J.M. Stedman, C.G.T. Blick, S.A. Nazir, S. Mallett, B.W. Turney, N.N. Onwu, I.S.D. Roberts, J.P. Crew, N.C. Cowan; Oxford/UK (jonathanstedman@doctors.org.uk)

Purpose: To evaluate diagnostic strategies for diagnosing bladder cancer (BCa) using CT urography (CTU) as additional, replacement or triage tests.



Methods and Materials: The clinical cohort was a consecutive series of 778 patients referred to a haematuria clinic with visible haematuria, age over 40 years with urinary tract infection excluded. All patients underwent CTU and flexible cystoscopy (FC), scored using 3-point systems and urine microscopy. Reference standard consisted of review of imaging, histopathology and medical notes. Follow-up was 21-66 months.

Results: The prevalence of BCa in the cohort=20% (n=156/778). For CTU as an 'additional-test' to FC, sensitivity (Se)=1.0 (95%CI,0.98-1.00), specificity (Sp)=0.94 (95%CI,0.91-0.95), positive predictive value (PPV)=0.80 (95%CI,0.73-0.85) and negative predictive value (NPV)=1.0 (95%CI,0.99-1.00). For CTU as a 'replacement-test' for FC, Se=0.95 (95%CI,0.90-0.97), Sp=0.83 (95%CI,0.80-0.86), PPV=0.58 (95%CI,0.52-0.64), and NPV=0.98 (95%CI,0.97-0.99). For FC for diagnosing BCa, Se=0.98 (95%CI,0.94-0.99), Sp=0.94 (95%CI,0.92-0.96), PPV=0.80 (95%CI,0.73-0.85) and NPV=0.99 (95%CI,0.99-1.0). For CTU and FC as a 'triage-test' for rigid cystoscopy (RC) and follow-up (normal and equivocal-scores referred for FC=option-1), Se=1.0 (95%CI,0.98-1.0), Sp=0.94 (95%CI,0.91-0.95), PPV=0.80 (95%CI,0.73-0.85), NPV=1.0 (95%CI, 0.99-1.0). For CTU and FC as a 'triage-test' for RC and follow-up (normal-score referred for follow-up=option-2), Se=0.95 (95%CI,0.90-0.97), Sp=0.98 (95%CI,0.97-0.99), PPV=0.93 (95%CI,0.87-0.96), NPV=0.99 (95%CI,0.97-0.99).

Conclusion: The optimum 'diagnostic-strategy' for diagnosing BCa uses CTU and FC as a 'triage-test' for RC and follow-up (option-1). Patients with positive CTU-scores for BCa go direct for RC, and normal and equivocal scores undergo FC. Diagnostic accuracy is the same as the additional test strategy with the advantage of a 17% reduction of the number of FCs performed.

14:00 - 15:30

Room F2

Breast

SS 202a

New technologies

Moderators:

P. Panizza; Milan/IT

E. Szabó; Szeged/HU

B-0210 14:00

Contrast-enhanced spectral mammography versus MRI in tumour size assessment: initial results

E.M. [Fallenberg](#), M. Krohn, J. Foerster, H. Wiebe, J.M. Singh, F. Diekmann, U. Bick; [Berlin/DE](#) (eva.fallenberg@charite.de)

Purpose: To compare contrast-enhanced spectral mammography (CESM) to mammography (MX) and MRI in detection and size estimation of histologically proven breast cancers using postoperative histology as gold standard.

Methods and Materials: The study was approved by health authorities and institutional review board and all patients enrolled provided written informed consent. All examinations and final histological results were available for 21 patients. CESM examinations were bi-lateral craniocaudal and mediolateral views with exposures starting 2 minutes after IV injection of 1.5 ml iodinated contrast agent per kg of bodyweight with a flow of 3 ml/sec. MRI was performed using a 1.5 T system and a dedicated 4 channel breast coil. Dynamic 3D T1-weighted gradient echo sequences were acquired before and after injection of 0.1 mmol/kgBW gadolinium contrast agent. MRI, MX and CESM images were read by two independent radiologists.

Results: The tumour was visible in 19 MX, 21 CESM and 20 MRI examinations. When visible, the average lesion size (largest dimension) was 28.5 mm (SD 18.7) in MX, 34.5 mm (SD 21.2) in CESM and 31.8 mm (SD 22.7) in MRI, versus 32.6 mm (SD 29.4) from postoperative histology. Breast density classes were ACR1: 1, ACR2: 7, ACR3: 7 ACR4 :6. Difference in lesion size measurements was significant between CESM and MX (p = 0.002) and not significant between CESM and MRI (p=0.47).

Conclusion: CESM showed a better lesion detection and size estimation compared to mammography. Initial results showed no difference between CESM and MRI in tumour detection and size assessment, both in good correlation with postoperative histology.

B-0211 14:09

Differential phase contrast mammography: a new tool for breast imaging

M. [Stampanoni](#)¹, Z. Wang¹, C. David¹, E. Roessl², M. Trippel³, G. Singer³, R.A. Kubik-Huch³, M.K. Hohl³, N. Hauser³; ¹Villigen/CH, ²Hamburg/DE, ³Baden/CH (marco.stampanoni@psi.ch)

Purpose: Phase-contrast and scattering-based x-ray imaging are known to provide additional and complementary information to conventional, absorption-based methods. We report on the first mammographic investigation of 5 native, that is, freshly dissected, breasts carried out with a grating interferometer and a conventional x-ray tube source. Four patients in this study had histopathologically proven invasive breast cancer. One male patient, without the presence of any malignant formations within the resected breast, was included as a control specimen.

Methods and Materials: We used a Talbot-Lau interferometer installed on a low-brilliance x-ray source; the interferometer was operated at the fifth Talbot distance, tube voltage of 40 kVp with mean energy of 28 keV, and current of 25 mA. The device simultaneously recorded absorption, differential phase and small-angle scattering. These quantities were combined into novel colour and high-frequency-enhanced radiographic images. Presurgical images (conventional mammography, ultrasonography, and MRI) supported the findings and clinical relevance was verified.

Results: Our approach yields complementary and otherwise inaccessible information on electron density distribution and small-angle scattering power of the sample at microscopic scale. This information can be used to answer clinically relevant, yet unresolved questions such as unequivocally discerning between malignant, premalignant changes and postoperative scars and distinguishing cancer-invaded regions within healthy tissue.

Conclusion: We present the first ex vivo images of fresh, native breast tissue obtained from mastectomy specimens using grating interferometry. This technique yields improved diagnostic capabilities when compared with conventional mammography, especially when discerning the type of malignant conversions and their breadth within normal breast tissue.

B-0212 14:18

Pilot study for the detection of simulated lesions at a 2D resp. 3D digital full-field digital mammography system with a new developed high-resolution detector on the base of two shifts of a-Se

R. [Schulz-Wendtland](#), M. Meier-Meitingner, M. Heinz, B. Adamietz, M. Uder, S. Schwab; [Erlangen/DE](#) (ruediger.schulz-wendtland@uk-erlangen.de)

Purpose: Experimental study at a new system for digital 2D resp. 3D full-field mammography with a high-resolution detector on the base of two shifts of a-Se.

Methods and Materials: The examinations were acquired at a new FFDM system Amulet® (FujiFilm, Japan): a-Se detector (receptor 24x30 cm², pixel size 50µm, memory depth 12 bit, spatial resolution 10 lp/mm, DQE > 0.50). Integrated in the detector there is a new method for data transfer, based on the optical switch technology. The object of investigation was the Wisconsin mammographic random phantom, model 152 A using the same parameters and exposure data (Tungsten, 100 mAs, 30 kV). We acquired 3 different images in c-c and oblique plane (2D) resp. in c-c and c-c plane with an angle of 4 degree (3D). Five in mammography experienced radiologists read the images (Monitor) randomly encoded (random generator) with regard to recognisability of details like specks of aluminium oxide (200 to 740 micrometers), fibres of nylon (0.4 to 1.6 mm) and round lesions/masses (diameters 5 to 14 mm) for decision and compared these results.

Results: 225 right positive decisions were possible to detect: we found for 2D and 3D in each case 222 (98.7%) right positive results.

Conclusion: The results of this phantom study demonstrate for 2D as well as 3D full field digital mammography the same detection rate. This must be proven in further clinical trials.

B-0213 14:27

Digital mammography with a new needle-based detector system: clinical results after a one-year trial

C.-P. [Wallner](#), M. Hittinger, M. Koerner, U. Linsenmaier, M. Reiser; [Munich/DE](#) (cwallner@med.uni-muenchen.de)

Purpose: To evaluate diagnostic image quality of digital mammography with a new needle-based detector system with respect to a 30% dose reduction.

Methods and Materials: We compared 160 mammographies with standard dose (n=80) and 30% dose reduction (n=80), performed on a GE Senographe DMR running the new Agfa DX-M needle-based imaging plate system (NIP) to their corresponding preliminary examinations (mean interval 1.76 y) which were acquired on the same GE mammography system with the Agfa CR85-X standard storage phosphor imaging plate system (PIP). For dose reduction the automatic exposure

control (AEC) settings were modified, dosimetry proved a dose reduction of 29.87%. According to the ACR Breast Imaging Reporting and Data System (BI-RADS), the mammograms were category 1-3, breast tissue density was ACR level 1-4. The mammograms were read twice by 2 experienced radiologists with a 3-point score on diagnostic image quality and the visualisation of parenchyma, cutis, benign lesions as well as calcifications.

Results: NIP compared to PIP at standard dose showed a better over-all image quality at ACR 1-3 which was significantly better at ACR 2 ($p < 0.038$). At ACR 4 image quality was similar with standard and reduced dose on NIP and PIP. With 30% dose reduction we found no significant loss of image quality within the NIP examinations. The reading showed a good intra- and interobserver agreement ($r=0.87/0.89$).

Conclusion: With the new needle-based imaging plate (NIP) technology in digital mammography, dose reduction of 30% is possible without loss of diagnostic image quality.

B-0214 14:36

Mammographic texture resemblance generalises as an independent risk factor of breast cancer

K. Chernoff¹, S. Christopher², G. Karemore¹, N. Karssemeijer³, C. Vachon², M. Nielsen¹; ¹Copenhagen/DK, ²Rochester, MN/US, ³Nijmegen/NL

Purpose: Breast density is an established risk factor of breast cancer. Mammographic-texture-resemblance (MTR) was shown to be a density independent risk factor, but only on a single study. We show that MTR generalises across different cohorts.

Methods and Materials: MTR was computed from digitalised mammograms of a 4-year prospective study (S1, Dutch screening program, 245/250 cancers/matched-controls, cancers were ascertained years prior to diagnosis 1993-2006), and from an independent cohort study (S2, Mayo Mammography Health Study cohort, 226/442 cancer/age-matched-controls). Mammographic percentage-density (PD) and other major risk factors were ascertained in S2. Finally, S2 was MTR-scored based on textures from S1 and S2 in a leave-two-out fashion. Scores on S2 were related to future breast cancer incidence by analysing AUC and quartiles adjusted for BMI, menopause status, and postmenopausal hormone (PMH) use.

Results: MTR-scores on S1 showed a significant capability to separate cancers from controls (AUC=0.63±0.02, $p < 0.001$). Age of S1 and S2 was 58.0±5.7, and 55.2±10.5 years, respectively. Differences in BMI, menopause status, and PMH between cases and matched controls in S2 were insignificant. S2 showed an AUC of 0.633, 0.613, and 0.600 based on percentage density, MTR-scores trained on S2 and S1, respectively. Adjusted for PD, MTR-scores of S2 trained on S1 showed OR in quartiles of ref; 1.10 (0.64-1.89); 0.93 (0.52-1.68); 1.96 (1.19-3.23), respectively, and a combined AUC of 0.654.

Conclusion: The heterogeneities that characterised breast cancer risk in S1 were also density independent risk factors in S2. Hence, the MTR-predicted risk persisted under differences in x-ray technology, population demographics and geography.

B-0215 14:45

Tomosynthesis elastography: evaluation of a novel elastography technique on simulated tumours in breast-mimicking phantoms

F. Engelken, I. Sack, D. Klatt, T. Fischer, E. Fallenberg, F. Diekmann; Berlin/DE (florian.engelken@charite.de)

Purpose: To evaluate whether measurement of strain under static compression in tomosynthesis of breast-mimicking phantoms can be used to distinguish tumour-simulating inclusions of different elasticities. To compare the results of this technique to ultrasound elastography as well as values predicted by rheometric analysis.

Methods and Materials: We prepared three soft breast-mimicking phantoms containing simulated tumours of different elasticities varying within a range typical for benign and malignant lesions. The phantoms were imaged using a wide angle tomosynthesis system with compression settings ranging from 0N-105N in steps of 15N. Strain of the inclusions was measured in two planes. Ultrasound elastography of the inclusions was performed using two different ultrasound elastography algorithms. In a separate experiment, the elasticity of the phantom matrix and inclusion material was determined by rheometry.

Results: The mean strain ratios obtained for the soft, intermediate, and firm inclusions were 0.72±0.13, 1.02±0.21 and 2.67±1.70, respectively, for tomosynthesis elastography, 0.91, 1.64 and 2.07, respectively, for ultrasound tissue strain imaging, and 0.97, 2.06 and 2.37, respectively, for ultrasound real-time elastography. The strain ratios predicted by rheometry were 0.41, 0.83 and 1.26 for the soft, intermediate, and firm inclusions, respectively.

Conclusion: Tomosynthesis elastography is a novel elastography method that allows differentiation of tumour-simulating inclusions in breast-mimicking phan-

toms by elasticity. The results are similar to ultrasound elastography and to the gold standard, rheometry. This technique may in future be useful for assessing elasticity of breast lesions. Initial results from clinical experiments appear promising; examples will be shown.

B-0216 14:54

Functional infrared imaging of the breast: automatic breast cancer detection using multiparametric computer analysis

M. Sklair-Levy¹, T. Sella², M. Cohen³, M. Rosin⁴, T. Allweis⁵, M. Shapiro⁶, E. Libson², D. Izhaky⁷; ¹Ramat Gan/IL, ²Jerusalem/IL, ³Petach Tiqva/IL, ⁴Tel Aviv/IL, ⁵Rehovot/IL, ⁶Kfar Sava/IL, ⁷Air Port City/IL (Miri.SklairLevy@sheba.health.gov.il)

Purpose: A novel prototype system performing functional three-dimensional (3D) infrared imaging (RUTH), coupled with multi-parametric computer analysis (MIRA), was evaluated for non-invasive detection of breast cancer. The technique utilizes non-ionising radiation and automatically provides risk assessment based on parameters derived from a clinically known training set.

Methods and Materials: Following IRB approval, a prospective multicentre, two-armed blinded study, was performed on 118 women, which included 66 patients with histologically proven breast cancer and 52 women with a normal (BI-RADS 1) mammogram. RUTH imaging (Real Imaging Ltd, Israel) was acquired on a continuous temporal timeline for 1 minute at 9 Hz. Acquired data were analysed using multiple computed algorithms (MIRA) which were combined to develop a master algorithm for risk assessment of breast cancer. Analysis was blinded to the pathological diagnosis and mammography. Performance was evaluated using ROC analysis.

Results: Fifty-eight of 66 cancers (87.8%) were identified using this technology. The sensitivity and specificity of RUTH imager coupled with MIRA for detecting breast cancer were 87.8% and 73.1%, respectively. ROC-AUC was 0.872. Detected tumours ranged 5 mm-45 mm (mean 17.4 mm) in size.

Conclusion: This preliminary study shows high sensitivity and specificity of the novel technology examined for detecting breast cancer. Performance was better than the published sensitivity of mammography and comparable to the reported performance of new adjunctive breast imaging technologies. Our results warrant further evaluation of the RUTH imager in detecting and characterising breast cancer.

B-0217 15:03

Molecular breast imaging (MBI) dose lowered to match mammography: potential for screening dense breasts

J.W. Hugg¹, M.K. O'Connor², C.B. Hruska², A.L. Weinmann², A.L. Connors², D.J. Rhodes², F.P. DiFilippo², B.E. Patt¹; ¹Northridge, CA/US, ²Rochester, MN/US, ³Cleveland, OH/US (james.hugg@gammamedica.com)

Purpose: Molecular breast imaging (MBI) uses single gamma photons to visualise breast tumours that are often occult on mammography of radiographically dense breasts. Our purpose was to reduce the MBI dose and evaluate its potential for future screening of women with dense breasts.

Methods and Materials: We optimised the imaging physics for the LumaGEM MBI scanner (Gamma Medica) that uses two detector heads with pixellated CZT gamma detectors with 1.6 mm square pixels. We designed a low-dose collimator with tungsten septa and square holes that match the CZT detector pixels. We developed with a breast lesion phantom that facilitates measurement of contrast-recovery curves, useful for comparison of various MBI systems and for predicting lesion detectability.

Results: In clinical trials at Mayo Clinic we have demonstrated low-dose MBI with 99mTc-Sestamibi, at a whole body dose equivalent to screening mammography. We are conducting a clinical trial to evaluate MBI screening of about 1600 women with dense breasts. MBI has proven far more sensitive and specific at detecting biopsy proven cancers than mammography in dense breasts. The breast lesion phantom demonstrates that our 1.6 mm pixel size is optimal for MBI, enabling the lowest dose compared to systems using 2.5 mm or 3.2 mm pixels.

Conclusion: Dose has been effectively mitigated as an obstacle to MBI screening of radiographically dense breasts. An ongoing clinical trial suggests that MBI could be a very effective screening tool in the dense breast population (up to 40% of European and American women; more than 50% of Asian women).

B-0218 15:12



Non-invasive differentiation of small breast lesions via 3D MT imaging

G. Zografos¹, D. Koulocheri¹, P. Liakou¹, P. Grigoropoulos¹, M. Sofras¹, S. Hadjiagapis¹, V. Marmarelis²; ¹Athens/GR, ²Los Angeles, CA/US (marmarelis@hotmail.com)

Purpose: The 3D non-ionising diagnostic imaging technology of multimodal tomography (MT) was introduced in ECR 2011. MT was recently shown to differentiate breast lesions (down to 2 mm in size) in 103 BIRADS-4 volunteers.

Methods and Materials: The MT clinical prototype performs 3D tomographic scan of the pendulant breast in water-bath using transmission ultrasound in a fixed-coordinate system. Design details were presented in the EIBIR Workshop of ECR2011. MT reconstructs multiple images for each coronal slice, using measurements of refractivity and frequency-dependent attenuation and dispersion. MT detects and differentiates lesions using fusion of these multimodal images. This year, MT results from 103 BIRADS-4 female volunteers (ages 39-79, average: 54.7 years) were compared with histopathology results from biopsy of the suspicious lesions (sizes 2-28 mm, average: 7.1 mm) taken by minimally invasive core biopsy, FNA, Fischer Mammotome® and BLES®. The hypothesis that MT can detect and classify correctly malignant lesions down to 2 mm in size was tested.

Results: MT detected and correctly classified 33 out of 34 malignant lesions (97.1% sensitivity) in the biopsy samples. Among the 33 detected malignant lesions, 15 (45%) had maximum dimension <= 5 mm (mostly DCIS). The smallest detected malignant lesions (DCIS) had maximum dimension of 2 mm. There was only one false-positive MT result in the biopsied lesions (98.5% specificity).

Conclusion: Initial clinical results confirmed the ability of MT technology to detect and classify breast lesions (down to 2 mm in size) among 103 BIRADS-4 female volunteers with 97.1% sensitivity and 98.5% specificity.

B-0219 15:21

Fusion of US and FDG-PET/CT image for evaluation of loco-regional recurrence of breast cancer using real-time virtual sonography (RVS): first experience

S. Nakano, K. Fujii, K. Yorozuya, M. Yoshida, J. Kousaka, Y. Shiomi, T. Fukutomi, T. Ishiguchi, O. Arai; Aichi-gun/JP (snakano@aichi-med-u.ac.jp)

Purpose: F18-fluorodeoxyglucose (FDG) positron emission tomography/CT (PET/CT) is more sensitive than conventional imaging in detecting metastatic or recurrent disease of the breast. When incidental FDG uptake with high standard uptake value (SUV) is detected in loco-regional lesion by FDG-PET/CT, sonographic confirmation needs to be done immediately. We recently developed a real-time virtual sonography (RVS) system that enables simultaneous display of both a US and the CT images of the same site in real-time using magnetic position tracking system. The aim of this study was to evaluate the role of RVS in the sonographic localisation of FDG activity.

Methods and Materials: Between March 2009 and June 2011, we performed FDG-PET/CT for suspected recurrent breast cancer in 22 patients. The sonographic detection rate was determined for FDG uptake in loco-regional recurrence, with or without RVS.

Results: Of the 22 patients, a total of 14 FDG uptake lesions in seven patients were detected as loco-regional recurrence. The median tumour size was 14 mm (range 5-54 mm). Of the 14 lesions, 7 (50%) could be identified in targeted US without RVS, but 13 (93%) were identified in targeted US with RVS (p=0.031). The RVS was able to correctly project FDG uptake information onto a body surface without operator's skill, as we checked sonography form images.

Conclusion: Our results suggest that RVS can sonographically identify FDG uptake lesions with excellent accuracy.

14:00 - 15:30

Room G/H

Breast

SS 202b

MRI: contrast media and clinical applications

Moderators:

R.M. Mann; Nijmegen/NL

J.L. Raya Povedano; Córdoba/ES

B-0220 14:00

Influence of breast parenchyma density on malignant lesion detection with gadobenate dimeglumine-enhanced MRI compared to gadopentetate dimeglumine-enhanced MRI, mammography and ultrasound

F.J. Gilbert¹, H.C. van den Bosch², A. Pettilo³, K. Siegmann⁴, J.T. Heverhagen⁵, S. Corcione⁶, M. Faivre-Pierret⁷, C.M. Zechmann⁸, L. Martincich⁹; ¹Aberdeen/UK, ²Eindhoven/NL, ³Naples/IT, ⁴Tübingen/DE, ⁵Marburg/DE, ⁶Ferrara/IT, ⁷Lille/FR, ⁸Heidelberg/DE, ⁹Candiolo/IT (f.j.gilbert@abd.n.ac.uk)

Purpose: To determine the influence of breast parenchyma density on malignant lesion detection in patients undergoing gadobenate dimeglumine-enhanced MRI, gadopentetate dimeglumine-enhanced MRI, mammography and ultrasound.

Methods and Materials: One hundred and eight women (52.7±12.7 years) that underwent mammography and who had BIRADS 3/4/5 findings on mammography and/or ultrasound underwent two identical breast MRI exams in randomised order, one with gadobenate dimeglumine and the other with gadopentetate dimeglumine each at a dose of 0.1 mmol/kg BW. MRI was performed at 1.5 T using T2w and 3D spoiled T1w GRE sequences with a temporal resolution of <=2 min. Images were evaluated independently by three, unaffiliated, blinded radiologists for cancer detection. Imaging findings were matched with histology data by a fourth independent, blinded, radiologist. Malignant lesion detection rates were compared (McNemar's test) across different categories of breast tissue density.

Results: 122 malignant lesions were confirmed at histology in patients undergoing MRI and mammography/ultrasound. In predominantly fatty breasts (< 50% glandular) each reader detected 41/41 (100%) malignant lesions on gadobenate dimeglumine-enhanced MRI compared with 35-39/41 (85.4-95.1%) lesions on gadopentetate dimeglumine-enhanced MRI and 38/41 (92.7%) lesions on mammography/ultrasound. In heterogeneously dense and extremely dense breasts (> 51% glandular) the three readers detected 74-76/81 (91.3-93.8%) malignant lesions on gadobenate dimeglumine-enhanced MRI compared with 64-66/81 (79.0-81.5%) lesions on gadopentetate dimeglumine-enhanced MRI and 66/81 (81.5%) lesions on mammography/ultrasound. Gadobenate dimeglumine-enhanced MRI was significantly (p < 0.02) superior for malignant lesion detection particularly in heterogeneously dense breasts.

Conclusion: Gadobenate dimeglumine-enhanced breast MRI permits significantly improved cancer nodule detection regardless of breast tissue density.

B-0221 14:09

Intra-individual, randomised comparison of the MRI contrast agents Gadovist® 1.0 versus MultiHance® for pre-operative breast MR imaging, evaluated in a blinded read

F. Pediconi¹, R. Kubik², B. Chilla², C. Schwenke³, K. Kinkel⁴; ¹Rome/IT, ²Baden/CH, ³Berlin/DE, ⁴Chêne-Bougeries/CH (karen.kinkel-trugli@wanadoo.fr)

Purpose: To intraindividually compare 0.1 mmol/kg Gadovist® 1.0 (gadobutrol) and MultiHance® (gadobenate) by prospectively evaluating the agreement rate in breast lesion detection and characterisation at contrast-enhanced breast MR.

Methods and Materials: Two breast MRIs were performed for staging in 72 patients with biopsy-proven breast cancer with an interval of 24 hours and 7 days between the examinations. 1.0M Gadovist®1.0 or 0.5M MultiHance® was administered in a randomised order. Lesion detection and characterisation was performed by two independent blinded readers. Lesion tracking compared to on-site readings and to histology from surgery or biopsy was performed by a third reader. Differences in lesion detection for the known cancer and for all lesions with pathology, lesion characterisation and background enhancement in both breasts were compared between the two contrast agents.

Results: Among 133 lesions, 103 had pathology (96 malignant, 7 benign). The agreement rate for lesion detection by the blinded readers showed no difference between both contrast agents for the index lesion (94.41%) and all lesions (82.33% for Gadovist® 1.0, 81.60% for 0.5M MultiHance®). Sensitivity in lesion characterisation across readers showed no difference between Gadovist® 1.0 (92.63%) and MultiHance® (90.53%). There was no difference between contrast agents in the

Thursday

assessment of BIRADs, lesion enhancement curve or background enhancement. Morphology assessment differed significantly between the readers ($p=0.0002$) and both contrast agents ($p=0.0057$) with more non-focal enhancement for Gadovist® 1.0 than for MultiHance®.

Conclusion: Both contrast media showed no difference in breast lesions detection and sensitivity in lesion characterisation at contrast-enhanced breast MRI.

B-0222 14:18

Does preoperative MRI in breast cancer increase the rate of mastectomy?

A. Garcia-Illana, G. Viteri, I. Simon, I. Anton, A. Elizalde, L. Pina; Pamplona/ES (gviteri@unav.es)

Purpose: To evaluate whether preoperative-MRI in female patients diagnosed with breast cancer increases the rate of mastectomy.

Methods and Materials: Two series of consecutive women surgically treated for breast cancer were retrospectively reviewed: Group 1: 300 patients with preoperative-MRI; Group 2: 300 patients without preoperative-MRI. Patient age, menopausal status, tumour size, staging, surgical treatment, neoadjuvant chemotherapy and reinterventions due to affected margins were evaluated. Statistical analysis was performed with Student's t and Chi-square tests (SPSS 15.0).

Results: Both groups were similar in age (51.5 ± 0.6 and 51.8 ± 0.6 years; $p=0.71$) and menopausal status (150 and 158 women; $p=0.41$). The average pathological tumour size was smaller in group 1 (16.9 ± 13.5 mm vs 22.3 ± 15.3 mm; $p < 0.001$). Multifocal/multicentric tumours were more frequent in group 1 (28.7% vs 15.7%; $p < 0.01$). Bilateral tumours were diagnosed only in group 1 (5.3%). The rate of mastectomy was lower in group 1 (25% vs 49%; $p < 0.001$). Oncoplastic (16.7%) and bilateral surgeries (5.3%) were only performed in group 1. The rate of neoadjuvant chemotherapy was higher in group 1 (30.7 vs 9.3%; $p < 0.001$). Reinterventions due to margin infiltration were also more frequent in group 1 (7.3% vs 2.7%; $p < 0.01$).

Conclusion: Despite diagnosing more multifocal/multicentric cases in group 1 (preoperative-MRI), our study shows a decrease in the rate of mastectomy (from 49% to 25%) when oncoplastic surgery and neoadjuvant chemotherapy are available. However, the increase of tumorectomies has led to more reinterventions due to affected margins (from 2.7% to 7.3%).

B-0223 14:27

The role of preoperative MRI in breast cancer: is the menopausal status of relevance?

A. Garcia-Illana, I. Simon-Yarza, G. Viteri, I. Anton, A. Elizalde, L. Pina; Pamplona/ES (msyarza@unav.es)

Purpose: To evaluate the role of MRI in the preoperative setting of breast cancer according to the premenopausal vs. menopausal status.

Methods and Materials: 300 breast-MRI exams of patients with breast cancer diagnosed by percutaneous biopsy were retrospectively evaluated. They were divided into two groups: 150 premenopausal (group1) and 150 menopausal (group2). Changes in surgical management induced by MRI findings, surgical treatment, MRI staging (size, bilaterality, multicentricity and multifocality), free tumoral margins and requirement of neoadjuvant chemotherapy (NAQ) were evaluated. Statistical analysis was performed with Student's-T and Chi-square tests (SPSS 15.0).

Results: Initially planned surgery was modified in 30.3% of the patients due to MRI findings, with no significant differences between groups ($p=0.53$). This additional information given by MRI was proved to be malignant in 95.6% of the cases. 16 bilateral surgeries, 75 mastectomies, 50 oncoplastic surgeries and 157 tumorectomies were performed with more mastectomies carried out in Group1 (30% vs 20%; $p < 0.05$). MRI detected 16 bilateral cancers (5.3%) unsuspected with conventional techniques, 36 multicentric (12%) and 52 multifocality (17.3%), with no significant differences between groups ($p=0.91$). Mean size of the tumours was similar in both groups ($p=0.11$). Free margins were obtained in 91.7% with no significant differences ($p=0.06$). More women underwent NAQ in group1 (36.7% vs 24.7%; $p < 0.05$).

Conclusion: MRI is more sensitive than conventional techniques for staging breast cancer, changing initial planned treatment in up to one-third of the patients. Both menopausal and premenopausal patients may benefit from preoperative MRI. Premenopausal women undergo more mastectomies and NAQ.

B-0224 14:36

Impact of T-stage on lesion characteristics and overall diagnostic accuracy of breast MRI: does size really matter?

M. Dietzel, H.P. Burmeister, R. Zoubi, T. Groeschel, M.R. Gajda, I.B. Runnebaum, W.A. Kaiser, P.A.T. Baltzer; Jena/DE (dietzelmatthias@hotmail.com)

Purpose: Histopathological characteristics of breast tumours change during their course of growth. However, in radiological practice, lesion characteristics are applied irrespective of tumour stage. We aimed to identify morphologic and dynamic profiles of breast tumours in correlation to the T-Stage and to evaluate the impact on overall diagnostic accuracy of breast-MRI (bMRI).

Methods and Materials: Basis of this investigation was a cross-sectional database of consecutive, histologically verified breast lesions imaged by bMRI (standardised protocols; ethical-board approval). All lesions were prospectively evaluated by two radiologist in consensus (> 1000 bMRI-exams) using 17 standardised morphological and dynamic descriptors. According to the TNM-systems, size of each lesion was categorised as "I" (< 2 cm; n:757), "II" (2-5 cm; n:267) and "III" (5 cm; n:60). Statistics addressed accuracy of individual descriptors in association with each size-subgroup (contingency-tables, Chi-square tests). Then, descriptors were combined into a multivariate model to identify overall accuracy of bMRI in association with the T-Stage (logistic-regression; histology/target-variable: benign vs. malignant). Finally, results between each subgroup were compared (AUC-comparison [area under the receiver-operating-characteristics curve]).

Results: Majority (76%) of bMRI descriptors were associated with T-Stage ($P < 0.05$), resulting in different accuracy of such features according to tumour size. This contributed to the higher performance of bMRI in advanced T-Stages (II: AUC=0.97; III AUC=0.99) compared to smaller tumours (I: AUC=0.90; $P < 0.05$).

Conclusion: Our results suggest that lesions characteristics in bMRI change during the tumour's course of growth. This causes characteristic morphologic and dynamic profiles in correlation with the T-Stage and further increases diagnostic accuracy of bMRI in larger lesions.

B-0225 14:45

Breast MRI and ductal carcinoma in situ: when can we expect to have no enhancement?

S. De Stefanì, C. Molinari, P. Clauser, A. Dal Col, V. Londero, R. Girometti, C. Zuiani, M. Bazzocchi; Udine/IT (silvia.destefani@gmail.com)

Purpose: To evaluate the characteristics of ductal carcinoma in situ not identified on dynamic MRI examination performed for breast cancer staging.

Methods and Materials: Two experienced breast radiologists retrospectively evaluated images of 86 patients with ductal carcinoma in situ (DCIS) histopathologically proven on surgical specimen, who had also performed a dynamic breast MRI investigation before surgery in 54 months. We divided the patients with DCIS into two groups, depending on the result of dynamic MRI investigation: the absence of suspicious contrast enhancement, including in the late phase, was considered to be a false-negative examination. The presence of enhancement was considered positive. Fisher exact tests was used for statistical analysis (statistically significant: p -value < 0.05).

Results: MRI correctly demonstrated the presence of 65/86 DCIS (sensitivity: 75.6%). In 21 patients no enhancement was identified in the area of neoplasm. DCIS smaller than or equal to 15 mm on mammography did not present enhancement during MRI investigation more often than those over 15 mm ($p < 0.05$). The absence of suspicious contrast enhancement at MRI was more frequently associated with low or intermediate histological grade compared with high grade ($p < 0.05$). Mammographic presentation was not a significant predictor of absence of suspicious contrast enhancement at breast MRI.

Conclusion: MRI demonstrated high sensitivity in the identification of breast cancer, even without invasive features. Malignant lesions in situ that do not show enhancement are more often small and low grade.

B-0226 14:54

Validation of EUSOMA criteria for selecting to MRI preoperative staging patients eligible for conservative surgery at conventional staging

S. Ciatto, D. Bernardi, M. Pellegrini; Trento/IT (stefano.ciatto@gmail.com)

Purpose: To verify the validity of EUSOMA criteria prompting MRI preoperative staging by magnetic resonance (MRI) in subjects eligible for breast conserving therapy (BCT): lobular histological type, size discrepancy > 1 cm between mammography and ultrasonography, high eredo-familial risk, and planned partial breast irradiation.

Methods and Material: We reviewed an unselected series of subjects eligible for BCT and consecutively undergoing MRI staging at Trento Breast Clinic. We

retrospectively simulated how many MRI procedures would have been spared and how many BCT would not have been converted to mastectomy (MX) indication had MRI staging been performed only in cases fulfilling EUSOMA criteria.

Results: MRI indication for MX was observed in 25 of 119 cases (21.0%) in the total series. Based on EUSOMA criteria MRI staging would have been indicated only in 47 cases (39.5%) generating 11 (23.4%) MX indications. MRI would have been spared in 72 subjects in whom it did actually generate 14 MX indications (56.0% of total MX indications). EUSOMA criteria, single or combined, were not efficient in selecting subjects at higher risk of MRI indication to MX, in particular lobular histological type which in the presence series was associated with lower risk. Applying EUSOMA criteria would only reduce MRI staging procedures (by 60.5%) and indication to MX with a comparable rate (by 56.0%).

Conclusion: We question the validity of EUSOMA criteria for selecting patients to MRI staging prior to BCT. They should be validated in controlled studies of greater statistical power before being adopted in current practice.

B-0227 15:03



Dynamic contrast enhancement MRI as a predictive and surrogate marker of pathological complete response of neoadjuvant treatment for locally advanced breast cancer

S. [Drisis](#), M. Capelan, S.-I. Chao, M. Paesmans, M. Lemort; *Brussels/BE (steliosdrisis@yahoo.com)*

Purpose: To evaluate the pharmacokinetic parameters of DCE-MRI as a predictive and surrogate marker for patients receiving neoadjuvant chemotherapy (NAC) for locally advanced breast cancer.

Methods and Materials: A retrospective study of 90 patients was performed where all patients underwent two DCE-MRI examinations, before (EX1) and during NAC (EX2). Maximum diameter (Dmax), and pharmacokinetic parameters from DCE-MRI such as Ktrans, Kep, Ve and Vp were concerned. Post-operative pathological examination was used as the golden standard with a binary response: responders, patients showing complete remission or "in situ" residual disease and non-responders for the rest of the patients. Wilcoxon test, ROC curves, comparison of ROC were employed for the statistical analysis.

Results: From the 90 patients 74 were non-responders (82.5%) and 16 (17.5%) showed complete pathological response. At EX1, a significant difference was found between the response groups only for the KtransEX1 ($p=0.035$) and at EX2 for Dmax ($p < 0.001$) and all pharmacokinetic parameters: Ktrans ($p < 0.001$), Kep ($p=0.011$), Ve ($p=0.003$) and Vp ($p=0.043$). Moreover, a significant difference was found between the response groups for the absolute changes of Ktrans, Ve and Vp and for the percentage changes of Dmax, Ktrans and Ve and Vp between EX1 and EX2. The ROC curve analysis showed the best performance for Ktrans at (EX1), for Dmax at EX2 and for % decrease of Ve between the two examinations.

Conclusion: DCE-MRI pharmacokinetic parameters could be a potential predictive and surrogate marker of neoadjuvant treatment in locally advanced breast cancer.

B-0228 15:12

Conventional and diffusion-weighted magnetic resonance imaging in predicting residual disease after neoadjuvant chemotherapy in patients with breast cancer

F. [Priolo](#), G. Petralia, L. Bonello, S. Raimondi, R. Di Filippi, M. Colleoni, E. Cassano, M. Bellomi; *Milan/IT (francesca.priolo@ieo.it)*

Purpose: To evaluate the role of conventional magnetic resonance imaging (MRI) and diffusion-weighted (DW)-MRI in predicting residual disease after neoadjuvant chemotherapy (NACT) in patients with locally advanced breast cancer (LABC).

Methods and Materials: we enrolled patients with LABC who underwent conventional MRI and DW-MRI at baseline, during and after completion of NACT. Two readers carried out a qualitative analysis for conventional MRI and DW-MRI performed after completion of NACT, alone and in combination, in order to evaluate the presence of residual disease. We evaluated the potential of the baseline apparent diffusion coefficient (ADC), and its changes after 12 weeks, to predict residual disease.

Results: We enrolled 56 patients, of whom 40 patients with 42 breast cancers underwent surgery. The qualitative analysis of conventional MRI alone, DW-MRI alone, and of conventional MRI and DW-MRI in combination was performed in 34 tumours, showing a diagnostic accuracy (DA) for predicting residual disease of 85.3%, 88.2% and 91.2%, respectively. Patients with pathological complete response (pCR) showed a lower baseline ADC ($p=0.0177$) when compared to those with residual disease. The change in ADC after 12 weeks of NACT was significant ($p=0.005$) in patients with pCR; no significant change was observed in patients with residual disease.

Conclusion: conventional MRI and DW-MRI showed comparable DA in predicting residual disease after NACT. Baseline ADC and its changes after 12 weeks predicted residual disease in our cohort.

B-0229 15:21

Diffusion weighted imaging (DWI) as a mammary carcinoma characteristic: association of apparent diffusion coefficient (ADC) and pathological outcome in patients treated with neoadjuvant chemotherapy

V.H.P. [Tran](#), M. Volmerink, A. Imholz, M. Louwen, R. van Dijk; *Deventer/NL*

Purpose: The role of DWI is currently under investigation in tumour response evaluation in patients with neoadjuvantly treated mammary carcinoma. However, the role of DWI prior to treatment as a tumour characteristic in relation to pathological outcome is still unclear.

Methods and Materials: In this retrospective study, we first investigated the association between baseline ADC and pathological outcome (either complete or incomplete response) by logistic regression in 44 consecutive patients with neoadjuvantly treated mammary carcinoma in our hospital between 2006 and 2010. Second, we investigated if change of ADC and change of tumour size were mediating factors.

Results: High baseline ADC (b-value 600) was associated with pathological complete response (odds ratio= 1.7×10^{-5} , 95%-CI= $0.1 \times 10^{-5} - 41.4 \times 10^{-5}$, $p=0.01$). Mean ADC in responders was 1.57×10^{-3} mm²/sec and in incomplete responders 1.33×10^{-3} mm²/sec (unpaired Student's t-test $p < 0.01$). This association was independent of changes in tumour size (RESIST, washout) and changes in ADC after neoadjuvant chemotherapy.

Conclusion: High baseline ADC was associated with complete pathological response, independent of changes in ADC and tumour geometry during the course of neoadjuvant chemotherapy. Therefore, there is a potential role for ADC as a tumour characteristic in predicting pathological outcome.

14:00 - 15:30

Room I/K

Abdominal Viscera

SS 201b
CT technique

Moderators:

A. [Alcalá-Galiano](#); *Madrid/ES*
S. [Stojanovic](#); *Novi Sad/RS*

B-0230 14:00



Variability of CT contrast enhancement in the pancreas: a cause for concern?

L. [Delrue](#)¹, P. Blanckaert¹, D. Mertens², P. Duyck¹; ¹*Gent/BE*, ²*Brussels/BE (louke.delrue@uzgent.be)*

Purpose: Multidetector CT is a valuable technique for diagnosis/staging in several pancreatic pathologies. Diagnosis is usually based on tissue density measurements. Recently, newer functional CT techniques were introduced. The aim of this study was to assess variability on perfusion and dual energy CT data, and to compare these data with density measurements in the pancreas of a healthy population.

Methods and Materials: Two groups were included: twenty patients underwent perfusion CT imaging, ten patients were scanned using a dual energy protocol. In both groups, tissue density (Hounsfield units) was measured in pancreatic head, body and tail. Functional data were calculated (blood flow/blood volume in the perfusion CT group, iodine concentration in the dual energy group), and variability was assessed.

Results: Density measurements were comparable for the perfusion and dual energy CT groups, and ranged from 14 to 60 HU. Maximal enhancement differences between head/body/tail of the pancreas ranged between 2 and 21 HU. Considerable variability was observed, both on density measurements (ranging from 3% to 34%) and on functional parameters (mean variability on perfusion CT parameters blood flow and blood volume was 21.3% and 10%, respectively; mean variability on dual energy iodine mapping results was 24.4%).

Conclusion: This study demonstrated the presence of important intra-individual variability in pancreatic tissue contrast enhancement, regardless of the CT technique used. Considering the variability observed in this study, the use of cut-off values to characterise pancreatic pathologies seems troublesome, and morphologic primary and secondary changes will remain important, even when using novel functional imaging techniques.

B-0231 14:09

Measurement of transplanted pancreatic volume by computed tomography: reliability by intra- and inter-observer variability

E. Lundqvist, A.-R. Biglarnia, M. Segelso, A. Magnusson; *Uppsala/SE* (eva.lundqvist.8954@student.uu.se)

Purpose: The aim of this study was to evaluate the reliability of measurement of pancreatic volume by CT in transplanted patients. Today there is no sufficient prognostic method for predicting failure of transplanted pancreas. The hypothesis is that measurement of pancreatic volume by CT volumetry could be a useful method for clinical purpose as a prognostic method and to follow the natural cause of pancreatic transplants.

Methods and Materials: CT examination was performed on twenty-one consecutive patients that had undergone pancreas transplantation. Volume measurements were performed by two observers who traced the pancreatic contours in all slices. The corresponding volume was then automatically calculated. Observer 1 performed measurement for each patient twice. Observer 2 performed the measurements once for each patient. Differences in volume measurement were used to evaluate intra- and inter-observer variability.

Results: Intra-observer variability of pancreatic volume measurement, on CT, was found to have an almost perfect agreement with ICC 0.90. The inter-observer variability was also found to have an almost perfect agreement. ICC for the first measurements of observer 1 versus the measurements of observer 2 was found to be 0.90. ICC for the second measurements of observer 1 versus the measurements of observer 2 was found to be 0.96.

Conclusion: Intra- and inter-observer variabilities of transplanted pancreatic volume measurement have been evaluated concluding the method is reliable and reproducible with almost perfect intra- and inter-observer variability agreement. Thereby, CT volumetry could be considered a proper method for following and evaluating size/volume development of pancreatic transplants.

B-0232 14:18

Evaluation of quantitative perfusion map, with CT-perfusion technique, as an early predictor for tumour response to radiofrequency ablation in patients with HCC lesions: initial results

D. Ippolito, P. Bonaffini, C. Capraro, M. Meloni, S. Sironi; *Monza/IT* (davide.atena@tiscalinet.it)

Purpose: To assess the role of CT-perfusion (CT-p) technique in detection of blood flow changes related to the therapeutic effects in HCC lesion treated with RFA.

Methods and Materials: A total of 27 patients with known cirrhotic liver disease and biopsy-proven diagnosis of HCC lesion, that underwent RFA treatment, were prospectively enrolled in our study. Perfusion study of hepatic parenchyma and of treated lesion was performed about 1 month after treatment on a multidetector 16 slice-CT (Philips Brilliance, 16p, NL). Contrast medium-enhanced dynamic-CT was performed with static table position acquiring 8 dynamic slice/scan for a total of 40 scans after intravenous injection of 50 ml of contrast medium. Treated lesion and surrounding parenchyma were evaluated using a dedicated perfusion software (CT Perfusion Philips 2.0). The following parameters were considered: hepatic perfusion (HP); arterial perfusion (AP); blood volume (BV); hepatic perfusion index (HPI) and time to peak (TTP). Univariate paired Wilcoxon signed ranked test was used for statistical analysis.

Results: Perfusion parameters of treated lesions could be quantitative assessed using CTP analysis. Seven out of 27 patients had a residual disease and values of perfusion parameters measured within tumour tissue were: HP 42.1±14.8 ml/sec/100 gr; AP 45.9±9.1 ml/min; TTP 19.06±3.7sec; BV 19.08±4.9 ml/100 mg; HPI 52.1 ±31.8%. The corresponding perfusion values calculated in patients without residual tumour were: HP 10.3±6.1 ml/sec/100 gr; AP 10.7±7.8 ml/min; TTP 34.5±12.6sec; BV 8.7±12.9 ml/100 mg; HPI 12.6±7.5%. A significant difference (p < 0.001) was observed in mean value of all parameters calculated between treated lesions with residual tumour and those successfully treated. CT-p technique has demonstrated highly perfused areas related to the presence of residual arterial vessels within the viable portion of treated HCC lesions.

Conclusion: Perfusion-CT in patients with hepatocellular carcinoma enables assessment of tumour vascularity after RFA, by adding quantitative information about viable tumour tissue.

B-0233 14:27

Hypervascular liver lesion at dual energy CT: enhancement evaluation at different tube voltages

A. Colloconi, A. Scrimieri, R. Maroldi, P. Cabassa; *Brescia/IT* (paolocob@libero.it)

Purpose: To compare attenuation values of hypervascular liver lesion with 80 kVp-images, 140 kVp-images and with weighted-average (WA) simulated 120 kVp-images, using dual energy CT (DECT).

Methods and Materials: In this prospective study thirty-five patients (29 males, age range 27-83) underwent (in a two-month period) abdominal DECT scanning for suspected or known hypervascular lesions. A non-enhanced sequence, an arterial phase with DE technique (80Kvp, 140Kvp and WA-0.3) and a venous acquisition (120 kVp) were performed. Arterial images were obtained after a standard triggered threshold. The attenuation values were calculated using ROIs placed in arterial DE images on 6 different areas: lesion, aorta, psoas muscle, subcutaneous fat, healthy right and left liver. The LLR (lesion-to-liver ratio) and the CNR (contrast-to-noise ratio) were calculated independently by two radiologists. The CNR by (ROI lesion - ROI right liver lobe)/(SD subcutaneous fat) and the LLR by mean value of the lesion/mean value of healthy right liver lobe. A t-student test was used for statistical analysis.

Results: Fifteen lesions were detected. The mean attenuation values of the lesions were 172.79±51.69 HU for 80kV-images, 95.46±19.98 HU for 140kV-images, 120.80±26.08 HU in WA images. LLR was 2.36 in 80kV-images, 1.57 in 140kV-images and 1.88 in WA images (p < 0.005). The mean CNR was 2.89 in 80kV-images, 1.31 in 140kV-images and 2.45 in WA images.

Conclusion: 80 kVp acquisition images of hypervascular lesions demonstrated a higher LLR than acquired images at 140kVp and at WA-120KVP. The 80 kVp images could be used in clinical practice to better evaluate hypervascular liver lesions.

B-0234 14:36

Multi-organ perfusion CT in the abdomen using a 320-detector row CT scanner: preliminary results of perfusion changes in the liver, spleen, and pancreas of cirrhotic patients

K. Sano, U. Motosugi, H. Morisaka, H. Sou, T. Ichikawa, T. Araki; *Chuo/JP* (snkthr@yahoo.co.jp)

Purpose: To compare the perfusion of multiple abdominal organs between patients with and without liver cirrhosis using perfusion CT with 320-detector row CT.

Methods and Materials: This study included 21 patients with cirrhosis and 20 without cirrhosis. The 320-detector row CT scanner enabled multi-organ perfusion CT without requiring the scanner table to be moved. Perfusion was calculated using the maximum slope model for the aorta, the portal vein, the right and left lobes of the liver, the head and body of the pancreas, the spleen, and the corpus and antrum of the stomach. Perfusion in each organ of patients with and without cirrhosis was compared.

Results: Portal venous perfusion of the right and left lobes of the liver in patients with cirrhosis (117 and 100 mL·min⁻¹·100 mL⁻¹, respectively) was significantly less than that in patients without cirrhosis (213 and 174 mL·min⁻¹·100 mL⁻¹, respectively; p = 0.0081 and 0.0294, respectively). Arterial perfusion of the spleen (111 mL·min⁻¹·100 mL⁻¹) and the body of the pancreas (112 mL·min⁻¹·100 mL⁻¹) in patients with cirrhosis was also significantly decreased compared with that in patients without cirrhosis (spleen, 162 mL·min⁻¹·100 mL⁻¹, p = 0.0020; body of pancreas, 133 mL·min⁻¹·100 mL⁻¹, p = 0.0405).

Conclusion: The results of the perfusion CT suggest that arterial perfusion of the spleen and the body of the pancreas, as well as portal perfusion of the liver, in cirrhotic patients was decreased compared with that in non-cirrhotic patients.

B-0235 14:45

Influence of different iteration levels in fourth generation iterative reconstruction technique on image noise in CT examinations of the abdomen

P. Stumpp¹, M. Fernau¹, K. van Daal¹, D. Gosch¹, H.-D. Nagel², T. Kahn¹; ¹Leipzig/DE, ²Buchholz/DE (patrick.stumpp@medizin.uni-leipzig.de)



Purpose: The objective of this study was to evaluate the effect of the fourth generation, raw data-based iterative reconstruction technique (IRT) iDose4 (Philips Healthcare) compared to traditional reconstruction with filtered back-projection (FBP) on image noise in a representative group of patients undergoing abdominal CT examinations.

Methods and Materials: In this prospective study, 21 consecutive patients underwent routine CT examinations of the abdomen (8 f, 13 m; mean age 56.6 yrs.; mean BMI 24.8). Patients were scanned on a Philips Brilliance 64 with the use of an automatic dose control system (120 kV, protocol mAs: 180). Raw data were

reconstructed using FBP as well as IRT with different iteration levels with a prototype image reconstruction system. Resulting images were analysed with objective noise measurements, defined as standard deviation of average density values in the liver as a homogenous organ.

Results: Absolute noise levels in image reconstructions with filter B were reduced from 14.19 (FBP) to 5.64 HU (highest level IRT). Relative noise in IRT images compared to FBP images was reduced by 60% with only minimal effects on subjective image quality.

Conclusion: By the use of a fourth generation IRT for CT examinations of the abdomen a reduction of image noise of up to 60% can be achieved.

B-0236 14:54

Reducing x-ray dose for liver perfusion on an extended coverage multi-slice CT with a relaxed temporal resolution

Y. Ge¹, Z. Zhou¹, T. Cheng¹, Y. Guo¹, X. Su¹, J. Li²; ¹Zhengzhou/CN, ²Beijing/CN (cjr.geyinghui@vip.163.com)

Purpose: To investigate the feasibility of reducing CT x-ray dose in liver perfusion using a relaxed temporal resolution (TR) in axial scan mode.

Methods and Materials: 60 patients underwent CT perfusion scans for suspicion of tumours. The first 30 patients (group 1) underwent 40 mm perfusion scans with 2s TR for 16 samples, while the second 30 patients (group 2) underwent 80 mm perfusion scans with 3s TR for 10 samples. Tube currents were 120 mAs and 96 mAs for groups 1 and 2, respectively. The regional cerebral blood flow (rCBF), regional cerebral blood volume (rCBV), mean transit time (MTT) and the radiation dose from the two groups were analysed by t-test. In addition, the detection rates for nodules with rich arterial blood supply were compared and verified by pathology.

Results: There were 49 sHCC, 1 RN, 8 CH and 2 liver abscess patients. The 80 mm scans detected 7 more sHCC focuses and 8 more CH cases. The rCBF (ml·100 g⁻¹·min⁻¹), rCBV (ml·100 g⁻¹) and MTT (s) for groups 1 and 2 were (191.94±20.36, 11.39±0.94, 6.18±0.69), and (160.30±20.29, 11.65±1.22, 4.52±1.21), respectively, with no statistical differences between these parameters (p> 0.05). The radiation dose from group 2 with 80 mm coverage was similar to group 1 with 40 mm coverage.

Conclusion: With the use of an appropriate TR (up to 3s), the 80 mm coverage axial perfusion scans provided higher nodule detection rate without dose increase compared to conventional 40 mm coverage MDCT perfusion scans.

B-0237 15:03

Abdominal CT with model based iterative reconstruction: comparison with adaptive statistical iterative and filtered back projection reconstruction

C. Suzuki, M. Nagata, K. Kitagawa, S. Murashima, N. Nagasawa, H. Sakuma; *Tsu, Mie/JP (chsuzuki@clin.medic.mie-u.ac.jp)*

Purpose: To investigate if model-based iterative reconstruction (MBIR) can improve the quality of abdominal CT images and volume-rendered (VR) CT portography in comparison with adaptive statistical iterative reconstruction (ASIR) and filtered back projection (FBP).

Methods and Materials: Twenty patients (69.0±10.9 years) underwent three phase contrast-enhanced 64-slice CT of the liver. Images were reconstructed with MBIR (Veo), ASIR 50% and FBP. The contrast-to-noise ratio (CNR) relative to muscle was calculated for the liver and portal vein on 0.625-mm-thick images acquired in portal venous phase. The image quality of 4th branches of the portal vein on VR images was assessed by two observers using a 4-point scale (1: poor, 2: fair, 3: good, 4: excellent with clear delineation of 5th branches).

Results: MBIR showed significantly improved CNR of the liver (4.3±1.8) in comparison with those by ASIR (2.9±1.5, p=0.013 by Mann-Whitney U test) and FBP (2.0±1.0, p=0.035). The CNR of portal vein was 12.1±3.4, being significantly higher than those by ASIR (7.4±1.9, p < 0.001) and FBP (5.0±1.3, p < 0.001). On qualitative analysis, the image quality score of portal vein branches on VR portography was significantly improved using MBIR (3.7±0.6) as compared with those by ASIR (2.9±0.9 p < 0.001 by Wilcoxon signed ranks test) and FBP (1.9±0.9, p < 0.001).

Conclusion: The new MBIR algorithm significantly enhances CNRs of abdominal CT, and can provide substantially improved visualisation of portal venous branches when compared with ASIR and FBP.



B-0238 15:12

Is it available, by iodine concentration of the active part of renal mass, for differentiation between renal angioleiomyolipoma and renal cell carcinoma?

J. Sun, X.-T. Li, C. Yong, X.-Y. Zhang, S.-Y. Gao, Z.-L. Wang, Y.-S. Sun, X.-P. Zhang; *Beijing/CN (xnqiuju@163.com)*

Purpose: To evaluate the potential of iodine concentration of the active part of the renal mass as a tool to differentiate angiomyolipoma (AML) and renal cell carcinoma (RCC).

Methods and Materials: Of these twenty-two patients with highly suspected renal disease who underwent single source-dual energy CT scanning between July 2010 and April 2011, seventeen (eight patients had AML; nine RCC) underwent corticomedullary, nephrographic and excretory phase enhanced scanning. The regions of interest (ROI) were manually placed on the active part of the renal mass and the abdominal aorta. The average iodine concentrations of (ROI)s and abdominal aorta were obtained. Repeated measure analysis was conducted with SPSS, and Bonferroni adjusted p was used for multiple comparisons.

Results: The average iodine concentrations of the active part of AML in three enhanced phases were 3.11±1.91 mg/cc, 2.65±1.49 mg/cc and 2.24±0.50 mg/cc, respectively. And those of RCC were 6.55±3.41 mg/cc, 4.71±2.32 mg/cc and 3.73±1.79 mg/cc. The average iodine concentrations were significantly different between AML and RCC in all enhanced phases (p=0.024, p=0.049, p=0.040), especially in corticomedullary phase. The iodine concentration change patterns of three phases between AML and RCC were also significantly different (p=0.024).

Conclusion: These preliminary results suggest that iodine concentration could provide another helpful method to differentiate AML and RCC in addition to conventional CT. If these results are confirmed, this approach could potentially differentiate AML and RCC with the active part of the mass no matter the fat in AML are minimal or much.

B-0239 15:21

Low dose unenhanced MDCT with radiation dose equivalent to abdominal radiograph in evaluation of acute flank pain

S. Goel, A. Tandon, G. Mehrotra, S.K. Bhargava, S. Bhatt, I. Singh, A. Srivastava; *New Delhi/IN (docsandeepgoel@gmail.com)*

Purpose: To determine the diagnostic efficacy of low dose unenhanced MDCT delivering radiation dose equivalent to abdominal radiograph in evaluation of patients with acute flank pain in comparison to standard dose CT.

Methods and Materials: A prospective study was conducted in 50 patients presenting with acute flank pain, after ethical committee clearance and informed consent. All patients underwent unenhanced low dose CT (LDCT) (effective mAs = 20) and followed by ultrasound and standard dose CT (SDCT) (effective mAs=165). Three reviewers, who were blinded to clinical findings independently reviewed LDCT, ultrasound and SDCT for pathology and image quality (graded as good, acceptable or poor).

Results: 58% of patients had calculus disease while 28% had non-calculus urological causes and 10% had extra-urinary causes responsible for pain. No cause was found in 4% patients. Calculus detection rate was 91.5% for LDCT, 100% for SDCT and 76% for ultrasound. The mean size of calculus missed on LDCT was 1.2 mm. Interobserver agreement in calculus detection amongst three reviewers was excellent. The sensitivity for detection of non-calculus causes was 66.6% for LDCT, 80.9% for SDCT and 85.7% for ultrasound. Mean radiation dose in LDCT and SDCT was 0.44 mSv and 6.00 mSv, respectively. Only 2-4% of low dose scans were rated as of poor quality.

Conclusion: Low dose unenhanced MDCT revealed a high sensitivity for urolithiasis and moderate sensitivity for diagnosing alternate causes of acute flank pain. Thus, it has potential to be used as a first line modality in evaluation of these patients.

14:00 - 15:30

Room L/M

Cardiac

SS 203a

Perfusion, CT and MRI

Moderators:

M. Francone; Rome/IT

M. Gardarsdottir; Reykjavik/IS

B-0240 14:00

Quantification of regional myocardial perfusion at different levels of coronary flow in a large animal model using dynamic perfusion CT

A. Rossi¹, E. Klotz², D. Merkus¹, A. Uitterdijk¹, N. Mollet¹, P. de Feyter¹, D. Duncker¹, G.P. Krestin¹; ¹Rotterdam/NL, ²Forchheim/DE

Purpose: To quantify regional changes of several myocardial perfusion parameters at different levels of coronary flow using ECG-triggered dynamic contrast-enhanced CT (DCE-CT).

Methods and Materials: In seven pigs, an adjustable hydraulic occluder was placed around the LAD to induce various degrees of coronary flow reduction. 28 scans were performed under maximum adenosine vasodilatation (no obstruction and flow reduced by 12% to 90%). Dynamic data were acquired for the whole heart after bolus injection using a dedicated ECG-triggered scan mode on a dual source CT. Using a two-compartment deconvolution technique 3D-maps of myocardial blood flow (MBF), first pass distribution volume (FPDV), perfused capillary blood volume (PCBV) and flow-extraction-product (FE) were calculated. All parameters were measured in the downstream LAD area and were correlated with relative input flow.

Results: MBF (baseline 257±27 ml/100 ml/min, r=0.78, slope=0.66), FPDV (baseline 24.6±2.8 ml/100 ml, r=0.84, slope=0.76) and PCBV (baseline 16.2±4.6 ml/100 ml, r=0.78, slope=0.83) significantly decreased proportional to the reduction of coronary flow in the LAD (p < 0.0001). FE (baseline 106±19 ml/100 ml/min), on the other hand, remained constant until coronary flow was reduced to less than 30%. FE values below 30% coronary flow were significantly lower than FE values above 30% (Mann-Whitney, p < 0.01). This agrees with the assumption that parenchymal flow does not decrease until the coronary flow reserve is exhausted. **Conclusion:** DCE-CT is suitable for the assessment of regional myocardial perfusion parameters and can be used to study microcirculatory changes at various degrees of clinically relevant coronary flow reductions in a large animal model.

B-0241 14:09

Myocardial perfusion MRI at 3 T using kt-BLAST in patients with coronary artery stenoses of unclear haemodynamic relevance

P. Bischoff, R.L. Duschka, F. Himmel, K. May, P.W. Radke, A. Kovacs, F.M. Vogt, J. Barkhausen, P. Hunold; Lübeck/DE

Purpose: To evaluate high-field myocardial perfusion MRI using kt-BLAST for ischaemia detection in known coronary stenosis of unclear haemodynamic relevance.

Methods and Materials: Twelve patients (age, 74±11 yrs; 5 males) with known coronary artery disease (CAD) and angiographically (cath) proven stenosis of indefinite haemodynamic relevance were included. First-pass myocardial perfusion stress MRI (3 T, Achieva, Philips) was performed including Cine SSFP in long and short axes, accelerated kt-BLAST perfusion (spatial resolution, 1.1x1.1 mm) in 3 short axes during adenosine stress and at rest with 0.05 mmol/kg gadobutrol each, followed by 3DIR-TFE late enhancement imaging. MRI perfusion data were compared to cath results (suggested medium to high-grade stenosis) on a coronary vessel basis.

Results: In total, 36 coronary territories (LAD, RCA, RCX) were evaluated. In 6/36 coronary territories with suggested high-grade stenosis, MRI corresponded (LAD: n=4, RCX: n=1, RCA: n=1). MRI perfusion defects in anticipated low-grade stenoses were detected in 3/36 vascular areas (LAD:1, RCA:2), whereas positive cath findings without ischaemia were detected in 3/36 vascular areas (LAD:1, RCX:1, RCA:1). In 24/36 vascular territories, MRI and angiography showed negative results. Thus, MRI discovered discrepancies between visual grading of stenosis (cath) and the haemodynamic relevance (MRI) in 4/12 patients (6/36 vascular areas).

Conclusion: Myocardial perfusion MRI at 3 T using kt-BLAST provides relevant information for indicating coronary intervention in known CAD solving mismatch problems between visual stenosis grading (anatomy) and perfusion (physiology). The combination of high-field and rapid acquisition yields improved diagnostic quality. Prospective MRI studies in comparison with coronary flow reserve are needed to assess the diagnostic benefit.

B-0242 14:18

Quantification of myocardial ischaemia and infarcts by adenosine stress 128-high-pitch DSCT

T. De Zordo¹, F. Vega-Higuera², R.P. Goetti³, A. Plass³, F. Plank¹, A. Klausner¹, S. Leschka⁴, H. Alkadhi⁵, G. Feuchtner¹; ¹Innsbruck/AT, ²La Coruña/ES, ³Zurich/CH, ⁴St. Gallen/CH, ⁵Boston, MA/US

Purpose: To evaluate quantification of adenosine myocardial stress/rest CTP using a combined high-pitch 128-dual source CTP/coronary CTA protocol with a new volumetric 3-D prototype software.

Methods and Materials: Adenosine stress high-pitch 128-slice dual source myocardial CTP (pitch, 3.4) and CMR (1.5 T)/DE was performed in 30 patients. Myocardial perfusion defects by CTP were classified as complete or partial reversible and fixed during stress and rest. A new prototype (SiemensTM) was used for quantification of CT-density (HU) of the myocardium based on automated 3-D volume segmentation into 16 AHA-myocardial segments. The total, subendo- and subepicardial HU were quantified. Image quality was evaluated (score 1-4).

Results: The total and subendocardial HU of myocardial segments with complete (n=49) and partial (n=58) reversible ischaemia were lower during stress as compared to rest (total: 88.5vs100.2; subendocardial: 85vs97 HU). For fixed perfusion defects, HU were total: 103.7vs114.4 HU; subendocardial: 99.5vs109.7 HU during stress and rest (n=55). As compared to CMR-DE, total and subendocardial HU of segments with myocardial infarcts were slightly lower during stress (98 and 101 HU) as compared to normal myocardium (111 and 115 HU). During stress, none of LAD and LM segments were non-diagnostic, whereas 4/169 of CX and 23/113 of RCA segments were nondiagnostic and rest CTA was needed for assessment. Radiation dose CTP was 0.93mSv±0.18.

Conclusion: Quantification of ischaemic myocardium during adenosine stress high-pitch 128-DSCT is possible at an ultra-low radiation dose of < 1mSv. Rest CTA is required to characterise myocardial perfusion defects and to ensure coronary CTA, and DE for viability.

B-0243 14:27

Dynamic CT perfusion imaging of the myocardium using a wide detector CT scanner: first results

D. Muenzel¹, P.B. Noel¹, V. Renz¹, B.M. Gramer¹, M. Vembar², A.A. Fingerle¹, E.J. Rummeny¹, A. Huber¹; ¹Munich/DE, ²Highland Heights, OH/US

Purpose: To evaluate the feasibility of CT dynamic myocardial perfusion imaging (MPI) at a wide detector CT scanner.

Methods and Materials: 12 pigs underwent stress CT MPI at a 256-slice MDCT scanner. In 6 pigs a stenosis of a coronary artery (LAD n=4 LCX n=1, diagonal branch n=1) was induced by subtotal balloon occlusion (stenosis group), 6 pigs were examined without intervention (control group). The semiquantitative parameters time-to-peak (TTP), peak enhancement (PE), upslope (US), and the area-under-the-curve (AUC) were compared intra- and interindividually in post-stenotic and normal myocardium. Radiation dose was estimated by CTDIvol.

Results: The intra-individual evaluation showed significantly (p < 0.01) higher mean values for TTP (19.5±7.9 s) and lower mean values for PE (14.5±14.0 HU), US (1.1±0.9 HU/s), and AUC (119.3±114 HU*s) in the hypoperfused myocardium compared to the remote myocardium in the septum and lateral wall (TTP: 13.5±6.4 s/12.4±5.9 s, PE: 77.0±16.0 HU/75.9±8.9 HU, US: 6.5±2.4 HU/s/7.3±4.2 HU/s, AUC: 467.9±198 HU*s/415.1±79 HU*s). The inter-individual evaluation showed significantly (p < 0.05) lower mean values for TTP (9.7±1.8 s) and higher mean values for PE (75.3±24.3 HU), US (8.4±3.7 HU/s) and AUC (362.0±71 HU*s) in the control group. CTDIvol was 88.5 mGy.

Conclusion: Dynamic stress CT perfusion imaging offers the potential assessment of the physiological significance of coronary artery stenosis, thereby overcoming one of the limitations of cardiac CT

B-0244 14:36

Dynamic CT perfusion imaging of the myocardium: comparison of reconstructions from 180° and 360°

D. Muenzel¹, P.B. Noel¹, B.M. Gramer¹, V. Renz¹, M. Vembar², A.A. Fingerle¹, E.J. Rummeny¹, A. Huber¹; ¹Munich/DE, ²Highland Heights, OH/US

Purpose: To compare the image quality and z-axis coverage using standard 180° and 360° reconstruction analysis for CT dynamic myocardial perfusion imaging (MPI).

Methods and Materials: In 8 pigs coronary artery stenosis was induced by balloon occlusion. CT dynamic MPI was performed using a 256-slice MDCT. Image noise and signal-to-noise-ratio (SNR) were assessed. The semiquantitative parameters time-to-peak (TTP), peak enhancement (PE), upslope (US), and the area-under-

the-curve (AUC) were compared intra-individually in post-stenotic and normal myocardium. Z-axis coverage of reconstructed 3D scan volumes was estimated in coronal reformations.

Results: The intra-individual evaluation showed significantly ($p < 0.01$) higher values for TTP (26.9 ± 7.4 sec) and lower values for PE (1.3 ± 3.5 HU), US (0.1 ± 0.2 HU/s), and AUC (13.1 ± 3.7 HU*s) in the hypoperfused myocardium compared to the remote myocardium (TTP: 9.9 ± 10.4 sec/ 8.6 ± 9.9 sec, PE: 56.3 ± 27.1 HU/ 58.8 ± 26.8 HU, US: 4.4 ± 2.5 HU/s/ 5.1 ± 2.6 HU/s, AUC: 372 ± 182 HU*s/ 351 ± 174 HU*s). 360° filtered reconstruction analysis significantly reduced image noise with 5.5 ± 1.8 HU compared to 14.3 ± 3.9 HU in 180° reconstructed images ($p < 0.001$). SNR was increased with 28.9 ± 19.9 (360°) versus 10.8 ± 6.9 (180°), $p < 0.01$. Z-coverage was increased of about 1 cm using 360° reconstruction (360° : 77.8 ± 0.3 mm vs. 180° : 67.7 ± 1.9 mm), $p < 0.001$.

Conclusion: Reconstructions from 360° improve image quality of dynamic CT MPI and increase z-axis coverage of 3D imaging volumes using a 256-slice MDCT scanner.

B-0245 14:45

Association between myocardial blood flow as measured by dynamic adenosine-mediated stress perfusion computed tomography and coronary artery flow in a large animal model

R.P. Marcus, F. Bamberg, T. Sander, F. Schwarz, E. Baloch, R. Hinkel, D. Theisen, K.J. Hildebrandt, K. Nikolaou; Munich/DE (fabian.bamberg@med.uni-muenchen.de)

Purpose: To determine the association between myocardial blood flow (MBF) as measured by CT-based dynamic stress perfusion imaging and coronary artery flow by sensor-tipped flow-wire in a porcine model with variable degrees of induced coronary stenosis.

Methods and Materials: Seven domestic pigs received stents in the LAD, distal to first diagonal branch, in which a balloon catheter was inflated to simulate luminal narrowing (50% and 75% diameter stenosis). Intra-arterial flow measurements were performed at each perfusion state. All models underwent adenosine-mediated ($140 \mu\text{g/kg/min}$) dynamic stress and rest myocardial perfusion CT imaging, using a dual source CT (shuttle-mode, 100 kV/300 mAs, 20 ml Iopromide). MBF was calculated for each myocardial segment using a model-based parametric deconvolution method and correlated with results of coronary flow measurement.

Results: At rest, measured coronary flow in 50% and 75% coronary artery stenosis were 18.8 ± 1.3 and 14.0 ± 1.5 cm/sec, respectively. Under stress condition, coronary flow increased to 20.2 ± 1.6 cm/sec at 50% stenosis and decreased at 75% coronary stenosis to 11.0 ± 0.7 cm/sec, similar to MBF derived by CT (1.10 ± 0.25 vs. 0.80 ± 0.28 ml/g/min, $p < 0.001$). The increase in coronary flow of 1.4 cm/sec at 50% stenosis under stress was associated with an increase of 0.7 ml/g/min in MBFCT; the decrease in coronary flow at 75% under stress (3.0 ml/sec) was associated with a decrease in MBF of 0.10 ml/g/min.

Conclusion: Our results indicate that CT-derived eMBF measurements at rest and stress with varying degrees of coronary stenosis associate well with results of coronary flow measurements in a large animal model.

B-0246 14:54

Evaluation of myocardial CT perfusion in patients presenting with acute chest pain to the emergency department: comparison with SPECT-MPI

G. Feuchtnner¹, F. Plank¹, J. Battle², J. Leipsic³, T. Dezordo¹, J. Min⁴, J. Ziffer², B. Katzen², R. Cury²; ¹Innsbruck/AT, ²Miami, FL/US, ³Vancouver, DC/CA, ⁴Los Angeles, CA/US (Gudrun.Feuchtnner@i-med.ac.at)

Purpose: To evaluate resting myocardial CT perfusion (CTP) from coronary CT angiography (CTA) datasets in patients presenting with chest pain (CP) to the ED, in comparison with myocardial SPECT.

Methods and Materials: 76 patients (mean age 54.9 ± 13 ; 42% females; 13% prior coronary revascularisation and 16% with prior MI) presenting with CP to the ED underwent coronary 64-slice CT-angiography (CTA). Myocardial perfusion defects were evaluated for CTP employing an AHA 17-segment model. CTP results were compared to rest sestamibi SPECT myocardial perfusion imaging (MPI) per-patient and per-segment. CTA was assessed for $> 50\%$ stenosis per vessel and compared to stress/rest SPECT. Combined CTA/CTP approach was tested using vessel territory-based method.

Results: CTP demonstrated an sensitivity of 92% and 89%, specificity of 95% and 99%, positive predictive value (PPV) of 80% and 82%, and negative predictive value (NPV) of 98% and 99% on a per-patient and per-segment basis, respectively. The intermodality agreement of CTP to SPECT-MPI was $\kappa = 0.82$ ($p < 0.001$). CTA showed an accuracy of 92%, sensitivity of 70.4%, specificity of 95.5%, PPV

67.8%, and NPV of 95% as compared to SPECT-MPI. Addition of CTP findings to CTA improved the PPV from 67% to 90.1%, primarily by reduced false positives.

Conclusion: In patients presenting to the ED with CP, the evaluation of rest myocardial CTP demonstrates high diagnostic performance as compared to SPECT-MPI. Addition of CTP to CTA improves the diagnostic accuracy of CTA, primarily by reducing rates of false positive CTA.

B-0247 15:03

Perfusion deficits of the myocardium: a comparison of dynamic CT perfusion imaging and coronary computed tomography angiography

B.M. Gramer¹, D. Muenzel¹, P.B. Noel¹, V. Renz¹, M. Vembar², A.A. Fingerle¹, E.J. Rummeny¹, A. Huber¹; ¹Munich/DE, ²Highland Heights, OH/US

Purpose: To compare the potential of detection of myocardial perfusion deficits using CT dynamic myocardial perfusion imaging (MPI) and "single shot" coronary CT angiography (CCTA) for detection of hypoperfused myocardium in an animal model.

Methods and Materials: 8 pigs underwent rest CT MPI (100 kV, 150 mAs) and retrospectively ECG-gated CCTA (120 kV, 210 mAs) using a 256-slice multidetector computed tomography scanner (MDCT). Complete balloon occlusion of a coronary artery (LAD n=4, LCX=2, diagonal branch n=1) was induced. Attenuation values of post-stenotic and normal myocardium were compared intra-individually for MPI and CCTA. Image noise and signal-to-noise-ratio (SNR) for normal myocardium and hypoperfused myocardium were assessed.

Results: Mean densities between both groups were not significantly different for CCTA (136.8 ± 15.5 HU) and MPI (137.6 ± 11.9 HU) at peak enhancement ($p = 0.976$). Hypoperfused territories showed significantly lower HU compared to remote myocardium in the septum and lateral wall in CCTA (56.1 ± 34.1 HU vs 134.6 ± 12.0 HU and 139.1 ± 18.9 HU, respectively, $p < 0.0001$) and MPI (42.0 ± 26.2 HU vs 138.1 ± 11.7 HU and 135.0 ± 13.8 HU respectively, $p < 0.0001$). Image noise was 17.4 ± 4.7 HU in CCTA and 11.0 ± 3.6 HU in MPI, $p < 0.001$. SNR was higher in MPI (15.0 ± 9.9) compared to CCTA (8.3 ± 2.1), $p < 0.05$.

Conclusion: Hypoperfused coronary territories supplied by completely occluded arteries can be detected in both single shot CCTA at one time point and with dynamic CT MPI.

B-0248 15:12

Myocardial perfusion imaging using adenosine-induced stress dual energy computed tomography of the heart: comparison with single-photon emission computed tomography and conventional coronary angiography

S. Qu, S.-n. Li, G.-m. Peng, Y.-x. Guo; Guangzhou/CN (lhq2008xxh@163.com)

Purpose: To evaluate the feasibility and diagnostic accuracy of adenosine-stress dual energy computed tomography (DECT) for detecting haemodynamically significant stenosis causing reversible myocardial perfusion defect (PD) compared with SPECT myocardial perfusion imaging (SPECT-MPI) and conventional coronary angiography (CCA).

Methods and Materials: Thirty-four patients with known coronary artery disease (CAD) detected by dual source CT (DSCT) were investigated by contrast-enhanced, stress DECT with high- and low-energy x-ray spectra settings during adenosine infusion. Dual source computed tomography (DSCT) was performed as follows: 1) stress CT: contrast-enhanced scan during adenosine infusion; 2) rest CT: contrast-enhanced scan using prospective triggering.

Results: The DSCT protocol was successfully completed for 33 of 34 subjects (average age 55.4 ± 10.7 years; 82% male; body mass index 24 ± 3 kg/m²) with an average radiation dose of 12.7 mSv. A total of 561 myocardial segments and 99 vascular territories of 34 patients were analysed. 249 segments and 59 vascular territories in 29 patients showed reversible PDs on stress DECT. Stress DECT had 89% sensitivity, 78% specificity and 82% accuracy for detecting segments with reversible PDs seen on SPECT-MPI (n = 28). Compared with CCA (n = 29), stress DECT had 89% sensitivity, 76% specificity and 83% accuracy for the detection of vascular territories with reversible myocardial PDs that had haemodynamically relevant CAD.

Conclusion: Adenosine stress CT can identify stress-induced myocardial perfusion defects with diagnostic accuracy comparable to SPECT, with similar radiation dose and with the advantage of providing information on coronary stenosis.

B-0249 15:21

Benefit of combining quantitative cardiac CT parameters with troponin I for predicting right ventricular dysfunction and adverse clinical events in patients with acute pulmonary embolism

M. Meyer, C. Fink, S. Roeger, P. Apfaltrer, D. Haghi, W. Kaminski, M. Neumaier, S.O. Schönberg, T. Henzler; *Mannheim/DE (mr.meyer.mathias@gmail.com)*

Purpose: To prospectively evaluate the diagnostic accuracy of quantitative cardiac CT parameters alone and in combination with troponin I for the assessment of right ventricular dysfunction (RVD) in patients with acute pulmonary embolism (PE).

Methods and Materials: This prospective study had institutional IRB approval and was HIPAA compliant. 598 consecutive patients with suspected PE underwent pulmonary CT angiography. In total, 83 patients with confirmed PE underwent echocardiography and troponin I serum level measurements within 24 hours. Three established cardiac CT measurements for the assessment of RVD were obtained (RV/LVaxial, RV/LV4-CH, and RV/LVvolume). CT measurements and troponin I serum levels were correlated with RVD found on echocardiography and adverse clinical events according to MAPPET-3 criteria.

Results: 39 of 83 patients with PE had adverse clinical events and 31 of 83 patients had RVD on echocardiography. A RV/LVvolume ratio > 1.43 showed the highest area under the curve (AUC) (0.65) for the prediction of adverse clinical events when compared to RV/LVaxial, RV/LV4Ch and troponin I (0.57-0.61). Patients with RVD showed significantly ($p=0.0001$ - $p=0.042$) higher RV/LV ratios and troponin I levels compared to those without RVD. The AUC of RV/LVaxial, RV/LV4Ch, RV/LVvolume, and troponin I for the detection of RVD were 0.86, 0.86, 0.92, and 0.69, respectively. A combination of RV/LVaxial, RV/LV4Ch, RV/LVvolume with troponin I increased the AUC to 0.87, 0.87 and 0.93, respectively.

Conclusion: A combination of cardiac CT parameters and troponin I measurements improves the diagnostic accuracy for detecting RVD and predicting adverse clinical events if compared to either test alone.

14:00 - 15:30

Room N/O

Vascular

SS 215

New aspects in vascular imaging

Moderators:

V. Cantisani; *Rome/IT*

P. Vilares Morgado; *Porto/PT*

B-0250 14:00

Estimated radiation dose reduction for prospective electrocardiography-triggered dual source CT angiography of the thoracic aorta using iterative reconstruction: a prospective study

P. Blanke, S. Bulla, G. Pache, B. Rylski, M. Langer; *Freiburg/DE (philipp.blanke@uniklinik-freiburg.de)*

Purpose: To prospectively investigate image quality and radiation dose reduction for prospective ECG-triggered sequential dual source (DS) CTA using iterative reconstruction of the thoracic aorta in comparison to prospective ECG-triggered sequential dual source (DS) CTA with standard filtered back-projection (FBP).

Methods and Materials: Two-hundred and sixty consecutive patients referred for ECG-assisted DS CTA of the thoracic aorta were prospectively enrolled. Tube voltage was adjusted to body mass index (< 25.0 kg/m², 100 kV, n=95; 25.0 kg/m², 120 kV, n=165). Patients were randomly assigned to a CT-protocol with reduced reference tube current of either 100, 150 or 200 mAs/rot employing iterative reconstruction and were compared to a reference cohort previously examined with our institutional standard protocol (250 mAs/rot, FBP). Image noise and subjective image quality were assessed. Effective radiation dose was calculated from the dose-length product.

Results: Mean estimated effective dose was significantly lower for protocols with reduced tube current (200, 150, 100 mAs/rot) compared to the standard protocol with 250 mAs/rot (100 kV, 1.6±0.4mSv, 1.2±0.3mSv, 0.8±0.3mSv vs. 1.9±0.6mSv, $p < 0.001$; 120 kV, 3.9±1.1mSv, 2.9±0.9mSv, 1.8±0.4mSv vs. 4.7±1.1mSv, $p < 0.001$). With decreasing tube current, image noise increased but did not reach level of the standard protocol. Subjective image quality decreased with decreasing tube current, but image quality of the 100 mAs/rot subgroups was equivalent to the standard protocol (100 kV, 1.9 vs. 2.0; 120 kV, 2.0 vs. 2.0, $p=n.s$).

Conclusion: Iterative reconstruction allows for reduction of applied tube current and thereby for dose reduction of approximately 60% in CTA of the thoracic aorta while maintaining objective and subjective image quality when compared to a standard protocol with filtered back-projection.

B-0251 14:09

Clinical evaluation and potential radiation dose reduction of the novel sinogram-affirmed iterative reconstruction technique (SAFIRE) in abdominal computed tomography angiography

C. Schabel¹, D. Ketelsen¹, M. Fenchel¹, B. Schmidt², T.G. Flohr², A. Korn¹, C. Thomas¹, C.D. Claussen¹, M. Heuschmid¹, C. Schraml¹; ¹Tübingen/DE, ²Forchheim/DE

Purpose: To evaluate the novel sinogram-affirmed iterative reconstruction algorithm (SAFIRE) with respect to clinical usability and potential reduction of radiation exposure.

Methods and Materials: Forty-six patients underwent routine contrast-enhanced CT follow-up after endovascular aneurysm repair. The examination was performed with a dual source CT running both x-ray tube detector systems at the same voltage. Raw data were reconstructed using the projections of both tubes (FD) with filtered back projection (FBP) and using only the projections of one tube (HD) with FBP and SAFIRE, corresponding a synthetic half-dose acquisition. Image sets were objectively compared with regard to image noise and edge sharpness. Two independent radiologists assessed a set of subjective criteria.

Results: HD SAFIRE images showed significantly lower noise than FD FBP ($p < 0.0001$) and equal edge sharpness ($p=0.56$). Most of the subjectively assessed parameters, like diagnostic usability and depiction of contrasted vessels, were rated similar in HD Safire and FD FBP images. FD FBP images depicted fine anatomic structures more clearly ($p < 0.05$) while HD SAFIRE datasets had subjectively less noise ($p < 0.001$). HD FBP images were significantly worse in every subjective and objective criterion ($p < 0.001$). The image texture of the HD SAFIRE reconstructed images was regarded equal to FD FBP datasets. Inter-rater agreement was found to be good (FD FBP $\kappa=0.74$, HD FBP $\kappa=0.8$, HD SAFIRE $\kappa=0.77$).

Conclusion: Using the SAFIRE algorithm, the radiation dose of high-contrast abdominal CTA can be reduced from a routine clinical level by up to 50% while maintaining good image quality and diagnostic accuracy.

B-0252 14:18

Higher iodine concentration permits dose reduction while increasing contrast-to-noise-ratio in high-pitch, wide-range CT angiography

F. Schwarz, K. Grandl, A. Arnoldi, W.H. Sommer, F. Bamberg, M.F. Reiser, C.H. Becker; *Munich/DE (florian.schwarz@med.lmu.de)*

Purpose: To compare contrast-to-noise-ratio (CNR) and effective dose at different iodine concentration in high-pitch, wide-range CT-angiography.

Methods and Materials: All scans were performed on a 128-slice CT-system using a high-pitch acquisition technique ($p=3.2$). A software algorithm optimising kV and mAs settings on the basis of adjustable reference values and attenuation on the initial topogram was applied. Two scan protocols were compared: Protocol_A used 300 mg/ml contrast injected at 4.0 ml/sec and reference values for kV and mAs set to 120 and 330. Protocol_B used 400 mg/ml contrast injected at 4.0 ml/sec and reference values for kV and mAs set to 120 and 275. 100 patients who had undergone CT-angiography of the chest, abdomen and pelvis using either protocol_A (n=50) or protocol_B (n=50) were included in this analysis. Two readers measured intravascular enhancement and standard deviation at 18 different points within the arterial system. For dose estimation, the dose-length-product (DLP) was recorded.

Results: There were no significant differences in sex-ratio or BMI (25.5 vs. 26.2, $p=0.72$) between both groups. Automatic kV selection used 100 kV, 120 kV and 140 kV in 5, 19 and 26 patients in group A and in 17, 30 and 3 patients in group B ($p < 0.05$). Overall, datasets of group B showed significantly higher levels of noise (27 HU vs. 20.6 HU, $p=0.0001$) but also of signal (334 HU vs. 208 HU, $p=0.0001$), resulting in higher CNR in group B (12.8 vs. 10.8, $p < 0.05$). Applied DLP was significantly lower in group B (370 vs. 595 mGycm, $p=0.01$).

Conclusion: In high-pitch, wide-range CT-angiography, higher iodine concentration permits significant dose reductions while increasing contrast-to-noise-ratio.

B-0253 14:27

Low-dose multidetector-row CT angiography in the evaluation of infrarenal aorta and peripheral arterial occlusive disease

M. Nestola, R. Iezzi, M. Santoro, R. Marano, C. Di Stasi, L. Bonomo; *Rome/IT*

Purpose: To investigate the possibility to reduce x-ray exposure during CTA of peripheral arteries and to evaluate the impact of radiation dose on diagnostic accuracy. We also compared the diagnostic performance achieved by three CTA acquisition protocols using pre-treatment DSA as gold standard.

Methods and Materials: We performed a prospective, single-centre, randomised comparison of 3 different x-ray exposure CT-acquisition protocols enrolling 60

patients with PAOD referred to our department to undergo a lower limb 64-MDCT angiography (0.625 mm-collimation; 100 ml iomeprol 400 mgI/mL; @4 ml/s). Patients were randomised into three x-ray exposure acquisition protocols: A (standard-dose): noise-index: 26 (SMARTmA); 120 KV; B (low-dose): noise-index: 26 (SMARTmA); 80 KV; C (ultra-low-dose): noise-index: 30 (SMARTmA); 80 KV. Axial and 3D-images were qualitatively and quantitatively compared. The three protocols were also compared in terms of diagnostic performance using pre-interventional DSA as gold standard.

Results: Statistically significantly higher attenuation values were measured in the low-dose and ultra-low-dose acquisition protocol. Qualitatively, image quality was judged slightly better with the standard protocol than with the low-dose and ultra-low-dose protocol without significant differences on 3D images. No significant differences were found between the three protocols in terms of contrast-to-noise ratio (CNR). No significant differences were also found among the three groups of patients concerning the diagnostic performance. An overall dose reduction of 48% and 64% was observed for the low-dose and ultra-low-dose protocol, respectively. **Conclusion:** Ultra-low-dose MDCT-angiography of peripheral arteries provides substantially reduced radiation exposure while maintaining a constant CNR, good image quality and an adequate diagnostic performance.

B-0254 14:36



Imaging findings in a distinct lethal inherited arteriopathy syndrome associated with a novel mutation in Fibulin4 gene

R. Rajeshkannan¹, K. Mahesh¹, C. Kulkarni¹, S. Moorthy¹, K.P. Sreekumar¹, A.D. paepe², S. Nampoothiri¹; ¹Cochin/IN, ²Gent/BE (rajeshkr@aims.amrita.edu)

Purpose: We present the imaging findings of a new lethal inherited arteriopathy syndrome associated with novel mutation in FBLN4 gene occurring in a distinct community from South India.

Methods and Materials: Twenty-four infants from a distinct population subgroup, presenting with characteristic arterial dilatation and tortuosity during the period August 2004 to August 2011 were studied. All infants belonged to unrelated families from an ethno-religious group (Muslim) from the northern coastal belt of the southern Indian state of Kerala. All patients underwent 64 slice CT angio and echocardiography.

Results: Dilatation and elongation of aortic root, arch, descending aorta and main pulmonary arteries with narrowing of isthmus were seen in all patients. Folding of the elongated thoraco abdominal aorta was seen in all patients. Stenosis of arch branches, abdominal visceral branches and pulmonary artery branches were seen in 13 (54%), 15 (62.5%) and 11 (46%) cases, respectively. Cerebral arterial involvement was seen in 9 (82%) out of 11 cases scanned. In 9 (90%) out of 10 patients who were more than 8 months old showed poor opacification of distal aorta in the first run due to slow circulation. Echo showed very slow forward flow in dilated arteries. Genetic studies revealed an identical c.608 A>C (p.Asp203 Ala) mutation in exon 7 of the FBLN4 gene in all 24 patients.

Conclusion: We describe imaging findings of a new lethal arteriopathy syndrome from a distinct population subgroup.

B-0255 14:45

Perfusion system for ex-vivo investigation of human vessels

G. Edelhauser, G. Erman, C. Domenig, D. Berzaczky, M. Popovic, R. Borny, J. Lammer, M. Funovics; Vienna/AT (gundula.edelhauser@meduniwien.ac.at)

Purpose: For the understanding of biological processes in the vessel wall after interventional procedures, an ex-vivo tissue culture model of human vascular segments accessible to interventional procedures and sufficient cultivation time to study their effects is highly desirable. We developed a system to suit these requirements and assessed morphologic characteristics of cultivated human vessel segments for up to 15 days.

Methods and Materials: 15 saphenous vein segments were harvested from patients undergoing bypass surgery of the leg. The vessel segments were placed in a customised glass chamber connected to a regulated roller pump. Customised culture medium was pumped at a set flow rate and transmural pressure. The vessel segments were cultured for 5 and 15 days. The samples were histologically examined with uncultivated segments of the original vessel serving as controls. Morphology and integrity were investigated after transmission electron microscopy and immunohistochemistry for CD31, 1 A4 and Ki 67.

Results: 14 samples were cultivated without detectable infection for the planned time period. Temperature, medium pH, and transmural pressure remained constant during the cultivation. Compared to the controls, medial thickness remained within 10% of the original values, no changes in elastin content, intimal morphology, or receptor distribution and density were detectable.

Conclusion: An ex-vivo tissue culture model was created that can maintain basic biomorphology and receptor status of human venous segments in vitro over 15 days. This model potentially allows for long-term investigation of human vessel segments including studying the effects of interventional procedures in a convenient, cost-effective, controlled environment.

B-0256 14:54

Interobserver agreement of whole body MR angiography for the depiction of atherosclerosis

T.C. Lauenstein, C. Odenhausen, A. Quinsten, M. Forsting, S. Ladd; Essen/DE (thomas.lauenstein@uni-due.de)

Purpose: To evaluate the interobserver agreement for the depiction of arteriosclerotic changes in different anatomical areas as a marker for the quality of MR angiography (MRA).

Methods and Materials: 25 patients were referred for whole body MRA either for screening purposes or for suspected atherosclerotic disease. Imaging was performed on a 1.5-T MR system (Magnetom Avanto, Siemens). For signal reception a combination of several surface coils was used. After the intravenous injection of Gadobutrol (Gadovist, Bayer; weight-adjusted dose of 0.1 mmol/kg) four to five overlapping 3D GRE T1w sagittal data sets were collected from head to the calves. Images were evaluated by two readers independently for the presence of stenotic lesions in 40 arterial segments using a 5-point scale (0-no stenosis; 1-stenosis < 50% of vessel diameter; 2-stenosis 50-90%; 3-stenosis 90-99%; 4-occlusion). Interobserver agreement was calculated using the Cohen's kappa value.

Results: 1000 arterial segments were assessed. Mean Kappa value amounted to 0.84. Lowest Kappa values were found for the assessment of the aortic arch (0.58) and the ascending aorta (0.61). Highest Kappa values (1.0) were found for the evaluation of the iliac and femoral arteries.

Conclusion: Interobserver agreement of MRA differs substantially within various anatomical segments. The only moderate values for the thoracic aorta may be explained by the complex depiction of the vessel wall due to (cardiac) motion artefacts. However, large arteries in the pelvic and femoral region proved best agreement probably because of an easy and robust delineation.

B-0257 15:03

Intraindividual comparison of whole body MR angiography at 1.5 and 3 Tesla in high risk patients with hereditary hyperlipidaemia

C. Weber, J. Buhk, T. Bley, A.-K. Fink-Wedel, A. Kooops, G. Adam, P. Bannas; Hamburg/DE (c.weber@amalie.de)

Purpose: To prospectively and intraindividually compare image quality and detectability of stenoses in contrast-enhanced whole body MRA (WBMRA) at 1.5 and 3 Tesla (T) in patients with hereditary hyperlipidaemia.

Methods and Materials: 27 patients with hereditary hyperlipidaemia received a 1.5 and 3 T gadobutrol contrast-enhanced WBMRA. 43 defined arterial segments were analysed regarding depiction of target vessels, image quality according to a 5-point scale ("not evaluable" to "excellent"), degree of stenosis (0%, 1-49%, 50-99% and 100%) as well as vessel alterations such as aneurysms. Wilcoxon-matched pair test and Chi-square test were performed for comparison of the two field strengths.

Results: 1.5 T and 3 T scans yielded high-quality WBMRA in all patients. Mean image quality of all arterial segments at 3.0 T was rated significantly higher (3.8 ± 0.9) to image quality at 1.5 T (3.6 ± 0.9) (p = 0.001). Field inhomogeneity artefacts deteriorated image quality at 3 T in 16 patients and venous overlay was described more often at 3 T (n=9) than at 1.5 T (n=3). All relevant stenoses (50-99%) (n=5), occlusions (n=6) and aneurysms (n=3) were evaluated similarly at both field strengths.

Conclusion: WBMRA can be performed at 1.5 and 3 T with diagnostic image quality. Due to technical drawbacks observed at 3 T, overall image quality was rated only modestly higher for 3 T examinations. In order to effectively take advantage of the higher field strength, further optimisation of sequence parameters and injection protocols for WBMRA at 3 T is necessary.

B-0258 15:12

Pulse wave velocity measurements in 5-point velocity encoded radially undersampled 4D phase contrast MR data (PC-VIPR)

A. Frydrychowicz¹, A.L. Wentland², K.M. Johnson², C.J. Francois², T.A. Grist², O. Wieben²; ¹Madison, WI/US, Lübeck/DE, ²Madison, WI/US (alex.frydrychowicz@uksh.de)

Purpose: Pulse wave velocity (PWV) is a non-invasive measure of vascular stiffness and biomarker of atherosclerosis. We compared four different measurements of

14:00 - 15:30

Room Q

Cardiac

SS 203b

Valvular and congenital heart diseases

Moderators:

M. Oudkerk; Groningen/NL

E. Woo; Aylesbury/UK

B-0260 14:00

Aortic valve calcium scoring (AVCS) is a predictor of significant paravalvular aortic insufficiency in transapical aortic valve implantation (TAVI)

L. Lehmkühl, M. Haensig, A.J. Rastan, J. Kempfert, C. Mukherjee,

D.M. Holzhey, M. Grothoff, F.W. Mohr, M. Gutberlet;

Leipzig/DE (lukas.lehmkuhl@med.uni-leipzig.de)

Purpose: Transapical aortic valve implantation (TA-AVI) has evolved as a routine for selected high-risk patients. However, paravalvular leaks remain an unsolved issue using current generations of transcatheter valve devices. The purpose of this study was to investigate the impact of native aortic valve calcification on paravalvular leaks and outcome using the Edwards SAPIENTM prosthesis and transapical approach.

Methods and Materials: 120 consecutive patients (out of 307 TA-AVIs) with preoperative computed tomography, age 82.6±6.2 years, 75.0% female, were included. Implanted prosthetic valve sizes were 23 mm (n=31), and 26 mm (n=89), respectively. Mean logistic EuroSCORE was 30.1±15.5 and mean STS-Score 12.8±7.9. ECG-gated cardiac CT allowed to quantify the amount of calcification of aortic valve leaflets using a scoring analogous to the Agatston calcium scoring of coronary arteries (AVCS). Paravalvular leaks were assessed intraoperatively by echocardiography and root angiography.

Results: All valves were implanted successfully. Mean AVCS in patients without paravalvular leaks (n=66) was 2704±1510, with mild paravalvular leaks (n=31) 3804±2739 (p=0.05) and with moderate paravalvular leaks (n=4) 7387±1044 (p=0.002). There was a significant correlation between AVCS and paravalvular leaks (r=0.334; p=0.001) and a trend towards a higher incidence of new pacemaker implantation (r=0.117, p=0.232). No correlation was found to 30-day mortality, major cardiac events and stroke-rate (r=0.040, p=0.671; r=-0.050, p=0.593 and r=-0.025, p=0.792).

Conclusion: Severe native valve calcifications are predictive for postoperative relevant paravalvular leak. AVCS prior to TA-AVI might serve as an additional tool to reconsider the TAVI indication to reduce the risk of paravalvular leaks especially in so-called operable patients.

B-0261 14:09

Morphological assessment of the aortic valve using cardiovascular computed tomography and cardiovascular magnetic resonance in patients with severe aortic stenosis: comparison with intraoperative finding

S. Bak, S. Ko, J. Choi, M. Song, J. Shin, H. Ji; Seoul/KR (20090057@kuh.ac.kr)

Purpose: To compare the accuracy of cardiovascular CT (CVCT) and cardiovascular MR (CMR) for the morphological assessments of the aortic valve (AV) in patients with severe aortic stenosis (AS) and to assess accuracy of the CVCT features differentiating between bicuspid AV (BAV) and tricuspid AV (TAV).

Methods and Materials: Ninety-four patients with severe AS underwent CVCT and CMR before surgery. Two radiologists assessed morphologic pattern as definite BAV, definite TAV, and borderline type. In borderline type on CVCT, uneven cusp size, round-shaped opening, midline calcification, and length of cusp fusion were analysed. Diagnostic accuracy of CVCT and CMR for discriminating BAV from TAV was compared with surgical finding.

Results: At surgery, 46 patients had TAV and 48 patients had BAV. Definite BAV, definite TAV or borderline type was present in 38, 41, and 15 patients on CVCT and 41, 40, and 13 patients on CMR. In borderline type on CVCT (BAV 11, TAV 4), only round-shaped opening was strongly associated with BAVs (P < 0.009). Sensitivity, specificity, positive and negative predictive values for assessment of AV morphology were 98%, 87%, 89%, 98%, respectively, on CVCT and 100%, 87%, 89%, and 100%, respectively, on CMR.

Conclusion: CVCT and CMR are accurate for differentiation between BAV and TAV in patients with severe AS. Further studies are needed for assessment of CVCT features differentiating between BAV and TAV in borderline AV type.

PWV based on radially undersampled 4-dimensional phase contrast (4D-PC) MRI using high-temporal-resolution 2D-PC as standard of reference.

Methods and Materials: In eighteen healthy volunteers (9men/9women; 38.4±14.8years; BMI<30) 5-point velocity-encoded 4D-PC-VIPR data and 2D-PC-MRI were acquired at 3 T with a 32-channel body coil. Key parameters were (4D/2D) 26-34/63±13 time frames and 1.5x1.5x1.5 mm/1.6x1.6x7 mm spatial resolution. 2D slices were prescribed from a contrast-enhanced MRA using 0.03 mmol/kg gadofosveset trisodium. 2D and 4D-PC data were analysed with a MATLAB-based software. PWV was computed using time-to-peak (TTP), time-to-foot (TTF), cross-correlation (XCorr), and time-to-upstroke (TTU). Bland-Altman analysis was used to compare 2D and 4D results and intra- and interobserver reproducibility (in 10/18 subjects). Data variability was assessed with a model of age-dependence. Residuals of data were compared with a Brown-Forsythe ANOVA test.

Results: Overall results (2D: 4.6-5.3m/s, 4D: 3.8-5.0m/s) were similar. Results based on different algorithms differed non-significantly with average biases: 1.8±3.15m/s (TTU), 0.68±3.98m/s (TTF), and 0.84±3.37m/s (XCorr). TTP showed significant differences with unphysiological values. Overall interobserver (0.30±2.83m/s) and intraobserver variability (0.01±2.51m/s) were low. Brown-Forsythe-test resulted in p=0.609 for TTU, TTF, and XCorr data indicating equal variability. Binning into age groups (><35years) revealed that TTU and XCorr (as opposed to TTF) were able to detect the expected increase with age.

Conclusion: PWV calculations from radially undersampled 4D-PC-VIPR are feasible and may thus be useful in comprehensive vascular diagnosis. TTU and XCorr were the preferred algorithms.

B-0259 15:21

Image quality and radiation dose of BMI-adjusted peripheral CT-angiography with 80/100 kVp compared to a standard protocol with 120 kV

K.M. May, M. Simon, F.M. Vogt, P. Hunold, J. Barkhausen, A. Kovacs;

Lübeck/DE (Katharina.may@uk-sh.de)

Purpose: To compare the image quality and radiation dose of a peripheral CT-angiography (pCTA) performed with low-kVp and BMI-adjusted mAs to the standard protocol.

Methods and Materials: Retrospective and prospective gained data of 111 patients receiving 128-slice-CTA were analysed. 54 patients analysed retrospectively, received a standard pCTA (120 kV, 250 mAs and CareDose) of those 14 were assigned to BMI-group.i. < 25 kg/m², 28 to BMI-group II 25-30 kg/m² and 12 to BMI-group III > 30 kg/m². 57 patients included prospectively were examined with a BMI-adjusted protocol: group.i. (n=16) using 80 kV/200 mAs, II (n=28) 80 kV/250 mAs and III (n=13) 100 kV/250 mAs, respectively. Contrast administration was identical in all patients (80 ml Iomeprol® 400, 50 ml NaCl 0.9%, flow-rate 4 ml/s). The arterial enhancement (SI), SNR, CNR and the image quality (5-Point-Scale) were analysed at 7 defined levels of the peripheral arteries. The effective radiation dose was calculated for all scans.

Results: The arterial enhancement was significantly higher (mean 345 HU vs 232 HU) at all vascular levels using the low-kVp protocols. Although background noise level significantly increased, SNR and CNR were comparable and the image quality was non-inferior to the standard protocol. The modified protocol significantly reduced the radiation dose in all BMI-groups: group.i. (2±2 vs 7±2mSv; p<.0001), II (5±1 vs 10±2mSv; p<.0001) and group III (11±1 vs 20±3mSv; p<.0001).

Conclusion: The image quality of pCTA with low-kVp and BMI-adjusted tube current is not compromised when compared to a standard protocol. However, radiation dose can significantly be reduced by 40-63% depending on the patients BMI.

B-0262 14:18

Cardiac magnetic resonance for evaluation of bicuspid aortic valve morphology

R. Faletti¹, G. Schivazappa¹, A. Paolino¹, F. Angelino¹, F. Cesarani², G. Gandini¹; ¹Turin/IT, ²Asti/IT (riccardo_faletti@yahoo.it)

Purpose: The most common aortic valve abnormality is the bicuspid aortic valve (BAV) (1-2%). The role of CMR to evaluate aortic valve morphology, diameters of the ascending aorta and the arrangement of the sinuses of Valsalva was investigated.

Methods and Materials: Forty-two of 134 consecutive patients with aortic diseases who underwent CMR presented with BAV. BAV were presented with different phenotypes: BAV without raphe and BAV with raphe. Within these subgroups different phenotypes are identified: BAV without raphe is subdivided into AP (antero-posterior) and LA (lateral-anterior). In BAV with raphe we have identified 3 phenotypes: RL (left and right cusp fusion), RN (fusion of right and non-coronary cusp) and LN (fusion of the left and non-coronary cusp). The results were compared with recent literature. We also evaluate the possible association between BAV and ascending aorta dilatation.

Results: We observed prevalence of BAV with raphe (71.43%), and within this group, the phenotype RL (76.67%). The results have shown partly in agreement with the study of Buchner and colleagues. Both studies showed the prevalence of the group with BAV with raphe (71.43% in our study, 85.71% for Buchner, $p = 0.07$) and the subgroup RL (76.67% vs 84.44%, $p = 0.49$). In our study prevalence AP phenotype (75%) vs LA (73.3%). There was no significant correlation ($p = 0.66$) within BAV and ascending aorta dilatation.

Conclusion: CMR is currently the most complete imaging technique for classification and characterisation of BAV.

B-0263 14:27

MR assessment of pulmonary (QP) to systemic (QS) flow using 4D phase contrast technique: comparison with conventional through-plane 2D phase contrast technique

B.J. Wintersperger, M. Sivagnanam, N.S. Paul, D. Diva, E. Nguyen, A.M. Crean, L. Jimenez Juan, R.M. Wald, S. Ley; Toronto, ON/CA (Bernd.Wintersperger@uhn.ca)

Purpose: To evaluate 4D phase contrast (PC) MRI in assessment of possible intracardiac shunts by simultaneous assessment of pulmonary (Qp) and systemic (Qs) flow.

Methods and Materials: 21 patients with suspicion of intracardiac shunts underwent cardiac MRI at 1.5 Tesla. Assessment of Qp and Qs was performed using free-breathing retro-gated 2D PC GRE (1.6x1.6x5 mm³; TR 40 ms) imaging with 1D through-plane velocity encoding gradient (venc=150 cm/s) in consecutive measurements for the main pulmonary artery (MPA) and ascending aorta (AA), respectively. In addition, a prospectively triggered 3D PC GRE technique (2.4x1.8x3 mm³; TR 46 ms) with three orthogonal venc directions was employed with volume coverage of MPA and AA. 2D PC GRE was post-processed using a commercially available software algorithm and 4D PC GRE was analysed using custom-built software. Both approaches were compared for absolute Qp and Qs values and Qp/Qs ratio.

Results: Heart rates during 2D PC measurements for AA and MPA were 70.4±14.5 bpm and 68.5±11.5 bpm, respectively ($P=0.146$) while heart rate during 4D PC was significantly lower (65.5±10.7 bpm; $P < 0.005$). Qp assessed by 4D PC correlated highly with the 2D PC ($R=0.92$; $P < 0.0001$) but demonstrated a significant systematic and random error (-21.9±12.2 ml; $P < 0.0001$). 4D PC Q values also demonstrated high correlation ($R=0.67$; $P < 0.0001$) with significant systemic and random error (-10.7±13.1 ml; $P=0.0023$). Resulting Qp/Qs ratios of 4D and 2D PC acquisitions showed high correlation ($R=0.78$; $P < 0.0001$) and no significant differences (1.19±0.51 vs. 1.28±0.51; $P=0.14$).

Conclusion: 4D volumetric PC flow assessment allows for accurate assessment of Qp/Qs ratios in the evaluation of possible intracardiac shunts. Further investigations of the accuracy of individual flow volumes are warranted.

B-0264 14:36

Computed tomography evaluation of possible intraprocedural obstruction of the coronary ostia by the aortic valve leaflets during transapical aortic valve implantation

L. Lehmkühl, B. Foldyna, K. von Aspern, M. Haensig, C. Luecke, C. Andres, S. Nitzsche, M. Grothoff, M. Gutberlet; Leipzig/DE (lukas.lehmkuehl@med.uni-leipzig.de)

Purpose: To compare the distance of the coronary ostia from the basal attachment of the aortic valve leaflets and the length of the aortic valve leaflets prior to transapical

cal valve implantation (TA-AVI) with focus on possible, intraprocedural obstruction of the coronary ostia using computed tomography (CT).

Methods and Materials: CT scans of 56 patients (40/16 m/w, mean age 81±6.8y) with severe AS, scheduled for TA-AVI were included retrospectively. Distances of the coronary ostia to the aortic annulus were measured in systolic and diastolic phase and compared to the leaflet length measured in diastolic phase. Possible overlap distance (POD) was calculated using pairwise analysis.

Results: The mean POD indicated the risk of a potential occlusion of parts of the right coronary artery (RCA) ostium by the right leaflet (POD 1.7 ±2.2 mm, $p < 0.001$) due to the TA-AVI procedure. The mean distance from the most basal attachment of the LCL to the left coronary ostium did not differ significantly ($p = 0.66$) from the mean LCL length with a mean difference of 0.2 (±2.7) mm.

Conclusion: Right coronary leaflet may theoretically overlap and occlude a large part of the RCA ostium due to the TA-AVI procedure.

B-0265 14:45

Right ventricular hypertrophy after atrial switch operation and its role in a systemic RV: normal adaptation process or risk factor? A cardiovascular magnetic resonance study

M. Grothoff, J. Hoffmann, M. Gutberlet; Leipzig/DE (Matthias.Grothoff@herzzentrum-leipzig.de)

Purpose: Systemic RV hypertrophy and impaired systolic function occur after atrial switch (AS) in d-transposition of the great arteries (d-TGA). Echocardiography has limitation in the assessment of the right ventricle (RV). In this study, we sought to evaluate systemic RV myocardial mass and function after AS for d-TGA and to analyse the role of excessive hypertrophy for ventricular function under special consideration of the interventricular septal (IVS) movement.

Methods and Materials: Thirty-seven patients after AS were studied at a 1.5 T scanner (Intera CV, Philips) using a dedicated 5-channel-phase-array surface cardiac-coil. Cine steady-state-free-precession sequences were acquired to obtain biventricular myocardial masses and function. The systolic movement of the IVS was defined as positive (PSM), when moving towards the centroid of the RV, or else as non-positive. Patient parameters were compared to age-matched controls.

Results: Systemic RVs were significantly larger ($p < 0.001$) than LVs of the control group, systolic function significantly impaired ($p < 0.001$) and myocardial mass index (MMI) was comparable ($p = n.s$). RV-MMI and RV-EF demonstrated a quadratic correlation ($r=0.6$, $p < 0.001$), meaning that patients with RV-MMI below 29 g/m² and above 68 g/m² had a reduced systolic function. Patients with PSM had a better RV function compared with the non-PSM subgroup ($p=0.024$).

Conclusion: A certain amount of RV hypertrophy after AS is a normal adaptation process after AS and a sufficient RV-EF can be expected within a range of 29-68 g/m². PSM is probably the result of hypertrophic septal RV fibres, which is beneficial for RV function and might be regarded as the physiological contraction pattern.

B-0266 14:54

Cardio-vascular MSCT angiography in newborns with known or suspected congenital heart disease applying mean effective doses of 0.36 mSv

T. Klink, G. Müller, J. Weil, G. Adam, T.A. Bley; Hamburg/DE (t.klink@uke.uni-hamburg.de)

Purpose: To investigate the diagnostic capability of cardio-vascular 256-MSCT angiography in cardio-pulmonary compromised newborns and infants with suspected or known congenital heart disease, and to compare different scan protocols with regard to radiation doses.

Methods and Materials: Nine newborns and infants (mean weight, 3700 g ±1800; age range 7 days to 8 months) were included in this retrospective study. Clinically indicated, non-ECG-triggered, cardio-vascular CTA was performed utilising a 256-MSCT scanner. Vendor-specific preset scan protocols were initially used and progressively adapted. Images were acquired with helical or a single axial rotation scan and tube voltages of 120 kV or 80 kV, respectively. Two observers evaluated thoracic cardiovascular findings and image quality. Effective radiation doses were estimated from dose length product.

Results: All major cardio-vascular defects could be detected, and all images were of diagnostic quality. Two small atrial septal defects and one persistent foramen ovale were seen on echocardiography only. Image quality of axial scans covering the entire heart and great thoracic vessels within a single rotation were superior to images acquired with a helical scanning protocol. Reducing the tube voltage from 120 kV to 80 kV resulted in a mean effective dose of 0.36mSv ±0.09.

Conclusion: Cardio-vascular CT examinations can be performed in cardio-pulmonary compromised newborns and infants with radiation doses as low as 0.36mSv and diagnostic image quality. A protocol utilising a single-shoot, axial, non-ECG triggered 256-MSCT scan is most favourable. Tube voltage of 80 kV reduced radiation significantly without relevant degradation of image quality when studying the heart and great thoracic vasculature.

B-0267 15:03

In-vivo imaging characteristics of a transcatheter heart valve prosthesis with multislice computed tomography

L.M. de Heer, J. Habets, J. Kluin, W.P.T.M. Mali, P.R. Stella, L.A. van Herwerden, R.P.J. Budde; *Utrecht/NL (L.M.deheer-2@umcutrecht.nl)*

Purpose: Transcatheter heart valve (THV) prostheses are explored as an alternative to conventional aortic valve replacement. Post-implant echocardiographic follow-up findings can be complemented by multislice computed tomography (MSCT). However, little is known on image quality (IQ) of these stented THV prostheses that may be hampered by metal induced artefacts. We assessed the CT image quality of the commonly implanted Edwards Sapien THV prosthesis (with a cobalt-chromium stent) in patients after transcatheter aortic valve implantation (TAVI).

Methods and Materials: Twenty-two patients after TAVI underwent retrospectively ECG-gated cardiac CTA on a 256-slice CT-scanner (120 kV, 250-600 mAs). After reconstruction in three perpendicular planes, The general IQ and IQ of the supra-prosthetic, sub-prosthetic, peri-prosthetic, intra-prosthetic and valvular regions was scored on a four-point scale (1=non-diagnostic, 2=moderate, 3=good and 4=excellent) in the best systolic and diastolic phase.

Results: Twenty-two patients underwent a cardiac CTA (12 female patients, age 79±9 years). Mean heart rate during scanning was 74±12 beats per minute. The general IQ score was moderate (23%) and good (77%) during systole and moderate (23%), good (68%) and excellent (9%) during diastole (p=0.7). A significant difference between the systolic and diastolic IQ in the supra-prosthetic (diastolic better, p < 0.001), peri-prosthetic (systolic better, p=0.004) and intra-prosthetic region (systolic better, p=0.005) existed. A significant correlation between the heart rate and general systolic IQ was present (p=0.03).

Conclusion: The commonly implanted Edwards Sapien THV prosthesis and the peri-prosthetic regions can be visualised with moderate to good image quality by MSCT, despite the presence of a cobalt-chromium stent frame.

B-0268 15:12

The diagnostic value of dual source CT in complex congenital heart disease

S.-X. Qu, D.-S. Luo, G.-M. Peng, M. Qian; *Guangzhou/CN (lhq2008xxh@163.com)*

Purpose: To discuss the diagnostic value of three-dimensional reconstructed technique with contrast enhancement of dual source CT (DSCT) in complex congenital heart disease (CCHD).

Methods and Materials: The MSCT data of 121 patients with CCHD confirmed by surgery were retrospectively analysed. All patients were performed with transthoracic echocardiograms (TTE) and 68 were compared with cineangiocardiograms (CAG) before surgery.

Results: A total of 425 cardiac deformities were found by operation. The accuracy of DSCT, TTE and CAG in detecting deformities was 96.9%, 71.3%, and 95.8%, respectively. There were 238 intracardiac deformities, 4 missed by DSCT, 3 missed by TTE, and 1 missed by AG. There was no significance difference in diagnosis accuracy with three methods (P> 0.05). There were 187 extracardiac anomalies. The definite diagnosis rate of MSCT, TTE and CAG for extracardiac anomalies were 97.5%, 56.2%, and 96.6%, respectively. MSCT and CAG were superior to TTE in the identification of extracardiac deformities (P < 0.01), and the diagnosis accuracy of MSCT and CAG showed no difference (P> 0.05). MSCT combined with TTE could increase the definite diagnosis rate to 98.3%.

Conclusion: MSCT may be used to clearly display the pathologic anatomy of CCHD, which is superior to TTE remarkably in the diagnosis of extracardiac anomalies. Therefore, as a non-invasive technique, MSCT has a very higher diagnostic value in CCHD.

B-0269 15:21

X-ray-induced DNA double-strand breaks in lymphocytes of children undergoing cardiac flat-panel CT and angiography

M. Brand, M. Gloeckler, M. Sommer, C. Engert, M. Uder, M.A. Kuefner; *Erlangen/DE (michael.brand@uk-erlangen.de)*

Purpose: Flat-panel CT (DynaCT®) enables CT-like cross-sectional imaging by creating 3D soft tissue data sets by rotation of the detector around the patient's

body. Purpose of this study was to investigate the effect of cardiac flat-panel CT on x-ray-induced DNA double-strand breaks (DSBs) in blood lymphocytes in children.

Methods and Materials: Blood samples were obtained from thirteen children before and 5 minutes after cardiac flat-panel CT. Lymphocytes were isolated, stained against the phosphorylated histone variant H2 AX, and foci representing DSBs were visualised using fluorescence microscopy. Dose area product (DAP) was registered as provided by the patient protocol.

Results: DAP ranged from 50.5 to 1070.5 μGym^2 (median 304.4 DSB/cell). DSB levels ranged from 0.06 to 0.29/cell (median 0.11 DSB/cell) before, and from 0.08 to 0.36/cell (median 0.15 DSB/cell) after flat-panel-CT, the increase of DSBs was statistically significant (p=0.0002). A correlation was obtained between the induced DSB and the DAP (r=0.60).

Conclusion: In every patient a significant increase of DSBs was detectable after flat-panel-CT. x-ray induced DSBs depend on the delivered dose. In conclusion, immunofluorescence microscopy is a valid method to detect distinct DNA damages even after rather low diagnostic doses and therefore it can be used as a measure of biological radiation effects.

Friday, March 2

10:30 - 12:00

Room D1

Chest

SS 504

CTPA, dual energy and dose reduction

Moderators:

T. Frauenfelder, Zurich/CH

B. Ghayé, Brussels/BE

B-0270 10:30

Evaluation of dual energy CT lung perfusion-maps: a correlation with V/Q scan and lung parenchymal changes

M. Lefere, M. Demeter, F. De Keyzer, J. Coolen, J. Verschakelen, W. De Wever; Leuven/BE (mathieu.lefere@uzleuven.be)

Purpose: Dual energy computed tomography (DECT) perfusion-maps can be used to visualise pulmonary perfusion in the diagnostic work-up of pulmonary embolism (PE) and other pulmonary diseases. Study purpose are: (1) to observe inter-observer variability in perfusion-map reading, (2) to compare perfusion-maps with V/Q scan, (3) to correlate perfusion-defects (PD) with lung-parenchymal changes on DECT-images.

Methods and Materials: Twenty-six patients underwent DECT angiography and V/Q scan to exclude PE. DECT perfusion maps were evaluated by two radiologists. Iodine distribution patterns were rated as homogeneous perfusion (HP), wedge-shaped defect (WSD), patchy defect (PaD), circumscribed defect (CD) or artefact. Dual energy perfusion findings were correlated with CT findings (normal, emphysema, mosaic-perfusion, ground-glass opacities (GGO), and consolidation) and V/Q findings (normal, perfusion defect (PD) with and without ventilation defect (VD)) in per-segment analyses.

Results: There was a good inter-observer agreement reading perfusion-maps ($\kappa=0.655$). Perfusion-maps showed HP, WSD, PaD, CD, artefacts in 65.7%, 3.5%, 23.2%, 4.2% and 3.4%, respectively. V/Q showed 27.1% PD (24.9% without and 2.2% with VD) for HP, 50% PD (all without VD) for WSD, 56.6% PD (2.8% without and 53.8% with VD) for PaD and 50% PD (19.2% without and 30.8% with VD) for CD. Normal lung showed 79.1% HP and 15.8% PaD. Emphysematous lung showed 75% PaD and 18.8% HP. Mosaic-perfusion showed 45.4% HP and 36.7% PaD. GGO showed 42.1% HP and 42.1% PaD. Consolidation showed 38.1% HP or 42.9% CD.

Conclusion: There is a good inter-observer agreement in reading DECT perfusion-maps. WSD correspond with real perfusion-defects. PaD and CD can correspond with perfusion defects; however, they are more likely corresponding with other parenchymal abnormalities.

B-0271 10:39

Usefulness of vascular iodine distribution maps in the diagnosis of pulmonary embolism

J.I.E. Bosco, H.S. Teh; Singapore/SG

(bosco.jerome.ie@alexandrahealth.com.sg)

Purpose: To evaluate the value of vascular iodine maps (VID) maps in dual energy CT pulmonary angiogram for detection of pulmonary embolism.

Methods and Materials: One hundred and twenty-six consecutive patients with suspected PE underwent CT pulmonary angiography (CTPA) with dual energy CT (DECT) (Siemens Somatom Definition Flash) in our Department since December 2010 were evaluated. VID maps were obtained for all patients using standard Siemens software. CT images were assessed and compared for lung pathology, angiographic findings and VID.

Results: Thirty-three of 126 patients had PE based on the CTPA findings. Of these, 6 were initially reported as normal, but showed evidence of segmental/subsegmental thrombi after angiographic images were reviewed when VID images revealed WPD. WPD was absent in 3 patients who had PE on CTPA. Underlying diffuse lung pathology was present in these patients, which probably obscured the WPD. Nine patients showed WPD, but negative CTPA. Three had extensive parenchyma abnormality; 3 had paucity of pulmonary vessels in the corresponding areas. In the remaining 3, no obvious parenchyma or vascular abnormalities were noted. On per patient basis, positive predictive values, negative predictive values, sensitivity, specificity and accuracy were 76.9%, 96.3%, 90.9%, 89.7% and 90.0%, respectively.

Conclusion: VID analysis made possible by DECT when used with the angiographic images significantly improves the accuracy of PE detection.

B-0272 10:48

Pseudo-embolic perfusion defects in COPD: evaluation with dual energy CT angiography (DECT) in 170 patients

F. Pontana, C. Chalayer, J.-B. Faivre, C.-F. Murphy, M. Rémy-Jardin, J. Remy; Lille/FR (francois.pontana@chru-lille.fr)

Purpose: To investigate the frequency of pseudo-embolic perfusion defects secondary to the underlying bronchopulmonary disease in COPD patients.

Methods and Materials: 170 patients with stable COPD and no history of acute and/or chronic pulmonary vascular disease, underwent DECT with reconstruction of diagnostic and perfusion scans. This volumetric acquisition at deep inspiration was completed by sequential expiratory scans. Two radiologists evaluated, by consensus, (1) the presence of pseudo-embolic perfusion defects (i.e., triangular, pleural-based and sharply marginated hypoattenuated areas) on lung perfusion scans; (2) with systematic depiction of morphological changes in the corresponding areas on inspiratory and expiratory diagnostic images.

Results: A total of 143 pseudo-embolic perfusion defects were depicted in 47 patients (27.6%) with (a) a predominant distribution in the lower lobes (89/143; 62.2%); (b) observed with the concurrent presence of small airways disease alone (120/143; 83.9%), emphysematous lesions alone (11/143; 7.7%), a variable association of small airways disease and emphysema (n=9; 6.3%) or the exclusive finding of central airways abnormalities (n=3; 2.1%) in the corresponding anatomical zones. The CT features of small airways disease depicted in the areas of pseudo-embolic perfusion defects included air trapping (81/120; 67.5%), focal hypoattenuated area (67/120; 55.8%), mucoid impactions (59/120; 49.2%) and/or bronchiolectasis (8/120; 6.7%). No statistically significant difference was found in the frequency of pseudo-embolic defects between the CT phenotypes of COPD ($p=0.12$).

Conclusion: Pseudo-embolic perfusion defects were identified in 27.6% of COPD patients, mainly seen in association with CT features of small airways disease.

B-0273 10:57

Frequency and origin of lung perfusion defects on dual energy computed tomography (DECT) in an unselected patient group

A.E. Odink¹, M. Rossius¹, W. Vermeule¹, C.M. Schaefer-Prokop², I. Hartmann¹;

¹Rotterdam/NL, ²Amersfoort/NL

Purpose: Lung perfusion defects seen on DECT are not necessarily caused by acute pulmonary embolism (APE) and therefore may cause interpretation difficulties. Purpose of the study was to assess frequency and underlying cause of perfusion defects on DECT in an unselected patient group.

Methods and Materials: The study group consisted of 200 consecutive patients who underwent DECT for suspected APE between May 2009 and February 2011. State-of-the-art protocols were used with a second generation DECT scanner. All scans were retrospectively revised by two radiologists with respect to the presence, morphology and location of perfusion defects and to the presence and type of artefacts. Findings were correlated with the findings at lung window settings and the CTA findings.

Results: In 189 (94%) of the included 200 patients perfusion maps were available for evaluation. Twenty-three patients (12%) were positive for APE, of whom 14 had wedge shaped perfusion. In 140 of the 175 patients (80%) underlying lung diseases were identified causing perfusion defects. These included emphysema (18%), pleural fluid with compression atelectasis and/or pneumonic consolidations (62%). 162 DECT perfusion maps (93%) showed some type of perfusion defects caused by artefacts such as beam hardening or pulsation artefacts, none of them were found to interfere with the diagnosis.

Conclusion: In an unselected study group, the majority of patients show perfusion defects on DECT which are not caused by APE and correct interpretation requires close correlation with lung parenchymal findings and CTA findings.

B-0274 11:06

Impact of iodine delivery rate with varying flow rates on dual energy CT image quality in patients with suspected pulmonary embolism

J. Hansmann, C. Fink, M. Meyer, P. Apfaltrer, S.O. Schönberg, T. Henzler;

Mannheim/DE (jan.hansmann@medma.uni-heidelberg.de)

Purpose: To prospectively compare 4 different contrast material injection protocols for dual energy CT pulmonary angiography (DE-CTPA) in patients with suspected pulmonary embolism (PE).

Methods and Materials: 100 consecutive patients who underwent CTPA for exclusion of PE were randomised into 4 different contrast material (CM) injection protocols defined by different iodine concentrations and iodine-delivery-rates (IDR) (A: 80 ml Iopromide 370/4 mL/s (IDR-1.4 gI/s); B: 80 ml Iopromide 370 at 3 mL/s (IDR-1.1 gI/s); C: 98 ml Iopromide 300 at 4.9 mL/s (IDR-1.4 gI/s); D: 98 ml Iopro-

mid 300 at 3.7 mL/s (IDR-1.1 gI/s)). Attenuation values were measured on "virtual" 120 kV images in the inflow tract (subclavian vein; superior vena cava; right atrium), target tract (right ventricle; pulmonary trunk; pulmonary arteries) and outflow tract (left atrium; left ventricle; ascending aorta) and compared using the Wilcoxon rank sum test. Subjective image quality of "virtual" 120 kV images and calculated iodine perfusion maps was assessed by two readers (5-point-Likert-scale; κ -statistics).

Results: Target tract attenuation was highest for protocol A with 388 ± 116 Hounsfield Units (HU) (highly concentrated CM, high IDR) if compared to all other protocols (all $p < 0.05$). No statistically significant difference was found between protocol B (311 ± 87 HU), protocol C (333 ± 112 HU) and D (335 ± 78 HU). Image quality of protocol A was rated significantly higher compared to all other protocols with a median-score of 5; ($p < 0.001$). Interreader agreement was good with a kappa of 0.63.

Conclusion: Highly concentrated iodinated contrast material in combination with high flow rates provides improved diagnostic image quality and has the highest target-tract attenuation for a DE-CTPA protocol.

B-0275 11:15

Pulmonary embolism at dual source CT angiography: do we overdose?

R. Oca, G. Tardaguila, C. Delgado, C. Trinidad, A. Fernandez Del Valle, F. Tardaguila Montero; *Vigo/ES*



Purpose: To compare the radiation dose of dual source 128-multidetector CT (128-DSCT) with conventional 16-multidetector CT (16-MDCT) in pulmonary angiography for the diagnosis of pulmonary embolism (PE).

Methods and Materials: The local ethics committee approved this study. We retrospectively reviewed 100 patients with clinical suspicion of pulmonary embolism (PE); 50 underwent 128-DSCT and 50 underwent 16-MDCT. Effective doses were compared with estimates based on the most commonly used method in clinical literature: multiplying dose-length product (DLP) by a general conversion coefficient ($0.014 \text{ mSv} \cdot \text{mGy}^{-1} \cdot \text{cm}^{-1}$), determined from Monte Carlo simulations of chest CT.

Results: The two groups matched well for clinical characteristics (there were included 28 men and 72 women, with an average of age of 65 ± 19 years). The percentage of patients with PE diagnosis was 20% for each group. Mean effective doses with 128-DSCT and 16-MDCT were $4.5 \pm 1.07 \text{ mSv}$ and $4.8 \pm 0.41 \text{ mSv}$, respectively ($p < 0.05$).

Conclusion: Mean effective doses do not increase using a double source CT protocol compared with conventional multidetector CT in the PE studies. Despite the widespread idea that double source studies could increase radiation dose, we found there is no increase but a slight reduction of mean effective dose with dual energy technique. According to the additional information provided for the dual source techniques (iodine maps and lung perfusion), we recommend using this method routinely, if available.

B-0276 11:24

80-kVp 16-MDCT to diagnose pulmonary embolism with minimised radiation dose

U. Nyman¹, P. Bjorkdahl¹, B. Goldman¹, M.-L. Olsson², S. Wettemark¹; ¹Trelleborg/SE, ²Malmö/SE (ulf.nyman@bredband.net)

Purpose: To compare radiation dose and image quality of 80 kVp 16-multirow detector computed tomography (MDCT) to diagnose pulmonary embolism (PE) with that of 100 and 120 kVp with all other scanning parameters being equal, while 350 instead of 300 mg I/kg were used at 80 kVp to compensate for the decreased theoretical contrast-to-noise ratio (CNR).

Methods and Materials: Patients with an estimated GFR $\geq 50 \text{ mL/min}$ underwent 80 (maximum weight 100 kg), 100 and 120 kVp (50 patients in each group) 16-MDCT using the same scanner and 100 "Quality reference" effective mAs. Pulmonary artery attenuation, image noise (1 standard deviation) and CNR (providing a clot of 70 HU) were evaluated. Subjective image quality was assessed. Computed-tomography-dose-index (CTDIvol) and dose-length-product (DLP) were recorded and effective dose calculated based on published conversion factors.

Results: Median patient weight and BMI at 80/100/120 kVp were: 76/75/73 kg and 26/25/25 kg/m². Median pulmonary artery attenuation, image noise, CNR, CTDIvol, DLP and effective dose at 80/100/120 kVp were: 653/467/332 HU, 49/32/22 HU, 13/12/12, 2.7/4.8/7.5 mGy, 78/139/234 mGy \cdot cm and 1.2/2.2/4.0 mSv. At 80 kVp all examinations were adequate; 92% classified as excellent compared with 70% and 36% at 100 and 120 kVp.

Conclusion: Radiation dose to patients may be decreased to about one-third by reducing x-ray tube potential from 120 to 80 kVp without deterioration of diagnostic image quality if the decreased CNR is compensated with a slightly increased iodine dose. The protocol may be of special benefit in young individuals < 100 kg with adequate GFR.

B-0277 11:33

Dose reduction in CT pulmonary angiography: is it safe to limit scan coverage?

J. Halperin, J. Rajchgot, D. Odedra, K. Hany, M. Hashemi, N.S. Paul; Toronto, ON/CA (jhalperin@qmed.ca)

Purpose: To determine if scan length restriction during CT pulmonary angiography (CTPA) results in non-detection of significant findings.

Methods and Materials: Retrospective reviews of 461 consecutive patients 253 F mean age 57.8y (17-99) having CTPA from 2010 to 2011. Two observers reviewed all images in each study (full scan) and then only images superior to the aortic arch and inferior to the heart (limited scan) to detect radiological abnormalities. It was determined whether the abnormalities would be missed on limited scans and if they were significant; indeterminate or insignificant based on imaging features, chart review and previous imaging. Dedicated on-line software (Radimetrics Inc, Toronto) calculated patient and organ-specific dose for full and limited scans.

Results: Mean scan length: full; 290 mm, limited 169.3 mm, average change, 122 mm ($p < 0.05$). 43.8% (202/461) patients had abnormalities missed on limited CTPA, 16.3% (33/202) were significant but only 6% (2/33) were new. Overall, 0.4% (2/461) patients had new significant findings missed; renal carcinoma (1) and peritoneal disease (1). Limited scan CTPA produces patient radiation dose reduction of 34.4%, from 11.1 to 7.25mSv (ICRP 103) and organ dose reduction > 70%: kidneys (81.6%), colon (74.0%), thyroid (70.2%), > 50%: testicles (69.3%), skin (68.7%), small intestine (55.8%), > 30%: spleen (48.0%), stomach (48.4%), oesophagus (45.4%), red marrow (42.6%), brain (41.2%), eye lens (32.8%) and breasts (30.1%).

Conclusion: Limited scan length CTPA is a safe procedure in 99.6% of patients, results in 34% reduction in patient dose and significant reductions in organ dose to radiosensitive tissues.

B-0278 11:42

Raw-data-based iterative reconstruction for chest computed tomography (CT) angiography: comparison of low-dose low-kV iterative reconstruction CT and standard-dose filtered back projection CT in 80 patients

J. Pagniez, F. Pontana, J.-B. Faivre, T. Flohr, M. Rémy-Jardin, J. Remy; Lille/FR (martine.remy@chru-lille.fr)

Purpose: To evaluate the image noise and image quality of a raw-data-based iterative reconstruction technique in low-kV pulmonary CT angiograms in comparison with standard-dose filtered back projection (FBP) CT.

Methods and Materials: 80 consecutive patients, referred for a follow-up chest CT angiographic examination, underwent a low-dose CT examination (i.e., T2 scan) in similar technical conditions to those of the initial examination (i.e., T1 scan), except for (a) the kilovoltage selection reduced by 20 kV with adaptation of the milliamperage to ensure a 50% reduction of the CTDI; and (b) the replacement of regular FBP by iterative reconstructions (SAFIRE).

Results: Despite a mean decrease of 52.8% in the DLP (T1: 163.6 mGy \cdot cm; T2: 77.3 mGy \cdot cm), T2 scans showed: (a) significantly less objective noise measured at the level of the trachea on mediastinal (T2: 18.33 \pm 5.89; T1: 21.48 \pm 9.41) ($p < 0.0001$) and lung images (T2: 41.28 \pm 10.39; T1: 49.77 \pm 11.73) ($p < 0.0001$); (b) significantly higher signal-to-noise (T2: 12.92 \pm 3.80; T1: 10.86 \pm 3.15) and contrast-to-noise (T1: 11.68 \pm 3.64; T2: 9.42 \pm 3.13) ratios ($p < 0.0001$); (c) a similar visual perception of noise on mediastinal ($p=0.1317$) and lung images ($p=0.3657$), mainly rated as moderate; and (d) a similar overall image quality, rated as excellent in 23% (18/80) (vs T1: 21/80; 26%) and good in 77% (62/80) (T1: 59/80; 74%) of CT examinations ($p=0.4054$).

Conclusion: The raw-data-based iterative reconstruction technique allowed better objective and similar subjective image quality of low-kilovoltage CT angiograms compared to standard-dose FBP CT examinations.

B-0279 11:51

Image quality and radiation dose optimisation for high-resolution CT pulmonary angiography using 100 kVp and automatic exposure control

S. Alrajhi¹, S. Alhumayyd¹, H. Kashani¹, D. Odedra¹, J. Blobel², N.S. Paul¹; ¹Toronto, ON/CA, ²Zoetermeer/NL (Sulaiman.Alrajhi@uhn.on.ca)

Purpose: To analyse patient exposure and image quality (IQ) uniformity for high-resolution (1 mm) 100 kVp CT pulmonary angiography (CTPA) comparing constant mAs to automatic exposure control (AEC) variable mAs with equivalent image noise (IN).

Methods and Materials: Two readers independently measured IN (R1-4): R1=pulmonary artery, R2=aortic arch, R3=proximal descending aorta, R4=distal

thoracic aorta. Gp1: 30 consecutive patients (age 54.3±20.5y, 19 F) scanned using 100 kVp and 175 mAs. For each patient, mean IN was averaged for both readers at each ROI and subsequently averaged over all patients for R1-R4. Gp1 averaged IN=36.8 HU. Gp2: 30 subsequent patients (mean age 56.1±14.9y, 16 F) had CTPA with 100 kVp and AEC determined variable mAs with matched target IN=40 HU. 480 measurements tested for normal distribution (Kolmogorov-Smirnov test) and reader agreements (paired Wilcoxon Test). IN R1-R4 and patient DLP (mGy*cm) were compared between Gp1 and Gp2 using the Mann-Whitney test for IN agreement and Bartlett test for standard deviation (1σ) agreement of IN.

Results: Mean ± 1σ body weight [kg] Gp1: 67.3±13.0, Gp2: 67.2±13.3; IN[HU] Gp1: R1=37.4±15.1, R2=32.0±14.1, R3=36.1±14.6, R4=42.6±18.8; Gp2: R1=38.8±7.7, R2=31.2±5.9, R3=38.8±7.5, R4=42.8±8.4; DLP[mGy*cm] Gp1: 473.8±128.2 and Gp2: 474.7±164.4. No significant differences in patient bodyweight (p=0.894) and DLP (p=0.734), in inter-reader results of IN for R1-R4, (p=0.082-0.459) or in IN for R1-R4 (all p > 0.55). Significant differences in 1σ-standard deviation (p < 0.0005) for R1-R4 with 49% 1σ-reduction of averaged R1-R4 values in Gp2.

Conclusion: High-resolution 100 kVp CTPA using AEC provides more uniform image quality adapted to patient body habitus across the entire chest with 49% reduction in standard deviation (1σ) of image noise compared with a fixed mAs-technique at equivalent patient exposure.

10:30 - 12:00

Room D2

Interventional Radiology

SS 509

CT and MR-guided interventions

Moderators:
P. Almeida; Coimbra/PT
S. Kos; Basle/CH

B-0280 10:30

CT fluoroscopy-guided percutaneous vertebroplasty in spinal malignancy: technical results, PMMA leakages and complications in 202 patients

C.G. Trumm¹, T.K. Helmberger¹, T.F. Jakobs¹, C.J. Zech¹, R. Stahl¹, T.A. Sandner¹, P.M. Paprottka¹, M.F. Reiser¹, R.-T. Hoffmann²; ¹Munich/DE, ²Dresden/DE (christoph.trumm@med.uni-muenchen.de)

Purpose: To retrospectively evaluate the incidence and clinical impact of local polymethylmethacrylate leaks and pulmonary cement embolisms (PCE), occurring under CT fluoroscopy-guided vertebroplasty of malignant vertebral compression fractures (VCF) and osteolyses.

Methods and Materials: From 12/2001 to 06/2009, 202 cancer patients (116 women, 86 men; age 63.2±8.6) with painful VCF and spinal osteolyses underwent vertebroplasty. 331 vertebrae were treated in 231 sessions under CT fluoroscopy guidance (120 kV; 10-25 mA; single slice, 4-, 16-, and 128-row CT). Osteolytic involvement (i.e., none, ≤25%, ≤50%, ≤75%, or ≤100%) of the vertebral cross-sectional area and the posterior wall were assessed in the pre-vertebroplasty CT. Local PMMA leaks were analysed using the post-vertebroplasty CT. Presence and location of PCE were evaluated in all patients having undergone conventional radiography (CR; n=53) or CT (n=88) of the chest after vertebroplasty due to their underlying tumour disease. Patient charts were reviewed regarding adverse events related to vertebroplasty.

Results: 32% and 20.2% of 331 treated vertebrae showed more than 50% osteolytic involvement of the vertebral cross-sectional area and the posterior wall, respectively. Local PMMA leakage rate was 58.6% (194 of 331 vertebrae). PCE (segmental, n=10; central, n=1) were seen after 7.8% of the procedures with follow-up imaging of the chest. No major complications occurred within a 30-day period after vertebroplasty.

Conclusion: Vertebroplasty of spinal malignancy can be safely performed under CT fluoroscopy guidance even in patients with substantial osteolytic involvement. In our patient collective, local PMMA leaks and PCE visualised in post-procedural radiography and CT images had no clinical impact.

B-0281 10:39

Accuracy of CT-guidance for lumbar facet blocks

M. Weininger, J. Mills, Z. Rumboldt, W. Huda, A. Cianfoni; Charleston, SC/US (weininge@muscu.edu)

Purpose: Lumbar facet joint blocks (FJB) require precise intra-articular injection for diagnostic specificity efficacy. Our purpose was to assess the procedural success profile of FJB under CT-guidance and to estimate periprocedural radiation doses. **Methods:** We retrospectively reviewed clinically indicated FJB procedures in 37 consecutive patients (13 men; mean age 60±12 years; 47 procedures; 84 targeted facet joints). Under CT-guidance a posterior paravertebral access was used. A pre-procedure localising scan was followed by intermittent low dose (120 kV/30 mAs) guidance scans (3 slices, 2.5/1.25 mm slice thickness/overlap; 3.75 mm coverage). Presence of posterior facet osteophytes overlying a direct joint access, needle direction for joint access (oblique ipsilateral, straight ipsilateral, oblique contralateral), and number of CT-guidance scans needed for final needle placement and dose length product (DLP) were recorded. Intra-articular needle placement was confirmed by joint space contrast opacification.

Results: FJB were technically successful in 79/84 cases. Access side and direction were as follows: 73/84 ipsilateral (53 straight, 20 oblique), 11/84 contralateral oblique (13%). 46 FJB were at L4/L5, 29 at L5/S1, 5 at L3/L4, and 4 at L2/L3. 40/84 facet joints presented posterior osteophytes. Average number of guiding scans needed to obtain final needle position was 4±2. Average DLP per FJB was estimated at 16 mGy-cm, corresponding to an effective dose of 0.2mSv.

Conclusion: FJB using CT-guidance is safe and rapid, ensures reliable needle guidance, individual to each facet joint's anatomy, and allows precise intra-articular injection, with extremely high procedural accuracy. The effective dose is comparable to that of one minute of fluoroscopy guidance.



B-0282 10:48

Extrapleural paravertebral CT-guided fine needle biopsy of subcarinal lymph nodes

W.H. Tantawy, A.S. Ibrahim, M.A. Mohamed, E.H. El-Gemeie; Cairo/EG (tantawyw@yahoo.com)

Purpose: To report our experience in CT-guided extrapleural paravertebral subcarinal lymph biopsy using a thin 25-gauge (25G) thin needle without the need of injection of saline to widen the mediastinum.

Methods and Materials: Biopsy was performed using a 25G needle which was advanced lateral to the vertebral body between the endothoracic fascia and the parietal pleura to gain access to subcarinal lymph nodes. One hundred and forty-one patients were included in the study (74 females, 57 males). No artificial widening of the mediastinum using saline injection was required. The study was performed in the presence of a cytopathologist; sensitivity and specificity rates were calculated. Complications were documented for each case especially for pneumothorax and haemorrhage.

Results: Cytopathological diagnosis was reached in all cases. All re-aspirations were done in the same session to reach a primary diagnosis at the time of the biopsy. Immunophenotyping study was done in 94 cases to confirm the primary diagnosis and to classify the malignant lesions. No pneumothorax was encountered. Small haematomas were noted in 5 cases (3.5%). Cytopathology showed a sensitivity of 97.2% and specificity of 100%. By adding immunophenotyping a 100% sensitivity and specificity was achieved.

Conclusion: Fine needle aspiration cytology (FNAC) using a 25-gauge needle for subcarinal lymph nodes via a percutaneous extrapleural paravertebral CT-guided approach is a safe, minimally invasive, and tolerable procedure yielding a high sensitivity and specificity rates without the need of artificial widening.

B-0283 10:57

Initial experience of a novel CT fluoroscopy-guided percutaneous gastrostomy technique with loop gastropexy and peel-away sheath trocar technique in amyotrophic lateral sclerosis patients

M. de Buccourt, F. Colletini, C. Althoff, F. Streitparth, J. Greupner, B. Hamm, U. Teichgräber; Berlin/DE (mdb@charite.de)

Purpose: To report our initial experience of a novel CT fluoroscopy-guided percutaneous gastrostomy technique with loop gastropexy and peel-away sheath trocar technique.

Methods and Materials: A consecutive series of 31 amyotrophic lateral sclerosis patients in whom endoscopic gastrostomy was considered too dangerous or impossible underwent CT-guided percutaneous gastropexy and gastrostomy, and prospective follow-up. All procedures were performed with a 15 FR Freka® Pexact gastrostomy kit (Fresenius Kabi, Bad Homburg, Germany), 16-row scanner

(Aquilion 16, Toshiba Medical Systems Europe, The Netherlands) and single shot CT fluoroscopy mode.

Results: The procedure was performed successfully in 30 of 31 patients (20 men, 11 women; median age 60 years, range 38-80). In the remaining case the stomach was punctured under CT-fluoroscopy and CO2 insufflation was initiated thereafter, leading to successful gastrostomy without prior gastropexy and without further adverse events during follow-up. Two patients reported unproblematic exchange of a balloon tube due to skin irritations with no further adverse events. One patient reported accidental displacement of an exchanged new balloon tube in domestic environment due to balloon leakage: A new balloon tube was easily re-inserted in a hospital the same day. No serious adverse events such as peritonitis, persistent local bleeding, or any local infection requiring surgical intervention were observed. Until Aug. 11th 2011 follow-up resulted in 7473 cumulative gastrostomy-days from the date of first placement.

Conclusion: Initial results suggest the outcome of the described technique to be comparable to conventional radiologic gastrostomy and it can be successfully performed where endoscopic gastrostomy and sedation are contraindicated.

B-0284 11:06

Sphenopalatine ganglion alcohol neurolysis under CT guidance in the management of craniofacial pain in 53 procedures

A. Kastler¹, S. Aubry², G. Cadel², B. Kastler²; ¹Clermont-Ferrand/FR, ²Besancon/FR

Purpose: The purpose of this study is to describe and evaluate the safety and effectiveness of alcohol neurolysis of the sphenopalatine ganglion under CT guidance in the management of facial various pain syndromes.

Methods and Materials: Thirty-eight patients were included in this retrospective study between December 1995 and June 2011. A total of 53 sphenopalatine neurolysis (SPN) were performed using absolute alcohol. The SPN was considered to be effective when pain relief was equal to or greater than 50% lasting for at least one week. The mean pain relief period following the procedure for each patient was noted. In case of recurring pain, both duration and intensity of pain were noted. All procedures were realised on an outpatient basis under local anaesthesia.

Results: Mean duration of facial pain before procedure was 6.1 years. Thirty six out of the 53 SPN (67.9%). procedures performed were successful. The overall mean duration of pain relief was 8.7 months after SPN procedure. In 26/36 successful SPN, recurring pain occurred with a mean duration of 5.4 months after initial procedure. Success rate of SPN depending of pain type are as follows: atypical facial pain 85.7% (p < 0.05); cluster headache: 83.3% (P < 0.05), trigeminal neuralgia 50% (p < 0.05), compression by neoplasm: 100% (p < 0.05).

Conclusion: CT-guided alcohol neurolysis of the sphenopalatine ganglion is a safe and effective treatment of refractory chronic craniofacial pain syndromes especially in cases of cluster headaches, atypical facial pain and trigeminal neuralgia.

B-0285 11:15

Tailored interactive sequences for continuous MR-image-guided freehand biopsies of different organs in an open system at 1.0 Tesla: preliminary results

M. de Bucourt¹, F. Streitparth¹, U. Teichgräber²; ¹Berlin/DE, ²Jena/DE (mdb@charite.de)

Purpose: To assess feasibility, image quality and accuracy of freehand biopsies of lung, liver, soft tissue and bone lesions using bFFE (gradient + spin echo), FFE (fast gradient echo) and TSE (fast spin echo) sequences for interactive continuous navigation in an open MRI system at 1.0 T.

Methods and Materials: 24 MR-guided biopsies (1 lung, 13 liver, 3 bone, 7 soft tissue and other organs) were performed in a 1.0-T open magnetic resonance (MR) scanner (Panorama HFO; Philips Healthcare, Best, The Netherlands). 14-to-18-gauge MR-compatible biopsy sets (Somatex Medical, Teltow, Germany), semi-automatic biopsy guns (Invivo, Schwerin, Germany) or 11-gauge MR-compatible bone marrow biopsy needles (Somatex Medical, Teltow, Germany) were employed. Complications and pathological biopsy reports as an indicator for lesions hit were recorded. Average patients' age was 49 (min. 28; max. 70). 13 female and 11 male patients were included. The mean intervention time was 27 min.

Results: Our initial results indicate that bFFE is particularly suitable for fast moving organs (pulmonary, paracardial), moving organs are targeted better with T1W TSE, T1W FFE (liver) or T2W TSE (adrenal glands), and static organs are successfully approached with PD (spine) or T1W TSE (peripheral bones, musculoskeletal system). No major complications occurred. Average lesion size was 35 mm (min. 15; max. 65).

Conclusion: Applying tailored interactive dynamic imaging sequences for continuous navigation with arbitrary slice selection for maneuvering even to delicate locations improves interventional accuracy and feasibility of freehand MR-guided biopsies and may hence reduce the risk of complications.

B-0286 11:24

Percutaneous drainage under CT-guidance of deep abscess using a blunt-tip introducer

C. de Bazelaire, F. Sabatier, M. Chapellier, A. Scemama, A. Pluvinage, P. Bourrier, A.-M. Zagdanski, E. de Kerviler; Paris/FR (cedric.de-bazelaire@sls.aphp.fr)

Purpose: Deep abscess drainages under CT guidance are usually difficult to reach because of vital structures intervening in the needle pathway. Our purpose is to evaluate the efficacy and the safety of deep drainages under CT guidance using a blunt-tip introducer.

Methods and Materials: Two hundred and seven consecutive patients referred for CT-guided abscess drainage were included in this retrospective study. In fifty patients, a blunt-tip introducer was used to reach the abscess and in 157 a standard needle was used (control group). Procedures were analysed in term of duration, irradiation, success and complications.

Results: The procedure duration was longer in the blunt-tip group (29 min vs 22 min, p < 0.0001). However, patient's dosimetry was not significantly higher in the blunt-tip group (950 vs 870 mGy.cm). No side effect was observed in the blunt-tip group whereas 2 haematomas and 2 bowel perforations were seen in the control group. During the follow-up, a second drainage was necessary in 17% in the blunt-tip group and 8% in the other group (p=0.04).

Conclusion: Blunt-tip introducers represent a viable a safe alternative to standard needles when performing CT-guided percutaneous drainages of deep abscess.

B-0287 11:33



Towards cardiovascular interventions guided by magnetic particle imaging (MPI): first instrument characterisation

J. Haegele, S. Biederer, H. Wojtczyk, M. Graeser, T. Knopp, T.M. Buzug, J. Barkhausen, F.M. Vogt; Lübeck/DE (haegele@radiologie.uni-luebeck.de)

Purpose: Magnetic particle imaging (MPI) is a new tomographic imaging method and a very promising application for cardiovascular interventional radiology. We evaluated the MPI-performance of various commercially available instruments and a self-coated catheter using magnetic particle spectroscopy (MPS).

Methods and Materials: Seventeen commercially available interventional devices were selected: nine catheters (five braided (one nitinol, four stainless-steel) and four non-braided) and eight guide wires (four stainless-steel, three nitinol, one polyetheretherketone, PEEK). 2-mm-sized pieces were taken from the tip, the distal part (20-30 mm proximal the tip) and from the shaft of each device and evaluated using MPS. As a measure of performance the total harmonic distortion (THD) was determined. In a second step, one commercially available catheter without signal response in MPS was experimentally coated at the tip with SPIOs to evaluate the traceability of a SPIO-coating.

Results: Signal-generating and non-signal-generating devices could be distinguished reliably using MPS. The THD of signal-generating instruments was significantly higher than of non-signal-generating instruments (-41.03, SD 17.54 dB vs. -114.33, SD 7.62 dB, p < 0.0001). 7 of 8 stainless-steel containing devices generated a signal response whereas nitinol-containing (1 of 4) and metal-free instruments (0 of 5) did not. Furthermore, the SPIO-coated catheter generated a signal in contrast to the same uncoated catheter (-56.76 vs. -109.51 dB).

Conclusion: It is possible to reliably distinguish signal-generating and non-signal-generating instruments and to label instruments with SPIOs for a better traceability using MPI. This is a precondition for further development of suitable instruments.

B-0288 11:42



Percutaneous MR-guided cryoablation of prostate cancer: technical feasibility and preliminary results

G. Tsoumakidou, H. Lang, O. Abdelli, X. Buy, M. de Mathelin, D. Jacqmin, A. Gangi; Strasbourg/FR (gtsoumakidou@yahoo.com)

Purpose: We herein report our initial experience and technical feasibility of transperineal prostate cryoablation under magnetic resonance guidance.

Methods and Materials: From July 2009 till July 2011 percutaneous MR-guided cryoablation was performed in 11 patients with prostatic adenocarcinoma contraindicated for surgery (mean age: 72-years, mean Gleason-score: 6.45, mean PSA: 6.21 ngr/ml, T1-2c/N0/M0, mean prostate-volume: 36.44 ml). Free-hand probe positioning was performed under real-time MR-imaging. Four to seven cryoprobes were inserted in the prostate, depending on the total gland volume. The ice-ball was monitored using real-time Trufi and high-resolution T2W-Blade multi-planar imaging. Patients were followed at 1, 3, 6, 9, 12 months after the procedure with serum PSA-level and post-ablation MRI.

Results: Prostate cryoablation was technically feasible in 10 out of 11 patients. The ice-ball was clearly and sharply visualised in all cases as a signal-void area. Mean ice-ball volume was 53.3 ml. Mean follow-up was 15 months (range: 1-25 months). Mean PSA-nadir was 0.33 ngr/ml (range: 0.02-0.94 ngr/ml). Mean hospitalization was 5 days (range: 3-13 days). Complications included a urethra-rectum fistula, urinary infection, transient dysuria and scrotal pain.

Conclusion: MR-guided prostate cryoablation is feasible and promising, with excellent monitoring of the ice-ball. Future perspectives could include the use of MR-guidance for the focal prostate cancer cryotherapy.

B-0289 11:51

Clinical importance of CT-assisted sympathectomy in primary, focal palmar and palmar hyperhidrosis

F. Scheer¹, A. Wins², P. Kamusella¹, P. Wiggermann³, C. Wissgott¹, R. Andresen¹; ¹Heide/DE, ²Rostock/DE, ³Regensburg/DE (CWissgott@wkk-hei.de)

Purpose: The objective of this study was to evaluate the benefit of thoracic and lumbar computed tomographic-assisted sympathectomy (CTS_y) in patients with primary, focal hyperhidrosis.

Methods and Materials: Thoracic and/or a lumbar CTS_y was conducted on 101 patients (average age 37.5 ± 15.5 years) with primary, focal hyperhidrosis of the hands and/or feet, who experienced persistent symptoms after all conservative treatment options had been exhausted. The patients were divided into groups with palmar, palmoplantar and plantar hyperhidrosis. The patients evaluated the severity of their symptoms prior to the intervention, 2 days, 6 months and 12 months after the intervention using a Dermatology Quality of Life Index (DLQI) and side effects experienced.

Results: The interventions performed led to a statistically significant decrease in the follow-up after CTS_y in all groups (p < 0.01). The technical success rate of the CTS_y was 100%. No major complications occurred. As the most common side effect, 39/101 of the patients reported compensatory perspiration over the course of treatment. Neuralgia experienced by 15/101 and paraesthesia by 13/101 of the patients subsided spontaneously in all of those affected after a period of 4 weeks at most. The differentiated assessment of the strength of perspiration of the hands and feet showed statistically significant differences between the foot and hand region, whereby the decrease in sweat secretion of the feet was stronger and more lasting (p < 0.02).

Conclusion: After conservative measures have been exhausted, CTS_y represents a therapeutic option low in side effects for patients with primary, focal hyperhidrosis.

10:30 - 12:00

Room E1

Musculoskeletal

SS 510
Ultrasound

Moderators:
D. Miklič; Zagreb/HR
G. Turóczy; Budapest/HU

B-0290 10:30

Sonoelastography can help in the evaluation of supraspinatus tendon degeneration

C. Martini, E. Fabbro, G. Ferrero, D. Orlandi, E. Silvestri; *Genoa/IT* (chiarapio@libero.it)

Purpose: To describe utility of sonoelastography in the evaluation of supraspinatus tendon (SSP) degeneration in two groups of young and elderly asymptomatic volunteers

Methods and Materials: Sixty asymptomatic subjects were included in our evaluation (thirty young subjects, group A, mean age 26, range 18-32; thirty elderly subjects, group B, mean age 72, range 63-84). All subjects were screened by US (13-6 MHz probe, MyLab 70 XvG, Esaote, Italy). Two young shoulders were found to have partial-thickness tear of the SSP, while 21 elderly shoulders were found to have partial/full-thickness tear of the SSP. Thus, our study group was made by 58 young and 39 elderly shoulders. For each shoulder, we detected the presence of signs of tendon degeneration (fibre interruption, fragmentation, and calcifications). Then, all tendons were evaluated by sonoelastography, whose outcome was translated into a semi-quantitative scale (hard=1 to soft=5). Chi-square, Kruskal-Wallis, and Spearman's statistics were used.

Results: In group A, we found interruption (n=2), fragmentation (n=2), and calcifications (n=4), while in group B, n=21, n=24, and n=12, respectively (p < .01).

The median sonoelastography score in group A was 2 (1-3 [25th-75th percentile]) while it was 4 in group B (3-5) (p < .01). Group A tendons presented with a relatively homogeneous colour pattern, while group B tendons presented with a relatively patchy colour pattern. Correlation between US and sonoelastography was high (r=.810, p < .01).

Conclusion: Sonoelastography was able to detect degenerative changes of SSP tendons in elderly volunteers, with good correlation to US, so it could help in increasing US diagnostic accuracy in detection of SSP tendon degeneration.

B-0291 10:39

Clinical indications for musculoskeletal ultrasound: consensus paper of the European Society of Musculoskeletal Radiology

A. Klausner¹, A. Tagliafico², G.M. Allen³, N. Boutry⁴, R. Campbell⁵, M. Court-Payen⁶, A.J. Grainger⁷, H. Guerini⁸, E.G. McNally⁹, P.J. O'Connor⁷, S. Ostlere⁹, P. Peetrons⁹, M. Reijnen¹⁰, L.M. Sconfienza¹¹, E. Silvestri², D.J. Wilson³, C. Martinoli²; ¹Innsbruck/AT, ²Genoa/IT, ³Oxford/UK, ⁴Lille/FR, ⁵Liverpool/UK, ⁶Copenhagen/DK, ⁷Leeds/UK, ⁸Paris/FR, ⁹Brussels/BE, ¹⁰Leiden/NL, ¹¹Milan/IT (atagliafico@sirm.org)

Purpose: To develop clinical guidelines for musculoskeletal ultrasound (MSKUS) referral in Europe.

Methods and Materials: Sixteen musculoskeletal radiologists from seven European countries participated in a consensus-based interactive process (Delphi method) using consecutive questionnaires and consensus procedure at European meetings. First evidence validity was confirmed by literature research, followed by consensus on clinical utility in evaluation of musculoskeletal diseases in three consensus meetings. This involved a thorough, transparent, iterative approach, employing quantitative and qualitative research techniques including interview, questionnaire, Delphi and standard setting methodologies. All relevant stakeholders were engaged, including European MSK experts with special focus on MSKUS. Two different expert groups worked on a consensus in a first and second meeting. The third consensus meetings resolved questions that did not achieve consensus (limit 67%) by the first two questionnaires.

Results: On general consensus, musculoskeletal ultrasound is indicated to detect joint synovitis, fluid and septic effusion for potential aspiration and poorly indicated to detect loose bodies. Recommendations for most appropriate use of musculoskeletal ultrasound are reported in six areas relevant to musculoskeletal ultrasound: hand/wrist, elbow, shoulder, hip, knee, ankle/foot.

Conclusion: A comprehensive evidence-based, expert consensus-defined educational framework is presented. This should facilitate referrals for musculoskeletal ultrasound throughout Europe.

B-0292 10:48

Factors influencing quantitative values of contrast-enhanced ultrasound and correlations with clinical values in rheumatoid arthritis

C. Cyteval; *Montpellier/FR* (c-cyteval@chu-montpellier.fr)

Purpose: To evaluate the reliability of quantitative parameters of the time/intensity curves in contrast-enhanced ultrasound (CEUS) for the assessment of synovial vascularisation in RA and their correlation with clinical and biological signs of inflammation during the follow-up of the disease.

Methods and Materials: 21 patients with active RA and 6 control patients were recruited. Two acquisitions of a selected joint with Doppler synovitis were performed at 1-hour interval for each patient by the same investigator after injection of microbubble contrast agent. In addition, in patients with RA a third acquisition was performed 3 months later. Synovial vascularisation was quantified using time/intensity curve parameters (maximum signal intensity; AUC: area under the curve; TTP: time-to-peak). Correlations of the curve parameters with the following variables: patient, acquisition, size and localisation of ROI, as well as with clinical and biological signs of inflammation were analysed using logistic regressions and Pearson or Wilcoxon tests.

Results: RA patients presented the following features: median age 55: (16-80) years, median disease duration: 11.8 (0.25-31) years. No signal intensity increase was observed in control patients (median age 65 (58-75) years). The curve parameters were independent from the acquisition and the ROI localisation (p < 0.001). At the 3-month follow-up variation of AUC was correlated with DAS28 variation (r=0.74 [0.65-0.82]) and with CRP variation (r=0.69 [0.41-0.80]).

Conclusion: Our preliminary findings show that synovitis may be reliably followed using CEUS time/intensity curve parameters and suggest that AUC are correlated with the variation of the DAS28 in patients with RA.



B-0293 10:57

CEUS evaluation in the pseudarthrosis before and after treatment with autologous transplantation of bone marrow stem cells: preliminary results

S. Pozza¹, A. De Marchi¹, M. Petrazz¹, D. Aloj¹, G. Biino², C. Faletti¹; ¹Turin/IT, ²Pavia/IT (simona.pozza@tin.it)

Purpose: To demonstrate the effectiveness of CEUS in evaluating the process of reparative bone regeneration by monitoring angiogenesis around the fracture site in patients with pseudarthrosis who were treated with transplantation of marrow-derived mesenchymal stem cells.

Methods and Materials: The method was used in 15 patients of the Traumatology Centre in Torino, Italy from February 2009 to May 2011. All patients were treated for delayed multifragmentary fracture evolved in pseudarthrosis. Autologous concentrate of bone marrow stem cells was applied into the area of bone defect. CEUS examination was performed before the gelatinous compound was applied and at one-, four- and twelve-week follow-up time points, in order to evaluate the physiological formation of new blood vessels. At the end of the study an X-ray confirms the presence of callus.

Results: Ecographic signs of neo-vascularisation were noted at one week in 13 of 15 patients; a steady increase in vascularity was demonstrated in 13 patients in subsequent tests; repeated measures ANOVA demonstrated statistically significant differences in the extent of vascularisation at subsequent follow-up time points ($P < 0.0001$). At the end of the study x-ray examination revealed initial attachment of calcified callus in those patients who demonstrated an increase in vascularity at CEUS. The other two patients showed no improvement because of the presence of haematoma.

Conclusion: Transplantation of stem cells is a new treatment of pseudoarthrosis; our results demonstrate that CEUS has a good predictive value on the formation of callus in that it affords the monitoring of the reparative tissue vascularity.

B-0294 11:06

Visualisation of myofascial trigger points in low back muscles by real-time sonoelastography

N.M. Abdel Razek, O. Kattabei, M.K. Nassif, M. El Lithey; Cairo/EG (naglaabdelrazek@yahoo.com)

Purpose: Myofascial trigger points (MTrPs) are a common source of pain and has been reported to vary from 30% to 93% in musculoskeletal pain. However, there is still a lack of objective means to either quantify or visualise their core features. Purpose is to examine the ability of vibration sonoelastography (E-colour mode) to visualise MTrP; superficial as well as deep ones and to differentiate them from their immediate surrounding myofascial structure. Also, to compare between active and latent MTrPs, in the quadrates lumborum, longissimus thoracis, iliocostalis lumborum, piriformis and gluteus medius muscles.

Methods and Materials: Thirty eight (38) subjects with more than two (6) MTrPs were randomly assigned to an active MTrP group and a latent MTrP group. MTrP identification was based on their essential and confirmatory criteria; also, a hand-held digital electronic algometer was used to measure MTrPs tenderness, through pressure pain threshold value. A hand-held vibrator (50 Hz) was used over MTrPs while sonoelastography readings were taken. Outcome measures; percentage of tissue stiffness of MTrP and their immediate surrounding myofascial structure, as well as their strain ratio.

Results: Vibration sonoelastography clearly differentiated with statistically significant difference between MTrPs stiffness and their immediate surrounding myofascial structure stiffness with a P-Value = 0.000 (P-Value<0.05). However, there was no significant difference between tissue strain ratios of both active and latent MTrPs with a P-Value = 0.929 (P-Value> 0.05).

Conclusion: These preliminary results indicate that vibration sonoelastography can actually visualise MTrPs and can differentiate them from its surrounding myofascial structure through tissue strain. However, it could not differentiate between active and latent MTrPs where tissue strains yield similar values.

B-0295 11:15

Sonographic-guided treatment of rotator cuff delamination tears using autologous blood: a one-year follow-up study assessing radiological features, pain scores and shoulder function

W.A. Bashir, D. Connell; London/UK (wabashir@doctors.net.uk)

Purpose: To assess ultrasound-guided autologous blood injection (ABI) as an effective treatment for rotator cuff interstitial delamination tears which are difficult to diagnose by arthroscopy and are therefore problematic to treat. ABI offers a

new alternative minimally invasive treatment that actually targets pathophysiology of rotator cuff tendon pathology that has failed traditional non-surgical remedies.

Methods and Materials: 36 patients with clinical suspicion of rotator cuff tear underwent MRI examination. When evidence of a supraspinatus longitudinal split tear was confirmed, the patient was prospectively enrolled in the study and had US assessment; diagnosis confirmed according to echotexture, interstitial tearing and neovascularity. Individuals randomised into 2 groups; first group (18 patients, age 18-39) received standard treatment with 3 mL Bupivacaine and 40 mg triamcinolone into the subacromial-subdeltoid bursa. The second group (18 patients, age 19-39) received the standard therapy as well as ABI into the site of interstitial tearing and fibrillar discontinuity. We performed two injections and monitored any changes in the tendon with ultrasound and assessed pain scores and functional improvement using the validated Oxford Shoulder Score (OSS).

Results: Pre-procedural OSS and those at 10 days, 6 weeks, 3 and 12 months post-procedure were compared. Differences in sonographic echogenicity, neovascularity, and interstitial tear size noted. Patients in the ABI group showed statistical and clinical long-term pain relief and functional improvement as assessed by the overall OSS.

Conclusion: Autologous blood injection appears to be a viable alternative and more clinically effective when compared to standard steroid injection therapy for rotator cuff delamination tearing.

B-0296 11:24

Evaluation of echo-guided autologous platelet gel (APG) treatment in patients with tendinosis

S. Battisti, L. Gregori, F. Arrigoni, A. La Marra, L. Zugaro, A. Barile, C. Masciocchi; L'Aquila/IT (antonio.barile@cc.univaq.it)

Purpose: Purpose of our study was to evaluate the effect of platelet gel treatment in patients with tendinosis, that today is not surgically treated. The evaluation was based on observation of clinical improvement and MRI-imaging. The platelet gel shows anti-inflammatory and regenerative effects which allow recovery of the functionality.

Methods and Materials: We evaluated 72 patients with tendinosis of supraspinatus (40 pts), Achilles' (20 pts) and patellar tendons (12 pts). Clinical as well as functional evaluations of the patients were performed, using the visual analogue scale (VAS), for pain, and Constant Scale, VISA-A and VISA-P, for functionality. The instrumental evaluation was based on US and MRI. The protocol included three infiltrations performed at a distance of 21 days the one from the other. The control MRI was performed before treatment and 30 days after the last infiltration.

Results: The VAS mean value of the supraspinatus tendon at the end of treatment improved overall by 75%, and the Constant scale by 55.4%. In the patients with tendinosis of Achilles tendons, we found an improvement of 75% (VAS) and 43% (VISA-A). The patellar tendon VAS value increased of 71% and the VISA-P value of 50%. Compared with these good clinical results, the imaging findings were less significant.

Conclusion: Besides producing very satisfactory results in terms of symptoms and functionality in patients with tendinosis, the use of platelet gel also gives signs of morphological recovery. However, further investigations are needed to confirm consistency of these results.

B-0297 11:33

Combined ultrasound (US)-guided percutaneous treatment of epitrochleitis: a randomised controlled trial

D. Orlandi¹, E. Fabbro¹, C. Martini¹, G. Ferrero¹, L. Sconfienza², G. Serafini³, E. Silvestri¹; ¹Genoa/IT, ²San Donato Milanese/IT, ³Pietra Ligure, SV/IT (theabo@libero.it)

Purpose: Epitrochleitis is a common cause of elbow pain that could be treated with conservative or surgical intervention. The purpose of our work was to compare patients with clinical diagnoses of epitrochleitis treated with a combined US-guided percutaneous approach (dry needling and steroid) and similar patients treated with either local steroid injection or dry needling.

Methods and Materials: 30 patients suffering from epitrochleitis underwent to US-guided percutaneous treatment: 10 (7 males; age 38.7±7.4 [mean±st.dev]) were treated with dry needling and local steroid injection together, 10 (6 males; age 43.2±6.8) with dry needling only and 10 (3 males; age 35.2±9.4) with local steroid injection only. A visual analogue scale (VAS from 0 to 10) was used to evaluate the degree of pain at baseline and at 2, 12, 24, 36, 48 weeks after the procedure; US scanning was performed at baseline, 24, 48 weeks.

Results: No immediate or delayed complications were observed. Patients who underwent steroid injection only had a prompt pain decrease but limited effects on a long-term basis (baseline VAS=6.9±0.3; 2 weeks VAS=1.8±0.5; 12 VAS=4.0±0.3;

24 VAS=4.8±0.7; 36 VAS=5.3±0.6; 48 weeks=7.1±0.3). Patients treated with dry needling only had a delayed decrease of symptoms but permanent long-lasting effects (baseline VAS=7.6±0.4; 2 weeks VAS=7.4±0.3; 12 VAS=3.1± 0.5; 24 VAS=1.1±0.8; 36 VAS=0.8±0.4; 48 VAS=0.2±0.3). Patients treated with the combined procedure had a faster and more permanent decrease of symptoms (baseline VAS=7.1±0.4; 2 weeks VAS =2.3±0.6; 12 VAS= 2.6; 24 VAS=1.0±0.9; 36 VAS=0.7±0.6; 48 VAS=0.3±0.2; p <.01 for all).

Conclusion: Patients treated with the US-guided combined procedure had a better outcome than other groups and pain relief was faster and more permanent.

B-0298 11:42

A new minimally invasive safe and reproducible technique for management of cervical radiculopathy: ultrasound-guided cervical transforaminal epidural nerve root injections

W.A. Bashir, D.A. Connell; London/UK (wabashir@doctors.net.uk)

Purpose: Cervical radiculopathy is a common problem leading to intolerable debilitating pain. In refractory cases invasive therapies include CT and fluoro-guided transforaminal epidural steroid injections (TF-ESIs) as well as surgery. Unfortunately, there is increasing literature illustrating potential for brain and spinal cord injury following injection. Ultrasound allows safe, accurate and real-time injection.

Methods and Materials: This pilot study involved 40 patients who were referred to the radiology department following appropriate anaesthetic and surgical assessment with requirement for cervical TF-ESIs. Normally patients would have undergone fluoroscopic or CT-guided injection but were enrolled in this study after fully informed written consent. A 25-gauge spinal needle was advanced under sonographic guidance to a transforaminal position - nerve root levels mapped by identifying transverse processes and counting nerve roots cranially. The nerve root under investigation clearly showed thickening and was bathed in corticosteroid and anaesthetic.

Results: Pre- and post-pain scores performed regularly till 6 months post-therapy. All patients had significant reduction in pain scores at 6 months with sonographic evidence of reduction in nerve thickness. No complications were reported during this study.

Conclusion: Ultrasound TF-ESIs avoid the risks of ionising radiation. Sonographic guidance allows accurate real-time visualisation with high resolution of local anatomy and needle trajectory. Needle tip position is seen clearly. Colour Doppler allows scrutiny of vascular flow and therefore the investigator can have greater confidence in avoiding intravascular injection. Cervical nerve root injection has been shown to be a feasible and effective therapy for patients with chronic symptoms.

B-0299 11:51

Meralgia paresthetica: ultrasound-guided injection with 12-month follow-up data

R. Faschingbauer¹, C. Siedentopf¹, G. Feuchtner¹, C. Martinoli², W. Jaschke¹, A. Klausner¹; ¹Innsbruck/AT, ²Genoa/IT (christian.siedentopf@i-med.ac.at)

Purpose: To evaluate the efficacy of ultrasound-guided injections around the lateral femoral cutaneous nerve (LFCN) in patients complaining of meralgia paresthetica nocturna, and to document long-term results at 12 months.

Methods and Materials: This HIPPA compliant study was approved by our local Institutional Review Board; informed oral and written consent were obtained. Between 2008 and 2011 seventeen patients with symptoms of meralgia paresthetica nocturna, including 8 men (mean age, 61.38 years; range 47-70 years, SD: 9.16) and 9 women (mean age 61.57 years; range 46-75 years, SD: 8.60) were treated with US-guided injection of steroids along the LFCN. A visual analog scale (VAS) measure of symptoms before treatment and after 12 months was compared.

Results: Complete resolution of symptoms was documented in 12/17 patients (70.6%; 95% CI [0.44, 0.90]) and partial resolution in the remaining 5. These patients remained symptom-free or maintained their symptomatic improvement at 12-month follow-up. When compared with historical controls (60% failure of treatment), our ultrasound-guided technique resulted in statistically significant improvement in patient outcome (p < 0.05).

Conclusion: US-guided injection of steroids along the LFCN in patients complaining of Meralgia paresthetica results in more frequent long-term improvement in symptoms as compared with historical controls treated by injection without ultrasound guidance.

10:30 - 12:00

Room F1

Genitourinary

SS 507

Gynaecological MR imaging

Moderators:

C.D. Alt; Heidelberg/DE

S. Barter; Cambridge/UK

B-0300 10:30

MR imaging of the normal endometrium: do apparent diffusion coefficient values change among the portions of the uterus and over the phases of the menstrual cycle?

F. Fornasa, F. Pantalone, A. Dibenedetto, N. Schio, A. Quaglia; S.Bonifacio/IT (francescaforfornasa@libero.it)

Purpose: To establish whether the apparent diffusion coefficient (ADC) measured with diffusion-weighted magnetic resonance imaging (DWI) in the endometrium of healthy women significantly varies between the fundus and the isthmus of the uterus and from the early proliferative to the periovulatory phase of the menstrual cycle.

Methods and Materials: A series of healthy fertile women (minimum endometrial thickness: 4 mm; no endometrial fluid) underwent DWI (1.5 T; b values: 0 and 800 mm²/sec²). In 81 women (5th through 18th menstrual day) the endometrial ADCs measured at the fundus (as high as possible) were compared to those taken at the isthmus (2-3 cm from the internal cervical os). The fundal endometrial ADCs were moreover calculated, in 17 women, both at the 5th day after the beginning of the cycle and at the 14th day before the subsequent cycle. Each ADC value was obtained through the average of three different measurements. The statistical significance of the differences (fundal vs. isthmus; proliferative vs. periovulatory phase ADCs) was determined using the Student's t-test per paired data.

Results: The ADCs at the fundus (mean: 1.132 mm²/sec; range: 0.68-1.80) were lower than at the isthmus (mean: 1.420; range: 0.83-1.96). The fundal ADCs in the proliferative phase (mean: 0.923; range: 0.68-1.16) were lower than in the periovulatory phase (mean: 1.256; range: 1.10-1.80). Both differences were highly significant at statistical analysis (p < 0.001).

Conclusion: The magnitude of the variations in endometrial ADCs occurring in normal women should make the radiologists cautious when interpreting DWI examinations in patients with disease.

B-0301 10:39

Scaled signal intensity of uterine fibroids in T2-weighted MR images; new objective parameter to determine the suitability for magnetic resonance-guided focused ultrasound surgery of uterine fibroids

S.-W. Yoon; Gyunggi-Do/KR (jansonsrad@gmail.com)

Purpose: MR-guided focused ultrasound surgery (MRgFUS) is a non-invasive treatment for symptomatic uterine fibroids. Patient selection is the most important step to achieve good result. The purpose of this study is to assess the initial efficacy of scaled signal intensity (SSI) of uterine fibroids in T2-weighted MR images as a new objective parameter to determine the suitability for MRgFUS.

Methods and Materials: Twenty-four uterine fibroids in twenty premenopausal Asian patients were treated using MRgFUS. Treatments were performed from October 2008 to January 2010 and mean age of the patients was 37.9±6.1 years. SSI was measured at T2-weighted MR images by standardising its mean pixel intensity to a 0-100 scale, using reference intensities of muscle (0) and fat (100), respectively. SSI in each fibroid was retrospectively analysed, according to the non-perfusion volume (NPV) ratio.

Results: Mean NPV ratio in uterine fibroid of SSI, less than 10 (n=13), was 63.5±14.9%. In the case of uterine fibroid of SSI more than 10 (n=11), mean NPV ratio was 53.5±19.3%. Uterine fibroids of SSI less than 10 in T2 weighted MR images showed higher NPV ratio than uterine fibroids of SSI more than 10.

Conclusion: Scaled signal intensity of uterine fibroids in T2-weighted MR images can be suggested as a new objective parameter for the patient selection in MRgFUS. Uterine fibroids of SSI less than 10 is more eligible for MRgFUS.

B-0302 10:48

Deeply infiltrating endometriosis: evaluation of retrocervical space on MRI after vaginal opacification

V. Fiaschetti, A. Meschini, S. Crusco, V. Cama, L. Di Vito, G. Simonetti; *Rome/IT (a.mesko@libero.it)*

Purpose: To prospectively investigate diagnostic value and tolerability of MRI with intra-vaginal gel opacification for diagnosis and preoperative assessment of deeply infiltrating endometriosis.

Methods and Materials: One hundred and six women with clinical suspicion of deeply infiltrating endometriosis were previously examined with trans-vaginal ultrasonography and with MRI pre- and post-administration of vaginal gel. We evaluated the tolerability of this procedure with a scoring scale from 0 to 3. We also assessed with a score from 1 to 4 the visibility of four regions: Douglas-pouch, utero-sacral-ligaments, posterior-vaginal-fornix and recto-vaginal-septum. All patients underwent laparoscopic surgery after MRI.

Results: Nine patients considered procedure intolerable. Visibility of utero-sacral-ligaments and posterior-vaginal-fornix showed to be increased with gel ($p < 0.001$). In 75 out of 106 patients MRI has allowed us to diagnose deeply infiltrating endometriosis. The percentages of MRI-sensitivity, specificity, positive predictive value and negative predictive value were, respectively, 67.5%, 95.4%, 89.5 and 83.5% without gel, and 90.3%, 94.4%, 90.3% and 94.4% with gel; trans-vaginal ultrasonography sensitivity, specificity, positive predictive value and negative predictive value were 57%, 96.4%, 90.3% and 79.5%. In evaluation of utero-sacral-ligaments trans-vaginal ultrasonography, MRI without gel and with gel sensitivity was, respectively, 62.9%, 48.1% and 81.5%; for recto-vaginal-septum these values were 15%, 70% and 95%; for pouch of Douglas 82.6%, 86.5% and 90.3%; for posterior-vaginal-fornix 26.7%, 33.3% and 80%.

Conclusion: MRI with gel opacification of vagina should be recommended for suspicion of deep infiltrating endometriosis, in particular, for the added value in evaluation of recto-vaginal septum, utero-sacral ligaments and posterior vaginal fornix.

B-0304 10:57

MRgFUS treatment of uterine leiomyomas: results on quality of life, non-perfused volume ratio and size reduction over 12 months

F. Ciolina, A. Napoli, M. Anzidei, F. Zaccagna, G. Cartocci, L. Bertaccini, V. Noce, F. Boni, C. Catalano; *Rome/IT (federica.ciolina@gmail.com)*

Purpose: To investigate the efficacy of sonication in symptoms relief and volume reduction over time.

Methods and Materials: 36 leiomyomas in 30 women (average age 40 years, range 32-46) were treated with MRI-guided focused ultrasound (MRgFUS). The system (ExAblate2100, InSightec), equipped with a phased-array transducer, computer-controlled positioning system, radiofrequency amplifier system, operates in conjunction with a 3 T MR unit (GE). We scored severity of symptoms (as menorrhagia, urinary frequency, pelvic pain or bulk symptoms) using a 0- to 3-point scale before and after treatment. We also measured their impact on quality of life using a visual analog scale, the choice-based waiting trade-off and the time trade-off. Pre-treatment imaging set (T2-w, T1-w, pre- and post-Gd-BOPTA images) were obtained to measure leiomyoma volume. Immediately after treatment, T1-w contrast-enhanced fat-suppressed MR images in three planes were used to measure non-perfused volume (NPV). The average volume of treated fibroids was 63 ± 55 (SD) cm³. Follow-up images were obtained 3, 6 and 12 months after treatment to determine leiomyoma shrinkage. Qualitative and quantitative relations between fibroid volume, NPV ratio at treatment, and 6-month shrinkage were measured.

Results: All patients showed a complete relief of symptoms related to uterine fibroids and an increased quality of life. The average NPV ratio was $70\% \pm 25\%$ immediately after treatment. At follow-up treated fibroids showed volume decrease to 54 ± 40 cm³ with an average volume reduction of $20\% \pm 15\%$. A linear regression model showed highly significant correlation between post-treatment non-perfused volume ratio and shrinkage at 6 months.

Conclusion: MRgFUS therapy of leiomyoma shows as a noninvasively and safe method to obtain significant relief of symptoms, good NPV ratio and in mild shrinkage at 3, 6 and 12 months.

B-0305 11:06

Combined diffusion-weighted magnetic resonance imaging and MR lymphography reliably detect and evaluate sentinel lymph node in cervical cancer

Z. Zhou, H. Yu, B. Zhu, Y. Hong, J. Fang; *Nanjing/CN (zyzhou@nju.edu.cn)*

Purpose: To evaluate whether DWI and MR lymphography (MR-LG) reliably detect and evaluate sentinel lymph nodes (SLNs) metastasis in cervical cancer.

Methods and Materials: Thirty-eight patients with cervical cancer were preoperatively underwent interstitial MR-LG with Omniscan after completing the conventional MRI and DWI examinations, and the first lymph node in the lymphatic drainage pathway was defined as the SLN. Blue dye SLN biopsy was performed on all patients. The morphologic features of all the SLNs on MR lymphographic images were analysed. The relative apparent diffusion coefficient (rADC) of each SLN was measured. Diagnostic accuracies of the combined MR-LG and DWI approach compared with only MR-LG without DWI versus histopathology were evaluated.

Results: All localised SLNs corresponded well with SLNs identified on SLN biopsy. In patients with non-metastatic SLNs, oval enhanced SLNs were visualised by MR-LG. In patients with metastatic SLNs, the enhanced SLNs were visualised with or without filling defects in all patients except three in which SLNs were not enhanced. The sensitivity, specificity, accuracy, and positive and negative predictive values (PPV and NPV) for using filling defects on MR-LG as a diagnostic criterion were 78%, 72%, 90%, 65%, and 89%, respectively. Meanwhile, there were statistically significant differences between metastatic and non-metastatic SLNs in rADC ($P < 0.01$). With the addition of DWI, the diagnostic accuracies increased: sensitivity, 80%; specificity, 87%; accuracy, 91%; PPV, 78%; NPV, 94%.

Conclusion: The combination of DWI and MR-LG was useful in detecting the SLNs and in improving the diagnostic accuracy of SLN metastases in cervical cancer.

B-0306 11:15

Evaluation of therapeutic response to concurrent chemoradiotherapy in cervical cancer using blood oxygenation level-dependent MR imaging at 3 T: preliminary experience

A. Kim, C. Kim, B. Park, S. Huh, Y. Chong, Y. Choi, J. Park; *Seoul/KR (ahyeong.kim@samsung.com)*

Purpose: To investigate the changes in the rate of spin dephasing ($R2^*$) values at blood oxygenation level-dependent (BOLD) MRI in cervical cancer patients receiving concurrent chemoradiotherapy (CCRT), and to assess the relationship between tumour $R2^*$ values and final tumour responses to treatment.

Methods and Materials: 29 consecutive patients with biopsy-proven cervical cancer were examined by T2-weighted and BOLD MRI at 3 T. BOLD MRI was performed using a multiple fast field echo (mFFE) sequence to acquire 12 T2*-weighted images within a single breath-hold. All patients who treated with CCRT performed two serial MR examinations [i.e., prior to therapy (pre-Tx) and 1 month after the completion of therapy (post-Tx)]. At each therapeutic point, $R2^*$ value (1/sec) was calculated in the tumour and normal myometrium. Final tumour response as determined by changes in tumour size using MRI $\{(pre-Tx - post-Tx)/pre-Tx\}$ was correlated with tumour $R2^*$ values at pre-Tx.

Results: The final tumour size response was 69.9%. The mean $R2^*$ values of the tumours were 21.1 ± 6.7 at pre-Tx and 39.4 ± 8.6 at post-Tx, respectively, which showed a significant difference ($P < 0.001$). However, the mean $R2^*$ values of normal myometrium were 24.9 ± 3.7 at pre-Tx and 24.1 ± 2.8 at post-Tx, respectively, which did not show a significant difference ($P = 0.36$). At pre-Tx, tumour $R2^*$ values showed significantly negative correlation with final tumour size response ($P = 0.028$, Spearman's coefficient = -0.416).

Conclusion: BOLD MRI at 3 T may be helpful to evaluate therapeutic response in cervical cancers. These possibilities await further studies.

B-0307 11:24

Preoperative staging of patients with cervical carcinoma: comparison of magnetic resonance imaging and histopathologic evaluation

B. Banko, R. Milenkovic, M. Kratovac-Dunjic, G. Lilic, J. Djokic-Kovac, R. Maksimovic; *Belgrade/RS (bojanbanko@yahoo.com)*

Purpose: Magnetic resonance imaging (MRI) is recommended for preoperative assessment of local tumour extension in patients with FIGO stage IB or higher, after histological confirmation. The purpose of this study was to evaluate diagnostic value of MR in preoperative assessment of patients with cervical tumours and to optimise further therapeutic approach.

Methods and Materials: This prospective study included 43 patients, with preoperative MRI and cervical biopsy that confirmed cervical carcinoma. Therefore, the patients were divided into two groups: group 1, patients with FIGO \leq IIa who undergo surgery, and group 2, FIGO \geq 2b, who did not have surgery. In addition, in patients who underwent surgery, MR findings were compared with the histopathological report of the hysterectomy specimen.

Results: According to MRI findings, 18 (42%) patients were classified as T1, 7 (16%) patients were classified as T2a, 7 patients (16%) as T2b, 6 (14%) as T3, and 5 patients (12%) as T4, while on pathohistological specimens after surgery 20 (47%) were classified as T1, 5 (12%) as T2a, 7 as T2b (16%), 8 (19%) as T3 and



3 (7%) patients were classified patients as T4. There was a significant correlation between MR staging and histopathological findings of biopsy specimens ($\rho = 0.71$, $p < 0.01$). Furthermore, sensitivity and specificity for MRI for group 1 was 91% and 58%, respectively, while for group 2 was 100% and 73%, respectively.

Conclusion: MR is a useful diagnostic method in preoperative assessment and further therapeutic decision-making process in patients with cervical carcinoma.

B-0308 11:33

Dynamic contrast-enhanced imaging for evaluation of therapeutic response to concurrent chemoradiotherapy in cervical cancer

Y. Kim, J. Min, C. Kim, B. Park; *Seoul/KR (y.kim@samsung.com)*

Purpose: To evaluate the changes of quantitative parameters of dynamic contrast-enhanced imaging (DCEI) in cervical cancers before, during, and after concurrent chemoradiotherapy (CCRT), and to assess relationship between quantitative parameters of the tumours and final tumour responses to treatment.

Methods and Materials: 35 consecutive patients with biopsy-proven cervical cancer were enrolled. DCEI was obtained using T1-weighted 3D fast-field-echo sequence at 3 T. Pharmacokinetic analysis using an extended Kety model was performed. All patients who treated with CCRT performed three serial MR examinations [i.e., prior to therapy (pre-Tx), at the fourth week of therapy (mid-Tx), and 1 month after the completion of therapy (post-Tx)]. At each therapeutic point, quantitative parameters (i.e., Ktrans, Ve and Kep) were calculated in the tumours and normal gluteus muscles. Final tumour responses as determined by changes in tumour size or volume using MRI ((pre-Tx - post-Tx)/pre-Tx) was correlated with quantitative parameters of the tumour.

Results: Between therapeutic points, all quantitative parameters of the tumours revealed a significant difference ($P < 0.05$), while those of normal gluteus muscles showed no significant difference ($P > 0.05$). The mean value of final tumour response for the size and volume was 82.1% and 97.9%, respectively. Quantitative parameters of the tumours at pre-Tx or mid-Tx were not statistically associated with final tumour size or volume responses.

Conclusion: Quantitative parameters of DCEI revealed the therapeutic changes to CCRT in cervical cancers, compared with normal gluteus muscles. However, the parameters in cervical cancers were not associated with final tumour size or volume responses.

B-0309 11:42

Correlation between tumour size and surveillance of lymph node metastasis for Ib and IIa cervical cancer by MRI

B. Kwon, S. Kim, B. Rho, E. Ahn; *Daegu/KR (radoriya@naver.com)*

Purpose: To assess the feasibility of preoperative MRI-based measurement of tumour size with regard to lymph node (LN) metastasis in early uterine cervical cancer.

Methods and Materials: A retrospective review of patients with FIGO stage IB-IIA cervical cancer who underwent lymphadenectomy was performed. Diagnostic accuracy of MRI in detecting LN metastasis and rate of LN recurrence in terms of tumour size (≤ 4 cm versus > 4 cm) were analysed. ROC curve analysis was used to determine LN size for differentiating LN metastasis in terms of tumour size. $P < 0.05$ was considered statistically significant.

Results: Of the 200 patients, 45 (22.3%) had LN metastasis. There was no statistical difference between patients-based and region-specific analysis. The patients with tumour size with > 4 cm revealed higher diagnostic accuracy of MRI in detecting LN metastasis (85.4% versus 50.6%, $P=0.023$) and rate of LN recurrence (20.0% versus 6.4%, $P=0.031$) in than those with size with ≤ 4 cm, the differences was statistically significant. Discriminant analysis of LN size for the differentiation of metastasis from non-metastasis resulted in cut-off values (11.8 mm; size with > 4 cm versus 8.3 mm; size with ≤ 4 cm) and diagnostic accuracy (84.0% of size with > 4 cm versus 72.0% of size with ≤ 4 cm).

Conclusion: MRI has limited sensitivity, but high specificity in predicting surveillance of LN metastasis in the preoperative early cervical cancer, especially useful tool for patients with tumour size with > 4 cm.

10:30 - 12:00

Room F2

Breast

SS 502

Ultrasound: new developments

Moderators:

U. Bick; *Berlin/DE*

S. Ganau Macias; *Sabadell/ES*

B-0310 10:30

Additional breast ultrasonography (US) to negative mammography: impact on cancer detection and invasive assessment rate

V. Girardi, M. Tonegutti, E. Manfrin, F. Bonetti; *Peschiera del Garda/IT (giravero@yahoo.it)*

Purpose: To evaluate the outcome of lesions detected by US in asymptomatic women with negative mammography.

Methods and Materials: Out of 23,508 self-referring women undergoing to clinical examination, mammography and ultrasound (period: 2009-2011), 22,546 asymptomatic women were screened with bilateral US. US characterisation was based on BI-RADS criteria (negative-benign: BI-RADS 1-2, probably benign: BI-RADS 3, indeterminate-suspicious: BI-RADS 4-5). All indeterminate/suspicious US findings underwent invasive assessment. Fine needle aspiration cytology (FNAC; 22-27 gauge needle) was currently the first step followed by needle core biopsy (NCB; 14-gauge needle). The malignant and atypical lesions were referred to surgery. The pathological results represented the reference standard.

Results: Overall, there were 162 cancers: 134 (83%) cancers were detected by mammography and 28 (17%) only by US. Of 837 total invasive procedures, 428 (51%) were prompted by mammography and 409/837 (49%) were prompted only by US (403 FNAC, 6 NCB). Lesions detected by mammography resulted malignant in 134/428 (31%) and benign in 294/428 (69%). Lesions detected by US resulted malignant in 28/409 (7%) and benign in 381/409 (93%). The benign to malignant open surgical biopsy ratio by US was 0.25 (7 benign versus 28 malignant). Compared to mammography, the relative incremental breast cancer detection rate by US was +20.8% (28/134) and the relative incremental benign lesions detection rate by US was +129.6% (381/294%).

Conclusion: Addition of US to negative mammography allows for a substantial cancer detection increase of +20.8%. US generated a major increment of invasive diagnostic assessment. It took about 800 US examinations and 15 invasive procedures to detect one additional cancer. If the costs were sustainable, women may benefit from US screening.

B-0311 10:39

Diagnostic assessment of digital mammography screening: evidence on incremental breast cancer detection by bilateral ultrasound examination

S. Weigel, W. Heindel, C. Biesheuvel;

Muenster/DE (biesheuvel@referenzzentrum-ms.de)

Purpose: To evaluate the contribution of bilateral ultrasound (US) in detecting additional breast cancer at diagnostic assessment of lesions detected with digital mammography screening.

Methods and Materials: 2,803 women underwent additional mammographic imaging and bilateral whole-breast US examination at our screening assessment unit. We calculated the incremental breast cancer detection rate and associated false positive rate for US and mammography per assessment participant and per breast side (recall and contralateral).

Results: 393 women were diagnosed with 414 cancer lesions. Seven patients were diagnosed with a cancer lesion detected by US only, yielding an incremental breast cancer detection rate of 0.25% per assessment participant. For an additional two patients, US changed the diagnosis from unilateral to bilateral breast cancer. Thus, a total of nine cancer lesions were detected by US only; four were detected in recall sides, five in contralateral sides, resulting in incremental breast cancer detection rates of 0.13% and 0.20%, respectively. The associated false positive biopsy rates were 73.3% (11/15) in recall sides and 58.3% (7/12) in contralateral sides, compared to 80.0% (527/659) and 100% (6/6), respectively, for mammography-only indicated biopsies. The proportion of invasive cancers ≤ 10 mm was significantly lower among US-only detected cancers (44.4%) compared to those detected with mammography only (79.2%) ($p=0.035$).

Conclusion: We showed that supplemental whole breast US detected additional breast cancer lesions in both recall and contralateral breast sides that were occult on mammogram. This extra cancer yield should be weighed carefully against the associated false positive biopsies and substantial costs of bilateral US.

B-0312 10:48

Additional breast ultrasonography (US) in asymptomatic women with negative mammography: are there risk categories that benefit more than others?

V. Girardi, M. Tonegutti, E. Manfrin, F. Bonetti; *Peschiera del Garda/IT (giravero@yahoo.it)*

Purpose: To assess the cancer detection of US in addition to negative mammography in asymptomatic women and to correlate with age, risk factors, mammographic density.

Methods and Materials: During a 2-year period (2009-2011), a series of 23,508 self-referring women underwent to clinical examination, mammography and ultrasound. 22,118 asymptomatic women (no breast/axillary sign) with negative mammography constituted the population study (age < 40 years in 9%, 40-49 years in 41%, ≥50 years in 49%; previous history of breast cancer in 10%). Cancers detected by US was assessed in the population, as well as in subpopulations grouped by age (< 50 years; ≥50 years), breast density (BI-RADS ACR categories: fatty breasts D1-2, dense breasts D3-4), patient history (previous breast cancer, no previous cancer), hormonal status (fertile, menopausal). Fisher's exact test was used for statistical analysis (significant p value < 0.05).

Results: Overall, 162 breast cancers were diagnosed. 134/162 cancers (83%) were identified by mammography. The remaining 28 cancers (17%) were diagnosed by US alone. The US detection rate for total population was 1.3%. In the subgroups it was: 1.45% in women ≤50 years vs 1.03% in women > 50 years (p=0.29); 1.47% in dense breasts vs 1.06% in fatty breasts (p=0.24); 5.04% in women with previous cancer vs 0.85% in women without previous cancer (p=0.03).

Conclusion: The addition of ultrasound to mammography resulted in an increase of breast cancer detected of 17%. The age and the breast density have no significant effect on US performance. Most US-detected cancers occurred in women with personal history of breast cancer.

B-0313 10:57

Lesion detection in 3D-US automated breast volume scans (ABVS): correlation with breast MRI

T.A. Fassaert, I.J.M. Dubelaar, M.D.F. de Jong, G.J. Jager, M.J.C.M. Rutten; *Den Bosch/NL (tfassaert@hotmail.com)*

Purpose: To determine the diagnostic accuracy of 3D-US automated breast volume scanning (ABVS) related to MR breast imaging, using BI-RADS classification as discriminator.

Methods and Materials: During a 5-month period, all patients who underwent breast MRI were requested to have additional ABVS conducted of their breasts. Patients under 18 years of age, males, patients unable to undergo MRI, or give informed consent were excluded. Time between breast MRI and ABVS was < 7 days. Scan protocol depends on breast size: In cup A-C 3 scans and in size D and D+ 5 scans per breast are obtained. Resulting 3D-US data is evaluated on a dedicated workstation by an experienced radiologist, who is blinded for MRI findings. The 3D-US findings are evaluated using the BI-RADS classification for ultrasound. MR findings are used as gold standard and, when available, also histopathologic correlation was performed.

Results: Out of 281 consecutive scanned patients with MR imaging of the breasts 201 patients participated in our study. In nearly all patients, ABVS was technically successful and breast tissue was visible from skin to thoracic wall. The axillary region could not sufficiently be visualised for evaluation in most patients. So far, 104 patients are evaluated: 3D-US evaluation of the breast shows a sensitivity of 80% and specificity of 97%, compared to MR imaging findings. In coming months all 201 patients will be evaluated.

Conclusion: Compared to MRI, 3D-US shows high sensitivity and specificity in the detection of suspicious lesions. ABVS seems a promising new ultrasound technique in breast evaluation.

B-0314 11:06

Automated whole breast ultrasound: radiologists' detection performance and interobserver variability

H. Kang, S. Kim, B. Kang; *Seoul/KR (hera@catholic.ac.kr)*

Purpose: To evaluate the detection performance of automated whole breast ultrasound (AWUS) in comparison with hand-held breast ultrasound (HHUS) and to evaluate the interobserver variability in the interpretation of AWUS.

Methods and Materials: From October of 2009 to March of 2010, bilateral automated whole breast ultrasound was performed in consecutive 38 breast cancer patients who were scheduled for breast MRI. Total 66 lesions were included: 38 index cancers, 12 additional malignancies, and 16 benign lesions. Three breast radiologists independently reviewed AWUS data and analysed the breast lesions according to the BI-RADS classification. Detection rate, sensitivity and specificity of benign and malignant lesion detections were calculated and interobserver variabilities were calculated using Cohen's kappa statistics.

Results: Detection rate of index lesion and additional malignancy was 98.0% (45/50) in HHUS, 90.0% (45/50), 88.0% (44/50) and 96.0% (48/50) for three readers of AWUS. Sensitivity and specificity were 100% (50/50), 62.5% (10/16) in HHUS, 92.0% (46/50), 87.5% (14/16) in reader 1, 90.0% (45/50), 81.3% (13/16) in reader 2, and 96.0% (48/50), 93.8% (15/16) in reader 3. There was no significant difference in radiologists' detection performance, sensitivity and specificity among HHUS and AWUS (p < 0.05). The interobserver agreement was fair to almost perfect agreement for US features, categorisation, size and location of index masses.

Conclusion: AWUS is thought to be useful for detecting breast lesion. AWUS showed no significant difference of detection rate, sensitivity and specificity in comparison with HHUS and there were high degrees of interobserver agreement.

B-0315 11:15

What is pathology underlying stiffness? Ultrasound elastography of a human breast cancer model, with pathological correlation

F. Chamming's, H. Latorre, V. Fitoussi, M.-A. Le Frère-Belda, L. Pidial, J.-L. Gennisson, C.-A. Cuenod, O. Clement, L.S. Fournier; *Paris/FR (foucauld.chammings@egp.aphp.fr)*

Purpose: The purpose of this study was to assess stiffness using shear-wave elastography (SWE) during tumour growth in a human breast cancer implanted in mice, and to correlate the results with pathology.

Methods and Materials: A human invasive ductal carcinoma was implanted subcutaneously in 30 athymic female mice. Ultrasound was longitudinally performed during growth in 22 tumours, using a 15 MHz probe, every 1-2 weeks. Maximum diameter and mean elasticity value were collected. Seven tumours were measured in vivo and ex vivo. For pathological analysis, tumours of different sizes were removed. The following elements were quantified: the proportion of 'viable' and 'non-viable' tissue, the 'overall cellularity', the 'overall fibrosis rate', and the 'overall MicroVascular Density (MVD)'. A 'pathological stiffness score' (PSS), combining these pathological elements was calculated.

Results: A total of 69 SWE longitudinal measurements were performed. The mean elasticity value increased during tumour growth with an excellent correlation with size (r = 0.90, p < 0.0001). We found no significant differences between the values of elasticity in vivo and ex vivo (p=0.81). There was a significant correlation between elasticity and MVD (r=0.63, p = 0.006) and cellularity (r = 0.49, p = 0.05) but no significant correlation with fibrosis (r = 0.41 p=0.1). The correlation between elasticity and the 'PSS' was very good (r = 0.74 p = 0.0007).

Conclusion: SWE measured stiffness changes during tumour growth in a human breast cancer model implanted in mice, reflecting underlying pathological changes. There was a good correlation between elasticity and a 'PSS'.

B-0316 11:24

ShearWave™-elastography worldwide breast trial model - can additional SWE-features support downgrading BI-RADS 3 to BI-RADS 2?

F.K.W. Schaefer, W. Berg, D. Cosgrove, J. Gay, M.S. Henry, O. Wolf, C. Cohen-Bacrie, International BE-1-collaborative study group; *Kiel/DE (fschaefer@email.uni-kiel.de)*

Purpose: To determine the added value of ShearWave™-Elastography (SWE) in the characterisation of BI-RADS 3 breast-lesions as compared to conventional-ultrasound alone in an international-multicentre-study (BE1-collaborative-study-group)-world wide trial.

Methods and Materials: Patients scheduled for a breast-ultrasound were recruited to the BE1-study which was approved by the IRB of each centre. 939 lesions from 18 centres worldwide were entered, all histological/cytological confirmed. Significant SWE-features to add BI-RADS to improve lesion characterisation: 2 qualitative-

variables: elastography-shape, elastography-homogeneity/ 5 quantitative-variables: lesion dimension/maximum stiffness (kPa), median-elasticity-mean, lesion/fat ratio, mean-elasticity-diameter-ratio. All standard calculations of sensitivity/specificity, negative and positive predictive value and p-value were performed.

Results: 650 (69.2%) lesions were benign, 289 (30.8%) malignant. 303 lesions were scored BI-RADS 3. The reference test was BIRADS 2 < 0 and BIRADS 3-5 > 0. There were no cancers in the BIRADS 2-group. Therefore, the reclassification of the lesions consisted only in downgrading BI RADS 3 to a new BIRADS 2' -group when the SWE feature was not suspicious. BI-RADS alone had a sensitivity of 100%, specificity 16%, PPV 35%, NPV 100%. Round shape on SWE appears to be a helpful finding to alter clinical management (no malignant lesions/ $p < 0.001$). No malignancies were found with maximum-stiffness < 20kPa (gain of specificity 48%/ $p < 0.001$)/median-elasticity-mean < 1.6kPa (gain of specificity 8%/ $p < 0.01$)/lesion/fat ratio < 0.5kPa (gain of specificity 14%/ $p < 0.001$)/mean-elasticity-diameter-ratio < 0.7kPa (gain of specificity 14%/ $p < 0.001$).

Conclusion: All SWE-features taken separately increased specificity of breast ultrasound in case of BI-RADS 3 findings and reclassification in BI-RADS 2'. Best model with highest clinical impact: BI-RADS+SWE-maximum stiffness<20kPa.

B-0317 11:33

Is shear wave elastography (acoustic radiation force impulse) able to improve the assessment of BIRADS 4 breast solid lesions?

W. Ben Hassen, S. Canale, P. Vielh, M.-C. Mathieu, S. Delalogue, C. Balleyguier, Villejuif/FR (wagih@yahoo.fr)

Purpose: To evaluate the performance of shear wave elastography in breast lesions for the characterisation of BI-RADS 4 solid lesions.

Methods and Materials: Solid mass lesions categorised as BI-RADS 4 on ultrasonography were prospectively included. B mode images and results of acoustic radiation force Impulse (ARFI) imaging - both qualitative (suspicious elastogram image or not) and quantitative (shear wave speed m/s) - were correlated with cyto/histological results (FNA or biopsy). Values of the shear wave velocity were determined in both the solid masses and normal surrounding tissue with measurements performed at the same depth and with the same probe pressure. Percentage of speed increase was calculated, to limit the bias due to variable pressure, and correlated to pathology.

Results: 82 solid mass lesions were studied (39 benign, 43 malignant, mean size 13.7 mm) in 78 patients. The mean shear wave velocity in benign masses was statistically significantly lower than in malignant lesions (respectively, 2.105m/s and 3.279m/s ($p < 0.0001$)). Using the receiving operating characteristic curve, a cutoff level for shear wave speed of 2.96m/s predicted malignancy with 90% specificity and 56% sensitivity, with an area under the curve (AUC) of 0.834. A 100% speed increase had 85% specificity and 45% sensitivity with an AUC of 0.77. In addition, all cancer cases exhibited a suspicious appearance using ARFI qualitative imaging.

Conclusion: ARFI, in combination with B-mode imaging, can improve the assessment of breast lesions, especially for benign lesions miscategorised as BIRADS4 and might help decreasing the number of benign lesions referred for biopsy.

B-0318 11:42

Lesion characteristics and histopathological factors affecting diagnostic performance of breast ultrasound elastography

L.C.H. Leong, L.S. Sim, S.M.C. Fook-Chong, A.R. Jara-Lazaro, P.H. Tan; Singapore/SG (lester.leong.c.h@sgh.com.sg)

Purpose: To identify factors affecting the diagnostic performance of breast ultrasound elastography.

Methods and Materials: 701 sonographically visible breast masses that were referred to our department for image-guided biopsy were evaluated with ultrasound elastography. Elastographic assessment interpreted as probably benign or malignant based on a combination of elastographic size ratios and grey-scale strain pattern assessment. Using histological diagnosis as the gold standard, the sensitivity and specificity for various lesions were assessed.

Results: There was no statistically significant difference in the sensitivities of well-defined vs ill-defined lesions, regular vs irregular shaped lesions and lesions with and without acoustic shadowing. Statistically significant difference was noted in the specificities of well-defined lesions (90.0%) vs ill-defined lesions (63.8%) ($p < 0.0001$), regular (90.3%) vs irregular shaped lesions (71.9%) ($p < 0.0001$), no acoustic shadowing (83.5%) vs posterior shadowing (66.7%) vs combined shadowing (100%) ($p=0.003$). Sensitivity and specificity of lesions measuring 10 mm or less were 84.3% and 78.6% vs 98.1% ($p=0.001$) and 87.1% ($p=0.009$), respectively, for lesions more than 10 mm. There was no statistically significant difference in sensitivity and specificity for lesions with and without calcifications, lesions of different echogenicity and lesions in mammographically dense or fatty

breasts. Sensitivity of mucinous carcinomas (50.0%) and LCIS (33.3%) was lower than the other malignancies. Specificity of papillomata (64.9%) and fibrocystic change (77.4%) was lower than for other benign conditions.

Conclusion: Ill-defined lesions, irregular shaped lesions, lesions with posterior acoustic shadowing, small lesions, mucinous carcinomas, LCIS, papillomata and fibrocystic change appear to be related to poorer ultrasound elastographic diagnostic performance.

B-0319 11:51

Utility of second-look US with real-time virtual sonography (RVS) for MRI-detected lesions of the breast

S. Nakano¹, K. Yorozuya¹, K. Fujii¹, M. Yoshida¹, J. Kousaka¹, Y. Shiomi¹, T. Fukutomi¹, T. Ishiguchi¹, O. Arai²; ¹Aichi-gun/JP, ²Kashiwa/JP

Purpose: The aim of this study was to verify the utility of second-look US with using real-time virtual sonography (RVS) for the identification of MRI-detected lesions of the breast.

Methods and Materials: From 196 breast MRI, all MRI-detected lesions and subsequent biopsy were identified between February 2006 and December 2009. All patients were examined using RVS that could synchronise a US image and the MRI of the same site in real time. In order to achieve the same position of patient's body as in US, MRI was obtained on a 1.5-T imager in the supine position using a body surface coil. We searched all cases for MRI-detected lesions and investigated second-look US with or without RVS in identifying the lesions.

Results: Of 196 patients, MRI-detected suspicious lesions were detected in 55 (28%) patients. A total of 67 MRI-detected lesions in 55 patients comprised this analysis. Of 67 lesions, 24 (36%) were malignant and 43 (64%) were benign. Overall mean lesion size was 6.7 mm. A total of 46 mass lesions were identified, compared with 16 foci and 5 nonmasslike lesions. 18 (27%:18/67) lesions were detected in second-look US without RVS and were revealed as cancers in eight, benign lesions in 10. In contrast, 60 (90%:60/67) lesions were detected in second-look US with RVS and were revealed as cancers in 21, benign lesions in 39.

Conclusion: The present results suggest that second-look US with RVS can identify a large part of MRI-detected lesions without operator's skill.

10:30 - 12:00

Room G/H

Neuro

SS 511

Ageing, degenerative disorders and epilepsy

Moderators:

T. Stosic-Opincal; Belgrade/RS
T. Tourdias; Bordeaux/FR

B-0320 10:30

Regional cortical thickness deterioration in elderly healthy persons from AIBL MRI 3 T data: a MRI study using brain surface intensity model (BSIM)

Z. Lin¹, K. McMillan¹, L. Yan¹, U. Avinash²; ¹Waukesha, WI/US, ²Menomonee Falls, WI/US (zhongmin.lin@ge.com)

Purpose: Cortical thinning may be an effective biomarker for normal ageing process. Traditional methods used for measuring this biomarker on people over 60 have shown very small decline rates. A new method was developed to measure cortical thickness consistently and was used to study cortical deterioration rates of normal ageing between 60 and 89.

Methods and Materials: 30 healthy men and 30 healthy women of the age groups between 60 and 69, 70 and 79, and 80 and 89 from Australian Imaging Biomarkers and Lifestyle (AIBL) study were used to measure individual and average cortical thickness in 15 functional brain regions using BSIM. Regional cortical thickness of individuals and group averages were studied to evaluate thickness deterioration of normal ageing. BSIM registers brain images to a standardised atlas with 15964 predefined brain surface points. From each point a MR intensity profile perpendicular to the brain surface is extracted and modelled to calculate cortical thickness at the point.

Results: Regional cortical thickness within an age group was widespread and overlapped between groups. Compared to people in their 60's, thickness lost at different rates in functional regions- 0.1 mm/decade in temporal and medial-parietal and 0.3 mm/decade in posterior cingulate were observed. Results also show people in their 80s lost cortex at faster rates than in the 70s.



Conclusion: Widespread cortical thickness shows diversified distribution of cortical thickness among individual healthy persons. The normal ageing decline rates measured from AIBL 3 T data using BSIM are higher than what has been previously reported.

B-0321 10:39



Arterial spin labelling perfusion magnetic resonance (MR) imaging contributes to the early diagnosis of dementia

R.M.E. Steketee, S. Ooms, M. Luijten, G. Houston, J.C. van Swieten, M. Smits; Rotterdam/NL (*r.steketee@erasmusmc.nl*)

Purpose: Early diagnosis of dementia is challenging as brain atrophy may not yet be apparent. Changes in cerebral blood flow (CBF) preceding atrophy may be detected with arterial spin labelling (ASL). This study aims to assess ASL for diagnosing early dementia.

Methods and Materials: Fifteen patients with suspected diagnosis of dementia (mean age 63y, 7 males, mean Mini Mental State Examination 26) and 15 controls (mean age 59y, 8 males) underwent 3D PCASL and T1w MR scanning at 3 T (GE Healthcare, US). Data were coregistered and normalised using SPM8 (London, UK). ROI analysis of the CBF maps, masked for grey matter only, was performed with MarsBaR (Marseilles, FR), in regions involved in dementia and regions initially spared. Mean CBF values were compared between groups using 2-sample t-tests.

Results: Age and gender were not different between groups ($p > 0.05$). Mean CBF values in dementia-related brain regions were significantly lower in patients than controls ($p < 0.05$, right/left medial temporal lobe: 30/30 versus 37/38; right/left precuneus: 29/29 versus 43/42; right/left posterior cingulum: 35/34 versus 56/58 s ml-1100 g-1). No difference was found in regions not implicated in dementia (right/left precentral gyrus: 29/30 versus 35/36; right/left occipital gyri: 24/25 versus 31/29 s ml-1100 g-1 for patients and controls, respectively).

Conclusion: Patterns of hypoperfusion assessed with ASL in early dementia are concordant with those in established dementia and those assessed with positron emission tomography, indicating the contribution of ASL in the early diagnosis of dementia. Future aims are to assess ASL for early differentiation between types of dementia.

B-0322 10:48



1H MRS and DWI for differentiation of Parkinson's disease (PD) from parkinsonian syndromes (PS)

Z.Z. Rozhkova, M. Shkliar; Kiev/UA (*invivo@ukr.net*)

Purpose: We try to find diagnostic markers to differentiate PD from multiple system atrophy (MSA) and progressive supranuclear palsy (PSP) using ADC's and T2 values in the basal ganglia (BG) and in middle cerebral peduncles (MCP).

Methods and Materials: Four groups of patients (PDG, MSAG, PSPG, CG) are studied with 1.5 T SignaExcite (GE). The PDG includes 19 patients with PD, the MSAG includes 16 patients with MSA, the PSPG includes 14 patients with PSP, and CG group includes 15 controls. 1H spectra are obtained in BG and in MCP with SVSSTEAM:TR/TE=1500/144, 164, 184, 204 ms. From the echo-time dependence of the signal peak areas AM (M = Cho, Cr, NAA) T2M are calculated.

Results: The mean values of T2M in BG are: 67.1, 40.5, 98.6 ms (in PDG); 145.2, 59.3, 207.5 ms (in MSAG); 210.1, 185.3, 263.4 ms (in PSPG); 204.2, 198.0, 331.2 ms (CG). These differences in T2M allow us to distinguish subjects of CG from patients of PDG, and PSG, but they are not specific for differentiation of MSA from other patients. The mean values of T2M in MCP are: 63.3, 56.5, 101.8 ms (PDG); 58.2, 49.0, 90.2 ms (MSAG); 134.1, 152.3, 233.1 ms (PSPG); 215.0, 114.0, 320.1 ms (CG). The shortening of T2M in MCP for the patients of MSAG is extremely specific. ADCs (mm²/s) for the patients of PDG, MSAG, PSPG, CG in the region of BG are: 0.65, 0.54, 0.64, 0.44. More pronounced differences of ADC are found in MCP: 0.82, 0.96, 0.79, 0.8 for PDG, MSAG, PSPG, CG, respectively. Increasing ADCs in MCP for the patients of MSAG allows us to differentiate MSA from PSP and PD with high sensitivity.

Conclusion: ADC and T2M in MCP for MSA in comparison with PD and PSP are the in vivo diagnostic markers of MSA.

B-0323 10:57

Test-retest reliability of resting-state networks in healthy elderly subjects and MCI patients

J. Blautzik¹, D. Keeser¹, A. Berman¹, M. Paolini¹, V. Kirsch¹, S. Mueller¹, M. Reiser¹, S. Teipel², T. Meindl¹; ¹Munich/DE, ²Rostock/DE (*janusch.blautzik@med.uni-muenchen.de*)

Purpose: Longitudinal studies investigating the reliability of the brain's resting-state networks (RSNs) have focused on young healthy subjects; data on healthy elderly subjects and various patient groups, which represent individuals of clinical and

scientific interest, are lacking. Therefore, we aimed to investigate the test-retest reliability of RSNs in amnesic mild cognitive impaired (aMCI) patients, a prodromal stage of Alzheimer's disease, and healthy elderly controls (HC).

Methods and Materials: Fourteen aMCI patients and 11 HC underwent resting-state fMRI (rs-fMRI) and neuropsychological testing (CERAD battery) at baseline and on a follow-up examination after 13-16 months. Resting-state fMRI data were decomposed into independent components (ICs) using FSL's temporal concatenation group ICA (TC-GICA) and dual regression. The within-group test-retest reliability was determined by calculating spatial normalised correlation coefficients (SNCCs) for the corresponding averaged group-level components deriving from both MRI examinations.

Results: Both groups remained cognitively stable over time. The TC-GICA approach produced 15 ICs considered as RSNs and 9 ICs considered as artefacts. Overall SNCCs were low/moderate to high ranging from 0.20 to 0.81 and did not differ significantly between groups ($p > 0.55$). Group-level components considered as RSNs expressed SNCCs ranging from 0.62 to 0.81. Highest test-retest reliability was observed in two sub-networks of the default-mode network, two sensorimotor networks, and a visual network.

Conclusion: The long-term test-retest reliability of RSNs is moderate to high in cognitively stable healthy elderly and aMCI patients. This finding is essential to establish rs-fMRI as a tool in the diagnosis and follow-up of neuropsychiatric and neurodegenerative disorders.

B-0324 11:06

Multi-tracer PET early frames as a functional marker in Alzheimer's disease

V. Abreu¹, S. Carter², A. Nordberg²; ¹Geneva/CH, ²Stockholm/SE

Purpose: We investigated whether the distribution of (11)C-Pittsburgh compound B (PIB) and (11)C-L-deprenyl (DEP) in dual-tracer PET early frames is flow-dependent and its potential clinical use.

Methods and Materials: Dual-tracer PET scans were performed in a group of 7 patients with clinical diagnosis of "probable AD" (mean age \pm SD, 64.1 \pm 6.1y; mean Mini-Mental State Examination [MMSE] score \pm SD, 22.2 \pm 6.0) and a group of 7 age-matched controls (mean age \pm SD, 60.3 \pm 9.3y; mean MMSE score \pm SD, 28.7 \pm 1.0), both recruited from Karolinska University Hospital. Quantitative data were obtained by summing all early PIB and DEP frames and an iterative algorithm generated normalised perfusion images with standard uptake values for selected regions of interest (frontal, parietal, temporal and posterior cingulate cortex). We calculated Pearson's correlation coefficient for the combined frames in all brain tissue voxels and group differences were analysed with two-tailed t-tests.

Results: PET frames between minutes 1-3 produced the only voxelwise correlation found ($R=0.78\pm0.05$) in both groups. In this 3-min window were the lowest PIB and DEP uptake values measured, but the binding/flow ratio was significantly higher ($p < 0.05$) in most AD patients ($n=6$) than in the control group, suggesting that tracer distribution may be flow-dependent. No correlation was found in the other frames studied (minutes 4-10). Brain regions of interest identified as significant discriminators ($p < 0.05$) of AD disease were posterior cingulate and temporal cortex.

Conclusion: The distribution of PET tracers in the very early frames is likely flow-dependent, which may be useful to derive clinical estimates of cerebral blood flow and neuroinflammation from a single multi-tracer PET scan.

B-0325 11:15

T2 relaxometry (on 3.0 T MR) made temporal lobe epilepsy diagnosis easy

H.P. Parekh, D.P. Vasavada; Jamnagar/IN

Purpose: The purpose of this study was to evaluate whether T2 relaxometry made hippocampal pathology diagnosis easy and lateralise the epileptic focus in patients with intractable temporal lobe epilepsy.

Methods and Materials: Our study includes 40 patients with unilateral temporal lobe epilepsy who had unilateral hippocampal atrophy and 10 patients with unilateral temporal lobe epilepsy who had no evidence of atrophy on MRI. On a 3.0 T MR scan using a dual echo sequence, 25 contiguous oblique coronal slices in all 50 patients and in 25 healthy subjects were taken. Averages of six slices containing the head, body, and tail of the hippocampus were used to calculate hippocampal T2 relaxation times

Results: All first 40 patients with hippocampal atrophy and 6/10 (80%) patients with normal MRI had abnormally high hippocampal T2 relaxation ipsilateral to the epileptic focus. Bilateral abnormal hippocampal relaxation values were found in 8/40 (20%) patients with unilateral hippocampal atrophy and 2/10 (20%) patients with normal MRI. However, this increase was always greater ipsilateral to the epileptic focus

Conclusion: Hippocampal T2 mapping provides evidence of hippocampal damage in the majority of patients with intractable temporal lobe epilepsy who may or may not have hippocampal atrophy on MRI and can correctly lateralise the epileptic focus in most patients. Adding T2 relaxometry in MR protocol for suspected temporal lobe epilepsy helps in establishing the diagnosis and lateralisation of epilepsy.

B-0326 11:24

Hippocampal malrotation: not everything is mesial sclerosis

R. Pastor Toledo, J.L. Leon Guijarro, I. López Blasco, S. Paz Maya, L. Ariño Montaner, D. Soriano Mena, A. Llanes Rivada, J. Uchiyamada, R. Sanchez Oro; Valencia/ES

Purpose: Demonstrate the imaging finding in Magnetic Resonance Imaging (MRI) in patients with epilepsy and hippocampal malrotation using high-resolution volumetric sequences.

Methods and Materials: Review of studies of MRI brain patient's with epilepsy of our hospital diagnosed with mesial sclerosis from January 2005 through December 2011. For now, we have obtained 78 patients. The studies were conducted on a high field 1.5 T and 3 T, according to the protocol of epilepsy include: sagittal T1, axial T1 and T2, coronal FLAIR, coronal T2 (high resolution) and 3D volumetric sequences IR (1.5 mm thick).

Results: We have obtained 12 patients with hippocampal malrotation in which there had been a misdiagnosis. Common features found in hippocampal malrotation were hippocampus abnormally situated in a medial location, which has not rotated to the normal depth within the wall medial temporal lobe. The vertical diameter is similar or greater than the transverse. The temporal horn appears enlarged and choroidal fissure is prominent and empty. The collateral sulcus is often verticalizes altering its angle, causing a temporary imprint on the pole known as temporal eminence. The internal structure of the hippocampal gyrus is blurred, keeping the size and normal internal signal and changes in surrounding structures appear as parahippocampal gyrus (decrease in its upper transverse), the subiculum, the fimbria and fornix (thinning and flow position), but all in a temporal lobe maintains its normal size.

Conclusion: Hippocampal malrotation built a malformation that should be considered in the differential diagnosis of patients with epilepsy.

B-0327 11:33

Cerebellar changes in essential tremor patients detected by magnetic resonance spectroscopy

I. Latnerova, J. Keller, A. Rulseh, F. Jiru, A. Skoch, M. Hoskovcova, E. Ruzicka, J. Vymazal; Prague/CZ (iva.latnerova@gmail.com)

Purpose: Essential tremor (ET) is one of the most common movement disorders in humans, characterised by a kinetic tremor of arms, head and even the voice. The prevalence of ET is dependent on the increasing age. The aim of our study was to find out, if the metabolite concentrations measured in cerebellum are also age-dependent.

Methods and Materials: Patients with ET (n=28, 20 M, 8 F, age=50±31) and healthy volunteers (n=23, 15 M, 8 F, age=50±31) were divided into 4 age-groups: ≤30 years (controls=4, patients=5), 30-50 years (c=7, p=6), 50-70 years (c=9, p=12), > 70 years (c=3, p=5). We focused on the cerebellum and measured N-acetyl aspartate (NAA), creatine (Cr) and phosphocholine (Pch) concentrations. Spectroscopy was performed on 1.5 Siemens Avanto scanner using single-slice CSI sequence (TR=1500 ms, TE=135 ms) and processed using Sipro software package with LCModel. Only voxels with low fitting error were chosen. Double-tailed Welch two sample t-test was used for statistical analysis.

Results: We found NAA (controls=5.0345, patients=4.6110, p-value=6.7922E-4) and Pch (controls=1.0851, patients=0.9468, p-value=0.0038) reduction in ET patients, no Cr reduction was found. The greatest difference between controls and patients was found in the age-group 40-50 years. We found all concentration values with no drop in increasing age.

Conclusion: We found the significant reduction of NAA and Pch concentrations in ET compared to healthy controls; however, these changes were not related to age. Supported from grants IGA MZ CR, NS9654-4/2008, NT11328-4/2010, MŠM 0021620849 and MŠM 0021620816, IGA MZ CR NS10336-3/2009.



B-0328 11:42

Diffusion tensor imaging and voxel-based morphometry in Parkinson disease

A. Efimtsev, V. Fokin, A. Trufanov, A. Pashkova, D. Khaimov; Saint Petersburg/RU (atralf@mail.ru)

Purpose: The purpose of this study was to find out if a microstructural damage to cerebral white matter correlates with grey matter volume changes and cognitive symptoms in idiopathic Parkinson disease (PD).

Methods and Materials: 36 patients with de novo PD were examined (Hoehn and Yahr stages I, III; two age subgroups, 41 to 60 (A) and 63 to 80 (B) years old; with and without cognitive impairments). T1-weighted images (gradient echo, voxel 1 mm3), diffusion tensor images (DTI) were obtained. Total brain, grey matter (GM), white matter (WM) volumes were defined from T1-weighted images, fractional anisotropy (FA) meanings were calculated using FSL.

Results: Patients of A age subgroup also did not show any significant difference with controls, despite that duration of illness was twice longer than in patients 63 to 80 years. Subgroup B had shown decreased volume in medium temporal gyrus, fronto-temporal area, pons. Putamen, thalamus, caudate nucleus, amygdala volumes did not demonstrate difference with controls. FA, measured in all patients was unaltered in the midbrain, lowered in the corticospinal tract, in splenium of corpus callosum, front lobes, centrum semiovale, pons (in projection of substantia nigra). There were lower FA meanings in corpus callosum and internal capsule in patients with cognitive impairments and III Hoehn and Yahr stage, not depending on age or duration of illness.

Conclusion: Correlation of FA decrease and worse cognitive state in patients of any age, without brain structure volume changes can be proved that widespread neurodegeneration is already present at the time of clinical onset.

B-0329 11:51

The relation of neuroimaging findings in carbonic anhydrase type II deficiency syndrome to cognitive disturbance and visual loss

I.A. Alorainy, T.M. Bosley, M.A. Salih, D.T. Oystreck, S. Al-Malki, A.H. Al-Suhaibani, H. Khiari, K.K. Abu-Amero; Riyadh/SA (alorainy@ksu.edu.sa)

Purpose: This work describes the neuroimaging findings in carbonic anhydrase type II deficiency syndrome (CADS) and the relation of these findings to cognitive disturbance and visual loss.

Methods and Materials: Retrospective analysis of serial neuroimaging studies performed in 18 individuals from 10 unrelated consanguineous families with CADS followed for 10 years was performed and correlated with visual loss and mental retardation.

Results: Brain calcification was present in patients as young as two years old, but absent in patients as old as nine years, and was generally progressive and followed a distinct distribution, involving predominantly basal ganglia and thalami and grey-white matter junction in frontal regions more than posterior regions. Patients with more severe cognitive disturbance had less profound brain calcifications. In general, basal ganglia and thalami were spared in individuals with more severe mental retardation, although grey-white junction calcification still occurred. Progressive calcification was noted even in individuals with minimal or no cognitive disturbance. Small optic canal was always associated with very poor vision, while canal size greater than 3 mm was associated with normal optic disk appearance. Optic canal size was correlated with visual acuity (r = -0.578; p = 0.001) and with degree of optic atrophy (r = -0.477; p = 0.003).

Conclusion: Brain calcification in CADS may not be present during childhood. Worse mental retardation is associated with less brain calcification, especially in the deep grey matter. Variability of brain calcification and cognitive disturbance may imply additional genetic or epigenetic influences affecting the course of the disease.

10:30 - 12:00

Room L/M

Abdominal Viscera

SS 501

Liver (non primary lesions)

Moderators:

B.J. Op de Beeck; Antwerp/BE

A. Siemianowicz; Piekary Śląskie/PL

B-0330 10:30

Paradoxical uptake of Gd-EOB-DTPA on the hepatobiliary phase in the evaluation of hepatic metastasis from breast cancer: is the "target sign" a common finding?

J. Shim, C. Lee, A. Kim, K. Kim, J. Choi, J. Lee, Y. Park, C. Park; Seoul/KR (kikookie@hanmail.net)

Purpose: To describe MRI findings of breast cancer liver metastasis using gadoteric acid with an emphasis on the added value of the hepatobiliary phase (HBP).

Methods and Materials: Nine patients with 13 liver metastases were included in the study after reviewing the medical records of 29 breast cancer patients who underwent Gd-EOB-DTPA-enhanced MRI between February 2008 and June 2010. The diagnoses of liver metastasis were established by percutaneous liver biopsy or surgery and on the basis of image findings. Two radiologists retrospectively evaluated SI and sizes of metastases and patterns of enhancement in HBP. The SI ratio was calculated as the SI of the central hyperintense portion in "target" lesions divided by the SI of nearby normal liver parenchyma on HBP. We also measured ADC values from DWI.

Results: Liver metastases were all hypointense (100%) on T1WI, and many lesions had "target" appearances with central high SI and peripheral low SI rim (47%) on T2WI. Dynamic study showed rim enhancement on arterial phase (85%), and "target" appearance, consisting of central enhancing portion with peripheral wash-out or hypointense rim, on HBP (62%). The mean SI ratio was 0.7. The mean ADC value of "target" appearing metastases was $1.25 \times 10^{-3} \text{mm}^2/\text{s}$; (1.3-1.6), compared with a mean value of $0.8 \times 10^{-3} \text{mm}^2/\text{s}$; (0.8-1.4) in homogeneous defect on HBP. There was statistically significant difference ($p < 0.05$).

Conclusion: Breast cancer liver metastases commonly demonstrated as peripheral ring enhancement on arterial dominant phase and target sign with central round enhancing portion and peripheral hypointense rim on HBP.

B-0331 10:39

Detection of colorectal hepatic metastases using Gd-EOB-DTPA MR imaging and diffusion-weighted imaging (DWI) alone and in combination in patients after chemotherapeutic treatment

A. Macera, M. Petracchini, A. Balbo Mussetto, A. Fornari, C. Lario, T. Gallo, S. Cirillo; Turin/IT (macera.annalisa@gmail.com)

Purpose: To compare the accuracy and sensitivity of Gd-EOB-DTPA MR imaging and DWI, alone and in combination, for detecting colorectal liver metastases in patients with metastatic disease after chemotherapeutic treatment.

Methods and Materials: 32 consecutive patients, with a total of 166 lesions, underwent MR imaging. Out of 166 lesions, 144 (86.8%) were metastases on histopathology and/or intraoperative sonography. Three image sets (Gd-EOB-DTPA, DWI, and combined Gd-EOB-DTPA and DWI) were reviewed independently by two observers. Statistical analysis was performed on a per lesions basis.

Results: MRI scans evaluated by the image set 1 (unenhanced sequences and after intravenous administration of Gd-EOB-DTPA) correctly identified 127/166 lesions with accuracy of 76.5% (95% CI 69.3-82.7) and 106/144 metastases with a sensitivity of 73.6% (95% CI 65.6-80.6). MRI scans evaluated by the image set 2 (unenhanced sequences and DWI) correctly identified 108/166 with accuracy of 65.1% (95% CI 57.3-72.3) and 87/144 metastases with a sensitivity of 60.4% (95% CI 51.9-68.5). MRI scans evaluated by the image set 3 (unenhanced sequences, after intravenous administration of Gd-EOB-DTPA and DWI) correctly identified 148/166 with accuracy of 89.2% (95% CI 83.4-93.4) and 131/144 metastases with a sensitivity of 91% (95% CI 85.1-95.1).

Conclusion: The sensitivity and accuracy of set 3 is significantly better than both sets 1 and 2 ($p < 0.0001$). The sensitivity and accuracy of set 1 is significantly better than set 2 ($p=0.0001$).

B-0332 10:48

Multi-center, randomised comparison study to evaluate outcomes and resource needs of imaging and treatment following Gd-EOB-DTPA-enhanced MRI of the liver in comparison to extracellular contrast media (ECCM)-enhanced MRI and contrast-enhanced multidetector computed tomography (MDCT) in patients with a history of colorectal cancer and known or suspected metachronous liver metastases: the value study

C.J. Zech¹, S. Gschwend², A. Ba-Ssalamah³, T. VALUE-Study Group²;

¹Munich/DE, ²Berlin/DE, ³Vienna/AT (Christoph.Zech@med.uni-muenchen.de)

Purpose: To compare gadoteric-acid-enhanced MRI (Gd-EOB-DTPA-MRI), MRI with extracellular contrast media (ECCM-MRI) and contrast-enhanced MDCT (CE-MDCT) as initial diagnostic modalities in the local work-up of patients with colorectal liver metastases.

Methods and Materials: 34 study centres included 342 patients with suspected liver metastases from 10/2008 to 09/2010. The initial imaging technique to be used was randomised. The primary variable was the proportion of patients for whom further imaging was required after initial imaging. For this decision a consensus between a liver surgeon and radiologist on-site was reached. Secondary variables included confidence, diagnostic efficacy parameters and impact on the surgical plan in the sub-group of patients with histopathology and/or intraoperative ultrasound.

Results: Further imaging was required in 0/118 (0%), 19/112 (17%) and 44/112 (39%) cases after Gd-EOB-DTPA-MRI, ECCM-MRI and CE-MDCT, respectively ($p < 0.0001$). Diagnostic confidence was high/very high in 98.3%, 85.7% and 65.2%, respectively. In the sub-group of patients who underwent surgery (112/342) sensitivity for detection of metastases was 93.8%, 89.4% and 84.1% for Gd-EOB-DTPA-MRI, ECCM-MRI and CE-MDCT, respectively. Surgical plan was changed and surgery time increased in 12.8%, 16% and 29.4% of patients after Gd-EOB-DTPA-MRI, ECCM-MRI and CE-MDCT, respectively. Gd-EOB-DTPA-MRI as second imaging avoided unnecessary surgeries in 4/24 patients (16.6%) scheduled for surgery.

Conclusion: The results show superiority of Gd-EOB-DTPA-MRI over CE-MDCT and ECCM-MRI for evaluating patients for liver surgery. Patients randomised for Gd-EOB-DTPA-MRI as initial staging strategy needed no further imaging to assess operability with implications for work-flow and costs. The comparison of diagnostic efficacy parameters demonstrates the diagnostic benefit of Gd-EOB-DTPA-MRI.

B-0333 10:57

Kinetics of Gd-EOB-DTPA in liver lesions suspect for metastases: a systematic comparison of raw data with arterial-input-function corrected data

P.A.T. Baltzer, M. Benndorf, W.A. Kaiser, M. Dietzel;

Jena/DE (pascal.baltzer@med.uni-jena.de)

Purpose: Gd-EOB-DTPA is a liver-specific contrast agent for differentiation of focal liver lesions. Herein, our aim is to compare Gd-EOB-DTPA kinetics among benign and malignant lesions and to assess the effect of arterial-input-function (AIF) correction on this comparison.

Methods and Materials: Two blinded observers retrospectively reviewed consecutive examinations of 40 patients and identified 116 focal liver lesions (49 benign, 67 malignant). Reference standard was established on the basis of histopathology and follow-up examinations. Signal intensities (SI) were obtained for all identified lesions, healthy liver parenchyma, aorta and noise. For each lesion, these signal intensities were measured in the precontrast images as well as in the arterial, portalvenous, venous and late phase. Lesion signals now were evaluated using two different approaches (M1 and M2). M1 employed the lesions' absolute SI and was corrected for the AIF with the aorta's SI. M2 employed the lesions' contrast-to-noise ratio and was corrected for the AIF with the aorta's signal-to-noise ratio. M1 and M2 were compared.

Results: In M1 there was a significant difference between benign and malignant focal liver lesions in the late phase ($P < 0.01$). In M2 there was a difference in the arterial phase ($P < 0.01$). No other significant differences occurred in M1 and M2. Visual comparison showed that correction leads to more streamlined kinetics among all lesions.

Conclusion: AIF-correction may lead to further information about focal liver lesions, depending on what kind of correction is performed. Whether this information is diagnostically relevant needs to be determined.

B-0334 11:06

Detection of colorectal liver metastases: sensitivity of T2-weighted and diffusion-weighted imaging using pathological examination as method of reference in a rat model

M. Wagner, L. Maggiori, M. Ronot, V. Vilgrain, Y. Panis, B.E. Van Beers; Clichy/FR (wagner.mathilde@gmail.com)

Purpose: To compare the sensitivity of T2-weighted and diffusion-weighted imaging (DWI) in detecting colorectal liver metastases in a rat model.

Methods and Materials: Eighteen BDIX rats had surgery with 4 injections of 0.5 million DHDK12 cells in the left liver. MR examination included RARE T2-weighted imaging and SE-DWI (b = 0, 20 and 150 s/mm²). Sacrifice was performed immediately after MRI procedure. Images were analysed by two independent readers. Pathological examination was performed after slicing the whole left liver every 0.4 mm. Average diameter of each liver metastasis was computed. Cochran Q-test was used to compare the detection rates.

Results: A total of 166 liver metastases were identified on pathological examination. Mean average diameter was 1.05 ± 0.8 mm. For both readers, a significantly higher number of metastases was detected on DWI than on T2-weighted images (99/166 (60%) vs. 77/166 (46%), p < 0.001 for reader 1 and 92/166 (55%) vs. 77/166 (46%), p = 0.001 for reader 2). After stratification according to metastasis average diameter, DWI had a significantly higher detection rate than T2-weighted imaging for metastases with an average diameter between 0.3 and 1.2 mm (42/78 (54%) vs. 24/78 (31%), p < 0.001 for reader 1 and 36/78 (46%) vs. 24/78 (31%), p = 0.001 for reader 2). No difference was found between the two imaging techniques for metastases larger than 1.2 mm or smaller than 0.3 mm.

Conclusion: This experimental study with MR and pathological correlations shows the better sensitivity of DWI relative to T2-weighted imaging for detecting liver metastases, especially those of small size.

B-0335 11:15

Impact of contrast-enhanced intraoperative ultrasound on operation strategy in case of colorectal liver metastasis

A. Schulz, J.B. Dormagen, A. Drolsum, B.A. Bjørneth, K.J. Labori, N.E. Klow; Oslo/NO (anselm.schulz@gmail.com)

Purpose: To evaluate the current impact of contrast-enhanced intraoperative ultrasound (CE-IIOUS) on the initial surgical strategy for resection of colorectal liver metastasis (CRLM).

Methods and Materials: Eighty-six consecutive patients undergoing open liver resection for CRLM were evaluated retrospectively over a 2.5 years period. The patients underwent 97 operations. Preoperative staging was performed with contrast-enhanced CT and MRI (70 of 97 operations). Acuson Sequoia™ 512 ultrasound system was used in all cases. Contrast agent used was 2-4 ml SonoVue®. Transducers were curved array 4C1 and linear 15L8. CE-IIOUS was performed in all patients with standardised examination technique. CRLM were identified in venous phase as hypoechoic lesions. CE-IIOUS findings were compared with preoperative staging.

Results: Combined CT/MRI identified preoperative 328 CRLM. Seventy-two additional lesions were identified during the operation. Intraoperatively 41 additional CRLM were identified by inspection, palpation and CE-IIOUS (10%), and another 31 CRLM were identified by CE-IIOUS alone (8%). All additional CRLM detected by CE-IIOUS were confirmed by histology. CE-IIOUS changed planned operation strategy in 29.9% of operations. A larger resection was necessary in 13.4% of cases, reduced liver resection was found sufficient in 11.3% and 5.2%, and was found inoperable. For patients diagnosed preoperatively staged solitary lesions CE-IIOUS changed operation strategy in 19%. Thus, radical tumour resection would have failed in 4.8% without CE-IIOUS.

Conclusion: CE-IIOUS is still an essential tool to ensure optimal and complete tumour resection. In case of a solitary CRLM the additional value of CE-IIOUS might be debatable.

B-0336 11:24

Diffused-weighted MRI for quantification of liver fibrosis

J.M. Alustiza¹, J. Arenas¹, M.A. Von Wichmann¹, A. Castiella², J.I. Emparanza¹, E. Salvador¹, M. Garcia-Bengochea¹, E. Zapata²; ¹San Sebastian/ES, ²Mendaro/ES (jmalustiza@osatek.es)

Purpose: To evaluate the accuracy of diffused-weighted (DW) MRI for assessing the different stages of liver fibrosis.

Methods and Materials: 103 consecutive patients suffering different chronic liver diseases were studied by liver biopsy and by MRI. Patients with decompensated liver diseases were excluded. Diffusion-weighted MRI sequence was performed

with 0, 150, and 450 b values and 0-150, 0-450, and 150-450 ADC (apparent diffusion coefficient) values were obtained. Variance analysis was applied by Krause Wallis (K-W) formula with unilateral signification for the diffusion measures. The AUROC were calculated with a CI of 95% for significative liver fibrosis detection (Metavir Scale->F1).

Results: 40 patients were HIV+, 70 HCV+, 2 HBV, 2 HBV-HCV, 9 had autoimmune liver diseases, and 20 other causes. Stages Metavir Scale: F0-47; F1-33; F2-8; F3-4; F4-11. The ADC values (10³ xmm²/seg) were as follows: 0-150 (F0-F4): 2.5; 1.7; 0.2; 0.2; and 0.7, with K-W=7.67 and p=0.1. 0-450: 2.6; 1.6; 0.2; 0.2; 0.7 with K-W =7.81 and p=0.09. 150-450: 2.7; 1.5; 0.4; 0.2; 0.4 with K-W=4.68 and p=0.3. The AUROC for significative liver fibrosis detection for the three ADC, respectively, were of: 0.50 (CI95%: 0.4-0.6; p=0.96), 0.52 (CI95%: 0.42-0.62; p=0.08) and 0.58 (CI95%: 0.48-0.67; p=0.23).

Conclusion: DW-MRI with b values of 0, 150 and 450 ms do not adequately discriminate the different liver fibrosis stages. This technique is not useful for significative liver fibrosis detection.

B-0337 11:33

Magnetic resonance assessment of functional changes in liver perfusion related to intrahepatic islets transplantation (islet-tx) and clinical outcome: preliminary results

A. Palmisano, A. Esposito, F. De Cobelli, P. Maffi, T. Canu, P. Magistretti, G. Ironi, A. Secchi, A. Del Maschio; Milan/IT

Purpose: Pancreatic islet transplantation (islet-tx), through intra-portal vein infusion, is a promising therapeutic approach for T1DM, but most islets are lost in the first phases after transplantation. A potential crucial factor for islets engraftment seems to be vascularisation. A previous preclinical study found a strong correlation between dynamic-contrast-enhancement magnetic resonance imaging (DCE-MRI) parameters and immunohistochemical measures of islets neovascularisation. Aim of our study was to assess the changes in the liver perfusion occurring at 7days from intrahepatic islets infusion, in humans, and correlate this data with islet-tx outcome.

Methods and Materials: 4 diabetic patients (pts) received islet-tx. DCE-MRI studies were performed before islet-tx and at 1 week from transplantation on a 1.5 T, using a T1w-3D-TRIVE sequence (slice thickness:4 mm; 45 dynamic scans; temporal resolution 4.2sec) encompassing the entire liver, during intra-venous gadolinium injection. DCE-MRI was quantitatively analysed to obtain maximum enhancement (ME) and area under curve (AUC). DCE-MRI-parameters modifications were compared with metabolic function [C-peptide, glycated haemoglobin (HbA1c)] at 4 months after transplantation.

Results: DCE-MRI parameters increased 7 days after transplantation in 2 pts (pt#1:ΔME+5%, ΔAUC:+13%; pt#3:ΔME+17%,ΔAUC+38%). These 2 pts showed a good graft function at 4 months after transplantation (pt#1:C-pep:1.1 ng/ml; ΔHbA1c:-2.3%; pt#3:C-pep1.36 ng/ml; ΔHbA1c:-1.9%). DCE-MRI parameters strongly decreased in the other 2 pts at 1 week after transplantation (pt#2:ΔME-30%;ΔAUC-28%;pt#4:ΔME-33%,ΔAUC-39%). They experimented graft failure, respectively, 1 and 4 months after transplantation (C-pep secretion after arginine stimulus pt#2:0.01;pt#4< 0.2).

Conclusion: From our preliminary results DCE-MRI changes appear to predict islets-tx outcome, supporting the hypothesis that early islets vascularisation is crucial for engraftment.

B-0338 11:42

Evaluation of efficiency and image quality between a manual and a novel automated MR scanner interface in liver MR imaging

C. Kloeters¹, L. Umütlu¹, C. Moeninghoff¹, M. Ladd¹, A. Sombetzki², G. Antoch², M. Schlamann¹, M. Forsting¹, T.C. Lauenstein¹; ¹Essen/DE, ²Düsseldorf/DE (christian.kloeters@uk-essen.de)

Purpose: To evaluate the potential benefits of an automated MRI algorithm in patients with contrast-enhanced liver examinations (1.5 T) under consideration of examination efficiency and image quality.

Methods and Materials: Seventy patients (34-71 years) were prospectively enrolled and referred to a contrast-enhanced MR examination of the liver. Patients were randomised to one of the following scanners: 1.5 T MAGNETOM Aera including a completely automated user interface or a 1.5 T MAGNETOM Avanto with manually operated scanner software (Siemens, Germany). Two blinded readers rated the image quality in different categories:1) angulations/FOV, 2) image contrast, 3) image noise, 4) artefacts and 5) presentation of the target organ from excellent ("5") to insufficient ("1"). The degree of diagnostic confidence to depict liver lesions was rated from "certain" ("5") to "uncertain" ("1"). Above-named categories were assessed for the following sequences: 1) TrueFISP, 2) T2w TSE, 3) HASTE, 4)

In-/opposed phase, 5) MRCP, 6) 3D and 2D FLASH. Total examination time was recorded. Chi-square test and U-test were used for statistical analysis.

Results: The mean image quality for the automated processed examinations was rated higher for all categories and showed statistical significant difference in assessment of image contrast (meanautomated4.5 vs meanmanual4.1) and presentation of target organ (meanautomated4.4 vs meanmanual4.1) (* = p < 0.05). The diagnostic confidence was 4.5/4.0 (p < 0.05), respectively. Mean examination time was 25.01 min in the automatically and 20.48 min in the manually processed examinations.

Conclusion: The completely automated MR scanner user interface shows an increase in image quality and diagnostic confidence. The examination time was higher in the automatically processed examination due to longer lasting MR sequences.

B-0339 11:51

Alveolar echinococcosis of the liver: diffusion-weighted MR imaging findings

A. Pomoni, S. Schmidt, E. Uldry, N. Halkic, A. Denys, R. Meuli, F. Becce; Lausanne/CH (npomoni@hotmail.com)

Purpose: To report the diffusion-weighted MR imaging (DWI) findings in hepatic alveolar echinococcosis (AE). To evaluate the usefulness of apparent diffusion coefficients (ADCs) for differentiating the 5 types of AE lesions (as reported by Kodama, Radiology, 2003).

Methods and Materials: We retrospectively included 17 patients (10 women, mean age 64.3years) with 48 AE liver lesions (> 1 cm²) that had been investigated by 3-Tesla MR imaging between March 2008 and August 2011 performing our standard protocol including DWI (b-values: 0, 300 and 600s/mm²). In consensus, two radiologists assessed lesion characteristics such as diameter, cystic and/or fibrotic components including Kodama classification, signal intensity, contrast enhancement, calcifications (on CT), and measured the ADC of each lesion. AE was confirmed by serology, biopsy and/or surgery in all patients.

Results: Seventeen lesions of Kodama type 1, 10 of type 2, 19 of type 3, 1 of type 4 and 1 of type 5 were found. Mean (±SD) ADC of all AE lesions was 1.75±0.45 ×10⁻³ mm²/s. Mean (±SD) ADCs of Kodama type 1, 2, 3, 4 and 5 lesions were 1.74±0.55, 1.71±0.49, 1.82±0.36, 1.46±0 and 1.43±0 ×10⁻³ mm²/s, respectively. No significant difference was noted between the different Kodama types (p=0.89). Presence of fibrotic (p=0.24) and/or calcified (p=0.90) components, or contrast enhancement (p=0.84) of AE lesions were not correlated with significant differences in ADCs.

Conclusion: ADCs of AE lesions are relatively low compared to other cystic liver lesions, which is helpful in suggesting the diagnosis. However, ADCs were not found to be useful for differentiating Kodama types of AE lesions.

10:30 - 12:00

Room N/O

Vascular

SS 515

Imaging in vascular diseases

Moderators:

H.K. Ahlström; Uppsala/SE
O. Pellerin; Paris/FR

B-0340 10:30

Impact of cardiovascular risk factors and vessel wall inflammation on atherosclerotic disease progression: a PET/CT study

T. Saam, A. Rominger, M. Habs, L. Walter, P. Bartenstein, C. Rist, M.F. Reiser, M. Hacker, K. Nikolaou; Munich/DE (Tobias.Saam@med.uni-muenchen.de)

Purpose: We hypothesised that atherosclerotic risk factors and vessel wall inflammation are associated with an accelerated progression of atherosclerotic disease as assessed by [18 F]fluorodeoxyglucose (FDG)-PET/CT.

Methods and Materials: 94 tumour patients underwent whole body FDG-PET and contrast-enhanced CT twice within 12 months. Clinical risk factors for atherosclerosis and medications were documented. Blood pool-corrected standardised uptake value (TBR) and calcified wall volume (CWV) were measured in the aorta and both iliac and carotid arteries. Furthermore, pericardial fat volume (PFV) and mean aortic lumen area in the thoracic aorta were measured. The one-sample t-test and multiple regression analysis were used for statistical comparisons.

Results: On average, aortic lumen area decreased by 1.7%/year (P=0.002), PFV increased by 3.1%/year (P=0.03) and CWV increased by 14.2%/year (P < 0.001). TBR values did not change significantly within 12 months (-1.0%/year). Multiple regression analysis demonstrated that i) higher TBR values (P=0.009) and higher

BMI values (P=0.004) at baseline were associated with a significant decrease of mean aortic lumen area; ii) hypertension (P=0.003) was associated with a significantly increased rate of progression in mean CWV; iii) male gender (P=0.043) was associated with a significantly increased rate of progression in mean PFV and iv) smoking (P=0.002) was associated with a significantly increased rate of progression in mean TBR values. All other documented risk factors were not significantly associated with changes in atherosclerotic disease progression.

Conclusion: Atherosclerotic disease progression, as assessed by whole body FDG-PET/CT, is associated with a number of factors, such as arterial FDG-uptake, high BMI, hypertension, male gender and smoking.

B-0341 10:39

Diagnosis of large vessel vasculitis with 18 F-FDG PET/CT: single centre experience on 64 patients

U. Rozzanigo, A. Pellegrin, M. Centonze, G. Casagrande, M. Cetrulo, D. Donner; Trento/IT (andrea.pellegrin@apss.tn.it)

Purpose: This is a retrospective study that aims to assess the diagnostic performance of 18F-FDG PET/CT in large vessel vasculitis (LVV); comparing four different standards of image evaluation and taking into account concomitant immunosuppressive therapy.

Methods and Materials: Consecutive patients (n=64; 28=male, 36=female, mean age 55yo, range 14-86yo) sent with clinical suspicion of LVV; with at least 2 symptoms among: fever, weight loss, arthralgia-myalgia underwent 18F-FDG PET/CT examination. At the moment of PET/CT scan, 32 on 64 patients were under immunosuppressive therapy. Final diagnosis of LVV was obtained on clinical consensus in 31 of 64 patients. Four types of analysis were used and compared with McNemar test: 1) semiquantitative maximal standardised uptake value (SUVmax), 2-3) qualitative evaluation on maximum intensity projection (MIP) images with a four-grade scale (0 to 3) repeated with two different cut-offs, 4) qualitative evaluation with collegial clinico-radiological correlation (considering: concurrent vascular pathology, focal distribution, age/cardio-vascular risk factors).

Results: Quantitative analysis with SUVmax cutoff value= 2.5 (sens 74.19%, spec 78.78%, acc 76.56%) did not show statistical significant differences compared to semiquantitative evaluation with higher cut-off (grade ≥2) (sens 64.51%, spec 84.84%, acc 75.00%). Semiquantitative analysis with lower cut-off (grade ≥1) had superior sensitivity but reduced specificity (sens 93.54%, spec 75.75%, acc 84.37%). Evaluation with collegial clinico-radiological correlation showed increase specificity, without a decrease in sensibility (sens 93.54%, spec 93.93%, acc 93.75%).

Conclusion: Interpretation of 18F-FDG PET/CT exams in LVV needs to be based on efficient integration of clinico-radiological data, customised for each patient.

B-0342 10:48

Contrast-enhanced magnetic resonance angiography in management of pulmonary arterio-venous malformations in patients with HHT (Osler disease)

G.K. Schneider, A. Massmann, A. Buecker, P. Fries; Homburg a.d. Saar/DE (dr.guenther.schneider@uks.eu)

Purpose: To evaluate contrast-enhanced magnetic resonance angiography (CE-MRA) for management of pulmonary arterio-venous malformations (PAVM) in patients with hereditary haemorrhagic telangiectasia (HHT), as well as a screening procedure for the detection and for follow-up after embolisation therapy.

Methods and Materials: 286 patients (mean age 45.9y, male 118, female 168) with confirmed HHT or their first degree relatives underwent screening pulmonary CE-MRA (Gadolinium-BOPTA 0.1 mmol/kg bodyweight) for the presence of PAVM. Patients with at least one PAVM > 5 mm or a feeding pulmonary artery diameter > 3 mm were referred for catheter angiography (DSA) for embolisation therapy and underwent follow-up MRA for detection of reperfused PAVMs.

Results: Overall, CE-MRA detected 323 PAVM in 97 of 286 patients (149 in 44 men, 174 in 53 women, 89 in 32 women of childbearing age). Most PAVMs detected on CE-MRA were small (< 10 mm). 74 of 97 patients with 263 PAVMs detected on CE-MRA underwent global or selective DSA. Significantly (p < 0.001) fewer PAVMs (205/263 [78%]) were demonstrated on global DSA of which 191 were embolised. Follow-up CE-MRA showed 57 newly developed PAVM in 14 patients (interval 1-6years), and 32 reperfused PAVM (due to recanalisation, insufficient packing) in 24 patients (interval 3 months-7 years) of which 5 patients were embolised elsewhere. All reperfused PAVMs were confirmed by DSA and reembolised successfully.

Conclusion: CE-MRA should be the method of choice for the management of PAVMs in HHT patients. Due to the high sensitivity and the lack of ionising radiation MR should be preferred to CT if available.

B-0343 10:57

Evaluation of acute pulmonary embolism detection using non-linear blending in dual energy computed tomography

F. Al-Butmeh, L. Kroker, J.M. Kerl, M.C. Larson, B. Bodelle, B. Schell, M. Beeres, T.J. Vogl, R.W. Bauer; Frankfurt a. Main/DE (Firas.Albutmeh@gmail.com)

Purpose: To compare non-linear blending with standard linear blending (virtual 120 kV) and low kV images of dual energy CT pulmonary angiography for improved diagnostic image quality.

Methods and Materials: We compared 35 dual energy CT datasets of central and peripheral acute pulmonary embolism. A non-linear blending method based on a modified sigmoid function was compared with the low kV image series and the standard linear blending method that simulates the attenuation of a 120 kV scan. For the non-linear blending method we evaluated 37 different parameter settings with different blending centre and width. Contrast-to-noise-ratio (CNR) was calculated. Two independent radiologists evaluated the totally 39 image sets for their visual preference. Overall subjective image quality was rated with a 6-point-scale (1 = excellent image, 6 = non-diagnostic).

Results: With either one of the non-linear blending settings, the CNR was significantly higher compared with the low kV (CNR=27.4 ±16.6 and 3.35 ±0.88 subjective overall image quality) and linear blending series (CNR=26.5 ±18.1 and 2.55 ± 1.00 subjective overall image quality). The optimal blending centre and width for highest CNR (CNR=63.8 ±38.0 and 2.7 ± 1.08 subjective overall image quality) results strongly depended on the level of contrast enhancement in the pulmonary arteries. However, on subjective image quality rating, the image series with the highest CNR was rated in 21 of 35 cases (60%) as the best in terms of optimal image quality.

Conclusion: Non-linear blending of dual energy pulmonary computed tomography allows significant increase of CNR and image quality.

B-0344 11:06

Imaging findings in arterial stenosis and mural involvement in Takayasu arteritis on CEMRA

A.K.S. Sharma; Noida/IN (shokie@hotmail.com)

Purpose: To assess vessel involvement and activity of Takayasu arteritis with whole body MRA.

Methods and Materials: 25 patients with diagnosis of TA were subjected to whole body MRA with Gadolinium dimeglumine. According to vasculitis activity score, 19 patients were classified as having active/persistent disease and 6 patients as having remissive disease. The arterial system was divided into 32 segments of 5 regions. The image quality, wall thickness and wall signal intensity were evaluated by three radiologists who were not knowing clinical data. Quality analysis was performed, statistically significant differences in SI values of AD and RD were tested on a per region basis.

Results: A total 750 arterial segments with good to excellent image quality were assessed. 5 extravascular manifestation were identified. In 8 patients monostation could not depict vessel involvement. The vessel wall thickness of the AD group was thicker than that of RD group. Post-contrast SI ratio was significantly different for both the groups. Per region analysis revealed higher signal intensity in carotid and subclavian regions in both groups.

Conclusion: Whole body MRA allows a complete and comprehensive documentation of the vessel involvement. MRA is very useful modality for Takayasu arteritis staging, whether disease is active or not and is also in follow-up for therapy management.

B-0345 11:15

Usefulness of CT angiography of celiac axis prior to pancreaticoduodenectomy

M. Belgrano, B. Petronio, W. Toscano, M.A. Cova; Trieste/IT (belgranom@libero.it)

Purpose: To perform a CT angiography of the celiac axis (CA), to detect the presence of stenosis due to atherosclerosis (AS) or to the median arcuate ligament (MAL), and to correlate it with the prevalence of complication after surgery.

Methods and Materials: We revised retrospectively 46 patients who underwent to pancreaticoduodenectomy between 2006 and 2010 in the Surgery Department of our Institution. Each patient underwent to a CT angiography (within 2-18 days before the surgery) with a 64 slice (64 x 0.5 mm slices) scanner after administration of 90 ml of iodinated contrast media to detect the presence of stenosis of CA (> 50% of lumen reduction). The prevalence of pancreatic fistula (PF) was collected from the Patient's clinical history.

Results: Of the 46 patients included, 17 presented a CA stenosis (10 due to MAL, 7 due to AS). After the surgery 18 patients developed a PF, of this group 13 presented a stenosis of CA.



Conclusion: We observed a significant correlation (P < 0.0001) between the presence of stenosis of CA and the development of PF that is a major complication of pancreaticoduodenectomy and is related to a mortality rate of 20-40%. A stenosis of CA is easily treated during the surgery and must be therefore included in the report of the pre-surgery CT exam.

B-0346 11:24

Vascular anomalies in a population with Turner syndrome: real adjunctive diagnostic role and clinical impact of magnetic resonance angiography (MRA) vs echocardiography (ECHO)

G. Rinaldi, G. Mineo, F. Montanari, L. Mazzanti, D. Prandstraller, V. Russo, F. Buia, L. Lovato, M. Zompatori; Bologna/IT

Purpose: Turner syndrome (TS) is associated with congenital heart diseases (CHD), aortic dilation and dissection, but also with a high prevalence of vascular anomalies, not easily depicted by ECHO. We tested the adjunctive diagnostic value of MR versus ECHO to identify the prevalence of vascular anomalies in a TS population echocardiographically pre-selected for the absence of CHD, excepting bicuspid aortic valve (BAV).

Methods and Materials: Retrospective analysis of MR aortic study of 111 TS patients was performed to evaluate minor and major vascular anomalies. All MR studies included thoracic axial and oblique sagittal spin-echo sequences, and 98/111 thoraco-abdominal MRA.

Results: MR showed vascular anomalies in 44 patients (39.6%): the most frequent is aortic arch elongation (32 patients, 29%). Among major anomalies misdiagnosed by ECHO, MR analysis identified 10 partial anomalous pulmonary venous returns (PAPVR) (9%), 3 inferior hollow vein interruption, 5 peripheral arteries aneurysms (4.5%). The subgroup with BAV (20 patients) shows higher prevalence of malformations (55%; p < 0.05), especially elongation and PAPVR (35%). Among patients not affected by BAV, comparative analysis between groups with and without vascular malformations (PAPVR excluded) showed higher aortic dilation prevalence in the malformation group (p < 0.05). MR analysis identified 4 PAPVR not reported at first evaluation.

Conclusion: MR has an adjunctive diagnostic power versus ECHO, identifying several vascular malformations otherwise misdiagnosed and a potential clinical impact on TS natural history. MRA must always be performed in TS to integrate ECHO study. MR evaluation, especially in BAV patients, must be extended to all the thoracic vasculature.

B-0347 11:33

3D reconstructed contrast-enhanced MR angiography: 1.5 Tesla vs 3 Tesla in detection of the different branches of the internal iliac artery in females scheduled for uterine artery embolisation

N.N.N. Naguib, N.-E.A. Nour-Eldin, T. Lehnert, T. Gruber-Rouh, M. Harth, T.J. Vogl; Frankfurt a. Main/DE (nagynnn@yahoo.com)

Purpose: To compare the ability of the 1.5-Tesla (1.5 T) MRI versus the 3-Tesla (3 T) MRI in detecting the different branches of the internal iliac artery (IIA) before UAE using 3D-reconstructed contrast-enhanced MR-angiography (CE-MRA).

Methods and Materials: Pre-embolisation CE-MRA from 84 females (mean age: 44.9 years) were retrospectively evaluated by 2 radiologists in consensus. Studies were done using a 1.5 T (n=49, 98 IIA) and 3 T (n=35, 70 IIA) MRI and 3D-images were reconstructed using Syngo-VesselView. A scoring system of 3 Grades was used: score 0 means that the artery was not seen, interrupted or its origin was not identified, score 1 means that the artery was faintly seen but can be traced with no missing segments till it gives off its first branch, score 2 means that the artery was clearly seen. Differences between both systems were tested using Mantel-Haenssel-Test.

Results: The superior-gluteal artery was detected in the 1.5 T in 98 arteries (sensitivity (S)=1), in the 3 T in 70 arteries (S=1), no statistically significant difference was noted between both systems (p=0.82). Inferior-gluteal: 1.5 T (n=98, S=1), 3 T (n=70, S=1), no difference (p=0.4). Internal-pudendal: 1.5 T (n=96, S=0.98), 3 T (n=70, S=1), no difference (p=0.055). Middle-rectal: 1.5 T (n=11, S=0.11), 3 T (n=17, S=0.24), no difference (p=0.12). Iliolumbar: 1.5 T (n=84, S=0.86), 3 T (n=69, S=0.99), significant difference noted (p=0.0047). Lateral-sacral: 1.5 T (n=86, S=0.89), 3 T (n=70, S=1), significant difference noted (p=0.0079). Uterine: 1.5 T (n=95, S=0.97), 3 T (n=70, S=1), significant difference noted (p=0.017). Obturator: 1.5 T (n=81, S=0.83), 3 T (n=67, S=0.96), significant difference noted (p=0.0006). Superior-vesical: 1.5 T (n=21, S=0.21), 3 T (n=32, S=0.46), significant difference noted (p=0.0009).

Conclusion: The 3 T was superior to the 1.5 T in detecting all IIA branches except the internal pudendal, middle rectal, superior and inferior gluteal arteries in which both systems showed similar performance.

B-0348 11:42

Low dose contrast-enhanced time-resolved MR angiography at 3 T: diagnostic accuracy for treatment planning and follow-up of body vascular malformations

P. Lucatelli, M. Anzidei, B. Cavallo Marincola, A. Napoli, F. Fanelli, R. Passariello; *Rome/IT*

Purpose: To assess the accuracy of low dose contrast-enhanced time-resolved 3 T MR-angiography (MRA) for the morphological and functional assessment of vascular malformations (VM) and to evaluate its diagnostic potential in planning treatment and for the depiction of treatment-induced changes.

Methods and Materials: Twenty-five patients with known VM underwent MRA to evaluate the location and extent of lesions and their haemodynamic characteristics. 3D T1-weighted time-resolved sequences were acquired following the administration of 0.05 mmol/kg of gadobenate dimeglumine (Bracco, Milan, Italy). VM were classified according to their morphology and haemodynamic characteristics (high flow or low-flow). This lead to the subsequent patient's management: transarterial embolisation for high flow VM, percutaneous sclerotisation in case of low-flow VM, or combined approach for artero-venous VM. Follow-up MRA was performed 30 days after treatment to assess morphological and functional changes.

Results: Based on haemodynamic characteristics, VM were classified as predominantly arterial (4 [16%]), artero-venous (19 [76%]) or venous (2 [8%]). Twenty-three (92%) lesions were classified as high-flow VM and 2 (8%) as low-flow VM. Complete exclusion of the nidus was obtained in 20 patients (80%) of patients, leading to a dimensional reduction and regression of aesthetical impairment or symptoms.

Conclusion: Low dose contrast-enhanced time-resolved 3 T MRA can accurately define morphological and functional aspects of VM during treatment planning and follow-up, and can identify post-therapy changes that positively correlate with treatment outcome. Moreover, MRA can avoid radiation exposure considering the youth age of these patient.

B-0349 11:51

Automated Doppler angle correction in liver transplant ultrasound

O. Kolokythas¹, T.P. Gauthier², C. Cuevas¹, P. Bhargava¹, L.M. Mitsumori¹, D.E. Green¹, A.A. Saad³; ¹Seattle, WA/US, ²Eindhoven/NL, ³Bothell, WA/US (*orpheus@uw.edu*)

Purpose: To evaluate the clinical feasibility of automatically corrected Doppler angle in hepatic vessels.

Methods and Materials: This prospective study was approved by the institutional review board; all patients gave their written consent to participate. 150 hepatic vessels were evaluated in 15 patients (total of 10 arteries and veins per patient) after liver transplant with ultrasound using a curvilinear 5-1 MHz transducer; manual Doppler angle correction was performed as the gold standard, followed by automated Doppler angle correction, both performed by the same operator with 10 years of experience in abdominal Doppler ultrasound, blinded to the measurements of the competing method. Doppler angles and peak velocities using manual and automated correction of Doppler angle were recorded. Results were analysed using regression analysis and a Bland-Altman (Difference) plot. Case-by-case analysis was performed for Doppler angles discrepant by more than 9 degrees to evaluate for possible aetiologies.

Results: 141 vessels were successfully examined. A strong correlation was found between the manually adjusted and the automated angle correction. The mean discrepancy of Doppler angles was 1.67 degrees (SD=9.95 degrees, correlation coefficient = 0.88). The mean discrepancy of peak velocities was 0.72 cm/s (SD=14.1 cm/s, correlation coefficient = 0.95). Causes for discrepant angles above 9 degrees included curved and bifurcating vessels, low eccentricity merged vessels, user's preference of Doppler gate placement and other. Discrepancies were deemed clinically non significant.

Conclusion: Automation of Doppler angle correction is clinically feasible in the evaluation of hepatic vasculature. It may enhance standardisation and reproducibility of Doppler measurements.

10:30 - 12:00

Room P

Physics in Radiology

SS 513

Interventional radiology and mammography

Moderators:

E. Atalar; *Ankara/TR*

Y. Kyriakou; *Forchheim/DE*

B-0350 10:30

Development of in-hospital x-ray radiographic system using rotating cerium anode for coronary and cerebral microangiography

H. Mori, C. Tanaka, Y. Ikeya, T. Fujii, T. Shizuma, N. Fukuyama; *Isehara/JP*

Purpose: As conventional angiography cannot visualise small arteries with a diameter of < 500 µm, we developed an in-hospital microangiographic system and evaluated its performances in basic experiments.

Methods and Materials: The microangiographic system consists of a rotating cerium anode and a large heat unit (5MHU) x-ray generator. The quasi-monochromatic x-ray spectra has a peak at 34.6 KeV and have a narrow energy band of 20 KeV in half maximum, which can efficiently detect small amount of iodine-contrast in small vessel. The high x-ray photon flux generated by 5MHU generator allows to maintain enough photon number at the surface of a flat panel detector of spatial resolution of 50 µm even after passing through the adult body. Canine heart and brain of which arterial beds are filled with iodine-containing microspheres with a diameter of 15 µm was used as the test samples.

Results: The angiographic system visualised intramural small coronary arteries entirely from their epicardial origin to subendocardial terminal portions in the excised heart, and the perforating branches of cerebral arteries arising from the middle cerebral arteries and reaching to the deep subcortical lesions in the brain model. Vascular diameter measurement revealed a step-wise narrowing with a fixed reduction ratio as branching in the range of 50-500 µm.

Conclusion: The present angiographic system will lead to better prediction of therapeutic effects of percutaneous coronary intervention and/or coronary bypass surgery, and better understanding of cerebral white matter disease related to vascular cognitive impairment in clinical settings.

B-0351 10:39

4D Guidance in interventional radiology: prototype development and feasibility study

J. Kuntz¹, S. Sawall², M. Socher¹, W. Semmler¹, M. Kachelriess², S. Bartling¹; ¹Heidelberg/DE, ²Erlangen/DE (*s.bartling@dkfz.de*)

Purpose: To allow for volumetric (3D+time) radiological guidance of interventions at the same low dose levels as conventional projection fluoroscopy (2D+time) guidance.

Methods and Material: Today, radiological guidance of interventions is limited to projection fluoroscopy and repetitive full-dose volumetric CT scans. The use of continuous CT imaging, allowing true 4D intervention guidance suffers from prohibitive radiation dose. To reduce its dose to acceptable levels a compressed sensing CT reconstruction algorithm using prior information was developed and implemented. Guided interventions were simulated in phantoms and pig models. During interventions, continuous rawdata acquisition using a prototype flat-panel CT system was performed. 4D datasets of the intervention process were reconstructed with various undersampling ratios corresponding to various dose levels. Image quality was evaluated for the use in 4D interventional guidance by visual inspection. X-ray doses were compared to biplane fluoroscopy.

Results: Reconstruction results showed sufficient image quality for high contrast materials allowing as few as 12 projections per reconstruction. Guidewires and stents were visible in a 3D setting, could be followed while moving and located clearly with respect to vessels and their surrounding. Radiation doses of 4D guidance (47µGy/s), albeit slightly higher, were still in the order of biplane fluoroscopy (24µGy/s).

Conclusion: 4D interventional guidance is possible without exceeding acceptable x-ray dose values. Using prior information and compressed sensing image reconstruction techniques, real-time 4D guidance approaches may become an attractive method for intervention guidance with a great potential to make interventions faster, safer and to make more complex interventions possible; with a significant benefit for patient health.

B-0352 10:48

4D interventional guidance: a technical feasibility consideration

J. Kuntz¹, S. Sawall², W. Semmler¹, M. Kachelriess², S. Bartling¹;
¹Heidelberg/DE, ²Erlangen/DE (j.kuntz@dkfz.de)

Purpose: To investigate the overall feasibility of 4D interventional guidance using current flat-panel CT technology.

Methods and Materials: Recent research suggests that 4D interventional guidance may become feasible by the use of novel reconstruction algorithms and prior information. To this end, continuous 3D data acquisition using circular trajectories might be the most straight-forward solution. Total dose of update scans can be distributed among various amounts of projections. Mathematical simulations as well as real phantom scans were performed; FDK reconstructions were used for high resolution prior images, temporal updates were reconstructed using compressed sensing algorithms (including PICCS and ASD-POCS). For temporal update reconstructions, various noise levels per projection and different undersampling ratios were used, while the overall dose for every reconstruction was kept constant. Electronic detector noise was not included into simulations. Image quality was evaluated automatically (e.g. by a modified universal quality index) and by visual inspection.

Results: Image quality varied largely between algorithms and reconstruction parameters. For the distribution of the total dose to various amounts of projections a maximum image quality was found to be reached at the order of 20 to 40 projections per update reconstruction in simulations of typical interventional situations (e.g. stent placement, 100 ASD-POCS iterations). Both, more and less projections suffered from larger noise and undersampling effects.

Conclusion: These data suggest that with current flat-panel technology (readout rates 30 to 60 fps) and gantries rotating at about one to two rotations per second a sufficient 4D intervention guidance with up to three updates per second can be realised.

B-0353 10:57

2D curvelet spatio-temporal filtering applied to x-ray digital flat panel detector imaging

J. Pescatore, C. Amiot, Moirans/FR (jeremie.pescatore@thalesgroup.com)

Purpose: x-ray interventional imaging is particularly challenging in terms of dose reduction and de-noising. Indeed, cardiac and respiratory motion coupled with dense anatomies are among the major reasons for low signal-to-noise ratio in fluoroscopic imaging (< 20 nGy/frame detector entrance dose). Our work consists in developing a novel method to enhance interventional devices (needles and catheters) while preserving the anatomical boundaries. For this, we developed a spatio-temporal filter based on the 2D curvelet transform.

Methods and Materials: The proposed method consists of two steps: a temporal and a spatial filtering. The temporal filter is based on the time evolution of pixel's value. This filter has a limited de-noising power, tends to erase the objects of interest and introduces spike noise in the image. Therefore, our approach combines a 2D curvelet spatial filter to the temporal filter. This spatial filter is based on the wrapping discrete curvelet implementation. The curvelet coefficients shrinkage is performed according to a scale-dependent hard thresholding scheme.

Results: The 2D curvelet spatio-temporal filtering is applied on x-ray images representing guidewires and stents. Input contrast-to-noise ratio is between 0.5 and 2.5. We demonstrate that our method outperforms wavelet-based spatio-temporal filter. The proposed method removes most of the gaussian noise and leaves some minor spike noise induced by the temporal filtering.

Conclusion: Our work demonstrates that combined curvelet and temporal filtering improves significantly low dose fluoroscopic image quality. Interventional devices and bone visibility is increased while the image background noise is decreased.

B-0354 11:06

Radiation exposure in vascular angiographic procedures

R. Kloeckner, C. Dueber, J. Schneider, A. Bersch, C. Ruckes, M.B. Pitton;
 Mainz/DE (roman.kloeckner@googlemail.com)

Purpose: To investigate the radiation exposure in vascular angiographic procedures and to search strategies for dose reduction.

Methods and Materials: 764 consecutive vascular interventional procedures performed over 1 year were analysed including diagnostic DSA, recanalisation and PTA/stent in the pelvis and leg, EVAR, embolisation of lumbar arteries, PTA/stent of renal arteries, embolisation of diverse bleedings and other rarely performed interventions. They were analysed with respect to the fluoroscopy time and the resulting fluoroscopy radiation dose, the radiation dose of the radiographic frames, and the overall dose. Additionally, the investigators experience on the total dose was investigated.

Results: Overall, 70% of the total radiation dose was due to the acquisition of radiographic frames leaving only 30% of the total dose being applied by fluoroscopy ($p < 0.001$). The investigators experience had no significant impact on the total dose applied, most likely since there was no stratification to intervention-complexity.

Conclusion: Image grabbing of fluoroscopy should be used for documentation whenever possible. Interventional radiologists should be aware of the radiation exposure of different procedure types. A registry of radiation exposure should not only comprise a sufficiently large number of interventions but also the different intervention types in order to develop reference levels.

B-0355 11:15

A new method of real time skin dose visualisation: clinical evaluation of fluoroscopy-guided interventions

F. Boujan, N. Clauss, C. Jahn, M. Habashy, M. Manisor, H. Benjamel, V. Mardakhayeva, L. Mertz, R. Beaujeux; Strasbourg/FR (fazel.boujan@chru-strasbourg.fr)



Purpose: The radiation exposure in fluoroscopy-guided interventions (FGI) is a major issue for the Public Health. The increasing complexity of FGI enhances the risk of creating side effects for patient such a radiation induced skin injuries. Currently dose area product (DAP) estimate the patient skin dose. This study evaluates an innovative awareness tool that displays directly the real time peak skin dose information.

Methods and Materials: We have tested during 6 months a new machine parameter-based dose calculations method (MAPDOC) on 50 patients population scheduled for head and neck, thoracic and abdominal FGI. Currently, angiographic system provides a basic cumulative air kerma value. MAPDOC method provides a real time air kerma mapping on a sphere patient model. It takes into account all relevant acquisition parameters (table height, angulation, collimation). This method is prospectively compared to radiochromic films for every patient, for monoplane and biplane angiographic systems.

Results: Findings between MAPDOC and radiochromic films are closely correlated with a constant correction factor depending on procedure type (average ratio 1.30 for monoplane thoracic and abdominal procedures, 0.95 for monoplane cerebral procedures and 1.65 for biplane cerebral procedures) and procedure parameters (patient weight, C-arm angulations, collimation, ...). Mapping on a sphere patient model is closely correlated to radiochromic films dose mapping and allow to optimise skin dose repartition during FGI.

Conclusion: MAPDOC provides a reliable real time feedback on patient skin dose and mapping during FGI. This innovative tool allows physician to optimise FGI procedures and prevents skin injuries.

B-0356 11:24

Study of a real-time dosimetry system and its impact on current practices in an angiography room

F. Boujan¹, N. Clauss¹, A. Hornbeck², C. Jahn¹, L. Mertz¹, R. Beaujeux¹;
¹Strasbourg/FR, ²Toulouse/FR (fazel.boujan@chru-strasbourg.fr)

Purpose: The radiation exposure in fluoroscopy-guided interventions (FGI) is a major issue for the Public Health. In our institution, we studied the impact of a new real-time dosimetry system (Philips DoseAware) on operators' exposure.

Methods and Materials: The Dose Aware System allows operators to see their personal dose-rate at a glance, during a procedure. Each Personal Dose-Meter (PDM) measures Hp (10) which is send wirelessly to a Base Station, a screen mounted next to the radiology monitors. The study consisted on the comparison of two measurements periods. First, the blinded stage, consisting radiation measurements by core lab with the screen off for operators. Then a regular stage, consisting measurements with the screen on.

Results: More than 21.000 elements of information have been treated during 6 months. The interpretation on cerebral angiography procedures showed a dose reduction for all operators: 45% for physicians, 25% for technicians and 8% for nurses.

Conclusion: The Philips DoseAware is an interesting optimisation tool for the operators' exposure during cerebral angiography procedures. We intend to study this system on others FGI procedures. However, this system could be used also to estimate operators eye lens exposure, especially in the context of new recommendations project of International Commission of the Radiological Protection (ICRP) to reduce the eye lens' exposure limit (150 to 20 mSv per year).

B-0357 11:33

Quantra, BIRADS scale and breast density correlation: preliminary results

F. Cavagnetto¹, R. Rosasco¹, M. Calabrese¹, A. Tagliafico¹, G. Taccini¹, B. Mongero², G. Massari²; ¹Genoa/IT, ²Turin/IT (*francesca.cavagnetto@istge.it*)

Purpose: Many studies proved that radiological breast density can be a predictive element of cancer risk. Radiologists evaluate breast density according a visual analysis of the images, using BIRADS classification. A dedicated software, Quantra 1.3, can reduce errors associated with this qualitative method. The software makes a numeric measure, on mammography views, of breast and fibroglandular tissue volume, then it calculates the volumetric percentage of fibroglandular tissue of breast. The aim of this work is to provide a calibration in order to correlate the numerical result of Quantra with the BIRADS scale and then with the real breast density.

Methods and Materials: Four compressible phantoms were made, filled with substances of known density between 0.79 and 1.0 g/cm³, to simulate typical densities of real breasts. Mammographic images of phantoms were processed by the software. Finally digital mammograms of 24 patients was submitted to Quantra and then to radiologists in order to derive estimations of breast density according to BIRAD system.

Results: The numerical evaluation provided by Quantra on phantom breasts has been related with known densities (R=0.96). Using this calibration, the breast densities of 24 were calculated. These values show a correlation with the radiologists evaluations based on BIRADS scale (R²=0.97).

Conclusion: Quantra help radiologists to estimate volumetric percentage of the fibroglandular tissue of breast, but it is necessary a proper calibration of this software to obtain the correct relation between Quantra results and real breast densities. This method enables to relate Quantra numbers with quantitative evaluations with BIRADS scale.

B-0358 11:42

Physical characteristics and image quality of reconstructed planes in digital breast tomosynthesis (DBT) - a system comparison

N. Oberhofer; Bolzano/IT (*nadia.oberhofer@asbz.it*)

Purpose: In Europe there are three commercial systems for digital breast tomosynthesis (DBT) which differ by acquisition technique (angular range, number and spacing of projections) and reconstruction algorithm. This work compares the systems by characterisation of the physical properties and the image quality of the reconstructed 3D planes.

Methods and Materials: The studied units are Hologic Selenia Dimensions, Siemens Mammomat Inspiration and IMS Giotto. Besides 2D MTF, NPS and DQE, the systems have been characterised in terms of homogeneity, signal difference to noise ratio (SDNR) behaviour throughout the volume, in-plane resolution and z-resolution. Image quality has been assessed by means of contrast detail evaluation with the phantom CDMAM and the software CDMAM Analyser. Average glandular dose (AGD) was calculated according to Dance. Performances have been evaluated for various PMMA phantom thicknesses in clinical setup using automatic exposure control modality (AEC).

Results: In all systems the AGD for a tomo-scan was clearly inferior to twice the AGD for a standard 2D projection, the ratio ranking from 0.85 to 0.55 depending on the compressed breast thickness. Although the single tomo-projections were characterised by lower image quality with respect to standard 2D images and in one system by lower spatial resolution, too, the reconstructed image in the central plane was never inferior to 2D images.

Conclusion: The methodology for DBT performance assessment is not well established; reconstruction algorithms seem to play a dominant role in the image quality of reconstructed planes. Further investigation and international harmonisation on protocol and phantom are desirable.

B-0359 11:51

Breast tomosynthesis: physical characterisation and comparison between two systems

S. Pasetto, P. Colombo, A. Torresin, M. Tagliabue; Milan/IT (*stefano.pase@gmail.com*)

Purpose: In our work, some image quality parameters have been proposed, as a way to characterise a tomosynthesis system, concerning image quality and dose. This protocol was applied to two different systems, Mammomat Inspiration (Siemens) e Selenia Dimensions (Hologic).

Methods and Materials: Dose measurements were performed in agreement to average glandular dose formulation proposed by Dance et al. (Phys. Med. Biol 2011). Image quality evaluation was carried out considering the following parameters: signal and noise uniformity, MTF, NPS, CNR, presence and propagation

of artefacts (ASF), reconstructed slice thickness and geometrical distortion. A semi-clinical evaluation on CIRS phantom (Model 020 BR3D) was also performed.

Results: The dose delivered by the two systems does not show remarkable differences, neither in its absolute value nor in relation to the dose delivered by a standard mammographic projection. The ratio between tomosynthesis and standard mammography has a mean value of 1.7. With respect to projection mammography, in tomosynthesis we found: a strong loss in spatial resolution; a CNR improvement; a strong presence of artefacts, especially along vertical direction; a geometric distortion at detector edges. Finally, just small differences between the two systems have emerged from the semi-clinical evaluation.

Conclusion: Average glandular dose delivered in tomosynthesis is smaller than dose delivered by two standard projections, for both systems. Tomosynthesis advantage with respect to standard mammography lies in the tomographic representation, which entails a CNR improvement, particularly for small objects, whereas the disadvantage is a decrease in high contrast resolution correlated with artefacts propagation, particularly along vertical direction.

10:30 - 12:00

Room Q

Cardiac

SS 503

CT coronary angiography: stenosis assessment

Moderators:

G. Feuchtner; Innsbruck/AT

N.-E. Klow; Oslo/NO

B-0360 10:30

The area stenosis measurement of significant coronary artery lesions by quantitative computed tomography coronary angiography (QCTA) correlates better with quantitative invasive coronary angiography (QCA) than diameter stenosis measurement

B. Laskowicz, B. Krupinski, T. Miszalski-Jamka, B. Guzik, M. Andres, R. Banyas, M. Urbanczyk - Zawadzka, M. Kostkiewicz; Krakow/PL

Purpose: To date most studies evaluated the diagnostic value of computed tomography coronary angiography (CTCA) to detect significant diameter coronary artery stenoses, but there is paucity of data comparing CTCA to invasive coronary angiography for area stenosis assessment. The aim of this study was to compare the variance of quantitative area and diameter stenosis measurement in significant obstructive coronary artery lesions between CTCA and invasive coronary angiography.

Methods and Materials: Fifty patients with significant coronary artery stenoses (?70% area stenosis) in dual source CTCA (Somatom Definition) were included and underwent invasive coronary angiography (ICA) within 3 months after CTCA. Area and diameter stenosis, minimal lumen area (MLA) and diameter (MLD), reference lumen area (RLA) and diameter (RLD) were evaluated in quantitative CTCA (QCTA) and quantitative invasive coronary angiography (QCA).

Results: Of 65 quantitatively evaluated significant stenotic lesions 19 were calcified, 17 were mixed and 29 were non-calcified. The Spearman's rank correlation between QCTA and QCA area and diameter stenosis measurements was: a) good (r=0.68, p < 0.0001) and moderate (r=0.58, p < 0.0001) for all lesions, b) very good (r=0.80, p < 0.0001) and good (r=0.72, p < 0.0001) for non-calcified plaques, c) very good (r=0.80, p < 0.0001) and good (r=0.65, p=0.005) for mixed lesions, and d) none for calcified plaques (r=0.26, p=NS and r=0.17, p=NS), respectively.

Conclusion: The area stenosis measurement of significant coronary artery lesions provided by quantitative CTCA closely correlates with QCA and yields higher correlation than diameter stenosis measurement. This correlation depends on plaque composition and is highest for non-calcified and mixed lesions.

B-0361 10:39

Is there a role for 64-row MDCT in the follow-up of heart transplanted patients? A comparison study with echocardiography and MR performed on the same day

V. Silvestri, R. Marano, G. Savino, B. Merlino, G. Verrillo, A. Meduri, L. Natale, L. Bonomo; Rome/IT (*valentina_silvestri@hotmail.it*)

Purpose: To evaluate the accuracy of 64-MDCT in the F/U of heart-transplanted patients assessing the LVF in comparison with echocardiography and MR, performed on the same day.

Methods and Materials: Sixteen patients with transplanted hearts were investigated by echocardiography, MR, and 64-MDCT. Two independent readers blind evaluated EF, EDV, ESV, SV, CO, and Mass of the LV on MDCT using a dedicated

software (TeraRecon, CA, USA) in comparison with MR and Echo, both performed on the same day. During all the examinations HR has been recorded. MDCT interobserver-agreement was also assessed.

Results: HR recorded during the examinations resulted lower for MDCT (74.2±8.0) ($p < .01$). EF resulted lower for MDCT (MDCT:57.1%±7.5, MR:61.3%±10.0, Echo:60.7%±6.1) (NS). In comparison with MR for the assessment of LV volumes, MDCT showed higher EDV (MDCT:159.2±22.9 mL; MR:135.0±31.2 mL, $p < .01$), ESV (MDCT:70.4±17.9 mL; MR:59.7±27.2 mL, $p < .01$) and SV (MDCT:88.8±16.7 mL; RM:76.1±16.0 mL, $p < .01$), but with moderate-to-good correlation ($r=0.647$, $r=0.565$, $r=0.815$, respectively) ($p < .05$ to $.01$). Slightly higher CO for MDCT was found (MDCT:6.6±1.3L, MR:6.3±1.3L, $p < .01$), with a high correlation coefficient value (0.959, $p < .01$). MDCT showed slightly higher values of Mass (MDCT:120.6±25.9 g/m², MR:105.7±23.4 g/m²) ($p < .01$), but with a high correlation ($r=0.795$, $p < .01$). Excellent was the MDCT interobserver-agreement (CCC>0.95).

Conclusion: MDCT allows the evaluation of heart-transplanted patients, obtaining diagnostic images with a relatively good agreement and correlation with MR for LVF assessment. It seems sufficiently reproducible to consider its application in the F/U and to support therapeutic strategies, with the advantage to perform LVF assessment within a global diagnostic approach including coronary arteries evaluation in one single very fast acquisition.

B-0362 10:48

Can segmented 3D images be used for stenosis evaluation in coronary CT angiography?

C. Wang, A. Persson, J. Engvall, J. De Geer, W. Czekierda, A. Bjorkholm, S.-G. Fransson, Ö. Smedby; *Linköping/SE*

Purpose: To retrospectively evaluate the diagnostic accuracy of coronary CT angiography (CCTA) using segmented 3D data for the detection of significant stenoses.

Methods and Materials: CCTA datasets from 30 patients were acquired with a 64-slice CT scanner and segmented using the region growing (RG) method and the "virtual contrast injection" (VC) method. Three types of images of each patient were reviewed by different reviewers for the presence of stenoses with diameter reduction of 50% or more. For the original series, the reviewer was allowed to use all the 2D and 3D visualisation tools available (conventional method). For the segmented results (from RG and VC), only maximum intensity projection was used. Evaluation results were compared with catheter angiography (CA) for each artery in a blinded fashion.

Results: Thirty-four arteries with significant stenosis were identified by CA. The percentage of evaluable arteries, accuracy and negative predictive value for detecting stenosis were, respectively, 86%, 74% and 93% for the conventional method, 83%, 71% and 92% for VC, and 64%, 56% and 93% for RG. Accuracy was significantly lower for the RG method than for the other two methods ($p < .01$), whereas there was no significant difference in accuracy between the VC method and the conventional method ($p = 0.22$).

Conclusion: Diagnostic accuracy for RG-segmented 3D data was lower than with access to 2D images. However, as a screening step, 3D methods may be a useful complement to 2D reviewing. The VC-based method is more promising for this purpose than the RG-based method.

B-0363 10:57

Diagnostic accuracy of coronary CT angiography for stenosis detection according to calcium score: systematic review and meta-analysis

M.A.M. den Dekker¹, K. de Smet², G.H. de Bock¹, R.A. Tio¹, M. Oudkerk¹, R. Vliegenthart¹; ¹Groningen/NL, ²Brussels/BE (m.a.m.Dekker@umcg.nl)

Purpose: The presence of coronary calcification is considered to negatively influence diagnostic accuracy of coronary CT angiography (cCTa). No consensus exists on whether cCTa can accurately diagnose coronary artery disease in case of an elevated calcium score (CS).

Methods and Materials: We performed a systematic review and meta-analysis to assess sensitivity and specificity of cCTa for significant stenosis at different degrees of coronary calcification. A literature search was performed with inclusion of studies describing test characteristics of cCTa for significant stenosis, performed with minimally 16-MDCT, by CS. Invasive coronary angiography was the reference standard. Pooled sensitivity and specificity of cCTa by different CS categories and scanner generations were calculated.

Results: Of 14,121 articles on cCTa, 53 studies reported on the impact of calcium scoring on diagnostic accuracy of cCTa and could be included in the systematic review. 27 of these studies (5,234 participants) were suitable for meta-analysis. In patient-based analysis, sensitivity of cCTa for significant stenosis was 95.8% (95%CI, 93.8-97.2), 95.6% (93.7-97.1), 97.6% (95.9-98.7) and 99.0% (97.0-99.8) for CS 0-100, 101-400, 401-1000 and > 1000, respectively. Specificity was 91.2%

(89.3-92.9), 88.2% (84.8-91.0), 50.6% (39.5-61.7) and 84.0% (76.5-89.9), respectively. Specificity of cCTa was significantly lower for CS 401-1000 due to lack of patients without significant stenosis. Sensitivity and specificity of 16-MDCT was significantly lower compared to newer CT generations.

Conclusion: Even in case of severe coronary calcification, sensitivity and specificity of cCTa for significant stenosis is high. With 64-MDCT and newer scanner generations, a CS cutoff for performing cCTa seems no longer indicated.

B-0364 11:06

Evaluation of left main coronary in-stent restenosis by dual source CT: comparison with invasive angiography and intravascular ultrasound

T. Adla, J. Veselka, D. Zemanek, P. Cadova, V. Suchanek, L. Miksik, M. Rodek; *Prague/CZ (theodor.adla@lfmotol.cuni.cz)*

Purpose: To evaluate the diagnostic accuracy of dual source computed tomography coronary angiography (CTCA) compared to invasive coronary angiography (ICA) and intravascular ultrasound (IVUS) for detection and quantification of in-stent restenosis.

Methods and Materials: Fifty-one patients with percutaneous coronary intervention of the LM were prospectively evaluated. Thirty-four of them underwent 56 complete follow-up examinations (median 6 months after intervention; CTCA, ICA and IVUS as gold standard examination) that focused on detection and quantification of restenosis.

Results: Sensitivity, specificity, positive and negative predictive values of ICA and CTCA were 100%, 94%, 50%, 100% and 100%, 74%, 18%, 100%, respectively. There was a moderate correlation between the minimal luminal areas (MLA) measured by CTCA and IVUS ($r=0.63$; $p < .01$). A Bland-Altman analysis showed that the MLA measured by CTCA was underestimated (mean difference 2.14±2.24 mm²).

Conclusion: These results suggested that dual source CTCA has a high negative predictive value and might be considered a less invasive alternative to ICA for exclusion of LM in-stent restenosis. However, there was only a moderate correlation between the measurements of MLAs by IVUS and CTCA in the stented LMs. Therefore, finding of any restenosis according to CTCA should be re-evaluated by ICA or, better, by subsequent IVUS.

B-0365 11:15

Coronary computed tomography angiography for detection of occult coronary artery disease in asymptomatic patients

A. Hidalgo, M. Descalzo, R. Leta-Petracca, L. Segura, S. Pujadas, F. Carreras, G. Pons-Llado; *Barcelona/ES (alhidalgo@gmail.com)*

Purpose: The purpose of this study is to assess the accuracy of coronary computed tomography angiography (CTA) for detecting significant coronary artery disease (CAD; ≥70% lumen reduction) and evaluate the impact in the risk stratification of middle aged asymptomatic patients.

Methods and Materials: A total of 310 consecutive middle aged asymptomatic individuals (87 men; mean age 55±9 years) underwent CTA (320-slice multidetector row computed tomography) as part of a general health screening. Medium follow-up was 3.8±2 years (1-7.5 years).

Results: Atherosclerotic plaques (AP) were identified in 163 (55.3%) individuals. 19 individuals (6.4%), luminal stenosis was significant (≥70%). Aged (decade), male gender ($p=0.005$), diabetes ($p=0.025$), serum cholesterol, smoking and hypertension ($p=0.0001$) were related with the presence of atherosclerosis. The patient group with AP had a medium of cardiovascular risks greater (2.1±1.1 vs 1.2±1, $p=0.0001$). In the midterm follow-up 1 patient died because of a cardiovascular cause, 1 patient had myocardial acute infarct and required stent implantation. Both had non-obstructive AP at CTA. 3 patients had atypical chest pain.

Conclusion: The prevalence of subclinical atherosclerosis shown by CTA in an asymptomatic population is high and it was related with a higher number of cardiovascular risks. Nevertheless, the number of major events in the midterm follow-up was low.

B-0366 11:24

Utility of computed tomography coronary angiography (CTCA) in diagnosis of cardiac allograft vasculopathy (CAV)

K.E. Tweed, C. Lewis, J. Parameshwar, D. Gopalan; *Cambridge/UK (katharinetweed@doctors.org.uk)*

Purpose: 1. Evaluate cardiac allograft coronary artery vasculopathy using CTCA. 2. Compare CTCA to catheter angiography.

Methods and Materials: Retrospective analysis of 26 cardiac transplant patients selected on the basis of CTCA performed on 64 slice dual source CT, over a four-year period in a tertiary cardiothoracic centre. CTCA and matched catheter

angiography in 11 patients were examined using International Society of Heart and Lung Transplantation (ISHLT) criteria segmental analysis. CAV grading of each patient was completed using ISHLT criteria in both modalities.

Results: Patient cohort mean age is 54 years and assessed at a mean of 11.7 years post-transplant. The mean coronary artery calcium score (Agatston) was 2.7 excluding a confounding patient with calcium score of 2030. 50% of patients had CAV on CTCA and of these 85% had grade 1 CAV, the remainder grade 2 CAV. CAV was demonstrated using CTCA with sensitivity of 92% and specificity of 95% on ISHLT segmental analysis, compared with catheter angiography. There was 100% concordance of patient CAV grading between CTCA and catheter angiography.

Conclusion: Cardiac allograft vasculopathy is reliably demonstrated using CTCA compared with catheter angiography. Coronary artery vasculopathy is differentiated from atherosclerotic disease. Routine use of less invasive CTCA for surveillance post-heart transplant may be feasible but needs further study.

B-0367 11:33

Impact of different levels of coronary calcium score on the prevalence of coronary artery stenosis in patients with an intermediate pre-test likelihood of coronary artery disease

T. Henzler, N. Vogler, M. Meyer, P. Apfaltrer, S. Sudarski, S.O. Schoenberg, c. Fink; Mannheim/DE (thomas.henzler@medma.uni-heidelberg.de)

Purpose: To investigate the prevalence of significant coronary artery stenosis on coronary catheterization in patients with an intermediate pre-test likelihood of coronary artery disease at different levels of coronary calcium score (CCS).

Methods and Materials: 87 patients (33 females, 66 ± 10 years) with an intermediate pre-test likelihood of coronary artery disease underwent CCS-CT prior to coronary catheterization. The prevalence of significant coronary artery stenosis (> 50%) on coronary catheterization was correlated to 5 different CCS levels using the Agatston score (AS) (AS: > 0; AS: > 10; AS: > 100; AS: > 200; AS > 400).

Results: Mean AS was 571 ± 599. Coronary catheterization revealed stenosis > 50% in 55 of 87 patients. Mean AS of patients with confirmed stenosis > 50% was 637 ± 484; range 3 - 1775. The sensitivity, specificity, positive predictive value (PPV) and negative predictive value (NPV) to predict significant stenosis on coronary catheterization was 100%, 15.6%, 67.1% and 100% using an AS cut-off value > 0; 96.4%, 25%, 68.8%, 80% using an AS cut-off value > 10; 87.3%, 40.6%, 71.6, 65% using an AS cut-off value > 100; 83.6%, 50%, 74.2%, 64% using an AS cut-off value > 200 and 60%, 65.6%, 75% and 48.8% using an AS cut-off value > 400, respectively.

Conclusion: In patients with an intermediate pre-test likelihood of coronary artery disease an AS between 0-10 makes a significant coronary artery stenosis very unlikely. Thus, CCS-CT provides additional information in combination with traditional clinical risk factors e.g. Framingham score to accurately predict the risk of those patients.

B-0368 11:42

Influence of intra-coronary enhancement on performance of second generation dual source CT coronary angiography

E. Maffei¹, C. Martini¹, S. Seitun², F. Cademartini¹; ¹Monastier di Treviso/IT, ²Genoa/IT

Purpose: To assess the effect of intra-coronary attenuation on diagnostic accuracy using second generation dual source computed tomography coronary angiography (CCT).

Methods and Materials: 142 patients with suspected coronary artery disease who underwent conventional coronary angiography (CA) and CCT were evaluated. CCT was performed with collimation 64x2x0.6 mm and rotation time 280 ms using 100 ml of high concentration contrast material (Iomprol 400; 400 mg/ml) administered at 6 ml/s. The study population was divided into two groups of 71 patients based on median (332 HU) vascular attenuation measured at the origin of the coronary arteries (group 1 = men attenuation < median value; group 2 = attenuation > median value). Image quality and diagnostic accuracy for the detection of significant coronary artery stenosis was determined and compared for both groups.

Results: No significant differences between groups 1 and 2 were noted in terms of age, gender, heart rate, coronary calcium score and body mass index. Overall, 258 significant stenosis (134 in group 1 and 124 in group 2) were detected in 1709 assessable coronary artery segments. The average intra-coronary attenuation was significantly (p < 0.05) higher for group 2 (396±46 HU) compared to group 1 (298±33 HU). Image quality and corresponding sensitivity/specificity values were higher for group 2 (99.2% and 97.6%, respectively) than for group 1 (85.1% and 93.0%, respectively).

Conclusion: Higher intra-coronary attenuation results in higher image quality and diagnostic accuracy for detection of coronary artery stenosis using second generation dual source computed tomography coronary angiography.

B-0369 11:51

Role of CT coronary angiography in suspected ab-extrinsico coronary compression in patients with pulmonary hypertension

V. Russo, E. Gobbi, G. Rinaldi, G. Mineo, F. Buia, L. Lovato, N. Galie, M. Zompatori; Bologna/IT (vi-rus@fastwebnet.it)

Purpose: Pulmonary artery hypertension (PAH) is a rare disease in which the increased blood pressure cause thickening, stiffening and, thus, the enlargement of the pulmonary artery. Such growth of the pulmonary artery could rarely cause "ab-extrinsico" compression of the coronary artery, in most of the cases the left main. The aim of this study is to evaluate the role of coronary CT angiography (CCTA) in the diagnosis of such complication.

Methods and Materials: from January 2009 to June 2011, 43 pts (19 M and 24 F, mean age 43aa) with PAH and angina underwent CCTA.

Results: in 30 pts (70%) coronary artery compression (n=13) or coronary artery displacement without significant compression (n=17) have been observed. In 10 pts (23%) other potential causes of angina have been discovered, such as coronary anomalies, coronary stenoses, myocardial bridges. All of 13 pts with coronary compression at CCTA and 6 with significant displacement were further examined with conventional coronary angiography which confirmed results in 16 pts (84%): 7 have been treated with coronary stenting, 2 with heart transplant and 2 with remodeling of the pulmonary artery; 4 pts are waiting for treatment and 1 it is deceased.

Conclusion: In pts with PAH and suspected ab-extrinsico coronary artery compression, CCTA is able to identify those which need a treatment.

10:30 - 12:00

Room Z

Computer Applications

SS 505

Image processing (part 2)

Moderators:

L. Fischer; Vienna/AT
E. Neri; Pisa/IT

B-0370 10:30

Semi-automated segmentation and characterisation of liver and liver lesions in contrast-enhanced CT images

C. Orsini, D. Della Latta, I. Bernardeschi, G. Di Girolamo, M. Patronelli, M. Guadagni, V. Positano, D. Chiappino, A. Monteleone; Massa/IT (orsini.chiara@gmail.com)

Purpose: Computed tomography is the most commonly used imaging technique for the inspection of liver lesions. Its spatial resolution allows a reliable extraction of liver and lesions features, such as their boundaries, size and density. The high variability of these parameters renders the segmentation task especially challenging.

A multi-stage semi-automatic hepatic tumour segmentation method is introduced.

Methods and Materials: Abdominal CT images with the use of venous contrast agent were acquired from 15 patients. Both liver segmentation and liver lesions segmentation were realised using information from portal and arterial phase and applying thresholding algorithm, region growing algorithm and morphological operators. A minimal user involvement is required to guide liver segmentation and lesions identification. The software framework was implemented in Java on NetBeans IDE.

Results: The software detects all liver lesions diagnosed by Physician (114 lesions) and their linear size (1.5-30 mm). Lesions segmentation allows the extraction of objective parameters (mean CT number, standard deviation, normalised contrast and CNR) in the different contrast phases. In addition to the evaluation of Recist protocol standard dimensions, lesion wash-out curves were considered. Through lesions density and CNR is possible to discriminate different kind of lesion and define a recognising decisional algorithm.

Conclusion: The developed method is able to identify all liver lesions. Lesions wash-out curves allow to obtain an attenuation profile in the three acquisition phases, so that we can have a response to therapy not only in volume terms but also in terms of lesions density variation.

B-0371 10:39

Automated detection and measurement of uterine peristalsis in cine MR images

K. [Yano](#)¹, K. Watanabe², M.Y. Kataoka², A. Kido², K. Togashi²; ¹*Osaka/JP*, ²*Kyoto/JP (kyano@is.oit.ac.jp)*

Purpose: Changes in direction and incidence of uterine peristalsis, namely wavy conduction of subendometrial myometrium (junctional zone), are supposed to strongly affect conditions such as infertility and dysmenorrhoea. In this study, we have developed and evaluated software to detect and quantify the peristalsis in cine MR images.

Methods and Materials: A total of 60 serial HASTE images in a midsagittal plane of the uterus of 11 healthy females were obtained every 3 seconds. Uterine peristalsis was defined as rhythmic changes of signal intensities and their propagations in junctional zone. Our software first calculated cross-correlation between time courses of pixel intensities in a section of junctional zone and those of neighbouring sections. The cross-correlation was high with appropriate time-lag when travelling wave was present. For the sections where the travelling waves were detected, the software calculated auto-correlation of time course of the signal intensities and obtained wave periods from peak intervals of the auto-correlation. Two radiologists, meanwhile, visually assessed uterine peristalsis using the same image series.

Results: The results from the automated method were consistent with those of visual assessments and had less variance (mean counts by software, observers A and B were $6.6 \pm 0.8SD$, $6.6 \pm 1.3SD$ and $5.2 \pm 2.1SD$, respectively). Weighted kappa between software and observer A, software and observer B, and observers A and B were 0.95, 0.72 and 0.71, respectively, indicating variations between software and humans were smaller than that between humans.

Conclusion: Uterine peristalsis can be detected and counted by automated evaluations. Our method may be used for a routine functional assessment of uterus.

B-0372 10:48

Digital perfusion phantoms and their use in perfusion validation

O.S. [Pianykh](#); *Newton Highlands, MA/US (opianykh@bidmc.harvard.edu)*

Purpose: Despite the increasingly broad use of perfusion applications, we still have no generally accessible means for their objective validation. To solve this problem, we introduce digital perfusion phantoms (DPP) - simulated DICOM images sequences, specifically designed to have known perfusion maps with simple visual patterns.

Methods and Materials: Let S be a temporal perfusion image sequence $S = \{I_0, I_1, \dots, I_n, \dots, I_N\}$. We define digital perfusion phantom (DPP) as a computer-simulated image sequence S , where each temporal pixel value $I_n(x, y) = I_n(x, y; t_n)$ is generated to have predefined visual perfusion map patterns. That is, given blood flow FB , blood volume VB and mean transit time TM maps, we build DPP image sequence S to produce these maps. While any perfusion algorithm works a numerical solver for perfusion convolution equation, DPP becomes a known solution to it, which can be used to verify the algorithm correctness.

Results: We developed a 45-image DPP where FB , VB and TM maps consist of simple linear patterns. We then processed our DPP with several perfusion packages, comparing the resulting maps to the expected. This comparison provided an instantaneous and objective visualisation of perfusion algorithms' deficiencies, as well as their sensitivity to noise and small details. DPP, used with different perfusion software and protocols, can clearly visualise processing errors and discrepancies.

Conclusion: Processing DPP perfusion sequence with any perfusion algorithm/software of choice, and comparing the results to the expected DPP patterns provides a robust and straightforward way to control the quality of perfusion analysis, software, and protocols.

B-0373 10:57

Automated semantic navigation and synchronised alignment in baseline and follow-up full body CT scans: clinical feasibility and accuracy

P. [Dankerl](#), M. Hammon, M. Suehling, A. Tsybal, M. Uder, A. Cavallaro; *Erlangen/DE (peter.dankerl@uk-erlangen.de)*

Purpose: Comparing findings from initial and follow-up examinations in increasing full body CT data is a challenging and time-consuming task for radiologists. We evaluated practicability and performance of automated semantic navigation and synchronised alignment in routine clinical follow-up CT data.

Methods and Materials: Initial and follow-up CT studies from 16 oncological patients undergoing routine CT staging were retrospectively incorporated into THESEUS-MEDICO-software (German federal project-number 01MQ07026) which automatically detects organs and anatomical landmarks, used for automatic semantic alignment and prediction of findings locations in follow-up data from base-

line findings locations. 205 relevant reported findings, e.g. lymph nodes or vessel junctions, were evaluated. Manual navigation by two experienced radiologists to corresponding findings in follow-up data was taken as gold standard and compared to system-based navigation. Error in mm between manual and automatic navigation was documented as craniocaudal-, ventrodorsal-, lateral-left or lateral-right deviation. Mean deviations and intra-class correlation coefficient (ICC) were evaluated.

Results: The mean deviation of the reported 205 lesions for reader 1 was 9.6 mm with similar deviations in all directions (4.4 mm cranial; 5.7 mm caudal; 5.1 mm ventral; 5.2 mm dorsal; 4.5 mm lateral-left; 4.0 mm lateral-right), and 9.2 mm for reader 2 (4.1 mm cranial; 5.4 mm caudal; 5.1 mm ventral; 4.8 mm dorsal; 4.4 mm lateral-left; 4.2 mm lateral-right). ICC was 0.9. For both readers there was no deviation bias into a particular direction.

Conclusion: Automated semantic navigation in CT follow-up data provides clinically sufficient accuracy and reproducibility allowing automated side-by-side viewing of corresponding locations in baseline and follow-up data. It should improve handling large datasets and speed up radiological reading.

B-0374 11:06

An automated method for visualising changes in vessel wall dynamics

E. [Schwartz](#)¹, G. Langs¹, J. Holfeld², M. Czerny³; ¹*Vienna/AT*, ²*Innsbruck/AT*, ³*Berne/CH (Ernst.Schwartz@meduniwien.ac.at)*

Purpose: The study of effects of vascular interventions is today mostly limited to static vessel models. This represents an over-simplification in the case of the thoracic aorta, which is strongly influenced by the motion of the myocardium.

Methods and Materials: In this paper, we propose a framework enabling the quantification and visualisation of the motion of the thoracic aorta from ECG-gated CTA sequences during the cardiac cycle. The vessel is segmented and tracked automatically through a heartbeat. The extracted motion of the aorta is decomposed in measures of pulsation, bending and stretching. We further generate a novel 2D representation of the vessel dynamics for quick visual assessment.

Results: We used the proposed method to evaluate the effects of stent-grafting in the aortic arch after supra-aortic rerouting in 5 cases. The obtained measurements and their visual representation give detailed insight into of patterns of movement in the thoracic aorta as well as changes induced by stent-grafting of the aortic arch. Elevated strain due to diffuse motion at the beginning of the prosthesis could be observed in all cases. The influence of stent-length and placement could also be quantified using the proposed method.

Conclusion: We developed an automated method to aid the visual inspection of the effects of vascular interventions in the aortic arch. As a first example of the application of the proposed method, we could describe the influences of the length and location of a stent graft in the aortic arch in 5 cases.

B-0375 11:15

Towards efficient simultaneous multi-patient annotation of 3D imaging data

W. [Lang](#), R. Donner; *Vienna/AT (e0726752@student.tuwien.ac.at)*

Purpose: Manual segmentations of medical data are tedious and time intensive - multiple segmentations quickly become prohibitively expensive (especially on 3D data). Observing this, we developed an interactive, incremental annotation tool for generic medical image data, focusing on simultaneous, weakly supervised classification based, multi-patient segmentations.

Methods and Materials: We use an initial over-segmentation methods such as Superpixels to cluster spatially coherent, homogeneous structures while retaining edge information. User-guided brush strokes mark representatives for each label class within the image, which are passed to a random forest, learning implementation. Resulting priors combined with local descriptors and optimised by a MRF solver, give a first estimation of desired appearances in all multi-patient views. Successive interactions refine the annotation, making maximal use of each user input.

Results: The resulting framework provides a multi-patient view, allowing to interact with all individual annotation simultaneously. We evaluate the segmentation results on 25 left-hand CTs, we calculate the Dice coefficient between our ground truth and segmentation results. We reach an overlap of 92.1% in metacarpals, 91.7% in proximal phalanges and 86.0% in intermediate phalanges on 800x500 pixel sized images with approximately 500 oversegmentation primitives (Superpixels). **Conclusion:** Using over-segmentation through Superpixels combined with local descriptors makes the labelling problem in multi-patient segmentations tractable. Consistent with our goal of providing whole image labelling annotations, not individual object delineations, by lowering accuracy (due to the Superpixels) the annotation time for a whole set of patient data (e.g. hand CTs) is a fraction of the time required using current annotation tools.

B-0376 11:24

Retrieving positive findings in radiological images with the aid of textual hints in reports

P. Daumke, K. Simon, C. Simon, E. Kotter, A. Gerstmair;
Freiburg/DE (daumke@averbis.de)

Purpose: To build and evaluate a retrieval system for German radiology reports enabling improved access to radiological image and free-text data.

Methods and Materials: A scalable text analysis platform is used to extract relevant information from German radiology reports and to create semantic links between images and textual descriptions. The platform consists of domain-specific analysis components dealing with different aspects of medical language such as negations, abbreviations, dimensions, proper names and the morphological analysis of word compounds. Additionally, it contains an image reference and context recognition component allowing the creation of semantic links between text and image data. Given an explicit picture reference mentioned in a report, e.g. 'IMA 12-15', and its surrounding description this component tries to deduce the corresponding DICOM series ID based on explicit or implicit hints and loads the referenced image (s) from the local PACS server. Finally, key images and relevant text passages are subsequently made available to radiologists in a search engine for ad-hoc querying.

Results: On a corpus of 113.325 radiology reports the system was able to identify 32.533 image references and successfully retrieve 32.157 images from the local PACS server. Randomised validations of identified image references showed that the extraction component is able to resolve the correct reference with mean-average precision of P:0.97.

Conclusion: Our analysis shows that comprehensive syntactic and semantic text analysis is required to achieve high-quality information extraction from radiology reports. It is the basis for a number of value-added applications such as image search, data mining and decision support.

B-0377 11:33

Rapid semiautomatic liver segmentation using a new user-friendly, prototypic software tool: initial experience

F.I. Martínez Gambaro¹, F.O. Henes², H.D. Nagel², G. Adam², M. Regier²;
¹Santiago/CL, ²Hamburg/DE (femartinezg@gmail.com)

Purpose: To evaluate the accuracy of a new software-tool for semiautomatic liver segmentation in the analysis of liver segments, vessels and tumour lesions and to assess its the user-friendliness.

Methods and Materials: In 10 healthy liver donors and 20 patients suffering from hepatic tumours thin-sliced MDCTs (256-iCT, Philips; 1 mm slice-thickness) were acquired. Based on a level set method for automatic contour identification the segmentation was performed following Couinauds anatomical classification. The volumetry of segments, vessels and lesions was assessed automatically using a 2D-based voxel classification algorithm with propagational learning and, afterwards, manual correction was performed. The time necessitated for segmentation and manual correction was recorded. The time to execute all measurements and corrections was quantified.

Results: The semiautomatic segmentation rapidly performed precise determination of all segments with averaging correctness of 97.4% in healthy donors. In tumour patients the correctness for all segments was 95.5%. The mean time for semiautomatic liver segmentation and manual correction was 6:31 min and 5:48 min, respectively. Rapid assessment of tumour volume was achieved with correctness of 92%. The accuracy was limited if prior resection or large necrotic areas were present. The recognition of liver vessels was highly precise (> 90%) using a standard contrast injection protocol.

Conclusion: The new semiautomatic software tool evaluated allows for the segmentation of the liver, vessels and tumour lesions with remarkably high precision and efficiency. Furthermore, due to its easy-to-handle approach and the rather short time for manual correction this tool might meet the broad demands of modern cross-sectional imaging of the liver in daily clinical routine.

B-0378 11:42

Image registration in a hybrid routine using Shannon-Tsallis entropy for the statistical parametric mapping (SPM)

H.T.A.S. Amaral, L.O. Murta Jr., L. Wichert-Ana, A.C. Sakamoto,
P.M. Azevedo-Marques; Ribeirão Preto/BR (henriquetomaz@uol.com.br)

Purpose: The automatic co-registration of medical images based on similarity measures have been suggested in several studies using different cost function approaches; which have presented relevant results for many kind of biomedical images. Based on previous results showing the contribution of the Tsallis entropy on the alignment of magnetic resonance imaging (MRI) and single photon emis-

sion computed tomography (SPECT), this project proposes the implementation of a hybrid routine using the combination of the Shannon and the Tsallis entropies in the Statistical Parametric Mapping co-registration.

Methods and Materials: MRI and SPECT of 1 morphologically normal patient were used for the construction of simulators which were co-registered with the original images using the proposed hybrid routine and the individual ones. The comparative analysis between the routines reliability was performed based on the root mean square (RMS) error of the rotation and translation parameters.

Results: Preliminary results showed that the hybrid routine led to a more reliable inter-modality co-registration for simulators with small transformations based on the RMS error, as expected. More co-registrations are being performed to confirm these results for the simulators with larger transformations.

Conclusion: The initial results showed strong evidences that the hybrid routine using Shannon and Tsallis entropies jointly performed most reliable inter-modality co-registration using statistical parametric mapping and therefore could be a new available cost function approach in the image processing tools.

B-0379 11:51

Integration of diffusion and perfusion images of human breast cancer by registration and dissimilarity-based clustering

C.A. Méndez¹, F. Pizzorni Ferrarese¹, P. Summers², G. Petraia², G. Menegaz¹;
¹Verona/IT, ²Milan/IT (andres.mendezg@gmail.com)

Purpose: To introduce a new patient-specific pipeline for the integration of breast diffusion and perfusion MRI for surgical planning.

Methods and Materials: We propose a two-step process for the integration of information derived from DCE-MRI and DW-MRI modalities. First, voxel-wise dissimilarity-based clustering is performed on DCE images to identify different tumoral subregions, which are then projected to the DW-MRI following a patient-specific registration protocol consisting of a preliminary multiresolution rigid transformation followed by an elastic B-Spline deformation focused on the lesion area. The probability density functions in the ADC map of the subregions are then extracted and compared through non-parametric testing (Wilcoxon-signed-rank test, p=0.05). The pipeline was demonstrated using DCE-MRI and DW-MRI acquired from 7 patients, ranged in age 42-70 (median 48 years), affected by primary ductal carcinoma.

Results: Non-parametric tests show that ADC values from the subregions corresponding to different clusters in the DCE volume have statistically different characteristics, which indicates the consistency of the information obtained from the two modalities while providing a posterior validation of the registration method.

Conclusion: In this work we have employed dissimilarity-based representations instead of classic features to integrate the information provided by both diffusion and perfusion MRI images of the breast. Preliminary results are quite promising and suggest the exploitation in future works of this combined information in the registration process through the definition of an ad-hoc objective function. Moreover, after spatial registration, the diffusion information can be incorporated into the classification process yielding a truly multimodality integration of imaging data.

14:00 - 15:30

Room A

Neuro

SS 611a

Interventional neuroradiology

Moderators:
B. Gómez-Ansón; Barcelona/ES
S. Puchner; Vienna/AT

B-0380 14:00

Single centre experience of intracerebral artery thrombectomy using TREVO device in 60 patients with acute ischaemic stroke

L. San Roman, V. Obach, J. Macho, J. Blasco, A. Lopez,
A. Tomasello, J. Perandreu, J. Branera, A. Chamorro; Barcelona/ES
(lsrmanzanera@gmail.com)

Purpose: To describe the effectiveness and safety and of a mechanical stent-like device TREVO in the endovascular treatment of acute ischaemic stroke.

Methods and Materials: Prospective, single-centre study of 60 patients with an acute ischaemic stroke attributable to a large cerebral artery occlusion. Median National Institutes of Health Stroke Scale, 17. Arterial occlusion was in the anterior circulation in 86% of cases and in vertebrobasilar territory 14%. Mean time from symptom onset to endovascular treatment was 263 minutes. Endovascular treatment was ruled out when established ischaemic lesions were greater than



one-third of the middle cerebral artery territory, measured by multimodal computed tomography (CT) or magnetic resonance (MRI).

Results: 46% of patients were deemed to show good outcome (modified Rankin Scale score 0-2) at 90 days. Of the 49 patients treated using Trevo as the sole treatment technique, 76% showed complete thrombolysis in cerebral infarction score (TICI, grade 3) or partial (TICI 2b) reperfusion, and this increased to 86% if additional treatments were used. The mean time from groin puncture to recanalisation was 78 min. Symptomatic intracranial haemorrhage was found in 8 (13%) patients and 16 (28%) patients died within the 90-day follow-up period. There were 4 distal embolisations of a previous uninvolved territory. No arterial rupture or other major complications occurred.

Conclusion: Our findings indicate that mechanical intracranial thrombus extraction using TREVO is effective and has a reasonable morbidity and mortality rate in the treatment of acute ischaemic stroke.

B-0381 14:09

Endovascular reperfusion for acute ischaemic stroke (AIS). Preliminary results of a single centre retrospective study

E. Puglielli, M. Fuschi, V. Di Egidio; *Teramo/IT (edopug@hotmail.com)*

Purpose: Aim of this preliminary study was to assess the safety/efficacy of the multiple endovascular modalities (pharmacologic/mechanical) that can be used in the reperfusion therapy for AIS to improve the rates of recanalisation.

Methods and Materials: 52 consecutive patients with AIS (mean age 57y, from April 2009 to September 2011), on-set less than 8 hours for the anterior circulation and 12 for the vertebro-basilar one, underwent to intra-arterial pharmacologic or mechanical therapy with recanalisation. CT/CT-perfusion/MRI/DSA were used for the assessment of ischaemic area and causes. Patient's age, sex, aetiology of occlusion, symptom before/after mechanical/pharmacologic treatments with modified Rankin Scale (mRS), recanalisation rates evaluated with TICI (thrombolysis in cerebral ischaemia): grade 0 (no-flow) grade 3 (normal-flow), and haemorrhagic transformations (HT) were recorded and correlated using a multiple logistic regression analysis.

Results: The sites of arterial occlusion before treatment were: M1=28 patients (53.84%), intracranial carotid=4 (7.69%), M2=7 (13.46%), tandem occlusion=3 (5.76%), extracranial internal carotid isolated occlusion=5 (9.61%), P1=2 (3.84%), basilar trunk=3 (5.76%). Therapeutic interventions included: multimodal therapy=28 (54.84%), pharmacologic cheap with tissue-plasminogen activator (t-PA)=11 (21.15%), mechanical therapy with embolectomy using solitaire (ev3-TM)=13 (25.00%). The recanalisation rate with multimodal therapy was significantly higher TICI 2-3 recanalisation rate (23 patients [82.14%]) compared to pharmacologic therapy only (6 patients [54.54%]) or mechanical one (8 patients [61.53%]), $p < 0.001$. Haemorrhagic perfusion occurred in one patient with M1 occlusion that spontaneously resolved.

Conclusion: Multimodal therapy showed significantly higher recanalisation rates vs pharmacologic or mechanical ones while the prevalence of hemorrhage does not exceed that which occurs in the natural history. These preliminary results show potential for the endovascular management of AIS.

B-0382 14:18

Results of mechanical thrombolysis for acute ischaemic stroke: comparison with intra-arterial urokinase infusion

A. Im, S. Jeon, S. Choi; *Iksan/KR*

Purpose: To evaluate the efficacy and safety of mechanical thrombolysis in acute ischaemic stroke compared with results of intra-arterial (IA) pharmacologic thrombolysis.

Methods and Materials: We retrospectively reviewed patients who were performed IA thrombolysis for acute thromboembolic occlusion of major vessels. Total patients were 101 and divided in to 3 groups: group 1 (pure urokinase [UK] infusion, n=31), group 2 (mechanical thrombolysis [clot disruption] using microwire and microcatheter, n=40), group 3 (mechanical thrombolysis using angioplasty balloon, retrievable self-expandable stent, or aspiration thrombectomy catheter, n=30). We assessed treatment results which were compared by recanalisation rate, clinical outcome, mortality, and symptomatic haemorrhage rate.

Results: The recanalisation rate was 51.6% in group I, 75% in group II, and 78.6% in group III. Mechanical thrombolysis groups had higher recanalisation rate and group III had the best result of recanalisation rate ($p < .05$). We assessed clinical outcome using modified Rankin Scale (mRS) after 3 months and favourable outcome was the best in group III, followed by groups II and I ($p < .05$). The symptomatic haemorrhage rate and mortality was 12.9%, 19.4%, in group I, 15%, 17.5% in group II, and 3.3%, 6.7% in group III, respectively. This difference was not

statistically significant ($p > .05$). However, group III has tendency that symptomatic haemorrhage and mortality are low.

Conclusion: Mechanical thrombolysis has higher rate of recanalisation and good clinical outcome than UK thrombolysis. From among two different mechanical thrombolytic therapies, using mechanical devices have lower rate of haemorrhage and mortality than using microwire and microcatheter.

B-0383 14:27

Mechanical thrombectomy with the trevo stent device in proximal intracranial arterial occlusions

M.M.A.C. Van Santen-Van Doorn¹, R. Van Den Berg¹, B. Van Der Kallen², G.L.A. Nijeholt², W. Van Zwam³, R. Van Oostenbrugge³, A. Van Der Lugt⁴, Y. Roos¹, C.B.L.M. Majoie¹; ¹Amsterdam/NL, ²Den Haag/NL, ³Maastricht/NL, ⁴Rotterdam/NL

Purpose: To evaluate the safety and effectiveness of a self-expanding and fully retrievable stent (Trevo; Concentric Medical Inc, Mountain View, CA, USA) in revascularisation of patients with acute ischaemic stroke.

Methods and Materials: Prospective multicentre case series of 22 patients (mean age 54Y; M:F = 17:5) with an acute ischaemic stroke caused by proximal intracranial arterial occlusion treated with a fully retrievable stent within the first 8 hours from symptom onset (median National Institutes of Health Stroke Scale 19 [range 10-28]). Thrombectomy was used as rescue therapy in patients who were refractory to, had contraindications for or were too late for IV rtPA. The occlusion site was the MCA in 7, terminusICA in 2, cervical ICAMCA in 4 and basilar artery in 9 patients. Complications related to the procedure and outcome at 3-6 months were assessed.

Results: Stent placement was feasible in all procedures and successful recanalisation defined as thrombolysis in cerebral ischaemia (TICI) grade 2b or 3 was achieved in 19 of 22 treated vessels (86%). The mean number of passes for maximal recanalisation was 2 (range 1-5). The median time from groin puncture to recanalisation was 84 (range 26 - 199) minutes. One significant procedural event occurred (carotid artery occlusion after stent removal). Forty-one% of all patients had a good outcome (mRS 0 to 2), 6% a moderate outcome (mRS 3), and 53% a poor outcome (mRS 4 to 6).

Conclusion: These results suggest that with the Trevo device, clots can be safely and effectively removed from intracranial large vessel occlusions in acute ischaemic stroke.

B-0384 14:36

Cerebral vasospasm (CV) after aneurysmal subarachnoid haemorrhage (A-SAH): intra-arterial management

E. Puglielli, M. Baffie, M. Fuschi, V. Di Egidio, M. Monina; *Teramo/IT (edopug@hotmail.com)*

Purpose: The purpose of this work is to evaluate predictors of recanalisation and a favourable neurological outcome in patients with CV after acute A-SAH.

Methods and Materials: From May 2004 to September 2011, we embolised 149 aneurysm in 145 patients (age ranged from 19 to 87 years, mean age 57) with A-SAH, using metal detachable coils/stenting; in 55 (36.91%) of these patients we report clinical and/or angiographic signs of CV. MRA, CT and DSA have been used to evaluate SAH. We discuss the use of neuroendovascular techniques and the recent advances in the local therapy of CV following A-SAH. Patient's age, sex, aetiology, perfusion, recanalisation and symptom pre- and post-treatment with modified Rankin Scale (mRS) were analysed using a multiple logistic regression analysis.

Results: In 21 (38.18%) of the 55 patients we have observed regularisation of the narrowed vessel using local i.a. infusion of papaverine (4 cases) or nimodipine (17 cases) at the 3 weeks control. In 25 (45.45%) patients we report the use of local i.a. nimodipine before and after large vessel percutaneous transluminal balloon angioplasty (PTA) with recanalisation after procedure and improvement of clinical condition at the 3-6 months of follow-up. Recanalisation favoured a better outcome with a pre- and post-treatment mRS improvement at 6- to 9-month follow-up ($p=0.005$), especially in those who received early treatment.

Conclusion: Earlier treatment is usually associated with better patient survival and outcome but continued efforts are necessary to improve and refine endovascular strategies as well as develop new treatment modalities.

B-0385 14:45

Angiographic outcome after endovascular treatment of intracranial aneurysms with the silk flow diverter

A. Ringelstein, M. Schlamann, S. Gricke, C. Moeninghoff, I. Sandalcioglu, M. Forsting, I. Wanke; *Essen/DE (adrian.ringelstein@uk-essen.de)*

Purpose: Wide-necked and fusiform aneurysms are technically challenging for EVT. FD may occlude the aneurysms by endoluminal reconstruction of the parent

artery and reducing the blood flow into the aneurysms. The purpose of this study was to assess the rate of intervention-associated complications and the midterm outcome after Silk stent implantation.

Methods and Materials: We retrospectively analysed 17 patients with unruptured aneurysms treated with 21 Silk FD between 05/2008 and 12/2010. Treatment indications were fusiform aneurysms, circumferential aneurysms, and giant aneurysms presented with embolic events or a progressive mass effect.

Results: Technical success was reached in 17/17 patients. Three aneurysms were immediately occluded, one of these with additional coiling. All aneurysms showed immediately inflow reduction. After three months, occlusion was observed in all cases except one aneurysm of the ICA. The overall complication rate including technical, thromboembolic complication or in-stent-thrombosis was 6 of 21 FD (29%). Clinical outcome in 17 patients included one with not severe and 2 with severe neurological deficits. 1-year follow-up did not show any reperfusion of the aneurysm.

Conclusion: Despite a not low complication rate the FD treatment of complex aneurysms is effective with a high occlusion rate of the aneurysm also in the midterm follow-up. The overall complication rate may be higher than in conventional stent-assisted coiling but we have to consider that the aneurysms were difficult to treat with conventional endovascular methods, had recurred after previous treatments, or showed a disease progression.

B-0387 14:54

Computational fluid dynamics in patients treated with flow-diverter devices

T. Baptista¹, P. Watton², E. Holland², J. Penrose³, A. Chiarini A⁴, J. Byrne², J. Reis¹; ¹Lisbon/PT, ²Oxford/UK, ³Abingdon/UK, ⁴Casalecchio di Reno/IT (jtbaptista@gmail.com)

Purpose: Flow-diverter devices have been demonstrated to be of high efficacy in treatment of intra-cranial aneurysms, especially those with wide necks. This project attempts to identify if pre-treatment flow characteristics are of assistance in predicting whether a specific aneurysm is more prone to thrombose, and if there are any haemodynamic indices that correlate with the regions which thrombose first.

Methods and Materials: Two cavernous aneurysms were modelled from 3D pre-treatment angiographic studies. Patients were treated using flow-diverter devices and were followed over the subsequent 2 to 12 months with contrast-enhanced 3D time of flight magnetic resonance angiography. Images were segmented using @neuFuse 7.3 TS software. @neuFuse was also used to virtually deploy a flow-diverter in both aneurysms. Flow with/without the flow-diverter was simulated using ANSYS CFX 13.0 software.

Results: Computational fluid dynamic (CFD) analysis and 3D angiographic follow-up studies enabled us to observe that thrombus formation within the aneurysm sacs initiated in regions of significant flow reversal; indicated by high Oscillatory Shear Index (reaching values near 0.5) and negative values of minimum aneurysm formation index (close to -1).

Conclusion: In this study, CFD analysis was performed on pre-treatment aneurysm geometries before and after the virtual deployment of a flow-diverter device. It was observed that thrombosis is more prone to occur in regions of significant flow reversal. We conclude that CFD may prove useful in predicting which regions of an aneurysm treated with a flow diverter will thrombose first.

B-0388 15:03

Silent ischaemic lesions after stent-assisted coiling

M.L. Hahnemann, M. Ho, M. Schlamann, S. Goericke, I. Wanke, C. Moeninghoff, M. Forsting, A. Ringelstein; Essen/DE (mariahahnemann@gmx.de)

Purpose: Stent-assisted coiling has improved the ability to treat difficult and complicated aneurysms. The present study aims to investigate the rate of silent embolic lesions after stent-assisted coiling and to define associated predictors.

Methods and Materials: The study includes a total of 69 patients treated with 70 stent-assisted coilings. DWI MR imaging of the brain was performed after stent-assisted coiling to detect intervention-associated silent ischaemic lesions. Demographic data, aneurysm characteristics and angiographic parameters were correlated with the frequency, the distribution, and the size of the ischaemic lesions.

Results: After 70 stent-assisted coilings 40 DWI MRI analyses after intervention revealed 161 bright lesions in a pattern consistent with embolic events. 147 lesions were smaller than 10 mm in diameter, whereas 14 lesions were larger than 10 mm. More than the half of the treated patients (54%) displayed embolic events without new neurological deficit. We presume a correlation of these ischaemic lesions with the duration of the procedure and with the patient's age. Furthermore, higher DWI rates tend to appear in the anterior brain circulation.

Conclusion: Silent embolic events are much more frequent than the apparent neurological complication rate after stent-assisted coiling. However, individual and aneurysm-specific parameters may predict the safety of the intervention and presumably, the subsequent rate of neurological complications.

B-0389 15:12

New ischaemic brain lesions on diffusion-weighted MRI after carotid artery stenting with protection: a single-centre study

D.A. Stojanov, M. Ilic, P. Bosnjakovic; Nis/RS (drstojanov@gmail.com)

Purpose: Carotid artery stenting (CAS) with distal protection is now considered an alternative to carotid endarterectomy. Despite cerebral protection, the risk of cerebral embolisation still persist during the procedure. Diffusion-weighted imaging (DWI) is considered the most sensitive tool for early detection of cerebral ischaemia. The purpose of this study was to evaluate the appearance of new ischaemic cerebral lesions by DWI after protected CAS in patients with severe internal carotid artery (ICA) stenosis.

Methods and Materials: Fifty CASs were performed with the use of distal protection. Mean age of the patients was 65.13±7.08 years and 74.5% were symptomatic. In 8.51% patients procedure was done on an emergency basis. All patients were unsuitable for CAE. DWI was performed immediately before CAS and within 24 hours after the procedure.

Results: There were 15 new lesions in 7 patients (14.89%) (mean 2.14±1.12 per patient). In 3 of them (42.86%) there were single lesions, and in 4 (57.14%) patients multiple lesions. Four patients (57.14%) developed ipsilateral new lesions, two patients (28.58%) developed contralateral new lesions and one patient (14.28%) developed bilateral new lesions. Patients with fibrolipid plaques had a significantly higher number of new lesions compared to patients with fibrocalcified plaques (p=0.025).

Conclusion: New ischaemic lesions were observed in 14.89% of our patients. There was a significant relationship between plaque characteristics and the appearance of new lesions. The low percentage of new lesion suggests that CAS with protection is safe and effective in patients with severe ICA stenosis.

14:00 - 15:30

Room B

Cardiac

SS 603

CT and MRI: reconstruction algorithms and dose reduction

Moderators:
K. Nikolaou; Munich/DE
P.K. Vanhoenacker; Aalst/BE

B-0390 14:00

Reconstructions with identical filling (RIF) of the heart: a physiological approach to image reconstruction in coronary CT angiography

S.D. Reinartz¹, B.S. Diefenbach¹, T. Allmendinger², C.K. Kuhl¹, A.H. Mahnken¹; ¹Aachen/DE, ²Erlangen/DE (sreinartz@ukaachen.de)

Purpose: The aim of the study was the comparison of image quality in coronary CT angiography (cCTA) between routine reconstructions with automated phase detection and Reconstructions computed with Identical Filling of the heart (RIF). The timing is provided RIF-formula, which is deducted from cardiac physiology.

Methods and Materials: From November 2009 until July 2010, 74 patients undergoing ECG-gated DSCT were included in the study for suspected coronary heart disease (n=40) or planning of interventional aortic valve replacement (n=34). RIF formula and the manufacturer's software (BestDiastole) were used for calculating the datasets. Two radiologists assessed in consensus coronary artery segments according to the 15 segments AHA model. Image quality was stratified using a 5 grade Likert scale. Continuous variables were expressed as mean ± standard deviation, categorical variables additionally as frequencies or percentages. Differences in categorical data were analysed using the Wilcoxon test for paired variables.

Results: 31 men and 43 women with an average age of 71.86±13.1 years and with a mean heart rate of 69.2±14.8 were examined. In the BestDiastole group 590 segments achieved diagnostic quality compared to 693 segments in the RIF group. In corresponding AHA segments RIF was superior in 342 segments (30.8%), BestDiastole scored higher in 155 cases (14.0%). In the arrhythmic subgroup the mean RIF images scored 2.40 ± 0.53 in comparison to BestDiastole with 1.84 ± 0.41.

Friday

Conclusion: RIF reconstruction is superior to standard reconstruction, especially in patients with atrial fibrillation. Furthermore, RIF provides a theory for the optimal image reconstruction point.

B-0391 14:09

CT coronary artery calcium scoring and iterative image reconstruction techniques: reproducibility, accuracy, and potential for radiation dose reduction

A. Schindler¹, P. Apfaltrer¹, R. Vliegenthart¹, T. Allmendinger², S. Vogt³, R. Raupach², F. Bamberg⁴, K. Nikolaou⁴, U. Schoepf¹;
¹Charleston, SC/US, ²Forchheim/DE, ³Malvern, PA/US, ⁴Munich/DE (andreas.schindler@med.uni-muenchen.de)

Purpose: The effect of iterative-reconstruction on CT coronary calcium scoring (CCS) has not been investigated. We evaluated in-vivo and in-vitro the reproducibility of CCS across different reconstruction methods and the potential for radiation-dose reduction.

Methods and Materials: 33 consecutive patients (17 men; 58.5±9.5 yrs) underwent CCS studies on a 2nd generation dual source CT (DSCT) system. In-vitro data were obtained using a moving anthropomorphic cardiac phantom containing calcium inserts of different sizes. Full-dose reconstructions were based on projections from both DSCT tube-detector configurations. Half-dose acquisition was simulated by discarding raw data from one tube. Full-dose and half-dose series were reconstructed with iterative-reconstruction-in-image-space (IRIS) and sinogram-affirmed-iterative-reconstruction (SAFIRE) using dedicated CCS kernels. Calcium was measured using a conventional CCS application and compared with traditional filtered-back-projection (FBP) series by Wilcoxon-Mann-Whitney-testing.

Results: No significant differences in overall CCS were found between full-dose FBP, IRIS, and SAFIRE (mean CCS (25th/75th-percentile) 101 [0/62] vs. 98 [0/59], and 98 [0/62]; p> 0.05). The mean effective dose was 1.42±0.54mSv. Differences in overall CCS between full-dose FBP, half-dose IRIS (95 [0/63]), and half-dose SAFIRE (96 [0/63]) were also not significant (p> 0.05). In two patients with a CCS of zero based on FBP, the CCS became positive on iterative-reconstruction. Likewise, in-vitro the smallest (1 mm) insert was recognized as calcium only on iterative-reconstruction, but not on FBP.

Conclusion: Overall CCS obtained by FBP and iterative-reconstruction are comparable, even if the radiation dose is reduced by 50%. Likely through noise suppression, iterative-reconstruction may enable detection of smaller calcium deposits, and thus of earlier coronary atherosclerosis.

B-0392 14:18

How different levels of 4th generation iterative reconstruction influence image quality in low-dose cardiac CT

P. Kroepil¹, H.D. Nagel², A.H. Bigdeli³, P. Heusch¹, R.S. Lanzman¹, G. Pentang¹, G. Antoch¹, M. Cohnen³; ¹Düsseldorf/DE, ²Buchholz/DE, ³Neuss/DE (Patric.Kroepil@med.uni-duesseldorf.de)

Purpose: To investigate effects of an advanced 4th generation iterative reconstruction (IR) technique on subjective and objective image quality (IQ) in low-dose cardiac CTA.

Methods and Materials: Five datasets of prospectively triggered coronary CTA in "step-and-shoot" mode were acquired on a 256-slice CT-scanner with optimised exposure settings. Each dataset was processed 16 times resulting in n=80 image stacks. Data were processed on a prototype IR-system using filtered back projection (FBP) and 4 levels of an advanced IR technique (IDose4, Philips) providing incremental rate of IR (level 2,4,6,7) involving both raw and image data space. Image noise was measured in the contrast-enhanced ascending aorta. Contrast-to-noise and signal-to-noise ratios (CNR, SNR) were compared at 9 coronary locations in all image stacks. Subjective IQ was rated on a 3-point scale with "natural" image appearance and noise-related artefacts as main criteria.

Results: Mean effective dose of cardiac CTA was 1.5mSv. Mean CNR and SNR were significantly improved with IR when compared to FBP and with every increasing level of IR (range CNR: 9.8-19.8; range SNR: 7.7-15.2; p < 0.0001) with best objective IQ at highest level of IR (IDose level 7). Subjective IQ, however, was rated best at medium level of IR (IDose level 4) with fewer artefacts when compared to FBP and more "natural" image appearance compared to higher levels of IR.

Conclusion: Objective IQ (CNR, SNR) improves with increasing level of IR in low dose cardiac CTA. Best subjective IQ, however, is reached at medium levels of IR with minimal artefacts and "natural" image appearance.

B-0393 14:27

Iterative reconstruction (IR) improves image quality and diagnostic confidence of CT delayed enhancement imaging for the detection of myocardial infarction: preliminary results

A. Rossi, M. van Straten, A. Dharampal, R. Booij, B. Russo, T. Springeling, R.J. van Geuns, A. Weustink, G.P. Krestin; Rotterdam/NL (a.rossi@erasmusmc.nl)

Purpose: To determine the effect of iterative reconstruction (IR) on CT image quality and diagnostic confidence of myocardial infarction detection on delayed enhancement scans.

Methods and Materials: Nineteen patients with prior history of myocardial infarction were enrolled in the study. Prospectively triggered CT-delayed enhancement imaging was performed eight minutes after CT coronary angiography using dual source CT scanner. Scans were reconstructed using filtered back projection (FBP) with a smooth-medium kernel (B26) and Sinogram Affirmed IR (SAFIRE, Siemens Healthcare) at strength 60% and 100% with kernel I26 and I36. Signal and noise were measured in the descending aorta. Attenuation within the infarcted myocardium was measured and the contrast-to-noise ratio (CNR) was calculated. Two blinded readers graded the images in terms of image quality and diagnostic confidence in infarction detection using a four point scale (1: poor and 4: excellent). MR delayed enhancement was used for comparison.

Results: In comparison with FBP, the use of IR (strength 60%) resulted in a significant reduction of image noise of 26±4% for I26 and 20±7% for I36 (p < 0.001). Increasing the strength to 100% a further decrease of noise was observed: 39±9% for I26 and 45±14% for I36 (p < 0.001). An equivalent increase of CNR from 1.9±0.7 (B26) to 2.6±0.7 (I26-100%) and 2.82±1.0 (I36-100%) was also observed (p < 0.05). The overall image quality and the diagnostic confidence significantly improved using IR.

Conclusion: The use of IR reduces image noise, improving CNR of the infarcted myocardium thus providing better image quality and having the potential to decrease radiation dose.



B-0394 14:36

The effect of iterative reconstruction on computed tomography coronary artery calcium score

M.C. Williams, N.W. Weir, N. Uren, G. McKillop, D.E. Newby, J.H. Reid; Edinburgh/UK (michelle.williams@ed.ac.uk)

Purpose: Iterative reconstruction enables the reduction of radiation dose with maintained image quality in computed tomography (CT). We aimed to assess the effect of iterative reconstruction on the calculation of coronary artery calcium score (CACS).

Methods and Materials: One hundred patients underwent electrocardiogram-gated CT coronary calcium scans as part of the SCOTHEART study using a 320-multi-detector scanner. Tube voltage was 120 kV and tube current was selected based on body mass index. Images were reconstructed using standard reconstruction and an iterative reconstruction algorithm (AIDR). Both Agatston score and calcium volume were calculated. The estimated percentile for a particular CACS based on age, sex and ethnicity was calculated using the MESA CACS reference values.

Results: Thirty-seven patients had a calcium score of zero and were excluded from further analysis. There was a small but significant difference in median Agatston score and calcium volume between standard and iterative reconstructions (179 vs 171, p0.008 and 157 vs 155, p0.044, respectively). Image noise was significantly reduced with iterative reconstruction (26 HU (95% CI 23 to 29) vs 21 HU (19 to 24), p < 0.001). There was no significant difference in estimated percentile with iterative reconstruction (85.5 vs 86, p0.84).

Conclusion: Iterative reconstruction reduces image noise in CT coronary calcium scans. The application of AIDR could lead to significant reduction in radiation dose. The absolute values of both Agatston score and calcium volume are slightly reduced using iterative reconstruction. However, the estimated percentile for the individual patient is not altered.

B-0395 14:45

Coronary CT angiography: comparison of a novel iterative reconstruction with filtered back projection for reconstruction of low-dose CT

R.A.P. Takx¹, U. Schoepf², J.W. Nance², A. Moscariello³, M. Das¹, C. Fink⁴, T. Henzler⁴; ¹Maastricht/NL, ²Charleston, SC/US, ³Rome/IT, ⁴Mannheim/DE (r.takx@student.maastrichtuniversity.nl)

Purpose: To compare image noise between a novel iterative reconstruction algorithm (SAFIRE) and traditional filtered back projection (FBP).

Methods and Materials: Twenty consecutive patients underwent coronary CT angiograms (cCTA) using pECGdual_step scan protocol, a scan mode that applies full-radiation at an adjustable, limited phase of the cardiac cycle while low-radiation (20% tube current) is performed over 10-90% of the cardiac cycle. The images were reconstructed with regular FBP at full-dose (Group 1a) and low-dose (Group 1b) and with SAFIRE with 5 iterations at low-dose (Group 2). Three regions of interest (ROI) were evaluated for signal intensity, image noise, signal-to-noise-ratio (SNR) and contrast-to-noise-ratio (CNR). Subjective image quality was assessed on a 4-point scale based upon image sharpness and noise.

Results: Objective image noise was reduced by 22% ($P < 0.0001$) on average in Group 2 compared to Group 1b. There was also a significant ($P = 0.0156$) improvement in overall subjective image quality in Group 2 compared to Group 1a.

Conclusion: Iterative reconstruction enabled significant reduction in image noise without loss in subjective image quality and holds potential to improve image quality in low-dose functional cCTA and possibly reduce radiation dose even further.

B-0397 14:54

Stenosis quantification using different kV: a phantom study comparing volume CT to micro-CT

A. Ursani¹, H. Mehrez², J. Blobel³, H. Kashani¹, N.S. Paul¹; ¹Toronto, ON/CA, ²Markham, ON/CA, ³Neuss/DE (ali.ursani@uhn.on.ca)

Purpose: To determine the impact of in-stenosis contrast on accurate lumen assessment in calcified coronary plaques comparing two high-resolution CT; a phantom study.

Methods and Materials: A 10x10 cm static coronary artery phantom with tissue equivalent (40 HU) material contained 6 vessels of 3.5 mm (G1) and 5 mm (G2) diameter each. Circumferential lumen stenosis 0, 30, 50, 70, 90 and 100% were created using 800 mg/cc Hydroxyapatite (HA). The lumen contained diluted iodinated contrast 350 mg/ml (Visipaque) reaching 400 HU. CT scans performed using 200µm (MicroCT, mCT) and 350µm (VolumeCT, vCT) spatial resolution with 0.5 mm slice reconstruction at 80 and 135 kVp. Varied tube current maintained image noise of 30 HU. The maximum HU value of the plaque and the minimum value of the vessel lumen were measured by in-line histogram (HU) and contrast (C [HU]) was calculated.

Results: Contrast (HU) for vCT/mCT at 80 kV in G1: C30%: 894/705; C50%: 910/602; C70%: 784/550; C90%: 60/400 and G2: C30%: 919/550; C50%: 915/500; C70%: 864/400; C90%: 413/360.

Contrast (HU) for vCT/mCT at 135 kV in G1: C30%: 675/502; C50%: 650/452; C70%: 640/410; C90%: 10/200, and G2: C30%: 645/550; C50%: 600/450; C70%: 525/400; C90%: 300/350.

vCT showed 51% higher mean contrast compared with mCT for 30-70% stenosis (paired t-test, $p = 1.54 \times 10^{-5}$).

Conclusion: vCT reliably visualises 30-70% lumen stenosis in 3.5 and 5 mm arteries and 90% stenosis in 5 mm arteries. mCT visualises 90% lumen stenosis in 3.5 mm vessels. For 30-70% lumen stenosis vCT contrast is 51% higher than mCT, this capability promises superior potential for detection of coronary plaque composition including dual energy techniques.

B-0398 15:03

A randomised study to test the diagnostic performance of 128-slice dual source CT coronary angiography in patients with various heart rates using 3 low-dose scan protocols

A. Rossi, L.A. Neefjes, A.S. Dharampal, A.C. Weustink, G.P. Krestin, K. Nieman, P.J. de Feyter, N.R. Mollet; Rotterdam/NL (alexia.rossi@aliceposta.it)

Purpose: To compare radiation dose and diagnostic performance of 3 CT coronary angiography (CTCA) protocols using a 128-slice dual source CT scanner (Siemens): a prospective high pitch spiral (HPS), a prospective step-and-shoot (SAS), and a retrospective (RS) scan protocol.

Methods and Materials: We prospectively included 459 symptomatic patients with a regular heart rate (HR). Patients with a pre-scan HR < 65 bpm (group A: 231 patients, 146 men, mean HR 58±7 bpm) were randomised to have a HPS or SAS (scan window 62-74% of the RR-interval) scan. Patients with a pre-scan HR ≥ 65 bpm (group B: 228 patients, 132 men, mean HR 75±11 bpm) were randomised to have a SAS (scan window 31-75%) or RS scan (pulsing window 31-75%). The presence of a significant stenosis was assessed (segment-level) and compared with quantitative coronary angiography.

Results: Group A: sensitivity was significantly lower using HPS than using the SAS protocol (89% vs. 97%, $p < 0.05$). Specificity, positive predictive value (PPV) and negative predictive value (NPV) were similar. The estimated radiation dose was significantly lower with the HPS than with the SAS protocol (0.74±0.15 vs. 2.65±1.0mSv, $p < 0.001$). Group B: sensitivity, specificity, PPV and NPV were not

significantly different using a SAS or RS protocol. The estimated radiation dose was significantly lower with the SAS than with the RS protocol (4.05±1.46 vs. 5.66±2.30mSv, $p < 0.001$).

Conclusion: A step-and-shoot CTCA scan protocol is the preferred protocol in patients with regular heart rates using 128-slice dual source CT, providing optimal diagnostic accuracy with an "as-low-as-reasonably-achievable" radiation dose.

B-0399 15:12

Computed tomography coronary angiography (CTCA) radiation dose: a systematic review of the application of conversion factors

M.C. Williams, D.S. Maclachlan, S. Mirsadraee, D.E. Newby, N.W. Weir; Edinburgh/UK (michelle.williams@ed.ac.uk)



Purpose: Tissue weighting factors used to calculate effective dose (E) were updated by ICRP in 2007. Recent work suggests that, due to the increased weighting factor for breast tissue, conversion factors should be increased when calculating E from dose length product (DLP) in CTCA. We aimed to assess the application of conversion factors in CTCA literature.

Methods and Materials: Peer-reviewed articles on CTCA in English or with an available translation were identified on MEDLINE using an online search tool (PubMed). Articles were included if they commented on radiation dose in title or abstract. Reviews, editorials, phantom and paediatric studies were excluded. Between 1979 and September 2011 there were 205 suitable papers.

Results: Conversion factor was not stated in 24 papers (12%), with 6 of these being published in the first half of 2011. There is a non-significant trend towards presenting DLP and conversion factors in abstracts (2010 16% vs 2008 13%, $p = 0.777$ and 2010 14% vs 2008 5%, $p = 0.223$, respectively). The most frequent conversion factors are 0.017 (61%) and 0.014 (37%). However, the use of 0.017 is decreasing (2007 90% vs 2010 56%) and 0.014 is increasing (2008 10% vs 2010 40%, $p = 0.013$). The use of scanner-specific conversion factors has recently emerged but currently accounts for only 2% of papers.

Conclusion: The use of the lower 0.014 conversion factor is increasing despite the change in ICRP recommendations. A significant proportion of current literature does not report the conversion factor making it impossible to compare radiation doses between studies.

14:00 - 15:30

Room C

Neuro

SS 611b

Functional MRI, resting state and DTI

Moderators:

N. Bargallo; Barcelona/ES
M. Smits; Rotterdam/NL

B-0400 14:00

Target map individualisation for thalamus neurosurgery: possible applications of diffusion tensor tractography and statistical shape models

A. Jakab¹, R. Blanc¹, A. Morel¹, E.L. Berenyi², G. Szekely¹; ¹Zurich/CH, ²Debrecen/HU (jakaba@med.unideb.hu)

Purpose: Neurosurgical interventions of the thalamus rely on transferring stereotactic 3D coordinates from an anatomical atlas onto the patient's MR brain images. We aimed to develop a software application for thalamus target map individualisation that fuses information from patient-specific thalamus geometry and diffusion tensor tractography.

Methods and Materials: Previously, our workgroup developed a thalamus atlas by fusing anatomical information from 7 histologically processed thalami. The atlas was transferred to a standard neuroimaging space and DTI scans of 40 healthy subjects were accessed; thalamo-cortical connectivity maps were generated using a previously described procedure. Visible outlines and connectivity-based internal landmarks were incorporated in a statistical shape model respecting the inherent variability of the individual examples. This information was used to deform the atlas to individual images. Postmortem MRI scans were used to quantify the geometric accuracy of nuclei predictions.

Results: Reliable tractography-based markers were located in the ventro-lateral thalamus, with the somatosensory connections coinciding with the VPLa and VPLp nuclei, and motor/premotor connections with VLP and VL a nuclei, the uncertainty of localisation was less than 2 mm. The error of predicting geometry, expressed in surface-to-surface distances, was 0.56 mm for the visible thalamus outlines and

Friday

varied from 0.5 to 1.5 mm depending on the information utilised during predictions (e.g. connectivity-based landmarks or thalamus outlines).

Conclusion: Previous studies have already applied DTI to the thalamus. As a further step in this direction we demonstrate a hybrid approach using statistical shape models that has the potential to cope with variations in individual thalamus geometry.

B-0401 14:09

DTI tract-specific evaluation of the corpus callosum in patients with diagnosed systemic lupus erythematosus

P. Podgorski, A. Zimny, P. Szewczyk, J. Bladowska, M. Szmyrka-Kaczmarek, M. Sasiadek; *Wroclaw/PL (p.podgorski@onet.pl)*

Purpose: Assessment of the potential white matter damage in patients with diagnosed systemic lupus erythematosus (SLE) using diffusion tensor imaging (DTI) and tract-specific morphometry.

Methods and Materials: Thirty-one patients (mean age 35.8 yrs) with diagnosed SLE and normal appearing brain in conventional MRI were included in this study. The study also included a control group composed of 12 age- and sex-matched healthy volunteers. All subjects underwent conventional brain MRI with typical protocol consisting of T1, T2, FLAIR and DWI images performed on a 1.5 T MR scanner. All subjects also underwent DTI examination with the following parameters (25 diffusion directions, $b=1000s/mm^2$, slice thickness 4 mm, no gap). Obtained DTI images were preprocessed by applying 12-parameter affine transformation using AiR (<http://bishopw.loni.ucla.edu>) and then analysed in DtiStudio (<https://www.mristudio.org>). Multiple ROI approach was applied to select: genu, splenium and entire corpus callosum tracts. Obtained minimal, maximal and mean values of fractional anisotropy (FA) were then compared in patients and controls by using Mann-Whitney U and t-test.

Results: Compared to controls, SLE patients showed significantly ($p < 0.05$) lower mean FA values within genu and splenium tracts of the corpus callosum. FA mean values within entire corpus callosum showed lower values in SLE patients compared to the control group but did not reach the statistical significance.

Conclusion: Tract-specific DTI study showed statistically significant reduction of FA value in the corpus callosum suggesting white matter damage in patients with SLE.

B-0402 14:18

New non-linear colour look-up table to visualise fractional anisotropy changes: demonstrated on multiple system atrophy

J. Keller, A.M. Rulseh, A. Komarek, I. Latnerova, R. Rusina, K. Zarubova, H. Brozova, J. Vymazal; *Prague/CZ (jiri.keller@homolka.cz)*

Purpose: To facilitate the assessment of fractional anisotropy (FA) in daily clinical practice by defining a new, non-linear color look-up table (LUT).

Methods and Materials: FA was calculated for 76 healthy volunteers (age 44.4 years \pm 18 SD, range 15-80. 1.5 T, 2.2 mm isotropic voxel, 12 motion probing gradients (MPG)). A subset of 59 subjects was additionally scanned using 30 MPG. FA in the corpus callosum, frontal grey matter, thalamus, and in the basal ganglia was measured and analysed using the random intercept linear mixed model to calculate the population means and 95% prediction intervals, which were used to create a non-linear colour LUT. Unique colours were assigned to inflection points and continuous ramps were generated to create a colour transition between them. The LUT was applied to groups of 17 patients with multiple system atrophy (MSA) and matching volunteers. Four blinded radiologists classified subjects as norms/MSA. Thirteen patients with Parkinson disease were then added to anonymised cohort.

Results: The LUT generated from 12 MPG data is comparable with that from 30 MPG, and provides 82% sensitivity and specificity in differentiating MSA subjects from healthy volunteers. MSA patients can be separated from parkinsonians and norms with 76% sensitivity and 86% specificity.

Conclusion: Our LUT, based on the normative data, can accentuate abnormal FA values as well as anatomy. The radiologist can differentiate between MSA and norms just using LUT information. The new LUT can be potentially useful as a screening method for other neurological disorders. Supported by grants IGA-NT11328-4/2010, NS9654-4/2008, MSM0021620816 and MSM0021620839

B-0403 14:27

Assessment of the degradation of the selected projectile, commissural and association white matter tracts in asymptomatic HIV-positive nontreated, HIV-positive HAART-treated and HIV-HCV-positive patients using diffusion tensor MR imaging

J. Bladowska, A. Koltowska, P. Szewczyk, A. Zimny, B. Hendrich, B. Krnysz, M. Sasiadek; *Wroclaw/PL (mbladow@wp.pl)*

Purpose: HIV infection may affect cerebral white matter. The aim of the study was to evaluate the selected white matter tracts in asymptomatic HIV-positive patients using diffusion tensor imaging (DTI).

Methods and Materials: Forty-eight HIV-positive asymptomatic patients: 21 HIV-positive nontreated (mean age 33 yrs), 18 HIV-positive HAART-treated (mean age 39.3 yrs), 9 HIV-HCV-positive (mean age 36.6 yrs), and 17 normal control subject (mean age 34.6 yrs) were enrolled in the study. DTI examinations were performed on 1.5 T MR scanner. Fractional anisotropy (FA) and average diffusion coefficient (average DC) values were obtained with a small ROI method in middle cerebellar peduncles (MCP), inferior longitudinal fasciculi (ILF), inferior frontooccipital fasciculi (IFOF), genu (GCC) and splenium (SCC) of the corpus callosum, posterior limbs of the internal capsules (PLIC), superior longitudinal fasciculi (SLF) and posterior cingula (CG).

Results: Significant decrease of FA ($p < 0.05$) compared to the normal subjects was found in all HIV-positive patients in the left MCP, both ILF, both IFOF, GCC, SCC and both SLF, while there were no such differences in the right MCP and both CG. Significant reductions of FA in both PLIC were observed only in HIV-positive HAART-treated patients ($p=0.001$). Significant increase of average DC ($p < 0.05$) was found only in GCC and right SLF in HIV-positive nontreated and HIV-HCV-positive subjects.

Conclusion: The FA value could be a noninvasive neuroimaging biomarker for assessing the microstructural changes within the white matter tracts in asymptomatic HIV-positive patients. HIV-positive HAART-treated patients seem to present the most significant changes.

B-0404 14:36

Passive range-of-motion functional MRI paradigms are useful in the pre-surgical workup of childhood epilepsies

L.R. Kozak, M. Hegyi, P. Barsi, G. Rudas; *Budapest/HU (lkozak@mrkk.sote.hu)*

Purpose: Performing pre-surgical functional MRI (fMRI) in epileptic children poses challenges due to the relatively young age of the patients and/or their possible mental retardation or paresis. Passive range-of-motion (RoM) paradigms were suggested for sensory-motor cortex mapping in this population, as these paradigms do not require patient cooperation. Retrospective analysis of our passive RoM examinations is presented to evaluate the utility of the method in the paediatric epilepsy population.

Methods and Materials: Nine fMRI examinations of seven children (mean age 9.2 yrs, range: 3-15; 6 boys; 2 cases of cortical dysgenesis, 2 of tumour, and 3 of porencephalic cysts) performed at 3 T (Philips Achieva 3 T, Philips Healthcare, Best, The Netherlands) in our institute is reviewed. Four patients were scanned in intravenous propofol sedation using passive RoM, one of them was scanned without sedation, as well. The remaining three patients were examined without sedation both with active and passive RoM paradigms.

Results: We were able to clearly identify the main sensory-motor foci in all cases. Moreover, we could show variable amount of functional reorganization to the healthy hemisphere in three cases. Nevertheless, the distribution of activations obtained with and without sedation, and with passive and active RoM differed to some extent, and in one case ongoing epileptic activity interfered with fMRI.

Conclusion: Passive RoM fMRI paradigms are useful for the evaluation of sensory-motor cortex in paediatric epilepsy patients. Moreover, our results show that these paradigms are able to describe cortical reorganisation, thus they have clear prognostic value in a pre-operative setting.

B-0405 14:45

f-MRI study of smell: perceptual, cognitive and semantic component of cortical elaboration of four familiar aromas

L. Romoli, M. Ukmar, F. Casagrande, M. Naccarato, P. Battaglini, M. Cova; *Trieste/IT (majaukmar@alice.it)*

Purpose: To investigate the changes in cortical activation during the administration of four familiar aromas.

Methods and Materials: 11 volunteers have been enrolled in the study. All the examinations have been performed on a 1.5 T magnet using an f-MRI EPI sequence (TR/TE= 2171/45, 25 slices, 288 dynamics, session duration=10.51 min). Four

stimuli were chosen: citrus fruit, chocolate, coffee, flower plus neutral one (air). The experiment consisted of 3 sessions and each session consisted of 24 trials (3 stimulations for each aroma and 12 for pure air). Timing, amount and order of presentation were controlled by an MRI compatible olfactometer. The data were analysed using SPM5 package. The analysis were conducted for each aroma compared to the neutral during the timing in which the subjects received the aroma and the few seconds immediately after.

Results: Each aroma seems to stimulate different cerebral regions. In particular, citrus is characterised by the perceptual aspect, especially visual (BA 17-18 bilaterally); chocolate involves mainly the cingulate and frontal cortex; coffee seems to be the most recognisable odor (orbital gyrus, medial cingulate cortex, left inferior frontal gyrus); flower seems to be the most difficult stimulus to recognise and describe, involving areas implicated in the recollection of autobiographical memory. **Conclusion:** This study shows that odours can affect a variety of perceptual, motor and cognitive functions. The evaluation of olfactory system in order to demonstrate olfactory dysfunction could be used to assess the possible risk of developing neurodegenerative disorders in healthy individuals.

B-0407 14:54

Functional MRI for neurosurgical intervention planning: retrospective analysis of 87 examinations performed with our standardised language task panel

L.R. Kozak, A. Szabo, V. Toth, C. Borbely, P. Barsi, G. Rudas; *Budapest/HU* (*kozak@mrkk.sote.hu*)

Purpose: Functional MRI (fMRI) gained importance in the neurosurgical assessment of brain tumour and epilepsy patients despite the ongoing debate regarding its clinical usefulness. A retrospective analysis of our pre-surgical language-mapping protocol is presented.

Methods and Materials: Blood-oxygenation level-dependent fMRI with picture naming, synonym decision, speech comprehension, and auditory word/non-word decision tasks was analysed from 87 sessions of 83 epilepsy and brain tumour patients (36 females; 47 lesions near eloquent areas) using SPM8. Spatial normalisation was performed with the lesions masked for analysing all patients in a common framework. First- and second-level results and probabilistic maps were calculated from general linear model fits. Lateralisation indices were calculated for Broca, Wernicke and whole-hemisphere regions of interest (ROIs), in threshold-independent and thresholded manners.

Results: The paradigms probed different aspects of language processing, therefore their perceived difficulty, and mapping performance varied across subjects. Generally, picture naming resulted in widespread bilateral activations not restricted to core language areas, while synonym task was the most lateralised in the Broca and Wernicke regions. Auditory tasks showed the expected preference for temporal structures and the Wernicke area. Lateralisation differences were significant at the group level ($p < 0.0001$ ANOVA for factors paradigm and ROI), but lateralisation indices were highly ($r^2=0.71$, $p < 0.0001$) correlated regardless of ROI and paradigm. **Conclusion:** Due to individual differences there is no single "best" paradigm for language mapping, thus performing more tasks enhances accuracy. Nevertheless, performing the synonym and the word/non-word task seems sufficient for determining language lateralisation in most cases if time-availability is limited.

B-0408 15:03

Visualising hippocampal BOLD activity in humans at 3 and 7 Tesla

N. Theysohn¹, S. Qin², S. Maderwald¹, B.A. Poser², J.M. Theysohn¹, M.E. Ladd¹, E.R. Gizewski³, G. Fernandez², I. Tendolkar²; ¹Essen/DE, ²Nijmegen/NL, ³Giessen/DE (*nina.theysohn@uk-essen.de*)

Purpose: High-field strength functional MRI has developed rapidly due to its advantages such as increasing SNR and BOLD contrast. Nevertheless, it suffers from artefacts in brain regions close to tissue air boundaries such as the mediotemporal lobe (MTL). These deficits have challenged functional imaging of the hippocampus though optimised high-resolution imaging is particularly useful for this region both from a clinical and cognitive neuroscience perspective. Therefore, we set out to visualise MTL activity during an associative memory encoding task at 3 and 7 tesla.

Methods and Materials: 28 healthy volunteers were examined either with 3 T or with 7T while performing a blocked-design face-professional name associative memory encoding task and a visual-motor judgment as control condition. Whole brain EPI images were acquired. 3 T and 7T data were compared and analysed with SPM 5.

Results: EPI images at 7T were of high quality, showing a good white/grey matter contrast. Signal dropouts and artefacts at the lower MTL were acceptable at 7T. Assessing the memory-related neural activity in both groups, the results revealed

robust functional activations in the bilateral MTL at both field strengths and a significantly higher hippocampal BOLD sensitivity at 7T.

Conclusion: The associative memory encoding task resulted in robust functional activity in the MTL at both field strengths and higher BOLD sensitivity in hippocampal structures at 7T. These preliminary results will be used for further high-resolution region of interest analysis concentrating on the hippocampal substructures, its role in memory encoding and in MTL disorders.

B-0409 15:12

Acute effects of modafinil on cognition and brain resting state network activity in young healthy subjects

R. Esposito, F. Cilli, V. Pieramico, A. Ferretti, A. Macchia, A. Saggino, A. Tartaro, G. Romani, S.L. Sensi; *Chieti/IT* (*resposito@sirm.org*)



Purpose: There is growing debate on the use of drugs that promote cognitive enhancement. Most of the cognitive enhancing drugs, including amphetamine-like drugs, have important side effects and show the risk of addiction. We investigated the use of modafinil, a drug approved for the treatment of narcolepsy that may also act as a cognitive enhancer and appears to have fewer side effects compared to other psycho stimulants. The aim of this study was to evaluate whether modafinil can influence the cognitive performance as well as the brain resting state network activity of healthy young subjects.

Methods and Materials: 30 subjects were included in a double-blind, placebo-controlled study in which a single dose (100 mg) of Modafinil was administered. Both groups were tested before and three hours after the administration of modafinil or placebo for their neuropsychological performances by employing the Raven's progressive matrices and the Trial making test. With fMRI, also after three hours, we studied the activity of resting state brain networks. Finally, diffusion tensor imaging (DTI) was also performed via tract-based spatial statistics (TBSS).

Results: Our results indicate that a single acute dose of modafinil improves fluid intelligence while BOLD-fMRI data show that the drug increases the activation of the frontal parietal control (FPC) system and of extra-striate visual networks. No changes were observed as far as anatomical connectivity.

Conclusion: Taken together, our findings support the idea that modafinil can increase cognitive performance, modulate the activity of resting state networks, and be an effective cognitive enhancer.

14:00 - 15:30

Room D1

Chest

SS 604

Airway diseases

Moderators:
I. Hartmann; *Rotterdam/NL*
N.J. Scaleton; *Cambridge/UK*

B-0410 14:00

Can CT help recognise a link between left atrial volume, impacting left ventricular preload, and the severity of emphysema?

L. Cassagnes, E. Algeri, J.-B. Faivre, T. Santangelo, J. Remy, M. Rémy-Jardin; *Lille/FR* (*lucie.cassagnes@aliceadsl.fr*)



Purpose: To evaluate left atrial (LA) volume in smokers according to the severity of emphysema and total lung volume (TLV).

Methods and Materials: 121 consecutive smokers, free of clinical cardiovascular disease, underwent a high-pitch and high-temporal resolution CT angiographic examination of the chest with dual source, single energy CT enabling quantification of emphysema, lung volumes and LA volume measurements normalised to body surface area.

Results: The CT phenotypes of the studied population were as follows: emphysema-predominant (Group 1; n=57); airway-predominant (Group 2; n=30); a mixed pattern of emphysema and airways disease (group 3; n=15), and absence of CT abnormalities (group 4; n=19). A negative correlation was found between the indexed LA volume and the percentage of emphysema: (a) in the overall study group ($p=0.032$; $r=-0.19$); (b) in group 1 ($p=0.0163$; $r=-0.32$); and (c) in groups 1 and 3 when analysed together ($p=0.0492$; $r=-0.23$). In group 1, we found a negative correlation between the indexed LA volume and the percentage of emphysema in the right upper and right middle lobes ($p=0.03$; $r=-0.29$). A negative correlation was also found between the indexed LA volume and TLV in the overall study group ($p=0.039$; $r=-0.19$) and in group 1 ($p=0.048$; $r=-0.26$) while no correlations

Friday

were found in Group 2 ($p=0.44$; $r=-0.15$) and group 3 ($p=0.52$; $r=-0.17$) nor when gathering patients from groups 1 and 3 ($p=0.14$; $r=-0.17$).

Conclusion: The LA volume, impacting left ventricular preload, is significantly reduced in patients with severe emphysema.

B-0411 14:09

Krypton ventilation imaging using dual energy CT in COPD patients: initial experience

A.-L. Hachulla, S. Khung, L. Wemeau, J.-F. Cazaubon, J. Remy, M. Rémy-Jardin; Lille/FR (anne-lise.hachulla@chru-lille.fr)

Purpose: To evaluate the level of lung enhancement achievable after inhalation of stable krypton whose atomic number (36) and lack of anaesthetic properties make it eligible for ventilation imaging using dual energy CT.

Methods and Materials: 32 patients with severe emphysematous lesions were included in this study aimed at comparing the level of attenuation within normal lung (presumed to be normally ventilated) with that of emphysema (presumed to be poorly or not ventilated) after inhalation of a mixture of krypton (80%) and oxygen (20%). They underwent a dual source, dual energy chest CT examination with reconstruction of diagnostic and ventilation images. The statistical analysis was defined on the following assumption: the level of attenuation within the emphysematous lung was expected to be reduced in comparison to the level of attenuation within the normal lung; when present, this result was defined as a "success".

Results: All studies were successfully performed, without adverse effects. Analysis of ventilation images showed differences in lung attenuation between normal lung and emphysematous areas in 28 patients (87.5%; 95% CI= [71%-96.5%]), thus demonstrating the feasibility of lung ventilation with krypton. The maximal level of attenuation within normal lung was 18.5 HU. Krypton attenuation difference between normal and emphysematous lung was statistically significant with a median value of 51.8% ($p < 0.001$). The mean (\pm SD) DLP value of this protocol was 387.1 ± 32.15 mGy.cm.

Conclusion: Dual energy CT of the lungs after inhalation of stable krypton was found to be technically feasible and well tolerated by all patients.

B-0412 14:18

A genome-wide association study of COPD with lung volumetry and airway measurement using MDCT

L.K.Y. Lee¹, K. Kim¹, J. Lee¹, E. Kang², Y. Oh³, B. Je¹, J. Choo¹; ¹Ansan/KR, ²Guro/KR, ³Anam/KR (mynef33@daum.net)

Purpose: The ratio of forced expiratory volume in one second to forced vital capacity (FEV1/FVC) is a measure used to diagnose airflow obstruction and is highly heritable. The aim of this study is to investigate genetic association of SNPs (single nucleotide polymorphism) in COPD genes for association with 3D-CT lung volume and airway measurement.

Methods and Materials: We have the GWAS results for 4,530 participants for lung function-related genes. FAM13 A SNPs (single nucleotide polymorphism) on chromosome 4 including rs2609264 were associated with FEV1/FVC value. On the 3D-MDCT images, the software semi-automatically calculates total lung volume (TLV) and emphysema volume (EV), emphysema percentage (EP), mean lung density (MLD) including bronchial wall area (WA)%. We will compare the CT parameters between minor (TTCA) and major (CCTG) alleles. We did CT scans targeting 200 adults (aged 40-69 years) representative of T and C alleles for the acquisition of TLV, EV, MLD and bronchial WA%.

Results: The subjects with T allele had significantly smaller emphysema volume and emphysema volume % than those with C allele. However, total lung volume, mean lung density and bronchial WA% showed no significant difference between subjects with T and C allele.

Conclusion: The subjects with T allele were associated with emphysema volume and emphysema volume %. This might be important implication concerning the prevention of chronic lung function impairment caused by interventions directed at risk factors such as ongoing COPD, smoking, infection, and socioeconomic factors.

B-0413 14:27

The performance of CT severity scores determined from paired expiratory/inspiratory high-resolution CT in predicting the severity of airflow obstruction

T. Suwatanapongched, P. Pornsuriyasak, W. Sukkasem, S. Rattanasiri; Bangkok/TH (rattspoom@yahoo.com)

Purpose: To assess the performance of CT severity scores from paired expiratory/inspiratory high-resolution CT (HRCT) in predicting the severity of airflow obstruction (AFO).

Methods and Materials: We retrospectively assessed paired expiratory/inspiratory HRCT scans of 26 patients (6 men and 20 women; mean age (SD), 59.6 (11.0) years) having AFO from pulmonary function testing at the six chosen levels (i.e. five vessels, aortic arch, tracheal carina, 1 cm below the right bronchus intermedius origin, right inferior pulmonary vein, and 1 cm below the right hemidiaphragm dome). The severity grading of expiratory air-trapping (AT, 0-4), bronchial wall thickening (0-3) and bronchial dilatation (0-3) multiplied by its extent ($I < 25\%$; $II \geq 25-50\%$; $III \geq 50-75\%$; and $IV \geq 75\%$) of involvement were considered as AT, bronchial wall thickening, and bronchial dilatation scores, respectively. The sums of all scores were considered as AT-Br scores. Receiver-operating-characteristic (ROC) analysis was applied to assess the performance of AT and AT-Br scores in discriminating patients with mild AFO (FEV1 $\geq 65\%$ predicted) from those with moderate to severe AFO (FEV1 $< 65\%$ predicted).

Results: The areas under ROC curves of AT and AT-Br scores were 0.74 (95%CI: 0.53, 0.94) and 0.79 (95%CI: 0.59, 0.99), respectively. The cut-off values of AT and AT-Br scores of 101 and 104 had a power to discriminate patients with mild AFO from those with moderate to severe AFO with a sensitivity of 85.7% and 85.7% and specificity of 57.9% and 57.9%, respectively.

Conclusion: The AT and AT-Br scores determined by our methods had the ability to predict the severity of AFO in most cases.

B-0414 14:36

Reproducibility of automatic airway measurements with multidetector computed tomography (MDCT) in inspiratory and expiratory scans

M. Amato, A. Larici, A. del Ciello, E. Devicienti, G. Corbo, S. Valente, L. Bonomo; Rome/IT (michele.amato61@gmail.com)

Purpose: Software for post-processing MDCT images allow to obtain automatic measurement of airway parameters until the fifth bronchial generation. Aim of the study was to assess the inter- and intra-observer reproducibility of airway measurements using an automated commercial software.

Methods and Materials: Forty patients with functional diagnosis of chronic obstructive disease (21 males, 19 females; age range: 48-85 years) were prospectively included. All the patients underwent two consecutive 64-rows CT scans of the chest (slice thickness/interval 0.625 mm; pitch 1.375) at full inspiration and at the end of forced expiration, respectively. Datasets were independently analysed by two chest radiologists in two distinct sessions (30 days apart) using an automated commercial software for the airways analysis (Lung VCAR, GE Healthcare). Operators reported for both acquisitions the values of lumen area (LA), automatically calculated on axial images reformatted along the perpendicular axis of the airway from the lobar (second generation) to the sub-segmental bronchi (fifth generation). The inter- and intra-operator differences were expressed as percentages over means (Bland-Altman). Mean values of differences (Δ) and standard deviations (SD) were assessed

Results: Automatic measurements of LA has shown high reproducibility (mean \pm SD%) on both inspiratory and expiratory scans. For LA we observed: Δ inter-insp \pm SD Δ inter-insp = $-3.7/1.6 \pm 4/14\%$; Δ intra-insp \pm SD Δ intra-insp = $1.4/2.8 \pm 0.9/2.7\%$; Δ inter-exp \pm SD Δ inter-exp = $-2.7/1.8 \pm 5/11\%$; Δ intra-exp \pm SD Δ intra-exp = $-1.3/0.9 \pm 1.1/4.9\%$.

Conclusion: Automatic measurement of lumen area on MDCT demonstrated high inter- and intra-operator reproducibility in both inspiratory and expiratory scans. Thus, it has the potential of being used as a complementary tool in the assessment of obstructive airways disease.

B-0415 14:45

Automatic airway analysis on MDCT in cystic fibrosis: correlation with pulmonary function testing

M.O. Wielpuetz¹, M. Puderbach¹, M. Eichinger¹, O. Weinheimer², S. Ley¹, M.A. Mall¹, A. Bischoff¹, H.-U. Kauczor¹, C.-P. Heussel¹; ¹Heidelberg/DE, ²Mainz/DE (mark.wielpuetz@web.de)

Purpose: Software tools allow for quantitative airway analysis on multi-detector computed tomography (MDCT) of the chest. Aim of this study was to evaluate generation-based airway parameters in patients suffering from cystic fibrosis (CF) lung disease in correlation with predicted forced expiratory capacity in 1s (FEV1%).

Methods and Materials: MDCT acquired in parallel to FEV1% (median gap 0d, range 0-10d) from n=14 infant (CFinfant) and n=16 adult (CFadult) CF patients were subjected to fully automatic airway analysis. N=4 infants and n=22 adults with normal airways and FEV1% served as controls (NORMALinfant, NORMALadult). Total diameter (TD), lumen area (LA), and wall thickness (WT) of proximal to distal airways were separately correlated with FEV1%.

Results: No significant correlations with FEV1% existed for TD and WT of proximal and distal airways in both NORMAL (R ranging from -0.12 to 0.38), but for LA of the 2nd generation in NORMALadult (R=0.60). In CF infant moderate inverse correlations were found for TD and LA of 2nd generation airways (R=-0.53 and -0.64, respectively), but not for WT. In CF adult TD and WT of 5th generation airways inversely correlated with FEV1% (R=-0.86 and -0.90, respectively), but not of the 2nd generation (R=-0.11 and -0.31, respectively). LA correlated best for 7th generation airways (R=-0.70).

Conclusion: TD, LA and WT of distal airways showed strong correlations with FEV1% in adult CF patients, indicating a shift of major airway resistance to distal bronchi in chronic CF. Fully automatic software tools could introduce user independent quantitative parameters into the assessment of obstructive lung disease.

B-0416 14:54

Contrast-enhanced MRI (CE-MRI) is more sensitive to detect small airways disease than proton-MRI (MRI): a comparative study in cystic fibrosis (CF) lung disease

P. Ciet¹, P. Wielopolski¹, E. van der Wiel¹, G.P. Krestin¹, M.H. Lequin¹, G. Morana², H.A.M.W. Tiddens¹; ¹Rotterdam/NL, ²Treviso/IT (p.ciet@erasmusmc.nl)

Purpose: Chest-CT is the most sensitive technique to monitor progression of CF-related bronchiectasis and trapped-air (TA) reflecting small airways disease. Chest-MRI is a radiation-free alternative for CT, but its sensitivity for TA is poor. Hypoperfusion (HP) often coincides with TA and thus CE-MRI might be more sensitive to identify TA. Aims: 1) to compare volume of HP on CE-MRI with volume of AT on MRI, 2) to compare volume of HP and TA to spirometry parameters sensitive to small airway disease.

Methods and Materials: 26 stable CF patients (13 M, mean age 14 yrs, range 8-18 yrs). Spirometry and CE-MRI were done on the same day. 1.5 T Scanner (Signa, GE). Protocol: SSFP-2D PD-w axial, coronal and sagittal (TR/TE/SL = 5.7/1.4/8 mm). GRE-3D axial and coronal (TR/TE/SL= 3/1/3 mm; 0.1 mmol/kg). Images were anonymised and scored in random order with CF-MRI score (expressed as % of max). Descriptive statistics, T-test and Spearman correlation (r) were used.

Results: Mean (SD) HP and TA scores were, respectively: 4.4 (3.94) and 3.3 (2.75). Correlations: TA vs HP (r=0.413; p=0.045); HP vs FEF25 (r=-0.69; p=0.0001); HP vs FEF75 (r=-0.46; p=0.02), HP vs FEV1/FVC (r=-0.51; p=0.01); TA vs FEF75 (r=-0.48; p=0.016); TA vs FEF25 (ns) or FEV/FVC (ns).

Conclusion: HP but not TA showed highly significant negative correlations with spirometry parameters sensitive for small airway disease. HP areas did not always match TA areas. CE-MRI seems to improve the diagnostic value of MRI to detect small airways disease.

B-0417 15:03

A scoring system for tomosynthesis in pulmonary cystic fibrosis

K. Vult von Steyern¹, I. Bjorkman-Burtscher, P. Hoglund, G. Bozovic, M. Wiklund, M. Geijer; Lund/SE (kristina.vult_von_steyern@med.lu.se)

Purpose: No scoring system for tomosynthesis (digital tomography) in pulmonary cystic fibrosis (CF) has been published. The purpose was to introduce and validate such a system.

Methods and Materials: 88 paired chest radiography and tomosynthesis examinations on 69 patients with CF (33 children and 36 adults) and 7 paediatric oncology patients were scored independently by three radiologists. Tomosynthesis studies were scored for overinflation, bronchial wall thickening, atelectasis or consolidation, number and severity of bronchiectases, and large and small mucus plugs with a maximum score of 100. The Brasfield scoring system was used for radiographs.

Results: Correlation between the score for tomosynthesis and Brasfield score for radiography was good (Kendall's rank correlation tau 0.68, 0.77 and 0.78 for the three raters). Tomosynthesis was generally scored higher in percentage of maximum score. Observer agreements for total scores were high in both systems (weighted kappa > 0.90 for the three pairs of radiologist raters for the tomosynthesis score, and 0.80, 0.81 and 0.85 for the Brasfield score). 29 patients (33%) were scored normal for nodular-cystic lesions on radiographs by all raters, but were scored positive for bronchiectases or mucus plugging with tomosynthesis.

Conclusion: The proposed tomosynthesis score correlates well with the Brasfield scoring system, with good observer agreements for the total score. Tomosynthesis is more sensitive to CF changes, in particular bronchiectases and mucus plugging, and shows them in more detail than radiography. Therefore, the new scoring system, having a higher maximum score, offers the possibility for a more accurate scoring of disease severity.

B-0418 15:12

Small airway and interstitial lung involvement in asymptomatic patients with antiphospholipid syndrome

A. Oikonomou, A. Tzouvelekkis, P. Skendros, I. Mitroulis, E. Apostolidou, A. Thomaidi, K. Ritis, D. Bours, P. Prassopoulos; Alexandroupolis/GR (aoikonom@med.duth.gr)

Purpose: Antiphospholipid syndrome (APS) is a systemic autoimmune disorder characterised by vascular thrombosis. Activation of the coagulation cascade is thought to be associated with induction and maintenance of inflammation, which leads to tissue injury and fibrosis. Our aim was to determine the prevalence of nonthrombotic lung manifestations in asymptomatic patients with APS.

Methods and Materials: Ten patients free of respiratory symptoms who met the criteria for APS (5 primary APS and 5 secondary to systemic lupus erythematosus-SLE) were prospectively identified. All patients underwent high-resolution computed tomography (HRCT) of the chest and functional assessment. HRCT scans were evaluated for the presence of air-trapping, fibrosis, micronodular pattern, cysts, emphysema, atelectasis, consolidation and pleural effusion. The total extent of air-trapping was estimated based on a subjective semi-automated HRCT scoring system. Functional assessment included FVC, TLC, MMEF25/75, DLCO, 6-minute walking distance and systolic pulmonary artery pressure.

Results: All patients exhibited both a radiological and functional pattern compatible with small airway disease, irrespective of smoking. Mean score of air-trapping was 45.3% (range: 20-75%). HRCT findings and reduced levels of MMEF25/75%pred were negatively correlated (r=-0.936, p < 0.0001). Subpleural basal reticular pattern consistent with fibrosis was seen in 3 patients. Thin-walled cysts were seen in 3 patients, while upper-lobe hazy micronodular pattern was detected in 4 patients.

Conclusion: Asymptomatic patients with APS may present with small airway and interstitial lung involvement irrespective of smoking history and SLE coexistence. Chest HRCT and routine functional tests maybe valuable tools for physicians when evaluating patients with APS.

B-0419 15:21

MDCT evaluation of the tracheobronchial tree anomalies in children with congenital heart disease

A.G. Shin, Z.A. Vakhidova, N.I. Safonova, T. Shinkareva, V. Makarenko; Moscow/RU

Purpose: To assess the value of multidetector computer tomography (MDCT) in diagnostics of anomalies of the tracheobronchial tree in children with congenital heart disease (CHD).

Methods and Materials: 32 children with CHD referred for MDCT evaluation were examined (mean age: 9 months, range: 14 days to 16 months). Patients were examined using ECG-gated 128-MDCT-angiography. We employed 3-dimensional (3D) image reconstruction in patients who were suspected of having complicating external vascular compression as a cause of respiratory symptoms. To all patients x-ray study of the chest was performed.

Results: Lung anomalies caused by pulmonary underdevelopment were recognised in 8 cases which had not been diagnosed by means of x-ray examination. The lobar emphysema was identified in 3 patients and it was the result of a check-valve mechanism at the bronchial level caused by external vascular compression. Critical tracheal stenosis in one patient was caused by pulmonary artery sling. In 2 cases bronchial stenosis was due to compression by the right aortic arch and Kommerell's diverticulum. The stenosis of the left main bronchus was observed in 15 cases due to compression between the descending aorta and the left upper pulmonary vein. Arteriovenous malformations were diagnosed in 3 patients, one of which led to compression of segmental bronchus of lower lobe of the right lung.

Conclusion: MDCT evaluation of anomalies of the tracheobronchial tree in children with congenital heart disease (CHD) identifies the causes of respiratory disorders and allows predicting possible respiratory complications in the early post-operative period.



14:00 - 15:30

Room D2

Interventional Radiology

SS 609

Vascular interventions

Moderators:

L. Mailli; Athens/GR

R. Morgan; London/UK

B-0420 14:00

Directional atherectomy of calcified stenotic lesions of the lower limb in segments with high biomechanical stress: 3-year results

P. Minko, S. Jaeger, A. Buecker, M. Katoh;

Homburg a.d. Saar/DE (peterminko@yahoo.com)

Purpose: To evaluate the long-term outcomes (3 year) of patients with peripheral occlusive disease (POD) and calcified stenotic lesions in segments with high biomechanical stress after atherectomy.

Methods and Materials: Patients suffering from POD (Rutherford 2 to 6) were treated with the Silverhawk atherectomy device (ev3 Endovascular, MN, USA) if calcified stenotic lesions in the most proximal or distal 3 cm of the superficial femoral artery and/or popliteal artery were present. Overall 42 patients with 46 lesions (15 females, 27 males; mean age: 69±8.8) were included into this prospective study. Patients underwent clinical re-evaluation every 6 months for 36 months including the measurement of the maximum walking distance and the ankle brachial index (ABI). In addition, duplex sonography was performed.

Results: The primary success rate of the procedure was 89%. In five cases additional PTA and/or stenting was necessary. Procedure-related complications namely peripheral embolism occurred in 3 cases (6%). The mean Rutherford score decreased significantly from 4.1 to 0.75, while the mean ABI increased from 0.62 to 0.85 after 36 months. The primary and assisted primary patency rate was 66% and 79%, respectively. Target lesion revascularisation was performed in five patients.

Conclusion: Directional atherectomy should be considered as an alternative for treatment of calcified stenotic lesions in segments with high biomechanical stress as in most cases stenting can be avoided. Results after three years demonstrated a significant decrease of the Rutherford score and an increase of the ABI and a reasonable patency rate.

B-0421 14:09

Intra-arterial infusion of allogenic mesenchymal stem cells for critical limb ischaemia and foot ulcers safety and efficacy

B.J.J. Abdullah, S.S. Dhillon, A. Das, A.C. Roslani; Kuala Lumpur/MY (basrij@ummc.edu.my)



Purpose: To determine safety, technical feasibility and clinical efficacy of intra-arterial allogenic mesenchymal stem cells (AMSC) for critical limb ischaemia (CLI) and foot ulcers

Methods and Materials: A prospective single arm Phase II non-randomised study was carried out in 8 patients with untreatable lower limb peripheral arterial disease (surgical bypass or angioplasty) diagnosed by CE MRI. Uncontrolled DM, renal/hepatic failure or any previous malignancy was cause for exclusion. Only single injection of 100 million cells into the common femoral artery under US guidance. No repeat injections allowed. AMSC isolated from unrelated healthy donors analysed using flow cytometry. AMSC upscaled according to cGMP. The type of adverse events (AEs), number of AEs and percentage AEs were noted. Primary endpoints were rest pain and ulcer healing at end 6 months while secondary endpoints were increased transcutaneous partial oxygen saturation (TcPO₂), ankle brachial pressure index (ABPI), vasculogenesis (CE MRI) and limb preservation. Approval obtained from hospital ethical review board.

Results: To date, a total of 10 limbs treated. 1 patient each (1 limb) did not respond to treatment (pain persistent) with 1 patient having BKA. 2 patients died from unrelated causes (1 limb at 10 months; 2 limbs at 2months). At 6 months, 4 patients (5 limbs) have limb preservation (improved TcPO₂ and ABPI within 1 month) and peaking at 3 months. No increased vasculogenesis seen on CE MRI. No AEs documented during the FU period.

Conclusion: These preliminary data show intra-arterial AMSC is a safe, technically feasible and efficacious in untreatable CLI.

B-0422 14:18

DEB vs PTA for multilevel lower limb revascularisation: 6-month results from a randomised trial

A. Cannavale, F. Fanelli, A. Bruni, M. Allegritti, E. Boatta, R. Passariello; Rome/IT (alessandro.cannavale@hotmail.com)

Purpose: Drug-eluting balloons have shown promising results in recent trials improving the patency rate in steno-obstructive disease of the femoro-popliteal region. We would like to evaluate mid-term patency of peripheral angioplasty with paclitaxel-coated balloons (DEB) in comparison with conventional balloons (PTA).

Methods and Materials: Fifty consecutive patients (mean age 66±4 years), with stenosis or occlusion of a femoro-popliteal artery were enrolled and randomly assigned to treatment with DEB (25 pts, 50%; IN.PACT Amphirion, Invatec, Italy) and to treatment with uncoated balloons (25 pts, 50%; control group). Patients' characteristics were similar in both groups: 28% smokers, 45% diabetes and 59% hypercholesterolemia. Thirty-eight% were TASC B while 34% were C and 10% D. The primary end point was late lumen loss at 6 months.

Results: Twenty-two percent of the lesions were total occlusions, and 36% were stenotic lesions. The mean lesion length was 5.5±3.5 cm. There were no adverse events correlated with the paclitaxel-coated balloons. At 6 months, USCD follow-up showed neointimal thickness of 1.6±1.7 mm in the control group, as compared with 0.5±1.4 mm (P=0.001) in the group treated with DEB. The rate of revascularisation of target lesions at 6 months was 9 of 25 (36%) in the control group, 2 of 25 (8%) in the DEB group (P=0.001 vs. control group). Thrombosis rate was 12% (PTA) vs 7% (DEB) p < 0.01. Amputation rate was 8% (PTA) vs 3% (DEB) p < 0.01.

Conclusion: Use of DEB in femoropopliteal disease is associated with significant reductions in late lumen loss and target-lesion revascularisation.

B-0423 14:27

Concomitant use of endovenous laser and foamed sclerosant in treatment of lower limb varicosities: 3-year follow-up results

M. Bhalla¹, N. Bhalla¹, H. Vasavada²; Ahmedabad/IN, ²Jamnagar/IN

Purpose: To report mid-term results (upto 3 years) of concomitant use of two modes of treating varicose veins - endovenous laser treatment for great saphenous vein (GSV) reflux and sclerotherapy for incompetent perforators and accessory venous channels.

Methods and Materials: 253 lower limbs (76 left, 43 right, 134 bilateral) of 186 patients (66 women, 120 men; mean age 45.5 yrs) were treated with concomitant use of endovenous laser and sclerotherapy. 5 patients (18 legs; 7%) had ulcers. GSV was mapped using 10MHZ linear Ultrasound (US) probe. Following local anaesthesia, 0.035 inch J-Guidewire was introduced in GSV from lowest point of reflux. A 5 F sheath and 610µm laser fibre was used. Laser energy was delivered intraluminally at 14 W continuous mode. Fibre was uniformly withdrawn. Sclerosant mixed with air to produce foam was introduced through needle in perforators and additional venous channels under US guidance. All patients were advised ibuprofen and class II stockings. Follow-up was done at 1 week, 3, 6, 12, 24 and 36 months.

Results: 98% laser-treated GSV remained ablated at 3-year follow-up. 7% limbs in first year and additional 3% limbs in next 2 years (i.e., 10 % limbs in 3 years) required one more sclerotherapy session for new incompetent perforators. No complications were noted. 90% patients complained of tightness along the course of treated GSV. Patients resumed routine activities immediately.

Conclusion: Laser has already proven its use in treating GSV. Sclerotherapy is effective in dealing with perforators and provides rapid healing of chronic venous ulcers. Concomitant use of both modes limits the need of subsequent procedure.

B-0424 14:36

PTA the other way: US-guided SAFARI technique

I. Kogan, M. Leiderman, R. Rozenberg, A. Engel, A. Ofer; Haifa/IL (radurosenberg@yahoo.com)

Purpose: To describe the benefits of ultrasound (US)-guided subintimal arterial flossing antegrade-retrograde intervention (SAFARI).

Methods and Materials: We retrospectively analysed patients who were treated with the SAFARI technique due to failure of classical antegrade PTA to recanalise occluded femoral and tibial arteries. Between 2009 and 2011, 226 patients underwent 263 PTA procedures in our hospital for treatment of limb ischaemia. We used the SAFARI technique on 16 patients in whom antegrade PTA failed to provide direct flow to the ischaemic site. In all patients the retrograde puncture was performed under US guidance. In 93.7% of patients the ensuing puncture site was in the dorsalis pedis artery and in one patient we punctured the tibialis anterior artery. The guide wire was pushed in a retrograde manner through the previously inserted antegrade catheter. The balloon dilatation was performed using both puncture sites.

Results: In all patients the US-guided puncture of a distal artery was successful. Combined antegrade and retrograde (SAFARI technique) PTA was successful in 87.5% of the patients in which the antegrade PTA alone did not provide satisfactory recanalisation and was considered failed. As a minor complication, temporary DP artery spasm was seen in 12.5% of the cases.

Conclusion: SAFARI technique is usually used when the classic antegrade PTA fails. This procedure necessitates a hollow distal artery, angiographers with ultrasonographic skills and it is time consuming. However, it provides a good last alternative in patients in which the antegrade PTA has failed.

B-0425 14:45

Silverhawk directional atherectomy in the treatment of de novo femoropopliteal atherosclerotic steno-obstructive disease: single centre experience

M. Citone, M. Rossi, L. Greco, G.M. Varano, A. Zolovkins, V. David; Rome/IT (mi.citone@inwind.it)

Purpose: To evaluate the role of percutaneous directional atherectomy (DA) in the treatment of femoropopliteal atherosclerotic lesions, in symptomatic PAD patients.

Methods and Materials: Between 2008 and 2011, 62 patients (42 males, ma72) with symptomatic PAD (intermittent claudication 23 cases, rest pain 17, tissue loss 22) underwent DA with SilverHawk catheter for 62 atherosclerotic lesions (38 obstructions: 26 SFA, 12 popliteal artery; 24 stenoses: 4 CFA, 12 SFA and 8 popliteal artery). Average angiographic lesion length was 7.5 cm (3-11) occlusion and 4 cm (2.5-8) stenoses. Pre-procedural evaluation consisted of CD-ultrasound and in selected cases CT-angiography to better characterise lesions. If lesions were low calcified. In 8% cases embolic protection device was employed.

Results: Technical success was 98% (61 pts). Adjunctive pta was performed in 32% cases. In 12% pts associated tibial vessel treatment was performed. No perioperative mortality was observed. One complication (distal embolisation) occurred (2%). Average ABI increased from 0.51 ± 0.07 to 0.85 ± 0.08. At 30 days clinical status evaluation was: improvement 84% invariable 14% and worst 1%. At 19 mts mean FU (range 6-29) Kaplan-Meier analysis showed primary patency of treated vessels at 12 and 24 months of 92% and 81%. Assisted patency was 96% and 90%, respectively.

Conclusion: Percutaneous directional atherectomy is a safe and effective technique in lower limb revascularisation. Preliminary results supported by short-term data encourage use of DA with SilverHawk catheter in the femoro-popliteal steno-obstructive lesions also in traditionally "forbidden districts". Long-term data are missing.

B-0426 14:54

Endovascular treatment of extracranial carotid artery aneurysms

K.D. Mathias, A. Ranft; Dortmund/DE (klaus.mathias@klinikumdo.de)

Purpose: Efficacy and durability of endovascular treatment of carotid artery aneurysms with covered stents were investigated.

Methods and Materials: 41 patients with extracranial aneurysms of the internal and common carotid artery were treated with covered stents. 23 men, 18 women, mean age 56±16 years. The patients suffered from fibromuscular dysplasia, traumatic and spontaneous dissection, whiplash injury, tumour invasion, atherosclerosis, and direct trauma. The diameter of the smallest aneurysm measured 8 mm, the largest 64 mm, on an average 38 mm. Self-expandable covered stent were used in all cases. Three patients received 2 stents. Platelet inhibitors were administered during and after the procedure. Follow-up examinations are available up to 7 years.

Results: In 40 of the 41 patients the stents sealed the aneurysms. In one patient a giant aneurysm could not be crossed. One patient developed a major stroke immediately after treatment. One patient needed a second intervention due to an endoleak 9 months later. In two tumour patients the carotid artery occluded within 2 years after the intervention without a stroke, but with migration of the endograft. 38 of the 41 patients had a good long-term outcome without adverse events.

Conclusion: Endovascular treatment of carotid artery aneurysms is highly effective and replaces open surgical repair in nearly all cases with a long-term cure rate of 93% and without the cranial nerve palsies seen after surgery.

B-0427 15:03

Type-II endoleaks after endovascular abdominal aortic aneurysm repair: fate of the aneurysm sac during long-term follow-up

R. Nolz, H. Teufelsbauer, D. Beitzke, M. Funovics, U. Asenbaum, A. Wibmer, C. Plank, J. Lammer, M. Schoder; Vienna/AT (richard.nolz@meduniwien.ac.at)

Purpose: To evaluate frequency of type-II endoleaks after endovascular AAA repair and to compare sac diameter changes to endoleak free AAAs in patients with at least three-years CT-follow-up.

Methods and Materials: The study cohorts consist of a no EL (nEL)-group (n=60) and a type-II-EL group (n=49). According to their course and vessel origin, type-II ELs were splitted in subgroups. Maximum sac diameter changes were measured in defined groups and also according to different stentgraft devices. Additionally, reintervention and death rates were evaluated.

Results: Mean follow-up was 68.1 ± 23.8 months. In the type-II-EL group sac diameters increased significantly in comparison to the first postoperative CT. In the nEL there was a not significant tendency to decreasing sac diameters. In progradient and equal type-II ELs the mean difference of sac diameter increase was significant in comparison to the nEL (p < 0.005). By means of the overall type-II-EL group there was no significant diameter change in comparison to the nEL. Also, the difference of diameter change was not significant comparing the EL subgroups according to their vessel origin. Regarding different stentgraft devices, the Excluder endoprosthesis showed a significant mean difference of sac diameter increase in comparison to the Talent and Zenith endoprosthesis (p < 0.005). Reinterventions were performed in 18.3% (n=20) of patients and there were 6.3% (n=2) aneurysm-related deaths.

Conclusion: Progradient and equal type-II ELs result in significant aneurysm sac enlargement during long-term follow-up. Based on our results, routinely follow-up of patients with type-II ELs remains mandatory.

B-0428 15:12

Excimer laser atherectomy in arteries of the lower limb with TASC C and D lesions

C. Wissgott, P. Kamusella, C. Luedtke, R. Andresen; Heide/DE (cwissgott@gmx.de)

Purpose: The study objective was to examine the application of excimer laser atherectomy (ELA) in patients with refractory occlusions in femoropopliteal arteries, where previous conventional recanalisation attempts, using percutaneous transluminal angioplasty (PTA), were unsuccessful.

Methods and Materials: The average age of the 40 patients (32 men, 8 women) included in this study was 65.4 years. The average occlusion length was 17.5 cm (range: 12-25 cm). The initial recanalisation attempts were performed with stiff Terumo guidewires (curved or straight) supported by various catheters (straight/multipurpose/Cobra). After the unsuccessful attempt, an excimer laser catheter (catheter diameters from 1.7 to 2.5 mm) was used for recanalisation using the step-by-step method of crossing. After successful crossing, balloon dilatation was performed in all cases. Stent implant was required in 10% (4/40) of procedures. Patients were followed for 12 months with CCDS.

Results: The initial technical success rate of 90% (36/40) resulted in primary, primary-assisted and secondary-assisted patency rates of 58.9%, 67.8% and 83.2%, respectively, after 12 months. No serious complications occurred that were attributable to the intervention.

Conclusion: According to these results, ELA recanalisation provides a low stent rate alternative to surgical procedures for refractory occlusions. This would offer patients, with increased operative risks, a promising and low-risk therapeutic procedure. The option of a subsequent vascular operation would not be compromised.

B-0429 15:21

Long-term volumetric follow-up of abdominal aortic aneurysms after endovascular aneurysm repair to determine the effect of endoleaks on aneurysm volume

W.H. Sommer, M. Haack, R. Weidenhagen, F. Meinel, M.F. Reiser; Munich/DE (wieland.sommer@med.uni-muenchen.de)

Purpose: To determine the effect of different types of endoleaks on long-term changes of aneurysm volume in patients after abdominal endovascular aneurysm repair (EVAR).

Methods and Materials: We determined the volume of the abdominal aneurysm size in 103 patients who underwent EVAR between 2002 and 2009 in all pre-therapeutic and follow-up CTs using the software Osirix 3.8. Mean increase of the aneurysm volume was determined for patients without endoleaks and with different types of endoleaks at different time points (3 months (M), 12M, and 36M after

EVAR). Patients with low-flow (type II) and with high-flow (type II/III) endoleaks were analysed separately to determine the effect of endoleak on aneurysm volume. **Results:** Overall 576 CT-datasets were evaluated by volumetry (patient age 69±14 y; no. of follow-up CTs: 5.6±1.6; mean follow-up time: 43±9 months). Among these patients, there were 6 type I, 19 type II and 5 type III endoleaks. The aneurysm volume in patients without endoleaks after 3M, 12M and 36M was 95±10%, 86±9% and 76±8% of the initial aneurysm volume, respectively. Low-flow (type II) endoleaks showed the following volumes: 110±5% (3M), 107±7% (12M) and 106±11% (36M). High-flow (type II/III) endoleaks showed the following volumetries, compared to the initial volumetry: 108±8% (3M), 113±12% (12M) and 121±14% (36M) ($p < 0.05$). **Conclusion:** Both low- and high-flow endoleaks have a significant impact on regression of aneurysm volume in patients after EVAR. Type II endoleaks rather lead to stable volumes over years, type I and III endoleak continuously increase aneurysm size.

14:00 - 15:30

Room E1

Musculoskeletal

SS 610

Cartilage and osteoarthritis

Moderators:

A. Platkajis; Riga/LV
G. Scheurecker; Linz/AT

B-0430 14:00

Biomechanics of human knee cartilage-loading of knee during 3 T MRI

T. Shiomu, P. Szomolanyi, V. Juras, S. Zbyn, S. Trattnig; Vienna/AT
(t-shiomu@ka2.so-net.ne.jp)

Purpose: As reported previously, MRI measurements of knee cartilage morphology are not sensitive to changes associated with early stage of osteoarthritis development. Biochemical MRI provides information on cartilage composition, dominantly on proteoglycan content and collagen matrix. We hypothesise that changes in T2 values of human knee cartilage observed during biomechanical MRI correlate with cartilage functionality.

Methods and Materials: Multi-slice multi-echo was performed on 10 volunteers. After load-free measurements, load of half body weight was applied with the MR compatible custom-made pneumatic controlled compression device for 3 T. At the end, load-free measurement was repeated. Offline post-processing was used to evaluate T2 maps. ROIs were drawn manually by experienced radiologist in deep and superficial zone of the weight-bearing area. Mean, standard deviation and pixel count were recorded and statistically analysed by T-test.

Results: T2 values of human knee cartilage exhibit significant decrease in loading phase (57.04 ms → 52.45 ms, $p = 0.00045$), and significant increase in unloading phase (51.86 ms → 56.58 ms, $p = 0.00004$). T2 values exhibit nonlinear dynamic change over time and reached stable values after 20 minutes of loading/unloading. Changes of T2 values were more obvious in superficial layer.

Conclusion: Loading of knee during MRI can provide biomechanical characteristics of human knee cartilage. Statistically significant change of cartilage T2 in loading and unloading phase provides insight into cartilage function. This can help in diagnostics of early stages of osteoarthritis development, when morphological changes and degenerations are not visible. Next step will be application of loading MRI to the patients after cartilage surgery.

B-0431 14:09

Knee joint configuration: the implication of severe osteoarthritis and ACL injury

E. Vassalou, P. Matalliotaki, K. Spanakis, P. Maldas, E. Magkanas, A. Karantanas; Iraklion/GR (vassalou.e@hotmail.com)

Purpose: To assess the effect of severe osteoarthritis (OA) and ACL injury on the knee joint configuration.

Methods and Materials: MR images for 206 patients were reviewed. Group.i consisted of 101 patients (11-71y) with MRI diagnosis other than severe OA (chondral defects < stage II) and ACL injury. Group IIa included 40 patients (14-67y) with complete, chronic or recent, ACL tear and IIb 25 patients (14-76y) with partial, chronic or recent ACL tear. Group III encompassed 40 patients (39-93y) with severe OA (chondral defects > stage II). The femoral angle was defined in the axial plane, by drawing a horizontal line and a line tangent to the posterior aspect of the cortex of the femoral condyles at their maximum anteroposterior diameter. The tibial angle was measured similarly one slice above the head of the fibula. The

femorotibial angle (FTA) was defined as the femoral angle minus the tibial angle. All patients' ages were recorded.

Results: There was significant difference regarding the FTA between group.i and groups IIa, IIb and III (independent samples, t-test, $p < 0.005$). 91% and 22% of the patients in group.i and IIa respectively, had an FTA < 4.40. No significant correlation between the FTA and patients' age was observed, in any of the groups.

Conclusion: ACL injury and severe OA induce alteration in the femorotibial anatomical relationship by means of rotation of the femur in relation to the tibia. The above finding could be of value in assessing ACL tears with equivocal direct signs on MRI.

B-0432 14:18

Multi-parametric MRI of talar and tibial cartilage in cadaver ankles at 7T: correlation with immuno-histological findings

S. Zbyn, S. Apprich, V. Juras, P. Szomolanyi, S. Domayer, S. Trattnig; Vienna/AT (stefan.zbyn@meduniwien.ac.at)

Purpose: To evaluate biochemical MRI techniques at 7 Tesla, such as sodium imaging and T2 mapping, as potential markers for biochemical composition of talar and tibial cartilage in upper ankle-joint, by correlating MRI parameters with immuno-histologically assessed glycosaminoglycan and water content of cartilage in cadaver ankles.

Methods and Materials: Seven fresh cadaver ankles from a local anatomy department were used in this study. Sodium MRI was performed with gradient echo sequence optimised for articular cartilage using sodium-only 15-channel transmit/receive knee coil. The T2-relaxation times were obtained using a multi-echo spin echo technique with 28-channel transmit/receive knee coil. Talar and tibial cartilage of each cadaver ankle was divided into lateral, central and medial part and region-of-interest analyses were performed on corresponding MR images. Resultant sodium signal-to-noise ratio (SNR) and T2-relaxation times were correlated with each other, as well as with immuno-histologically assessed glycosaminoglycan and water content of talar and tibial cartilage.

Results: Strong Pearson correlation coefficient was found between sodium SNR and glycosaminoglycan content in talar ($r = 0.716$) and tibial ($r = 0.780$) cartilage as well as between T2-relaxation times and water content in tibial cartilage ($r = 0.761$). Low correlation was observed between T2-relaxation times and water content in talar cartilage ($r = 0.434$).

Conclusion: Obtained high correlation between MRI parameters and immuno-histological results validates the findings of progressive MRI methods at 7T. A contrast-free, glycosaminoglycan-specific sodium imaging, as well as water- and collagen-sensitive T2 mapping, are feasible for the noninvasive biochemical evaluation of the talar and tibial cartilage in reasonable scan times.

B-0433 14:27

UCSF score: a novel quantitative assessment score for cartilage lesions in early osteoarthritis - data from the osteoarthritis initiative

H. Alizai, W. Virayavanich, G.B. Joseph, L. Nardo, H. Liebl, P. Jungmann, M.C. Nevitt, C.E. McCulloch, T.M. Link; San Francisco, CA/US (hamzaalizai@gmail.com)



Purpose: In this study, we describe a quantitative scoring system for cartilage lesions, test its reliability and validity and compare it with established semiquantitative scoring systems.

Methods and Materials: Forty-seven individuals with and 27 without risk factors for knee OA were randomly selected from the osteoarthritis initiative cohort. Inclusion criteria were age 45-55, BMI 19-27 kg/m², no knee pain and no radiographic OA at baseline. Baseline and 24-month follow-up right knee 3 T MR images were analysed using WOMBS, BLOKS and UCSF-Score with an interval of 3 weeks between each analysis. Progression of cartilage lesions using each scoring system was calculated and compared using multilevel, mixed-effect linear-regression models. Weighted Kappa values were calculated to determine reliability.

Results: The UCSF-Score assesses 5 features of cartilage defects: diameter, number of sections, section thickness, depth and shape, in 6 knee compartments. The inter- and intra-observer reliability for the total UCSF-Score were calculated as 0.80 and 0.84. Inter-observer Kappa for individual features ranged from 0.87 to 0.94. UCSF-Score had a significantly higher rate for detecting cartilage lesion progression than WOMBS and BLOKS ($p < 0.0001$); 43%, 18% and 13% of the lesions progressed when analysed with UCSF-Score, WOMBS and BLOKS, respectively. Using UCSF-Score, the subjects with OA risk factors had higher odds of progression than subjects without risk factors (OR 2.78, $p = 0.005$).

Conclusion: The UCSF-Score is a novel reproducible and valid quantitative scoring system for cartilage lesions, which provides an improved detection rate for monitoring early OA progression compared to the semi-quantitative WOMBS and BLOKS.

B-0435 14:36

T2 relaxation time measurements are limited in monitoring advanced cartilage degeneration of the knee - longitudinal data from the osteoarthritis initiative

P.M. Jungmann, H. Liebl, H. Alizai, L. Nardo, G. Joseph, J. Lynch, C.E. McCulloch, M.C. Nevitt, T.M. Link; *San Francisco, CA/US* (*hans.liebl@ucsf.edu*)

Purpose: To analyse the natural two-year development of knee cartilage T2 relaxation time measurements in relation to the extent of morphological cartilage abnormalities, assessed with 3 Tesla MR images from the osteoarthritis initiative incidence cohort.

Methods and Materials: Right knee MRIs of 245, 45 - 60 year old individuals (122 males, 123 females) with risk factors for osteoarthritis (OA) but without radiographic OA or knee pain at baseline were included in this study. Cartilage was segmented and T2 maps were generated in five compartments (patella, medial and lateral femoral condyle, medial and lateral tibia plateau) at baseline and two-year follow-up. T2 changes over 2 years were correlated with baseline T2 values as well as cartilage degenerative changes assessed with whole organ MR imaging scores (WORMS). Statistical analysis was performed with ANOVA and two-sided Students t-tests.

Results: Longitudinal T2 changes were significantly negatively correlated with both baseline ($P=0.038$) and follow-up ($P=0.002$) cartilage WORMS. Patients that developed new cartilage defects had significantly smaller increase in T2 values than patients without new lesions (0.50 ms (± 1.69) versus 1.63 ms (± 1.24); $P=0.045$). Further, individuals with higher baseline T2 showed smaller T2 increases over time in all compartments ($P < 0.001$).

Conclusion: An inverse correlation of longitudinal T2 relaxation time changes versus baseline T2 values and morphological cartilage abnormalities was found; suggesting that T2 values may not be well suited for monitoring advanced degenerative disease. This may be due to a true negative correlation in T2 measurements, ceiling effects, or regression to the mean.

B-0436 14:45

Baseline mean and heterogeneity of MR knee cartilage T2 are associated with morphologic degeneration of cartilage, meniscus, and bone marrow over three years: data from the osteoarthritis initiative

T. Baum, G.B. Joseph, H. Alizai, J. Carballido-Gamio, L. Nardo, W. Virayavanich, C.E. McCulloch, S. Majumdar, T.M. Link; *San Francisco, CA/US* (*thbaum@gmx.de*)

Purpose: (i) To study the natural progression of morphologic changes of the cartilage, meniscus, and bone marrow using a semi-quantitative score and (ii) to determine whether the mean and heterogeneity of MR knee cartilage T2 at baseline are associated with morphologic degeneration of these tissues over three years in subjects with risk factors for knee osteoarthritis (OA).

Methods and Materials: Subjects with risk factors for knee OA ($n=289$) with an age range of 45-55 years were selected from the osteoarthritis initiative (OAI) database. 3.0 Tesla MR images of the right knee at baseline and 3-year follow-up were analysed using morphological gradings of cartilage, meniscus, and bone marrow (WORMS scoring). A T2 mapping sequence was used to assess baseline mean and heterogeneity of cartilage T2 (grey level co-occurrence matrix (GLCM) texture analysis). Regression models were used to assess the relationship between baseline T2 parameters and changes in morphologic knee WORMS scores over three years.

Results: The prevalence of knee abnormalities in the cartilage, meniscus, and bone marrow significantly ($p < 0.05$) increased from baseline to 3 years in all compartments combined. The mean and heterogeneity of baseline cartilage T2 was significantly ($p < 0.05$) elevated in subjects whose cartilage, meniscus, and bone marrow WORMS scores increased over three years compared to subjects whose scores did not change.

Conclusion: The prevalence of knee abnormalities significantly increased over three years; increased cartilage T2 at baseline is associated with longitudinal morphologic degeneration in the cartilage, meniscus, and bone marrow over three years in subjects with risk factors for OA.

B-0437 14:54

MR-based baseline T2 relaxation time predicts progression of knee osteoarthritis

L. Nardo, A. Prasad, J. Schooler, H. Liebl, T.M. Link; *San Francisco, CA/US*

Purpose: To evaluate whether T2 relaxation times of knee cartilage determined with 3 T MRI at baseline predicted longitudinal progression of cartilage degenerative changes.

Methods: Quantitative analysis of cartilage was performed using 3 T MRI with both T2 mapping techniques in 55 individuals with mild OA (Kellgren-Lawrence [KL] score of 1-2), divided into two groups of progressors (27 subjects) and non-progressors (28 subjects). Morphological abnormalities of cartilage, menisci, ligaments and bone marrow were analysed on sagittal fat-saturated T2-weighted fast spin echo (FSE) sequences and progression of degenerative disease was assessed over a period of two years. Differences between T2 relaxation time in progression and non-progression cohorts were compared using one-way analysis of variance (ANOVA) and t tests.

Results: Significant differences in baseline T2 values were found between progression and non-progression cohorts in all compartments ($p < 0.05$) except the lateral tibia: medial femur ($p=0.0171$), medial tibia ($p=0.012$), lateral femur ($p=0.0179$), and patella ($p=0.01$).

Conclusion: T2 mapping techniques differentiated individuals with and without progression of degenerative abnormalities and may therefore be used as predictors for progression of knee OA.

B-0438 15:03

MRI-based and clinical long-term results of isolated osteochondral transplantation (OATS) of the knee joint

J.S. Bauer, L. Kohn, J. Penzel, P.U. Brucker, A. Imhoff, E. Rummeny, K. Woertler, M. Sauerchnig; *Munich/DE* (*jsb@roe.med.tum.de*)

Purpose: OATS is an established therapy for osteochondral lesions at the knee joint. However, long-term results regarding clinical and morphological outcome do not exist in a uniform patient set so far.

Methods and Materials: We followed up 22 patients (16m, 6f, \bar{o} age 24.7y) in average 8.8 years (6-13) after isolated OATS therapy of the medial or lateral femoral condyle. Clinical scores (WOMAC-, Lysholm-, IKDC-, Tegner-score, VAS) were obtained and MR imaging was performed at 1.5 T pre-surgery and at 3.0 T at follow-up, using standard morphological sequences (triplanar fat saturated intermediate weighted fast spin echo, sagittal T1-weighted fast spin echo sequence, spatial resolution 0.21x0.21x3.0 mm) and T2-mapping (multiecho spin echo, $TE=13/27/41/55/69/82$ ms, $TR=2160$ ms, resolution 0.46x0.42x2.5 mm). Exclusion criteria were ligament reconstructions, wedge osteotomies, meniscal resections and kissing lesions. Progression of osteoarthritis was quantified in MR images using the BLOK-score. Transplant integration was evaluated using the MOCART score. Cartilage quality was assessed using T2-relaxation times.

Results: Comparing pre-surgery with follow-up, significant improvement was found in case of VAS, WOMAC- and Lysholm-score. The Tegner-score did not show differences ($p > 0.9$). BLOKS increased in OA-associated findings like osteophytes. Average T2-relaxation times of the OATS cylinders (48.5 ± 8.0) did not show significant differences to normal cartilage (47.1 ± 5.2). However, the adjacent cartilage next to the cylinder demonstrated significantly higher T2-values (50.9 ± 7.6 , $p < 0.01$).

Conclusion: Isolated OATS therapy shows good long-term results, both clinically and morphologically. The T2-elevation of the surrounding cartilage may suggest a preexisting defect in cartilage ultrastructure, larger than the replaced area, not visible for the surgeon.

B-0439 15:12

Long-term results 8 years after autologous osteochondral transplantation: 7T gagCEST and sodium magnetic resonance imaging with morphological and clinical correlation

B. Schmitt, I. Krusche-Mandl, S. Apprich, V. Juras, S. Trattnig; *Vienna/AT* (*benjamin.schmitt@meduniwien.ac.at*)

Purpose: The aim of the study was to compare morphological (MOCART), biochemical (T2-mapping, gagCEST and sodium imaging) and clinical long-term results after autologous osteochondral transplantation (AOT).

Methods and Materials: Nine patients, treated with AOT at their knee joints, consented to participate in clinical (IKDC, modified Lysholm and VAS) and radiological long-term follow-up at a median of 7.9 years (IQR: 7.7-8.2). Morphological MRI was performed on a 3 T-MR unit and included PDw imaging with and without fat suppression, T2w and T1w imaging, from which the MOCART score was derived. T2 mapping was performed at 3 T using a multi-echo, spin-echo approach. Sodium and CEST MRI were performed on a 7T whole body MR scanner.

Results: The difference between native and repair cartilage was statistically significant regarding median T2 values, median CEST asymmetry and median sodium SNR. The median MOCART score revealed 75 points, the median modified Lysholm score 90 and the median VAS was 1.0. The strongest correlation between MRI parameters was found between sodium SNR ratios and CEST asymmetry ratios ($\rho = 0.952$, $p < 0.001$), showing consistent proteoglycan assessment at 7T.

A correlation between MRI parameters and clinical scores was only found between T2 ratios and modified Lysholm ($p = -0.690$, $p = 0.04$).

Conclusion: Our results imply that the hyaline character of AOT grafts seems to degenerate in the long term. AOT can still be recommended as an option for the treatment of limited sized cartilage defects due to few correlations found between MRI and clinical scores.

14:00 - 15:30

Room F1

Abdominal Viscera

SS 601

MRI (high field)

Moderators:

K. Holzapfel; Munich/DE
O. Lucidarme; Paris/FR

B-0440 14:00

Optimisation of liver intravoxel incoherent motion imaging protocol at 3.0 T for chronic liver diseases assessment

B. Leporq, F. Pilleul, O. Beuf; Villeurbanne/FR
(benjamin.leporq@creatis.insa-lyon.fr)

Purpose: To optimise a 3.0 T acquisition protocol for liver intra-voxel-incoherent motion (IVIM) imaging to be included in a clinical study focused on chronic liver diseases. Four set of parameters were evaluated on fifteen healthy volunteers.

Methods: Invariant parameters were: eDWI sequence with 11 b-values (0-20-40-60-80-100-200-300-400-600-800s.mm⁻²); 2000 ms TR; 21 axial slices; 400x300 mm² FOV; 128x96 matrix; 8 mm slice thickness, 250KHz bandwidth. Variable parameters according to the four settings were: a) respiratory-triggering, 6NEX, 48 ms TE, 3 perpendicular diffusion gradients applied simultaneously (option "3-in-1") and 6' average scan duration. b) Free-breathing, 9NEX, 48 ms TE, 3-in-1 option and 5'35" scan duration. c) Free-breathing, 9NEX, 55 ms TE, 3 perpendicular diffusion gradients applied sequentially ("all" option) and 9'40" scan duration. d) Variable NEX according to b-values (2-2-2-2-3-3-4-5-6-7-8-9NEX from 0 to 800s.mm⁻²); additional 10s.mm⁻² b-value, 55 ms TE, "all" diffusion option and 5'26" scan duration. Pure molecular diffusion coefficient (Dslow), perfusion-related coefficient (Dfast) and perfusion fraction (f) were obtained by a non-linear least-square fit to the IVIM model.

Results: Mean IVIM parameters were: $f=21.0\pm6.0$, 16.9 ± 6.2 , 17.9 ± 5.0 and $22.4\pm10.6\%$; $D_{Slow}=1.03\pm0.14$, 1.12 ± 0.10 , 1.09 ± 0.08 , $1.09\pm0.08\times 10^{-3}$ mm².sec⁻¹; $D_{Fast}=56.4\pm22.2$, 71.6 ± 26.3 , 86.0 ± 26.6 , $75.8\pm44.7\times 10^{-3}$ mm².sec⁻¹ for protocol a), b), c), d), respectively. Bland-Altman plots were not shown significant differences between settings.

Conclusion: High signal averaging restricted motion artefacts caused by free-breathing imaging and allowed free-breathing technique. The smart-averaging procedure reduces significantly the scan duration with similar SNR for the highest numbers of b-values and three perpendicular diffusion gradients sequentially applied. This setting is a suitable compromise to be added in a clinical protocol between acquisition time, modelling reliability, reproducibility and patient acceptance.

B-0441 14:09

Can we differentiate infiltrative hepatocellular carcinoma and confluent fibrosis in background liver cirrhosis with Gd-EOB-DTPA-enhanced 3 T MRI?

Y. Park, C. Lee, K. Kim, J. Choi, J. Lee, C. Park; Seoul/KR
(pys797979@naver.com)

Purpose: To retrospectively determine the significant MRI features for the differentiation of infiltrative hepatocellular carcinoma (HCC) from confluent fibrosis in liver cirrhosis.

Methods and Materials: After search of pathologic and radiologic databases, 16 of infiltrative HCC and 8 of confluent fibrosis evaluated with Gd-EOB-DTPA-enhanced 3 T MRI from 2008 to 2010 were reviewed. Two radiologists retrospectively reviewed MR images in consensus for morphologic change, signal intensity, enhancement pattern, apparent diffusion coefficient (ADC) value, and presence of portal vein thrombosis, duct dilatation, and metastatic lymph node. Clinical findings such as tumour marker and symptom also were recorded. Univariate analyses were used to differentiate these entities.

Results: All infiltrative HCC showed preservation of contour or contour-bulging and all confluent fibrosis showed capsular retraction. Infiltrative HCC manifested arterial enhancement (9/16) and portal vein thrombosis (14/16). Confluent fibrosis appeared delayed enhancement (6/8). ADC was significantly lower in infiltrative HCC

than in confluent fibrosis ($0.96\pm0.14 \times 10^{-3}$ mm²/s and $1.47\pm0.17 \times 10^{-3}$ mm²/s, $p=0.0001$). Compared with T2-weighted image, hepatobiliary phase showed more discrete margin and nodular configuration in infiltrative HCC and more indistinct and wedge shape in confluent fibrosis.

Conclusion: Preservation of liver contour or contour-bulging, portal vein thrombosis, and low ADC value were found to be highly suggestive MR findings for differentiation of infiltrative HCC from confluent fibrosis in liver cirrhosis. Hepatobiliary phase improves characterisation and determination of extent and margin of the lesion to distinguish these two entities.

B-0442 14:18

Gd-EOB-DTPA-enhanced 3.0 T MRI for the evaluation of hepatic metastasis from colorectal cancer: is metastasis always seen as a "defect" on the hepatobiliary phase?

A. Kim, C. Lee, K. Kim, J. Choi, J. Lee, Y. Park, C. Park; Seoul/KR
(arkim.rad@gmail.com)



Purpose: To determine specific imaging features of hepatic metastasis from colorectal cancer, focusing on the hepatobiliary phase (HBP) of Gd-EOB-DTPA-enhanced MRI.

Methods and Materials: Over a 2-year period, 79 hepatic metastatic lesions were identified from 32 patients (22 men and 10 women) who proven colorectal cancer and underwent Gd-EOB-DTPA-enhanced 3.0 T MRI. Hepatic metastases were proven pathologically in 16 patients: by surgical liver resection (n=14) and by US-guided biopsy (n=2). The remaining 16 patients were considered to have hepatic metastasis based on imaging studies and clinical information. Two radiologists evaluated the imaging features of each MRI sequence, including high-resolution T2WI, dynamic contrast enhancement study with hepatobiliary phase, and diffusion-weighted image. We also compared SI of the lesions on T2WI and HBP.

Results: T2WI showed homogeneous high SI (n=25; 31.7%), target appearance (n=3; 3.8%), reversed target appearance (n=2; 2.6%), and heterogeneously high SI (n=49; 62%). On HBP, homogeneous defect was seen in 22 lesions (27.9%), target appearance in five lesions (6.4%), reversed target appearance in two lesions (2.5%), and heterogeneous defect in 50 lesions (63.3%); including reticular (70%), partially globular (26%), and diffuse GGO-like (4%) patterns. According to the imaging features on HBP, the homogeneous defect and heterogeneous defect groups had a mean ADC value of 0.99×10^{-3} and 1.07×10^{-3} mm²/sec, respectively, without statistically significant difference.

Conclusion: Hepatic metastasis from colorectal cancer usually showed as a heterogeneous defect on HBP and a heterogeneous high SI on T2WI. The generally accepted "true defect" was not a common finding in hepatic metastasis from colorectal cancer.

B-0444 14:27

Quantification of liver fat content by 3 Tesla spectroscopy magnetic resonance (3 T SRM) in nonalcoholic fatty liver disease: correlation with serum levels of alanine aminotransferase (ALT)

J.L. Martin-Rodriguez, J.J. Jimenez-Moleon, J. Machado Gallas, M.R. Navarro-Labrat, M. Velasco Torres, J. Sanchez-Gonzalez, J.L. Gonzalez-Calvin; Granada/ES
(joseluismartin.rx@hotmail.com)

Serum levels of ALT is a biomarker nonalcoholic fatty liver disease (NAFLD). Only a proportion of patients with NAFLD have elevated serum ALT levels.

Purpose: To know if there is a relationship between liver fat content and serum levels of ALT, as well as to study if there is a threshold within de current normal ALT values, from which we could suggest the presence of NAFLD.

Methods and Materials: This is a community, prospective, cross-sectional, random study. Group A: 22 subjects with elevated serum ALT levels (> 40 U/L) without any known cause: alcohol, viral hepatitis, autoimmune, drugs and others were excluded. Group B: 23 subjects with serum ALT levels between 20 and 40 U/L. Group C: 11 subjects with serum ALT < 20 U/L. Quantification of liver fat by spectroscopy 1H MR 3 T. We used a cut off value > 5% of liver fat content for the diagnosis of hepatic steatosis.

Results: The proportion with hepatic steatosis was: group A: 88%; group B: 87%. Group C: 0% ($p < 0.001$ for group B or C vs. group A). A significant positive correlation was observed between liver fat content and ALT serum levels ($r: 0.576$; $p < 0.001$).

Conclusion: Our study shows that there is a positive significant correlation between liver fat content and serum ALT levels in subjects with NAFLD. 87% of subjects with "normal" ALT levels (20-40 U/L) had hepatic steatosis. We suggest that serum ALT could be a useful biomarker of NAFLD if the normal threshold is established at ALT levels < 20U/L.

B-0445 14:36

Liver intravoxel incoherent motion imaging at 3.0 T: comparison with conventional dual b-values method

B. Leporq, F. Pilleul, O. Beuf, Villeurbanne/FR
(benjamin.leporq@creatis.insa-lyon.fr)

Purpose: To report our experience about intra-voxel incoherent motion (IVIM) imaging on human liver and phantom to compare the bi-exponential diffusion pattern with the conventional dual-b values ADC method.

Methods and Materials: Acquisitions were performed at 3 T, in free breathing, on fifteen healthy volunteers then on a doped 2.5% agar gel phantom using eDWI sequence (GEHC). Parameters were: 11 b-values (0-20-40-60-80-100-200-300-400-600-800 s.mm⁻²); 2000 ms TR; 48 ms TE; 21 axial slices; 400x300 mm² FOV; 128x96 matrix; 8 mm slice thickness, 9NEX, 250 kHz bandwidth. Three perpendicular diffusion gradients were applied simultaneously. Pure molecular diffusion coefficient (Dslow), perfusion-related coefficient (Dfast) and perfusion fraction (f) were obtained by a non-linear least-square fit to the bi-exponential IVIM model. ADC was computed using conventional mono-exponential method with two pair of b-values: 0/600 and 40/600.

Results: Mean IVIM parameters were DSlow=1.12±0.10x10⁻³ mm.s⁻²; DFast=71.6±26.3x10⁻³ mm.s⁻²; f=16.9±6.20%; mean ADC was D=1.66±0.26x10⁻³ mm.s⁻². A strong correlation was found between absolute (D-DSlow) value and perfusion fraction (Pearson's coefficient 0.86; p < 0.001). Bias between D and DSlow increased when zero b-value was used for ADC quantification (37.3% and 4.85% for 0/600 s.mm⁻² and 40/600 s.mm⁻², respectively). Quantification from phantom acquisition gave the same values for D and DSlow (2.0x10⁻³ mm.s⁻²) and diffusion followed a simple mono-exponential pattern.

Conclusion: The bi-exponential pattern of diffusion encountered in liver was linked to perfusion-related diffusion and explained the bias between ADC measured with mono-exponential approach and pure molecular diffusion coefficient extracted from IVIM modeling. Dual b-values method for ADC measurement could be an alternative method to assess the DSlow component choosing appropriate pair of b-values (> 40).

B-0446 14:45

Apparent diffusion coefficient values of healthy pancreas from diffusion-weighted imaging of upper abdomen at 3.0 T

C. Ma, C. Pan, H. Zhang, H. Wang, J. Wang, S. Chen, J. Lu; Shanghai/CN
(mengqih@gmail.com)

Purpose: To clarify the apparent diffusion coefficient (ADC) values in different anatomical regions (head, neck, body and tail) of normal pancreas.

Methods and Materials: The study subjects comprised 383 patients with confirmed healthy pancreas. Echo-planar diffusion-weighted imaging (DWI) of upper abdomen was performed by applying two b-values of 0 and 500 s/mm² at a 3.0-T magnetic resonance imaging (MRI) system. ADC values were obtained in 1532 various regions of pancreas. Dependency of ADC on the anatomical regions was analysed using Kruskal-Wallis test and Wilcoxon sign rank test.

Results: The mean ADC value of the whole healthy pancreas is 1.60±0.33 x10⁻³ mm²/s. The results of Kruskal-Wallis test showed a significant difference of the ADC values among the anatomical regions and the lowest values were obtained in the pancreatic head (head 1.52±0.29, neck 1.64±0.34, body 1.67±0.35, and tail 1.58±0.31 x10⁻³ mm²/s; Chi-square = 44.8748, Df = 3, P < 0.0001). The results of Wilcoxon sign rank test showed the mean ADCs differed remarkably between head and neck (P < 0.0001), head and body (P < 0.0001), head and tail (P=0.0008< 0.05), neck and tail (P=0.0062< 0.05), body and tail (P < 0.0001), respectively, but the mean ADCs of neck and body (P=0.1181> 0.05) showed no significant difference.

Conclusion: The mean ADC values of normal pancreas varied significantly within the different anatomical regions. Therefore, it is necessary to utilise these results in related studies or clinical applications for differentiating between different pancreatic diseases.

B-0447 14:54

1.5 Tesla vs 3 Tesla versus 7 Tesla abdominal MRI: the more Tesla, the better?

L. Umutlu, O. Kraff, A. Fischer, M. Forsting, M.E. Ladd, S. Maderwald, T.C. Lauenstein; Essen/DE (Lale.Umutlu@uk-essen.de)

Purpose: The aim of our study was to investigate and compare the diagnostic ability of 1.5, 3 and 7 Tesla abdominal MRI.

Methods and Materials: 12 healthy volunteers were each examined on a 1.5 T (Magnetom Aera), a 3 T (Magnetom Skyra) and a 7T MR system (Magnetom 7T, Siemens). The following sequences were obtained: 1) T1w fs 2D FLASH, 2) T1w

fs VIBE 3) T1w 3D FLASH, 4) T1w 2D in-and-opposed phase 5) True-FISP and 6) T2w TSE. Qualitative image analysis was performed using a four-point scale (1 = non-diagnostic to 4 = excellent image quality) regarding 1) overall image quality; 2) delineation of abdominal vasculature, 3) delineation of the biliary duct system as well as 4) image impairment due to artefacts. For correlation of signal intensities, regions-of-interest were placed in parenchymatous organs. For statistical analysis, a Wilcoxon rank test was used.

Results: With increasing magnetic field strength, all sequences could be obtained at higher spatial resolution at equivalent acquisition times. While overall image quality was rated comparably high for T1w imaging in all three field strengths, 7T T1w MRI showed its superiority in the assessment of non-enhanced abdominal vasculature (mean 1.5 T 1.2, mean 3 T 1.2, mean 7T 3.6). Quantitative analysis revealed an average increase of the mean organ signal from 1.5 T to 3 T of 1.45, and 1.19 from 3 T to 7T.

Conclusion: Our results demonstrate the benefits and the limitations of an increase of the magnetic field strength, offering improved and highly detailed delineation of anatomical and vascular structures in T1w imaging.

B-0448 15:03

Implementation of dual source RF excitation techniques with 3 T imaging systems allows for nearly identical ADC values in comparison to 1.5 T MR scanners when imaging the abdomen

P. Riffel¹, R. Rao², M. Meyer¹, P. Kettner¹, A. Lemke¹, S. Haneder¹, S.O. Schönberg¹, H.J. Michaely¹; ¹Mannheim/DE, ²Galveston, TX/US

Purpose: To retrospectively and prospectively compare apparent diffusion coefficient (ADC) values obtained within clinically relevant abdominal regions in a 1.5 T system and 3 T systems with and without dual source parallel RF excitation techniques.

Methods and Materials: Diffusion-weighted images of the abdomen were obtained on three different MR systems (1.5 T, first generation 3 T, and second generation 3 T which incorporates dual source parallel RF excitation) on 150 patients retrospectively and 19 volunteers prospectively. Seven regions of interest (ROI) were selected to represent areas of clinical significance.

Results: In the patient population the differences in mean ADC values between first generation 3 T and the other two MR scanners ranged from 5% (kidneys) up to 200% in the left lobe of the liver (1.5 T: 1.09 x 10⁻³ s/mm², first generation 3 T: 0.35 x 10⁻³ s/mm², second generation 3 T: 1.11 x 10⁻³ s/mm²). The ADC values measured between the 1.5 T and second generation 3 T systems were nearly identical, with no significant differences between the two systems. In the volunteer population correlation between 1.5 T and second generation 3 T systems in the kidneys ranged from r = 0.64-0.88 and in the remaining regions (besides the spleen), r > 0.85. The mean ADC values from most anatomical distributions obtained with the first generation 3 T scanner disagreed with the other two scanners.

Conclusion: A second generation 3 T scanner, which incorporates dual source parallel RF excitation provides nearly identical ADC values compared with the 1.5 T imaging system in abdominal imaging.

B-0449 15:12

Evaluation of T1, T2* and T2 relaxation times in young and aging rat liver at 9.4T

R. Seidel, K. Matthes, A. Mueller, A. Buecker, P. Fries; Homburg/DE (drolandseidel@schlau.com)

Purpose: To assess T1, T2 and T2* relaxation times in healthy rat liver at 9.4 T in vivo and to correlate the influencing effect of aging for determination of an experimental standard.

Methods and Materials: In 20 WAG-Rij rats of 2 different age groups (group 1-N=10: age of 12 weeks, group 2-N=10: age of 2years) liver MRI was performed on a 9.4 T MR animal scanner (Bruker BioSpec, Germany) using 16-channel volume coil. A RARE sequence with four different repetition and echo times was acquired for T1 relaxation time measurement. T2* relaxation time was measured by a multi-gradient echo (MGE) sequence. A multi-slice multiple echo sequence (MSME) was used for T2 relaxation time measurement. T1 and T2 mapping was performed with an image sequence analysis tool. A student t- test and Mann-Whitney rank sum test were performed for statistical analysis (p < 0.05).

Results: The animal groups differed statistically significant regarding all investigated relaxation characteristics. Mean T1 relaxation time for group 1 was 843.80 ms (SD 141.56) and for group 2 663.43 ms (SD 68.96); p=0.001. Mean T2* relaxation time for group 1 was 8.37 ms (SD 0.51) and group 2 6.07 ms (SD 0.75); p < 0.001. Mean T2 relaxation time for group 1 was 23.22 ms (SD 2.48) and group 2 35.81 ms (SD 8.64); p=0.006.

Conclusion: At 9.4 T liver relaxation characteristics in rat liver vary with the age of the animal as a consequence of tissue transformation and have to be considered in experimental settings.

14:00 - 15:30

Room F2

Breast

SS 602

Tomosynthesis and FFDM

Moderators:

M. Michell; London/UK
E. Siopis; Bologna/IT

B-0450 14:00

Specificity: digital breast tomosynthesis versus mammography

G. Gennaro¹, E. Bezzon¹, E. Baldan¹, R. Chersevani², C. di Maggio¹, M. La Grassa³, L. Pescarini¹, I. Polico¹, A. Proietti¹; ¹Padua/IT, ²Gorizia/IT, ³Aviano/IT (gisella.gennaro@ioveneto.it)

Purpose: To analyse the impact of breast tomosynthesis (DBT) on specificity compared to standard digital mammography (MX).

Methods and Materials: The study included 250 consenting women with breast lesions classified as suspicious at mammography and/or ultrasound. A reader study comparing two-view (CC, MLO) mammography, one-view (MLO) tomosynthesis, and the combination of DBT and MX CC-view (DBT+MXCC) was conducted with six breast radiologists and a sample of 469 breasts. Mean area under the receiver operating characteristics curves, sensitivity and specificity were calculated for each modality by averaging results across the readers. Specificity analysis is presented here, refined separately for the two subsets of 201 normal breasts and 200 breasts with benign lesions.

Results: Overall, mean specificity was significantly higher with DBT than MX (86.9% vs. 83.1%, $p=0.025$), while the combined protocol led to higher specificity (not significantly) than MX, but slightly lower than DBT alone (DBT+MXCC: 84.9%). The proportion of benign lesions correctly scored with tomosynthesis, either one-view or with the addition of MXCC, was significantly higher than standard mammography (36.8% MX, 43.4% DBT, 45.6% DBT+MXCC; p -value (DBT vs. MX) = 0.017; p -value (DBT+MXCC vs. MX) = 0.002). The proportion of normal breasts correctly assessed was similar with MX and DBT (87.6% vs. 86.7%, p -value = 0.723), with a small decrease with the combined protocol (84.3%).

Conclusion: Tomosynthesis significantly increased specificity compared to digital mammography. More in detail, DBT significantly improved capability in characterising benign lesions, reducing the number of false positives.

B-0451 14:09

MRI in the pre-operative breast cancer staging before and after the introduction of digital breast tomosynthesis (DBT): has anything changed?

J. Giglio, G. Ghione, E. Regini, M. Durando, A. Luparia, M.C. Eandi, P.P. Campanino, G. Mariscotti, G. Gandini; Turin/IT (jacopo.giglio@gmail.com)

Purpose: To compare the diagnostic accuracy of MRI and conventional imaging techniques (digital mammography [DM] and ultrasound [US]) combined or not with DBT in pre-operative breast cancer assessment and to determine the effects on surgical treatment.

Methods and Materials: We retrospectively reviewed 132 newly diagnosed breast cancer patients (146 operated breasts), who underwent pre-operative conventional imaging modalities and MRI between January 2009 and June 2011. The patients were divided into two groups: those who had DBT in addition to DM and US (group-1:76/132, 88 operated breasts) and those who did not undergo DBT (group-2:56/132, 58 operated breasts). Statistical analyses were performed to compare the diagnostic accuracy of imaging techniques and to evaluate MRI impact on surgical management in the two groups.

Results: In group-1 MRI overall sensitivity was 94.1% (DM+DBT:80.6%, DM+DBT+US:83.1%; $p < 0.05$) and in group-2 93.6% (DM:66.3%, DM+US:73.6%; $p < 0.05$); for multifocal/multicentric lesions was, respectively, 80% (DM+DBT:65%, DM+DBT+US:70%; $p > 0.05$) and 73.3% (DM:46.7%, DM+US:46.7%; $p < 0.05$); for contralateral lesions was 100% in both groups (group-1:DM+DBT:57%, DM+DBT+US:57%; $p < 0.05$; Group-2:DM:50%, DM+US:50%; $p < 0.05$). In group-1 MRI specificity was 72.2% (DM+DBT:77.7%, DM+DBT+US:83.3%; $p > 0.05$) and in group-2 72.7% (DM:81.8%, DM+US:81.8%; $p > 0.05$). Pre-operative MRI changed surgical treatment in 12/88 (14.7%) in group-1 and in 12/58 (20.6%) in group-2, with a conversion from breast conservative surgery into mastectomy, respectively,

in 7/88 (9.0%) and 10/58 (17.2%) ($p < 0.05$). Overall pathologic confirmation of malignancy was, respectively, 8/12 (66.7%) and 9/12 (75%) in surgical specimens. **Conclusion:** DBT combined with DM and US improved conventional imaging accuracy, but MRI still showed the highest sensitivity in detecting and staging breast cancer.

B-0452 14:18

The role of breast tomosynthesis combined with digital mammography

P. Martínez¹, A. Garcia-Lallana², R. Sainz-Mendiguren², C. Minguillon¹, L. Pina²; ¹Zaragoza/ES, ²Pamplona/ES (paulamartinezmiravete@yahoo.es)

Purpose: To evaluate the detection rate of breast cancer using digital tomosynthesis as an additional tool combined with digital mammography in ACR density patterns 2, 3 and 4 in a clinical setting.

Methods and Materials: Retrospective study. From December 2010 to August 2011, 3300 Combo studies (2D-digital mammography plus tomosynthesis) were performed in ACR density patterns 2, 3 and 4 to evaluate the role of the tomosynthesis in the detection of additional cancers. Statistical analysis was performed calculating the Pearson Chi-square test and using the SPSS software.

Results: 54 breast tumours were detected on conventional digital mammography (detection rate 1.63%). Thirty-one additional cancers were detected on tomosynthesis and not seen on standard mammograms: 6 cases on ACR 2 (the detection rate was increased 0.75%), 11 cases in ACR 3 (0.87%) and 14 cases in ACR 4 (1.18%). No statistical differences were found in the detection rate among the three patterns ($p=0.62$). Tomosynthesis increased the detection rate 0.94%, so the total detection rate using the combo studies was 2.57%.

Conclusion: The addition of digital tomosynthesis increases the detection rate from 1.63% to 2.57%. There are not significant differences among the three ACR density patterns, so tomosynthesis can be useful not only in dense patterns but also in pattern 2.

B-0453 14:27

Role of breast tomosynthesis in the morphological analysis of breast lesions

B. Raghavan, M. Rajmohan, G. Sivaramalingam; Chennai/IN (drbagem@gmail.com)

Purpose: To assess the role of breast tomosynthesis (by 3D combo view) versus 2D full field digital mammogram alone in the morphological analysis of breast lesions. To evaluate the potential role of tomosynthesis in BIRADS categorisation and final histopathology.

Methods and Materials: Patients who were referred to our department for mammogram from May 2011 (900 patients) underwent full field digital mammogram and 3D tomosynthesis (combined view). Craniocaudal and mediolateral oblique views of both breasts were acquired for all patients. Of these our study population includes 100 patients with abnormal 2D digital mammogram. 2D digital mammogram and 3D tomosynthesis were analysed for the following features mass, margins, calcification asymmetric density, focal asymmetry and architectural distortion. Following the mammogram all patients were subjected to ultrasound and image-guided FNAC or trucut core tissue biopsy for correlation. Statistical analysis was done to evaluate the performance of tomosynthesis versus 2D digital mammogram in terms of morphology, BIRADS categorisation and histopathology.

Results: There was significant difference between 2D and tomo for feature analysis ($p < 0.05$) and for BIRADS significant difference ($p < 0.05$) was found between 2D and USG/final and no significant difference ($p < 0.05$) was found between 3D and USG/final.

Conclusion: Tomosynthesis was useful in majority of patients in terms of lesion conspicuity and feature analysis. It approximated the final BIRADS after ultrasound and HPE better than 2D digital mammogram alone.

B-0454 14:36

Does combining 3D breast tomosynthesis with digital mammography improve diagnostic accuracy?

N.H. Said, H. Abol Magd, M. Mokhtar, L. Bassam, S. Waheed, D. Salem, A. Selim; Cairo/EG (norranhussein@yahoo.com)

Purpose: To assess the value of adding 3D breast tomosynthesis (BT) to full field digital mammography (DM), for improving lesion visibility and BIRADS assessment in relation to pathological outcomes.

Methods and Materials: 929 cases were evaluated with DM and BT in a dedicated breast imaging unit with diagnostic and screening services. Both DM and BT were performed in craniocaudal and mediolateral oblique views in different exposures using a Siemens Mammomat Inspiration unit. Evaluation and BIRADS scoring was

given to DM followed by BT. A final BIRADS score considering both interpretations and any additional information by ultrasound was later decided.

Results: 70.8% of cases were screening and 29.2% were diagnostic. According to the final assessment categories; 25.3%, 53.3%, 11.2%, 5.5%, 4.7% of cases were given a BIRADS score of 1, 2, 3, 4, 5, respectively. Accuracy, +PP and -PP of DM alone were 96.77, 89.71, 97.33%. On adding BT results were 98.06, 87.5, 99.17%, respectively. Agreement between BT BIRADS and Final BIRADS score was 91.8% (Kappa 0.872). Between DM and Final BIRADS was 81.1% (Kappa 0.710). Between BT and DM BIRADS was 84.8% (Kappa 0.764). Regarding the cancers detected in very dense breasts (more than 75% glandular tissue) DBT could diagnose 76.4%, while only 5.8% were diagnosed by DM. BT added new information in 20% of cases by visualisation of margins, analysis of focal asymmetry and detecting multifocality/multicentricity of cancers.

Conclusion: Adding BT to DM improves accuracy of BIRADS categorisation and radiologic-pathologic correlation

B-0455 14:45

Dutch digital breast cancer screening: implications for breast cancer care

J. Timmers¹, G. den Heeten², E.M. Adang¹, J.D. Otten¹, A.L.M. Verbeek¹, M.J.M. Broeders¹; ¹Nijmegen/NL, ²Amsterdam/NL (j.timmers@lrbc.nl)

Purpose: In comparison to other European population-based breast cancer screening programmes, the Dutch programme has a low referral rate, similar breast cancer detection and a high breast cancer mortality reduction. The referral rate in the Netherlands has increased over time and is expected to rise further, mainly following nationwide introduction of digital mammography. This study explores the consequences of the introduction of digital mammography on the balance between referral rate, detection of breast cancer, diagnostic work-up, and associated costs.

Methods and Materials: Detailed information on diagnostic work-up (chart review) was obtained from referred women (n=988) in 2000-2006 (100% analogue mammography) and 2007 (75% digital mammography) in Nijmegen, the Netherlands.

Results: The average referral rate increased from 15 (2000-2006) to 34 (2007) per 1000 women screened. The number of breast cancers detected increased from 5.5 to 7.8 per 1000 screens, whereas the positive predictive value fell from 37% to 23%. A sharp rise in diagnostic work-up procedures and total diagnostic costs was seen. On the other hand, costs of a single work-up slightly decreased, as less surgical biopsies were performed.

Conclusion: Our study shows that a low referral rate in combination with the introduction of digital mammography affects the balance between referral rate and detection rate and can substantially influence breast cancer care and associated costs. Referral rates in the Netherlands are now more comparable to other countries. This effect is therefore of value in countries where implementation of digital breast cancer screening has just started or is still under discussion.

B-0456 14:54

Dramatic increase in stereotactic core needle biopsy rate and ductal carcinoma in-situ detection after conversion from analogue to digital screening mammography

J. Nederend¹, A.C. Voogd², J.H. Groenewoud³, M.W.J. Louwman¹, L.E.M. Duijm¹; ¹Eindhoven/NL, ²Maastricht/NL, ³Rotterdam/NL (joost.nederend@gmail.com)

Purpose: To determine the impact of implementation of digital screening mammography on stereotactic core needle biopsy (SCNB) rate and ductal carcinoma in-situ (DCIS) detection.

Methods and Materials: We included a consecutive series of 47,737 analogue and 49,946 digital screening mammograms, obtained at a Dutch breast screening region between, respectively, January 2008-July 2009 and July 2009-January 2011. SCNB rate and DCIS detection were determined for both populations.

Results: Referral rate and overall cancer detection rate at digital screening were 3.0% (1502/49,946) and 6.9 (343/49,946) per 1,000 screened women, compared to 1.5% (737/47,737, p < 0.001) and 4.9 (233/47,737, p < 0.001) at analogue screening. At digital screening mammography, 8.1 SCNB procedures (406/49,946) per 1,000 screened women had been performed, compared to 2.4 SCNB procedures (115/47,737) per 1,000 analogue screens (p < 0.001). Positive predictive value of SCNB for breast cancer was 27.3% (111/406) and 37.4% (43/115), respectively, for digital and analogue screening mammography (p=0.04). DCIS was diagnosed in 1.8 women (88/49,946) per 1,000 digital screens, compared to 0.8 (36/47,737) per 1,000 analogue screens (p < 0.001) and DCIS comprised 25.7% of cancers (88/343) detected at digital screening and 15.5% of breast cancers (36/233) detected at analogue screening (p=0.003). Compared to DCIS at analogue screening, DCIS at digital screening tended to be more frequently low grade DCIS or intermediate grade DCIS (63.6% (56/88) vs 47.2% (17/36), p=0.09).

Conclusion: Conversion from analogue to digital screening mammography resulted in a dramatically increased SCNB rate, with a concomitant increased DCIS detection. Over-diagnosis of breast cancer is more profound at digital than at analogue screening mammography.

B-0457 15:03

Conversion from analogue to digital screening mammography results in a more favorable tumour stage and tumour biology of screen-detected cancers

J. Nederend¹, M.W.J. Louwman¹, J.H. Groenewoud², A.C. Voogd³, L.E.M. Duijm¹; ¹Eindhoven/NL, ²Rotterdam/NL, ³Maastricht/NL (joost.nederend@gmail.com)

Purpose. To determine the impact of conversion from analogue to digital screening mammography on tumour stage and tumour biology of screen-detected cancers. **Methods and Materials.** We included a consecutive series of 47,737 analogue and 49,946 digital screening mammograms, obtained at a Dutch breast screening region between, respectively, January 2008-July 2009 and July 2009-January 2011. Tumour stage and biology characteristics were determined for screen-detected cancers.

Results. The overall cancer detection rate was 6.9 (343/49,946) per 1,000 screened women at digital screening (255 invasive cancers and 88 ductal carcinomas in-situ (DCIS), compared to 4.9 (233/47,737) at analogue screening (197 invasive cancers and 36 DCIS, p < 0.001). The proportion of advanced cancers (defined as T2+ and/or lymph node positive cancers) was significantly lower at digital screening (20.4% versus 34.8%, p < 0.001), but tumour size (either T1a-c or T2+) of invasive cancers was comparable to those detected at analogue screening (p=0.7). At digital screening, significantly fewer invasive cancers showed lymph node metastasis (18.8% (48/255) versus 32.0% (63/197), p=0.002). Tumour histology of invasive cancers (either ductal or lobular cancer) was comparable (p=0.6), but invasive cancers detected at digital screening showed a more favourable Nottingham gradation (p=0.01). Proportions of estrogen receptor positive or Her2/Neu receptor positive invasive cancers were similar (p=0.2 and p=0.2, respectively), but the proportion of progesterone receptor positive invasive cancers was larger at digital screening (72.9% (186/255) versus 61.9% (122/197, p=0.01).

Conclusion. Replacement of analogue screening mammography by digital screening mammography had a favourable impact on both tumour stage and tumour biology of screen-detected cancers.

B-0458 15:12

What do we gain by changing from screen film to full field digital mammographic screening?

S. Hofvind¹, C.I. Lee², J.G. Elmore³; ¹Oslo/NO, ²Los Angeles, CA/US, ³Seattle, WA/US (solveig.hofvind@krefregisteret.no)

Purpose: To analyse the effect of prior and current use of screen film mammography (SFM) and full field digital mammography (FFDM) on early outcome measures in screening mammography.

Methods and Materials: Data from women aged 50-69 years screened in the Norwegian Breast Cancer Screening Programme between 1996 and 2009 were included in the study. Recall and detection rate, and positive predictive value from 525,092 initial SFM, 74,420 initial FFDM, 964,853 SFM after a prior SFM, 197,426 FFDM after a prior SFM, and 168,410 FFDM after a prior FFDM were analysed using two-sided Chi-square tests.

Results: The recall rate was 5.5% for initial FFDM (p < 0.001) and 4.6% for initial SFM (p < 0.001). Either the detection rate of DCIS or DCIS and invasive differ statistically significant by initial screening technique. In subsequently screened women, the recall rate was 2.4% for SFM after SFM and for FFDM after SFM, and 2.7% for FFDM performed after a prior FFDM (p < 0.001). The detection rate of DCIS was 0.08% for SFM after SFM, 0.11% for FFDM after SFM (p < 0.001), and 0.11% for FFDM after FFDM (p < 0.001). The rate of invasive cancer was 0.39 for SFM after SFM, 0.41 for FFDM after SFM (p=0.030), and 0.46 for FFDM after FFDM (p < 0.001). The interval cancer rate was 0.15% for SFM after SFM, 0.20% for FFDM after SFM, and 0.20% FFDM after FFDM (p < 0.001 for both).

Conclusion: Early outcome measures in mammographic screening seem to be influenced by the prior and current screening technique.

B-0459 15:21

Improving detection rates of DCIS with digital DR mammography

C.S. Mameri¹, J. Mameri Filho¹, A.C.P. Nazario²; ¹Vitoria ES/BR, ²Sao Paulo/BR (claudiamameri@hotmail.com)

Purpose: To evaluate detection rates of pure ductal carcinoma in situ (DCIS) by film screen mammography and by digital radiographic (DR) mammography in women submitted to annual screening for breast cancer.

Methods and Materials: Prospective study of 17,606 asymptomatic women submitted to annual mammographic screening in two centres. Ten thousand two hundred and ninety-four women in the first group had film screen mammograms and 7,312 women in the second group had digital DR mammograms. All exams were read by the same radiologists. All women on first screening examination were excluded. Biopsy was recommended for lesions suspicious for malignancy, in accordance with BI-RADS® categorisation, and was submitted to pathological examination.

Results: Mean age was 54.3 years in the first group and 52.5 years in the second group. Dense breasts were present in 44.8% of women in the first group and in 46.2% of those in the second group. In the film screen group, 49 of 175 women recommended for biopsy were diagnosed with breast cancer (positive predict value [PPV] =28%), 9 of 49 with pure DCIS (18%). In the digital group, 51 of 152 women recommended for biopsy were diagnosed with breast cancer (PPV=33.5%), 13 of 51 had pure DCIS (25.5%), which was significantly higher than with film screen mammography.

Conclusion: In women undergoing annual screening for breast cancer, digital DR mammography improves detection rates of preinvasive stage compared to that achieved by film screen mammography.

14:00 - 15:30

Room G/H

Head and Neck

SS 608

Oncology

Moderators:

C.Z. Karaman; Aydin/TR
R. Kohler; Geneva/CH

B-0460 14:00

Incidental F-18 FDG positive focal thyroid nodules on PET/CT: evaluation and outcome

J.B. Straiton, S. Bethapudi, F.W. Poon; Glasgow/UK (jack.straiton@nhs.net)

Purpose: 18-F-fluorodeoxyglucose (FDG) accumulation within normal thyroid tissue is low or absent on whole body FDG-PET/CT. As a result of increasing use of this hybrid imaging modality, incidental thyroid FDG uptake is increasingly identified.

Methods and Materials: 6536 cases of FDG-PET/CT performed at our institution between January 2008 and May 2011 were retrospectively reviewed by searching for keyword 'thyroid' within the clinical information/body of report. These cases were reviewed by two independent observers. Patients with established/suspected thyroid malignancy or previous thyroid surgery were discarded. Cases with focal or diffuse thyroid FDG uptake were correlated with clinical, biochemical and cytopathology/histopathology records. 29% (8/28) were malignant (six papillary carcinomas, one anaplastic carcinoma, one squamous cell metastasis). 11% (3/28) were potentially malignant on FNA. 14% (4/28) were indeterminate.

Results: The prevalence of incidental thyroid FDG uptake was 3.7% (242 of 6536) on FDG-PET/CT. Of these, 2.4% (154/6536) demonstrated focal uptake and 1.3% (88/6536) were diffuse. 28 of cases with focal uptake had ultrasound-guided fine-needle aspiration (FNA), core biopsy or post-surgical pathological diagnosis. 46% (13/28) were benign nodules. 29% (8/28) were malignant (six papillary carcinomas, one anaplastic carcinoma, one squamous cell metastasis). 11% (3/28) were potentially malignant on FNA. 14% (4/28) were indeterminate.

Conclusion: The prevalence of incidental thyroid FDG uptake on FDG-PET/CT was 3.7%. The overall incidence of malignancy for focally FDG-avid thyroid nodules was 29%. This study reiterates the importance of obtaining a tissue diagnosis in such patients to exclude synchronous or clinically occult malignancy.

B-0461 14:09

SPECT-CT for the depiction of sentinel lymph nodes in cutaneous head and neck tumours

T.C. Lauenstein, C. Boy, T. Poeppel, I. Stoffels, D. Schadendorf, A. Bockisch, J. Klode; Essen/DE (thomas.lauenstein@uni-due.de)

Purpose: The value of sentinel lymph node excision (SLNE) in patients with cutaneous head and neck malignancies has been controversially discussed. We aimed to assess the diagnostic impact of preoperative SPECT-CT in direct comparison to standard SLNE without SPECT-CT.

Methods and Materials: Data of 48 clinically lymph node-negative patients (age range: 12-86 years) were analysed. Primary tumours included malignant melanoma (n=27) and high risk cutaneous squamous cell carcinoma (n=21). In group A (n=10) a lymphoscintigraphy was performed with either 16 MBq or 80 MBq of Tc-99m-nanocolloid depending on the schedule of the surgical procedure. In group B (n=38) an additional SPECT-CT scan (matrix: 128x128, 128 frames, 25s per frame) of the head and neck region was obtained immediately after lymphoscintigraphy. SLNE was performed during surgery according to the previous imaging results. Operating times for both groups were compared.

Results: 78 SLN were removed in 44/48 patients. The operating time in group B was significantly shorter (median 40 min) than in group A (median 108.6 min; P < 0.001). Due to the exact anatomical localisation of the SLN determined by SPECT-CT, the surgical approach was changed in 9 of 34 patients (26.5%).

Conclusion: SPECT-CT is an innovative imaging technique providing additional information to detect and to excise SLN in patients with head and neck malignancies.

B-0462 14:18

Dose and image quality of high-pitch dual source CT for the evaluation of cervical lymph node status: comparison to regular 128-slice single source CT

R.W. Bauer, L. Holthaus, B. Schell, M. Beeres, F. Al-Butmeh, T.J. Vogl, J.M. Kerl; Frankfurt a. Main/DE (ralfwbauer@aol.com)

Purpose: Patients with malignant lymphoma regularly undergo CT of the neck for the evaluation of lymph node status with relevant dose exposure. We compared a novel high-pitch dual source CT (DSCT) protocol with our standard single-source CT protocol in terms of dose and conspicuity of cervical lymph node levels.

Methods and Materials: Each 30 patients underwent either contrast-enhanced high-pitch DSCT (group 1; pitch 3.0) or regular single-source CT (group 2; pitch 0.8) of the neck on the same CT device (Definition Flash, Siemens) at 120 kV/180 mAs. Automated exposure control was used in both groups. Images were reconstructed at 2-mm thickness with a medium soft kernel (B30f). CT DIvol, DLP and background noise (BN) were compared. Two radiologists rated diagnostic image quality and artefact burden (1 = excellent image quality/no artefacts, 5 = no reliable diagnosis possible/heavy artefacts).

Results: Mean CT DIvol (5.6±0.9 vs. 12.9±1.1 mGy) and DLP (182±34 vs. 357±39 mGycm) were significantly (p = 0.003) lower in group 1, while BN was significantly higher (6.7±1.4 vs. 4.2±0.4 HU; p = 0.001). This did not affect diagnostic image quality, since subjective image quality (1.2±0.4 vs. 1.1±0.3) and artefact burden (1.7±0.7 vs. 1.3±0.5) were not rated significantly different between both groups (p = 0.54 and 0.29).

Conclusion: High-pitch DSCT of the neck allows for a significant reduction of dose while diagnostic image quality is preserved in patients undergoing cervical lymph node staging for malignant lymphoma. Especially in young adults radiation delivered to the thyroid gland and eye lens is of important matter.

B-0463 14:27

Management of head and neck carcinoma of unknown primary: the diagnostic accuracy of F-18 FDG-PET/CT in detection of the clinically occult tumour

J.B. Straiton, S. Bethapudi, A. McCallum, S. Han; Glasgow/UK (jack.straiton@nhs.net)

Purpose: Carcinoma of unknown primary (CUP) represents 3-7% of all head and neck malignancies and poses significant demands on otorhinolaryngology departments. Squamous cell carcinomas account for 70-90%. Traditional evaluation of metastatic cervical lymphadenopathy includes clinical examination, fiberoptic-laryngoscopy/nasopharyngoscopy, cross-sectional imaging (CT/MRI) and panendoscopy with directed biopsies ± tonsillectomy. The disease follows an aggressive course with median survival of 2-10 months. Our aim was to review the diagnostic accuracy of FDG-PET/CT in cases of CUP in the West of Scotland.

Methods and Materials: Clinical records and imaging reports of 63 consecutive patients with metastatic cervical lymphadenopathy and occult primary tumour

(despite clinical/radiological workup) presenting to our institution for FDG-PET/CT were retrospectively reviewed. There were 43 males and 20 females with a mean age of 58.3 years (range = 37-86). FDG/PET-CT images/reports were independently reviewed by two observers and compared with gold standard histopathology.

Results: FDG-PET/CT correctly detected 26 occult primary tumours in 63 patients (detection rate 41.3%). There were 17 true negatives, in which no extranodal malignancy was proven. There were 11 false negatives in which an underlying primary tumour was established by other methods despite negative PET/CT. There were 9 false positives in which directed search established no histological diagnosis at the site of concern on FDG-PET/CT. Sensitivity and specificity were 70.3% and 65.4%, respectively. Positive predictive value 74% and negative predictive value 61%. Overall accuracy 68%.

Conclusion: For a majority in this challenging subgroup of patients, FDG-PET/CT contributes positively when conventional diagnostic pathways have failed to establish a primary tumour.

B-0464 14:36

Comparison of contrast-enhanced PET-CT and MRI in patients with head and neck cancer

T.J. Vogl, N. Rode, T. Stoeber, R. Sader, I. Burck, M. Harth, F. Gruenwald; Frankfurt/DE (t.vogl@em.uni-frankfurt.de)

Purpose: To retrospectively compare combined 18F-fluorodeoxyglucose positron-emission-tomography/computed-tomography (18F-FDG PET-CT) to contrast-enhanced magnetic-resonance-imaging (MRI) in the diagnosis of head and neck cancer regarding diagnostic accuracy and tumour volumetry.

Methods and Materials: Within 13 days 18F-FDG PET-CT and MRI were performed in oral cavity SCC (n=41;23 primaries/18 recurrent tumours) and within 5 days in Hodgkin lymphoma (n=12;10 primaries/2 recurrent tumours). Evaluated parameters were tumour localisation, tumour diameter, tumour volume, lymph nodes, distant metastases.

Results: In oral cavity SCC diagnostic accuracy was as follows: accordance of MRI=PET-CT:78%; MRI-positive/PET-CT-negative:9.8%, MRI-negative/PET-CT-positive:0%, MRI-positive/PET-CT-unclear:4.9%, MRI-negative/PET-CT-unclear:2.4%; PET-CT-positive/MRI-unclear:2.4%, PET-CT-negative/MRI-unclear:2.4%. Average maximum standardised uptake-values (SUV-max) in PET-CT findings were measured to be 6.43. In tumour volume and expansion PET-CT vs. MRI showed larger volume in 39%, MRI vs. PET-CT larger volume in 39%, PET-CT equaled MRI in 19.5%. In 2.4% no evaluation was possible. Regarding lymph node evaluation MRI equaled PET-CT. In 19.5% distant metastases were detected via 18F-FDG PET/CT. In Hodgkin lymphoma there was no statistically significant difference between the two modalities regarding pathological findings. Concerning lymphoma expansion PET-CT was superior to MRI in 13.9%, MRI was superior to PET-CT in 19.4% and in other patients MRI equaled PET-CT. Concerning lymph node numbers MRI equaled PET-CT in size and morphology. In 8.3% suspect extra-cervical findings were revealed by 18F-FDG PET/CT.

Conclusion: In summary, MRI was equal to PET-CT regarding accuracy. Concerning volumetry MRI had some advantages vs. PET-CT. 18F-FDG PET/CT easily identified distant lymph node metastases. Maximum standardised uptake-values (SUV max> 2.5) in PET-CT is reliable for evaluating lymph node metastases.

B-0465 14:45

Pre- and intraoperative determination of tumour extent and bone infiltration in the head-and-neck region: a comparison of multislice computed tomography (MSCT), high-resolution flat-panel volumetric CT (VCT), and histopathologic methods

E. Alejandro Lafont, H. Schaaf, T. Mueller, M. Obert, H.-P. Howaldt, G. Krombach, E. Gizewski; Giessen/DE

Purpose: To assess if VCT, as a high-resolution bone imaging modality, can intraoperatively supplement frozen-section analysis to establish the depth of tumour infiltration. To validate the VCT-approach, we compared CT, VCT, and histopathology results for tumour-extent.

Methods and Materials: Head-and-neck tumours of 92 patients were preoperatively staged with CT. Perioperative VCT of the resected specimen was used to supplement frozen section analysis. Bone destruction was compared for the VCT, CT, and frozen-section methods before the results were relayed to the surgeon, who adjusted the resection procedure as necessary. Staging-CT and final histopathology results were compared postoperatively. 51 patients were not included in the final evaluation because either histopathology or CT results were incomplete.

Results: CT determined a larger tumour size than histology in 13 cases (mean difference 7 mm), a smaller size in 14 cases (mean difference 10 mm), and approximately equal sizes in 25 cases. In a comparison of tumour extent with CT,

VCT, and histopathologic methods, results were approximately equal in 34 cases, although VCT best visualised the extent of bone destruction. In 18 cases, the CT results differed from those determined by VCT and histology.

Conclusion: Computed tomography is a sound method for determining tumour extent. VCT can accurately determine bony infiltration. It is thus a valid intraoperative supplement to frozen section analysis and can aid the resection and reconstruction strategy. Secondary reconstructive surgery can be avoided, thereby increasing patients' life-quality and decreasing total therapy costs.

B-0466 14:54

Radiochemotherapy-induced changes of local tumour blood supply estimated by DCE-CT in head and neck tumours

A. Abramjuk, V. Hietschold, K. Zoepfel, S. Appold, R. von Kummer, N. Abolmaali; Dresden/DE (Andrij.Abramjuk@Uniklinikum-Dresden.de)

Purpose: Radiochemotherapy (RChT) is considered standard treatment for non-operable head and neck tumours (HNT). Primary aim of our study was to investigate RChT-induced changes of local tumour blood supply parameters relative tumour blood volume (rTBV) and transfer coefficient (Ktrans) derived from DCE-CT in HNT.

Methods and Materials: 15 patients with non-operable HNT (Stages III-IV) scheduled for RChT were included. Chemotherapy consisted of cisplatin during all 6 weeks of radiotherapy and 5-fluorouracil during first week only. DCE-CT was performed before RChT, in two weeks (20Gy) and five weeks (50Gy) using Biograph 16 (Siemens). rTBV and Ktrans were determined by modified Patlak analysis using pixel-based software (VPCT, Siemens). Dynamics of rTBV and Ktrans were analysed during RChT and in 12 months follow-up.

Results: In 11 patients an increase of rTBV and/or Ktrans after 20Gy, followed by a decrease of both parameters after 50 Gy was noted. Except for one patient with local recurrence, complete tumour response during follow-up was diagnosed in 10 patients. In 3 patients an increase of rTBV with concomitant drop of Ktrans under RChT was detected. Morphologically, in all 3 patients a partial tumour response was established. In 1 patient showing an elevation of both rTBV and Ktrans during RChT local tumour progress was detected during follow-up.

Conclusion: Estimated by DCE-CT radiochemotherapy-induced changes of rTBV and Ktrans may represent a modification of local tumour blood supply as a function of intratumoral oxygen distribution and, consequently, reveal clinical impact allowing individualisation of RChT strategy in patients with HNT.

B-0467 15:03

Dynamic contrast-enhanced T1-weighted MR imaging to distinguish tumour recurrence from scar after treatment in patients with head and neck neoplasms: a pilot study

C. Gaudino, R. Csernus, S. Heiland, M. Bendszus, S. Rohde; Heidelberg/DE (chiara.gaudino@med.uni-heidelberg.de)

Purpose: In follow-up imaging of patients with head and neck neoplasms it is often difficult to distinguish tumour recurrence from scar after treatment. Aim of this study is to analyse if perfusion curve-patterns help to differentiate tumour from scar.

Methods and Materials: MRI-perfusion data of 31 patients (17 men; mean age 64 years) with suspicious enhancing lesions of the oropharynx or the oral cavity were analysed. In 17 patients primary or recurrent squamous-cell carcinoma was diagnosed histologically, in 14 patients scar was diagnosed histologically (n=4) or by long-term radiological follow-up (> 6 months). Dynamic contrast-enhanced MRI were performed on a 3-Tesla-scanner (Tim-Trio, Siemens, Erlangen/Germany) using a volumetric interpolated breath-hold examination (VIBE) T1-weighted sequence (TR/TE 4.66/1.53 msec; slice 3 mm; FOV 220 mm; 38 measurements of 7.8s; flow 3.5 ml/s). Perfusion data were post-processed on a region-of-interest (ROI) basis using the mean-curve software (Siemens, Erlangen/Germany) obtaining signal intensity-time S (t) curves. In each suspect lesion four ROIs were positioned in consensus of two radiologists. For each S (t)-curve (1) maximal intensity value (Pmax) and (2) time to peak (TTP) were analysed.

Results: Mean S (t)-curves of the two groups were significantly different. Tumour showed a fast wash-in (TTP= 22.5±17s) with a high Pmax (1.83±0.80; range 0.73-3.48); scar had a slower wash-in (TTP= 98.1±76s; p < 0.001) with a lower Pmax (0.77±0.57; range 0.3-1.81; p < 0.001).

Conclusion: Perfusion S (t)-curve pattern of head and neck squamous-cell carcinomas is significant different to perfusion S (t)-curve pattern of scar following treatment. Dynamic contrast-enhanced MRI could be helpful in follow-up of patients with head and neck tumours.

B-0468 15:12

Do apparent diffusion coefficient and histological characteristics of squamous cell carcinoma of the oral cavity correlate?

L. Bonello, L. Preda, G. Petralia, P. Summers, C. Giannitto, M. Bellomi; *Milan/IT* (luke.bonello@ieo.it)

Purpose: To correlate apparent diffusion coefficient (ADC) with histological characteristics of squamous cell carcinoma of the oral cavity.

Methods and Materials: 66 patients with untreated histologically proven squamous cell carcinoma underwent conventional (including T2-weighted and T1 pre- and post-contrast) and diffusion-weighted MRI (b-values 0, 50, 250, 500 and 900s/mm²). The ADC for oral cavity tumours were calculated from regions of interest drawn manually on the highest b-value images using the ImageJ (ImageJ, NIH) and fsl (fsl 4, University of Oxford) image processing packages. The ADC for the tumour volume obtained was correlated with histological characteristics (TNM, Grading).

Results: Of the eligible patients, 53 (35 males, 18 females, mean age 56.0, range 26-77 years) were suitable for ADC calculation. Nine patients were excluded due to the presence of artefacts, and 4 due to inability to visualise the tumour on the diffusion-weighted sequences. The mean ADC value was 1123 ± 163 mm²/s, and mean size 33.5 ± 13.3 mm. ADC did not correlate with tumour stage or grade. ADC was significantly lower (p=0.025) for N2 (n=26) stage tumours when compared to N1 (n=8) stage. No other differences were observed between T stages, N stages or tumour Grading.

Conclusion: In our cohort we did not observe clinically relevant differences in ADC values in squamous cell carcinoma of the oral cavity.

B-0469 15:21

Macrobiopsies for head and neck cancers

J. Janssens¹, M. Deleu²; ¹Hasselt/BE, ²Tienen/BE (jaak.janssens@interventionaloncologysociety.org)

Purpose: Contemporary medical treatments for head and neck (H&N) cancers increasingly use targeted therapies that are selected by molecular biomarkers. To allow these personalised diagnostics macrobiopsies are preferred. This study evaluates the use of the Spirotome macrobiopsy system in H&N cancers for providing high-quality tissue specimen.

Methods and Materials: 49 patients with a mass in the H&N region were selected for biopsy in 3 regional hospitals. Mild anticoagulation was allowed. The biopsy site was studied with regard to access route and critical organs by ultrasound, CT and/or MRI. The Spirotome (MedInvents NV, Belgium) was used as macrobiopsy system. Sample quality was evaluated with regard to volume, length, diameter and histological/immunohistochemical diagnosis and molecular biology. Patient tolerance and both early and late complications were recorded.

Results: In all 49 patients the anticipated procedure could be performed without complications or major side effects. Tolerance was good with only minimal pain in 6 patients. In all cases minimal bleeding could be stopped during the procedure. No hospitalisation or prolonged stay was necessary. Where appropriate (n= 34) complete histological, immunohistochemical and molecular biology could be performed. In 9 patients only benign reactive lymph node tissue could be harvested. In 1 patient an abscess was recorded. In 8 patients an incomplete pathological protocol was given due to reimbursement restrictions.

Conclusion: The Spirotome macrobiopsy provides sufficient and high-quality tissue volume in H&N cancers to allow all molecular biology and histological tests for optimal diagnosis without hospitalisation or major side effects.

14:00 - 15:30

Room L/M

Molecular Imaging

SS 606

Hybrid imaging: PET-CT and MR-PET

Moderators:

K. Åhlström Riklund; *Umeå/SE*
L.S. Politi; *Milan/IT*

B-0470 14:00

Role of 18FDG PET-CT in the follow-up of paediatric patients with Ewing sarcoma and primitive neuroectodermal tumour

E.A. Al-alawi, A. Al-sugair, A. Javed, A. Al-Gafri, A.I. Almuhaideb, A. Fathala, M. Tuli, M.M. Abouzied; *Riyadh/SA* (zied@buffalo.edu)

Purpose: We are aiming to evaluate the diagnostic performance of 18F FDG PET-CT in the follow-up of paediatric patients with Ewing Sarcoma and primitive neuroectodermal tumour (PNET).

Methods and Materials: Eighty two consecutive PET-CT scans were performed in thirty-nine paediatric patients with histopathological proof of Ewing's sarcoma in 36 patients and PNET in three patients (28 males, 11 females) average age of 14 years (range 2-14 years). FDG-PET-CT was performed to evaluate a suspected local recurrence and to rule out distant metastases. Histology (n=10) or follow-up clinically and radiologically (n=29) for at least 6 months (range 6- 62 months) were employed as the standard of reference for imaging findings.

Results: PET-CT was true negative in 30 patients in excluding local recurrence. Only one false negative study in a patient developed local recurrence at four months post-scanning with an overall negative predictive value of 91%. On the other hand, PET-CT was true positive in five patients and false positive in one patient in whom the histopathological examination revealed fibroblastic proliferation, giant cell reaction and no viable tumour with an overall positive predictive value of 83%. Overall, PET/CT had an accuracy of 89.7%. PET/CT depicted distant lung metastatic disease in ten patient and bone metastases in two patients requiring further chemotherapy.

Conclusion: PET/CT is a useful diagnostic tool in the follow-up of patients with Ewing sarcoma particularly in excluding local and distant disease with high diagnostic accuracy. False positive findings might be related to therapy-induced inflammation.

B-0471 14:09

Low-dose non-enhanced CT versus full-dose contrast-enhanced CT in integrated FDG-PET/CT studies for the diagnosis of ovarian cancer recurrence

K. Kitajima, Y. Ueno, K. Suzuki, Y. Onishi, M. Kita, T. Yoshikawa, Y. Ohno, M. Senda, K. Sugimura; *Kobe/JP* (kitajima@med.kobe-u.ac.jp)



Purpose: To evaluate low-dose non-enhanced CT (ldCT) and full-dose contrast-enhanced CT (ceCT) in FDG-PET/CT studies for restaging of ovarian cancer.

Methods: One hundred women who had undergone treatment for ovarian cancer underwent a conventional PET/CT scans with ldCT, and then ceCT. Two observers interpreted and decided in consensus on the PET/ldCT and PET/ceCT images by a 3-point scale (N: negative, E: equivocal, P: positive) per patient and lesion. Final diagnoses were obtained by histopathological examinations, or clinical follow-up for at least six months.

Results: Patient-based analysis showed that the sensitivity, specificity, and accuracy of PET/ceCT were 86.8% (33/38), 95.2% (59/62), and 92.0% (92/100), respectively, whereas those of PET/ldCT were 78.9% (30/38), 91.9% (57/62), and 87.0% (87/100), respectively. Sensitivity, specificity, and accuracy did not significantly differ between two methods (McNemar test, p=0.25, p=0.48, and p=0.073, respectively). There were 86 sites of lesion recurrence: 28 peritoneum, 15 pelvic lymph node (LN), 14 para-aortic LN, 11 local recurrence, 6 liver, 6 supraclavicular LN, 4 mediastinal/hilar LN, and 2 lung. The scales of detecting 86 recurrent regions were N:11, E:5, P:70 for PET/ceCT, and N:12, E:14, P:60 for PET/ldCT, respectively. Nine equivocal regions (2 local, 2 peritoneum, 2 pelvic LN, para-aortic LN, supraclavicular LN and liver) and one negative regions (liver) by PET/ldCT were correctly interpreted as positive by PET/ceCT.

Conclusion: PET/ceCT is an accurate imaging modality for the assessment of ovarian cancer recurrence with certainty, reducing the frequency of equivocal interpretations.

B-0472 14:18



Early bone marrow (BM) metastases: metabolic data using 18 F-fluorodeoxyglucose (FDG) PET/CT versus CT imaging

A. Panunzio, L. Evangelista, A.R. Cervino, M. Gregianin, G. Salandri, P.C. Muzzio, R. Polverosi; *Padua/IT (annaloripanunzio@libero.it)*

Purpose: To assess the diagnostic role of FDG-PET/CT vs. CT in early metastatic deposit in BM.

Methods and Materials: 198 patients, 33% with lung cancer, 33% with breast cancer, 29% with lymphoma and 5% with multiple myeloma were retrospectively examined. All patients underwent FDG-PET/CT and CT for disease evaluation. At the time of PET/CT none of the patients were receiving cytokine therapy. All scans were reviewed by a radiologist and a nuclear medicine physician. BM metastases were confirmed by sequential PET/CT or MRI when available. The images of PET/CT and CT were compared. A patient-based analysis was performed.

Results: 94 (48%) patients had positive and 104 (52%) negative CT scan, whereas 110 (56%) had positive and 88 (44%) negative PET/CT for bone lesions. The imaging findings were concordant in 178/198 (90%) patients, while 20/198 (10%) had discordant imaging results (Chi-square test; $p < 0.001$). 21/178 (12%) concordant patients had BM lesions at PET/CT, whereas 9 out of 20 (45%) patients had BM involvement. Therefore, PET/CT was able to identify 27/198 (14%) patients with confirmed BM lesions. In these latter patients, the standardised uptake value for BM metastases was 7.9 ± 4.5 (range: 3.1-19.0), resulting weakly higher in patients with negative than positive CT scan (8.3 ± 5.1 vs. 7.8 ± 4.3 , respectively; t-student test $p=0.79$).

Conclusion: PET/CT is more accurate than CT in detection of BM metastases; its inclusion in diagnostic algorithms changed the staging in about 15% of patients. PET/CT detects BM lesions directly based on their degree on metabolic activity either than by altered anatomy.

B-0473 14:27

CT protocols in [18 F]-FDG-PET/CT examinations: is there an additional benefit of contrast-enhanced CT in the differentiation of incidental gastrointestinal FDG uptake?

C. Brendle, C. Schraml, T. Kratt, M. Reimold, C. Pfannenbergl; *Tübingen/DE (cornelia.brendle@med.uni-tuebingen.de)*

Purpose: Evaluation of the possible benefit of contrast-enhanced (CE) CT in comparison to low dose (LD) CT in [18 F]-FDG-PET/CT for the further evaluation of incidental gastrointestinal FDG uptake.

Methods and Materials: From a database of 5045 patients with FDG-PET/CT, a subgroup of 60 patients with incidentally detected gastrointestinal PET lesions and a PET/CT scan including a multiphase (LD for AC + CE) CT protocol was retrospectively analysed. The PET lesions were categorised concerning their CT patterns (mass/inflammation/unspecific/normal) separately for both CT protocols. The imaging findings were correlated with the results of endoscopy or surgery.

Results: 62 incidental gastrointestinal PET lesions were found in the group of 60 patients. The PPV for a corresponding endoscopic pathology in these lesions was 0.81 for CECT and 0.70 IDCT. All 17 malignancies were correctly detected by CECT (sensitivity 100%) in comparison to only 5 detected malignancies by IDCT (sensitivity 29%). Premalignant lesions in endoscopy (10/62) were detected in 50% by CECT and 10% by IDCT, the 18 benign findings (inflammations and benign masses) in 44% by CECT and 6% by IDCT. The false negative rate in IDCT was higher than in CECT (69% versus 31%). False positive results due to physiological FDG uptake (17/62 lesions) could be excluded neither by CECT nor by IDCT.

Conclusion: CECT provides additional benefit in detecting incidental gastrointestinal malignancies. However, endoscopy of incidental gastrointestinal PET lesions cannot be spared due to a substantial percentage of false negative results in both CT protocols regarding premalignant and benign lesions.

B-0474 14:36

Additional value of "dual phase" 18 F-FDG PET-CT in recurrent gynaecological malignancies

G. D'Angelo, P. Mirk, V. Rufini, M. Calcagni, A. Di Legge, A. Testa, G. Scambia, A. Giordano, L. Bonomo; *Rome/IT (pmirk@rm.unicatt.it)*

Purpose: To prospectively evaluate the usefulness of "dual phase" PET-CT in suspected recurrences from gynaecological malignancies.

Methods and Materials: 45 patients with suspected recurrences from previously treated gynaecological cancer underwent both whole body PET-CT at 1 hr after 18 F-FDG injection (standard PET-CT) and delayed PET-CT of the abnormal area at 3 hrs post-18 F-FDG injection (dual phase PET-CT). Besides qualitative evalu-

ation, semiquantitative criteria used were standardised uptake value of early and delayed images, and retention index of the lesions.

Results: Per-patient analysis: 32/45 patients were confirmed to have recurrence and 13 to have benign lesions. Standard PET-CT detected recurrent tumour in 27/32 patients (84%), whereas delayed scan was true positive in 32/32 (100%). Standard PET-CT correctly excluded malignancy in 6/13 patients (46%) and was false positive in 7/13 (54%), whereas delayed scan was true negative in 10/13 (77%) and false positive in 3/13 (23%). Per-lesion analysis: 49 lesions were confirmed to be malignant and 18 benign. Standard PET-CT correctly identified 39/49 tumour lesions (79%) whereas at delayed scan all 49 lesions were true positive (100%). Standard PET-CT correctly excluded malignancy in 7/18 (39%) and was false positive in 11/18 (61%), whereas delayed scan was true negative in 13/18 lesions (74%) and false positive in 5/18 (26%). Mean RI was +33.1% (range +5.2-+104%) in malignant lesions and -7.03% (range -77.8% - +80%) in benign lesions. **Conclusion:** Dual phase PET-CT is a valuable tool in patients with suspected recurrence of gynaecological cancer and may impact on patient management.

B-0475 14:45

Whole body PET/CT compared to whole body MRI in the diagnosis of sclerotic bone metastases

S.M. Shaikh; *Hyderabad/IN*

Purpose: Aim of the study was to evaluate the diagnostic value of contrast-enhanced PET/CT using F-18 FDG compared to whole body MRI (WB-MRI) in the diagnosis of sclerotic bone metastases.

Methods and Materials: In a retrospective blinded study 58 patients with suspected sclerotic skeletal metastases underwent PET/CT as well as WB-MRI with the use of parallel imaging. PET/CT was acquired after administration of F-18 FDG, which followed by with a MR by 1.5 T MRI system coronal T1-weighted- and STIR-sequences of the entire body and sagittal imaging of the spine were performed.

Results: Sclerotic bone metastases were confirmed in 46 patients WB-MRI, but was missed in 2 patient during initial PET/CT reading. WB-MRI rated 102 lesions as suspicious for malignancy, out of them 96 lesions turned out to be metastatic. PET/CT described a number of 84 lesions as metastatic, which was lower as compared to WB-MRI. Most malignant lesions missed by PET/CT were located in the extremities. PET/CT was more sensitive in detecting malignant lesions of the lumbar spine (WB-MRI n=9 vs PET/CT n=10). The lesions missed by WB-MRI were located in the spine (n=8) and rib cage (n=4). 25 lesions were identified as benign during follow-up. PET/CT rated 20 of these 25 lesions correctly as probably benign, WB-MRI only 19. WB-MRI falsely diagnosed metastatic bone disease in one healthy patient.

Conclusion: WB-MRI delineates more sclerotic bone metastases compared to PET/CT.

B-0476 14:54

Diagnostic accuracy of virtual FDG-PET/CT bronchoscopy for the detection of lymph node metastases in non-small cell lung cancer patients

T.A. Heusner¹, J. Treffert², B. Geiger³, V. Hartung⁴, M. Herbrich⁴, M. Forsting⁴, G. Antoch¹; ¹Düsseldorf/DE, ²Knoxville, TN/US, ³Princeton, NJ/US, ⁴Essen/DE (heusner@med.uni-duesseldorf.de)

Purpose: The aim was to determine: (a) the diagnostic accuracy of the FDG-PET/CT bronchoscopy for the detection of mediastinal, hilar, interlobar and lobar lymph node metastases in non-small cell lung cancer (NSCLC) patients; (b) the smallest bronchus diameter accessible by virtual FDG-PET/CT bronchoscopy; (c) the time duration from starting the viewing tool until virtual FDG-PET/CT images were displayed.

Methods and Materials: 61 NSCLC patients underwent FDG-PET/CT. From these source data virtual FDG-PET/CT bronchoscopies were reconstructed. The time duration from starting the tool till the display of virtual bronchoscopy images was determined. The diagnostic accuracy of FDG-PET/CT bronchoscopy for the detection of regional lymph node metastases was evaluated on a lesion basis. Axial FDG-PET/CT scans served as the standard of reference. The smallest bronchus diameter accessible by FDG-PET/CT bronchoscopy was measured.

Results: The sensitivity, specificity, positive predictive value (PPV), negative predictive value (NPV) and accuracy of virtual FDG-PET/CT bronchoscopy for the detection of lymph node metastases was 76%, 87%, 85%, 79% and 81%. The mean smallest diameter of accessible bronchi by FDG-PET/CT bronchoscopy was 3 mm. The mean time duration from starting the virtual FDG-PET/CT bronchoscopy tool till the display of the images was 22 ± 7 seconds.

Conclusion: Virtual "fly-through" 3D FDG-PET/CT bronchoscopy is feasible in clinical routine, yields a relatively high diagnostic accuracy for the detection of regional lymph node metastases and has access to bronchi even in the periphery of the lung.

B-0477 15:03

Does simultaneous image acquisition by a hybrid MR-PET system result in a better registration quality of PET and morphologic data compared to sequential image acquisition by PET-CT?

C. Brendle, C. Pfannenberger, H. Schmidt, C. Wuerslin, N. Schwenzer; Tübingen/DE (*cornelia.brendle@med.uni-tuebingen.de*)

Purpose: Recently established hybrid MR-PET allows for simultaneous acquisition of PET and MR data in contrast to conventional sequential PET-CT. The purpose of this study was to evaluate the registration quality of MR-PET compared to PET-CT in abdominal organs.

Methods and Materials: The datasets of 10 patients with MR-[18 F]-FDG-PET and [18 F]-FDG-PET-CT examinations at the same day were separately fused by automatic rigid registration and then displayed on a viewing station (TrueD, Siemens Healthcare, Erlangen, Germany). The exterior slice positions of liver, spleen, kidneys and urinary bladder were assigned blinded for the two PET and the two morphologic datasets in x-, y- and z-direction. Cumulative deviation vectors of the alignment were calculated for each organ and both modalities. Significance was tested with Wilcoxon test.

Results: The alignment in MR-PET as well as PET-CT images was very exact. The mean cumulative deviation (mm) of MR-PET/PET-CT was 5.6/11.1 for liver ($p=0.019$); 6.1/9.4 for spleen ($p=0.2159$); 5.2/7.2 for right kidney ($p=0.9095$); 4.9/5.3 for left kidney ($p=0.5194$) and 5.5/9.3 for urinary bladder ($p=0.0467$). PET-CT showed distinctly worse alignment of the data for one patient in the upper abdominal organs and for another patient in the urinary bladder.

Conclusion: In single cases PET-CT shows large deviations of the whole dataset. The simultaneous data acquisition of hybrid MR-PET leads to a significantly improved alignment of metabolic and morphologic datasets in the liver and urinary bladder and can reduce anatomical deviations due to breathing and patient movement as well as different filling states of the urinary bladder.

B-0478 15:12

Molecular imaging of breast tumours with MR-PET

K. Pinker-Domenig, H. Bickel, W. Bogner, S. Gruber, H. Magometchnigg, B. Brueck, M. Scherthner, T.H. Helbich; Vienna/AT (*katja.pinker@meduniwien.ac.at*)

Purpose: To prove that that molecular imaging of breast tumours with proton MR spectroscopy, diffusion-weighted imaging, contrast-enhanced MRI and positron-emission tomography improves diagnostic accuracy, sensitivity and specificity in cancer diagnosis.

Methods and Materials: 49 patients with a suspicious breast were included in this IRB approved prospective study. All patients were examined with dedicated 18 FDG-PET-CT and 3 T multiparametric MRI of the breast. MRI protocol included: a diffusion-weighted sequence (DWI), a T2-w sequence and a contrast-enhanced 3D-T1-w sequence (CE-MRI) before and after application of a standard dose Gd-DOTA. After injection of approx. 300 MBq 18 F-FDG based on the patients weight PET-CT was acquired in the prone position allowing the same patient geometry in breast MRI. CT data were used for attenuation correction. Co-registration of imaging data and image fusion were performed. MR-PET was assessed for lesion morphology and EH-kinetics according to BIRADS, restricted diffusivity, increased Choline (Cho)-levels and 18 FDG-avidity. An ADC threshold $1.25 \times 10^{-3} \text{ mm}^2/\text{s}$ and a signal-to-noise ratio of the Cho resonance peak > 2.55 were defined as a marker of malignancy. Lesions classified as positive when 18 F-FDG-uptake was greater than blood-pool activity. All lesions were histopathologically verified.

Results: Multimodal multiparametric MR-PET achieved an excellent sensitivity of 100% and good specificity of 81% in the diagnosis of breast cancer. Diagnostic accuracy was 94%. MR-PET increased sensitivity in the diagnosis of lymphnode metastases from 71% to 88% compared to MRI alone.

Conclusion: Molecular imaging of breast lesions with MR-PET increases sensitivity, specificity and diagnostic accuracy in the diagnosis of breast cancer and lymphnode metastases.

B-0479 15:21

Bone tissue and body region-specific variability of errors in SUV values: implications on attenuation correction methods in MR-PET

A. Samarin, C. Burger, D.W. Crook, I.A. Burger, D.T. Schmid, G.K. von Schulthess, F.P. Kuhn; Zurich/CH (*andrei.samarin@regionaalhaigla.ee*)

Purpose: The purpose of this study was to evaluate the need for accurate bone segmentation in MR-based AC for whole body MR-PET imaging.

Methods and Materials: In 22 patients who underwent integrated sequential PET/CT-3 T MR imaging, modified CT AC maps were produced by replacing pixels with

values > 100 HU representing mostly bone structures, by tissue with a constant value of 36 HU corresponding to soft tissue, thereby simulating current MR-derived AC maps. The error of mean standardised uptake value (SUVmean) of 141 osseous lesions and 50 soft tissue lesions adjacent to bones for modified PET images was calculated using standard PET image as reference.

Results: Substitution of bone by soft tissue values in AC maps resulted in an underestimation of SUVmean in osseous and soft tissue lesions adjacent to bones of $11.2 \pm 5.4\%$ (min 1.5%, max 30.8%) and $3.2 \pm 1.7\%$ (min 0.2%, max 4%), respectively. Analysis of the spine and pelvic osseous lesions revealed a substantial dependence of the error on lesion composition. For predominantly sclerotic and osteolytic spine lesions, the average underestimation was $15.9 \pm 3.4\%$ and $7.2 \pm 1.7\%$, respectively.

Conclusion: CT-simulation of treating bone as soft tissue in MR-AC maps for PET leads to a substantial underestimation of tracer uptake in bone lesions and depends on lesion composition, the largest error being seen in sclerotic lesions. Therefore, depiction of cortical bone and calcified areas in MR AC maps is necessary for accurate quantification of tracer uptake values in MR-PET imaging.

14:00 - 15:30

Room N/O

Emergency Radiology

SS 617

Trauma and chest pain

Moderators:

R. Polverosi; Padua/IT

H. Ringl; Vienna/AT



B-0480 14:00

Whole body CT for trauma: strategies to justify radiation dose using the injury severity score

A.A. Lemos, R. Brambilla, M. Firetto, P. Biondetti; Milan/IT (*alessandrolemos@hotmail.com*)

Purpose: Patients who have sustained multiple trauma are often young and the radiation doses confer a lifetime cancer risk of up to 1/500. These scans have to be fully justified either in terms of imaging findings or in potential change in management. The purpose of our study was to evaluate whether targeted region-specific CT (focused CT) can replace whole body CT (WBCT) using the Injury Severity Score (ISS).

Methods and Materials: A series of 170 patients (mean age 35.2 years) were included. All patients underwent WBCT with a 64-slice scanner equipped with an automatic tube current modulation system (Care Dose 4D). The ISS of each patient was retrospectively evaluated and compared to the discharge diagnosis. Radiation dose was calculated using a mathematical phantom (ImpACT CT Patient Dosimetry Calculator, version 0.99x 01/02/2006).

Results: The effective dose associated with WBCT ranged from 16 to 42 mSv, depending upon how many phases are incorporated. The effective dose for focused CT ranged from 5 to 14 mSv, depending upon how extended is the FOV. 40% of the WBCT scans had an ISS ≤ 15 , and revealed no trauma-related pathology. Analysis of our data confirms that many of these negatives scans were clinically indicated, but in a proportion, a more focussed scan, aimed at specific areas of clinical concerns, would have been more appropriate.

Conclusion: The associated radiation dose with WBCT is high and patients should be carefully selected using the ISS. When the ISS is ≤ 15 , a more targeted region-specific CT is recommended.

B-0481 14:09

Prospective study on immediate total body CT in severe trauma patients

L.F.M. Beenen, J.C. Sierink, T.P. Saltzherr, M.J.A.M. Russchen, J.S.K. Luitse, J.C. Goslings; Amsterdam/NL (*l.f.beenen@amc.uva.nl*)

Purpose: In polytrauma patients rapid and adequate evaluation of injuries is essential. In recent years a tendency to use total body CT (TBCT) in trauma has become apparent. An international multicenter randomised trial (REACT-2) has been initiated to determine the effect of immediate TBCT in severe trauma patients. The aim of our pilot study was to evaluate the work up of immediate TBCT in trauma patients.

Methods and Materials: All trauma patients meeting the inclusion criteria and admitted to our hospital in the period January 2009 - April 2011 were evaluated. Inclusion criteria were suspicion of severe injury based on predefined vital parameters or clinically suspicious diagnosis. Exclusion criteria were age < 18 years, known pregnancy, referral from other hospitals or CPR required. Included patients

underwent an immediate TBCT from vertex to pubic symphysis. For the first 50 patients during day time several clinical important time points were registered.

Results: In total, 159 patients were included, of which 112 were males, 152 had blunt trauma. Median age was 42 years, median Injury Severity Score was 19.5. After TBCT 93 patients received additional imaging and 84 underwent radiological or surgical intervention. Median time to imaging was 11.7 min (acquisition time 7.4 min), all diagnoses were known 29.6 min after admission. Mortality in the 159 patients was 16.4%.

Conclusion: With the use of immediate TBCT in severe trauma patients complete diagnoses can be achieved within 30 minutes.

B-0482 14:18

Ultrasound follow-up of polytrauma patients after initial computed tomography: an analysis of role and costs

M.H. Maurer, A. Winkler, M. Powerski, F. Elgeti, B. Hamm, R. Roettgen, T. Marnitz; Berlin/DE (martin.maurer@charite.de)

Purpose: To assess the costs and diagnostic gain of abdominal ultrasound follow-up of polytrauma patients initially examined by whole body computed tomography (CT).

Methods and Materials: A total of 176 polytrauma patients (126 men, 50 women; age 43.5±17.4 years) were retrospectively analysed with regard to supplementary and new findings obtained by ultrasound follow-up compared with the results of exploratory FAST (focused assessment with sonography for trauma) on admission and the findings of whole body CT. A process model was used to document the staff, material, and total costs of the ultrasound follow-up examinations.

Results: FAST yielded 26 abdominal findings (organ injury and/or free intra-abdominal fluid) in 19 patients, while the abdominal scan of whole body CT revealed 32 findings in 25 patients. FAST had 81% sensitivity and 100% specificity. Follow-up ultrasound examinations revealed new findings in two of the 25 patients with abdominal injuries detected at initial CT. In the 151 patients without abdominal injuries on the initial CT scan, ultrasound follow-up yielded no supplementary or new findings. The total costs of an ultrasound follow-up examination were EUR 29.61. The total costs of all follow-up ultrasound examinations performed in the study population were EUR 5211.36.

Conclusion: Follow-up abdominal ultrasound shows a very low overall diagnostic gain in polytrauma patients in whom initial CT fails to detect any abdominal injuries but causes high personnel expenses for radiologic departments. In contrast, sonographic follow-up appears to be indispensable in patients diagnosed with an abdominal injury on admission.

B-0483 14:27

The value of contrast-enhanced ultrasound (CEUS) in the follow-up of post-traumatic abdominal injuries submitted to nonoperative management

F. Pinto, R. Farina, A. Pinto, C. Acampora, L. Romano; Naples/IT (fpinto1966@libero.it)

Purpose: To evaluate the role of contrast-enhanced ultrasound (CEUS) in the follow-up of post-traumatic abdominal injuries nonoperatively managed.

Methods and Materials: One-hundred and forty-two patients (87 males and 55 females, age range 18-63 years old) with post-traumatic injuries of solid abdominal organs were followed-up by means of CEUS. All the diagnostic exams were performed at variable time intervals (in the range between 1 and 30 days from patients hospitalisation), depending on the clinical needs and until complete clinical resolution was reached. Low-mechanical index techniques and a sulphur-hexafluoride-filled microbubbles contrast agent were used. After 30 days after trauma, all the enrolled patients also underwent a multidetector computed tomography (MDCT) abdominal exam.

Results: At CEUS, the absence of vascular complication was seen in 132/142 (93%) cases until complete clinical resolution: in these patients, nonoperative management was favourable. In 4/142 (2.8%) cases, an hepatic pseudoaneurysm was detected at CEUS: subsequent angiographic embolisation was successfully performed. In 3/142 (2.1%) cases, CEUS depicted wide contrast agent extravasation or pooling, both in the splenic organ and out the capsule: all of these 3 patients underwent subsequent emergent splenectomy. Finally, in 3/142 (2.1%) cases, a splenic arteriovenous fistula was seen at CEUS: subsequent angiographic embolisation was performed.

Conclusion: CEUS represents an accurate technique in the evaluation of post-traumatic injuries of solid abdominal organs. The technique is not only able to detect active bleeding and vascular lesions, avoiding overexposure to ionising radiation, but also proves particularly useful for monitoring patients undergoing nonoperative management.

B-0484 14:36

The volume of free intraperitoneal fluid influences the sensitivity of primary focused assessment with sonography in trauma (FAST), whereas radiologist's experience does not

R.J.V. Loekke, A. Schulz, S. Groven, C. Gaarder, P.A. Naess, J.B. Dormagen; Oslo/NO

Purpose: Focused assessment with sonography in trauma (FAST) is a rapid, non-invasive method designed to detect free intraperitoneal fluid in trauma patients. However, in recent years, some studies on the sensitivity of FAST report values below 50%. The aim of this study was to evaluate how the volume of intraperitoneal free fluid and the radiologist's experience influence the sensitivity of FAST.

Methods and Materials: Over a two-year period, 1379 trauma patients underwent FAST performed by 35 radiologists with different levels of experience (2 to 36 months, performing 4 to 92 exams each). CT volumetry, diagnostic peritoneal lavage, laparotomy and clinical observation were considered the reference standard in 800, 14, 40 and 525 patients, respectively. FAST results were correlated with four different levels of blood volume (negligible, 100, 200 and 500 ml) and with three different levels of experience with FAST (less than 12 months, 12 to 36 months and more than 36 months).

Results: FAST sensitivity was 0.53, specificity was 0.98, positive and negative predictive values were 0.74 and 0.95 and accuracy was 0.94 for the whole study population. With increasing volumes of intraperitoneal fluid FAST sensitivity increased successively to 0.80 at 500 ml. In the subgroup of patients with a volume of 200 ml at CT volumetry, sensitivity was 0.84 and reached 0.90 for volumes over 500 ml. The radiologist's experience did not influence the sensitivity of FAST significantly, irrespectively of the measured volume.

Conclusion: The volume of free intraperitoneal fluid influences accuracy of FAST, whereas the radiologist's experience does not.

B-0485 14:45

Coronary atherosclerosis in cocaine abusers presenting with acute chest pain: characterisation with coronary CT angiography

H. Ebersberger¹, S. Sudarski¹, U.J. Schoepf¹, F. Tricarico¹, R. Vliegenthart¹, G.F. Headden¹, A. Leber², E. Hoffmann², P. Apfaltrer¹; ¹Charleston, SC/US, ²Munich/DE (ebersberger@gmx.net)

Purpose: Cocaine-associated chest pain accounts for a substantial proportion of emergency department (ED) visits. Such patients are known to be at increased risk for acute coronary syndrome (ACS). We aimed to use coronary CT angiography to evaluate the prevalence, extent, and composition of atherosclerotic lesions in patients with acute chest pain and history of cocaine abuse.

Methods and Materials: 68 patients (48 men, 44±6.9 yrs) with a history of cocaine abuse (18 under acute influence) who had undergone coronary CT angiography for acute chest pain were included. Each coronary artery segment was evaluated for the presence of atherosclerotic plaque, composition (calcified, non-calcified, mixed), and the presence and degree of stenosis. Findings were compared with a matched control cohort (48 men, 45±7.0 yrs) without a history of drug abuse using T- and Chi-square testing.

Results: There was no significant difference between patients with and without history of cocaine abuse with respect to the presence of significant stenosis (17 (25%) vs. 14 (21%), p> 0.05). History of cocaine use was not associated with a higher prevalence of overall plaque (25 (38.8%) vs. 20 (29.4%), p> 0.05), calcified plaque (12 (17.6%) vs. 16 (23.5%), p> 0.05) or non-calcified plaque (4 (5.9%) vs. 2 (2.9%), p> 0.05). However, patients with history of cocaine abuse had a higher prevalence of mixed plaque (18 (26.5%) vs. 6 (8.8%), p=0.02).

Conclusion: Higher risk for ACS in patients with a history of cocaine abuse might be associated with a higher prevalence of mixed coronary atherosclerotic plaque. This association may be explained by the mechanical properties of mixed plaque, which may predispose to rupture during cocaine-induced vasospasm.

B-0486 14:54

Standard vs high-pitch CT of the chest in ventilated patients: comparison of motion artefacts, image noise and effective dose

F. Schwarz, T. Goelz, A. Arnoldi, K. Nikolaou, M.F. Reiser, C.H. Becker; Munich/DE (florian.schwarz@med.lmu.de)

Purpose: To compare motion artefacts, image noise and effective dose between a high-pitch and a routine chest CT protocol in ventilated patients.

Methods and Materials: All analysed studies were performed on a 128-slice CT-system. 35 consecutive ventilated patients who underwent high-pitch chest CT (p=3.2) were included in this analysis. As control group, 35 ventilated patients matched for sex and body mass index (BMI) who had undergone routine chest CT

($p=1.2$) were identified. Two blinded readers assessed all datasets for the extent of motion artefacts on 3.0 mm axial lung reconstructions. A compound-motion-score (range: 0-12) was calculated based on signs of motion at four standardised positions. For image noise, the average standard deviation within ROI's in air was calculated. The dose length product (DLP) was used to estimate applied dose.

Results: All 35 high-pitch acquisitions had been performed without complications and no dataset had to be excluded. There were no significant differences in BMI or ventilation frequency between both groups. Interobserver agreement for compound-motion-scores was excellent ($\kappa=0.81$). Compound-motion-score was significantly lower in the high-pitch group (0.9 vs. 3.3, $p=0.004$). The highest motion scores observed in the high-pitch group and control group were 5 and 11, respectively. High-pitch datasets had a tendency towards higher image noise (24 HU vs. 20 HU, $p=0.7$) and lower DLP (445 vs. 507 mGycm, $p=0.6$).

Conclusion: For CT scans of the chest in ventilated patients, a high-pitch acquisition technique significantly reduces motion artefacts while maintaining similar degrees of image noise. This has considerable potential to improve detection of pulmonary infiltrates without increases in applied dose.

B-0487 15:03

High-pitch dual source CT pulmonary angiography with 30 cc of contrast material

J.M. Kerl, B. Schell, M. Larsson, T. Lehnert, T.J. Vogl, R.W. Bauer; Frankfurt a. Main/DE (matthias.kerl@kgu.de)

Purpose: To compare different low contrast material injection protocols using high-pitch dual source CT pulmonary angiography in patients with suspected pulmonary embolism.

Methods and Materials: Data of 60 consecutive patients referred for CTPA for exclusion of PE were evaluated. All scans were performed on a 128-channel dual source CT scanner with a high-pitch protocol (pitch 3.0, 100 kV, 180 mAs). In group 1 ($n=20$) contrast enhancement was achieved by injecting 50 cc CM followed by a saline chaser of 50 cc, in group 2 ($n=20$) contrast enhancement was achieved by 40 cc of CM followed by a saline chaser of 50 cc and in group 3 ($n=20$) contrast enhancement was achieved by 30 cc of CM followed by a saline chaser of 50 cc. In all studies iomeprol (400 mgI/cc) was used injected at a rate of 4 cc/s. Attenuation profiles in the pulmonary trunk and on segmental level were measured to evaluate the enhancement within the pulmonary arteries.

Results: In all patients an adequate and homogeneous contrast enhancement of more than 250 HU was achieved in the pulmonary arteries. However, a significant different level of enhancement within the pulmonary system between group 1 and group 2 versus group 3 was observed ($p < 0.05$). No statistically significant difference between groups 1 and 2 was found regarding attenuation of the pulmonary arteries.

Conclusion: A homogeneous opacification of the pulmonary arteries and sufficient image quality can be achieved with 30 cc of contrast material in high pitch DSCT pulmonary angiography.

B-0488 15:12

Accuracy of multidetector computed tomography to evaluate acute aortic syndromes: 5-year experience in a cardiovascular center

A.R. Martinez, H. Paladini, M.J. Mela, F.M. Perea, M. Cerda, G. Ganum, M. Castignola, E. Dulbeco, D. Haberman; Caba/AR (armartinez@ffavaloro.org)

Purpose: To assess the accuracy of multidetector computed tomography (MDCT) performed in acute patients with clinical diagnosis of aortic syndrome.

Methods and Materials: Emergency MDCT was performed in 72 patients suspected of having acute aortic syndrome. From these patients 51 met inclusion criteria and were enrolled for this study. From 21 refused patients, 5 had previously known and treated aortic disorders and 16 did not undergo surgery or second comparative method. MDCT was compared with surgery ($n=22$). In patients without surgery, second method was ultrasound ($n=20$), digital angiography ($n=8$), both ($n=1$). In all patients not only second comparison method but also clinical follow-up was considered.

Results: MDCT was positive for acute aortic syndrome in 31 of 51 patients. Diagnosis included type A dissection ($n=9$), type B dissection ($n=6$), aortic rupture ($n=4$), type A intramural haematoma ($n=4$), ulcer ($n=3$), type A dissection and intramural haematoma ($n=3$), type B dissection and rupture ($n=1$), type B intramural haematoma and ulcer ($n=1$). MDCT was negative for acute aortic syndrome in 20 patients. 11 patients with normal aorta, 9 patients had unknown aneurysm without complication. Sensitivity, specificity, positive predictive value and negative predictive value for detection of acute aortic syndrome and correct characterisation for each subtype was 100% in all cases.

Conclusion: MDCT depicts an excellent imaging method to evaluate acute aortic diseases and represents a fundamental tool to properly stratify patients in this critical situation.

B-0489 15:21

Emergency CTPA performed in one year: clinical results

C. Martino, G.A. Zamboni, G. Salvagno, R. Pozzi Mucelli; Verona/IT (gzamboni@hotmail.com)

Purpose: To review the CTPA scans performed on patients with clinical suspicion of acute PE in one year, and assess final diagnosis and presence of unexpected findings.

Methods and Materials: All the emergency CTPA scans performed in 12 months (January-December 2010) were reviewed and evaluated for the presence of pulmonary embolism and/or other thoracic findings. The presence of PE was correlated to D-Dimer levels. When the abdomen was scanned to search for thrombosis, the presence of thrombosis and/or other abdominal findings was assessed.

Results: Over 12 months, 239 emergency CTPA scans were performed (128 F/121M, mean age 67.1 years). 97% patients had D-Dimer > 500 ng/dl. 74 patients (31%) were diagnosed with PE: 48/74 involving the pulmonary trunk, the main pulmonary arteries or lobar arteries. 73/74 patients had D-Dimer > 500 ng/dl. In 51/74 patients the abdomen was scanned: 5 cases of DVT were observed. Collateral findings in these 74 patients with PE included pleural effusion (27/74), parenchymal consolidation (15/74) and tumours (7/74). 165 scans were negative for PE: 75/165 patients had no significant findings at CT, while 90 had pleural effusion (66) and/or parenchymal consolidation (36) and/or tumours (10). 160/165 patients had D-Dimer > 500 ng/dl. In 72/165 the abdomen was scanned: 8 cases of DVT were observed.

Conclusion: Even in a population with a relatively high prevalence of PE, most of the patients who undergo CTPA for clinically suspected PE will not have PE. Scanning the abdomen to search for DVT shows a DVT prevalence around 10% both in patients with and without PE.

14:00 - 15:30

Room P

Radiographers

SS 614

Experiencing the complexity of the radiographers' role

Moderators:

W. Heindel; Münster/DE
K. Németh; Budapest/HU

B-0490 14:00

Educational programme for radiography students at CT

K. Heggen, E. Johansen, R. Silkset; Oslo/NO (k_liveltel@hotmail.com)

Purpose: An educational program was designed to improve relevant competence in brain anatomy, pathology, CT technique and physics among radiography students training at Oslo University Hospital, Ullevål.

Methods and Materials: The educational program consisted of lectures, a compendium, practical lessons and competence testing. The lectures and compendium focused on brain anatomy, pathology, CT technique and physics. All second year radiography students at the University College in Oslo completed the same competence tests before and after their hospital training. This allows a comparison of the competence improvement among students who followed the educational program, with students training elsewhere (the control group). The second year class comprises 40 students. 29 took the initial test. Out of this number 12 participated in the project while the remaining 17 (the control group), did not. 30 students took the final test. 3 students who actually took part in the project opted out of the final test, reducing the number to 9 while the number of students in the control group was increased to 21 because 4 students who did not take the initial test joined the control group at the final test.

Results: Radiography students who participated in the educational program improved their test score from 31% to 61%, while the control group improved their score from 33% to 34%.

Conclusion: This study demonstrates a pronounced improvement in level of competence among students who followed the educational program.

B-0491 14:09

Impact of a radiographic positioning doll on developing skills in skeletal radiology: a study on radiography students

R. Girometti, C. Zuiiani, S. Da Dalt, A. Moretti, R. Fazzini, M. Bazzocchi; Udine/IT (rgirometti@sirm.org)

Purpose: To investigate the subjective impact of a radiographic positioning doll (RPD) in developing main skeletal radiology (SR) skills in radiography students.

Methods and Materials: Before starting the clinical internship in skeletal radiology, 30 radiography students were involved in a preliminary 100-hours training program using an anthropomorphic RPD. The training was supervised by two expert radiographers in order to develop 7 main skills in performing a SK examination. After completing the clinical internship, students were asked to subjectively quantify how the use of RPD impacted on developing each of the established skills using a 1 to 3 score (1=no impact; 2=moderate impact; 3=high impact). We calculated the proportion of 2-3 scores for each skill, by testing statistical significance with the Chi-square test.

Results: Regardless of the specific skill, the large majority of the students subjectively attributed a 2-3 impact score to the use of the RPD ($p < 0.0015$). RPD was found more impacting in developing capabilities in post-processing procedures (100%; 95%CI. 86.7-100), patient positioning (92.5%; 95%CI. 75.7-99.0), and individuation of radiographic reference points (92.5%; 95%CI. 75.7-99.0). RPD was found less useful in training to perform radiographic projections (73.0%; 95%CI. 52.2-88.4), patient preparation (71.4%; 95%CI. 51.3-86.7), and exposure regulation (62.9%; 95%CI. 42.3-80.6). High proportion of students found the use of RPD of value in preparing for clinical practice (81.4%; 95%CI. 61.9-93.7).

Conclusion: A training with a RPD is subjectively of value in developing main SK skills of radiography students before the clinical internship.

B-0492 14:18

Image quality system for radiographers

S. Geers-van Gemeren; Utrecht/NL (s.geers@nvmb.nl)

Purpose: The Dutch Society of Medical Imaging and Radiotherapy has developed in cooperation with Rogan Delft a system to analyse rejected images, retakes, image quality and radiation dose. The aim of the Image Quality System (IQS) is to evaluate, improve and audit patient positioning and radiographic exposure conditions in a digital radiology department.

Methods and Materials: In 1998 a instrument is implemented for radiographers to analyse and evaluate retakes in the department. In 2004 a first step was made to investigate the possibilities to change the instrument from conventional images to digital images. In 2009 the Dutch Society started with a inventory of the requirements for the Image Quality System. A questionnaire was constructed and sent out to all the radiology departments in the Netherlands.

Results: With the outcome of the survey the Dutch Society developed requirements for the Image Quality Tool. The IQS is tested in different hospitals and is available on a licency base agreement between the department and the Dutch Society.

Conclusion: It is possible in a full digital environment to use the IQS to evaluate, improve and audit patient positioning and radiographic exposure conditions. International agreements should be made for standardisation of the information in the DICOM header to assure a high-quality service. The IQS can be used in quality assurance programme in the department, as a benchmark tool between departments and for clinical audits performed by the radiographer society.

B-0493 14:27

The evaluation of patient's anxiety levels undergoing magnetic resonance imaging examination

F.D.F.R. Medeiros, K.B. Azevedo, L.P.V. Ribeiro, A.F.C.L. Abrantes, S. Rodrigues, C.A. Silva, R.P.P. Almeida; Faro/PT (filipa_medeiros@hotm.com)

Purpose: To analyse possible differences between the anxiety levels of patients who receive additional information about the MRI scan, and patients who receive only basic instructions from the hospital, and to verify if there is variation in anxiety levels of patients before and after the examination, and relate them to gender, age, education level, and previous MRI examinations.

Methods and Materials: The total sample of 60 patients was divided into a control group and an experimental group, and each one divided into two subgroups before and after the exam, and then it was applied STAI form Y-1 to both, after the sociodemographic questions.

Results: At a 95% confidence interval, the mean difference between the control group, before and after, ranged from 7.210 and 20.624. The value of the Student's t test was 4.153 (df=58 and 2-tail sig=0.000). The mean difference between the

experimental group before and after, ranged from 6.112 and 19.305. The value of the Student's t test was 3.856 (df=58 and 2-tail sig=0.000). Using Spearman's Ro, there are some correlations between the sociodemographic variables and their levels of anxiety. The level of anxiety can be changed by many reasons, one and the most important is when the patient has already performed a MRI scan.

Conclusion: The main results suggest a significant difference in both groups, among the subgroup before and after, that let us concluded that after the MRI exam patients are less anxious. We also conclude that who has previously performed an MRI scan has smaller values of anxiety.

B-0494 14:36

Children's and parents' perception of a MRI examination

J. Gaardling, M. Edwinston Maansson; Lund/SE (jenny.gaardling@med.lu.se)

Purpose: To describe children's and parents' perception of a MRI examination.

Methods and Materials: Children and parents were selected consecutively. Inclusion criteria were that they could understand and speak Swedish. The children should be of both genders and aged 6-10 years. It should be children who did a MRI examination for the first time and they would be able to carry out an interview of 30-40 minutes. The parents who followed were also interviewed. Semi-structured interviews with 8 children, 5 girls and 3 boys, and their parents were carried out. The interviews were analysed using a phenomenographical approach.

Results: The children perceived security through preparation/information, parental presence and that it was a light inside the MRI. The parents perceived security through information about the procedure and being present while their child was examined. Both children and parents felt a sense of security by the positive behaviour from health professionals. The children perceived anxiety when too little preparation/information had been given, the design of the MRI, the sound and to obtain a peripheral venous catheter. The parents perceived anxiety from the sound, a failed examination and the insertion of a peripheral venous catheter. The children talked much about the difficulty to lie still. Parents wanted more information so that they could prepare their children and themselves.

Conclusion: An information leaflet before an MRI examination that is produced for children could contribute to reduced anxiety, greater understanding of what they are going through and lead to improved quality of the examination.

B-0495 14:45

Information to the parents in connection with their child's diagnostic examination

O. Muharemovic; Hvidovre/DK (omarradiograf@hotmail.com)

Purpose: To identify parents' need for information in connection with their child's diagnostic examination, and to prepare radiographers better to communicate to satisfy those needs.

Methods and Materials: A qualitative approach was applied, and the data were collected from twenty parents who participated in the semi-structured face to face or focus group interviews. Constant comparative technique was utilised to analyse the data, where answers and conclusions were categorised and then compared and related to one another. The categories were critically reviewed and revised to improve the reliability of the analysis. A follow-up focus group was created to validate, clarify and refine the collected data.

Results: Parents' knowledge about diagnostic examinations and the risk connected to them are very limited. Most of them have prejudices and their thoughts about radiation are very confused. Information about the risk their children are exposed to is highlighted as the most important need parents have. They have a need to be involved verbally and practically in examination of their children. Participants who did not received adequate information showed signs of stress.

Conclusion: Radiographer should involve the parents in examination using clear instructive information, as their resources can be very useful as psychological support to the child and practical help. The risk of radiation should be explained in a way parents can relate to. More detailed information will contribute to better procedure understanding and concerns will be eliminated. By defining and standardising information some minimum quality should be guaranteed to the parents.

B-0496 14:54

Hypnosis in the management of claustrophobic MRI patients

N. Alexandre¹, M.A. Fontaine¹, B. Suarez¹, D. Mompoint², J. Becchio³; ¹Thiais/FR, ²Garches/FR, ³Villejuif/FR (nachwan.alexandre@gmail.com)

Purpose: Claustrophobia is responsible for the cancellation of a significant number of MRI examinations. We prospectively evaluated the usefulness of hypnosis in the management of claustrophobic patients scheduled for an MRI.



Methods and Materials: Two MRI technicians and a radiologist learned eriksonian hypnosis. Over a period of twenty months, 3920 patients were explored by MRI. Fifty-two patients were identified as claustrophobic, refusing the scheduled MRI. Seven patients experienced a panic attack. A brief single session of hypnosis was proposed.

Results: Among the 52 identified claustrophobic patients, 48 accepted hypnosis and underwent MRI. Four patients declined the proposed treatment and were unable to withstand the MRI procedure.

Conclusion: Hypnosis appears to be a suitable, efficient, rapid and inexpensive tool for the care of patients suffering from claustrophobia during MRI. With this drug-free method, MRI of claustrophobic patients can be performed in the best conditions.

B-0497 15:03

Practices to control infection related to chest radiography in intensive care unit

M.M.C.P. Ribeiro¹, A.L. Resendes¹, F.P. Rodrigues¹, J.E.G. O'Neill¹, J.C. Mauricio²; ¹Lisbon/PT, ²Tomar/PT (margarida.ribeiro@estes.ipl.pt)

Purpose: To analyse the process of carrying out chest radiography at the intensive care unit (ICU), regarding the control infection practices applied by radiographers.

Methods and Materials: The study took place in a public hospital which carries out chest radiography in bedridden in the ICU. Fifteen radiographers were observed (observational empirical component) and filled, by the researchers, one check-list with eleven items. Thirteen different radiographers filled one survey with eight questions (exploratory empirical component).

Results: Most of radiographers gave only three correct answers. 15.2% of the radiographers presented practices suspicious to conduct to an infection process, 1.9% led to practices of an effective infection while the remaining (82.9%) did not present any risk behaviour related to the development of infection. Most of radiographers had more than 5 years of work experience and 29.5%, 0-2 years. Disinfection procedures were not carried out on the image plates (Ip's) or portable equipment in the Imaging Department, before to arrive on the ICU. Most of the radiographers (71.4%) used gloves, did not use any personal utensils (94.3%) or did not come into contact with the patient or the bed without disinfect first (62.9%), during the procedures; the Ip's protection was used in 57.1% of the cases. The following procedures never were applied by half sample: wearing of a white coat/impermeable apron or mask, and disinfection of the Ip's at the end.

Conclusion: The results, far from following the recommendations or guidelines, suggested that the matter about prevention and control infection among radiographers should be improved through theoretical and training initiatives.

B-0498 15:12

Are UK radiographers more emotionally intelligent than a normative comparison group? An age- and gender-matched analysis

S.J. Mackay¹, P. Hogg¹, G.T. Cooke¹, R.D. Baker¹, T. Dawkes²; ¹Salford/UK, ²Chester/UK (s.mackay@salford.ac.uk)

Purpose: Emotional intelligence (EI) has been identified as a beneficial phenomenon in medicine, nursing, radiography and has been shown to be positively associated with a greater amount of compassionate and empathic patient care. This paper will compare EI data from a UK wide survey of radiographers with a normative sample group to determine whether radiographers have higher emotional intelligence than a normative group.

Methods and Materials: In 2010, a UK-wide survey of radiographer trait emotional intelligence (n=1997) was undertaken to determine the global and four factor EI levels of radiographers. This data were compared with a normative group (n=866) from the national Trait EI database. The mean, age range and gender proportion of these two datasets differed so age and gender matching by group was undertaken followed by ANOVA with post hoc Tukey tests.

Results: Statistically significant difference was observed for age group between datasets on global trait EI and all factors. Post hoc tests indicated differences lay mainly with 18-29 age group. Radiographers scored more highly than normative group for all but the emotionality factor. Highly statistically significant differences were observed in gender between data sets for global and all factors. Post hoc tests indicated differences between females across global and all factors but for males this was limited to global trait EI, well being and self-control.

Conclusion: The UK radiographer sample scored more highly in emotional intelligence than a normative sample group.

B-0499 15:21

Radiographer's role in teleradiology

E. Metsala¹, A. Henner²; ¹Helsinki/FI, ²Oulu/FI (anja.henner@oamk.fi)

Purpose: Teleradiology is one of the most important areas of telemedicine. Change from conventional film-screen imaging systems to the digital ones has changed radiographers' job description a lot. Some tasks such as developing images or achieving the films have disappeared and new work areas such as PACs work has emerged.

Methods and Materials: Systematic literature review was made from Finnish and English language electronic health care databases and Thesis database of universities of applied sciences. Volumes of Journal of Digital Imaging were reviewed. No time limit was set because phenomenon on the focus of search is relatively new. Inclusion criterion was that selected studies described radiographers' role as an active actor or beneficiary. Studies describing radiographers' role in diagnostic or therapeutic teleradiology were searched. Studies comprising final data were analysed by inductive content analysis.

Results: Most central areas forming radiographers' job description in teleradiology were: patient data management and combining patient data to imaging data, radiotherapy and/or image production, processing and saving images, taking care of safety, quality assurance and dose optimisation, lifelong education, developing oneself and ones' work, multiprofessional teamwork, client centred patient education and nursing, data safety and security and planning and managing economy were part of PACS administrators work.

Conclusion: Radiographers' job description in teleradiology should be taken into account when radiographers' education is planned on the first and second cycle and in life long education. Competences should be recognised when planning imaging units' job descriptions, evaluating work demands and rewarding.

Saturday, March 3

10:30 - 12:00

Room A

Neuro

SS 911

Stroke diagnosis

Moderators:

D.R. Hadizadeh; Bonn/DE

M. Mechl; Brno/CZ

B-0500 10:30

Distinction of antegrade flow across intravascular thrombus from retrograde collateral flow in occluded cerebral arteries: initial experience using time-resolved CT angiography

A.M.J. Erölich¹, R. Schramm¹, E. Klotz², M. Knauth¹, P. Schramm¹;

¹Göttingen/DE, ²Forchheim/DE

Purpose: Acute stroke patients with intracranial vessel occlusion may demonstrate subocclusive thrombus, typically characterised by antegrade opacification distal to an occlusion on catheter angiography. This finding has been associated with higher rates of vessel recanalisation. We sought to determine whether antegrade flow can be demonstrated on near-whole-brain time-resolved four-dimensional CT angiography (4D-CTA) and whether it can be distinguished from retrograde collateral flow.

Methods and Materials: Thin-section 4D-CTA data from 43 consecutive stroke patients with acute terminal internal carotid or middle cerebral artery occlusion were assessed for pre-treatment thrombolysis in cerebral infarction (TICI) grade and the presence of antegrade or retrograde contrast opacification at the distal thrombus end. Digital subtraction angiograms were reviewed for pre-treatment TICI grade, presence of antegrade opacification distal to the thrombus as well as post-intervention TICI grade.

Results: On 4D-CTA, there was evidence of antegrade flow in 5 of 43 cases (11.6%). Compared to angiography, 4D-CTA correctly classified antegrade flow in 4 cases (80.0%), there was 1 false positive and no false negatives. Recanalisation (TICI 2a or greater) was achieved in all 5 cases with evidence of antegrade flow on 4D-CTA versus 34 out of the 38 cases (89.5%) without evidence of antegrade flow.

Conclusion: 4D-CTA can distinguish antegrade flow across a cerebral artery occlusion from retrograde collateral flow. Further studies, preferably with a larger sample size are needed to confirm our findings and assess whether 4D-CTA can be used to predict success of recanalisation procedures in select cases.

B-0501 10:39

Poor collateral status on timing-invariant CTA is a strong predictor of poor clinical outcome in acute stroke patients with large vessel occlusion

E.J. Smit¹, E.-j. Voncken¹, T. van Seeters¹, J.W. Dankbaar¹, I.C. van der Schaaf¹,

B.K. Velthuis¹, B. van Ginneken², M. Prokop²; ¹Utrecht/NL, ²Nijmegen/NL

(ewoudsmit@gmail.com)

Purpose: To assess whether collateral status in acute stroke patients with large vessel occlusion predicts clinical outcome and to compare standard CT angiography (CTA) to a timing-invariant CTA for this purpose.

Methods and Materials: We selected 40 consecutive ischaemic stroke patients with ICA and/or MCA occlusion from our clinical database. CTA and CT perfusion (CTP) at admission and clinical outcome data (modified Rankin Scale, mRS) after three months were available. CTP source images were used to reconstruct timing-invariant CTA (TI-CTA), a technique that is insensitive to delayed contrast arrival. Four experienced observers assessed collateral status on CTA and TI-CTA in an independent, blinded, randomised manner. Collateral status was rated good if $\geq 50\%$ of collaterals were present or poor if $< 50\%$ were present. Clinical outcome was defined as good for mRS ≤ 2 or poor for mRS > 2 .

Results: Collateral status was rated significantly more often as good on TI-CTA (84%) than on CTA (49%; $p < 0.05$). Inter- and intraobserver agreement were good for assessing collateral status on CTA and TI-CTA (mean kappa = 0.63 and 0.76, respectively). Poor collateral status on TI-CTA had a predictive value of 100% for poor outcome. This number was only 69% for CTA. Good collateral status on CTA or TI-CTA predicted good outcome in only 64% and 56%, respectively.

Conclusion: Poor collaterals status on timing-invariant CTA is a strong predictor of poor clinical outcome in acute stroke patients with large vessel occlusion. TI-CTA detects more collaterals than standard CTA due to its insensitivity to delayed contrast arrival.

B-0502 10:48

CT angiography "Spot Sign" predicts haematoma expansion in patients with acute spontaneous ICH

I. Havsteen, L. Christensen, A. Christensen, J. Nielsen, D. Krieger,

H. Christensen; Copenhagen/DK (anderschristensenemail@hotmail.com)

Purpose: Spontaneous intracerebral haemorrhage (P-ICH) expands in up to 50% of cases and spot sign detection on CT-angiography (CT-A) enables prediction of haematoma expansion which has been linked to death and bad outcome. The aim is to investigate the strength in the correlation between presence of spot-sign and haematoma expansion.

Methods and Materials: Six-hundred and twelve patients underwent standardised work up for i.v. thrombolysis at Bispebjerg University hospital, Copenhagen from April 2009 to May 2011 within 4.5 hours after stroke symptom onset A non-contrast CT scan (NC-CT) and CT-A was performed routinely in patients with ICH and NC-CT was control planned next day when possible. One radiologist reviewed all data for spot sign and estimated the haematoma volume in the acute and follow-up NC-CTs with the ABC/2 method of measurement. Samples were assessed with the Mann-Whitney test. The study was approved by the Danish Data Protection Agency file no 2009-41-313.

Results: CT-A was obtained in 69 patients and next day NCCT was obtained in 40 patients mainly due to early transferral of stable patients. In 43.5% of patients spot sign was observed. There was significant difference in haematoma expansion in groups with and without spot sign, $p=0.0008$. Mean acute volume was 65.8 ml (range 8.8-362.4 ml) in patients with spot sign vs. 15.9 ml (range 0.5-78.0 ml).

Conclusion: Spot sign identifies patients with later haematoma expansion and may be useful in identifying patients for proof of principle trials in acute spontaneous ICH aiming at preventing or stopping early haematoma expansion.

B-0503 10:57

Dual energy CT for detection of contrast leakage within high-density haematoma in patients with intracranial haemorrhage: iodine images versus combined images

Y. Watanabe, H. Tanaka, M. Nishizawa, Y. Kunitomi, A. Tsukabe, N. Tomiyama;

Suita/JP (watanabe@radiol.med.osaka-u.ac.jp)

Purpose: To elucidate the detectability of contrast leakage in high-density haematoma on early phase dual energy CTA and compare the results with those obtained on delayed-CT (reference standard).

Methods and Materials: Twenty-six patients with intracranial haemorrhage were retrospectively included in this study. All patients had undergone dual source dual energy CTA (100 kV and 140 kV) and delayed-phase-enhanced CT (2 minutes after contrast injection) between April 2010 and July 2011. Dual energy CT images were post-processed with commercial software applying a three-material-decomposition algorithm to calculate iodine images and virtual unenhanced images and also to generate combined CT images that create the impression of 120 kV CT images. One neuroradiologist, blinded to the patient's data, reviewed the iodine images and combined images to detect contrast enhancement or contrast leakage in the haematoma.

Results: The patients' diagnosis was as follows: 12 idiopathic intracerebral haemorrhage, 11 traumatic haemorrhage, 2 subarachnoid haemorrhage, and 1 brain tumour with haemorrhage. Contrast leakage or enhancement was detected in 15 of 26 patients (58%) on delayed-CT. Among these 15 patients, 5 patients showed an equivocal leakage on combined images, but the iodine images revealed clear contrast leakage in the haematoma. In 2 patients iodine leakage could be detected on both iodine and combined images, but iodine image was superior in depicting the leakage. Eight patients were equal to depict the contrast leakage in both iodine and combined images.

Conclusion: Dual energy CT is able to differentiate iodine contrast-medium from haematoma and facilitates the detection of contrast leakage especially in patients with faint iodine enhancement.

B-0504 11:06

Cerebral perfusion CT quantifying regional functional parameters at the onset of the stroke and 24hs after intravenous thrombolytic therapy

Z.M. Metafratzi, E. Alexiou, M. Fanariotis, P. Argiri, A. Chovas, A. Komnos;

Larisa/GR

Purpose: To assess the changes in regional functional parameters (rFPs) of ischaemic and normal brain at the onset of acute stroke (AS) and 24hs after thrombolytic therapy, correlate rFPs to NIHSS in both time frames and to evaluate utility of the initial rFPs to predict the clinical outcome at 24hs.

Methods and Materials: Seventeen AS patients who thrombolised underwent brain unenhanced CT and CT perfusion (CTP) at admission and 24hs after thrombolysis. All CT studies were reviewed and rFPs (CBF, CSV, MITT) of ischaemic and normal brain at both time frames were calculated. rFPs were correlated with baseline and 24hs NIHSS, respectively. A multivariate linear regression analysis was used to investigate the effect of the initial rFPs on the clinical outcome.

Results: Normal brain rFPs at 24hs were not significantly different compared to initial rFPs. CBF and MTT of diseased brain were significantly reduced ($p=0.003$) and increased ($p < 0.001$), respectively, compared to the contralateral healthy side. rFPs of the diseased brain were significantly improved at 24hs (MTT, $p < 0.001$ // CBF, $p < 0.015$ /CBV, $p < 0.034$). NIHSS was significantly improved at 24hs ($p < 0.001$). CBV was the strongest predictor of improvement of NIHSS followed by MTT ($R^2=0.718$, $p < 0.001$).

Conclusion: rFPs and NIHSS are significantly improved 24hs after thrombolysis at the settings of AS. The clinical severity expressed by NIHSS is strongly correlated to CBV of the diseased brain at presentation of the stroke and at 24hs later. Furthermore, patients with the lower CBV values at admission had a poorer clinical outcome as it is expressed by higher NIHSS.

B-0505 11:15

Dynamic perfusion CT (PCT) imaging and alteration of blood brain barrier permeability (BBB-P) after acute ischaemic stroke (AIS), prognostic significance

E. Puigueli, M. Bafile, M. Fuschi, V. Di Egidio, M. Monina; *Teramo/IT (edopug@hotmail.com)*

Purpose: Aim of the study was to assess the correlation between BBB permeability alteration and the final outcome in AIS.

Methods and Materials: From January 2009, sixty patients with AIS less than 6h for anterior or 12h for vertebrobasilar circulation, mean age 67y, evaluated by PCT were included. Increase on microvascular permeability (MP) of the BBB was detected and MP colour maps were retrospectively generated. Two expertise readers analysed each map by drawing 3 circular 10 mm regions of interest on the focal abnormality. The mean of these 3 regions of interest represented the MP of the infarct (MPI) and on the non-ischaemic hemisphere (MPC control). The modified Rankin score (mRS) test was performed. MPI and MPC were compared (exactWilcoxon test). MPI that developed HT on follow-up (MP-HT) was compared with all of the others (MP No-HT) (exactMann-Whitney test).

Results: Fifty-four infarcts (90%) showed focal MP elevation in the region of infarct. Cerebral blood flow (CBF) (ml/100 g/min), MPI ranged from 0 to 15 (mean: 3.7 ± 2.1) versus MPC of 0-0.9 (mean: 0.38 ± 0.15 ; $P < .0001$). Six infarcts (10%) developed HT, all of which were within the areas of MP elevation. MP-HT ranged from 4.9 to 14 (mean: 8.5 ± 2.4) versus MP No-HT of 0-5.7 (mean: 3.8 ± 2.0 ; $P < .0001$). Forty infarcts (66%) were treated with embolectomy and local rtPA. A significant difference between MP-HT and MP No-HT persisted with respect to local treatment.

Conclusion: PCT has an inverse correlation with the mRS, while elevated BBB-P was directly correlated with the outcome and PCT can predict HT.

B-0506 11:24

CT perfusion and CT angiography: can they better predict the final infarct?

M. Fernández Taranilla, C.R. Caracela Zaballos, I. Herrera, E. Barcena, J.M. García Benassi, R. Gonzalez-Gutierrez; *Toledo/ES*

Purpose: To evaluate cerebral CT-perfusion imaging (CCTP) predicting final infarcted cerebral areas (ICA). To review correlation of the imaging findings between non-enhanced-CT (NECT) and cerebral blood volume (CBV) maps, identifying the ICA. To assess the impact of collateral arteries (CA) in the development of the final infarct. To analyse the outcome of the cerebral areas at risk in fibrinolysis-treated patients (FTP) versus non-treated patients (NTP).

Methods and Materials: We reviewed retrospectively imaging findings of stroke in 48 patients, who underwent NECT, CCTP and follow-up NECT after 24 hours; using the Alberta Stroke Program Early CT Score (ASPECTS), as a measure of cerebral areas. CT-angiography was performed to evaluate the CA in the middle cerebral artery territory (absent, moderate and evident). We performed correlation and linear regression analysis between ASPECTS on: NECT, CBV, CBF, and follow-up CT (FCT) in FTP and NTP.

Results: There is a strong positive correlation between: ASPECT on CBV maps and ASPECT on FCT ($R^2=0.78$); and ASPECT on NECT and ASPECT on FCT ($R^2=0.70$), both in NTP. In FTP we observed a strong positive correlation ($R^2=0.87$) between cerebral areas at risk in CCTP and those that were not infarcted in the FCT. Less infarcted areas were seen in FTP versus NTP (0.95 versus 1.26). Compared with moderate or evident CA, absence of CA increments more than 50% the ICA.

Conclusion: In NTP the final ICA can be predicted by changes on CBV, but among FTP it varies significantly. Evident and moderate CA seem to be a good prognosis factor, reducing 50% the ICA.

B-0507 11:33

Automated assessment of regional CT perfusion in acute ischaemic stroke

A. Kemmling, R. Krumm, L. Feyen, T. Niederstadt, W.L. Heindel; *Münster/DE (akemmling@web.de)*

Purpose: To present a novel algorithm for fully automated user-independent assessment of regional relative cerebral CT perfusion (CTP) parameters in acute ischaemic stroke.

Methods and Materials: Acute stroke imaging (native CT and dynamic CTP) was performed in 83 consecutive acute middle cerebral arterial strokes on a 128-slice CT scanner (Somatom Definition AS+, Siemens Medical Solutions). Regional CTP values were obtained by a fully automated routine: (1) robust non-linear registration of CTP maps to MNI-152 space regardless of brain coverage was accomplished by rigid body transformation of native CT to the anatomical average CT perfusion image followed by inversion of the transformation matrix (CTPtoCT). The matrix CTPtoCT and the non-linear warped CTPtoMNI were concatenated (CTPtoMNI). The warped CTPtoMNI was applied to perfusion maps. (2) A probabilistic atlas covering 68 structures (Harvard-Oxford structural atlas) was used to calculate brain perfusion parameters weighted by the anatomical probability of a region. (3) An error correction term excluded non-significant voxels defined by cerebrospinal fluid and vessels. (4) Relative CT perfusion values were calculated (regional perfusion of ischaemic hemisphere divided by the contra-lateral side). Automated perfusion values were compared with selected manually traced perfusion values for reference.

Results: Registration of perfusion maps to MNI-152 space was robust and reliable. Automated and manually obtained regional brain perfusion values were not significantly different ($p < 0.01$). The average difference between automated and manual regional perfusion parameters was less than 4.3% (SD 3.1%).

Conclusion: The presented algorithm is robust and reliable for automated calculation of regional perfusion parameters.

B-0508 11:42

Recommendations for selecting the vascular input functions to optimise the validity in CT-perfusion imaging in 256 (or more)-slice scanners

J. Niesten, I. Van Der Schaaf, A. Riordan, H. De Jong, W. Mali, B. Velthuis; *Utrecht/NL (jniesten@hotmail.com)*

Purpose: To improve accuracy of quantitative perfusion measurements and reduce operator-dependent postprocessing steps by optimising the selection of the arterial input function (AIF) and the venous output function (VOF) in CT-perfusion (CTP).

Methods and Materials: Forty-four patients with acute middle cerebral artery (MCA) ischaemic stroke underwent non-contrast CT, CTP and CT-angiography on admission with a 256-slice CT-scanner. In CTP-measurements, different arteries were selected as the AIF and the area under the AIF-curve (AUCAIF) was calculated. To investigate the AIF accuracy, we compared the quantitative perfusion measurements in both symptomatic and asymptomatic hemisphere (repeated Measures' test) for each AIF location. To reduce operator steps and improve reproducibility we examined if selection of the VOF could be replaced by the AIF. The resulting quantitative measurements of both AIF and VOF were compared (paired t-test).

Results: The internal carotid artery (ICA) had significantly the largest AUCAIF, followed by the basilar artery (Abas), the MCA and the anterior cerebral artery (between all groups $p < 0.0001$). Selecting the ICA and Abas as AIF resulted in the most accurate values with lowest quantitative mean CBV and CBF and accordingly highest quantitative MTT (all $p < 0.0001$). Replacement of VOF by AIF showed significantly higher mean CBV (i.e. overestimation) on both the hemisphere ipsi- and contralateral to the thrombus ($p=0.003$ and $p=0.001$ respectively), and a significantly higher CBF ($p=0.016$) on the ipsilateral hemisphere.

Conclusion: To improve validity of quantitative perfusion values we recommend to select the ICA as the AIF and a large vein as the VOF.

B-0509 11:51



Effect of radiation exposure on quantitative evaluation of cerebral CT perfusion maps: results from a hybrid digital phantom

R. van den Boom¹, M.T.H. Oei¹, L.J. Oostveen¹, E.J. Smit², S.J. Lafebree¹, B. van Ginneken¹, R. Manniesing¹, M. Prokop¹; ¹Nijmegen/NL, ²Utrecht/NL (R.vandenBoom@rad.umcn.nl)

Purpose: To use a hybrid digital phantom to study the effect of mAs on quantitative evaluation of cerebral CT perfusion scans.

Methods and Material: The hybrid digital phantom consists of scans of a homogeneous skull phantom on which circular objects (10-15-20 mm) are digitally superimposed. Tissue perfusion curves derived from patient data were superimposed on the background (white matter) and on the objects (grey matter). We tested a CTP sequence using 30 scans every 2s over 60s (80 kV, 5 mm thickness) derived from a 320-row CT scanner. The mAs values per CTP sequence were varied per scan (10-230 mAs). A synthetic dataset without noise was the gold standard. CBF maps for each mAs setting and for the synthetic dataset were calculated using the ASIST CT program. Noise in CBF maps was measured in the background; contrast between background and objects was measured in circular ROIs with a diameter of half the object diameter. Size- and dose-dependence of absolute values and CNR in CBF maps was calculated.

Results: Above 45 mAs per scan, the CBF values for the 20 mm objects were within ±12% of the gold standard. At 10 mAs CBF was overestimated by > 100%. With smaller objects the estimation of CBF became less precise. CNR for CBF in 20 mm decreased rapidly: CNR at 230 mAs was 4.2 and decreased to 2.4 at 100 mAs and 0.4 at 10 mAs.

Conclusion: Absolute CBF values require sufficient dose to be correct: values at low dose are overestimated. In addition, CNR rapidly decreases with lower dose.

10:30 - 12:00

Room D1

Chest

SS 904

Image quality and dose reduction

Moderators:

M. Brink; Nijmegen/NL
M.-P. Revel; Paris/FR

B-0510 10:30

Improving breath hold during mobile radiography

N. Houssein¹, D. Al-azawi¹, M.F. McEntee²; ¹Dublin/IE, ²Sydney/AU (mark.mcintee@sydney.edu.au)

Purpose: The degree of inflation of the lung seen on a chest x-ray (CXR) is dependent on when the radiographer exposes the image receptor during the respiratory cycle. Exposing the radiography image receptor at the exact peak of inflation may be quite difficult because the inspiratory pause may be exceedingly brief. We aimed to test whether images taken with and without an incentive spirometer show different levels of image quality.

Methods and Materials: This is a paired, prospective, single blinded study of 30 patients undergoing a mobile CXR. The radiographs were taken with and without the use of the incentive spirometer (IS). Images were scored using the European Guidelines on Quality criteria for diagnostic radiographic images.

Results: The mean patients' age was 53 years. Sixty images were taken, half with the use of IS and half without the use of the IS. Post lung lobectomy was the main indication for the mobile CXR. Scoring the visualisation of the sixth rib, spine, trachea and the cardiac border was not affected significantly by the use of the IS. While improved visualisation of the tenth rib, the vascular pattern, the retro-cardiac lung, and the costo-phrenic angles was significantly associated with the use of the IS $p=0.004$, $p=0.0001$, $p=0.013$ and $p=0.005$, respectively.

Conclusion: This study provides a novel technique to improve the quality of mobile CXR images. The use of the IS has improved the inspiratory depth and image quality when used in patients requiring in-ward mobile CXR.

B-0511 10:39

Digital chest tomosynthesis: impact on patient management

E. Quaià, E. Baratella, A. Lorusso, F. Casagrande, V. Ulcigrai, M. Cova; Trieste/IT (quaia@units.it)

Purpose: To assess the clinical impact of digital tomosynthesis (DTS) in the management of patients with suspected pulmonary lesions on chest radiographic examination (CRE).

Methods and Materials: Three-hundred and thirty-nine patients (200 males, 139 females; age, 71.19 ± 11.9 years) with suspected pulmonary lesion (s) on CRE underwent DTS. Two readers (experience, 10 and 25 years) prospectively analysed CRE and DTS images and proposed a diagnosis according to a confidence score: 1 or 2=definite or probable benign pulmonary or extra-pulmonary lesion, or pulmonary pseudolesion deserving no further diagnostic work-up; 3=indeterminate; 4 or 5=probable or definite pulmonary lesion deserving further diagnostic work-up by CT. Mean interpretation time and effective dose were measured both for CRE and DTS.

Results: Final diagnoses included 128 pulmonary and 29 pleural lesions in 157/339 patients, and pulmonary pseudolesions in the remaining 182/339 patients. DTS resolved the CRE doubtful finding without requiring further diagnostic work-up in 256/339 (76%) patients, while 83/339 (24%) patients underwent chest CT. The mean interpretation time for DTS (mean±SD, 220 ± 40 secs) was higher ($P < .05$; Wilcoxon test) than for CRE (110 ± 30 secs). Mean effective dose was 0.06 mSv (range, 0.03 - 0.1 mSv) for CRE, and 0.2 mSv (range, 0.1 - 0.3 mSv) for DTS.

Conclusion: DTS avoided the need for chest CT in about three-fourth of patients with suspected pulmonary lesions on CRE with a slight increase in the interpretation time and effective dose compared to CRE.

B-0512 10:48

Ultra-low-dose CT for the detection and characterisation of the most common CT patterns of pulmonary disease

A. Christe¹, J. Charimo Torrente¹, P. Vock¹, J.E. Roos²; ¹Berne/CH, ²Winterthur/CH (andreas.christe@insel.ch)

Purpose: To assess the accuracy of ultra-low-dose CT for the detection and characterisation of the most common CT-patterns of pulmonary disease compared to middle-dose CT scans of the chest.

Methods and Materials: Ten patients with pulmonary infections, 20 with interstitial lung diseases and 30 with lung nodules were scanned according to an ultra-low dose (64x0.75 mm, 40 reference-mAs, 120 kVp) and a middle-dose (150 reference-mAs, 120 kVp) contrast-enhanced chest-CT protocol (Xenetix). Two radiologists with 3 and 10 years of thoracic imaging experience searched individually both dose images for the most common CT patterns consisting of 34 different subgroups of ground glass opacities, nodules, interstitial and airspace diseases. The standard of reference was established by two different expert radiologists in consensus.

Results: The 1080 lung segments showed 818 nodules, 596 ground glass opacities, 74 airspace and 575 interstitial diseases and 64 normal segments. Both readers' sensitivities, specificities and accuracies of ultra-low-dose CT did not drop significantly (McNemar) for 28 of the 34 patterns. The sensitivity of only one reader dropped for small ground glass nodules (< 5 mm) from 85% to 64% (p -value < 0.0001) and sensitivity for all interstitial lung diseases together was significantly lower for both readers with an average loss of sensitivity of 19% from 57% to 43% (Reader 1) and from 87 to 64% (Reader 2), respectively.

Conclusion: Except for small ground glass nodules and interstitial lung disease, the pattern detectability is not significantly impaired at ultra-low-dose CT. It is applicable for lung nodule or consolidation follow-up examinations.

B-0513 10:57

Impact of 4th generation iterative reconstruction technique on image quality in ultra-low-dose computed tomography of the lungs

A. Laqmani, F. Henes, J.-H. Buhk, H.-C. von Schultendorff, D. Hammerle, H. Nagel, G. Adam, M. Regier; Hamburg/DE (azien.laqmani@gmx.de)

Purpose: To intraindividually compare and evaluate the influence of the 4th generation iterative reconstruction (iR) technique iDose™ on ultra-low-dose MDCT of the lungs with regard to anatomical delineation, lesion conspicuity and artefact reduction.

Methods and Materials: In 23 immunocompromised patients with suspected pulmonary infection the raw data of unenhanced MDCT scans (120 kV, mean CT DIvol: 2.4 mGy, mean DLP: 125 mGyXcm) were reconstructed using a prototype reconstruction processor featuring iDose4™ (Philips, Best, the Netherlands). iDose™ level settings varied between 0, 2, 4, 6 and 7. Images were reconstructed with a slice-thickness of 1 mm. Three radiologists blinded to the reconstruction technique independently performed image analysis. A 4-point grading-scale was

applied regarding the depiction of anatomical details and the degree of artefacts observed (1, worst; 4, excellent). The signal-to-noise ratio (SNR) was assessed for each data set. Statistical evaluation included kappa-analysis and Wilcoxon-test.

Results: Best image quality was assessed with iDose™ level 6. Compared to filtered-back-projection, the high iDose™ level of 6 improved the conspicuity of subtle infiltrations, groundglass opacities and mosaic perfusion. Even at the lower iDose™ level of 2 image ratings scored superior to filtered-back-projection. With increasing iDose™ levels, reduction of streak artefacts was successfully quantified by a decrease of the standard deviation at constant mean attenuation values.

Conclusion: Iterative reconstructions obtained in ultra-low-dose MDCT substantially improve image quality, conspicuity of subtle lesions and decrease image noise even at lower iDose™ levels. Thus, the implementation of this technique into clinical routine imaging seems to be desirable, e.g. for immunocompromised patients, in whom the identification of subtle changes can be crucial.

B-0514 11:06

Upgrading to adaptive statistical iterative reconstruction (ASIR) in 64-row computed tomography (CT) of the chest: detailed analysis of the performance of different ASIR modes and levels by intra-individual comparison of dose-reduced ASIR scans to full-dose filtered back projection series

S. Wirth, L. Michael, D. Maxien, Z. Deak, M. Scherr, U. Linsenmaier, M. Reiser, M. Körner; *Munich/DE (stefan.wirth@med.uni-muenchen.de)*

Purpose: To compare image quality in dose reduced 64-row-CT of the chest at different levels of adaptive statistical iterative reconstruction (ASIR) to full dose baseline examinations reconstructed solely with filtered back-projection (FBP) in a realistic upgrade scenario.

Methods and Materials: A waiver of consent was granted by the IRB. Baseline examinations of the chest (noise index NI=29; LightSpeed VCT XT, GE) were intra-individually compared to follow-up studies on a CT with ASIR option (NI=45; other scan variables constant and as provided by the vendor; Discovery 750HD, GE), n=46. For this, images were calculated in ASIR slice and volume mode; with ASIR blendings of 0% to 100% in standard and lung kernel. Three experienced radiologists independently compared image quality of these 828 series to the corresponding full-dose baseline examinations (-2: diagnostically inferior, -1: inferior, 0: equal, +1: superior, +2: diagnostically superior). Statistical analysis used the Wilcoxon-, the Mann-Whitney-U-test and the intra-class-correlation coefficient (ICC).

Results: With standard kernel, image quality in dose-reduced studies was comparable to the baseline at ASIR 70% in volume mode (-0.07±0.29, p=0.29). Volume mode was superior to slice mode (significant for ASIR 70-100%; p < 0.05). For lung kernel every ASIR level outperformed the baseline image quality (p < 0.001), with ASIR 30% rated best (slice: 0.70±0.6, volume: 0.74±0.61). Mean CTDIvol decreased from 17.2±6.9 (FBP baseline) to 8.0±2.3 mGy (ASIR follow-up; p < 0.001). ICC was 0.70.

Conclusion: Vendors recommendation of 30-50% ASIR is fair. But for standard kernel ASIR 70% in volume mode and for lung kernel ASIR 30% performed best, allowing for 50% dose reduction.

B-0515 11:15

Intraindividual comparison of image quality using retrospective and prospective respiratory gating for the acquisition of thin sliced 4D MDCT of the thorax

M. Regier¹, F.O. Henes¹, D. Schwarz¹, M. Groth¹, G. Riesenberger¹, G. Adam¹, P.G.C. Begemann²; ¹Hamburg/DE, ²Düsseldorf/DE (mregier@uke.de)

Purpose: To intraindividually compare image quality and anatomical depiction of the lung and mediastinum using retrospective as well as prospective respiratory gating for the acquisition of 4D MDCT in a porcine model.

Methods and Materials: Five tracheally intubated pigs underwent 64-row MDCT of the thorax. For retrospective and prospective gating the frequency of the respirator was adjusted to 10, 14, 18 and 22 respiratory cycles/min. The table speed varied between 3.9, 5.7 and 7.6 mm/sec. Free-breathing scans of the lungs were performed with the same respiratory frequencies. After respiratory cut-off an additional scan in breathhold technique was acquired which served as the reference. Three reviewers independently analysed the CT data applying a 4-point-grading scale regarding the degree of artefacts observed and the anatomical depiction (1, excellent; 4, non-diagnostic). Comparison of different techniques was performed using Wilcoxon-matched paired test.

Results: Breathhold imaging allowed for the highest image quality (mean values: trachea, 1.00; bronchi, 1.10; lung parenchyma, 1.08; diaphragm, 1.00; pericardium, 1.80). Retrospective gating proved to be of superior image quality compared to prospective gating for all respiratory frequencies (p > 0.05). With the respiratory frequency set to 14/min and a table speed of 5.7 mm/sec retrospective gating

even enabled the same image quality as breathhold imaging. Performing image acquisition during free breathing lead to a minor image quality compared to all other techniques applied.

Conclusion: In an experimental setting, retrospective gating is superior to prospective gating and can even be of equivalent image quality as standard breathhold imaging when set to lower respiratory frequencies and table speed.

B-0516 11:24

Adaptive iterative dose reduction using three-dimensional processing (AIDR 3D) for reduced and low-dose CT examination: comparison with standard-dose CT of image quality and radiological finding assessment for patients with various pulmonary diseases

Y. Ohno¹, M. Nishio¹, H. Koyama¹, D. Takenaka¹, T. Yoshikawa¹, S. Matsumoto¹, N. Sugihara², H. Inokawa², K. Sugimura¹; ¹Kobe/JP, ²Ohtawara/JP (yosirad@kobe-u.ac.jp)

Purpose: To compare the image noise reduction capabilities and radiological findings assessments for reduced- and low-dose chest CT without and with adaptive iterative dose reduction using three-dimensional processing (AIDR 3D) with those for standard-dose CT for patients with various pulmonary diseases.

Methods and Materials: Chest CT examinations with three different tube currents and using 16- and 64-detector row CT were administered to 37 patients. 150 mAs (standard-dose) data was reconstructed as thin-section CT without AIDR 3D, and CT data at 25 mAs (low-dose) and 50 mAs (reduced-dose) as thin-section CT without and with AIDR 3D. To compare image quality, image noise of all CTs was quantitatively assessed by means of ROI measurements. For comparison of radiological finding assessments, probabilities of emphysema, ground glass opacity, reticular opacity, bronchiectasis, honeycomb pattern and nodules were evaluated on a 5-point scale. Then, image noise and agreements of radiological findings between standard-dose CT and others were statistically evaluated.

Results: Image qualities of reduced- and low-dose CTs without AIDR 3D were significantly lower than that of others (p < 0.05). All intra-method agreements for emphysema, GGO, bronchiectasis, honeycomb pattern and nodules, except for those observed on low-dose CT without AIDR 3D, were almost perfect (κ > 0.81). Agreements for reticular opacity of reduced-dose CT were also almost perfect, while the respective agreements of low-dose CT without and with AIDR 3D were moderate (κ=0.49) and substantial (κ=0.74).

Conclusion: AIDR 3D is useful for image noise reduction and radiological finding assessments obtained with reduced- and low-dose CTs for patients with various pulmonary diseases.

B-0517 11:33

Model-based iterative reconstruction technique for radiation dose reduction in chest CT

M. Katsura, I. Matsuda, M. Akahane, J. Sato, H. Akai, A. Kunimatsu, K. Yasaka, K. Ohtomo; *Tokyo/JP*

Purpose: To intraindividually compare image quality characteristics of low-dose chest CT reconstructed with model-based iterative reconstruction (MBIR) and adaptive statistical iterative reconstruction (ASIR), and standard-dose CT reconstructed with ASIR.

Methods and Materials: In this prospective study, 100 patients (male/female 55/45, age 65.6±12.4years) underwent unenhanced chest CT scan at standard-dose and low-dose with a 64-row multidetector CT scanner, which involved the use of automatic tube current modulation with fixed noise indexes (11.1/24.82 of 5 mm for standard-dose/low-dose CT). Images were reconstructed blending of 50% filtered back projection and 50% ASIR image data (ASIR50) for standard-dose, and at ASIR50 and MBIR for low-dose CT. Two radiologists assessed the images in a blinded and randomised manner for subjective image noise, artefacts, critical reproduction of visually sharp chest structures, and diagnostic acceptability. Objective image noise was measured in the lung parenchyma. Data were analysed by using the sign test and the pair-wised student t-test.

Results: There was a 79.0% decrease for dose-length product with low-dose CT, compared to standard-dose CT. Low-dose MBIR images had significantly lower objective image noise in the lung parenchyma (16.93±3.00), compared with low-dose ASIR (49.24±9.11, P < 0.01) and standard-dose ASIR images (24.93±4.65, P < 0.01). Diagnostic acceptable images were obtained with all low-dose MBIR images, although they tended to have motion artefacts and pixilated blotchy appearances.

Conclusion: In chest CT images acquired with nearly 80% radiation dose-reduction, MBIR significantly improves image quality compared to ASIR, and provides diagnostic acceptable images; however, image qualities of low-dose MBIR are not completely equivalent to those of standard-dose ASIR.

B-0518 11:42

Can iterative reconstruction restore image quality at 60% dose reduction? Clinical experience in 50 patients with simultaneous availability of low-dose and standard-dose images from dual source datasets

F. Pontana, D. Moureau, J.-B. Faivre, T. Flohr, M. Rémy-Jardin, J. Remy; Lille/FR (francois.pontana@chru-lille.fr)

Purpose: To compare image quality of low-dose images reconstructed with a raw-data-based iterative reconstruction technique (SAFIRE) with standard-dose filtered back projection (FBP) CT.

Methods and Materials: 50 consecutive dual source chest CT datasets, acquired in the conditions of routine clinical practice (120 kVp; 110 mAs) with (a) both tubes set at similar energy, (b) the total reference mAs split up in a way that 40% of the reference mAs was applied to tube A (i.e., 44 mAs); (c) while 60% of the reference mAs was applied to tube B (i.e., 66 mAs). Two series of images were generated: (a) full-dose images (generated from both systems) reconstructed with FBP (group 1); and (b) low-dose images (generated from tube A) reconstructed with SAFIRE (group 2).

Results: On group 2 images, there was: (a) a significant reduction in the objective image noise measured at the level of the trachea on mediastinal (16.04 ± 5.66 vs 17.66 ± 5.84) ($p=0.0284$) and lung images (29.77 ± 6.79 vs 37.96 ± 9.03) ($p < 0.0001$); (b) a similar visual perception of noise on mediastinal ($p=1$) and lung images ($p=1$), mainly rated as minimal; and (d) a similar overall image quality, rated as excellent in 66% (33/50) of examinations, without loss of diagnostic information as assessed by the comparative analysis of individual CT features of lung infiltration (98.4%; 95% CI=[96.9%-99.9%]).

Conclusion: Despite 60% dose reduction, the raw-data-based iterative reconstruction technique allowed better objective and similar subjective image quality of low-dose images compared to full-dose FBP images.

B-0519 11:51

Evaluation of dose reduction and image quality in chest CTs using adaptive statistical iterative reconstruction with the same group of patients

L. Qi, L. Tang, X.-P. Zhang, Y. Li, Y. Li; Beijing/CN (tanglei@bjcancer.org)

Purpose: To compare the image quality and radiation dose of chest CT images reconstructed with a blend of adaptive statistical iterative reconstruction (ASIR) and filtered back projection (FBP) with images generated using conventional FBP.

Methods and Materials: Patients with chest CT reexaminations were alternately assigned to two scanners with different reconstruction techniques. The study groups included noise index (NI) 11 with 30% ASIR (A30), NI 13 with 40% ASIR (A40), NI 15 with 50% ASIR (A50) and NI 17 with 60% ASIR (A60), sequentially changed every two months. The control images were obtained using FBP and NI 11. All acquisitions were performed with automatic dose modulation. Paired-t and non-parameters tests were applied to compare the difference.

Results: The radiation doses were significantly lower in the examinations used ASIR ($p < 0.001$). The mean dose reduction rate for each group (A30-60) was 27.7%, 45.2%, 57.1% and 71.8%, respectively. The image quality of groups A30-A50 was not inferior to those of the control examinations. The image noise of group A60 was greater and subjective image quality was inferior to that of the control.

Conclusion: ASIR enabled the use of a higher NI with automatic dose modulation. With 50% ASIR and a NI of 15, the effective radiation dose was reduced by 57%, without compromising image quality.

10:30 - 12:00

Room D2

Interventional Radiology

SS 909

Hepatocellular carcinoma: endovascular

Moderators:

G. Antoch; Düsseldorf/DE

R. Golfieri; Bologna/IT

B-0520 10:30

Predictive factors of downstaging of hepatocellular carcinoma (HCC) beyond the Milan criteria treated with intra-arterial chemoembolisation

V. Bova, L. Maruzzelli, R. Miraglia, G.B. Vizzini, F. Tuzzolino, A. Luca; Palermo/IT (valentinabova@inwind.it)

Purpose: The present study was undertaken to retrospectively analyse the long-term clinical results in patients suitable for liver transplantation, who underwent transarterial chemoembolisation (TACE), with hepatocellular carcinoma (HCC) who exceeded the Milan criteria, to determine predictive factors of successful downstaging.

Methods and Materials: Between January 2004 and December 2010, 304 consecutive patients with HCC were treated by repeatedly performed TACE, 80 of them exceeding the Milan criteria. Patients with infiltrative HCC, hypovascular HCC, portal vein thrombosis, were excluded, with a final study population of 48 patients. Tumour response to TACE was evaluated at 1 month with CT/MR according to amended Response Evaluation Criteria in Solid Tumours (RECIST) guidelines. Successful downstaging was defined as a reduction in the number and size of viable tumours to within the Milan criteria and AFP < 400 ng/ml for at least 6 months.

Results: After TACE, 19 patients (39%) had their tumours successfully downstaged; 29 patients (61 %) did not. No intergroup differences existed with respect to patient characteristics or types and number of treatments. However, at multivariate analysis, alpha-fetoprotein levels < 100 ng/ml and 3-years Metroticket were significant independent prognostic variables of successful downstaging ($p < 0.023$, $p < 0.049$, respectively). Kaplan Meyer patient survival rate was significantly higher in the downstaged group than in the not-downstaged group ($p < 0.00113$)

Conclusion: In patients with HCC beyond the Milan criteria, biological characteristics of the tumour may predict a good response to downstage after TACE.

B-0521 10:39

Balloon-occluded percutaneous radio-frequency thermal ablation (RFA) plus transcatheter arterial chemoembolisation (TACE): a new combined single-step therapy for treatment of single large hepatocellular carcinoma

M. Nestola, R. Iezzi, M. Santoro, R. Dattesi, M. La Torre, L. Bonomo; Rome/IT

Purpose: To evaluate the feasibility and safety of combined single-step therapy with balloon-occluded RFA followed by superselective TACE in patients with single unresectable hepatocellular carcinoma larger than 3 cm.

Methods and Materials: 10 consecutive patients with single unresectable large HCC (mean diameter 4.43 ± 1.27 cm; range: 3-6.5 cm), not suitable to thermal ablation alone for size and site of the lesion, were enrolled in our single-centre multidisciplinary pilot study. The schedule of treatment consisted of: percutaneous RFA (single 3-cm monopolar needle insertion) of the target lesion during occlusion of the hepatic artery supplying the tumour followed by superselective TACE with epirubicin (Farmorubicin® 50 mg Powder)-loaded DC Bead (100-300micron). Adverse events as well as intra/periprocedural complications were clinically assessed. Early local efficacy in target lesions in terms of persistence of contrast enhancement and presence of necrotic diameter was evaluated on 1-month follow-up multiphasic CT basing on m-RECIST criteria.

Results: Technical success was achieved in all patients. No major complications occurred. Overall technical success, defined as complete devascularisation during the arterial phase of the target lesion, was achieved in 8/10 patients with 2 partial response (persistence of vital tissue less than 30%), with a nonenhancing area corresponding in shape to the previously identified HCC (mean necrotic diameter 5.62 ± 1.07 cm; range: 4.2-8 cm).

Conclusion: Balloon-occluded-RFA plus TACE seems to be a safe and effective combined therapy for the treatment of advanced unresectable single large HCC, allowing to obtain a high complete local response rate also in patients not suitable to thermal ablation alone.

B-0522 10:48

Long-term recurrence rates of HCC treated with doxorubicin eluting DC bead

E. Bouma, A. Pomoni, A. Charokopakis, E. Karagiannis, H. Moschouris, M. Pomoni, L. Thanos, K. Malagari, D. Kelekis; *Athens/GR*

Purpose: The objective was to report on the long-term recurrences of HCC that presented complete response after treatment with 2-4 scheduled sessions of chemoembolisation with doxorubicin-loaded DC bead.

Methods and Materials: 45 patients not suitable for curable treatments that had been treated with DC bead loaded with doxorubicin and achieved complete response were included. Doxorubicin loading was done at 37.5 mg/ml of reconstituted beads. Child Pugh class was A/B (28/17;62.2%/37.8%), Okuda stage was 0/1 (28/17;62.2%/37.8%).

Results: Local recurrences and new lesions considered as recurrent disease were separately recorded. Recurrence rates were: new lesions in Child A patients with dominant lesion ≤ 5 cm occurred in 23%/53.8%/84.6%, with dominant lesion > 5 cm occurred in 25%/50%/87.5% during 1st, 3rd, 5th year, respectively. Local lesions in Child A patients with dominant lesion ≤ 5 cm occurred in 30.7%/61.5%/61.5%, with dominant lesion > 5 cm occurred in 37.5%/62.5%/87.5% during 1st, 3rd, 5th year, respectively. New lesions in Child A patients with multinodular lesions occurred in 57.1%/100% during 1st and 2nd year, respectively. Local lesions in Child A patients with multinodular lesions occurred in 71.4%/100% during 1st and 2nd year, respectively. New lesions in Child B patients with dominant lesion ≤ 5 cm occurred in 36.4%/63.6%/90.9%, with dominant lesion > 5 cm occurred in 33.3%/100% during 1st, 3rd, 5th year, respectively. Local lesions in Child B patients with dominant lesion ≤ 5 cm occurred in 36.4%/54.5%/72.7%, with dominant lesion > 5 cm occurred in 33.3%/83.3%/83.3% during 1st, 3rd, 5th year, respectively. Overall survival at 1-yr, 2-yr, 3-yr, 4-yr and 5-yrs was 100%,100%,97.8%, 88.9% and 62.2%, respectively. **Conclusion:** DEB-DOX achieves high rates of 5-yr survival for patients that yielded CR after initial scheduled treatments but cannot be classified among curative treatments.

B-0523 10:57

Single-step balloon-occluded percutaneous radio-frequency thermal ablation (RFA) plus transcatheter arterial chemoembolisation (TACE) for treatment of "complex" unresectable hepatocellular carcinoma

M. Santoro, R. Iezzi, R. Dattesi, M.F. la Torre, M. Nestola, L. Bonomo; *Rome/IT* (*dott.santoromarc@gmail.com*)

Purpose: To evaluate the feasibility and safety of single-step balloon-occluded-RFA followed by TACE in patients with "complex" unresectable HCC, previously not suitable to RFA alone due to their localisation.

Methods and Materials: 15 consecutive patients with single HCC (mean diameter 4.17 \pm 1.02 cm), adjacent to the diaphragm (7 lesions), proximal to the hepatic portal Glisson's capsule (6), or located on the intra-abdominal free surface (2), considered as "complex" for their unfavourable location, and not suitable for RFA alone, were enrolled in our single-centre multidisciplinary pilot study. The treatment was composed by RFA (single 2-cm or 3-cm monopolar needle insertion) during occlusion of the feeding artery followed by superselective TACE (conventional-TACE or with DC-BEAD). Adverse events and intra/periprocedural complications were clinically assessed. Tumour response was evaluated on 1-month follow-up multiphasic CT based on mRECIST criteria.

Results: Technical success was achieved in all patients. No major complications occurred. A mean total treated diameter (necrotic diameter plus circumferential peripheral lipiodol uptake for conventional TACE; mean necrotic diameter for TACE with DC-Bead) of 4.67 \pm 1.43 was obtained. Based on mRECIST criteria, a tumour response was obtained in all patients, with a complete response achieved in 11 out of 15 patients (73.3%), with a partial response in the last 4 patients (residual tumour $< 30\%$), without any progressive disease.

Conclusion: Balloon-occluded-RFA plus TACE seems to be a safe and effective therapy for the treatment of "complex" HCC, allowing to obtain a high complete local response rate, without complications, also in patients not suitable to RFA alone.

B-0524 11:06

Radioembolisation of hepatic tumours: hepatopulmonary shunt reduction by administration of Sorafenib

J.M. Theysohn, J.F. Schlaak, J. Ertle, S. Mueller, A. Bockisch, T.C. Lauenstein; *Essen/DE* (*jens.theysohn@uni-duisburg-essen.de*)

Purpose: An emerging therapy option for unresectable liver malignancies is radioembolisation (RE) using the beta emitter 90 Yttrium. Contraindications, however, may represent high hepatopulmonary shunt fractions (i.e. due to tumorous

AV-fistulae). A systemic drug approved for the treatment of advanced primary liver cancer is the protein kinase inhibitor Sorafenib. Aim of this study was to assess if reduction of the hepatopulmonary shunt fraction can be achieved by the administration of Sorafenib prior to RE.

Methods and Materials: 130 patients suffering from hepatocellular carcinoma were studied. Patients consecutively underwent hepatic digital subtraction angiography (DSA) with the administration of Technetium-99m-labelled macroaggregated albumin (99mTc-MAA) and a SPECT/CT, from which data the pulmonary shunt fraction was calculated. Eight patients with a contraindication for RE due to an estimated pulmonary radiation dose of over 30 Gy resulting from high shunt values were enrolled. These patients received Sorafenib (Nexavar, Bayer) for 12 weeks on average. Afterwards, DSA and shunt fraction calculation was repeated.

Results: In all eight patients a reduction of the hepatopulmonary shunt fraction of MAA was achieved (average shunt reduction of 62.7%; range 15-87%). Following Sorafenib administration, RE therapy was possible in 7/8 patients. In one patient, however, reduction of hepatopulmonary shunt fraction was not sufficiently high for subsequent RE therapy.

Conclusion: Reduction of hepatopulmonary shunt fraction in patients with advanced HCC can be successfully induced by the administration of Sorafenib. Even patients with high hepatopulmonary shunt fractions may become eligible for radioembolisation therapy.

B-0525 11:15

Five-year survival of HCC patients treated with doxorubicin eluting DC bead

E. Bouma, A. Charokopakis, H. Moschouris, A. Pomoni, K. Malagari, J. Kornezos, S. Tandeles, V. Tsagouli, M. Pomoni; *Athens/GR*

Purpose: Five-year survival of hepatocellular carcinoma (HCC) patients treated with DC Bead loaded with doxorubicin (DEB-DOX) was the purpose of this study.

Methods and Materials: 173 patients not suitable for curable treatments have been prospectively enrolled (mean age 70.4 \pm 7.4 years). Child Pugh class was A/B (102/71; 59% / 41%), Okuda stage was 0/1/2 (91/61/19; 53.2%/35.7%/11.1%), and mean lesion diameter was 7.6 \pm 2.1 cm. Lesion morphology was one dominant ≤ 5 cm (22%), one dominant > 5 cm (41.6%), multifocal ≤ 5 (26%) and multifocal > 5 (10.4%). Patients had scheduled embolisations until 3 sessions and then on demand (scheduled sessions were every 2 months in 112 patients and every 3 in 61). Follow-up ranged between 2 and 68 months until time of death or time of the analysis.

Results: Overall survival at 1-yr, 2-yr, 3-yr, 4-yr, 5-yrs was 93.6%, 83.8%, 62%, 41.04% and 22.5%, with higher rates achieved in the Child A patients compared to Child B (95%, 88.2%, 61.7%, 45% and 29.4% vs 91.5%, 75%, 50.7% 35.2% and 12.8%). Mean overall survival was 43.8 months (1.2-64.8). Cumulative survival was better for Child A compared to Child B patients (p=0.029). For dominant lesions ≤ 5 cm 1-, 2-, 3-, 4- and 5-year survival rates were 100%, 95.2%, 71.4%, 66.6% and 47.6% for Child A patients, and 94.1%, 88.2%, 58.8%, 41.2%, 29.4% and 23.5% for Child B. Regarding DEB-DOX treatment multivariate analysis identified number of lesions (p=0.033), lesion vascularity (p < 0.0001), initially achieved CR (p < 0.0001) and OR (p=0.046) as significant and independent determinants of 5-year survival.

Conclusion: DEB-DOX results with high rates of 5-yr survival for dominant tumours ≤ 5 cm.

B-0526 11:24

Blood flow redistribution: infusion strategy before radioembolisation

C. Spreafico, R. Lanocita, C. Morosi, E. Civelli, M. Maccauro, R. Romito, L.F. Frigerio, A. Marchianò, V. Mazzaferro; *Milan/IT* (*carlo.spreafico@istitutotumori.mi.it*)

Purpose: Problems arise when performing a 90Y-particle infusional therapy in tumours with multiple arterial supplies. We aim at demonstrating that tumours can be treated via one main feeding artery achieving flow redistribution by embolising all accessory vessels.

Methods and Materials: From Jan. 2007 to March 2011, 100 90Y-radioembolisations were carried out on patients with intermediate to advanced HCC using glass microspheres TheraSphere. In 19 lesions/17 pts, mean diameter 65 mm, 18 (9 intra 9 extra hepatic) accessory branches were found and embolised. Within the next 4 weeks all pts were treated by 90Y infusion. The 17 lesions with flow redistribution were chosen as target lesions and their radiological response was evaluated according to mRECIST criteria.

Results: In all pts the 90Y-infusion was satisfactory, the complete tumour perfusion was assessed prior to radioembolisation by angiography in all pts and after the 90Y-infusion (exploiting the Bremsstrahlung effect) by SPECT-CT in 15/17 pts. In

the 15 assessable pts the mean follow-up was 6 months and the response rate in their 17 lesions was 3 CR, 8 PR and 6 SD.

Conclusion: All embolisation procedures were successfully carried out with no complications and responses were encouraging: objective response rate (CR+PR) in 11/17 lesions (64.7%). No correlation emerged between the residual active lesion and the accessory artery territory. Our findings confirmed the actual intra-tumoral flow redistribution after embolising the accessory arteries, which makes it possible to treat the tumour through its single main feeding artery.

B-0527 11:33

Transarterial chemoembolisation (TACE) with mitomycin and cisplatin in hepatocellular carcinoma: curative, palliative and neoadjuvant therapy protocol

T.J. Vogl, K. Auerbach, K. Engels, K. Ochs, S. Zangos, N.N.N. Naguib, T. Lehnert, N.E. Nour-Eldin; *Frankfurt/DE (t.vogl@em.uni-frankfurt.de)*

Purpose: To evaluate the effect of transarterial chemoembolisation (TACE) on local response and survival of patients with hepatocellular carcinoma (HCC) in a curative, palliative and neoadjuvant protocol.

Methods and Materials: In a retrospective study, 356 patients (male:259/female:97) with histopathologically proven HCC were treated with repetitive TACE (mitomycin, cisplatin, lipiodol) between April 2003 and February 2011. The underlying liver pathology, Child-Pugh score, tumour volume, number of tumours, local response and survival since first diagnosis and first TACE were analysed. Local tumour response was evaluated by MRI and CT volumetric measurements, and survival rates from first TACE and last TACE were calculated according to the RECIST criteria.

Results: Local tumour control showed partial response (PR) in 113 patient (31.74%), stable disease (SD) in 123 patients (34.55%) and progressive disease in 120 patients (33.71%). Local response rate per patient was 0% CR, 29% PR, 37% SD and 34% PD. The survival rates of all patients since first diagnosis and first TACE were 35.45 months (median) and 26.22 months (median), respectively. For neoadjuvant intervention and resection survival rates since first diagnosis and first TACE were 12.0 months and 6.6 months, for neoadjuvant intervention and transplantation 21.88 months and 21.12 months and for neoadjuvant intervention followed by different ablation techniques (LITT, MW, RFA) 28.55 months and 19.58 months.

Conclusion: TACE for the treatment of HCC is an effective therapy for all three therapy protocols. In neoadjuvant therapy it can be used as a bridging therapy, in palliative therapy it stabilises the tumour load.

B-0528 11:42

Preprocedural 3D-CT image blending with fluoroscopy to guide catheterisation of proper hepatic artery during transarterial chemoembolisation: a feasibility study

I. Bargellini, E. Bozzi, A. Cicorelli, A. Lunardi, F. Turini, R. Cioni, C. Bartolozzi; *Pisa/IT (irenebargellini@hotmail.com)*

Purpose: To assess feasibility of preprocedural computed tomography 3D model fusion with fluoroscopy to guide the catheterisation of the proper hepatic artery during transarterial chemoembolisation (TACE) of hepatocellular carcinoma (HCC).

Methods and Materials: Twenty consecutive cirrhotic patients with HCC undergoing TACE were prospectively enrolled in the study. The early arterial phase axial images of the preprocedural CT were post-processed on an independent workstation connected to the angiographic system (Innova 4100, GE Healthcare), obtaining a 3D volume rendering image (VR) that included: abdominal aorta, celiac trunk, common, proper, left and right hepatic arteries, superior mesenteric artery, origin of the renal arteries, first and second lumbar vertebrae. The VR image was manually registered to the 2D fluoroscopic image using the lumbar spine as reference. The VR image was then used as guidance to selectively catheterise the proper hepatic artery using an adequately shaped 5 Fr hydrophilic catheter and a 0.035" hydrophilic guidewire. The procedure was considered successful when performed with no need for intra-arterial contrast injections or angiographic acquisitions.

Results: The procedure was successful in 19/20 patients (95%). In one patient, celiac trunk angiography was required for the presence of a severe ostial stenosis that was under-estimated at CT. Time for image reconstruction and registration was < 10 minutes in all cases.

Conclusion: The use of preprocedural CT image blending to fluoroscopy enables confident and direct catheterisation of the proper hepatic artery with no need for celiac trunk angiography or other acquisitions, thus reducing radiation exposure, contrast media administration and procedural time.

B-0529 11:51

Radioembolisation with Y-90 glass microspheres in hepatocellular carcinoma: safety and long-term survival

T.A. Heusner¹, P. Hilgard², S. Mueller², J. Ertle², A. Bockisch², G. Antoch¹; ¹Düsseldorf/DE, ²Essen/DE (heusner@med.uni-duesseldorf.de)

Purpose: Radioembolisation with glass microspheres allows effective locoregional therapy of patients with hepatocellular carcinoma (HCC) not eligible for local therapies. The aim of this study was to validate evidence on safety and efficacy of this treatment in a European sample of patients with advanced HCC.

Methods and Materials: 108 consecutive patients with advanced HCC were included in this prospective open label study. Y-90 microspheres were administered in a lobar fashion over the right or left branch of the hepatic artery. Response to treatment was evaluated by CT imaging applying RECIST and WHO criteria with recent EASL/NCI amendments. Time to progression and overall survival were estimated by the Kaplan-Meier method.

Results: 106/108 patients had underlying liver cirrhosis, with Child-Pugh scores between 4 and 8. 176 treatment sessions were performed ranging between 1 and 3 treatments per patient. The mean radiation dose per treatment was 120 (±18) Gy. According to EASL criteria, complete responses were determined in 3%, partial responses in 37%, stable disease 53% and primary progression in 6%. Time to progression (TTP) was 10.0 months, the median overall survival was 16.4 months. No lung or visceral toxicity was observed. The most frequent adverse event was a transient fatigue-syndrome.

Conclusion: Radioembolisation with Yttrium-90 glass microspheres for patients with advanced HCC is a safe and effective treatment which can be utilised even in cases with compromised liver function.

10:30 - 12:00

Room E1

Musculoskeletal

SS 910

Spine and peripheral nerves

Moderators:

I.W. McCall; *Oswestry/UK*
M.-A. Weber; *Heidelberg/DE*

B-0530 10:30

The assessment for the intervertebral foramen in the lumbar disk herniations using 640-slice dynamic volume CT: a pilot study

Y.-I. Song, Z. Jia, X.-s. Li, Z. Wang, Y. Tian; *Beijing/CN (ylsong²⁰⁰⁶@sohu.com)*

Purpose: To evaluate the dynamic changes of intervertebral foramen during lumbar extenso-flexal movement in the patients of lumbar disk herniations (LDH) using Toshiba Aquilion ONE 640-slice dynamic volume CT (AQ-ONE).

Methods and Materials: AQ-ONE was used to perform the scanning for the continuous lumbar spine movement for 39 patients group with LDH, who were positive cases for routine MRI static scanning, central type of projecting backward. The Cobb angle was measured to determine the reference image of 0 degree in the movement process. The LDH (L3-S1) and foramen intervertebrale in the static and dynamic situations were measured and compared through MPR, MIP and VR processing in different angles. The effective radiation dose is 5~12mSv.

Results: Among the 39 patients, totally 66 disk protrusion were classified by Spangler method. At the 20 degree of hyperextension position, the intervertebral disc in grade III and IV increased 48% than static. Compared with the images of routine MRI, the discs increased 1.33 mm per 10 degree extension and decreased 0.85 mm per ten degrees flexion. LDH in hyperextension position had more influence than hyperflexion, otherwise, intervertebral foramen showed different characteristics in hyperflexion position. The foramens decreased 12.15 mm²per 10 degrees during lumbar extension. At the 10 degree hyperflexion position, 88% foramens are reduced by 6.58 mm². Ninety-one percent foramens of 20 degree hyperflexion are larger 7.71 mm² than the ones of 10 degree.

Conclusion: CT dynamic lumbar scan can reflect the continuous variations of LDH during the movement, which will provide important information for the treatment.

B-0531 10:39

Sodium imaging of the lumbar intervertebral disc at 7 Tesla: correlation with T2 mapping and modified Pfirrmann score at 3 Tesla

I.-M. [Noebauer-Huhmann](#)¹, V. Juras¹, C.W.A. Pfirrmann², P. Szomolanyi¹, S. Zbyn¹, A. Messner¹, J. Wimmer¹, K. Friedrich¹, S. Trattinig¹; ¹Vienna/AT, ²Zurich/CH (iris.noebauer@meduniwien.ac.at)

Purpose: To compare sodium imaging of lumbar intervertebral discs in asymptomatic volunteers at 7 Tesla with quantitative T2 mapping and morphological scoring at 3 Tesla.

Methods and Materials: In 10 asymptomatic volunteers (9m, 1f; mean age 30 years, range, 23-43), the discs L2/3 to L5/S1 were examined. At 7 Tesla, normalised sodium signal-to-noise ratios were calculated, using region-of-interest analysis. At 3 Tesla, T2 mapping was performed with a multi-echo-spin echo sequence (TR/TE 1200/13.8, 27.6, 41.4, 55.2, 69.0 and 82.8 msec). T2 values were calculated over the nucleus, with a pixel-wise, mono-exponential non-negative least squares fit analysis. Morphological grading according to a modified Pfirrmann score was assessed, and Pearson's correlation analysis of the covariates was performed.

Results: In total, 40 discs were evaluated. The mean normalised sodium signal intensity was 275.5 (SD 115.4). The T2 mapping showed a mean value of 89.8 ms (SD 19.34 ms). The median modified Pfirrmann score was 2b (with 90% < 3c). The Pearson correlation coefficient showed a near moderate inverse correlation between sodium imaging and the Pfirrmann score ($r=-0.49$), a moderate inverse correlation between T2 mapping and the Pfirrmann score ($r=-0.62$), and no correlation between sodium imaging and T2 mapping ($r=0.06$).

Conclusion: Our results suggest that MR imaging of the intervertebral disc, using sodium imaging and T2 mapping, characterises different, measurable biochemical component changes, and that both of these methods affect the Pfirrmann score.

B-0532 10:48

MR imaging of the lumbar spine: comparison of 3D isotropic turbo spin-echo SPACE sequence versus conventional 2D sequences at 3.0 T

S. [Lee](#), W.-H. Jee, J.-Y. Jung, S.-Y. Lee, K.-Y. Ha, C.-K. Park; *Seoul/KR* (sungwonlee@gmail.com)

Purpose: To compare isotropic three-dimensional (3D)-T2-weighted-turbo-spin-echo sequence (TSE-SPACE) with conventional two-dimensional (2D)-TSE-sequences for evaluating the neural foramina and nerves of the lumbar spine at 3.0 T MR imaging.

Methods and Materials: The institutional ethics committee approved this retrospective study and waived the requirement of informed consent. 43 patients who had spine surgery for disc herniation and had 3.0 T-spine-MRI were included. In addition to conventional 2D-TSE sequences, sagittal-3D-T2-weighted-TSE-SPACE was obtained to produce multiplanar intermediate-weighted images with 0.6-mm isotropic resolution along the axial, coronal, and oblique coronal planes. Each 2D and 3D-TSE images were independently scored for the degree of lumbar neural foraminal stenosis, nerve compression, and nerve swelling by two reviewers. These scores were compared with operative findings and initial symptoms. Interobserver agreements were compared with kappa statistics and correlation with the surgery was done by McNemar test.

Results: 33 neural foraminal stenoses in 30 patients and 60 nerve compromise in 39 patients were found at surgery. The mean diagnostic sensitivity and accuracy of 2D-TSE sequences versus 3D-TSE-SPACE were 73% and 82% versus 84% and 92% for neural foraminal stenosis; 66% and 56% versus 79% and 81% for nerve compression. Coronal and oblique coronal reformatted images of 3D-TSE-SPACE demonstrated higher correlation with the laterality of the symptom than 2D-TSE sequences (73% versus 49%). The interobserver agreements were substantial ($\kappa = 0.72$) on 3D-TSE-SPACE and moderate ($\kappa = 0.44$) on 2D-TSE sequences.

Conclusion: Isotropic 3D-T2-weighted-TSE-SPACE sequence was comparable to conventional 2D-TSE sequences for diagnosing foraminal stenosis and nerve compression at 3.0 T-lumbar spine MRI and showed better symptomatic correlation.

B-0533 10:57

Multi-echo MRI for muscle-fat quantification in patients with low back pain: comparison to spectroscopy

M.A.F. [Fischer](#), R. Guggenberger, D. Nanz, G. Andreisek; *Zurich/CH* (michaelalexander.fischer@usz.ch)

Purpose: To prospectively compare fat-signal-fractions derived from spoiled-gradient dual-echo (SPGR-DE) and multi-echo (SPGR-ME) MRI with and without correction of T2*-bias for quantification of muscle-fat content (MFC) in patients with low back pain (LBP) using single-voxel spectroscopy as the standard of reference.

Methods and Materials: 41 patients (24 women; 56±16 years) suffering of LBP underwent clinically indicated MRI at 1.5-Tesla including SPGR-DE and SPGR-ME for quantification of fatty degeneration of the erector spinae muscle in a predefined region-of-interest (ROI) at the level L4/5. Fat-signal-fractions (FSF) were determined from signal intensities (SI) on automatically generated fat-/water-only images from both datasets (FSFDE, FSFME) as well as from T2*-corrected fat-/water-only images derived from SPGR-ME (FSFME*) and compared to spectroscopically determined fractions (FSFSPEC). Student's t-test and the method of Bland-and-Altman were used to study the agreement between FSF derived from SPGR-DE, SPGR-ME and spectroscopy.

Results: Spectroscopic results were obtained in 34/41 patients bilaterally. Mean FSFSPEC was 20.79±12.85 (range, 0.2-76.5; n=75). Correlation between FSF-SPEC and FSFDE, FSFME was significant with correlation-coefficients of $r = .814-.828$. Mean FSFDE, FSFME values significantly differed from FSFSPEC (both, $p < .01$), whereas mean FSFME* showed no significant differences ($p = .90$) and a small mean measurement bias of -0.2% (95% limits-of-agreement, -15.78 - 15.55) compared to FSFSPEC.

Conclusion: Fat-signal fractions as obtained from both SPGR-DE and standard SPGR-ME were significantly larger than determined by spectroscopic analysis, whereas FSF from T2*-corrected SPGR-ME images may allow fast and accurate quantification of MFC in patients suffering of LBP.

B-0534 11:06

Influence of weight-bearing and lumbar lordosis on the dural sac in patients with severe stenosis of the lumbar spinal canal

P. [Niggemann](#)¹, E. Stoetzel², J. Hoeffler², H.K. Beyer², H.H. Schild¹; ¹Bonn/DE, ²Cologne/DE (pascal.niggemann@ukb.uni-bonn.de)

Purpose: Moderate correlation between clinical complaints and imaging in patients with lumbar spinal canal stenosis (SCS) could be due to the lack of applied body weight during horizontal imaging. Positional MRI allows visualising the spine under weight-bearing conditions. The purpose of this study is to analyse the influence of weight-bearing and lordosis on the dural sac (DS) in patients with severe SCS.

Methods and Materials: 211 segments in 127 patients with severe SCS were examined. The size of the DS and the degree of lordosis were measured in supine, extension (standing) and neutral sitting position. The findings were compared for all segments and for segments with stable and unstable slips. Patients were divided into two groups, one with severe claudication and one with less severe or no claudication. The findings were compared for the most narrowed segment.

Results: The spinal canal was most narrowed in extension, whereas the lordosis was most prominent in supine position. The differences between the positions were significant for all parameters. Lordosis is the main factor contributing to the narrowing of the spinal canal. Weight-bearing is an important factor for segments with unstable slips. SCS was less functional in patients with severe claudication compared to the SCS in patients with less severe or no claudication.

Conclusion: Horizontal MRI is reliable to diagnose lumbar SCS since no segment with SCS was missed. Positional MRI seems useful in segment with unstable vertebral slips. The functionality of SCS seems to better correlate with clinical complaints than the maximum SCS.

B-0535 11:15

Correlation between strength of paraspinal lumbar muscles, muscle degeneration and diffusion properties

C.C. [Much](#), J.D. Busch, S. Schlampp, N.D. Forkert, G. Adam, C.R. Habermann; *Hamburg/DE* (cmuch@uke.de)

Purpose: The aim of this study was to evaluate correlations between visible degeneration, diffusion properties and strength of the paraspinal muscles.

Methods and Materials: 15 patients (6 females, 9 males, mean age: 43 years) were imaged with a 1.5 T MR-Scanner (Symphonie, Siemens) and underwent measurements with a specific machine developed for isolated lumbar muscle strength quantification (DELPHEX-Medical LE). T1- and diffusion-weighted imaging (DWI) were performed at the L4/5 level. Fatty and fibrotic degeneration of the muscle compartment and apparent diffusion coefficient (ADC) values of the paraspinal muscles were measured using an in-house developed semi-automatically analysis method. Spearman's rank correlation coefficient (SCC) was used to determine correlations between patient strength (Nm), muscle fat/fibrous fraction (%) and ADC ($\times 10^{-3}$ mm²/s).

Results: Muscle strength showed a moderate negative correlation with fat fraction (SCC: -0.63 to -0.79, $p < 0.05$) and moderate positive correlation with ADC values (SCC: 0.67 to 0.76, $p < 0.05$). Fat/fibrous fraction correlates negatively with ADC (SCC: -0.63, $p < 0.05$).

Conclusion: Our results suggest that the percentage of degenerated muscle and diffusion properties can be used as an indirect marker for muscle strength. Muscular function has, in turn, been demonstrated to be associated with the development and persistence of lower back pain. Quantification of muscular degeneration and ADC values may offer important benefits to MR-based morphologic analysis of the lumbar spine.

B-0536 11:24

Diffusion-weighted MR imaging of the spine at 3-T: feasibility, optimization of b-value and utility to differentiate benign from pathological vertebral compression fractures

G. Fetz¹, N. Theumann¹, C. Federau¹, D. Richarme¹, P. Hagmann¹, J. Pfeuffer², R. Meuli¹, F. Becce¹; ¹Lausanne/CH, ²Erlangen/DE

Purpose: To evaluate the feasibility, determine the optimal b-value, and assess the utility of 3-T diffusion-weighted MR imaging (DWI) of the spine in differentiating benign from pathologic vertebral compression fractures.

Methods and Materials: Twenty patients with 38 vertebral compression fractures (24 benign, 14 pathologic) and 20 controls (total: 23 men, 17 women, mean age 56.2 years) were included from December 2010 to May 2011 in this IRB-approved prospective study. MR imaging of the spine was performed on a 3-T unit with T1-w, fat-suppressed T2-w, gadolinium-enhanced fat-suppressed T1-w and zoomed-EPI (2D RF excitation pulse combined with reduced field-of-view single-shot echo-planar readout) diffusion-w (b-values: 0, 300, 500 and 700s/mm²) sequences. Two radiologists independently assessed zoomed-EPI image quality in random order using a 4-point scale: 1=excellent to 4=poor. They subsequently measured apparent diffusion coefficients (ADCs) in normal vertebral bodies and compression fractures, in consensus.

Results: Lower b-values correlated with better image quality scores, with significant differences between b=300 (mean±SD=2.6±0.8), b=500 (3.0±0.7) and b=700 (3.6±0.6) (all p < 0.001). Mean ADCs of normal vertebral bodies (n=162) were 0.23, 0.17 and 0.11×10⁻³ mm²/s with b=300, 500 and 700s/mm², respectively. In contrast, mean ADCs were 0.89, 0.70 and 0.59×10⁻³ mm²/s for benign vertebral compression fractures and 0.79, 0.66 and 0.51×10⁻³ mm²/s for pathologic fractures with b=300, 500 and 700s/mm², respectively. No significant difference was found between ADCs of benign and pathologic fractures.

Conclusion: 3-T DWI of the spine is feasible and lower b-values (300s/mm²) are recommended. However, our preliminary results show no advantage of DWI in differentiating benign from pathologic vertebral compression fractures.

B-0537 11:33

High-resolution magnetic resonance imaging of the brachial plexus using an isotropic-enhanced scan of 3D-STIR sequence

F. Yang, D. Liu, Y. Lv, X. Kong; Wuhan/CN (fyang@vip.163.com)

Purpose: To investigate the feasibility of imaging brachial plexus in enhanced scan of 3D-STIR sequence in MRI and its diagnostic accuracy in the evaluation of brachial plexopathies.

Methods and Materials: The 3D-STIR sequence scanning and 3D-STIR sequence of enhanced scan were used in 68 patients in the diagnosis of brachial plexus pathologies involving primary and secondary brachial plexus lesions, and in 30 volunteers. All patients had clinical, nerve conduction, and electromyographic findings consistent with brachial plexus lesions.

Results: 3D-STIR sequence and enhanced scan can clearly display all the volunteers from the brachial plexus, course, continuity, shape, signal, and the enhanced scan can improve the suppression effects of background, it is the case that trauma and tumour can be clearly seen involving the brachial plexus due to a variety of signs.

Conclusion: We conclude that the enhanced scan of 3D-STIR sequence is a useful technique in evaluating patients with brachial plexus lesions, and receive a better suppression effects of the background. Magnetic resonance imaging may have significant potential to provide more information about problems such as brachial plexus injuries and peripheral nerve compression.

B-0538 11:42

Diffusion tensor imaging of the median nerve in patients with recurrent carpal tunnel syndrome after surgical release

P. Lindberg, A. Feydy, M.A. Maier, J.-L. Drape; Paris/FR (pavel.lindberg@cch.aphp.fr)

Purpose: Preliminary studies suggest that diffusion tensor imaging (DTI) may be of use for the quantification of structural integrity of the median nerve in patients with carpal tunnel syndrome (CTS). However, how DTI relates to electromyog-

raphy (EMG) and behavioural measures remains unclear. We hypothesised that DTI measures of the median nerve would correlate with slowed nerve conduction and impaired grip force control in patients with postoperative recurring symptoms.

Methods and Materials: Cohort: 16 patients with EMG evidence of recurrent CTS after surgical release (mean post-op time=4 years). The median nerve DTI sequence consisted of 6 noncollinear diffusion gradients (b=1000s/mm²). Anatomical MR images were also collected. Fractional anisotropy (FA) and apparent diffusion coefficient (ADC) values were extracted. Regions of interest were drawn on the median nerve 1.5 cm proximal to and in the carpal tunnel (ratio=distal/proximal).

Results: The median nerve was identified successfully through fibre tracking in all patients. Diffusion parameters for the median nerve were (mean±SD): FA=0.60±0.06 and ADC=0.96±0.11. Mean distal/proximal ratios were: FA=0.87±0.09 and ADC=1.2±0.2. EMG revealed reduced motor conduction (< 50 m/s) in 8 and reduced sensory conduction in 15 patients. Grip force tracking error was higher than normative values in all patients. Sensory nerve conduction correlated with FA ratio (R=0.51, P=0.05). Tracking error correlated with mean FA for the median nerve (R=-0.60, P=0.02) and with FA ratio (R=-0.56, P=0.03).

Conclusion: The results suggest that DTI may be useful for the evaluation of the median nerve in patients with recurrent CTS.

10:30 - 12:00

Room F1

Oncologic Imaging

SS 916

New applications for US and CT in evaluating patients with cancer

Moderators:

T. Bäuerle; Heidelberg/DE
M. Bellomi; Milan/IT

B-0539 10:30

Multicentric prospective study of DCE-US for the evaluation of antiangiogenic treatments: determination of criteria with correlation to overall survival

N. Lassau¹, V. Vilgrain², J. Lacroix³, S. Taieb⁴, A. Sarran⁵, R. Aziza⁶, M. Kind⁷, A. Lucian⁸, S. Koscielny¹; ¹Villejuif/FR, ²Clichy/FR, ³Caen/FR, ⁴Lilles/FR, ⁵Marseille/FR, ⁶Toulouse/FR, ⁷Bordeaux/FR, ⁸Creteil/FR (lassau@igr.fr)

Purpose: A prospective study of dynamic contrast-enhanced ultrasound (DCE-US) with quantification for the evaluation of antiangiogenic treatments was launched (19 centres), supported by the French National Cancer Institute. The objectives were the diffusion of the standardised method, a cost evaluation and the identification of perfusion parameters predicting tumour response.

Methods and Materials: All patients had DCE-US at baseline, D7, D14, D30, D60 and every two months. Each examination included a bolus injection of sonovue (Bracco®) and 3 minutes of raw linear data with an Aplio (Toshiba). Raw data were analysed with a mathematical model (patent PCT/IB2006/003742) to evaluate 7 parameters characterising the tumour perfusion curve. Response to treatment was evaluated every 2 months with RECIST criteria. In order to have sufficient follow-up data, the statistical analysis has to be performed more than 6 months after the inclusion of the last analysed patient. Inclusions were closed in March 2010.

Results: A total of 539 patients have been included (mainly RCC (157) and HCC (107)); more than 2000 DCE-US and 1700 CT-scan were performed. A follow-up more than 12 months showed that 3 parameters have a strong significant difference (P < 0.0003) according to the response at 6 months. The decrease of more than 40% of AUC at one month is correlated to the TTP (P < 001) and OS (P < 0.04)

Conclusion: Final results confirm the usefulness of this tool to monitor antiangiogenic treatments. The criteria : the decrease of more than 40% of AUC at one month is predictive of response.

B-0540 10:39

Parametric maps of tumoral perfusion with dynamic contrast-enhanced ultrasound versus histology: multimodalities melimage project

S. Pitre-Champagnat¹, J.-B. Castaigne¹, L. Calmels¹, A. Leroy-Willing², I. Leguierney¹, J. Thalmensi¹, G. Bonniaud¹, N. Lassau¹, J. Coulot¹; ¹Villejuif/FR, ²Orsay/FR (stephanie.pitre@u-psud.fr)

Purpose: To identify correlations between dynamic contrast-enhanced ultrasonography (DCE-US) and histology in the assessment of the tumoral perfusion with specific methodological tools we developed.

Methods and Materials: Study was conducted on 26 melanoma-bearing nude mice and on 5 patients with metastatic node of melanoma. For preclinical study, DCE-US exam was realised after a 0.1 ml bolus injection of SonoVue® (Bracco, Italy). From the linear raw data, we established parametric maps using the mathematical model of the time intensity curve of tumoral perfusion patented by the team. Two parameters were considered: area under the curve (AUC) and peak intensity (PI). Histological study evaluated microvessel density (MVD) and vessel diameter. These data were obtained within 3 to 6 distinct sections in each tumour and confronted to the parametric maps from DCE-US. For clinical study, DCE-US was performed before surgery with a 4.8 ml bolus injection of SonoVue®.

Results: Among the 26 studied mice, 17 were evaluable with 67 analysed sections. Spatial distribution of AUC and PI was significantly correlated with MVD (respectively, $R_2=0.54$ $p < 0.0001$ and $R_2=0.63$ $p < 0.001$). 12 hypervascularised sections from DCE-US corresponded to a weak MVD but with large vessel diameter. Correlation was also significant (AUV: $R_2=0.69$ $p < 0.001$ PI: $R_2=0.60$ $p=0.003$). From the 5 patients included, 4 could be studied with a contrast uptake between 30 and 100%. Histological analyses are in progress and results will be presented.

Conclusion: Our study shows a correlation between the spatial distribution of perfusion parameters (AUC and PI) and the MVD associated with the vessel size.

B-0541 10:48

Evaluation of the reliability and repeatability of dynamic contrast-enhanced tumour perfusion imaging parameters with high-frequency ultrasound

D.B. Husarik¹, R.C. Nelson², D. Marin², L.W. Hedlund², G.A. Johnson²; ¹Zurich/CH, ²Durham, NC/US

Purpose: To evaluate the reliability and repeatability of dynamic contrast-enhanced tumour-perfusion-imaging with high-resolution-ultrasound in colon-cancer-xenografts in mice.

Methods and Materials: 8 mice with subcutaneous colon-cancer-xenograft tumour models were examined with a Vevo770 ultrasound system (Visualsonics Inc., Toronto, CA) using a RMV 706 40-MHz high frequency transducer and three different microbubble concentrations (2x10⁸, 1x10⁹, 1.2x10¹⁰ microbubbles/mL). Three separate 150 µL bolus injections of each microbubble concentration were examined in each tumour. The recording of each dynamic study was triggered 3 seconds prior to the contrast agent injection and a total of 750 images were recorded over a 64sec period. The following semi-quantitative perfusion parameters were extracted from the time-intensity curves: peak intensity (in arbitrary units=AU), time to peak intensity (in sec), area under the time-intensity curve (AUC) during wash in (in AU), and slope coefficient of the wash in (in AU/sec). The coefficient of variation was calculated for each dynamic parameter of each set of microbubble-concentrations for each tumour.

Results: Peak intensity, time to peak, as well as AUC values correlated significantly ($P < 0.05$) with microbubble-concentration while slope coefficient values did not ($P=0.22$). The semi-quantitative perfusion parameters following 3 injections with the same microbubble-concentration were obtained with varying reliability with a coefficient of variation for peak intensity values of 0.26 ± 0.18 , for time to peak values of 0.26 ± 0.25 , for AUC values of 0.23 ± 0.13 , and for slope coefficient values of 0.32 ± 0.22 .

Conclusion: The evaluated semi-quantitative perfusion parameters demonstrate a varying reliability and repeatability during dynamic contrast-enhanced tumour-perfusion-imaging with high-resolution ultrasound.

B-0542 10:57

Dual source dual energy CT scan to evaluate the mediastinal lymph node metastases in non-small cell lung cancer: feasibility study

Y. Rao, W. Yang, B. Liu, L. Cao, Y. Bu, W. Chai, K. Chen; Shanghai/CN (roy_0326@hotmail.com)

Purpose: To evaluate the accuracy of the weighted iodine concentration from second generation dual source dual energy (DSDE) CT scan in diagnosing mediastinal lymph node metastases in patients with non-small cell lung cancer (NSCLC).

Methods and Materials: A contrast-enhanced dual energy CT scan was performed 30 seconds after the contrast injection (60 ml CM at 3 ml/s) on 21 patients with histopathologically proven NSCLC. The size of lymph nodes and the iodine concentrations (mg/ml) of the mediastinal lymph nodes as well as the aorta on the same image plane were measured in a DE post-processing workstation. The iodine concentrations from the lymph nodes were normalised by the iodine concentrations of aorta according to the blood supply of mediastinum to minimise the patient variation. Statistical analysis was performed to investigate the radiologic-pathologic correlation.

Results: 83 mediastinal lymph nodes from the 21 patients were analysed with 25 proved to be malignant at pathology examination and 58 benign. By comparing the size of lymph nodes and the weighted iodine concentrations, statistically significant differences was found (both with $p < 0.01$). The weighted iodine concentration was 0.10 ± 0.09 mg/ml for malignant lymph nodes group and those for benign group was 0.21 ± 0.13 mg/ml.

Conclusion: The weighted iodine concentrations from DE scan correlated with pathological results of lymph nodes in patients with NSCLC. The weighted iodine concentrations could be a new method to evaluate the mediastinal lymph node metastases in NSCLC.

B-0543 11:06

Is blood flow-blood volume mismatch in colorectal cancer associated with advanced disease?

V.J. Goh¹, K. Miles², B. Ganeshan², M. Rodriguez-Justo¹, A. Engledow¹, A. Groves¹; ¹London/UK, ²Falmer/UK

Purpose: Vasodilatation in the presence of low blood flow represents an adaptation to hypoxia which, in tumour, may reflect an aggressive phenotype. This study uses perfusion CT to undertake a preliminary assessment of whether such blood flow-blood volume (BF-BV) mismatch in primary colorectal cancer is associated with the presence of advanced disease.

Methods and Materials: IRB approval and informed consent were obtained. Perfusion CT blood flow and blood volume measurements were acquired prospectively in primary colorectal cancers from 35 patients. Nodal and metastatic disease status were determined from pathological examination of the resection specimen and 18F-fluorodeoxyglucose PET. Tumours with blood flow values below the median and blood volume measurements above the median were considered to exhibit BF-BV mismatch. The frequency of mismatch amongst node-positive and M1 tumours was compared to N0 and M0 tumours using Fischer's exact test.

Results: Median BF and BV were 81.0 ml/min/100 g and 5.1 ml/100 g, respectively. 5 of 35 tumours demonstrated BF-BV mismatch. Mismatch was significantly more common amongst M1 tumours (3/7 versus 2/24; $p=0.044$) but not amongst node-positive tumours (3/15 versus 2/20; $p=0.063$).

Conclusion: This study provides preliminary evidence of an association between BF-BV mismatch and the presence of distant metastases in colorectal cancer. BF-BV mismatch may potentially provide a marker of tumour adaptation to hypoxia.

B-0544 11:15

Dual source dual energy CT for lung cancer evaluation: correlation study between weighted iodine concentrations and pathological results of tumour lesion

Y. Rao, W. Yang, B. Liu, L. Cao, Y. Bu, W. Chai, K. Chen; Shanghai/CN (roy_0326@hotmail.com)

Purpose: To evaluate the correlation between pathological subtypes of lung cancer and the weighted iodine concentration in the tumour lesion from second generation dual source dual energy (DSDE) CT scan.

Methods and Materials: 51 patients with lung cancer underwent contrast-enhanced dual energy CT scan which was performed 30 seconds after the contrast injection (60 ml CM at 3 ml/s). The CT values (blended value from high and low kV images) and iodine concentrations (mg/ml) from the tumour as well as those from pulmonary artery and aorta on the same image plane were measured in a DE post-processing workstation. The iodine concentrations from the lesion were normalised by the iodine concentrations of pulmonary artery and aorta due to the dual blood supply of lung tumour to minimise the patient variation. Statistical analysis was performed to investigate the correlation between the weighted iodine value of tumour and corresponding pathological results.

Results: 28 patients were pathologically proved with adenocarcinomas and 23 patients with squamous cell carcinoma. The mean CT values provided no difference between the two groups ($p=0.708$). However, by comparing the weighted iodine concentrations, statistically significant differences was found ($p < 0.01$). The mean value of weighted iodine concentration was 0.30 ± 0.30 mg/ml for adenocarcinomas group and that for squamous cell carcinoma was 0.12 ± 0.11 mg/ml.

Conclusion: Dual energy CT scan could be a useful tool in differentiation of pathological lung cancer subtypes as the weighted iodine concentration for lung tumour lesion correlates with the tumour pathological subtypes.

B-0545 11:24

Development of non-necrotic tumour volumetry criteria for evaluation of therapy response in hepatocellular carcinoma
A.K. Singh, V. Kurra, W. Cai, G. Harris, D. Sahani; *Boston, MA/US*
(VKURRA@PARTNERS.ORG)

Purpose: To compare statistical variables derived by existing RECIST1.1 and, total tumour volumetry (TTV) criteria's and proposed non-necrotic tumour volumetry (NNV) criteria for assessing therapy response in hepatocellular carcinoma's (HCC).

Methods and Materials: In this study, pre- and post-treatment MDCT of 45 patients with pathologically proven HCC were used. Interval change in TTV and NNV was estimated on a 3D workstation using 3D quantification tools on MDCT axial slices. RECIST1.1 measurements were compared to the interval change in total tumour volume (TTV) and non-necrotic volume criteria's (NNV). Inter-method Kappa for predicting partial regression, stability and progression was derived and statistical estimates of Kaplan Meier curve survival curves derived by each method were compared. Logistic regression analysis was used to derive the most accurate response assessment criteria.

Results: The kappa coefficients for therapy response agreement remained poor between these methods ($\kappa \leq 0.354$). The overall median survival was 11 months. Kaplan Meier curves were more optimal for predicting survival by proposed NNV [median survival (ms): response (R) =36months, no-response (NR) =10months; $p < 0.0001$] than existing TTV (ms: R=18m, NR=5m; $p=0.0047$) and RECIST 1.1 (ms: R=14m, NR=11m; $p=0.9236$) criteria's. Stepwise logistic regression analysis revealed odds ratio (OR) for NNV (0.01) as the most optimal in the model compared to TTV (0.1131) and RECIST (0.3712).

Conclusion: Quantification of interval change in non-necrotic tumour volume may be a more objective and reliable measure for predicting therapy response in HCC's compared to the existing total tumour volume and RECIST 1.1 criteria's and deserves validation on a larger cohort.

B-0546 11:33

Angiogenesis in non-small cell lung cancer: early assessment of therapeutic response to antiangiogenic chemotherapy with perfusion multidetector-row CT (MDCT)
N. Tacelli, T. Santangelo, A. Scherpereel, A.-L. Hachulla, J. Remy, M. Rémy-Jardin; *Lille/FR* (nunzia.tacelli@chru-lille.fr)

Purpose: To evaluate temporal changes in CT perfusion parameters under antiangiogenic drugs.

Methods and Materials: 40 patients with non-small cell lung carcinoma, treated by chemotherapy (platinum-based and third generation drugs) alone (group 1; n=23) or combined with bevacizumab (group 2; n=17) underwent quantitative CT perfusion examinations with 64-slice MDCT before (T0: n=40) and after chemotherapy (T1: n=40; T2: n=33; T3: n=24) with an interval of 3 weeks between therapeutic sessions. The CT parameters evaluated included: (a) tumour blood volume (BV) and capillary permeability (CP) indexed to tumour volume; (b) RECIST measurements. The link between therapeutic response according to RECIST criteria and changes in CT functional parameters was investigated.

Results: Comparing T0 and T1: (a) the median values of BV and CP were significantly reduced in group 2 (BV at T1: 1.392 vs BV at T0: 4.368 mL; $p=0.0395$; CP at T1: 1.495 vs CP at T0: 4.335 mL/min; $p=0.0150$) without any change in tumour size, (b) functional parameters did not change in group 1. Comparing T0 and T2, both groups demonstrated reduction in BV (group 1, $p=0.0546$; group 2 $p=0.0043$) and CP (group 1, $p=0.0546$; group 2 $p < 0.0001$). In the overall population, a significant decrease in CP at T1 was found to be strongly related to the reduction in tumour size ($p=0.0192$) at T2.

Conclusion: Perfusion CT demonstrates restoration of the neovessel walls after the first therapeutic session of antiangiogenic chemotherapy, enabling assessment of therapeutic response before changes in RECIST criteria.

B-0547 11:42

Early diagnosis of recurrence of peritoneal carcinomatosis: MDCT correlated with serum tumour markers
M.T. Maccarone, R. Basilio, E. Rodolfo, V. Calamita, A. Ferri, M. De Tursi, A.R. Cotroneo; *Chieti/IT*

Purpose: To assess the value of MDCT in the early detection of peritoneal recurrence in patients with peritoneal carcinomatosis (PC) treated by means of cytoreductive surgery and HIPEC, in comparison to serum tumour markers.

Methods and Materials: Thirty-five patients with PC from ovarian (n=21), colorectal (n=9) tumours, uterine sarcoma (n=2), fallopian tube tumours (n=2) and peritoneal liposarcoma (n=1) treated by means of cytoreductive surgery and HIPEC were in-

cluded. They underwent serum tumour marker measurements (CEA, CA 125) every month after surgery and MDCT follow-up at 3 and 6 months interval. Two readers in consensus evaluated axial and multiplanar reconstructed MDCT images of the abdomen obtained during the portal venous phase of contrast material enhancement, with a collimation of 4 x 2.5 mm and a slice-width of 3 mm. MDCT findings were correlated with tumour markers measurements obtained within 15 days.

Results: Sensitivity, specificity and diagnostic accuracy were, respectively, 75%, 100% and 77% for serum tumour markers and 94%, 66% and 91% for MDCT. In 8/11 patients with normal tumour markers, MDCT showed peritoneal neoplastic implants confirmed at pathology and MDCT follow-up. In 1/11 patients with normal tumour marker levels, MDCT revealed one peritoneal nodule demonstrated to be necrotic lesion at pathology.

Conclusion: MDCT is able to early detect peritoneal recurrence in patients treated by means of cytoreductive surgery and HIPEC and can predate rising tumour markers levels.

B-0548 11:51

Multimodal imaging for therapy monitoring of loco-regional alpha therapy (213Bi-DOTATOC) in patients with hepatic metastases of neuroendocrine tumours

F.L. Giesel¹, C. Zechmann¹, S. Wulfert¹, H.-U. Kauczor¹, F. Bruchertseifer², A. Morgenstern², U. Haberkorn¹, C. Kratochwil¹, F.L. Giesel¹; ¹Heidelberg/DE, ²Karlsruhe/DE (f.giesel@dkfz.de)



Purpose: Radiolabelled somatostatin analogs play an emerging role in the therapy of patients with neuroendocrine cancers. The first-in-human peptid receptor alpha-therapy with 213Bi-DOTATOC was assessed with multimodal imaging (MRI, PET/CT and US) for initial therapy monitoring and surveillance of possible local side effects of this new approach.

Methods and Materials: In 12 patients the recently introduced alpha-particle-emitting 213Bi-DOTATOC was administered loco-regional in the liver. Multi-modal imaging of liver metastases was assessed using MRI with standard sequences and diffusion-weighted imaging (DW-MRI) before and after therapy. This modality delivers the lesion diameter (LD), apparent diffusion coefficient (ADC) as a surrogate of tumour integrity as a surrogate of tumour perfusion. In addition, contrast-enhanced ultrasound (CEUS) was accomplished as an onsite imaging modality to assess tumour microvascularisation (time-to-peak (TTP)).

Results: In the early MR analysis, most metastases demonstrated only a moderate decrease in LD, whereas median tumour ADC as a representative of tumour integrity increased from 1.21x10⁻³ mm²/sec to 1.47x10⁻³ mm²/sec 4-6 weeks after last loco-regional therapy. Prior to therapeutic intervention CEUS presented a pronounced enhancement in the liver metastases compared to the adjacent liver parenchyma (median TTP metastasis = 26.6 sec; median TTP liver parenchyma = 53.6 sec). 2 months after intervention the i.a. 213Bi-treated patients showed a decline in contrast enhancement in 56%.

Conclusion: In this ongoing study, CEUS, diffusion-weighted and perfusion MRI were able to demonstrate such tumour changes also early after treatment with alpha-therapy. Therefore, this functional tumour imaging assessment seems to be a reliable bio-surrogate of treatment response and might predict in an early stage lesion responses.

10:30 - 12:00

Room F2

Breast

SS 902

Screening mammography and CAD

Moderators:
E.M. Fallenberg; *Berlin/DE*
P. Skaane; *Oslo/NO*

B-0549 10:30

Variations in screening outcome among pairs of radiologists at independent double reading of screening mammograms: a population-based study

V. van Breest Smalenburg, J. Nederend, E.G. Klompenhouwer, L.E.M. Duijm; *Eindhoven/NL* (LEMDuijm@hotmail.com)

Purpose: To determine variations in screening outcome among unique pairs of radiologists at independent double reading of screening mammograms.

Methods and Materials: We included pairs of screening radiologists with a minimum of 7500 screening examinations per pair, obtained at a Dutch screening

mammography region between January 1997 and August 2009. During 2-year follow-up, breast imaging reports, surgical reports and pathology results were collected of all screen detected cancers and interval cancers. Screening outcome parameters were calculated for each screening couple.

Results: A minimum of 7500 screens for each pair of radiologists had been read by 26 unique combinations of two screening radiologists, totalling 300154 screens. The number of screening mammograms per pair of radiologists varied from 7500 screens to 20633 screens. Breast cancer incidence did not differ significantly among these 26 couples and ranged from 6.0 (95%CI 4.7-7.4) to 8.8 (95%CI 6.7-10.9) per 1000 screens. The referral rate among couples ranged from 0.9% (95%CI 0.7-1.1%) to 1.5% (95%CI 1.3%-1.8%), whereas the sensitivity for breast cancer detection and the positive predictive value of referral ranged from 55.1% (95%CI 44.5%-65.6%) to 84.1% (95%CI 74.9%-93.4%) and from 28.9% (95%CI 21.1%-36.9%) to 50.6% (95%CI 40.0%-61.2%), respectively.

Conclusion: Screening outcome varied significantly among pairs of screening radiologists. We advise a continuous monitoring of screening outcome parameters for each screening couple that participates at screening mammography. Regular feedback of this outcome to each couple may avoid screening of women by pairs of radiologists with suboptimal screening performance.

B-0550 10:39

Tailored breast cancer screening program in 40-49ers: results from an Italian single centre pilot study

E. Schiani, P. Panizza, M. Rodighiero, I. Fedele, E. Venturini, C. Losio, F. De Cobelli, A. Del Maschio; *Milan/IT (schiani.elena@hsr.it)*

Purpose: The aim of our study was to assess the feasibility of a screening program on 40-49ers; usually, 40-49ers are not included in screening program due to the low sensitivity and negative predictive value of mammography in this population. Our innovative screening program is tailored on individual risk profile and breast tissue density and implements mammography with further assessment (US/MRI), usually not included in evaluation of first level.

Methods and Materials: From September 2010 to May 2011 we invited 2,709 women from the town of Segrate (Milan, Italy). Low-dose photon-counting digital mammography (Sectra) was performed in 2 views (CC/MLD). The US and MRI were performed when needed.

Results: 1,345 women were enrolled (participation rate: 49.65%). The average glandular dose was 0.745 with an average breast thickness of 50 mm. The recall rate for US was 57.84%. The recall rate for MRI was < 0.008% (7/792). The US early recall rate was 6.56%. The cancer detection rate was 7.43% (10 cases). Eight cancers were diagnosed with mammography and two were detectable only at US (US-ICDR 0.31%, US-false positives 0.90%).

Conclusion: Preliminary results demonstrated an elevated breast cancer detection rate (7.43%) in women 40-49ers, higher than the incidence reported by the Italian Cancer Registry (0.15-0.2%). The US examination performed for high breast tissue density allows to detect other two cases of cancer.

B-0551 10:48



Phenotypic characteristics of interval breast cancers diagnosed in a population-based screening program in Catalonia, Spain. Correlation with radiological findings

D. Leon Guevara¹, A. Guma Martinez², L. Prieto Alvarez¹, R. Ortega Martinez¹, A. Valdivielso¹, C. Vidal Lancis¹, M. Garcia Martinez¹; ¹Barcelona/ES, ²Hospitalet de Llobregat/ES

Purpose: To analyze if there are phenotypic differences between prevalent, incident and interval cases of breast cancers, diagnosed in a breast cancer screening program in Catalonia, Spain. To Correlate the data with the radiographic presentation of these tumors.

Methods and Materials: We performed a retrospective study of all breast cancers diagnosed in the screening program between 2006-2010: analyzing histological type, prognostic factors and radiological findings. Subgroups were made of prevalent, incident or early interval cases.

Results: We have studied 424 cases, 372 invasive carcinomas and 52 intraductal carcinomas. Interval breast cancer cases were invasive carcinomas in 89% and 11% in situ. Analysis of radiological findings and prognostic factors was achieved in 364 cancer cases. The triple-negative phenotype was more frequent in interval invasive carcinomas cases (17.4%) than in cancers detected at screening (7.8%). This difference was statistically significant (p = 0.006). Phenotypic type Her2 (5.7%) and luminal A (69.4%) tumors were more frequent in breast cancer cases detected in screening compared to interval cases (0% and 60.5% respectively), although not statistically significant. Radiologically, triple negative tumors were more often

circumscribed and had ill-defined margins without microcalcifications, with areas of necrosis and posterior acoustic enhancement.

Conclusion: Analysis of prognostic factors in breast carcinomas confirms that interval cases are more aggressive than those diagnosed in screening. The radiological presentation may predict clinical characteristics and histological type.

B-0552 10:57

Stage-specific incidence rates of breast cancer in participants and non-participants of a population-based mammographic screening programme

S. Hofvind¹, C.I. Lee², J.G. Elmore³; ¹Oslo/NO, ²Los Angeles, CA/US, ³Seattle, WA/US (solveig.hofvind@krefregisteret.no)

Purpose: To compare stage-specific incidence of breast cancer in the target population of the Norwegian Breast Cancer Screening Programme.

Methods and Materials: We compared the incidence among 640,347 invited women aged 50-69 years who received 1,925,727 invitations and stratified the analyses by invited participants and invited non-participants. Two-sided chi-square tests were used to determine statistical significance between groups.

Results: The incidence of breast malignancy (DCIS or invasive breast cancer) was 1.6 times higher in invited participants compared with invited non-participants; 659.0/100,000 versus 409.3/100,000 (p < 0.001). For invasive breast cancers only, the rate ratio was 1.5. The incidence of stage I cancer was two times higher for participants (345.9/100,000 invitations) compared with non-participants (173.2/100,000 invitations, p < 0.001), while the incidence of stage III cancer was 50% lower and stage IV cancer 70% lower (p < 0.001 for both). The rate of mastectomy was 1.3 higher in participants than in non-participants compared with invited non-participants.

Conclusion: Participants in an organised breast cancer screening program run a higher risk of stage 0 and I breast cancer and lower risk of advanced breast cancer compared with invited non-participants. Efforts to support early detection of breast cancer in non-participants in organised screening are needed.

B-0553 11:06

Proportional incidence and review of T2+ screen detected carcinomas: a new measure of diagnostic accuracy?

S. Ciatto¹, D. Bernardi¹, M. Pellegrini¹, F. Caumo², A. Frigerio³, M. Gentilini¹; ¹Trento/IT, ²Verona/IT, ³Turin/IT (stefano.ciatto@gmail.com)

Purpose: Large size (T2+) screen detected that carcinomas might be assumed as screening failures and monitored for quality control as interval cancers (IC).

Methods and Materials: Based on T2+ cancers screen detected during 2001-2009 at Trento screening programme, we a) assessed the proportional incidence as compared to pre-screening (1999-2000) incidence, and b) reviewed previous screening tests preceding diagnosis. Blind review of films mixed (3:1) to negative controls was performed by a panel of three external reviewers, screening errors being defined according to majority (cancers seen by at least two reviewers). A subset of IC diagnosed during 2008-2010 was included in the review set.

Results: Proportional incidence (271,385 women year) was 68% (168/247 observed/expected, 95% confidence interval 61-9-73.5, higher as compared to 20.3% (101/495, 17-24.1) recently determined for IC in the same centre. Review of 54 T2+, 50 IC and 170 controls classified 14/50 screening errors among IC (28%, 17.4-41.7) and 15/54 among T2+ (28%, 17.6-40.9; p=0.84). Differences in detection and recall rate observed among reviewers were not statistically significant.

Conclusion: Assessing T2+ proportional incidence and review is feasible as a modality for screening surveillance. T2+ assessment is easier as compared to IC, but no reference standards are available yet, particularly for proportional incidence which was higher as compared to IC. Comparable review findings between T2+ and IC cases might suggest to adopt the EC standard (<20%) also for T2+. Further studies are needed to confirm the present results.

B-0554 11:15

Incidence and review of interval cancers in a community biannual mammographic screening programme

L.A. Carbonaro¹, B. Babaei Paskeh¹, G. Brambilla², P. Malerba², L. Menicagli¹, G. Vadala³, L. Fantini⁴, S. Ciatto⁵, F. Sardanelli¹; ¹San Donato Milanese/IT, ²Rozzano/IT, ³Vizzolo Predabissi/IT, ⁴Lacchiarella/IT, ⁵Padua/IT (luca.carbonaro@gmail.com)

Purpose: To assess the performance of an Italian mammographic screening programme in terms of interval cancers (ICs) observed from 2001 to 2006.

Methods and Materials: ICs were identified by matching the screening archives with local cancer registry, pathology archives, and hospital discharge records.

Saturday

Proportional incidence was determined according to breast cancers expected in the absence of screening, estimated on the basis of patients/year at risk and age-specific incidence. Three offsite high-experienced reviewers blindly evaluated the screening mammograms prior to the diagnostic ones, randomly mixed with age and breast-density-matched negative controls with a 1:2 ratio.

Results: 86,276 first-level mammograms in 6 centers were acquired; the mean recall rate was 6.8 at first screening and 4.6 at repeat screening. A total of 476 screen-detected cancers and 145 ICs were diagnosed. The IC proportional incidence was 46/234 (19.6%) for the first year, 99/234 (42.3%) for the second year, and 145/468 (31%) for the two-year interval. Of 145 CI mammograms, a total of 130 of them (89.7%), randomly mixed with 287 negative controls, were reviewed; 28/130 (21.6%) were recalled by 2 or 3 reviewers (errors), 31/130 (23.8%) were recalled by only 1 reviewer (minimal signs), and 71/130 (54.6%) were not recalled (occult).
Conclusion: Our screening programme can be considered within EC standards for what concerns IC analysis.

B-0555 11:24

Presorting by CAD according to lesion type: increasing the reader's awareness of mammographic lesions in a screening environment

R. Lederman, I. Leichter, M. Greenberg; *Jerusalem/IL (izhak@hadassah.org.il)*

Purpose: To explore the capability of CAD run in the background to automatically presort prioritised subgroups with higher prevalence of either malignant masses or clusters. Knowing that prevalence is increased for either lesion type, readers should review the tagged cases with higher suspicion.

Methods and Materials: Since breast cancers are usually visible in both views, CAD can presort cases with matching CAD marks of the same type in both views, creating prioritised subgroups with increased prevalence of malignant clusters or masses. Although false marks tend to occur randomly, these subgroups will also include normal cases, since matching false marks may also be generated in both views coincidentally. 15892 FFDM cases (280 cancers-182 masses) culled retrospectively from 6 facilities were run with a prototype CAD algorithm (Siemens) and presorted by matching CAD marks according to lesion type, to explore the cancer prevalence in the prioritised subgroups.

Results: Of normal cases, 16.2% (2527 cases) had coincidentally matching mass marks and 5.1% (798) matching cluster marks. Conversely, of the malignant cases, 70.3% (128) had matching mass marks, and 80.6% (79) had matching cluster marks. In the subgroup with matching mass marks, cancer prevalence, thus, increased 4.2 times, from 1.15% to 4.82% (128 of 2655), while for clusters, cancer prevalence increased 14.61 times, from 0.62% to 9.0% (79 of 877).

Conclusion: Presorting by matching CAD marks substantially increases the breast cancer prevalence in the prioritised subgroups of cases, especially in the cluster subgroup, thereby focusing the readers' attention on cases which are more suspicious.

B-0556 11:33

Can CAD be used as a preliminary reader in screening mammography?

R. Lederman, I. Leichter, M. Greenberg; *Jerusalem/IL (izhak@hadassah.org.il)*

Purpose: To explore the potential of CAD as a preliminary reader run in the background in screening mammography, to reduce reading time by creating for the radiologist subsets of normal cases and of cases considered suspicious for a specific lesion type.

Methods and Materials: 12675 FFDM cases were run with a prototype CAD device (Siemens), with separate algorithms for detecting masses and clusters. The malignant cases included 319 masses, 79 clusters and 75 masses with micro-calcifications. When using CAD as a preliminary reader, the algorithm is designed to create subsets of cases suspicious for either masses or clusters, directing radiologists to select the appropriate visual process for finding the specific lesion type. The remaining cases with no marks for that lesion type bypass review.

Results: CAD found only 43.7% of the normal cases, to be suspicious for clusters, and 48.6% to be suspicious for masses. For malignant cases with clusters, the algorithm suspected clusters in 94.9%, for malignant cases with masses, 90.3% were suspicious for masses, and for cases of masses with calcifications, 98.7% were suspicious for either lesion type or both.

Conclusion: CAD as a preliminary reader in screening mammography could substantially reduce the workload by nearly half for either lesion type. Using CAD as a preliminary reader for clusters might warrant consideration, since only about 1% of masses with calcifications and 5% of clusters would be missed. Recent algorithm modifications to improve detection of masses and clusters should make this approach practical for masses as well.

B-0557 11:42

Standalone computer-aided detection compared to human readers for the detection of breast cancer in screening mammograms

N. Karssemeijer¹, R. Hupse¹, M. Samulski¹, M. Lobbes², A. den Heeten¹; ¹Nijmegen/NL, ²Maastricht/NL (n.karssemeijer@rad.umcn.nl)

Purpose: We developed a computer-aided detection (CAD) system aimed at decision support for detection of malignant masses in screening mammograms. In contrast to current CAD systems, which have many false positives due to their focus on high sensitivity, this system is aimed to operate at high specificity comparable to that of radiologist. The purpose of this study was to compare the performance of this CAD system to that of radiologists and residents.

Methods and Materials: In a retrospective study eight certified screening radiologists and three residents with mammography experience read 200 screening mammograms without the use of CAD. Cases included 63 screen-detected cancers, 17 missed cancers, 20 false positives from screening, and 100 normals. Microcalcification cases were excluded. Readers and CAD were compared using localisation ROC (LRROC) analysis, by computing the mean true positive fraction (MTPF) at a false-positive fraction (FPF) less than 0.2.

Results: CAD performance (MTPF=0.518) was similar to that of the residents (MTPF=0.484) but still significantly below the performance of the radiologists (MTPF=0.596). However, at very high specificity (FPF< 0.1) and for the subset of cases missed in screening CAD standalone performance was similar to that of the radiologists.

Conclusion: The performance of a novel CAD system aimed at decision support is approaching the level of performance of experienced human readers. These results show the potential of CAD to be used as second or third reader in breast cancer screening.

B-0558 11:51

Retrospective comparison of the accuracy of two different computer-aided detection systems for detecting malignant lesions on mammography

M. Lobbes, K. Keymeulen, M. Smidt, R.G. Beets-Tan, J.E. Wildberger, C. Boetes; *Maastricht/NL*

Purpose: To retrospectively compare the accuracy of two computer-aided detection (CAD) systems (SecondLook versus AccuDetect Galileo) for the detection of malignant breast lesions on full-field digital mammograms.

Methods and Materials: Digital mammograms of 326 patients were analysed (117 patients with breast cancer, 209 negative cases). Positive cases consisted of 85 masses, 6 calcifications, and 26 masses plus calcifications. Each set of cases was read by both CAD systems and true positive fraction (TPF) for both systems and per image, case, and total cancers was assessed. Operating points for both systems was set at comparable false positive rates per image and case. One-sided, exact McNemar's tests were used to assess statistical significance of the results.

Results: When compared to SecondLook, AccuDetect Galileo significantly increased TPF per image for masses (increase of 10.6% to 72.2%, p=0.0001) and calcifications (increase of 12.8% to 61.5%, p=0.03). Per case, AccuDetect Galileo did not significantly increase TPF for masses and calcifications. AccuDetect Galileo achieved higher TPF for all cancers (per image increase to 6.9% to 72.2%; per case increase to 4.3% to 84.6%). Most interestingly, AccuDetect Galileo, using a new voting methodology algorithm, had a significant performance improvement in detecting masses on extremely dense breasts over SecondLook, increasing TPF with 15.4% to 69.2% (p=0.0156).

Conclusion: AccuDetect Galileo showed significantly better overall performance than SecondLook in detecting masses, microcalcifications and all cancer types, even in extremely dense breasts.

10:30 - 12:00

Room I/K

Abdominal Viscera

SS 901 Pancreas

Moderators:

K. Coenegrachts; Bruges/BE
R. Pozzi-Mucelli; Verona/IT

B-0559 10:30

Diffusion-weighted MRI of pancreas cancer: comparison of free-breathing, respiratory-triggered and breath-hold sequences

N. Kartalis, L. Loizou, N. Edsberg, R. Segersvard, N. Albiin; *Stockholm/SE*
(nikolaos.kartalis@me.com)

Purpose: To compare respiratory-triggering (RT), free-breathing (FB), and breath-hold (BH) diffusion-weighted imaging (DWI) techniques regarding a) subjective image quality, and b) signal intensity (SI) characteristics and ADC measurements in patients with pancreatic adenocarcinoma.

Methods and Materials: Prospectively, 15 consecutive patients with histopathologically proven disease (mean size 3.2 cm), underwent DWI at 1.5 Tesla with 5 b-values (0, 50, 300, 600, and 1000 s/mm²) with the 3 different techniques. Two radiologists, independently and blindly, assessed image quality, by assigning a total quality score [score sum of rating diffusion images (lesion detection, anatomy, presence of artefacts) and ADC maps (lesion characterisation, overall image quality)] per sequence and by ranking them (sequences viewed simultaneously). Lesion signal intensity (SI), signal-to-noise ratio (SNR), mean ADC and coefficient of variation (CV) were compared. A p-value < 0.05 was considered significant.

Results: Total quality score for RT, FB, and BH was 17.9, 16.5, and 17.1, respectively (RT significantly higher than FB but not than BH). RT had a significantly higher ranking compared to both FB and BH. SI on all b-values and SNR on b300 and b600 were significantly higher for RT compared to FB and BH. Mean ADCs for RT, FB, and BH were 1.201, 1.132, and 1.253, respectively (BH significantly higher than FB but not than RT). Mean CV for RT, FB, and BH were 8.9, 10.8, and 14.1 respectively (RT significantly lower than BH but not than FB).

Conclusion: In both analyses, RT-DWI showed superiority and seems the optimal technique for DWI of pancreas adenocarcinoma.

B-0560 10:39

Comparison of abdominal MRI including diffusion-weighted sequences with 68Ga-DOTATATE PET/CT in detecting neuroendocrine tumours of the pancreas

C.M. Schmid-Tannwald, C. Schmid-Tannwald, R. Neumann, A. Haug, M. Reiser, C. Rist; *Munich/DE* (christoph⁸¹²@hotmail.com)

Purpose: To compare abdominal MRI including diffusion-weighted MRI (DW-MRI) with 68Ga-DOTATATE-PET/CT (PET/CT) in detecting neuroendocrine tumours (NET) of the pancreas.

Methods and Materials: 19 patients were retrospectively included with pancreatic NET who underwent MRI including DW-MRI and PET/CT within 6 weeks. Two blinded reader compared T2-weighted (T2w), T2w+DW-MRI, T2w+contrast-enhanced T1-weighted (CE T1w) sequences and PET/CT images for NET detection and confidence level using a 5-point-scale. Sensitivity, confidence level and ADC of NET and normal pancreatic tissue was compared.

Results: 9/25 (36%) and 15/25 (60%) NET were detected on T2w images and T2w+DW-MRI by both observers, respectively. Observers 1 and 2 detected 15/25 (60%) and 16/25 (64%) NET on their review of T2w+CE T1w image combination, respectively, and all 25 NET (100%) were detected on PET/CT by both observers. Detection rate and confidence level improved significantly by combined interpretation of T2w images and DW-MRI or CE T1w images (p < 0.04). There was no significant difference between the NET detection rate of T2w+DW-MRI and T2w+CE T1 image combinations (p > 0.05). Detection rate and confidence level of PET/CT were significantly higher than MRI (p=0.02). Mean ADC of NET (1.02±0.26 x 10⁻³ mm²/s) was significantly lower than mean ADC of normal pancreatic tissue (1.47 ± 0.39 x 10⁻³ mm²/s).

Conclusion: DW-MRI is a valuable adjunct to T2w and comparable to CE T1w images in detection of NET of the pancreas and ADC measurements provide a quantitative differentiation between NET and normal pancreatic tissue. PET/CT seems to improve significantly the detection of pancreatic NET compared to MRI.

B-0561 10:48

Are pancreatic calcifications predictive of impairment of pancreatic exocrine function? A retrospective study with S-MRCP and abdominal CT in patients with known or suspected pancreatic disease

G. Restaino¹, M. Missere¹, D. Distefano², R. Casale², A. Pierro¹, G. Sallustio¹;
¹Campobasso/IT, ²Rome/IT (gennares@hotmail.com)

Purpose: To establish correlation between pancreatic calcifications detected by CT and pancreatic exocrine function evaluated with S-MRCP in subjects with known or suspected pancreatic disease.

Methods and Materials: 197 consecutive patients (M:F=98:99, mean age: 49±16 y/o) underwent S-MRCP and upper abdominal helical CT for suspected or known pancreatic disease. S-MRCP were evaluated for the presence and grade of chronic pancreatitis according to Cambridge classification and for assessment of pancreatic exocrine reserve according to Matos classification. CT examinations were evaluated for the presence or absence of pancreatic calcifications. The findings were compared with Fisher's exact test.

Results: Cambridge score was 1 in 73 patients, 2 in 13 patients, 3 in 20, 4 in 66, and 5 in 25 patients. Matos score was 3 in 159 cases, 2 in 32 cases, 1 in 4 subjects and 0 in 1 patient. Pancreatic calcifications were detected by CT in 23/197 patients (11.6%). There was a significant correlation between prevalence of calcifications and grade of chronic pancreatitis (p < 0.0001) and pancreatic exocrine reserve (p < 0.0001). Calcifications were observed in 10/159 (6.3%) patients with normal pancreatic exocrine reserve (Matos:3) versus 13/37 (35.5%) patients with impaired reserve (Matos: 2,1,0), with significant difference (p < 0.0001), even after adjusting for sex and age. Among patients with mild and severe chronic pancreatitis (Cambridge score 3 and 5), the presence of pancreatic calcifications was a significant indicator of impaired exocrine function (p=0005 and, respectively, p < .0001).

Conclusion: Unlike previously published papers, our study shows that pancreatic calcifications are independent predictors of impairment of pancreatic exocrine function.

B-0562 10:57

Comparative performance of CT and MRI in prognostication of acute pancreatitis: correlation with clinical outcome

K. Rahul, K. Mandeep, B. Deepak K, G. Rajesh, K. Naveen, B. Ashish, S. Surinder, N. Khandelwal; *Chandigarh/IN* (rahu⁸⁸mona@rediffmail.com)

Purpose: To compare the diagnostic and prognostic performance of computed tomography (CT) and magnetic resonance imaging (MRI) in acute pancreatitis.

Methods and Materials: In this institution review board approved prospective study, patients with clinical suspicion of acute pancreatitis were enrolled after taking informed consent. All patients underwent a contrast-enhanced CT (CECT) and contrast-enhanced MRI (CEMRI). A CT severity index (CTSI) and MR severity index (MRSI) was assigned in all cases by two different radiologists based on Balthazar scoring system. The CTSI and MRSI were compared with each other and with various clinical outcome parameters.

Results: 40 patients (male:female 30:10; mean age: 40.93 years; age range: 12 - 80 years) were enrolled from January 2010 to April 2011. There was excellent inter-observer agreement for assessing CTSI (kappa value: 0.754) and good interobserver agreement for MRSI (kappa: 0.745). Both CTSI and MRSI showed statistically significant correlation with the need for percutaneous intervention, development of infection or organ failure and duration of hospital stay. MRSI also showed a statistically significant correlation with mortality. Patients with signs of pancreatic/peripancreatic haemorrhage on MRI showed a statistically significant correlation with all parameters of clinical outcome. Pancreatic duct disruption could only be diagnosed on MR; however, poor image quality (motion artefacts) was seen more often on MRI.

Conclusion: MRI and CT are equally efficient modalities for assessing severity and predicting complications of acute pancreatitis. MRI is superior in demonstrating ductal pathology and haemorrhage.

B-0563 11:06

CT assessment of sarcopenia in patients with pancreatic cancer and chronic pancreatitis

E. Bulanova, V. Lyadov, E. Mershina, V.E. Sinitsyn; *Moscow/RU*

Purpose: As metabolic disorders, such as cachexia and sarcopenia (muscle wasting), are common conditions in patients with pancreatic cancer and chronic pancreatitis, we studied the role of CT in assessing sarcopenia in these two groups of patients.

Methods and Materials: We evaluated 42 CT-images of patients with pancreatic cancer (20) and chronic pancreatitis (22), which underwent operative treatment in

2010-2011. An axial CT-image on the level of L3 vertebrae was assessed to measure cross-sectional areas of skeletal muscle. The values were normalised for height to get Lumbar skeletal muscle index (cm²/m²). Sex-specific sarcopenia cut-offs were 52.4 cm²/m² for men and 38.5 cm²/m² for women (Prado et al). The range of body-mass index (BMI) was from 15.9 kg/m² to 37.9 kg/m² (MV 25.01±3.1 kg/m² for 1 group and 22.5 ±2.98 kg/m² for 2 group).

Results: 14/20 patients with pancreatic cancer were found sarcopenic (70%). Mean value of L3-index was 44.7±5.6 cm²/m² for men and 35.7±3.8 cm²/m² for women. There were 15/22 sarcopenic patients with chronic pancreatitis (68%), mean values of L3-index for men and for women were 47.6±7.5 cm²/m² and 39.0±10.8 cm²/m², respectively. Sarcopenia was diagnosed not only in patients with decreased BMI but also with normal and increased BMI.

Conclusion: CT is a useful tool to evaluate sarcopenia in patients with pancreatic cancer and chronic pancreatitis using L3-index. The use of CT for body composition analysis opens up new possibilities in metabolic disorders research in these groups of patients.

B-0564 11:15

Relationship between clinicopathological factors and total lesion glycolysis in pancreatic cancer

M. Shinagawa, H. Kaida, Y. Kunou, M. Uchida, M. Ishibashi, N. Hayabuchi, M. Yasumoto, Y. Naito; *Kurume/JIP (bokuceleb@gmail.com)*

Purpose: The purpose of this study was to investigate the relationship between fluorine-18-fluorodeoxyglucose (FDG) uptake [maximum standardised uptake value (SUVmax), total lesion glycolysis (TLG)], and clinicopathological factors associated with pancreatic cancer.

Methods and Materials: FDG-positron emission tomography/computed tomography was performed on 33 patients with pancreatic cancer for initial staging prior to surgery. Diagnosis was histopathologically confirmed for all cases. The relationship between clinicopathological factors (i.e., tumour size, pathological T-stage, lymph node metastasis, pathological stage, tumour differentiation, lymphatic invasion, venous invasion, intrapancreatic neural invasion, and tumour growth pattern (INF)), TLG, and SUVmax was investigated. TLG was calculated by multiplying mean SUV and metabolic tumour volume.

Results: TLG significantly correlated with tumour size (TLG, $r = 0.573$, $p < 0.001$; SUVmax, $r = 0.333$, $p = 0.06$) and associated with tumour differentiation (TLG, $p = 0.042$; SUVmax, $p = 0.078$), whereas SUVmax did not. In contrast, SUVmax associated with INF, whereas TLG did not (SUVmax, $p = 0.034$; TLG, $p = 0.163$). No significant difference was observed between clinicopathological features and SUVmax or TLG.

Conclusion: Tumour size and differentiation were more highly correlated with TLG than SUVmax, suggesting that TLG is more reflective of clinicopathological factors and likely to be useful in the clinical management of pancreatic cancer.

B-0565 11:24

Timing bolus dynamic contrast-enhanced magnetic resonanced imaging for characterization of solid focal pancreatic lesions

J. Lee¹, J. Kim¹, J. Han¹, I. Joo¹, B. Choi¹, B. Keifer²; ¹Seoul/KR, ²Erlangen/DE (*jms@snuc.ac.kr*)

Purpose: To assess the feasibility of dynamic contrast-enhanced (DCE) MRI timing bolus data using a three-dimensional radial gradient-echo technique with K-space-weighted image contrast (Radial-KWIC) can be postprocessed for characterisation of solid pancreatic diseases.

Methods and Materials: A total of 45 patients with suspected pancreatic diseases who underwent pancreatic MRI at 3 T scanner, which included a low-dose (2 mL gadopentetate) timing bolus using a radial-KWIC technique. There were 24 patients with pancreatic cancers, 8 with PNETs, 3 with chronic pancreatitis, and 10 with normal pancreas. Using the dedicated, post-processing software program for DCE-MRI, the several perfusion parameters were measured for tumour and nontumorous parenchyma.

Results: The K-trans, Kep and iAUC values in patients with pancreatic cancer (0.042 min⁻¹, 0.76 min⁻¹.2.841 mmol/s, respectively; $P < 0.05$ were significantly lower than those with normal pancreas (0.387 min⁻¹, 6.376 min⁻¹, 7.156 mmol/s, respectively; $P < 0.05$). In addition, the kep values of PNETs and normal pancreas were also different ($P < 0.0001$). Furthermore, the Ktrans, kep, iAUC values of pancreatic cancers and PNETs were significantly different ($P < 0.05$). The prevalent TIC patterns of the pancreatic cancer, PNETs, chronic pancreatitis and normal pancreatic parenchyma were different: pancreatic cancers showed a slow gradual enhancement pattern (18/24, 75%) while PNETs showed a rapidly increasing and gradually decreasing enhancement pattern (4/8, 50%).

Conclusion: Timing bolus DCE MRI using the radial-KWIC sequence from routine examinations can be postprocessed to yield potentially useful perfusion parameters for characterisation of pancreatic diseases.

B-0566 11:33

Single energy low-voltage arterial phase scans for the detection of adenocarcinoma of the pancreas

G.A. Zamboni, M. Ambrosetti, E. Zivelonghi, R. Pozzi Mucelli; *Verona/IT (gzamboni@hotmail.com)*

Purpose: To test a single energy low-voltage protocol for detecting adenocarcinoma of the pancreas.

Methods and Materials: 22 patients with pathology-proven pancreatic adenocarcinoma underwent MDCT with arterial phase at 80 kVp (group A) on a 64-row scanner and were compared to a similar group of 22 patients scanned with a 120 kVp arterial phase protocol (group B). Except for tube voltage, all other scan parameters were kept constant. Scans were compared for quantitative image parameters (attenuation and standard deviation in the liver, pancreas, aorta and tumour), CTDI and DLP using an unpaired t-test. Image noise values for each protocol (SD of the HU from 3 ROIs drawn outside the body) were compared using an unpaired t-test. Effective dose for the two protocols was calculated with TLD measurements.

Results: Mean attenuation was significantly higher in group A in the aorta (525.6±126.8 vs 292.9±87.4 HU), liver (94.4±17.8 vs 75.3±14 HU) and normal pancreas (162.1±42 vs 89.9±19.7 HU) (all $p < 0.0001$), while no significant difference was observed for adenocarcinoma (67.8±39.2 vs 50.5±20.5 HU; $p = n.s$). CTDI and DLP were significantly lower in group A (6.0±1 vs 9.7±2.8 mGy, and 184.6±40.3 vs 369.6±133.4 mGy, respectively; all $p < 0.0001$). Tumour conspicuity (HUpancreas-HUtumour) was significantly higher in group A (94.2±39.3 vs 39.5±22 HU; $p < 0.0001$). Mean image noise was significantly higher in group A (12.3±3.6 vs 9.5±2.9 HU; $p < 0.0001$). TLD effective dose was significantly lower for the test protocol (0.157 vs 0.201 mSv; $p = 0.0083$).

Conclusion: The use of 80 kVp arterial phase for abdomen CT increases the conspicuity of adenocarcinoma thus potentially improving its identification.

B-0567 11:42

Quantification of pancreatic fat fraction and confounding factors in an adult population-based study using magnetic resonance imaging

J.P. Kuehn, S. Baumeister, P.-O. Behrmdt, K. Hegenscheid, H. Voelzke, J. Mayerle, N. Hosten, R. Puls; *Greifswald/DE (kuehn@uni-greifswald.de)*

Purpose: To establish the proportion of pancreatic fat fraction and their correlates in an ongoing population-based cohort-study using T2* corrected Dixon magnetic resonance imaging (MRI).

Methods and Materials: MRI was performed in a 1.5 T system (Avanto, Siemens) using a work in progress T2* corrected three-echo-Dixon technique. Fat phantom was constructed using fat fractions of 0, 25, 50, 75, and 100% to test the accuracy of fat quantification. In addition, a total of 2,136 healthy volunteers (1,008 men, 1,128 women, mean age: 52.7±14.25 years, mean BMI: 27.8±15.1 kg/m²) underwent an abdominal MRI, including the study sequence. Fat fractions of the pancreas (head, body, and tail) were calculated using a region-of-interest-based image evaluation. Pancreatic fat (log-transformed) was regressed on demographic, behavioural, and cardiometabolic factors.

Results: The correlation between predicted fat content by MRI and true fat content in phantom was very high ($r_{\text{Pearson}} = 0.989$). The median pancreatic fat fraction among volunteers was 6.7% (25th percentile (Q1): 5.1%; 75th percentile (Q4): 9.1%). There are no significant changes in fat distribution between head: 6.2%, body: 7.2%, and tail: 6.7% ($p = 0.53$). In multivariable linear regression models, male gender, age, obesity, dyslipidemia, and triglycerides were associated with pancreatic fat. For example, men had 14% higher values than women; those with BMI larger than 25 32%; and subjects with dyslipidemia 8.5% higher pancreatic fat.

Conclusion: MRI is a useful tool to quantify the pancreatic fat fraction. Sex, age, BMI, dyslipidemia, and triglycerides are associated with pancreatic fat, whereas smoking status, alcohol consumption, hypertension, diabetes, and fasting glucose are not.

B-0568 11:51

Preoperative CT findings predicting the recurrence of pancreatic cancer after surgical resection

Y. Lee, Y. Kim, K. Lee; *Seongnam-si/KR (yoonjin²¹⁹@gmail.com)*

Purpose: To determine useful preoperative CT findings for predicting the recurrence of pancreatic cancer after surgical resection.

Methods and Materials: From October 2005 to March 2009, multiphasic multidetector CT data were acquired in patients undergoing curative resection for ductal

adenocarcinoma of the pancreas. Forty consecutive patients were divided into recurrence or recurrence-free groups. Two radiologists retrospectively reviewed the CT findings in consensus with regard to the size of the tumour, local invasion, vascular invasion, regional lymph node enlargement and the presence of associated pancreatitis. The results from CT were analysed to identify the risk factors associated with tumour recurrence after surgery. Kaplan-Meier method and Cox proportional hazards regression model were used for evaluation.

Results: Presence and number of regional lymph node enlargement on CT were important predictors of tumour recurrence ($p=0.019$ and 0.002 , relative risk estimate 3.75 and 1.47, respectively). The presence of retropancreatic lymph node enlargement was a significant predictor ($p=0.0006$, relative risk estimate 5.95) in multivariate analysis. The median tumour recurrence times were 7 months and 21 months in patients with and without lymphadenopathy, respectively ($p=0.001$). However, other CT findings were not statistically significant predictors of tumour recurrence.

Conclusion: The presence of regional, especially retropancreatic lymph node enlargement on CT may improve predicting patients at high risk of tumour recurrence after surgical resection of pancreatic cancer.

10:30 - 12:00

Room L/M

Cardiac

SS 903

Cardiomyopathies: CT, MRI and PET

Moderators:

A. Esposito; Milan/IT
M. Gutberlet; Leipzig/DE

B-0569 10:30

Myocardial late enhancement in hypertrophic cardiomyopathy: spread more than amount predicts evolution towards heart failure

M. Cava¹, F. De Cobelli¹, A. Esposito¹, S. Ravelli¹, A. Damascelli¹, G. Ligabue², R. Fattori³, A. Del Maschio¹; ¹Milan/IT, ²Modena/IT, ³Bologna/IT (cava.mariangela@hsr.it)

Purpose: This study aimed to explore by cardiac magnetic resonance (CMR) relative relevance of morpho-functional and structural informations related to potentially life-threatening clinical events in hypertrophic cardiomyopathy (HCM) patients.

Methods and Materials: 50 HCM patients (pts) (mean age 52 ± 16) underwent CMR between 2004 and 2011, performed on a 1.5 T magnet (Achieva Philips) with assessment of left ventricular end-systolic/diastolic volumes, ejection fraction, end-diastolic-wall-mass, maximum-wall-thickness (MWT), outflow-tract-obstruction, mitral regurgitation, diastolic function (DF) and late-enhancement (LE) after i.v. injection of gadolinium-based contrast-medium. During 39 ± 24 months follow-up, cardiac events (CE) were recorded and divided into two groups: arrhythmic CE [sustained ventricular tachycardia, ventricular fibrillation, sudden cardiac death, ICD discharge] and heart failure (HF)-related-CE [atrial fibrillation (AF), unplanned hospitalisation, progression to NYHA class III/IV, HF-related death].

Results: 43 pts showed LE ($10\pm 8\%$ mean) with mean number of involved segments (LENS) 4 ± 3 . We recorded HF-related events in 10 pts; no arrhythmic CE occurred. According to events (E), we divided pts into two groups ($E=10$, $noE=40$): data assessed by CMR showed significant differences about MWT ($E=22\pm 4$ vs $noE=19\pm 5$, $p=0.045$), LE% ($E=14\pm 7$ vs $noE=9\pm 9$, $p=0.038$) and LENS ($E=6\pm 3$ vs $noE=3\pm 3$, $p=0.002$), number of patients with DF impairment ($E=9/10$ vs $noE=14/40$, $p=0.002$). At multivariate analysis, apart from age ($p=0.025$), number of LE involved segments seems to be the best predictor of HF-related events; the involvement of any segment increased the risk of HF-related events ($p=0.032$, $OR=1.6$).

Conclusion: Myocardial LE could predict evolution towards HF in HCM: LE spread seems stronger than its amount.

B-0570 10:39

Feasibility, reproducibility and reliability for the T2* iron evaluation at 3 T in comparison with 1.5 T

C. Tudi¹, A. Meloni², G. Valeri³, E. Chiodi⁴, M. Missere⁵, A. Carollo⁶, M. Lombardi², M. Midiri¹, A. Pepe²; ¹Palermo/IT, ²Pisa/IT, ³Ancona/IT, ⁴Ferrara/IT, ⁵Campobasso/IT, ⁶Trapani/IT

Purpose: We aimed to determine the feasibility, reproducibility and reliability of the T2* magnetic resonance imaging (MRI) at 3 T for heart and liver iron burden quantification and the relationship between T2* values at 3 T and 1.5 T.

Methods and Materials: 38 transfusion-dependent patients underwent MRI. Segmental and global cardiac T2* values were calculated after developing a cor-

rection map to compensate the artefactual T2* variations. The hepatic T2* value was determined over a region of interest.

Results: The intra- and inter-operator reproducibility at 3 T was good ($ICC>0.949$). Segmental correction factors were significantly higher at 3 T ($P=0.002$). A strong linear relationship was found between 3 T and 1.5 T R2* values for both liver and heart: the 3 T R2* values were about twice with an intercept depending on the non-iron tissue component. The concordance between global and mid-septum values confirmed the consistence of measurements. The reliability for 3 T T2* assessment was full for the mid-septum (sensitivity, specificity and accuracy 100%) and high for global heart (sensitivity 100%, specificity and accuracy 97%). For the segmental measurement of iron levels at 3 T, the accuracy was no optimal. The accuracy was high to identify patients with mild to no-iron liver burden (97%) but dropped to 94% in patients with heavy-moderate iron burden. The sensitivity was unsatisfactory (67%) to detect patients with heavy liver iron burden.

Conclusion: T2* quantification of iron burden in the mid-septum, global heart and no heavy-moderate livers resulted to be feasible, reproducible and reliable at 3 T. Challenge was the segmental heart T2* analysis due to significantly higher susceptibility artefacts at 3 T.

B-0571 10:48

Relationship between myocardial T2* values and right and left ventricular volumetric and functional parameters in thalassaemia major (TM) patients evaluated by cardiac magnetic resonance (CMR)

I. Di Giampietro, C. Liguori, I. Sansoni, A. Feliziani, P. Cianciulli, B. Beomonte Zobel; Rome/IT

Purpose: CMR has become the most useful imaging technique in TM patients thank to T2* acquisition in order to quantitatively evaluate myocardial iron overload. The aim of the study was to assess the relationship between the myocardial T2* value and left-right ventricular functional parameters and to examine the associations between the degree of cardiac iron load and ventricular function impairment.

Methods and Materials: A retrospective analysis of 50 patients (24 M and 26 F mean age 34.57 ± 2.20 ys) with TM was performed. Myocardial iron load was assessed by T2* measurements and volumetric functions were analysed using the steady state free precession (SSFP) sequences.

Results: In patients with myocardial iron deposition ($T2^* < 20$ ms), the mean LVEF was $58.75\pm 6\%$ resulting significantly lower compared to LVEF measured in patients without iron deposition $64.73\pm 2.38\%$. Statistically significant correlations were founded between both the LV volumes and the myocardial T2* value: inverse correlations between both the LV end-systolic volume index ($r=-0.3$, $P < 0.01$) and the left ventricular LV end-diastolic volume index ($r=-0.28$, $P < 0.01$) were observed. In contrast cardiac T2* values were not associated with functional modifications in the right ventricle functional parameters.

Conclusion: Myocardial iron load assessed by CMR is associated with deterioration LVEF and the degree of the overload is inversely correlated with the T2* values. Non-correlation has been founded between T2* values and right ventricle functional parameters.

B-0572 10:57

Septal late gadolinium enhancement at the right ventricular insertions: more frequent than expected in hypertrophic and dilative cardiomyopathy

P. Bischoff, R.L. Duschka, S. Hollmann, M. Simon, A. Kovacs, P.W. Radke, F.M. Vogt, J. Barkhausen, P. Hunold; Lübeck/DE

Purpose: The particular pattern of septal Late Gd-enhancement (LGE) at the right ventricular-(RV)-insertions has been described in conjunction with pulmonary hypertension. Aim of this retrospective study was to characterise the distribution and prevalence of septal LGE at the RV-insertions in cases of hypertrophic and dilative cardiomyopathy (HCM/DCM).

Methods and Materials: A total of 517 contrast-enhanced cardiac MRI studies were performed (1.5 T and 3.0 T, Achieva, Philips) for different clinical indications. The MRI protocol consistently contained Cine SSFP in long and short axes and 3D T1w IR-LGE in long and short axes 8-15 min after double dose (0.2 mmol/kg) gadobutrol. All cases were reviewed in a retrospective analysis. DCM and HCM patients with LGE at the anterior and/or inferior septal RV-insertion were evaluated and compared to cardiomyopathy patients without LGE.

Results: In total, DCM or HCM were found in 46/517 pts (8.9%). Hypertrophic-non-obstructive cardiomyopathy (HNOCM) was detected 15/517 pts (2.9%), hypertrophic-obstructive cardiomyopathy (HOCM) was detected in 12/517 pts (2.3%). Thereof, anterior and inferior LGE at the RV-insertions was found in 8/27 pts (29.6% -HNOCM: 4/15 pts, 26.7%/ HOCM: 4/12 pts, 33.3%), only inf. LGE was found in 5/27 pts (18.5% -HNOCM: 3/15 pts, 20%/ HOCM: 2/12 pts, 16.7%). 19/517 pts

(3.7%) presented DCM, thereof 4/19 pts (21%) demonstrated ant. and inf. LGE at the RV-insertions, 2/19 pts (10.5%) had only an inferior LGE.

Conclusion: LGE at the septal right ventricular anterior and inferior insertions is a frequent finding in dilative and hypertrophic cardiomyopathy. This specific LGE pattern seems to be useful in the differential diagnosis of myocardial disease. However, its clinical relevance remains unclear.

B-0573 11:06

Visualisation of amyloid deposition in the heart of familial systemic amyloidosis using [11C]BF-227 PET

M. Tashiro¹, S. Ikeda², K. Furukawa¹, N. Okamura¹, S. Furumoto¹, R. Iwata¹, K. Yanai¹, Y. Kudo¹, H. Arai¹; ¹Sendai/JP, ²Matsumoto/JP (mtashiro@cyric.tohoku.ac.jp)

Purpose: The purpose of this study was to examine whether an amyloid-imaging tracer, [11C]BF-227, usually used for early diagnosis of Alzheimer's disease, can visualise the β -amyloid deposition in the cardiac muscle of a familial systemic amyloidosis patient.

Methods and Materials: The subject was a man with familial systemic amyloidosis, confirmed by biopsy of gastroduodenal specimen. Cardiac amyloidosis was also strongly suspected by echocardiography and MRI. For this patient, PET with [11C]BF-227, that sensitively and specifically binds to aggregated amyloid fibrils, was conducted. PET imaging was conducted using SET-2400 W (Shimadzu Inc., Kyoto, Japan). SUV values in the heart and lung were compared with those of normal database.

Results: The PET images revealed significantly robust retention of [11C]BF-227 in the heart of the patient compared to the normal control. His biopsy specimens from the duodenum also showed high signals of [11C]BF-227. SUV value of the heart was significantly higher than the normal database, while those of the lung showed no-significant difference.

Conclusion: To our knowledge, this is the first report showing the usefulness of a β -pleated sheet structure-specific PET in investigating visceral organ amyloidosis. None of the previous tracers was able to specifically bind to aggregated amyloid which forms a β -pleated sheet structure. It is truly important to detect the accumulation of real amyloid fibrils for early and accurate diagnosis of amyloidosis. Our result may provide a new evidence that our amyloid-specific PET tracer, [11C]BF-227, can successfully detect amyloid deposition in the heart, as well.

B-0574 11:15

Multidetector computed tomography with late enhancement (MDCT-LE) for pre-treatment planning of ventricular tachycardia (VT) RF-ablation

C. Colantoni, A. Esposito, F. De Cobelli, A. Palmisano, R.N. Cavallin, G. Maccabelli, S. Colombo, P. Della Bella, A. Del Maschio; Milan/IT

Purpose: Myocardial scars are the common substrate of VT; radio-frequency ablation (RFA) guided by electro-anatomical map (EAM) is frequently the therapy of choice. An imaging tool providing an anatomical and structural substrate to guide EAM and subsequent RFA should be an important help to reduce procedural time and improve success rate. We aimed to evaluate MDCT for this role, being MRI use mainly precluded from defibrillators (ICD) implanted to prevent sudden death.

Methods and Materials: 13 pts with recurrent-VT underwent 64-slice-MDCT before EAM and RFA, including an angiographic-scan and a low-energy (80 kV) delayed-scan (10 minutes after contrast-media injection). MDCT scans were merged with EAMs.

Results: MDCT scans were prospectively-ECG-triggered in 10 pts and retrospectively gated in 3 pts. 8 pts had ICD. 6 pts showed subepicardial LE suggestive for post-myocarditis scars. EAM, performed with epicardial approach, confirmed scars identified at MDCT-LE (voltage < 0.5mV) in all these pts. 6 pts had LE suggestive for post-ischaemic scars with subendocardial (4 pts) or transmural (2 pts) involvement. Low voltage areas at EAM performed with endocardial approach matched with LE areas. 1pt did not show LE areas and underwent RFA in areas with voltages between 0.5 and 1.5 mV (border zone) at EAM.

Conclusion: In most of enrolled patients MDCT-LE allowed us to map the scars responsible for electrical substrate of VT. MDCT-LE may be proposed to provide anatomic and structural substrate for guiding EAM and RFA in patients with recurrent-VT, also suggesting the more appropriate approach (endocardial vs epicardial). MDCT-LE, instead of MRI, may allow imaging guide also in patients with ICD.

B-0575 11:24

Late gadolinium-enhanced cardiac magnetic resonance (LGE-CMR) quantification of myocardial damage as a predictor of arrhythmic events

S. Bertugno, G. Ligabue, F. Flocchi, L. Nocetti, S. Vasaturo, R. Lugli, A. Barbieri, P. Torricelli; Modena/IT



Purpose: To investigate the prognostic value of LGE-CMR, throughout the association between LGE extension and the occurrence of sustained ventricular tachyarrhythmias (SVT) and implantable cardioverter defibrillator shock (ICDS) in HCM patients.

Methods and Materials: 62 patients (mean age: 55.6±16.0; 67.7% males) with documented HCM underwent 1.5 T cardiac magnetic resonance. LGE-MR images were obtained 15 min after injection of 0.2 mmol/kg of gadolinium-based contrast agent. Indexed end-diastolic left ventricular mass (IEDLV mass) was assessed and myocardial damage (expressed as percentage of total IEDLV myocardial mass) was quantified and defined as intensity 6SD above the mean signal of a non-enhanced myocardium area. Occurrence of SVT and ICDS during 32.1±11.2 months follow-up were recorded.

Results: The mean IEDLV mass was 89.8±28.5 g/m². On LGE-CMR, 53 (85.5%) patients exhibited myocardial scar. The mean LGE was 7.0±7.4% of IEDLV mass (median 5.25%; range 0-34%). During the follow-up 9 (14.5%) patients presented SVT. 8 (12.9%) patients implanted ICD and 4 of those had one or more ICDS. Patients who presented SVT had significantly higher LGE%, compared to those without: [12.3±6.9] vs. [6.1±7.1], P=0.009. Patients who presented one or more ICDS had significantly higher LGE%, compared to those without any shocks: [16.6±5.7] vs. [6.4±7], P=0.003.

Conclusion: Extension of LGE predicts the occurrence of SVT and ICDS in HCM patients.

B-0576 11:33

Increased late gadolinium enhancement of the left atrium by cardiovascular magnetic resonance in cardiac amyloidosis

F. Secchi¹, A. Jabbour², F. Sardanelli¹, D. Pennell², R. Mohiaddin²; ¹Milan/IT, ²London/UK (francescosecchimid@gmail.com)

Purpose: Our aim was to determine the prevalence of left atrial late gadolinium enhancement (LGE) by cardiac magnetic resonance (CMR) in patients with cardiac amyloidosis.

Methods and Materials: The CMR studies of 110 patients (aged 56±5 years) with known cardiac amyloidosis were reviewed. ECG-triggered four-chamber and long-axis views were acquired using an inversion recovery sequence 10 minutes after administration of contrast (Gadovist, 0.1 mmol/kg). Balanced steady-state free precession cine images were used to determine left ventricular end-diastolic and systolic indexed volumes (LVEDVi, LVESVi), ejection fraction (EF), stroke volume (SV) and mass index. Only patients with the classic diffuse circumferential pattern of left ventricular LGE were included in the study.

Results: Of 110 patients with cardiac amyloidosis, 26 patients (24%) displayed left atrial LGE. All three atrial were involved in 17 (65%), both septal and free walls in 7 (27%), and isolated septal wall involvement in 2 (8%). Patients with left atrial LGE also had significantly higher LVEDVi (143±35 mL vs. 124±50 mL, [mean±SD], p=0.033). However, no significant differences in LVESVi (69±35 mL vs. 70±40 mL, p=.462), EF (54%±14% vs. 68%±15%, p=.367), SV (74±17 mL vs. 68±25 mL, p=.125) and mass (123±31 g/m² vs. 126±40 g/m², p=.248) were observed.

Conclusion: Patients with cardiac amyloidosis have an increased prevalence (24%) of left atrial LGE. Patients with atrial LGE also had more dilated left ventricles those without atrial DE. Atrial LGE in cardiac amyloidosis may be a marker of disease severity and its prognostic implications require further evaluation.

B-0577 11:42

Does exist a correlation between late enhancement mass and left ventricular function in hypertrophic cardiomyopathy?

C. De Cecco, G. Muscogiuri, M. Di Girolamo, S. Fierro, M. Maurizi Enrici, V. David; Rome/IT (g.muscogiuri@hotmail.it)

Purpose: To correlate left ventricular volumes and function with late enhancement (LE) mass in patients with hypertrophic cardiomyopathy (HCM).

Methods and Materials: We retrospectively evaluated 106 patients with HCM diagnosis. All patients were studied with a 1.5 T MR. Study protocol included cine True-Fisp sequences (TR:3.09 ms, TE:1.3 ms, FA:80, thick: 8 mm in four-chamber, vertical long axis and short-axis) followed by inversion recovery Turbo-Flash sequences for LE evaluation (TR:8 ms, TE:4 ms, TI:250-340 ms, thick: 8 mm in four-chamber, vertical long axis and short-axis) acquired 10-15 minutes after iv administration of 0.2 mmol/kg of gadolinium. Left ventricular volumes (EDV, end-

diastolic volume; ESV, end-systolic; SV, stroke volume), ejection fraction (EF) and myocardial mass were calculated by manual planimetry with a dedicated software. LE mass was measured on short axis by manual planimetry as an area with SI > 6SD from normal tissue. Patients were divided into two different subgroups with LE (group 1) and without LE (group 2). For statistical analysis we used Spearman's correlation.

Results: In group 1 we observed the following **Results:** EDV 125±40 ml, ESV 36±22 ml, EF 72±10%, SV 88±25 ml and LE mass 10±14 g; in group 2 we observed: EDV 110±32 ml, ESV 27±21 ml, EF 77±7%, SV 85±24 ml. A significant positive correlation between LE mass and EDV (p=0.007), ESV (p=0.001) was obtained, meanwhile a negative correlation with EF (p=0.001). A correlation between SV and LE mass was not reported (p=0.6).

Conclusion: Patients with LE present a worst left ventricular function compared to control group. LE mass is correlated with a progressive systolic dysfunction. This finding could be relevant in terms of therapeutic approach especially in case of early HCM onset.

B-0578 11:51

Black blood versus bright blood T2* acquisition in cardiovascular magnetic resonance (CMR) for thalassaemia major (TM) patients: which can do better?

I. Di Giampietro, C. Liguori, I. Sansoni, P. Cianciulli, L. Mortato, B. Beomonte Zobel; *Rome/IT*

Purpose: To assess between black blood and bright blood T2* CMR acquisition which is superior in terms of images artefacts presence and to establish if significant differences can be founded in terms of T2* values, intra and inter-observer variability.

Methods and Materials: In a setting of 50 TM patients we performed both conventional bright blood and black blood T2* CMR sequences to determine intra and inter-observer variability and the presence of artefacts. In all patients, 2 separate studies of both techniques were performed to assess interstudy reproducibility. Image quality was assessed using a 5-point grading scale (0-very poor quality; 5-excellent quality) and image analysis was in all cases conducted by 2 experienced observers.

Results: Cardiac T2* values ranged from 5.30 to 50.63 ms. The mean T2* values were not different between black blood and bright blood acquisitions (32.04± 1.80 vs 34.52 ± 2.02 ms, p < 0.001). Compared with the conventional bright blood diastolic acquisition, the coefficient of variance of the black blood technique was superior for intra-observer reproducibility (p < 0.001), inter-observer reproducibility (p < 0.001) and inter-study reproducibility (p=0.001). Assessment of artefacts showed a superior score for black blood vs white blood scans (p < 0.001).

Conclusion: Black blood T2* CMR has superior reproducibility and reduced imaging artefacts for the assessment of cardiac iron, in comparison with the conventional bright blood technique, which make it the preferred technique for clinical practice.

10:30 - 12:00

Room P

Radiographers

SS 914

Dose and technique optimisation from the radiographer's perspective

Moderators:

P. Blackburn Andersen; *Kolding/DK*
D. Tack; *Baudour/BE*

B-0579 10:30



Patient's knowledge about radiation and radiological protection

J.P. Pinheiro, L.P.V. Ribeiro, S. Rodrigues, A.F.C.L. Abrantes, C.A. Silva, R.P.P. Almeida; *Faro/PT* (joao.pinheiro@gmail.com)

Purpose: To obtain and analyse patient's knowledge and perceptions regarding radiation exposure, from both natural and man-made radiation of medical procedures and interventions. Verify if patients worry about their exposure when undergoing medical exams, are aware of associated risks and means of radiological protection and if their knowledge on medical radiation exposure affects their own decisions.

Methods and Materials: On a medical environment a self-applied questionnaire was used as instrument and assigned to patients who would undergo medical imaging exams involving ionising radiation. A total of 300 valid questionnaires were interpreted and statistically analysed through descriptive statistics and Phi & Cramer's V correlation tests.

Results: 44.3% of patients believe most of their exposure derives from electronic appliances and 25% from medical imaging exams, while patient's with higher edu-

cation levels tend to consider is comes from the environment. The great majority of patients (95%) consider that only certified personnel should operate medical imaging equipment, but 74% never ask for their qualifications. 66.3% of patients claim that Technologists have more education on radiological protection and about 60% of patients rarely or never worry about radiation exposure when undergoing medical imaging exams.

Conclusion: Patients overestimate the risks of industrial radiation exposure while they underestimate the associated risks of medical radiation exposure and the Technologist's ability to reduce the inherent radiation exposure of medical imaging exams. Patient's knowledge on radiation and radiological protection is based more on perceptions and beliefs, rather than factual knowledge.

B-0580 10:39

A study of the awareness of x-ray radiation doses among Norwegian student radiographers

S. Kada; *Bergen/NO* (sundaran.kada@hib.no)

Purpose: To assess the level of student radiographers' knowledge concerning both the radiation doses received by patients undergoing commonly requested radiological investigations and the associated risks of these doses.

Methods and Materials: A survey was sent to all radiography program teachers in charge (n=6) in Norway, along with a request to administer the survey to final year student radiographers in their final term of study. The questionnaires pertained to radiation-related issues and demographic information.

Results: The response rate was 79% (122/155). The majority of the student radiographers reported poor knowledge of radiation doses. They were either ignorant of or underestimated the radiation doses used in the various imaging examinations. Only 4 student radiographers answered more than 50% of the items in a questionnaire designed for assessment of their level of knowledge correctly. Overall 63% (n=77) of the student radiographers were not aware of the radiation dose received from a chest x-ray, and 64% (n=78) of the students were ignorant of the annual dose limit for the patients. The study identified no statistically significant differences among radiography institutions (p=0.08) and between genders (p=0.61).

Conclusion: Overall, final year student radiographers' knowledge regarding radiation doses and the risks associated with ionising radiation is reported to be poor.

B-0581 10:48

Radiographer's role in dose optimisation in co-operation with dentists in orthopantomography

A. Henner¹, H. Poysko¹, A.-R. Pietila²; ¹*Oulu/FI*, ²*Haukipudas/FI* (anja.henner@oamk.fi)

Purpose: To find out consequence of referral in orthopantomographic imaging of the teeth in order to decrease patient's dose. Follow-up of doses was made in order to find out how permanent is the manner of dentists to ask partial OPTG.

Methods and Materials: Dose area product (DAP) of different programs was measured without patient. The variation in different program is large, e.g. when using partial program instead of whole mandible to seven-year-old child, dose is only one third (from 6.13 cGycm² to 2.31 cGycm²). The radiographers and dentists evaluated critically the present procedures: very poor referrals without any focused indication and due to this orthopantomogram was always taken as whole mandible. Dentists have been reminded of the possibility of partial OPTG also later. Form of OPTG was analysed from digital archive in two-month periods.

Results: After meeting the dentists started to write better referrals with clear indications and detailed information. On the basis of this information radiographer takes whole or partial mandible and set the kV and mA according to the required image quality. The dentists have to be reminded of this possibility to make the procedure permanent.

Conclusion: It is easy to decrease patient dose in co-operation the referral dentists. It requires radiographer's professional attitude and activity to remind the dentists of the importance of referral and its affect to patient's dose and harms due to ionising radiation to children. Multiprofessional co-operation, open discussions and awareness of the dose levels are the key points.

B-0582 10:57

Radiographic imaging: image quality and radiation dose optimisation in digital imaging

M.P. Possakka, V.J. Oksanen; *Oulu/FI* (mika.possakka@gmail.com)

Digital imaging applications have been increasing rapidly in the past years. Implementation of digital imaging systems has introduced a need to study the possibilities that digital imaging has to offer. Traditional tradeoffs between image quality and dose no longer exist.

Purpose: The purpose of the study was to make a standard of activity for optimising image quality and radiation dose with the CDRAD analyser program and contrast-detail phantom. The product is intended for radiographers, students and professionals working in the field of radiographic imaging. The functional aim was to create a standard of activity that enabled uniform procedure in optimising the image quality and radiation dose.

Methods and Materials: Images were taken using different parameters (mA, kVp filtration, etc). Three images were taken with the same parameters to achieve better reliability. The images taken of the contrast-detail phantom were evaluated with CDRAD analyzer program. The study revealed how different imaging parameters affected the image quality.

Results: According to the results, image quality was better and radiation exposure was lower when kVp was added to 75 from 66 and when 2 mm Al added filtration was used.

Conclusion: The results of the project can be utilised by radiographer students as part of evidence-based learning. Oulu University of Applied Sciences can also implement the results of the study in the curriculum. Thus, radiation safety can be improved in the School of Health and Social Care in accordance with the regulations of the Ministry of Social Affairs and Health.

B-0583 11:06

Mammography image quality in Switzerland

N. Richli Meystre¹, J.-L. Bulliard²; ¹Lausanne/CH, ²Epalinges/CH
(nicole.richli@hesav.ch)

Purpose: Although image quality in mammography has been positively associated with screening performance, mammography quality has seldom been assessed. In Switzerland, regional screening programmes undergo strict quality management procedures, which include continued training of radiographers. This study aimed at evaluating quality of mammograms in Switzerland, its evolution over time, and at identifying its determinants.

Methods and Materials: 7352 mammograms, performed between 1999 and 2007, were randomly drawn from 6 hospitals in 2 cantons with and without a screening program, and evaluated according to the PGMI (P: Perfect, G: Good, M: Moderate, I: Inadequate) classification system. Determinants of quality were assessed by multivariate logistic regressions for 2 indicators of quality.

Results: Overall, the inadequate image rate decreased over time (-0.8%/year, CI95% : - 1.14;-0.45) while the proportion of good or perfect images increased (+0.51%/year, CI95% : +0.18;+0.84). Higher image quality was associated with a mammogram being performed recently, for a cranio-caudal view, in a hospital with a high output (> 250 mammographic images/radiographer/year) and within a screening program. The inadequate image rate was 28% (95%CI: 12-42) lower with a digital mammogram and a perfect or good image classification twice as likely in the canton with an organised screening program (OR=1.96, 95%CI: 1.65-2.34).

Conclusion: Mammography image quality is steadily improving since 1999. Although quality-assurance procedures for screening programmes has contributed to the higher quality, the difference across settings has decreased. The annual volume of images performed per radiographer appears to be a strong predictor of image quality.

B-0584 11:15

Study of the scattered x-ray distributions around a mammography unit

P.E. Lima, P. Sousa, S. Rodrigues, A.F.C.L. Abrantes, C.A. Silva, L.P.V. Ribeiro, R.P.P. Almeida, K.B. Azevedo; Faro/PT (patriciaeneslima@gmail.com)

Purpose: To measure the distribution of scattered radiation in a mammography unit for shielding design purposes.

Methods and Materials: Measurements were carried out with an anthropomorphic phantom used to simulate a body from one adult patient. The dose rate for scattered radiation was recorded by placing a solid state sensor (Unfors Xi Survey Detector) every 10 degrees at 1 m distance from the FOV centre, in the axial and coronal planes of the breast. The scattered radiation distribution was treated as isodose curves, specifying the amount of radiation that will be delivered to a specific point in the room around the equipment (GE Senographe DMR). More than 50 exposures were made with a tube voltage of 30 kVp, anode-filter combination Mo/Mo and large focus.

Results: In the axial plane, results show that the scattered radiation is absorbed up to 73% on the back of the anthropomorphic phantom, at the potter bucky plane height. In the coronal plane, the scattered radiation significantly increases with the angle due to backscattering effect. Assuming the direction of the incidence beam is 0 degree, results show that the scattered radiation is 86% higher at 160 degrees than at 90 degrees.

Conclusion: The type of mammographic view and the patient's body strongly influence the distribution of scattered x-ray radiation. These results can be used to improve the shielding design of a mammographic unit with less resources and less spending on shielding barriers.

B-0585 11:24

Optical guidance in percutaneous CT-guided procedures

N. Greenbaum¹, L. Appelbaum¹, A. Hirschenbein², Y. Applbaum¹, Y. Libson¹, J. Sosna¹; ¹Jerusalem/IL, ²Ra'anana/IL

Purpose: A post-marketing prospective study was performed to assess accuracy and safety of a CT-based video guidance system. We also looked at shortening of procedure time and reduction of radiation exposure of the patients.

Methods and Materials: All participants signed an informed consent form. Percutaneous biopsy/RF ablation was conducted on 20 patients including both soft tissue and bone lesions. Eight procedures were RF ablations and 12 were biopsies/FNA. All procedures were performed using ActiSight needle guidance system. The miniature video camera of the system fitted all needles used for the procedures: 11G-20G according to common practice. Procedure-related data, including accuracy, time to reach lesion, number of scans, and complication rates, were compiled. ActiSight Needle Guidance System (ActiViews, Haifa, Israel) is designed to assist CT-guided interventions. It incorporates skin-attached reference markers and a miniature video camera mounted on the needle. Registration of the video image with the CT image allows showing the location of the needle in real time.

Results: Accurate access was achieved in all 20 lesions (100% success). Lesion diameter ranged 4 mm-38 mm (median 13 mm). Mean time for correct needle placement was 15 min. Total number of CT scans until beginning of actual procedure (biopsy and/or RFA) was 3.6.

Conclusion: Our preliminary experience shows that ActiSight-assisted procedures yield an accurate, fast process with less confirmation scans during needle placement. Accuracy of needle placement was independent of the lesion size or difficulty to reach the specific location. There were no system-related complications.

B-0586 11:33

A novel optimisation strategy in CT results in significant dose reductions

F. Zarb¹, M.F. McEntee², L. Rainford³; ¹Msida/MT, ²Sydney/AU, ³Dublin/IE
(francis.zarb@um.edu.mt)

Purpose: To compare optimisation of CT protocols using quality assurance phantoms and anatomical structures within a porcine model: a radiation dose and image quality study.

Methods and Materials: Three scan protocols were applied: current clinical protocols; phantom protocols (based on the use of lowest mA, kV and highest pitch settings before significant changes were objectively measured on images produced from a Catphan® 600 CT QA phantom) and further optimised protocols. These were applied in 4 CT suites, for 4 anatomical regions: posterior fossa; cerebrum; abdomen and chest. Image quality was evaluated using relative visual grading analysis based on EU image quality criteria guidelines, then critically reviewed with respect to CTDI and DLP findings.

Results: Current clinical protocols were retained in 5 out of 16 protocols. Catphan® 600-based protocols were retained in 2 cases with a dose reduction between 19% and 38% over current clinical protocols. Further optimisation was achieved in the remaining 9 cases with further dose reductions of 14% - 38%.

Conclusion: This study demonstrates that dose optimisation based on objective phantoms can improve CT protocols efficacy; however, if used in conjunction with animal models further dose and image quality optimisation can be attained. The use of animals in dose optimisation strategies allows the use of multiple exposures without radiation risks to patients facilitating experimentation and evaluation of image quality using anatomical structures comparable to those of patients.

B-0587 11:42

Paediatric CT scanning parameters used in Greek hospitals

D. Koumarianos, M. Salonikidou, E. Zaloni; Athens/GR (elizaloni@yahoo.gr)

Purpose: To determine if specific protocols related with children ages are used in CT.

Methods and Materials: The survey consisted of 14 questions addressing scanner details and scanning parameters used for three examinations (brain, chest, and abdomen CT) for four age groups (1, 5, 10 years and adults).

Results: The survey was sent to 133 radiographers and 135 hospitals. The web-based questionnaire was filled out by 110 people, yet only 38 questionnaires were fully completed. The scanner was mainly in public hospital (52.6%), multislice (65.8%) with 16 detectors (26.3%). The paediatric CT examination was applied

without any parameter change with respect to adult protocol in 12.4% of cases. Paediatric CT parameters were not adjusted on the basis of the age of the child in 52.6% of cases. For children 1, 5, and 10 years old and for adults correspondingly, the third CTDI quarter was calculated at 42.7, 50.9, 55.4 and 66.9 mGy for brain CT, 12, 13.5, 15.6 and 24.9 mGy for chest CT and 16.9, 17.7, 17.7, and 27.7 mGy for abdomen CT.

Conclusion: There is a considerable potential for dose reduction by optimisation of scan protocols and better education of the personnel. A reduction of CTDI in adult protocols (up to 38%) is required which will result in a significant dose reduction in paediatric protocols.

B-0588 11:51

The control infection in a mammography setting: a looking over practices and analysis of microorganisms

M.M.C.P. Ribeiro¹, E.L. de Oliveira¹, J.S. Gomes¹, M.L. Goncalves¹, J.P. Costa¹, L. Lanca¹, J.G. O'Neill¹, J.C. Mauricio²; ¹Lisbon/PT, ²Tomar/PT (margarida.ribeiro@estesl.pt)

Purpose: The cleaning and disinfection of medical surfaces and equipments, as well the hand hygiene are basic measures to guarantee safe practices in the control infection of health care. This study aimed to identify the steps in mammography CR (computerized radiology) process, characterising them according to the presence of microorganisms and identify the practices that lead to their transmission.

Methods and Materials: The observational data were collected in a form from WHO in order to characterise the hygiene practices applied by radiographers. In addition, for 3 different times, microorganisms were collected from five surfaces in the mammography room (analytic component). Before performing each examination, the radiographer never washed her hands. Using water and soap, she always washed her hands, after the examinations, except in 1 case. Only one time she used an alcohol-based antiseptic solution. The equipment was disinfected in 88.9% of the cases. The microorganisms found in the mammography surfaces were: coagulase-negative Staphylococcus; Micrococcus spp; Suspected Enterococcus spp (6.7%); Streptococcus spp (13.3%); Bacterial contamination of surfaces (40%) and the pathogenic microorganism-Escherichia Coli (6.7%) collected on the keyboard.

Results: The hands hygiene should be performed before and after the contact with the patient, using an alcohol-based antiseptic solution. The mammography's equipment and other medical surfaces must be disinfected between each patient at the beginning and end of each work session.

Conclusion: Although x-ray examinations, such as mammography, are undervalued in this matter due to the procedures mostly with ambulatory patients, this study allowed the identification of the many types of microorganism being one of these pathogenic.

10:30 - 12:00

Room Q

Paediatric

SS 912

Heart and chest

Moderators:

C. Balassy; Vienna/AT
C. Owens; London/UK

B-0589 10:30



Quantitative evaluation of chronic lung disease in infant with thin-section CT

F. Tsushima, S. Ono, H. Fujita, T. Tokuda, S. Kakehata, H. Seino, K. Shibutani, H. Miura, Y. Takai; Hiroshima/JIP (fmystshm@yahoo.co.jp)

Purpose: A clinical chronic pulmonary disorder group of infant is named with chronic lung disease (chronic lung disease; CLD). CLD is defined that a respiratory distress symptom to need oxygenation follows infancy ahead of opening, day instars 28. We evaluated above-mentioned thin-section CT findings and performed objective quantification of emphysema in patients with CLD.

Methods and Materials: Very or extremely low birth weight infants of 19 cases in this hospital in September, 2009 since May, 2011 were listed. Their mean birth weight was 976.5 (32.3-1646) g and mean gestational age was 26.7 (22.6-32.3) weeks. Thin-section CT were performed at 40 weeks corrected age in all cases. The entire lung was scanned with 0.625-mm section thickness with a MDCT scanner (LightSpeed16; GE, USA). The total lung volume (CT number <400 HU) and volume of emphysematous change (CT number <900 HU) were measured using the threshold method on a workstation.

Results: Eleven of all cases that were clinically diagnosed as CLD. All cases had CT findings of emphysematous change. Their mean total lung volume was 71.2 (56.6-97) ml and mean volume of emphysematous change was 11.3 (0.2-93.4) ml. Six infants had a severe initial respiratory course and went home on oxygen. Five of six cases who had large amount of emphysematous change had consequently become with home oxygen therapy. Their mean volume of emphysema was 21.6 ml. There was no difference between each illness type and lung volume measurement.

Conclusion: Quantitative evaluation of emphysematous changes classification of prognosis in infant with CLD.

B-0590 10:39



Coronary artery abnormalities in Kawasaki disease: comparison between CT and MR coronary angiography

J. Kim, H. Goo; Seoul/KR (ewooya@empal.com)

Purpose: To compare visibility and diagnostic performance of coronary artery abnormalities between CT and MR in children and adolescents with Kawasaki disease.

Methods and Materials: Between 1989 and 2010, a total of 56 children and adolescents (38 males; range 1-21 years) with Kawasaki disease who performed CT (n=58) or MR (n=39) coronary angiography were included in this study. In 17 of them, both CT and MR were performed. Visibility was graded on a 4-point scale (1:excellent, diagnostic≤3) for 11 coronary arterial segments of each patient. Coronary artery abnormalities (aneurysm, stenosis, and occlusion) were evaluated on CT and MR, based on reference standard obtained from cardiac catheterisation (n=29), echocardiography (n=56), follow-up CT and MR, and clinical history. Coronary artery visibility and diagnostic performance were compared between CT and MR.

Results: On CT and MR studies, 84.6% and 71.3%, respectively, of coronary arterial segments were assessable (P < 0.001). In 17 patients with both CT and MR, 89.2% and 68.9%, respectively, of them were assessable (P < 0.001). On CT and MR studies, sensitivity, specificity, positive predictive value (PPV), negative predictive value (NPV), and accuracy were 93.1% vs. 77.9% (P < 0.001), 99.2% vs. 99.7% (P=0.653), 96.8% vs. 98.7% (P=0.652), 98.2% vs. 94.1% (P < 0.001), and 98.0% vs. 94.9% (P=0.008), respectively. In the 17 patients, they were 91.8% vs. 70.4% (P < 0.001), 99.5% vs. 99.5% (P=1.000), 98.5% vs. 98.0% (P=1.000), 97.2% vs. 91.1% (P=0.006), and 97.6% vs. 92.3% (P=0.004), respectively.

Conclusion: CT shows significantly higher coronary artery visibility, sensitivity, NPV, and accuracy in evaluating coronary artery abnormalities of Kawasaki disease.

B-0592 10:48

Iterative image reconstruction techniques in paediatric cardiovascular CT angiography: image quality and potential for radiation dose reduction

F. Tricarico¹, P. Apfaltrer¹, U. Schoepf¹, R. Vliegenthart¹, J.R. Spears¹, G. Savino², R. Marano², L. Bonomo², A. Hlavacek¹; ¹Charleston SC, SC/US, ²Rome/IT (ftrix@libero.it)

Purpose: We assessed image quality, image noise, and the potential for further radiation dose reduction in children undergoing ultra-low radiation dose cardiovascular CT angiography (cCTA) using iterative reconstruction techniques.

Methods and Materials: Twenty-four children (median age: 4 months) with suspected or known congenital cardiovascular anomalies underwent dual source cCTA with (n=10) or without (n=14) ECG-synchronisation. Data were reconstructed with filtered back projection (FBP), iterative reconstruction in image space (IRIS), and sinogram-affirmed-iterative-reconstruction (SAFIRE). For ECG-synchronised studies, half-dose image acquisition was simulated by discarding projections from one tube. Signal/noise was measured within the ascending and descending aorta, left atrium, main pulmonary artery, and the trachea. Image quality was graded from 1 (non-diagnostic) to 5 (excellent) for the ventricular septum, mitral valve, and all structures described above. Effective dose (ED) was estimated using age/weight-specific conversion factors. Results were compared using T- and Chi-square testing.

Results: Image noise with IRIS and full-dose-SAFIRE was lower than with FBP (30.5±18.9 and 32.2±15.7 versus 44.9±24.4; all p < 0.001), while SNR was higher (19.0±8.4 and 17.6±8.5 versus 12.8±5.3; p < 0.01). Image quality scores were higher for IRIS and full-dose-SAFIRE than for FBP (3.7±0.6 and 3.6±0.6 versus 3.4±0.5; p < 0.05). Average ED was 0.28mSv without and 1.6mSv with ECG-synchronisation. In half-dose ECG-synchronised SAFIRE studies (estimated average ED: 0.8mSv), image-noise (38.4±21.9) was still significantly (p < 0.01) lower and SNR (15.9±7.9) higher than in full-dose-FBP studies, while image quality (3.8±0.5) was maintained.

Conclusion: At ultra-low radiation dose paediatric cCTA, iterative reconstruction techniques improve image quality and hold potential for substantial further reductions in radiation exposure.

B-0593 10:57

New conversion coefficients for dose reconstruction in high-resolution computed tomography (HR-CT) of the chest in neonates and infants

M.C. Seidenbusch, K. Schneider;
Munich/DE (michael.seidenbusch@med.uni-muenchen.de)

Purpose: Reconstruction of organ and tissue doses achieved during computed tomographic (CT) examinations is performed by applying conversion coefficients (synonymously: normalised organ doses) to basic dose indicators like the CTDI or the dose length product. The calculations of conversion coefficients published so far consider only slice thicknesses of more than 5 mm. As a consequence, especially in small organs the tissue doses are greatly underestimated. As HR-CT examinations of the lungs in neonates and infants are performed with slice thicknesses of 1 - 1.5 mm new conversion factors are needed.

Methods and Materials: For the calculation of new conversion coefficients, a new algorithm named CTX was developed by the authors in order to apply the commercially available PCXMC Monte Carlo algorithm developed by the Finnish Radiation and Nuclear Safety Authority STUK for dose calculations in CT.

Results: New conversion coefficients for organ dose reconstruction in HR-CT of neonates and young infants are presented with a slice resolution of 1 mm and an angular resolution of 1° with a formal consideration of various bow tie filters. In small organs such as the thyroid gland and the mammary glands organ doses calculated by applying the new method can exceed the tissue doses, predicted by the conversion coefficients published so far, by more than 50%.

Conclusion: After implementation of real bow tie filtration data, the new conversion coefficients should allow a realistic reconstruction of organ doses achieved during HR-CT examinations in neonates and infants.

B-0594 11:06

Radiation dose reduction in chest CT with the adaptive statistical iterative reconstruction (ASIR) technique in children

S. Lee; Seoul/KR

Purpose: To retrospectively compare radiation dose and image quality of pediatric chest CT taken with adaptive statistical iterative reconstruction (ASIR) and with routine protocol.

Methods and Materials: Twenty-six paediatric patients (M:F = 13:13, age 0-17 years; mean 11.7) had separate chest CT with low dose 50% ASIR and routine dose on different days between January 2010 and June 2011 (mean follow-up interval 148 days). Volume CT dose indices (CTDIvol), dose length products (DLP) were recorded, and effective dose were calculated to estimate radiation dose. The image quality was evaluated subjectively by three radiologists for noise, sharpness, artefacts, and diagnostic acceptability with a four-point scale (1-4). Objective noise and CT number were measured in the descending aorta and paraspinal muscle at the level of carina.

Results: The ASIR studies presented 56%, 60%, and 55% reductions in CTDIvol (from 18.73 to 7.43 mGy), DLP (from 307.42 to 134.50 mGy x cm), and effective dose (from 4.11 to 1.84 mSv), respectively, compared to the routine dose studies. The subjective image quality was not different between the ASIR and routine protocol. The objective noise was higher in the paraspinal muscle of ASIR group (20.81 vs. 16.67), but not different in the aorta (18.23 vs. 18.72).

Conclusion: The use of 50% ASIR lowers the radiation dose in paediatric chest CT more than 55%, while maintaining image quality.

B-0595 11:15

Comparison of non-breathheld single phase CT and 3D reconstructed bronchoscopic images with bronchoscopy for diagnosing airway malacia in infants

H. Hong, S.-A. Im; Seoul/KR (daydreamer.hong@gmail.com)

Purpose: The clinical diagnosis of airway-malacia in children is difficult and an accurate and non-invasive method is being required. The purpose of our study is to compare the accuracy of free-breathing CT scans of the airway in children, for the diagnosis of airway-malacia using bronchoscopy as the "gold-standard".

Methods and Materials: This retrospective study includes 90 children who received both bronchoscopy and CT scan of the airways in our institution. CT scans included the chest, 3 dimension (3D) CT bronchoscopy, neck, and brain CT scans. All patients were scanned with a non-breath-held protocol, using a 64-detector-multislice-helical-CT-scanner. Anteroposterior (AP) and transverse (Tr) diameters of the supra-glottic-larynx, glottis, trachea and bronchus were measured in the axial CT scans. Air-trapping and airway narrowing in the 3D-reconstructed-images were checked. Bronchoscopy was used as the gold standard and airway-malacia was

defined as more than 50% narrowing of the airway. Logistic-regression model was used for correlation between CT measurements and the bronchoscopic finding, and receiver-operating-characteristic curve was used to find cut-off values.

Results: 90 children under 16 years (32 infants) were included, of which 26 had airway-malacia. CT measurements which demonstrated significant correlation with bronchoscopic findings, included the supra-glottic-laryngeal-AP (AUC 0.952), tracheal-AP (AUC 0.825), bronchial-AP (AUC 0.808), tracheal-AP/tracheal-Tr ratio (AUC 0.922), bronchus-AP/distal-tracheal-Tr ratio (AUC 0.827) and airway narrowing in 3D-reconstructed-images (p=0.000).

Conclusion: The accuracy of free-breathing CT scan of the airway in detecting airway-malacia in children is comparable to the bronchoscopy, with lesser radiation dose compared to dual phase or cine-CT scans of the airway.

B-0596 11:24

Chest MRI in the evaluation of pulmonary alterations detected by CT in the follow-up of paediatric patients with middle lobe syndrome (MLS): comparison with XR

G. Serra, G. Ciarlo, V. Massaccesi, A. Fiorelli, S. Liberali, M. Paoletti, C. Catalano, F. Macri, F. Fraioli; Rome/IT

Purpose: To assess the most frequent pulmonary alterations detected by CT in a group of pediatric patients affected by middle lobe syndrome (MLS) at the time of diagnosis and the possible role of chest-MRI, in comparison with XR, in their follow-up.

Methods and Materials: 17 patients with MLS (mean age 6.2 years) underwent a chest CT at time of diagnosis (100 kV, CAREdose with quality reference: 70 mAs; collimation: 24 x 1.2 mm; rotation-time: 0.33 sec; scan-time: 5 sec). At follow-up (mean time: 15.2 months) all patients were evaluated with chest MRI (respiratory triggered DP weighted BLADE sequence; TR: 2000; TE: 27; FOV 400 mm; flip angle: 150; slice-thickness 5 mm; axial and coronal plane) and XR. The following lung alterations were assessed: bronchiectasis; bronchial-wall-thickening; atelectasis/consolidation; mucus-plugging. Lymphadenopathies were evaluated on CTs and MRIs; frequencies of each alteration were recorded for each examination in all patients.

Results: CT at diagnosis reported bronchiectasis in 35% of patients; bronchial-wall-thickening: 53%; atelectasis/consolidation: 100%; mucus-plugging: 35%; lymphadenopathies: 47%. Follow-up MRI: bronchiectasis in 35% of patients (XR: 29%); bronchial-wall-thickening: 59% (XR:6%); atelectasis/consolidation: 65% (XR: 35%); mucus-plugging: 25% (XR: 0%); lymphadenopathies: 47%. The most frequent localisation was middle lobe for all alterations both at baseline and follow-up.

Conclusion: CT evaluation showed that MLS can be characterised by various parenchymal and airways alterations already at diagnosis; at follow-up, XR underestimated the number of alterations compared to chest-MRI. MRI might represent a feasible option in the follow-up of patients affected by MLS.

B-0597 11:33

Flow-sensitive 4D MRI of aortic blood flow in patients with Marfan syndrome

J. Geiger¹, M. Markl², R. Arnold¹, B. Jung¹, D. Hirtler¹, L. Herzer¹, B. Stiller¹, M. Langer¹; ¹Freiburg/DE, ²Chicago, IL/US (julia.geiger@uniklinik-freiburg.de)

Purpose: To apply flow-sensitive 4D MRI for the characterisation of flow pattern changes in patients with Marfan syndrome (MFS) compared to normal controls.

Methods and Materials: Flow-sensitive 4D MRI of the thoracic aorta (temporal resolution~45 ms, spatial resolution~2.4 mm, venc=200 cm/s) was performed in 24 patients (mean age 18y) with confirmed MFS and 10 healthy volunteers (mean age 24y). Aortic haemodynamics was visualised by 3D particle traces and streamlines. Abnormal flow patterns (helix and vortex flow) in the ascending aorta (AAo), aortic arch, and descending aorta (DAo) were graded in three categories (blinded reading, 2 observers). Quantitative evaluation comprised the calculation of regional time-averaged absolute wall shear stress (WSS) and peak velocities at eight sites.

Results: Local helical flow in the AAo was significantly (p < 0.05) increased in MFS patients and was associated with aortic sinus dilatation. The incidence of global and vortex flow in the DAo was increased in patients (77% and 50%) compared to volunteers (none and 10%). Interobserver agreement was substantial (κ =0.7). Quantitative analysis revealed a significant increase in regional aortic WSS (0.38±0.10N/m² in patients vs. 0.34±0.07N/m² in volunteers, p < 0.01) at the location of local helix flow.

Conclusion: 4D flow analysis revealed marked differences of the aortic flow patterns between MFS patients and controls. The presence of local helix flow and the increased WSS in the MFS patients' AAo may be associated with the increased incidence of aortic root dilatation. The high prevalence of vortex and helix flow in the proximal DAo may promote Type-B dissection originating from this site.

B-0598 11:42

Quantitative pulmonary perfusion imaging at 3.0 T of 2-year-old children after congenital diaphragmatic hernia (CDH) repair

W. Neff, K. Zahn, T. Schaible, S.O. Schoenberg, L.R. Schad, F.G. Zoellner; Mannheim/DE (wolfgang.neff@umm.de)

Purpose: To investigate whether dynamic contrast-enhanced MR imaging (DCE-MRI) of the lung in survivors after CDH-repair at 3.0 T is feasible in 2-year-old children.

Methods and Materials: 12 children with a mean age 2.0 ± 0.2 years and 9-12 kg of body weight after CDH-repair, including 5 female and 7 male children, underwent DCE-MRI at 3.0 T using a time-resolved angiography with stochastic trajectories (TWIST) sequence. Quantification of lung perfusion was performed using a pixel-by-pixel deconvolution approach implemented in an in-house OsiriX plug-in. Six ROIs were carefully placed in the upper, middle, and lower part of the right and left lung to access differences in pulmonary blood flow while avoiding the inclusion of larger pulmonary arteries and veins.

Results: Average regional pulmonary blood flow (rPBF) for the hypoplastic lungs was 43 ± 16 mL/100 mL/min and 72 ± 18 mL/100 mL/min for the contralateral side. The difference between hypoplastic and contralateral lung was significant ($p=0.0003$). Also, the differences in rPBF measured in the apical, middle and lower lung were significantly different between hypoplastic lungs and contralateral sides (apical: $p=0.0001$, middle: $p=0.0118$, low: $p=0.014$). Significant differences between upper, middle and lower lung regions of the same side could not be detected.

Conclusion: DCE-MRI of the lung in 2-year-old patients is feasible at 3.0 T. Ipsilateral lung hypoplasia with reduced perfusion is reflected by significant lower rPBF values compared to the contralateral lung. DCE-MRI of the lung in CDH can help characterising lung hypoplasia initially and in long-term follow-up of children after CDH-repair.

10:30 - 12:00

Room Z

Computer Applications

SS 905

Computer assisted diagnosis (CAD)

Moderators:

B. Merlino; Rome/IT

R. van 't Klooster; Leiden/NL

B-0599 10:30

A simple and robust classification tree for differentiation between benign and malignant lesions in MR mammography

P.A.T. Baltzer, T. Groeschel, H.P. Burmeister, W.A. Kaiser, M. Dietzel; Jena/DE (pascal.baltzer@med.uni-jena.de)

Purpose: A multitude of lesion descriptors has been proposed in order to improve differential diagnosis in breast MRI. In clinical routine, a practical algorithm for lesion classification is needed. Such an algorithm should be as simple as possible and include only the most important lesion features with the highest power to differentiate benign from malignant lesions. This investigation was performed in order to develop a simple classification tree for differential diagnosis in a large database and estimate its diagnostic accuracy.

Methods and Materials: 1084 lesions in standardised breast MRI (1.5 T, dynamic T1w after 0.1 mmol Gd-DTPA, T2w-TSE) with histological verification (648 malignant, 436 benign) were investigated. 17 categorical lesion descriptors were assessed by 2 experienced readers. Classification analysis was performed using the Chi-squared automatic interaction detection (CHAID) method. Results include the probability for malignancy for every descriptor combination in the classification tree.

Results: A classification tree incorporating 5 lesion descriptors with a depth of 3 ramifications (1: root (rootlike border dendrite), 2: delayed enhancement (Persistent, Plateau, Washout), 3: border, internal enhancement, oedema) and 11 terminal nodes was calculated. 82.6% of all benign and 80.3% of all malignant lesions were correctly identified. 262 malignant (24.1%) and 107 benign (9.8%) lesions could be classified with an accuracy above 95%.

Conclusion: The classification algorithm used was able to reduce the number of categorical descriptors to be analysed from 17 to 5 (29.4%), resulting in a high classification accuracy. More than one-third of all lesions could be classified with an accuracy above 95%.

B-0600 10:39

"Magnetic resonance mammography has a high sensitivity but low specificity!": new thoughts and fresh data on an old mantra

M. Dietzel, K. Schoen, R. Zoubi, H.P. Burmeister, M. Gajda, I.B. Runnebaum, W.A. Kaiser, P.A.T. Baltzer; Jena/DE (dietzelmatthias@hotmail.com)

Purpose: Even in its 3rd decade of clinical application, diagnostic-accuracy of MR-mammography (MRM) is still not well understood and remains discussed controversially. To a major part - this is certainly due to different standards-of-reference (SOR: histological verification, follow-up, etc.) and composition of patient collectives in previous studies: particularly the group of true-negative MRM-results is challenging to analyse, as such often do not get histological sampling anymore and are followed-up clinically/radiologically. In this scenario, only long-term MRM-follow-up is able to provide a valid SOR. Accordingly, we designed this investigation to identify the accuracy of MRM as interpreted by non-expert readers defining histological verification and long-term MRM follow-up as SOR.

Methods and Materials: Over 3 years all consecutive patients receiving MRM with subsequent histological verification or MRM-follow-up > 2years were included into this prospective cross-sectional investigation (exclusion: BI-RADS VI, adjuvant/neoadjuvant chemotherapy or any other breast-treatment between initial- and follow-up MRM). Initial-MRM was interpreted by non-expert readers (~500 MRM). Primary MRM-diagnosis and results of the reference-standards (histology, findings upon long-term follow-up: SORhistology/SORfollow-up) were assessed by contingency tables.

Results: 448 patients were included (SORhistology: 321; SORfollow-up: 175). Pretest-probability was 0.28. Main indication for initial-MRM was screening for recurrence of breast-cancer (22.9%), or BI-RADS II (7.7%), III (13.8%) and IV (37.1%) classification in conventional-imaging. The non-expert readers achieved high specificity (86.3%) and positive-likelihood-ratio (7.0). Overall accuracy reached excellent odd's-ratio (160.1), Sensitivity (96.2%), negative-predictive-value (98.3%) and negative-likelihood-ratio (0.04).

Conclusion: MRM provides excellent overall diagnostic accuracy, sensitivity and negative predictive. Even in non-expert readers MRM has a high specificity.

B-0601 10:48

Computer-aided diagnosis (CADx) is a feasible prognostic biomarker for the noninvasive prediction of axillary lymph node metastases

M. Dietzel, R. Zoubi, H. Habrecht, M. Gajda, I.B. Runnebaum, W.A. Kaiser, P.A.T. Baltzer; Jena/DE (dietzelmatthias@hotmail.com)

Purpose: Computer-aided diagnosis (CADx) allows semiautomatic assessment of breast lesion in MR-mammography (MRM). Previous investigations suggested that such CADx -data might not only be used for differential diagnosis of benign vs. lesions but could also provide some prognostic information. We aimed to further evaluate this approach and evaluated the potential of CADx to predict the most single important prognostic factor in primary breast cancer, i.e. axillary lymph-node-metastasis, by CADx-based analysis of MRM.

Methods and Materials: 82 consecutive patients with primary invasive breast-cancer receiving pre-therapeutic staging-MRM according to EUSOBI-guidelines were included into this prospective cross-sectional study. Surgical axillary-staging was defined as reference-standard. Breast MRI was analysed using commercial CAD-software: It evaluates semi-automatically functional tissue-parameters of the most-suspect-voxel as well of the whole tumour, e.g.: initial-enhancement, wash-out, peak-enhancement, time-to-peak-enhancement, etc. Significant and independent predictors for lymph-node-metastasis were identified (logistic-regression, backward feature-selection) and combined into a multivariate model to predict nodal-positive breast-cancers (AUC: area under the ROC curve).

Results: There were 24 nodal-positive and 58 nodal-negative cancers. BLRA identified 6 CAD-parameters as significant independent predictors for the prediction of lymph-node-metastasis ($P < 0.001$). Multivariate analysis reached high accuracy (AUC: 0.81; standard error: 0.05) and moderate model fit (r^2 : 0.35) to predict nodal-positive cancers.

Conclusion: CADx-based interpretation of MR-mammography is a significant predictor of axillary lymph-node-metastasis. Accordingly, it could be used as a prognostic biomarker and should be further investigated for potential noninvasive risk stratification of breast cancer patients in future studies.

B-0602 10:57

Computer-aided decision support for the characterisation of liver lesions in CT scans

M. [Hammon](#), P. Dankerl, M. Costa, A. Tsybmal, S. Seifert, M. Sühling, M. Uder, A. Cavallaro; *Erlangen/DE (matthias.hammon@uk-erlangen.de)*

Purpose: Daily routine of radiologists includes differentiating a variety of lesion types in CT-scans - a challenging and time-consuming task. We evaluated an innovative THESEUS-MEDICO CBIR-CAD (content-based image retrieval+computer-aided-decision) system that assists the reader in discriminating liver lesions by retrieving, scoring, ranking and displaying similar lesions according to user-defined similarity criteria including lesion benignancy, density and type.

Methods and Materials: A set of 523 CT scans containing 854 liver lesions annotated by 2 experienced radiologists were used for generation and evaluation of the learning-based models in the system. A ranked list of lesions showing similar benignancy (benign/malignant), density (hypodense/hyperdense) or lesion type (cyst/haemangioma/metastasis) can be retrieved from just a region of interest as input query. Additional input (e.g. characterising semantic features) has shown to improve the performance, especially for indeterminate sub-centimeter lesions.

Results: Algorithm runtime is within a few seconds per lesion. On unseen test data, the classification accuracy obtained was 95.5% for retrieval with similar density, 85.5% for similar benignancy, and 91.2% in the lesion type case. The data collection used is the biggest sample compared to similar studies and the predictive performance achieved is competitive with respect to state of the art.

Conclusion: As proven by this study, the investigated system automatically discriminated reliably between different types of liver lesions. The system assists reading and decision-making process by quick retrieval, ranking and displaying similar lesions with related radiological report information. This serves as a second opinion and provides valuable additional information for radiological decision making especially when MRI is contraindicated.

B-0603 11:06

Automated detection of osteolytic thoracolumbar spine lesions in CT scans

M. [Hammon](#), M. Wels, P. Dankerl, M. Kelm, A. Tsybmal, S. Seifert, M. Sühling, M. Uder, A. Cavallaro; *Erlangen/DE (matthias.hammon@uk-erlangen.de)*

Purpose: Osteolytic spinal bone lesion assessment in CT-scans is a challenging and important task in routine radiology. We evaluated the sensitivity and number of false positive results of a novel, fully automatic computer-aided detection (CAD) system featuring an innovative algorithm from THESEUS-MEDICO.

Methods and Materials: We retrospectively evaluated the CAD-system on CT-scans of 34 patients (including diagnosis such as osteoporosis, degenerative spine disorders, and vertebral fractures) with 105 osteolytic spine lesions larger than 0.5 cm³. The software is based on the principles of machine learning and automatically detects and highlights osteolytic lesions. Detected degenerative processes, e.g. Schmorl's nodules or haemangiomas were not considered as false positive findings. Manual lesion annotation was performed by an experienced radiologist (gold standard). Sensitivity and false-positive rates on unseen data were calculated (9-fold cross-validation).

Results: Algorithm runtime is less than 3 minutes per data set. Our system achieves a sensitivity of 75% at 3.0 false positives per spine on average. The median sensitivity is 86% at 2.0 false positives per spine. The difference between the two sensitivity values is due to the different data quality which is contributing to the degree of difficulty of the detection task.

Conclusion: The presented CAD-system successfully detects osteolytic thoracolumbar spine lesions even in challenging data sets. It can therefore be applied as a fully automatic pre-processing step to indicate suspicious areas and thus support the radiologist. This is extremely valuable during the reading of CT-scans as osteolytic bone lesions are at the risk of being missed even by experienced radiologists.

B-0604 11:15

Computed-aided stenosis detection on coronary CT angiography in chest pain patients with an intermediate pre-test likelihood for acute coronary syndrome

T. [Henzler](#), M. Meyer, P. Apfaltrer, S.O. Schoenberg, C. Fink; *Mannheim/DE (thomas.henzler@medma.uni-heidelberg.de)*

Purpose: To compare the performance of an automated computed-aided algorithm for stenosis detection on coronary CT angiography (cCTA) with expert human interpretation in patients with acute chest pain and an intermediate pre-test likelihood for acute coronary syndrome (ACS).

Methods and Materials: This retrospective study was approved by our IRB and in compliance with HIPAA regulations. Among 93 consecutive cCTA examinations, 74 were of adequate quality for automated evaluation by COR-Analyser (Rcadia Medical Imaging, Haifa, Israel). Findings were compared to human expert interpretation for detection of stenosis defined as $\geq 50\%$ vessel diameter reduction in the left main (LM), left anterior descending (LAD), circumflex (LCx), right coronary artery (RCA), or arterial side branches.

Results: Among 74 cases evaluated by the COR-Analyser, human expert interpretation identified 37 patients with stenosis $\geq 50\%$. On a per-patient/per-vessel level the COR-Analyser revealed a sensitivity of 100%/79%, a specificity of 78%/89%, a negative predictive value of 100%/94% and a positive predictive value of 82%/65%. With respect to individual segments, the COR-Analyser detected 1/3 LM lesions, 22/23 LAD lesions, 7/13 LCx lesions, 8/11 RCA lesions, and 5/7 arterial side branches. False-positive interpretations were localised to the LM (n=5), LAD (n=5), LCx (n=5), RCA (n=10), and arterial branches (n=4), and were related predominantly to overestimation of stenotic lesions with less than 50% diameter and calcified vessels.

Conclusion: An automated computed-aided detection algorithm of stenotic lesions on cCTA provides a high negative predictive value to rule-out ACS in patients with acute chest pain and an intermediate pre-test likelihood for ACS.

B-0605 11:24

A computer-assisted method for the rapid and accurate assessment of left ventricular volumes, ejection fraction and mass by MRI

M. [Mazonakis](#), K. Pagonidis, J. Damilakis; *Iraklion/GR (mazonak@med.uoc.gr)*

Purpose: To develop and evaluate a computer-assisted stereological method for the assessment of left ventricular (LV) size and function from MRI data.

Methods and Materials: Short-axis MRI slices covering the entire LV were obtained from 23 consecutive subjects with suspected coronary artery disease. A computer-generated systematic grid of test points was randomly superimposed on each slice. Cross-sectional LV areas were estimated using the semiautomatic stereological point-counting method. The LV volumes, ejection fraction and mass were calculated through the systematic slice sampling procedure. The reproducibility of stereological method was determined by three independent observers. The parameters derived from manually traced LV contours served as reference values.

Results: Stereological volume assessments obtained by samples consisting of every third slice depicting LV differed significantly from those by manual tracing ($p < 0.05$). Samples of 4-5 slices arising from the 1/2 systematic sampling scheme provided volume estimations with a mean coefficient of error of $6.8 \pm 2.1\%$ in less than 3 min. No difference was found between the reference values and LV parameters estimated by the 1/2 sampling intensity ($p > 0.05$). These stereological estimations were highly correlated with the reference values ($r = 0.86-0.95$). The 95% limits of agreement between the two methods were clinically acceptable (end-diastolic volume: -15.8 to 10.0 cm³; end-systolic volume: -6.9 to 8.7 cm³; ejection fraction: -8.7 to 5.0%; mass: -10.3 to 17.9 g). The intraobserver and interobserver variabilities associated with the stereological estimations were 2.8-5.4% and 4.2-7.6%, respectively.

Conclusion: Stereological analysis on 4-5 systematically sampled MRI slices allows the reproducible and accurate assessment of LV parameters with reduced user intervention.

B-0606 11:33

Automated branch name labelling system of tracheobronchial tree by computational anatomy

H. [Natori](#)¹, M. Mori¹, H. Takabatake¹, H. Honma¹, Y. Nimura², K. Mori²; ¹Sapporo/JP, ²Nagoya/JP (hnatori@sapmed.ac.jp)

Purpose: For computational anatomy, we proposed the system that automatically assigned anatomical names to the bronchial branches extracted from multi-detector CT (MD-CT) data. Designed system was able to process variant cases of branching types of tracheobronchial tree.

Methods and Materials: NewVES viewer developed by co-author K.M. was used for virtual bronchoscopy. Bronchial models based on MD-CT datasets were made using recognition of branching pattern, and directions of those branches. Machine-learning approach was employed for this system. MD-CT data of 65 cases were used as training data. For evaluation of the automated branch name labelling system, new external 25 cases of MD-CT data were used.

Results: In virtual bronchoscopy, bronchial names were automatically overlaid on navigation images. Bronchial names sequentially appeared from trachea, main bronchi, lobar bronchi, to segmental bronchi. Names of sub-segmental bronchi were also shown frequently, and sub-sub-segmental bronchi were shown in some cases. Automated branch name labelling system worked properly even for the variant

type of branching. In some cases, sequential shift of assigned names to proximal occurred in the belonging bronchi at the deleted site of the expected bronchus by poor reconstruction of a bronchial image and by congenital or operative deletion of the bronchus was present. Strict name matching to doctors' interpretation revealed 100% matched for the trachea and main bronchi. For the distal bronchi, overall results of 80% of labelled names were correct.

Conclusion: According to the knowledge of computational anatomy, automated assignment of bronchial branch names may help doctors during virtual bronchoscopy.

B-0607 11:42

Development of a computer-aided independent monitor unit verification system using Clarkson's sector integration routine

M. [Matsushima](#)¹, R. Tanaka², Y. Kikuchi³; ¹Kurobe/JP, ²Kanazawa/JP, ³Fukui/JP (linac@med.kurobe.toyama.jp)

Purpose: To develop a computerised method for verification of monitor unit (MU) based on geometrical factors in radiation treatment planning, and to investigate the clinical effectiveness of our system.

Methods and Materials: Shape information on Xjaw, Yjaw, and multi-leaf collimator (MLC) was read from the planning data, and radial direction distance (ri) of the division for integration of 36 segments was calculated. Clarkson's sector integration routine was used to calculate the mean phantom scatter correction factor (Sp) and mean tissue-maximum ratio (TMR) for external photon beams of irregular and conformal fields with MLC. Our system with a user-friendly graphical interface was installed on a personal computer (1.5GHz CPU) to verify its accuracy in 51 cases, including five square fields, six rectangular fields, four kinds' wedge-shaped fields, eight irregular fields, and three conformal fields.

Results: Average ri difference, the difference in MU, and measured absorbed dose were < 0.3 mm, 0.5%, and -0.2%, respectively. Maximum values were ±1.5 mm, 1.5%, and -0.9%, respectively. The time to calculate one field was < 1 s. Our system provided fully automated MU verification without any manual "hand calculation."

Conclusion: It is necessary to ensure disagreement between verification and primary calculations with homogeneous conditions or heterogeneity corrections is < 2%-5% by independent MU verification, according to the report of AAPM Task Group 114. The results indicated that our system will aid operators in MU verification with high accuracy and less complexity for external radiation therapy.

B-0608 11:51

Fully iterative reconstruction algorithm for MDCT: initial results

M. [Dobritz](#)¹, T. Koehler², K.M. Brown³, A. Fingerle¹, E.J. Rummeny¹, P.B. Noel¹; ¹Munich/DE, ²Hamburg/DE, ³Cleveland, OH/US (dobritz@roe.med.tum.de)

Purpose: To evaluate fully iterative reconstruction (IR) in MDCT with respect to image quality and diagnostic value compared with conventional FBP.

Methods and Materials: The study was performed prospectively with patients who had suffered from malignant diseases in a tumour follow-up. Data were acquired on a Philips Brilliance iCT and reconstructed using conventional FBP and IR. IR uses edge-preserving regularisation to trade off noise and resolution. Noise texture is controlled by a parameter and by fading the FBP image to the IR result. To determine the diagnostic value of IR, experienced radiologists independently defined pathological and anatomical features in the reconstructions.

Results: An extreme choice of IR parameters resulted in almost complete removal of image noise while producing an unfamiliar image texture. Without FBP fading, sharpness of some organ edges was found to be difficult to rate. In one case, the surface of the liver seems to have nodular-like cirrhotic changes. Less extreme parameters for IR led to still strongly reduced noise, less unfamiliar texture and no artificial changes. In the portal venous phase, vascular structures are better delineated in IR reconstructions compared to FBP. All pathological and anatomical features could be detected and defined in FBP and IR images. However, these features are more clearly visible in IR images. Overall, IR was assessed to be superior to FBP.

Conclusion: In this study, we illustrate the clinical value of IR. IR has the potential to reduce patient dose and improve diagnostic value for any clinical protocol.

Sunday, March 4

10:30 - 12:00

Room A

Oncologic Imaging

SS 1316

Whole body MRI in cancer patients

Moderators:

M. Mayerhöfer; Vienna/AT

H.-P. Schlemmer; Heidelberg/DE

B-0609 10:30

Bone marrow lesions in patients with myeloma: whole body DWIBS vs T1-weighted contrast-enhanced MR imaging

E. Squillaci, F. Bolacchi, C. Ciccio', M. Antonicoli, G. Manenti, G. Simonetti; Rome/IT (ettoresquillaci@tiscali.it)

Purpose: The purpose of our study was to compare T1-weighted contrast material-enhanced fat-suppressed spin-echo magnetic resonance (MR) sequences and DWIBS for depiction of bone marrow abnormalities in patients with myeloma.

Methods and Materials: One hundred and thirty-five patients with previously diagnosed MM underwent 3 T WB-MRI for pre-treatment staging. morphological (T1W), Diffusion-weighted imaging with background suppression (DWIBS) and contrast-enhanced 3D T1W sequences were performed. Volume and signal difference-to-noise ratio (SDNR) were measured. Staging determined with MR findings with each sequence were compared with the results of a review panel.

Results: Regarding volume of bone marrow abnormalities, a low correlation ($r(2) = 0.5$) of both sequences was found. SDNR was substantially higher on DWIBS images than on 3D T1-weighted contrast-enhanced (mean, 117.7 vs 89.3; $P < .001$). The qualitative analysis demonstrated the same imaging pattern with both sequences in 12% ($\kappa = 0.035$) of normal-appearing marrow with limited disease, in 96% ($\kappa = 0.74$) of focal infiltration, and in 10% ($\kappa = 0.041$) of diffuse infiltration. Inter-observer reproducibility of the three imaging patterns was similar for both sequences. The kappa values for these three zones with T1-weighted contrast-enhanced MR sequence were 0.61, 0.58, and 0.63, and those for the DWIBS sequences were 0.32, 0.64 and 0.22, respectively. Staging determined with MR findings were equal with both sequences in 85% of involved bones.

Conclusion: T1-weighted contrast-enhanced fat-suppressed MR images are superior to DWIBS in the demonstration of the diffuse and limited disease. However, staging determined with both sequences is comparable.

B-0610 10:39

Whole body MRI for response assessment of multiple myeloma after stem cell transplantation

C. Weber, H. Hentschel, T. Bley, N. Kroeger, G. Adam, P. Bannas; Hamburg/DE (hannahhentschel@gmx.de)

Purpose: Comparison of whole body MRI (WBMRI) with serum analyses to determine whether WBMRI enables reliable therapy response assessment in patients with multiple myeloma after stem cell transplantation (SCT).

Methods and Materials: 33 patients (19 men, 14 women; mean age 52±11.8 years) with multiple myeloma after SCT were examined with WBMRI at two time points after SCT. Extent of intra- and extramedullary myeloma manifestations from both WBMRI examinations was correlated with hematological parameters and with medium-term patient outcome. McNemars's test was used for statistical analysis.

Results: WBMRI identified new or progressive lesions in 10 of 33 patients (30.3%), 8 patients (24.2%) had only intramedullary lesions and 2 patients (6.1%) had intra- and extramedullary lymphoma manifestations. Results of WBMRI and serum analyses agreed in 26 of all 33 patients (78.8%), 19 patients (57.6%) were classified concordantly as responders and 7 patients (21.2%) as non-responders. The remaining 7 patients (21.2%) were classified unequally with both methods, however without being statistically significant ($p=1.0$)

Conclusion: WBMRI enables response assessment in patients with multiple myeloma after SCT, but without additional benefit compared to routinely performed serum analyses. However, WBMRI allows exact localization of intra- and extramedullary lymphoma manifestations, which advocates WBMRI particularly for symptomatic patients or patients with non-secretory myeloma.

B-0611 10:48

Whole body diffusion-weighted imaging at 3 Tesla field-strength for early treatment assessment and treatment prediction in lymphoma

K.N. de Paepe, C. Bevernage, F. de Keyzer, P. Wolter, R. Oyen, G. Verhoef, V. Vandecaveye; Louvain/BE

Purpose: To evaluate 3 T whole body diffusion-weighted imaging (WB-DWI) for early assessment of chemotherapy in aggressive non-Hodgkin lymphoma (NHL).

Methods and Materials: Fourteen patients with NHL treated with standard chemotherapy underwent 3 T WB-DWI with 2 b-values ($b=0-1000$ s/mm²) prior to, 2 and 4 weeks after initiation of treatment. The apparent diffusion coefficient (ADC) was calculated from regions-of-interest (ROI) drawn on lymphoma locations on transverse b0- and b-1000-images. Pretreatment ADC, ADC-change to pretreatment ADC (ADCbase) at 2 weeks (ADCratio2w) and at 4 weeks (ADCratio4w) during treatment of responding and non-responding lesions were compared using a Mann-Whitney-U-test. The predictive value of ADCbase, ADCratio2w and ADCratio4w was correlated with progression-free survival (PFS) with a log rank test, including the effect of the international prognostic index (IPI).

Results: Eight patients showed complete remission after 18 months of follow-up, whereas 6 patients showed persistent or recurrent disease within 5 to 15 months. The ADCbase, ADCratio2w and ADCratio4w were significantly different in lesions showing recurrence versus remission (ADCbase= $1.19 \pm 0.33 \times 10^{-3}$ mm²/s versus $0.96 \pm 0.28 \times 10^{-3}$ mm²/s, $p < 0.0001$; ADCratio2w= increase %: 4 ± 21 versus 119 ± 68 , $p < 0.0001$; ADCratio4w= increase %: 18 ± 61 versus 155 ± 78 , $p < 0.0001$). Per-body-region, the ADCratio2w demonstrated highest accuracy of 91% with a negative predictive value of 100% and positive predictive value of 91%. Differences in ADCbase, ADCratio2w and ADCratio4w between patient groups correlated significantly with PFS (ADCbase - $p=0.028$, ADCratio2w - $p=0.0002$ and ADCr4w- $p=0.004$), in contrast to the IPI.

Conclusion: WB-DWI may allow for treatment prediction and early treatment assessment of DLBCL using differences in ADCbase, ADCratio2w and ADCratio4w.

B-0612 10:57

Is whole body diffusion-weighted imaging at 3 Tesla field-strength feasible for staging lymphoma?

K.N. De Paepe, F. De Keyzer, P. Wolter, R. Oyen, G. Verhoef, V. Vandecaveye; Leuven/BE

Purpose: To determine the feasibility of 3 T whole body diffusion-weighted imaging (WB-DWI) for staging of non-Hodgkin lymphoma (NHL).

Methods and Materials: 16 patients with NHL underwent 3 T WB-DWI with 2 b-values (0-1000 s/mm²). Regions-of-interest (ROI) were drawn on coronal reformatted b-1000 images in every hyperintense lesion, in normal tissue (iso/hypointense) and in the surrounding air to determine background noise. Signal-to-background ratio (SBR=Slesion/Sbackground) was determined for every ROI. Additionally, apparent diffusion coefficient (ADC) was calculated from ROIs drawn on transverse b0- and b1000-images in hyperintense lesions and normal or benign tissue. SBR and ADC of malignant and benign tissue were compared using Mann-Whitney-U-tests while receiver-operating-characteristic-curves were constructed to determine sensitivity (s), specificity (sp) and accuracy (acc). Agreement between WB-DWI and PET-CT for Ann Arbor classification was assessed by calculating kappa scores.

Results: SBR and ADC of benign and malignant tissue differed significantly ($p < 0.001$), with ADC being the best discriminator for lymph nodes ($n=184$, $s=94\%$, $sp=92\%$, $acc=93\%$) and SBR for bone and soft tissue (bone: $n=82$, $s=94\%$, $sp=96\%$, $acc=95\%$; soft tissue: $n=16$, $s=100\%$, $sp=100\%$, $acc=100\%$). PET-CT and WB-DWI showed good to excellent agreement (?lymph nodes=0.80, ?bone=0.92, ?soft tissue=1) for lesion differentiation and agreed on Ann Arbor stage in 88% of patients. WB-DWI correctly downstaged one patient (stage IV to II) and incorrectly downstaged another (stage II to I).

Conclusion: WB-DWI is feasible for staging NHL showing comparable results to PET-CT. SBR is most accurate for characterising bone and soft tissue lesions while ADC is preferred to characterise lymph nodes.

B-0613 11:06

Whole body magnetic resonance imaging with diffusion-weighted sequences for the follow-up of stage III melanoma patients

G. Petralia¹, M. Padrenostro¹, S. Alessi¹, R. Di Filippi¹, S. Raimondi¹, L. Bonello¹, J. Garcia-Bennett², M. Bellomi¹; ¹Milan/IT, ²Reus/ES (giuseppe.petralia@ieo.it)

Purpose: To evaluate the feasibility and the potential of whole body magnetic resonance imaging (WB-MRI) with diffusion-weighted (DW) sequences as a substitute of whole body computed tomography (CT) for the follow-up of stage III melanoma patients.

Methods and Materials: we evaluated seventy-one WB-MRI in 19 patients with stage III melanoma, performed at baseline and every 3 months during adjuvant therapy. Findings were classified benign or suspicious for metastasis and divided into 9 body regions: brain, neck, thorax, upper abdomen, liver, pelvis, soft tissues, bone and lymph nodes. Biopsy or follow-up was considered as gold standard for diagnosis. The sensitivity (SE), specificity (SP), positive predictive value (PPV), negative predictive value (NPV) and diagnostic accuracy (DA) of WB-MRI were calculated per patient and per single body region.

Results: All patients well tolerated the exam. One-hundred and forty findings were considered for analysis, with the following per patient values: SE (93%), SP (89%), PPV (52%), NPV (99%), DA (90%). The DA per single body region was: brain (55%), neck (78%), thorax (85%), upper abdomen (85%), liver (100%), pelvis (100%), soft tissues (97%), bone (85%) and lymph nodes (60%). The smallest metastasis detected was 3 mm in the liver; the largest metastasis missed was 5 mm in the brain. **Conclusion:** WB-MRI was feasible in the follow-up of patients with stage III melanoma. WB-MRI achieved acceptable diagnostic performance per patient and per single body region, making it comparable to other whole body imaging techniques, including computed tomography and positron emission tomography, however, avoiding ionising radiation.

B-0614 11:15

Whole body MRI with DWI and 3D-CE-T1w in tumour staging: comparison with PET-CT

E. Squillaci, C. Cicci, G. Manenti, F. Bolacchi, O. Schillaci, G. Simonetti; Rome/IT (ettoresquillaci@tiscali.it)

Purpose: To assess the diagnostic performance of whole body magnetic resonance imaging (WB-MRI) with diffusion weighted whole body imaging with background body signal suppression (DWBS) in malignant tumour detection and to explore the potential diagnostic advantages in generating fused DWBS/3D-contrast-enhanced T1w (3D-CE-T1w) images.

Methods and Materials: 45 cancer patients underwent WB-MRI for staging purpose. Fused DWBS/3D-CE T1w images were generated off-line. 3D-CE-T1w, DWBS images alone and fused with 3D-CE T1w were compared by two readers groups for detection of primary diseases and local/distant metastases. Diagnostic performance between the three WB-MRI datasets was assessed using receiver operating characteristic (ROC) curve analysis. 18 F-FDG PET-CT and histopathological results were used as standard of references.

Results: Areas under the ROC curves of DWBS vs 3D-CE-T1w vs both sequences in fused fashion were 0.97, 0.978, and 1.00, respectively. The diagnostic performance in tumour detection of fused DWBS/3D-CE-T1w images were statistically superior to DWBS ($P < 0.001$) and 3D-CE-T1w ($P \leq 0.002$), while the difference between DWBS and 3D-CE-T1w did not show statistical significance difference. There was no statistically difference in detection rates of malignancy between WB-MRI with DWBS and 18 F-FDG PET-CT.

Conclusion: WB-MRI with fused DWBS/3D-CE-T1w images is to be considered as a valid and economic alternative tool to PET-CT for tumour staging and follow-up in cancer patients.

B-0615 11:24

FDG-PET-CT and whole body MRI for early detection of tumour recurrence in asymptomatic breast cancer patients with tumour marker kinetics

G.P. Schmidt, P. Stieber, D. Di Gioia, V. Heinemann, D. Nagel, C. Rist, M.F. Reiser, A. Baur-Melnyk; Munich/DE (gerwin.schmidt@med.uni-muenchen.de)

Purpose: To evaluate the diagnostic potential of integrated imaging with FDG-PET-CT and whole body MRI (WB-MRI) combined with tumour marker monitoring for the early detection of asymptomatic tumour recurrence in breast cancer patients.

Methods and Materials: After curative surgery, 40 asymptomatic breast cancer patients underwent regular tumour marker monitoring for CEA, CA 15-3 and CA-125 at 6-week intervals within an intensified diagnostic aftercare algorithm. A reproducible previously defined increase (100%) of single or combined markers was considered as a strong indicator of recurrent disease. All patients with pathologic marker increase underwent WB-MRI on a 1.5 T scanner and FDG-PET-CT in addition for verification (median: 3 days). Presence and distribution of local recurrence, lymph node involvement and distant metastatic disease were assessed. All patients underwent WB-MRI or FDG-PET-CT follow-up exams within 6 months after individualised therapy.

Results: WB-MRI and FDG-PET-CT detected tumour recurrence in 65% (26/40) of patients, 15% (6/40) had secondary malignancies and 22.5% (9/40) had no detectable malignancy. Limited disease (1 organ/< 5 metastases) was found in

39% of patients. WB-MRI and PET-CT equally detected 23/24 metastases, PET-CT was superior detecting local recurrence (PET-CT 2/2 vs WB-MRI 0/2). Secondary tumours detected were: ovarian-, gastric-, lung-, parotid cancer and multiple myeloma. Concordance between both modalities was 52%.

Conclusion: Monitoring of tumour marker kinetics combined with whole body imaging is effective for early detection of tumour recurrence in clinically asymptomatic breast cancer patients. Both FDG-PET-CT and WB-MRI are reliable methods for metastases detection, PET-CT shows advantages in local recurrence.

B-0616 11:33

Whole body MRI and FDG-PET-CT for triage in patients planned for radioembolisation therapy

G.P. Schmidt¹, P.M. Paprottka¹, T.F. Jakobs¹, R.-T. Hoffmann², A. Baur-Melnyk¹, A. Haug¹, M.F. Reiser¹, C. Rist¹; ¹Munich/DE, ²Dresden/DE (gerwin.schmidt@med.uni-muenchen.de)

Purpose: To evaluate the potential of whole body MRI (WB-MRI) and FDG-PET-CT as diagnostic triage methods for patients planned for radioembolisation (RE) of liver metastases.

Methods and Materials: 135 patients with multifocal liver metastases were evaluated for potential palliative therapy with RE using 90-Yttrium microspheres. All patients were examined with PET-CT and WB-MRI for exclusion of extra-hepatic tumour manifestations. All patients underwent 99mTc-albumine angiography followed by scintigraphy to exclude significant hepato-pulmonary shunting.

Results: Out of the 135 patients included into the pre-therapeutic diagnostic algorithm, 56% were eligible and received RE, while 44% could not be treated. In 91% exclusion criteria was diagnosis of significant extra-hepatic metastatic disease. In 85% diagnosis was made concordantly by both FDG-PET-CT and WB-MRI, in 9% by PET-CT, in 6% by WB-MRI alone. Patient-based sensitivity for detection of extra-hepatic disease was 94% for PET-CT and 91% for WB-MRI. False-positive diagnosis of extrahepatic disease leading to exclusion for RE was made in 2% of patients, in one patient by PET-CT and in one patient by WB-MRI alone. Overall, specificity for inclusion to RE by combining both modalities was 99%. In 9% of patients angiographic diagnosis made RE impossible.

Conclusion: Both FDG-PET-CT and WB-MRI are efficient diagnostic triage methods for patients planned for RE of liver metastases. Overall, FDG-PET-CT shows a higher diagnostic accuracy compared to WB-MRI and may be used as imaging method of choice as a standalone examination. In combination, both modalities exhibited high sensitivity for the diagnosis of extra-hepatic tumour manifestations and result in high specificity.

B-0617 11:42

Diagnostic capability of whole body diffusion-weighted imaging in malignant tumours compared with whole body 18F-FDG PET-CT

X.Y. Wang, N. Wu, Y.F. Zhao; Beijing/CN (oliverwxy_zz@sina.com)

Purpose: We studied the diagnostic capability of whole body diffusion-weighted imaging (WBDWI) with 1.5 T MR scanner in malignant lesions with comparison to whole body 18F-FDG PET-CT.

Methods and Materials: 35 patients with pathologically proved malignant tumours were enrolled. All patients underwent both WBDWI and 18F-FDG PET-CT, and then were followed up for 6 months. Three experienced MR radiologists who were blinded to the final diagnosis read the WBDWI respectively, analyse the 636 lesions identified by PET-CT and all radiologic examinations. Probability of malignant lesions was assessed using a 5-point visual scoring system. The receiver operating characteristic (ROC), sensitivity and specificity were compared between the two methods. Kappa analyses were used to compare the diagnostic consistency between both methods.

Results: The area under the ROC curve of WBDWI, PET-CT, ADC, and SUVmax were 0.949, 0.967, 0.846, and 0.864, respectively. There is no statistically significant difference between WBDWI and PET-CT ($P > 0.05$). The sensitivity, specificity and accuracy were 86.6%, 95.3%, and 89.5%, respectively, in WBDWI, and 94.4%, 94.3%, and 94.3%, respectively, in PET-CT. Kappa value of the diagnostic consistency between WBDWI and PET-CT was 0.745. In analysis of the impact of lesion size on the accuracy, there was statistical significance between WBDWI and PET-CT in a group of 9-18 mm diameter ($P = 0.000$). According to the location of lesions, the accuracy of WBDWI was similar to or sometimes better than PET-CT in sternum, clavicle, scapula, vertebral column, pelvis, and bones of extremities.

Conclusion: WBDWI had a higher sensitivity, specificity and accuracy in detecting malignant lesions.

10:30 - 12:00

Room D1

Chest

SS 1304

Interaction: lung, heart and circulation

Moderators:

J. Bremerich; Basle/CH
N. Karabulut; Denizli/TR

B-0619 10:30

High-pitch dual source CT pulmonary angiography in freely breathing patients

R.W. Bauer, B. Schell, M. Beeres, J. Wichmann, B. Bodelle, T. Lehnert, T.J. Vogl, J.M. Kerl; Frankfurt a. Main/DE (ralfwbauer@aol.com)

Purpose: Breath hold may lead to Valsalva's manoeuvre-inducing contrast artefacts in the pulmonary arteries such as inhomogeneous enhancement or loss of the contrast bolus during pulmonary CT angiography. We investigated a novel high-pitch dual source CT protocol that does not require a breath hold phase.

Methods and Materials: 76 consecutive patients underwent CT pulmonary angiography (CTPA) in dual source high-pitch mode (pitch 3.0, 100 kV, 180 mAs, 50 ml contrast material) without breathing command. Pulmonary arterial (PA) enhancement, image noise, signal-to-noise ratio, overall image quality, incidence of total or partial interruption of the contrast column in the PA tree, motion artefacts of the aortic root, diaphragm and pulmonary structures were recorded.

Results: Mean central and peripheral PA attenuation was 404 ± 104 HU and 453 ± 119 HU, mean image noise 11 ± 2 HU. Mean examination time was 0.67 ± 0.09 s, mean DLP 142 ± 31 mGycm. There were no motion artefacts of the diaphragm or the pulmonary vessels related to breathing. There was no case of partial or total interruption of the contrast column in the PA tree, no examination was rated non-diagnostic. In 62/76 cases, the aortic root was pictured without any motion artefact and with satisfying contrast enhancement to rule out dissection.

Conclusion: High-pitch dual source CTPA in freely breathing patients effectively avoids artefacts related to breath hold or breathing as well as to cardiac motion and thus represents a reliable tool to rule out pulmonary embolism. With further optimised contrast injection, aortic dissection may be additionally ruled out within the same examination without the use of ECG-synchronisation.

B-0620 10:39

Breath-hold at ease: a method of improving the diagnostic quality of CT pulmonary angiogram

K.K. Lau, J. Li, N. Ardley, T. Lau; Melbourne, Victoria/AU (kenkplau@yahoo.com.au)

Purpose: 6-8% of CT pulmonary angiography (CTPA) is inconclusive due to poor contrast enhancement of pulmonary arteries (PA). Typically, CTPA is undertaken after patient taking fully inspiration and breath-holding. The sudden negative intrathoracic pressure during quick inspiration increases venous return to the heart and dilutes the contrast in PA (transient interruption of contrast). The Valsalva associated with breath-holding lowers the cardiac output and delays the peak contrast opacification of PA. The aim of this study was to assess the efficacy of breath-hold at ease during CTPA on the contrast enhancement of PA.

Methods and Materials: CTPAs were undertaken in 51 consecutive patients who deeply inspired and breath-held during scanning, and 73 consecutive patients who simply breath-held at ease. Hounsfield units (HU) in pulmonary trunk, main pulmonary arteries and proximal branches were measured by 2 blinded readers. Results were compared between 2 patient groups. PE and co-existing lung diseases were also recorded.

Results: Suboptimal contrast enhancement was found in 15.6% of the deeply inspired group and 2.8% of the at ease group. HUs ranged from 320 to 337 in different part of PAs in the inspired group and 375 to 400 in the at ease group, with 18.8% mean increase of contrast density ($p = 0.001$). Images of the lung parenchyma in both groups were considered adequate. Less breathing artefact was noted in the at ease group.

Conclusion: Breath-holding at ease during scanning improves the overall contrast density in the PA, and therefore, the diagnostic quality of the CTPA.



B-0621 10:48

Evaluation of pulmonary blood flow using new method of dynamic x-ray examination: comparison with 99mTc-MAA perfusion scintigraphy

T. Abe, T. Izuka, N. Motohashi, E. Uema, Y. Akiyama, Y. Shiraiishi, H. Ogata, M. Ito, S. Kudou; Tokyo/JP

Purpose: To evaluate the pulmonary blood flow using dynamic chest x-ray without contrast enhancement in comparison with 99mTc-MAA scintigraphy.

Methods and Material: Dynamic chest pulsed x-ray at 7.5 frames per second in total 10 second of tidal breathing was performed in 30 patients with pulmonary disease. The institutional review board approval and written informed consent was obtained in all patients. Image datasets were extracted by signal intensity pixels of blood flows using a band-pass filter optimised for heart beats. Determined blood flows was divided into eight fields (upper, middle, lower, subphrenic in right and left) in each arterial and capillary phases, and was compared with the 99mTc-MAA scintigraphy.

Results: All patients were performed technically with the total exposed dose of 0.131 mGy. The blood flows in each upper, middle, lower, and subphrenic fields were $14.2\% \pm 4.6$, $20.0\% \pm 5.2$, $16.3\% \pm 4.6$, and $1.1\% \pm 0.8$ in the right, and $18.1\% \pm 5.2$, $21.3\% \pm 8.0$, $21.3\% \pm 8.0$, $7.7\% \pm 4.5$ and $1.3\% \pm 1.3$ in the left in arterial phase. The capillary blood flow signals were $17.7\% \pm 4.5$, $21.3\% \pm 3.3$, $19.5\% \pm 3.4$, and $1.5\% \pm 0.9$ in the right and $15.1\% \pm 3.3$, $15.7\% \pm 5.7$, $7.3\% \pm 3.1$, and $1.9\% \pm 1.7$ in the left in this study. In those cases, The 99mTc-MAA uptake was $6.3\% \pm 2.8$, $18.0\% \pm 6.5$, $22.8\% \pm 7.5$, $4.3\% \pm 1.9$ in the right and $8.9\% \pm 4.2$, $19.2\% \pm 9.0$, $15.3\% \pm 5.3$ and $5.2\% \pm 3.2$ in the left, respectively. Comparison of the examinations had good correlations with $R=0.742$ in arterial phase and $R=0.714$ in capillary phase.

Conclusion: Dynamic chest x-ray blood flows had good collation with 99mTc-MAA scintigraphy. This method may allow measurement and quantification of pulmonary blood flows without contrast.

B-0622 10:57

'Stunned lung': a novel observation of resolving pulmonary embolism on lung perfusion CT

J.H. Reid, E. van Beek, M. Williams, M. Connell, J.T. Murchison; Edinburgh/UK (john.reid@borders.scot.nhs.uk)

Purpose: Pulmonary emboli (PE) frequently resolve in an inconsistent manner. A pilot study was carried out to assess CT perfusion patterns of PE resolution and to potentially identify viable parenchyma exhibiting delayed perfusion similar to the phenomenon of 'stunned' myocardium.

Methods and Materials: Following institutional approval, a pilot study of 12 patients (6M:6 F, mean 62 years) with CTPA diagnosis of major PE were prospectively evaluated by CT lung perfusion after an average of 4 months. Thrombus load (modified Miller score MMS) and RV:LV ratio were determined. Perfusion maps were visually scored and correlated with residual endoluminal filling defects. Defects were further assessed by generating time/perfusion curves using regions of interest.

Results: The mean initial thrombus load was MMS 15 and mean RV:LV ratio was 1.36:1. The mean residual thrombus load was MMS 2 (range 0-7) with no post-treatment RV dilatation. Only 4 (33%) patients were clear of residual thrombus, and only 2 patients (16%) had no residual perfusion defects after a minimum of three months treatment. Perfusion defects ranged from 10% to 80% of the affected lung. CT perfusion defects matched areas showing residual embolic material in only 3 patients. In 4 (33%) patients perfusion defects showed delayed contrast enhancement.

Conclusion: Most patients have perfusion defects at three months, often substantial and these may not correspond with the areas of residual endoluminal material. Some defects exhibit delayed enhancement (which we have termed 'stunned' lung) suggesting they may potentially respond to revascularisation techniques.

B-0623 11:06

Volume rendering reconstruction of right ventricle improves interobserver agreement and accuracy of interventricular septum bowing sign in patients with acute pulmonary embolism

G. Staskiewicz, E. Czekajska-Chehab, J. Przegaliński, S. Uhlig, K. Torres, R. Maciejewski, A. Drop; Lublin/PL (grzegorz.staskiewicz@gmail.com)

Purpose: Bowing of interventricular septum (IVS) is one of the signs of severe PE adapted from echocardiography; however, it is affected by high interobserver variability. The aim of the study was to evaluate application of volumetric reconstruction of the right ventricle for improvement of reliability of this sign.

Methods and Materials: 60 consecutive patients with CTPA diagnosis of acute PE and echocardiographically measured pulmonary artery systolic pressure (PASP) were included into the study. IVS bowing was evaluated with multiplanar reforma-

tions (MPR) and volume rendering (VR) reconstructions. Two readers graded the position of IVS as normal, flattened or bowed. Interobserver agreement was measured for both methods of identification of IVS position. ROC analysis was performed to compare accuracy of both methods for identification of increased PASP. **Results:** Interobserver agreement was found to be fair ($\kappa = 0.381$; $p < 0.001$) for the MPR-based grading of IVS position as normal or abnormal. For the VR-based assessment, κ was good (0.629; $p < 0.001$). ROC analysis for both methods showed insignificantly better performance of VR-based method for identification of increased PASP, with area under ROC curve 0.656 for MPR-based method, and 0.705 for VR method. Sensitivity and specificity were 94% and 52% for VR method and 93% and 48% for MPR method, respectively. **Conclusion:** VR-based evaluation of IVS position is characterised by good interobserver agreement, and moderate accuracy for identification of increased PASP. Results indicate that this method may improve use of this valuable additional sign evaluated in patients with acute PE.

B-0624 11:15

Assessment of the correlation between CT angiographic clot load score, pulmonary perfusion defect score and global right ventricular function by dual source CT for acute pulmonary embolism
Y.-F. Zhou, P. Han, Y. Wang, H. Shi; *Wuhan/CN (zhouyunfeng08@yahoo.cn)*

Purpose: To investigate the correlation between CT angiographic clot load (CTACL) score, pulmonary perfusion defect (PPD) score and the global right ventricular function in the assessment of the severity of pulmonary embolism (PE).

Methods and Materials: Forty-nine patients with acute PE, who underwent dual source CT scan, were included in the study. CT angiography and perfusion imaging were performed. The data from ECG-gated coronary angiography scanning protocol were used for right ventricular function analysis. Two readers evaluated the CTACL and PPD scores according to the Qanadli and Chae methods, respectively, and their results were in consensus.

Results: The PPD score had a strong positive correlation with the CTACL score ($r = 0.72$, $p < 0.001$) and both scores, in turn, had a strong positive correlation with the right ventricular/left ventricular (RV/LV) diameter ratio ($r = 0.60$, $r = 0.62$, $p < 0.001$). However, the PPD score had a strong negative correlation with ejection fraction (EF) ($r = -0.63$, $p < 0.001$) while the CTACL score had a low negative correlation with EF ($r = -0.33$, $p = 0.02$). Between the RV/LV < 1 group ($n = 35$) and the RV/LV > 1 group ($n = 14$), the PPD score, CTACL score, pulmonary artery trunk diameter, EF and reflux of inferior vena cava were significantly different, all with $p < 0.001$. The end-systolic volume ($p = 0.01$) was significantly different but the end-diastolic volume ($p = 0.11$) and stroke volume ($p = 0.08$) showed no statistically significant difference between the two groups.

Conclusion: Therefore, considering PPD scores, CTACL scores and cardiovascular manifestations together may be helpful in the evaluation of PE severity (accepted by BJR).

B-0625 11:24

Comparison of high sensitive troponin I and quantitative CT parameters for prediction of adverse clinical events in patients with acute pulmonary embolism
P. Apfalter¹, F. Weilbacher¹, M. Meyer¹, T. Henzler¹, T. Walter¹, J. Gruettner¹, U.J. Schoepf², C. Fink¹; ¹Mannheim/DE, ²Charleston, SC/US

Purpose: To compare high sensitive troponin I (hsTnI) and quantitative CT parameters for prediction of adverse clinical events in patients with acute pulmonary embolism (PE).

Methods and Materials: Pulmonary CTA studies of 629 patients were retrospectively evaluated. 65 patients (67 years [20 - 90]) had acute PE and hsTnI measurements within 24 hours of CT. Right ventricular dysfunction (RVD) was assessed on CT by calculating the right ventricular/left ventricular (RV/LV) diameter ratios on transverse sections (RV/LVtrans), four-chamber views (RV/LV4ch), RV/LV volume ratio (RV/LVvol). Pulmonary CTA obstruction scores (OS) (Qanadli, Mastora) were calculated. HsTnI, RV/LV ratios, and OS were compared for predicting adverse clinical events.

Results: 12 patients with PE had at least one adverse clinical event (intensive care treatment $n = 11$, death $n = 2$); those patients showed significantly higher RV/LV ratios and OS compared to those without (RV/LVtrans 1.63 ± 0.48 vs. 1.15 ± 0.31 ; RV/LV4ch 1.67 ± 0.41 vs. 1.3 ± 0.34 ; RV/LVvolume 2.29 ± 1.16 vs. 1.34 ± 0.58 ; Mastora $61.5 [26.5-92]$ vs $6.5 [4-15.5]$, and Qanadli $20 [13-20]$ vs. $11 [3.5-31]$; ($p < 0.0058$). Elevated hsTnI was significantly associated with adverse clinical events (14% vs. 9%; $p < 0.05$; adjusted OR = 4.88; 95% CI 1.3-18.7; $p < 0.05$). HsTnI showed no correlation with RV/LV ratios or OS. The AUC for the prediction of adverse clinical

events of RV/LV4ch, RV/LVvolume, and hsTnI were 0.77, 0.75, and 0.64. The combination of hsTnI and RV/LV ratios revealed no increases in the AUC.

Conclusion: HsTnI is associated with adverse clinical events. A combination of hsTnI with CT parameters showed no further improvement in the prediction of adverse clinical events.

B-0626 11:33

Contrast-enhanced MDCT vs. time-resolved MR angiography vs contrast-enhanced perfusion MRI: assessment of treatment response by patients with chronic thromboembolic pulmonary hypertension

Y. Ohno, M. Nishio, H. Koyama, T. Yoshikawa, D. Takenaka, S. Matsumoto, K. Sugimura; *Kobe/JP (yosirad@kobe-u.ac.jp)*

Purpose: To compare therapeutic effect assessment capability of MDCT, time-resolved MR angiography, dynamic perfusion MRI and conventional parameters for chronic thromboembolic pulmonary hypertension (CTEPH) patients.

Methods and Materials: Twenty-four consecutive CTEPH patients (12 men and 12 women; mean \pm standard deviation age, 68.1 ± 8.6 years) treated with conventional therapy underwent pre- and post-therapeutic MDCT, time-resolved MR angiography, dynamic perfusion MRI and cardiac US and right heart catheterisation. All patients were divided into two groups, response ($n = 13$) and non-response ($n = 11$). CTEPH indexes for MDCT (CTEPHCT) and MR angiography (CTEPHMRA) were calculated on the basis of embolic burden. Pulmonary blood flow (PBF), pulmonary blood volume (PBV) and mean transit time (MTT) maps were generated from all perfusion MR data, followed by determination of improvements in mean PBF, PBV and MTT at ROIs for each patient. Receiver operating characteristic (ROC)-based positive tests were performed to determine the feasible threshold values for distinguishing response from non-response groups. Finally, diagnostic capabilities were compared by means of the McNemar's test.

Results: When each of the feasible threshold values was used, specificity (90.9%, $p < 0.05$) and accuracy (95.8%, $p < 0.05$) for improvement in PBF were significantly higher than those for improvements in 6-MWD (specificity: 36.4%, accuracy: 70.8%) and CTEPHCTA (specificity: 36.4%, accuracy: 70.8%).

Conclusion: Dynamic perfusion MRI and time-resolved MR angiography have equal or better capability for assessment of therapeutic effect on CTEPH patients than do conventional parameters and MDCT.

B-0627 11:42

Incidence and aetiology of mosaic lung attenuation (MLA) in a large cohort of patients with right heart catheter (RHC) corroborated pulmonary hypertension (PH)

L. Woods, A. Nair, D. Patel, A. Devaraj, B. Madden, I. Vlahos; *London/UK (liamwoods@doctors.org.uk)*

Purpose: To determine the extent, severity and aetiology of MLA detected at thin-section CT in a large RHC corroborated PH group.

Methods and Materials: CT scans of 168 patients with RHC confirmed PH referred to a tertiary centre were retrospectively evaluated. Inspiratory and expiratory imaging was reviewed from the same time-point where available/technically adequate or from metachronous studies if not. Three chest radiologists determined by consensus MLA severity (absent-0, minor/physiologic-1, mild-2, moderate-3, severe-4). For paired inspiratory-expiratory studies predominant aetiology was determined as air-trapping (A-MLA), vascular (V-MLA) or mixed/indeterminate (M-MLA).

Results: 149/168 (89%) of patients had technically adequate inspiratory imaging. MLA was present in 60% (severity 1-3: 17%, 20%, 17%, 6%, respectively). 103/168 (61%) of patients had paired inspiratory-expiratory imaging with a comparable percentage demonstrating at least mild MLA (63%). The MLA aetiology was A-MLA in 45%, V-MLA in 37% and M-MLA in 18%. When considering patients with at least mild MLA the proportion of V-MLA increased (50%). The proportion of patients with MLA due to V-MLA was significantly higher in patients with chronic thromboembolic PH (CTEPH) than other causes combined (46% v 17%, Fisher exact test $p < 0.01$). However, vascular predominant mosaicism also occurred in 46% of idiopathic PH, 36% of obstructive lung disease, and 11% of left heart disease PH aetiologies. Overall 58% of vascular mosaicism was not due to CTEPH.

Conclusion: In this cohort MLA is commoner than previously reported. Although usually due to air-trapping a significant proportion is vascular in aetiology, though not necessarily due to CTEPH.

B-0628 11:51

Use of pulmonary CT angiography to diagnose anaemia

C.S.L. Jung, M. Groth, T.A. Bley, F.O. Henes, A. Treszl, G. Adam, P. Bannas; Hamburg/DE

Purpose: Anaemia is associated with increased mortality in patients with acute symptomatic pulmonary embolism (PE). The purpose of this study was to evaluate the feasibility of Hounsfield unit (HU) measurements on a single unenhanced trigger scan of pulmonary CT angiography scans for the diagnosis of anaemia as a potential prognostic marker.

Methods and Materials: 150 consecutive patients with suspected PE underwent pulmonary CT angiography. Two radiologists, blinded to laboratory results, performed HU measurements in the single unenhanced trigger scan independently by region-based analysis (ROI). HU values from ascending and descending aorta and the calculated mean of both were correlated with serum haemoglobin levels. Inter- and intraobserver variability was determined for HU measurements, and receiver operating characteristic (ROC) analysis was performed for diagnosis of anaemia. Calculated linear models were used to assess formulas for estimation of haemoglobin levels from HU measurements.

Results: HU measurements revealed high intra- and interrater reliability (ICC > 0.981 and ICC > 0.965, respectively). Calculated mean HU values showed a moderate correlation with serum haemoglobin levels ($r=0.734$), which allowed generation of different formulas for calculation of haemoglobin levels from HU measurements. ROC analyses confirmed a high sensitivity (80.4 for men; 91.3 for women) and specificity (84.0 for men; 84.9 for women) for diagnosing anaemia.

Conclusion: Diagnosis of anaemia and quantification of haemoglobin levels upon a single unenhanced trigger scan of pulmonary CT angiography is feasible. We suggest disclosing the anaemic state in the radiological report, independent of the presence of PE, since anaemia carries increased risks of morbidity and mortality.

10:30 - 12:00

Room D2

Interventional Radiology

SS 1309

Special indications

Moderators:

E. Criado Paredes; Sabadell/ES
M.J. Lee; Dublin/IE

B-0629 10:30

Predictors and volume measurement of residual flow in embolised intracranial aneurysms at follow-up

Z. Serafin, P. Strzeżniewski, W. Lasek, W. Beuth; Bydgoszcz/PL
(serafin@cm.umk.pl)

Purpose: The possibility of recanalisation and the need for retreatment are the most important drawbacks of intracranial aneurysm embolisation. The volume of residual flow at follow-up is a key factor that determines decision on the aneurysm re-embolisation. The purpose of the study was to determine factors predicting the presence of residual flow at follow-up and to compare volumes of the flow measured with 3D digital subtracted angiography (DSA) and magnetic resonance angiography (MRA).

Methods and Materials: In 72 consecutively examined patients 26 aneurysms were found incompletely occluded. Independent predictors of the residual flow were determined including anatomical and clinical factors. Diameters and volume of residual flow areas were compared between three-dimensional DSA (3D-DSA), time-of-flight MRA (TOF-MRA), contrast-enhanced TOF-MRA (CE-TOF-MRA), and contrast-enhanced MRA (CE-MRA).

Results: Aneurysm neck size and sack-to-neck ratio were independent predictors of residual flow ($P < 0.0001$). A ROC curve cut-off points were 2.8 mm for aneurysm neck size, and 1.73 for sack-to-neck ratio. The mean recanalisation volume ranged from 16.3 mm³ in TOF-MRA to 30.5±44.6 mm³ in 3D DSA ($P < 0.04$, ANOVA). A direct comparison revealed significant differences in the volumes measured with 3D DSA and CE-MRA as compared to TOF-MRA and CE-TOF-MRA ($P < 0.05$).

Conclusion: The presence of the residual flow within the embolised aneurysm is predicted by the aneurysm anatomy. TOF-MRA and CE-TOF-MRA tend to underestimate the size of the flow. The definitive decision on re-embolisation should be made basing on 3D DSA.

B-0630 10:39

Diagnostic digital-subtraction dacryocystography: criteria of evaluation, frequency and localisation of pathological findings

D.K. Filippiadis¹, A. Weissbach², C. Meyer², A. Mazioti¹, H.H. Schild², K.E. Wilhelm²; ¹Athens/GR, ²Bonn/DE (dfilippiadis@yahoo.gr)

Purpose: To evaluate the frequency and localisation of pathological findings in patients suffering from epiphora.

Methods and Materials: Retrospective analysis of 355 diagnostic dacryocystograms in 281 patients suffering from epiphora. Stenosis was defined as early reflux through the punctum with residual flow of contrast material to the nasal cavity. Complete obstruction was assumed, if no flow of contrast material to the nasal cavity was seen, even after forced irrigation.

Results: In 104 (29%) cases no tear duct obstruction was found. In 251 (71%) cases a tear duct obstruction was seen. In 82 (33%) cases there was a stenosis, whilst in 169 (67%) cases there was a complete obstruction. Localisation of the stenosis included junction of the nasolacrimal sac and nasolacrimal duct at 31 cases (38%), post-saccal level at 26 cases (32%), common canaliculus at 24 cases (29%) and lower canaliculus at 1 case (1%). Localisation of complete obstructions included junction of nasolacrimal sac and nasolacrimal duct at 99 cases (59%), common canaliculus level at 29 cases (17%), postsaccal level at 27 cases (16%) and lower canaliculus at 14 cases (8%).

Conclusion: Epiphora is mostly caused by stenosis or complete obstruction of the nasolacrimal duct system. The most common site of obstruction is the junction of the nasolacrimal sac and nasolacrimal duct. Complete obstructions are more common than stenosis.

B-0631 10:48

Embolisation techniques for post-traumatic splenic injury: Grenoble's experience

J. Frandon, O. Eker, F. Thony, M. Rodiere, C. Sengel, P. Durand, M. Sahin, A. Vendrell, I. Bricault; Grenoble/FR (jfrandon@chu-grenoble.fr)

Purpose: Non operative management of splenic injury is now the standard in stable trauma patient. Our objective is to compare the outcomes of proximal, distal or combined embolisation procedures in patients with splenic injury.

Methods and Materials: Between 2005 and 2010, all patients admitted in our center for post-traumatic splenic injury requiring embolisation were reviewed. They underwent proximal (group A), distal (group B) or combined, proximal and distal, (group C) embolisation procedures. Rebleeding requiring splenectomy or not, and complications after embolisation (as splenic infarction, abscess, pancreatitis, pancreatic pseudocyst or hematoma, large hemoperitoneum, pseudoaneurysm, fistula, pleural effusion, or distal coil migration) were assessed in all groups. A Fisher's exact test was used.

Results: Forty seven patients underwent embolisations, as 36% (n=17), 47% (n=22) and 17% (n=8) in groups A, B and C, respectively. Rebleeding was observed in 15% of all patients (n=7/47) without any significant difference between all groups (n=2 in A, n=4 in B, n=1 in C; p=0.7). Splenectomy was required in 6.4% of patients, only in group B (n=3), without any statistically significant difference (p=0.23). Twenty nine complications after embolisation were observed in 42.6% of patients (n=20/47), 13 in group A (n=8), 12 in group B (n=9) and 4 in group C (n=3) without any statistically significant difference (p=1).

Conclusion: Proximal, distal and combined embolisation techniques for post-traumatic splenic injury presented no statistically different rates of rebleeding and complications after embolisation. Splenectomy was needed in few cases only for patients who underwent distal embolisation.

B-0632 10:57

Nasolacrimal polyurethane stent: improving outcomes with the Wilhelm-type Wilhelm tear leader stent

D.K. Filippiadis¹, A. Weissbach², C. Meyer², A. Mazioti¹, H.H. Schild², K.E. Wilhelm²; ¹Athens/GR, ²Bonn/DE (dfilippiadis@yahoo.gr)

Purpose: To evaluate the effectiveness and long-term results of nasolacrimal duct stent implantation in the treatment of epiphora.

Methods and Materials: 54 patients (mean age 64 [range 26-85]; 15 males and 30 females) with severe epiphora underwent nasolacrimal duct stenting (Wilhelm-type polyurethane stent) under fluoroscopic guidance after dacryocystography as a treatment for obstructions of the nasolacrimal system. The aetiology of the obstruction was chronic infection (chronic dacryocystitis) in all cases.

Results: The overall technical success rate of stent placement was 97%. No cases of palpebral haematoma were recorded, neither were there cases of acute dacryocystitis following the procedure. Secondary patency was achieved in 67%



during a mean follow-up period of nine months (range 3 months to 3 years). Stents malfunction occurred in 7 cases and all these stents were easily withdrawn; in the rest of the cases the stents remain in place and functional.

Conclusion: Treatment of epiphora with polyurethane stents is a technique that is well tolerated by patients and achieves a high long-term success rate comparable to surgical dacryorhinostomy.

B-0633 11:06

The 100 classical papers of interventional radiology - the evolution of a speciality

M.T. Crockett, O. Buckley, W. Torreggiani, R. Browne; *Dublin/IE* (CROCKETTMT@GMAIL.COM)

Purpose: The value of a scientific paper is defined by its impact on the biomedical field in which it is published. Papers which impact greatly on their field achieve classical status. This may be defined using the concept of a citation classic: the number of times a paper is cited reflects its impact and relevance. The purpose of this study was to identify and analyse the 100 most cited interventional radiology papers of the last 70 years.

Methods and Materials: Using the JCR database the 50 highest impact factor radiology journals were selected for review. From these journals the 100 most cited interventional radiology publications were chosen and further analysed

Results: The most cited paper received nearly 2500 citations whilst the average number of citations was 320. The oldest paper was published in 1953 and most recent in 2005. Most papers originated in the USA followed by Italy, France and Germany. The three most prolific institutions were Harvard University (USA), Ospedale Civile (Italy) and Massachusetts General Hospital (USA). The 100 most cited papers were published in 10 journals with Radiology & AJR making up the majority. Five authors have > 3 first name papers in the top 100 with SN Goldberg on top with 6. > 70% of papers were published after 1990. The older papers focus mainly on cardiovascular interventional techniques with more recent papers dominated by advances in interventional neuroradiology.

Conclusion: This analysis identifies many of the landmark interventional radiology papers of last six decades and provides a fascinating insight into the changing discourse within the field. It also identifies the topics, authors and institutions which have had the greatest impact on the speciality.

B-0634 11:15

Percutaneous arterio-venous shunting in patients with severe COPD: a novel interventional treatment

T. Schlosser, M. Burbelko, M. Ulrich, G. Antoch, R. Adamus; *Essen/DE* (thomas.schlosser@uni-due.de)

Purpose: The aim of this study was to evaluate the technical feasibility and safety of a new interventional-radiological technique to create a shunt between the external iliac vein and artery in patients with severe COPD. The creation of this fistula aims improving pulmonary oxygenation, reducing systemic vascular resistance and increasing cardiac output in these patients.

Methods and Materials: Thirty-seven patients were included in this multicentre trial. Two patients had to be excluded from the study based on too large distance between the iliac vessels on both sides. In 35 patients the artery was punctured from the vein with a novel crossing needle. Using a special delivery system a novel nitinol device (anastomotic coupling system, ROX medical) was implanted between the artery and vein to maintain a fistula between both vessels. All shunts were dilated with a 4 mm balloon and documented by DSA.

Results: Shunt implantation was successful in all 35 patients. The perfused arterio-venous shunts could be well documented in DSA and the diameter was measured between 3 and 4 mm in all cases. Peri-interventional dissection of the iliac artery occurred in one patient. This dissection was not flow limiting. Post-interventional venous bleeding in one patient was treated successfully by local compression.

Conclusion: The new interventional-radiological technique to create an arterio-venous shunt in the iliac vessels presented in this study has proven to be feasible and safe. The intended improvement of pulmonary oxygenation to reduce dyspnoea in patients with severe COPD has to be evaluated.

B-0635 11:24

The safety and efficacy of flow diversion treatment of intracranial aneurysms: preliminary results

D. Bagatto, B. Petralia, R. Girometti, M. Bazzocchi; *Udine/IT* (daniele.bagatto@gmail.com)

Purpose: To illustrate monocentric experience of flow diversion approach for endovascular treatment of intracranial aneurysms. To assess the safety and efficacy of this alternative and promising technique in comparison with coil and stent-assisted coil embolisation.

Methods and Materials: We retrospectively reviewed one-hundred and fourteen consecutive patients (36 males, 78 females; mean age, 56.2 years; s.d., ±13.8) with 125 intracranial aneurysms treated in our Institution with endovascular approach between January 2009 and July 2011. Efficacy in deployment procedure and angiographic outcomes at follow-up (in terms of complete aneurysm occlusion) were compared using Fischer's exact test between patients treated with a flow diverter device (SILK flow diverter (SFD)), patients treated with coil and those treated with stent-assisted coil embolisation.

Results: Among all cases, 10 (8%) were treated with SFD, 97 (77.6%) with coiling and 18 (14.4%) with stent-assisted coiling. Endovascular treatment was successfully performed in 114/125 (91.2%) aneurysms. SFD could not be delivered in 2/10 (20%) cases while coil embolisation failed in 8/97 (8.2%) cases and stent-assisted coil embolisation in 1/18 case (5.5%) (p=0.04). We obtained a complete aneurysm occlusion in all cases treated with SFD and no significant statistical difference (p>0.05) was found at 8.3±4.7 months (mean±s.d.) angiographic follow-up between the three different groups.

Conclusion: Although some difficulties in deployment procedure in comparison with coil and stent-assisted coil embolisation the treatment of intracranial aneurysms with SFD seems to be highly efficacious and early angiographic follow-up results are quite encouraging.

B-0636 11:33

Post-traumatic epistaxis treated with embolisation

K. Pyra, T. Jargielto, P. Trojanowski, M. Jarzabek, M. Szczermo-Trojanowska; *Lublin/PL* (k.pyra@poczta.fm)

Purpose: Epistaxis is a common consequence of craniofacial injury, involving damage to the external carotid artery branches. Depending on the intensity and the site of bleeding and also on the experience of the medical team conservative treatment, surgical or endovascular treatment is applied. In this paper, the possibility of endovascular embolisation and its effectiveness in the treatment of epistaxis following craniofacial injury is evaluated.

Methods and Materials: There were 24 patients (16 males and 8 females) in the mean age 41 years (21-64) with post-traumatic epistaxis. In 14 patients angiography. Disclosed pseudoaneurysms of the external carotid branches, in 7 extravasation of contrast media, in 3 caverno-carotid fistulae. Following diagnostic angiography the risk of endovascular embolisation was regarded to be too high in 3 patients. Remaining 21 patients were embolised using gelatin foam, polyvinyl alcohol particles, particles of acrylic polymer and platinum microcoils.

Results: In all embolised patients immediate arrest of epistaxis was achieved. In 4 cases (19%) the bleeding recurred, and in 2 was controlled with repeated embolisation. In 9 patients (43%) the side effect of the procedure was transient facial pain and swelling, paraesthesia, trismus and fever. Those symptoms disappeared within a few days. In 3 patients (14%) sensory disturbances in the cheek area were permanent. One patient developed a small ulceration of the palate, successfully treated conservatively. There were no serious neurological complications in any of the patients.

Conclusion: Endovascular embolisation is an effective method of posttraumatic epistaxis and should be considered in planning of the treatment.

B-0637 11:42

Tracheobronchial stenting for malignant airway disease: long-term results from a single centre

R. Inchingolo¹, S.C. Spiliopoulos², M. Krokidis³, I. Ahmed³, A. McGrath⁴, P. Gkoutzios³, R. Salter³, T. Sabharwal³; ¹Rome/IT, ²Patras/GR, ³London/UK, ⁴Dublin/IE

Purpose: To investigate the immediate and long-term outcomes of covered and uncovered self-expandable metallic stent (SEMS) insertion for the management of tracheobronchial malignant disease.

Methods and Materials: We retrospectively searched our department database for patients treated with covered or uncovered SEMSs for the management of tracheobronchial pathology owing to local or metastatic disease. Between January 2009 and December 2010, in total, 49 patients (27 males, mean age 60.9±15 years) underwent 77 SEMS insertions (57 uncovered, 20 covered). The hybrid procedure was performed under bronchoscopic and fluoroscopic guidance. The study's primary endpoints included technical success, and symptomatology recurrence rates, while secondary endpoints included patients' survival and complication rates. Baseline demographics and procedural details were recorded.

Results: Technical success rate was 97.9% (48/49 cases). In total 14 kissing (both bronchus), 23 main bronchus, 1 distal bronchus, 9 tracheal and 2 tracheal plus main bronchus stenting deployments were performed. The mean time follow-up was 5.5±5.9 months (range 0.03-24 months). The symptomatology recurrence rate

was 14.5% (7/48 patients) and was attributed to stent occlusion due to tumour ingrowth (4/48, 8.3%), stent migration (2/48, 4.1%) and bronchospasm (1/48, 2%). The estimated patients' survival rate according to the Kaplan-Meier statistical analysis was 21.5%, up to 2 years of follow-up, while the overall complications rate was 3.8% (3/77 stents).

Conclusion: Tracheobronchial SEMSs provide safe and effective minimally invasive management of patients suffering from symptomatic malignant airway disease.

B-0638 11:51

Follow-up of radiologically inserted TCVAP of the upper arm: long-term complications in 127750 catheter days

J.D. Busch, F. Heller, J. Herrmann, B.P. Schoennagel, G. Adam, C.R. Habermann; *Hamburg/DE (jd.busch@uke.de)*

Purpose: To retrospectively evaluate radiologically placed totally implantable central venous arm ports (TCVAP) in terms of safety, technical feasibility and device-related complications.

Methods and Materials: 507 consecutive patients (mean age 59.2 years, range 19.5-88.5 years, male/female ratio 236/271), who received a TCVAP between January 2005 and July 2010 at our university hospital, were included into this study. The insertion procedure was performed in an interventional radiology suite. Two different vascular access systems (Titanium Vital-Port® Mini, Cook Medical Inc., Bloomington/USA (n = 465); Titanium Vital-Port® Petite, Cook Medical Inc., Bloomington/ USA (n = 58)) were used. No antibiotic prophylaxis or long-term anticoagulant medications were routinely administered.

Results: In 507 patients in total 523 devices were implanted. All procedures were completed without major complications with a primary technical success of 99.04%. During follow-up and a total number of 127750 days (in mean 248±279 days per patient; range 1-1687 days) of TCVAP implantation, 50 patients had to be revised due to complications (9.9%). Those were observed after a mean duration of 114±183 days (range, 1-1113 days): 21 (4.1%) early complications and 29 (5.7%) late complications. Complications were as follows: 25 patients (4.9%) had local infection; two had systemic infection (0.4%); eight patients developed venous thrombosis (1.4%); three had paralysis of the median nerve (0.6%), one suffered from skin dehiscence at the port site (0.2%) and eleven patients (2.2%) required revision owing to mechanical problems.

Conclusion: Radiologically inserted TCVAP can be safely used and has a low complication rate during follow-up.

10:30 - 12:00

Room E1

Musculoskeletal

SS 1310

Tumours

Moderators:

G.M. Allen; *Oxford/UK*
C. van Rijswijk; *Leiden/NL*

B-0639 10:30

DCE MRI in differential diagnosis of soft tissue masses

T. Robba¹, V. Clementi², M. Stratta¹, G. Regis¹, A. Gallo¹, A. Linari¹, R. Piana¹, C. Faletti¹; ¹Turin/IT, ²Bologna/IT (tizianarobba@yahoo.it)

Purpose: The role of DCE MRI (dynamic contrast-enhanced magnetic resonance imaging) in differential diagnosis between benign/malignant soft tissue masses.

Methods and Materials: During standard MRI we performed DCE MRI in 33 soft tissue mass using 3D FSPGR (fast-spoiled-gradient-recalled-acquisition-in-steady-state) multi-phase sequences (temporal resolution ranging from 4 sec - to 10 sec after contrast-media MultiHance 2.5 ml/s) and saline (20 ml at 2.5 ml/s) injection. The signal-intensity/time curves were obtained from regions of interest on arterial and venous vessels, skeletal muscle and the areas with higher and earliest contrast-enhancement. We evaluated the morphological patterns of signal-intensity/time curves and correlated them with histological diagnosis data, except for 1 angioma, 1 myositis ossificans and 2 haematoma.

Results: We obtained four patterns of curves: 1) an exponential curve parallel to arterial curve followed by a plateau or a further increase of enhancement: 7 sarcoma and 1 myositis ossificans; 2) gradual progression of enhancement with the peak between arterial and venous curve, followed by a plateau: 4 sarcoma; 3) gradual progression of enhancement with the peak after the venous curve, followed by a further increase of enhancement: 5 sarcoma and 4 benign tumours (2 neurinoma,

1 angioma, 1 desmoid tumour); 4) none or equal to muscle enhancement: 9 benign lesions, 3 liposarcoma lipoma-like.

Conclusion: In our experience the presence of an exponential curve parallel to arterial is highly suspicious for malignant lesion, while an enhancement equal to that of muscle excludes the malignancy, except for the liposarcoma lipoma-like. DCE MRI may confirm the diagnosis of neurinoma.

B-0640 10:39

Diffusion-weighted imaging as a non-invasive predictor of tumour grading in soft tissue sarcoma

M.C. Herbrink, L. Umutlu, J. Kalkmann, S. Bauer, L. Podleska, F. Grabelius, G. Taeger, T. Lauenstein; *Essen/DE (m.herbrink@gmx.de)*

Purpose: Tumour grading is a valuable predictor with regard to prognosis and therapy management of soft tissue sarcomas (STS). Histopathology has been considered the gold standard of tumour grading. The aim of our study was to assess the diagnostic potential of diffusion-weighted MRI as a non-invasive predictor of tumour grading.

Methods and Materials: 17 patients with histologically proven STS were enrolled in this trial and were examined prior to isolated limb perfusion (ILP) on a 1.5 Tesla scanner. Beyond clinically applied sequences, a transversal EPI-DWI sequence was collected. Sequence parameters included TR/TE = 9700/78 ms, slice thickness 7 mm, voxel size: 2.0x2.0x7.0 mm, acquisition time 6:18 min, b-values: 50, 500, 1000). All malignant lesions were assessed by acquiring ADC (apparent diffusion coefficient) values in transversal plane by polygonal region-of-interest placement. The results were compared to histopathologic grading of pre-therapeutic specimens (G2 to G4). ADC-values were compared by Wilcoxon signed rank test. A p-value < 0.05 was determined to be statistically significant.

Results: According to histopathology 5 tumours were rated as G2 and 6 tumours were rated as G3 and G4 each. Correlation of histopathologic grading and ADC values allowed for a statistical significant differentiation of G2 (ADC 0.009) and G3 tumours (ADC 0.01) (p=0.04). However, assessment of ADC values did not show a statistical significant difference in the differentiation of G2 to G4 or G3 to G4 tumours (p> 0.06).

Conclusion: Diffusion-weighted imaging can be a non-invasive predictor of tumour grading for differentiation between G2 and G3 soft tissue sarcoma.

B-0641 10:48

Comparison of viable tumour volumes estimated on dynamic MRI by computer-aided quantification technique with the tumour viability scores of pathology following excision of soft tissue sarcoma's: prospective study

A.K. Singh, V. Kurra, Y.-L.E. Chen, W. Cai, G. Nielsen, D. Harmon, F.J. Hornicek; *Boston, MA/US (VKURRA@PARTNERS.ORG)*

Purpose: To assess the accuracy of viable tumour volume estimated using computer-aided technique on dynamic MRI datasets.

Methods and Materials: In this on-going prospective study, viable tumour estimates obtained by pathologist on 16 slices of soft tissue sarcoma specimens, post-excision were compared to tumour viability volumes estimated by computer-aided post-processing of post-gadolinium, dynamic T1-weighted fat-saturated (FS) sequence from MRI datasets. The MRI for these patients was performed after undergoing pre-operative chemotherapy or radiation treatment and within 7-10 days before excision. Computer-aided quantification of viable tumour was aided by estimation of contrast wash-in and wash-out curves. Care was taken to match the MRI axial images to the corresponding locations of cut-sections during pathology tumour slicing for reporting of viable tumour estimate that served as standard of reference. Pearson's correlation and Bland Altman (BA) analysis was used.

Results: The viable-appearing tumour volume percentage derived from dynamic MRI contrast acquisitions was within 1.96 standard deviation (SD) [-82.0 to 115.7] of the BA plot indicating similarity to pathological tumour viability estimates and good correlation (r = 0.804; p < 0.0001; 95% confidence interval= 0.7309 to 0.9455). There were no outliers in the BA plot.

Conclusion: The viable tumour fractions obtained by computer-aided quantification methods on dynamic MRI datasets for soft tissue sarcoma show similar results to surgical pathology estimates of viable tumour fraction after excision of soft tissue sarcoma. These findings warrant validation on a larger cohort of patients.

B-0642 10:57

DWI in differential diagnosis of enchondroma and central chondrosarcoma

T. Robba¹, V. Clementi², M. Stratta¹, G. Regis¹, A. Gallo¹, R. Piana¹, A. Linari¹, V. Ciccone¹, C. Faletti¹; ¹Turin/IT, ²Bologna/IT (tizianarobba@yahoo.it)

Purpose: The role of DWI (diffusion-weighted imaging) in differential diagnosis between enchondroma and central chondrosarcoma.

Methods and Materials: We performed DWI (November 2008-July 2011) in 14 patients with an intramedullary chondral lesion of the bone. During standard MRI, a spin-echo echo-planar-imaging (b: 0-900 s/mm²) was performed. The ADC (apparent diffusion coefficient) colorimetric map was matched against the corresponding axial FRFSE T2. Large regions of interest were plotted on the lesion at least in three consecutive slices. The average ADC of each lesions was calculated and correlated by ANOVA (analysis of variance) test with the histological data: in four I/II grade and in six III/IV grade chondrosarcoma the diagnosis was histologically proven, while in four enchondroma a 2- to 4-year follow-up was done.

Results: The ANOVA test shows a statistically significant difference (p < 0.05) in ADCs (F: 4,465, critical F:3,982) of the three groups: enchondroma (average ADC: 2.39x10⁻³ mm²/s), I/II grade chondrosarcoma (average ADC: 1.96x10⁻³ mm²/s) and III/IV grade chondrosarcoma (average ADC: 1.50x10⁻³ mm²/s).

Conclusion: Even if statistically significant, there is only a slight difference among chondroma and chondrosarcoma ADCs and many data are necessary to investigate the utility of DWI in differential diagnosis of I grade chondrosarcoma and enchondroma.

B-0643 11:06

Assessment of diffusion-weighted imaging for therapy monitoring in neoadjuvant isolated limb perfusion - therapy of soft tissue sarcoma

M.C. Herbrink, L. Umutlu, J. Kalkmann, S. Bauer, F. Grabellus, G. Taeger, T. Lauenstein; Essen/DE (m.herbrink@gmx.de)

Purpose: Assessment of therapy response is an inevitable aspect of neoadjuvant isolated limb perfusion (ILP) therapy of soft tissue sarcoma (STS). Morphologic assessment by means of RECIST criteria has been shown to provide limited accuracy. We aimed to evaluate diffusion-weighted imaging (DWI) for assessment of cancer response in correlation with morphological RECIST criteria and histopathologic regression.

Methods and Materials: 19 patients with histologically proven STS were enrolled in this trial and were examined (1) prior as well as (2) 7 days and (3) 6 weeks after the initiation of neoadjuvant ILP. MRI was performed on a 1.5 Tesla scanner. Beyond clinical sequences, a transversal EPI-DWI sequence was collected. Sequence parameters included TR/TE = 9700/78 ms, slice thickness 7 mm, voxel size: 2.0x2.0x7.0 mm, acquisition time 6:18 min, b-values: 50, 500, 1000). Morphologic analysis was assessed according to RECIST-criteria. For functional analysis ADC-values as well as CNR (in correlation to healthy muscle tissue) were evaluated. Results were correlated with histopathologic regression after surgery. The changes in ADC values were compared by Wilcoxon signed rank test.

Results: According to histopathology 14 patients were determined as responders. While morphologic assessment of therapy response did not show statistical significant correlation with histopathologic response, the evaluation of DWI imaging showed a statistically significant increase of mean ADC values, in terms of a regression of diffusion disruption. CNR values confirmed positive pathologic response, by means of a significant decrease under therapy.

Conclusion: DWI can be used for the assessment of therapy response of STS after ILP.

B-0644 11:15

MRI with diffusion-weighted imaging and apparent diffusion coefficient (ADC) in the assessment of response to treatment in patients with multiple myeloma: preliminary results

P.A. Bonaffini, D. Ippolito, I. Macchi, F. Rossini, A. Di Lelio, S. Sironi; Monza/IT (pa.bonaffini@gmail.com)

Purpose: To assess the added value of ADC in the evaluation of response to chemotherapy (CT) in patients with multiple myeloma (MM).

Methods and Materials: 20 patients with MM underwent 1.5 T WB-MRI (Achieva, Philips) from vertex to feet, before and after CT, with the following protocol: coronal and sagittal short tau inversion recovery (STIR) T2, T1 TSE and axial DWIBS sequences (b factor: 0, 500, 1000 mm²/sec). DWIBS images were compared with T1 and STIR images in five districts (skull; spine; sternum and ribs; pelvis; upper and lower limbs) to evaluate response to treatment. ROI were manually drawn along contours of tumours on ADC maps. The mean ADC values of lesions and percent-

age variation of ADC (Δ ADC) before (MR1) and after (MR2) CT were calculated and compared between responders and non-responders.

Results: All primary tumours were correctly detected on MRI and response to CT was established as intensity signal decrease over a period of time during follow-up. Compared to normal bone marrow, tumour showed high signal intensity on DWI. The mean ADC values were on MR1: 0.54 \pm 0.22 x10⁻³ mm²/sec and on MR2: 0.99 \pm 0.25 x10⁻³ mm²/sec. The mean percentage of tumour ADC changes in responders (Δ =66%) was significantly different (p < 0.05) than that in non-responders (Δ =15%), in relation to the higher cellularity of neoplastic bone marrow involvement.

Conclusion: MR DWI is a non-invasive tool able to predict early therapeutic response in patients with MM, by determining individual changes of ADC values corresponding to biological changes in tumour tissue.

B-0645 11:24

Diagnostic value of qualitative and quantitative diffusion-weighted MRI and chemical-shift imaging in the differentiation of benign and malignant vertebral body fractures: evaluation in a prospective group of patients

T. Geith, G. Schmidt, A. Biffar, O. Dietrich, H.R. Duerr, M. Reiser, A. Baur-Melnyk; Munich/DE (tobias.geith@med.uni-muenchen.de)

Purpose: To compare the diagnostic value of qualitative diffusion-weighted imaging (DWI), quantitative DWI, and chemical-shift imaging in a single prospective cohort of patients with acute osteoporotic and malignant vertebral fractures.

Methods and Materials: Patients with 26 osteoporotic (18 women, 8 men, mean age 69, 31.5-86.2 years) and 20 malignant vertebral fractures (9 women, 11 men, mean age 63.4, 24.7-86.4 years). T1-weighted, STIR and T2-weighted sequences were acquired at 1.5 T. A diffusion-weighted steady-state free-precession sequence (PSIF) at different delta values was evaluated qualitatively. A diffusion-weighted echo-planar imaging (EPI) and diffusion-weighted single-shot turbo spin echo (ssTSE) sequence at different b-values were evaluated qualitatively and quantitatively, using the apparent diffusion coefficient. Opposed-phase sequences were used to assess signal intensity qualitatively. The signal loss between in-/opposed-phase images was determined quantitatively. Two-tailed Fisher's exact and Mann-Whitney tests, and ROC-analysis were performed. Sensitivities, specificities and accuracies were determined.

Results: Qualitative DW-PSIF showed the highest accuracy (delta=3 ms: sensitivity 100%, specificity 88.5%, accuracy 93.5%). Qualitative DW-EPI and DW-ssTSE indicated no significant differences between benign and malignant fractures (p > 0.05), except DW-EPI at b=500s/mm² (p < 0.05). Quantitative DW-EPI and qualitative opposed-phase imaging exhibited no significant differences (p > 0.05), quantitative DW-ssTSE and quantitative chemical-shift imaging showed significant differences between benign and malignant fractures (p < 0.05).

Conclusion: DW-PSIF (delta=3 ms) had the highest accuracy in differentiating benign and malignant vertebral fractures. Quantitative chemical-shift imaging and quantitative DW-ssTSE had a lower accuracy in comparison with DW-PSIF because of a large overlap. Qualitatively assessed opposed-phase, DW-EPI and DW-ssTSE and quantitative DW-EPI were not suitable to differentiate between benign and malignant vertebral fractures.

B-0646 11:33

Magnetic resonance-guided focused ultrasound (MRgFUS) for the treatment of osteoid osteoma

A. Napoli, M. Anzidei, B. Cavallo Marincola, L. Molisso, G. Cartocci, F. Boni, L. Bertaccini, V. Noce, C. Catalano; Rome/IT (alessandro.napoli@uniroma1.it)

Purpose: The aim of our study was to evaluate the safety and efficacy of the MRg-FUS as a non-invasive method for the treatment of pain caused by osteoid osteoma.

Methods and Materials: Selected and informed patients with limited joint function and reduced quality of life due to painful osteoid lesion, confirmed at work-up MR and CT exam underwent MRgFUS (ExAblate 2100, InSightec, Haifa, Israel) housed into a 3 T MR system (GE). Clinical evaluation was assessed using visual analogue scale (VAS). Each patient was planned with a maximum of 5 sonications to complete nidus ablation. Clinical and imaging follow-up was performed 1 and 3 months after treatment. 3 patients with osteoid lesion underwent MRgFUS treatment. In two patients we treated a small and subperiosteal-located osteoma; one patient had a larger lesion (osteoblastoma).

Results: After treatment, VAS questionnaires demonstrated in two patients with typical osteoma the complete disappearance of painful symptoms, while third patient referred an initial reduction of pain and a gradual recurrence of symptoms. There were no observed treatment-related complications peri and post-procedure.

Conclusion: In our experience, MRgFUS represents a safe and effective treatment for the ablation of osteoid osteoma.

B-0647 11:42

Pain palliation of bone metastasis: initial clinical experience using high-intensity focused ultrasound therapy with magnetic resonance guidance

A. Napoli, M. Anzidei, E. Marotta, G. Brachetti, G. Cartocci, F. Boni, L. Bertaccini, V. Noce, C. Catalano; *Rome/IT (alessandro.napoli@uniroma1.it)*

Purpose: To determine the efficacy of non-invasive high-intensity MR-guided focused ultrasound (MRgFUS) treatment for palliation of bone metastasis pain in patients not candidates for external beam radiotherapy (EBRT).

Methods and Materials: Under the IRB approval 18 patients with 21 lesions underwent MRgFUS treatment using the ExAblate 2000 system (InSightec). Treatments were done in a single session, in an ambulatory setting. 12 patients underwent prior EBRT with a mean 6 months recurrent pain. In 6 patients MRgFUS treatment was performed as first treatment modality. Effectiveness of pain palliation was evaluated at follow-up using the visual analog pain score (VAS) and measurable changes in analgesics intake. For tumour control perfusion T1w-images were obtained pre- and post-treatment in order to determine the non-perfused sonication-related area.

Results: All patients and all lesions were treated. Mean follow-up time was 4 months. At baseline VAS was 7.1; it was 4.8 at 3 days, 3.0 at two weeks and 2.6 and 2.4 at one and four months, respectively. No heating-related adverse event was recorded during this clinical application; patient medication intake was considerably reduced. Variable degree of non-perfused volume was observed after treatment, mainly within the pericortical region. Deeper penetration of the acoustic energy is at present desirable even if technically difficult to achieve with the current system.

Conclusion: MRgFUS is a promising non-invasive treatment modality for successful palliation of bone metastasis pain in patients who are not candidates for EBRT.

B-0648 11:51

Iterative decomposition of water and fat with echo asymmetry and least-squares estimation (IDEAL) fast spin-echo imaging of the vertebral column metastasis: initial clinical experience

S.L. Juvvekar, A. Mahajan, S. Desai, A. Puri; *Mumbai/IN (sjuvvekar@gmail.com)*

Purpose: Our purpose was to test reliability and accuracy of iterative decomposition of water and fat with echo asymmetry and the least-squares estimation (IDEAL) method in combination with fast spin-echo imaging, in detecting vertebral metastasis and comparison of IDEAL and routine sequences in detection of the metastasis.

Methods and Materials: We compared IDEAL fast spin-echo with conventional fat-suppressed fast spin-echo imaging in 22 patients, who came for metastatic work up in the vertebral column. Routine spin echo and STIR sequences were acquired in all the cases. Each lesion was documented as benign or malignant based on the routine sequences and IDEAL sequence, and a corroborative data were also generated. Statistical correlation was performed.

Results: 6 subjects demonstrated breast metastases, 4 showed prostatic metastasis and 3 from unknown primary and one had a large presumptive schwannoma. 15 subjects demonstrated degenerative disc disease with associated Modic Type I or II changes at one or more levels. In all cases, marrow signal abnormalities could be particularly well characterised with IDEAL-derived images and parametric ratio maps. Marrow signal abnormalities could be particularly well characterised with IDEAL-derived images and parametric maps. Correlation of the lesion detection by routine spin-echo sequences and IDEAL sequence, a significant statistical difference was found in characterisation of the marrow signal abnormalities and lesion characterisation.

Conclusion: IDEAL sequence provides robust water-fat separation with optimised SNR performance. IDEAL imaging is a promising MRI technique affording a rapid automated high-resolution, high-contrast survey of the entire spine with optimised tissue characterisation.

10:30 - 12:00

Room E2

GI Tract

SS 1301a

Rectal and gastro-oesophageal cancer

Moderators:

A. Dieguez; *Buenos Aires/AR*
C. Kulinna-Cosentini; *Vienna/AT*

B-0649 10:30

Nodal restaging after chemoradiation for locally advanced rectal cancer: predictive factors

M. Maas, D.M.J. Lambregts, M. Berkhof, G.L. Beets, R.G.H. Beets-Tan; *Maastricht/NL (moniquemaas@live.nl)*

Purpose: Restaging N-stage after CRT is more accurate than N-stage prediction at primary staging of rectal cancer. A ypN0 status after CRT is mandatory to allow for less invasive treatment after CRT (e.g. local excision). Aim was to identify predictive factors which can help a radiologist in predicting yN-stage.

Methods and Materials: For 39 patients with locally advanced rectal cancer all visible nodes in the mesorectum were measured and recorded before and after CRT on a 3D-T1W-GRE-sequence with 1 mm³ voxels. Baseline characteristics were collected and compared between patients with and without nodal involvement at histopathology. With regression analyses predictive factors for nodal involvement were identified. ROC curves were constructed for a predictive model based on the regression analyses.

Results: 882 nodes were identified, of which 380 (43%) disappeared after CRT. Patients with ypN+ had larger nodes than ypN0-patients: mean 6.3 vs 3.6 mm before CRT and 4.5 vs 2.3 mm after CRT, respectively (both p < 0.0001). Regression analyses identified pre- and post-CRT size, T-downstaging and higher age as predictive factors for ypN0. AUCs for the regression-based model, pre-CRT size and post-CRT size were 0.86, 0.78 and 0.78, respectively (p < 0.05).

Conclusion: Nodal size (both pre- and post-CRT), T-downstaging and higher age at primary staging are predictors of ypN0-stage. With this knowledge and by use of these criteria a radiologist could select ypN0-patients with higher sensitivity than when size is used as a single criterion. With a higher sensitivity less invasive treatment after CRT can be applied more safely.

B-0650 10:39

Gadofosveset-enhanced MRI for nodal staging in rectal cancer: pitfalls and learning curve

L. Heijnen, D.M.J. Lambregts, G.L. Beets, M. Maas, M.H. Martens, V.C. Cappendijk, F.C.H. Bakers, R.G.H. Beets-Tan; *Maastricht/NL (d.lambregts@mumc.nl)*

Purpose: Nodal staging in rectal cancer remains insufficiently accurate. In a recent pilot-study we have shown improved performance in expert hands using gadofosveset-enhanced MRI (sensitivity 80%, specificity 97%). For the current study, gadofosveset-MRI was implemented in clinics (as part of ongoing research) and assessed by 'non-expert' abdominal radiologists. Aim was to identify the pitfalls of gadofosveset-MRI for nodal staging.

Methods and Materials: 44 patients underwent standard (T2W-FSE) and gadofosveset-MRI. Treatment-planning was based on T2W-MRI: 16 patients underwent (5x5 Gy+) immediate surgery, 28 underwent chemoradiation + a restaging MRI and surgery. Patients were scored as cN0/N+ based on the presence/absence of nodal gadofosveset-enhancement on the pre-surgical MRI. Histology was the gold-standard. In case of FP/FN findings, nodes were re-evaluated by a pelvic MR-expert on a per-node basis and compared with histology to identify the pitfalls.

Results: 27 patients were pN0.17 pN+. Thirty-three were correctly staged on gadofosveset-MRI (sensitivity 82%, specificity 70%); 3 pN+ patients were understaged, 8 pN0 were overstaged. FN-findings were due to: N+ node obscured by adjacent vessel (n=1), microscopic tumour cells too small to detect with MRI (n=2). FP-findings were due to: decreased gadofosveset-uptake in presacral/peri-vascular nodes (n=4), interpretation errors that were corrected after re-evaluation by the expert (n=3) and absence of gadofosveset-uptake (n=1).

Conclusion: Pitfalls mainly occur due to readers' inexperience and insufficient uptake of gadofosveset in nodes located between vessels (high in the mesorectum). Gadofosveset-MRI can improve radiologists' performance for nodal staging. Understanding the pitfalls and learning curve is crucial to allow broad clinical implementation.

B-0651 10:48

DW-MR and D-CE-MR: evaluation of the response in rectal cancer before, during and after neoadjuvant treatment

R. Del Vesco¹, V. Di Paola, S. Battisti, I. Sansoni, R. Grasso, B. Beomonte Zobel; *Rome/IT (r.delvesco@unicampus.it)*

Purpose: To evaluate the response of rectal adenocarcinoma to chemoradiation therapy (CRT) calculating changes of apparent diffusion coefficients (ADCs) before, during and after treatment and to correlate with the changes of dynamic contrast-enhanced MR (D-CE-MR) values.

Methods and Materials: we enrolled 28 patients (pts) with primary rectal carcinoma who were undergoing preoperative CRT. DWI and D-CE-MR were performed with a 1.5-T system in all patients before, during and after preoperative CRT. All patients underwent histopathologic postoperative staging. ADCs values were calculated through the specific formula, while tumour-perfusion was calculated by a semi-quantitative perfusion software (DYCHO), developed on Matlab. We evaluated the changes of ADCs and D-CE-MR dividing patients into two groups: not-downstaged group (NR) and downstaged group (R) at histologic postoperative staging.

Results: 6 patients were NR while 22 patients were R. Pretreatment ADCs values were significantly low; we observed a progressive increasing of ADCs values during treatment in R, while there was no significant ADCs increase in the NR ($p = 0.003$). The mean values of tumour ADCs change in the R was significantly higher than that in the NR at each time point ($p < 0.001$). The R showed 48% increase of local peak intensity (LPI) with respect to LPI before treatment; on opposite, the NR showed 18% decrease of LPI compared to LPI before treatment.

Conclusion: Tumour response more likely occurs in pts who report higher LPI values on D-CE-MR analysis during treatment with respect to pre-treatment.

B-0652 10:57

Standardised index of shape (SIS): a novel semi-quantitative DCE-MRI parameter based on pattern analysis (PA) able to divide responder (R) by not responder (NR) after preoperative radio-chemotherapy (pCRT) in locally advanced rectal cancer (LARC)

R. Fusco, M. Petrillo, S. Setola, M. Sansone, A. Rotondo, A. Petrillo; *Naples/IT (roberta.fusco@unina.it)*

Purpose: MRI is considered the best available tool for LARC staging after pCRT although in most cases to tumour response does not correspond a size reduction. To identify a DCE-MRI index based on PA which could differentiate between responders (R, TRG1 or TRG2) and not responders (NR, TRG3 or TRG4) after pCRT.

Methods and Materials: 40 patients underwent DCE-MRI examination before and after pCRT. Pre- and post-contrast T1w scans were acquired after Gd-DOTA injection. Regions of interest (ROI) were drawn inside the tumour and after time intensity curves (TIC) were plotted. Basing on PA 13 shape descriptors were computed and individual percentage changes were calculated.

Results: Performing Kruskal Wallis and Wilcoxon test for percentage change before and after pCRT in responders, maximum slope deviation (MSD), wash-in slope, wash-out intercept, area under the curve (AUC), AUC wash out (AUCWO) and heights ratio (HR) showed statistically significant differences ($P < 0.05$). According to the hotelling trace criterion (HTC) Δ MSD & Δ AUCWO match provided the best results and a cut-off value change of 11.6% divided R from NR with SEN of 85.0%, SPE of 83.3%, NPV of 71.4% and PPV of 91.7%.

Conclusion: Δ MSD & Δ AUCWO match, defined "standardised index of shape" (SIS) seems to be a promising semi-quantitative numerical parameter capable to evaluate residual tumour activity after pCRT in LARC, defining a robust cut-off value of 11.6% to separate R by NR.

B-0653 11:06

Reproducibility of 2D and 3D fractal analysis techniques for the assessment of spatial pattern of perfusion CT regional blood flow in rectal cancer

V.J. Goh¹, D. Banerjee², B. Sanghera², A. Khan², I. Simcock², J. Stirling², R. Glynn-Jones²; ¹London/UK, ²Northwood/UK

Purpose: To determine the reproducibility of 2D and 3D fractal analysis techniques for the assessment of spatial pattern of perfusion CT regional blood flow in rectal cancer.

Methods and Materials: Following institutional review board approval and informed consent, 10 prospective patients (8 males, 2 females, mean age 70.6years) with rectal adenocarcinoma underwent two repeated volumetric helical perfusion CT studies (4D adaptive spiral; 11.4 cm z-axis coverage; dual source CT; Siemens Healthcare) without intervening treatment within 24 hours, deriving regional blood flow by deconvolution analysis (VPCT, Siemens Healthcare). 2D and 3D fractal

analysis of the rectal tumour were performed following segmentation from surrounding structures by thresholding, deriving fractal dimension (FD) and fractal abundance (FA). 2D and 3D fractal parameters were compared by t-testing. Reproducibility was assessed by Bland-Altman statistics. Statistical significance was at 5%.

Results: Mean (SD) blood flow was 63.50 (8.95) mL/min/100 mL. Fractal dimension and fractal abundance were significantly lower for 2D than 3D analysis: 1.648 versus 2.488; $p < 0.0001$; and 7.278 versus 10.338; $p < 0.0001$ respectively. Good agreement was noted between the repeated studies for fractal dimension (mean difference (95% limits of agreement): 0.079 (-0.027 to +0.371) and 0.024 (-0.307 to +0.355)) and fractal abundance mean difference (95% limits of agreement): 0.354 (-0.091 to +0.802) and -0.043 (-1.154 to +1.239) for 2D and 3D fractal analysis, respectively. The 95% limits of agreement were narrower for 3D than 2D analysis.

Conclusion: As a measure of spatial heterogeneity, fractal analysis complements perfusion CT, and is a reproducible technique.

B-0654 11:15

Accurate identification of complete responders after CRT for rectal cancer with endoscopy and MRI

M. Maas¹, D.M.J. Lambregts¹, J.W.A. Leijtens², M. Sosef³, K.W.E. Hulsewe⁴, G.L. Beets¹, R.G.H. Beets-Tan¹; ¹Maastricht/NL, ²Roermond/NL, ³Heerlen/NL, ⁴Sittard/NL (moniquemaas@live.nl)

Purpose: Chemoradiation (CRT) for rectal cancer leads to complete tumour response (CR) in 15-25%. Accurate identification of a CR is necessary to allow for less invasive treatment (e.g. local excision or wait and see). Standard imaging cannot accurately identify a CR. Aim was to evaluate the accuracy of endoscopy for identification of a CR and compare it to T2W- and diffusion-weighted MRI (DWI).

Methods and Materials: 20 patients who underwent CRT and T2W-MRI, DWI and endoscopy 8 weeks after completion of CRT were included. One reader scored the T2W images followed by immediate evaluation of the DWI images with the T2W images at his disposal. A second reader scored the endoscopy images. Readers were blinded for histology and each others' results. Scoring was performed with a confidence level score (0=definitely residual tumour, 4=definitely CR).

Results: Of the 20 patients, 9 had residual tumour and 11 had a CR. The AUCs for T2W-MRI, T2+DWI and endoscopy were 0.65, 0.65 and 0.91, respectively. Corresponding sensitivities and specificities were 36% and 78% for T2W, 46% and 89% for T2+DWI and 73% and 89% for endoscopy.

Conclusion: Endoscopy is more accurate in identifying a CR after CRT than MRI (\pm DWI), mainly because of a higher sensitivity, which corrects for the understaging of a CR with MRI. MRI remains crucial to evaluate the presence of any extramural residual tumour and/or involved nodes. A combination of endoscopy and MRI+DWI is therefore recommendable to identify patients with a CR after CRT, making less invasive treatment after CRT feasible.

B-0655 11:24

Preoperative locoregional (T and N) staging of gastroesophageal cancers (GEC): comparison between magnetic resonance (MR) including diffusion-weighted sequences (DWI), computed tomography (CT), endoscopic ultrasound (EUS)

F. Giganti, F. De Cobelli, M. Cellina, R. Nicoletti, C. Martinenghi, P. Arcidiacono, E. Orsenigo, C. Staudacher, A. Del Maschio; *Milan/IT (giganti.francesco@hsr.it)*

Purpose: Preoperative GEC cancers staging is widely performed with CT and EUS; MR has limitations (motion artefacts, long acquisition time) partially overcome by technological development. We evaluated the usefulness of MR, included DWI, compared with CT and EUS.

Methods and Materials: During a 18-month period, 43 patients with GEC (7 oesophageal, 11 cardiac, 25 gastric) underwent preoperative EUS, multidetector-64-channels CT and 1.5 T MR, including DWI (b0-600 s/mm²). All the images were analysed in blind and the results were compared with histological findings after resection assuming T1-T2 as organ-confined GEC and T3-T4 as infiltrating GEC. Lymphnodes were staged as negative (N-) or positive (N+). Sensitivity, specificity, positive (PPV) and negative predictive value (NPV) were calculated.

Results: Sensitivity, specificity, PPV, NPV calculated for T were for MR: 73% 77% 79% 71%; while for CT: 79% 74% 79% 74% and for EUS: 80%, 76%, 76%, 80%; for N status: for MR 83% 89% 83% 89%; for CT: 48% 50% 62% 36%; for EUS: 72%, 52%, 54%, 71%. Mean apparent diffusion coefficient of primary tumours was $1.58 \times 10^{-3} \text{ mm}^2/\text{s} \pm 0.39$, of lymphnodes was $1.47 \times 10^{-3} \text{ mm}^2/\text{s} \pm 0.56$.

Conclusion: EUS is slightly superior to CT and MR for T stage, while, regarding N stage, MR results are superior to both CT and EUS, thanks to the addition of DWI. We can conclude that MR can be a valid diagnostic tool if used in standard protocols in the staging of oesophageal and gastric neoplasms.

B-0656 11:33

Apparent diffusion coefficient (ADC) modifications in assessing gastroesophageal cancer (GEC) response to neoadjuvant treatment (NT): comparison to tumour regression grade (TRG) at histology

M. Cellina, F. De Cobelli, F. Giganti, L. Albarello, E. Orsenigo, D. Chiari, A. Esposito, C. Staudacher, A. Del Maschio; *Milan/IT (cellina.michaela@hsr.it)*

Purpose: To evaluate whether modifications in the ADC before and after NT (Δ ADC) for locally advanced GEC are related to TRG, an objective histological parameter of treatment response scoring the residual neoplastic in 5 grades, obtained after radical resection, predictor for disease-free survival.

Methods and Materials: 20 patients affected by a biopsy-proved locally advanced EGC underwent 1.5 T diffusion-weighted imaging pre- and post-NT. Mean lesion ADCs, lesion volumes (V), Δ ADC, V changes pre- and post-NT (Δ V) were calculated. Patients with TRG 1-3 were considered responders (R), patients with TRG 4-5 non-responder (NR).

Results: No correlation between Δ V and TRG ($R=0.078$) was found. The difference in Δ V between the two groups was not statistically significant different ($P=0.333$). After NT, 14/20 patients (70%) showed an increase in ADC values; 1/20 patients (5%) did not show significant changes; 5/20 patients (25%) showed decreasing ADC values. ADCs changes showed a significant inverse correlation with response to NT ($r = -0.67$). R showed a statistically significant lower pre-NT ADC ($1.21 \pm 0.37 \times 10^{-3}$ mm²/s) than NR ($1.77 \pm 0.30 \times 10^{-3}$ mm²/s) ($P=0.010$) and higher post-NT ADC ($2.20 \pm 0.49 \times 10^{-3}$ mm²/s vs $1.76 \pm 0.6 \times 10^{-3}$ mm²/s) ($P=0.028$). Δ ADC was statistically significant higher for R than for NR ($+105.89 \pm 101\%$ vs -3.77 ± 25.02) ($P=0.002$).

Conclusion: The only dimensional criteria Δ V is not a good indicator of response. ADC can be considered a predictor of treatment response even before the beginning of NT. Δ ADC can be used to assess tumour response to NT, as a reliable indicator of the TRG classification.

B-0657 11:42

PET-guided prognosis: a promising role of metabolic imaging in oesophageal cancer

L. Evangelista, A.R. Cervino, R. Alfieri, C. Castoro, P.C. Muzzio, F. Pomerri; *Padua/IT (laura.evangelista@ioveneto.it)*

Purpose: To evaluate the prognostic value of FDG-PET/CT after neo-adjuvant therapy in locally advanced oesophageal cancer (EC) patients.

Methods and Materials: Among 108 EC patients who underwent FDG-PET/CT after neo-adjuvant treatment, we selected 56 patients without evidence or suspicious for distant metastases. All patients were followed for a mean period of 13 ± 9 months from nuclear imaging. PET/CT findings were correlated with patient management and long-term prognosis. Chi-square test was used for comparison of categorical variables and t-Student test for continuous data. Survival curves were computed using Kaplan Meier method. A p value of < 0.05 was considered statistically significant.

Results: 15 patients had negative and 41 positive (27 vs. 73%) PET/CT after neo-adjuvant therapy. 6/15 patients underwent radical-intent surgery and 9/15 did not, whereas 31/41 performed surgery and 10/41 did not ($p < 0.05$). After a median time of 10 months, 28 patients were disease-free, 15 relapsed and 11 died. The event-free survival was significantly higher in patients with negative than with positive PET/CT after neo-adjuvant treatment (73 vs. 41%; log rank $p < 0.05$). Considering patients with positive PET/CT, in non-surgery subset only 1 patient was alive without evidence of disease while in surgery subset 17 patients were disease-free (10 vs. 55%, $p < 0.001$).

Conclusion: PET/CT could stratify the recurrence risk of EC patients based on treatment efficacy. After 13 months from PET/CT, 89% of patients with negative PET/CT who did not undergo surgery resulted disease free. A positive PET/CT after neo-adjuvant therapy should be followed by surgery for improving the event-free survival.

B-0658 11:51

Spectral pre-saturation inversion-recovery MR imaging sequence after gadolinium injection to identify mesorectal fascia infiltration in patients with rectal carcinoma after neoadjuvant chemo- and radiation therapy

E. Quaià, V. Ulcigrai, L. De Paoli, B. Cabibbo, E. Pantano, M. Cova; *Trieste/IT (quaià@units.it)*

Purpose: To retrospectively assess the value of spectral pre-saturation inversion-recovery (SPIR) MR imaging sequence after gadolinium injection to identify mes-

orectal fascia infiltration in patients with rectal carcinoma undergoing MR restaging after neoadjuvant chemo- and radiation therapy (CRT).

Methods and Materials: Fifty-five consecutive patients (mean age: 65.8 years; range: 46 - 85 years; M:F 33:22) with locally advanced rectal carcinoma involving the higher, middle or lower rectum underwent CRT followed by surgery. MR imaging was performed before and after completion of CRT using T2-weighted fast spin-echo and T1-weighted SPIR sequences before and after gadolinium injection, and MR images were assessed by two radiologists in consensus. The evidence of reticular (interwoven within the mesorectal fat creating a meshwork) or linear-shaped (travelling separately through the mesorectal fat) enhancing strands within the mesorectal fat on MR images were retrospectively correlated with the histopathologic findings.

Results: After CRT the disease was either limited to the rectal wall ($n=24$ patients) or presented mesorectal fat infiltration ($n=31$) on histology. In 31 patients reticular or linear-shaped mesorectal enhancing strands were observed. In 10 patients the reticular-shaped enhancing strands reached the mesorectal fascia and a positive circumferential resection margin after total mesorectal excision was found on the histologic analysis (OR=170.1, 95% CIs: 4.1-4220.29; logistic regression), whereas linear-shaped enhancing strands either reaching or not reaching the mesorectal fascia revealed no correlation with mesorectal fascia infiltration (OR 0.25 or 0.1; 95% CIs: 0.01-1.07).

Conclusion: Reticular-shaped enhancing strands reaching the mesorectal fascia were significantly related to mesorectal fascia infiltration.

10:30 - 12:00

Room F1

Genitourinary

SS 1307

Adrenal and kidney imaging

Moderators:

M. Ramalho; Almada/PT
D.H.M. Szolar; Graz/AT

B-0659 10:30

Evidence-based medicine: decision-making on renal lesions based on meta-analysis of MR diffusion-weighted imaging

E. Lassel¹, R. Rao², C. Schwenke³, S.O. Schönberg¹, H.J. Michaely¹; ¹Mannheim/DE, ²Galveston, TX/US, ³Berlin/DE

Purpose: Commonly performed contrast-enhanced MRI can only distinguish to a limited extent between malignant and benign focal renal lesions. The aim of this meta-analysis is to review renal diffusion-weighted imaging to compare ADC-values for different renal lesions, which can be applied in clinical practice.

Methods and Materials: A search on PubMed was performed to identify relevant articles published on renal DWI of focal renal lesions between 2004 and 2011 by two independent reviewers. These reviewers extracted the ADC-values from the selected studies by lesion type to determine the dignity of a lesion within the kidney. The data table was finalised in a consensus read. The ADC-values were evaluated statistically by a meta-regression based on a linear mixed model. A two-sided p-value of less than 5% indicated statistical significance.

Results: The meta-analysis is based on 17 studies with a cumulative number of 764 patients. Renal cell carcinomas have significant lower ADC-values than benign tissue (1.61 ± 0.08 s/mm² vs. 2.10 ± 0.09 s/mm²; p -value < 0.01). Uroepithelial malignancies can be differentiated by lowest ADC-values (1.30 ± 0.11 s/mm²; p -value < 0.01). There is a statistically significant difference between the ADC-values of renal cell carcinomas and oncocytomas (1.61 ± 0.08 s/mm² versus 2.00 ± 0.08 s/mm²; p -value < 0.01).

Conclusion: The evaluation of ADC-values can help to determine between benign and malignant lesions, in general, but also seems able to differentiate oncocytomas from malignant tumours hence potentially reducing the number of unnecessarily performed nephrectomies.

B-0660 10:39

Comparison of 15-minute delayed contrast-enhanced CT and chemical shift MR in the evaluation of adrenal masses

H.J. Koo, H.J. Choi, M.-H. Kim, K.-S. Cho; *Seoul/KR (elfin⁹@gmail.com)*

Purpose: To retrospectively compare the diagnostic performance of delayed enhanced computed tomography (CT) and chemical shift magnetic resonance (MR) imaging for evaluating adrenal masses.



Methods and Materials: 15-minute delayed adrenal protocol CT (unenanced, 60 second and 15 minute delayed CT) or chemical shift MR images for 900 adrenal masses in 835 patients were retrospectively reviewed for the period from January 2000 through August 2011. 562 hyperattenuating adrenal masses (> 10 HU) on unenhanced CT images in 532 patients (287 men and 255 women; mean age, 51.7 years) analysed using absolute percentage washout (APW) and relative percentage washout (RPW) for evaluating CT, and 49 hyperattenuating adrenal masses were analysed with chemical shift MR by calculating adrenal-to-spleen ratio (ASR) and signal intensity index (SII). Receiver operating characteristic (ROC) analysis was performed to compare the diagnostic performance of CT and MR.

Results: All adrenal masses included 404 adenomas and 158 nonadenomas. The sensitivity and specificity for the APW at CT were 81.8% and 84.1%, respectively, and those for the RPW were 91.4% and 78.8%, respectively. And at MR, the sensitivity and specificity for the SII were 93.3% and 84.2%, respectively. Areas under the ROC curve were 0.882, 0.898 and 0.944 for the APW, RPW and SII, respectively. However, there was no significant difference for diagnostic performance between APW, RPW and SII ($P>.05$).

Conclusion: Chemical shift MR shows a high sensitivity and specificity for evaluating adrenal masses, but is of no additional diagnostic value compared to the 15-minute delayed contrast-enhanced CT.

B-0661 10:48

Evaluation of adrenal metastases from renal cell carcinoma or hepatocellular carcinoma using unenhanced and delayed contrast-enhanced CT

Y. Choi, C. Kim, B. Park, S. Park, J. Park, H. Yoon, A. Kim; *Seoul/KR (ya24.choi@samsung.com)*

Purpose: To retrospectively measure the attenuation values and percentage enhancement washout of adrenal metastases at delayed contrast-enhanced CT in patients with RCCs and HCCs and to compare with those of adrenal adenomas.

Methods and Materials: Fifteen patients with 18 adrenal metastases and 20 patients with 21 adrenal adenomas underwent dedicated adrenal CT. The attenuation values and percentage enhancement washout were calculated. The change in size of adrenal masses was also assessed. The final diagnosis was made by surgery or biopsy, a decrease in size after targeted chemotherapy (2 metastases), and stability in size on follow-up imaging at least 30 months (12 adrenal adenomas).

Results: The mean absolute percentage washout value of metastases (67 HU \pm 11) was not significantly different from that of adenomas (72 HU \pm 9). The mean relative percentage washout value of metastases (44 HU \pm 10) was significantly lower than that of adenomas (62 HU \pm 19), but 94% of metastases had APW of > 60% or RPW of > 40%. On unenhanced CT, the mean attenuation value of metastases and adenomas was 40 HU \pm 7.5 and 18 HU \pm 19.2, respectively; all metastases had > 10 HU. All metastases showed a measurable growing in size.

Conclusion: In patients with RCCs and HCCs, the percentage enhancement washout of adrenal metastases was similar to that of adrenal adenomas. Thus, if an adrenal mass in those patients has CT findings suggesting a lipid-poor adrenal adenoma, careful serial imaging follow-up is recommended to exclude a possibility of metastasis.

B-0662 10:57

Value of functional MRI with diffusion-weighted imaging in characterisation of indetermined adrenal lesions: comparison with chemical shift imaging

C.R. Talei Franzesi, D. Ippolito, L. Monguzzi, C. Capraro, A.C. Cadonici, S. Sironi; *Monza/IT (ctfdoc@hotmail.com)*

Purpose: To assess the value of adding functional sequences, using diffusion-weighted imaging and apparent diffusion coefficient value, to conventional MR imaging examination, in the differential diagnosis of adrenal lesions.

Methods and Materials: A total of 60 patients with a variety of adrenal lesions (adenomas, myelolipomas, adrenal metastasis and primitive carcinomas) were prospectively investigated with MRI scan (1.5 T, Achieva, Philips). The study was performed with a phased array multi-coil using a conventional protocol that included also diffusion-weighted imaging (DWI) with b-value of 0, 300, 500 and 1000 mm²/sec. DWI images were compared with T1 FFE in- and opposed phase. The mean ADC value of adrenal lesions was calculated and correlated with MRI findings. ROI were manually drawn along the contours of adrenal lesion on ADC maps and statistical analysis was performed.

Results: Lesions were proved either by follow-up (size increase of over a period of time) or biopsy (oncologic patients). All adrenal lesions presented restriction of diffusion and motion of water protons on diffusion-weighted images. There was no significant difference in obtained ADC values between adenomas (mean value:

1144 \pm 89.3 mm²/sec), myelolipomas (mean value:1240 \pm 204.9 mm²/sec) and primitive carcinomas (mean value:1133 \pm 63.9 mm²/sec). A higher ADC value was seen in the adrenal metastasis (mean value: 1451 \pm 145.9 mm²/sec) compared to the other adrenal lesions ($p < 0.05$), in relation to the presence of more homogeneous water protons diffusion.

Conclusion: We could not obtain differential diagnosis between benignant and malignant adrenal lesions using diffusion-weighted images and ADC map. Quantitative DWI evaluation by ADC maps offers a further non-invasive tool in terms of characterisation only of metastatic lesions against the other adrenal lesions. The chemical shift images remain the most helpful sequences in characterisation of adrenal lesions.

B-0663 11:06

Quantitative 23Na, and DW-imaging of the healthy human kidney for establishing norm values for the 23Na, concentrations at 3.0 T

S. Haneder, S. Konstandin, P. Kettner, L.R. Schad, S.O. Schönberg, H.J. Michaely; *Mannheim/DE (haneder@googlemail.com)*

Purpose: The purpose of this prospective study was to establish physiological ranges for the renal cortico-medullary 23Na-concentration ([23Na]) gradient, the correlation with DW-imaging at 3.0 T and physiological parameters in a collective of healthy volunteers.

Methods and Materials: 45 healthy volunteers (18f, 27m; mean age: 29a) were included in this IRB-approved study. For 23Na-imaging a 3D-density adapted, radial GRE-sequence (TE=0.55 ms; TR=120 ms; projections=8000; spatial resolution=5x5x5 mm³) was used at 3.0 T (TimTrio Magnetom, Siemens) in combination with a dedicated 23Na-coil and 0.6% reference 23Na-phantoms with 2% agarose. Axial diffusion-weighted images (TE=87.3 ms; TR=4435 ms; b-values=0-800; spatial resolution=0.6x0.6x5 mm³) were acquired with a standard body-coil. Mean values \pm standard deviations for [23Na] and ADC-values were calculated for each volunteer and as overall values. Pearson correlation coefficients were calculated to check for statistically significant correlations with ADC values, gender, serum [23Na], body mass index (BMI) and glomerular filtration rate (GFR).

Results: The mean cortico-medullary [23Na] for all healthy volunteers increased from cortical 60.4 \pm 7.8 mmol/l to medullar location 120.4 \pm 13.5 mmol/l. Inter-individual differences ranged from cortical/medullary 49.7 \pm 15.0/94.0 \pm 15.1 mmol/l to 71.5 \pm 11.9/137.6 \pm 15.6 mmol/l, with significant higher values for women ($p=0.004$). The mean cortico-medullary [23Na] gradient was 4.2 \pm 0.5 mmol/l/mm. The mean renal ADC value was 1.8x10⁻³ mm²/s and ranged inter-individually from 1.6x10⁻³ mm²/s to 1.9x10⁻³ mm²/s. No statistically significant correlations were found between the renal cortico-medullary 23Na-concentration and ADC values, serum [23Na], BMI and GFR.

Conclusion: Despite intra-individual differences a range of normal values for the cortico-medullary [23Na] could be defined and the lacking correlation with other physiological parameters could be shown.

B-0664 11:15

Tumour necrosis on magnetic resonance imaging correlates with aggressive histology and disease progression in clear cell renal cell carcinoma

P. Beddy, E. Genega, L. Ngo, N. Hindman, J. Wei, A. Bullock, R.S. Bhatt, M.B. Atkins, I. Pedrosa; *Boston, MA/US (pbeddy@eircom.net)*

Purpose: The aim of this study was to correlate the MR imaging features of clear cell renal cell carcinoma (ccRCC) with the pathological appearance and to assess if the MR imaging features correlate with disease progression.

Methods and Materials: Initial staging MRIs of patients with ccRCC were retrospectively assessed by two radiologists for the presence of tumour necrosis, cystic degeneration, intravoxel fat, haemorrhage, retroperitoneal collateral vessels and renal vein thrombosis. Quantitative analysis of the MR imaging for intracellular lipid within the tumours was also performed. These findings were correlated with histopathologic findings of clear cell percentage, growth pattern and time to disease progression.

Results: 76 patients with ccRCC were included, 69 patients had follow-up data available for progression analysis. The presence of tumour necrosis, retroperitoneal collaterals and renal vein thrombosis on MRI were significantly associated with low clear cell percentage for both readers ($p < 0.01$). MRI evidence of necrosis, retroperitoneal collaterals and renal vein thrombosis was associated with disease progression ($p < 0.01$). Multivariable analysis demonstrated that when tumour size, necrosis, retroperitoneal collaterals and renal vein thrombosis were analysed together, necrosis was the only feature that remained statistically associated with disease progression ($p=0.03$, adjusted odds ratio=24.2, CI 95%=1.3-453.8 for reader one and $p=0.02$, adjusted odds ratio=32.2, CI 95%=1.8-569.1 for reader two).

Conclusion: MRI features of ccRCC closely correlate with the percentage of clear cell features in the tumour at histopathology. MRI evidence of necrosis is a poor prognostic indicator irrespective of tumour size and this finding may be useful in guiding therapeutic management.

B-0665 11:24

Diagnostic performance of multi-detector CT for detecting renal sinus invasion in patients with renal cell carcinoma

C. Kim, H. Choi, M.-h. Kim, K.-S. Cho; *Seoul/KR (cherrykim83@dreamwiz.com)*

Purpose: The purpose of our study was to evaluate the accuracy of multidetector CT for detecting renal sinus invasion in the preoperative assessment of patients with renal cell carcinoma.

Methods and Materials: 433 patients with surgically renal cell carcinoma patients who underwent MDCT were included in this study. Contrast-enhanced acquisitions were obtained during arterial, corticomedullary, and nephrographic phase. Image analysis was first performed with only axial CT images. A second analysis was then performed with both axial and coronal CT images. Presence of renal sinus invasion of perirenal fat was evaluated in axial images and combined axial and coronal reformatted images. Histological evaluation has been the diagnostic standard. The value of addition of coronal images to axial images was evaluated by means of receiver operating characteristic (ROC) analysis.

Results: The mean tumour size was 4.9 cm. The sensitivity, specificity, accuracy of axial images and combined images were 85%, 91%, 91% and 81%, 94%, 93%, respectively. The AUCs of ROC analysis were 0.915 for axial images and 0.881 for combined images ($p = 0.237$).

Conclusion: MDCT is accurate in the preoperative evaluation of renal sinus invasion in the patients with renal cell carcinoma, but there was no additional diagnostic value of coronal reformatted image to axial images.

B-0666 11:33

Utility of 3 Tesla diffusion-weighted magnetic resonance (DWMR) imaging for the characterisation of small solid renal tumours

F. Agnello¹, J. Charton², M.-Y. Jeung², G. La Tona¹, M. Galia¹, M. Midiri¹, C. Roy²; ¹Palermo/IT, ²Strasbourg/FR

Purpose: To determine the utility of apparent diffusion coefficients (ADCs) for the characterisation of small solid renal lesions.

Methods and Materials: 26 patients (GFR 30-60 mL/min) with 39 small (1-3 cm) solid renal masses [16 RCCs (10 clear cell types; 6 other types); 18 AMLs (10 fat-containing; 8 minimal-fat) and 5 oncocytomas] were examined on a 3 T system using DW-SS-EPI (b-values 0, 1000 s/mm²). The ADC of the lesions and the ADC of kidney were evaluated. Receiver operator characteristic analysis was performed to evaluate the diagnostic value of ADC for differentiating clear cell RCCs from other type RCCs, AMLs and oncocytomas.

Results: The mean ADC of the lesions [1.22±0.27 28 mm²/sec (0.76-1.96)] was lower than that of kidney [1.85±0.12 mm²/sec (1.38-2.13)] ($p < 0.005$; Mann-Whitney test). The mean ADC was different between RCCs [1.23±0.34 mm²/sec (0.76-1.73)], AMLs [1.07 ± 0.1 mm²/sec (0.85-1.28)] and oncocytomas [1.66±0.28 mm²/sec (1.1-1.96)] ($p < 0.05$, Kruskal-Wallis test). The mean ADC of clear cell RCCs was significantly higher than that of other RCCs [1.46±0.34 mm²/sec (1.04-1.73) vs 0.83 ± 0.34 (0.76-1.01)] ($p < 0.005$; Student t-test). There was no significant difference between mean ADC of fat-containing [1.06 ± 0.48 mm²/sec (0.86-1.28)] and minimal-fat AMLs [1.11 ± 0.33 mm²/sec (1.04-1.22)] ($p=0.46$; Student t-test). The best cut-off ADC value for differentiating clear cell RCCs from other RCCs, AMLs and oncocytomas were 1.5.1.12 and 1.73 mm²/sec, respectively.

Conclusion: DWI is useful to differentiate benign from malignant small solid renal lesions.

B-0667 11:42

Central scar in renal oncocytomas: late contrast enhancement with MR imaging

F. Cornelis, A.-S. Lassere, T. Tournias, C. Deminiere, J.-M. Ferriere, Y. Le Bras, N. Grenier; *Bordeaux/FR (francoiscornelis@hotmail.com)*

Purpose: The purpose of this study was to evaluate the late Gd-enhancement of central area of renal tumours, compatible with fibrous scar or necrosis.

Methods and Materials: This retrospective study was institutional review board approved; informed consent was waived. Based on the thesaurus of our institutional RIS, 63 tumours in 59 patients, imaged with late Gd-enhanced MR sequences between 2006 and 2011 presented with high signal intensity (SI) central area on T2w sequences compatible with central scar. SI was measured in all renal tumours and spleen on in- and opposed-phase images. SI index (SII) and tumour-to-spleen ratio

(TSR) were calculated. Two experienced radiologists visually assessed presence and distribution of late enhancement in central areas (median: 10 mm, SD: 3.7).

Results: Among these 63 tumours, there were 18 oncocytomas in 15 patients were identified presenting with a central scar, 44 renal cell carcinomas (RCC) in 43 patients with a central necrosis, and 1 leiomyoma. Complete late enhancement of the central zone was observed in 13 oncocytomas (72%) and in 7 RCCs (16%) ($p=0.24$). SII and TSR were significantly different ($p=0.005$ and $p=0.002$, respectively) between oncocytoma and RCC groups. Combination of complete enhancement and SII or TSR provided sensitivity of 40% and 50%, specificity of 95% and 97%, positive predictive value of 67% and 53% and negative predictive value of 85% and 88%, respectively.

Conclusion: Central scar of oncocytomas and central necrosis of RCCs may both enhance on late Gd-enhanced MR images. However, a complete enhancement is highly evocative of oncocytoma.

B-0668 11:51

Study of renal iron overload by T2* MRI in a large cohort of thalassemia major patients

E. Grassettonio¹, A. Meloni², G. Restaino³, G. Valeri⁴, L. Natale⁵, G.R. Giugno⁶, M. Lombardi², M. Midiri¹, A. Pepe²; ¹Palermo/IT, ²Pisa/IT, ³Campobasso/IT, ⁴Ancona/IT, ⁵Rome/IT, ⁶Caltagirone/IT (egrassettonio@gmail.com)

Purpose: This study aimed to describe the renal T2* values in patients with thalassemia major (TM), to investigate the correlation between renal and cardiac or hepatic siderosis and biventricular cardiac function.

Methods and Materials: 119 TM patients (58 men, 30.7±8.2 years) underwent MRI. Multiecho T2* sequences were used for iron overload assessment. In the heart segmental and global T2* values were calculated. The liver T2* value was assessed in a single ROI. For each kidney, T2* values were calculated in three different ROIs and were averaged to obtain a representative value for the kidney. The mean T2* value over the kidneys was also calculated. Biventricular morphological and functional parameters were evaluated by cine images.

Results: T2* values in the right kidney were significantly lower than in the left kidney (40.3±11.9 ms vs 44.1±12.7 ms, $P < 0.0001$). The mean T2* value over the kidneys was 42.2±11.9 ms and 40 patients (33.6%) had a pathological value (T2* < 36 ms). Mean renal T2* values increased with age ($r=0.321$, $P < 0.0001$) and were significantly negatively correlated with serum ferritin levels ($r=-0.446$, $P < 0.0001$). Significant positive correlations of the mean T2* values were demonstrated for liver ($r=0.511$, $P < 0.0001$) and global heart ($r=0.262$, $P=0.004$) T2* values. No correlation was found between renal iron overload and bi-ventricular function parameters.

Conclusion: Systemic T2* differences between left and right kidneys were found, with significant lower values in the right one. Mean T2* value increased with age. Renal iron deposition was not very common in TM, but it was correlated with iron deposition in liver and heart.

10:30 - 12:00

Room F2

Breast

SS 1302

Interventional procedures

Moderators:

S. Allen; *Sutton/UK*

M. Álvarez-Benito; *Córdoba/ES*

B-0669 10:30

Multicentre cooperative study of the effectiveness of fine needle aspiration cytology (FNAC) of axillary lymph nodes under sonographic guidance in the pre-treatment management of breast cancer patients: results after 792 consecutive cancer cases

P. Palana¹, J. del Riego¹, M. Villajos¹, M. Teixido², M. Vilagrà³, M. Diaz-Ruiz⁴, L. Canales⁵, J. Ribe⁶, M. Sentsis¹; ¹Sabadell/ES, ²Terrasa/ES, ³Granollers/ES, ⁴Manresa/ES, ⁵Terrassa/ES, ⁶Vic/ES (ppalana@tauli.cat)

Purpose: To determine the sensitivity of FNAC in a consecutive series of patients with breast cancer. To evaluate the sensitivity of FNAC broken down by tumour size, volume and phenotype. To propose recommendations for the use of FNAC in this clinical setting.

Methods and Materials: From April 2010 to June 2011, we studied 792 patients with breast cancer using a protocol for lymph node evaluation. FNAC was performed on lymph nodes with morphologic changes according to the Bedi classification or, when lymph node appeared normal, on the node closest to the index tumour.

Patients were stratified according to the final nodal staging obtained by axillary dissection or sentinel node biopsy, histology, tumour phenotype and prognostic factors.

Results: FNAC was positive in 27% and sentinel node biopsy was avoided in all these cases. The prevalence of lymph node metastases in the series was 44.7%. The sensitivity of FNAC was 54% and the specificity was 100%. The odds ratio was 45% (0.8) and the pre-test negative likelihood ratio was 0.46 (95% CI, 0.40-0.52). In tumours < 10 mm in size or 524 mm³ in volume, only 2.1% of cases were positive. Triple-negative cancers had a high percentage of positive lymph node (52%) regardless of tumour size.

Conclusion: The sensitivity of FNAC is lower than previously reported. Triple-negative cancers had a high prevalence of lymph node impairment regardless of tumour size. FNAC has low specificity and can be avoided when: tumour size < 10 mm or tumour volume < 524 mm³ unspecific lymph nodes non-triple negative cancer.

B-0670 10:39

Staging the axilla with ultrasound and biopsy: maximising diagnostic yield whilst minimising unnecessary biopsy

K.A. Taylor, M.G. Wallis, J. Foreman, P.D. Britton; *Cambridge/UK* (*kathryn.taylor@addenbrookes.nhs.uk*)

Purpose: The use of ultrasound-guided needle biopsy of axillary lymph nodes in breast cancer can avoid unnecessary sentinel lymph node biopsy in node positive patients. We wished to establish a practical protocol for axillary node biopsy in a busy clinical setting that maximised diagnostic yield whilst minimising unnecessary biopsy.

Methods and Materials: Based upon a previously published study from this institution the axillary node biopsy criteria for patients with suspected breast cancer were determined. Axillary and breast core biopsies (CB) were performed in the same clinic session by any one of 8 practitioners. This protocol was undertaken throughout 2008-2010 and its effectiveness evaluated.

Results: 595 invasive cancers presented during the study period of which 251 (42%) were lymph node positive at surgical histology. CB was performed in 130 (22%) of patients. 85% of malignant nodes with TS diameter >or = 10 mm were malignant at CB. 87% of nodes with a cortex > or = 4 mm were malignant at CB. 92% of nodes with an absent hilum were malignant at CB and 77% of nodes with a lobulated cortex were malignant at CB. Overall pre-operative diagnosis of axillary metastases was 44%.

Conclusion: The suggested biopsy protocol can be successfully implemented into a busy clinical setting undertaken by a number of practitioners. Adoption of such a protocol enabled over 40% of patients with lymph node metastases to be diagnosed pre-operatively whilst minimising the number of unnecessary biopsies.

B-0671 10:48

Pre-operative staging of the axilla: UK audit of screen detected breast cancer 2008/9 and 2009/10

M.G. Wallis¹, S. Cheung², P.D. Britton¹, O. Kearins²; ¹Cambridge/UK, ²Birmingham/UK (*matthew.wallis@addenbrookes.nhs.uk*)

Purpose: Axillary nodal status is still the most powerful predictor of breast cancer survival. The introduction of sentinel lymph node biopsy has resulted in repeat operations for definitive treatment. We report the first nationally based screening audit of pre-operative staging with ultrasound and needle biopsy.

Methods and Materials: Data on axillary staging were first included in the annual United Kingdom audit of screen-detected cancers in 2008/09 and repeated in 2009/10. Scotland is unable to provide data and Wales only provided data for 2009/10.

Results: Of the 26,299 surgically treated invasive breast cancers, 5,720 (22%) were node positive. In 2008/9 there was an axillary ultrasound record for 49% of invasive cancers, this rose to 59% in 2009/10. Of the 2,054 abnormal ultrasound records, 1,758 (85.6%) underwent axillary biopsy. Of the 2,956 node positive patients with an ultrasound record, 610 (20.6%) were correctly staged pre-operatively. In 2008/9, 259 (11%) of women confirmed to be node positive at surgery were correctly staged pre-operatively, avoiding a repeat operation, rising to 401 (16%) in 2009/10. In the original data 40 false positive needle biopsies were reported. Individual records were available for 39 patients. Data entry errors accounted for 31 cases with 8 true false positives (6 cytology and 2 core biopsy).

Conclusion: Data entry and completeness have improved but require further improvement. Our rate of successful staging is equivalent to published data when the underlying rate of node positivity is taken into account. Care needs to be taken in interpreting cytology from the axilla.

B-0672 10:57

Management of flat epithelial atypia diagnosed at vacuum-assisted breast biopsy performed on suspicious microcalcifications.

Comparison between 9G and 11G devices

A. Villa¹, F. Chiesa¹, I. Rosenberg¹, M. Calabrese²; ¹La Spezia/IT, ²Genoa/IT (*chiesa.fabio@gmail.com*)

Purpose: We intended to establish if women with diagnosis of flat epithelial atypia (FEA) at stereotactic vacuum-assisted breast biopsy (VABB) without residual microcalcifications could be managed with mammographic follow-up (FU) instead of surgery, and whether better results could be achieved with 9G device compared with 11G.

Methods and Materials: VABB performed in two breast units in the same metropolitan area were reviewed. From October 2003 to January 2011, 121 FEA were found, 57 in centre 1 with 9G device and 64 in centre 2 with 11G. Patients were sub-grouped in those without (group A) and with (group B) residual microcalcifications. The underestimations rate (UR) of malignancy for each group and the proportion of group A patients were compared between the two centres.

Results: The UR of FEA was 3.5% (2/57) with 9G (centre 1) and 8% (5/64) with 11 G (centre 2). For patients considered as a whole, the UR of group A was 0% (0/85), the UR for group B was 19% (7/36) (p < 0.05). In centre 1 the UR for group A was 0% (0/46), the UR for group B was 18% (2/11). In centre 2 the UR for group A was 0% (0/39), the UR for group B was 16% (5/25); the proportion of patients in group A was 80% (46/57) in centre 1 and 60% (39/64) in centre 2 (p < 0.05).

Conclusion: Women with FEA without residual microcalcifications could be managed with mammographic FU. 9G VABB is associated with a lower prevalence of residual microcalcifications compared to 11G.

B-0673 11:06

Accuracy of minimal invasive breast biopsy in an incipient screening program: analysis of 2477 consecutive percutaneous interventions

S.H. Heywang-Koebrunner, J. Naehrig, H. Hfler, A. Hacker, S. Sedlacek, N. Hintermeier; *Munich/DE* (*HEYWANGKOE@aol.com*)

Purpose: To countercheck correlation of PPV and tumour stage with lesion type and biopsy method in 2477 consecutive minimal invasive biopsies.

Methods and Materials: 2477 (1425 US-guided core needle biopsies=US-CNB, 68 stereotactic cores needle biopsies=MX-CNB, 984 stereotactic vacuum-assisted biopsies = MX-VAB) were prospectively documented in a country-wide screening-RIS-database. Evaluation after 1.5-2.5 years follow-up and cancer registry matching.

Results: PPV clearly correlated with lesion type (70% for architectural distortion, 58% for mass w/wo microcalcifications, 33% for microcalcifications only, 26.7% for (focal) asymmetries. The PPV was highest for US-guided CNB (62%), followed by MX-guided CNB (35%) and VABB (29%). The earliest stages were detected by VABB (52% DCIS, 16% T1a, 13% T1b), followed by MX-CNB (38% DCIS, 9.5% T1a, 28.6% T1b) and by US-CNB (3% DCIS, 4% T1a, 26% T1b).

Conclusion: Different lesions are examined by the available imaging methods. Detection of very early malignancy is associated with a lower PPV. We thank all interventionalists for their cooperation with this evaluation supported by Ethicon, Norderstedt.

B-0674 11:15

Is image-guided biopsy always necessary in women under 30 years with solid, palpable breast masses?

A.E. Corr, D.M. Duke, N. Hambly, J.D. Cunningham; *Dublin/IE* (*alicorr@rcsi.ie*)

Purpose: To evaluate the need for percutaneous needle biopsy in women < 30 yrs with symptomatic breast lesions.

Methods and Materials: According to our current protocols solid palpable breast masses are biopsied under image-guidance irrespective of patient age. We reviewed all core needle biopsies over a four-year period in a symptomatic breast service. 2097 patients (F:M 2087:10) underwent image-guided biopsy in this period. 417 of whom (all female) were < 30 yrs. 391/417 (94%) were categorised BI-RADS 3/4a, 26/417 (6%) were categorised BI-RADS 4b and above. Imaging, pathological findings and decisions from multi-disciplinary meetings were examined.

Results: All biopsies were performed under ultrasound-guidance, with 14G tru-cut core needles. Costs, excluding medical man hours for an ultrasound-guided breast biopsy in our institution is €58 with a further €140 for pathological processing of specimen. Pathological results of the 391 patients scored as BI-RADS 3 or 4a, < 30 yrs of age, included fibroadenoma 317/391 (81%), other benign findings 71/391 (18.3%), invasive carcinoma 0/391 (0%), DCIS 0/391 (0%). In 3/391 (0.7%) findings suggested likely fibroadenoma but could not exclude phyllodes. All 3 underwent surgical excision where the final pathology demonstrated fibroadenoma

only. 63/391 (17%) underwent surgical excision post-biopsy, as a result of patient or surgical preference, with all lesions benign on excision. The negative predictive value of ultrasound assessment and BI-RADS categorisation of symptomatic breast lesions in a population under 30 yrs of age was 100%.

Conclusion: In experienced hands US combined with BI-RADS scoring of palpable breast lesions safely predicts women < 30 yrs not requiring percutaneous biopsy with significant financial savings.

B-0675 11:24

Incidence of cancer in consecutive negative core needle breast biopsy cases submitted to surgery

R.M. Trimboli¹, E. Gombos², D. Sippo², I. Fernandez², S. Raza²; ¹Milan/IT, ²Boston, MA/US (trimboli.rm@gmail.com)

Purpose: To evaluate the incidence of cancer in consecutive negative core needle breast biopsy cases submitted to surgery.

Methods and Materials: We reviewed consecutive 518 patients with negative core needle biopsies performed under stereotactic mammographic or ultrasound guidance that underwent subsequent surgery during a period between January 1, 2005 and March 15, 2009. Indications for surgery were: high-risk/borderline pathologic result (HR), radiologic-pathologic discordance (RPD), pathologist's recommendation (PR), fibroepithelial lesion (FEL), or patient's preference (PP). The incidence of cancer in the pathology of surgical excisions was calculated for each group and overall. Chi-square test was used to compare groups with and without cancer at excision.

Results: Final pathologic assessment revealed an overall incidence of 72/518 (14%) malignancy. In particular, there were 71/354 (17%) cancers in the HR group, 9/95 (9%) in the RPD group, 2/26 (8%) in the PR group, 0/21 (0%) in the FEL group, and 0/22 (0%) in the PP group. Significant difference was found between HR, RPD, PR groups (8-17% cancer incidence) and FEL and PP groups (0% cancer incidence) (p=0.006).

Conclusion: A non-negligible cancer incidence (14%) was found among negative core needle biopsies submitted for surgery. Sub-group analysis of indications for surgery showed that the cancer incidence was null for the patient's preference and fibroepithelial lesions groups, and moderate (8-17%) for the high risk lesion, radiologic-pathologic discordance and pathologist recommendation groups. Therefore, these latter three indications should prompt surgical excision.

B-0676 11:33

US-guided 14G core needle biopsy of breast masses categorised as BI-RADS 3, 4 and 5: can the radiologist predict the adequacy of tissue sampling?

V. Londero, E. Di Gaetano, C. Zuiani, G. Graziani, C. Di Loreto, M. Bazzocchi; Udine/IT (londero.viviana@aoud.sanita.fvg.it)

Purpose: To investigate whether radiologist can predict the 'probably diagnostic' core sample on the basis of gross appearance when performing US-guided 14 g core-needle-biopsy (US-CNB).

Methods and Materials: In a prospective study, 303 consecutive US-CNBs were performed on BI-RADS category 3.4 and 5 breast masses in 283 women. A mean of five core samples per lesion (range 3-7) were obtained and the first specimen showing dense material was predicted to be diagnostic and was analysed separately. This was compared with the final histological diagnosis. Positive predictive values (PPVs) of the 'probably diagnostic' core sample were calculated.

Results: Diagnostic material representative of the lesion was obtained with the dense specimens in 285 (94%) of the 303 lesions. PPVs of dense core samples was 29/29 (100%; 95% confidence interval [CI] 88%-100%) for B1, 127/132 (96%; 95% CI 91%-99%) for B2, 15/21 (71%; 95% CI 48%-89%) for B3 and 114/121 (94%; 95% CI 88%-98%) for B5 lesions. The remaining 18 (6%) specimens containing dense but nondiagnostic material showed focal fibrosis and had missed the lesions (4% of benign, 29% of B3 and 6% of malignant lesions). 1 (5%) of 21 B3 lesions and 4 (3%) of 121 malignant lesions were diagnosed only in the dense specimen.

Conclusion: At the time of US-CNBs of breast masses, the gross appearance of core specimens helped us: 1) predict the adequacy of tissue sampling; 2) determine the number of core samples needed for a reliable diagnosis.

B-0677 11:42

Stereotactically guided vacuum assisted breast biopsy: diagnostic reliability and complication rate

S. Kapsimalakou, A. Waldmann, A. Katalinic, I. Grande-Nagel, A. Kovacs, P. Hunold, S. Hollmann, J. Barkhausen, F.M. Vogt; Luebeck/DE (Smaragda.Kapsimalakou@uk-sh.de)

Purpose: The use of large core stereotactically guided vacuum-assisted biopsy (VAB) has shown multiple advantages over core needle biopsy. Purpose of this study is to evaluate the accuracy as well as the complications of VAB.

Methods and Materials: 415 VABs were performed on patients with microcalcifications detected on mammogram and rated as intermediate to suspicious (BI-RADS IV) or highly suspicious (BI-RADS V). VAB was performed according to a strict quality assurance protocol on a digital prone table, using 11- and 8-gauge vacuum probes. Specimen radiographs were obtained, for the detection of presentable microcalcifications.

Results: In 415 women with a mean age of 57 (SD: 11) years, we identified 4.6% invasive carcinomas (19/415), 18% ductal carcinomas in situ (DCIS; 77/415), < 1% atypical ductal hyperplasia (ADH; 3/415) and 2.9% lobular carcinoma in situ (12/415). After 111 surgical interventions, the final result needed an upgrading in 3 patients (3.1%) from ADH to DCIS and in 11 patients (2.7%) from DCIS to invasive carcinoma. However, 10 patients with DCIS after VAB had a benign diagnosis after surgery, indicating that DCIS was completely removed by VAB. Side-effects, such as bleeding occurred in 14.9% (62/415) patients: 11% (36/327) with 11G needle versus 29.5% (26/88) with 8G needle.

Conclusion: VAB is an effective tool for clarification of dignity of microcalcifications seen on mammograms and provides early cancer detection. Side effects were significantly less using 11 G needle for VAB.

B-0678 11:51

Bleeding, haematoma and scar formation after vacuum-biopsy under stereotactic guidance: MammotomeR-system 11G/8G vs ATECR-system 12G/9G

J. Neelsen, J. Biernath-Wuepping, P.J. Schaefer, K. Kroj, B. Order, M. Heller, W. Jonat, F.K.W. Schaefer; Kiel/DE (julianeelsen@yahoo.com)

Purpose: To evaluate the correlation of scar formations after vacuum-assisted biopsy (VAB) with different VAB-systems and needle sizes and peri-interventional bleeding/haematoma.

Methods and Materials: Between 01/2008 and 12/2009, 479 patients underwent VAB under stereotactic-guidance, using the MammotomeR-system with 11/8-gauge and ATECR-system with 12/9-gauge, whereas in 178 cases with representative benign histology no surgical-biopsy after VAB was performed and at least a 2-plane follow-up-mammogram after 6-month post-VAB was available. Bleeding during intervention, haematoma post-intervention and scar-tissue was scored as minimal and moderate/severe. Statistical analysis included Chi-square trend test, p-value < 0.05 was considered to be significant.

Results: Significantly more small/moderate bleedings/post-interventional haematomas for 8-gauge-MammotomeR-system vs 11-gauge-MammotomeR-system (41.9% vs 8.4%, p < 0.001/p=0.029), no significant-differences for the ATECR-systems (26.9% vs 29.9%, p=0.799/p=0.596). 11-gauge-MammotomeR-system vs ATECR-12-gauge-system revealed significantly less bleedings/haematomas (8.4% vs 29.7%, p=0.015/p=0.001), no significant differences for the large-systems (p=0.135/p=0.352). Follow-up of MammotomeR-11/8-gauge-system system has shown 13.1%/16.1% minimal scar formation and 1.2%/3.2% moderate/severe scars, whereas ATECR-12/9-gauge-system has shown 10.8%/3.8% minimal scar formation and 0%/11.5% moderate/severe scars, no significant differences. No significant difference comparing MammotomeR-11/8-g-systems vs ATECR-12/9-g-systems (p=0.609/p=0.823).

Conclusion: Using larger needle sizes significantly (MammotomeR) /not significant for ATECR) more bleedings and post-interventional haematomas were detected, only a tendency concerning scar formation.

10:30 - 12:00

Room G/H

Head and Neck

SS 1308

Lymph nodes and temporal bone

Moderators:
H.P. Burmeister; Jena/DE
S. Robinson; Vienna/AT

B-0679 10:30

Shear wave elastography of cervical lymph nodes: preliminary experience for detection of malignancy

K.S.S. Bhatia, C. Tong, C. Cho, Y. Lee, E. Yuen, J.K. Wong, A.T. Ahuja; Shatin/HK (drkbhatia@cuhk.edu.hk)

Purpose: Shear wave elastography (SWE) is a novel technology that permits real-time display and quantitative estimation of shear modulus, equating to tissue stiffness. A study was conducted to evaluate its potential for discrimination between malignant and benign cervical lymph nodes.

Methods and Materials: SWE was performed in 110 cervical lymph nodes undergoing US-guided needle aspiration for cytology in a routine ultrasound clinic. Shear modulus indices were measured on elastograms and correlated with cytological result.

Results: Shear modulus within the stiffest 2-3 mm diameter circular region within nodes was higher in malignant nodes (n=65, median 27.3kPa, interquartile range 16.2-40.2kPa, range 4.3-210.5kPa) than benign nodes (n=45, median 15.3kPa, interquartile range 11.6-20.3kPa, range 6.6-41.0kPa) (p < 0.0001, Mann Whitney U test). A cut-off of 22.3kPa attained highest average of sensitivity and specificity, with 56.3% sensitivity, 86.4% specificity and 0.75 AUC (95% CI 0.63-0.82). Qualitatively, SWE elastograms of benign nodes appeared homogeneous whereas malignant nodes were either homogeneous or markedly heterogeneous including areas lacking elasticity signal. This study is ongoing and presented data will be updated to evaluate different methods of SWE measurement within nodes, increased total sample size exceeding 200 lymph nodes, and SWE data according to histological subtype.

Conclusion: SWE is feasible for cervical nodes although preliminary data suggest it offers only modest discrimination between malignant and benign nodes. It appears unsuitable for screening of nodal malignancy but may detect a subset of malignant nodes with high specificity. The cause of marked spatial heterogeneity using SWE in some malignant nodes is yet to be determined.

B-0680 10:39

Percutaneous US-guided interstitial laser ablation of metastatic lymph nodes in the neck from papillary thyroid carcinoma following thyroidectomy and lymphadenectomy

G. Mauri¹, L. Cova², T. Ierace², T. Tondolo³, G. Lomuscio², A. Baroli², C.M. Pacella⁴, L. Solbiati²; ¹Milan/IT, ²Busto Arsizio/IT, ³Como/IT, ⁴Rome/IT

Purpose: We report our experience with percutaneous US-guided interstitial laser ablation for metachronous cervical nodal metastases from papillary thyroid carcinoma following total thyroidectomy and central + laterocervical lymph node.

Methods and Materials: Twenty-three metachronous metastatic nodes (mean size 1.2 cm; range 0.6-2.6 cm) in 19 patients were treated. A 1,064 nm Nd:YAG laser (EchoLaser X4, Esaote, Genoa, Italy) was used. All cases were negative at 131I whole body scan, but had positive 18 F-FDG PET and elevated serum levels of thyroglobulin. Under local anaesthesia a 300 mm quartz fiberoptic guide was placed into the node through a 21G needle. Nodes were treated with one (17 cases) or two (6) fibre insertions, each one with 3 W power for 400-600 sec (total energy 1,200-1,800 joules). All cases were followed at 3 and 6 months with B-mode US, CEUS, 18 F-FDG PET and assessment of serum levels of Tg.

Results: Laser ablation was technically feasible and well tolerated in all patients, with no either immediate or late complications. In 21/23 (91.3%) nodes complete ablation (lack of enhancement at CEUS, negative 18 F-FDG PET with normalisation of SUV and > 90% decrease of Tg serum levels) was achieved. In 2 cases residual uptake at 18 F-FDG PET with abnormal SUV was found and laser ablation was repeated.

Conclusion: Percutaneous US-guided interstitial laser ablation seems to be an effective, low cost and safe therapeutic tool for the treatment of metachronous nodal metastases from papillary thyroid carcinoma in the neck which would otherwise require often challenging further resections.

B-0681 10:48

Comparison of the ultrasound findings of biopsy-proven tuberculous lymphadenitis and Kikuchi disease

K. Kim, S.-i. Suh, K. Son, Y. Lee, H. Seo, H. Seol; Seoul/KR (rudals97@hanmail.net)

Purpose: The purpose of this study was to analyse the sonographic features that can contribute in differentiating between tuberculous lymphadenitis and Kikuchi disease.

Methods and Materials: Sonographic findings of 101 patients with biopsy-proven tuberculous lymphadenopathy and 175 patients with biopsy-proven Kikuchi disease were reviewed. Lymph nodes were assessed by their size, shape (shortest/longest axis ratio), location, echogenicity, presence of conglomeration, gross necrosis, calcification, echogenic nodal hilum, increased perinodal echogenicity and vascular pattern.

Results: The mean diameter of the lymph nodes was 2.2 cm for tuberculous lymphadenitis and 1.6 cm for Kikuchi disease. Most tuberculous lymph nodes were located in levels II and V; most Kikuchi disease lymph nodes in levels IV and V. Patients with tuberculous lymphadenitis manifested gross necrosis in 97 (96%) cases and patients with Kikuchi disease in 17 (10%) cases. 97 (96%) lymph nodes showed calcification in patients with tuberculous lymphadenitis, and none showed calcification in patients with Kikuchi disease. Increased perinodal echogenicity was seen in 69% of the tuberculous lymph nodes and 76% of the Kikuchi lymph nodes. Conglomeration of lymph nodes was seen in 62 (61%) of the tuberculous lymphadenitis cases and 5 (3%) of the Kikuchi disease cases. On power Doppler study, normal hilar vascularity was seen in 20 (20%) of the tuberculous lymph nodes and 161 (92%) of the Kikuchi lymph nodes.

Conclusion: Gross necrosis, conglomeration, and normal hilar vascularity on power Doppler study showed a significant difference between the tuberculous lymphadenitis and Kikuchi disease groups (p < 0.005).

B-0682 10:57

Tuberculosis, Kikuchi

C. Park, J. Han, S. Jo, Y. Youn; Cheon-an/KR (parksam-f@hanmail.net)

Purpose: To assess the differential imaging findings of necrotising lymphadenitis in tuberculous lymphadenitis and Kikuchi disease on neck CT, to facilitate the diagnosis the diseases without performing a biopsy.

Methods and Materials: We retrospectively analysed 46 patients (29 women, 17 men, mean age 26.6 years) with Kikuchi disease (group I) and 53 patients (26 women, 27 men, mean age 36.1 years) with tuberculous lymphadenitis (group II), performing neck CT from September 2007 to December 2010. We evaluated sex, age, nodal involvement sites, bilaterality, features and size of necrotic lymph nodes, fat infiltration, nodal distribution, WBC and ESR in all patients, and analysed statistically the differentiations of the imaging findings and blood factors between the two groups using independent Samples T-test for continuous parameters and Chi-square and McNemer tests for categorical parameters.

Results: Lymphadenopathies of group.i. were more common in levels II, III, V (58.7%, 56.5%, 82.6%), compared with those of group II were more common in level IV (49.1%). The incidences of fat infiltration around lymph node (63%), leukocytopenia (30.4%), increased ESR (41.3%) of group.i. were higher than those (9.4%, 5.7%, 17%) of group II. The incidence of irregular thick necrotic lymph node of group.i. (76.2%) was higher than that of group II (27%), but the incidence of regular thin necrotic lymph node of group II (73%) was higher than that of group.i. (23%).

Conclusion: Nodal involvement site, fat infiltration, necrotic nodal feature, WBC and ESR are useful in the differentiation between Kikuchi disease and tuberculous lymphadenitis.

B-0683 11:06

Dual energy CT-derived iodine content and iodine overlay for characterisation of enlarged cervical lymph nodes

A.M. Tawfik¹, N.-E.A. Nour-Eldin², N.N. Naguib², J. Kerl², A.A. Abdel Razek¹, T.J. Vogl²; ¹Mansoura/EG, ²Frankfurt/DE (ahm_m_tawfik@hotmail.com)

Purpose: To evaluate whether dual energy CT (DECT)-derived iodine content and iodine overlay could be used to differentiate between enlarged metastatic and inflammatory cervical lymph nodes.

Methods and Materials: Eighteen patients with enlarged pathologically proved metastatic lymph nodes and 17 patients with enlarged lymph nodes draining deep cervical inflammations underwent contrast-enhanced DECT. Only one enlarged node per patient was identified. DE software was used to reconstruct iodine overlay images. Iodine content and overlay of the pre-identified node was calculated by means of circular regions of interest. Iodine content of muscle and internal jugular

vein were also obtained as control. Iodine content and overlay of metastatic and inflammatory lymph nodes were compared. Receiver operator characteristic (ROC) curve was used to determine sensitivity and specificity of iodine content and iodine overlay for diagnosis of metastatic nodes.

Results: Iodine content was significantly lower for metastatic (2.39 ± 0.41) than inflammatory lymph nodes (3.48 ± 0.63), $p < 0.0001$. Iodine overlay was also significantly lower for metastatic than inflammatory nodes, $p < 0.0001$. No significant differences were observed between iodine content for muscle and internal jugular vein of both groups, $p=0.072$ and 0.716 . ROC curve of iodine content had larger area under the curve (0.948) than that of iodine overlay (0.913) denoting higher diagnostic accuracy in diagnosis of nodal metastases. Optimal threshold value for iodine content ≤ 2.8 to diagnose nodal metastases had 88.2% sensitivity and 100% specificity.

Conclusion: DECT-derived iodine content and overlay might help in characterisation of enlarged cervical lymph nodes.

B-0684 11:15

First experience with tri-exponential analysis of DWI signal attenuation in normal cervical lymphnodes: feasibility study

M. Ravanelli, D. Farina, E. Botturi, A. Marconi, V. Mazza, R. Maroldi; *Brescia/IT (marcoravanelli@hotmail.it)*

Purpose: Bi-exponential model (IVIM) postulates two distinct components influencing the DWI signal attenuation: a very-slow (diffusion) and a fast component (b -values < 200 s/mm²), related to arterial perfusion. When DWI dataset is acquired with b -values > 1000 s/mm², the accuracy of the bi-exponential model decreases. A third component, probably related to slow flows, could explain model inaccuracy. The study purpose is to assess the feasibility of tri-exponential analysis of DWI signal decay in cervical lymphnodes.

Methods and Materials: Four healthy volunteers had the neck examined by 1.5 T MR using EPI-DWI sequences with 13 b -values (0-2500s/mm²). The DWI signal attenuation of 13 cervical lymphnodes was analysed by mono-exponential (ADC), bi-exponential (IVIM) and the hypothesised tri-exponential model. This model extracts three parameters: fast-perfusion-fraction ($ffast$), slow-perfusion-fraction ($fslow$) and slow-pseudodiffusion-coefficient (D^*slow). All three analyses were performed on 0-1000s/mm² and 0-2500s/mm² intervals; mono- and bi-exponential analyses were also performed on 500-2500s/mm² interval. Accuracy of fitting was measured by R2 coefficient.

Results: The bi-exponential model fitted 500-2500 s/mm² DWI signals better than the mono-exponential model (R2 0.996vs0.982). In the 0-2500 s/mm² interval, the tri-exponential analysis was superior to bi-exponential (R2 0.998 vs 0.992). Tri-exponential parameters in this interval were: $ffast$ (0-2500) $7 \pm 2\%$, $fslow$ (0-2500) $53.9 \pm 0.8\%$, D^*slow $1.05 \pm 0.13 \times 10^{-3}$ mm²/s. The perfusion fraction extracted by bi-exponential model in the 500-2500s/mm² interval ($f500-2500$) and $fslow$ (0-2500) showed high positive correlation (r 0.96).

Conclusion: Tri-exponential analysis of lymphnodes DWI signals is feasible and accurate using very high b -values. It could provide new parameters (probably linked to venular and lymphatic flow) potentially valuable in the characterisation of the tissues microstructure and functionality.

B-0685 11:24

Comparative study of MDCT and CBCT of the temporal bone: anatomy-otosclerosis-superior semicircular canal dehiscence, early experience and preliminary results

D. Volders¹, N. Peters¹, B. De Foer², K. Bacher³, J.W. Casselman¹; ¹Bruges/BE, ²Antwerp/BE, ³Gent/BE (david.volders@azzintjan.be)

Purpose: Multidetector CT (MDCT) is the current standard for radiologic examination of the temporal bone. This study wanted to verify the non-inferiority or superiority of conebeam CT (CBCT) over MDCT in the temporal bone for detecting anatomical structures, otosclerosis and superior semicircular canal dehiscence (SSCD).

Methods and Materials: Patients (100 patients - enrolment in progress) in three centres were prospectively studied, after informed consent and ethical committee approval. Both CBCT and MDCT, with a spatial resolution of, respectively, 0.125 and 0.23 mm, were performed in every patient. Two readers scored 28 small anatomical structures (score 1-5), otosclerosis stage (score 1-6) and SSCD (score 1-3) in a blinded randomised manner.

Results: Preliminary results showed that CBCT has an overall superiority for the visualisation of every anatomical structure in the axial and coronal plane of the temporal bone, most significant in the coronal plane. CBCT corrected a false negative diagnose of MDCT for otosclerosis in 12.5% (3 out of 24 cases) and a false positive diagnose of MDCT for SSCD in 25% (6 out of 24 cases). The average radiation dose (CTDIvol) of CBCT and MDCT was, respectively, 26.84 mGy and 56.05 mGy.

Conclusion: CBCT allows studying the temporal bone anatomy in more detail. Moreover, the sensitivity to detect otosclerosis and especially the specificity to detect SSCD is higher compared to MDCT. The average radiation dose of an examination of the temporal bone with CBCT is less than half the dose of an examination with MDCT, making it the technique of choice.

B-0686 11:33

Prevalence of anterior internal auditory canal "diverticulum" on CT in patients with otosclerosis

M.C. Hoeberigs, J.J. Waterval, R.J. Stokroos, A.A.R. Stadler; *Maastricht/NL (christiannehoebe@gmail.com)*

Purpose: In patients with otosclerosis an otosclerotic hypodense cavitating plaque at the medial margin of the otic capsule, seen as an indentation or "diverticulum" of the anterior margin of the internal auditory canal (IAC), might be present. We aimed to determine the prevalence of this easily identifiable anterior IAC indentation on CT in patients with otosclerosis.

Methods and Materials: 222 consecutive high-resolution CT scans (0.4-0.6 mm) of the mastoid bone in patients with conductive or mixed hearing loss from January 2008 to December 2010 were retrospectively reviewed by 2 neuroradiologists and 1 ENT surgeon. A total of 444 ears were scored for the presence and severity of otosclerosis (graded according to the Symons/Fanning classification: 1 fenestral; 2 patchy pericochlear; 3 extensive pericochlear) and for the presence of anterior IAC diverticulum/plaque (defined as an obvious notch in the anterior IAC margine, isodense to the IAC itself; a faint curvature of the wall was scored negative).

Results: Anterior IAC diverticulum was observed in 9/92 ears (10%) with only fenestral otosclerosis; in 9/35 (25%) of grade 2 patchy cochlear otosclerosis and in 14/20 (70%) with grade 3 otosclerosis. Only 1 patient without CT-signs of otosclerosis, but with clinical stapedial fixation, demonstrated bilateral IAC hypodensity (2/297 ears or 0.6%).

Conclusion: Evaluation of the anterior IAC might aid in the detection of not only cochlear but also in the more subtle fenestral otosclerosis.

B-0687 11:42

Improved in vivo visualisation and evaluation of endolymphatic hydrops using high-field MRI in Menier's disease and correlation with audiovestibular function

W.H. Flatz, R. Guerkov, B.B. Ertl-Wagner, O. Dietrich, M.F. Reiser; *Munich/DE (wilhelm.flatz@med.uni-muenchen.de)*

Purpose: To improve detection and evaluation of endolymphatic hydrops in Meniere's disease in vivo using MRI and to determine whether the degree of endolymphatic hydrops as it is detected in vivo in patients with definite Meniere's disease correlates with audiovestibular functions.

Methods and Materials: 37 patients suffering from clinical symptoms of Meniere's disease according to AAO-HNS criteria were examined in a prospective study. Diluted gadolinium was administered intratympanically 24 hours prior to the MR-scan. MRI was performed using a 3 T-scanner using a dedicated 8-channel surface-coil and a head-coil acquiring a 3D-FLAIR sequence, a 3D-IR TSE sequence and a high-resolution True-FISP dual excitation sequence (CISS). Correlation with clinical symptoms and audiovestibular function testing was performed using audiometric hearing tests, caloric stimulation, electrocochleography (ECoChG) and vestibular-evoked myogenic potentials (VEMP).

Results: There was a significant correlation between the degree of hydrops, on the one hand, and the averaged hearing level at 0.25-1 and 0.5-3 kHz and the vestibular evoked myogenic potential interaural amplitude ratio, on the other hand. A trend towards a correlation was noticed between the hydrops and the caloric response, no correlation was noticed between the hydrops and the SP/AP ratio. The degree of endolymphatic hydrops correlates with a progressive loss of auditory and sacculus function in patients with Meniere's disease.

Conclusion: The degree of endolymphatic hydrops in patients with definite Meniere's disease, as it is detected by in vivo MRI imaging, correlates with a loss of audiovestibular function. This underlines the usefulness of this technique in the evaluation of Meniere's disease.

B-0688 11:51

Middle ear cholesteatoma: compared diagnostic values of incremental MRI protocols including non-echo-planar diffusion-weighted imaging performed on 3 T and 1.5 T scanners

J. Lincot¹, S. Riehm², N. Babay², J.-F. Matern², N. Meyer², F. Veillon²; ¹Paris/FR, ²Strasbourg/FR (julienlincot@gmail.com)

Purpose: To evaluate diagnostic values of incremental MRI protocols performed on 3 T and 1.5 T scanners.

Methods and Materials: Retrospective study conducted on a cohort of 53 patients suspected with acquired or residual/recurrent cholesteatoma. All patients underwent 3 T and 1.5 T non-EP DWI and 39/53 patients had additional unenhanced T1-, delayed gadolinium-enhanced T1- and high-resolution T2-weighted standard acquisitions. On the basis of initial clinical and imaging findings, patients whether benefited from tympanoplasty or from a strict otoscopic survey. Imaging, surgical and follow-up findings concluded to a total of 55 middle ear lesions including 28 cholesteatomas. For each case 4 radiologists reviewed 3 incremental MRI protocols differing on the magnetic field of the DWI acquisitions interpreted (3 T, 1.5 T, 3T+1.5 T) and comprising the three non-DW ordained standard sequences. At each step diagnostic performances were expressed as sensibility, specificity, positive and negative predictive values and accuracy. Univariate and multivariate analyses assessed reader, sequence adding and magnetic field effect upon diagnostic performances. Cholesteatomas' ADC values and DWI signals were compared according to magnetic field using paired t and binomial tests.

Results: Univariate and multivariate analyses concluded to no significant reader or sequence adding effect over diagnostic performances obtained by non-EP DWI alone. Univariate analysis showed no significant magnetic field effect either. Cholesteatomas' ADC values and DWI signals did not differ significantly according to magnetic field.

Conclusion: In 3 T and 1.5 T MRI a self-sufficient non-EP DWI protocol could be employed for cholesteatoma diagnosis. This needs to be confirmed by further studies over a wider and less heterogeneous cohort.

10:30 - 12:00

Room I/K

Abdominal Viscera

SS 1301b
HCC diagnosis

Moderators:

C. Ayuso; Barcelona/ES
A. Furlan; Pittsburgh, PA/US

B-0689 10:30

Hypervascular hepatocellular carcinoma showing hyperintensity on gadoxetic acid-enhanced MR imaging: a less malignant subtype with low production of AFP and PIVKA-II

A. Kitao, N. Matsui, N. Yoneda, K. Kozaka, S. Kobayashi, W. Koda, T. Gabata, Y. Nakanuma, S. Kaneko; Kanazawa/JP (azusa@med.kanazawa-u.ac.jp)

Purpose: To analyse the correlation between tumour markers production, histological features and signal intensity on the hepatobiliary phase of gadoxetic acid enhanced MR imaging in hepatocellular carcinomas (HCCs).

Methods and Materials: Surgically resected or biopsy diagnosed 178 hypervascular HCCs were classified as hypointense HCCs (n=146) or hyperintense HCCs (n=32) compared to the background liver on the hepatobiliary phase of gadoxetic acid-enhanced MR imaging. We analysed the alpha fetoprotein (AFP) and protein induced by vitamin K absence or antagonist-II (PIVKA-II) production by serum analysis and immunohistochemical staining, then compared between hypointense HCCs and hyperintense HCCs. We also analysed the pathological features such as macro growth pattern, differentiation grade, vessel invasion and intrahepatic metastasis. Statistical analyses were performed in each result.

Results: The serum levels of tumour markers were lower in hyperintense HCCs than in hypointense HCCs. The average value of AFP was 19.2 ng/ml to 1160.0 ng/ml (P=0.0007), AFP-L3 fraction 3.5% to 14.3% (P=0.0015) and PIVKA-II 90.1 mAU/ml to 170 mAU/ml (P=0.0017). The immunohistochemical AFP and PIVKA-II expressions were also decreased in hyperintense HCCs compared to that of hypointense HCCs (P < 0.0001 and P=0.009). Pathologically, the grade of differentiation was higher (P=0.0063) and the portal vein invasion was fewer in hyperintense HCCs than in hypointense HCCs (31.9% vs 11.1%, P=0.035).

Conclusion: The tumour markers production was repressed in hyperintense HCCs on gadoxetic acid-enhanced MR imaging with high grade of differentiation and few portal vein invasions. It indicated that hyperintense HCCs would be classified into a less malignant subtype than that of hypointense HCCs.

B-0690 10:39

Comparison of contrast-enhanced US to 64-row multidetector CT and MR with Gd-BOPTA in the depiction of diagnostic vascularity pattern in hepatocellular carcinoma nodules ≤ 2 cm in diameter

E. Quaia, L. De Paoli, S. Pulvirenti, B. Cabibbo, M. Cova; Trieste/IT (quaia@units.it)

Purpose: To assess contrast-enhanced US (CEUS) in the depiction of the hepatocellular carcinoma (HCC) diagnostic vascularity pattern (hypervascularity during arterial phase followed by hypovascularity during portal venous-late phase) in small HCC nodules (≤2 cm) in comparison to contrast-enhanced 64-row multidetector CT and MR imaging with Gd-BOPTA.

Methods and Materials: One hundred-and-twenty cirrhotic patients (68 males, 52 females; mean age±SD, 70±7 years) with 131 small HCCs were included. Each nodule was scanned by CEUS after sulphur hexafluoride-filled microbubble, multiphase contrast-enhanced 64-row multidetector CT, and contrast-enhanced MR imaging after Gd-BOPTA injection (15-25 days from CEUS and CT). Nodule vascularity at CEUS, CT, and MR imaging was evaluated side-by-side by 2 independent blinded readers.

Results: CEUS vs CT did not differ in the depiction of hypervascularity followed by hypovascularity (reader 1 vs 2, CEUS=57/131 vs 56/131; CT=60/131 vs 59/131 nodules; P>0.05, Wilcoxon test) with high inter-reader agreement (k statistics, .89 for CEUS and .91 for CT), while MR imaging revealed this pattern in 85/131 nodules for both readers (P < 0.05). Other vascularity patterns included hypervascularity followed by isovascularity (reader 1 vs 2, CEUS=58/131 vs 58/131; CT=58/131 vs 50/131; MR=25/131 nodules for both readers), isovascularity followed by hypovascularity (reader 1 vs 2, CEUS=14/131 vs 15/131; CT=11/131 vs 20/131; MR=14/131 nodules), and persistent hypovascularity (CEUS=2/131, CT=2/131, and MR=7/131 nodules for both readers).

Conclusion: CEUS did not differ from multiphase contrast-enhanced 64-row multidetector CT in the depiction of diagnostic vascularity pattern in small HCCs, while MR imaging with Gd-BOPTA revealed this pattern in an higher number of nodules.

B-0691 10:48

Spectral CT of hypervascular liver lesions in patients with HCC: investigation of image quality and sensitivity

P. Lv¹, X. Lin², K. Chen², J. Gao¹, Y. Shen³; ¹Zhengzhou/CN, ²Shanghai/CN, ³Beijing/CN

Purpose: To investigate monochromatic imaging from spectral CT of hypervascular liver lesions in patients with HCC.

Methods and Materials: Twenty-three patients with small hepatocellular carcinomas underwent Spectral CT scanning during the late arterial phase (AP) and portal venous phase (PP). Both conventional 120 kVp polychromatic images (protocol A) and a set of monochromatic images with energy level ranging from 40keV to 140keV with 10keV increments (protocol B) were reconstructed. Image noise for normal liver or tissue was measured and the contrast-to-noise ratio (CNR) for tumours was calculated for both protocols. The highest CNR and the lowest image noise were chosen from protocol B and compared with protocol A with Student t test (SPSS 13).

Results: The highest CNR from monochromatic images distributed at 40keV (38.46%), 50keV (26.92%) and 70keV (69.23%) energy levels for AP and 40keV (30.77%) and 70keV (69.23%) for PP. The CNR values from the optimal monochromatic images for AP (3.44±2.00) and PP (2.15±2.33) were significantly higher than those from the protocol A (1.49±0.81 and 1.52±1.81 for AP and PP, respectively) (p < 0.02). In addition, the lowest image noises in the protocol B during the two phases occurred at 70keV (AP: 100%?PP: 93.33%), lower than those in protocol A.

Conclusion: The optimal monochromatic energy level of spectral imaging can increase the sensitivity in detecting hypervascular liver lesions without image quality loss.

B-0692 10:57

HCC wash-out at contrast-enhanced ultrasonography (CEUS): isoechoogenicity or hypoechoogenicity? A comparison with MDCT

P. Rizzardi, M. Ravanelli, L. Sottocornola, A. Giardini, R. Maroldi, P. Cabassa; Brescia/IT (jam.91@virgilio.it)

Purpose: To compare the pattern of enhancement of HCC at CEUS and MDCT, focusing on the CEUS wash-out features.

Methods and Materials: One-hundred and twenty-three patients affected by HCC underwent CEUS and subsequent MDCT within 1 month. The HCC diagnosis was based on histology in 73/123 patients (31/73 surgery, 42/73 biopsy), on imaging in 50/123 patients. In the case of multifocal disease, one target-lesion for each patient was evaluated. CEUS was performed using Sonovue (Bracco Imaging, Milano,

Italy). The echogenicity of HCC compared to liver parenchyma was assessed in three phases: arterial (15-30s), portal (70-90s) and late (120s). The results were compared with those from multiphase MDCT and matched with histological grade, when available. Typical pattern (TP) was defined as: arterial iper-echogenicity/density associated with portal and late ipo-echogenicity/density.

Results: At CEUS, only 39% of HCC (48/123) showed a TP; 55%(67/123) were isoechoic in the portal phase and 60% of these (40/67) showed isoechoogenicity also in the late phase. Conversely, a TP was demonstrated in 92% of HCC (113/123) at MDCT. Multivariate analysis including several nodule- and patient-related characteristics showed that only histological grade influenced vascularisation pattern at CEUS: well-differentiated HCC were more likely to show a slow or absent wash-out at 120s.

Conclusion: HCC shows different enhancement pattern at CEUS and MDCT. The presence of isoechoogenicity in the portal or both portal and late phase is prevalent in well-differentiated lesions. For this reason, the association of CEUS to MDCT could provide adjunctive information in the characterisation of hypervascular HCC nodules.

B-0693 11:06

Dynamic CT perfusion technique in the evaluation of neoangiogenesis tumour-related phenomenon in diagnosis and treatment of HCC lesion in cirrhotic patients

D. Ippolito, P. Bonaffini, C. Capraro, F. Meloni, R. Corso, S. Sironi; *Monza/IT (davide.atena@tiscalinet.it)*

Purpose: To determine the value of perfusion computed tomography (CT-p) in the quantitative assessment of tumour-related neoangiogenesis for the evaluation of diagnosis and treatment of HCC lesions.

Methods and Materials: A total of 97 CT-p study were performed in cirrhotic patients by analysing 56 biopsy-proven HCC lesions and 41 HCC-treated lesion with TACE or RFA. Dynamic study was performed on 16 multidetectorCT (Brilliance 16, Philips, NL) by acquiring 8 dynamic slices/scan for a total of 40 scans, at fixed table position, during injection of 50 ml of non-ionic contrast agent at flow rate of 6 ml/sec. A dedicated perfusion software which generated a quantitative map of arterial and portal perfusion by means of colour scale was employed. The following perfusion parameters for the whole liver and HCC lesions were considered: hepatic perfusion (HP), arterial perfusion (AP), blood volume (BV), hepatic perfusion index (HPI) and time to peak (TTP).

Results: In HCCs lesions evaluated, the following quantitative data were obtained: HP (ml/sec/100 gr) 47.0±13.8; BV (ml/100 mg) 22.5±4.6; AP (ml/min) 42.9±8.7; HPI (%) 75.3±31.3; TTP (sec) 18.7±4.1. The perfusion values calculated in lesions correctly treated were: HP (ml/sec/100 gr) 13.6±5.6; BV (ml/100 mg) 6.8±4.8; AP (ml/min) 13.1±7; HPI (%) 13.6±9.2 and TTP (sec) 29±16.1; while in partially or incompletely treated lesions were: HP (ml/100 gr/sec) 32.5±15; BV (ml/100 gr) 17.6±9.5; AP (ml/min) 38.4±8.8; TTP (sec) 19±5.7; HPI (%) 61.3±32.7. A statistical difference was obtained for all the perfusion parameters evaluated with a significant lower (p < 0.001) values in correctly treated lesion or in surrounding parenchyma than in viable HCC tissue, in relation to the presence of arterial structures that develop in viable neoplastic tissue.

Conclusion: Our results suggest that CT-p technique can help in non-invasive quantification of tumour blood supply, related to the formation of new arterial structures (neoangiogenesis), which are essential for tumour growth, allowing also the assessment of therapeutic response.

B-0694 11:15

Can contrast-enhanced MRI differentiate malignant from benign hepatocellular tumour in the non-cirrhotic liver?

M.A.F. Fischer, D.A. Raptis, O.F. Donati, S. Breitenstein, P.-A. Clavien, H. Alkadhhi, M.A. Patak; *Zurich/CH (michaelalexander.fischer@usz.ch)*

Purpose: To retrospectively evaluate whether MR imaging findings can be used to differentiate hepatocellular-carcinoma (HCC) from hepatocellular-adenoma (HA) and atypical focal-nodular-hyperplasia (FNH) in non-cirrhotic patients.

Methods and Material: In total, 107 consecutive patients (46 men; 45±14 years), who underwent liver resection for HCC (n=55), HA (n=24) and FNH (n=28) were included in this international-multi-centre study. Preoperative liver-MRI was analysed by two independent radiologists for the following **Imaging Findings:** lesion-diameter, lesion-demarcation; presence of satellite-lesions, central-scar, lesion-capsule, fat, haemorrhage, signal-intensity (SI) on unenhanced T1- and T2-weighted images, arterial-enhancement and contrast-media wash-out. Differences between both readers were resolved in a consensus reading and independent diagnostic parameters for diagnosis of HCC were determined by multivariate analysis.

Results: HCC showed a significant higher frequency (all, p < .01) of a) T1-hypointensity (69.4% vs 30.6%), b) T2-hyperintensity (64.4% vs 35.5%), c) presence of fat (86.7% vs 13.3%), d) satellite-lesions (64.4% vs 35.5%), e) lack of arterial-enhancement (73.1% vs 26.9%) f) contrast-media wash-out in the equilibrium-phase (67.7% vs 32.3%) as compared to both HA and FNH. Significant predictors for diagnosis of HCC (R, odds ratio; p < .05) were T1-hypointensity (R=6.0), presence of satellite-lesions (R=4.9) and contrast-media wash-out (R=3.8).

Conclusion: MR-imaging characteristics in primary non-cirrhotic liver tumours show significant differences. Independent parameters for diagnosis of HCC are T1-hypointensity, presence of satellite-lesions and contrast-media wash-out which might help to differ this entities in the future.

B-0695 11:24

Comparison of prospectively triggered (PT) FLASH with retrospectively self-gated (RSG) FLASH sequences for imaging of experimental liver tumours in rats at 9.4 T

P. Fries, K. Matthes, A. Mueller, G. Denda, A. Massmann, J. Sperling, G. Schneider, A. Buecker, R. Seidel; *Homburg/DE (drpeterfries@googlemail.com)*

Purpose: To compare prospectively triggered FLASH (PT) (using respiratory signals monitored by an external pressure transducer) with retrospectively self-gated FLASH (RSG) sequences (based on a navigator technique / IntraGate, Bruker, Germany) for unenhanced and contrast-enhanced T1w imaging of experimental liver tumours in rats at 9.4 T.

Methods and Materials: 8 rats (WAG-Rij) with experimentally induced hepatic colon cancer metastases were subjected to MRI using a 9.4 T animal scanner (Bruker, BioSpec, Germany) with a 16-channel volume coil. We acquired a PT (TR/TE: 45/2.5, FA=45°, FOV 5x5 cm, matrix=256x256) and a RSG (TR/TE: 45/2.5, FA=45°, FOV 5x5 cm, matrix=256x256, slice thickness: 1 mm each) sequence at identical positions. After intravenous injection of 0.2 mmol/kg BW Gd-DTPA we performed an alternating acquisition of either sequences at four consecutive time points (up to 12 min. after injection). SNR and CNR were calculated based on ROI measurement within the tumour and adjacent normal liver tissue for both sequences. A Wilcoxon-matched pairs signed-rank test and a paired t-test were performed for statistical analysis (p < 0.05).

Results: No statistically significant differences were obtained between the PT and the RSG sequence after CM injection regarding SNR (tumour: RSG (mean±SD): 11.5±6.0 / PT:12.5±2.5, p=0.31), SNR (liver: RSG:7.0±3.0, PT: 7.8±1.1, p=0.5) and the CNR (Tu/liver: RSG: 2.0±2.3, PT: 2.7±1.2, p=0.5).

Conclusion: PT and RSG FLASH sequences provide comparable SNR and CNR of normal liver tissue and experimentally induced liver tumours. Being independent of external trigger devices the retrospectively self-gated approach may be a favourable alternative for abdominal imaging in small rodents.

B-0696 11:33

Single-energy low-voltage arterial phase scanning increases conspicuity of hypervascular lesions of the liver: an intra-patient study

G.A. Zamboni, M.C. Ambrosetti, E. Zivelonghi, R. Pozzi Mucelli; *Verona/IT (gzamboni@hotmail.com)*

Purpose: To compare intra-patient a single-energy low-voltage arterial phase protocol and a 120 kv protocol for detecting hypervascular focal liver lesions (hFLL).

Methods and Materials: 27 patients with chronic liver disease and ≥1 hFLL underwent abdominal MDCT with 80 kV arterial phase (test group) on a 64-row scanner. This was compared to a previous 120 kV scan. The mean interscan interval was 139 days; lesions were not treated between exams. Scans were compared for attenuation and standard deviation in the liver, aorta and largest hFLL, image noise, CNR, CTDI and DLP, (paired t-test). Effective dose was calculated with TLD measurements.

Results: All scans were of diagnostic quality, according to the reporting radiologist. Mean attenuation was significantly higher in the test group than in the control group in the aorta (501.7±148.3 vs 273.6±82.9 HU), liver (78.5±14.3 vs 60.9±11.9 HU) and hFLL (160.0±32.2 vs 107.9±23.2 HU) (all p < 0.0001). CTDI and DLP were significantly lower in the test group (6.4±0.4 vs 12.96±4.3 mGy and 194.3±27.5 vs 405.4±117.4 mGy x cm, respectively; all p < 0.0001). Lesion conspicuity (HU/nodule -HU/liver), was significantly higher in the test group (83.8±35.5 vs 48.8±21.5 HU; p= 0.0008). Mean image noise was significantly higher in the test group than in control group (12.3±3.6vs 8.5±2.4 HU; p < 0.0001). Lesion CNR was not significantly different between the two protocols. TLD effective dose was significantly lower for the test protocol (0.158 vs 0.202mSv; p=0.0083).

Conclusion: The use of a 80 kVp arterial phase protocol for abdominal CT increases conspicuity of hFLL, possibly improving identification, while allowing significant dose reduction.

B-0697 11:42

Accuracy of differentiating hepatocellular carcinoma (HCC) from dysplastic nodule (DN) at gadobenate dimeglumine-enhanced hepatobiliary-phase (Gd-BOPTA) magnetic resonance imaging

A. Gatto¹, A.M. De Gaetano¹, M. Giuga¹, L. Siciliani², L. Riccardi¹, F. Pizzolante¹, F.M. Vecchio¹, M. Pompili¹, L. Bonomo¹; ¹Rome/IT, ²Pavia/IT

Purpose: To investigate whether Gd-BOPTA-enhanced hepatobiliary phase MRI could predict the histologic grade of HCC and dysplastic nodule (DN) in patients with cirrhosis.

Methods and Materials: We retrospectively evaluated MRI of 30 patients with 15 HCCs (10 well differentiated-5 moderately differentiated) and 15 DNs (6 low grade-9 high grade), all histopathologically proved. MR T1w 3D GRE images were acquired before, 30s-60s-180s-90 min after bolus injection of Gd-BOPTA (0.1 mmol/kg). Each lesion was defined as iso-hypo-hyperintense compared with the surrounding liver parenchyma on the DPI (delayed-phase-imaging). The tumour-liver contrast-to-noise ratio (CNR) of each lesion on the DPI was calculated (quantitative analysis).

Results: HCC nodules were hypointense in a greater percentage than DNs (14/15 HCC and 10/15 DNs were hypointense); 1 HCC (well differentiated) and 5/15 DNs (2 high grade-3 low grade) were isointense. There was a significant signal intensity difference between HCCs and DNs on the DPI (mean CNR of -15.86±13.58 and -7.07±6.4, respectively; p=0.03), between low-grade and high-grade DNs (mean CNR of -2.6±3.7 and -10.05±6.17, respectively; p=0.02) and between low-grade DNs and HCC (p=0.03). There was no significant difference between high-grade DNs and HCCs and between well and moderately differentiated HCCs (mean CNR of -14.2687±12.69 and -19.06±16.27, respectively; p=0.5).

Conclusion: The relative hypointensity of a lesion to normal surrounding liver on the DPI is helpful to distinguish HCC-high-grade DN from low-grade DN. There is no significant difference between high-grade DN and HCC and between the different pathologic grades of HCC.

B-0698 11:51

Intraoperative high-resolution linear contrast-enhanced ultrasound (IOUS) for detection of microvascularisation of malignant liver lesions before surgery or radiofrequency ablation

E.M. Jung, M. Loss; Regensburg/DE (emjung@gmx.de)

Purpose: To evaluate the value of linear contrast-enhanced intraoperative ultrasound to improve detection of malign liver tumours lesions before surgery or radiofrequency ablation (RFA).

Methods and Materials: 50 patients were included for surgery of malignant liver tumours (mean age 61 years (19-80); male n=35, female n=15), suffering from HCC (n=15), colorectal liver-metastasis (n=28), CCC (n=2) or other malign liver lesions (n=5). Preoperative CE-CT (n=38), CE-MRI (n=23) or PET-CT (n=8) confirmed hepatic tumour manifestation. Before undergoing surgery, intraoperative conventional (IOUS) as well as CE-IOUS were performed by one experienced examiner in all cases using multifrequency linear probes (6-9 MHz, 6-15 MHz; LOGIQ E9; GE) CE-IOUS was performed after bolus injection of 5 ml up to 15 ml SonoVue® (Bracco, Italy). Digitally stored images of CE-IOUS were compared with preoperative imaging.

Results: In 28 of 50 patients (56%), additional lesions were found using CE-IOUS (mean tumour size 8 mm, range 4-12 mm). This resulted in a change of surgical strategy or the intraoperative application of RFA in 27 patients (54%). Modification of therapy due to additionally found liver lesions was statistically significant (p < 0.05). Comparing conventional IOUS and CE-IOUS, 14 additional lesions in 10 patients were seen by CE-IOUS. All lesions seen in B-scan could also be detected with CE-IOUS.

Conclusion: This is the first study using contrast-enhanced ultrasound with high-resolution linear probes for intraoperative detection of malignant liver lesions. Compared to preoperative imaging and also conventional IOUS more than 40% additional lesions were found leading to therapeutic consequences of patients.

10:30 - 12:00

Room L/M

Contrast Media

SS 1306

Safety and diagnostic value

Moderators:

R. Lagalla; Palermo/IT

Y.W. Nielsen; Copenhagen/DK

B-0699 10:30

Nephrogenic systemic fibrosis: a review of published cases and results from three prospective observational studies

G. Pirovano¹, J. Munley¹, C. Schultz¹, J. Parker¹, M.A. Kirchin², K. Quince¹, A. Spinazzi¹; ¹Princeton, NJ/US, ²Milan/IT (gianpaolo.pirovano@diag.bracco.com)

Purpose: To assess the profile of nephrogenic systemic fibrosis (NSF) in the medical literature and evaluate the incidence of NSF in three prospective studies.

Methods and Materials: For published peer-reviewed cases of NSF (2000-2010), we recorded country, age, gender, renal impairment, gadolinium-based contrast agent (GBCA) exposure (type/dose), date of onset, and time from GBCA exposure to onset. In three prospective observational studies we assessed NSF incidence in CKD patients exposed to gadoteridol (G), gadobenate dimeglumine (GD), or without gadolinium exposure for 10 years. Patients were stratified into 2 cohorts (eGFR of 30-59 mL/min/1.73 m² [Cohort 1] or < 30 mL/min/1.73 m² [Cohort 2]) and were followed for up to 2 years.

Results: 711 published NSF cases from 28 countries (NAmerica=75%; Europe=20%) were identified in patients (8-87yr). 709 cases reported renal status (CDK=639 cases; ARF=70 cases). The specific GBCA (s) administered was known in 486 cases, including 444 unconfounded cases (gadodiamide=348; gadopentetate dimeglumine=88; gadoversetamide=6; gadobutrol=2). Exposure to gadodiamide or gadopentetate dimeglumine occurred in all confounded cases. In about 50% of cases, symptoms developed within 2 months of the last GBCA exposure. No case was reported with an NSF onset date of 2010 or later. In the prospective studies, 839 patients have been enrolled (GD=293, G=141, control= 405). At least 1yr follow-up has been completed in 524 subjects and 2yr+ in 102. No NSF case has been identified to date.

Conclusion: Improved screening has apparently halted new NSF cases. In the prospective studies with gadobenate dimeglumine and gadoteridol, no NSF case has been reported.

B-0700 10:39

Prevalence of nephrogenic systemic fibrosis in dialysis patients: the Pro-FINEST study

S. Amet¹, G. Choukroun², V. Launay-Vacher¹, C. Frances¹, A. Tricotel³, B. Stengel⁴, G. Deray¹, O. Clement¹; ¹Paris/FR, ²Amiens/FR, ³Saint-Denis/FR, ⁴Villejuif/FR (sabine.amet@psl.aphp.fr)

Purpose: NSF is a cutaneous and systemic disorder characterised by widespread tissue fibrosis. It has been suggested that gadolinium-based contrast agents (GBCA) may be responsible for NSF, especially in dialysis patients. The Pro-FINEST study is a national prospective study endorsed by the French Drug Agency (Afssaps), and the French Societies of Nephrology, Dermatology, and Radiology. It aims at determining the prevalence of NSF after a magnetic resonance imaging (MRI) examination, ± GBCA, in dialysis patients.

Methods and Materials: The study is based on a 3-section patient form. Section 1: demographics and dialysis; Section 2: MRI examination; Section 3: any dermatological event (DE). Further investigations are planned in case of DE. When a NSF diagnosis is confirmed, an ancillary study is to be performed, with random selection of 4 patients (same gender, dialysis technique, centre, and without any DE after MRI with the same GBCA, if injected).

Results: Since 01/2009, 570 patients have been included (112 centres): mean age 63.3 years, 58.4% males, 443 forms received: 56% received GBCA among whom 89.9% received Gadoterate. Twenty patients reported a DE. Dermatological diagnoses did not report any evidence of NSF.

Conclusion: So far thus, no case of NSF has been reported in 570 dialysis patients among whom the majority received a GBCA. Most patients received a macrocyclic gadolinium chelate for which no unconfounded case of NSF has been observed yet worldwide (Gadoterate). Final results will be available at the time of the congress.

B-0701 10:48

Tolerability and diagnostic value of gadoteric acid in general and in patients with risk factors: results in more than 84,000 patients

M.H. Maurer¹, O. Heine², M. Wolf³, T. Durmus¹, M. Wagner¹, B. Hamm¹;
¹Berlin/DE, ²Sulzbach/Taunus/DE, ³Püttlingen/DE (martin.maurer@charite.de)

Purpose: To review the tolerability and the diagnostic effectiveness of gadoteric acid under daily practice conditions in the general population and at-risk patients.

Methods and Materials: A total of 84,621 patients (45.4% male, 54.6% female, mean age 52.0±16.9 years) were studied in 129 German centres. Patients underwent contrast-enhanced magnetic resonance imaging (MRI) using gadoteric acid (Gd-DOTA, Dotarem, Guerbet, Roissy CdG, France) as IV contrast medium (mean volume, 16.4 ml). 22.9% of the patients had at least one risk factor (e.g., allergies, previous allergic reaction to a contrast medium, renal impairment). Forty-six patients received antiallergic pretreatment before contrast medium administration (0.1%). Adverse events were documented and image quality was assessed.

Results: A diagnosis was possible in 99.7% of all cases. Image quality was rated good or excellent in 97.1%. Adverse events (e.g., nausea, vomiting, and urticaria) were observed in 0.34% of the examinations and were mostly rated as minor. There were 8 patients with severe adverse events. The adverse event rate was significantly higher in patients with a history of allergies (0.62%; $p < 0.001$) and in patients with a previous allergic reaction to contrast medium (1.23%; $p < 0.001$). There was no elevated risk for adverse events in patients with renal or hepatic impairment.

Conclusion: Gadoteric acid was shown to be a well-tolerated MRI contrast medium in patients with and without risk factors associated with a low rate of adverse events and a good or excellent image quality in most patients.

B-0702 10:57

Observational post-marketing study on the safety of meglumine gadoterate: interim safety analysis on 17,193 patients

B. Kress; Frankfurt/DE (kress.bodo@khnw.de)

Purpose: To prospectively assess the general safety profile of meglumine gadoterate (Gd-DOTA) and evaluate the overall incidence of nephrogenic systemic fibrosis (NSF).

Methods and Materials: A worldwide post-marketing study (PMS) was conducted to collect safety data in 40,000 patients with or without renal insufficiency who had routine contrast-enhanced magnetic resonance (MR) imaging using Gd-DOTA. For each patient, risk factors at inclusion, indications for MR imaging examination, and conditions of use and administration of the contrast material were recorded. For any patient identified as renally impaired at the time of inclusion (i.e., estimated creatinine clearance or estimated glomerular filtration rate < 60 mL/min/1.73m²), at least a 3-month follow-up evaluation was performed in order to detect any suspicion or occurrence of NSF.

Results: As of July 05, 2011, the cut-off date for the interim safety analysis, this ongoing PMS included data from 17,193 patients (mean age: 50.3 years; range: 0-98 years; female, 53.5%). MR imaging examinations were mainly performed to image the central nervous system (50.7%), whole body (23.1%) and musculoskeletal (17.4%). The main risk factors were hypertension (13.5%) and allergies (9.7%). Moderate to severe impaired renal function was reported in 487 patients (2.8%). Among them, 298 (61.2%) had no suspicion of NSF (follow-up evaluation not yet completed at the time data were collected for 189 patients). Thirty patients (0.17%) had at least one adverse event (mainly urticaria, nausea, vomiting).

Conclusion: This interim safety analysis already confirms a very good safety profile of Gd-DOTA.

B-0703 11:06

Safety and diagnostic efficacy of gadobenate dimeglumine (MultiHance) in MR imaging of paediatric patients

G.K. Schneider, H. Schuerholz, P. Fries, A. Buecker;
 Homburg a.d. Saar/DE (dr.guenther.schneider@uks.eu)

Purpose: To retrospectively evaluate the safety and diagnostic efficacy of gadobenate dimeglumine in CE imaging in different indications.

Methods and Materials: 200 paediatric subjects (age: 0 - 18 years) underwent CE MRI as part of clinical routine. Patients received a dose of either 0.05 mmol/kg bodyweight (liver, abdominal, musculo-skeletal, brain and other rare indications) or 0.1 mmol/kg bodyweight (cardio-vascular imaging, MR-urography). Young patients underwent MRI either in sedation or general anaesthesia, in case of MRA studies in CHD, patients generally underwent imaging in intubation with controlled ventilation. Monitoring for adverse events was performed up to at least 24 hours post-injection. Depending on the clinical necessity, laboratory measurements, and in some cases vital sign and ECG determinations were made before and after the CE examination.

Determination of the safety of gadobenate dimeglumine was thereafter made by age-group, clinical indication and dose administered.

Results: No clinical adverse events were reported either amongst patients who underwent only a solitary MR or multiple examinations. There were no alterations in creatinine levels even in very young subjects whose kidney function is not yet fully developed. Likewise, there were no changes in bilirubin levels despite the elimination of 3-5% of the injected dose through the hepatobiliary pathway.

Conclusion: Gadobenate dimeglumine is a safe and efficient contrast agent for imaging of paediatric patients. Concerning the current discussion on the safety of Gd-based MR contrast agents, the lower dose of gadobenate dimeglumine needed for diagnostic abdominal imaging (0.05 mmol/kg) and contrast-enhanced MR-angiograph (0.1 mmol/kg) seems beneficial.

B-0704 11:15

Parstatin averts development of contrast-induced nephropathy in an in-vivo experimental model

A. Diamantopoulos, K. Katsanos, S. Spiliopoulos, A. Karatzas, D. Karnabatidis, N. Tsopanoglou, D. Siablis; Patra/GR (adiamantopoulos@gmail.com)

Purpose: To present the preliminary results of an experimental study investigating the hypothesis that parstatin, the N-terminal 41-amino-acid peptide cleaved by thrombin from the protease-activated receptor 1, may hold a protective role against contrast-induced nephropathy (CIN). Parstatin, has previously been shown to protect against rat myocardial ischaemia and reperfusion injury.

Methods and Materials: CIN was experimentally induced in New-Zealand-White (NZW) rabbits by intravenous administration of a high dose (10 mg I/kg) of iodinated contrast medium (Iopromide 370 mg I/ml) infused over a 30 min period. Subjects received either pre-treatment with 10 µg/kg parstatin exactly 15 minutes before initiation of contrast infusion (group P), or an equal volume of normal saline (control, group C). Blood serum creatinine (sCr) was measured at 48 hours in all subjects. CIN was defined as an increase of subject's sCr above 1.5 mg/dl. Animals were euthanised at 48 hours, kidneys were removed and sectioned for histological examination with haematoxylin and eosin staining.

Results: Thirty three subjects were assigned in either group P (n=18, 3.1±0.3 kg) or group C (n=15, 3.0±0.2 kg). At 48 hours CIN was detected in a statistically significant higher proportion of subjects in the control group C (86.7%, 13/15) compared to the parstatin pre-treated group P (27.8%, 5/18), $p < 0.001$. Histology demonstrated more extensive tubular necrosis in group C compared to group P.

Conclusion: Parstatin successfully inhibits CIN in an animal model of contrast-induced nephropathy. Further studies are necessary to validate the protective role of parstatin against contrast nephrotoxicity and find the optimal dose for the best possible result.

B-0705 11:24

Clinical and pathological effects and in vivo stability of all categories of gadolinium chelates on a new model of renal failure in rats

N. Parmentier¹, N. Fretellier¹, P. Bruneval², C. Wallon¹, G. Jestin¹, C. Hollenbeck¹, C. Factor¹, J.-M. Idee³, C. Corot¹; ¹Roissy/FR, ²Paris/FR (ideej@guerbet-group.com)

Purpose: Compare the clinical, pathological effects and the in vivo stability of all currently marketed categories of gadolinium chelates (GC) in rats with adenine-induced renal failure.

Methods and Materials: Wistar rats (4-6/group) received a 0.75% adenine-enriched diet for 16 days and received 5 daily intravenous injections of gadoterate (Dotarem®), gadobutrol (Gadovist®), gadopentetate (Magnevist®), gadobenate (MultiHance®), gadodiamide (Omniscan®) (all 2.5 mmol/kg/day) or saline from day 14. Rats were sacrificed 4 weeks after the first injection of GC. A clinical, histopathological (blinded examinations), biochemical and analytical (measurement of total Gd concentration in various tissues, ICP-mass spectrometry) follow-up was carried out, as well as relaxometry measurements (skin, liver, and femur) (Minispec, 60 MHz).

Results: Gradual mortality was found in the gadodiamide-treated group (3 out of 4 rats). Early and transient punctiform skin lesions appeared in gadopentetate-treated rats (4/6 animals). Moderate dermis inflammation, overexpression of TGFβ1 and tissular inhibitor of matrix proteinase-1 were found in the skin of the gadodiamide survivor at sacrifice. Gradual increase in r1 relaxivity values was found in the skin of gadopentetate rats (4.0 ± 0.1, 6.5 ± 1.2 and 10.6 ± 3.8 mM⁻¹.sec⁻¹ at days 14, 23 and 39, respectively, ex vivo reference range = 3.5-5.6 mM⁻¹.sec⁻¹) and gadodiamide (8.9 mM⁻¹.sec⁻¹ for the survivor at sacrifice vs. 4.1 ± 0.1 mM⁻¹.sec⁻¹ at day 14), an effect consistent with gradual in vivo GC dissociation.

Conclusion: The adenine model of renal failure allows to discriminate between GCs as regards their skin toxicity and in vivo stability profiles.

B-0706 11:33

Renal function of outpatients undergoing contrast-enhanced CT: what have we learned from universal eGFR testing?

H. Chalian, H.G. Tore, K. Ghadjar, V. Yaghmai; *Chicago, IL/US (v-yaghmai@northwestern.edu)*

Purpose: To determine the frequency of abnormal renal function in all outpatients undergoing contrast-enhanced CT and to correlate this with the patients' knowledge of their renal function.

Methods and Materials: This retrospective HIPAA compliant study was approved by our IRB. eGFR (ml/min/1.73 m²) values for 2404 consecutive outpatients obtained immediately before CT were recorded. eGFR values were obtained for all patients regardless of their risk factors. Results were compared to the patients' self reporting of the history of renal disease. eGFR values were also compared to the serum creatinine (mg/dL) levels. eGFR < 60 ml/min/1.73 m² was defined as abnormal.

Results: 1923 (80%) patients were younger than 70 years. 648 patients (27.0%) had abnormal eGFR (mean: 48.7±10.0 ml/min/1.73 m²). The average and median age for those with abnormal eGFR were 65.5±11.9 and 66.0, respectively. 550 (84.9%) patients with abnormal eGFR reported no history of renal disease. 121 (69.5%) of those with eGFR < 45 ml/min/1.73 m² reported no history of renal disease. Of those who indicated history of renal disease (164), 66 (40.0%) had normal eGFR. 505 patients (77.9%) with abnormal eGFR had creatinine levels below 1.5 mg/dL.

Conclusion: Patients referred for -enhanced CT are frequently unaware of their abnormal renal function status. Conversely, patients who report history of renal disease commonly have normal renal function. Universal eGFR testing may be necessary to determine the renal function in this population.

B-0708 11:42

Evaluation of contrast injection protocols for thoraco-abdominal high-pitch dual source CT angiography: a phantom study

G.D. Puippe, A. Winklehner, A. Plass, T. Frauenfelder, S. Baumüller; *Zurich/CH (gilbert.puippe@usz.ch)*

Purpose: To experimentally evaluate three contrast protocols for thoraco-abdominal high-pitch dual source CT angiography (CTA), with regard to level and homogeneity of vascular enhancement at different cardiac outputs.

Methods and Materials: Uniphase, biphasic and tailored contrast injection protocols were tested using a human vascular phantom. Protocols were scanned at 5 different cardiac outputs (3-5L/min, steps 0.5L/min) using a centrifugal pump. Thoraco-abdominal vascular enhancement was measured every 5 cm. Overall mean enhancement of each protocol and mean enhancement for each cardiac output within each protocol were calculated. Enhancement homogeneity along the z-axis was evaluated for each cardiac output and protocol. Amounts of administered contrast agent were noted.

Results: Overall mean enhancement was significantly higher in the uniphase than in the other protocols (all p < .05), whereas the difference between the biphasic and tailored protocol was not significant (p = .76). Cardiac output inversely influenced the level of vascular enhancement. Changing cardiac outputs lead to significantly different mean vascular enhancements (all p < .05), with the exception at cardiac outputs of 3.5L/min vs. 5L/min (484±25 HU vs 476±19 HU, p = .14) and 4 vs 5L/min (443±49 HU vs 476±19 HU, p = .05) at the tailored protocol. Homogeneous enhancement was feasible at all cardiac outputs with the uniphase and tailored but not with the biphasic protocol. Amounts of contrast agent were significantly lower at the tailored (53±5 mL) than at the uni- (100 mL) or biphasic (80 mL) protocol (all p < .05).

Conclusion: Results suggest that homogeneous enhancement at thoraco-abdominal high-pitch dual source CTA is achievable with either uniphase or tailored contrast protocol, the latter being favourable of needing significantly less contrast agent.

10:30 - 12:00

Room N/O

Vascular

SS 1315

Peripheral and renal arteries

Moderators:
G. Carratiello; *Varese/IT*
K. Katsanos; *Patras/GR*

B-0709 10:30

Accuracy of dynamic contrast-enhanced ultrasound and transient arterial occlusion for diagnosis of peripheral arterial disease

E. Amarteifio, S. Wormsbecher, M. Krix, S. Demirel, S. Braun, S. Delorme, D. Boeckler, H.-U. Kauczor, M.-A. Weber; *Heidelberg/DE (erick.amarteifio@med.uni-heidelberg.de)*

Purpose: To ascertain the accuracy of dynamic contrast-enhanced ultrasound (CEUS) and transient arterial occlusion for diagnosis of peripheral arterial disease (PAD).

Methods and Materials: 40 patients with PAD, Rutherford classification grade I, category III (mean age, 65 years) and 40 healthy volunteers (mean age, 54 years) were included. The dominant lower leg was examined with CEUS (7 MHz; MI, 0.28) during continuous intravenous infusion of 4.8 mL microbubbles containing sulphur hexafluoride. Transient arterial occlusion at the thigh level simulated physical exercise. Regions of interest (ROI) were placed in the selected muscle and several parameters were obtained from time-CEUS-intensity curves: Maximum CEUS signal after occlusion, and its time (tmax), resulting slope to maximum (m), and vascular response after occlusion (AUCpost). Accuracy, receiver operating characteristic (ROC) curves, and correlations of these parameters with ankle-brachial index (ABI) and walking distance were analysed.

Results: All parameters significantly differed for patients compared to volunteers (p < 0.014). tmax was markedly delayed in PAD (31.2±13.6 vs. 16.7±8.5s, p < 0.0001), and was significantly negatively correlated with ABI (r = -0.65). Highest diagnostic accuracy was found using m, which was significantly smaller for patients (4.3±4.6□mL/s) compared to volunteers (13.1±8.4□mL/s, p < 0.0001) with a sensitivity of 75% and specificity of 93% for detection of diminished muscular micro-perfusion in PAD (cut-off value, m < 5~mL/s). Discriminant analysis and receiver operating characteristic (ROC) curves revealed that a parameter combination of m, and AUCpost is optimal for diagnosis of PAD.

Conclusion: Dynamic CEUS and transient arterial occlusion quantifying muscular micro-perfusion is suitable for diagnosis of PAD providing accurate sensitivity and specificity.

B-0710 10:39

Comprehensive MR angiography of the lower limbs: comparison of performance of gadobenate dimeglumine, gadobutrol and gadofosveset trisodium

S. Chandramohan, G. Roditi; *Glasgow/UK (dr.schandramohan@gmail.com)*

Purpose: Comprehensive lower limb MRA protocol incorporating dynamic, first pass 3 station and high-resolution imaging with results comparable to bloodpool contrast agents (BPCA) could be achieved with non-BPCAs. We aim to evaluate this in a prospectively comparing gadofosveset with gadobutrol and gadobenate.

Methods and Materials: 60 patients, claudicants (n=30) and critical limb ischaemics (n=30) are recruited for this study. CE-MRA acquired in 3 phases; initial dynamic MRA (TWIST) of the infrapopliteal vessels, standard 3 station first pass MRA then immediately followed by imaging in 'extended phase' with high-resolution acquisitions of the thigh and calf vessels. Critical patients were imaged once only with BPCA (10 ml gadofosveset, 15 patients) or either of the 2 ECS agents gadobenate dimeglumine or gadobutrol (15 ml, 15 patients). Claudicant patients are imaged twice on separate attendances - with BPCA and either gadobenate dimeglumine or gadobutrol, or gadobenate dimeglumine and gadobutrol to allow intra-individual comparison. Evaluation of image quality for arteries and veins using a Likert scale and ROI measurements for CNR on high-resolution images.

Results: For arterial diagnosis dynamic and first-pass images obtained with gadobenate dimeglumine and gadobutrol are not significantly different to those obtained with gadofosveset trisodium. High spatial resolution extended phase images are also comparable to arterial disease although venous signal is significantly reduced in non-BPCAs.

Conclusion: Comprehensive lower limb vascular imaging including dynamic acquisitions and extended phase imaging can be performed with similar diagnostic

utility for arterial disease using all 3 agents. Venous enhancement is significantly less conspicuous with the non-BPCAs.

B-0711 10:48

Efficacy of Dotarem®-enhanced mra in the diagnosis of peripheral artery disease compared to Gadovist®-enhanced MRA

C. Loewe¹, J. Arnaiz², D. Krause³, L. Marti-Bonmati⁴, M. Aschauer⁵, A. Tartaro⁶, M. Lombardi⁷, M. Burrel⁸, R. Izzillo⁹; ¹Vienna/AT, ²Santander/ES, ³Dijon/FR, ⁴Valencia/ES, ⁵Graz/AT, ⁶Chieti/IT, ⁷Pisa/IT, ⁸Barcelona/ES, ⁹Saint-Denis/FR (christian.loewe@meduniwien.ac.at)

Purpose: To compare the diagnostic performance of Dotarem®-enhanced MRA and Gadovist®-enhanced MRA at 3 T.

Methods and Materials: In this prospective, multi-countries, randomised, parallel group, double-blind, phase IV trial, 189 patients (66.4±10.7 years) with peripheral arterial disease (PAOD) (stages II-IV Leriche and Fontaine classification) were included. Patients randomly underwent MRA of the lower legs during injection with 0.1 mmol/kg of either Dotarem® (15.4±3.1 mL) or Gadovist® (7.6±1.3 mL). A total of 21 vascular segments were explored (from infrarenal aorta to peroneal artery). The primary criterion was the degree of agreement (within patient accuracy) of each type of MRA examination as compared to the gold standard, DSA, using a non-inferiority analysis, evaluated in a blinded manner by on-site reading. Main secondary criteria included specificity, sensitivity, positive/negative predictive values (PPV/NPV), diagnostic confidence, and safety.

Results: The agreement in stenosis detection between Dotarem®-MRA and DSA was similar to that of Gadovist®-MRA (75.8%±18.9% vs 69.0%±24.2%, respectively, Δ=6.8%), and the 95%CI excluding the non-inferiority limit (-6.5%) demonstrated the non-inferiority. The MRA sensitivity for detecting significant stenosis (> 50%) was 73.7% with Dotarem® and 69.5% with Gadovist®; whereas the specificity (92%), PPV (75.8% versus 72.5%), NPV (91%), and diagnostic confidence (86.3% vs 86.2%) were similar in both groups. Two patients (2.2%) in each group experienced adverse events (mostly mild and unrelated).

Conclusion: Dotarem®-MRA can be used with similar diagnostic accuracy as Gadovist®-MRA in the diagnosis of PAOD at 3 Tesla. This trial suggests that there is no direct correlation between higher intrinsic relaxivity and/or gadolinium concentration and improved clinical diagnosis.

B-0712 10:57

Peripheral MRA at 3 T: intraindividual comparison between nonenhanced ToF and SSFP sequences vs contrast-enhanced MRA for the detection of clinically relevant stenosis

M. Anzidei¹, A. Napoli¹, F. Zaccagna¹, L. Saba², G. Cartocci¹, L. Bertaccini¹, V. Noce¹, F. Boni¹, C. Catalano¹; ¹Rome/IT, ²Capri/IT (michele.anzidei@gmail.com)

Purpose: To compare diagnostic accuracy of two nonenhanced MRA (NE-MRA) sequences (ToF and SSFP) vs conventional contrast-enhanced MRA (CE-MRA) at 3.0 T in patients with peripheral arterial obstructive disease (PAOD), using CT-angiography (CTA) as reference standard.

Methods and Materials: 30 patients symptomatic for PAOD underwent NE-MRA of the femoral and calf regions with 3D ECG-gated ToF and ECG-gated SSFP sequences followed by CE-MRA with Gd-BOPTA. All patients underwent CTA as reference standard. Three blinded observers separately reviewed all MRA datasets in random order; one independent observer evaluated CTA images for the assessment of relevant stenosis (> 50%), extent and location. Image quality was evaluated by an independent observer for all MRA datasets. Intraobserver and interobserver agreement for the three MRA techniques were analysed using Cohen-k statistics. Sensitivity, specificity, accuracy, positive predictive value (PPV) and negative predictive value (NPV) were calculated for each technique. The McNemar's test was used to assess statistically significant differences in the diagnostic accuracy of each MRA technique.

Results: Intraobserver and interobserver agreement were substantial for stenosis assessment. The sensitivity, specificity, accuracy, PPV and NPV values of ToF/SSFP/CE-MRA sequences for stenosis assessment compared to CTA were, respectively, 90/92/97%, 78/87/94%, 85/86/97%, 94/93/97%, 72/83/94%. Diagnostic performance of CE-MRA was superior to ToF and SSFP sequences (p < 0.001); SSFP sequences were better for stenosis assessment compared to ToF sequences (p < 0.001).

Conclusion: 3 T CE-MRA is superior to NE-MRA techniques for image quality and diagnostic performance. The diagnostic performance of SSFP sequences is significantly higher than that of ToF sequences and may be considered as a potential alternative diagnostic tool in selected patients.

B-0713 11:06

How should renal artery stenoses be measured?

M. Andersson, K. Jägervall, P. Eriksson, A. Persson, G. Granerus, Ö. Smedby; Linköping/SE

Purpose: To determine which morphological measures from CTA and MRA are best in predicting whether a renal artery stenosis affects renal haemodynamics or not.

Methods and Materials: Forty-seven patients with hypertension or anti-hypertensive treatment and a clinical suspicion of renovascular hypertension were examined with computed tomography angiography (CTA), magnetic resonance angiography (MRA), captopril-enhanced renography (CER) and captopril test (Ctest). The CTA and MRA images of the renal arteries were analysed by two readers using fuzzy connectedness segmentation. The measures used were minimum diameter, minimum area, diameter reduction and area reduction. In addition, two radiologists measured the diameter reduction without using automated segmentation. The results were then correlated with the results from CER combined with Ctest using receiver operating characteristics (ROC) analysis.

Results: A total of 68 kidneys had all three investigations (CTA, MRA and CER+Ctest), where 11 kidneys (16%) got a positive result on the CER+Ctest. Area reduction on MRA had the greatest area under ROC curve (AUROC): 0.91 (95% confidence interval 0.82-0.99). The AUROC for the radiologists' measurements on CTA and MRA were 0.90 (0.82-0.98) and 0.91 (0.83-0.99), respectively. None of the differences were statistically significant.

Conclusion: No significant differences were found between the morphological measures in their ability to predict positive renographic findings, but a tendency of MRA having higher AUROC than CTA. There was no significant difference between the measurements made by the radiologists and the measurements made with fuzzy connectedness segmentation. Further studies are required to definitely identify the optimal measurement.

B-0714 11:15

Duplex evaluation of distal renal artery to predict the presence of proximal significant acceleration: an experience of 2,200 explorations

J. Leal, R. Rodriguez, J. Peinado, S. Vicente, C. Salgado, A. Flores, J. Gil, A. Orgaz, M. Doblas; Toledo/ES (j_i_leal@wanadoo.es)

Purpose: The aim of this study was to determine the accuracy of indirect haemodynamic parameters obtained by evaluation of the segmental or interlobar arteries within the kidney as predictors of the presence of haemodynamically significant proximal renal artery stenosis.

Methods and Materials: We performed a retrospective analysis of all consecutively studied patients at our centre with suspected RAS. Direct haemodynamical measures (renal peak systolic velocity-RPSV-and end diastolic velocity-EDV-) determined in the proximal and middle segments of the main renal artery were measured with the association of four indirect Doppler parameters obtained in the renal hilum (Resistive Index-RI- Acceleration Index-AI-,Systolic Acceleration Time-AT-and Pulsatility Index-PI-). The population was classified by the presence or absence of direct haemodynamical criteria of RAS (RPSV> 200 cm/s) and the distal indirect parameters were compared in these two populations.

Results: A total of 2,200 explorations in 1,419 patients were analysed. A predictive binary logistic regression model was developed in order to determine the accuracy of distal indirect parameters to predict the presence of a proximal significant RPSV. The area under the curve of the receiver operating characteristic analysis of the predictive model was 0.84 (95% confidence interval [CI] 0.703 - 0.924), indicating good discrimination power between those with and without significant proximal values of RPSV. Only PI (prevalence odds ratio [POR] 4,109 95% CI 1.74-9,695) and AT (POR 1,031 95% CI 1,021 -1,041) were significantly associated with highest RPSV.

Conclusion: These results suggest that distal indirect haemodynamic parameters PI and TA could provide good diagnostic accuracy in the prediction of proximal significant RPSV values, being useful when main-vessel velocities cannot be determined reliably.

B-0715 11:24

Non-enhanced magnetic resonance angiography (MRA) of the renal arteries: comparison with contrast enhanced MRA

D. Lumia, M.G. Angeretti, A. Cani, A.M. Maresca, E.A. Genovese, C. Fugazzola; Varese/IT (domenicolumia@gmail.com)

Purpose: To assess the diagnostic accuracy of non-enhanced steady-state-free-precession (SSFP) magnetic resonance angiography (NE-MRA) for detection of renal artery stenosis (RAS), in comparison with breath-hold contrast-enhanced MR angiography (CE-MRA) as the reference standard.

Methods and Materials: Sixty-three patients (33 males, 30 females) with suspected renovascular hypertension were examined with NE-MRA using a ECG-gated SSFP sequence and a 1.5 T MR scanner; in 26/63 patients a respiratory trigger was used in addition to cardiac gating. During the same examination, CE-MRA was performed in all patients and its results used as reference standard. MIP image quality, number of main renal arteries, accessory arteries and presence of stenoses were independently assessed by two readers. Sensitivity, specificity, positive (PPV) and negative predictive values (NPV) of NE-MRA in the identification of significant ($\geq 50\%$) RAS were calculated.

Results: MIP image quality was considered better for NE-MRA by both readers. NE-MRA identified 143/144 arteries detected by CE-MRA (1 accessory missed). Fourteen stenoses were identified by CE-MRA (11 atherosclerotic, 3 dysplastic) with 4 significant RAS. Sensitivity, specificity, PPV and NPV of NE-MRA were, respectively, 100%, 100%, 100% and 100% for reader 1, and 100%, 98.2%, 87.5% and 100% for reader 2. Overestimation of the stenosis grade occurred in two cases for reader 2 (< 50% vs. normal in one case, $\geq 50\%$ vs. < 50% in the other case).

Conclusion: NE-MRA has become a viable alternative to CE-MRA for the study of the renal arteries. In case of significant stenosis, given the risk of overestimation, the use of CE-MRA is still indicated.

B-0716 11:33

Evaluation of renal artery aneurysm by non-contrast magnetic resonance angiography: a SLEEK sequence comparison with CTA

Y. Pei; Changsha/CN (tjpyg2027@163.com)

Purpose: To determine the performance of a new non-contrast magnetic resonance angiography (NC-MRA) sequence (spatial labelling with multiple inversion pulses, SLEEK) in its ability to present the renal artery aneurysm (RAA) and to investigate whether a suitable multiple blood suppression inversion time (BSP TI) can help to improve RAA visibility in SLEEK.

Methods and Materials: 32 RAAs confirmed by CTA was carried out NC-MRA using SLEEK on a 1.5 T MR system with various BSP TI. A suitable BSP TI to increase RAA visibility was determined and RAA was evaluated for each patient by two experienced radiologists in their consensus, and were compared with CTA results using a joint reading performed in consensus.

Results: 32 RAAs consisted of 13 right and 19 left RAAs (12 RAAs were performed by surgery), including 4 RAAs with < 0.5 cm, 13 RAAs with > 0.5 cm and < 1.0 cm, 9 RAAs with > 1.0 cm and < 2.0 cm, 6 RAAs with > 2.0 cm. The excellent correlation between SLEEK and CTA was found in presenting RAA size ($R_s=0.889$, $p < 0.05$). The suitable BSP TI was 1100 ms for displaying RAA with < 0.5 cm, 1400 ms for RAA with > 0.5 cm and < 1.0 cm, 1700 ms for RAA with > 1.0 cm and < 2.0 cm, and 2000 ms for RAA with > 2.0 cm.

Conclusion: A suitable BSP TI in SLEEK may increase the RAA visibility. SLEEK represents a non-renal complication, relatively inexpensive, and reliable diagnostic method for evaluating RAAs. It can be as an alternative choice of CTA for evaluating RAAs, especially in subjects with renal insufficiency.

B-0717 11:42

Symmetry of atherosclerotic lesions at the lower extremities arteries on magnetic resonance angiography (MRA)

V. Nardella, F. Secchi, A. Giardino, E. Resta, G. Di Leo, F. Sardanelli; Milan/IT (gaia.nardella@gmail.com)

Purpose: Our aim was to quantify the symmetry between right and left lower extremities atherosclerotic arteries lesions on MRA.

Methods and Materials: We retrospectively evaluated a consecutive series of reports concerning 82 patients (aged 70 ± 9 years, 22 females) who underwent lower extremities MRA. We performed a three-step MRA from aortic bifurcation to tibial arteries using a 3D gradient-echo sequence before/after intravenous administration of 0.1 mmol/kg of gadobenate dimeglumine. Disease grade (DG) was evaluated for each artery using a 4-point score: 0=normal; 1=stenosis < 50%; 2=stenosis $\geq 50\%$ or aneurysm; 4=occlusion. Moreover, after exclusion of normal bilateral vessels, disease symmetry (DS) was evaluated for each artery compared with the contralateral: we calculated DS as absolute difference of left and right leg DG for each vessel (0=max symmetry and 4=min symmetry). Absolute median DS was calculated for artery and for patient. Median DS per patients was weighted for the number of pathological arteries (weighted DS, WDS, 0=max and 17=min symmetry). We compared the left leg global DG with right leg global DG through Wilcoxon test.

Results: Comparing the global DG between the two legs, no significant difference was found ($P=.506$). Median DS score was 1 for the femoral profunda and superficial, poplitea, anterior tibial and peroneal arteries. Median patient DS score was 1.5 while median patient WDS score was 6.7.



Conclusion: Patients showed a symmetrical distribution of atherosclerotic lesions, in particular, for the femoral profunda and superficial, poplitea, anterior tibial and peroneal arteries. Patient's analysis showed a symmetrical lesions and severity distribution.

B-0718 11:51

Study of the left renal vein variations and inferior vena cava variations by means of spiral computed tomography

A. Dilli¹, U.Y. Ayaz², B. Hekimoglu²; ¹Çankaya/TR, ²Mersin/TR (umityasarayaz@gmail.com)

Purpose: A retrospective study was designed to evaluate the percentages of the left renal vein variations, inferior vena cava variations and the effect of gender on their frequencies, using spiral computed tomography (CT).

Methods and Materials: Between January 2010 and August 2011, the study population was recruited from 1204 patients who would undergo a contrast-enhanced abdominal spiral CT examination for various abdominal problems.

Results: As the left renal vein variations, retroaortic left renal vein (RLRV) and circumaortic left renal vein (CLR) were detected. The number of cases with the correspondent percentages of the total left renal vein variations, RLRV and CLR was 63/1204 (5.23%), 38/1204 (3.15%) and 25/1204 (2.08%), respectively. There is a correlation between female gender and frequency of the left renal vein variations ($P = 0.02$). RLRV is 1.7 times more frequent in females than in males (95% confidence interval, 1.06-2.84). As the inferior vena cava (IVC) variations, duplication of IVC and transposition of IVC were detected. The number of cases with the correspondent percentages of the total IVC variations, duplication of IVC and transposition of IVC was 5/1204 (0.42%), 3/1204 (0.25%), 2/1204 (0.17%), respectively. There was no effect of gender on the frequencies of IVC variations ($P = 0.769$).

Conclusion: Abdominal spiral CT is useful in detecting the left renal vein variations (RLRV, CLR) and the IVC variations. Radiological recognition of these variations is crucial when an IVC surgery and a left renal or retroperitoneal surgery are considered.

10:30 - 12:00

Room P

Radiographers

SS 1314

Radiographers in the clinical setting

Moderators:

H.H. Hjemly; Oslo/NO
W. Hruby; Vienna/AT

B-0720 10:30

Digital mammography: training, technical/clinical practices and workflow issues

C. Reis, L. Radu, T. Sakellaris, S. Carrasqueiro, A. Pascoal; Rio de Mouro/PT (claudia.reis@estesl.ipl.pt)

Purpose: To assess current practices in digital mammography (DM) in Portuguese hospitals/clinics, to investigate compliance with European standards and to identify optimisation needs.

Methods and Materials: Three questionnaires, targeted at breast-radiologists, breast-radiographers, and chief-radiographer, were designed and applied in 45 imaging departments offering DM. Institution and staff profiles, technology/quality control (QC), technical/clinical practices, workload and certification matters were investigated.

Results: A participation rate of 35.5% was achieved (68.8% private; 31.2% public) representing a total of 34 radiographers, 20 radiologists and 16 chief-radiographers participating. The training survey revealed 38.2% of radiographers and 20% of radiologists without specific training in DM. Regarding practices most (97%) radiographers enquired use AEC for standard breast imaging. The existence of an exposure indicator was ignored by 23.5% of radiographers. Most sites (81.2%) perform equipment QC. Rejected analysis was rare (18.8%). EUREF guidelines were followed in 31.25% of the sites with manufacturer recommendations frequently (50%) driving practices. 56.25% of the centres still print all images while 18.75% never does. Overall, the participant centres represented an estimated production of 12000 mammographic examinations/month with noticeable variations in workload and work-efficiency (1.7 to 6 mammography/hour). Radiologists (90%) agreed with the need for certification in DM and the 70% would join a volunteer program.

Conclusion: On-the-job dosimetry training and reject analysis may contribute to improve practices in DM. European guidelines are used in a limited number of sites. Manufacturer's recommendations drive current practices in most sites. Efficient/financial gains may be obtained from standardising digital image output.

B-0721 10:39

How to increase the participation rate among non-European immigrants in the mammography screening programme in Oslo, Norway

E. Røstad, R. Gullien, H. Linnestad; *Oslo/NO (roeb@uus.no)*

Purpose: To increase the participation among non-European immigrants at the mammography screening. Studies shows that less than 1 in 4 woman from minority groups knows about mammography screening and breast cancer despite the fact that breast cancer is a common cause of death among women in the group. Non-European immigrants in Oslo have low participation rate in the screening programme.

Methods and Materials: The department focused on the largest minority groups with women speaking Urdu, Arabic and Somali. Posters in these languages and Norwegian with a summary about mammography screening were printed and sent to all general practitioners in Oslo and hung up in public places and health offices in districts with many women from minority groups. Radiographers from the department visited women's groups and informed about mammography screening and breast cancer. Not all women can read their native language so there were broadcasted several radio shows in Urdu, Arabic and Somali.

Results: The general practitioners are pleased with the posters and inform their patients about mammography screening. The response at the meetings in the women's groups has been successful. The attendances at the meetings were doubled; the women were involved and asked relevant questions. During the radio show women called to comment on the topic. There has been increased participation from non-European immigrants at the mammography screening.

Conclusion: It is important to continue the ongoing work and include new initiatives to increase the participation among non-European immigrants in the mammography screening programme.

B-0722 10:48

Echoes from Estonia: introduction of sonography as a specialism for radiographers

J. Dodgeon¹, A. Lukken², P. Vahtramae²; ¹Salford/UK, ²Tartu/EE (*J.r.dodgeon@salford.ac.uk*)

Purpose: An EU-funded project was initiated by the Estonian Society of Radiographers and Tartu Healthcare College to train 45 radiographers in one of three specialist areas, Radiotherapy, nuclear medicine and diagnostic ultrasound. This presentation focuses on one aspect of the project, designed to create an education programme for a new group of radiographers in Estonia - sonographers.

Methods and Materials: The sonography project started in 2010, the first year being devoted to curriculum design, based on EFSUMB guidelines. International links were made with Sweden, the UK and the USA. The education was implemented from February 2011, and this presentation examines the visit by a UK ultrasound educationalist. A bespoke educational programme, comprising lectures and hands-on practical training sessions, was delivered over one week. Subsequently the knowledge of the students was tested and the teaching evaluated.

Results: The students' knowledge and skills were enhanced by the input. The Estonian staff acquired teaching resources and were assisted in developing ultrasound examination protocols. Successful students graduated in January 2012, and sonography specialism has been approved as new occupation by the Estonian Qualifications Authority.

Conclusion: There is now a workforce of radiographer-sonographers, who can work to reduce waiting list times and enhance health care delivery in Estonia. The host educationalists have acquired considerable resources and skills, which will enable them to develop curricula and continue training radiographers for advanced practice roles.

B-0723 10:57

Evaluation of the first radiographers with additional degree in ultrasound: to what extent are the learning objectives achieved 6 months after graduation?

K.G. Vikestad¹, E.N. Eikefjord², B.M. Hofmann¹; ¹Oslo/NO, ²Bergen/NO (*uxvkar@ous-hf.no*)

Purpose: The purpose of this study was to compare ultrasound (US) findings of advanced radiographer practitioner (APR) and experienced radiologists. To see if APR manage to separate positive and negative examinations from each other,

number of pictures, time to exam, technical image quality, significant findings and ability to perform reports.

Methods and Material: The study was conducted as a quantitative prospective controlled study including 244 patients, five APRs and four experienced radiologists. All patients underwent ultrasound examinations by an APR and a radiologist. The APR were not given the opportunity to consult a radiologist during the examinations and they were blinded for each others findings. They separately registered, time per examination, number of images, incomplete examinations, confidence in own findings. The examinations performed by the APR were evaluated by radiologists for technical image quality, the ability of the APR to make significant findings and additional findings, ability to perform diagnostic reports, and an overall evaluation of their examinations. Statistics in the study: Cohens Kappatest, Chi-square tests and paired t-test.

Results: The radiologist and APR showed findings conform at 95.1%. In 99.2% of the examinations the radiologists gave the APRs "best" or "medium best" score in overall confidence. 99.2% of the examinations had a technical quality superior or equal to the examinations performed by radiologists.

Conclusion: This study indicates that APR are qualified to perform US examination in upper abdomen in safe way in Norway, equal to radiologist given that they undergo a qualified education.

B-0724 11:06

Can radiologic technologists be trained to triage CT colonography for extracolonic findings?

T.N. Boellaard, C.Y. Nio, P.M.M. Bossuyt, S. Bipat, J. Stoker; *Amsterdam/NL (t.n.boellaard@amc.uva.nl)*

Purpose: Technologists have been shown to be capable CT colonography observers and we evaluated whether radiologic technologists can be trained to triage screening CT colonography for extracolonic findings.

Methods and Materials: Eight consenting technologists participated in a structured training program that consisted of study assignments and a 16-hour course with presentations, observation of expert reading and reading 100 unblinded cases. Subsequently, they reported extracolonic findings in 280 low-dose CT colonographies without intravenous contrast medium. This dataset contained 66 and 27 scans with a possibly (E3) or probably important (E4) finding as highest classified finding (C-RADS). The first and last 40 cases were identical examination cases. Immediate feedback was given after each case from the reference standard, except for examination cases. Technologists reported C-RADS classification, reporting time, and the need for a radiologist to read. We constructed learning curves for correct scan triaging using a moving average technique.

Results: For the final exam 70%(84/120) of scans with E3 or E4 findings and 69.5%(139/200) without E3 or E4 findings were correctly triaged. There was improvement between the first and final exam in identifying E3 scans (52.3%(46/88) vs 70.5%(62/88); p < 0.05). There was no improvement for identifying E4 scans (both 68.8%(22/32)). The technologists' average reading time decreased from 11:51 to 4:13 minutes (p < 0.0001).

Conclusion: Technologists have an increased capability in triaging extracolonic findings at CT colonography after training. A higher number of cases and/or a modified training program is needed to determine whether technologists can reach sufficient competence.

B-0725 11:15

Proposed CT diagnostic reference levels for Ireland

S.J. Foley¹, M.F. McEntee², L.A. Rainford¹; ¹Dublin/IE, ²Sydney/AU (*shane.foley@ucd.ie*)

Purpose: Computed tomography (CT) is recognised as the largest contributor to population dose from medical exposures, accounting for 56% of the total dose, but only 10% of the total examinations in Ireland. Diagnostic reference levels (DRLs) are crucial to dose optimisation, facilitating the identification of abnormally high doses. DRLs should be based on local, regional or national data and reflect local practices; however, current Irish values are based on international data from 1991. Given the advances that have occurred in CT technology since then and its increasing application, this research proposes updated DRLs for the most common CT examinations.

Methods and Materials: Forty-four CT scanners in Ireland from various manufacturers and with various multidetector capabilities were surveyed. Each CT centre was asked to record CT dose data (DLP, CTDIvol, tube voltage and current) prospectively, on 10-20 anonymised adult patients of average size (70±10 kg) presenting for eight common CT examinations. Mean results from each site were pooled and the 75th percentile was used to set DRLs using both CTDIvol and DLP.

Results: Dose data on 3,118 patients were collected. The DRLs for brain, sinuses, cervical spine, chest, HRCT, pulmonary angiography, abdomen and pelvis as well as trunk examinations, using CTDIvol were 69/59, 16, 20, 10, 9, 14, 13 and 11/13 mGy and using DLP were 940, 210, 420, 390, 280, 430, 600, 850 mGy/cm, respectively. These are up to 42% below current Irish and EU recommendations and compare favourably with other international studies.

Conclusion: DRLs should be regularly updated to facilitate optimisation of radiation doses.

B-0726 11:24

Comparison of automatic exposure control in CT equipment 64 slices

M. Monteiro, J. Santos, C. Silva, N. Santos; Coimbra/PT
(mmonteiro@estescoimbra.pt)

Purpose: To evaluate the influence of the technical parameters related to the AEC in the dose received by the patients and diagnostic image quality.

Methods and Materials: CT scans were acquired in two chest phantoms (adult and paediatric) in 2 different 64-CT equipments, with changes in technical parameters, related to their AEC. Six different protocols were used for adult and 2 for paediatric and chosen two images from each one to be evaluated using a Table specified for that. To evaluate their influence in the final image quality, CTDIw and DLP were analysed.

Results: The changes made in the technical parameters did not induce significant changes in the diagnostic quality imaging. With the used protocols 50% dose reduction was achieved, without producing images enable to diagnose.

Conclusion: The noise and mAs may still be handled in a more meaningful way in order to decrease the dose values, without interfering in the image quality. However, this analysis must be appropriate for the patient and the anatomic region under study.

B-0727 11:33

Identification of sentinel nodes during radiographer performed lymphoscintigraphy prior to sentinel lymph node biopsy

G. Camilleri, F. Zarb, K. Borg Grima; Msida/MT (francis.zarb@um.edu.mt)

Purpose: The concept that malignant disease primarily affects the sentinel node/s before being disseminated into the axillary nodes (ALNs) has dramatically evolved towards minimally invasive approaches in breast cancer management. Radiographer-performed lymphoscintigraphy using the cutaneous (subdermal) peri-areolar approach prior to SLNB is rapidly emerging as the technique for axillary staging in breast cancer limiting the dissection to the sentinel node/s (SN). The objective of this study was to define the role of radiographer-performed lymphoscintigraphy prior to SLNB and to establish the correlation between the numbers of SNs visualised on lymphoscintigraphy and the number of surgically identified SNs.

Methods and Materials: A quantitative approach was chosen for this non-experimental, correlation type of study. Between May 2009 and December 2010, a total of 55 female breast cancer patients (mean age, 58.35 years) who underwent SLNB with partial or total back-up axillary node dissection (ALND) were enrolled in this study. Lymphoscintigraphy reports and histology results were retrospectively evaluated.

Results: A minimum of 1 sentinel node was visualised on lymphoscintigraphy in 52 out of 55 patients (94.5%). Successful imaging was highly predictive ($p < 0.001$) of a successful SLNB. Results showed a significant association ($p < 0.05$) between the number of SN/s visualised on lymphoscintigraphy and the number of surgically identified SN/s during SLNB, with a concordance rate of 50.91%.

Conclusion: Lymphoscintigraphy performed by radiographers was shown to be indispensable in the reliable performance of SLNB.

B-0728 11:42

Ring-like contrast enhancement in liver metastases from rectal tumours - typical findings?

M. Kiss, B. Lombay; Miskolc/HU

Purpose: Rectal cancer can metastasize to almost any location in the body, most commonly the liver, lung, and peritoneum. The long-term results have improved, but long-term survival remains elusive for most. There are several therapeutic options - surgical, local or systemic chemotherapy - to manage metastases.

Methods and Materials: Between 01.10.2008 and 01.02.2011 we examined 1720 oncological patients with a known primary tumour and histologically established liver metastases. These patients underwent contrast-enhanced CT (a Siemens Somatom Definition AS+ 2x64 detector, row MDCT) and/or a contrast-enhanced liver MRI (a Siemens Magnetom Symphony 1.5 T). We analysed the visual ap-

pearance, the vascularisation of the metastases and studied how they changed during the course of treatment.

Results: We found liver metastases in 343 patients, with 84 (24.48%) patients who had primary rectal tumours. We divided the metastases into two groups, based on the pattern of their vascularity: hypervascular and hypovascular metastases. All these patient received systemic chemotherapy. In the hypovascular metastases we found 2 (2.38%) regression whereas 8 patients (9.52%) had unchanged status. On further evaluation and correlation of images, we found a "typical ring-like contrast enhancement" in liver metastases. Every patient with these metastases suffered progression independent of chemotherapy treatment.

Conclusion: CT and MRI scan has proved to be an excellent and widely used modality for the detection of liver metastases. The hypervascularised liver metastases with typical ring-like contrast enhancement are more likely to progress, independent of systemic chemotherapy.

10:30 - 12:00

Room Q

Neuro

SS 1311

Tumours

Moderators:

E. Avdagic; Sarajevo/BA

F.W. Cartes-Zumelzu; Innsbruck/AT

B-0729 10:30

Role of multimodal MR in brain glioma grading

P.A. Mattei, S. Salice, D. Tortora, V. Panara, C. Briganti, A.R. Cotroneo, M. Caulo, A. Tartaro; Chieti/IT (pamattei@unich.it)

Purpose: To evaluate the diagnostic accuracy of optimised cut-offs determined in pre-established regions of interest (ROI) with advanced MR techniques (perfusion, spectroscopy, diffusion and DTI) for differentiating between glioma WHO grade II vs. III and II vs III and IV.

Methods and Materials: 149 consecutive patients with cerebral glioma were retrospectively evaluated with a 3 T MR scanner. Gold standard was histology in 103 (30 low and 73 high grade). Four ROI were analysed: area of contrast enhancement (CE), T2 signal lower than that of liquor (T2-), T2 signal greater than or equal to liquor (T2+), and area with reduced diffusion (RD). Several parameters were determined for each ROI: rCBV, rMTT, Cho/Cr, Cho/NAA, Lip/Cr, Lac/Cr, ADC and FA. Statistical differences were evaluated with t-test ($p < 0.05$) and ROC analysis.

Results: The parameters which were capable of distinguishing between the low and high grade gliomas were: rCBV in CE (cut-off > 2.60, sensibility=72%, specificity=100%, AUC=0.85, $p=0.0001$), T2- (cut-off > 1.679, sensibility=73%, specificity=48%, AUC=0.705, $p=0.0004$), DR (cut-off > 2.615, sensibility=47%, specificity=90%, AUC=0.722, $p=0.0058$), Cho/Cr in T2- (cut-off > 1.93, sensibility=61%, specificity=75%, AUC=0.71, $p=0.0006$), Cho/Cr in DR (cut-off > 1.08, sensibility=94%, specificity=63%, AUC=0.809, $p=0.0001$). A statistically significant difference in rCBV was not observed between grades II ODG and WHO grade III gliomas or between grade II ODG and grade III astrocytomas. Cho/Cr in CE was higher (cut-off > 1.83, sensibility=100%, specificity=55%, AUC=0.872, $p=0.024$) in grade III ODG compared to grade II.

Conclusion: The integration of advanced MR quantitative biomarkers in the differential diagnosis between low and high grade gliomas can significantly improve diagnostic accuracy.

B-0730 10:39

DSC-MRI in glioblastomas: correlation of whole tumour histogram analysis of cerebral blood volume and vascular permeability (Ktrans) with biomarkers of tumour aggressiveness

R. Liserre, P.L. Poliani, M. Ferrara, S. Grisanti, L. Buttolo,

M. Buglione di Monale, R. Gasparotti; Brescia/IT (rliserre@libero.it)

Purpose: To examine the relationship between rCBV and contrast transfer coefficient (Ktrans) values obtained with dynamic susceptibility-contrast MR imaging (DSC-MRI) and histopathological features associated with tumour aggressiveness.

Methods and Materials: DSC MR imaging (Siemens Avanto 1.5 T) was obtained in a consecutive series of 30 patients with histologically confirmed glioblastoma (GBM), with a whole-brain T2*gradient-echo echo planar sequence during I.V. injection of a bolus of gadolinium-DTPA. Perfusion data were processed off-line with a dedicated software (NordicIce) to create colour-coded maps of rCBV and Ktrans. Regions of interest (ROIs) were manually drawn encompassing the whole

contrast-enhancing lesion and nonenhancing peritumoral area. Data analysis was performed with the histogram analysis of normalised CBVs and Ktrans from the entire tumour volume. The following histopathological variables were included into the statistical analysis: proliferation index (Mib-1/Ki67), tumour angiogenesis (enhancer of Zeste 2, EZH2), epidermal growth factor receptor (EGFR) and p53. **Results:** For whole tumour histogram analysis mean rCBV ($p < .001$ $r = .605$) and rCBV maximum values ($p < .05$, $r = .460$) were found to be significantly associated with EGFR expression. Mean and maximum rCBV values tended to be higher in patients showing increased overexpression of EGFR, with significant differences between subgroups as shown by post-hoc analysis ($p < .05$). No significant associations were found between Ktrans and histopathological markers. **Conclusion:** According to our findings EGFR overexpression, a molecular marker associated with tumour invasiveness, angiogenesis and radioresistance, is positively correlated with rCBV values, which could represent a new potential preoperative predictor of GBM response to therapy.

B-0731 10:48

High diagnostic accuracy of dynamic susceptibility contrast (DSC) magnetic resonance (MR) perfusion imaging to distinguish radiation necrosis from recurrent tumour in high-grade glioma patients

R. Tijong, M. Van den Bent, M. Smits; Rotterdam/NL

Purpose: To assess diagnostic accuracy and optimal relative cerebral blood volume (rCBV) ratio thresholds of dynamic susceptibility contrast-enhanced (DSC) perfusion to distinguish radiation necrosis from recurrent high grade glioma (HGG). **Methods and Materials:** From 157 HGG patients scanned at 3-month intervals between April 2010 and July 2011 with a standardised MR imaging protocol, 43 (27 males, mean age 51y) who had undergone radiotherapy and showed newly developed contrast-enhancing lesions were included in this retrospective study. DSC perfusion images were obtained at 1.5 T (GE Healthcare, US) with a 3 ml pre-load and 12 ml Gadovist 1.0 (Bayer Pharma) bolus administered at 5 ml/s using gradient-echo echo-planar imaging (TR 2000 ms). Ratios of maximum rCBV in contrast-enhancing lesions and contralateral white matter were calculated. The outcome measure was tumour progression, defined as clinical and/or radiological progression during 6-month follow-up. With logistic regression analysis the influence of patients' age, sex, tumour type and rCBV values on outcome was determined. A receiver operating characteristic (ROC) curve was created using sensitivity and specificity of different rCBV ratio thresholds for progression. **Results:** Only the rCBV ratio influenced outcome ($p < 0.01$). At an rCBV ratio of 1.35 100% sensitivity was obtained with specificity of 61%. At an rCBV ratio of 2.18 100% specificity was obtained with sensitivity of 72%. The area under the ROC curve (diagnostic accuracy) was 0.928 (SE 0.036). **Conclusion:** DSC perfusion MR imaging has high (93%) diagnostic accuracy to differentiate recurrent HGG from radiation necrosis. Maximum sensitivity is obtained at an rCBV ratio threshold of 1.35.

B-0732 10:57

Diagnostic accuracy of multimodal MR (MRS, DWI, DTI and DSC-PWI) tumour recurrence and radionecrosis

V. Panara, P.A. Mattei, D. Tortora, S. Salice, C. Briganti, A.R. Cotroneo, M. Caulo, A. Tartaro; Chieti/IT (valepana@libero.it)

Purpose: Conventional MR often fails in the differentiation between tumour recurrence and alterations induced by therapy (radiation therapy and chemotherapy) in primitive brain tumours. The aim of this study was to determine the cut-offs of perfusion (PWI), spectroscopy (2D-MRS), diffusion (DWI) and diffusion tensor (DTI) with a high field scanner (3 T) and the relative diagnostic accuracy in determining between tumour recurrence and post-adjuvant treatment cerebral modifications. **Methods and Materials:** 56 patients who had undergone surgery and adjuvant radiation therapy for cerebral gliomas were retrospectively evaluated. Exams were acquired with a 3 T. Four regions of interest (ROI) were analysed: area of contrast enhancement (CE), T2 signal lower than that of liquor (T2-), T2 signal greater than or equal to liquor (T2+) and area with reduced diffusion (RD). Several parameters were determined for each ROI: rCBV e rMTT, Cho/Cr, Cho/NAA, Lip/Cr, Lac/Cr, ADC and FA. Differences were evaluated with t-test and ROI analysis for optimal cut-offs. Gold-standard for was either histology or two-year follow-up. **Results:** Parameters which yielded statistically significant differences were rCBV in CE (cut-off > 0.5, sensibility=96%, specificity=100%, area under curve (AUC) 0.87, $p=0.04$), T2- (cut-off > 0.58, sensibility=96%, specificity=55%, AUC=0.80, $p=0.0001$) and T2+ (cut-off > 0.54, sensibility=64%, specificity=88%, AUC=0.78, $p=0.002$), Cho/Cr in T2- (cut-off > 2.17, sensibility=66%, specificity=100%, AUC=0.84, $p=0.0001$), and Lip/Cr in CE (cut-off ≤ 18.59, sensibility=94%, specificity=100%,

AUC=0.869, $p=0.04$) and T2+ (cut-off ≤ 1.045, sensibility=70%, specificity=86%, AUC=0.78, $p=0.017$). **Conclusion:** Given the elevated diagnostic accuracy observed for the indicated cut-offs, multimodal MR (MRS, and DSC-PWI) can be an instrumental method for the non-invasive differentiation between tumour recurrence and radionecrosis.

B-0733 11:06

Non-invasive differentiation of high- and low-grade glioma: a pulsed arterial spin labelling study using bolus arrival times

J. Furtner, V. Schoepf, G. Kasprian, M. Weber, G. Widhalm, S. Wolfsberger, M. Preusser, J.A. Hainfellner, D. Prayer; Vienna/AT (julia.furtner@meduniwien.ac.at)

Purpose: Pulsed arterial spin labelling (pASL) is a non-invasive MRI perfusion method using the water in the arterial blood as endogenous contrast agent. The purpose of this study was to determine the most suitable pASL inversion time point (TI) for the differentiation between high-grade and low-grade glioma, using a multi-TI-pASL approach which tracks the labelled bolus dynamically over time. **Methods and Materials:** Thirty-five patients with gliomas, histologically classified as low-grade ($n = 10$) or high-grade ($n = 25$) according to the WHO brain tumour classification were included. A 3 Tesla MR scanner (Trio Tim; Siemens Medical Solution, Erlangen, Germany) was used to perform pASL sequences at eight different inversion time points (370 ms, 614 ms, 864 ms, 1114 ms, 1364 ms, 1614 ms, 1864 ms, 2114 ms). The bolus arrival time, reflecting the maximum of tumour perfusion for all fixed inversion time points was calculated. A three-way mixed ANOVA was used to reveal potential differences in the bolus arrival time between high-grade and low-grade gliomas. **Results:** The difference of measured signal intensities between high-grade and low-grade gliomas obtained statistically significant results exclusively at 614 ms. ($p=0.005$). For all other determined inversion time points there was no significant difference of signal intensity between high-grade and low-grade gliomas (p -values ranged from 0.158 to 0.793). **Conclusion:** Our findings suggest that, using pASL for the evaluation of tumour perfusion, the most suitable inversion time point for differentiation of high-grade from low-grade glioma is 614 ms. Use of this pASL-TI may facilitate a non-invasive characterisation of such tumours, in the future.

B-0734 11:15

Simultaneous [18 F]-FET MR/PET in patients with cerebral tumours: comparison with conventional PET/CT

M. Souvatzoglou, S. Fuerst, C. Kruschke, S. Nekolla, S. Ziegler, C. Ganter, E. Rummeny, M. Schwaiger, A. Drzezga; Munich/DE (msouvatz@yahoo.de)

Purpose: To compare performance between PET/CT and recently introduced whole body MR/PET concerning evaluation of brain tumours. **Methods and Materials:** Twelve patients, referred to [18 F]FET-PET for brain tumour diagnostics, underwent a single-injection/dual-imaging protocol, including a PET/CT scan (Siemens-Truepoint 64, 34 ± 7 min p.i., 10 min 3D acquisition) and a subsequent MR/PET scan (Siemens mMR, 53 ± 11 min p.i., 15 min 3D acquisition), after injection of 171 ± 42 MBq [18 F]FET. Images were reconstructed with filtered backprojection (Hann 4.9 mm, zoom 2.5), attenuation correction was performed using low-dose CT for the PET/CT and Dixon-MR sequences for MR/PET. Images were interpreted visually and by semiquantitative analysis. The respective lesion and Bg SUVs were compared as well as the lesion/background ratios (T/Bg) using the Wilcoxon test. **Results:** Visual interpretation turned out suspicion of tumour tissue in 9/12 scans with both MR/PET and PET/CT, 3/12 patients were read as negative. Overall, T/Bg ratios as well as lesion- and Bg-SUVmax values were not different between PET/CT and MR/PET. However, the mean lesion- and Bg-SUVs were significantly higher for PET/CT, as compared to the respective MR/PET-values (lesions: 2.6 ± 1 vs. 2.2 ± 0.8 ; $p=0.01$; Bg: 1.19 ± 0.3 vs. 1.04 ± 0.2 ; $p=0.003$). There was a significant correlation between the respective max and mean lesion and Bg SUVs as well as between the respective T/Bg ratios. **Conclusion:** Imaging of brain tumours with [18 F]FET is feasible with the integrated whole body MR/PET-scanner with high image quality. Despite technological differences, the quantitative evaluation of [18 F]FET-PET data with MR/PET reveals comparable results as with PET/CT, indicating that established lesion/background ratio thresholds for distinguishing malignant brain tumour tissue, can be transferred.

B-0735 11:24

Contribution of diffusion and perfusion-weighted magnetic resonance imaging in the differential diagnosis of sellar and parasellar tumours: preliminary report

J. Bladowska, A. Zimny, P. Szewczyk, M. Guzinski, P. Tabakow, M. Kozba-Goszyta, W. Jarmundowicz, M. Sasiadek; *Wroclaw/PL (mbladow@wp.pl)*

Purpose: The most common pituitary tumours are adenomas, which, however, may be mimicked by other tumours that can show very similar appearance in plain MRI. The aim of our study was to evaluate usefulness of diffusion (DWI) and perfusion-weighted MR imaging (PWI) in the differential diagnosis of sellar/parasellar tumours.

Methods and Materials: Twenty-eight sellar/parasellar tumours (15 adenomas, 9 meningiomas, 1 intrasellar haemangioblastoma, 1 suprasellar glioma, 1 pituitary abscess, and 1 hamartoma) underwent standard MRI as well as DWI and PWI using 1.5 Tesla MR unit. In each tumour min. rADC and max. rCBV measurements were calculated. The relative peak height (rPH) and the relative percentage of signal intensity recovery (rPSR) were also evaluated.

Results: The mean values of min. rADC, max. rCBV, rPH and rPSR for different tumour types were as follows: adenomas (0.77; 5.19; 3.49; 0.36), meningiomas (1.07; 9.52; 3.91; 0.38), haemangioblastoma (2.0; 8.14; 9.05; -0.30), glioma (0.86; 7.48; 8.52; 0.93), abscess (0.68; 0.79; 1.26; 1.01), hamartoma (1.36; 1.07; 4.20; 0.57), respectively. There were significant differences between adenomas and all other tumour types in perfusion parameters and also in min. rADC values. There were no significant differences in rPH and rPSR between adenomas and meningiomas, while other tumours revealed significantly different values of rPH and rPSR, compared to pituitary adenomas.

Conclusion: PWI and DWI seem to be very useful in differential diagnosis of sellar/parasellar tumours, what may be of high importance in the clinical practice, especially in proper choice of surgical approach.

B-0736 11:33

Isolated cerebral susceptibility artefacts in patients with malignant melanoma: metastasis or not?

C. Gramsch, S. Goericke, F. Behrens, A. Krasny, L. Zimmer, D. Schadendorf, M. Forsting, M. Schlamann; *Essen/DE (Carolin.Gramsch@uk-essen.de)*

Purpose: At initial staging patients with malignant melanoma often show isolated cerebral susceptibility artefacts in T2*-weighted/SWI sequences without corresponding lesion in contrast-enhanced T1-weighted MR images. Cavemomas, microhaemorrhages and melanin-containing metastases without contrast enhancement represent possible differential diagnoses for these findings. Purpose of this study was to evaluate, if these lesions already represent metastases.

Methods and Materials: MR images (1.5 T) of 20 patients (6w, 14m) with malignant melanoma and no history of cerebral metastasis but signal intensity loss in T2*/SWI at initial staging by MRI were reviewed retrospectively. MRI protocol consisted of a T2*/SWI, a FLAIR sequence, non-enhanced T1w and contrast-enhanced MPR. Patients were followed by MRI in mean 19.6 months (range, 6 - 46 months, 2006 - 2009).

Results: All patients showed in mean 2.1 (range, 1-5) hypointense lesions in T2*/SWI. None of these lesions could be confirmed as cerebral metastases by follow-up.

Conclusion: Isolated cerebral susceptibility artefacts in T2*/SWI sequences without correlate in contrast weighted T1 images do not seem to indicate cerebral metastases.

B-0737 11:42

Evaluation of susceptibility weighted imaging in distinguishing of high-grade gliomas from primary central nervous system lymphomas

D. Cao, Y. Ding, Z. Xing, J. Li, M. Xiong; *Fuzhou/CN (caodr.87983593@yahoo.com.cn)*

Purpose: To analyse the findings of high-grade gliomas and PCNSL on SWI and conventional MR imaging, and to evaluate SWI in differentiating between these two tumours.

Methods and Materials: This study was approved by the institutional review board, and informed consent was obtained from all patients. 27 patients with high-grade gliomas 12 patients with PCNSL who had undergone conventional MR imaging and SWI were confirmed by histopathology. The number of lesions which were found haemorrhage was separately counted on the conventional MR imaging and SWI, then haemorrhage detection rate within tumours between these two sequences was separately compared, haemorrhage rate between these two tumours on SWI was also statistically analysed. Furthermore, the volume of haemorrhage and the number of intralesional vessels of these two tumours were statistically analysed.

Results: There was a statistically significant difference in the detection of haemorrhage between the conventional MR imaging and SWI ($P < 0.05$) in high-grade gliomas, but not in PCNSL ($P > 0.05$). There was a statistically significant difference in the haemorrhage rates of these two tumours on SWI ($P < 0.05$). The haemorrhagic volume of high-grade gliomas was statistically higher than PCNSL on SWI. No vessels were found in all the lesions of PCNSL. The number of intralesional vessels of high-grade gliomas was statistically higher than PCNSL on SWI.

Conclusion: SWI is more sensitive than the conventional MR imaging in detecting haemorrhage in high-grade gliomas. SWI is helpful to differentiate high-grade gliomas and PCNSL.

B-0738 11:51

Subependymal nodules and giant cell tumour prevalence in genetically studied tuberous sclerosis complex patients

C. Michelozzi¹, F. Galli¹, G. Di Leo², F. Silva Barbosa¹, F. Sardanelli², G. Cornalba¹; ¹Milan/IT, ²San Donato Milanese/IT (caterina.michelozzi@gmail.com)

Purpose: To estimate the association among the presence of subependymal nodules (SEN), subependymal giant cell tumour (SGCT) and gene mutation in tuberous sclerosis complex (TSC) patients.

Methods and Materials: Contrast-enhanced brain MRI studies of 81 TSC patients were retrospectively reviewed by two neuroradiologists in consensus. The number of SENs was recorded. Any enhancing SEN \geq 1 cm in diameter and placed near the foramen of Monro was considered as SGCT. Two brain MRI follow-up exams for each patient with SGCT were evaluated to assess tumour growth in terms of diameter and volume. Patients were categorised into three subgroups according to genetic assessment: TSC1, TSC2 and no mutation identified (NMI) patients. Wilcoxon and Chi-squared tests were used.

Results: Out of 81 patients, 17 were NMI, 20 TSC1, 44 TSC2. Fifty showed at least one SEN. A higher trend of SEN and SGCT among TSC2-patients was observed ($p=0.251$ and $p=0.187$, respectively). There was a significant association between SGCT and SEN: all of the 12 SGCT patients had at least one further SEN, while none of the 31 patients without SEN showed an SGCT ($p=0.003$). At follow-up, the median SGCT diameter significantly increased from 14 mm to 15 mm ($p=0.017$), while the median volume significantly increased from 589 mm³ to 791 mm³ ($p=0.006$).

Conclusion: TSC patients with SENs are more likely to present with SGCT and a closer follow-up is suggested, in particular, if affected with TSC2 mutation. Volume assessment is more sensitive than diameter to evaluate tumour growth.

Monday, March 5

10:30 - 12:00

Room A

Neuro

SS 1711

Vascular and perfusion imaging

Moderators:

H. Aronen; Turku/FI

J. Frühwald-Pallamar; Vienna/AT

B-0740 10:30

Time-resolved imaging of contrast kinetics does not improve performance of follow-up MRA of embolised intracranial aneurysms

Z. Serafin, P. Strzeńniewski, W. Lasek, W. Beuth; Bydgoszcz/PL
(serafin@cm.umk.pl)

Purpose: The use of contrast media and the time-resolved imaging of contrast kinetics (TRICKS) technique has some theoretical advantages over time-of-flight magnetic resonance angiography (TOF-MRA) in the follow-up of intracranial aneurysms after endovascular treatment. We prospectively compared the diagnostic performance of TRICKS and TOF-MRA with digital subtracted angiography (DSA) in the assessment of occlusion of embolised aneurysms.

Methods and Materials: Seventy-two consecutive patients with 72 aneurysms were examined 3 months after the embolisation. Test characteristics of TOF-MRA and TRICKS were calculated for the detection of the residual flow. The results of the quantification of the flow were compared with weighted kappa. Intraobserver and interobserver reproducibility was determined.

Results: The sensitivity of TOF-MRA was 85% (95% CI, 65-96%) and of TRICKS, 89% (95% CI, 70-97%). The specificity of both methods was 91% (95% CI, 79-98%). Accuracy of the flow quantification ranged from 0.76 (TOF-MRA) to 0.83 (TRICKS). There was no significant difference between the methods in the area under the ROC curve regarding both the detection and the quantification of the flow. The intraobserver reproducibility was very good with both techniques (kappa, 0.86-0.91). The interobserver reproducibility was moderate for TOF-MRA and very good for TRICKS (kappa, 0.72-0.81).

Conclusion: In this study, TOF-MRA and TRICKS presented similar diagnostic performance. Therefore, the use of time-resolved contrast-enhanced MRA is not justified in the follow-up of embolised aneurysms.

B-0741 10:39

Follow-up after embolisation of ruptured intracranial aneurysms: a prospective comparison of two-dimensional digital subtracted angiography, three-dimensional digital subtracted angiography, and time-of-flight magnetic resonance angiography

Z. Serafin, P. Strzeńniewski, W. Lasek, W. Beuth; Bydgoszcz/PL
(serafin@cm.umk.pl)

Purpose: The most appropriate method for follow-up of intracranial aneurysms after endovascular treatment is still being discussed. The purpose of the study was a prospective comparison of the diagnostic performance of digital subtracted angiography (DSA) and time-of-flight magnetic resonance angiography (TOF-MRA) at follow-up.

Methods and Materials: A total number of 72 consecutive patients with 72 aneurysms were examined 3 months after the embolisation. The index tests included: two-dimensional DSA (2D-DSA), three-dimensional DSA (3D-DSA), and TOF-MRA. The reference test was a consensus between 2D-DSA and 3D-DSA. The evaluation included detection of the residual flow, quantification of the flow, and validity of the decision on the retreatment. Intraobserver and interobserver reproducibility was determined.

Results: Sensitivity and specificity in the detection of the residual flow ranged from 84.6% (2D-DSA and TOF-MRA) to 92.3% (3D-DSA) and from 91.3% (TOF-MRA) to 97.8% (3D-DSA). Accuracy of the evaluation of the flow degree ranged from 0.78 (2D-DSA) to 0.92 (3D-DSA, Cohen kappa). 2D-DSA presented lower performance in the decision on re-embolisation than 3D-DSA ($P < 0.05$, ROC analysis). The intraobserver reproducibility was very good with all techniques (kappa, 0.86-0.97). The interobserver reproducibility was moderate for TOF-MRA and very good for 2D-DSA and 3D-DSA (kappa, 0.72-0.94).

Conclusion: The most precise method of aneurysm follow-up is 3D-DSA. 2D-DSA shows a lower diagnostic value with regard to the decision on re-embolisation. Considering the invasiveness of DSA and the minor difference in the diagnostic performance between 3D-DSA and TOF-MRA, the latter method should be the basic modality for follow-up after aneurysm embolisation.

B-0742 10:48

Positional venous MR angiography: an operator independent tool to evaluate cerebral venous outflow haemodynamics

P. Niggemann¹, M. Seifert¹, A. Foerg², H.H. Schild¹, H. Urbach¹, T. Krings³; ¹Bonn/DE, ²Aschheim/DE, ³Toronto, ON/CA
(pascal.niggemann@ukb.uni-bonn.de)

Purpose: Chronic cerebrospinal venous insufficiency (CCSVI) has been proposed as a cause for multiple sclerosis (MS). According to this theory, strictures of the internal jugular veins (IJV) are amongst the described causes for CCSVI. Little is known about their influence on the haemodynamics of the cerebral venous blood outflow (CVBO). We employed positional MRI to describe the influence of positional changes on the CVBO.

Methods and Materials: Using the FONAR Upright MRI a venous time of flight angiography of the cervical region was acquired in supine and sitting positions in fifteen healthy volunteers. The image quality was rated; the positional findings and interindividual variances in the CVBO were analysed.

Results: A venous time of flight angiography of the cervical spine was feasible with good image quality. Strictures of one or both IJV were found in 8 of 15 healthy volunteers in supine position; however, none was visible in upright position. The IJV was not the main outflow route in the erect position.

Conclusion: IJV strictures are a common finding in healthy volunteers in supine position. They seem to be of no relevance in the erect position. This questions the validity of this criterion for the diagnosis of CCSVI. Reflux into the venous system was not visualised and it remains to be seen whether it can be identified in patients with MS. Positional MRI enables operator independent evaluation of the CVBO and may help to clarify the validity of the criteria for CCSVI.

B-0743 10:57

7 Tesla MRI of the intracranial arterial vasculature: non-enhanced versus contrast-enhanced MPRAGE imaging

L. Umutlu, N. Theysohn, S. Maderwald, K. Wrede, P. Dammann, M.E. Ladd, S.L. Goericke, M. Forsting, M. Schlamann;
Essen/DE (Lale.Umutlu@uk-essen.de)

Purpose: Non-enhanced 7T MPRAGE-imaging is known to provide a homogeneous hyperintense vessel signal of the intracranial arteries. Aim of this trial was to assess a possible diagnostic benefit of the application of contrast-media in an intraindividual comparison setting of non-enhanced versus contrast-enhanced MPRAGE imaging.

Methods and Materials: 12 subjects were examined on a 7T whole body MR system (Magnetom 7T, Siemens) utilising a 32-channel head coil (Nova). For intracranial vessel delineation an MPRAGE sequence was obtained pre- and post-contrast (1-molar Gadobutrol, Bayer Healthcare). The following arteries and arterial segments were assessed utilising a five-point scale: (1) anterior cerebral artery, (2) arteria pericallosa, (3) internal carotid artery, (4) middle cerebral artery (segments M1-3), (5) posterior communicating artery, (6) posterior cerebral artery and (7) basilar artery. For statistical analysis, a Wilcoxon rank test was used.

Results: Visual analysis demonstrated a high-quality assessment of non-enhanced MPRAGE imaging for the complete intracranial arterial vasculature (mean 3.85), due to a homogeneous hyperintense vessel signal. The application of contrast media allowed only for a mild improvement of the delineation of central vessel segments, such as the carotid T (mean (ne) 4.83; mean (ce) 4.95). Yet, the conspicuity of smaller vessel segments was significantly improved in the contrast-enhanced MPRAGE images (e.g. anterior communicating artery: mean (ne) 3.33 to mean (ce) 4.50; $p=0.04$).

Conclusion: Exclusive non-enhanced 7T MPRAGE imaging provides a high-quality assessment of the intracranial arterial vasculature and may be beneficial in assessing the intracranial arterial vasculature in patients with contraindications to the application of contrast media (e.g. renal insufficiency).

B-0744 11:06

Asymmetry of carotid artery wall thickness between carotid arteries

L. Saba¹, S. Sannia¹, E. Raz², G. Ledda¹; ¹Cagliari/IT, ²New York, NY/US
(lucasaba@tiscali.it)

Purpose: Previous publications demonstrated that the CT angiography (CTA) can evaluate the carotid artery wall thickness (CAWT). The purpose of this work was to compare the asymmetry of CAWT between carotids in symptomatic and asymptomatic patients.

Methods and Material: Sixty consecutive symptomatic (males 44; median age 64) patients and sixty non-symptomatic patients matched for gender and age, were analysed using a 40-detector-row CT angiography. Each patient was analysed by injecting 80 ml of contrast material at a 5 ml/sec flow rate. CAWT was calculated

for both carotids and for each patient the ratio between the biggest CAWT and the contra-lateral was calculated to obtain an index. Bland-Altman, logistic regression and ROC curve analysis were calculated.

Results: The Bland-Altman plot demonstrates a very good agreement between measurements with a mean difference value of only 3.4% and 95% CI from -8% to 14.8%. A statistically significant difference in ACAWT between symptomatic and asymptomatic patients (with a p value of 0.0001) was found. The ROC area under the curve was 0.742 (p = 0.001). Logistic regression model indicated that ACAWT, stenosis degree and fatty plaques were independent variables associated with cerebrovascular symptoms (p value, respectively, 0.0057, 0.0003 and 0.0178).

Conclusion: Results of our study indicated that the index of asymmetry in the CAWT may be used as further parameter to stratify the risk of symptoms related to carotid artery.

B-0745 11:15

Detection of cerebral vasospasm using dynamic CT: analysis of volume perfusion CT maps and 4D-CT angiography

P. Schramm¹, K. Dolatowski¹, R. Schramm¹, A. Froelich¹, E. Klotz², M. Knauth¹; ¹Göttingen/DE, ²Forchheim/DE (p.schramm@med.uni-goettingen.de)

Purpose: Cerebral vasospasm with a raised risk for secondary ischemia is a frequent complication after subarachnoid haemorrhage (SAH). We tested, whether "whole brain" volume perfusion CT (VPCT) delivers relevant information about the localisation and characteristics of arterial vasospasm and the volume at risk of secondary infarction.

Methods and Materials: 11 consecutive patients with suspicion of cerebral vasospasm due to SAH underwent VPCT of the brain. CT angiographic maximum-intensity projections were generated from thin slice reconstructions of the VPCT dataset at peak arterial time. Images were assessed for the presence of arterial vasospasm and compared with conventional CTA or DSA. The distribution of ischaemic lesions was analysed on 3D perfusion parameter maps of cerebral blood flow (CBF), cerebral blood volume (CBV), mean transit time (MTT) and time to drain (TTD).

Results: In all 11 patients, focal areas of cerebral hypoperfusion were detected on colour-coded VPCT parameter maps. The highest sensitivity was found for MTT and TTD. Focal reductions of CBV strongly correlated with infarction on follow-up CT. 8 patients (73%) had vasospastic lesions of intracranial arteries on MIP reconstructions of the 4D CTA. All of these stenotic lesions were also visible on conventional CTA or DSA, resulting in 100% sensitivity of the 4D CTA reconstructions.

Conclusion: VPCT is a non-invasive method that allows detecting cerebral vasospasm in patients suffering from SAH. It has the potential to demonstrate focal perfusion deficits as well as vasospastic arterial segments and might therefore improve diagnosis and treatment decisions in those patients.

B-0746 11:24

Relationship between thrombus density and different stroke subtypes

J. Niesten¹, I. Van der Schaaf¹, G. Biessels¹, L. Kappelle¹, T. Van Seeters¹, Y. Van Der Graaf¹, W. Mali¹, B. Velthuis¹, A. Horsch²; ¹Utrecht/NL, ²Arnhem/NL (jniesten@hotmail.com)

Purpose: To determine the relationship between thrombus density and different stroke subtypes in patients with acute ischaemic stroke.

Methods and Materials: We prospectively included 91 patients with acute ischaemic anterior circulation stroke and a visible occlusion on CTA that was presumed to be caused by cardioembolism (n=35), large artery atherosclerosis (LAA, n=39) or dissection (n=17). All patients underwent non-contrast CT (NCCT), CT-perfusion and CT-angiography on admission within 9 hours after stroke onset. Presence or absence of a dense vessel sign (DVS) was assessed on NCCT and thrombus density was measured in Hounsfield Units (HU) on NCCT. Subsequently, DVSs and thrombus density were related with stroke subtypes.

Results: The presence of DVSs differed significantly among subtypes. DVS was found in 46% of patients with cardioembolism, in 59% of patients with LAA, and in 94% of patients with dissection (X2-test; p=0.002). The mean HU-value was significantly higher in dense vessels than in non-dense vessels: 50.1 (95% confidence interval (CI) 47.5-52.7) versus 40.2 (95%CI 37.8-42.6). The mean HU-value of all vessels with thrombus was 39.9 (95%CI 37.9-42.0) in cardioembolism, 47.1 (95%CI 43.0-51.2) in LAA and 57.0 (95%CI 51.9-62.1) in dissection (ANCOVA-test, p < 0.0001). We found the same significant ranking order in the density of thrombi with DVSs (mean HU-value: cardioembolism 43.3 (95%CI 40.0-46.5); LAA 49.3 (95%CI 46.0-52.6); dissection 58.2 (95%CI 53.3-63.1), ANCOVA-test; p=0.003).

Conclusion: Thrombus density is related to stroke subtype and probably reflects different thrombus composition. The predictive value of thrombus density for recanalisation-rate should be further investigated.

B-0747 11:33

Total cerebral blood flow from childhood to early senescence as assessed with phase-contrast imaging

I. Koerte¹, A. Pomschar¹, R.P. Laubender¹, D. Steffinger¹, F. Heinen¹, M. Reiser¹, N. Alperin², B. Ertl-Wagner¹; ¹Munich/DE, ²Miami, FL/US (inga.koerte@med.uni-muenchen.de)

Purpose: Cerebral blood flow changes with increasing age; however, no normative values in childhood and adolescents are available until present. We aimed to investigate and quantify the total cerebral blood flow in physiological development and ageing by phase contrast MR imaging.

Methods and Materials: After informed consent, 147 healthy subjects (66 males, 81 females, age 3 to 69 years) were investigated on a 3 T MRI. Cine-phase contrast sequences were performed at an axial plane perpendicular to the neck vessels to quantify arterial inflow through the left and right carotid (LCA, RCA) and left and right vertebral artery (LVA and RVA). Total cerebral blood flow was defined as the sum of flow through these four cervicocranial arteries. Data were analysed with linear regression models relying on fractional polynomials of second degree.

Results: Total cerebral blood flow significantly decreased with increasing age (p < 0.0001) in a non-linear fashion (ranged 1670-500 ml/min). This was also true for the quantitative flow through each of the investigated arteries (LCA, RCA, LVA and RVA (p < 0.0001)). Gender had no significant effect on arterial cerebral blood flow.

Conclusion: Total cerebral blood flow is age-dependent and decreases with age. This decrease already starts in childhood. Gender does not have a significant impact on cerebral blood flow. These age-related changes need to be taken into consideration when interpreting MR-based quantifications of cerebral blood flow in patients.

10:30 - 12:00

Room D1

Chest

SS 1704

Tissue characterisation

Moderators:

R. Cesar; Golnik/SI
M. Wielpütz; Heidelberg/DE

B-0748 10:30

CT findings of pneumonic type adenocarcinoma: comparison between invasive mucinous adenocarcinoma and nonmucinous adenocarcinoma

S. Nakamura; Shimabara/JP (snakamura662@gmail.com)



Purpose: Invasive mucinous adenocarcinoma (IMA) formerly classified as mucinous BAC usually presents consolidative opacities mimicking pneumonia on CT, on the contrary such pneumonic type adenocarcinoma may occur in nonmucinous adenocarcinoma (NMA) formerly classified as nonmucinous BAC. These tumours should be separated into different categories, because they have clinical, pathologic and genetic differences. The purpose of this study was to compare the CT findings of pneumonic type adenocarcinoma between IMA and NMA.

Methods and Materials: We retrospectively studied twenty patients with pathologically proven pneumonic type adenocarcinoma at four institutions from 1999 to 2011. They consist of 11 females and 9 males with ages ranging from 40 to 87 years (mean 71 years). CT findings of IMA (n=14) and NMA (n=6) were compared based on the characteristics of consolidation: peripheral distribution, lower lung predominance, multifocal distribution, air bronchogram, cavitation or cyst, heterogeneity, surrounding ground-glass opacity (GGO), bulging fissure, and CT angiogram sign. Accessory opacities (centrilobular nodules, cavities, GGO), pleural effusion, and lymphadenopathy were also analysed.

Results: CT showed peripheral distribution (6/14), cavitation or cyst (12/14), bulging fissure (9/14), and CT angiogram sign (5/9) in IMA type, while, those findings were not seen in NMA type. The former three findings were statistically significantly different between them. Lower lung predominance, multifocal distribution, air bronchogram, heterogeneity, surrounding GGO, and centrilobular nodules were seen in both types with no significant difference.

Conclusion: The absence of CT findings such as peripheral distribution, cavitation or cyst, and bulging fissure indicates the possibility of pneumonic type NMA.

B-0749 10:39

Dynamic perfusion MRI in patients suffering from primary lung cancer: a novel approach to tumour characterisation?

M. Regier, F.O. Henes, D. Schwarz, A. Laqmani, H. Kooijman, G. Adam; Hamburg/DE (mregier@uke.de)

Purpose: To evaluate the accuracy of dynamic magnetic resonance perfusion imaging (DCE-MR) in the differentiation of histological subtypes of primary lung cancer and to determine whether tumour localisation effects perfusion kinetics.

Methods and Materials: In 28 patients suffering from primary lung cancer dynamic contrast-enhanced MRI was performed for six minutes using a T1w 3D-GRE sequence (TR/TE, 4.9/2.4 ms; FOV, 375 mm; in-plane-resolution, 1.9x2.2x2 mm; scan-time, 17sec) at 1.5 Tesla. Density-time curves were determined by placing a region-of-interest (ROI) on the entire tumour as well as high-enhancing areas. The perfusion and peak enhancement were calculated using the maximum-slope method. Results were compared according to histological subtype, differentiation, size and allocation. The statistical analysis included Wilcoxon-test and Spearman's correlation coefficient.

Results: Tumour perfusion determined for both the entire tumour ($p < 0.0001$) and the maximum enhancing area ($p < 0.0001$) was significantly higher in smaller tumours than in larger ones. Peripheral carcinomas revealed a slightly higher perfusion than central tumours ($p=0.07$). The small cell carcinomas (SCLC) showed a significantly higher perfusion ($p=0.02$) and peak enhancement ($p=0.03$) than the adenocarcinomas. The comparison of SCLC with other non-small cell lung cancers (NSCLC) did not reveal any significant perfusion differences. In six patients tumour signal intensity showed an increase prior to aortic signal increase alluding to distinct tumour blood supply from pulmonary vessels.

Conclusion: DCE-MR depicts kinetic differences in perfusion between common histological subtypes of primary lung cancer. Additionally, DCE-MR can raise information about origin of tumour blood supply, perfusion and peak enhancement and might therefore be considered for therapy response monitoring.

B-0750 10:48

Conventional 18 FDG/PET-CT combined with first-pass CT-perfusion technique in lung cancer patients: clinical staging and functional information in a single study

C. Capraro, D. Ippolito, L. Guerra, E. De Ponti, C. Messa, S. Sironi; Monza/IT (cristinacapraro@hotmail.it)

Purpose: To assess the additional functional information and the relationship between perfusion measurements and glucose metabolism, obtained including CT-perfusion study (CTp) into whole body contrast-enhanced PET/CT protocol for lung cancer staging.

Methods and Materials: A total of 49 patients with biopsy-proven lung cancer, who were referred for cePET/CT staging, were prospectively enrolled in our study. Low-dose unenhanced PET/CT was acquired first. The position of CTp study was defined on PET/CT, and CTp was performed with following parameters: Kv120; mAs80; scan30, i.v. injection of 50 ml contrast-agent, 5 ml/sec. Then another bolus of contrast media (3 ml/sec; 80 ml, 60sec delay) was applied to assure the full diagnostic ceCT for clinical staging. CTp data were used to calculate a range of tumour vascularity parameters (BF, BV, and MTT) and tumour FDG uptake (SUVmax) was used as a metabolic indicator. Quantitative and functional parameters were compared and statistically analysed in relation to location, histology and tumour size.

Results: The perfusion images were analysed using a commercially available software (Perfusion 3.0; Advantage; GE) which generated a quantitative map of arterial perfusion. Significant differences with lower perfusion parameters were noted in tumours > 30 mm than in tumours < 30 mm ($p < 0.05$): BV 6.7 vs 15.4 ml/100 g; BF 7.7 vs 14.2 ml/min/100 g, MTT 5.7 vs 9.2sec, respectively. Interestingly, highest correlations (linear regression) were detected between BV and SUVmax for tumours with diameter > 3 cm. No significant differences were noted according to location and pathological tumour type. These results may indicate that large tumours exhibit significantly lower perfusion and higher metabolism in relation to their aggressiveness, showing that not only histological type but also size and presence of necrosis could determine the enhancement characteristics of lung carcinomas.

Conclusion: CT-p combined with PET/CT is feasible technique that can provide additional functional information about vascularity and tumour aggressiveness, thus helping in assessing the prognosis and proper treatment choice.

B-0751 10:57

Lung cancer perfusion: can we measure pulmonary and bronchial circulation simultaneously?

X. Yuan¹, G. Ao¹, J. Zhang²; ¹Beijing/CN, ²Shanghai/CN (yuanxiaodongzj@163.com)

Purpose: To report a new CT perfusion technique and its primary findings in assessing double blood supply in advanced bronchial carcinomas (ABCs).

Methods and Materials: Based on 320-detector row CT, a dual-input lung cancer perfusion model (DILCP) was established: Pulmonary trunk and descending aorta (representing bronchial artery) were appointed input arteries for pulmonary and bronchial circulation, respectively, peak time point of left atrium served as boundary between the two. Then pulmonary flow (PF), bronchial flow (BF), and perfusion index (PI, = PF/(PF+BF)) was figured out according to maximum slope method. After written informed consents were acquired 31 consecutive subjects with advanced bronchial carcinomas underwent the DILCP test. Haemodynamics of ABCs was compared with localisation (peripheral or central) and histology.

Results: Haemodynamics of the 31 ABCs were as follows: PF, 19.84±13.11 ml/min/100 ml; BF, 48.89±25.44 ml/min/100 ml; PI, 0.31±0.19. Both central (n=14) and peripheral (n=17) tumours have a predominant systemic circulation (PI: 0.23, 0.37, respectively; both statistically less than 0.5, the latter is bigger than the former, $p=0.038$). All kinds of histology of ABCs showed PIs less than 0.5 without significant difference between each other.

Conclusion: A new CT perfusion technique was established for assessing double blood supply in lung cancer. Our primary findings suggest that 1) advanced bronchial carcinoma is fed simultaneously by pulmonary and systemic circulation, 2) the latter is dominant independent of localisation and histology, furthermore 3) the proportion of pulmonary circulation with peripheral tumours is higher than that with central tumours.

B-0752 11:06

CT findings predicting EGFR gene mutation in patients with non-small-cell lung cancer

M.-P. Revel, C. Bordonne, H. Blons, A. Lupo, A. Cazes, G. Chatellier; Paris/FR (marie-pierre.revel@egp.aphp.fr)

Purpose: To compare computed tomography (CT) findings in non-small -cell lung cancer (NSCLC) patients with and without epidermal growth factor receptor (EGFR) gene mutations

Methods and Materials: Initial CT findings in 151 NSCLC patients, 62 with and 89 without EGFR gene mutation were retrospectively reviewed by two radiologists in consensus. The patient group mainly included patients with TTF1+ adenocarcinomas (110/151, 72.8%). The presence of ground glass opacity (GGO), of tumour density heterogeneity, of lymph node enlargement was analysed together with the presence of multiple nodules (>6) associated with the main tumour. The maximum diameter of the tumour was also measured.

Results: No significant correlation was found between EGFR gene mutation and GGO (30.2% in the mutation group vs 20.0%) ($p=0.32$), tumour density heterogeneity (32.0% vs 32.5%) ($p=0.97$) or lymph node enlargement (30.6% vs 34.8%) ($p=0.6$). The maximum diameter of the tumour was not significantly different in patients with and without EGFR gene mutation (40 vs 43 mm) ($p=0.21$). The presence of multiples nodules associated with the main tumour was more frequent in the mutation group (13/62, 20.9% vs 7/89, 7.9%) ($p=0.03$). Men proportion was significantly lower in the EGFR gene mutation group (29.0% vs 47.1%) ($p=0.03$).

Conclusion: The presence of multiple nodules associated with the main tumour is the only CT finding suggesting EGFR mutation at initial presentation of patients with NSCLC.

B-0753 11:15

Radiation dose to the radiologist during continuous CT-fluoroscopy-guided lung biopsy using different HandCARE options: how safe is it?

W.F.M. De Wever, F. Zanca, A. Jacobs, N. Bergans, R. Bogaerts, J. Coolen, J. Verschakelen, H. Bosmans; Leuven/BE (walter.deweever@uzleuven.be)

Purpose: CT-Fluoroscopy-guided lung biopsy (CTFLB) involves direct operator irradiation. Occupational limits (skin: 500-, eye-lens: 150-mSv/year) were reached at our department. Study purpose was to assess occupational body, hand and eye doses during CTFLB for routine and low dose protocol, using different HandCARE (HC) positions. HandCARE interrupts x-ray at selectable positions (10, 12 or 2 o'clock).

Methods and Materials: Data from 30 CTFLB biopsy-procedures were prospectively collected. Twenty were performed using the routine protocol (120 kV, 30 mAs, 10 mm slice) with HC-12 (10 patients), HC-10 (5 patients) and HC-2 (5 patients). A



low-dose protocol (80 kV, 30 mA, 10 mm slice) was used with HC-12 o'clock for last 10 patients. One radiologist, at 10 o'clock position of the CT-table, wearing apron, finger dosimeter, collar and goggle, performed all interventions. Body-, hand- and eye lens (unshielded) operator doses were monitored; total fluoroscopic time (TFT) and total hand time entering primary beam (THT) were recorded.

Results: Median TFT was 84s (range, 36-660s), median THT was 35s (range, 13-138s). Average operator doses per procedure at different HC for routine protocol were comparable (range 0.049-0.063mSv, average 0.056mSv); low-dose protocol showed 42% dose reduction (0.032 mSv). Maximum average dose to hands and eyes were 19.84mSv and 0.38mSv, 15.22mSv and 0.31mSv, 17.54mSv and 0.51mSv for HC-12, -10 and -2o'clock. They were 4.57mSv and 0.17mSv for the 80 kV protocol.

Conclusion: Compliance with occupational limits can be reached by matching radiologist and HC position and using low-dose protocols.

B-0754 11:24

Percutaneous transthoracic needle biopsy of pulmonary nodules with Xper-CT and Xper-Guide: a new technical approach

D. Leni, F. Vacirca, D. Ippolito, R. Corso; Monza/IT (dalenit@tin.it)

Purpose: To evaluate feasibility and efficacy of percutaneous transthoracic needle biopsy of pulmonary nodules with Xper-CT and Xper-Guide.

Methods and Materials: From 11/2009 to 6/2011 148 patients were scheduled for percutaneous transthoracic needle biopsy of pulmonary nodules using Xper-CT and Xper-Guide, new software applications provided by Philips Allura FD20. All procedures were performed with local anaesthesia in the angiographical suite. Before puncture patients underwent Xper-CT scan that allows to obtain images of small body volumes of conical shape due to cone beam acquisition. On the basis of 3D reconstruction, using Xper-Guide, we planned the path of the needle to the target lesion. 2-4 samples were obtained in each case with a coaxial technique. After the procedure, patients underwent again a Xper-CT scan to assess any complications. Samples were classified as adequate (identification of histotype, grade and prognostical factors), intermediate (diagnosis of benignity/malignancy; histotype < 50%) and inadequate. Complications and mean time of execution were also recorded.

Results: In 130 patients samples were adequate, in 11 patients were intermediate and in 7 inadequate. Pneumothorax was recorded in 14.8% of patients but external drainage was never required. Perinodular haemorrhagic suffusion was observed in 32 patients and in only one case self-limiting hemoptysis was registered. Mean time of execution was 18 minutes.

Conclusion: Percutaneous transthoracic needle biopsy of pulmonary nodules with XperCt and Xper-guide is a safe and accurate procedure and can be performed in every patient with a high percentage of adequate samples and with a low risk of severe complications.

B-0756 11:33

Response monitoring for lung cancer therapy using dynamic contrast-enhanced CT scan: a correlation with PET-CT

M. Yoo; S. Hwang, T. Kim, S. Kim, Seoul/KR

Purpose: To assess the usefulness of dynamic contrast-enhanced computed tomography (DCE-CT) for prediction of treatment response and to compare the results of DCE-CT with those of integrated positron emission tomography-computed tomography (PET-CT) in patients with lung cancer.

Methods and Materials: Twenty-four patients who had chemotherapy or radiotherapy for lung cancer (22 with NSCLC and 2 with SCLC) were enrolled into this study. A total of 39 tumours (mean size, 3.1 cm; range 1.3-7.2 cm) were revealed on follow-up DCE-CT, obtained at 30, 60, 90, and 120 seconds following administration of contrast media and PET-CT less than 4 weeks apart. We measured relative enhancement ratio (RER) at each time point on DCE-CT and maximum standardised uptake value (SUVmax) on PET-CT. According to the response evaluation criteria in solid tumour (RECIST), 39 tumours were classified into 3 groups as progressive disease (PD, n = 25), stable disease (SD, n = 6), and partial response (PR, n = 8).

Results: RER at 60 seconds of PD (mean, 98.0% ±36.4%) was higher (P < 0.01) than those of SD (mean, 40.4%, ±30.5%) and PR (mean, 38.3%; ±24.1%). SUVmax revealed significant correlation with RER at 60 seconds (r = 0.48, P < 0.01, respectively). 13 (92.8%) of 14 tumours classified as PR or SD showed SUVmax of 2.5 or less and RER at 60 seconds of 80% or less.

Conclusion: DCE-CT can provide the information about treated tumour, functional composition as well as anatomic change in the post-treatment evaluation for patients with lung cancer.

B-0757 11:42

Clinical application of tissue permeability factor for differentiation of benign and malignant pulmonary mass on dynamic contrast material-enhanced (DCE) MRI

S.H. Baik, G.Y. Jin, Y.M. Han; Jeonju/KR (lovegumatm@hanmail.net)

Purpose: To determine whether tissue permeability factor on dynamic contrast material-enhanced (DCE) MRI can help to discriminate between malignant and benign pulmonary mass.

Methods and Materials: From June 2010 to May 2011, 30 patients (14 women, 16 men; median age, 64 years; age range, 41-80 years) with suspected lung cancer agreed to undergo DCE MR imaging at 3.0 T. 15 patients were lung cancer and 15 patients were benign lung lesions. A two-compartment kinetic model was used to calculate the perfusion parameters including: volume transfer constant (Ktrans, in min⁻¹), extravascular extracellular space volume fraction (Ve), efflux rate constant (Kep), initial area under curve (iAUC). An unpaired T-test was used to calculate the statistical significance of quantitative perfusion parameters between malignancy and benign lung lesions. Receiver operating characteristic (ROC) analysis was also performed for evaluation of sensitivity and specificity of perfusion parameters.

Results: Malignant lesions had higher Ktrans value than benign lesions (0.22 vs 0.14, p=0.0031). But there were no significant differences in other parameters (mean Ve; 0.37 vs 0.05, mean Kep; 0.69 vs 0.83, mean iAUC; 19.1 vs 24.9, respectively). A Ktrans value of more than 0.22 (min⁻¹) was optimal for predicting malignancy (sensitivity 93.3% and specificity 40%).

Conclusion: Ktrans value of perfusion parameters on DCE MRI can help to discriminate between malignant and benign lung lesions.

10:30 - 12:00

Room D2

Interventional Radiology

SS 1709

Oncology

Moderators:

F. Melchiorre; Milan/IT

T. Rand; Vienna/AT

B-0758 10:30

Segmental radioembolization using Yttrium 90 and its effect on hepatic volume changes

J.M. Theysohn, S. Mueller, J.F. Schlaak, S. Sipilae, A. Bockisch, T.C. Lauenstein; Essen/DE (jens.theysohn@uni-duisburg-essen.de)

Purpose: Yttrium 90 is a beta emitter used for radioembolisation as an emerging therapy option for unresectable liver malignancies. After radiation therapy of one liver lobe, the other lobe is expected to compensate the therapy-induced loss of liver function. Aim of this study was to assess the amount of volume gain induced in the untreated liver lobe.

Methods and Materials: Thirty patients (21m, 9f, mean age 70.3y) suffering from hepatocellular carcinoma were studied. All patients underwent radioembolisation of the right liver lobe with Yttrium 90. A mean dose of 109Gy was delivered to the target hepatic volume (range 100-160Gy). Absolute volumes of the right (RLV) and left liver lobe (LLV) were assessed using CT: before, 3, 6 and 9 months after radioembolisation of the right liver lobe. Furthermore, the relative volume of the left liver lobe (LLV/[RLV+LLV]) was calculated.

Results: Baseline volumes of the right and left liver lobe amounted to 1039 ml (RLV) and 562 ml (LLV) on average. The absolute LLV showed an increase on average 28.3% after 6 months. However, the absolute RLV decreased significantly during follow-up (mean change: -17.8%). The average relative LLV was 35.1% before and 45.8% six months after radioembolisation.

Conclusion: Constraints of liver function after radioembolisation of one liver lobe can be partially compensated through hypertrophy of the contralateral lobe. This observation may be the basis to introduce the concept of a radiation lobectomy using radioembolisation. Contralateral hypertrophy of the liver following single lobe radioembolisation reduces the danger of liver failure.

B-0759 10:39

Long-term survival data of patients with liver metastases of colorectal cancer after MR-guided laser-induced thermotherapy (LITT)

T.J. Vogl, A. Dommermuth, K. Eichler, S. Zangos, M.G. Mack; Frankfurt/DE (t.vogl@em.uni-frankfurt.de)

Purpose: To evaluate retrospectively long-term survival of 594 patients with colorectal liver metastases treated with MR-guided laser-induced thermotherapy (LITT) depending on different factors.

Methods and Materials: 594 patients with liver metastases from colorectal carcinoma treated with MR-guided LITT between 01/99 and 12/10 were included. For survival analysis tumour localisation, TNM classification, number of metastases, diameter and volume of metastases and necrosis, lobular spread, number of treatment sessions, performance of adjuvant chemotherapy and transarterial chemoembolisation were considered. The Kaplan-Meier method was used to conduct this survival analysis.

Results: Log-rank test showed statistically significant differences between survival curves, multivariate Cox-regression-analysis ($p < 0.05$) showed prognostic factors regarding overall survival like number of metastases pre intervention, adjuvant chemotherapy, diameter of metastases, ratio of volumes of necrosis and metastases, and affected lymph nodes. Median overall survival rate at the time of first LITT was 25 months, 1-year survival: 78%, 2-year survival: 50.1%, 3-year survival: 28%; 4-year survival: 16.4%; 5-year survival: 7.8%. Numbers of metastases pre-intervention: 1-2 metastases with a median survival rate of 60 months; 3-4 metastases: 45 months; ≥ 5 metastases: 42 months. Median survival rate for metastases < 20 mm in diameter 36 months; 20-30 mm 27 months, 30-40 mm 24 months and > 40 mm 21 months. Affected lymph nodes: median survival rate for patients with N0-classification 30 months, N1-classification 24 months; N2/N3/N4-classification 22 months.

Conclusion: The multivariate Cox-regression-model provided the minimal number of significant variables with the maximal prognostic value concerning overall survival for MR-guided LITT, i.e. diameter and number of metastases and primary classification of lymph nodes.

B-0760 10:48

MR-guided radiofrequency ablation using a wide bore 1.5 T system: clinical results of 226 treated liver tumours

H. Rempp¹, R. Hoffmann¹, L. Waibel¹, P. Pereira², C.D. Claussen¹, S. Clasen¹; ¹Tübingen/DE, ²Heilbronn/DE

Purpose: To evaluate the effectiveness of MR-guided radiofrequency (RF) ablation of liver malignancies using a wide-bore 1.5 T MR-system.

Methods and Materials: In 110 patients (27 females, 83 males) a number of 226 liver lesions were treated in 157 sessions by percutaneous RF ablation. Patient mean age was 64 (range 29-92). 69 lesions were primary liver tumours, 157 lesions were liver metastases, including 114 colorectal liver metastases. Other primary tumours were melanoma, breast cancer and neuroendocrine tumours. Mean lesion diameter was 20 mm (range 5-69 mm). MR-compatible bi- or multipolar internally cooled RF-probes were used. Planning, targeting and post-interventional control imaging were carried out in a wide bore 1.5 T MR scanner (bore: 72 cm). Technical success was assessed by a contrast-enhanced MR liver examination directly subsequent to the intervention. Technique effectiveness was assessed by dynamic MR liver studies; mean follow-up period was 23.8 months (range 5-44 months).

Results: Complete ablation was achieved in 222/226 lesions (98%). In 21/226 lesions (8.1%) local tumour recurrence occurred 4-28 months after therapy. 11/25 lesions could be treated in a second session with complete ablation, 6 others were referred to surgery. Overall RF technique effectiveness rate was 212/226 (94%), overall therapy success (including surgery) 218/226 (96%). Subsequent to 157 interventions, two major complications (1.3%) (bleeding and infected bilioma) and 8 (5.1%) minor complications occurred. In 41/110 patients (37%) new intra- or extrahepatic manifestations of the disease occurred during the follow-up period.

Conclusion: Wide-bore MR-guided RF ablation is a safe and effective treatment option for liver lesions.

B-0761 10:57

New combination of mitomycin and cisplatin for transarterial chemoembolisation (TACE) of unresectable hepatocellular carcinoma: different aetiologies and local response rate

T.J. Vogl, K. Auerbach, K. Ochs, S. Zangos, T. Lehnert, N.N.N. Naguib; Frankfurt/DE (t.vogl@em.uni-frankfurt.de)

Purpose: To evaluate the effect of conventional transarterial chemoembolisation (TACE) on local response rates of hepatocellular carcinoma (HCC) patients with different aetiologies of liver cirrhosis using a new chemoembolisation.

Methods and Materials: In this prospective study, 177 patients (male:131 (74.01%)/female:46 (25.99%)) with histopathologically proven HCC were treated with repetitive TACE (mitomycin/cisplatin/lipiodol) from March 2006 to March 2011. Underlying liver pathology, Child-Pugh score, tumour volume, number of tumours and local response were included. Initial and end therapy local tumour response was evaluated according to the RECIST criteria, MRI and CT volumetric measurements.

Results: Local tumour control showed complete response (CR) in 0.56% of patients (n=1), partial response (PR) in 22.6% (n=40), stable disease (SD) in 48.02% (n=85), progressive disease (PD) in 28.81% (n=51). Local response rates of patients with underlying hepatitis C (HCV) (n=53) were CR in 1.89% (n=1), PR in 30.19% (n=16), SD in 45.28% (n=24), PD in 22.64% (n=12) and of patients with underlying hepatitis B (HBV) (n=17) PR in 17.64% (n=3), SD in 58.82% (n=10), PD in 23.53% (n=4). In patients with both HCV and HBV (n=5) local response showed PR in 60% (n=3), SD in 40% (n=2). Patients with haemochromatosis (n=8) showed PR in 25% (n=2), SD in 12.5% (n=1), PD in 62.5% (n=5) and patients with nutritive-toxic liver cirrhosis (n=36) PR in 16.67% (n=6), SD in 66.67% (n=24), PD in 16.67% (n=6).

Conclusion: The new TACE protocol yields respectable response rates in patients with liver cirrhosis-caused HCC independent of the underlying aetiology of the liver cirrhosis.



B-0762 11:06

Antiangiogenesis effect of arsenic trioxide on synergising the transarterial chemoembolisation effect in the treatment of rabbit VX2 tumours

X. Dai, K. Xu, H. Shao, Y. Cheng, Q. Wang; Shenyang/CN (daixudex@vip.sina.com)

Purpose: To study the effect and mechanism of arsenic trioxide (As₂O₃) combined with transarterial chemoembolisation (TACE) on the growth and metastasis of rabbit VX2 tumours.

Methods and Materials: After 2 weeks of inoculation of VX2 tumour into the livers, 40 rabbits were randomly divided into 5 groups. Group A is control group, group B with UFLP embolisation, group C with UFLP and ADM, group D with UFLP and As₂O₃ and group E combined UFLP with ADM and As₂O₃. Two weeks after treatment, all rabbits were examined with contrast-enhanced CT and the tumour and necrotic were measured and compared with pathological findings. VEGF and MVD were detected by immunohistochemical staining and quantitative comparison of tumour VEGFmRNA in different groups was done by RT-PCR.

Results: Compared with control group, tumours in the other four groups grew slowly ($p < 0.01$) and with larger necrosis ($p < 0.01$). Compared with no As₂O₃ group as B and C, group D and E grew slowly ($p < 0.01$). There are less intrahepatic and distant metastasis found in group D and E with As₂O₃ than the other groups ($p < 0.05$). MVD and VEGFmRNA expression in groups D and E with As₂O₃ are significantly reduced than no As₂O₃ groups ($p < 0.05$). MVD in group E combination with As₂O₃ and ADM is significantly lower than the other two groups C and D with ADM or As₂O₃, respectively ($p < 0.01$).

Conclusion: Combination of As₂O₃ and routine chemotherapeutic drugs can synergy the antitumour effects of TACE. As₂O₃ may reduce the expression of VEGFmRNA and prevent tumour growth and metastasis by inhibiting the angiogenesis process.

B-0763 11:15

Transarterial chemoembolisation (TACE) in patients with unresectable cholangiocarcinoma: results and prognostic factors

T.J. Vogl, N.N.N. Naguib, T. Lehnert, N.E.A. Nour-Eldin, W.O. Bechstein, S. Zeuzem, J. Trojan, T. Gruber-Rouh; Frankfurt a. Main/DE (t.vogl@em.uni-frankfurt.de)

Purpose: To evaluate the effectiveness of transarterial chemoembolisation (TACE) with four chemotherapeutic protocols regarding local tumour control and survival of patients with unresectable cholangiocarcinoma (CCC) and to identify the prognostic factors determining treatment success.

Methods and Materials: 115 patients (mean: 60.4 years) with unresectable CCC were repeatedly treated with TACE. In total, 819 sessions (mean, 7.1 sessions/patient; range, 3-30) were performed in 4-week intervals. The chemotherapeutic agent used was mitomycinC in 20.9% (24/115) of patients, gemcitabine in 7% (8/115), mitomycinC/gemcitabine in 47% (54/115) and gemcitabine/mitomycinC/cisplatin in 25.1% (29/115). Embolisation was performed with lipiodol and embocept. Local tumour response was evaluated by MRI according to the RECIST criteria. Survival data were calculated according to the Kaplan-Meier method. Prognostic factors for survival were evaluated using log-rank-test.

Results: Local tumour controls were: partial response 8.7% (10/115), stable disease 57.4% (66/115), progressive disease 33.9% (39/115) of patients. Median and mean survival times from the start of TACE were 13 and 20.8 months. Survival rate from the start of TACE was 52% after 1 year, 29% after 2 years, and 10% after 3 years. Initial tumour response, high tumour vascularity, and Child-Pugh class A were statistically significant factors for survival, and number of tumour lesions and location in liver were not statistically significant. No statistically significant difference between patients treated with different chemotherapy protocols was documented.

Conclusion: TACE is a palliative and safe treatment option for patients with unresectable CCC. Child Pugh class B, tumour hypovascularity, initially progressive disease were poor prognostic factors for survival.

B-0764 11:24



DC-beads chemoembolisation of HCC and evaluation of the results using CEUS and MDCT: a two-year study

V. Tsagkouli, T. Soldatos, S. Kampanarou, S. Tanteles, L. Thanos, K. Malagari, M. Pomonis, D.A. Kelekis; Athens/GR (mkampanarou@gmail.com)

Purpose: The purpose was to compare the accuracy of contrast-enhanced ultrasound (CEUS) and multidetector CT (MDCT) for evaluating the outcome of transarterial chemoembolisation with doxorubicin beads in patients with HCC.

Methods and Materials: We retrospectively studied the follow-up imaging studies of a total of 33 nodules, observed in 21 patients (13 males and 8 females that ranged in age from 56 to 78) with biopsy proven HCC, who had undergone chemoembolisation with DC-beads. All patients were examined with multiphase contrast-enhanced MDCT and CEUS approximately 4 weeks after DC-beads chemoembolisation. Contrast enhancement appearing within the tumour was interpreted as incomplete treatment or tumour recurrence. MDCT was used as reference standard and angiography in case additional DC-beads treatment was performed due to incomplete response. All examinations were interpreted blindly by two radiologists and afterwards CEUS findings were compared with MDCT by an experienced radiologist in abdominal imaging.

Results: In 33 nodules a complete response revealed in 26 nodules and incomplete in the other 7. Percentage of complete response was 78.7%. Post DC-beads chemoembolisation, CEUS was able to detect 6 of 7 cases with residual tumour. The results obtained with CEUS agreed with those obtained with MDCT in all cases, rendering a diagnostic accuracy of 100%. There was not any statistically significant difference in overall diagnostic accuracy between MDCT and CEUS in the evaluation of residual tumour ($p > .05$).

Conclusion: CEUS represents a cost-effective and valuable tool in the evaluation of the outcome of chemoembolisation with DC-beads in HCC.

B-0765 11:33

Transpulmonary chemoembolisation (TPCE) as a regional oncological treatment for non-resectable lung metastases

T.J. Vogl, S. Lindemayr, N.E. Nour-Eldin, T. Dauda, S. Zangos; Frankfurt/DE (t.vogl@em.uni-frankfurt.de)

Purpose: To evaluate tumour response with volumetric assessment for tumour size after treatment of unresectable lung metastases with repetitive transpulmonary chemoembolisation (TPCE) in palliative intention.

Methods and Materials: Between 2001 and 2011, 223 patients (mean 57.3 years; 111 males/112 females) suffering from 4,202 unresectable lung metastases were treated with TPCE (range: 1-16 sessions, mean: 3.8). They featured a mean of 18.8 metastases of different origins: colorectal carcinoma (n=82), breast cancer (n=32), sarcoma (n=19), renal cellular carcinoma (n=14), melanoma (n=8), thyroidal (n=5), and others (n=63). Lipiodol, mitomycin C and microspheres (Spherex) were administered via balloon protection. At 4-week intervals, diagnosis and follow-up were accomplished using unenhanced and contrast-enhanced computed tomography.

Results: All patients tolerated the repeated treatments without adverse effects. In 20.6% (n=46) moderate to high lipiodol uptake was found while 79.4% (n=177) of the treated tumours showed a low storage. In 21.1% (n=47) of embolised metastases, tumour volume was resolved to 45.2 ml on average, in 26.0% (n=58) it remained unchanged while in 52.9% (n=118) it increased to 18.8 ml on average.

According to the RECIST criteria 47 patients had "partial response", 58 had "stable disease" and 118 "progressive disease". Mean survival was 811 days in patients with colorectal carcinoma, 892 days in breast cancer, 599 days in sarcomas, 556 days in renal cell carcinoma, 399 days melanoma, 647 days in thyroid cancer, and 797 days in other cancers using the Kaplan-Meier method.

Conclusion: According to these findings TPCE might be a well-tolerated procedure for the palliative treatment of non-resectable lung metastases.

B-0766 11:42

Trans-arterial chemoembolization (TACE) using drug-eluting bead preloaded with irinotecan (DEBIRI) in the treatment of metastases from uveal melanoma (UM) confined to the liver: preliminary assessment of tumour response and predictive value of angiographic pattern and diffusion-weighted magnetic resonance imaging (DW-MRI)

M. Venturini, G. Agostini, L. Pilla, C. Losio, S. Cappio, A. Del Maschio; Milan/IT (venturini.massimo@hsr.it)

Purpose: UM, very aggressive/rare tumour, gives metastases confined to the liver in more than 60% of the patients. Systemic/regional chemotherapy (fotemustine) is usually ineffective. Our purpose was to assess feasibility, complications, tumour response, and predictive value of angiographic pattern and DW-MRI in 10 patients submitted to TACE with DEBIRI.

Methods and Materials: In 2010/11, 10 patients affected by UM metastases confined to the liver histologically diagnosed were enrolled. 5 patients with > 5 lesions were submitted to TACE with DEBIRI as second-line approach, in case of disease progression after systemic/regional fotemustine; 5 patients with < 5 lesions were directly submitted to TACE with DEBIRI as first-line approach. Tumour response was assessed by contrast-enhanced CT (Recist); at baseline, predictive value of angiographic pattern (hypervascular/nodular vs. hypovascular/infiltrative pattern) and apparent-diffusion-coefficient (ADC) at DW-MRI was considered.

Results: TACE with DEBIRI (24 total procedures, mean=2.4) was feasible with a low complication rate (one cholecystitis spontaneously resolved) in all patients. PD occurred in all 5 patients submitted to fotemustine. Tumour responses to TACE with DEBIRI were as follows: 1CR, 3PR, 4SD, 2PD (second-line DEBIRI: 1PR, 3SD, 1PD; first-line DEBIRI: 1CR, 2PR, 1SD, 1PD). PD was correlated with hypovascular/infiltrative angiographic pattern and high baseline ADC values of lesions ($p=0.03$).

Conclusion: In our preliminary experience, TACE with DEBIRI was feasible, safe, and effective in all patients; it can be proposed as first-line treatment in patients affected by UM metastases confined to the liver. Hypovascular/infiltrative angiographic pattern and high baseline ADC are predictive of a low response.

B-0767 11:51

Impact of hepatic steatosis and fibrosis on segmental liver hypertrophy after pre-operative portal vein embolisation

A. Koops, E. Ramcic, H. Itrich, C. Habermann, G. Adam; Hamburg/DE (kooops@uke.uni-hamburg.de)

Purpose: Portal vein embolisation (PVE) allows the induction of segmental liver hypertrophy in initially irresectable liver malignancies. Purpose of this study was to determine the impact of preexisting hepatic steatosis and portal fibrosis on the relative and absolute hypertrophy of the left lateral segments in patients scheduled for extended right hepatectomy.

Methods and Materials: Histology from pre-interventional biopsy or the resection specimen was evaluated in 67 patients that received PVE because of primarily irresectable malignancies (34 colorectal metastases, 6 other metastases, 24 cholangiocarcinoma, 3 HCC). All accessible portal branches of segments 4-8 were embolised with cyanoacrylate glue. CT-volumetry was performed prior and 4 weeks after embolisation, if necessary repeated every 2-4 weeks, until the future liver remnant weight exceeded 0.8% body weight. Diagnosis of hepatic steatosis and portal fibrosis were compared with hypertrophy rates calculating Levene-T-tests and Student's T-tests.

Results: Steatosis was found in 39 (58%) patients (graded mild, 35; moderate, 3; and severe, 1), fibrosis in 26 (39%) patients (graded mild, 18; moderate, 2; severe, 2; and cirrhosis, 2). Without stenosis volume gain was 74% after 28 days (2.45%/d), with stenosis only 50% after a mean of 39 days (1.61%/d). These absolute and relative differences reached statistical significance ($p < 0.05$), whereas no significant difference ($p=0.543$) was found in the left-lateral segmental volume increase between non-fibrotic (58%) and fibrotic (64%) livers.

Conclusion: Hepatic steatosis reduces the hypertrophy capability after PVE. However, the more chronic liver damage of - in this study mostly mild - portal fibrosis did not limit liver hypertrophy.

10:30 - 12:00

Room E1

Musculoskeletal

SS 1710

From foot to hip

Moderators:

M.P. Aparisi Gomez; Valencia/ES
F. Kainberger; Vienna/AT

B-0768 10:30

Femoral length assessment on prenatal MRI

U. Nemeč, S.F. Nemeč, M. Weber, P.C. Brugger, D. Prayer; Vienna/AT
(ursula.nemec@gmail.com)

Purpose: This study sought to demonstrate normal femoral length development on prenatal magnetic resonance imaging (MRI) by constructing a foetal growth chart. **Methods and Materials:** This retrospective study included the MR scans of 232 fetuses (19+0 to 35+5 gestational weeks [GW]) with normal anatomy or minor abnormalities. On echoplanar MRI, femoral length was measured from the proximal to the distal end of the shaft (diaphyseal length), and from the outer margin of the proximal to the outer margin of the distal epiphysis (total length). Statistical description, Pearson correlation and linear regression analysis were used to evaluate femoral length in relation to gestation. T-tests were calculated to compare diaphyseal/total femoral length on MRI with published US normative data.

Results: Minimum and maximum length values, mean values, and 95% confidence intervals and percentiles were defined for the gestational age. Femoral length as a function of gestational age was expressed by the regression equation: diaphyseal length = $-13.913 + 2.256^* \cdot GW$, and total length = $-15.373 + 2.977^* \cdot GW$. The correlation coefficients were statistically significant ($p < .001$). There was no significant difference between diaphyseal length on MRI and US data, whereas total length was significantly longer than the US measurements ($p < .001$).

Conclusion: Our study provides MRI reference data of normal femoral length in utero, which, in addition to US, may be helpful to determine normal long bone growth as well as abnormalities. Diaphyseal length on MRI and US are equivalent, whereas total length, including the epiphyses, is significantly different from US findings.

B-0769 10:39

3D-hindfoot alignment measurements based on low-dose biplanar x-rays: comparison to standard radiographic measurements

R. Sutter, C.W.A. Pfirrmann, N. Espinosa, F.M. Buck; Zurich/CH
(reto.sutter@balgrist.ch)

Purpose: To establish a robust and reproducible hindfoot alignment (HA), measurement technique based on low-dose biplanar x-rays and compare to HA measurements on standard radiographs.

Methods and Materials: A phantom consisting of a human foot skeleton embedded in acrylic glass was imaged with long axial view radiographs and in a low-dose biplanar x-ray scanner (EOS) in neutral position and different rotations (from 20° internal to 20° external rotation). Two independent readers measured HA on radiographs and performed 3D measurements of HA on EOS data using a custom-made Matlab code in two different readout sessions. Time for 3D measurements was determined. Intraclass correlation coefficients (ICC) were calculated.

Results: Measurements on reference standard radiographs at all rotations showed a large variation in HA (range, 13°/12° valgus to 22°/27° varus for reader 1/reader 2, respectively). 3D hindfoot angle EOS measurements at all rotations resulted in a mean angle of $8.7^\circ \pm 1.4/8.9^\circ \pm 0.5$ (for first and second readout by reader 1). For reader 2, these measurements were $8.1^\circ \pm 0.6/7.9^\circ \pm 0.8$. Differences between repeated EOS measurements were only 0.2° for both readers. Interreader agreement and agreement between different readouts was high (ICC = .926/ ICC = .995). Mean duration of 3D measurements was 2:55 min/ 2:42 min (for readers 1 and 2).

Conclusion: 3D-HA measurements based on biplanar x-rays are fast and reliable. They are independent of foot-positioning during image acquisition and reader-independent. In this phantom study, the 3D-measurements were superior to measuring HA with the reference standard radiographs.

B-0770 10:48

Is it possible to identify a pathologic hindfoot alignment on non-weight-bearing coronal MR-images? An attempt using different measurement techniques

F.M. Buck¹, A. Hoffmann¹, N. Mamisch¹, M. Farshad¹, N. Espinosa¹, D. Resnick², J. Hodler¹; ¹Zurich/CH, ²San Diego, CA/US

Purpose: To investigate the ability to discriminate between patients with normal and pathologic hindfoot alignment (HA) on coronal non-weight-bearing MR images.

Methods and Materials: IRB approval and informed consent of all patients was obtained. HA was quantified on HA view radiographs of 49 patients (mean age, 48 years; range, 21-76 years) using three different measurement techniques (calcaneal axis, medial and lateral calcaneal contour). These measurements were used to define a group of patients with a normal HA (0°-10° valgus) and a group with a clearly pathologic HA (> 10° valgus or varus). HA was then measured on coronal MR images using six different measurement techniques (calcaneal axis, medial and lateral calcaneal contour, sustentaculum-tangent, fibulocalcaneal distance, talar offset). ROC analysis was performed to find the one MR measurement technique with optimal sensitivity and specificity for discrimination between normal and pathologic HA.

Results: If on the HA view radiographs the measurements using the medial calcaneal contour were defining the assignment of the patients into the normal or the pathologic group, all measurements on MR images could clearly ($p < 0.05$) identify the pathology. MR measurement with the calcaneal axis, however, reached the best combination of sensitivity (86%) and specificity (79%) with a cutoff of > 11° valgus.

Conclusion: It is possible to discriminate between patients with normal and pathologic HA on coronal non-weight-bearing MR images with a sensitivity of 86% and a specificity of 79%.

B-0771 10:57

Screw-home mechanism and its influence on tibial tuberosity-trochlear groove (TTTG) distance: measurement on MR examinations of the knee in asymptomatic volunteers in full extension, 15° flexion and 30° flexion

T.J. Dietrich, M. Betz, C.W.A. Pfirrmann, P.P. Koch, S.F. Fucentese; Zurich/CH
(tdiet@gmx.net)

Purpose: Increased tibial tuberosity-trochlear groove (TTTG) distance leads to patellar instability. The so-called screw-home mechanism refers to an outward rotation of the tibia when the knee reaches full extension. We hypothesised that the so-called screw-home mechanism of the knee in end stage extension increases the distance of the TTTG distance of the knee on MRI.

Methods and Materials: Transversal spin-echo T1-weighted MR images of the knee were acquired in full extension, 15° and 30° flexion of the knee in 19 asymptomatic volunteers (patients' mean age: 28.9 years, range: 19.9-37.6 years, 10 left, 9 right) using a flexible coil. Following parameters were used: slice thickness: 3 mm, matrix: 256 x 384, FOV: 150 x 150 mm. The TTTG distance was measured in all three positions. The Student's t-test served for statistics.

Results: The mean TTTG distance was 15.3 ± 3.4 mm (range: 8.4-19.9 mm) in full extension, 10.4 ± 3.8 mm (range: 4.0-15.6 mm) in 15° flexion and 8.8 ± 3.4 mm (range: 2.5-13.3 mm) in 30° flexion. The mean values were significantly different (p -value < 0.001) between three positions.

Conclusion: The TTTG distance increases significantly in the endstage extension of the knee. Therefore, the comparability of published TTTG values measured on radiographs, CT and MRI at various flexion/extension angles of the knee is limited.

B-0772 11:06

Femoral and tibial torsion measurements using 3D models based on low dose biplanar x-ray in comparison to standard CT measurements

F.M. Buck, R. Guggenberger, P.P. Koch, C.W.A. Pfirrmann; Zurich/CH

Purpose: To compare femoral and tibial torsion measurements and interreader agreement of measurements using 3D models based on low dose biplanar x-ray in comparison to standard CT measurements and evaluate interchangeability of the two methods.

Methods and Materials: Institutional review board approval was obtained and all patients signed an informed consent. Femoral and tibial torsion were measured based on 3D models based on low dose biplanar x-rays (EOS imaging system) and on axial CT images by two independent readers, respectively. The two measurement modalities were compared by means of Bland-Altman plots and descriptive statistics. Interreader agreement was quantified by of intraclass correlation coefficients (ICC).

Results: The maximal measurement difference between the two CT readers (femur 11°/Tibia 12°) was slightly bigger than the maximal measurement difference between the two readers using 3D models based on biplanar x-rays (Femur 9°/Tibia 10°). Bland-Altman plots showed no relevant differences between the results of the two measurement modalities. Except for one measurement of the femoral torsion and one measurement of the tibial torsion all results based on the 3D models were within the 95% limit of agreement (mean ± 1.96 standard deviation). Interreader agreement was significant (p 0.9).

Conclusion: Femoral and tibial torsion measurements using 3D models based on biplanar x-rays are interchangeable with CT measurements.

B-0773 11:15

Is the alpha-angle able to discriminate between symptomatic patients with femoroacetabular impingement (FAI) and asymptomatic volunteers?

R. Sutter, T.J. Dietrich, C.W.A. Pfirrmann; Zurich/CH (reto.sutter@balgrist.ch)

Purpose: To assess diagnostic characteristics of different alpha-angle thresholds in volunteers and FAI patients.

Methods and Materials: 106 individuals (20-50 years) were included (53 patients with cam-deformities and 53 age- and gender-matched asymptomatic volunteers). The patient group consisted of 33 cam-type FAI and 20 mixed-type FAI. Alpha-angles were measured on a radially reformatted T2-weighted true-FISP 3D-MRI-sequence of the proximal femur by two independent readers. Intraclass correlation coefficients (ICC) and receiver operator characteristics (ROC) were calculated.

Results: Mean alpha-angles were highest in the anterosuperior segment with 65.4°±11.5/ 65.2°±7.3 (for reader 1/2) for patients and 53.3°±9.6/ 55.0°±8.8 for volunteers. Alpha-angles > 55° were measured in 20 and 33 out of 53 volunteers (38%/63% for reader 1/2). Most elevated alpha-angles in volunteers were found anterosuperiorly (32%/51%) and superiorly (19%/32%). The maximal alpha-angle in any segment was significantly different (p <.001) in patients and volunteers (70.3°±11.2 vs. 57.9°±10.5 for reader 1; 69.4°±8.8 vs. 58.7°±8.9 for reader 2), albeit with a large overlap. Interobserver agreement was good (ICC=0.712). ROC showed the largest area under the curve at the anterosuperior segment (area=0.791/0.824 for reader 1/2; p <.001); a 55° alpha-angle threshold gave a sensitivity/specificity of 82%/65% for reader 1 and 90%/47% for reader 2, while a 60° threshold gave 72%/76% for reader 1 and 80%/73% for reader 2.

Conclusion: The alpha-angle is suboptimal to discriminate volunteers and FAI patients with cam-type deformities. Discrimination is most reliable at the anterosuperior segment. Raising the alpha-angle threshold from 55° to 60° reduces false-positives and might result in less overtreatment.

B-0774 11:24

Is there a relationship between T2-mapping of knee cartilage or the whole-organ MRI scoring method (WORMS) for knee osteoarthritis and the patient's pain, symptoms, function in daily life (ADL), function in sport and recreation (Sport) and knee-related quality of life (QOL) as given by the knee osteoarthritis outcome score (KOOS) questionnaire?

G. Scheurecker, C. Scheurecker, A. Scheurecker, J. Kramer; Linz/AT (georg.scheurecker@inode.at)

Purpose: Both T2-mapping of cartilage and the WORMS method are established research tools for knee osteoarthritis: is there a relationship with the patients' KOOS-questionnaire?

Methods and Materials: After introducing T2-mapping and the KOOS-questionnaire in our routine protocol for knee MRI, we included the first 50 females and males, respectively (female mean-age 41y, range 18-57y; male mean-age 42y, range 27-58y). We employed a sagittal multi-echo-spin-echo-sequence for T2-mapping together with the routine-knee-protocol (sagittal T1w and sagittal-/coronal-/axial-Pdw-fatsat) on a 3 T-MRI-unit. The T2-maps were analysed with ROIs with a standardised length of 4 mm for the full-thickness-cartilage on three consecutive images of the central medial and lateral femoral condyle (MFC, LFC), the patella and the trochlea. The repeated T2 measurements were averaged for each region. R2 were calculated with linear regression to look for relationships between T2 values or the WORMS and the KOOS-questionnaire (R2 graded as > 0.9 very strong, > 0.7 strong, > 0.5 moderate, > 0.3 weak, > 0.1 very weak).

Results: For females the WORMS had a very weak relationship with pain, symptoms, Sport and QOL, for males there was no relationship. T2 mapping had a very weak relationship regarding the LFC and symptoms in females, in males it was very weak for MFC and symptoms, patella and pain, and trochlea and pain. Beside these relationships there were none more.

Conclusion: Although T2 mapping of cartilage and the WORMS are valuable in knee osteoarthritis research, both of them show only a very weak if any relationship with the patients' pain, symptoms, ADL, function in sport and QOL.

B-0775 11:33

Comparison of 3D-SPACE vs. 2D-FSE sequence for the evaluation of internal knee derangement at 3.0 T

P. Van Dyck, J.L. Gielen, K. Wouters, F.M. Vanhoenacker, L. Dossche, P.M. Parizel; Edegem/BE (pieter.van.dyck@uza.be)

Purpose: To assess the diagnostic performance of the 3D-SPACE (sampling perfection with application-optimised contrast using variable flip-angle evolutions) fast spin-echo (FSE) sequence, as compared to routine 2D FSE in the evaluation of internal knee derangement at 3.0 T.

Methods and Materials: From January to July 2011, a sagittal isotropic fat-saturated 3D-SPACE FSE sequence was added to a conventional 2D knee MR imaging protocol. Sequence parameters of 3D-SPACE were: TR=1200 ms; TE=47 ms; voxel size=0.6 mm3. Subsequent knee arthroscopy was performed in 40 patients. Two radiologists, blinded to operative results, independently evaluated multiplanar 2D-FSE and 3D-SPACE data sets, with a 4-week interval, for the presence of meniscal tears, anterior cruciate ligament (ACL) and cartilage lesions. Accuracies were calculated for each reader, using arthroscopy as the reference standard. McNemar's test was used to identify significant differences (p < 0.05) between 2D and 3D sequences. Interobserver agreement was determined using Cohen's kappa test.

Results: For the diagnosis of tears of medial and lateral meniscus, and ACL lesions, accuracy of both sequences ranged from 78% to 88%, 88% to 95%, and 92% to 100%, respectively, for both readers. For the detection of cartilage lesions, accuracy of both sequences ranged from 75% to 81% for both readers. We found no significant differences in diagnostic yield between 2D and 3D sequences. Interobserver agreement was excellent for meniscus and ACL lesions (kappa > 0.81), and it was moderate for cartilage lesions (kappa=0.60).

Conclusion: The diagnostic performance of 3D-SPACE is similar to routine 2D-FSE for the detection of meniscal, anterior cruciate ligament and cartilage lesions of the knee at 3.0 T.

B-0776 11:42

Through-plane distortion correction and view-angle tilting for reduction of metal artefacts at MR imaging in patients with total hip arthroplasty: performance of STIR and T1 sequences

R. Sutter¹, E.J. Ulbrich¹, V. Jellus², M. Nittka², C.W.A. Pfirrmann¹; ¹Zurich/CH, ²Erlangen/DE (reto.sutter@balgrist.ch)

Purpose: To determine the performance of the new WARP sequence for reduction of both through-plane and in-plane artefacts in patients after total hip arthroplasty (THA).

Methods and Materials: 40 patients with THA were prospectively included. Slice encoding metal artefact correction (SEMAC), view-angle-tilting (VAT), and increased bandwidth were applied by the "WARP"-TSE sequence at 1.5 T. Coronal STIR-WARP and transverse T1-WARP images, standard coronal STIR and transverse T1 images optimised with high bandwidth (STIR-hiBW/T1-hiBW) were acquired. Signal void was quantified. Qualitative criteria (anatomy, distortion, blurring, noise) were assessed on a five-point scale (1, no artefacts; 5, not visible due to severe artefacts) by two readers. Clinical findings were recorded. Quantitative data were analysed with a t-test and qualitative data with a Wilcoxon signed rank test.

Results: Signal void around the prosthesis head was smaller for STIR-WARP than STIR-hiBW (21.6 cm2/42.4 cm2), and for T1-WARP than T1-hiBW (17.6 cm2/20.2 cm2; p=.0001 for all). Anatomic distinction was better on STIR-WARP compared to STIR-hiBW (1.9-2.8 vs. 3.6-4.6; p=.0001), and on T1-WARP compared to T1-hiBW (1.3-2.8 vs. 1.8-3.2; p <.002). Distortion, local blurring and noise were lower at WARP than in the standard sequences (p=.0001). Generalised blurring was higher for STIR-WARP compared to STIR-hiBW (p=.23) and for T1-WARP compared to T1-hiBW (p=.0001). Almost half of the clinical findings were missed on STIR-hiBW compared to STIR-WARP (55 and 105 findings; p=.0001), while T1-hiBW was similar to T1-WARP (50 and 55 findings; p=.06).

Conclusion: STIR-WARP and T1-WARP were statistically significantly better for most image criteria, but the clinically relevant advantage in artefact reduction was only present for STIR images and not for T1 images.

B-0777 11:51

7 Tesla hip imaging in avascular necrosis using a multi-channel transmit array and RF shimming

J.M. Theysohn, O. Kraff, S. Orzada, S. Landgraeber, M.E. Ladd, T.C. Lauenstein; Essen/DE (jens.theysohn@uni-duisburg-essen.de)

Purpose: MRI of hip joints plays an important role in staging especially young patients with hip disease (i.e. avascular necrosis, AVN). Aim of this study is the evaluation of ultra-high-field imaging (7 Tesla) of the hips using a new multi-channel transmit technology to compensate the inherent B1 inhomogeneities of 7T MRI in comparison to 3T.

Methods and Materials: Ten patients with AVN were imaged at 7T (Magnetom 7T, Siemens) using a self built eight channel transmit-receive coil. After RF shimming, identical sequences (MEDIC, DESS, PD/T2w TSE, T1w TSE, and STIR) were acquired at 7T and 3T (Skyra, Siemens). Robustness against B1 inhomogeneities (4-point scale: 3/0=no/strong degradation), and CNR between cartilage, cortical bone, and fluid were evaluated.

Results: Overall, regions of interest could be imaged with reproducible high quality at 7T (except STIR). While almost absent at 3T (grade 2.7), all 7T sequences showed signal variations with DESS most robust (grade 1.8) and STIR least favourable (grade 0.7). For MEDIC, PD, T2w, and T1w strong signal dropouts were sufficiently shifted away from the FOV. 7T exhibited stronger cartilage/fluid contrasts especially for MEDIC and DESS. Pathologies were depicted with slightly more detail at 7T.

Conclusion: Application of new transmit technologies (RF-Shimming) allows the high-resolution imaging of the hips with 7T MRI. Pathologies of the femoral head can be displayed in more detail, while sacrificing image quality of the surrounding soft tissue. 7 Tesla MRI of the hip joint might help improve diagnostic and staging accuracy of avascular necrosis.

10:30 - 12:00

Room E2

Oncologic Imaging

SS 1716

PET for cancer patient management

Moderators:

J. Grimm; New York, NY/US
D. Miletić; Rijeka/HR

B-0778 10:30

Assessment of the metabolic-flow phenotype of primary colorectal cancer: correlations with microvessel density are influenced by the histological scoring method

V.J. Goh, M. Rodriguez-Justo, A. Engledow, M. Shastry, R. Endozo, M. Meagher, S. Taylor, S. Halligan, A. Groves; London/UK

Purpose: To investigate how different methods of histological scoring of microvessel density ('Hotspot' versus Chalkley) affect correlation between integrated 18F-FDG-PET/perfusion CT parameters and CD105 microvessel density.

Methods and Materials: Institutional review board approval was obtained for this prospective study. 53 patients were enrolled from April 2007 to October 2010. Integrated 18F-FDG PET/perfusion CT was successful in 45 patients (26 males; 19 females; mean 67.6 years), 35 of whom underwent surgery without intervening neo-adjuvant treatment. Tumour SUVmax, SUVmean, and regional blood flow (BF) were derived for the entire tumour. Immunohistochemical staining for CD105 expression and analysis for 2 hotspots, 4 hotspots and the Chalkley method were performed. Correlations between metabolic and flow parameters and CD105 expression were assessed by Spearman rank correlation with statistical significance at 5%.

Results: Mean (SD) tumour size was 38.5 (20.5) mm. Mean (SD) for SUVmax, SUVmean and BF were 19.1 (4.5), 11.6 (2.5), and 85.4 (40.3) mL/min/100 g tissue, respectively. The mean (SD) for CD105 microvessel density was 71.4 (23.6), 66.8 (22.9) and 6.18 (2.07), respectively, for 2 hotspot, 4 hotspot, and Chalkley methods. The positive correlation between BF and CD105 expression was modest but higher for Chalkley than 4 hotspot analysis ($r=0.33$; $p=0.05$; $r=0.38$; $p=0.03$, respectively). There was no correlation with 2 hotspot analysis ($r=0.20$, $p=0.26$). There were no significant correlations between metabolic parameters (SUVmax or SUVmean) and CD105 expression (r 0.08 to 0.22, p 0.21-0.63).

Conclusion: The histological analysis method affects correlations between tumour CD105 expression and BF but not SUVmax or SUVmean

B-0779 10:39

Diffusion-weighted MRI and (68)Ga-DOTATOC PET for early monitoring of response to loco-regional (90)Y-(177)Lu-DOTATOC therapy in patients with neuroendocrine liver metastases

F.L. Giesel¹, S. Wulfert¹, T. Kuder¹, L. Schwartz², H.-U. Kauczor¹, U. Haberkorn¹, C. Kratochwil¹; ¹Heidelberg/DE, ²New York, NY/US (f.giesel@dkfz.de)

Purpose: Monitoring response to therapy is predominantly based upon evaluating tumour size before and after treatment, for example, in the response evaluation criteria in solid tumours (RECIST). Therefore, we evaluated if diffusion-weighted MR imaging (DW-MRI) and (68)Ga-DOTATOC PET are potential surrogate biomarkers for providing earlier information about a possible treatment response to intraarterial DOTATOC therapy.

Methods and Materials: In 12 consecutive patients with 29 liver metastases of gastroenteropancreatic neuroendocrine cancer (GEP-NET) were evaluated. All patients underwent both diffusion-weighted and dynamic contrast-enhanced magnetic resonance imaging (DWI-/DCE-MRI) including breath-hold echoplanar DWI sequences (b-values 50, 300, 600s/mm²) as well as (68)Ga-DOTATOC PET before therapy (baseline) and after last intervention (follow-up). Largest diameter (LD), intratumoral apparent diffusion coefficient (ADC) and maximal standardised uptake value (SUVmax) were measured in all target lesions as well as in normal liver parenchyma and spleen.

Results: Tumour metastases were subclassified, based upon change in tumour size in responding lesions (RL, n=7) and non-responding lesions (NRL, n=22). In NRLs, baseline median tumour ADC increased from 1.21x10⁻³ mm²/sec to 1.47x10⁻³ mm²/sec while the responding lesion increased from 1.06x10⁻³ mm²/sec to 1.32x10⁻³ mm²/sec after last loco-regional intervention ($p < 0.001$) whereas the change in SUVmax of (68)Ga-DOTATOC was not significantly different.

Conclusion: After loco-regional DOTATOC therapy non-responder and responder subgroups both presented a change in ADC, prior to SSR2-receptor expression changes and although morphological response according to RECIST criteria was only measurable in few lesions. Therefore, this work suggests that diffusion-weighted imaging is an earlier tumour integrity surrogate for therapeutic intervention and possible early indicator for treatment response.

B-0780 10:48

Simultaneous whole body MR/PET in patients with oncological diagnoses: comparison to PET/CT

M. Souvatzoglou, A. Beer, M. Eiber, S. Fuerst, S. Ziegler, S. Nekolla, E. Rummeny, M. Schwaiger, A. Drzezga; Munich/DE (msouvatz@yahoo.de)

Purpose: To evaluate comparability of the clinical performance of PET/CT and MR/PET in patients with oncological diagnoses.

Methods and Materials: Thirty-two patients underwent a single-injection/dual-imaging protocol, consisting of a PET/CT and subsequent MR/PET scan. PET/CT was performed according to standard clinical protocols (85±9 min p.i. of 400±44 MBq [18 F]FDG, 2 min/bed position (BP)). Subsequently (140±24 min p.i.), MR/PET was performed (4 min/BP). PET-images of both modalities were reconstructed iteratively (OSEM 3D), attenuation correction and regional allocation was performed using low dose CT-data for PET/CT and Dixon-MR sequences for MR/PET. MR/PET and PET/CT were compared visually by rating number and location of suspicious lesions, image quality and alignment. For quantitative comparison, SUV-based assessment of the detected lesions and different organs was performed.

Results: Simultaneous MR/PET acquisition was feasible. No significant difference was found between the numbers of suspicious lesions (n=80) or lesion-positive patients (n =22) detected with MR/PET or PET/CT. Anatomical allocation of PET-findings obtained by MR/PET was sufficiently feasible on the basis of the non-diagnostic Dixon-MR sequences, with comparable performance as with low-dose CT for PET/CT. Quantitative evaluation revealed a high correlation between mean SUV measured in lesions and organs with MR/PT or PET/CT ($\rho = 0.93$; $\rho = 0.92$, respectively).

Conclusion: Simultaneous whole body MR/PET imaging is feasible with high quality in short time, allowing the detection of hypermetabolic lesions with comparable reliability as with PET/CT. Despite different attenuation-correction approaches, the tracer-uptake correlated well between MR/PET and PET/CT. The Dixon MR-sequences acquired for attenuation correction may serve for anatomical allocation of PET findings.

B-0781 10:57

Staging of neuroendocrine tumours: comparison of 68Ga-DOTATOC-PET/CT and MRI

C. Schraml, N.F. Schwenzer, M.K. Werner, C. Brendle, M. Mueller, C.D. Claussen, C. Pfannenberger; Tübingen/DE (christina.schraml@med.uni-tuebingen.de)

Purpose: To compare 68Ga-DOTATOC-PET/CT and whole body (WB) MRI regarding metastatic lesion detection in patients with neuroendocrine tumours (NET).

Methods and Materials: In 51 patients with histologically proven NET 68Ga-DOTATOC-PET/CT and WB MRI were performed. PET/CT was performed after administration of 150 MBq 68Ga-DOTATOC. CT protocol comprised multiphase contrast-enhanced imaging, MRI protocol standard sequences (pre/post Gadolinium) at 1.5 T. Each modality (PET, CT, PET/CT, WB MRI) was evaluated independently by two experienced readers. Consensus-decision based on imaging, histology, surgery and clinical follow-up served as standard of reference. Detection rates of each modality were compared using McNemar test. P values < 0.05 were considered significant.

Results: In 41 of 51 patients, metastatic lesions were detected (lung: 54, liver: 266, bone: 131, lymph node (LN): 99, other: 43). 68Ga-DOTATOC-PET was false negative in 5/41 patients due to lack of receptor expression. Of all 593 detected lesions, PET identified 370 (62%), CT 482 (81%), PET/CT 545 (92%) and WB MRI 540 (91%). Organ-based detection rates of PET/CT were significantly higher for LN (100% vs 73%; p < 0.0001) and pulmonary lesions (100% vs 87%; p=0.0233) while WB MRI had significantly higher detection rates for liver (99% vs 92%; p < 0.0001) and bone lesions (96% vs 82%; p < 0.0001). Of all 593 lesions, 22 were found only in PET, 11 only in CT and 47 only in WB MRI.

Conclusion: PET/CT and WB MRI showed comparable overall detection rates in NET, but significantly differed in organ-based detection rates with superiority of PET/CT for LN and pulmonary lesions and of WB MRI for liver and bone metastases.

B-0782 11:06

Comparison of lesion detection in patient with cranial meningiomas using 68Ga-DOTATOC-PET/CT and contrast-enhanced MRI

A. Afshar-Oromieh, C. Kratochwil, H. Linhart, U. Haberkorn, F.L. Giesel; Heidelberg/DE (f.giesel@dkfz.de)



Purpose: PET imaging with somatostatin receptor ligands, such as 68Ga-DOTATOC-PET/CT, is a well-established method for detection and target volume definition of meningiomas prior to radiotherapy. Since DOTATOC-PET appears to detect more meningiomas than MRI, we conducted a retrospective analysis to compare the diagnostic accuracy of contrast-enhanced MRI (CE-MRI) with 68Ga-DOTATOC-PET/CT in patients with cranial meningiomas prior to radiotherapy.

Methods and Materials: Over a period of six years 134 patients (20-82yo, 107, 27) in our hospital underwent cranial CE-MRI and 68Ga-DOTATOC-PET/CT prior to radiotherapy of cranial meningiomas. Both methods were compared by a side by side read counting the detected meningiomas and recording the localisation and the SUVmax of those detected by PET/CT only.

Results: Within the 134 patients investigated by both modalities 190 meningiomas were detected by 68Ga-DOTATOC-PET/CT and only 171 by CE-MRI (90.00%). Therefore, 19 meningiomas were detected by PET/CT only. Meningiomas, detected in PET/CT only but located close to areas of previous craniotomy (possible relapses or remnants of former meningiomas) were excluded from further analysis.

Conclusion: 68Ga-DOTATOC-PET/CT presented with a higher sensitivity in detecting meningiomas when compared to CE-MRI. Especially tumours adjacent to the falx cerebri, located in the skull base or tumours obscured by imaging artefacts are difficult to detect by MRI.

B-0783 11:15

Diagnostic performance of PET/MR versus PET/CT in the abdomen

D.W. Crook, C. Mader, F.P. Kuhn, A. Samarin, T.F. Hany, J. Hodler, G.K. von Schulthess, D. Schmid; Zurich/CH (caecilia.mader@usz.ch)

Purpose: To compare the diagnostic performance of PET/MR versus PET/CT in the abdomen.

Methods and Materials: Sixty-six oncologic patients (mean age 61) were examined on a TOF-PET/CT and 3 T-MR platform (GE Discovery 690 & 750, respectively) integrated by a shuttle system. Unenhanced CT and T1w (LAVA) 3D-GRE images of the abdomen were acquired, co-registered with PET data and analysed independently by two double board certified radiologists/nuclear physicians. PET-positive lesions were characterised at CT and MR using a 3-point scale to grade image quality and lesion conspicuity. Cohen κ -statistics were calculated for interobserver agreement and the Wilcoxon rank-sum test was employed for intraobserver conspicuity grading.

Results: A total of 147 PET positive lesions were evaluated in the liver (n=49), bone (n=26), lymph nodes (n=21), lung (n=13), GI-tract (n=10), soft tissues (n=8), pleura (n=6), adrenal glands (n=5), pancreas (n=4), spleen (n=1), peritoneum (n=1), chest wall (n=1) and breast (n=1). Lesions were characterised and graded based on conspicuity in CT and MR with good ($\kappa=0.72$) and moderate ($\kappa=0.46$) interobserver agreement, respectively. In the overall lesion-based comparison, no significant difference was found. However, in the organ-based comparison, MR performed significantly better than CT in the liver (p < 0.001 for both readers) while CT tended to perform better than MR in depicting basal lung lesions (p < 0.05 and p < 0.32).

Conclusion: Unenhanced PET/MR outperforms unenhanced PET/CT in the depiction and characterisation of liver lesions. However, in the evaluation of extrahepatic abdominal pathology in oncologic patients, no significant difference between these modalities is seen.

B-0784 11:24

Staging and restaging Hodgkin's disease: low-dose non-enhanced FDG-PET/CT versus full-dose contrast-enhanced FDG-PET/CT

C. Capraro, D. Ippolito, L. Guerra, E. De Ponti, C. Messa, S. Sironi; Monza/IT (davide.atena@tiscalinet.it)

Purpose: To compare the agreement between low-dose non-enhanced PET/CT with full dose contrast-enhanced PET/CT in the staging and restaging Hodgkin's disease (HL).

Methods and Materials: A total of 42 patients with histologically proven HL underwent a 18 F-FDG-PET/CT study that included low-dose non-enhanced CT and full-dose contrast-enhanced CT studies, performed in a single step procedure. 30 studies were performed for staging and 40 for the evaluation of residual disease after first line of chemotherapy (restaging). For every patient, each modality of PET/CT images was evaluated by either of 2 pairs of expert readers blinded about the clinical data and unaware of the results of the other type. Finally, the stage of the disease was defined according to PET/IdCT and PET/ceCT following the Ann Arbor classification. For restaging studies, images were interpreted considering the presence of residual mass with or without residual activity according to the International Harmonization Project.

Results: Of 630 sides considered as potentially involved by the disease, PET/IdCT and PET/ceCT were concordant in 622/630 (98.7%) sides in staging studies and in 40/40 (100%) patients of restaging studies. PET/IdCT and PET/ceCT were concordant with standard reference in 28/30 (88.9%) and in 29/30 (94.4%) patients, respectively, in staging studies. In restaging studies, both PET/IdCT and PET/ceCT results were concordant with standard reference in 38/40 (92.8%) studies.

Conclusion: Our study showed a good correlation between PET/IdCT and PET/ceCT both in staging and, in particular, in restaging studies. If these results are confirmed in a larger patients' population, PET/IdCT might suffice as the only imaging technique for staging and restaging HD, sparing addicted radiation burden and iodinate contrast administration to the patient and reserving ceCT for selected cases.

B-0785 11:33

Prognostic value of residual CT masses in HD patients with a negative FDG PET after chemo/radiotherapy

M. Magagnoli, E. Lopci, M. Rodari, K. Marzo, L. Giordano, F.R. Lutman, A. Anastasia, A. Santoro, A. Chiti; Rozzano/IT (egesta.lopci@gmail.com)

Purpose: To properly define the negative predictive value of residual CT masses in HD patients with PET negative at the end of treatment and define its correlation with disease-free survival (DFS).

Methods and Materials: For our study we retrospectively analysed data deriving from patients (n=105; M:F =62:43; median age 58 years) who underwent FDG-PET and CT scan at the end of treatment. For study purpose, we identified those presenting a negative PET scan and a residual mass on CT: 72 patients after first line treatment, while 31 after salvage therapy. All patients were followed up for a median period of 45 months.

Results: The five-year DFS for PET-/CT- Vs PET-/CT+ patients was 89.4% and 68.7%, respectively (p=0.053). The prognosis of residual mass at CT scan was significantly worse also when considering the dimension of the masses: the larger the mass, the lower the DFS (p=0.007). An optimal cut-off point was identified, with regard to maximal diameter, namely 4 cm. When introducing this cut-off, the DFS in this setting of patients was 50% vs 82% (p < 0.0029). Also, other potential prognostic factors have been analysed (number of masses, first Vs salvage treatment program, sex, bulky disease, B-symptoms), but among them no correlation with DFS or overall survival (OS) emerged.

Conclusion: These data suggest that the presence of residual mass, independently from the FDG PET result, should be carefully followed up and the patients should be considered at an increased risk for relapse/progression of the disease.

B-0786 11:42

Comparison of MR/PET and PET/CT in the assessment of pulmonary masses

C. Schraml, H. Schmidt, C. Brendle, A. Sauter, M. Mueller, C. Pfannenber, C.D. Claussen, N.F. Schwenger; *Tübingen/DE*

Purpose: Comparison of the hybrid modalities MR/PET and PET/CT in the assessment of pulmonary lesions regarding FDG-uptake, lesion characterisation and tumour staging.

Methods and Materials: The study was approved by the local ethics committee. Ten patients with suspected or proven bronchial carcinoma were evaluated. MR/PET was performed with a new hybrid whole body system consisting of a 3 T MR scanner with an integrated PET system. Results were compared to those gained by a directly preceding [18 F]-FDG-PET/CT. Segmentation-based attenuation correction of PET data recorded in MR/PET was conducted with DIXON-based fat-water separation. Tumour and lymph node staging based on PET/CT and MR/PET studies was performed by two readers in consensus. Tumour-to-liver (T/L) ratios calculated in MR/PET and PET/CT were compared. Statistical testing was carried out using Pearson's correlation and Bland-Altman analysis.

Results: In all patients, diagnostic MR/PET image quality with good tumour delineation was achieved. Most lesions (9/10) showed a pronounced FDG uptake. One lesion was morphologically suspicious for malignancy in CT and MRI but showed no FDG uptake. MR/PET showed higher T/L ratios than PET/CT (8.0 ± 3.9 vs 4.4 ± 2.0); however, significant correlation regarding T/L ratio was found between both scanners ($r = 0.90$, $p = 0.0008$). TNM score discrepancies occurred in 3/10 patients mainly due to modality-inherent differences in lesions size measurement.

Conclusion: MR/PET imaging of the lung is feasible and provides diagnostic image quality in the assessment of lung masses. Similar lesion characterisation and tumour stage was found comparing PET/CT and MR/PET in the majority of patients.

B-0787 11:51

The impact of acquisition time on image in whole body 18 F-FDG-PET CT for cancer staging

D. Hausmann, D. Dinter, S.O. Schönberg, J. Brade, M. Sadick, K. Buesing; *Mannheim/DE* (daniel.hausmann@umm.de)

Purpose: To evaluate the impact of acquisition time on image quality, lesion detection rate, standard uptake values and lesion volume in F-18 fluorodeoxyglucose positron emission tomography (18 F-FDG PET) in cancer patients.

Methods and Materials: Over a time period of 7 months, 33 cancer patients were included in this study. In these patients, a total of 63 lesions were independently evaluated by two radiologists (experienced and beginner). A whole body 18 F-FDG PET-computed tomography scan with 3 min and 1.5 min acquisition time per bed position was performed in each patient. Lesions were visually identified and lesion locations compared. Lesion volumes and standard uptake values (SUV) of the primary tumour, lymph nodes and metastases were obtained and compared. For all parameters, interrater agreement was assessed.

Results: All relevant lesions were identifiable at both acquisition times. Image quality was significantly reduced in scans with an acquisition time of 1.5 min ($p < 0.001$). Nevertheless, the image quality was rated excellent/good in 91% of the scans with an acquisition time of 1.5 min. The quality of lesion visualisation was excellent regardless of the acquisition time. Lesion volume on PET images and SUVmax were not significantly different between both acquisition times ($p < 0.001$). Interrater agreement was good ($\kappa > 0.8$).

Conclusion: Despite significant decrease in image quality, a reduction of acquisition time per bed position seems to be clinically feasible without reduction of the lesion detection rate even for less experienced observers.

10:30 - 12:00

Room F1

Genitourinary

SS 1707

Transplant imaging and special topics

Moderators:

P. Hallscheidt; Heidelberg/DE

J.Å. Jakobsen; Oslo/NO

B-0788 10:30

Pre-operative assessment of living renal transplant donors with computed tomography angiography versus magnetic resonance angiography in 118 patients

F. Engelken, F. Friedersdorff, B. Hamm, G. Diederichs; *Berlin/DE* (florian.engelken@charite.de)

Purpose: To compare modern multislice computed tomography angiography (CTA) with magnetic resonance angiography (MRA) in the pre-operative evaluation of vascular anatomy of living renal transplant donors.

Methods and Materials: 118 renal transplant donors were examined with both a modern multislice CT-scanner (≤ 1 mm slice thickness) and a 1.5 T MRI scanner. 236 kidneys were included in the CTA- and MRA-analysis. Renal vasculature was evaluated independently by two readers in each modality with a delay of 4 weeks between reading sessions. Surgical correlation on the operated side was available in all patients. Gold-standard was defined by surgical correlation and consensus reading of both modalities.

Results: There were 316 renal arteries and 267 renal veins in total. Sensitivity of CTA for arteries was 99.1% and 94.9% for readers 1 and 2, respectively. Sensitivity of MRA for arteries was 95.3%/94.6%. Most of the overlooked arteries were ≤ 1 mm diameter (reader 1: 2 of 3 in CTA and 12 of 15 in MRA; reader 2: 12 of 16 in CTA, and 10 of 17 in MRA). Sensitivity for arteries ≥ 2 mm was 99.7%/98.7% in CTA, and 99.1%/97.8% in MRA. Sensitivity for veins was 99.6%/97.8% in CTA, and 97.0%/95.1% in MRA. Both readers misdiagnosed between 1 and 3 non-present arteries and between 2 and 4 non-present veins in both modalities.

Conclusion: Modern multislice CT- and MRI-scanners allow highly accurate evaluation of the vascular anatomy of living renal transplant donors, especially for vessels of ≥ 2 mm diameter. CTA may provide slightly better depiction of very small arteries; however, this may be reader-dependent.

B-0789 10:39

Diagnostic performance of a non-contrast-enhanced MR imaging protocol for potential living-related kidney donors

G.D. Puipe, S. Baumüller, H. Alkadhi, T. Pfammatter, R. Hunziker, M. Schiesser, R.P. Goetti; *Zürich/CH* (gilbert.puipe@usz.ch)

Purpose: To prospectively evaluate the performance of a non-contrast-enhanced magnetic resonance (MR) imaging protocol for preoperative screening of living-related kidney donors.

Methods and Materials: Forty consecutive subjects (mean age 52.2 ± 11.3 years, range 29-73 years) underwent MR imaging with T2-weighted sequences (coronal and axial plane), with a non-contrast enhanced respiratory-gated 3D steady state free precession (SSFP) angiography (NCE-MRA) sequence and with contrast-enhanced magnetic resonance angiography (CE-MRA) sequences in the arterial and venous phase. Two blinded readers independently assessed arterial and venous anatomy and potential kidney lesions. Results of non-contrast-enhanced images were compared to CE-MRA, and in a subgroup of 21 subjects to surgery as standard of reference.

Results: Regarding arterial anatomy NCE-MRA yielded sensitivity, specificity and accuracy of 100%, 89% and 91% compared to CE-MRA. Three kidneys were found to have more accessory renal arteries at NCE-MRA but not at CE-MRA. In the subgroup of 21 subjects one surgically proven accessory artery was depicted with NCE-MRA but not with CE-MRA. Accuracy of T2-weighted images regarding accessory veins or variant venous course was 99%, with one missed circumaortic vein at T2-weighted images. Two simple cysts were missed on T2-weighted and NCE-MRA but not on CE-MRA images.

Conclusion: A non-contrast-enhanced MR imaging protocol including NCE-MRA and T2-weighted images allows for the accurate screening of living-related kidney donors and may serve as an alternative to CE-MRA.

B-0790 10:48

Diffusion-tensor imaging (DTI) for functional assessment of transplanted kidneys at 3 T

R.S. Lanzman, A. Ljimini, G. Pentang, P. Kropil, P. Heusch, F.R. Miese, D. Blondin, G. Antoch, H.-J. Wittsack; *Düsseldorf/DE (rotenshlomo@yahoo.de)*

Purpose: The purpose of our study was to investigate diffusion tensor imaging (DTI) for functional assessment of transplanted kidneys at 3 T.

Methods and Materials: 40 renal transplant recipients (mean age 49.6 ± 14.9 years) were included in this study and examined on a 3 T MR scanner using a body array coil. Recipients were divided into two groups according to allograft function: group a, patients with good allograft function ($GFR > 30 \text{ ml/min/1.73m}^2$); group b, patients with poor allograft function ($GFR \leq 30 \text{ ml/min/1.73m}^2$). The DTI sequence was acquired in the coronal plane with 5 b-values (0, 200, 400, 600, 800 s/mm²) and 20 direction (FOV 400 mm, matrix 192, slice thickness 6 mm, 10 slices, TR/TE 1500/90 ms). FA (fractional anisotropy) and ADC (apparent diffusion coefficient) maps were calculated and a ROI-based analysis was performed.

Results: Mean FA of the renal medulla was significantly higher in group a (0.39 ± 0.06) as compared to group b (0.27 ± 0.05). Furthermore, mean ADC values of the renal cortex and medulla were significantly higher in group a (1856.6 ± 107.4 and $1816.9 \pm 126.4 \text{ } 10^{-6} \text{ mm}^2/\text{s}$, respectively) than in group b (1722.8 ± 164.2 and $1698.5 \pm 148.8 \text{ } 10^{-6} \text{ mm}^2/\text{s}$, respectively). Medullary FA values correlated significantly with allograft function as assessed by GFR ($r=0.65$).

Conclusion: DTI is a promising nonenhanced technique for functional evaluation of renal allografts. FA values of the renal medulla correlate significantly with allograft function. Further studies are required to determine the clinical value of DTI for monitoring transplanted kidneys.

B-0791 10:57

DWI with mono- and biexponential analysis in kidneys allografts early after transplantation

U. Navarro, M. Ravanelli, P. Rizzardi, S. Sandrini, R. Maroldi; *Brescia/IT (navarrougo@gmail.com)*

Purpose: To evaluate if DWI-related parameters, obtained by mono- and bi-exponential analysis early after transplantation, correlate with kidney allografts function and biopsy results.

Methods and Materials: Twenty-two consecutive kidney allograft recipients were examined by MR between 7 and 9 days after transplantation. MR protocol included EP-DWI sequences with 11 b-values (0-1000s/mm²). DWI ROI-measurement were performed by two radiologists with different experience in abdominal MR. One radiologist analysed twice ten datasets to assess the intra-observer variability. DWI-related parameters were: ADC (mono-exponential analysis); diffusion-coefficient (D) and perfusion-fraction (f) (bi-exponential analysis). Fourteen allografts showed normal function recovery. 6/8 patients with delayed function recovery underwent biopsy: 3/6 had acute rejection (AR), 2/6 had acute tubular necrosis (ATN) and one presented specific findings. T-test was used to compare mean values between patients groups. Inter- and intra-observer variability was assessed by Bland-Altman test.

Results: ADC, D and f values were significantly ($p < 0.005$) higher in normal-function allografts ($2.10 \pm 0.13 \times 10^{-3} \text{ mm}^2/\text{s}$, $1.71 \pm 0.12 \times 10^{-3} \text{ mm}^2/\text{s}$, $12.3 \pm 2.3\%$) compared to the impaired-function group ($1.90 \pm 0.17 \times 10^{-3} \text{ mm}^2/\text{s}$, $1.51 \pm 0.21 \times 10^{-3} \text{ mm}^2/\text{s}$, $9.5 \pm 2.2\%$). Compared with the 2 ATN, the 3 AR had lower D ($1.3 \pm 0.1 \text{ vs } 1.67 \pm 0.13 \times 10^{-3} \text{ mm}^2/\text{s}$), ADC ($1.77 \pm 0.11 \text{ vs } 1.92 \pm 0.01 \times 10^{-3} \text{ mm}^2/\text{s}$) and f ($8.6 \pm 2.4\% \text{ vs } 9.9 \pm 0.1\%$). The three patients with impaired renal function without AR or ATN, had ADC values greater than the ATN group ($2.02 \pm 0.02 \text{ vs } 1.92 \pm 0.01 \times 10^{-3} \text{ mm}^2/\text{s}$). Intra- and inter-observer variability was adequate.

Conclusion: These preliminary results suggest that DWI could represent a reliable non-invasive tool to evaluate the allograft status early after transplantation. Bi-exponential analysis is feasible and useful to confirm the results of mono-exponential analysis. Differentiation between AR and ATN, critical for patients management, seems to be feasible.

B-0792 11:06

Quantitative CT imaging of renal perfusion for assessment of renal allograft dysfunction

A. Helck¹, F. Schoen¹, U. Schoenermarck¹, M. Wessely¹, M. Fischereider¹, E. Klotz², M. Reiser¹, K. Nikolaou¹, C. Becker¹; ¹Munich/DE, ²Forchheim/DE (andreas.helck@med.uni-muenchen.de)

Purpose: To assess the feasibility of a quantitative CT-perfusion technique for the differential diagnosis between renal allografts with acute tubular necrosis (ATN) and graft rejection.

Methods and Materials: This study was performed with institutional review board approval. 21 patients suffering from acute unexplained kidney allograft dysfunction were included in the study. A dynamic multi-phase CT-angiography protocol (128 slice CT-scanner, 12 phases, temporal resolution 3.5 s) including the entire renal graft was performed to exclude post-operative or vascular complications. Dynamic CT data were used for the calculation of parenchymal blood flow and parenchymal blood volume using dedicated software. Renal biopsy (n = 15) or clinical follow-up (n = 6) served as the standard of reference.

Results: Renal parenchymal blood flow values were substantially lower in allografts with acute rejection ($48 \pm 15 \text{ ml/100 ml/min}$, n = 7), compared to ATN ($76 \pm 24 \text{ ml/100 ml/min}$, n = 14). In addition, renal parenchymal blood volume was reduced in case of renal graft rejection ($8.7 \pm 5 \text{ ml/100 ml}$) compared to subjects suffering from ATN ($13.8 \pm 5.5 \text{ ml/100 ml}$).

Conclusion: CT-perfusion has the potential to improve assessment of renal allograft dysfunction.

B-0793 11:15

Comparison of diffusion-weighted MRI and histopathologic findings in kidney transplant patients with deteriorating renal function

P. Steiger, M. Ith, M. Gugger, A. Kruse, J. Fröhlich, D. Chong, H. Thoeny; *Berne/CH*

Purpose: To determine whether diffusion-weighted MRI (DW-MRI) can be used to stratify patients for biopsy (BI) or follow-up (FU) based on various diffusion parameters.

Methods and Materials: Thirty-five consecutive kidney transplant patients (8w/27m) with deteriorating renal function underwent DW-MRI (EPI-sequence; ten b-values: 0-900s/mm²) on a 1.5 Tesla MR-scanner (Siemens Sonata) within ten days before or after biopsy. DW-MRI data were processed applying either mono-exponential (yielding ADC-values [$\times 10^{-5} \text{ mm}^2/\text{s}$]) or bi-exponential fitting (yielding values for pure diffusion ADCD [$\times 10^{-5} \text{ mm}^2/\text{s}$] and perfusion fraction FP [%]). If renal biopsy yielded at least one result with a direct implication for clinical management, e.g. rejection, patients were assigned to the BI-group. Statistical evaluation was performed using STATA and values are given as mean \pm SEM. Unpaired t-tests were used to compare the DW-MRI parameters between BI- and FU-group.

Results: Of the 35 patients who underwent renal allograft biopsy 22 were classified into the BI-group and 13 into the FU-group. Histopathologic findings in the BI-group included cellular rejection (n=8), humoral rejection (n=2), glomerulonephritis (n=1), IGA nephropathy (n=1), BK virus nephropathy (n=2), acute tubular necrosis (n=2), cyclosporine toxicity (n=8) and chronic allograft-nephropathy (n=3), whereas findings in the FU-group included chronic changes such as vascular or glomerular sclerosis, fibrosis, atrophy or minor interstitial inflammation. DW-MRI parameters of the BI-group were significantly lower compared to the FU-group: ADC ($183 \pm 1 \text{ vs } 195 \pm 1$; $p < 0.01$), ADCD ($177 \pm 12 \text{ vs } 188 \pm 12$; $p < 0.01$) and perfusion fraction FP ($16 \pm 3\% \text{ vs } 18 \pm 5\%$; $p < 0.01$), respectively.

Conclusion: DW-MRI in kidney transplant patients with deteriorated renal function might improve the diagnostic workup by stratifying patients for renal biopsy.

B-0794 11:24

High-field MRI in assessment of murine placental functional morphology and comparison to histology

C.C. Much, E. Solano, T. Ernst, J. Yamamura, G. Adam, P. Arck, U. Wedegaertner; *Hamburg/DE (cmuch@uke.de)*

Purpose: To date, insights on placental architecture are achieved by tedious histomorphological analysis. The purpose of our study was to evaluate MRI as a tool to examine placental morphology in a murine model.

Methods and Materials: MRI Imaging was performed on 20 formalin-fixed and gadolinium-treated mouse placentas on a 7T animal scanner (ClinScan, Bruker) using a T2-weighted 3D-TSE sequence. 10 placentas were taken from prenatally stressed (well-established model of sound challenge) foetuses and 10 placentas served as controls. Total placental volume and volume of functional zones (junctional zone and labyrinth) was calculated. For comparison 20 formalin-fixed and paraffin-embedded placentas (10 stressed, 10 controls) were morphologically assessed for functional zones upon histology by an experienced foeto-maternal pathologist, according to the to date 'gold standard protocol' for placental analyses. Differences between groups were analysed by Mann-Whitney U-test.

Results: Placental functional zones could be easily identified with MRI. Further, placental functional alterations could be detected, as tissue from prenatally stressed mice displayed a bias towards an increased labyrinth zone (ratio 1.9 vs. 1.3 controls, $p < 0.01$), whilst the overall placental volume remained unaltered. These observations could be independently appreciated upon histological assessment.

Conclusion: Our preliminary results demonstrate that in vitro imaging of murine placental functional morphology with MRI is feasible and results are comparable to time-consuming histological analysis.

B-0795 11:33

Magnetic resonance diffusion tensor imaging identifies histopathological changes in a rat model of diabetic nephropathy

K. Hueper¹, D. Hartung¹, M. Gutberlet¹, F. Wacker¹, H. Sann², B. Husen³, D. Reiche⁴; ¹Hannover/DE, ²Barsbüttel/DE, ³Saarbrücken/DE, ⁴Ingelheim/DE

Purpose: To investigate whether magnetic resonance (MR) diffusion tensor imaging (DTI) allows assessment of renal pathologies in a rat model of diabetic nephropathy.

Methods and Materials: Twenty-one Sprague-Dawley rats were divided into three groups: controls, diabetes (DM), diabetes with uninephrectomy (DM UNX). UNX is known to accelerate renal impairment. Eight weeks after diabetes induction with streptozotocin MRI was performed on a 1.5-T scanner using an 8-channel wrist-coil. Morphological images and echoplanar DTI were obtained (b=0, 300 s/mm², 6 diffusion directions). Renal ADC and fractional anisotropy (FA) were calculated for each of the different layers of the kidney. Imaging results were compared to laboratory parameters and histology.

Results: All diabetic animals developed significant hyperglycemia and hypoin-sulinemia. Albuminuria and histopathological changes were more pronounced in DM UNX. ADC values were not different between groups except for cortical ADC, which was higher in DM UNX than in controls. FA of different layers of the kidney was significantly reduced in DM UNX when compared to controls and to DM group. In DM without UNX only cortical FA was significantly lower than in controls. Cortical FA negatively correlated with glomerulosclerosis (p < 0.001, R²=0.42). In animals with tubulo-interstitial fibrosis and tubular enlargement, FA was significantly reduced in comparison to animals without those findings.

Conclusion: MR DTI identified renal pathologies of diabetic nephropathy such as glomerulosclerosis, interstitial fibrosis and tubular damage by reduction of FA. DM and DM UNX animals, representing different stages of disease, could be differentiated. Thus, DTI may be valuable for detection and monitoring of renal nephropathy in diabetic patients.

B-0796 11:42

MRgFUS treatment for uterine myomas: safety, effectiveness and pathogenesis

Y. Kurashvili, A. Stepanov, V. Bytchenko, E. Kulabuchova, O. Batarchina, I. Lugina; Moscow/RU (leri@me.com)

Purpose: Clinical safety evaluation of MRgFUS treatment for uterine fibroids. Retrospective and prospective study. 664 patients suffering uterus fibromyoma had underwent MRgFUS treatment since March 2006 for March 2011 I group: 487 randomised included patients; II group: 177 patients according to patient selection criteria. Follow-up period up to 3.5 years.

Methods and Materials: Standard and specifying. Clinical effect was measured in scores using The Pictorial Blood Assessment Chart (Higham, Janssen), UFS-QOL chart and McGill pain questionnaire. MRgFUS ablation procedures were conducted using ExAblate-2000 system (InSightec*, Israel), guided by MRI 1.5 [[Unsupported Character - Т]] (GE, USA).

Results: Results of the study proved MRgFUS technology to be a safe enough method for treatment of uterus fibromyoma. Complications and adverse effects were revealed in the course of first two years of the method's clinical use and 5 cases (1.02%) of these were: temperature-induced lesion of the small intestine - 1 (0.2%), temperature-induced local oedema of the anterior abdominal wall (without burn) - 1 (0.2%), sciatica - 2 (0.4%), passage of FUS-detritus via uterine body cavity - 1 (0.2%). There were no complications afterwards provided patient selection criteria were used.

Conclusion: Despite the fact that the method is sufficiently safe and has a short list of rare complications it should be remembered that curative agent of the technology is focused coagulating ultrasound. Patient selection criteria and regulations governing the procedure should be followed strictly in order to prevent complications and adverse effects.

B-0797 11:51

Detection of localised prostate cancer using contrast-enhanced MRI and 11C-acetate PET/CT

I. Jambor, R. Borra, J. Kemppainen, V. Lepomki, K. Dean, K. Alanen, M. Nurmi, H.J. Aronen, H. Minn; Turku/FI (ivjamb@utu.fi)

Purpose: We assessed the ability of contrast-enhanced MRI at 1.5 Tesla and 11C-acetate PET/CT to detect localised prostate cancer. In addition, fusion of 11C-acetate PET with MRI was performed.

Methods and Materials: Thirty-six patients (mean age, 65 years; range, 46-78 years) with untreated localised prostate cancer were prospectively enrolled. A pelvic 11C-acetate PET/CT scan was performed in all patients, and a contrast-enhanced MRI scan in 33 patients (6 examinations using both endorectal coil and surface coils, and 27 examinations using surface coils only). Obtained PET/CT and MRI data were evaluated visually and compared with biopsy findings on a lobar level. In addition, PET data were fused with MRI data using in-house developed software. The lobe with the highest percentage of cancer in biopsy samples was determined to be the dominant lobe.

Results: The sensitivity, specificity and accuracy for the visual detection of prostate cancer on a lobar level by contrast-enhanced MRI were 85%, 37%, 73% and 11C-acetate PET/CT was 88%, 41%, 74%, respectively. Fusion of PET data with MRI increased diagnostic performance with sensitivity, specificity and accuracy of 90%, 72% and 85%, respectively. The accuracy of dominant lobe detection was 70%, 75% and 82% for contrast-enhanced MRI, PET/CT and fused PET/MRI, respectively. Maximal and average SUV values normalised to benign sextants correlated significantly with PSA only (p=0.0005 and 0.0002, respectively).

Conclusion: Fusion of sequentially obtained PET/CT and MRI data was feasible and superior in localisation of prostate cancer compared to both imaging modalities alone.

10:30 - 12:00

Room F2

Breast

SS 1702

MRI sequences: advances and applications

Moderators:

E. Taheri; Tehran/IR
S.J. Vinnicombe; Dundee/UK

B-0798 10:30

Initial maximum slope of the contrast enhancement versus time curve for dynamic evaluation of breast lesions on ultrafast breast MRI

R.M. Mann¹, R.D.M. Mus¹, C. Geppert², C.P.M. Frenzt¹, N. Karssemeijer¹, H. Huisman¹, B. Platel¹; ¹Nijmegen/NL, ²Erlangen/DE (r.mann@rad.umcn.nl)

Purpose: Modern viewsharing sequences allow dynamic whole breast MRI at diagnostic spatial resolution within 5 seconds, showing the inflow of contrast in breast abnormalities. We evaluate the maximum slope of initial contrast enhancement as a heuristic parameter for differentiating benign from malignant disease and compare its value to classic 3 timepoint analysis.

Methods and Materials: We employed a bi-temporal breast MRI protocol on a 3 T MRI using a 16 channel bilateral breast coil. High-resolution VIBE acquisitions (0.8*0.8*1.0 mm, temporal resolution 94s) were interleaved with a series of ultrafast TWIST acquisitions (1*1*2.5 mm, temporal resolution 4.2s) during the inflow of the contrast agent. Forty-two consecutive patients with 43 enhancing abnormalities (21 benign and 22 malignant) presenting between November 2010 and July 2011 were included. We measured the maximum slope of the relative enhancement versus time curve on the TWIST acquisitions and recorded curve type of the lesions on the VIBE acquisitions. ROC analysis was performed to compare diagnostic performance.

Results: The maximum slope of the relative enhancement versus time curve was significantly better in discriminating between benign and malignant disease than the curve type (Az 0.865 vs. Az 0.723, p = 0.036). Cutoff values of 15%/sec and 3.15%/sec can be used to differentiate high-risk lesions (> 85% malignancies) from intermediate and low-risk lesions (< 10% malignancies). This simplification yields an Az of 0.808.

Conclusion: The initial maximum slope provides more diagnostic information than the curve types and can therefore be used to assess lesion dynamics. This can substantially shorten current scan protocols.

B-0799 10:39



Diagnostic performance of a dedicated breast MR system using spiral acquisitions

S.E. Harms¹, B.J. Hillman², G. Stevens³, R. Stough⁴, A. Hollingsworth⁴, K. Kozlowski⁵, L. Moss⁶; ¹Fayetteville, AR/US, ²Philadelphia, PA/US, ³Bastrop, TX/US, ⁴Oklahoma City, OK/US, ⁵Knoxville, TN/US, ⁶Worcester, MA/US (seharms@earthlink.net)

Purpose: To assess diagnostic performance of breast MRI at dedicated breast imaging centers using a dedicated 1.5 T breast MR system that employed high resolution, high contrast spiral trajectory acquisitions.

Methods and Materials: We retrospectively assessed diagnostic performance for 1,100 consecutive screening (n=348) and diagnostic (n=752) cases performed from April 2006 to December 2007 for women aged 25-89 from four sites for which dedicated breast MRI reports and ground truth (biopsy for cancer cases; one year negative follow-up for negative cases). The study was IRB approved and HIPAA compliant. The sensitivity, specificity, and ROC for the breast MRI, mammography, and ultrasound were calculated and compared to each other to determine if there were statistically significant differences between the modalities with respect to these parameters.

Results: The sensitivity and specificity for the dedicated breast MRI system were 0.966 (p=0.0006) and 0.862 (p < 0.0001). For all cases, the negative predictive value (NPV) was 0.984, for screening cases, 1.0. The area under the receiver operating characteristic (ROC) curve was 0.956. Of the 120 false positives seen on dedicated breast MRI, thirteen (11%) were high risk histologies.

Conclusion: We demonstrate high diagnostic accuracy in breast MRI.

B-0800 10:48

Evaluation of the ability of parametric dynamic contrast-enhanced MRI and diffusion tensor imaging to detect breast malignancies

E. Furman-Haran¹, M. Feinberg-Shapiro², N. Weisenberg², N. Nissan¹, T. Zehavi², D. Grobgeld¹, E. Eyal¹, H. Degani¹; ¹Rehovot/IL, ²Kfar Saba/IL (edna.haran@weizmann.ac.il)

Purpose: To compare the ability of perfusion parameters and of diffusion parameters, obtained from breast DCE-MRI and DTI datasets, respectively, to identify IDC, ILC and DCIS.

Methods and Materials: High-resolution DCE and DTI breast datasets of 43 patients with breast malignancies (24 IDC, 9 ILC and 13 DCIS) confirmed by histopathology were analysed. Axial images of the two breasts were recorded at 3 T using high spatial resolution (DCE: 0.8x0.8 x2-2.5 mm³, ~ 10 min; DTI: 1.9x1.9x2-2.5 mm³, ~6 min).

Results: All malignancies were enhanced and were correctly diagnosed using morphological and dynamic features of enhancement. Most of the lesions exhibited high wash-in rate indicating high transcappillary transfer contrast, followed by constant enhancement or reduced enhancement (washout). In part of the lesions (6 IDC, 1 ILC and 6 DCIS) slow enhancement patterns were observed with no washout. Two DTI parameters, the prime diffusion coefficient and the maximum anisotropy index, were significantly lower in the cancers than in the normal breast tissue, enabling cancer delineation. In 4 IDC, 1 ILC and 6 DCIS, the two DTI parameters did not reveal clearly the boundaries of the lesions, primarily due to low S/N and partial volume effects in fatty breasts. In part of the slow enhancing cancers the DTI parameters helped identify correctly the lesion.

Conclusion: The results confirm the high sensitivity of DCE-MRI and show the potential of DTI to provide high sensitivity as a standalone method in dense breasts. Further studies are required in order to incorporate DTI into the clinical setting.

B-0801 10:57

Correlation between apparent diffusion coefficient and molecular and histological prognostic factors in breast cancer: observations in 94 patients

L. Bonello, G. Petralia, P. Summers, L. Preda, S. Raimondi, G. Renne, G. Bardo, G. Curigliano, M. Bellomi; Milan/IT (luke.bonello@ieo.it)

Purpose: To correlate apparent diffusion coefficient (ADC) with molecular and histological prognostic factors for breast cancer.

Methods and Materials: 94 female patients (mean age 48.6, range 28-81 years) with histologically proven breast cancer underwent conventional (including T2-weighted and T1 dynamic imaging post-contrast) and diffusion-weighted MRI (b-values 0, 250, 500 and 1000s/mm²). The ADC for breast cancer, as defined manually on the highest b-value images, was correlated with molecular and histological prognostic factors. ADC values were assessed for difference between gene profiling subtypes (Luminal A, Luminal B, HER-2, triple receptor negative), vascular

invasion (present/absent), grading (G1/G2/G3), ER/PgR/HER-2 expression (positive/negative), Ki67 (14%) and TNM staging using analysis of variance (ANOVA). Spearman coefficient was used to assess correlation between ADC values and continuous variables (age, percentage of ER, PgR, HER-2, Ki-67).

Results: The ADC of breast cancer visible on the high b-value image was 1.158±0.23 x 10⁻³ mm²/sec. The ADC for T4 tumours was higher than in T2 and T3 tumours (p < 0.05). The ADC for lymph node positive tumours (N1/N2) was lower than lymph node negative tumours (p < 0.02). The ADC value for triple receptor negative tumours was higher than other subtypes, only reaching significance when compared to Luminal B (p = 0.014).

Conclusion: Our results showed differences in ADC for different histological prognostic factors and genetic subtypes of breast cancer. The ADC differences in patients with different lymph nodes status encourages further studies to explore its clinical utility as an additional prognostic factor for breast cancer.

B-0802 11:06



Differentiating invasive and non-invasive breast carcinomas using diffusion-weighted MRI: a feasibility study

A.M. Chow, V. Ai, P.S.Y. Cheung, R. Lee, S.K. Yu, G.G. Lo; Happy Valley/HK (aprilcmk@gmail.com)

Purpose: To establish threshold apparent diffusion coefficient (ADC) value for differentiating invasive and non-invasive breast carcinomas using diffusion-weighted imaging (DWI) at 3 T.

Methods and Materials: 73 female patients with biopsy-proven malignant breast lesions (N = 100) were prospectively evaluated. All MRI examinations were performed on a 3 T MRI scanner (MAGNETOM Trio, Siemens) using a dedicated 4-channel phased array coil. A single-shot echo-planar imaging DWI protocol was performed to obtain images axially using b-values = 0, 1000 s/mm². A circular ROI was defined in the DW images over the breast lesions and used for ADC measurements. Threshold ADC values were determined using receiver operating characteristic (ROC) analysis.

Results: Pathological results showed that 67 lesions were invasive carcinomas, while 33 lesions were non-invasive carcinomas. ADC of invasive carcinomas (0.97 ± 0.14 x 10⁻³ mm²/s) was significantly lower (p < 0.001, two-tailed paired Student's t test) than that of non-invasive carcinomas (1.19 ± 0.13 x 10⁻³ mm²/s). The area under the receiver operating characteristic curve was 0.874, indicating a good diagnostic performance of ADC in differentiating invasive and non-invasive breast carcinomas. An ADC threshold value of 1.09 x 10⁻³ mm²/s was determined, allowing differentiation between invasive and non-invasive breast carcinomas with sensitivity, specificity and accuracy of 80.6%, 84.9% and 82.0%, respectively.

Conclusion: DWI is a feasible method to characterise breast lesions quantitatively, offering promise as a robust non-invasive tool to differentiate between invasive and non-invasive breast carcinomas.

B-0803 11:15

Is 3D proton spectroscopic imaging at 3 Tesla able to discriminate benign and malignant breast lesions?

B. Brueck, K. Pinker-Domenig, H. Magometschnigg, W. Bogner, H. Bickel, T.H. Helbich, S. Gruber; Vienna/AT (benedikt.brueck@meduniwien.ac.at)

Purpose: To assess whether 3D proton spectroscopic imaging at 3 Tesla (3 T 3D-1H-MRSI) is able to differentiate between benign and malignant breast lesions.

Methods and Materials: 89 patients with a suspicious breast lesion were included in this prospective IRB approved study and underwent 3 T 3D-1H-MRSI using a dedicated breast coil. For 3 T 3D-1H-MRSI, a point-resolved spectroscopy sequence with the following sequence parameters was used: TR/TE=750/145 ms; FOV 12 x 12 x 12 cm³; matrix size 12 x 12 x 12 interpolated to 16 x 16 x 16; TA 11:17 min. 8 Patients had to be excluded due to insufficient quality of data due to motion artefacts. Signal-to-noise ratio (SNR) of choline (Cho) was calculated using JMURUI and a self-written software. MRSI voxels were assessed for the maximum SNR of Cho by an experienced spectroscopist and an SNR threshold of > 2.55 was defined as indicative of malignancy. All lesions were histopathologically verified.

Results: 53 malignant and 28 benign lesions were confirmed in 81 patients. 3D-1H-MRSI had a sensitivity of 89% and a specificity of 93%. NPV was 0.81, PPV was 0.96 and diagnostic accuracy was 90%. The median SNR of Cho in was 5.7 in malignant and 2.0 in benign breast lesions.

Conclusion: 3D-MRSI at 3 T yields high diagnostic sensitivity and specificity for discrimination of benign and malignant breast lesions within clinically feasible scan times.

B-0804 11:24

Role of proton MR spectroscopy in the high field magnet (3 T) in diagnosis of indeterminate breast masses (BIRADS 3&4)

N.M. Abdel Razek, A.O. Azab; Giza/EG (naglaabdelrazek@yahoo.com)

Purpose: To evaluate the role of MR spectroscopy using the state-of-art high field magnet (3 Tesla) as a diagnostic method in indeterminate breast lesions (BIRADS 3&4 lesions) aiming at decreasing the unnecessary breast intervention.

Methods and Materials: In this study, 240 female patients classified as BIRADS 3&4 by sono-mammography (Sono-MX) were examined by MRI using the multiphase dynamic sequence and proton MR spectroscopy using a high field magnet (3 Tesla). Single voxel technique after adequate shimming was used. The graphs were interpreted for the presence of choline peak in the spectrum and the results were correlated to the results of the dynamic MRI. All lesions were histopathologically proven (FNB, CNB, VAB&OB).

Results: 88 cases (35%) of cases were malignant (based on the presence of high choline peak in the spectrum) and 152 cases (65%) were benign (no choline peak). Malignant cases were DCIS, IDC, medullary colloid and lobular carcinomas. Benign cases were fibroadenoma, papilloma, sclerosing adenosis and breast cysts. MR spectroscopy has increased the sensitivity and specificity of dynamic MR mammography for diagnosis of probable lesion from 94% to 78% to 97% to 95%. False-positive results were found in lactating females and in only one case of atypical fibroadenoma; however, the choline peak in such case was short and bifid. There was a strong agreement between the results of MRS and the histopathology (p value < 0.01).

Conclusion: MR proton spectroscopy in the high field magnet (3 T) offered additional information that increased the sensitivity and specificity of the conventional dynamic MRI in evaluating probable breast lesions and hence reduced the need for unnecessary intervention.

B-0805 11:33

To compare MR spectroscopy at 3 T with tumour type and grading of breast cancers

M. Luciani, F. Pediconi, M. Telesca, F. Vasselli, V. Casali, E. Miglio, C. Catalano; Rome/IT (marialauraluciani@gmail.com)

Purpose: To evaluate the diagnostic performance of magnetic resonance (MR) spectroscopy at 3 T to detect different cancer types and prognostic factors in patients with biopsy-proven breast cancer.

Methods and Materials: Breast MR spectroscopy was performed at 3 T in patients with biopsy-proven malignant lesions measuring 6 mm or larger at MR imaging. Single-voxel MR spectroscopy data were collected from a single rectangular volume of interest that encompassed the lesion. MR spectroscopy findings were defined as positive if the signal-to-noise ratio of the choline resonance peak was ≥ 2 and as negative in all other cases. MR spectroscopy findings were then compared with histologic findings. Lesion size, histotype, nuclear-grade, receptor status (ER, PgR), and Ki67 and HER2 expression were evaluated.

Results: 25 patients with 30 lesions were evaluated. Pathology confirmed 24 IDC, 5 ILC and 1 DCIS. Choline peak occurred in 17/30 lesions (16 IDC and 1 ILC). Three IDC with no choline peak presented with large central area of necrosis. Thus, a choline peak was more frequently associated with IDC than with ILC, DCIS and necrosis. No statistically significant association of choline peak with receptor status (ER, PgR), Ki67 and HER2 was found, although the choline peak was always present in triple negative patients.

Conclusion: Proton MR spectroscopy at 3 T was successfully incorporated into breast MR imaging studies for lesions measuring 6 mm or larger. MR spectroscopy could be an additional tool to predict tumour aggressiveness. Results need to be validated in larger-scale studies.

B-0806 11:42

Diagnostic performance and interobserver variation in quantitative proton magnetic resonance spectroscopy of the breast at 1.5 T: a prospective single-centre cross-sectional study

P.A.T. Baltzer¹, J. Schelhorn², M. Benndorf¹, W.A. Kaiser¹, M. Dietzel¹; ¹Jena/DE, ²Weimar/DE (pascal.baltzer@med.uni-jena.de)

Purpose: An increase of choline metabolites in proton MR-spectroscopy (MRS) is associated with malignancy. One approach for differentiation of breast lesions is quantification of the choline resonance at 3.23 ppm normalised to the water resonance. As postprocessing is a subjective task, this investigation was performed to investigate interobserver variation and diagnostic performance of quantitative MRS of breast lesions.

Methods and Materials: 98 patients (mean age 54.8y) with enhancing lesion > 8 mm on contrast-enhanced MRI (1.5 T, 0.1 mmol/Gd-DTPA/kg) were investigated using single voxel MRS (PRESS, TR 2000 ms, TE 270 ms). Reference standard (RS) was histopathology or follow-up of > 24 months. Spectra were analysed and postprocessed by two independent observers (O1, O2) using MRUI software. For Choline/water quantification, the AMARES algorithm was applied. Statistical analysis included interobserver correlation coefficient and receiver operating characteristics (ROC) analysis.

Results: 71 malignant and 27 benign lesions were investigated. Interobserver correlation coefficient was high with 0.974. Accuracy for discrimination between benign and malignant findings determined by ROC analysis was O1: 79.6%, S.E. 4.9%; O2: 79.9%, S.E. 5.0%; differences not significant (P> 0.05). A significant overlap of choline concentration between benign and malignant findings was observed.

Conclusion: According to the presented results, MRS quantification showed high interobserver correlation and no significant differences between the diagnostic performance of both observers. A quantitative and reliable diagnostic tool may be able to reduce diagnostic variation in breast MRI. However, elevated choline concentration seems not to be restricted to malignant findings and is also observed in benign lesions, limiting diagnostic power of MRS.

B-0807 11:51

Ex-vivo MRI of breast specimen: an innovative technique for the management of only or better MRI-detected cancer

G. Trecate, R. Agresti, D. Vergnaghi, B. Valeri, C. Ferraris, S. Bohm, I. Maugeri, M. Carcangiu, D. Scaramuzza; Milan/IT (gio@doghunter.org)

Purpose: When better staged with MRI, breast malignancies rise the radiological problem to be localised and the surgical issue of their complete resection. This mainly happens with lobular histotypes, where growth pattern shows minimal or absent desmoplastic reaction, or by in situ disease, especially if not associated with calcifications. The aim of our study was to invent a new strategy that firstly enabled the localisation of cancer and secondly demonstrated their true excision.

Methods and Materials: We enrolled 43 cases of better or only MRI emphasised lesions. We localised the disease by means of a careful three-dimensional reconstruction of breast parenchyma, made with a post-processing elaboration of images and combined with the measurement of the distances from the nipple and skin outlines. Later, we injected contrast medium (Gd-DTPA) before surgical incision and finally performed ex-vivo MRI of surgical specimen within 15' after resection by means of a surface coil and SPAIR sequences. Informed consent was requested for both diagnostic and ex-vivo examinations.

Results: All enhancing lesions were retrieved in breast specimen after resection. The new technique reproduces primary disease even if associated with dendritic branches or small satellite nodes and the surface coil magnifies malignancies with a representation that is very similar to the pathological gross examination.

Conclusion: To our knowledge, this procedure is the first that re-enhances breast lesions within a surgical specimen. The technique reproduces morphology and extension of the disease by means of the same procedure that had previously provided the most accurate staging of cancer, giving the certainty of its true remotion.

10:30 - 12:00

Room G/H

Head and Neck

SS 1708

New technical applications

Moderators:

H.B. Eggesbø; Oslo/NO

R. Ljumanovic; Amsterdam/NL

B-0808 10:30

MR microscopy of the human eye: correlation with histology

P.-C. Krüger¹, S. Langner¹, K. Falke², R. Guthoff², O. Stachs², N. Hosten¹;

¹Greifswald/DE, ²Rostock/DE

Purpose: Magnetic resonance imaging (MRI) at 1.5 and 3 Tesla with small surface coils is a well-established procedure in the diagnosis of space-occupying lesions of the eye and orbital cavity. Until now histological examination has been required to reliably assess tumour extent and possible infiltration of surrounding structures. With ultra-high-field MRI, however, it has become possible to evaluate tumour morphology as well as infiltration into surrounding structures with sub-millimeter resolution.

Methods and Materials: Ten human eyes with different space-occupying masses were examined ex vivo to compare the standard clinical examination (ultrasound) with ultra-high-field micro-MRI using a small surface coil. Imaging parameters

were: slice thickness 500 μm ; matrix size 1024 x 1024 pixels; in-plane resolution 39 x 39 x 500 $\mu\text{m}/\text{pixel}$; acquisition time 8:20 min per plane. Finally, the specimens were examined histologically, and the histological and MRI results were correlated.

Results: Ultra-high-field MRI at 7.1 Tesla provided images of anatomical structures of the bulb as well as different benign and malignant intraocular masses with high resolution, enabling reliable assessment of tumour morphology and extent. Subsequent histological examination confirmed MRI findings regarding origin, internal structure and extent of the masses.

Conclusion: This study demonstrates the potential of MR microscopy for imaging small anatomical structures. The findings correlate strongly with histology, making MRI of central importance in determining tumour morphology, extent and potential infiltration of surrounding structures. This work was performed *ex vivo*, but with wider availability, ultra-high-field MR microscopy is expected to become an essential tool not only in experimental studies but also for daily routine.

B-0809 10:39

Contrast-enhanced ultrasonography (CEUS) using early dynamic in microcirculation for localization of pathological parathyroid glands: first-line or complimentary diagnostic modality?

E.M. Jung, A. Agha; *Regensburg/DE*

Purpose: Contrast-enhanced ultrasonography (CEUS) represents a new diagnostic tool to localize pathological parathyroid glands. The aim of this study was to differentiate the capability of CEUS as first-line or complimentary modality for the detection of hyperfunctioning parathyroid glands.

Methods and Materials: 70 patients with pHPT were admitted to the University Hospital Regensburg between 8/2009 and 8/2011. Conventional and contrast-enhanced ultrasonography (CEUS) using a linear probe (6-9 MHz, LOGIQ E9/GE) was performed in all patients preoperatively. The sensitivity of CEUS was analyzed to determine its potential as first line or complimentary diagnostic procedure.

Results: Using CEUS 97 % of all pathological glands could be detected in the correct quadrant whereas conventional ultrasonography (70%) ($p < 0.001$) revealed less sensitivity. In all patients CEUS indicated a correct side localization of the hyperfunctioning parathyroid gland. The advantage of CEUS was the detection of the early dynamic on the capillary level immediately after contrast injection. Overall, CEUS permit minimally invasive video-assisted parathyroidectomy in 52 patients. 18 patients required conventional procedure due to concomitant goiter. All patients showed normal calcium and parathyroid hormone serum levels three months after surgery.

Conclusion: CEUS represents a highly sensitive diagnostic modality for localization of pathologic parathyroid glands in patients with pHPT. Nevertheless, it can only be recommended as first-line diagnostic procedure in specialized clinical centers with experienced investigators.

B-0810 10:48

Ventilation imaging of the paranasal sinuses using xenon-enhanced dual energy CT

T.R.C. Johnson¹, S.F. Thieme¹, W. Moeller², S. Becker¹, U. Schuschnig³, O. Eickelberg¹, A.D. Helck¹, M.F. Reiser¹; ¹Munich/DE, ²Neuherberg/DE, ³Gräfelfing/DE (*Thorsten.Johnson@med.uni-muenchen.de*)

Purpose: To show the feasibility of dual energy CT (DECT) and dynamic single energy CT for the visualisation of the ventilation of the paranasal sinuses.

Methods and Materials: For a dynamic quantification and visualisation of sinus ventilation, xenon gas was administered to a nasal cast with a laminar flow of 7 L/min. Repeated dynamic single energy CT measurements of the nasal cavity and the sinuses were performed. This procedure was repeated with pulsating xenon flow. The xenon-related enhancement level in the different compartments of the model was quantified and local xenon concentrations were determined. Additionally, using DECT, CT measurements were performed both during laminar and pulsating xenon administration. The xenon concentration in the different compartments was quantified directly based on the spectral information.

Results: Neither with single energy CT nor with DECT xenon-related enhancement could be detected in the paranasal sinuses during laminar air flow, while the xenon concentration in the nasal cavity reached 100%. Using pulsating air flow, the dynamic measurements showed a xenon wash-in and wash-out in the sinuses that followed a mono-exponential function with time constants of a few seconds. Accordingly, DECT images revealed xenon enhancement in the sinuses only after pulsating xenon administration.

Conclusion: DECT and dynamic xenon-enhanced CT imaging demonstrated the superiority of pulsating gas flow over laminar flows for the administration of gas or aerosols to the paranasal sinuses. DECT with xenon ventilation may represent an attractive option for therapy planning before medical aerosol treatment or surgery.

B-0811 10:57

Reducing the radiation dose for low-dose CT of the paranasal sinuses using organ-specific dose reduction (X-CARE) and iterative reconstruction: feasibility and image quality

S. Bulla, G. Pache, P. Blanke, F. Hasepess, M. Langer; *Freiburg im Breisgau/DE (stefan.bulla@uniklinik-freiburg.de)*

Purpose: To prospectively evaluate image quality of dose-reduced CT of the paranasal sinus using organ-specific dose reduction (X-CARE) and iterative reconstruction technique (IRIS).

Methods and Materials: In this prospective study, 100 patients (mean age: 47.9 \pm 18 years) underwent low-dose CT of the paranasal sinus (Siemens Definition, Forchheim, Germany) using iterative reconstruction technique with either standard settings (A: 120 kV, 48 mAs, bismuth eye-lens shield protection) or with tube voltage and tube current-time product lowering using organ-specific dose reduction (X-Care) in groups of 20 patients each (B: 120 kV, 48 mAs, C: 120 kV, 37 mAs, D: 100 kV, 74 mAs and E: 120 kV, 37 mAs). Objective image quality was evaluated and subjective image quality was independently assessed by two blinded observers using a semiquantitative five-point grading scale (1=poor, 5=excellent). Effective radiation dose was calculated. Mann-Whitney-U-test was used for statistical analysis.

Results: Best image quality was observed at 100 kV, 74 mAs (4.98), whereas scores for bismuth-shielded standard low-dose CT (A) and maximum dose reduction with X-CARE (E) provided nearly the same subjective image quality (4.78/4.73; $p=0.69$). Mean effective doses were 0.22 \pm 0.02mSv (A), 0.21 \pm 0.02mSv (B), 0.17 \pm 0.01mSv (C), 0.22 \pm 0.02mSv (D) and 0.11 \pm 0.01mSv resulting in a maximum dose reduction of 50% without loss in diagnostic image quality. Background noise was moderately higher in dose reduced areas when employing X-Care (perinasal 56.7 \pm 8.9 HU vs. periauricular 54.4 \pm 8.3 HU, $p=0.018$). Interobserver agreement was excellent (κ values 0.89).

Conclusion: As compared with bismuth-shielded CT, application of iterative reconstruction and organ-specific dose reduction allows for significant dose reduction of up to 50% for paranasal-sinus low-dose CT without loss in diagnostic image quality.

B-0812 11:06

Quantification of metal artefacts on cone beam computed tomography images

R. Pauwels¹, H. Bosmans¹, R. Jacobs¹, R. Bogaerts¹, H. Stamatakis², K. Tsiklakis², K. Horner³; ¹Leuven/BE, ²Athens/GR, ³Manchester/UK (*hilde.bosmans@scarlet.be*)

Purpose: To quantify metal artefacts obtained from a wide range of cone beam computed tomography (CBCT) devices and exposure protocols, to compare their tolerance to metals of different densities, and to provide insights regarding the possible implementation of metal artefact analysis into a QC protocol for CBCT.

Methods and Materials: A customised polymethyl methacrylate (PMMA) phantom, containing titanium and lead rods, was fabricated. It was scanned on 13 CBCT devices and 1 multi-slice computed tomography (MSCT) device, including high dose and low dose exposure protocols. Artefacts from the rods were assessed by two observers by measuring the standard deviation of voxel values in the vicinity of the rods, and normalising this value to the percentage of the theoretical maximum standard deviation.

Results: For CBCT datasets, artefact values ranged between 6.1% and 27.4% for titanium, and between 10.0% and 43.7% for lead. Most CBCT devices performed worse than MSCT for titanium artefacts, but all of them performed better for lead artefacts. In general, no clear improvement of metal artefacts was seen for high dose protocols, although certain devices showed some artefact reduction for large FOV or high mAs protocols.

Conclusion: Regions in the vicinity of the metal rods were moderately or gravely affected, particularly in the area between the rods. In practice, the CBCT user has very limited possibilities to reduce artefacts. Researchers and manufacturers need to combine their efforts in optimising exposure factors and implementing metal artefact reduction algorithms.

B-0813 11:15

A customised dental CT software for automatic correction of patient positioning error and detection of jaw midline

A. Lo Casto, G. Petrucci, P. Gallo, P. Purpura, F. Barreca, G. La Tona; *Palermo/IT (antoniolocasto@hotmail.com)*

Purpose: To develop a dental CT reformatting software for automatic correction of patient positioning error and detection of jaw midline for panoramic and cross-sectional reformations.

Methods and Materials: Axial CT images of the jaws from a volumetric acquisition were elaborated by a software developed in Matlab® language. To correct patient positioning errors, 2 rotations were assigned to the voxel coordinates in order to dispose the voxel relative to the sagittal plane parallel to the axial plane. This is accomplished using the characteristics of symmetry of the jaws with respect to the sagittal plane, allowing to determine the central inertial axes of the jaws, to identify the sagittal plane and determine the rotation angles to be assigned to the voxels. Once the positioning correction is done the optimal jaw midline is automatically traced, dividing in 3 parts an axial referral reformatted image to identify the midline equation by the ordinary least squares method. Then panoramic, reformatted along the central inertial axes of all cross-sectional images of the jaw, and cross-sectional images are automatically generated.

Results: The panoramic and cross-sectional reformatted images obtained were judged of good quality by 3 radiologists who compare the reformations obtained with those ones they obtained manually with a commercially available dental CT reformatting software.

Conclusion: An useful tool was developed to overcome patient positioning errors and cut time consuming procedure of manually tracing the jaw midline for panoramic and cross-sectional reformations.

B-0814 11:24

PET/CT and PET/MR image quality in the presence of dental implants

M.K. Werner¹, J. Wiegand¹, J. Kupferschlaeger¹, C. Lois², I. Bezrukov¹, H. Schmidt¹, C. Pfannenberg¹, N. Schwenzler¹, T. Beyer¹; ¹Tübingen/DE, ²Santiago de Compostela/ES (Matthias.Werner@med.uni-tuebingen.de)

Purpose: Combined PET/MR imaging has the potential to provide diagnostic image quality of anatomical regions adjacent to dental implants, which cause intense artefacts in PET/CT and often handicap proper diagnosis. We evaluated PET/MR for head and neck imaging using a dental phantom and patient images.

Methods and Materials: The phantom (filled with uniform background) contained real human teeth, some with dental implants, and one tooth gap, in a plastic carrier resembling the jaws. Phantom scans were performed on a clinical PET/CT (Biograph HiRez16) and integrated whole body PET/MR (Biograph mMR, Siemens). Images were reconstructed with and without CT- and MR (Ultrashort-Echo-Time UTE-) based attenuation correction (AC). Phantom data and five patient datasets from both PET/CT and PET/MR were evaluated visually and quantitatively (ROI-based analysis).

Results: MR-based attenuation correction using UTE sequences yielded significant inhomogeneities in MR images and, consequently, biased μ -maps with erroneous assignment of voxels to tissue electron densities. An enlarged photopenic area around the location of the implants was detectable in PET/MR, regardless of prior AC. There were no additional artefacts after AC even with hampered μ -maps. In contrast, severe streaking artefacts in CT images translated into non-uniform PET images in PET/CT after AC (only mild photopenia without AC). The analysis of PET/MR patient images revealed a significantly improved visualisation of structures such as the floor of the mouth and the submandibular regions usually affected by PET/CT artefacts.

Conclusion: Combined PET/MR head and neck imaging promises improved visibility and diagnosis for structures adjacent to dental implants compared to PET/CT.

B-0815 11:33

Magnetic resonance parameters and clinical scores in thyroid-associated orbitopathy: which one to trust for the extra-ocular muscles evaluation?

C. Godi¹, S. Bianchi Marzoli¹, G. Cammarata¹, A. Ambrosi¹, A. Falini¹, G. Scotti¹, L.S. Politi¹; Milan/IT (claudia.godi@collegiodimilano.it)

Purpose: 1) To find the magnetic resonance imaging (MRI) parameter best representing extra-ocular muscles dysfunction and disease activity in thyroid-associated orbitopathy (TAO); 2) to compare baseline and follow-up clinical and MRI measures of TAO patients.

Methods and Materials: 74 patients with TAO underwent MRI with T2-SPIR, post-gadolinium T1-SPIR (T1Gad) and DWI (b=0-700) sequences following ophthalmologic evaluation. According to the Clinical Activity Score (CAS), patients were divided into inactive (CAS<3) or active disease. A functional score (1=normal; 4=severe impairment) was assigned to every rectus muscle. Signal intensities and apparent diffusion coefficient (ADC), measured on all recti-muscles and normalised to thalamus (SIRs), were compared with those from 26 healthy subjects and with Patients' clinical scores. The data after intra-venous steroid treatment were available for 35/74 patients. Mann-Whitney, Wilcoxon Signed Rank Test and Spearman correlation were applied.

Results: Patients had T2, T1Gad, ADC SIRs higher than healthy subjects ($p < 0.001$), with significant signal decrease from active, inactive disease to healthy controls (except of ADC, not different between active/inactive groups). T2 and T1Gad SIRs, but not ADC, showed good correlation with the muscle dysfunction and CAS levels in the affected subjects. In addition, T2 and ADC SIRs of patients' normally functioning muscles were significantly higher than those of healthy controls. All SIRs significantly reduced in muscles that had clinical improvement after therapy; interestingly, even in the group of clinically stable-functioning muscles, a significant reduction in MRI parameters was detected over time.

Conclusion: MRI shows even clinically silent muscle involvement and could be more sensitive than ophthalmologic scores to changes in muscle involvement.

B-0816 11:42

Evaluation of a 32-channel versus a 12-channel head coil for MRI diagnostics in giant cell arteritis

P.A. Franke¹, M. Mark², S. Heinzelmann¹, P. Vaith¹, M. Langer¹, J. Geiger¹; ¹Freiburg/DE, ²Chicago, IL/US (philipp.franke@uniklinik-freiburg.de)

Purpose: To evaluate the diagnostic value of a 32-channel head coil in comparison with a 12-channel coil for evaluation of superficial cranial arteries' inflammation in patients with giant cell arteritis (GCA).

Methods and Materials: 55 patients with suspected GCA underwent 3 T MRI. 27 patients were examined with a 32-channel head coil first and a 12-channel head coil second, 28 patients in the other coil order. T1-weighted post-contrast images were evaluated by two blinded readers regarding image grading, artefact level and arteries' inflammation. SNR measurements were performed for both coils in the brainstem, the cerebellum and the galeal tissue. Inter-observer agreement was measured with the Cohen κ -test. Comparison between the two coils was calculated with Wilcoxon-rank test and t-test. Significant levels were $p < 0.01$.

Results: Both coils identified arteries' inflammation reliably, the inter-observer agreement was excellent ($\kappa = 0.89$ for 12-channel coil, $\kappa = 0.96$ for 32-channel coil). We obtained a statistically significant higher SNR ($p < 0.01$) with the 32-channel coil independently of the coil order. Image grading and artefact level were significantly higher with the 32-channel coil in either examination order. Regarding the image grading, the inter-observer variability was moderate ($\kappa = 0.5$) for the 12-channel coil and substantial ($\kappa = 0.63$) for the 32-channel coil.

Conclusion: The 32-channel head coil is superior to the 12-channel coil in depicting the superficial cranial arteries and, in general, image quality because of a higher SNR which is independent of coil order and delay of vessels' contrast enhancement. For GCA diagnosis, however, the 12-channel coil seems to be sufficient.

B-0817 11:51

Comparison of true real-time MR imaging with radial k-space sampling to videofluoroscopy exams in the follow-up evaluation of velopharyngeal dysfunction treated by surgery

M.C. Larson¹, M.J. Kerl¹, R.W. Bauer¹, T. Block², S. Zhang³, R. Hammerstingl¹, S. Zangos¹, T.J. Vogl¹, M.G. Mack¹; ¹Frankfurt am Main/DE, ²Erlangen/DE, ³Göttingen/DE (maycriss.larson@web.de)

Purpose: Velopharyngeal dysfunction can have many causes and is often treated by surgery. After surgery the resulting improved closure of the velopharyngeal port during speaking and swallowing is the manoeuvre of interest which is usually monitored by videofluoroscopy. The aim of our study was to show that rapid MRI protocols using equal temporal resolution to fluoroscopy (27 Hz) is as accurate as videofluoroscopy without exposure to x-rays.

Methods and Materials: With the approval of our institutional review board 26 patients (12 males, mean age 10.6 years) underwent 3.0 T MR functional imaging and videofluoroscopy exams. Our approach concerning the MRI scan protocol was to use a fast low-angle shot (FLASH) gradient-echo sequence with radial k-space sampling and sliding-window reconstruction (5 subframes) for achieving an image update rate of 27 Hz (27 frames per second). Sagittal views with 8 mm slabs were obtained during speech with a TE of 1.97 ms, a TR of 3.95 ms, a flip angle of 20°, and a matrix size of 128 pixels. The closure of the velopharyngeal port during speaking was compared by 2 radiologists in both diagnostic methods.

Results: The obtained real-time MR cinematics were equal to the videofluoroscopic images to evaluate the closure of the velopharyngeal port during speech to assess the postoperative results. Both radiologists rated the overall image quality in consensus as diagnostic.

Conclusion: Functional MRI is to consider equal to fluoroscopic imaging in the evaluation of the closure of the velopharyngeal port during postoperative follow-up exams without exposure to x-rays.

10:30 - 12:00

Room I/K

Abdominal Viscera

SS 1701

MRI of focal liver lesions

Moderators:

S. Bohata; Brno/CZ

P. Huppert; Darmstadt/DE

B-0818 10:30

Diffusion-weighted imaging of focal liver lesions: lesion size and image technique used have significant influence on diagnostic performance

P.A.T. Baltzer¹, J. Schelhorn², M. Benndorf¹, W.A. Kaiser¹, M. Dietzel¹; ¹Jena/DE, ²Weimar/DE (pascal.baltzer@med.uni-jena.de)

Purpose: To compare diagnostic performance of two commonly available diffusion-weighted imaging (DWI) techniques for detection and differentiation of focal liver lesions (FLL) suspect for metastases.

Methods and Materials: This retrospective cross-sectional study investigated consecutive patients with suspected liver metastases. All patients underwent Gd-EOB-DTPA-enhanced liver MRI including two different DWI techniques: a spectrally fat saturated breath hold EPI sequence (DWIbh, time of acquisition (TA): 0:23 min). and a free breathing spectrally fat saturated EPI sequence (DWIfb; TA: 5:28 min). DWI images were analysed by two readers in consensus. In identified lesions, signal intensities (SI) at lowest and highest b-values were measured using a user defined region of interest. Subsequently calculated apparent diffusion coefficient (ADC) values were analysed by receiver operating characteristics (ROC) analysis. The reference standard included histopathology and follow-up examinations.

Results: 37 of 45 included patients presented with 113 FLL (46 benign, 67 malignant). Of these, DWIfb detected significantly more malignant lesions compared to DWIbh (P=0.002). Lesion size ≤ 10 mm was significantly associated with FLL missed by DWIbh (P=0.018) but not with DWIfb (P=0.920). ROC analysis revealed a significantly higher area under the ROC curve for ADC values of DWIfb (0.801) compared to DWIbh (0.669, P < 0.0113).

Conclusion: Due to a higher lesion detection rate, DWIfb performed better than DWIbh. However, both DWI techniques did not depict all malignant FLL. This finding and overlaps between benign and malignant lesions limits the applicability of these techniques as a standalone diagnostic tool in imaging of hepatic FLL.

B-0819 10:39

Focal liver lesions in the right and left hepatic lobes on diffusion weighted MR imaging: is there a difference?

C. Schmid-Tannwald, F. Dahi, Y. Jiang, I. Sethi, A. Oto; Chicago, IL/US (christine.schmid-tannwald@med.uni-muenchen.de)

Purpose: To determine possible differences between ADC values of benign and malignant FLLs and normal liver parenchyma in the left vs. right hepatic lobes.

Methods and Materials: Thirty-six patients (16 males, 20 females, mean age: 56.8 years) with FLLs of the same aetiology in both the left and right lobes of the liver (13 patients with 26 benign FLLs and 23 patients with 46 malignant FLLs) who underwent 1.5 T MRI including DW-MRI (b values of 0 and 800 mm²/s) were included in this HIPAA-compliant and IRB-approved study. ADC values of normal liver parenchyma and FLLs in each hepatic lobe were calculated and compared using Student's t-test for paired data.

Results: ADC values of normal liver parenchyma, benign FLLs, and malignant FLLs were significantly higher (p < 0.001, p = 0.004, and p = 0.007, respectively) in the left hepatic lobe (1.74 x 10⁻³, 1.81 x 10⁻³, and 1.48 x 10⁻³ mm²/s, respectively) than in the right hepatic lobe (1.48 x 10⁻³, 1.54 x 10⁻³, and 1.24 x 10⁻³ mm²/s, respectively).

Conclusion: ADC values of benign and malignant FLLs and normal liver parenchyma are significantly higher in the left hepatic lobe compared with the right hepatic lobe. This is likely due to cardiac motion, and may limit the reliability and reproducibility of FLL ADC value estimates and the clinical usefulness of non-cardiac gated DW-MRI in characterising FLLs.

B-0820 10:48

Characterisation of focal liver lesion with quantitative techniques: comparison of apparent diffusion coefficient values and T2 relaxation times

A. Cieszanowski, A. Grodzicka, W. Szeszkowski, B. Kaczynski, E. Maj, B. Gornicka, M. Grodzicki, M. Krawczyk, O. Rowinski; Warsaw/PL (andrzej.cieszanowski@wum.edu.pl)

Purpose: To compare efficacy of two quantitative methods for discrimination between benign and malignant focal liver lesions (FLLs): apparent diffusion coefficient (ADC) values and T2 relaxation times.

Methods and Materials: Seventy-three patients with 215 confirmed FLLs including 115 benign ((42 cysts, 47 haemangiomas, 13 FNHs, 12 abscesses, 1 cystadenoma) and 100 malignant (65 metastases, 19 HCCs, 13 haemangioendotheliomas, 2 CCAs, 1 cystadenocarcinoma) underwent 1.5-T MRI with respiratory-triggered single-shot SE DWI (b=50,400,800) and dual-echo T2TSE (TR=3000 ms; TE1=84 ms; TE2=228 ms). ADC values and T2 relaxation times of FLLs were calculated and then optimal threshold values and accuracies for each method were assessed.

Results: Following, mean ADC values were obtained for all types of FLLs: cysts 2.52x10⁻³ mm²/s, haemangiomas 1.55x10⁻³ mm²/s, abscesses 1.5x10⁻³ mm²/s, FNHs 1.177x10⁻³ mm²/s, cystadenoma 3.3x10⁻³ mm²/s, metastases 1.05x10⁻³ mm²/s, HCCs 0.94x10⁻³ mm²/s, haemangioendotheliomas 1.30x10⁻³ mm²/s, CCAs 0.89x10⁻³ mm²/s, cystadenocarcinoma 2.93x10⁻³ mm²/s. With the use of optimal threshold value of 1.25 10⁻³ mm²/s sensitivity for diagnosis of benign lesion was 84.4%, specificity 79%, accuracy 81.9%, PPV 82.2%, NPV 81.4%. Following, mean T2 times were calculated: cysts 1029.1 ms, haemangiomas 124.33 ms, abscesses 406.84 ms, FNHs 2.79 ms, cystadenoma 458.98 ms, metastases 66.3 ms, HCCs 59.09 ms, haemangioendotheliomas 64.9 ms, CCAs 55.67 ms, cystadenocarcinoma 117.49 ms. At the threshold of 107 ms sensitivity for the diagnosis of benign lesion was 80.9%, specificity 99%, accuracy 89.3%, PPV 98.9%, NPV 81.8%.

Conclusion: The difference between sensitivities for the diagnosis of benign lesion was not statistically significant between both quantitative techniques, whereas the analysis of T2 relaxation times yielded significantly better specificity (99%) than ADC values (79%).

B-0821 10:57

Sensitivity and specificity of DWI-related parameters, apparent diffusion coefficient (ADC), diffusion coefficient (D) and perfusion fraction (PF), in distinguishing among benign and malignant focal liver lesions (Flls)

F. Regini¹, F. Pasquinelli¹, C. Nardi¹, L. Mazzoni¹, G. Belli², S. Colagrande¹; ¹Florence/IT, ²Arezzo/IT

Purpose: A workflow (acquisition and sampling methods, quantitative analysis) less site dependent as possible is proposed, to determine the combination of DWI parameters that maximises sensitivity and specificity in differentiating benign and malignant Flls.

Methods and Materials: 67 patients with known Fll (21 haemangiomas, 21 FNH, 25 metastasis) underwent free-breath MR-DWI (b-values: 0-1000, step of 200 s/mm²). Two ROIs were defined, including the Fll and a part of the surrounding parenchyma, respectively. ADC, PF and D were estimated in the Fll (ADCl, PFI, DI) and in the surrounding parenchyma; the ratios between Fll and parenchyma values were calculated (ADCr, PFr, Dr). T-test and ROC analysis were performed to identify the best set of DWI-related parameters in distinguishing benign and malignant Flls (significance threshold p=0.05).

Results: T-test showed significant differences between benign and malignant Flls values for ADCl, PFI, DI, ADCr, and Dr, more pronounced for ADCl (2048±760 vs 1307±467, p value < 0.0009) and ADCr (1.13±0.43 vs 0.79±0.26, p =0.001). Sensitivities with 95% confidence interval (CI) of ADCl and ADCr, corresponding to a specificity of 80%, were 79% (47%-95%, ADCl=1579 10-6-mm²/s) and 69% (20%-90%, ADCr=0.98).

Conclusion: Results in differentiating Flls with DWI are encouraging (very low p values), but the CIs of ADCl and ADCr sensitivity estimations are still too wide: a larger cohort of Flls should be evaluated, possibly with multicentric studies, given the low dependency on the site of the workflow proposed.

B-0822 11:06

Comparison of three methods of apparent diffusion coefficient evaluation in assessing solid focal liver lesions with diffusion-weighted imaging (DWI)

R. Girometti, S. Pullini, L. Cereser, M. Del Pin, G. Como, M. Bazzocchi, C. Zuiani; Udine/IT (rgirometti@sirm.org)

Purpose: To compare the performance in diagnosing solid focal liver lesions (FLLs) malignancy of the apparent diffusion coefficient (ADC) thresholding (ADC-T) method vs. two variants of the lesion-to-liver ADC ratio (ADC-R).

Methods and Materials: Examinations were performed on a 1.5 T system. Analysis was applied to 50 FLLs proven to be malignant and benign in 34 and 16 cases, respectively. Cysts and haemangiomas were excluded from the analysis. We estimated the positive-predictive value (PPV) and negative-predict value (NPV) for malignancy of ADC-T and two variants of the ADC-R, calculated without (ADC-R1) and with (ADC-R2) the inclusion of the parenchymal ADC standard deviation value, respectively. An ADC-R < 1 was considered as malignant. A receiver-operating-characteristic (ROC) analysis was carried out to establish a threshold for malignancy and to compare the area under the curve (AUC) values.

Results: The threshold for malignancy of ADC-T was $\leq 1.09 \times 10^{-3} \text{ mm}^2/\text{sec}$. The PPV and NPV were 87.5% (95%CI. 74.4-94.7) and 50.0% (95%CI. 35.7-64.3) for ADC-T vs. 75.0% (95%CI. 60.4-85.7) and 36.7% (95%CI. 23.9-51.5) for ADC-R1 vs. 90.9% (95%CI. 78.5-96.8) and 38.5% (95%CI. 25.4-53.3) for ADC-R2, respectively. Most false-negative FLLs were represented by hepatocellular carcinoma. ADC-T showed an AUC (0.71) significantly higher ($p < 0.05$) than ADC-R1 (0.56), but not than ADC-R2 (0.61).

Conclusion: The NPV for FLLs assessment were low, regardless of the ADC evaluation method, while the PPV was high, especially by comparing lesion and parenchymal ADCs with the ADC-R2 method. However, the use of an ADC threshold provided higher diagnostic performance in terms of AUC.

B-0823 11:15

Comparison of the apparent diffusion coefficient thresholding method vs. lesion-to-liver ADC ratio in discriminating solid benign and malignant focal liver lesions (FLLs)

S. Pullini, R. Girometti, M. Del Pin, L. Cereser, G. Como, M. Bazzocchi, C. Zuiani; Udine/IT (serepul@libero.it)

Purpose: A threshold-independent method to assess focal liver lesions (FLLs) is needed because of the apparent diffusion coefficient (ADC) variability linked to equipment-related factors. Our purpose was to compare the diagnostic performance of the ADC-thresholding (ADC-T) method vs. lesion-to-liver ADC ratio (ADC-R) in differentiating solid benign and malignant FLLs.

Methods and Materials: Thirty-two patients were evaluated on a 1.5 T system. Corresponding 50 FLLs included hepatocellular carcinoma (n=22), metastases (n=12), hepatocellular adenoma (n=6), focal nodular hyperplasia (n=6), dysplastic nodules (n=3) and atypical haemangioma (n=1). Cysts and typical haemangiomas were excluded from the analysis. Lesions ADC was used to establish a threshold for malignancy with a receiver-operating-characteristic (ROC) analysis (ADC-T) and to calculate the ADC-R as the ratio of lesion ADC and liver parenchyma ADC. An ADC-R < 1 was considered as malignant. By comparing ADC-T and ADC-R results with the standard of reference, we estimated the sensitivity, specificity, positive- and negative predictive values (PPV, NPV) for malignancy. ROC analysis was used to compare the area under the curve (AUC) of both methods.

Results: ADC threshold for malignancy was $1.09 \times 10^{-3} \text{ mm}^2/\text{sec}$. Sensitivity, specificity, PPV and NPV were 61.8% (95%CI. 46.9-74.8), 81.3% (95%CI. 67.2-90.4), 87.5% (95%CI. 74.4-94.7) and 50.0% (95%CI. 35.7-64.3) for ADC-T vs. 44.1% (95%CI. 30.4-58.8), 68.8% (95%CI. 53.9-80.7), 75.0% (95%CI. 60.4-85.7) and 36.7% (95%CI. 23.9-51.5) for ADC-R, respectively. ADC-T showed a significantly higher AUC (0.71) than ADC-R (0.56) ($p < 0.05$). Main source of false-negative cases was hepatocarcinoma.

Conclusion: ADC-R has not the capability to replace ADC-T in assessing FLLs.

B-0824 11:24

Sensitivity of visual assessment vs apparent diffusion coefficient quantification in differentiating malignant and solid benign focal liver lesions with diffusion-weighted imaging

R. Girometti, M. Del Pin, S. Pullini, L. Cereser, G. Como, M. Bazzocchi, C. Zuiani; Udine/IT (rgirometti@sirm.org)

Purpose: To compare the sensitivity of diffusion-weighted imaging (DWI) visual analysis (VA) vs. apparent diffusion coefficient quantification (ADC-Q) in diagnosing malignancy of solid focal liver lesions (FLLs).

Methods and Materials: Two radiologists in consensus retrospectively assessed as benign or malignant 50 FLLs on 32 patients examined on a 1.5 T. Two different methods were used in separate reading sessions: a) visual analysis of signal intensity on DWI images at $b=800 \text{ sec/mm}^2$ and ADC-map; b) lesion ADC measurement on the ADC-map. FLLs showing a signal intensity pattern of restricted diffusion were assessed as malignant. Lesions included metastases (n=12), hepatocarcinomas (HCC) (n=22), dysplastic nodules (n=3), focal nodular hyperplasias or hepatocellular adenomas (FNH/HA) (n=12), and atypical haemangioma (n=1) as confirmed by histology, TACE or 1-year follow-up. A receiver-operating characteristic (ROC) analysis was performed to determine the sensitivity and to establish an ADC threshold for malignancy.

Results: The overall sensitivity for malignancy was 32.4% (95%CI.20.2-47.2) for VA and 61.8% (95%CI. 46.9-74.8) for ADC-Q (threshold: $1.09 \times 10^{-3} \text{ mm}^2/\text{sec}$). According to stratified analysis, VA and ADC-Q showed a sensitivity of 9.1% (95%CI. 1.4-9.2) and 54.4% (95%CI. 32.2-75.5) for HCC, and 75.0% (95%CI. 54.8-88.6) and 66.7% (95%CI. 32.2-75.5) for metastases, respectively. A large overlap in ADC and VA features was found between benign and malignant FLLs.

Conclusion: Although the overall sensitivity is low, ADC-Q should be preferred to VA in assessing FLLs (especially HCC). However, VA is more sensitive than ADC-Q for metastases. The T2-shine-through phenomenon was hypothesised to cause this discrepancy by affecting the VA of HCC.

B-0825 11:33

Is white-blood (2-min)-phase in dynamic liver MRI using hepatobiliary contrast agent (Gd-EOB-DTPA) really useless compared with black-blood (20-min)-phase? A preliminary study

S. Kim, C. Lee, S. Choi, K. Kim, J. Choi, C. Park, J. Lee, Y. Park; Seoul/KP (chlee@korea.ac.kr)



Purpose: To determine the value of white-blood (2-min)-phase (WBP) for detection of hepatic metastasis by comparing with black-blood (20-min)-phase (BBP) of liver MRI using Gd-EOB-DTPA.

Methods and Materials: During March 2009 to February 2010, 35 patients (19 men, 16 women: age, 25~77 years) with extrahepatic malignant tumours and liver metastasis have undergone liver MRI. Three radiologists blind to primary tumour, number and location of liver lesions reviewed MRI of 35 patients twice with an interval of at least two weeks. Detection rate between WBP and BBP, and interobserver variability was also evaluated.

Results: Among 120 hepatic metastatic nodules, 33 nodules in 19 patients were confirmed pathologically, and other nodules were considered as metastasis after review of follow-up CT or MRI. Sensitivity of WBP and BBP was 91.7%, 91.7%, and 90.0%; and 92.5%, 95.0%, and 93.3% for three observers, respectively. There was no significant difference between detection rate of two phases in all of three observers ($P=1.00, 0.22, \text{ and } 0.29$). Average sensitivity was 91.1% in WBP, and 93.6% in BBP and no significant difference was found ($P=0.78$). Interobserver agreement was good or excellent ($\kappa=0.891, 0.700, \text{ and } 0.700$ in WBP, and 0.787, 0.848, and 0.937 in BBP). Most nodules missed in WBP appeared iso-intense to liver parenchyma. One nodule found only in WBP by all observers was small (4 mm) and adjacent to blood vessels.

Conclusion: WBP in liver MRI is never inferior to BBP in the detection of hepatic metastasis, and may be even superior for small nodules adjacent to blood vessels because of its white blood effect.

B-0826 11:42

How useful is a quantified analysis of hepatobiliary phase imaging for the characterisation of focal hepatic lesions? A comparison of dynamic gadoteric acid contrast-enhanced (Gd-EOB-DTPA) MRI versus apparent diffusion coefficient (ADC)

U.I. Attenberger¹, J. Morelli², H. Michaely¹, T. Rustemeier¹, S.O. Schönberg¹; ¹Mannheim/DE, ²Temple, TX/US (ulrike.attenberger@umm.de)

Purpose: To evaluate the value of quantified dynamic Gd-EOB-DTPA and apparent diffusion coefficient (ADC) imaging in the differentiation of hepatic lesions.

Methods and Materials: 57 consecutive patients referred for dynamic Gd-EOB-DTPA MR imaging of the liver were included in this institutional review board (IRB) approved retrospective study. A total of 57 lesions were evaluated. Of these, 21 haemangiomas, 18 hepatocellular carcinomas, 10 hepatic adenomas, and 8 cases of focal nodular hyperplasia were assessed. All patients underwent both Gd-EOB-DTPA scans (at arterial, portal-venous, venous, liver-specific phase at 15 and 25 min p.i.) and diffusion-weighted imaging (DWI, $b=0-400-800 \text{ s/mm}^2$) at 1.5 T with ADC calculation. The lesion contrast ratio (CR) was calculated as follows: $CR = (\text{signal intensity lesion post-contrast}) / (\text{signal intensity parenchyma post-contrast})$. ROC analyses were performed at all time points as well as for the ADC values.

The area under each ROC curve (AUC) was obtained. The ability of liver-specific phase imaging and ADC values to differentiate between the lesions was compared. **Results:** In both liver-specific phases, FNH CR was significantly higher than that of all other lesions ($p < 0.01$). Adenomas demonstrated significantly higher CR than haemangiomas ($p < 0.01$), but not HCC ($p = 0.1$). Haemangiomas demonstrated significantly lower CR ($p < 0.005$). ADC values allowed accurate differentiation between haemangiomas and all other lesions ($p < 0.05$), but the accuracy was in no case greater than that of liver-specific phase imaging. Neither adenomas and HCC nor FNH and HCC could be differentiated by ADC values **Conclusion:** Gd-EOB-DTPA outperforms ADC in the differentiation of hepatic lesions.

B-0827 11:51

Comparison of MR elastography and diffusion-weighted MR imaging for differentiating benign and malignant focal liver lesions

S.K. Venkatesh, G. Wang, K. Madhavan, A. Wee; *Singapore/SG* (sudhakar_k_venkatesh@nuhs.edu.sg)

Purpose: Comparative evaluation of MR elastography (MRE) and diffusion-weighted imaging (DWI) for differentiation of benign and malignant liver lesions. **Methods and Materials:** MRE and DWI were performed in 74 patients with a total of 109 lesions (benign-44, malignant-65). The lesions were hepatomas-57; haemangiomas-24, focal nodular hyperplasia-15, cholangiocarcinoma-7, cyst-5 and gallbladder carcinoma-1. DWI was performed with a free breathing technique (TR/TE 5000-6000/91 ms, matrix 160 x 160, 5 mm thickness, b=0.500). MRE was performed with modified gradient-echo sequence (TR/TE=100/27 ms, matrix 96 x 256, 5-10 mm thickness). The apparent diffusion coefficient (ADC) maps and elastograms were generated on workstation. Regions of interest (ROI) were placed on the focal lesions on the elastograms and ADC maps excluding large vessels, liver edges, and artefacts wherever possible. Mean stiffness values in kilopascals (kPa) and mean ADC values were derived for each lesion and tabulated. Receiver operating curve (ROC) analysis was performed to determine the area under curve (AUC) for accuracy of MRE and ADC for differentiation of benign and malignant lesions. **Results:** ROC analysis showed that AUC/sensitivity/specificity for MRE (cutoff, $> 4.54\text{kPa}$) and DWI (cutoff, $< 151 \times 10^{-3} \text{ mm}^2/\text{s}$) were 0.99/92.3%/95.5% ($p < 0.001$) and 0.85/78.5%/81.9% ($p < 0.001$), respectively, for differentiating malignant and benign lesions. The accuracy of MRE was significantly better than DWI ($p=0.008$). There was a negative correlation between stiffness and ADC values ($r=-0.48$, $p < 0.001$). Interestingly, a correlation between size and stiffness of lesions ($r=0.48$, $p < 0.0001$) was seen. **Conclusion:** Our study results show that MRE is more accurate than DWI for differentiation of benign and malignant focal liver lesions.

10:30 - 12:00

Room L/M

Cardiac

SS 1703

CT and MRI: risk stratification, prognosis and outcome

Moderators:
A. Bernardini; *Teramo/IT*
M. Pasowicz; *Krakow/PL*

B-0828 10:30

Gender differences in the prognostic value of cardiac CT angiography

J.W. Nance Jr¹, U. Schoepf², C.L. Schlett³, J. Barraza², F. Bamberg⁴;
¹McConnells, *SC/US*, ²Charleston, *SC/US*, ³Boston, *MA/US*,
⁴Munich/DE (Fabian.Bamberg@med.uni-muenchen.de)

Purpose: To determine gender differences in predictive value of cardiac CTA in patients presenting to the emergency department with acute chest pain but without acute coronary syndrome. **Methods and Materials:** Subjects with acute chest pain underwent cardiac CTA. The presence, extent (number of affected vessel segments), severity ($\geq 50\%$ or $< 50\%$ stenosis), and composition of atherosclerotic lesions (calcified, non-calcified, or mixed) were determined. Patients were followed for major adverse cardiac events (MACE: myocardial infarction, unstable angina, revascularisation, cardiac death). Hazard ratios were derived using univariate and multivariate cox regression (adjusting for risk factors) and stratified by gender if there was a statistically significant interaction ($p < 0.01$).

Results: Of 480 patients (65% female, mean age 55 ± 11 yrs), 70 (15%) incurred a MACE (3 cardiac deaths, 11 nonfatal MI's, 29 revascularisations, and 27 unstable angina) during median follow-up of 13 (IQR 9-18) months. On multivariate analysis, the presence and extent of obstructive disease predicted similar risks in males and females (all $p > 0.05$); however, presence (HR 49.3 vs 39.1) and extent (HR 133.9 vs 66.9) of any plaque was more hazardous in females ($p=0.03$). Plaque composition also portended variable risks ($p=0.03$), with extent of non-calcified plaque less hazardous in females and presence of exclusively calcified plaque more hazardous. **Conclusion:** The predictive value of cardiac CTA findings is gender-specific. Women with any atherosclerosis are at increased risk compared to men with equivalent disease; in addition, calcified plaque portends a higher risk in females while males are at increased risk with non-calcified lesions, indicating there may be gender differences in plaque progression/stability.

B-0829 10:39

Prognostic value of CT coronary angiography in subjects with suspected CAD: focus on severity of coronary artery disease and the presence of left main disease. Results from the CONFIRM Registry (coronary CT angiography evaluation for clinical outcomes: an international multicentre registry)

F. Cademartiri¹, E. Maffei¹, S. Seitun², J.K. Min³, H.-J. Chang⁴, D. Berman⁵, B. Chow⁶, S. Achenbach⁶, J. Hausleiter⁷; ¹Monastier di Treviso/IT, ²Genoa/IT, ³Los Angeles, *CA/US*, ⁴Seoul/KR, ⁵Ottawa, *ON/CA*, ⁶Giessen/DE, ⁷Munich/DE (filippocademartiri@gmail.com)

Purpose: To examine the association of all-cause mortality with the computed tomography coronary angiography (CCT) evidence of coronary artery disease (CAD), with focus on the presence and severity of left main (LM) disease. **Methods and Materials:** A total of 7700 patients (4120 men, age 57.5 ± 11.9 years) without known history of CAD from an International multicentre CCT registry (CONFIRM Registry) met the inclusion criteria (total database 27125 patients). 12 coronary artery segments analysis were performed. Cox proportional hazard models with adjustment for risk factors and after stratification according to LM disease were developed to predict outcome. **Results:** The prevalence of obstructive ($> 50\%$) CAD was 14.7%, whereas 33% of patients had non-obstructive CAD and 52.3% had normal coronary arteries. The presence of obstructive ($> 50\%$) and non-obstructive CAD in LM were, respectively, 0.9% ($n=69$) and 11% ($n=845$). A total of 95 deaths (1.2%) occurred after a mean follow-up of 29 ± 14 months. Multivariate analysis showed that CAD severity (HR:3.3; 95%CI:1.8-5.9, $p < 0.0001$) and the number of diseased segments (HR:1.13; 95%CI:1.05-1.22, $p=0.002$) were predictors of all-cause mortality with incremental prognostic value over Framingham risk and calcium score. Risk-adjusted survival showed that the presence of either non-obstructive or obstructive (cut-off $> 50\%$) LM disease was not associated with a significantly worse prognosis. However, after considering a cut-off value $> 70\%$ for obstructive CAD, patients with LM disease fared the worst ($p < 0.0001$). **Conclusion:** LM coronary artery disease presence and severity as detected by CCT seems to be poorly associated with worse prognosis.

B-0830 10:48

Prognostic value CT coronary angiography in subjects with suspected CAD: focus on severity of coronary artery disease and presenting symptoms. Results from the CONFIRM Registry (coronary CT angiography evaluation for clinical outcomes: an international multicentre registry)

E. Maffei¹, F. Cademartiri¹, S. Seitun², M. Hadamitzky³, P. Kaufmann⁴, K. Nasir⁵, L.J. Shaw⁶, G. Raff⁷, T. Villines⁸; ¹Monastier di Treviso/IT, ²Genoa/IT, ³Munich/DE, ⁴Zurich/CH, ⁵New Haven, *CT/US*, ⁶Atlanta, *GA/US*, ⁷Royal Oak, *MI/US*, ⁸Bethesda, *MD/US*

Purpose: The aim of this study was to examine the association of all-cause mortality with the computed tomography coronary angiography (CCT) evidence of coronary artery disease (CAD), with focus on the prognostic role of symptoms. **Methods and Materials:** A total of 7700 patients (4120 men, age 57.5 ± 11.9 years) without known history of CAD from the International CONFIRM CCT registry met the inclusion criteria. A 12 coronary artery segments analysis was performed. Survival analysis and Cox proportional hazard models with adjustment for risk factors according to presenting symptoms were developed to predict outcome. **Results:** 31.8% patients were asymptomatic, 48.5% had non-cardiac or atypical pain, 11.6% had typical pain and 8.1% had dyspnoea. The overall prevalence of obstructive ($> 50\%$) CAD was 14.7%, whereas 33% of patients had non-obstructive CAD and 52.3% had no CAD. A significant higher prevalence of obstructive CAD was observed among patients with typical pain with respect to other symptom

Monday

categories ($p < 0.001$). A total of 95/7700 deaths (1.2%) occurred after a mean follow-up of 29 ± 14 months. Multivariate analysis showed that CAD severity (HR:3.3; 95%CI:1.8-5.9 $p < 0.0001$) and the number of diseased segments ($p=0.002$) were predictors of all-cause mortality with incremental prognostic value over Framingham risk and calcium score. Risk-adjusted survival did not differ significantly between symptom categories; however, the worst prognosis was observed in patients with dyspnoea ($p=0.2$).

Conclusion: CCT is a valuable tool for risk stratification. Severity of CAD and typical chest pain appear to be the strongest predictors of mortality within symptoms groups.

B-0831 10:57

Coronary computed tomography angiography in the selection and evaluation of outlier patients: results from the international multicentre CONFIRM (coronary CT angiography evaluation for clinical outcomes: an international multicentre registry)

E. Maffei¹, F. Cademartiri¹, S. Seitun², J.K. Min³, M. Al-Mallah⁴, M.J. Budoff³, T.Q. Callister⁵, V. Cheng³, A. Delago⁶; ¹Monastier di Treviso/IT, ²Genoa/IT, ³Los Angeles, CA/US, ⁴Detroit, MI/US, ⁵Hendersonville, TN/US, ⁶Albany, NY/US (saraseitun@yahoo.com)

Purpose: To evaluate the presence and distribution of outlier patients with 64-slice coronary computed tomography angiography (CCT) in a large international multicentre registry (CONFIRM).

Methods and Materials: From a population of 27.125 consecutive patients (14.997 men, mean age 58 ± 13 years) underwent CCT, we analysed patients with suspected coronary artery disease (CAD) for whom the complete cardiac risk profile were available. We selected patient outliers in the fifth and sixth decades of life with the following criteria: ≥ 3 risk factors and absence of CAD, zero to one risk factors and ≥ 5 diseased coronary segments. Diabetes was excluded because of the different impact on CAD.

Results: The population consisted of 14.966 individuals with suspected CAD (8.379 men, age 57.7 ± 12.4 years). The prevalence of significant ($\geq 50\%$ stenosis) CAD was 19%. Patients with normal coronary arteries accounted for 46% of the total (3242 men, age 52.5 ± 11.9 years): 2.189 were in the fifth and 1.537 in the 6th decade (1.443 men, age 58.5 ± 5.6 years); of these, patients with ≥ 3 risk factors accounted for 3.7% of the total (men 186, women 370). Patients with ≥ 5 diseased coronary segments accounted for 15.4% of the total (1.623 men, age 65.2 ± 10.3 years): 502 were in the fifth and 919 in the sixth decade (men 1.062, women 359); of these, patients with zero to one risk factors accounted for 2.1% of the total (309/14.966; men 253, women 56).

Conclusion: CCT identifies outlier patients; this will enable dedicated trials aimed at characterising biomarkers and genomics of protective/antiprotective factors with respect to CAD.

B-0832 11:06

Increased left atrial or left atrial appendage volume: an independent risk factor for cardioembolic stroke in patients without atrial fibrillation? Cardiac computed tomography study

M. Taina, R. Vanninen, M. Hedman, P. Jakala, P. Sipola; Kuopio/FI (Mikko.Taina@kuh.fi)

Purpose: Intracardiac thrombus is an established high risk finding for cardioembolic stroke. We studied whether left atrium (LA) or left atrial appendage (LAA) volumes measured with cardiac computed tomography (cCT) provide additional information on risk factors in patients with suspected cardioembolic stroke without atrial fibrillation.

Methods and Materials: Consecutive patients ($n=138$, 94 males, mean age 60.2 years) with acute stroke of suspected cardioembolic origin underwent cCT. In cCT, LA and LAA volumes were calculated using Simpson's method. The control population constituted of 124 patients with low pre-test probability of coronary artery disease and $< 50\%$ coronary artery stenosis in cCT. A pairwise comparison was performed with 56 patients and 56 controls matched for age and gender.

Results: Twenty-two patients proved to have established cardiogenic risk factors (cardiac or aortic thrombus, LV aneurysm or tumour) for stroke. In pair-wise comparisons, both LA (83.8 ml vs. 61.6 ml; $p < 0.001$) and LAA (11.1 ml vs. 6.3 ml; $p < 0.001$) volumes were significantly larger in patients with suspected cardioembolic stroke than in control subjects. The upper limits (mean +2SD) for normal LA and LAA volumes were 97.5 ml and 10.8 ml in control subjects. By these criteria 76 (55.1%) stroke patients had enlarged LAA and 47 (34.0%) patients had enlarged LA. Sixty-one of the 76 patients (80.3%) with LAA dilatation had none of the previously described established risk factors for stroke.

Conclusion: LA and LAA volumes in patients with suspected cardiogenic stroke are significantly increased. Enlarged LA and/or LAA volume measured with cCT may constitute an independent risk factor for cardioembolic stroke.

B-0833 11:15

Frequent and widespread vascular abnormalities in human STAT3 deficiency detected by whole body MR and cardiac CT scan

A.A. Azarine, O. Chandesris, C. Picard, E. Mousseaux, P. Boutouyrie, Z. Mallat, A. Fischer; Paris/FR (arshid.azarine@egp.aphp.fr)

Purpose: To evaluate the prevalence and characteristics of cardio-vascular abnormalities in STAT3 deficiency, responsible for autosomal-dominant hyper-IgE syndrome.

Methods and Materials: We prospectively screened 21 adult STAT3-deficient patients (median age: 26 years; range 17 - 44) for vascular abnormalities. They were explored with whole body magnetic resonance imaging angiography, prospective coronary multislice computed tomography and echotracking-based imaging of the carotid arteries.

Results: Brain abnormalities (white matter hyperintensities, lacunar lesions suggestive of ischaemic infarcts, atrophy) were found in 95% of patients. Peripheral and cerebral artery abnormalities were reported in 84% of patients, whereas coronary artery abnormalities were detected in 50%. The most frequent vascular abnormalities were ectasia and aneurysm. The carotid intima-media thickness was markedly decreased, with a substantial increase in circumferential wall stress indicating the occurrence of hypotrophic arterial remodelling in this STAT3-deficient population.

Conclusion: Coronary and peripheral vascular abnormalities are highly prevalent in STAT3-deficient patients.

B-0834 11:24

Anomalous coronary artery originating from opposite coronary sinus frequently reveals multiple high risk anatomy features

M. Krupinski, T. Miszalski-Jamka, B. Laskowicz, B. Róg, R. Banys, M. Urbanczyk-Zawadzka, M. Kostkiewicz; Krakow/PL

Purpose: The aim of the study was to assess the prevalence of high risk anatomy features in patients with anomalous origin of coronary artery from opposite coronary sinus. High risk anatomy variants include interarterial course, narrowed slitlike orifice, acute angle of takeoff, intramural course and hypoplasia.

Methods and Materials: 3360 patients, who were scheduled for 64-slice or dual source computed tomography coronary angiography (CTCA) due to suspected obstructive coronary artery disease were screened for the anomalous origin of coronary artery from opposite coronary sinus. Patients were evaluated in terms of course of anomalous segment, presence of obstructive coronary artery disease and high risk anatomy.

Results: Anomalous origin of coronary artery at improper sinus of Valsalva was found in 33 (1%) patients (19 males, 14 females, mean age 62 ± 13 years). Eighteen patients presented circumflex artery originating at right coronary artery sinus (ALCx), 6 patients right coronary artery originating from left coronary sinus (ARCA) and 9 patients left coronary artery originating from right coronary sinus (ALCA). High risk anatomy was found in 21 (64%) of these subjects: interarterial course in 2, slitlike orifice in 11, acute angle of takeoff in 17, intramural course in 6 and hypoplasia in 6 individuals. Patients presenting obstructive coronary artery disease in anomalous segment had acute takeoff angle ($p=0.02$) and slitlike orifice ($p=0.001$) more frequently than others.

Conclusion: High risk anatomy is present in the majority of patients with anomalous origin of coronary artery at opposite coronary sinus and is often accompanied by obstructive coronary artery disease in the anomalous segment.

B-0835 11:33

Italian cardiac CT registry: preliminary results

F. Cademartiri¹, M. Francone², L. Patriarca³, I. Carbone², G. Ligabue⁴, L. Lovato⁵, E. Di Cesare³; ¹Monastier di Treviso/IT, ²Rome/IT, ³L'Aquila/IT, ⁴Modena/IT, ⁵Bologna/IT (filippocademartiri@gmail.com)

Purpose: Cardiac CT (CCT) is an imaging modality that is becoming a standard in clinical cardiology. We evaluated indications, safety, and impact on patient management of routine CCT in a multicentre national registry.

Methods and Materials: During a period of 6 months, 42 centres in Italy, we enrolled patients undergoing CCT for any indication.

Results: A total of 2,554 consecutive patients were enrolled. CCT was performed mainly with 64-slice CT scanners (1754; 68.7%) and with retrospective-ECG-gating (1764; 69%). In 95.2% (2432) of the cases CCT was performed with IV contrast material. In 59.7% (1524) of the cases pharmacological management of heart rate was performed (heart rate during CCT = 61 ± 10 bpm). Mean DLP was 753 ± 483

(10.5±6.8mSv). The most important indication for CCT was suspected CAD (1144; 44.8%) followed by evaluation of coronary stent (213; 8%). In 1167 (45.7%) patients there was a stress test prior to CCT. Most of the CCT were performed in outpatient settings (1890; 74%) and a minority in inpatients settings (527; 20.6%). We reported 23 (0.9%) clinical events (mainly related to contrast material) of which the majority (17/23; 74%) were mild and none was severe. In 44.8% (1146) of the cases CCT findings impacted patient management.

Conclusion: CCT is performed with different workloads and profile in participating centres. The most important indication for CCT is detection/exclusion of suspected CAD. CCT imaging is a safe procedure and its results have strong impact on patient management.

B-0836 11:42

Prevalence of MRI-detected unrecognised myocardial infarction and its relation to cerebral ischaemic lesions in both genders

C. Ebeling Barbier, R. Nylander, R. Themudo, H. Ahlstrom, L. Lind, E.-M. Larsson, T. Bjerner, L. Johansson; *Uppsala/SE (Charlotte.Ebeling_Barbier@radiol.uu.se)*

Purpose: To investigate the prevalence of unrecognised myocardial infarction (UMI) detected with magnetic resonance imaging (MRI) and whether it is related to cerebral ischaemic lesions on MRI in an elderly population-based cohort.

Methods and Materials: Cerebral MRI and cardiac late enhancement (LE) MRI were performed on 394 randomly selected 75-year-old subjects (188 women, 206 men). Images were assessed for cerebral ischaemic lesions and MI scars. Medical records were scrutinised. Subjects with MI scars, with or without a hospital diagnosis of MI were classified as RMI or UMI, respectively.

Results: UMIs were found in 120 subjects (30%) and RMIs in 21 (5%). The prevalence of UMIs (p=0.004) and RMIs (p=0.02) was greater in men than in women. Men with RMI displayed an increased prevalence of cortical and lacunar cerebral infarctions, whereas women with UMI more frequently had cortical cerebral infarctions (p=0.003).

Conclusion: MI scars are more frequent in men than in women at 75 years of age. The prevalence of RMI is related to that of cerebral infarctions. This might only apply to men, whereas women with UMI display an increased prevalence of cortical cerebral infarctions. Further studies are needed to clarify gender-specific morbidity correlations and risks.

B-0837 11:51

Age- and sex-related differences in outcome based on coronary computed tomography angiography; preliminary results from the Italian National PRORECAD Registry

E. Maffei¹, C. Martini¹, M. Midiri², S. Seitun³, M. Rengo⁴, V. Russo⁵, M. Francone⁶, F. Cademartiri¹; ¹Monastier di Treviso/IT, ²Palermo/IT, ³Genoa/IT, ⁴Latina/IT, ⁵Bologna/IT, ⁶Rome/IT

Purpose: To assess the prognostic value of 64-slice coronary computed tomography angiography (CCTA) in relation to age and gender.

Methods and Materials: We evaluated a cohort of 1.163 patients without known CAD who underwent a 64-slice CCTA. The primary endpoint was the occurrence of myocardial infarction, hospitalisation for unstable angina and death from all causes. Univariable and multivariable Cox proportional hazards models were developed to assess potential predictors.

Results: 546 patients had ≥65 years (262 male) and the remaining 617 had < 65 years (399 male). The prevalence of normal coronary arteries was 42% (n=489), whereas the prevalence of non-significant (1%-49% stenosis) and significant (≥50%) CAD was 29% (respectively, n=339 and n=335). At a mean follow-up of 831.8±310 days, 62 events had occurred (5.3%). In risk-adjusted analysis, obstructive (p < 0.0001) and nonobstructive (p=0.04) CAD conferred increased risk compared with patients without evident CAD. The number of diseased segments (p=0.006), and the number of segments (p=0.04) and vessels (p=0.003) with significant CAD were independent prognostic indicators. No significant differences in outcome were observed between male and female patients in each age categories (< or ≥65 years). Significant CAD was an independent predictor of events for both patients with < 65 years and ≥65 years and in male, but not for female patients. For female patients independent predictors were the number of vessels (p=0.01) and segments (p=0.01) with significant CAD.

Conclusion: Presence of significant CAD is associated with a poor prognosis. CCTA has the potential to improve risk stratification according to age and sex.

10:30 - 12:00

Room N/O

Emergency Radiology

SS 1717

Acute abdomen

Moderators:
J.M. Artigas; Zaragoza/ES
V. Vieth; Münster/DE

B-0838 10:30

Requesting radiological investigations - do junior doctors know their patients?

J. Cho, D.C. Bosanquet, N. Williams, D. Gower, K. GowerThomas, M.H. Lewis; *Llantrisant/UK (juncho2010@gmail.com)*

Purpose: To ascertain clinicians' knowledge of their patients when requesting radiological investigations, as required legally by government legislation "Ionising Radiation (Medical Exposure) Regulations 2000" (IRMER 2000), following the implementation of European Working Time Directive.

Methods and Materials: In our institution, all radiological investigation requests, excluding plain films, are required to be discussed with a consultant radiologist. All such requests received every Monday, following the weekend on-call, were collected prospectively over 8 weeks. Data included grade of requesting doctor, their specialty, types of modality requested, knowledge of their patient, addressograph signature confirming identity and appropriateness of investigation. There were no exclusion criteria. Statistical analysis using a two-tailed Fisher's exact test was performed for all data.

Results: 164 requests were received, the majority (61%) were made by Foundation Programme 1 (FP1) doctors and general medical specialties accounted for the highest proportion of requests (45%). Ultrasound scan was most frequently requested (47%), closely followed by computed tomography scans (42%). Almost a one-third (30%) of requests were made by doctors who had not seen the patient to be investigated, predominantly by FP1 doctors (p=0.003) and more frequently by general medical specialties (p=0.001). Signatures were absent in 20% of the addressographs and overall, 10% of requests were deemed inappropriate.

Conclusion: In almost a one-third of radiological requests, doctors have not seen patients to be investigated, most likely a result of shift working patterns. This does not fulfil the IRMER 2000 criteria and potentially exposes patients to unnecessary/inappropriate radiation.

B-0839 10:39

Acute pancreatitis: qualitative and quantitative evaluation using DW-MRI with parallel imaging technique and multiple b gradient factor values

P. Boraschi, F. Donati, R. Gigoni, F. Pacciardi, G. Gherarducci, C. Bartolozzi, F. Falaschi; *Pisa/IT (p.boraschi@do.med.unipi.it)*

Purpose: To determine the usefulness of qualitative and quantitative evaluation using diffusion-weighted MR imaging (DW-MRI) with parallel imaging technique and multiple b gradient factor values in patients with acute pancreatitis (AP).

Methods and Materials: A series of eighteen patients with a clinical diagnosis of AP underwent MR imaging at 1.5 T-device (Signa HDxt, GE Healthcare). After the acquisition of axial T1, T2w sequences, and coronal MRCP, DW-MRI was performed using an axial breath-hold single-shot spin-echo echo-planar (SE-EPI) sequence (parallel imaging factor, 3); the values of b factor were set at 0, 300, 500, 700, 1000s/mm². All DW images were blindly interpreted. Qualitative evaluation was performed by consensus reading of two reviewers that evaluated the presence or absence of AP and complications. Quantitative evaluation was performed by two other radiologists in conference that calculated mean ADC values for each patient using a b-value of 500s/mm².

Results: DWI could detect acute pancreatitis as persistent bright signal intensity at different b gradient factor values. The reviewers were able to differentiate inflammation from necrotic and haemorrhagic tissue and identified possible causes of AP (choledocholithiasis and pancreas divisum) on MR images in 9 cases. Furthermore, the mean pancreatic ADC value in the AP group was significantly lower than in the normal control group (p < 0.05).

Conclusion: DW-MRI with parallel imaging technique and multiple b gradient factor values can assess the manifestations of acute pancreatitis using no contrast material and has the potential of becoming a powerful tool for the evaluation and follow-up of these patients.

Monday

B-0840 10:48

Erect chest radiograph in the setting of the acute abdomen: essential tool or waste of resources and unnecessary

S. Alazzawi¹, W. Sprenger De Rover², G. Morris-Stiff³, M.H. Lewis⁴; ¹London/UK, ²Nottingham/UK, ³Cleveland, OH/US, ⁴Llantrisant/UK

Purpose: To review the quantity and quality of requests for emergency chest radiographs (CXR) in patients presenting with abdominal symptoms. The Royal College of Radiology (RCR) recommends a CXR with suspected viscous perforation to exclude air under the diaphragm but does not supersede a thorough clinical examination and should not be done routinely.

Methods and Materials: A retrospective analysis of all patients admitted to the Royal Glamorgan Hospital (UK) with acute abdominal pain was done for 12 months in 2004. Inclusion criteria: surgical admissions with abdominal pain, aged over 14. The requests and reports of the CXRs were evaluated and compared to nationally accepted guidelines produced by the RCR, to look at the appropriateness of the requests.

Results: 515 patients presented with acute abdominal pain. 65% had an erect CXR on admission. Of these 5% were clinically significant showing possible medical causes for the pain and altering management. Only 1% were surgically significant showing free gas under the diaphragm. It is arguable that 314 (94% of 334) had unnecessary CXRs which contributed no new information towards treating the patient. In fact if no old radiology records were available this could have been misleading as 53 (16% of 334) had abnormal findings of which none were new.

Conclusion: Vast room to reduce unnecessary CXRs being ordered. Stricter adherence to the RCR guidelines. Limiting the CXR requests in the presence of abdominal pain unless there are very clear indications or unless first reviewed by general surgery. By implementing guidelines and trusting clinical findings can reduce the financial, radiation and time costs.

B-0841 10:57

Prediction of bowel necrosis extent basing on the degree of bowel dilatation detected by CT reconstructions

M. Moschetta, A.A. Stabile Ianora, F. Lorusso, M. Telegrafo, A. Scardapane, G. Angelelli; Bari/IT (marco.moschetta@gmail.com)

Purpose: This study aims to correlate the degree of bowel dilatation detected by computed tomography (CT) and the extent of bowel necrosis in patients affected by mesenteric infarction.

Methods and Materials: Forty-seven patients affected by bowel infarction due to vascular obstruction were assessed by MDCT examination searching for pathognomonic signs of ischaemia and for the degree of bowel dilatation (subdivided into 4 groups: entire small bowel (SB); $\geq 50\%$ of SB; $< 50\%$ of SB; large bowel only). Two blinded radiologists evaluated multiplanar and 3D transparent wall reconstructions. Cohen's kappa statistics was used in order to assess inter-observer agreement. CT findings were then correlated with the mortality rate.

Results: Arterial vascular obstruction was found in 66% of cases and venous thrombosis in the remaining 34%. The overall mortality rate was 64%, with a 90% value for arterial forms and 10% in case of venous infarctions. The entire SB dilatation or a $\geq 50\%$ SB dilatation correlated with poor prognosis in all cases; a $< 50\%$ SB dilatation correlated with good prognosis in 87.5% of cases. A large bowel only dilatation did not show a significant prognostic value. Almost perfect agreement between the two readers was found ($k=0.84$).

Conclusion: Although bowel dilatation does not represent a specific sign of bowel ischaemia, when associated with other pathognomonic CT findings it can provide useful prognostic information, because a $\geq 50\%$ SB dilatation correlates with higher extent of bowel necrosis and with poor prognosis.

B-0842 11:06

Findings of sigmoid volvulus at CT

A. Fustier, M.-C. Jules, M. Zins; Paris/FR (annefustier@gmail.com)

Purpose: The objective of this study was to assess the features of sigmoid volvulus at CT.

Methods and Materials: This was a retrospective analysis of 18 cases of sigmoid volvulus in 13 men and four women, explored by CT within 24 hours before surgical (n=5) or endoscopic (n=13) treatment. In 14 cases, CT was associated with contrast enema. Two radiologists assessed in consensus the CT diagnostic signs and the topographical type of volvulus (organo-axial or mesenterico-axial). The clinical, radiological and evolutive features of the patients were correlated with the topographical type of volvulus (Fisher exact test and Mann-Whitney U test). The CT signs of severity were correlated with ischaemic findings in endoscopy or pathology (Fischer exact test).

Results: 72% (n=13) of sigmoid volvulus had an organo-axial configuration with one transition point. The whirl sign was the most frequent diagnostic sign, seen in 100% of the cases using multiplanar reconstructions and stack mode viewing. There was no significant difference between the mesenterico-axial and organo-axial form in terms of clinical severity, mean age, sigmoid loop opacification by enema, recidive rate after conservative treatment. Only parietal ischaemic signs (lack of enhancement, parietal thickening and pneumatosis intestinalis) were correlated with clinically proved ischaemia (p=0.04).

Conclusion: The most frequent configuration of sigmoid volvulus is the organo-axial type. The whirl sign is constantly found. Parietal ischaemic CT signs are associated with proved ischaemia.

B-0843 11:15

Abdominal CT in emergency: how to avoid the missed diagnosis of appendicitis

E. Pace, A. Filippone, R. Cianci, V. Bianco, G. Esposito, A. Cotroneo; Chieti/IT

Purpose: To establish the causes of missed diagnosis of appendicitis on multi-detector-row CT (MDCT).

Methods and Materials: We included 21 patients with proven appendicitis, for whom the diagnosis was missed on preoperative MDCT. A control group of 43 patients with a correct MDCT diagnosis of appendicitis was selected for comparison. Two experienced radiologists, who were aware of the diagnosis of appendicitis, re-evaluated MDCT images of the case and the control groups. The case and control group CT features were compared using the Fischer's exact test.

Results: Significant differences were found regarding the position of caecal pole (p < 0.0001), appendicolith (p=0.0001), appendiceal inflammatory changes (p=0.02), stranding of periappendiceal fat (p < 0.0001), fluid collection and/or gas bubbles (p=0.0001), small bowel obstruction or colonic diverticulosis (p < 0.0001), amount of pericaecal fat (p=0.0001), and clinical history (p=0.0001).

Conclusion: Knowledge of the causes of incorrect diagnosis of appendicitis allows to avoid false negative CT reports.

B-0844 11:24

Acute bowel ischaemia: analysis of diagnostic error by primarily overlooked findings at multidetector CT angiography

M. Firetto, A.A. Lemos, A. Marini, E. Contessini Avesani, P. Biondetti; Milan/IT (cristinaf@libero.it)

Purpose: To retrospectively evaluate the frequency and type of findings that were missed in the original report of multidetector CT angiography (MDCTA), in patients with suspected acute bowel ischaemia.

Methods and Materials: From January 2007 until March 2011, 35 patients (23 males, 12 females, mean age: 68.3 years) who underwent MDCTA (G.E. Light-Speed, Wisconsin, USA), and surgery, were included in the study. The reports of the initial CT were retrospectively compared to the discharge diagnosis and operation reports. Discrepant or missing findings were analysed for technical and/or diagnostic errors by reevaluating MDCTA images, and divided into (1) relevant, and (2) not relevant for the diagnosis.

Results: In 23/35 patients (67%), all findings were correctly diagnosed in the initial MDCTA. In the remaining 12/35 patients (33%) lesions that were not reported were present at surgery. In 10/12 (83%) patients, overlooked findings were relevant and subtle. In 2/12 (17%) patients with bowel dilatation and free fluid in whom the MDCTA overlooked findings were classified as non-relevant, bowel ischaemia was found at surgery. With retrospective image interpretation, almost all patients (83%) with bowel ischaemia were correctly identified, whereas the remaining patients (17%) with non-occlusive ischaemia at surgery showed non-relevant findings at MDCTA also at the retrospective analysis.

Conclusion: About 33% of relevant findings of bowel ischaemia were overlooked by the initial MDCTA interpretation; mostly were subtle findings. However, secondary reading of MDCTA scans revealed most of these findings and can serve to improve diagnostic performance.

B-0845 11:33

CT diagnosis of nature of bowel obstructions: morphological evaluation of the transitional point

M. Moschetta, T. Cosmo, F. Binetti, A. Scardapane, A.A. Stabile Ianora, G. Angelelli; Bari/IT (marco.moschetta@gmail.com)

Purpose: This study aims to evaluate the morphology of the transitional point in defining the nature of bowel obstructions.

Methods and Materials: CT examinations of 95 patients affected by severe bowel obstruction (23 of neoplastic origin; 72 of non-neoplastic origin) were retrospectively evaluated and the morphology of the transitional point was considered.

Results: The transitional point was detected in 89 patients (94%) and its morphology was concave in 64 cases (68%); linear in 5 (5%); convex in 20 (21%), as compared with the proximal loop. A concave morphology of the transitional point indicated a non-neoplastic condition, with sensitivity, specificity, positive predictive value (PPV), negative predictive value (NPV) and diagnostic accuracy values of 89%, 100%, 100%, 74% and 92%, respectively. A linear aspect presented almost the same incidence among neoplastic (60%) and non-neoplastic (40%) conditions. A convex aspect correlated with a neoplastic pathology with sensitivity, specificity, PPV, NPV and diagnostic accuracy values of 87%, 100%, 100%, 96% and 97%, respectively. **Conclusion:** In case of bowel obstruction, the detection of the transitional point indicates the site of obstruction, while its morphological evaluation can contribute to define the nature. A concave morphology indicates a non-neoplastic condition with a high probability; a convex morphology correlates with a neoplastic pathology, while a linearity is not significant.

B-0846 11:42

Abdominal paediatric trauma: radiologic findings and managing in solid viscera injury

J. Guibernau Lisitano¹, J.I. Ribo²; ¹Gerona/ES, ²Esplugues del Llobregat/ES

Purpose: The study aimed to investigate the method of management and diagnosis of paediatric blunt trauma with solid viscera injury, and determine the role of ultrasound and computed tomography image on it.

Methods and Materials: We undertook a 6-year retrospective audit of children admitted to the Sant Joan de Dèu Hospital, Barcelona, Spain, with a hospital-coded diagnosis which included hepatic, splenic, kidney, pancreatic and adrenal injury between 2005 and 2010. Data included patient demographics, results of any acute computed tomography and/or ultrasound imaging of the organs related, results of any surgical findings and outcome.

Results: 121 (67%) of the patients (n=179) were males and 58 (33%) females; the mean age was 11.5 years (0-18 range). Ultrasound was the first-line examination in 161 patients (91%) and computed tomography in 18 (9%). 45 patients (25%) went to have a computed tomography after ultrasound evaluation, (free fluid as the only ultrasound finding), most of them with questionable no impact in therapeutic decision. The radiologic findings included spleen injury in 43.9% of children, 26.3% kidney, 24.5% liver, 3.5% pancreas, and 2.6% adrenal glands. Conservative management was the choice in 172 cases, all they haemodynamically stable. 2 cases were undergoing acute intervention, both of the haemodynamically unstable. 17 cases had post-trauma complications such as urinoma and pancreatic pseudocysts.

Conclusion: Ultrasound is the first-line imaging in paediatric blunt abdominal trauma. The are no established guidelines to assess paediatric computed tomography, and most of the studies have questionable impact in therapeutic decision.

B-0847 11:51

CEUS usefulness in the characterisation of haemodynamic abnormalities associated with endoleak following endovascular treatment of abdominal aortic aneurysms

F. Pinto, C. Acampora, A. Pinto, R. Farina, S. Nicotra, L. Romano; Naples/IT (fpinto1906@libero.it)

Purpose: To reveal the usefulness of contrast-enhanced US (CEUS) in the detection and the characterisation of haemodynamic abnormalities associated with endoleak in patients previously submitted to endovascular treatment of abdominal aortic aneurysms (EVAR).

Methods and Materials: From January 2008 to July 2009, 88 consecutive patients (60 males and 28 females; mean age, 68.5 years old) underwent treatment of abdominal aortic aneurysms (EVAR). At diagnostic surveillance, both a multidetector computed tomography angiography (MDCTA) exam and a CEUS exam were performed in all the patients after 1 month, 12 months and 24 months, respectively.

Results: At MDCT, in 70/88 patients no complication was revealed, whereas in the remaining 18 cases the presence of a vascular complication was shown (a type II endoleak in 16/18 cases, and a type I endoleak in the remaining 2/18 cases). At CEUS, the diagnosis of a type II endoleak was obtained in all the 16 cases. Moreover, in 6/16 cases with type II endoleak, CEUS outperformed MDCTA findings by early depicting, since the first or the second control, an increase of the inflow/outflow ratio of the contrast agent in the sac followed by aneurysm diameter enlargement at the second or third follow-up exams.

Conclusion: CEUS represents a valid alternative tool in the surveillance of vascular complications in patients submitted to endovascular treatment of abdominal aortic aneurysms (EVAR). This method can be useful for better depicting endoleak features that may not be seen at MDCTA exam.

10:30 - 12:00

Room P

Physics in Radiology

SS 1713

Dose optimisation and assessment in CT

Moderators:
K. Bacher; Gent/BE
J. Geleijns; Leiden/NL

B-0848 10:30

Dose reduction with automated attenuation-based tube potential selection in patients with testicular cancer

R. Gnannt, A. Winklehner, D. Eberli, A. Knuth, H. Alkadhi; Zurich/CH (ralph.gnannt@usz.ch)

Purpose: To prospectively evaluate, in patients with testicular seminoma, the radiation dose saving potential and image quality of a novel algorithm which automatically selects tube potential based on the patients' attenuation from the topogram.

Methods and Materials: Forty consecutive patients (mean BMI 25.4±4.3 kg/m²) with testicular seminoma underwent contrast-enhanced thoraco-abdominal 64-section CT with automated-tube potential selection (CarekV); all had a foregoing thoraco-abdominal CT study at 120 kV (automated tube current modulation, 110ref.mAs). Two independent readers semi-qualitatively assessed image quality, two others measured objective image quality parameters. Dose information (CTDIvol) was noted.

Results: In the 120 kV scans, effective tube current was 134±30eff.mAs (range 54-235eff.mAs) for the chest and 204±59eff.mAs (range 88-444eff.mAs) for the abdomen. With CarekV, effective tube current significantly increased to 141±24eff.mAs (range 45-186eff.mAs) for chest and 304±82eff.mAs (range 47-444eff.mAs) for abdominal scans. Use of CarekV led to a tube potential reduction to 100 kV in 55 chest and abdominal and to 80 kV in 5 scans; tube potential increased to 140 kV in one patient (both chest and abdomen). Overall CTDIvol was significantly lower for CarekV (8.5±2.9 mGy; 12.8±5.0 mGy) compared to 120 kV (9.6±2.1 mGy; 14.7±4.0 mGy, p < 0.01). None of the datasets was of non-diagnostic image quality. With CarekV, signal-to-noise-ratio was significantly lower for both chest and abdomen (p < 0.05), contrast-to-noise ratio significantly higher in the abdomen (p < 0.05) and similar in the chest (p=0.152).

Conclusion: As compared to a protocol with fixed 120 kV, use of the automated tube potential selection algorithm for thoraco-abdominal CT yields comparable image quality at a reduced radiation dose by 13-15%.

B-0849 10:39

Screening CT colonography with 256-slice scanning: comparison of radiation risks and benefits

K. Perisnakis¹, I. Seimenis², A.E. Papadakis¹, A. Tzedakis¹, J. Damlakis¹; ¹Iraklion/GR, ²Alexandroupolis/GR (perisina@med.uoc.gr)

Purpose: To estimate and compare the cumulative lifetime attributable risk (LAR) of radiation-induced cancer for patients enrolled in a quinquennial screening CT colonography (CTC) program to corresponding nominal lifetime intrinsic risk (LIR) of cancer and the risk of not performing any screening test.

Methods and Materials: A Monte Carlo simulation software dedicated for CT dosimetry was used to determine absorbed doses to primarily exposed radiosensitive organs of 60 individuals subjected to screening CTC on a 256-slice CT scanner. Organ-specific and total LARs of cancer were determined. The cumulative LARs for 50-years-old individuals subjected to screening CTC every five years until the age of 80 years were estimated. The corresponding LIRs of cancer and the risk of not performing the screening test were estimated using the latest cancer statistics data.

Results: The cumulative LAR of radiation-induced cancer from repeated quinquennial screening CTC between the ages of 50 and 80 years was estimated to be 0.072%, with half of the radiation-induced cancers assumed to be fatal. The corresponding increase in the LIR of cancer incidence was increased by less than 0.2%. If not screened, 2.15% of the entire US population between 50 and 54 years are expected to develop colorectal cancer during their remaining life and die from it. The corresponding value for the screened population may drop down to 0.86%, at the expense of 0.036% additional theoretical radiation-induced cancer deaths.

Conclusion: Radiation risk does not constitute a barrier for accepting CTC as a first-line mass screening tool for colorectal cancer.

B-0850 10:48

Reduction of effective and organ dose to the eye lens in cerebral MDCT scans using iterative image reconstruction

J. Zizka, J. Jandura, T. Kvasnicka, J. Grepel; *Hradec Kralove/CZ*

Purpose: To compare effective radiation dose and dose to the eye lens in MDCT brain examinations utilising either standard filtered back projection (FBP) technique or iterative reconstruction in image space (IRIS).

Methods and Materials: Of 400 MDCT adult brain examinations, 200 were performed using standard FBP and 200 using IRIS. All scans were performed on Siemens Somatom Definition AS+ system with parameters: tube voltage 120 kV (FBP&IRIS); reference mAs value 300 (FBP) and 200 (IRIS), pitch factor 0.55, rotation time 1.0 sec. Doses were calculated from CT dose index (CTDIvol, mGy) and dose length product (DLP, mGy.cm) values utilising ImpACT software; the organ dose to the lens was derived from the actual tube current-time product value applied to the lens.

Results: The average CTDIvol was 33.29 in FBP and 22.41 in IRIS, respectively (32.7% decrease). The average DLP was 589.7 (FBP) and 396.2 (IRIS), respectively (32.8% decrease). The average effective scan dose was 1.47±0.26 mSv (FBP) and 0.98±0.15 mSv (IRIS), respectively (33.3% decrease). The average organ dose to the eye lens decreased from 40.0±3.3 mGy (FBP) to 26.6±2.0 mGy (IRIS, 33.5% decrease). No significant change in diagnostic image quality was noted between IRIS and standard FBP scans (p=0.17).

Conclusion: Iterative reconstruction of cerebral MDCT examinations enables reduction of the effective dose by at least one third. Corresponding reduction of the organ dose to the lens is of high importance due to both lens radiosensitivity and the fact that the lens is commonly exposed to the primary beam in MDCT examinations.

B-0851 10:57

Ultra-low radiation dose 64-row MDCT: multicentre clinical trial to assess the diagnostic feasibility of model-based iterative reconstruction (ultra-low Veo study)

R.C. Nelson¹, A.K. Hara², W.D. Foley³, E.K. Paulson¹, D. Sahani⁴, D.B. Husarik⁵; ¹Durham, NC/US, ²Phoenix, AZ/US, ³Milwaukee, WI/US, ⁴Boston, MA/US, ⁵Zurich/CH

Purpose: CT contribution to the collective radiation dose remains a dominant topic. Our purpose is to confirm the effectiveness of a full model-based iterative reconstruction (Veo) technique designed to significantly reduce radiation dose and improve image quality in patients.

Methods and Materials: The pilot study includes 120 patients from three institutions imaged in one of four anatomic arms: (1) anatomy/pathology in the posterior fossa, (2) lung cancer staging/restaging, (3) detection/characterisation of focal liver lesions, or (4) urolithiasis. For each patient, two datasets are acquired on the Discovery CT750 HD (GE Healthcare, trial sponsor): (1) standard-of-care radiation dose and (2) ultra-low radiation dose. Both acquisitions are reconstructed with filtered back projection (FBP), adaptive statistical iterative reconstruction (ASiR), and Veo. Two readers independently assess clinical value, lesion characterisation, diagnostic confidence and recommended treatment for each dataset. Quantitative measurements include CNR and noise. Initial pilot study results will be presented and will confirm design for the 800-patient global multi-centre trial to follow.

Results: Prior phantom results (quantitative and observer) indicate the ability to maintain routine diagnostic image quality at doses as low as 1-3 mSv using this new reconstruction technique. Initial study results demonstrate translation of these findings into the clinical population for each anatomic arm evaluated.

Conclusion: The pilot study demonstrates diagnostic image quality in patient datasets reconstructed with Veo using radiation doses down to 1-3 mSv. These results will be used as objective evidence for the design of a comprehensive global multi-centre trial to encourage appropriate introduction into clinical practice.

B-0852 11:06

Feasibility of 50% dose reduction in whole body lymphoma staging CT using iterative reconstruction

T. Henzler, H. Jafarov, M. Meyer, J. Shi, S.A. Klein, P. Apfalter, S.O. Schoenberg, C. Fink; *Mannheim/DE (thomas.henzler@medma.uni-heidelberg.de)*

Purpose: Patients with lymphoma are at higher risk of secondary malignancies due to radiotherapy and frequent follow-up-staging-CT. We aimed to systematically investigate quantitative and subjective image quality of full-dose-standard (FDS), full-dose-iterative (FDI) and half-dose-iterative (HDI) reconstructions in patients with lymphoma.

Methods and Materials: To acquire full-dose and half-dose CT simultaneously, contrast-enhanced whole body staging-CT was performed with a DSCT, operating

both tubes at 120 kV with the total mAs was equally distributed on both tubes. CTDI and dose length product of the scan were equal to the standard institutional protocol. For FDS and FDI reconstructions data of both tubes were used, whereas HDI reconstructions were calculated using only data from tube A of the DSCT-system (50% of total mAs). Quantitative image quality was assessed by measuring image noise in different tissues of the neck, thorax and abdomen. Overall diagnostic image quality was assessed by two radiologists using a 5-point Likert scale. Differences between reconstruction techniques were compared.

Results: Image noise significantly decreased in all anatomic regions when FDI and HDI (-33%; -20%, respectively) was compared to FDS reconstructions (all p < 0.05). Image quality of FDI (median 5) and HDI (median 4) was rated significantly higher when compared to FDS (median 3) reconstructions (both p < 0.05). FDI was rated as the best in 78%, HDI second best in 75% and FDS as the third best reconstruction technique in 94% regarding image quality (all p < 0.05).

Conclusion: Subjective and objective image quality of FDI and HDI appear to be superior to FDS reconstruction, thus enabling dose reduction in whole body lymphoma staging-CT.

B-0853 11:15

CT evaluation of coronary artery stents: potential for radiation dose reduction using iterative image reconstruction techniques

H. Ebersberger¹, F. Tricarico¹, P. Apfalter¹, R. Vliegenthart², T. Allmendinger³, G. Rowe¹, A. Leber⁴, E. Hoffmann⁴, U. Schoepf¹; ¹Charleston, SC/US, ²Groningen/NL, ³Forchheim/DE, ⁴Munich/DE (ebersberger@gmx.net)

Purpose: Patients with coronary stents require frequent follow-up, so that low radiation dose techniques are desirable. We compared diagnostic image quality for stent evaluation in full-radiation dose CT studies reconstructed with traditional filtered-back-projection (FBP) with studies at half the radiation dose using sinogram-affirmed-iterative-reconstruction (SAFIRE).

Methods and Materials: 15 implanted coronary stents were evaluated by 128-slice dual source CT (DSCT). Image data were reconstructed at full-dose with FBP and at half-dose with SAFIRE using corresponding kernels. Half-dose data were reconstructed using projection data from only one DSCT tube-detector configuration. In-stent signal-to-noise-ratio (SNR) was measured and image quality was graded on a five-point scale (5=excellent, 1=non-diagnostic). To objectively assess the effect on beam hardening artefacts, volumes of stents were measured using dedicated volume analysis software. Stent-lumen-attenuation-increase-ratio (SAIR) was calculated [(in-stent attenuation-vessel attenuation)/in-stent attenuation]. Statistical analysis used paired t- and chi-square testing.

Results: Mean full effective dose was 4.4±2.5mSv. Significant in-stent stenoses were present in 2 stents, which were correctly identified with both reconstruction methods compared with coronary angiography. In-stent SNR was higher for half-dose SAFIRE compared with FBP (15.3±9.1 vs. 11.2±6.0; p < 0.01) while the SAIR was considerably lower (11.9% vs. 29.3%; p < 0.01). In addition, image quality was found to be significantly (p < 0.01) better when iterative reconstruction was applied (4.1±0.8 vs. 3.8±0.8). Stent volumes tended to be lower when reconstructed with half-dose SAFIRE (170.1±110.1 mm³ vs. 183.7±115.9 mm³; p=0.11).

Conclusion: Despite using half-dose image data, iterative reconstruction improves evaluation of coronary stents by reducing image noise and beam-hardening artefacts and improving visualisation of the in-stent lumen.

B-0854 11:24

DNA damage repair kinetics from ionising radiation in the range of doses experienced in CT studies

S.R. Saxon, M. Khatonabadi, M.F. McNitt-Gray, S.G. Ruehm, K.S. Iwamoto; *Los Angeles, CA/US (s.robin.saxon@gmail.com)*

Purpose: To quantify the kinetics of the cellular response to a range of low, CT-relevant doses of ionising radiation (IR) in mouse tumour infiltrating lymphocytes (Til) in vitro.

Methods and Materials: Til cells were placed in the centre chamber of the CDTI head phantom and irradiated with 10 mGy, 20 mGy, 40 mGy, 80 mGy or 170 mGy (reported CTDIvol values) using a SIEMENS Somatom Sensation 64 CT scanner. Cellular kinetics of DNA damage and response were quantified by flow cytometric quantitation of gammaH2 AX foci at three time points (30 min, 1hr and 2 hrs post-IR at room temperature). A non-irradiated control was included for each sample. Collected flow cytometry data, corrected for debris and dead cells using side and forward scatter gating, were analysed with CellQuest Pro Software. Fluorescence histograms were generated and the median fluorescence of each treatment sample was compared to its respective control and reported.

Results: In cells exposed to 80 mGy or 170 mGy gammaH2 AX signal reached a peak value at approximately 1hr and then began to drop. In contrast, cells exposed to 10 mGy, 20 mGy and 40 mGy showed different repair kinetic patterns.

Conclusion: Our results suggest DNA damage may be repaired by different mechanisms in a dose-dependent manner. This altered kinetic response could have marked biological effects for current radio-diagnostic procedures. Our study, therefore, underscores the importance of understanding the different repair mechanisms at different dose regions in order to accurately assess risk estimates and biological dose.

B-0855 11:33

Organ dose correlation with an attenuation-based patient size metric

M. *Khatonabadi*¹, A. Turner², D. Zhang¹, G. Chu¹, A. Banola¹, D. Oria¹, J. DeMarco¹, C. Cagnon¹, M. McNitt-Gray¹; ¹Los Angeles, CA/US, ²Tucson, AZ/US (*mkhatonabadi@mednet.ucla.edu*)

Purpose: Previous work (including AAPM Task Group 204) have described the effect of size on patient radiation dose from CT exams. The purpose of this study was to investigate the relationship between organ dose from CT with different patient size metrics, including one based on patient attenuation.

Methods and Materials: Using Monte Carlo simulation methods, patient radiation dose from fixed and tube current modulated scans were estimated and normalised by scanner-reported CTDIvol for 39 adult male and female patient models. These models were generated from tube current modulated abdomen/pelvis CT scans. Doses were tallied in three organs: liver, kidneys and spleen. For each patient, several size metrics were calculated, including: the square root of the image attenuation area, perimeter, and maximum lateral width and A-P thickness. The correlation between normalised organ dose and each of these metrics was calculated and compared.

Results: For fixed tube current scans, the correlation with organ dose was greatest for image attenuation and perimeter (R2 = 0.75). However, for tube current modulated scans, image attenuation showed the best correlation with dose (R2=0.65), whereas perimeter, A-P thickness, and lateral width produced lower correlations (R2 of 0.4, 0.2 and 0.15, respectively).

Conclusion: An attenuation-based patient size metric can be used to estimate dose from both fixed and tube current modulated scans. It is a better patient size indicator for tube current modulated scans than perimeter due to its ability to take into account the attenuation of patients, which is also used in tube current modulating algorithms.

B-0856 11:42



The effect of CT dose reduction on performance of a diagnostic task

D. Zhang, M. Khatonabadi, C.M. Jude, E. Zaragoza, H. Kim, M. Lee, D. Andrews-Tang, C. Poon, M. Douek, M. Patel, L. Doepke, S. McNitt-Gray, C. Cagnon, J. DeMarco, M. McNitt-Gray; Los Angeles, CA/US (*skintchenzhang@gmail.com*)

Purpose: Several studies have investigated tradeoffs between radiation dose and image quality (noise) in CT imaging. This study took the analysis a step further by investigating the tradeoffs between radiation dose and diagnostic performance in a clinical task (diagnosis of appendicitis).

Methods and Materials: This preliminary study was IRB approved and utilised data from 20 patients who underwent clinical CT exams for indications of appendicitis. Medical record review established true diagnosis of appendicitis, with 10 positives and 10 negatives. Original (100%) and simulated reduced dose levels (70%, 50%, 30%, 20% of original) were created with a validated software tool using raw projection data from each scan. An observer study was performed with 5 radiologists reviewing each case at each dose level in random order over several sessions. Readers assessed image quality and provided confidence in their diagnosis of appendicitis, each on a 5-point scale. ROC curves were generated for each dose level. AUC (area under curve) was calculated for each dose level.

Results: Interim results of the study showed that the AUC for each of the dose levels was 0.996, 0.982, 0.970, 0.965, and 0.963 for dose levels at 100%, 70%, 50%, 30% and 20%, respectively. Only 2 out of 480 readings received "unacceptable" image quality ratings (1 patient at 20% dose level).

Conclusion: This preliminary study demonstrated tradeoffs between radiation dose and diagnostic performance and indicated that: (a) even small dose reductions may affect diagnostic performance slightly and (b) large dose reductions may still allow acceptable performance levels.

B-0857 11:51

Radiation dose reduction with model-based iterative reconstruction: evaluation in different patient sizes and tube voltage settings. A phantom study

D.B. *Husarik*¹, D. Marin², S. Richard², E. Samei², T.A. Jaffe², T.A. Jaffe², M.R. Bashir², R.C. Nelson²; ¹Zurich/CH, ²Durham, NC/US (*danielahusarik@yahoo.com*)

Purpose: To compare image quality of abdominal CT scans at different radiation dose levels reconstructed from the same raw datasets with a standard convolution filtered back projection (FBP) and a model-based iterative reconstruction algorithm (MBIR).

Methods and Materials: An anthropomorphic phantom in three sizes was used with a custom built liver insert simulating late hepatic arterial enhancement and containing hypervascular liver lesions of various sizes. Imaging was performed on a 64-section multidetector-row CT (MDCT) scanner (Discovery CT750 HD, GE Healthcare, Waukesha, WI) at 3 different tube voltages for each patient size, and 5 incrementally decreasing tube-current-time products for each tube voltage. Quantitative analysis consisted of contrast-to-noise ratio (CNR) calculations and image noise assessment. Qualitative image analysis was performed by three independent radiologists rating subjective image quality and lesion conspicuity.

Results: CNR on MBIR images was significantly higher and mean image noise was significantly lower than on FBP images in all patient sizes, at all tube voltage settings, and radiation dose levels (P <.05). Overall image quality and lesion conspicuity were rated higher for MBIR images compared to FBP images at all radiation dose levels. Image quality and lesion conspicuity on 25-50% dose MBIR images were rated equal to full dose FBP images.

Conclusion: Compared to FBP, MBIR allows for a 50 to 75% reduction in radiation dose for abdominal CT imaging without compromising quantitative and qualitative image quality.

10:30 - 12:00

Room Q

Paediatric

SS 1712

Body and bones

Moderators:
A.D. Calder; London/UK
H.-J. Mentzel; Jena/DE

B-0858 10:30

Additional value of FDG-PET in partial responders on CT: data deriving from a multicentric Italian paediatric HD study

E. *Lopci*¹, R. Burnelli², A. Cistaro³, A. Piccardo⁴, L. Guerra⁵, A. Chiti¹, P. Zucchetta⁶, S. Fanti⁷; ¹Rozzano/IT, ²Ferrara/IT, ³Torino/IT, ⁴Genoa/IT, ⁵Monza/IT, ⁶Padua/IT, ⁷Bologna/IT (*egesta.lopci@gmail.com*)

Purpose: In this study, we present our findings in paediatric Hodgkin's disease (HD) patients evaluated with the aim to establish FDG-PET role in the assessment of patients showing a partial response (PR) on CT both at interim and end-treatment evaluation.

Methods and Materials: We analysed 102 paediatric HD patients (mean age 13 years) underwent FDG-PET investigations at interim or after completion of therapy, and showing a PR on CT. PET data were reported as negative (no evidence of disease/no pathologic uptake) or positive for disease. All results were statistically analysed with respect to PFS, on a mean follow-up of 26.5 months.

Results: As expected, CT response, both at interim and at the end-treatment evaluation did not result significantly correlated with PFS (p=0.8991 and 0.1969, respectively). On the other hand, in this same pool of patients, also FDG-PET at interim did not result statistically significant (p=0.4727), whereas when performed at the end of treatment, PET data were highly predictive and resulted significantly correlated with PFS (p=0.0028). On the univariate analysis, data were confirmed as so, demonstrating that only end-treatment PET was predictive (p=0.0168), whereas on the multivariate analysis none of the imaging techniques was significant.

Conclusion: These results suggest that the most reliable value in differentiating real response in paediatric HD patients presenting with a PR on CT is FDG-PET performed after completion of therapy.

Monday

B-0859 10:39

Voiding urosonography with a second generation contrast agent as a first step study for the diagnosis and grading of vesicoureteric reflux in children

A. Ntoulia¹, F. Papadopoulou¹, F. Papachristou², E. Siomou¹, K. Darge³;
¹Ioannina/GR, ²Thessaloniki/GR, ³Philadelphia, PA/US

Purpose: To assess the efficacy of voiding urosonography (VUS) with a second generation contrast agent (CA) as a first step study for the diagnosis and grading of vesicoureteric reflux (VUR) in children.

Methods and Materials: Two hundred and ten consecutive children (86 boys, 124 girls, mean age 33.4 months) with 421 kidney-ureter-units (KUU) were evaluated with VUS to rule out (n=180) or follow-up (n=30) VUR. In all children VUS was performed with a contrast-specific-harmonic-imaging-mode and 1 ml of a second generation CA (SonoVue®, Bracco, Milan), according to ESPR working group recommendations. The VUS was recorded on digital clips and read twice by two blinded radiologists. The diagnosis in discordant cases was reached by consensus. The intraobserver and interobserver reproducibility was calculated by kappa coefficient.

Results: VUR was diagnosed in 178 KUU (42%) from 87 (41%) patients (34/84 boys and 53/126 girls). The rate of reflux was not significantly correlated with the sex, age, clinical indications and the presence or side of dilated pelvis. VUR was significantly more common in duplex than in single kidneys ($p < 0.001$). The intraobserver and interobserver reproducibility was excellent for the detection of VUR ($k > 0.85$) and moderate to excellent for the grading of VUR ($k = 0.75-0.84$).

Conclusion: VUS with a second generation CA is an efficient first step study for the diagnosis and grading of VUR in children and it can reliably be used as an alternative radiation-free imaging method for this purpose.

B-0860 10:48

Contrast-enhanced voiding urosonography for diagnosis of vesicoureteric reflux in comparison to conventional methods: a meta-analysis

F. Papadopoulou¹, E. Evangelou¹, M. Riccabona², A. Ntoulia¹, K. Darge³;
¹Ioannina/GR, ²Graz/AT, ³Philadelphia, PA/US (fpapadopoulou@hotmail.com)

Purpose: To assess the diagnostic performance of voiding urosonography (VUS) in vesicoureteral reflux (VUR) and urethral pathology detection compared to conventional methods published in medical literature.

Methods and Materials: Medline was searched by two independent observers for all possible articles published up to May 2011 on VUS in neonates-infants-children compared to VUCG or DRNC and performed with Levovist or SonoVue. The bivariate hierarchical model was chosen for statistical analysis. Individual study results were presented graphically by plotting estimates of sensitivity and specificity in receiver operating characteristics (ROC) and extended summary ROC. The 95% confidence intervals (CI) and the positive (LR+) and negative (LR-) likelihood ratios were calculated.

Results: 127 articles were found concerning "ultrasound contrast VUR". 30 comparative studies fulfilled the inclusion criteria: 26 VUS-studies in comparison with VUCG and 4 with DRNC, 26 performed with Levovist and 4 with SonoVue. Totally 2549 children with 5078 pelvo-ureteral-units were included for analysis. VUS compared to VUCG and DRNC had sensitivity 90% (CI: 85-93), specificity 92% (CI: 89-94), LR+ 11.7, LR- 0.11. VUS performance was better compared to DRNC than to VUCG (sensitivity 94%, specificity 95% versus 90%, 92%, respectively) as well as with SonoVue compared to Levovist (sensitivity 92%, specificity 91% versus 89%, 92.5%, respectively). Regarding urethral pathology detection 880 patients (682 boys) were included. Excellent imaging of urethral anatomy was reported in > 97% of patients.

Conclusion: From the published data there is convincing evidence for the diagnostic performance of VUS in VUR detection compared to VUCG and DRNC. For urethral pathology detection, although results are very promising, more comparative studies are needed.

B-0861 10:57

Diagnostic accuracy and clinical significance of magnetic resonance enterography of the small intestine in comparison with ileocolonoscopy in paediatric inflammatory bowel disease

U. Fagerberg¹, M.R. Torkzad², L. Blomqvist³, H. Hildebrand³, P. Hellström², U. Ullberg³; ¹Västerås/SE, ²Uppsala/SE, ³Stockholm/SE (michael.torkzad@radiol.uu.se)

Purpose: To study the diagnostic accuracy of magnetic resonance enterography (MRE) in paediatric inflammatory bowel disease (IBD) in diagnosing intestinal

inflammation and to evaluate the clinical significance of the MRE results on the management of paediatric IBD patients.

Methods and Materials: Forty prospective paediatric patients (median age 13.8 years, range 10.0-17.7) with suspected (n=35) or newly diagnosed (less than four weeks) confirmed IBD (n=5) were included and underwent gastroileo-colonoscopy with biopsies followed by MRE (median interval 20 days, range 6-55). The MRE results were compared with macroscopic (gold standard-based Paris classification 2010) and microscopic assessment of the ileum. The clinical importance of the MRE results was registered based on prospective alteration in diagnosis and management.

Results: Crohn's disease (CD) was diagnosed in 25 cases, ulcerative colitis (UC) in 12, and IBD unclassified (IBDU) in three. Macroscopic ileitis was detected in 15/25 (60%) of CD cases and in 2/12 (17%) of UC (backwash ileitis). Microscopic inflammation was found in another four CD cases and one IBDU patient. The discrepancy between gold standard and MRE was less than microscopy and gold standard. The sensitivity and specificity of MRI was 71% and 92%, respectively. MRE findings led to changes in diagnosis in 4/40 (10%) and treatment in 11/40 (28%).

Conclusion: MRE is a specific method for imaging of intestinal inflammation in paediatric IBD, and can be supportive or essential for clinical treatment decisions. MRE has lower sensitivity in patients with newly diagnosed IBD, perhaps due to less advanced changes.

B-0862 11:06



Multiphase contrast-enhanced MRI for control of subacute trauma of abdomen and chest in children

A. Petraikin, T. Akhadov, N. Semenova, O. Karaseva, I. Melnikov, S. Sidorin;
 Moscow/RU (petrai@rambler.ru)

Purpose: Traumatic damage of abdomen and chest organs in children (isolated as well as a part of multiple injuries) is not rare in radiological department of an emergency hospital. In order to control the trauma in subacute phase, we suggest multiphase contrast-enhanced MRI.

Methods and Materials: An MRI unit with 3.0 T was used in the research. We used T1 sequence e-THRIVE for pre- and postcontrast scans (Gd contrast agent, bolus). The scanning was of breath-hold type, with high spatial resolution (1x1 mm in plane, 1.7 mm slice thickness). Before contrast injection we used T2 sequences, MRCP, in synchronisation with breathing (Navigator method). 24 patients with subacute trauma scored from 9 to 50 on injury severity score (ISS) were examined.

Results: Examinations of subacute traumatic injuries in children revealed damages of parenchymal organs with various degrees of severity: liver (16 cases), kidneys (10), lungs (6), spleen (6) and pancreas (2). Eighteen patients (75%) had multiple injuries. All patients demonstrated positive dynamic of recovery. Ability of the patient to hold his breath is needed, comprising one of major restrictions for using this method. The particular strength of this method is opportunity to overcome ultrasonography limitations (good performance in lungs, subdiaphragmatic region of hepar etc).

Conclusion: Multiphase contrast-enhanced MRI is highly effective radiological method for control of recovery after chest and abdomen trauma in children. It reduces radiation exposure and may be suggested as a method of choice for children with major trauma undertaking treatment in an emergency hospital.

B-0863 11:15

The importance of advanced MRI techniques as the definitive diagnostic tool in the differentiation between osteomyelitis and osteonecrosis in children with sicklecell disease

A. Alavi, J. De La Fuente; London/UK (alavi_afshin@yahoo.de)

Purpose: Acute musculoskeletal pain due to marrow infarction is by far the most frequent clinical presentation for sicklecell, but symptoms can be similar to osteomyelitis. MRI has the highest sensitivity and specificity in detection of marrow and extraosseous changes in both infarction and infection. Although musculoskeletal changes are confidently detectable with MRI, they can be very similar. The purpose of this study was to illustrate the importance of MRI and the advanced protocols including unenhanced, dynamic-enhanced, multiphase subtraction and whole body DWI sequences.

Methods and Materials: We examined 22 children with sicklecell disease, acute musculoskeletal pain and noncharacteristic symptoms with our completed MRI protocol, and correlated our results with the clinical, microbiological and surgical details in order to determine the diagnostic value of our sequences.

Results: There was a significant correlation between our results and the clinical results, and except few cases with clear diagnosis through unenhanced sequences, in most cases postcontrast dynamic, subtraction and DWI sequences were required for the diagnosis.

Conclusion: Whole body DWI sequences are the most effective for detecting hot spots in multifocal process, which is the nature of sickle cell disease. Although unenhanced sequences are helpful to determine the extent of a local process, in most cases the musculoskeletal abnormalities are either in osteomyelitis or in marrow infarction, similar and dynamic postcontrast and subtraction sequences are required for the definitive differentiation. Our results show that advanced MRI protocol is an ultimate diagnostic tool for confidently differentiating between marrow infarction and infection in children with sickle cell disease.

B-0864 11:24

Pixel-by-pixel analysis of DCE-MRI curve shapes in knees of juvenile idiopathic arthritis patients

R. Hemke, C. Lavini, M.A.J. van Rossum, M. van den Berg, K.M. Dolman, M. van Veenendaal, D. Schonenberg, T.W. Kuijpers, M. Maas; *Amsterdam/NL* (*r.hemke@amc.nl*)

Purpose: To compare the relative number of time-intensity curve (TIC) shapes as derived from DCE-MRI in clinical active and clinical inactive juvenile idiopathic arthritis (JIA) patients.

Methods and Materials: DCE-MRI datasets of knees of JIA patients were prospectively obtained using an open-bore magnet (1T). Patients were classified into two clinical subgroups: active arthritis (n=8) and inactive disease (n=8). Every voxel with its TIC was classified into one of seven predefined TIC shape categories, which resulted in a colour-coded shape map. Spatial information of the synovial TIC shape distribution pattern and relative number of TIC shapes were calculated on a three-dimensional region of interest. Relative TIC shape numbers were compared using a nonparametric Mann-Whitney U test.

Results: No differences between active and inactive JIA patients were found regarding the relative number of type 2 TIC shapes (slow enhancement) and type 3 TIC shapes (fast enhancement followed by plateau phase) (p=0.645, p=0.600, respectively). However, a significant higher relative number of type 4 TIC shapes (fast enhancement followed by early washout phase) was seen in clinical active patients compared with the inactive group (9.2% vs. 4.1%, p=0.021). Type 5 TIC shapes (fast enhancement followed by slow enhancement increase) tended to be more present in clinical inactive patients compared with active JIA patients (16.1% vs. 12.3%, p=0.052).

Conclusion: Results obtained using the pixel-by-pixel DCE-MRI TIC-shape analysis differ in small cohorts of active and inactive JIA patients.

B-0865 11:33

Permanent muscular sodium overload and muscle oedema in Duchenne muscular dystrophy: a possible contributor of progressive muscle degeneration

M.-A. Weber¹, A.M. Nagel¹, M.B. Wolf¹, K. Jurkat-Rott², W. Semmler¹, H.-U. Kauczor¹, F. Lehmann-Horn²; ¹Heidelberg/DE, ²Ulm/DE (*MarcAndre.Weber@med.uni-heidelberg.de*)

Purpose: To assess the presence and persistence of muscular oedema and increased myoplasmic sodium (Na⁺) concentration in Duchenne muscular dystrophy (DMD), probably contributing significantly to its progressive muscle degeneration.

Methods and Materials: We examined 11 DMD patients (mean age, 10.2±4.7 years) and 11 healthy volunteers (mean age, 10.5±3.2 years) on a 3-Tesla MR-system with proton (1H) and 23Na density-adapted 3D-radial sequences. To ensure consistency, 5 patients were re-examined about 7 months later. We quantified muscle oedema on STIR images with background noise as reference and fatty degeneration on T1-weighted images using subcutaneous fat as reference. Na⁺ was quantified by a muscular tissue Na⁺ concentration (TSC) sequence employing a reference tube for standardisation, containing 51.3mM Na⁺ with 5% agarose gel. With a novel inversion-recovery (IR) sequence, which utmost suppresses extracellular 23Na signals, for instance, from vasogenic oedema, we determined mainly the myoplasmic Na⁺.

Results: The normalised muscular 23Na IR signal intensity was higher in DMD (0.77±0.13) than in volunteers 0.50±0.04 (p < 0.001) and persisted at second measurement (n=5, 0.75±0.06 vs. 0.73±0.02, p=0.38). When compared to volunteers (25.8±2.2 mmol/l), TSC was markedly increased in DMD (38.4±6.8 mmol/l, p < 0.001) and remained constant (n=5, 36.9±4.0 mmol/l vs. 36.3±2.8 mmol/l, p=0.38). Oedema (14.8±3.6 vs. 7.0±0.6, p < 0.001) and muscular fat content (0.49±0.09 vs. 0.38±0.01, p < 0.001) were elevated in DMD muscles when compared with volunteers. This could also be confirmed during follow-up (p=0.50, p=0.17).

Conclusion: The permanent muscular Na⁺ overload in DMD is likely osmotically relevant and responsible for the persisting, mainly intracellular muscle oedema. Both were present in all DMD patients.

B-0866 11:42

Evaluation of a radiation dose reduction strategy for paediatric abdomen CT: comparison between automatic exposure control and weight-based mAs

Y.-W. Kim¹, J.-Y. Jang¹, H. Kim²; ¹Yangsan/KR, ²Pusan/KR (*jycj008@daum.net*)

Purpose: The purpose of our study was to assess the effect of automatic exposure control system on radiation dose and image quality at paediatric abdomen CT.

Methods and Materials: We retrospectively selected 332 children who underwent abdomen CT: 221 for 128-slice single-source CT (Definition AS+) and 111 for dual source CT (Definition Flash). Automatic exposure control (Care dose 4D) was applied to 172 of the 218 patients and 80 of the 111, respectively. For each examination, the total mAs and the total dose-length product (DLP) were recorded and the effective dose was estimated using the DLP method (0.015xDLP). At last, signal-to-noise ratio (SNR=ROI/SD) and contrast-to-noise ratio (CNR=ROI at aorta - ROI at psoas muscle/SD) were calculated from those values.

Results: The effective dose (mAs) values were higher in the group who were adjusted AEC than the value in the group with weight-based fixed mAs and lower than the value in the group with randomised mAs. The higher the effective dose was, the better SNRs and CNR were. So, when we perform the paediatric abdomen CT with high mAs that does not consider their weights, the image quality was most desired. However, for most of cases with AEC or with weight-based mAs, image quality was acceptable.

Conclusion: Significant radiation dose reduction can be achieved for routine paediatric abdomen CT by weight-based fixed mAs. There was an acceptable trade-off between increased noise and decreased dose, and image quality was considered diagnostically adequate.

B-0867 11:51

Improvement of image quality in paediatric patients by lowering the tube voltage to 40 kV at fixed effective dose in digital radiography. Simulating radiography of extremities

J. Gronau¹, U. Neitzel², R. Hess², R. Wolf¹; ¹Bern/CH, ²Hamburg/DE

Purpose: With the advent of direct radiography imaging, conventional adjustments for paediatric imaging have often been adopted without change. Radiography of extremities of very young patients show only little intrinsic contrast because of the still immature bone development. In digital radiography, contrast-to-noise ratio is better at 40 kV compared to 60 kV. We examined whether the rate of correctly detected subtle fractures improves at 40 kV compared to 60 kV at fixed effective dose.

Methods and Materials: As a patient model, subtle greenstick fractures were generated in ribs from cadavers of foetal and newborn lambs. Ribs were submerged in a 3 cm water surrounding to simulate surrounding tissue. X-ray-imaging was done at 40 kV/5 mAs and 60 kV/1.6 mAs before and after fracturing. Presets at 40 kV and 60 kV led to a similar effective dose, as calculated by the Monte Carlo Simulation. The fractures could only be detected by irregularities in the spongiosa structure; x-rays from ribs with irregularities in their shape like angulation were excluded. Three radiologists analysed 320 x-rays each.

Results: The rate of correct diagnoses at 40 kV vs 60 kV was significantly higher with 71.25% vs 61.25%, 80% vs 65%, and 83.75% vs 70,625%.

Conclusion: In digital radiography, the image quality can be improved at fixed dose by lowering the tube voltage to 40 kV. Alternatively, this might be used to reduce patient dose maintaining sufficient image quality, which will be examined in following studies.

14:00 - 15:30

Room B

GI Tract

SS 1801a

CT colonography and beyond

Moderators:

P. Lefere; Roeselare/BE
A.M. Riddell; Sutton/UK

B-0868 14:00

Accuracy of computer-aided detection in detecting flat lesions in CT colonography

J.J. Nappi¹, H. Yoshida¹, D. Regge²; ¹Boston, MA/US, ²Turin/IT
(jnappi@partners.org)

Purpose: To evaluate the performance of an independently trained computer-aided detection (CAD) system in detecting flat adenomas and carcinomas from a large multi-centre CT colonography (CTC) screening population. Previous CAD studies have reported low detection performance and involved compromised training/testing schemes.

Methods and Materials: A total of 1,948 patients with cathartic preparation from 32 medical centres were included. For CAD training, 1,211 patients were collected from two CTC screening trials involving 20 US medical centres. Faecal tagging was used in 36% of cases. The CAD was trained with the 1,211 CTC cases to detect lesions ≥ 6 mm at 90% sensitivity. For CAD testing, 737 asymptomatic patients at increased risk of colorectal cancer were collected from a recent CTC screening trial involving 12 European centres. Iodine tagging without or with barium was used in 34% of cases. No intravenous contrast was administered. The pre-trained CAD system reviewed the 737 testing cases. Per-lesion and per-patient detection sensitivities and false positives (FPs) per patient were assessed with bootstrapping for biopsy-proven colonoscopy-confirmed lesions.

Results: There were 262 lesions, including 30 flat adenomas or carcinomas: 14 were ≥ 10 mm and 16 were 6-9 mm. Per-lesion (per-patient) sensitivity of CAD was 100% (100%) for flat lesions ≥ 10 mm in size and 81% (79%) for flat lesions 6-9 mm with median of 5 FPs per patient. CAD detected all 5 flat cancers.

Conclusion: Independently trained CAD can detect flat adenomas and carcinomas from unseen multi-centre CTC populations at clinically acceptable accuracy, comparable to that for polypoid lesions.

B-0869 14:09

Potential complications at CT colonography in asymptomatic and symptomatic patients: national survey of Italy

M. Ciolina¹, F. Iafrate¹, G. Iussich², D. Regge², M. Iannitti¹, P. Baldassari¹, A. Pichi¹, L. Corrales³, A. Laghi⁴; ¹Rome/IT, ²Candiolo/IT, ³Torino/IT, ⁴Latina/IT
(mariaciolina@gmail.com)

Purpose: To retrospectively evaluate the incidence of complication related to CTC performed in both symptomatic and asymptomatic patients undergoing CTC during the period ranging from 2000 and 2010.

Methods and Materials: With a national survey, an e-mail questionnaire about serious adverse events of virtual colonoscopy, particularly large bowel perforation, was sent to all Italian Public Health Centers performing a daily CTC service. Technical parameters related to complications and kind of treatment needed for adverse events were also investigated. The questionnaire was completed by clinical director from all radiology departments. Responses were analysed and raw frequencies were determined.

Results: All centres (13/13) interviewed, answered positively to the Survey. Among 13 centers, 40.121 CT colonography exams were performed. No deaths were reported. 39 (0.097%) patients experienced a complication during the procedure: 32 vasovagal self-limiting attack episodes (0.079%) and 7 perforations (0.017%). In 4 (57%) cases the site of perforation was within the rectum, in 3 (43%) cases within the sigmoid colon. No case of perforation within transverse, ascending colon and caecum. Three patients had to undergo surgery. The remaining four patients had a conservative treatment. Four out of seven cases of perforation had a conventional colonoscopy in the past seven days prior to CTC and on the same day of the exam, respectively.

Conclusion: In summary, we found a low rate of colonic perforation (0.017) that were associated with CT colonography. The rate of occurrence of luminal perforation, however, was more than four times lower than were equivalent rates published for colonoscopy.

also
EPOS

B-0870 14:18

Value of CT colonography as preliminary study prior to laparoscopic surgery in patients with colon malignancies and complicated diverticular disease

R. Rizzati¹, S. Tartari¹, C. Cavallini¹, M. Princivalle¹, R. Righi¹, G. Anania², G. Benea¹; ¹Lagosanto Ferrara/IT, ²Ferrara/IT (r.rizzati@ausl.fe.it)

Purpose: To investigate the clinical value of CT colonography (CTC) in the diagnosis and staging of colorectal cancer (CRC) and complicated diverticular disease, in order to properly plan the laparoscopic surgery.

Methods and Materials: From January 2009 until November 2010, 162 patients scheduled for surgery for CRC or complicated diverticulitis (known or suspected) underwent CTC. All patients were previously evaluated with optical colonoscopy (OC). Sensitivity in lesion location and detection was compared between OC and CTC and discrepancies analysed. Accuracy of CTC in CRC staging was determined.

Results: A total of 113 CRC and 49 complicated diverticulitis were classified by CTC. OC was incomplete in 37/162 (26%) cases. There were 17 cases of discrepancy of lesion location correctly identified by CTC and 7 polypoid (6-9 mm) lesions detected by CTC and missed by OC. Basing on CTC assessment, 5 cases of complicated diverticulitis were managed medically; 10 patients underwent conventional open surgery for CRC and 147 (103 CRC and 44 complicated diverticulitis) laparoscopic surgery. Sensitivity of CTC in TNM preoperative staging of patients with CRC resulted to be, respectively, 100%, 86% and 100%. In diagnosis of complicated diverticular disease CTC showed 100% agreement regarding location and extent of the lesion and 90% sensitivity for complications. Furthermore, CTC detected 34 extracolonic findings, 12 of whom of major clinical relevance.

Conclusion: CTC provides accurate staging of colon cancer and detailed evaluation of complicated diverticular disease, allowing an appropriate management of patient and making the laparoscopic surgical planning more precise and safer.

B-0871 14:27

Effective radiation dose in CT colonography: did we make progress?

T.N. Boellaard¹, H.W. Venema, G.J. Streekstra, J. Stoker; Amsterdam/NL
(t.n.boellaard@amc.uva.nl)

Purpose: To assess the effective radiation dose used for CT colonography and to compare these with previous inventories.

Methods and Materials: CT colonography institutions that had published on CT colonography were invited to participate. A questionnaire was sent concerning CT colonography scan protocols. Median effective doses were calculated (prone, supine and combined) for daily practice and screening protocols, and compared with earlier inventories. Separate analyses were performed for the use of intravenous contrast and academic versus non-academic. Differences in effective dose were tested for significance, using a Wilcoxon rank-sum or Wilcoxon signed-rank test where appropriate.

Results: In total, 62 of 109 (57%) institutions responded, providing 57 protocols. Median effective dose for daily practice protocols was 7.5 mSv (4.3 mSv and 2.0 mSv for supine and prone) and for screening 4.4 mSv (2.7 mSv and 2.0 mSv for supine and prone) ($p=0.013$). For daily practice with and without contrast median effective doses were 10.5 mSv ($n=29$) and 4.0 mSv ($n=32$) ($p < 0.001$). Academic and non-academic institutions used similar doses (daily practice: 7.8 vs. 6.1 mSv ($p > 0.05$) and screening: 4.7 vs. 3.8 mSv ($p > 0.05$)). For institutions, which also participated in a 2007 inventory, effective dose for both daily practice and screening protocols were similar ($p > 0.05$), but for daily practice lower than in a 2004 inventory ($p=0.037$).

Conclusion: Median effective dose of daily practice protocols has decreased as compared to 2004, but not to 2007. Further reduction is desirable to reduce radiation burden in CT colonography and increase its acceptance.

B-0872 14:36

Comparison of 64-slice CT colonography with conventional colonoscopy in patients with ulcerative colitis

N. Prabhakar, N. Kalra, D.K. Bhasin, S. Rana, R. Singh, N. Khandelwal; Chandigarh/IN

Purpose: Clinical and colonoscopic findings are used for the diagnosis of patients with ulcerative colitis and their follow-up. The purpose of the study was to compare the findings of CT colonography (CTC) with conventional colonoscopy (CC) in patients with ulcerative colitis.

Methods and Materials: In this prospective study, 20 consecutive patients proven to have ulcerative colitis on biopsy and presently in clinical remission underwent CTC and CC within one week of each other. The CC findings were considered as gold standard. The investigators performing CTC and CC were blinded to the

also
EPOS

findings of the other study. Chi-square test and kappa test were used to compare the findings on CTC and CC. Sensitivity and specificity on CTC for detecting pseudopolyps and granularity in a segment were also calculated.

Results: Good correlation was seen between CTC and CC for detection of granular appearance and pseudopolyps. Sensitivity and specificity on CTC for detecting pseudopolyps were 82.14% and 84.48%, respectively, and for granular appearance were 81% and 73.8%, respectively. Loss of haustral folds, pericolonic vascularity, pericolonic lymph nodes and wall thickening seen on CTC were found to correlate with intraluminal findings seen on CC. These can be used as additional markers of disease extent in association with intraluminal findings on CTC.

Conclusion: CTC can be used as an all-in-one technique for evaluating patients with ulcerative colitis who are in remission. It provides information about the bowel lumen, bowel wall and extraluminal abnormalities in these patients.

B-0873 14:45

Low-dose computed tomography to detect body packing: stepwise dose reduction in an animal model

M.H. Maurer, S.M. Niehues, D. Schnapauff, C. Grieser, J. Rothe, S.S. Chopra, B. Hamm, T. Denecke; Berlin/DE (martin.maurer@charite.de)

Purpose: To determine the value of low-dose computed tomography (CT) to detect body packing (ingested drug packets) as an alternative to plain radiographs in an animal model with stepwise CT-dose reduction.

Methods and Materials: Twelve packets containing cocaine (purity > 80%) were introduced into the intestine of an animal (crossbred pig, 21.5 kg), which was then repeatedly examined by abdominal CT with stepwise dose reduction (tube voltage, 80 kV; tube current, 10-350 mA, detector collimation, 64x0.625 mm; pitch, 1.5; rotation time, 350 ms; scan length, 35 cm). Three blinded readers independently evaluated the CT datasets (images reconstructed at 1.25 mm slice thickness; increment, 0.5) starting with the lowest tube current and noted the numbers of packets detected at the different tube currents used. One experienced reader determined the number of packets detectable on plain abdominal radiographs and ultrasound.

Results: The threshold for correct identification of all 12 drug packets was 100 mA for reader 1 and 125 mA for readers 2 and 3. Above these thresholds all 3 readers consistently identified all 12 packets. The effective dose of a low-dose CT scan with 125 mA (including scout view) was 1.0 mSv, which was below that of 2 conventional abdominal radiographs (1.2 mSv). The reader interpreting the conventional radiographs identified a total of 9 drug packets and detected 8 packets by abdominal ultrasound.

Conclusion: Extensive dose reduction makes low-dose CT a valuable alternative imaging modality for the examination of suspected body-packers and might replace conventional abdominal radiographs as the first-line imaging modality.

B-0874 14:54

Material decomposition of spectral CT: a new way in the prediction of response to chemotherapy in gastric carcinoma?

L. Tang, X.-P. Zhang, Y.-S. Sun, L.-P. Qi, Y. Cui, S.-Y. Gao, Y. Li; Beijing/CN (tanglei@bjcancer.org)

Purpose: To investigate the use of the iodine concentration (IC) derived from material decomposition of spectral CT as a response indicator in patients with gastric carcinoma treated with chemotherapy.

Methods and Materials: Twenty-two patients with gastric cancer were scanned on a GE Discovery CT 750HD using spectral imaging mode, before and 2-4 months after chemotherapy. Patients were divided into the good-response group (GoodR) and poor-response group (PoorR) according to RECIST criteria. The iodine-water basis material decomposition images and monochromatic images on arterial and venous phase covering the entire stomach were reconstructed. An oval regions-of-interest (ROI) was placed on the highest enhanced region of gastric carcinoma. The iodine concentrations (IC, mg/cc) in ROIs were recorded, and the decrease rate of IC was computed by the formula: % Δ IC = (IC_{before} - IC_{after}) / IC_{before} x 100%. The decrease rates of IC between two groups were compared using independent t test.

Results: We recorded a positive correlation between % Δ IC and the shrinkage rate of tumour size on both phases (arterial phase: r=0.698, P < 0.001; venous phase: r=0.760, P < 0.001). There were 9 cases of GoodR and 13 cases of PoorR. Statistical difference of % Δ IC was demonstrated between GoodR and PoorR at venous phase (Z=-2.771, P=0.004), but not at arterial phase (Z=-1.302, P> 0.05).

Conclusion: Our findings suggest that iodine concentration derived from spectral CT imaging could provide clinical information for the treatment evaluation of gastric carcinoma. Prospective studies with large samples are needed to test its reproducibility and to determine the diagnostic threshold.

B-0875 15:03

The accuracy of pre-operative CT in the assessment of the acute abdomen

J. Weir-McCall¹, D. Christodoulou², A. Shaw², A. Arya², A. Knight², D. Howlett³; ¹Dundee/UK, ²London/UK, ³Eastbourne/UK

Purpose: While there is a lot of data on the accuracy of CT in diagnosing specific causes of an acute abdomen, there is very little information on the accuracy of CT in the acute general surgical admissions workload. We look at the diagnostic accuracy of CT in patients presenting with an acute abdomen who ultimately required laparotomy.

Methods and Materials: Patients who underwent emergency laparotomy from 2008 to 2010 at our hospital with a pre-operative CT on the same admission were included. The CT report was compared with the laparotomy and histology findings, and where a discrepancy existed, the original scans were reviewed by a senior consultant blinded to the original report and laparotomy findings.

Results: 196 emergency laparotomies were performed over the 2-year period with 112 patients undergoing a preoperative CT. 15 patients were excluded due to missing notes. In the remaining 97 patients, 80 CT reports correlated with the final operative diagnosis giving a diagnostic accuracy of 82%. Of these, the oncall registrar was the initial reporter in 37 CTs with a diagnostic accuracy of 78%. On review of the CT scan by a second consultant this increased to 90 correlations yielding an accuracy of 93%. Delay between CT scan and operation did not significantly alter diagnostic accuracy, nor was there any statistically significant reduction in accuracy in reports issued by oncall registrars.

Conclusion: On first reporting CT misses 18% of diagnosis that ultimately require operative intervention. Reducing the threshold for obtaining a second consultant radiologist review significantly improves the diagnostic accuracy to 93%.

B-0876 15:12



Quantitative imaging biomarkers from PET-CT as potential correlates for angiogenesis and hypoxia in colorectal cancer

B. Ganeshan¹, Z. Ziauddin², V.J. Goh², M. Rodriguez-Justo², A. Engledow², S. Taylor², S. Halligan², K.A. Miles¹, A.M. Groves²; ¹Brighton/UK, ²London/UK (b.ganeshan@sussex.ac.uk)

Purpose: Integrated PET-CT systems allow measurements of tracer uptake on PET to be combined with quantitative imaging biomarkers from CT. This study aims to identify histopathological correlates for fluorodeoxyglucose (FDG) uptake, CT attenuation and CT heterogeneity in colorectal cancer.

Methods and Materials: 18 FDG-PET was performed prospectively in a series of 53 patients with colorectal cancer. FDG uptake (maximal standardised uptake value; SUV_{max}), CT attenuation and CT heterogeneity for unenhanced images were quantified in a region of interest (ROI) encompassing the primary tumour. Heterogeneity was expressed as the standard deviation (SD) of pixel values in CT images with and without filtration to highlight image characteristics ranging from fine detail to coarse features (as determined by the filter value). Using the Spearman-rank method, all imaging parameters were correlated with tumour microvessel density (MVD) and expression of vascular endothelial growth factor (VEGF) and Glut-1 on histological examination of resected tumours.

Results: Histological data were available in 32 cases. CT heterogeneity (filter value 2.0) was the best correlate for MVD (rs = 0.47, p = 0.006). SUV_{max} correlated significantly with expression of VEGF (rs = 0.42, p = 0.017) but not Glut-1 (rs=-0.35, p = 0.053). The ratio of SUV_{max} to CT heterogeneity (filter value 2.5) was the best correlate for expression of VEGF (rs = 0.45, p = 0.009) and Glut-1 (rs = -0.42, p = 0.018).

Conclusion: Addition of CT-based biomarkers has the potential to increase the utility of PET-CT by enhancing the imaging correlates for angiogenesis and hypoxia in colorectal cancer.

14:00 - 15:30

Room C

Oncologic Imaging

SS 1816

CE-MRI and DWI-MRI for cancer evaluation

Moderators:

S. Delorme; Heidelberg/DE
R. Girometti; Udine/IT

B-0877 14:00

Interscanner comparison of dynamic contrast-enhanced MRI in prostate cancer: 1.5T versus 3 T MR

M. Sertdemir, D. Dinter, D. Hausmann, H.J. Michaely, S. Schönberg, A. Weidner; Mannheim/DE (Metin.Sertdemir@umm.de)

Purpose: To compare the diagnostic potential of DCE-MRI to differentiate malignant vs. normal prostate and prostatitis tissue with special regard to different field strengths of 1.5 vs. 3 Tesla.

Methods and Materials: 68 patients with biopsy and/or prostatectomy of the prostate were included in the study. MRI was performed at 1.5 T in 22 patients with biopsy-proven prostate cancer (PC) and in 8 patients with prostatitis; at 3 T, MRI was undertaken in 27 patients before prostatectomy after histologically proven PC and in 11 patients with prostatitis. MRI was undertaken with combined body and endorectal coil protocol in all patients, using a 2D TurboFLASH T1W GRE sequence to calculate plasma flow (PF) and mean transit time (MTT) values.

Results: PC showed higher PF ($p < 0.0001$) and shorter MTT ($p < 0.0001$) at 3 T as well as at 1.5 T ($p < 0.0001$ for PF and $p=0.0016$ for MTT) compared to normal tissue. PC demonstrated higher PF than prostatitis ($p=0.0018$) and shorter MTT ($p=0.0006$) at 3 T, but only shorter MTT ($p=0.0034$) at 1.5 T without significantly higher PF values ($p=0.3604$). In comparison with normal tissue, prostatitis had a statistically significant higher PF at 1.5 T ($p=0.0156$) but not at 3 T ($p=0.1748$) and no significantly shorter MTT values both at 3 T ($p=0.1595$) and 1.5 T ($p=0.25$).

Conclusion: Both field strengths are capable to differentiate PC vs. normal tissue. Using 3 T, PC can be better delineated from prostatitis compared to 1.5 T. Nevertheless, the results are equivocal for differentiation of prostatitis and normal tissue.

B-0878 14:09

Contrast enhanced MRI features of early (microscopic) extracapsular disease in patients with known prostatic cancer

C. Sit, N. Dikaios, A. Kirkham, C. Allen, A. Freeman, C. Moore, M. Emberton, J. Kelly, S. Punwani; London/UK (cherryhysit@gmail.com)

Purpose: To assess contrast-enhanced MRI for detection of microscopic extracapsular disease in patients with known peripheral zone prostate cancer.

Methods and Materials: Pre-biopsy contrast enhanced MR images of 33 patients with histologically diagnosed peripheral zone tumour (without macroscopic extracapsular disease on imaging) were retrieved for prospective analysis. Histological confirmation of tumour was by standard 8 core TRUS biopsy; and 18 of the 33 patients underwent subsequent radical prostatectomy. An experienced radiologist aware of the histologically confirmed tumour site, unaware of presence or absence of microscopic extracapsular extension (ECE), contoured the tumour on contrast enhanced images, recording (i) total tumour volume, (ii) total area of capsular abutment, (iii) tumour-muscle signal intensity ratio, (iv) symmetry of peri-prostatic vascular enhancement, (v) symmetry of capsular enhancement, (vi) area under tumour signal intensity time curve, (vii) initial slope of enhancement of the signal intensity time curve, (viii) maximum enhancement ratio, (ix) enhancement curve shape (type I, II or III). Differences between mean values of continuous variables were assessed using t-test and Mann-Whitney statistics; and differences in categorical variables were assessed using chi-square and Fisher's exact tests for patients with and without histological ECE.

Results: 19/33 patients had histologically confirmed ECE. There was significantly increased vascularity on the same side as the prostatic tumour for patients with ECE ($p=0.002$). There was no significant difference between patients with and without ECE for any of the other parameters ($p=0.09$ to 0.67).

Conclusion: Increased ipsilateral peri-prostatic vascularity alone was associated with ECE on contrast enhanced MRI.

B-0879 14:18

MRI as an imaging surrogate to predict radiation dosimetry borders: a methodology feasibility study

A. Kovacs¹, P.O. Zinn², F.P. Schwarm³, F.A. Jolesz³, I. Repa¹, R.R. Colen³; ¹Kaposvar/HU, ²Texas, TX/US, ³Boston, MA/US (kovacs.arpad⁹⁷⁹@gmail.com)

Purpose: To develop a robust methodology using MRI for predicting radiation dosimetry borders of the tumour beyond the area of enhancement for radiation treatment planning.

Methods and Materials: We retrospectively identified 88 consecutive glioblastoma multiforme patients (2005-2010) whom had (presurgical, postsurgical, pre-radiation, and relapse) MRI studies and undergone radiation treatment (RT). 3D Slicer software 3.6 (slicer.org) was used for image analysis, manipulation and segmentation. Two neuroradiologists (RRC, FAJ) reviewed the images in consensus. Three structures were segmented (oedema/invasion, enhancing tumour, and necrosis). Subsequently, the models/quantitative volumes of oedema, tumour and necrosis were calculated. MR perfusion (MRP) scans (N=40) were registered to segmented images and quantitative perfusion parameters obtained. These were then registered to the radiation planning CT images and the dosimetry curves superimposed.

Results: Accurate registration (within 2 mm) occurred among the images and the radiation planning CT images. 23/40 patients demonstrated increases in perfusion (reflective of tumour infiltration) beyond the border of enhancement and corresponding to the regions of subsequent recurrence, suggesting that radiation planning to include those abnormal regions seen on advance imaging techniques (not on conventional MRI) might result in better tumour treatment and control of recurrence.

Conclusion: We present a robust image analysis methodology/platform for accurate registration of conventional and advanced MRI sequences and with the radiation planning CT images. MR perfusion abnormalities seen outside the area of enhancement predict regions of subsequent recurrence and thus registering and including these regions in the RT and dosimetry planning system can be expected to decrease tumour recurrence and increase survival.

B-0880 14:27



Diagnostic value of functional magnetic resonance imaging for differentiation of benign osteoporosis and multiple myeloma

M. Sumkauskaitė, J. Hillengass, C. Heiss, M. Dornisch, B. Stieltjes, H.-P. Schlemmer, H. Goldschmidt, S. Delorme; Heidelberg/DE (migles@gmail.com)

Purpose: The aim of our study was to assess the value of dynamic contrast-enhanced magnetic resonance imaging (DCE-MRI) and diffusion-weighted imaging (DWI) of the bone marrow for differentiating benign osteoporosis and multiple myeloma.

Methods and Materials: Between 2009 and 2011, twenty patients with untreated multiple myeloma and twenty patients with clinically confirmed, idiopathic or postmenopausal osteoporosis were prospectively examined using a 1.5 Tesla MR scanner (Magnetom Symphony, Siemens Erlangen, Germany). DWI and DCE-MRI of the lumbar spine were performed in all patients. DCE-MRI parameters amplitude A (associated with blood volume) and exchange rate constant kep (associated with vessel permeability) as well the DWI parameters (according to the intravoxel incoherent motion (IVIM) model) perfusion fraction f and diffusion constant D were evaluated for each lumbar vertebra separately by a radiologist blinded to the patient's history.

Results: A and kep in DCE-MRI were significantly higher in the myeloma group than in patients with osteoporosis ($P < 0.001$, Wilcoxon Rank Sum Test). Furthermore, a significantly increased diffusion constant D was found in patients with multiple myeloma ($P < 0.001$, Wilcoxon Rank Sum Test). No significant difference was found for the perfusion fraction f ($P=0.07$, Wilcoxon Rank Sum Test).

Conclusion: DCE-MRI and DWI may assist in differentiating benign osteoporosis from malignant bone disease caused by multiple myeloma.

B-0881 14:36

Early prediction of histopathological response to pre-operative chemotherapy in locally advanced gastric cancer by FDG PET-CT

F. Maggi, L. Leccisotti, G. Treglia, R. Persiani, A. Giordano, L. Bonomo; Rome/IT (fmaggi@sirm.org)

Purpose: Pre-operative chemotherapy can improve the prognosis of patients with locally advanced gastric cancer (LAGC). Aim of this prospective observational study is evaluate the role of FDG PET-CT to early predict histopathological response during pre-operative chemotherapy in a group of accurately staged LAGC patients.

Methods and Materials: Patients with resectable LAGC (cT4a-b any N or any cT with node metastases) were included in the study and underwent FDG PET-CT at baseline and 14 days after initiation of chemotherapy. Patients with non-avid

FDG tumour at baseline PET-CT were excluded. Clinical re-staging was repeated pre-operatively. Tumoral metabolic response was assessed according to EORTC criteria. Histopathological response was assessed qualitatively by T-downstaging and quantitatively by grading of tumour regression induced by pre-operative chemotherapy according to Becker's criteria.

Results: Twelve LAGC resectable patients (7 F/5 M; mean age: 63±9 years) were included. Five patients (42%) were classified as metabolic responders (reduction of 54±10% in tumoral SUVmax) and seven patients (58%) as metabolic non-responders (increase of 6±16% in tumoral SUVmax). All metabolic responders showed T-downstaging with 3 partial, 1 subtotal and 1 minimal tumour regression. All metabolic non-responders did not show T-downstaging and tumour regression analysis showed 6 minimal responses and 1 partial response. Additionally, 3 metabolic responders were ypN0 while 6 metabolic non-responders were ypN2-3. **Conclusion:** FDG PET-CT could be a reliable modality to predict histopathological response at an early stage of the pre-operative treatment in LAGC patients, thus allowing a change in the treatment for metabolic non-responders patients.

B-0882 14:45

ADC maps: differentiation of metastatic from non-metastatic lymph nodes in patients with endometrial cancer

G. Rechichi, S. Galimberti, A.C. Cadonici, C. Talei Franzesi, P. Perego, S. Sironi; Monza/IT (*gilda.rechichi@gmail.com*)

Purpose: To evaluate the usefulness of diffusion-weighted images with body background suppression (DWIBS) and apparent diffusion coefficient (ADC) to discriminate between metastatic and non-metastatic pelvic lymph nodes in endometrial cancer.

Methods and Materials: This prospective study included 32 patients with histologically proven endometrial cancer who underwent MR examination including T2-weighted, dynamic T1-weighted and diffusion-weighted images with background suppression (DWIBS) with b-values of 0 and 1000 s/mm². Then all patients underwent total hysterectomy and pelvic lymphadenectomy. All identifiable lymph nodes on DWIBS (n=94) were evaluated and for each lymph node mean ADC values, short- and long-axis diameters were measured and compared. Histopathological findings served as the reference standard.

Results: Mean (+SD) ADC values (10-3 mm²/sec) of metastatic lymph nodes (n=12; 0.851 ± 0.134) were significantly lower than those of non-metastatic lymph nodes (n=82; 1.062 ± 0.157) (p-value < 0.0001). Long- and short-axis diameters of metastatic vs non-metastatic lymph nodes were 13.6 ± 2.4 mm vs. 12.6 ± 3.1 mm and 9 ± 4.3 mm vs. 8 ± 2.5 mm, respectively.

Conclusion: In endometrial cancer patients, ADC measurements of pelvic lymph nodes allow to discriminate between metastatic and non-metastatic nodes.

B-0883 14:54

Multimodality quantification of tumour perfusion in diffusion-weighted MRI and dynamic PET in a rodent model

N. Mortazavi-Jehanno, D. Balvay, C. Bourillon, C. Badoual, M. Bernardini, M. Faraggi, C.-A. Cuenod, O. Clement, L.S. Fournier; Paris/FR (*nina.jehanno@egp.aphp.fr*)

Purpose: Development of new parameters of acquisition and treatment for the assessment of tumour perfusion using diffusion-weighted MRI and dynamic PET/CT with 18F-FDG, in a rodent model.

Methods and Materials: Experimentations were made on two models of epidermoid head and neck carcinoma implanted in nude rats, FaDu a highly vascularised tumour and A253 a poorly vascularised tumour. DW-MRI was performed with an acquisition of 20 different b values (0-2000), for which a "clinical ADC" (using only b=1000), a mono-exponential and a bi-exponential analysis of ADC and perfusion parameters (f, D*) were calculated. Dynamic PET/CT was performed, with visual analysis of enhancement curves, and a Patlak and compartmental analysis. All data were correlated pathology with semi-quantitative evaluation of vascularity, necrosis, inflammation and haemorrhage.

Results: DW-MRI data with bi-exponential analysis, allowed separation of two components, with a perfusion fraction f greater for FaDu than A253 (21.5 vs. 11.8; p=0.004), consistent with pathology. There was also a significant difference in diffusion between the tumour types (Dr 1.00 vs. 0.79, p= 0.013) but which did not correlate a specific pathological characteristic. Enhancement curves in dynamic PET showed an accumulation of tracer in the tumour starting from the first minute. Perfusion parameters extracted using Patlak or compartmental analysis did not yield a significant difference between the two groups.

Conclusion: Our study allowed optimisation of data acquisition and analysis for the evaluation of tumour perfusion using multi-b DW-MRI and dynamic PET.

B-0885 15:03

MRI-based liver segmentation for quantification of functional liver volume: evaluation of a threshold-based method facilitated by hepatobiliary contrast media (Gd-EOB)

J.H. Rothe, R. Papendieck, C. Grieser, D. Schnapauff, B. Hamm, T. Denecke; Berlin/DE (*jan-holger.rothe@charite.de*)

Purpose: Knowledge of the exact tumour volume is relevant in various oncological scenarios (assessment of tumour load, radioembolisation dosimetry, future liver remnant before major surgery). Purpose was the evaluation of this approach compared to manual segmentation with CT as reference.

Methods and Materials: A total of 20 patients (10 gastrointestinal primary malignancies, 10 hepatic primary tumours) were examined before selective internal radioembolisation with computed tomography and Gd-EOB (Primovist, BayerSchering)-enhanced MRI of the liver within one week. T1w 3D-sequences (THRIVE) were acquired in the hepatobiliary phase. The liver volume was measured by manual segmentation of the liver silhouette excluding intrahepatic tumour masses in the CT and MR dataset and by manually adjusted thresholding of the MR dataset followed by removal of extrahepatic structures. Mean absolute error, reproducibility and duration of each segmentation procedure by a threshold-based volumetry and manual slice segmentation were quantified.

Results: A MRI-based liver volumetry underestimated the calculated volume based on CT data with mean of 4.0% (maximum, 7.8%) for a manual segmentation, 5.8% (maximum, 7.5%) for the threshold-based method. For a MRI-based volumetry segmentation times between 2.5 and 5 minutes, mean 3.5 minutes with a manual slice segmentation, between 2.0 and 4.0 minutes, mean 3.0 minutes for the threshold-based method were observed. Segmentation times for a CT-based liver volumetry ranged between 4 and 8 minutes, mean 5.5 minutes.

Conclusion: With a small mean absolute error and the reduced segmentation time compared to manual segmentation, Gd-EOB volumetry offers quick and convenient segmentation of functional liver volume.

B-0886 15:12

Fusion of dynamic CE-MRI mammography at 3.0 Tesla with FFDM mammography: pilot study using a dedicated semi-automatic registration software

M. Dietzel¹, T. Hopp², P. Kreisel¹, N.V. Ruiter², H.P. Burmeister¹, W.A. Kaiser¹, P.A.T. Baltzer¹; ¹Jena/DE, ²Karlsruhe/DE (*dietzelmatthias@hotmail.com*)

Purpose: Image-fusion of x-ray mammography and MR-mammography (XR-M/ MR-M) allows correlation of pathological findings between these imaging-modalities (e.g. microcalcifications, architectural distortions, focal enhancements, etc). Thus, it has the potential to optimise diagnostic accuracy and clinical workflow of breast imaging. This pilot study evaluates the accuracy of a dedicated semi-automatic image fusion of XR-M and high-resolution/high-field MR-M.

Methods and Material: MR-M were acquired on a high-field scanner (3.0 Tesla: T1-weighted 3D-VIBE ± Gadolinium). XR-M were obtained with state-of-the-art full-field digital systems. Patients with clearly delineable mass lesions > 10 mm in XR-M and MR-M were enrolled (exclusion criteria: previous breast surgery; surgical intervention between XR-M/MR-M). XR-M and MR-M were matched using our in-house developed software allowing semi-automatic non-linear deformation of MR-M. Based on the MR-M a "virtual 2D Mammogram" was calculated to identify registration-errors (RE; with and w/o Gadodiamide/Gd) and compared to the corresponding XR-M. To quantify REs the geometric-centre of the lesions in the virtual vs. conventional mammogram were subtracted. Robustness of registration was quantified by registration of X-MRs to both MR-Ms with and w/o Gadodiamide.

Results: Image registration was performed successfully for all patients (n=7). Overall RE was 8.2 mm (w/o Gd; confidence-interval/CI: 2.0-14.4 mm) vs. 8.9 mm (1st minute after Gd; CI: 4.0-13.9 mm). Mean difference between pre- vs. post-contrast scans was 0.7 mm.

Conclusion: Semi-automatic image registration of high-field MR-mammography with x-ray mammography is feasible. For this study applying a high-resolution protocol at 3.0 Tesla, the registration was robust and the overall registration error was sufficient for clinical application.

14:00 - 15:30

Room D1

Neuro

SS 1811

New fields and developments

Moderators:

S.J. Bakke; Oslo/NO

J. Ramalho; Lisbon/PT

B-0887 14:00

Evaluation of diffusivity in anterior lobe of the pituitary gland: 3D turbo field echo with diffusion-sensitised driven-equilibrium preparation

A. Hiwatashi, T. Yoshiura, O. Togao, K. Yamashita, K. Kikuchi, M. Obara, H. Honda; Fukuoka/JP

Purpose: 3D turbo field echo (TFE) with diffusion-sensitised driven-equilibrium (DSDE) preparation is a novel non-echo planar (EPI) technique for diffusion-weighted imaging (DWI), which enables high-resolution DWI without field inhomogeneity-related image distortion. The purpose of this study was to evaluate the feasibility of this sequence to assess the normal pituitary gland.

Methods and Materials: First, validation of DSDE DWI was attempted by comparing with conventional EPI DWI. Five healthy volunteers were imaged using a DSDE DWI sequence and an EPI sequence. For both methods, a motion-probing gradient was applied in one direction (A-P) with b values of 0 and 500 s/mm². The imaging voxel size was 1.5x1.5x1.5 mm³ for the DSDE and 1.5x1.9x3.0 mm³ for the EPI. The apparent diffusion coefficient (ADC) measured by the two methods in 15 regions (6 in grey matter and 10 in white matter) were compared using Pearson's correlation coefficient. Then, the ADC in the pituitary anterior lobe was measured in 7 volunteers using the DSDE DWI sequence, and compared with those in the pons and cerebellum using the t test.

Results: ADC from the two methods showed good correlation ($r = 0.88$), confirming the accuracy in ADC measurement with the DSDE sequence. The ADC in the normal pituitary gland was $1.32 \pm 0.11 \times 10^{-3}$ mm²/s. This was significantly higher than that in the pons ($0.95 \pm 0.18 \times 10^{-3}$ mm²/s) and in the cerebellum ($0.84 \pm 0.14 \times 10^{-3}$ mm²/s) ($P < 0.05$, respectively).

Conclusion: We demonstrated that DSDE DWI is feasible to assess ADC in the pituitary gland.

B-0888 14:09

Sonographic evaluation of the intracranial pressure in adult brain injury

T. Soldatos, A. Karabinis, V. Tsagkoulis, S. Kampanarou, S. Tanteles, G. Economou, L. Thanos, M. Pomoni, D.A. Kelekis; Athens/GR
(mkampanarou@gmail.com)

Purpose: The optic nerve sheath diameter (ONSD) may be increased in brain-injured patients with elevated intracranial pressure (ICP). We evaluated whether ONSD measurements correlate with invasive and noninvasive ICP measurements in brain-injured adults.

Methods and Materials: We examined 106 brain-injured patients and 67 control subjects without intracranial pathology. Brain-injured patients were evaluated using Glasgow coma scale (GCS) and a semiquantitative (I-VI) neuroimaging scale (Marshall Scale, MS), and were divided into moderately (MS=I and GCS>8, n=35) and severely (MS=II-VI and GCS≤8, n=71) brain-injured subjects. Measurements of the ONSD and noninvasive ICP (eICP), using optic nerve sonography and transcranial Doppler sonography, respectively, were performed upon admission in controls and moderately brain-injured subjects, and three times during hospitalisation in severely brain-injured patients. Upon admission, 32 severely brain-injured patients also underwent invasive ICP measurement.

Results: In severely brain-injured patients, the ONSD correlated with the MS ($r=0.76-0.82$) and the eICP ($r=0.53-0.80$) in all three evaluations, whereas ONSD and eICP were significantly increased (6.2 ± 0.7 mm and 27.5 ± 6.9 mmHg) as compared with moderately brain-injured subjects (4.2 ± 0.9 mm and 12.2 ± 3.7 mmHg) and controls (3.5 ± 0.8 mm and 9.9 ± 3.7 mmHg) ($P < 0.001$). Invasive ICP measurements also correlated with ONSD measurements ($r=0.68$, $P=0.002$). The best cut-off ONSD value for predicting elevated ICP was 5.7 mm (sensitivity=74%, specificity=100%).

Conclusion: ONSD measurements correlate with invasive and noninvasive ICP measurements, and with neuroimaging findings in brain-injured adults. Optic nerve sonography could alert clinicians to the presence of elevated ICP, whenever invasive ICP evaluation is contraindicated and/or is unavailable.

B-0889 14:18

The human eye after lens replacement surgery

P.-C. Krüger¹, S. Langner¹, O. Stachs², R. Allemann², R. Guthoff², N. Hosten¹;
¹Greifswald/DE, ²Rostock/DE

Purpose: Today lens replacement is a basic method of cataract treatment. The evaluation of postoperative changes, especially in the area of the posterior circumference, is often inadequate using ophthalmologic standard methods such as ultrasound or optical coherence tomography. High-field magnetic resonance imaging (MRI) enables evaluation of the structures of the anterior eye segment before and after cataract surgery with high resolution and free of distortion.

Methods and Materials: Ten pseudophakic human eyes (cataract surgery) were examined ex vivo with ultra-high-field MRI (7.1 Tesla, ClinScan, Bruker BioScan) using a small surface coil and T2-weighted spin echo sequences. Different biometrical distances of the pseudophakic situation were measured and correlated with the crystalline lens situation.

Results: Ultra-high-field MRI at 7.1 Tesla provided excellent visualisation of anterior segment details especially in the area of the posterior circumference of the lens. It was possible to evaluate the postoperative changes after lens replacement without distortion and with high spatial resolution.

Conclusion: Our results suggest that MR microscopy has the potential to image small anatomical structures and to evaluate the results of surgical interventions. 7.1 T MRI provides an extremely high spatial resolution under absence of distortion artefacts. While our study was performed ex vivo, we expect that, with wider availability, ultra-high-field MR microscopy will evolve into an essential tool for both experimental studies and daily routine.

B-0890 14:27

Usefulness of perfusion-weighted MR imaging in the assessment of the effects of HIV brain infection in asymptomatic HIV-positive nontreated, HIV-positive HAART-treated and HIV-HCV-positive patients

A. Koltowska, J. Bladowska, P. Szewczyk, A. Zimny, B. Hendrich, B. Knysz, M. Sasiadek; Wroclaw/PL (annakoltowska02@gmail.com)

Purpose: HIV enters the brain early after initial exposure and can cause central nervous system (CNS) dysfunction leading to neuropsychological impairment. The aim of the study was to evaluate the impact of the HIV infection on the cerebral microcirculation in asymptomatic HIV-positive patients.

Methods and Materials: Forty-three HIV-positive asymptomatic patients: 18 HIV-positive nontreated (mean age 32.2 yrs), 18 HIV-positive HAART-treated (mean age 39.3 yrs), 7 HIV-HCV-positive (mean age 32.57 yrs), and 18 normal control subjects (mean age 33.87 yrs) were enrolled in the study. PWI was performed with a 1.5 T MR unit using dynamic susceptibility contrast (DSC) method. Cerebral blood volume (CBV) measurement relative to cerebellum (rCBV) was evaluated in the posterior cingulate region, temporoparietal and frontal association cortices as well as in the white matter of frontoparietal areas.

Results: Significantly lower rCBV values compared to normal subjects were found in temporoparietal (right $p=0.01$, left $p=0.03$) and frontal cortices (right $p=0.04$, left $p=0.03$) in all HIV-positive patients, while there were no such differences in the posterior cingulate region ($p=0.0535$) and in the white matter of frontoparietal areas (right $p=0.42$, left $p=0.92$). HIV-positive HAART-treated and HIV-HCV-positive patients demonstrated lower rCBV values in the right frontal cortex compared to HIV-positive nontreated subject.

Conclusion: The rCBV value, particularly measured in temporoparietal and frontal cortices could be a noninvasive neuroimaging biomarker for assessing the impact of HIV infection on the impairment of cerebral microcirculation in asymptomatic HIV-positive patients. These changes are the most significant in HIV-positive HAART-treated and HIV-HCV-positive patients.

B-0892 14:36

A subjective score for olfactory bulb injury in post-trauma anosmia

S. Sefidbakht, B. Khademi, H. Hoseini al Hashemi, M. Lotfi, Z. Zare, R. Jalli, M. Sefidbakht; Shiraz/IR (sepidsefidbakht@yahoo.com)

Purpose: To design a subjective grading system for olfactory bulb injury in post-trauma anosmia, and to compare it with objective measurement of olfactory bulb volume.

Methods and Materials: In 27 patients with post-trauma anosmia, olfactory bulb volumes were measured using manual tracing of the bulb in high-resolution coronal 3D FIESTA images (1.5 T GE Signa Excite). In a separate session 3 months later the olfactory bulbs were subjectively assigned to a 7-point scale by two radiologists in consensus, independently for T2 FSE and FIESTA coronal images. Bulbs were assigned a score of 0 if normal-looking, 1 if small but otherwise normal, 2 if

somehow high signal but otherwise normal, 3 if large and deformed, 4 if small and deformed, 5 if deformed and high signal, and 6 if not definitely identified. Subjective score was compared with volume using linear regression.

Results: The better and worse bulbs were $39 \pm 18 \text{ cm}^3$ and $37 \pm 31 \text{ cm}^3$ in volume, respectively. Subjective scoring in T2 FSE and FIESTA images did not correlate significantly with the better olfactory bulb volume. Subjective scoring in FIESTA images correlates significantly with the worse olfactory bulb volume ($p=0.002$). There were, respectively, 2, 17, 3, 2, 1 lesions within categories 0, 3, 4, 5, and 6.

Conclusion: A small deformed olfactory bulb is the most frequent findings in post-trauma anosmia. Subjective assessment of the olfactory bulb correlates well with objective measurement in the more severely injured bulb.

B-0893 14:45

Signal intensity profile analysis of the olfactory bulb and tract for evaluation of pathologic olfactory bulb changes in neurological and smelling disorders: comparison of 3 T, 9.4T MR microscopy, and histological sections

H.P. Burmeister¹, T. Bitter¹, P.M. Heiler², A. Irintchev¹, R. Froeber¹, P.A.T. Baltzer¹, J.R. Reichenbach¹, O. Guntinas-Lichius¹, W.A. Kaiser¹;
¹Jena/DE, ²Mannheim/DE (hartmut.burmeister@med.uni-jena.de)

Purpose: Neurological and smelling disorders (e.g. Alzheimer's disease, sino-nasal disease) negatively affect the microstructural integrity of olfactory bulb's (OB) paleocortical layers. Recovery processes depend on active restoration of this microstructural integrity enabled by neuroneogenesis in the OB. The aim of this study was to evaluate lamination patterns of the OB and adjacent tract (OT).

Methods and Materials: Twenty-four human OBs underwent in vitro standard and high-resolution T1w and T2w-imaging at 3 T. Based on signal intensity differences, OB lamination patterns were assessed by two observers in consensus. Results were compared using Wilcoxon test. Signal intensity profiles were compared to reference histological sections and imaging results using 9.4T MR microscopy. OT lamination patterns were assessed and different configurations of cross-sectional areas were compared to macroscopic results and OB lamination patterns.

Results: Standard resolution identified three (8.3%), two (83.3%), and one layer in 8.3%. High-resolution MRI (4 layers in 91.7%, 3 layers in 8.3%) significantly performed better ($P < 0.001$). Signal intensity profile analysis at 3 T and 9.4T (yielding up to 6 different signal intensities) correlated with histological sections. 3 T-MRI of the OT revealed two separate signal intensities in T2w in 75%, a hyperintense core and a hypointense sheath. Cross-sectional area configurations correlated with macroscopic results ($p=0.558$, $P=0.002$) and OB lamination patterns ($p=0.446$, $P=0.022$).

Conclusion: Signal intensity profile analysis at 3 T indicates the possibility to differentiate OB layers. Therefore, signal intensity profile analysis could be used as a future tool to assess OB recovery processes in neurodegenerative/neuropsychiatric and smelling disorders.

B-0894 14:54

Age and gender alterations in signal intensities of posterior pituitary gland on 3-dimensional T1-weighted magnetic resonance imaging

A. Yamamoto, H. Oba, J. Kotoku, S. Furui; Tokyo/JP
(asakonemurinomori@yahoo.co.jp)

Purpose: The posterior pituitary gland usually shows hyper signal intensity on T1-weighted MR images in healthy persons, but changes in the values caused by ageing or gender difference are not well recognised. This study aimed to clarify the differences in the signals of the posterior pituitary gland according to gender and age.

Methods and Materials: We retrospectively reviewed 2,255 consecutive patients who underwent cerebral sagittal 3-dimensional T1-weighted imaging on a 3 T-MRI unit between July 2010 and May 2011. We excluded patients with any endocrine, fluid balance abnormality or cysts, tumours, haemorrhages and atrophy of pituitary gland. We identified the posterior pituitary gland between the pars intermedia of pituitary gland and dorsum sellae, and regions of interest were drawn on the posterior pituitary gland and the pons. The maximum signal intensity of the posterior pituitary gland and average signal intensity of the pons were determined. We calculated the signal ratio, posterior pituitary gland/pons and analysed the changes in the signal ratio between the genders and ages.

Results: Female group showed significantly higher signal ratio than male group from 3rd to 8th decades ($r > 0.9$, $p < 0.05$). Disappearance of the high signal of the posterior pituitary gland was observed in 47 patients (36 males, 11 females, 22 - 88 years).

Conclusion: Differences in the signal intensity of the posterior pituitary gland between genders and ages exist in the general population with appropriate metabolic state and fluid balance.

B-0895 15:03

T1-weighted gradient-echo vs spin-echo sequences in gadolinium-enhanced brain imaging at 3 T: comparison in terms of image quality, flow artefacts and depiction of vessels

D. Floery, S. Kirchner, C. Ginthoer, R. Wunn, F.A. Fellner; Linz/AT
(daniel.floery@akh.linz.at)

Purpose: With 3 T MR units, T1-weighted gradient echo sequences, such as FLASH are often used instead of spin-echo (SE) sequences for brain imaging due to well-known disadvantages of SE sequences at this field strength. The purpose of this study was to evaluate contrast-enhanced FLASH vs. SE sequences in terms of image quality, flow artefacts in arterial and venous cerebral vessels, and depiction of small vessels.

Methods and Materials: In 50 patients, axial FLASH as well as SE sequences was acquired after gadolinium administration. Two radiologists assessed the following parameters in both sequences: Image quality, flow artefacts, and quality of depiction in large arteries, small arteries and dural sinuses, resp., cerebral veins (each assessed with a 3-tier scale).

Results: In all cases, overall image quality of FLASH sequence was superior to SE. In the depiction of larger arteries, FLASH was assessed superior to SE in 96% of cases whereas in the depiction of small vessels, SE was superior in 96%. Flow artefacts were completely absent in FLASH whereas SE demonstrated flow artefacts in 94% and 64%, respectively. In the visualisation of sinuses and cerebral veins, FLASH was found to be equal or superior to SE in 90%. Equally to arteries, flow artefacts were rarely found in FLASH (18% vs. 100% of cases).

Conclusion: At 3 T, T1w-GRE sequences demonstrate improved overall image quality and better depiction of large cerebral arteries and sinuses in comparison to SE sequences, while small vessels are significantly better seen with SE sequences.

B-0896 15:12

Sonographic evaluation of the intracranial pressure in adult brain injury

T. Soldatos; Athens/GR (soldatos@gmail.com)

Purpose: The optic nerve sheath diameter (ONSD) may be increased in brain-injured patients with elevated intracranial pressure (ICP). We evaluated whether ONSD measurements correlate with invasive and noninvasive ICP measurements in brain-injured adults.

Methods and Materials: We examined 106 brain-injured patients and 67 control subjects without intracranial pathology. Brain-injured patients were evaluated using Glasgow coma scale (GCS) and a semiquantitative (I-VI) neuroimaging scale (Marshall Scale, MS), and were divided into moderately ($MS=I$ and $GCS > 8$, $n=35$) and severely ($MS=II-VI$ and $GCS \leq 8$, $n=71$) brain-injured subjects. Measurements of the ONSD and noninvasive ICP (eICP), using optic nerve sonography and transcranial Doppler sonography, respectively, were performed upon admission in controls and moderately brain-injured subjects, and three times during hospitalisation in severely brain-injured patients. Upon admission, 32 severely brain-injured patients also underwent invasive ICP measurement.

Results: In severely brain-injured patients, the ONSD correlated with the MS ($r=0.76-0.82$) and the eICP ($r=0.53-0.80$) in all three evaluations, whereas ONSD and eICP were significantly increased ($6.2 \pm 0.7 \text{ mm}$ and $27.5 \pm 6.9 \text{ mmHg}$) as compared with moderately brain-injured subjects ($4.2 \pm 0.9 \text{ mm}$ and $12.2 \pm 3.7 \text{ mmHg}$) and controls ($3.5 \pm 0.8 \text{ mm}$ and $9.9 \pm 3.7 \text{ mmHg}$) ($P < 0.001$). Invasive ICP measurements also correlated with ONSD measurements ($r=0.68$, $P=0.002$). The best cut-off ONSD value for predicting elevated ICP was 5.7 mm (sensitivity=74%, specificity=100%).

Conclusion: ONSD measurements correlate with invasive and noninvasive ICP measurements, and with neuroimaging findings in brain-injured adults. Optic nerve sonography could alert clinicians to the presence of elevated ICP, whenever invasive ICP evaluation is contraindicated and/or is unavailable.



14:00 - 15:30

Room D2

Interventional Radiology

SS 1809

Experimental

Moderators:

J.H. Peregrin; Prague/CZ

M.A.A.J. van den Bosch; Utrecht/NL

B-0897 14:00

Experimental feasibility study on real-time ultrasound elastography of hepatic thermal lesions: first results

P. Wiggemann, E.-M. Jung, C. Stroszczynski;

Regensburg/DE (philippwiggemann@googlegmail.com)

Purpose: To evaluate the reliability of elastography, a new ultrasonographic method, for delineating thermal lesion boundaries in porcine liver tissue by comparing lesion dimensions determined by real-time elastography with the findings at gross pathology.

Methods and Materials: A total of 15 thermal lesions with diameters ranging from 17 to 60 mm were created using radiofrequency ablation (RFA). The new LOGIQ E9 elastography imaging technology (GE Healthcare, Wauwatosa, WI) was used with a 6-15 MHz high frequency linear transducer. Lesions were examined using B-mode and real-time elastography (RTE). Lesion detection, delineation and size were assessed using B-mode and RTE immediately after each thermal ablation. Measurements of the sections representing the same image plane used for elastography were taken at pathologic examination and compared with the measurements obtained from the elastograms.

Results: In our sample a statistically significant correlation in vitro between RTE and pathological measurements with respect to the lesions' principal axis and area ($r^2 = 0.9338$ long axis, $r^2 = 0.8998$ short axis, and $r^2 = 0.9676$ area). Overall, elastography slightly underestimated the lesion size, as judged by the digitalised pathologic images.

Conclusion: These results support that RTE outperforms conventional B-mode ultrasound and could potentially be used for routine assessment of thermal therapies.

B-0898 14:09

Radioembolisation with Y-90 glass microspheres: do we really need SPECT-CT to identify extrahepatic shunts?

T.C. Lauenstein, J. Theysohn, J. Schlaak, J. Ertle, S. Mueller, A. Bockisch, M. Forsting; Essen/DE (thomas.lauenstein@uni-due.de)

Purpose: Radioembolisation (RE) using the beta emitter ⁹⁰yttrium (Y-90) is an emerging therapy option for unresectable liver malignancies. A complication of RE may represent the nontarget embolisation of extrahepatic tissue, particularly the GI tract. We aimed to assess whether extrahepatic shunts can be reliably diagnosed based on hepatic digital subtraction angiography (DSA) or if subsequent SPECT/CT data provide additional information.

Methods and Materials: 205 patients with hepatocellular carcinoma (n=124), hepatic metastases (n=73) or cholangiocellular carcinoma (n=8) were studied. During hepatic digital subtraction angiography, 122 arteries representing shunts to extrahepatic tissue were coilembolised (right gastric artery n=86, falciform artery n= 13, branches to duodenum/pancreas n=23). Subsequently, Technetium-99m-labeled macroaggregated albumin (^{99m}Tc-MAA) was injected and patients underwent a SPECT/CT. SPECT/CT data were used to identify any additional shunt to extrahepatic tissue.

Results: 16/205 patients (7.8%) exhibited an unexpected increased MAA uptake in extrahepatic tissue (small bowel n=7, abdominal wall n=5, stomach n=4). These patients underwent repeated DSA and corresponding arteries could be identified and coilembolised in 13/16 patients.

Conclusion: Most extrahepatic shunts can be identified on DSA prior to Y-90 therapy. However, SPECT-CT data help to identify additional shunts that were initially not seen on DSA.

B-0899 14:18

Angiographic and pathological comparison of hydrogel-coated coils and fibered coils in a sheep model

A. Fohlen¹, J. Namur², M. Wassef², H. Ghegediban², A. Laurent², J.-P. Pelage¹;
¹Caen/FR, ²Paris/FR (pelage-jp@chu-caen.fr)

Purpose: To compare the angiographic and pathological features with hydrocoils and fibered coils at 24 hours and 7 days in terms of mechanism of occlusion and inflammatory response.

Methods and Materials: Six sheep had both internal iliac and renal arteries randomly embolised using fibered coils or hydrocoils. Renal arteries were embolised using 0.018 coils and internal iliacs using 0.035 coils. The number of coils and time to complete occlusion was recorded. Three animals were sacrificed after 24 hours and 3 after 7 days. Pathological evaluation consisted in characterising the mechanism of occlusion: percentage of the lumen occluded by the embolic (platinum + dacron fibres vs hydrogel) and thrombus, presence of inflammatory cells.

Results: No difference was found between hydrocoils and fibered coils for the number of coils and time to achieve vascular occlusion. At angiography, 75% of iliac arteries embolised with hydrocoils were occluded vs 67% of those embolised with fibered coils (NS). Recanalisation of the renal artery was observed in both groups. The percentage of thrombus was significantly lower for hydrocoils than for fibered coils at the 2 time points. For fibered coils, at pathology thrombus accounted for 69% of the occlusion vs 42% for hydrocoils. The presence of inflammatory cells was more frequent with fibered coils than with hydrocoils (71% vs 30%).

Conclusion: The percentage of thrombus was significantly less with hydrocoils as compared to fibered coils. Markedly lower inflammatory cell response was seen with hydrocoils. Both differences may translate into less long-term recanalisation. Further investigation is needed.

B-0900 14:27

Multipolar hepatic RFA: influence of electrode configuration on coagulation volume

P. Bruners, T. Penzkofer, P. Isfort, A. Hofmann, T. Schmitz-Rode, C.K. Kuhl, A.H. Mahnken; Aachen/DE (pbruners@ukaachen.de)

Purpose: For multipolar hepatic radiofrequency (RF)-ablation it is known that the amount of energy applied correlates with the generated coagulation volume. Our goal was to analyse whether the combination of electrodes also influences the ablation volume if the amount of applied energy is kept constant.

Methods and Materials: In total, 60 RF-ablations were performed in freshly excised bovine liver using a multipolar RF-system (CelonLabPower, Celon AG Medical Instruments, Teltow, Germany). Ten ablations were performed with each of the following RF-applicator combinations: 3x2 cm, 3x3 cm, 3x4 cm, 6x2 cm, 6x3 cm, 6x4 cm. RF-ablations were interrupted after application of 25 kJ. During the experiments time, tissue impedance and generator output were monitored using a dedicated software tool. Generated coagulation zones were dissected and macroscopically measured along x-, y-, and z-axis followed by calculation of the approximate coagulation volume. An ANOVA was applied followed by Student-Newman-Keuls tests to analyse for significant differences.

Results: The combination of 6x3 cm resulted in the largest mean coagulation volume (32 cm³). All other electrode combinations led to significant smaller coagulation volumes ranging from 25 cm³ (3x4 cm) to 29 cm³ (3x3 cm). Except for the 3x2 cm combination (13.26 min) there were no significant differences with regard to the application time (10.65 - 11.20 min).

Conclusion: Besides the amount of applied energy, the combination of RF-applicators shows an influence on the generated coagulation volume in ex-vivo liver experiments.

B-0901 14:36

Mid-term recanalisation after embolisation using hydrocoils vs fibered coils in an animal model

J.-P. Pelage¹, A. Fohlen¹, H. Ghegediban², J. Namur², A. Laurent², M. Wassef²;
¹Caen/FR, ²Paris/FR (pelage-jp@chu-caen.fr)

Purpose: To compare the angiographic and pathological effects (complete occlusion or recanalisation) of hydrogel-coated coils and fibered coils in 2 arterial territories after 7 days, 1 month and 4 months.

Methods and Materials: 12 sheep had one internal iliac and one renal artery randomly embolised using fibered coils or hydrocoils. Renal arteries were embolised using 0.018 coils and internal iliacs using 0.035 coils. All animals had control angiography performed at 7 days, 1 month and 4 months to assess recanalisation. All animals were sacrificed after 4 months. Tissue samples were embedded

in resin, sectioned and stained with methylene and toluidine blue. Recanalisation and inflammation were evaluated at pathology.

Results: After 7 days, no difference in terms of recanalisation was found between both products. At one month, 100% of the arteries embolised with hydrocoils were occluded vs 50% of those embolised with fibered coils ($p=0.004$). At 4 months, 80% of the arteries embolised with hydrocoils were occluded vs 25% of those embolised with fibered coils ($p=0.01$). A total of 60% of renal arteries embolised with hydrocoils were occluded vs 0% of those embolised with fibered coils.

Conclusion: After 4 months, 75% of the arteries embolised with fibered coils were recanalised vs 20% of those embolised with hydrocoils. It may be hypothesised that the difference is explained by the mechanism of initial occlusion (more thrombus with fibered coils).

B-0902 14:45

Portal vein ligation alone compared with portal vein and hepatic artery ligation in a rodent model

G. Jeon¹, B. Lee², S. Chung³, J. Yoon¹, J. Kim¹, J. Lee¹; ¹Seongnam/KR, ²Seoul/KR, ³Busan/KR

Purpose: Our study compared the volume change and regenerative capacity of portal vein ligation (embolisation) (PVL) and heterochronous PVL with hepatic artery ligation (HAL) in a rodent model.

Methods and Materials: Animals were separated into three groups. For group I, ligation of the left lateral and median portal vein branches was performed. For group II, ligation of the portal vein was completed, followed by ligation of the same branches of the hepatic artery after 48 h. For group III (control group), a laparotomy without ligation (sham operation) was performed. At least 5 rats from each group were sacrificed at 1, 3, 5, and 7 d after surgery. Liver volume change was measured and a liver function test performed. Using excised rat livers, we performed immunohistochemical analyses of c-kit and MIB-5. Histologic features were analysed.

Results: The volume of the nonligated lobe increased most in group II initially, but there was no significant difference at days 5 and 7. Mean AST and total bilirubin levels were significantly higher in group II and albumin levels were high in group I. C-kit positive cells were more presented on days 1 and 3 in group.i. versus group II, which was statistically significant. MIB-5-stained cells were more numerous in group.i. on days 1, 3, and 5. Necrotic changes in the ligated lobes were shown in large number of group II.

Conclusion: PVL alone is safe and effective for compensatory liver regeneration. Performing both PV and HA ligation does not result in additional benefit.

B-0903 14:54

Microwave ablation of the kidney: evaluation of cooled antegrade pyeloperfusion for protection of the collecting system in an in vivo porcine model

P. Isfort¹, T. Penzkofer¹, T. Tanaka², P. Bruners¹, T. Schmitz-Rode¹, C.K. Kuhl¹, A.H. Mahnken¹; ¹Aachen/DE, ²Nara/JP (isfort@ukaachen.de)

Purpose: To evaluate the effect of antegrade-cooled pyeloperfusion for the protection of the renal collecting system during microwave ablation.

Methods and Materials: CT-guided nephrostomy was performed in one kidney in each of 14 female house pigs using a 6 F pigtail nephrostomy catheter. Pyeloperfusion was performed using a cooled 5%-glucose solution that was infused via the nephrostomy catheter at 10 ml/sec (100 drops sec). Meanwhile microwave ablation was performed at 45 watts for 10 minutes in the irrigated and the non-irrigated kidneys creating a central and peripheral lesion. Maximum ablation diameters were measured and ablation volumes were calculated after sacrifice of the animals. The affection of the renal collecting system was assessed in the slice of maximal thermal injury (0%-100%; 10% intervals).

Results: Peripheral lesion sizes in the irrigated/ non-irrigated kidneys were 4.02±2.46 ml/ 3.49± 1.52 ml. Central lesion sizes in the irrigated/ non-irrigated kidneys were 4.81± 2.51 ml/ 3.14± 1.34 ml. Maximum thermal damage of the collecting system in peripheral lesions in irrigated/ non-irrigated kidneys were 10.0± 26.89%/ 2.1± 5.79%. Maximum thermal damage of the collecting system in central lesions in irrigated/ non-irrigated kidneys were 15.71± 26.74%/ 33.57± 34.11%. No statistically significant difference in ablation volume and affection of the collecting system was observed in central and peripheral lesions with or without cooled pyeloperfusion.

Conclusion: In microwave ablation cooled antegrade pyeloperfusion does not protect the collecting system from thermal damage. Therefore, ablation of central renal structures does not seem advisable using microwave ablation.

B-0904 15:03

An experimental study on multimodal visibility (angiography, CT and MRI) of embolisation particles performed in porcine kidneys

C.M. Sommer¹, U. Stampff¹, N. Bellemann¹, M. Holzschuh¹, N. Kortess¹, A. Kueller², J. Bluemmel², B.A. Radeleff¹, H.U. Kauczor¹; ¹Heidelberg/DE, ²San Antonio, TX/US (cmsommer@gmx.com)

Purpose: To analyse multimodal visibility of embolisation particles on angiography, CT and MRI in porcine kidneys.

Methods and Materials: As an evolution of the current available embolisation particles (Embozene® Microspheres, CeloNova BioSciences, USA), those particles were modified, that additional embedding of dense X-ray materials should result in good visibility on angiography and CT as well as additional embedding of magnetic substances should result in good visibility on MRI. Three different prototypes (Intensity A, B and C) as well as current available Embozene® Microspheres with sizes of 100±25µm and 700±50µm were tested. Without using any contrast material, renal arteries of four pigs were catheterised and each kidney was embolised with one milliliter of one type of particle. Subjective and objective particle visibility was evaluated on angiography, CT and MRI.

Results: On angiography, intensity A, B and C of 100±25µm particles as well as intensity B of 700±50µm particles were definitely visible. Current available Embozene® Microspheres given as control group were definitely not visible. On CT and MRI (T1 and T2), intensity A, B and C of 100±25µm particles as well as 700±50µm particles were definitely visible. On CT, signal-to-noise ratio for intensity A, B and C increased significantly (e.g. intensity A, 100±25µm particles: +66.5±23.7%, $P < 0.05$). On MRI (T1 and T2), signal-to-noise ratio for intensity A, B and C decreased significantly (e.g. intensity B, 700±50µm particles, T1: -73.0±8.9%, $P < 0.05$).

Conclusion: Modification of the current available Embozene® Microspheres was successful with multimodal visibility on angiography, CT and MRI.

B-0905 15:12

Ablation therapy of hepatic malignancy: a comparative study between radio-frequency and microwave ablation techniques

T.J. Vogl, A. Darvishi, P. Farshid, A. Azizi, B. Bazrafshan, N.N.N. Naguib, N.E. Nour-Eldin, S. Zangos, J. Trojan; Frankfurt/DE (t.vogl@em.uni-frankfurt.de)

Purpose: To compare the effects and outcome of radiofrequency (RFA) and microwave (MWA) ablation therapy in the treatment of primary and secondary liver malignancy.

Methods and Materials: In this prospective study approved by the institutional review board 57 patients with 63 lesions were treated with RFA and MWA. In the RFA group (21 patients), 10 patients suffered from HCC (12 lesions) and 11 patients from liver metastases (11 lesions). In the MWA group (36 patients) 40 lesions (15 HCC and 25 liver metastases) were documented. Response criteria, recurrence rate (RR) and survival indices were assessed after both procedures.

Results: In group 1, 9/12 HCC lesions (75%) showed complete response, 3/12 lesions (25%) had residual tumours. In group 2, 11/15 HCC lesions (73.3%) showed complete response, 4/15 lesions (26.6%) had residual tumours. Liver metastases showed complete response with no residual lesions after both procedures. All HCC lesions ≤2.0 cm showed complete response with no residual lesions in both groups. There was no significant difference in rates of residual HCC lesions > 2 cm between both groups ($P=0.15$, Log-rank test). Time-to-progression (TTP) in all patients treated with RFA compared with MWA was 5.6 versus 4.7 months and RR at 3, 6, 12 months were 0.0%, 16.7%, 25% versus 13%, 20%, 26.7%, respectively ($P=0.005$).

Conclusion: HCC lesions treated with RFA and MWA had statistically similar complete response rates of residual tumours, recurrence rate and survival indices. All liver metastases and all HCC lesions ≤2.0 cm had complete response with no residual tumours in both groups.

B-0906 15:21

Microwave ablation compared with radiofrequency ablation for breast tissue in an ex vivo bovine udder model

P. Isfort¹, T. Tanaka², T. Penzkofer¹, P. Bruners¹, T. Braunschweig¹, K. Kichikawa², T. Schmitz-Rode¹, C.K. Kuhl¹, A.H. Mahnken¹; ¹Aachen/DE, ²Nara/JP (isfort@ukaachen.de)

Purpose: To compare the effectiveness of microwave (MW) ablation with radiofrequency (RF) ablation for treating breast tissue in ex vivo bovine udder tissue.

Methods and Materials: MW ablations were performed at power outputs of 25 W, 35 W, and 45 W using a 915-MHz frequency generator and a 2-cm active tip antenna. RF ablations were performed with a bipolar RF system with 2- and 3-cm active tip electrodes. Tissue temperatures were continuously monitored during ablation.

Results: The mean short-axis diameters of the coagulation zones were 1.34 ± 0.14 , 1.45 ± 0.13 , and 1.74 ± 0.11 cm for MW ablation at 25 W, 35 W, and 45 W. For RF ablation, the corresponding values were 1.16 ± 0.09 and 1.26 ± 0.14 cm with electrodes having 2- and 3-cm active tips, respectively. The mean coagulation volumes were 2.27 ± 0.65 , 2.85 ± 0.72 , and 4.45 ± 0.47 cm³ for MW ablation of 25 W, 35 W, and 45 W and 1.18 ± 0.30 and 2.29 ± 0.55 cm³ for RF ablation with 2- and 3-cm electrodes, respectively. MW ablations at 35 W and 45 W achieved significantly longer short-axis diameters than RF ablations ($p < 0.05$). The highest tissue temperature was achieved with MW ablation at 45 W ($p < 0.05$). On histological examination, the ablation zone in MW ablations was less affected by tissue heterogeneity than in RF ablations.

Conclusion: MW ablation appears to be advantageous with respect to the volume of ablation and the shape of the margin of necrosis compared with RF ablation in an ex vivo bovine udder.

14:00 - 15:30

Room E1

Musculoskeletal

SS 1810a

Arthrography and advanced MR technology

Moderators:

S.G. Davies; Llantrisant/UK
M. Ruprecht; Maribor/SI

B-0907 14:00

MR arthrography of the shoulder: prospective tolerance evaluation of four different injection techniques

E. Perdikakis, A. Karantanas; Iraklion/GR (perdikakis_ev@yahoo.gr)

Purpose: To prospectively evaluate patient discomfort and technical success of four different arthrographic techniques for performing MR arthrography of the shoulder.

Methods and Materials: 125 consecutive patients (96 males and 29 females; age range, 16-67 years; mean age, 29.3) were referred for MR arthrography of the shoulder. The patients were randomly injected under fluoroscopic guidance (n1=37), with CT guidance using an anterior (n2=29) or a posterior route (n3=32) and with ultrasound guidance (n4=27). For each patient, absolute periprocedural pain on a numerical rating pain scale (0="no pain", 10="intolerable pain"), technical success of the method used and reason for MR arthrography referral were recorded. The unpaired Student t test was used to compare the patient's discomfort in the four arthrographic techniques.

Results: The technical success rate was 100% for all methods of injection (37/37, 29/29, 32/32, 27/27). The results regarding the absolute periprocedural pain were as following: fluoroscopic guidance showed a mean numerical rating pain score of 4.05 ± 1.24 , CT guidance using an anterior approach demonstrated a mean pain score of 3.87 ± 0.95 , CT guidance using a posterior route of injection showed a mean pain score of 1.59 ± 0.81 and ultrasound guiding injections a mean numerical rating pain score of 3.63 ± 1.12 . A significant difference in absolute ($P < 0.05$) pain was observed for the posterior route under CT guidance compared with the other methods.

Conclusion: No differences were found for the technical success rate of performing MR arthrography using either of the aforementioned techniques. A CT-guided posterior approach seems to be the most comfortable method for the patient.

B-0908 14:09

SLAP tears at 3.0 T shoulder MR arthrography: diagnosis with a 3D isotropic VIBE sequence versus 2D standard sequences

H. Song, W.-H. Jee, J.-Y. Jung, Y.-S. Kim; Seoul/KR (hyun0203@gmail.com)

Purpose: To retrospectively determine the reliability and accuracy of shoulder MR arthrography with a 3D isotropic T1-weighted gradient-echo sequence (volume interpolated breathhold examination, VIBE) for diagnosing SLAP tears compared with 2D standard sequences at 3.0 T.

Methods and Materials: Seventy-nine patients who underwent shoulder MR arthrography using 3.0-T imagers and subsequent arthroscopy were included. In addition to 2D standard sequences, 3D VIBE was obtained to produce multiplanar images with a 0.6-mm isotropic resolution. Each set of MR images from each method was independently scored for the SLAP tear and categorised. Diagnostic performances between 2D standard and 3D isotropic VIBE were compared with ROC curves. Interobserver agreements were assessed with kappa value.

Results: At arthroscopy, there were 33 SLAP tears: type II (n = 28), type III (n = 0), and type IV (n = 2), V (n = 3). Mean sensitivity, specificity and accuracy on 2D standard sequences were 92%, 87% and 89%, whereas mean sensitivity, specificity

and accuracy on 3D isotropic VIBE were 71%, 84% and 78%. The sensitivity was different between 2D standard and 3D isotropic VIBE in both readers. The areas under the ROC curves were statistically different: 2D standard vs 3D VIBE : 0.93 vs 0.84 for reader 1, 0.96 vs 0.87 for reader 2. Interobserver agreement was substantial: $\kappa = 0.72$ with 2D standard sequences, $\kappa = 0.68$ with 3D isotropic VIBE.

Conclusion: 3.0 T shoulder MR arthrography using a 3D isotropic VIBE has less diagnostic performance for SLAP tears compared with 2D standard MR sequences.

B-0909 14:18

Preoperative assessment of anterior shoulder instability, comparative study of MR arthrography and CT arthrography

S. Khedr; Jiddah/SA

Purpose: To compare direct MR arthrography and CT arthrography in assessment of anterior shoulder instability.

Methods and Materials: 41 consecutive patients (2 women and 39 men, age range 21-45 years) who underwent direct MRA followed by CTA within 1 hour before anterior shoulder instability repair were prospectively included in this study. MRA and CTA images were analysed by musculoskeletal radiologist and compared with arthroscopic results.

Results: In detection of glenoid rim fracture, sensitivity and specificity were 100% and 97.4% for CTA and 73.4% and 100% for MRA for HAGL lesions diagnosis; sensitivity, specificity were 100% and 100% for CTA, 100% and 96.3% for MRA. In detection of glenoid articular cartilage lesion sensitivity and specificity were 76.4% and 89.7% for CTA, and 74.8% and 93.5% for MRA. No difference was observed for detection of rotator cuff tendons tear.

Conclusion: CTA was superior to MRA in detection glenoid osseous lesions that are known to be decisional element in the surgical strategy. CTA and MRA WERE equivalent in demonstrating labroligamentous and cartilagenous lesions associated with anterior shoulder instability. CTA may be considered method of choice in preoperative evaluation of anterior shoulder instability.

B-0910 14:27

CT arthrography (CTA) of the hip and shoulder: optimisation of technique and of radiation burden in vitro and in cadavers

L. Scarciolla¹, C. Maréchal², A. Tromba², M. El Hachemi³, T. Thirion², B. Beomonte Zobel¹, P. Simon²; ¹Rome/IT, ²Liege/BE, ³Beaufays/BE

Purpose: To optimise the acquisition parameters of CTA of the hip and shoulder in order to minimise the radiation burden.

Methods and Materials: Cartilage defects were artificially created on a bovine femoral condyle. The specimen was scanned in a bath of iodinated contrast medium (meegluminie/sodium ioxagalte 320 mg/dl) changing parameters one at a time (kV, mAs). KV values spanned from 80 to 140 kV and mAs from 40 to 800. Using the same procedure, multiple acquisitions were carried out for the hips and the shoulders of 7 fresh cadavers. After imaging cadavers were frozen and multiple 4-mm slices were obtained in the coronal and axial planes with the bench saw. Anatomic specimens were compared to multiplanar reconstruction 2-mm section CTA images. Each set of values was qualitatively scored by two independent radiologists on the basis of the visibility of cartilage as following (poor=0, diagnostic quality=1, very good =2).

Results: CTA reformatted images on axial plane were judged of diagnostic value even when kV and mAs were decreased to a total dose reduction of 30% for the hip and of 50% for the shoulder, compared to the standard techniques. However, MPR coronal images obtained with a reduced dose gave a poor depiction of cartilage.

Conclusion: A reduction of the standard dose currently used to perform CTA did not influence the quality of reformatted axial MPR but was ineffective to generate MPR images of diagnostic quality in other planes.

B-0911 14:36

Capsular laxity of the hip: findings at MR arthrography

O. Magerkurth¹, J.A. Jacobson², Y. Morag², E.M. Caolli², D. Fessel², J. Sekiya²; ¹Basle/CH, ²Ann Arbor, MI/US

Purpose: To retrospectively describe MRA findings associated with capsular laxity of the hip joint found at surgery.

Methods and Materials: IRB approval was obtained. Patients with MRA and surgically assessed presence or absence of laxity of the hip joint were included. Axial T1w Images were randomised and reviewed twice by 2 independent, blinded readers. The widths of the anterior joint space lateral to the zona orbicularis and of the posterior joint space were assessed. The angle between femoral neck and ischium was measured to assess hip rotation. Statistical differences were calculated

with a t-test. Inter- and intra-reader agreement as well as correlation of widths of joint spaces with angles and volume of contrast was evaluated with a Pearson test.

Results: The study group consisted of 27 subjects of which 17 were positive and 10 negative for hip laxity at surgery. The mean width of the anterior joint space was significantly different ($p < 0.0001$) in the laxity group (6 mm) and in the group without laxity (4 mm). The mean width of the posterior joint space was significantly different ($p=0.0029$) in the laxity group (6 mm) and in the group without laxity (5 mm). There was no difference in mean femoral neck/ischium angles between the groups ($p=0.3$), mean volume of contrast ($p=0.2$). There was no correlation between the angle/volume to the widths of the joint spaces ($r:0.001-0.1$). Inter- and intra-reader agreement was high ($r:0.78-0.9$).

Conclusion: Distention of the anterior and posterior joint space was greater with hip laxity, independent of intra-articular contrast volume and hip rotation.

B-0912 14:45

MR-traction arthrography of the hip in femoroacetabular impingement

E. Schmaranzer, M. Kogler, M. Reichkendler, P. Vavron; *St. Johann/AT* (*schmaranzer@khsj.at*)

Purpose: The central compartment of the hip is usually difficult to assess by direct MR arthrography. Mostly a sufficient interface between acetabular and femoral cartilage is not achievable with traction procedures described in the literature. We therefore developed a dedicated device in analogy to the traction system for hip arthroscopy.

Methods and Materials: This dedicated traction device consists of a mobile aid made of chromium-nickel steel, not directly connected to the MR table, provided with an integrated deflection pulley for a cable winch (weight 15 to 18 kg) and a supporting plate for the contralateral lower extremity. A total of consecutive 35 patients (mean age 38 years; 18 women) were investigated after arthrography without and with traction on a 1.5 Tesla unit.

Results: Without traction the labrum was sufficient assessable in 31 patients (91.17%), the acetabular and femoral cartilage only in 2 patients (5.88%). Using traction an adequate separation of femoral and acetabular cartilage, with an average continuous interface of 2.6 mm (range from 0.7 to 6.7 mm), was achieved in 34 patients. And therefore the labrum, femoral and acetabular cartilage were sufficient detectable. Only in one case we were unable to differentiate femoral from acetabular cartilage. Excluding this patient chondral defects and labral lesions were accurately assessable.

Conclusion: These preliminary results show that the use of this traction system markedly improves diagnostic studies of the hip. The exact location of labrum and cartilage lesions is very significant as regards prognosis and of decisive importance for selection of therapy.

B-0913 14:54

Metal artefact reduction in MR-imaging at 1.5 Tesla in comparison to 3 Tesla using innovative sequence strategies

M. Reichert¹, A. Tao², M. Trelles³, R.K. Rao³, M. Nittka⁴, A. Padua⁵, S.O. Schoenberg¹, V.M. Runge³, U.I. Attenberger¹; ¹Mannheim/DE, ²Tongji/CN, ³Galveston, TX/US, ⁴Erlangen/DE, ⁵Malvern, PA/US (*Miriam.Reichert@umm.de*)

Purpose: The aim of this study is to show the feasibility of metal artefact reduction in MRI at 3 T in comparison to 1.5 T using innovative sequence strategies.

Methods and Materials: State-of-the-art techniques for metal artefact reduction including VAT and SEMAC were evaluated. T1, T2, PD and STIR images were acquired on a 1.5 T system as well as on a 3 T system. Agarose phantoms with stainless steel implants, tissue phantoms with metal implants and 3 volunteers were imaged with these techniques. Artefact reduction was assessed by measurement of the artefact volume and by blinded read.

Results: Compared to conventional acquisitions with a high bandwidth, metal artefacts judged by volume of artefact were reduced by 79%, 21%, 89% on T1 VAT, SEMAC and SEMAC-VAT at 1.5 T and 62%, 63% and 76% on T1 VAT, SEMAC and SEMAC-VAT at 3 T. T2, PD and STIR demonstrated similar artefact reduction. For artefact size, distortion of normal structures and ability to visualise the bone marrow, bone cortex and soft tissues, SEMAC-VAT were ranked superior to conventional acquisitions, as evaluated on the blinded read. For overall image quality, images were ranked as follows: SEMAC-VAT > VAT > SEMAC > conventional acquisition ($\kappa = 0.788$). SNR values were ranked SEMAC > SEMAC-VAT > conventional acquisition > VAT.

Conclusion: SEMAC-VAT substantially reduced metal artefacts for 1.5 T and 3 T scans for all evaluated image contrasts. The artefact volume is increased on 3 T but still substantially reduced by SEMAC-VAT.

B-0914 15:03

The accuracy of dynamic magnetic resonance imaging in evaluation of internal derangement of the temporomandibular joint: comparison with arthroscopic findings

M.F. Amin, A.M. Hassan, K.I. Barakat; *Elminy/EG* (*Mohammed_amin@yahoo.com*)

Purpose: To evaluate the correlation between dynamic MRI and arthroscopic findings in internal derangement of the temporomandibular joint.

Methods and Materials: The current prospective study was conducted on twenty-five patients (of 28 TMJs), eighteen females and seven males their age ranging from 20 to 42 years (mean 31 years). A control group of 10 adult volunteers (7 females and 3 males) - their age ranged from 22 to 46 years - was used to study the normal anatomical features of the TMJ as well as the dynamics of the joint. MRI was used to assess disc position, disc morphology, disc mobility, bone marrow oedema, condylar translation and joint effusion. Main outcome measures: Qualitative data were presented as frequencies and percentages.

Results: Concerning disc position, MR examination revealed 24 TMJs out of 28 (85.7%) with anteriorly displaced discs, while 4 TMJs (15.3%) showed normal disc position. When type of displacement was considered, MRI revealed 8 TMJs (28.7%) with ADDWR, while 16 TMJs (57.1%) with ADDWOR. MRI assessment of disc mobility revealed 12 out of 28 TMJs (42.8%) with limited asynchronous movements, while 3 TMJs (10.7%) with stuck disc, and 13 TMJs (46.4%) with normal mobility.

Conclusion: Both arthroscopy and dynamic MRI are statistically correlated to each other in detecting TMJ internal derangement. Nevertheless, reviewing the results highlighted the advantages of MRI augmented by dynamic protocol over arthroscopy in diagnosing disc position and mobility and hence we recommend using MRI as a first line diagnostic modality when internal derangement is suspected.

B-0915 15:12

Assessment of articular cartilage repair tissue after matrix-associated autologous chondrocyte transplantation or the microfracture technique in the ankle joint using diffusion-weighted imaging at 3 Tesla

S.R. Apprich¹, S. Trattnig¹, G.H. Welsch², I.M. Noebauer-Huhmann¹, S. Domayer¹; ¹Vienna/AT, ²Erlangen/DE (*sebastian.apprich@meduniwien.ac.at*)

Purpose: The purpose was to compare patients after matrix-associated autologous chondrocyte transplantation (MACT) and microfracture therapy (MFX) of the talus using diffusion-weighted imaging (DWI), with morphological and clinical scoring.

Methods and Materials: Twenty patients treated with MACT or MFX (ten per group) were examined using 3 T MRI at 48±21.5 and 59.6±23 months after surgery, respectively. For comparability, patients from each group were matched by age, body-mass index, and follow-up. AOFAS score served as clinical assessment tool pre- and postoperatively. DWI was obtained using a partially balanced, steady-state gradient-echo pulse sequence, as well as the MOCART score, based on a 2D-PDw-TSE-sequence and a 3D-iso-TrueFisp-sequence. Semi-quantitative diffusion quotients were calculated after ROI analysis of repair tissue (RT) and healthy control cartilage, and compared among both groups.

Results: The mean AOFAS-score improved significantly ($P=0.001$) for both groups (MACT: 48.8±20.4 to 83.6±9.7; MFX: 44.3±16.5 to 77.6±13.2). No differences in the AOFAS ($P=0.327$) and MOCART ($P=0.720$) score were observed between MACT and MFX postoperatively. DWI distinguished between healthy cartilage and cartilage RT in the MFX group ($P=0.022$), but not after MACT treatment ($P=0.208$). Correlation was found between MOCART score and DWI (Pearson: -0.461; $P=0.041$) and a trend for a correlation between BMI and DWI (Pearson: 0.435; $P=0.055$).

Conclusion: Whereas conventional scores reveal a similar outcome after MACT or MFX treatment in the ankle joint, DWI was able to distinguish between different RT qualities, as reported histologically for these diverse surgical procedures.

B-0916 15:21

Feasibility of gagCEST imaging on a clinical 3 T MRI system: initial results and comparison with sodium imaging at 7 Tesla

B. Schmitt, G.H. Welsch, S. Zbyn, S. Goed, S. Trattnig; *Vienna/AT* (*benjamin.schmitt@meduniwien.ac.at*)

Purpose: Evaluation of feasibility to perform gagCEST imaging on a clinical 3 T MRI system in nine patients with knee pain and three healthy volunteers.

Methods and Materials: Morphological MRI and gagCEST imaging were performed on a clinical 3-T-TimTrio. Sodium imaging was carried out on a Siemens 7-T whole body system using a modified GRE sequence. Signal distributions in healthy cartilage of volunteers were determined as a reference for pathological changes. Sodium imaging and gagCEST performed in patients were compared

with respect to cartilage signal intensities from ROIs in healthy cartilage (NT) and ROIs adjacent to apparent morphological lesions (AT, minimum distance: 3 mm). Evaluation was performed separately by two readers. Statistical relations between techniques were assessed using non-parametric tests.

Results: Absolute gagCEST values from ROIs in various cartilage areas of the volunteers significantly followed Gaussian distributions and exhibited positive mean values in the order of 3 to 5%. Patients exhibited consistently lower average gagCEST signals in AT (0.49±1.79%) compared to NT (2.76±2.93%). These results were confirmed by sodium imaging, where a mean signal intensity of 458.28±124.69 was measured in NT and 415.28 ± 124.69 in AT. Intra-class correlation between readers yielded $R^2 = 0.852$ for gagCEST values and $R^2 = 0.990$ for sodium signal intensities.

Conclusion: We demonstrated that it was possible to obtain 3D gagCEST datasets in reasonable scan time with the presented technique. The results of this study, especially the strong correlation of gagCEST with sodium imaging, clearly suggest the feasibility of gagCEST imaging in a routine clinical setting.

14:00 - 15:30

Room E2

Paediatric

SS 1812

Neuro and fetal imaging

Moderators:

J.-F. Chateil; Bordeaux/FR

J. Geiger; Freiburg/DE

B-0917 14:00

Effect of x-ray tube parameters and iodine concentration on radiation dose and image quality in paediatric and adult brain CT angiography: a phantom study

A.E. Papadakis, K. Perisinakis, M. Raissaki, J. Damilakis; Iraklion/GR

Purpose: To assess the effect of x-ray tube parameters and iodine concentration on radiation dose and image quality in paediatric and adult brain CT angiography.

Methods and Materials: A new type of brain vascular lesion phantoms was devised in our lab. Cylindrical vessels were bored along the brain equivalent plugs of physical anthropomorphic head phantoms that simulate the average individual as neonate, 1-year, 5-year, 10-year-old child, and adult. To simulate vascular lesions of different diameter, vessels of 0.6 mm, 1 mm, 2 mm, and 3 mm were created. These vessels were filled with iodine solutions of different concentration. Phantom heads were scanned using standard kVp and mAs settings prescribed by the routine examination protocol for each age and at reduced kVp and mAs exposure settings. Acquisitions were performed on a 16-slice CT scanner using i) fixed mAs and ii) automatic exposure control (AEC). Contrast-to-noise ratio (CNR) was calculated based on the Hounsfield Unit values measured within contrast-enhanced and unenhanced regions of interest.

Results: CNR values varied from 33 ± 2.1 for the 1-year-old child to 61 ± 3.4 for adult at standard exposure settings. CNR values increased linearly with mAs settings, vessel diameter, iodine concentration ($P < 0.0001$) and were optimum at 100 kVp. AEC activation reduced dose by up to 37% without significant degradation of CNR ($P > 0.05$).

Conclusion: Exposure settings and iodine concentration can be further reduced during paediatric and adult CT angiography without significantly affecting CNR. Our findings can be used to determine these minimum exposure settings and iodine concentration.

B-0918 14:09

Bismuth shielding and automatic tube current modulation during paediatric head CT

M. Raissaki, A. Papadakis, K. Perisinakis, J. Damilakis; Iraklion/GR (mraissaki@yahoo.gr)

Purpose: To study the effect of orbital bismuth shielding combined with ATCM on tube current and image noise.

Methods and Materials: Four anthropomorphic phantoms (ATOM phantoms, CIRS Inc., Norfolk), representing the average head of newborn, 1, 5, and 10-year old were scanned on a Siemens Somatom Sensation 16 scanner a) with fixed tube current b) with ATCM c) with ATCM and a shield on orbits before scout acquisition d) with ATCM and a shield on orbits after scout acquisition. Noise was measured as SD of HU by drawing 0.5 cm³ regions of interest in homogeneous-appearing areas at both orbits, temporal, frontal, parietal lobes for each scan.

Results: CDTIs were 20.21 mGy/100 mAs in all scans. Current reduction over the eyes was 5-43.5% (mean 22.5%) and overall 20.9-46.4% (mean 32.2) with the neonate-equivalent scans benefiting most from ATCM. Noise exhibited a statistically significant increase when AEC was employed compared to fixed mA with or without shielding. Noise exhibited further significant increase when shields were positioned after scout acquisition.

Conclusion: ATCM is a requisite during paediatric head CT and when employed, tube current is not affected by bismuth shield placement. Shields cause increase in image density over the eyes especially in neonates, irrespectively of fixed or reduced current. Brain density is minimally affected by shield placement.

B-0919 14:18

A local dose survey of cranial CT in children: comparison with different European DRL levels and possibilities for dose optimisation

T.H.E. Mulkens, P. Bellinck, R. Salgado; Lier/BE (tom.mulkens@scarlet.be)

Purpose: To compare the dose level of our cranial CT protocols in children with recent European DRL levels of 5 different European countries and propose objectives for dose optimisation.

Methods and Materials: Cranial CT is the most common CT examination in children. Although dose reduction and optimisation of CT in children is mandatory, there are, compared with adult CT, no established European dose reference levels (DRL). We reviewed the dose values of our cranial CT protocols in children of 2010 (n=124), according to age. They were compared with the mean DRL levels of 5 different European countries, published in the last years (2003-2009).

Results: Following mean cranial dose levels of CT in children were obtained: < 1 year (n=14): CTDI vol of 11.34 mGy, DLP of 177.86 mGy.cm and effective dose: 1.96 mSv, 1-5 year (n=37): CTDI vol of 19.12 mGy, DLP of 330.19 mGy.cm and effective dose 2.21 mSv, 5-10 year (n=31): CTDI vol of 27.37 mGy, DLP of 492.45 mGy.cm and effective dose of 1.97 mSv and 10-15 year (n=32): CTDI vol of 43.08 mGy, DLP of 755.48 mGy.cm and effective dose of 2.27 mSv. Compared with the mean DRL level of 5 different European countries our protocols showed following dose reduction: < 1 year: 62%, 1- 5 year: 49%, 5-10 year: 28% and 10-15: 9%.

Conclusion: Our local dose survey showed that dose reduction is possible in cranial CT of children, especially in younger children.

B-0920 14:27

Evaluating the diagnostic accuracy of ultrasound in craniostylosis among infants under 1 year

N. Najmi; Tehran/IR



Purpose: Various imaging modalities have been studied for accurate diagnosis of craniostylosis. Ultrasound is a non-invasive, available, low-cost modality, and above all is free of side effects (complications). The current study has been performed to assess the diagnostic accuracy of ultrasound compared to CT scan as a gold standard in the diagnosis of craniostylosis.

Methods and Materials: Forty four infants under 1 year were included in the study. All of the infants were clinically suspected to have craniostylosis and were referred to department of radiology in Tehran children medical centre. Data were gathered from 2007 to 2008. Infants were first sonographically examined by a paediatric radiologist and were later referred to another paediatric radiologist to examine CT scan with 3D reconstructed images of skull as gold standard modality. The second radiologist was blinded to results of the ultrasound.

Results: Seventeen girls and 27 boys were included in the study. There was no difference in head circumference and age between boys and girls. Sensitivity, specificity, positive and negative predictive values of ultrasound versus CT scan were 96.9%, 100%, 100%, and 92/3%, respectively. There was no significant difference in diagnostic accuracy of ultrasound between girls and boys, and between infants under 6 months and infants older than 6 months.

Conclusion: The high specificity of ultrasound helps to correctly rule out craniostylosis in clinically suspected cases and thus can prevent unnecessary exposure of healthy infants to CT scan ionising radiation.

B-0921 14:36

Magnetic resonance imaging of diffuse axonal injury in acute period of paediatric crano-cerebral trauma

I. Melnikov, T. Akhadov, N. Semenova, A. Petryaikin, S. Sidorin, S. Gur'yakov; Moscow/RU

Purpose: The true degree of brain injury with DAI can be fully assessed with MRI, which is more sensitive to acute damages, than other methods of radiological diagnostics.

Methods and Materials: We have retrospectively analysed medical records and imaging findings of 24 children with DAI, aged from 1 to 17 years, who admitted to our hospital in 2010. According to GCS in 4 cases we classified trauma as mild, in 4 cases as moderate and in 16 cases as severe. The average GCS score of all patients on admission was 6.9. In all cases MRI was performed in a period from several hours till 3 days from the moment of injury. For this study, we used the following protocols: axial T2-TSE, T2-FLAIR and T2-FFE, sagittal T2-FLAIR and T2-FFE, coronal T1-FLAIR. Diffusion-weighted imaging (DW-EPI with 3 encoding directions, $b=0$ s/mm² and $b=1000$ s/mm²) in axial projection was performed in 10 patients.

Results: Small haemorrhagic lesions on white matter of brain hemispheres were classified as grade I lesions (8 patients); in case when additional lesions in corpus callosum were present, they were classified as grade II (7 patients); combination of above-mentioned lesions with ones located in brainstem was classified as grade III (9 patients). Pathological changes, revealed with DWI in 10 patients, were typical: hyperintense signal on DW maps and hypointense signal on ADC maps.

Conclusion: In patients with severe clinical decompensation MRI more often reveals lesions in corpus callosum and brainstem, which indicates that grade III DAI is present. Diffusion-weighted imaging performed in acute period of paediatric cranio-cerebral trauma can reveal either the presence of perifocal oedema or the presence of ischaemic form of DAI, in cases where the haemorrhage in the lesions are not detected.

B-0922 14:45

Impairment of the branches of the deep cerebral veins on neonatal germinal matrix haemorrhage using susceptibility-weighted imaging

T. Niwa, N. Aida, Y. Fujii, T. Okabe, K. Nozawa, Y. Tachibana, J. Shibasaki; *Yokohama/JP (tniwa@kcmc.jp)*

Purpose: Germinal matrix haemorrhage (GMH) occurs with a hypoxic-ischaemic insult in preterm infants. The purpose of this study was to assess the relationship between GMH grade and the visualisation of the branches of the deep veins in infants using susceptibility-weighted imaging (SWI).

Methods and Materials: Thirty-three infants (gestational age, 23-36 weeks; corrected age at MRI, 33-46 weeks) with GMH, who underwent SWI, were retrospectively assessed. GMH was graded with associated finding: grade I; no intraventricular haemorrhage; II, GMH extending into the ventricle; III, intraventricular haemorrhage with ventricular enlargement; VI, parenchymal haemorrhage. Visualisation of each branch of the deep veins (i.e., anterior septal, anterior caudate, thalamostriate, medial and lateral atrial, internal cerebral, and basal veins) on SWI was rated using a four-point scale by two experienced paediatric neuroradiologists. GMH grade was compared to the score of the visualisation of the each deep vein branch. Interobserver agreement was also assessed.

Results: The grade of GMH included I in 12, II in 9, III in 2, and IV in 10. There was a significant difference in the score of visualisation of the thalamostriate vein among the infants according to the GMH grades (reader 1, 2; $p=0.02, 0.04$, respectively); the visualisation of the vein in infants with GMH-grade IV was significantly impaired compared to that with GMH-grade I (reader 1, 2; $p=0.01, 0.01$, respectively). Interobserver agreement was moderate to excellent (intraclass correlation coefficient, 0.63-0.86).

Conclusion: GMH with parenchymal haemorrhage may be accompanied with more frequent impairment of the branches of the deep veins.

B-0923 14:54

Fractional anisotropy of the foetal midbrain and myelination

R. Voitek, G. Kaspran, M. Weber, P.C. Brugger, D. Prayer; *Vienna/AT (ramona.voitek@meduniwien.ac.at)*

Purpose: In rat-pups diffusion anisotropy imaging has been shown to demonstrate postnatally increasing white matter myelination of the brainstem more sensitively than other conventional imaging modalities (Prayer D, *Neuroradiology* 1997). We investigated whether diffusion tensor imaging (DTI) in foetuses with normal CNS development is capable of showing changes in fractional anisotropy (FA) or apparent diffusion coefficient (ADC) in the midbrain correlated with gestational age. An increasing FA would point to ongoing prenatal myelination as myelin constrains diffusion perpendicular but not parallel to fibres.

Methods and Materials: During clinically indicated MRI (1.5T) in 63 foetuses (17-38 GW, normal CNS development) T2W-FSE sequences in three orthogonal planes of the foetal brain and an axial, single-shot, echo planar diffusion tensor sequence (32 non-collinear diffusion gradient encoding directions) perpendicular to the long axis of the foetal brainstem were acquired. After coregistering T2W-FSE axial images with axial FA colour-coded maps a region of interest (ROI) was drawn in the midbrain to calculate FA and ADC.

Results: A significant positive correlation between gestational age (GA) and FA was found ($r=.503, p<.001$) but no significant correlation was found between GA and ADC ($r=-.209, p=.103$).

Conclusion: We could show a significant positive correlation of GA with FA but not with ADC in the foetal midbrain. Increasing FA during gestation can be explained by increasing myelination. Therefore, FA measurements are capable of demonstrating prenatal myelination in foetuses with normal CNS development and might serve to investigate (ab-)normal myelination or brainstem compression in hydrocephalus or Chiari II malformations.

B-0924 15:03

Role of foetal MRI in the evaluation of cerebellar morphostructure and biometry

L. Manganaro, A. Tomei, F. Fierro, S. Bernardo, V. Vinci, P. Sollazzo, M.E. Sergi, E. Silvestri, M. Marini; *Rome/IT (sivvia@gmail.com)*



Purpose: Our study aimed to investigate the role of foetal MRI in the evaluation of cerebellar morphostructure in order to define main biometrical parameters which allow cerebellar pathologies detection.

Methods and Materials: From June 2006 to April 2011, we enrolled 59 women with previous US suspect of posterior cranial fossa alteration, we performed 59 foetal MRI exams of cerebral region. We excluded cases with diagnosis of Arnold Chiari Malformation and of space-occupying not cystic-like lesion. We evaluated main biometrical parameters of the cerebellum, vermis morphology and biometry, IV ventricle, brainstem, cerebellar pontine angle, cisterna magna and tentorium insertion.

Results: Foetal MRI detected alteration of the posterior cranial fossa in 39/59 cases, thus excluding the US suspect of pathologies in the remaining 20 cases. We diagnosed in 5/39 cases Dandy Walker malformation, in 13/39 cases partial vermis agenesis, in 7/39 vermis hypoplasia (4/7 secondary to cystic-like lesions), in 3/39 cases malrotation, in 6/39 cases cisterna-magna dilatation, in 1/39 cases ponto-cerebellar hypoplasia, in 2/39 ischaemic-haemorrhagic lesions of the cerebellum, at last in 1/39 cases we diagnosed a reduction of the cranial-cerebellar biometry. MRI results were compared with autopsy in 56 cases, our results were confirmed in 52 cases (18 TN and 36 TP), 4 were misconfirmed.

Conclusion: Foetal MRI of the cerebral region revealed useful as third level diagnostic technique in cases of posterior cranial fossa pathologies in order to confirm and characterise the various malformation thanks to the multiplanes orientation which allows to study biometry and morphology of all the structures involved.

B-0925 15:12

MR lung volume assessment at different times of gestation for prediction of survival, need for ECMO-therapy and development of chronic lung disease in fetuses with congenital diaphragmatic hernia

A. Walleyo, A. Debus, S. Kehl, C. Weiss, S.O. Schönberg, T. Schaible, K.A. Buesing, K.W. Neff; *Mannheim/DE (anna.walleyo@umm.de)*

Purpose: Purpose of the study was to investigate the prediction of survival, need for extracorporeal membrane oxygenation (ECMO) and development of chronic lung disease (CLD) in patients with congenital diaphragmatic hernia (CDH), regarding a classification in three different times of gestation (< 28, 28-32, > 32 weeks gestation), by assessing the observed/expected MR fetal lung volume (o/e MR FLV).

Methods and Materials: 226 foetuses with CDH were included for data analysis. MRI was performed at different times of gestation (56 foetuses < 28, 50 foetuses 28-32, 120 foetuses > 32 weeks gestation), using T2-weighted half-Fourier acquired single-shot turbo spin echo (HASTE) imaging. Receiver operating characteristic curve (ROC) analysis was applied to investigate the prognostic quality of the assessment of the o/e MR FLV at different times of fetal growth.

Results: For all reviewed times of gestation the o/e MR FLV yielded almost equivalent statistically significant differences for neonatal survival and nonsurvival ($p\leq 0.0029$), need for ECMO therapy ($p\leq 0.0195$) and development of CLD ($p\leq 0.0064$) or not. Complemented were these results by high prognostic accuracy for early likewise for late times of gestation. ROC analysis showed the highest area under the curve ($AUC\geq 0.819$) for neonatal survival.

Conclusion: In patients with CDH the o/e MR FLV is a valuable prognostic parameter to predict neonatal mortality, morbidity represented by the development of CLD and need for ECMO therapy already in early weeks gestation (< 28 w.g.) as well as in later times of gestation with no statistically significant differences.

B-0926 15:21

Utilisation of neonatal brain MRI: experience, variation and implications: a survey study of UK level 3 neonatal units

C. Sayer¹, L. Vitta²; ¹Brighton/UK, ²Hove/UK

Purpose: To compare the use, experience and variation of MRI for neonatal brain imaging in level 3 neonatal units in England, UK.

Methods and Materials: An electronic questionnaire was sent to neonatologists working in all level 3 units. Participants were asked 21 questions relating to their experience of MRI, indications for its use, practical aspects (sequences, timing, access and wait), procedure for reporting images and use of MRI in comparison to other tests.

Results: 34% (n = 71) of the survey population, representing all 44 separate units, responded. 49.3% had no local/regional guidelines. A significant number (19.3%) claimed that lack of clear guidelines contributes to prolonged wait for MRI. Ultrasound is still used as the first line in the majority of units. MRI is frequently second line based on scanner location, staffing issues and cost. 45% consider prolonged waiting times to be a problem. There is a significant association between MRI availability and lack of guidelines with a failure to utilise the optimal sequences and timing as recommended in the literature.

Conclusion: This important survey highlights a considerable variation in practice and availability. This may be resulting in delayed imaging in cases where MRI is vital for diagnostic and prognostic information as well as suboptimal use of a modality that has been well established in the research literature. It is vital to establish a more uniform and robust neonatal neuroimaging pathway and this work is a powerful tool for understanding current practice and working towards a set of national guidelines for the UK.

14:00 - 15:30

Room F1

Genitourinary

SS 1807

GU gems and jewels

Moderators:

M.A. Cova; Trieste/IT
D. Yakar; Nijmegen/NL

B-0927 14:00

Testis cancer: MDCT staging with histopathological correlation

A.M. Osborne¹, D. Halpenny¹, P. Burke², D.W. Good¹, W.C. Torreggiani¹;
¹Dublin/IE, ²Limerick/IE (osbornea@tcd.ie)

Purpose: To assess whether testis cancer metastasises to specific sites using MDCT according to specific primary histopathological diagnosis.

Methods and Materials: A ten-year retrospective database was created including patients who underwent orchiectomy for testicular tumour in a single institution. All patients underwent MDCT thorax, abdomen, pelvis. The histology of the primary tumour and the location of any metastases present on MDCT were categorised and recorded. Data are presented as median (interquartile range: IQR) and logistic regression analysis was used to identify risk factors.

Results: 255 patients were identified. The median (IQR) age was 32 (26-37) years. 23.9% of patients had nodal metastasis at the time of diagnosis with 5.1%, 21.6% and 2.7% having pelvic, abdominal and supra-diaphragmatic nodal metastasis, respectively. 5.5% had solid organ metastasis at diagnosis. Independent risk factors for abdominal nodal metastasis included having a teratoma (HR: 3.04, 95% CI: 1.31-7.06, P=0.009) and having an LDH over 500 at diagnosis (HR: 3.83, 95% CI: 1.68-8.78, P=0.001). Independent risk factors for supra-diaphragmatic nodal metastasis included having a mixed tumour (HR: 4.62, 95% CI: 1.02-21.06, P=0.048) and having a β -HCG over 10 mL/mL at diagnosis (HR: 4.40, 95% CI: 1.04-18.67, P=0.044).

Conclusion: Results indicate that the pattern of metastasis can vary according to histological subtype and staging of tumour. Results suggest that patients who present with mixed testis tumours and patients with a serum β -HCG over 10 mL/mL should undergo CT thorax as part of staging of disease.

B-0928 14:09

Diffusion-weighted magnetic resonance imaging in patients selected for radical cystectomy: detection rate of pelvic lymph-node metastases

R. Cazzato, R. Del Vecovo, E. Faiella, F. D'Agostino, R. Francesco Grasso, B. Beomonte Zobel; Rome/IT

Purpose: To evaluate whether DW-MRI improves the detection rate of pelvic lymph node metastases in a cohort of patients with muscle invasive bladder cancer selected for radical cystectomy.

Methods and Materials: Nineteen consecutive patients with muscle invasive bladder cancer were enrolled between April and September 2010. Patients pre-operatively underwent 1.5-T MRI using conventional sequences combined with DW-MRI. Radical cystectomies with extended lymphadenectomy were performed in all patients. Diagnostic accuracy of DW-MRI was compared with the histopathologic findings according to a chart where the following nodal stations were recorded: right- and left-side common, internal and external iliac vessels, right- and left-side obturator station, presacral station.

Results: The mean ADC value was of 0.85×10^{-3} mm³/sec in the nodal metastatic group and 1.00×10^{-3} mm³/sec in the nodal non-metastatic group (P 0.02, standard error, 0.06; 95% CI, 0.022 to 0.270). The ADC cut-off value, obtained by the ROC curve in order to show the best separation between metastatic and non-metastatic lymph nodes was 0.86×10^{-3} mm³/sec. With this threshold value the patient-based sensitivity, specificity, PPV and NPV of the Dw-MRI were 71%, 90%, 86% and 79%, respectively.

Conclusion: DW-MRI may be used to differentiate metastatic from non-metastatic lymph nodes in patients with high grade bladder cancer.

B-0929 14:18

Does USPIO-enhanced diffusion-weighted MRI enhance the diagnostic accuracy of lymph-node staging in normal sized lymph nodes of patients suffering prostate or bladder cancer?

J.M. Froehlich, M. Triantafyllou, D. Chong, A. Fleischmann, F.D. Birkhaeuser, H.C. Thoeny; Berne/CH (froehlich@klus-apotheke.ch)

Purpose: To prospectively determine whether diffusion-weighted MRI (DW-MRI) after the administration of ultrasmall superparamagnetic iron oxide nanoparticles (USPIO) increases the diagnostic accuracy for the detection of metastases in normal sized lymph nodes in patients with bladder and/or prostate cancer.

Methods and Materials: Seventy-five patients (9f,66m; mean age 64) with bladder (n=18), prostate cancer (n=49) or both (n=8) were examined preoperatively on a 3 T MR unit before and after administration of USPIO (Sinerem, Guerbet). T1- and T2-weighted 3D TSE Space sequences of the entire pelvis were performed besides axial EPI-DW-MRI with 3 b-values (0.500,1000sec/mm²) after spasmolysis with 1 mg iv glucagon. Suspicious hyperintensive structures on the post-contrast high b images were correlated with morphological pre-contrast images to check whether they corresponded to lymph nodes. Each visualised lymph node depending on its morphology was rated as malignant or benign. Readings were performed by three independent blinded readers and compared to histopathology.

Results: In 75 patients, 2993 lymph nodes (mean number 40/patient) were resected. 54 positive lymph node metastases were detected in 20 patients with 43 nodes beyond a short-axis diameter of 3 mm. Readings on a patient level yielded a mean sensitivity of 70%, specificity of 93.9%, positive predictive value of 80.8%, negative predictive value of 89.6% and diagnostic accuracy of 87.6%. No metastasis above a short-axis diameter of 5 mm was missed.

Conclusion: USPIO-enhanced DW-MRI allows for higher diagnostic accuracy in the detection of metastases in normal sized lymph nodes in patients with bladder and/or prostate cancer.

B-0930 14:27

Ultrasmall particles of iron oxide-enhanced MR-imaging of ischaemic acute renal failure in a rat model on a clinical 3 T scanner

H.J. Michaely, U. Benck, U. Goettmann, T. Runge, B.K. Kraemer, S. Haneder, S.O. Schönberg; Mannheim/DE (henrik.michaely@umm.de)

Purpose: To assess if the novel ultrasmall-particle-of-iron-oxide (P904) can be used to visualise ischaemic acute renal failure (IARF) in a rat model.

Methods and Materials: In this IRB-approved study 10 Lewis-rats underwent transient surgical clipping of the left renal artery for 45 min. 36 h after the surgical procedure the rats were injected 516 μ mol/kg P904 (Guerbet) and MR-imaging was performed another 36h after the P904-injection. Imaging was performed on a clinical 3 T scanner (Siemens TimTrio) with a dedicated 8-element rat coil (Rapid-Biomedical) with T2w-TSE sequences in coronal (TR/TE 2000/114 ms, acquisition time 2:33 min) and axial (3090/115 ms, 3:47 min) orientation with identical acquired

spatial resolution of 0.3x0.3x1.0 mm³. Signal-to-noise measurements (SNR) were performed in the cortex, medulla and pyelon of the IARF-kidney and the contralateral kidney as internal control. Immediately after the MR-exam the rats were sacrificed for histology and immunolabelling.

Results: Apparent differences between the IARF-kidneys and controls were encountered. Signal drop was mainly seen in the medulla of the IARF kidneys. The SNR of the IARF vs. control: cortex 19.6 vs.11.3 (p=0.007), medulla 4.5 vs. 21.3 (p < 0.001) and pyelon 14.6 vs. 34.0 (p=0.03). In all IARF-kidneys the histology confirmed the predominantly medullary presence of abundant iron and ED1-positive macrophages and typical changes of IARF while being normal in the control group.
Conclusion: P904 seems to be a suitable contrast agent to non-invasively detect IARF in a rat model with good correlation to histology. This suggests that P904-enhanced MR-imaging holds promise for non-invasive assessment of renal parenchymal diseases.

B-0931 14:36

Sonoelastography in patients with endometriosis of different location

N.A. Vorontsova, V.E. Gazhonova, S.O. Churkina, E.B. Savinova, I.A. Ponomorenko, A.V. Zubarev; *Moscow/RU (vornad@bk.ru)*

Purpose: The aim of this study was to assess the usefulness of SE (sonoelastography) for evaluation of patients with endometriosis.

Methods and Materials: 80 consecutive pts (with pelvic pain, dysmenorrhoea, urinary symptoms) range 18-45years with suspected diagnosis of endometriosis were referred for SE. All patients underwent conventional US and SE on HI VISION Preirus with an endocavity transducer (8-4 MHz frequency) and linear transducer (frequency 7.5-13 MHz). We used modified Tsukuba SE classification for evaluation of the SE data. 15 diagnostic biopsy, 39 diagnostic laparoscopies, 26 separate diagnostic scraping were performed with morphological study of the received material. US data (conventional B-mode, US angiography and SE) were assessed by comparing the findings with surgery results and MRI data. US data were retrospectively reviewed by 2 radiologists. Inter-observer agreement for endometriosis SE score, location of endometriosis (uterine, ovarium, cervix, urinary bladder's wall, soft tissue), endometriosis location by walls of the uterus, MRI data.
Results: Pathomorphological examination revealed 32/endometriotic cysts, 7/endometriosis the uterine wall, 26/endometrial polyps, 6/endometriosis of urinary bladder's wall, and 9/endometrial infiltrations of pelvic soft tissue. Endometriosis was characterised by reversed score 1, score 3 and score 5 of Tsukuba classification for lesions on SE. SE showed good to moderate inter-observer agreement for endometriosis evaluation by scoring (k=0, 8-0, 95), for endometriosis locations by walls of the uterus (k= 0.78-0.94), for locations of endometriosis by organs (k =0.74 -0.87), poor to moderate inter-observer agreement for endometriosis evaluation by MRI data (k=0.21-0.35).

Conclusion: US with SE offers a new possibility for definition of endometriosis.

B-0932 14:45

Possibilities of real-time sonoelastography in local staging of endometrial cancer

I.S. Belozeroval, V.E. Gazhonova, S.O. Churkina, A.L. Lozovator, T.S. Kurganskaya, A.V. Zubarev; *Moscow/RU (nibelozeroval@yandex.ru)*

Purpose: Possibilities of sonoelastography (SE) in local staging of endometrial cancer.

Methods and Materials: 42 pts with proven EC underwent real-time sonoelastography before surgery (age range 37-72 y.o.). US exams were performed on HI VISION Preirus and HI VISION 900 (Hitachi Medical Corporation). We used FIGO classification for local staging EC. US data were compared with final histopathology. The study was recorded and evaluated by 2 independent readers. Inter-observer agreement for tumour's location by walls (anterior, posterior, fundus, right, left), myometrial invasion (less than 1/2, more than 1/2), cervical and capsular involvement were studied. Sensitivity of SE in local staging was established.

Results: All patients have been operated (17 total hysterectomies, 25 radical hysterectomies with lymph node dissection). Histopathology revealed 17/stage IA, 15/stage IB, 5/stage IIA, 3/IB stage, 2/IIIAstage. The sensitivity of SE for local staging of EC: 89% - stage IA, 90% - stage IB, 84% - stage IIA, 94% - stage IIB, 93% - stage IIIA. The Kappa value between SE and location by walls was poor (k ranged 0.3 to 0.5), between SE and myometrial invasion was good (k ranged 0.76 to 0.84) and between SE and cervical invasion was poor too (k 0.4-0.66). SE increased the sensitivity of US (from 83% to 92.5%) and specificity (from 81% to 90.3%) in local staging EC.

Conclusion: Inclusion of SE in complex ultrasound scanning may help to evaluate myometrial invasion in pts with EC.

B-0933 14:54

Real-time compression elastography of the peripheral zone prostatic cancer: the impact in improving the diagnostic approach

G. Zacharopoulos, S. Yarmenitis; *Maroussi/GR (spyros.yarmenitis@gmail.com)*

Purpose: To evaluate the performance of real-time compression elastography (RTCE) in the diagnostic approach of the peripheral zone prostatic cancer.

Methods and Materials: Sixty-three male individuals were examined with both b-mode TransRectal Ultrasound (TRUS) and RTCE using a Hitachi/Preirus machine. Elastic properties of the Peripheral zone were classified as 1. normal tiffness, 2. inhomogeneous/inconclusive, 3. focal lesions of increased stiffness. The TRUS findings were categorised as 1. no focal lesion, 2. ill-defined focal lesion and 3. definite focal lesion. In 43 patients 10-12 core biopsies were taken. The rest 20 patients had 6-8 core biopsies. Ultrasound findings were compared to the results of the core biopsies.

Results: Nineteen of 63 patients (30%) were found with positive specimens for prostatic cancer. Sensitivity of prostate cancer detection was 84%(16/19) for the RTCE and 68%(13/19) for b-mode TRUS. RTCE score1 was found in 39 patients of whom none found with cancer, score2 was detected in 4 patients of whom 3 had cancer and score3 was assessed in 20 patients of whom 16 had cancer. Indeterminate score2 TRUS cases were found in 11 patients of whom 9 had RTCE score1 and negative core biopsy for cancer.

Conclusion: RTCE considerably improves the diagnostic yield of TRUS in detecting peripheral zone prostatic cancer.

B-0934 15:03

Diagnostic role of CT perfusion in the management of patients affected by prostate cancer

M. Osimani, D. Bellini, D. Caruso, D. Giansante, A. Laghi; *Latina/IT*

Purpose: To define the role of CT perfusion in the evaluation of patients with probable prostate cancer.

Methods and Materials: All 60 patients enrolled underwent CT perfusion exam, followed by radical prostatectomy and histopathological analysis of prostate. In 4320 prostatic areas available, we calculated numerical values of perfusion indices (blood flow, blood volume, mean transit time and permeability surface area product) by perfusion analysis, and the type of lesion in each areas by immunohistological assessment. Then, we had correlated the data, we had defined the threshold values for each perfusion index, and we had obtained values of diagnostic accuracy.

Results: Among the areas affected by cancer, and non-neoplastic areas, we obtained statistically significant differences in BV and PS (p < 0.05). The analysis revealed that for the threshold values considered, CTp has bought high specificity (Sp) and negative predictive value (NPV): Sp of 88% and NPV of 91% for PS> 27 mL/min/100 g; Sp of 82% and NPV of 89% for BF> 24 mL/min/100 g; Sp of 94% and NPV of 90% for BV> 11 mL/100 g; Sp of 77% and NPV of 91% for MTT> 21 (sec).

Conclusion: Results obtained demonstrated that CTp can be used for the exclusion of prostate cancer in doubtful areas (high NPV and Sp).

B-0935 15:12

Selective arterial embolisation of symptomatic giant renal angiomyolipoma: efficacy, complications and long-term outcomes

M. Abou El-Ghar, A. El-Assmy, H. Refaie, T. El-Diasty; *Mansoura/EG (maboelghar@yahoo.com)*

Purpose: To assess the efficacy, complications and long-term outcome of selective arterial embolisation (SAE) for treatment of giant angiomyolipoma (AML) > 10 cm.

Methods and Materials: The surgical records of 13 patients with giant AML managed by SAE between 1990 and 2010 were reviewed. Data collected included pre- and post-treatment AML size, creatinine level, technical success, complications and long-term clinical success.

Results: Our study included 4 men and 9 women, 6 of them (46.2%) had tubercous sclerosis (TS) complex. The tumour was bilateral in 53.8% and mean size of AML lesions was 14.8 cm. Indications of SAE were preoperative to avoid risk of haemorrhage during nephrectomy in 4 patients and to stop severe haematuria in the remaining 9. Among 9 patients with preserved kidneys; early complications occurred in 55.5% including post-embolisation syndrome in 1 patient, recurrent haematuria necessitating nephrectomy in 3 and acute renal failure in 1. Eventually, 5 (55.5%) patients preserved their kidneys with mean follow-up period of 2 years. During follow-up radiology showed decrease in size of the lesions in 60% of cases, remained stable in 20%, and increased in another 20%. During follow-up 60% of patients had recurrent haematuria which managed conservatively and all 5 patients had a stable serum creatinine.

Conclusion: SAE of giant renal AMLs can be done safely to stop bleeding in many cases. Additional treatment may be necessary in 1/3 of patients and preservation of involved kidneys is amenable in 1/2 of cases.

B-0936 15:21

Evaluation of dynamic contrast-enhanced MR-urography (DCE-MRU) for the determination of the split renal function in chronic and intermittent urinary obstruction in comparison to diuretic renal scintigraphy (DRS): results of a prospective, multicentre study

M. Claudon¹, E. Durand², F. Guillemain¹, E. Micard¹, N. Grenier³, P. Chaumet-Riffaud⁴, C. Pasquier¹, G. Sebag⁵, K. Chaumoitre⁶;
¹Vandoeuvre-les-Nancy/FR, ²Strasbourg/FR, ³Bordeaux/FR, ⁴Le Kremlin Bicetre/FR, ⁵Paris/FR, ⁶Marseille/FR (m.claudon@chu-nancy.fr)

Purpose: To compare dynamic contrast-enhanced MR urography (DCE-MRU) and renal scintigraphy for determination of the split renal function (SRF) in chronic and intermittent urinary obstruction (UO).

Methods and Materials: 369 children and adults presenting with chronic or intermittent UO were included in 14 centres. DCE-MRU consisted of a dynamic coronal T1-weighted sequence repeated for 10 minutes after administration of diuretics and Gd-chelate (0.1 ml/kg). Diuretic renal scintigraphy was performed within two months. MRU and scintigraphy data from 295 patients were judged in a blind review by a panel of 12 practitioners then 3 experts of each speciality: radiology and nuclear medicine. For DCE-MRU, signal intensity-time curves were obtained from ROIs on renal parenchyma and aorta. SRF was calculated successively by the area under the curve (AUC) and Patlak-Rutland (PR) methods, after normalisation by parenchymal volume. Reproducibility was assessed for intra- and interobserver agreement.

Results: Reproducibility was good to excellent for both methods, with κ values ranging from 0.75 to 0.90 for scintigraphy and 0.72 to 0.81 for DCE-MRU, and improved with the expert review. At the group level, equivalence between DCE-MRU and scintigraphy was demonstrated for calculation of SRF with both PR ($p < 0.001$) and AUC ($p = 0.029$) methods. The distribution of differences followed a Gaussian law 95%CI [-26.2; +30.2]. Underestimation of SRF by DCE-MRU was observed in severe hydronephrosis.

Conclusion: SRF estimated by DCE-MRU in obstructed kidneys was reproducible and equivalent to that one measured by with renal scintigraphy at the group level, but with individual differences. DCE-MRU provides both morphologic and functional information in UO.

14:00 - 15:30

Room F2

Breast

SS 1802

MRI: diagnosis and surgical settings

Moderators:
 M. Lobbes; Maastricht/NL
 R. Salvador; Barcelona/ES

B-0937 14:00

Potential of MR-mammography for the differential diagnosis of intraductal papillomas

M. Dietzel, R. Zoubi, H.P. Burmeister, T. Groeschel, M.R. Gajda, I.B. Runnebaum, W.A. Kaiser, P.A.T. Baltzer; Jena/DE (dietzelmatthias@hotmail.com)

Purpose: Even upon core biopsy, accurate classification of benign intraductal papillomas (IP) can be difficult. Accordingly, IP are still frequently surgically resected. Therefore, accurate assessment of IP by MR-mammography would potentially optimise patient management. However, the few investigations assessing MR-mammography of IP included small patient-collectives and overall-accuracy of this modality regarding the differential-diagnosis of IP is still unknown. We performed this investigation to analyse morphologic and dynamic MR-mammography profiles of IP in depth and to identify the overall-accuracy of MR-mammography for differential-diagnosis of IP from malignant breast-lesions.

Methods and Material: Consecutive patients receiving standardised MR-mammography (standardised-scanning protocols: dynamic-T1w-GRE before/after Gd-DTPA [0.1 mmol/kgBW]; T2w-TSE) with subsequent surgico-pathological verification were enrolled. For the detailed assessment of morphologic and dynamic profiles two experienced radiologists (> 500 examinations; blinded to surgico-pathological verification) performed prospective evaluation of MR-mammography in consensus

applying 17 predefined MR-mammography descriptors. Out of this database all patients showing IP (n=83) or malignant breast-lesions (n=648) upon surgico-pathological verification were further evaluated statistically: Univariate- (association of single-descriptors with IP/breast-cancer: contingency-tables-statistics) as well as multivariate analyses were performed to identify accurate descriptor-combinations (Chi-squared-Automatic-Interaction-Detection [CHAID]) and overall-accuracy of MR-mammography for differential-diagnosis of IP vs. malignant breast-lesions (logistic-regression; receiver-operating-characteristics [ROC], area-under-the-ROC-curve [AUC]).

Results: 82.4% of MR-mammography descriptors were significantly associated with IP (n=14; $P < 0.05$). Accuracy of single-descriptors (odd's-ratio [OR]: ≤ 10.6) could be further increased by descriptor-combinations (double-combination: $OR \leq 12.7$; triple-combination: $OR \leq 15.0$). With $AUC = 0.91$ (95%-confidence-interval: 0.88-0.94; $P < 0.001$) logistic-regression identified high overall-accuracy of MR-mammography for the differential-diagnosis of IP.

Conclusion: Detailed assessment of MR-mammography allows precise characterisation of benign intraductal-papillomas and accurate differentiation from malignant breast lesions.

B-0938 14:09

Reading MR-mammography between the lines: is the "constant-sharpness" a useful tool for prediction of benignity? Introduction, diagnostic accuracy and subgroup analysis of a new descriptor

M. Dietzel, R. Zoubi, T. Groeschel, H.P. Burmeister, M. Gajda, I.B. Runnebaum, W.A. Kaiser, P.A.T. Baltzer; Jena/DE (dietzelmatthias@hotmail.com)

Purpose: Accurate classification of benign lesions in MR-mammography (MRM) can be challenging and further descriptors might help to solve this problem. We performed a retrospective case-review and identified "constant-sharpness" (CS) as a useful new MRM-descriptor to predict benignity: Positive CS is defined as a lesion with smooth and sharp margins which are consistently present during the whole dynamic-series from the first to the last scan. Then, we conducted a prospective cross-sectional investigation to analyse diagnostic accuracy of CS for differential diagnosis of benign vs. malignant lesions.

Methods and Materials: 1014 consecutive patients (exclusion: breast-therapy ≤ 12 months before MRM) with histologically verified breast-lesions imaged by MRM according to standard-protocols (dynamic GRE-T1w scans after contrast-agent [0.1 mmol/kgbw Gd-DTPA] at 1-minute-intervals over 7 minutes). All MRM were read prospectively by two experienced (> 500 MRM) and blinded readers in consensus. Finally, CS was correlated with histology results (cross-tables, χ^2 -test).

Results: CS was a significant predictor of benignity ($P > 0.001$). It was typically associated with fibroadenomas and papillomas (63.1%, 45.8%). False negative cases were rare and CS accumulated within invasive-papillary (50%) and invasive-mucinous cancers (16.7%) as well as low-grade tumours (G1: 9.7%). Overall accuracy revealed sensitivity of 41.5% (95%-confidence-interval/CI: 37.0-46.2%), high specificity (93.2%; CI: 91.0-94.9%), Odd's-ratio (9.7%; CI: 6.8-14.0) and positive-likelihood ratio (L+: 6.1; CI: 4.5-8.3).

Conclusion: "Constant-sharpness" sixfold increases the likelihood of benignity in MRM. This accurate MRM-descriptor is typically seen in fibroadenomas and papillomas, whereas false-positives are uncommon and include rare histopathologies (invasive-papillary/mucinous carcinoma) and low-grade cancers (G1).

B-0939 14:18

Magnetic resonance imaging for assessing axillary lymph node status in breast cancer patients

E. Bui, M. Costantini, P. Belli, G.G. Giardina, P. Rinaldi, G. Franceschini, R. Masetti, L. Bonomo; Rome/IT (reagandus@alice.it)

Purpose: Although magnetic resonance imaging (MRI) is indicated for pre-operative breast cancer staging, assessment of the axillae is not routinely performed. Our aim was to investigate the ability of MRI in predicting axillary lymph node status in breast cancer patients.

Methods and Materials: Written informed consent and board approval were obtained. A retrospective analysis of breast cancer patients undergoing MRI before surgery from January 2009 to June 2011 was performed. Two experienced radiologists, blinded to the histopathologic findings, analysed size (short axis, longest axis-to-shortest axis ratio) and morphological features (presence/absence of fatty hilum, abnormal cortex) of axillary lymph nodes. Patients were divided into two groups according to the final pathologic axillary status: presence/absence of lymph nodes metastases. Sensitivity, specificity, positive and negative predictive value of MRI in predicting lymph node status were obtained.

Results: Out of 615 breast cancer patients, 168 were enrolled. Histopathologic results revealed 104 node-positive patients. Lymph node involvement was suspected

in 86 out of 168 cases. There were 75 true positive observations, 11 false positive, 29 false negative and 53 true negative. The MRI sensitivity, specificity, positive predictive value and negative predictive value in predicting axillary metastases were 72.1%, 82.8%, 87.2% and 64.6%, respectively. The MRI positive predictive value reaches 100% if we consider the association of at least two findings as suspicious for nodal involvement.

Conclusion: Although pathologic evaluation of lymph nodes still remains mandatory in all patients at risk for nodal involvement, MRI may be useful in predicting axillary lymph node metastases.

B-0940 14:27

Potential role of MRI in assessing the need for sentinel lymph node biopsy in patients undergoing contralateral prophylactic mastectomy

V. Freitas, S. Kulkarni, A. Scaranelo, K. Bukhanov, S. Ghai, P. Crystal; Toronto, ON/CA

Purpose: To evaluate accuracy of MRI in detecting otherwise occult breast malignancy in women undergoing contralateral prophylactic mastectomy (CPM).

Methods and Materials: With IRB approval, Institutional database review was performed to identify patients with newly diagnosed unilateral breast carcinoma who undergo CPM in 2004-2010. Sixty patients met inclusion criteria that were restricted to cases with mammography and breast MRI performed not more than six months before CPM. Retrospective review of MRI studies was performed by two experienced readers. Accuracy of MRI in detecting otherwise occult breast malignancy was evaluated. MRI specificity and negative predictive values (NPV) were calculated.

Results: The median patient age at the time of prophylactic mastectomy was 49 years (range 28-76 years). Breast carcinoma was diagnosed in 5% of patients (3 of 60). There was one case of invasive ductal carcinoma and two cases of ductal carcinoma in-situ (DCIS). The invasive cancer was 6-mm T1N0 tumour and it was confidently identified retrospectively by both reviewers. MRI in both cases of DCIS was negative. Specificity of MRI for detection of malignancy was 77% and NPV was 96%. MRI NPV for invasive disease was 100%.

Conclusion: MRI may be a reliable test in excluding contralateral invasive breast carcinoma in patients undergoing CPM. Based on the very high NPV of MRI in our series, an yield of sentinel lymph node biopsy in patients undergoing CPM should be re-evaluated.

B-0941 14:36

Breast MRI as a potential new biomarker to assess the axillary tumour load in patients with newly diagnosed breast-cancer: initial data using computer-assisted diagnosis (CADx)

M. Dietzel, H. Habrecht, R. Zoubi, H.P. Burmeister, M. Gajda, I.B. Runnebaum, W.A. Kaiser, P.A.T. Baltzer; Jena/DE (dietzelmatthias@hotmail.com)

Purpose: To stratify the individual risk of patients with newly diagnosed breast-cancer, numerous prognostic-factors have been proposed. Presence of axillary lymph-nodes metastases has been shown to be one of the most important prognostic-factors. Yet, it can be further improved, if the total number of metastatic lymph-nodes is addressed. This is usually done using the axillary-lymph-node-ratio (ALNR), being defined as the quantity of metastatic-nodes divided by the quantity of resected-nodes. Accordingly, we designed this prospective-cross-sectional investigation to investigate the potential of breast MRI to non-invasively assesses axillary tumour load and to predict ALNR using dedicated semiautomatic software.

Methods and Materials: Consecutive patients with primary invasive breast-cancer receiving preoperative breast-MRI at our institution were enrolled (IRB-approval). Reference-standard was surgico-pathological staging (breast, axilla) and ALNR was identified. Breast-MRI protocols were standardised according to EUSOBI-recommendations (T1w gradient-echo before and after [n=7] application of Gd-DTPA, flow: 0.3 ml/s; dosage 0.1 mmol/kg). For breast-MRI analyses a commercially available CAD-system was used (computer-assisted diagnosis), providing semiautomatic/semiquantitative analysis of breast-cancer enhancement profiles. Multiple-regression was used to assess possible correlation of such enhancement-profiles with the reference-standard (ALNR).

Results: 107 patients were enrolled (mean-age 57years; range 30-87years). Mean ALNR was 0.28 (range 0.03-0.97). Multiple-regression identified significant potential of breast-MRI to predict axillary tumour load (P < 0.05; r2: 0.18).

Conclusion: According to our data, CADx-based interpretation of breast MRI correlates with axillary tumour load. As the latter is amongst the most powerful prognostic factors in breast-cancer, such findings add further knowledge to the application of breast-MRI as a non-invasive prognostic biomarker.

B-0942 14:45

Detection of incidental vertebral fractures by MR-localiser in breast imaging

A. Bazzocchi, P. Spinnato, G. Garzillo, F. Ciccarese, F. Fuzzi, L. Miglio, L. Santilli, S. Mignani; Bologna/IT (ggarzillo@yahoo.it)

Purpose: Vertebral fractures (VFs) are the hallmark of osteoporosis, and the diagnosis of a VF may be essential in the assessment of women bone health status. Our purpose was to retrospectively evaluate MR-localiser (MR-loc) of breast MRI examinations as a potential tool in the detection of osteoporotic VFs.

Methods and Materials: MR-loc sagittal images of 536 breast MRI were reviewed by three expert skeletal radiologists with a semiquantitative diagnostic approach to detect VFs. Anamnesis and data of patients were collected as well as MRI original reports were read at the end of the MR-loc evaluation. Other available imaging exams were investigated to assess potential metastatic involvement of bone in all patients.

Results: 491/536 (91.6%) female patients undergoing MRI for oncologic reasons, and 45/536 (8.4%) for non-oncologic aims were recruited in the study (age 55.1±12.2 year-old). 38/536 (7.1%) MR-loc were considered to be inadequate for diagnostic purpose and these were excluded from the analysis. In 498/536 (92.9%) patients MR-loc allowed the evaluation of vertebral bodies between T4 and the upper lumbar spine (L1-L3). MR-loc was able to detect VFs in 39/498 (7.8%) patients. VFs were neither reported nor previously known in the clinical history of 34/39 (87.2%) patients. Moreover, no mention of VFs was found in all MRI breast reports. In 3/498 (0.6%) patients MR-loc could also identify vertebral metastases, as documented by other appropriate imaging methods.

Conclusion: In the female population submitted to breast MRI, a systematic evaluation of MR-loc can be proposed to offer additional clinical information in order to prevent unrecognised VFs.

B-0943 14:54

Are mammographic follow-up findings indeed more pronounced after intraoperative radiotherapy for breast cancer? Subgroup analysis of a randomised trial (TARGIT A)

D.B. Engel, A. Schnitzer, U. Kraus-Tiefenbacher, E. Blank, J. Brade, F. Wenz, S.O. Schönberg, K. Wasser; Mannheim/DE (dorothee.engel@medma.uni-heidelberg.de)

Purpose: Intraoperative radiotherapy (IORT) is increasingly used for breast-conserving therapy (BCT) offering a safe alternative to conventional BCT for selected patients with breast cancer. As using IORT increases structural changes in the tumour bed as previously observed in non-randomised patient groups, we aimed to further validate these results for the first time in a randomised subgroup of patients from the initial international TARGIT-A trial.

Methods and Materials: Including 48 patients, 27 patients received BCT with IORT (low-energy x-rays) and 21 patients had BCT with standard whole-breast radiotherapy served as controls. 258 follow-ups of postoperative mammograms (median follow-up 4.3 years, range 3-8) were retrospectively evaluated by two radiologists in consensus focusing on circumscribed changes and calcifications in the tumour bed.

Results: In patients after IORT fat necrosis was significantly more frequent (75% vs. 24%, p-value 0.0269) and larger (8.7 vs. 1.6 sqcm, median) than in controls. Haematoma and seroma appeared in the IORT group in 19% (20 sqcm, median) versus 0 in controls. Scar calcifications were also significantly more frequent after IORT (63% vs. 19%, p-value 0.0023) and specified as dystrophic in 37% vs. 14% and eggshell-like (i.e., typical for oil cyst) in 41% vs. 14%.

Conclusion: The study confirms the high incidence of circumscribed findings after IORT, specially large fat necrosis. The higher incidence of calcifications in the tumour bed after IORT represents a new finding which requires further attention.

B-0944 15:03

Radiological findings in mammary autologous fat injections: a multimodality evaluation

P. Belli, A. Cipriani, E. Bufi, R. Fubelli, P. Rinaldi, M. Costantini, M. Romani, L. Bonomo; Rome/IT

Purpose: Autologous fat injection (lipofilling) has recently been employed in breast plastic surgery. Our aim is to evaluate mammographic, sonographic and magnetic resonance imaging normal and pathological findings in breast lipofilling.

Methods and Materials: Informed consent and institutional review board approval were obtained. 25 patients underwent breast lipofilling from January 2008 to December 2010 at our institution. Site and amount of autologous fat injections were known. Mammography (MX), ultrasonography (US) and magnetic resonance

imaging (MRI) were prospectively obtained preoperatively and 12 months after lipofilling. US and MRI were repeated 6 months after procedure. Normal and pathological findings were described.

Results: 24 patients between 26 and 70 years old (M 50.8; SD 10.5) were enrolled in the study. 28 breasts underwent lipofilling: 13 after mastectomy, 8 after lumpectomy, 4 after DIEP flap reconstruction, 2 for asymmetry and 1 for Poland's syndrome treatment. Autologous fat injections amount ranged between 8 and 231 ml (M 114.8; SD 55.0). No severe complication after treatment was observed. At the end of the study, lipofilling normal outcomes ("oil cysts") were identified 26 times on US and 17 on MRI. Liponecrosis was detected 3 times on US and 8 on MRI. Injected fat average amount was 158.4 ml in patients with fat necrosis (104.6 ml in patients without, $p = 0.0043$). One cancer recurrence was diagnosed at 1 year follow-up by US-guided breast biopsy.

Conclusion: Lipofilling normal outcomes are best identified by US, pathological are by MRI. Liponecrosis occurs when large amounts of fat are injected. Lipofilling does not jeopardise cancer recurrence diagnosis.

B-0945 15:12

Breast-conserving surgery for non-palpable breast cancer: relationship of lumpectomy resection margins measurements between remote perioperative ultrasound and postoperative histopathology

C. Lutchmayer-Flick, F. Becce, L. Alamo, J.-F. Delaloye, R. Meuli, J.-Y. Meuwly; Lausanne/CH (linouflick@gmx.de)

Purpose: Tumour-free resection margins (RMs) are mandatory in breast-conserving surgery. On-site intraoperative ultrasound (US)-guided tumour resection with extemporaneous histopathological assessment of RMs has been described. Remote intraoperative US assessment of RMs is an alternative. The purpose of this study was to evaluate the relationship of lumpectomy RMs measurements between remote intraoperative US and postoperative histopathology.

Methods and Materials: In a retrospective IRB-approved review of 100 consecutive lumpectomies performed between October 2009 and April 2011 for presumed non-palpable breast cancer, 71 women (mean age 63.8years) were included. Twenty-nine patients were excluded because of absence of cancer at histopathology and/or incomplete data. Measurements of lumpectomy minimal RMs and tumour maximal diameter obtained on remote intraoperative US and postoperative histopathology were compared.

Results: Minimal RMs were 0.35 ± 0.32 (mean \pm SD) and 0.35 ± 0.32 cm on remote intraoperative US and postoperative histopathology, respectively. No significant difference was found between these measurements ($p=0.37$). Tumour maximal diameter was 1.02 ± 0.51 (mean \pm SD) and 1.33 ± 0.74 cm on remote intraoperative US and postoperative histopathology, respectively. US measurements were significantly smaller ($p < 0.001$). The 71 breast carcinoma (CA) consisted of: invasive canalicular (n=49), invasive lobular (n=11), in situ (n=3) and other types of CA (n=8). Twenty-nine patients had intraoperative re-excision (24 without residual CA), while 16 patients were re-operated due to insufficient histopathological RMs (12 without residual CA).

Conclusion: Good correlation of minimal RMs between remote intraoperative US and postoperative histopathology warrants use of both techniques in a complementary manner. Remote intraoperative US is helpful in taking rapid decision of re-excision and maintaining low re-operation rate after breast-conserving surgery for non-palpable cancer.

B-0946 15:21

Tumour to breast volume ratio as measured on MRI: a possible predictor of breast conservation surgery versus mastectomy

R. Faermann, F. Sperber, S. Schneebaum, D. Barsuk; Tel Aviv/IL (rfaermann@gmail.com)

Purpose: The surgical approach to breast cancer has changed dramatically in the past 20 years. Nowadays the surgical objective is to remove the tumour with negative margins and good cosmetic results. MRI of the breast has become an important imaging tool before surgery, proving to diagnose additional tumours, and to assess the tumour extent. Tumour to breast volume ratio is an important predictor of breast conservation, but was never accurately measured. MRI enables this ratio to be measured. Our purpose was to measure this ratio and to analyse if it can help in the planning of breast cancer surgery.

Methods and Materials: We conducted a retrospective hospital-based study of women diagnosed with breast cancer who underwent pre-surgery MRI. Breast volume was calculated with the AW software application. Tumour volume was calculated with the help of CAD software and the AW application. Tumour volume

was calculated including 10 mm margins. Afterwards the ratio between the volumes was calculated.

Results: 75 patients were included in our study. 63 patients had breast preserving surgery and 12 patients underwent mastectomy. Average tumour to breast volume ratio in the mastectomy group was 0.29 (29%). In the lumpectomy group, average tumour to breast volume ratio was 0.05 (5%).

Conclusion: Tumour to breast volume ratio as measured on MRI is an accurate measuring tool that can help the surgeon in the decision whether to perform breast conserving surgery or mastectomy. This tool should be introduced in the surgical planning of patients diagnosed with breast cancer.

14:00 - 15:30

Room G/H

Musculoskeletal

SS 1810b

Trauma and vertebroplasty

Moderators:

J. Raposo; Lisbon/PT
A. Vieira; Porto/PT

B-0947 14:00

The tibiofibular syndesmotom injury in acute ankle fracture: CT evaluation

Y. Kim, Y. Choi, M. Im, K. Lee, Y. Lee, J. Kim; Seoul/KR (yunnP1@eulji.ac.kr)

Purpose: To measure normal tibiofibular syndesmosis by CT and identify CT parameters that could aid in the diagnosis of syndesmotom injury after acute ankle fracture.

Methods and Materials: The study group comprised 50 patients with acute ankle fracture (mean age: 43 years) who underwent ankle CT and had syndesmotom tear along with 100 normal subjects (mean age: 38 years). The tibiofibular clear space (TFCS) and tibiofibular overlap (TFO) on the AP radiograph were measured. In the axial CT image, four parameters were measured, including the anterior tibiofibular width (ATFW), posterior tibiofibular width (PTFW), tibiofibular angle (TFA), and tibiofibular interval (TFI). We compared CT measurements between both groups and determined the optimal cut-off values for detecting syndesmotom injury.

Results: The mean TFCS and TFO were 3.8 mm and 5.1 mm for the normal group, 4.1 mm and 4.3 mm for the patient group, respectively. The mean ATFW was 3.2 mm, the PTFW was 6.1 mm, the TFA was 4.3 degrees, and the TFI was 3.3 mm for the normal group, while they were 4.9 mm, 10.4 mm, 13.7 degrees, and 5 mm for the patient group. The optimal cut-off values for syndesmotom injury were: ATFW 3.5 mm (42% sensitivity, 80% specificity), PTFW 8 mm (94% sensitivity, 99% specificity), TFA 7.2 degrees (92% sensitivity, 95% specificity), and TFI 4.2 mm (60% sensitivity, 91% specificity), respectively ($p < 0.05$).

Conclusion: CT measurements of PTFW and TFA aid in the diagnosis of syndesmotom disruption, which is difficult to detect by plain radiography in acute ankle fracture.

B-0948 14:09

Detection of bone marrow lesions with dual energy CT virtual noncalcium technique is not affected by dose reduction

G. Pache, S. Bulla, P. Blanke, T. Baumann, M. Langer; Freiburg/DE (gregor.pache@uniklinik-freiburg.de)

Purpose: To evaluate if dose reduction alters detectability of posttraumatic bone marrow lesions (BML) of the knee with dual energy (DE) CT virtual noncalcium technique (VNCA).

Methods and Materials: In this prospective, institutional review board approved study 50 patients with an acute knee trauma underwent DE-CT (Somatom Definition, Siemens) with either standard (group A) or with a dose equal to that of a single energy CT scan (group B, 28% dose-reduction) and MRI as the standard of reference. Calcium was virtually subtracted from the images (LiverVNC, Syngo Dual-Energy, Siemens). Presence of fractures was noted and presence of abnormal soft-tissue like attenuation in the bone marrow was rated on a 4-point scale for 6 femoral and tibial regions, each by 2 radiologists. HU measurements were performed in the same regions. Image ratings and HU values were subjected to ROC analysis.

Results: Mean age, number of fractures and attenuation values were not significantly different between both groups. MRI revealed 170 BML (femoral: 35, tibial: 135; A: 86, B: 84, $p=0.615$). Visual rating revealed overall AUC-values of 0.983 and 0.979 for observers 1 and 2, respectively. Visual judgement was superior over attenuation measurements for femoral regions regardless of the dosage applied. Anova-analysis of all CT values revealed a significant influence for the presence of oedema ($p < 0.001$) but no differences for the radiation dose used ($p=0.424$). Interobserver agreement was excellent (κ -value: 0.944).

Conclusion: Dose reduction does not affect detectability of posttraumatic BML with dual energy CT virtual noncalcium technique thereby providing potential additional information as compared to a single energy CT scan without additional radiation dose.

B-0949 14:18

Cone beam CT for quantitative assessment of bone defect healing: an animal study

P. Kroepil, A.R. Hakimi, C. Riegger, C. Rubbert, R.S. Lanzman, A. Scherer, P. Jungbluth, G. Antoch, M. Hakimi; Düsseldorf/DE (Patric.Kroepil@med.uni-duesseldorf.de)

Purpose: Cone beam CT (CBCT) is a rapidly expanding imaging modality for visualising osseous structures in the oral and maxillofacial (OMF) region. This study was done to evaluate CBCT beyond the OMF region for monitoring of tibial bone defect healing in an animal model.

Methods and Materials: Circumscribed tibial bone defects were created in 16 minipigs. Imaging of the tibia was performed on day 42 using a modern CBCT-scanner with flat-panel detector (PaX-Duo3D, Vatech, Korea). The extent of osseous consolidation was measured quantitatively by a CBCT-volumetry tool using commercially available imaging software (OsiriX, Pixmeo, Switzerland). Volumes of the entire defect (including all pixels), areas of osseous consolidation (density values > 2350) and non-consolidated areas (density values < 2350) of the defect were determined. The extent of bone consolidation was calculated and a correlation with histomorphometrical reference standard was performed. Independently, a visual semiquantitative CBCT-score was applied to assess bone defect healing.

Results: The mean extent of osseous consolidation in CBCT-volumetry was 63.4±17.6% (range 14-92%). A significant positive correlation was found between the extent of osseous consolidation on CBCT-volumetry and histologically visible newly formed bone ($r=0.74-0.79$, $p<0.001$). There was significant negative correlation between bone consolidation on CBCT and histological areas of persisting defect ($r=-0.82$, $p<0.0001$). The visual score matched with the volumetric results in 75% of the cases.

Conclusion: CBCT-volumetry allows for reliable, non-invasive quantitative monitoring of bone defect healing and correlates significantly with histological reference standard. CBCT is a promising technique for imaging of peripheral bones beyond the OMF region.

B-0950 14:27



Seemingly isolated greater trochanter fractures do not exist

D. Dunker¹, J.H. Gothlin¹, M. Geijer²; ¹Gothenburg/SE, ²Lund/SE (dennis.dunker@vgregion.se)

Purpose: To assess the frequency and extent of seemingly isolated greater trochanteric fractures as well as observer agreements in radiography, computed tomography (CT) and magnetic resonance imaging (MRI) of such fractures.

Methods and Materials: A review with interobserver variance was performed in 373 patients with suspected hip fracture with initial equivocal or negative radiography followed by CT (n=232) or MRI (n=170). Three reviewers scored extracapsular fractures as either complete trochanteric, avulsion of the greater trochanter with incomplete trochanteric extension, or isolated avulsion from the greater trochanter. Observer variation was quantified using linear weighted Kappa statistics.

Results: There was total agreement between three observers in 77% of the cases for radiography, 90% for CT, and 95% for MRI in classifying the cases as definite fracture, suspect or equivocal, or no trochanteric fracture. When classifying the cases as having a greater trochanteric avulsion fracture with or without a trochanteric extension there was 82% agreement for radiography, 93% for CT, and 84% for MRI. Agreements between the modalities ranged for the three observers between substantial and near-perfect ($k=0.61$, -0.92). When classifying cases as isolated trochanteric avulsions there was 100% agreement on no fractures with MRI.

Conclusion: Seemingly isolated avulsion fractures of the greater trochanter always have a trochanteric extension. CT and radiography are often adequate in diagnosing fractures of the greater trochanter but not always the extension. MRI reveals the intertrochanteric complexity but with uncertain clinical value as it may overestimate the need for internal fixation and thus an unnecessary procedure.

B-0951 14:36

Operative management of intra-capsular femoral fracture: is the requirement for additional imaging a barrier to operating within the 48-hour target?

R.G.E. Clement, Z. Davis, F. Perks; Edinburgh/UK (rhysclement@googlemail.com)

Purpose: Delay in management of patients with a femoral neck fracture of over 48 hours doubles mortality. The incidence of occult fractures that are not evident on plain radiography is up to 4.2%. Either CT or MRI can be used for further imaging but it has been suggested that waiting for these is the principle cause for delaying surgery.

Methods and Materials: Patients undergoing CT or MRI for suspected occult hip fractures at a major University hospital were identified during a one-year period. Timing of the patient admission, CT/MRI request, imaging and surgery were all recorded.

Results: 64 patients with suspected occult hip fracture were referred for further imaging during the study period. 32 underwent CT and the other 32 underwent MRI. The average wait from admission to MRI was 3.9 days with a delay from the request of 0.9 days. By comparison the average wait for CT from admission was 2.2 days with the average delay from request of 0.5 days. MRI identified 10 femoral fractures of which 2 were operated on within the 48-hour target. CT identified 12 femoral fractures of which 6 were operated on within 48-hours.

Conclusion: Over 50% of patients requiring additional imaging for suspected femoral fracture failed to be operatively managed within 48 hours. Radiology department delay is not often the cause for this and therefore clinicians should be encouraged to request additional imaging promptly.

B-0952 14:45

CT-guided minimally invasive musculoskeletal procedures augmented by a novel optical navigation system

Y. Applbaum¹, A. Hirschenbein², L. Appelbaum¹, Y. Libson¹, J. Sosna²; ¹Jerusalem/IL, ²Ra'anana/IL (avivh@hadassah.org.il)

Purpose: We employed an optical navigation system which uses video and 3-dimensional software to provide real-time needle position guidance during bone biopsies/RFA. We aimed at assessing system accuracy and safety in orthopaedic CT-guided procedures.

Methods and Materials: IRB was obtained and each patient signed informed consent. Eight percutaneous biopsies and 7 RFA of osteoid osteomas were conducted on 15 patients with lesions in the pelvis (6), spine (6), femur (2), and shoulder (1). The ActiSight (ActiViews, Haifa, Israel) guidance system was used for all cases. The system is a stereotactic accessory for CT-guided procedures which determines needle location in relation to the 3-D space of the CT images by registering a video image with the CT image. Procedure-related data, including accuracy, time to reach lesion, number of scans, and complication rates, were compiled.

Results: Patients were 19-82 of age, median 49.5. Technical success was achieved in 100% of cases. Lesion diameter ranged 4 mm-41 mm (mean 10 mm). Average distance skin-target was 64 mm (STD=25 mm) and navigation-based accuracy ranged between 0 and 10 mm (average 1.5 mm). Mean time for correct needle placement was 15 minutes (19 min for RFA and 14 min for biopsy). Total number of CT scans for needle placement averaged 3.6 (range 1-10). No complications occurred.

Conclusion: The use of the optical needle guidance system in CT-guided bone procedures is safe and accurate. Clinical relevance: The use of a stereotactic guidance system may improve the success rate in CT-guided procedures of bones; reduce time, complications and radiation associated with this procedure.

B-0953 14:54

Is there any preoperative MRI predictor in patients with degenerative lumbar stenosis?

B. Alicioglu¹, B. Yilmaz², N. Bulakbasi¹, C. Copuroglu², E. Yalniz², B. Aykac²; ¹Lefkosa-North Cyprus/TR, ²Edirne/TR (alicioglu.b@gmail.com)

Purpose: To identify any MRI predictor for surgical outcomes of patients with degenerative lumbar spinal stenosis (DLSS) having instrumented posterior decompression (IPD) surgery.

Methods and Materials: 70 patients with DLSS, who underwent IPD, were reviewed retrospectively. The clinical score of each patient were assessed using Japanese Orthopedic Association Scoring (JOAS) system, which is mainly based on the subjective symptoms and physical signs of the patients before (JOAS-I) and after (JOAS-II) surgery. Healing rate was calculated as: $[(JOAS-II)-(JOAS-I)] \times 100 / [15-(JOAS-I)]$. The HR greater than 50% was considered as clinical improvement.

At the laminectomy level the degree of disc degeneration, thecal sac compression, nerve root compression, foraminal stenosis, facet degeneration were graded from 0 to 3; the presence of alignment disorders, flaval ligament thickening were determined by MRI. The results of patients with/without clinical improvement were compared.

Results: Mean age was 59.4±7.9 (40-81), the duration of symptoms was 6.0 years. JOAS-I (5.2±3.8) was significantly different from JOAS-II (11.2±3.2)(p=0.001). Mean HR of the improved patients (n=39) was 81.94 ± 17.41; HR of the unimproved patients (n=31) was 34.75 ± 16.2, the difference was statistically significant. There was no statistical difference between the two groups by means of sex; the presence of alignment disorders; age and duration of complaints before the surgery; and radiologic stenosis parameters.

Conclusion: Although the degree of radiologic stenosis did not show any prediction about the surgical outcomes of patients having IPD, it does not mean that patients with severe stenosis will not benefit from decompression surgery.

B-0954 15:03

Percutaneous vertebroplasty with 3D-rotational fluoroscopy imaging vs CT with mobile C-arm fluoroscopy guidance

A. Cannavale, F. Fanelli, M. Corona, M. Allegritti, P. Lucatelli, R. Passariello; Rome/IT (alessandro.cannavale@hotmail.com)

Purpose: The development of rotational angiographic units (RAU) with flat detectors has markedly increased anatomic visualisation capabilities for interventional radiology procedures. We evaluated the reliability of RAU as a single technique to guide percutaneous vertebroplasty (PVP) vs CT with mobile C-arm fluoroscopy (CT-Carm).

Methods and Materials: Fifty consecutive patients (72 vertebral bodies, 40 lumbar and 32 thoracic) were treated under RAU-Artis zee with 2D/3D rotational acquisitions (N=25) and CT coupled with mobile C-arm fluoroscopy (N=25). We compared the two techniques about imaging quality, fluoroscopy time, patient and operator exposure dose, technical success, mean procedure time, mean number of rotational acquisitions and complications.

Results: RAU allowed a safe access and an accurate control of the bone-cement injection in all cases even at the thoracic levels and in case of vertebra plana. No cement leakages were encountered. The mean procedure time was 35.2 (RAU) vs 57 minutes (CT-Carm) p=0.02. Median fluoroscopy time was 14.58 (RAU) and 4.58 min (CT-Carm) p=0.02. Mean number of rotational acquisitions was 5 (RAU) and 10 (CT-Carm). Mean patient dose was 6 mSv (RAU) vs 9 mSv (CT-Carm). Mean operator dose (body/hands) was 0.004/0.3 mSv (RAU) vs 0.003/0.2 mSv (CT-Carm) p < 0.02.

Conclusion: Rotational fluoroscopy combines the most valuable interventional features of CT and fluoroscopy into one technology. It allows real-time visualisation of interventional procedures using 3D CT-like images. PVP with 3D-fluoroscopy with rotational acquisitions is a reliable and feasible technique reducing time of the procedure and allowing fast and cost-effective procedures with high rate of success.

B-0955 15:12

Coblation vertebroplasty as a means of treating high risk painful vertebral compression fractures

D.J. Wilson, S.E. Owen, R.A. Corkill; Oxford/UK (djwilson@herald.ox.ac.uk)

Purpose: It has become apparent that there are many cancer patients who would benefit from spinal cement augmentation to prevent pain and also to prevent catastrophic collapse despite the risk associated with posterior wall defect. A technique has been developed allowing the destruction of the tumour itself by cold ablation vaporising the tumour tissue and creating a cavity. This cavity can then be filled with cement at low pressure reducing the risk of displacing the tumour posteriorly.

Methods and Materials: We have now completed twenty-seven procedures. These include 5 patients with myeloma; 13 with malignancy, 8 with osteoporosis and 1 with trauma. Review of the outcome measures was based on routine baseline and post-procedure pain and disability scores using visual analogue pain scale and the Roland Morris 29 point disability score.

Results: The technique adds 10 to 15 minutes to the procedure time. The equipment is more complex and costs around 700 Euros more. We have not seen an increase in complications using this technique even though the patients are more difficult and complex. Our outcome measures are not as successful as those obtained by conventional vertebroplasty in the simpler patients where using our local anaesthetic and vertebroplasty protocol we would expect improvement in over 80%. Overall 68% obtained some improvement using coblation vertebroplasty.

Conclusion: This technique increases the safety of performing cement augmentation in patients with potentially catastrophic tumour invasion and treats patients who would otherwise be unsuitable for treatment by vertebroplasty.

B-0956 15:21

Dual energy CT myelography in patients with spinal osteosynthesis

A.E. Grams, J. Sender, R. Moritz, T. Schmidt, M. Stein, M. Oertel, G.A. Krombach, E.R. Gizewski; Giessen/DE (astrid.grams@googlegmail.com)

Purpose: The purpose was to evaluate benefits of CT myelography in dual energy (DE) technique in patients with previous lumbar osteosynthesis.

Methods and Materials: 30 patients were included. After intrathecal injection of iodine contrast agent, a DE-CT scan (Somatom Definition, Siemens) with tube voltages of 80 kV and 140 kV was performed and a virtual series of 120 kV was generated. In all series impact of metal artefacts on the visualisation of the spinal canal and the spinal foramina were evaluated. In addition, a VRT series of the dural sac was generated with "bone removal", which was compared to conventional myelography data.

Results: With tube voltages of 140 kV artefacts were least pronounced and did not limit evaluation of the spinal canal and the neural foramina. With 80 kV artefacts limited the evaluation moderately. In the virtual 120 kV series imaging quality was only slightly diminished compared to 140 kV. Visualisation of the dural sac in the VRT was comparable to the "gold standard" conventional myelography. In one patient with additional intervertebral material virtual myelography was better in visualisation of the dural sac in anterior-posterior view.

Conclusion: CT in DE technique provides minimal artefact disturbance with the 140 kV tube voltage in patients after osteosynthesis. It provides the possibility of "virtual myelography", which seems advantageous in patient with complex stabilisation. This could reduce the need of extensive conventional radiography after the injection of contrast agent and may shorten the entire examination time, unnecessary painful movements for the patients and shorten the radiation exposure for the radiologist.

14:00 - 15:30

Room I/K

Abdominal Viscera

SS 1801b

Abdomen

Moderators:

F.A. Arredondo; Guatemala City/GT
O. Buckley; Dublin/IE

B-0957 14:00

The amount of resected liver tissue determines velocity and completeness of liver regeneration after partial hepatectomy

P.G. Kele, M.T. De Boer, E.J. Van der Jagt, J.A. Lisman, R.J. Porte; Groningen/NL (p.g.kele@rad.umcg.nl)

Purpose: To evaluate liver regeneration following partial hepatectomy by computed-tomographic (CT) volumetry.

Methods and Materials: Ninety-one patients undergoing partial hepatectomy for different indications were included. Volumetry was performed semiautomatically on CT scans by drawing free-hand regions of interests in the portal-venous-phase on 2-mm thickness slices. Total liver, the part to be resected, tumour (s), future liver remnant (FLR) and liver remnants (LR) were measured. Three regeneration-velocity-indices (RVIs) were calculated: (1) RVI 7 days postoperatively (RVl early), defined as (VLR7days-VFLR)/VFLR*100, where VLR7days is the 7-day post-surgery LR-volume and VFLR is the FLR-volume; (2) RVI between the postoperative and subsequent scan (RVl late), calculated as (VLR3Months-VLR7days)/VFLR*100, where VLR3months is the ≥3-months-LR-volume; (3) RVI ≥3 months post-surgically (RVl total), calculated as (VLR3months-VFLR)/VFLR*100. Patients were classified into 5 groups: (1) patients with 0-19%, (2) 20-39%, (3) 40-59%, (4) 60-69% and (5) ≥70% resection of the total pre-operative liver volume.

Results: The RVl early ranged from a median of 11% in group 1 to 63% in group 5. The RVl late ranged from a median of 7% in group 1 to 121% in group 5. The RVl total ranged from a median 21% in group 1 to 216% in group 5. At postoperative day 7, the LR represented 97%, 87%, 70%, 58% and 41% of the total pre-operative liver volume for groups 1-5, after a median of 6 months, this was 102%, 99%, 88%, 82% and 87%, respectively.

Conclusion: Regeneration is proportional to the resected volume with higher RVIs after larger resections. Post-surgically, the liver does not regenerate to its original volume in most patients.

B-0958 14:09

Liver iron concentration quantification by MRI: are recommended protocols accurate enough for clinical practice?

J.M. Alustiza¹, A. Castiella², J.I. Emparanza¹, E. Zapata², B. Costero³, M.I. Dez³, E. Salvador¹; ¹San Sebastian/ES, ²Mendaro/ES, ³Alcala de Henares/ES (jmalustiza@osatek.es)

Purpose: To assess the quantification of liver iron concentration (LIC) by MRI using the Rennes University (URennes) model.

Methods and Materials: The LIC calculated by the URennes model in 171 patients were compared to LIC obtained by chemical measurement in liver biopsies.

Results: According to the biopsy, 107 patients had no overload (< 37 µmol Fe/g), 38 had moderate overload (37-79 µmol Fe/g), and 26 had high iron overload (HIO) (> 79 µmol Fe/g). There is a correlation between the LIC estimated with MRI and the measurement obtained with a biopsy (r=0.86). MRI correctly classified 105 patients in the various levels of LIC. Diagnostic accuracy is 61.4%, with a tendency to overestimate: 43% of patients with no overload were diagnosed as overloaded, and 44.7% of patients with moderate overload were diagnosed as having HIO. The sensitivity of the URennes method for HIO is 92.3%, and the specificity for absence of overload is 57.0%. The estimated concentrations > 170 µmol Fe/g revealed a PPV for HIO of 100%; estimated values < 60 µmol Fe/g had a NPV of 100% for HIO. The 44 patients with intermediate values remain in uncertainty.

Conclusion: The URennes model is able to correctly diagnose and rule out HIO in about 70% of patients with very specific cut-off points of 60 and 170 µmol Fe/g. For intermediate values the diagnosis is not as clear and an additional test to measure LIC or an empirical treatment should be evaluated.

B-0960 14:18

New regions of interest in body composition analysis by dual energy x-ray absorptiometry: liver "adiposity"

D. Diano, A. Andreone, G. Garzillo, G. Filonzi, C. Sassi, U. Albinini, G. Battista, E. Salizzoni, A. Bazzocchi; *Bologna/IT (giacomo.filonzi@gmail.com)*

Purpose: Hepatic steatosis is an increasing worldwide metabolic disease and the earliest biomarker for the liver fibrosis development. Thus, its detection and quantification during non-invasive examinations should be always considered as clinically relevant. Our aim was to test new designed regions of interest (ROIs) on whole body images acquired by dual energy x-ray absorptiometry (DXA) in comparison with DXA conventional ROIs and ultrasonography (US) in order to evaluate predictive values on liver steatosis detection and grading.

Methods and Materials: Ninety-nine subjects directed to body composition assessment by DXA were prospectively enrolled. All patients were submitted to whole body DXA scan (Lunar iDXA, software enCORE 12.0) and underwent US evaluation on the same day to assess hepatic steatosis (mild-moderate-severe). On every DXA image three new liver-suited ROIs were manually created by a skilled radiologist. Fat mass (FM) and FM percentage (Fmp) were investigated on whole body and regionally (android and new ROIs). FM and Fmp results were correlated with US

Results: Out of 99 patients, 70 (70.7%) resulted affected by liver steatosis on US evaluation (32/70-45.7% mild, 32/70-45.7% moderate and 6/70-8.6% severe). FM and Fmp of all ROIs were significantly correlated with presence and grading of steatosis (p < 0.001); however, they were able to predict and to distinguish steatosis absence from moderate and severe grade, but not mild. Fmp of one among the new liver-suited ROIs showed the best predictive value for liver steatosis.

Conclusion: New ROIs should be included in whole body DXA examinations to provide additional information and higher predictive value on liver steatosis.

B-0961 14:27

Reproducibility of two-point DIXON technique for measuring hepatic fat fraction

A.M. Chow, G.G. Lo, J.K.F. Chan, S. Lau, E. Wong, S.K. Yu; *Happy Valley/HK (aprilcmk@gmail.com)*

Purpose: To evaluate the reproducibility of two-point DIXON (2PD) technique for measuring hepatic fat fraction (HFF) in healthy subjects.

Methods and Materials: 15 healthy subjects (9M/6 F; age = 30.5±8.3 years; BMI = 25.3±3.0 kg/m²) were included. All MRI examinations were performed on a 1.5 T scanner (MAGNETOM Aera, Siemens). Breath-hold 2PD was performed axially using a gradient echo sequence with TE = 2.38/4.76 ms (out-of-phase (OP) and in-phase (IP), respectively). HFF maps were calculated as (Slin-Slout)/(2xSlin)x100%. Proton magnetic resonance spectroscopy (MRS) was also performed using breath-hold STEAM over a 2x2x2 cm³ voxel with TR/TE = 2000/20 ms and 4 averages. After T2 correction, HFF was then calculated as arealipid/(areawater+arealipid)x100%. Duplicate measurements were acquired after repositioning. Reproducibility

was assessed using coefficient of variation (CV), repeatability coefficient (RC) and intraclass correlation coefficient (ICC).

Results: HFF measured using 2PD and MRS for all subjects were 5.56±7.09% and 4.86±6.62%, respectively (r = 0.92; p < 0.001). CV for HFF using 2PD (5.2±4.3%) was significantly lower (p < 0.01, two-tailed Wilcoxon matched pairs test) than that using MRS (19.1±17.4%). Similarly, RC of 2PD (0.39±0.37%HFF) was significantly lower (p < 0.01) than that of MRS (1.55±2.56%HFF). Moreover, ICC for 2PD (1.00±0.00) was significantly higher (p < 0.01) than that for MRS (0.98±0.06).

Conclusion: 2PD shows higher reproducibility than MRS in measuring HFF non-invasively. Without extensive post-processing analysis, 2PD may offer promise as a robust tool to measure HFF for the entire liver reproducibly in diagnosis, treatment and follow-up of hepatic steatosis at clinical field strength within a single breath-hold.

B-0962 14:36

Early hepatic artery thrombosis after liver transplantation: the impact of onset and additional risk factors in a matched case-control study

J. Bekker¹, V. Fidler², K.P. de Jong²; ¹Rotterdam/NL, ²Groningen/NL (jasbekker@hotmail.com)

Purpose: In this study, we tested the hypothesis that early detection of eHAT and revascularisation of the graft is associated with a better graft survival. We analysed graft and patient survival in patients with intraoperative HAT - HAT detected and treated during transplantation - versus those with postoperative HAT. Additionally, we identified risk factors for eHAT by comparing eHAT patients with non-eHAT patients and by performing a case-control study in which patients were matched for the two most important risk factors for eHAT, transplantation in children and retransplantation.

Methods and Materials: Between January 2000 and August 2007, data of 376 liver transplantations in 304 patients were retrieved from our prospective database. HAT was present in 34 of 376 (9.0%) transplantations.

Results: The success rate of revascularisation attempts was comparable in the intraoperative HAT group (6/11; 55%) and the postoperative HAT group (3/11; 27%, P=0.4). Multivariate risk factors associated with an increased incidence of early hepatic artery thrombosis after liver transplantation were children, retransplantation and reduced size grafts. Independent risk factors for eHAT were: (CMV) mismatch (donor + recipient- combination), a lower prothrombin time, and a higher level of haemoglobin.

Conclusion: This suggests that early detection does not result in a better outcome of eHAT in terms of a lower retransplantation rate. As an additional potential risk factor for eHAT, we identified a high haemoglobin level in the immediate postoperative period.

B-0963 14:45

Body composition changes after liver transplantation

A. Bazzocchi¹, P. Spinnato¹, A. Cenni¹, P. Zappoli¹, F. Fuzzi¹, G. Filonzi¹, G. Bianchi¹, C. Rossi²; ¹Bologna/IT, ²Parma/IT (federica.fuzzi@gmail.com)

Purpose: The aim of the study was to evaluate body composition changes in patients undergoing orthotopic liver transplantation (OLT).

Methods and Materials: Twenty-three patients (12 males and 11 females; mean age 51.5, range 21-67 years) submitted to OLT were prospectively enrolled in the study. Patients started immunosuppressive therapy with different combinations of tacrolimus, azathioprine and steroids. In all patients a body composition analysis was performed by a new dual energy x-ray absorptiometry equipment (Lunar iDXA, GE Healthcare) before and after transplantation (1, 3, 6, 9 and 12 months). Fat mass (FM), non-bone lean mass (LM), bone mineral content and density were assessed in a three compartment whole body and regional model.

Results: All patients concluded the follow-up program. Four out of 23 (17.4%) patients presented with diabetes before OLT, and 11/23 (47.8%) were diabetic after surgery. Total and android FM/LM showed a slight decrease at 3 months, but ratios rose up in the subsequent months with statistically significant differences between 12-month values and baseline (p= 0.035 for total-body, 0.014 for android region). Android/gynoid index of fat distribution did not show any significant change after transplant. Insulin treatment did not significantly affect any body composition parameter, while steroid dosage was inversely correlated with android FM/LM ratio (p=0.004).

Conclusion: Body composition assessment is essential in the understanding of physiopathology and metabolic-related disorders and DXA is a valid tool at this aim. Patients submitted to OLT showed significant changes of their body composition that might be related to different metabolic destinies.



B-0964 14:54

Preoperative lymph node staging in patients with rectal cancer using dynamic magnetic resonance imaging: initial results

T. Vag, J. Slotta-Huspenina, U. Nitsche, R. Rosenberg, E. Rummeny; J. Gaa; Munich/DE (tiborvag@hotmail.com)

Purpose: To evaluate the accuracy of dynamic MRI for preoperative lymph node staging in rectal cancer using computerised analysis.

Methods and Materials: 19 patients received preoperative dynamic MRI (1.5 T system, VIBE-sequences in 1-minute intervals for a total of 6 minutes), identifying 51 lymph nodes located in the mesorectal fat. Contrast enhancement characteristics of identified lymph nodes were evaluated using computer-aided analysis software. The program analyses time-intensity curves voxelwise within a manually set volume of interest and summarises the percentual distribution of the different enhancement patterns in a profile map. All patients underwent rectal resection with total mesorectal excision. Identified lymph nodes on MRI were compared those from histopathologic examinations.

Results: 14 lymph nodes demonstrated metastatic involvement at histopathological examination, 37 lymph nodes were free of metastasis. Mean percentual distribution of enhancement patterns in malignant lymph nodes showed rapid initial enhancement followed by decrease in the late phase ("washout") in 23.5%, and rapid enhancement followed by flattening ("plateau") or by increase in the delayed phase ("persistent") in 14.6 and 61.2%, respectively. In comparison, distribution of enhancement patterns in negative lymph nodes demonstrated washout pattern in 56.8% ($P < 0.05$), plateau pattern in 17% ($P = 0.37$) and persistent pattern in 26.1% ($P < 0.05$).

Conclusion: Dynamic magnetic resonance imaging with computerised evaluation of enhancement characteristics might increase diagnostic accuracy in differentiating positive from negative lymph nodes in rectal cancer.

B-0965 15:03

Standardised cine loop in abdominal ultrasound yields high reliability of sonographic findings

J. Dormagen, M. Gaarder, A. Drolsum; Oslo/NO (jobador@frisurf.no)

Purpose: To compare abdominal grey-scale ultrasound findings of immediate bedside reading by performing radiologist with independent offline reading by a non-performing radiologist.

Methods and Materials: Over a six-month period, three radiologists performed dynamic ultrasound examinations in 43 outdoor patients. Examination protocols were standardised with predefined probe position and sequences of short cine loops of the liver, gallbladder, pancreas, kidneys and urine bladder, covering the organs completely in two plans. The studies were reviewed and read out immediately by the performing radiologist. Offline reading was performed blinded by a radiologist who had not performed the examination. Image quality was registered from 1 (no diagnostic value) to 5 (excellent cine loop quality). Bedside and offline reading were compared with each other and with consensus results.

Results: In 140 examinations, consensus reading revealed 21 cases with renal disorders, 17 cases with liver and bile pathology and 4 cases with bladder pathology. Overall interobserver agreement was 0.73 (95% CI 0.61-0.91), with lowest agreement for findings of the urine bladder (0.36) and highest agreement in liver examinations (0.90). Disagreements between the two readings were seen in nine kidneys, three bladder examinations, two pancreas and bile system examinations each and in one liver, giving a number of mismatches of 11%. Nearly all cases of mismatch were of minor clinical significance. The median image quality was 3 (2-5). Bedside-consensus discrepancies did not differ significantly from offline-consensus discrepancies.

Conclusion: Standardised dynamic cine loop technique in abdominal ultrasound yields high reliability of findings. Image interpretation can be performed independently from performing bedside-examination.

B-0966 15:12

Characterisation of adrenal masses using single-phase dual energy CT

A. Helck, N. Hummel, T. Johnson, M. Reiser, A. Graser; Munich/DE (andreas.helck@med.uni-muenchen.de)

Purpose: To evaluate the diagnostic accuracy of dual energy CT-based attenuation measurements in the characterisation of adrenal masses.

Methods and Materials: We retrospectively identified 55 patients with adrenal masses who had undergone single-phase abdominal contrast-enhanced dual energy CT (80 or 100 kVp / 140 kVp) on a dual source scanner (Siemens Somatom Definition/Definition Flash) for various indications. Using dedicated post-processing techniques, virtual nonenhanced and colour-coded iodine overlay images were

generated which allow direct measurement of pre- and post-contrast density on a single phase acquisition. Diagnosis of adrenal adenoma was made if CT density in the virtual nonenhanced image was lower than 10 HU. Long-term follow-up, noncontrast CT in- and opposed phase MRI served as the standard of reference.

Results: Based on follow-up imaging, 47/55 (85%) of the adrenal masses were benign adrenal adenomas. At a cut-off value of 10 HU virtual nonenhanced images allowed for correct diagnosis in 39 of 47 cases (83%), whereas 8 adrenal adenomas were lipid poor with a density higher than 10 HU.

Conclusion: Virtual nonenhanced images from dual energy CT allow for accurate characterisation of adrenal masses. DECT therefore helps to avoid unnecessary follow-up imaging (noncontrast CT, MRI).

14:00 - 15:30

Room L/M

Contrast Media

SS 1806

Applications in US, CT and MRI

Moderators:

C.U. Herborn; Hamburg/DE
P. Reimer; Karlsruhe/DE

B-0967 14:00

Contrast-enhanced ultrasound: errors and artefacts

M. Jedrzejczyk, K.T. Szopinski; Warsaw/PL (kszopinski@wum.edu.pl)

Purpose: Contrast-enhanced ultrasound (CEUS) is technically demanding, and many factors can influence the quality of the examination. A retrospective analysis was performed to assess the frequency and severity of errors and artefacts in CEUS examinations.

Methods and Materials: The films of 1690 CEUS examinations of the liver, kidneys, bowel, breast, thyroid, lymph nodes, soft tissue tumours and muscles were reviewed retrospectively. The examinations were performed with low mechanical index technique, using the SonoVue (Bracco/Altana) contrast agent (CA). The errors and artefacts were subdivided into: machine settings-related (incorrect machine settings), CA-related (preparation and administration of the contrast medium), patient-related (large body habitus, patient preparation, cooperation with the patient), examination technique-related, and archiving and interpretation errors. A serious error was defined as the one which could adversely affect the diagnosis or require a repeat examination.

Results: In 1690 reviewed files, 212 errors were detected (12.4% of examinations). Among the errors, 147 were serious (8.7% of the examinations, 69.3% of all errors). Most errors were machine settings related (81) and patient-related (62). However, the greatest percentage of serious errors was noted in CA-related (95%) and examination technique-related (83.3%) errors.

Conclusion: The errors and artefacts are common in CEUS. Often they can impair the final diagnosis. They have to be recognised, and taken into account, since the proportion of serious errors is substantial.

B-0968 14:09



Bolus versus continuous infusion of microbubble contrast agent for liver US using an automatic power injector

E. Quaia, B. Cabibbo, S. Pulvirenti, W. Toscano, M. Cova; Trieste/IT (quaia@units.it)

Purpose: To prospectively assess if continuous infusion of sulphur hexafluoride-filled microbubbles can prolong the duration of hepatic enhancement at ultrasonography over bolus injection.

Methods and Materials: 20 patients (15 males and 5 females; mean age \pm SD, 65 ± 10) received two injections - one bolus injection (2 mL/sec) and one continuous infusion (0.5 mL/min) - with the same dose (2.4 mL) of sulphur hexafluoride-filled microbubbles injected through a forearm or antecubital vein through an 18-gauge intravenous catheter using an automatic power injector. One unenhanced baseline sweep scan (mechanical index of 0.2) of the right liver lobe was acquired on the longitudinal plane followed by contrast-enhanced sweeps after bolus injection and continuous infusion. Each sweep was saved as DICOM cine-clips and analysed by a dedicated software which calculated the grade of contrast enhancement expressed as the percentage increase of echo-signal intensity in gray-scale levels over baseline scan.

Results: Duration of enhancement was prolonged by continuous infusion from 4.3 minutes \pm 2.5 at bolus injection to 8.3 minutes \pm 2.0 ($P < 0.005$). No difference in the maximal parenchymal enhancement was observed on bolus vs continuous

microbubble infusion, 50% increase over baseline \pm 15% (bolus injection) and 45% increase over baseline \pm 20% (infusion, $P < .05$).

Conclusion: Continuous infusion of sulphur hexafluoride-filled microbubbles, performed through automatic power injector, prolongs the hepatic enhancement without modifying the maximal parenchymal enhancement over the baseline.

B-0969 14:18

Prospective evaluation of vascular alterations in liver transplantation by intraoperative CEUS compared to conventional Doppler US: a pilot study

N. Leo, E. Vibert, O. Ciaccio, L. Ricca, R. Adam, D. Castaing, M. Lewin; Villejuif/FR (ustre@yahoo.it)

Purpose: To evaluate diagnostic performance of intraoperative microbubble contrast material-enhanced ultrasonography (CEUS) for assessment of vascular alterations in liver transplantation (LT), compared with intraoperative conventional Doppler ultrasonography (US).

Methods and Materials: Twenty patients were included (14 males, 6 females, average age: 48 years old). LT patients underwent both intraoperative conventional Doppler US and CEUS vascular examinations using an Aloka Alpha 7 device and intravenous microbubbles as a contrast agent.

Results: In two patients, Doppler US was normal while the CEUS was not: in one case CEUS showed flow reduction in hepatic veins and the other showed artery flow alteration due to a symptomatic arcuate ligament. These results had immediate medical and surgical implications. In another two patients Doppler US failed to visualise hepatic artery flow while this flow was shown by CEUS. Thus, Doppler US was wrong in 20 % of patients (4/20).

Conclusion: Intra-operative CEUS clearly improves the relevance of vascular imagery in LT patients as compared to conventional Doppler US. This technique should be recommended for a better management of these patients.

B-0970 14:27

Evaluation in vitro of new polymeric contrast microbubbles using Qontrast software

V. Migaleddu, V. Sanna, D. Scanu, G. Pintus, D. Sirigu, S. Uzzau, M. Marzo, M. Sechi, G. Virgilio; Sassari/IT (migaleddu@smirg.org)



Purpose: To evaluate in vitro, using ultrasound, the reflectivity of new prototypes of microbubbles (MBs) containing air, with the shell of different biocompatible and biodegradable copolymers: poly-lactic acid (PLA), poly-glycolic-lactic acid (PGLA), and PGLA conjugated with poly-ethylene-glycol (PGLA-PEG).

Methods and Materials: Using an experimental model of degassed and deionised water, each sample of MBs was evaluated with a 3.5-4 MHz convex probe (Sequoia Acuson-Siemens). Ultrasound imaging was obtained using a contrast-specific software (Cadence Contrast Pulse Sequencing). A quantitative analysis of the echoes intensity was performed through the specific Qontrast software (Advanced Medical Imaging Development, Bracco, Italy), selecting manually a region of interest.

Results: The intensity of signal produced by the different MBs has been compared to that of water. Each MBs prototype demonstrated a signal related to coating composition. Signal intensity increased in the order PLA < PLGA < PLGA-PEG, in particular $15 \pm 0.08\%$, $18 \pm 0.9\%$ e $34 \pm 1.8\%$, respectively, obtaining a significant statistical correlation ($p < 0.05$).

Conclusion: MBs with shell of PLGA-PEG resulted the most effective in terms of reflectivity after exposure to ultrasound. So they might be further optimised and used as potential carriers for selective drug delivery.

B-0971 14:36

The efficacy of contrast protocol in liver dynamic CT: multicentre prospective study in community hospitals in Japan

M. Okada¹, H. Kondo², H. Sou³, T. Murakami¹, M. Kanematsu², T. Ichikawa³, K. Awai⁴, K. Yoshimitsu⁵, Y. Yamashita⁶; ¹Osaka-Sayama/Jp, ²Gifu/Jp, ³Kofu/Jp, ⁴Hiroshima/Jp, ⁵Fukuoka/Jp, ⁶Kumamoto/Jp

Purpose: To compare the effects of contrast material (CM) with four different injection techniques on the conspicuity of hypervascular hepatocellular carcinoma (HCC) in patients with liver damage.

Methods and Materials: The survey was conducted in 91 institutions as post-marketing surveillance, and liver dynamic CT data of 415 patients with HCC (< 3 cm) were obtained. Four injection protocols (A; body weight (BW)-tailored dose of CM (300 mg/mL of Iohexol), fixed injection duration (30s), fixed arterial phase (AP) scan timing, B; BW-tailored dose of CM, fixed injection duration (30s), AP scan timing adjusted by bolus tracking, C; BW-tailored dose of CM, fixed injection flow rate, AP scan timing adjusted by bolus tracking, D; 100 mL constant of CM at

any BW, fixed scan timing) were used. Enhancement of the aorta and liver, and tumour-to-liver contrast (TLC) at AP and at equilibrium phase (EP) were compared between these protocols.

Results: Three hundred and forty of 415 patients had hypervascular HCC. The rate assessed "good or better" as TLC at AP were A; 81.3%, B; 79.6%, C; 80.7%, and D; 76.9%. In patients with higher BW (> 60 kg), qualitative TLC at AP and quantitative aortic enhancement in protocol A-C were significantly higher than those in protocol D, whereas quantitative TLC at AP in protocol A-C was significantly lower than that in patients with lower BW (≤ 50 kg). Enhancement of liver and TLC at EP showed no significant difference between 4 protocols.

Conclusion: In patients with higher BW (> 60 kg), protocols of BW-tailored dose of CM and/or fixed injection duration should be employed to diagnose hypervascular HCCs.

B-0972 14:45

Diagnostic utility of double-contrast MRI (DC-MRI) for evaluation of treatment response of hepatocellular carcinoma to ablative treatments (TACE, PEI, RFA)

A. Centola, L.P. Stoppino, C. Bristogiannis, G. Santangelo, P. Milillo, P. Lupo, R. Vinci, L. Macarini; Foggia/IT (annarita.centola@fastwebnet.it)

Purpose: To assess recurrence of disease in hepatocellular carcinoma (HCC) nodules after loco-regional treatment by sequential use of superparamagnetic iron oxide (SPIO) and the gadolinium-diethylenetriaminepentaacetic acid (Gd-DTPA) contrast agents compared with unenhanced MRI and SPIO-enhanced MRI (SPIO-MRI).

Methods and Materials: We enrolled 31 consecutive patients affected by hepatic cirrhosis with a total of 45 HCC nodules treated by loco-regional treatments. 6 patients were treated with transarterial chemoembolisation (TACE), 8 patients with radiofrequency ablation (RFA) and 17 patients were treated with percutaneous ethanol injection (PEI). DC-MRI study was performed one month after treatment.

Results: A viable HCC was found in 7 of 9 nodules (77.7%) treated by TACE, in 15 of 24 nodules (62.5%) treated by PEI and in 4 of 12 nodules (33.3%) treated by RFA. In all these cases DC-MRI technique clarified the MR picture, improving the possibility to diagnose the presence or absence of viable HCC within post-treatment liver fibrosis as well as an early detection of 12 dysplastic nodules by comparing unenhanced MRI, SPIO-enhanced and DC-MR images.

Conclusion: The combined use of two contrast agents (negative and positive) improved the diagnosis of viable tumour in treated HCC within post-treatment liver fibrosis.

B-0973 14:54

Magnetic resonance imaging contrast of brain tumours at 7 Tesla compared to 3 Tesla: enhancement after half and full routine contrast agent dose

I.-M. Noebauer-Huhmann, P. Szomolanyi, V. Juras, C. Kronnerwetter, M. Schmook, D. Payer, S. Trattnig; Vienna/AT (iris.noebauer@meduniwien.ac.at)

Purpose: To compare the diagnostic efficacy of a half and a full dose of gadolinium-based MR contrast agent in primary brain tumours at 7 Tesla MR versus 3 Tesla.

Methods and Materials: 11 patients (6m, 5f, mean age 55 years, range, 25-78) with malignant primary brain tumours were examined on both a 7.0 Tesla and a 3.0 Tesla MR whole body unit. Before and after intravenous administration of Gadobenate dimeglumine in a dosage of 0.05 mmol/kg and 0.1 mmol/kg body weight, a sagittal 3D GRE sequence with magnetisation preparation (MP-RAGE) with TR/TE/TI 4660/3.55/1700 msec at 7 Tesla, and TR/TE/TI 2190/3.02/1300 ms at 3 Tesla were performed. Signal intensities by region of interest measurements in the lesion and the contralateral normal white and grey matter were assessed, and the background noise was measured. The tumour-to-brain contrast was calculated. For statistical analysis two-way ANOVA tests for repeated measures and paired t-tests were used.

Results: The mean tumour-to-brain contrast after contrast agent administration was significantly higher at 7 Tesla than at 3 Tesla for both half the dose (85.4 ± 48.4 vs. 43.3 ± 24.3), and the full routine dose (118.5 ± 60.1 vs. 69.5 ± 32.85) ($p < 0.05$). The difference between half and full dose at each field strength was also statistically significant ($p < 0.001$). There was no difference between half the dose at 7 Tesla and the full dose at 3 Tesla ($p = 0.66$).

Conclusion: The results suggest that it is possible to reduce the contrast agent dose in the examination of brain tumours at 7 Tesla.

B-0974 15:03

Does higher gadolinium concentration play a role in the morphologic assessment of brain tumours? Results of a multicentre intraindividual crossover comparison of gadobutrol versus gadobenate dimeglumine (the MERIT study)

J. Vymazal¹, Z. Seidl¹, M. Mechl², M. Goyal³, M. Herman⁴, M. Pasowicz⁵, G. Schneider⁶, S. Bastianello⁷, J. Ruscalleda⁸; ¹Prague/CZ, ²Brno/CZ, ³Calgary, AB/CA, ⁴Olomouc/CZ, ⁵Krakow/PL, ⁶Homburg/Saar/DE, ⁷Pavia/IT, ⁸Barcelona/ES (josef.vymazal@homolka.cz)

Purpose: To intra-individually compare approved 0.1 mmol/kg doses of the high relaxivity MR contrast agent gadobenate dimeglumine (MultiHance) with the high concentration agent gadobutrol (Gadovist) for contrast-enhanced MRI of brain tumours.

Methods and Materials: Adult patients with suspected or known brain tumours underwent two identical MRI exams at 1.5 T, one with gadobenate dimeglumine and the other with gadobutrol both at a dose of 0.1 mmol/kg bodyweight. The agents were injected in randomised order separated by 3-14 days. Imaging sequences and acquisition timing were identical for the two exams. Three blinded readers evaluated images qualitatively for diagnostic information (lesion extent, delineation, morphology, enhancement, global preference) and quantitatively for % lesion enhancement, contrast-to-noise ratio (CNR) and lesion-to-background ratio (LBR).

Results: 114 of 123 enrolled patients successfully underwent both examinations. Final diagnoses were intra-axial tumours, metastases, extra-axial tumours, 'other' tumours and 'non-tumour' (49, 46, 8, 7 and 4 subjects, respectively). Readers 1, 2 and 3 demonstrated preference for gadobenate dimeglumine in 46 (40.7%), 54 (47.4%) and 49 (43.0%) patients, respectively, compared with 6, 7 and 7 patients for gadobutrol ($p < 0.0001$; all readers). Highly significant ($p < 0.0001$; all readers) preference for gadobenate dimeglumine was demonstrated for all other qualitative endpoints. Inter-reader agreement was good for all evaluations ($K=0.414-0.629$). Significantly superior % lesion enhancement, CNR and LBR was determined for gadobenate dimeglumine ($p \leq 0.019$; all readers).

Conclusion: High relaxivity rather than high gadolinium concentration results in significantly greater morphologic information and lesion enhancement when gadobenate dimeglumine and gadobutrol are compared at equivalent 0.1 mmol/kg doses.

B-0975 15:12

Iron oxide nanoparticles for magnetic particle imaging (MPI)

J. Haegeler, F.M. Vogt, J. Barkhausen, T.M. Buzug, K. Luedtke-Buzug; Lübeck/DE (haegeler@radiologie.uni-luebeck.de)

Purpose: Magnetic particle imaging (MPI) is a new tomographic imaging method measuring the spatial concentration of superparamagnetic-iron-oxide-particles (SPIOs). Due to the high sensitive and fast data acquisition capabilities MPI is perfectly suited for molecular imaging and dynamic measurements, e.g. quantitative assessment of myocardial perfusion. However, spatial resolution as well as sensitivity highly depend on the performance of the nanoparticles. Therefore, our study aimed to characterise different SPIOs with regard to their applicability as MPI tracer.

Methods and Materials: The spectral-signal-strength (SSS) and the total-harmonic-distortion (THD) of four different commercially available SPIOs (Resovist, Sinerem, Endorem and Lumirem) and self-synthesised, dextran-coated SPIOs were evaluated using a magnetic particle spectrometer (MPS). The magnetic amplitude was set to 20 mT; the excitation frequency was 25 kHz.

Results: The self-synthesised SPIOs performed best, but there was no significant difference to Resovist (THD -26.6 vs. -36.1 dB, average SSS 5.8×10^{-7} vs. 3.3×10^{-7} Am² Hz⁻¹, $p=0.75$). Sinerem (THD -47.6 dB, SSS 4.8×10^{-8}) and Endorem (THD -56.8 dB, SSS 1.64×10^{-8}) showed significantly inferior results, whereas Lumirem showed no signal at all. The differences in performance can be explained by different iron core sizes, and the presence of SPIO-aggregates.

Conclusion: Resovist and the self-synthesised SPIOs are well suited for MPI and may be applied in different clinical scenarios. However, compared to a perfect compound there is still room for improvement, and the results of this study will guide the development of new agents with optimised iron core size and aggregability.

B-0976 15:21

Contrast medium injection protocol for CT angiography with CT contrast medium dose adjusted to body surface area with simulation

K. Amakawa; Fukuoka/JP (kazutoshi_amakawa@ybb.ne.jp)

Purpose: The purpose of this study was to evaluate the efficiency of a computed tomography angiography (CTA) protocol with the contrast medium dose adjusted to body surface area (BSA) using a simulation model.

Methods and Materials: We produced a physiological pharmacokinetic model of a contrast enhancement simulation of the aorta based on a 7-compartment model using software. We fixed the cardiac index as 3.5 l/min/m². Simulated time-enhancement curves of CTA and peak CT attenuation values for body weights 30-120 kg were analysed using three different protocols: fixed iodine flux (1.11 g/sec), iodine flux based on body weight (17.35 mg/sec/kg), and iodine flux based on BSA (652 mg/sec/m²). A contrast agent at 370 mg/ml was postulated to be injected for 20 seconds in these two examinations.

Results: Unlike past studies, we excluded the effects of variable cardiac function by fixing the cardiac index. In this method, the protocol adjusted to BSA demonstrated the least uneven time-attenuation curve at different body weights and the least variation in enhancement peak of the three protocols, showing statistical differences.

Conclusion: The contrast material injection protocol adjusted to BSA provided aortic enhancement in patients with a wide variety of body weights more consistently than the other two protocols.

14:00 - 15:30

Room N/O

Vascular

SS 1815
Carotid arteries

Moderators:
E. Esteban; Alzira/ES
A. Spinelli; Rome/IT

B-0977 14:00

Characterisation of neovascularisation in carotid atherosclerotic plaques with contrast-enhanced ultrasound

D.A. Clevert, A. Helck, W. Sommer, T. Saam, M. Reiser; Munich/DE (Dirk.Clevert@med.uni-muenchen.de)

Purpose: To evaluate the use of contrast-enhanced ultrasound in the neovascularisation within carotid atherosclerotic plaques.

Methods and Materials: 35 patients with known atherosclerotic plaques in the carotid artery were examined with contrast-enhanced ultrasound to role out the features of neovascularisation within this plaque. Additionally, these plaques were analysed and correlated with plaque size and echogenicity. For contrast-enhanced ultrasound we injected 2.4 cc of SonoVue (Bracco, Italy) i.v. The examinations were performed using the S 2000 or Sequoia 512 (Siemens / Acuson, Mountain View) with an 9.15 MHz or 17 MHz probe using the CPS-software.

Results: There were 41 atherosclerotic plaques, 27 of which (19 soft and 8 mixed) enhanced after injection of SonoVue. The enhancement occurred from the carotid wall to the center of the plaque with a short-line pattern in 15 plaques, whereas 12 plaques enhanced from both the carotid wall and the carotid lumen, with just a little spot pattern. The arrival time of contrast was later in the plaques than in the carotid artery and the time to peak was longer in the plaques than in the carotid lumen. Among the 14 unenhanced plaques, 4 were hard, 3 were calcified, 2 were soft, and 5 were mixed. The unenhanced plaques had a thickness of < 2.7 mm.

Conclusion: In our small patient population, contrast-enhanced ultrasound allows the dynamic evaluation of neovascularisation within carotid plaques and neovascularisation may correlate with plaque morphology.

B-0978 14:09

Characterisation of atherosclerotic plaque of carotid arteries: high-resolution multisequence MR imaging vs colour Doppler ultrasonography (US)

S. Tartari¹, R. Rizzati¹, M. Princivale¹, K. Capello², G. Benea¹; ¹Lagosanto/IT, ²Legnaro/IT (s.tartari@alice.it)

Purpose: To investigate whether high-resolution multisequence MR Imaging of the vessel wall carotid arteries can differentiate at-risk soft plaque from solid fibrous plaque more accurately than colour Doppler ultrasonography (US).

Methods and Materials: This study included 55 carotid arteries in 52 consecutive patients who underwent carotid endarterectomy. MRI (1.5 T with neurovascular array coil) was performed using multiple sequences: diffusion-weighted imaging, fat-suppressed T1-weighted; first-pass CE-MRA; steady-state 3D T1 high-resolution (HR). Carotid plaques were grouped into three categories based on MR signal intensity and US pattern: at-risk soft plaque with large lipid-necrotic core (LNC) (group A); complex fibrotic-calcified including a segment of lipid-liquid component (B); hard plaque without soft content (C). Additional vulnerable plaque features like Intraplaque haemorrhage (IPH) and ulceration were registered. MR and US

findings were compared with findings of endarterectomy specimens considered as gold standard.

Results: Four patients were excluded from the study due to MR artefacts or because not US-assessable. Intraoperative findings and macroscopic examination of endarterectomy specimens revealed 15 at-risk soft plaques, 23 complex and 13 hard plaques. HR-MRI correctly classified 73%, 30% and 100% of plaques of group A, B and C; US identified 53%, 52% and 84% of group A, B and C, respectively. In 20/51 patients MR pinpointed 15 ulcerated plaques (8 of them identified by US) and 14 cases of IPH.

Conclusion: In patients undergoing CE-MRA, MR plaque characterisation could have a potential to more accurately diagnose soft plaque with large LNC or plaque with features of vulnerability in comparison with colour Doppler US.

B-0979 14:18

Ultra low-dose dual source computed tomography angiography of the supraaortic arteries using 100 kV tube voltage, a high pitch and iterative reconstruction: preliminary results

D. Beitzke, R. Nolz, G. Edelhauser, R.E. Scherthaner, F. Wolf, C. Plank, J. Lammer, C. Loewe; Vienna/AT (dietrich.beitzke@meduniwien.ac.at)

Purpose: To evaluate image quality, diagnostic confidence and radiation dose using 100 kV tube voltage and iterative image reconstruction for high pitch dual source CT angiography (DSCTA) of the supraaortic arteries in comparison to a 120 kV standard protocol.

Methods and Materials: DSCTA of the supraaortic arteries was performed in 20 patients randomly using either 100 kV, 3.2 pitch and iterative reconstruction or 120 kV, 2.4 pitch and filtered back projection. Contrast-to-noise ratio (CNR) and signal-to-noise ratio (SNR) calculations were performed to objectively evaluate image quality in 7 vascular segments. For subjective image quality a four-point scale was applied to 15 vascular segments in each patient by two readers. Effective dose was used to compare the differences in radiation dose.

Results: The use of 100 kV and iterative reconstruction showed significantly higher vessel opacification and reduced image noise in all segments resulting in significantly higher CNR and SNR values at the level of the carotid bifurcation ($p=0.02$) and significantly higher CNR values at the level of the internal carotid artery ($p=0.01$) compared to 120 kV and filtered back projection. There was no difference in the subjective image quality in all vascular segments. The effective dose was significantly lower using 100 kV (1.27 ± 0.39 vs. 2.82 ± 0.91 mSv; $p < 0.001$).

Conclusion: The use of 100 kV tube voltage, a high pitch and iterative reconstruction in DSCTA of the supraaortic arteries allows for radiation dose reduction down to 1.3 mSv without influencing diagnostic confidence.

B-0980 14:27

Comparison of 3 different evaluation criteria of carotid artery stenosis with 64-slice CT: role of cross-sectional area versus percent diameter stenosis

A.D. Annoni, G. Pontone, A. Formenti, D. Andreini, E. Nobili, F. Besana, G. Ballerini, M. Pepi, P. Montorsi; Milan/IT (andrea.annoni@ccfm.it)

Purpose: Aim of the study is to verify which of the daily used quantitative method of carotid stenosis evaluation [Common carotid artery (CCA), NASCET, ECST] better correlates with carotid stenosis area indexed to body surface area (Ai) of the patient, that is the real parameter of the blood flow in the carotid vessels

Methods and Materials: 112 patients underwent 64-slice CT (GE VCT) with evaluation of diameter and area, respectively, of common carotid artery (CC), carotid bulb and internal carotid (CI) at the site of stenosis and beyond the bulb. Stenosis degree was measured using, respectively, as reference diameter and area of CC (CC-d, CC-A), ECST method (ECST-d, ECST-A), and NASCET method (NASCET-d, NASCET-A) and correlated with Ai using Pearson test

Results: 179 carotid plaques were detected. Quantitative analysis showed mean $Ai=7.7\pm6.0$ mm². Stenosis degree using the 3 different methods was respectively: CC-d: $58\%\pm17$; CC-A: $71\%\pm19$; ECST-d: $55\%\pm16$; ECST-A: $62\%\pm23$; NASCET-d: $39\%\pm18$; NASCET-A: $66\%\pm25$. The agreement between Ai and each of the three different methods was: CC-A ($r:0.82$), ECST-A ($r:0.75$), NASCET-A ($r:0.82$).

Conclusion: CC-A method and NASCET-A method better correlates with Ai. Less agreement results between Ai and ECST method, maybe because of lower reproducibility of the measurements at the site of carotid bulb due to anatomical changes related to atherosclerosis

B-0981 14:36

Time-of-flight images: a viable alternative to contrast-enhanced MR angiography and fat suppressed T1w images for the diagnosis of cervical artery dissection?

E.M. Coppentrath, N. Lummel, J. Linn, K. Nikolaou, M.F. Reiser, M. Dichgans, T. Pfefferkorn, T. Saam; Munich/DE (Eva.Coppentrath@med.uni-muenchen.de)

Purpose: To compare the diagnostic performance of a non-enhanced time-of-flight sequence (TOF-MRA) with fat suppressed axial/coronal T1-weighted images and contrast-enhanced angiography (standard MRI) for the diagnosis of cervical artery dissection (CAD).

Methods and Materials: 26 consecutive patients (9 women, 17 men, age 24-66 years) with proven CAD on standard MRI had an additional TOF-MRA (3.0 T Siemens Verio) using dedicated surface coils (Machnet, Netherlands) within 7 days. Sensitivity (SE), specificity (SP), positive and negative predictive value (PPV, NPV) and accuracy of TOF-MRA were calculated using the standard protocol as gold standard. Image quality and diagnostic confidence were assessed by two raters in consensus decision on a 4-point scale. A p-value of < 0.05 was considered statistically significant.

Results: There was excellent agreement between TOF images and the standard protocol for the presence/absence of CAD, with a Cohen's kappa value of 0.96 ($p < 0.001$). On TOF images, 1 CAD in the V1 segment of the vertebral artery was missed. In addition, 1 CAD was found on TOF images which were not seen with the standard protocol. This resulted in a SE, SP, PPV, NPV and accuracy of 97%, 98%, 97%, 98% and 98%, respectively. Image quality did not differ significantly between the two methods. However, diagnostic confidence of the TOF sequence was rated significantly higher compared to the standard protocol (3.5 vs. 2.7; $p < 0.001$).

Conclusion: Findings of this study suggest that TOF imaging is a viable alternative to the standard contrast-enhanced protocol for the diagnosis of CAD.

B-0983 14:45

Head-to-head comparison of CTA and 3 T black-blood MRI for identification of symptomatic carotid plaques

J.M. Grimm, A. Schindler, F. Schwarz, C.C. Cyran, M. Dichgans, T. Freilinger, M.F. Reiser, K. Nikolaou, T. Saam; Munich/DE (jochen.grimm@med.uni-muenchen.de)

Purpose: The purpose of this prospective study was to compare multi-detector CT angiography (MDCTA) with black-blood 3 T-MRI (bb-MRI) with respect to their ability to identify symptomatic carotid plaques.

Methods and Materials: 22 patients with unilateral symptomatic carotid disease who underwent extensive clinical workup at our stroke unit to exclude other causes of ischaemic stroke underwent standard MDCTA and bb-MRI with TOF, pre- and post-contrast fsT1w-, fsT2w- and fsPDw- sequences within 7 days of symptom onset. Both symptomatic and contralateral asymptomatic sides were evaluated. By MRI, plaque morphology and composition and prevalence of complicated type VI lesions (AHA-LT6) with haemorrhage, thrombus and/or ruptured fibrous cap were evaluated. By MDCTA, plaque type (soft, mixed, hard), plaque density in HU and presence of ulceration and thrombus were evaluated. Sensitivity (SE), specificity (SP), positive and negative predictive value (PPV, NPV) were calculated using a four-by-four table.

Results: To distinguish between symptomatic and asymptomatic plaques AHA-LT6 was the best MRI variable and presence/absence of plaque ulceration was the best CT variable, resulting in a SE, SP, PPV and NPV of 80%, 80%, 80% and 80% for AHA-LT6 as assessed by bb-MRI, 40%, 95%, 65% and 71% for plaque ulceration as assessed by MDCTA and 90%, 80%, 78 and 94% for the combination of both MDCTA and bb-MRI.

Conclusion: Bb-MRI delivered a better sensitivity, NPV and PPV compared to MDCTA at identifying the symptomatic side, while MDCTA offered an excellent specificity. Best results were obtained using both techniques.

B-0984 14:54

Pulse pressure as risk factor for MRI-detected intraplaque haemorrhage in the carotid arteries: the Rotterdam study

M. Selwaness, Q. van den Bouwhuysen, G.C. Verwoert, A. Dehghan, M. Vernooij, A. Hofman, J.J. Wentzel, J.C.M. Witteman, A. van der Lugt; Rotterdam/NL (m.selwaness@erasmusmc.nl)

Purpose: Intraplaque haemorrhage (IPH), a high-risk characteristic of the vulnerable plaque, is considered to be an important predictor for ischaemic stroke. Yet, risk factors leading to plaque vulnerability and in specific IPH are unknown. We studied whether haemodynamic parameters are associated with presence of IPH.

Methods and Materials: Within the framework of the Rotterdam study, the carotid arteries of 1006 healthy participants 45 years and older and with wall thickening (> 2.5 mm) on ultrasound were imaged with a 1.5-T MRI scanner. IPH has been defined as a hyperintense signal on the 3D-T1w-GRE MR sequence. Generalised estimation equation analysis, adjusted for sex, age, intima-media thickness and other cardiovascular risk factors (smoking, diabetes, cholesterol, BMI) was used to assess the association between the main blood pressure parameters and IPH. **Results:** MR imaging of the carotid arteries revealed presence of IPH in 444/1866 (24%) plaques. Adjusted for age and sex, IPH was significantly associated with systolic blood pressure (SBP) and pulse pressure (PP). After adjustment for other cardiovascular risk factors, PP yielded the strongest association. The risk of IPH increased with 22% per SD increase in PP (95%CI 1.07-1.40, p=0.004) versus 13% per SD in SBP (95%CI 0.99-1.28, p=0.07). Furthermore, only PP remained significant after additional adjustment for other blood pressure components. **Conclusion:** Pulse pressure proved to be the strongest determinant for intraplaque haemorrhage independent of other blood pressure parameters and traditional cardiovascular risk factors. This association between pulsatile flow and IPH might provide novel insights into the aetiology of the vulnerable plaque.

B-0985 15:03

MRI-based quantification of adventitial contrast dynamics for the carotid artery as a marker for neovascularization in atherosclerosis: comparison of symptomatic and asymptomatic patients

F. Schwarz¹, M. Ingrisch¹, M. Hartmann¹, S.S. Sourbron², C.C. Cyran¹, J. Grimm¹, K. Nikolaou¹, M.F. Reiser¹, T. Saam¹; ¹Munich/DE, ²Leeds/UK (florian.schwarz@med.lmu.de)

Purpose: To compare contrast dynamics in adventitial tissue of the common and internal carotid artery between symptomatic and asymptomatic patients with atherosclerosis, calculated from time-resolved contrast-enhanced MRI datasets

Methods and Materials: 20 symptomatic patients (ischaemic stroke with DWI restriction on brain MRI) with atherosclerotic plaques on carotid ultrasound were included within 72h of symptom onset. 20 asymptomatic patients with familial hypercholesterolemia served as a control group. All patients were scanned on a 3 T-MRI-system using a dedicated surface-coil. Contrast kinetics were recorded on 2 representative axial slices at the level of the common and internal carotid artery with a temporal resolution of 1.8s for a total of 5 min. ROIs with a thickness of 2-3 pixels were positioned around the vessel wall, yielding time-dependent functions of signal. These were then fitted to a 2-compartment exchange-model and the parameters plasma-flow, plasma-volume, plasma-mean-transit-time (PMTT), extraction-flow (EF) and interstitial-mean-transit-time (IMTT) calculated.

Results: Contrast dynamics were analysed for 75 and 77 carotid segments in the symptomatic and asymptomatic group, respectively. The remaining 8 were excluded due to insufficient image quality. For symptomatic patients, significantly higher values for plasma-volume (6.5 vs. 4.2, p<0.001), extraction-flow (3.4 vs. 2.7, p=0.02) and IMTT (304 vs. 450s, p=0.04) were observed. There was a strong tendency for higher PMTT (11.4 vs. 9.1, p=0.05) and higher plasma-flow (41 vs. 35, p=0.18).

Conclusion: MRI-based quantitative assessment of contrast dynamics in the adventitial layer of the carotid artery reveals highly significant differences between symptomatic and asymptomatic patients. Further studies are needed to analyse the predictive value for future ischaemic cerebral events.

B-0986 15:12

Reproducibility and differentiation of cervical arteriopathies using in vivo high-resolution MRI

F. Schwarz, K. Nikolaou, C.C. Cyran, M. Hartmann, J. Grimm, M.F. Reiser, M. Dichgans, M. Pfefferkorn, T. Saam; Munich/DE (florian.schwarz@med.lmu.de)

Purpose: To evaluate the potential of high-resolution black-blood cervical magnetic resonance imaging (hr-bb-cMRI) to differentiate the most common cervical arteriopathies and to evaluate inter-observer reproducibility.

Methods and Materials: 43 patients underwent hr-bb-cMRI at 3.0-Tesla with fat-saturated pre- and post-contrast T1w-, PDw-, T2w- and TOF-images using specific surface-coils. 8 patients presented with cervical arthritis as confirmed by PET/CT and clinical response to steroid treatment. 23 patients showed atherosclerotic disease, causing high-grade stenoses in 12 (confirmed histologically after endarterectomy) while the remaining 11 showed no more than moderate stenosis (confirmed by ultrasound). 5 patients had arterial dissection (confirmed clinically and by follow-up imaging after 3 months). Furthermore, 7 control subjects with no evidence of disease were included. Two experienced readers blinded to all clinical information reviewed all MRI-series and classified both carotid and vertebral

arteries into either atherosclerosis, dissection, vasculitis or no-disease. Finally, a consensus reading was performed.

Results: On a per-vessel-level, agreement between both readers was excellent with a Kappa of 0.86 (p < 0.01). Compared to the gold standard both readers missed one patient with moderate atherosclerosis but correctly identified all cases of severe atherosclerosis, dissection and vasculitis. By consensus reading the correct diagnosis was made in 42 of 43 cases. Only one patient with moderate atherosclerosis was classified as disease-free. For the presence of disease this resulted in a sensitivity, specificity, PPR and NPR of 0.97, 1.0, 1.0 and 0.88.

Conclusion: This study demonstrates that hr-bb-cMRI is able to differentiate between the most common cervical arteriopathies non-invasively with excellent inter-reader reproducibility.

14:00 - 15:30

Room P

Physics in Radiology

SS 1813

New technologies and algorithms

Moderators:

O. Ciraj-Bjelac; Belgrade/RS
J.N. Vassileva; Sofia/BG

B-0987 14:00

CT image quality improvement using adaptive iterative dose reduction with wide-volume acquisition on 320-detector CT

A. Gervaise¹, B. Osemont², S. Lecocq², A. Noel³, E. Micard³, J. Felblinger³, A. Blum²; ¹Metz/FR, ²Nancy/FR, ³Vandoeuvre-Les-Nancy/FR (alban.gervaise@hotmail.fr)

Purpose: To evaluate the impact of adaptive iterative dose reduction (AIDR) on image quality and radiation dose in phantom and patient studies.

Methods and Materials: A phantom was examined in volumetric mode on a 320-detector CT at different tube currents from 25 to 550 mAs. CT images were reconstructed with AIDR and with FBP reconstruction algorithm. Image noise, contrast-to-noise ratio (CNR), signal-to-noise ratio (SNR) and spatial resolution were compared between FBP and AIDR images. AIDR was then tested on 15 CT examinations of the lumbar spine in a prospective study. Again, FBP and AIDR images were compared. Image noise and SNR were analysed using a Wilcoxon signed-rank test.

Results: In the phantom, spatial resolution assessment showed no significant difference between FBP and AIDR reconstructions. Image noise was lower with AIDR than with FBP images with a mean reduction of 40%. CNR and SNR were also improved with AIDR. In patients, quantitative and subjective evaluation showed that image noise was significantly lower with AIDR than with FBP. SNR was also greater with AIDR than with FBP.

Conclusion: Compared to traditional FBP reconstruction techniques, AIDR significantly improves image quality and has the potential to decrease radiation dose.

B-0988 14:09

Frequency-combined extended 3D reconstruction for multiple circular cone-beam CT scans

R. Grimmer¹, J. Baek², N. Pelc², M. Kachelriess¹; ¹Erlangen/DE, ²Palo Alto, CA/US (rainer.grimmer@imp.uni-erlangen.de)

Purpose: In circular cone-beam CT a single circle-scan often does not cover the complete z-range of interest. If this is the case, two or more circle-scans are acquired. The standard combination of the separate reconstructions has two disadvantages: 1) The reconstructable volume is smaller than possible, thus dose remains unused and the noise level is higher than necessary. 2) The cone-beam artefacts are increased at the edges of the partial volumes which have a large distance to the midplanes.

Methods and Materials: To overcome these disadvantages we developed a method that simultaneously reconstructs all circle-scans and thereby is able to reconstruct larger segments from each circle scan and furthermore that reduces cone-beam artefacts by combining the segments in frequency domain. The proposed method was evaluated using a simulation study as well as measured data from different flat-panel cone-beam CT scanners, as for example the Varian OBI scanner.

Results: In the example geometry the maximal reconstructable z-range can be increased by 25% and our approach additionally leads to a noise reduction of about 30% in the overlap region. Regarding the cone-beam artefacts, we were able to reduce the artefact level to a value as low as achievable by more complex

algorithms that perform a voxel-wise weighted backprojection to favour voxels seen under small cone-angles.

Conclusion: The proposed algorithm is able to significantly improve the reconstruction of sequence scans while the reconstruction time is kept equivalent to the standard approach. We further demonstrate that the method can be used in clinical practice.

B-0989 14:18

Beam-hardening and scatter removal with empirical cupping correction for primary modulation (ECCP)

R. Grimmer¹, R. Fahrig², W. Hinshaw², H. Gao², M. Kachelriess¹; ¹Erlangen/DE, ²Palo Alto, CA/US (rainer.grimmer@imp.uni-erlangen.de)

Purpose: x-Ray CT measures the attenuation of polychromatic x-rays through an object. The x-ray spectrum may vary as a function of the detector position, e.g. due to the heel effect, or a bowtie, or a primary modulator is used to modulate the primary intensity. We propose a new approach that allows handling all these effects.

Methods and Materials: Our ECCP corrects for artefacts, such as cupping artefacts or ring artefacts, that are induced by non-linearities in the projection data due to spatially varying filtration of the x-rays. To do so, ECCP requires nothing but a simple scan of a homogeneous phantom of arbitrary shape. Based on this information, coefficients of a polynomial series are calculated and stored for later use to precorrect patient data. We combine ECCP with the primary modulation scatter correction (PMSC) [IEEE TMI 25 (12):1573-1587.2006] to demonstrate the ECCPs ability of correcting for spatially varying x-ray spectra, and to show that PMSC+ECCP is a highly efficient method to correct for scatter artefacts.

Results: ECCP is applied to measurements and completely removes cupping and ring artefacts. It further guarantees well-calibrated CT-values even in cases of strong primary modulation. Our combination of ECCP+PMSC successfully performed scatter and beam-hardening correction. Ring artefacts were no more visible after combining these two methods; artefacts due to scatter or beam-hardening were removed.

Conclusion: ECCP is a highly effective pragmatic approach to compensate for strong detector channel-dependent changes of the detected spectrum. In combination with PMSC we achieve image results nearly free of scatter and beam-hardening artefacts.

B-0990 14:27

Exposition in CT-angiography: the impact of the new OPED algorithm in CT-angiography (CTA) - a phantom study

T. Werncke¹, B. Renger², O. Tischenko³, F. Wacker⁴, B. Meyer⁴; ¹Berlin/DE, ²Munich/DE, ³Neuherberg/DE, ⁴Hannover/DE (thomas.werncke@charite.de)

Purpose: The aim of this phantom study was to compare the quality of stenosis quantification for the novel OPED (orthogonal polynomial expansion on the disk) computed tomography reconstruction algorithm, which overcomes the radial decrease of image quality of the filtered back projection algorithm (FBP) with FBP.

Methods and Materials: To mimic stenosed abdominal vessels, acrylic tubes (inner diameter: small=4.0; large=6.5 mm) were filled with plaque material to create different degrees of stenosis and plaque composition (calcified [> 1000 HU], soft [~ 50 HU], inhomogeneous [50-1000 HU]). Lumen was filled with water-diluted contrast material (Iomeprol, Bracco) to enhance the lumen to 330 HU. Vessel phantoms were inserted in an anthropomorphic Alderson phantom and imaging was conducted on a 64-slice MDCT (Sensation 64, Siemens; collimation 12x0.6 mm, tube voltage: 120 kV, effective tube current: 210 mAs). Images were reconstructed using OPED and the standard kernel B31f. Agreement of measured (2 readers in consensus) stenosis area was correlated to the known value using KappaLin-Test (κ Lin).

Results: A total of 428 stenosis measurements were performed. Correlation of the OPED algorithm was superior to FBP. In large vessels, correlation was perfect for both reconstruction algorithms (OPED:0.97; FBP:0.91). In comparison, correlation was inferior in small vessels (OPED:0.82; FBP:0.81; substantial). Overall, best correlation was observed in calcified plaques (OPED: κ Lin=0.91; FBP: κ Lin=0.90) compared to soft (OPED: κ Lin=0.79; FBP: κ Lin=0.75) and inhomogeneous (OPED: κ Lin=0.81; FBP: κ Lin=0.75) plaques.

Conclusion: In large vessel phantoms, representing pelvic and renal arteries, the dose efficiency is higher with the OPED reconstruction compared to the standard filtered back projection. In smaller vessel phantoms, representing intestinal arteries, quality of luminal delineation is already limited due to the spatial resolution.

B-0991 14:36

Radiation dose and image quality at high-pitch CT angiography of the aorta: intra-individual and inter-individual comparison with conventional CT angiography

P. Apfaltrer¹, E. Hanna², U. Schoepf², J. Spears², G. Rowe², D. Harris², S. Schoenberg³, C. Fink³, R. Vliegghart⁴; ¹Mannheim/DE, ²Charleston, SC/US, ³Charleston, SC/US, ⁴Groningen/NL, ⁵Charleston, SC/US (paul.apfaltrer@umm.de)

Purpose: Latest generation CT systems enable acquiring the entire torso at high-pitch. We evaluated radiation dose and quantitative image-quality parameters at high-pitch CT-angiography (CTA) of the entire aorta, compared to conventional CTA.

Methods and Materials: 110 patients (65 males, mean age 64±15 years) with CTA of the entire aorta were retrospectively included. All patients underwent CTA on a 2nd-generation dual source CT system, 50 of which in high-pitch mode. Main indications were suspected aortic-syndrome (n=12), follow-up of aneurysm (n=37) or dissection (n=20), or post-aortic-repair (n=35). Mean arterial attenuation, signal-to-noise-ratio (SNR), contrast-to-noise-ratio (CNR), and figure-of-merit (FOM) were calculated at multiple aortic levels. A figure-of-merit (FOM) was computed to normalise the noise and CNR for each protocol to effective dose. Additionally, radiation exposure was compared.

Results: All studies were considered of diagnostic quality. At high-speed CTA, mean kV and mAs were 118±7 and 197±78, compared to 120±1 and 258±78 for conventional CTA ($p < 0.05$). Mean volume-CT-dose-index, dose-length-product, and effective dose were 8.1±2.4 mGy, 561±179 mGy*cm, and 9.6±3.0mSv at high-pitch CTA versus 18.3±7.7 mGy, 1163±480 mGy*cm, and 19.8±8.2mSv at conventional CTA ($p < 0.001$). Attenuation was similar for both protocols, while significantly less contrast medium was injected for high-pitch-CTA (87.3±16 mL vs. 97.9±16 mL, $p < 0.01$). SNR and CNR were significantly lower in the high-pitch-CTA group (< 0.01), while the FOM was non-significantly higher. 20 patients underwent both high-pitch and conventional CTA, radiation dose was reduced by 45% ($p < 0.001$).

Conclusion: High-pitch CTA of the aorta yields up to 50% reduction of radiation exposure as well as contrast medium savings with maintained vessel attenuation.

B-0992 14:45

A temporal resolution improvement method for cardiac CT using 120° of projections: initial patient experience

P. Apfaltrer¹, H. Schoendube², U.J. Schoepf¹, A. Schindler¹, T. Allmendinger², S. Vogt³, K. Stierstorfer², H. Bruder², H.U. Ebersberger¹; ¹Charleston, SC/US, ²Forchheim/DE, ³Malvern, PA/US (dr.apfaltrer@gmail.com)

Purpose: To evaluate the effect of a temporal resolution improvement method (TRIM) for cardiac CT on diagnostic image quality for coronary artery assessment.

Methods and Materials: The TRIM-algorithm employs an iterative approach to reconstruct images from less than 180° of projections and uses a histogram constraint to prevent the occurrence of limited-angle artefacts. This algorithm was applied in 11 obese patients (7 men, 67.2±9.8 yrs) who had undergone 2nd generation dual source cardiac CT with 120 kV, 175-426 mAs, and 500 msec gantry rotation time. All data were reconstructed with a temporal resolution of 250 msec using traditional filtered-back-projection (FBP) and of 200 msec using the TRIM-algorithm. Contrast attenuation and contrast-to-noise-ratio (CNR) were measured in the ascending aorta. The presence and severity of coronary motion artefacts was rated on a 5-point scale (1=no motion, 5=non-diagnostic).

Results: Mean body-mass-index was 35.1±4.3 kg/m². Average heart rate was 60±9 bpm. Mean effective dose was 13.5±4.6mSv. When comparing FBP- and TRIM-reconstructed series, the attenuation within the ascending aorta (392±70.7 vs. 396.8±70.1 HU, $p=0.182$) and CNR (13.2±3.2 vs. 11.7±3.1, $p > 0.05$) was not significantly different. A total of 110 coronary segments were evaluated. All studies were deemed overall diagnostic; however, there was a significant ($p=0.002$) difference in the occurrence and severity scores of coronary motion artefacts between FBP (mean=2.5) and TRIM (mean=2.0) reconstructions.

Conclusion: The TRIM-algorithm evaluated here allows clinically acceptable imaging of the coronary arteries despite 500 msec gantry rotation. Possible applications include improvement of cardiac imaging on slower gantry rotation systems or mitigation of the trade-off between temporal resolution and image noise in obese patients.

B-0993 14:54

Full field image reconstruction in high-pitch dual source CT

A.H. **Mahnken**¹, T. Allmendinger², M. Sedlmair², S. Reinartz¹, C. Kuhl¹, T. Flohr²;
¹Aachen/DE, ²Forchheim/DE (*andreas.mahnken@rwth-aachen.de*)

Purpose: The field-of-view (FOV) in high-pitch DSCT is limited by the size of the second detector. The goal of this study is to develop and evaluate a full FOV image reconstruction technique for high-pitch DSCT.

Methods and Materials: For reconstruction beyond the FOV of the second detector, raw data of the second system are extended to the full dimensions of the first system, utilising the partly existing data of the first system in combination with a very smooth transition weight function covering 50 detector channels. During the weighted filtered backprojection the data of the second system are applied with an additional weighting factor. This was tested for different pitch values from 1.5 to 3.5 on a simulated phantom and on 25 high-pitch DSCT data-sets acquired at pitch values of 1.6, 2.0, 2.5, 2.8 and 3.0 (Definition, Siemens, Forchheim, G). Images were reconstructed with FOV sizes ranging from 260x260 mm² to 500x500 mm². Image quality was assessed by two radiologists using a 5-point Likert scale.

Results: In phantom and patient data full FOV image quality depended on pitch. Where complete projection data from the second tube-detector system was available, image quality was unaffected by pitch changes. Full FOV image quality was not compromised at pitch values of 1.6 and remained fully diagnostic up to a pitch of 2.0. At higher pitch values a progressive depression of image quality occurred. **Conclusion:** With this new image reconstruction technique full FOV images should be used up to a pitch of 2.0.

B-0994 15:03

Detection of vascular map asymmetry in breast cancer using novel functional infrared imaging technique

D. **Izhaky**¹, M. Sklair-Levy², A. Mayer¹, Y. Pfeffer¹, E. Libson³, T. Sella³;
¹Air Port City/IL, ²Ramat Gan/IL, ³Jerusalem/IL

Purpose: Increased vascularity of the breast detected by MRI has been suggested as a marker for malignancy. Obtaining a breast vascular map requires contrast-enhanced injection during the examination. Here, we examined a non-invasive method for assessing vascular map density using a novel infrared imaging technique.

Methods and Materials: Ten patients with clinically proven cancer and 10 healthy volunteers were examined using a prototype system (RUTH Imager, Real Imaging Ltd). Multiple 3D image series were acquired. Computerised image processing generated 3D vascular maps. A special algorithm was developed to assign a score based on number, length and density of the visualised blood vessels. These scores were normalised for breast dimensions. Comparison between groups was done using a Student's t-test.

Results: There was no significant difference in age and average breast size between the two groups. For invasive cancer, the mean vascular map density score was 0.7453, with the affected breast showing increased overall vascularity (mean tumour size 11.8 mm ± 5). For healthy volunteers, the mean vascular map density score was -0.6405 ($p < 0.001$). Average image acquisition time on the RUTH scanner was 120 seconds.

Conclusion: The novel RUTH imager shows increased vascular map asymmetry in patients with malignant breast cancer with relatively fast, non-invasive acquisition. Further study should be performed to evaluate the role of monitoring of vascular map asymmetry using this technology for early detection of breast cancer.

B-0995 15:12

Low dose x-ray phase contrast computed tomography for breast cancer diagnosis

E. **Brun**¹, Y. Zhao², A. Sztrokay³, P. Diemoz⁴, Z. Huang², A. Mittone⁴, M.F. Reiser², J. Miao², P. Coan⁴; ¹Grenoble/FR, ²Westwood, CA/US, ³Munich/DE, ⁴Garching/DE (*emmanuel.brun@esrf.fr*)

Purpose: Mammography is the standard imaging modality for early breast cancer detection, but sensitivity is still limited, in particular, in dense breasts. Computed tomography (CT) has not yet been clinically implemented because of the high radiosensitivity of breast. In-vitro phase contrast CT has been proven capable of producing high contrast images potentially overcoming mammography limitations. We demonstrate that dose reduction for a given contrast/resolution can be achieved using a new reconstruction algorithm, known as equally sloped tomography (EST). Results of comparative experiments to explore radiation dose reduction in phase contrast mammography are reported.

Methods and Materials: Experiments were performed at European Synchrotron Radiation Facility. Three formalin-fixed full human breast samples were imaged using phase contrast CT (x-ray energy: 60 keV voxel size: 46*46*46 micron³).

Comparative reconstructions were produced using the standard filtered back-projection (FBP) algorithm.

Results: EST reconstruction with 512 projections has a signal-to-noise ratio comparable to FBP reconstruction with 2000 projections. No resolution or contrast degradation between tumour and normal glandular tissue is observed. Radiologist assessments blinded to the reconstruction parameters confirmed that the EST 512 reconstruction is superior to FBP. The mean glandular dose was estimated to be 2.3 mGy for the full volume EST reconstruction, which is less than the average dose in a dual-view screening routine exam.

Conclusion: Our results suggest that the EST method enables to reduce the radiation dose in phase contrast CT by 75% without sacrificing image quality. This study is an important step towards the clinical implementation.

B-0996 15:21

Human medical imaging with reformed x-ray interferometry using a practical x-ray tube: a preliminary study with normal volunteers

J. **Tanaka**¹, M. Niitsu¹, A. Momose², K. Kido³, M. Nagashima¹, F. Thiele¹; ¹Iruma-gun/JP, ²Kashiwa-city/JP, ³Hachioji-city, Tokyo/JP (*jtanaka@saitama-med.ac.jp*)

Purpose: To evaluate the image characteristics in normal volunteers obtained by reformed x-ray interferometry which uses a practical x-ray tube.

Methods and Materials: Reformed x-ray Talbot interferometry following the theory of Lau in which a practical incoherent x-ray source is used, i.e., Talbot-Lau interferometry was created based on a design with wave-optic simulation. In this system, source grating which consists of multiple slits of 10 µm or less in width, arranged periodically, is placed immediately after an incoherent x-ray source. Each slit emits coherent x-ray and if the pitch of the grating is set appropriately, an x-ray source with coherent light and enough power can be achieved due to the Lau effect. Since this system does not require either a synchrotron or a microfocus x-ray tube, the medical application of x-ray interferometry may be feasible. After confirming that the system worked with parts of human cadaveric bodies, we started to image parts of normal volunteers, such as the finger and hand under the approval of the university ethics committee. The resulting images were correlated with known macroscopic anatomical findings.

Results: Certain components of the finger and hand, such as ligaments, tendons and cartilage, which are scarcely seen by conventional x-ray imaging, were clearly depicted by this new system as expected through the ongoing work with human cadavers.

Conclusion: This new imaging technology may become clinically applicable. Further trials should study more normal volunteers and patients as well.

14:00 - 15:30

Room Q

Cardiac

SS 1803

Cardiac imaging: miscellaneous

Moderators:

T. **Leiner**; Utrecht/NL
N.H. **Strickland**; London/UK

B-0997 14:00

Incidental detection of coronary artery calcifications on non-gated chest CT: do radiologists report them?

G. **Rinaldi**, G. Mineo, P. Spinnato, V. Russo, L. Lovato, M. Zompatori; *Bologna/IT*

Purpose: Coronary artery calcifications (CAC) represent a cardiac risk factor, with relevant prognostic implications, occasionally discovered on non gated multidetector chest CT. Despite their clinical importance, they are very often not recognised and correctly reported by radiologists. The aim of this study is to evaluate the possible detection of CAC on non-gated chest CT studies not performed for coronaries or cardiac evaluation, and also to analyse their reporting rate.

Methods and Materials: We retrospectively reviewed 500 non-gated chest CT (16 multidetector-CT unit; conventional dose protocol) performed from January to December 2010 in our hospital. As a first approach, the four main coronary arteries were evaluated with a visual score to assess the presence and site of CAC. Then, radiological reports were checked to evaluate if CAC were reported and if the correct lesions site was indicated.

Results: In all patients (223 females and 277 males; mean age 52±10 years old) the evaluation of CAC was feasible. We recognised the presence of CAC in 215/500

(43.0%) patients; radiologists reported CAC only in 32/215 (14.9%) patients and in none of them the coronary arteries involved were indicated.

Conclusion: Non-gated chest CT is a valid tool for the evaluation of CAC. Nowadays radiologists are not confident in reporting this incidental finding. When the coronaries are not the aim of CT study, the reporting rate of CAC is very low. A systematic evaluation of CAC could be proposed in all chest CT studies to offer additional clinical information concerning heart disease risk.

B-0998 14:09

Progression of coronary artery calcifications during the first year after renal transplantation

L.V. Forzenigo, D. Cresseri, C. Alfieri, L. Longhi, M.G. Raciti, M. Garavaglia; Milan/IT (laura.v.f@libero.it)

Purpose: Cardio-vascular disease (CVD) is the most common complication after kidney transplant (KTx) and coronary artery calcifications (CAC) are claimed to play a key role. Scanty and contradictory results have been produced on this topic. In the present study, we looked at the CAC progression, evaluated according to Sevrukov's criteria, during the first year after KTx.

Methods and Materials: 86 consecutive KTx patients were evaluated within 3 months after KTx for CAC evaluation with CT. In 79 patients we repeated the CAC evaluation after 1 year. In 8 patients who did not perform the second control because of any clinical reason. The Agatstone score (AS) values and changes were put into relationship with the main biochemical and clinical variables, using univariate (UA) and multivariate analysis (MA).

Results: At basal evaluation 48/86 (56%) had significant AS values. The basal AS values were related only to the age of the patient, at either UA or MA ($p < 0.0001$). After 1 year, 8/79 (10.1%) patients significantly worsen their AS values, while the remaining 71 did not. No significant relationship was found between any clinical, instrumental or laboratory data and worsening of AS, nor there was any relationship of worsening in AS with any change in renal function.

Conclusion: The presence of CACs is a frequent finding at time of KTx. A worsening of CAC is also observed. However, the clinical meaning of this finding is equivocal and we need larger studies before deciding whether the CAC assessment is worth-doing on a routine basis.

B-0999 14:18

Sport category is an important determinant of cardiac adaptation: an MRI study

T. Luijckx, M.J. Cramer, N.H.J. Prakken, C.F. Buckens, F.J.G. Backx, W.P.T.M. Mali, B.K. Velthuis; Utrecht/NL (tluijckx@gmail.com)

Purpose: Physiologic cardiac adaptation in athletes is influenced by body surface area, gender, age, training intensity and sport type. This study assesses the influence of sport category and provides a reference framework for physiologic limits by sport category and gender.

Methods and Materials: 381 subjects (mean age 25 ± 5 years, range 18-39, 61% men) underwent a cardiac MRI (CMR) investigation: 114 healthy non-athletes (≤ 3 hours weekly exercise) and 267 healthy elite athletes (mean 17 ± 6.6 hours weekly exercise). Athletes performed either low dynamic-high static (LD-HS, $n=42$), high dynamic-low static (HD-LS, $n=144$) or high dynamic-high static sports (HD-HS, $n=81$).

Results: The left ventricular (LV) end-diastolic volume (EDV) (ml/m²) for non-athletes/LD-HS/HD-LS/HD-HS, respectively, was 101/107/122/129 in males and 90/103/106/111 in females. The LV end-diastolic mass (EDM) (g/m²) for non-athletes/LD-HS/HD-LS/HD-HS was 47/49/57/69 for males and 34/38/42/51 for females. Athletes' LV EDV/EDM ratios were not larger than in non-athletes, disproving selective ventricular wall thickening. LV/RV EDV ratios were similar in all groups (males/females range 0.90-0.92/0.90-1.01). Multivariate linear regression demonstrated a highly significant contribution of sport category with coefficients larger than that of training hours, gender and age ($p < 0.01$, LV EDV/EDM coefficients for sport category LD-HS 6/0.75, HD-LS 16/7, HD-HS 21/17).

Conclusion: This study demonstrates balanced cardiac adaptation for all sport categories, with preserved ratios of LV volume/LV wall mass and LV/RV volume. Sport category has a large impact on cardiac adaptation. HD-HS sports show the largest changes, whereas LD-HS sports show dimensions similar to non-athletes. This study's results can serve as a reference in clinical practice.

B-1000 14:27

Fully automated assessment of right ventricular functional parameters from ECG-gated coronary CT angiography data: evaluation of prototype software

R.W. Bauer¹, A. Wrzesniak¹, D. Bernhardt², T. Lehnert¹, F. Vega-Higuera², T.J. Vogl¹, J.M. Kerl¹; ¹Frankfurt a. Main/DE, ²Forchheim/DE (ralfwbauer@aol.com)

Purpose: Enlargement of the right ventricle is a sign of RV dysfunction, pressure or volume overload, or arrhythmogenic RV dysplasia and also a survival predictor in chronic pulmonary disease and pulmonary embolism. We evaluated the performance of prototype software for fully automated segmentation and volumetry of the right ventricle.

Methods and Materials: In 50 retrospectively ECG-gated coronary CT angiography scans the endsystolic (RVVmin) and enddiastolic (RVVmax) volume of the right ventricle was calculated fully automatically by prototype software. Manual slice segmentation by two independent radiologists served as the reference standard. Measurement periods were compared for these methods.

Results: Right ventricular volumes calculated with the prototype software were in excellent agreement with the results from manual slice segmentation (Bland-Altman $r = 0.95-0.98$; $p < 0.001$; Lin's correlation $Rho = 0.87-0.96$, $p < 0.001$) for RVVmax and RVVmin with excellent interobserver agreement between both radiologists ($r = 0.97$; $p < 0.001$). There was no need for manual correction of the RV borders as segmented by the software in a single case. Measurement period was significantly shorter with the software (153 ± 9 s) than with manual slice segmentation (658 ± 211 s).

Conclusion: The prototype software was able to demonstrate excellent performance in comparison to the reference standard. It promises not only to minimise postprocessing time but also to eliminate subjective selection of slices and cardiac phases.

B-1001 14:36

True real-time cardiac MRI in free breathing without ECG-synchronisation using radial k-space sampling: initial results

R.W. Bauer¹, I. Radtke¹, S. Zhang², T. Block¹, J.M. Kerl¹, M.G. Mack¹, T.G. Graf¹, T.J. Vogl¹, M.C. Larson¹; ¹Frankfurt/DE, ²Göttingen/DE (ralfwbauer@aol.com)

Purpose: We investigated a novel TrueFISP sequence based on radial k-space sampling (rTrueFISP) that does not require ECG-synchronisation or breathhold for cine cardiac MRI.

Methods and Materials: 12 healthy volunteers (heart rate 78 ± 12 bpm, range 57-100 bpm) underwent 1.5 T cardiac MRI. Single-shot short axis views were acquired with a) retrospectively ECG-gated segmented breathhold cine balanced steady-state free-precision (bSSFP) and b) with rTrueFISP sequences with sliding-window acquisition (5 subframes) with a temporal resolution of 15 fr/s and 40 fr/s. rTrueFISP were acquired during free breathing without ECG-synchronisation. Left ventricular functional parameters (EDV, ESV, EF) were determined according to the Simpson's rule with bSSFP representing the reference standard. Contrast-to-noise ratio (CNR) of myocardium/blood pool was calculated. Quality of wall motion depiction was assessed by two radiologists (1 = good, 2 = fair, 3 = non-diagnostic).

Results: EF showed strong correlation ($r=0.91$; $p < 0.001$) between bSSFP ($65 \pm 5\%$) and 40 fr/s rTrueFISP ($62 \pm 6\%$) but only moderate correlation ($r=0.67$) with 15 fr/s rTrueFISP ($52 \pm 6\%$). The reason for that was that ESV was significantly ($p=0.003$) overestimated with 15 fr/s rTrueFISP (15 fr/s: 43.9 ml; 40 fr/s: 36.2 ml; bSSFP: 33.9 ml). Mean CNR was significantly lower ($p = 0.002$) with 40 fr/s rTrueFISP compared to 15 fr/s rTrueFISP and bSSFP (7.5 vs. 12.6 vs. 14.2). However, due to the faster temporal resolution image quality for wall motion assessment was rated significantly better for 40 fr/s.

Conclusion: Left ventricular functional analysis with real-time non-ECG-synchronised free-breathing rTrueFISP is in good agreement with standard ECG-gated breathhold cine bSSFP sequences.

B-1002 14:45

Evidence of continuous helical structure of the cardiac ventricular anatomy assessed by diffusion tensor imaging magnetic resonance multi-resolution tractography

A. Hidalgo¹, F. Poveda¹, E. Marti¹, D. Gil¹, A. Andaluz¹, F. Carreras¹, M. Ballester²; ¹Barcelona/ES, ²Leida/ES (alhidalgop@gmail.com)

Purpose: Deep understanding of myocardial structure linking morphology and function of the heart would unravel crucial knowledge for medical and surgical clinical procedures and studies. Diffusion tensor MRI provides a discrete measurement of the 3D arrangement of myocardial fibres by the observation of local anisotropic

diffusion of water molecules in biological tissues. In this work, we present a multi-scale visualisation technique based on DT-MRI streamlining capable of uncovering additional properties of the architectural organisation of the heart.

Methods and Materials: We selected the John Hopkins University (JHU) Canine Heart Dataset, where the long axis cardiac plane is aligned with the scanner's Z-axis. Their equipment included a 4-element passed array coil emitting a 1.5 T. For DTI acquisition, a 3D-FSE sequence is applied. We used 200 seeds for full-scale tractography, while we applied a MIP mapping technique for simplified tractographic reconstruction. In this case, we reduced each DTI 3D volume dimensions by order-two magnitude before streamlining.

Results: Our simplified tractographic reconstruction method keeps the main geometric features of fibres, allowing for an easier identification of their global morphological disposition, including the ventricular basal ring. Moreover, we noticed a clearly visible helical disposition of the myocardial fibres, in line with the helical myocardial band ventricular structure described by Torrent-Guasp. Finally, our simplified visualisation with single tracts identifies the main segments of the helical ventricular architecture.

Conclusion: DT-MRI makes possible the identification of a continuous helical architecture of the myocardial fibres, which validates Torrent-Guasp's helical myocardial band ventricular anatomical model.

B-1003 14:54

Inaccuracies in cine SSFP MR LV volumetric measurements in patients with LV hypertrophy: correction applying the mass conservation principle

K.U. Bauner, M. Durand, A. Crean, E. Nguyen, S. Ley, R. Wald, H. Rakowski, N. Paul, B. Wintersperger; *Toronto, ON/CA* (Kerstin.Bauner@med.uni-muenchen.de)

Purpose: The study aim was to evaluate differences of LV mass and ESV assessment in patients with LV hypertrophy by comparing standard contouring methods with a total LV volume approach which includes application of the "conservation of mass" principle for myocardial volume.

Methods and Materials: 47 patients diagnosed with HCM/DCM (n=24/23) undergoing cardiac MR at 1.5 T/3 T were included. All patients underwent standard cine SSFP in short-axis orientation for LV volumetrics (6x1.3x1.3 mm³, TR30-35 ms). For the total LV volume approach, datasets were evaluated using semi-automated post-processing with epi- and endocardial contouring at end-diastole (ED) and epicardial contouring only at end-systole (ES). Calculation of ESV was based on total LV volume and the myocardial volume as assessed at ED applying the mass conservation principle (MCP). Analysis was performed for DCM and HCM patients and compared to standard LV volumetric assessment (STD) with epi- and endocardial contouring at ED/ES for EDV, ESV and myocardial mass.

Results: The HCM group showed smaller ESV using STD as compared to MCP (60.3±31.5 ml vs. 72.9±36.3 ml; p=0.0018) while no differences were found for the DCM group (175.7±79.9 ml vs. 176.5±77.2 ml; p=0.62). Average HCM EF declined from 65% (STD) to 56% (MCP) (p=0.0003). LV mass using STD approach differed by 2.6 g (1.2%) (95%CI:0.4-4.8 g/-0.4-2.9%) between ED and ES in DCM patients (p=0.03) but by 18.2 g (10%) (95%CI: 12.3-24.0 g/7.1-12.9%) in the HCM group (p < 0.001).

Conclusion: ESV and end-systolic mass assessment is challenging in HCM, due to problematic endsystolic endocardial contouring and underestimation of true ESV. Utilisation of the LV mass conservation principle may increase accuracy.

B-1004 15:03

Cardiac MRI using a new trigger method: MR compatible Doppler-ultrasound device to trigger the heart frequency in comparison to ECG

B. Schoennagel, C. Much, J. Yamamura, K. Tornquist, G. Adam, U. Wedegärtner; *Hamburg/DE* (wedegaer@uke.uni-hamburg.de)

Purpose: The aim was to assess a MR compatible Doppler-ultrasound device as a new method to trigger the heart rate for cardiac MRI in comparison to ECG triggering.

Methods and Materials: MR imaging was performed on 6 sheep on a 1.5 T MR scanner. The Doppler-ultrasound sensor was placed on the chest above the heart and fixed gently with a belt. The recorded signal was transferred to the ECG trigger unit of the MRI scanner and used for cardiac triggering. Additionally, conventional ECG triggering was recorded. Cardiac MRI was performed using both triggering methods consecutively. For cardiac MRI gradient echo sequences in 2- and 4-chamber view and in short axis view with cine sequences (25 phases) to determine left ventricular volumes (LV) and ejection fraction (EF) were generated. MR images acquired with Doppler-ultrasound and conventional ECG triggering were evaluated separately by two radiologists concerning image quality and functional assessment.

Results: Cardiac MR imaging was possible in all 12 examinations, 6 using the Doppler-ultrasound device and 6 using ECG triggering. Using Doppler-ultrasound for triggering image quality was comparable to ECG. All anatomical structures could be clearly evaluated. For functional evaluation the LV and the EF were assessed. There was no significant difference between both methods: LV 128 ml and EF 48% for Doppler ultrasound and LV 130 and 46% for ECG.

Conclusion: The MR compatible Doppler-ultrasound device is a new triggering method for cardiac MRI. It might be faster and easier in the application compared to ECG.

B-1005 15:12

Non-invasive cardiac vein mapping: role of MDCT-CA

R. Malago, A. Pezzato, C. Barbiani, U. Alfonsi, G. Sala, R. Pozzi Mucelli; *Verona/IT* (robertomalago@yahoo.it)

Purpose: Coronary venous anatomy is of primary importance when implanting a pacemaker or a defibrillator device because coronary sinus can be enlarged or stenotic depending on chronic heart failure. The aim of this study is to evaluate the usefulness of MDCT-CA in describing the coronary venous tree and in particular the coronary sinus and detecting main venous system variants.

Methods and Materials: 301 consecutive patients (196, mean age 63.74 YO) studied for coronary artery disease with 64 slice MDCT-CA were retrospectively examined. The cardiac venous system was depicted using 3D, MPR, cMPR and MIP post-processing reconstructions on an off-line workstation. For each patient image quality, presence and calibre of the coronary sinus (CS), great cardiac vein (GCV), middle vein (MV), anterior interventricular vein (AIV), lateral cardiac vein (LCV), posterior cardiac vein (PCV), small cardiac vein (SCV) and presence of variant of the normal anatomy were recorded.

Results and Conclusion: CS, GCV, MV and AIV were visualised in 100% of the cases. The LCV was visualised in 255/301 (84%) patients, the PCV in 248/301 (83%) patients and the SCV in 69/301 (23%) patients. Mean diameter of the CS was 8.69 mm in 276/301 (91.7%) patients without chronic heart failure and 9.93 mm in 25/301 (8.3%) patients chronic heart failure.

B-1006 15:21

Accelerated cine imaging of the heart in mice at 9.4 T: comparison of retrospectively self-gated and prospectively triggered FLASH sequences

P. Fries, J. Stroeder, A. Mueller, A. Massmann, R. Seidel, G. Schneider, A. Buecker; *Homburg/DE* (drpeterfries@googlemail.com)

Purpose: To compare prospectively triggered FLASH (PT) with retrospectively self-gated (RSG) and accelerated retrospectively self-gated FLASH (accRSG) cine sequences for the assessment of cardiac function in mice at 9.4 T.

Methods and Materials: 10 C57/BL6 mice were examined on a 9.4T animal scanner (Bruker BioSpec, Germany). We acquired 6 consecutive 1 mm short axis slices covering the left ventricle (LV) using a PT (TR/TE=5.7/2.1, α=20°, FOV=2.5x2.5 cm, matrix=256x256, frames=20, PI=1), a RSG (TR/TE=5.6/1.5, α=20°, FOV=2.5x2.5 cm, matrix=256x256, frames=20, PI=1), and an accRSG (TR/TE=5.6/1.6, α=20°, FOV=2.5x2.5 cm, matrix=160x160, cardiac frames=20, PI-GRAPPA=2). Two readers independently evaluated the different datasets in a blinded manner (twice, separated by 6 weeks) regarding LVEDV, LVESV, SV, EF, cardiac output (CO) and myocardial mass (MyoM). Total acquisition times (TA) for the complete examination of the heart were assessed for each sequence. Statistical analyses included a one-way ANOVA with Bonferroni multi-comparison test (p < 0.05) and Bland-Altman analyses for the assessment of intra- and inter-observer variability.

Results: There were no statistically significant differences between the different imaging approaches for all cardiac parameters (LVEDV (PT/RSG/accRSG (mean): 49.13/52.44/49.71 μl, p=0.06), LVESV (18.18/18.13/16.88 μl, p=0.26), SV (30.75/34.31/32.83 μl, p=0.06), EF (63.1/66.9/66.0%, p=0.7), CO (12.9/14.2/14.3 ml/min, p=0.07) and MyoM (67.6/65.2/64.8 mg, p=0.08)). TA was significantly shorter for accRSG (8:00±0:05 min, p=0.001) compared to PT (mean/SD: 19:24±4:41 min) and RSG (16:45±0:10 min).

Conclusion: Cine MRI with accRSG allows for an assessment of cardiac function in mice within 8 min while providing the same quantitative data as conventional PT and RSG FLASH sequences. This approach allows an expedition of MR studies in cardiovascular disease models.

14:00 - 15:30

Room Z

Computer Applications

SS 1805

Imaging informatics

Moderators:
M. Fatehi; Tehran/IR
P. Mc Laughlin; Cork/IE

B-1007 14:00

Combination of machine learning and computer-assisted diagnosis in breast MRI: systematic investigation identifies high potential to stratify survival outcome in primary breast cancer

M. Dietzel¹, A. Dietzel², R. Zoubi¹, O. Camara¹, M. Bogdan², W.A. Kaiser¹, P.A.T. Baltzer¹; ¹Jena/DE, ²Tübingen/DE (dietzelmatthias²@hotmail.com)

Purpose: Application of breast-MRI as a prognostic-biomarker remains challenging due to the multitude and complexity of information provided by one single examination. Machine-learning is a potential method to classify such data. Accordingly, we designed this investigation to systematically evaluate the potential of machine-learning algorithms to predict overall-survival of breast-cancer patients based on breast-MRI findings.

Methods and Materials: Patients receiving breast-MRI (standardised protocol: T1w-FLASH; 0.1 mmol/kgBW, Gd-DTPA) before surgery (BI-RADS IV-VI; no secondary/recurrent-cancer) were enrolled, treated and followed-up at our breast-cancer-centre. "Disease-related death" was defined as endpoint. A commercially available CAD-system (computer-assisted diagnosis) was used to semi-automatically evaluate 14 enhancement-parameters of the primary breast-cancer upon breast-MRI. Three machine-learning algorithms (artificial-neural-networks, k-nearest-neighbour, support-vector-machines) were optimised to predict the endpoint based on such enhancement-parameters. Predictions of the endpoint were compared with conventional-statistics (logistic-regression). To automatically optimise and validate (5-fold-crossvalidation) these classification-algorithms an in-house developed framework was used.

Results: 338 patients with primary invasive breast-cancer were enrolled (mean-age: 57.7 years). During a mean follow-up interval of 42 months "disease-related death" occurred in 41 patients. Compared to conventional statistics (logistic-regression: 68.4%), all machine-learning algorithms showed higher diagnostic accuracy ($\geq 80.9\%$) with support-vector-machines achieving the highest value (89.6%). Machine-learning showed particularly high specificity (artificial-neural-networks: 90.0%, k-nearest-neighbour: 88.7%, support-vector-machines: 100.0%) and negative-predictive-value to stratify the endpoint (artificial-neural-networks: 94.1%, k-nearest-neighbour: 94.3 %, support-vector-machines: 89.7%).

Conclusion: Machine-learning is a promising method for the individual risk-stratification of patients with primary breast-cancer. According to our results, it is superior to conventional-statistics and shows high specificity and negative-predictive-value to stratify the endpoint "disease-related death".

B-1008 14:09

RIS, PACS and archiving of images services and beyond delivered from the cloud: the greater Paris area experimentation

V.A. Dussaux, P. Boiron; Paris/FR (valere.dussaux@gcsdsisif.fr)

Purpose: The "Région Sans Film" ("Filmless Region") programme was launched in 2009 by the French Ministry of Health in order to help the generalisation to all healthcare structures, such as hospitals or general physician practices of PACS, RIS and systems of archiving of medical images. Recent achievements prove the concept of the delivering of such services from the cloud, after that both building of the platform of services and pilot phases of the program were completed. Moreover, new services of sharing of information are proved possible.

Methods and Materials: The services are delivered by means of a platform whom building and running has been confided to an industrial consortium. This platform implements the latest technologies of medical image processing and of cloud computing. It is built in order to support service-oriented enterprise architecture.

Results: The platform is innovative being the first one containing all the materials for the implementation of PACS services in the cloud, allowing for each healthcare structure to open these services beyond its borders. The platform has just been validated by the health structures involved in the pilot phase and the programme has entered industrial deployment phase. Additionally, new SuperPACS-like services are proposed, including access to the images produced in hospitals to the GPs and sharing of radiological advices services/workflows.

Conclusion: This also opens new opportunities for the implementation of new business processes/services such as teleradiology. By these means, the exercise of real filmless radiology can be more widely achieved.

B-1009 14:18

Are you keeping up to date? Over half of important radiological research is published in non-radiological journals

Y. Kwong, K. Latief; Nottingham/UK (dryune@hotmail.com)

Purpose: It is important for radiologists to practice evidence-based medicine, and identifying the latest research is crucial. With the growth in medical journals and the body of knowledge, radiologists need to be aware of strategies to identify up-to-date publications. We perform a bibliometric analysis to determine the range of journals where radiological research is published.

Methods and Materials: The 20 radiological journals with the highest impact factors were identified through the 2010 Journal Citation Reports. Systematic reviews over a 6-year period were retrieved and the primary studies constituting the systematic reviews were compiled to provide a database of high-quality unique publications. These were classified into four categories: 1. radiology journals 2. clinical sub-specialty journals 3. general medical journals 4. others.

Results: 101 systematic reviews were analysed and 1750 primary studies retrieved. These were classified as follows: 775 (45%) were published in radiological journals, 881 (50%) in clinical sub-specialty journals, 56 (3%) in general medical journals, and 38 (2%) in other journals. Amongst radiological journals, radiology had the highest number of original studies cited, with 179 (10%).

Conclusion: More than half of important radiological research is published in non-radiological journals. This can be explained by some clinical specialty journals having impact factors higher than radiology journals, collaboration between referring physicians and radiologists, and increasing involvement of referring physicians in directly acquiring imaging studies. The scatter of radiological research across a broad range of journals means that browsing selected radiological journals is not sufficient to keep up-to-date.

B-1010 14:27

Evaluation of pulmonary nodules on chest CT using iPad2®: preliminary experience

L. Faggioni, E. Neri, P. Sbragia, S. Angeli, L. Cini, D. Lauretti, D. Caramella, C. Bartolozzi; Pisa/IT (lfaggioni@sirm.org)



Purpose: To evaluate the effectiveness of the iPad2® as a mobile device for 2D reading of chest CT datasets for the assessment of pulmonary nodules.

Methods and Materials: We retrospectively reviewed 28 chest CT examinations performed in patients with pulmonary nodules, for a total of 325 nodules sized between 2 mm and 34 mm. CT images had been acquired using a 64-row CT and were wirelessly imported in DICOM format on an iPad2® 64GB (Apple Inc, Cupertino, CA) running OsiriX HD® (www.osirix-viewer.com) from a Macintosh desktop computer (iMac® 3.06GHz) connected to our hospital PACS and running OsiriX 3.9. Two experienced raters read CT datasets independently on the iMac® and on the iPad2®. Detection rate and segmental localisation of lesions were recorded for each dataset, as well as the time needed for complete reading of each chest CT examination. Image quality was also visually assessed using a three-point scale (1=poor, 2=fair, 3=good).

Results: All nodules detected on the iMac® were also identified on the iPad2®, and their segmental localisation was correctly assessed in 100% of cases. Image quality was good with both devices and image reading time was comparable between them (4.72±2.23 minutes for the iMac® vs 5.14±2.56 minutes for the iPad2®; p> 0.05).

Conclusion: The iPad2® can be successfully used for preliminary 2D reading of chest CT datasets in patients with pulmonary nodules, as well as for image sharing with non-radiology specialists and for teaching purposes.

B-1011 14:36

An ontology of magnetic resonance imaging sequences

J. Lasbleiz, A. Burgun, R. Duvauferrier, H. Saint-Jalmes; Rennes/FR (Jeremy.lasbleiz@laposte.net)



Purpose: The goal of this ontology is to improve the semantic interoperability for MRI sequences. Indeed every constructor has his own sequence name that could be unknown by radiologists or even PACS.

Methods and Materials: Concepts and definitions of MRI sequences had been extracted from domain experts, DICOM standard, DICOM headers and literature. DICOM headers had been extracted with OSIRIX. All those data had been organised with Protégé 4 owl2. The linkage between concepts had been made with relations and formal definitions.

Results: Every sequence is defined by its sequence family ancestor, timing diagram and description, parameters, artefacts and problems, clinical applications, duration, mathematical modelling and possible results, acronyms and DICOM description. We can interact with the ontology, making query. The ontology could be modified at any moment according to the last outcomes.

Conclusion: The obtained ontology gives a representation of MRI sequences that can be used for education or clinical exploitation.

B-1012 14:45

Considerations for sharing radiology reports and images on a national level in Luxembourg

U. Roth, N. Mack, B. Schroeder, H. Zimmermann; *Luxembourg/LU* (uwe.roth@tudor.lu)

Purpose: The exchange of radiology reports and images on a national level demands, in comparison to the exchange in ordinary in-house systems, additional and higher security requirements concerning data protection. In any case the communication should rely on current standards. The problem that has to be faced is the identification of gaps in these standards that arise from the shift into the national context.

Methods and Materials: Communication with the national platform will be mainly based on IHE XDS/XDS.I and PIX profiles, using document repositories for the storage of the reports and image-manifest files and a registry service for the storage of document references plus additional meta data. To protect data inside the repository against intentional or accidental misuse, it needs to be stored encrypted. For the protection of the document references and meta-data, this information has to be stored de-identified.

Results: Today IHE does not support de-identification and end-to-end document encryption. As a result, the in-house infrastructure is attached to the national platform via a connector that covers all aspects of de-identification and encryption. A trusted third party provides the de-identification. It allows the separation of demographic data from its pseudonym, which is never known in the in-house systems. If data are accessed, the trusted third party will also act as a rekey service for the individually used encrypted encryption keys.

Conclusion: The proposed national exchange platform combines the use of IHE profiles with additional security features like de-identification and encryption through the use of an additional connector component.

B-1013 14:54

Dedicated workflow solution to facilitate consistent, reproducible, and efficient patient monitoring in oncological trials and routine

M. Baumhauer, M. Seitel; *Heidelberg/DE* (m.baumhauer@dkfz-heidelberg.de)

Purpose: We introduce a new and dedicated software system to manage oncologic workflows. The working concept has been developed from ground up and optimised to meet the increasingly complex requirements of cancer therapy monitoring. Our work is motivated by the increasing amount and complexity of imaging criteria in oncologic radiology, and the lack of software that provides availability and easy access to preceding image assessments, automatically updated statistics, and a defined working concept to ensure consistency.

Methods and Materials: Background of the software is a general requirement analysis for oncological patient management workflows, conducted in 2009. Starting with an in-house development, identified deficits of commercially available software was addressed. Among them are: -An optimised data model: include relevant context information, like patient therapy scheme, clinical trial affiliation, imaging criteria, lesion characteristics. -Flexibility in quantitative lesion assessment: conduct unlimited correlated measurements in unlimited MR/CT/PET studies and series for unlimited follow-ups. - Consistency by automating routine procedures: clinical trial management, automated overall response evaluation, and criteria conformance validation.

Results: Since beginning of 2011, the software is available under the label of mint Lesion™ as CE-marked product in Europe by a newly founded spin-off company of German Cancer Research Centre. Mid-term feedback of our reference users attest the system's feasibility and show the high potential for a application in trials and routine patient care.

Conclusion: While improving consistency, quality, and safety, mint Lesion™ aims at leveraging the routine workload. Future research will assess the effectiveness of mint Lesion™ in practical routine.

B-1014 15:03

Managing IT services in a completely digitised radiological department with an in-house departmental IT group: a 7-year follow-up experience

H. Strube, S. Wirth, M.F. Reiser, M. Treitl; *Munich/DE* (hanna.strube@med.uni-muenchen.de)

Purpose: To evaluate the performance of a departmental information technology (IT)-group compared to hospital-IT and system manufacturer's support in a completely digitised radiological department based on seven years of experience. The potential to reduce manufacturer's service and to manage unknown IT-problems were investigated.

Methods and Materials: The departmental IT-group maintains the radiology information system (RIS) and picture archiving and communication system (PACS) using an intranet-based reporting system. IT-problems are specified according to urgency, responsibility and affected system. A new RIS/PACS and a speech recognition system were installed. The performance and mean time for troubleshooting by the different providers were evaluated.

Results: In 90 months, 14681 IT-problems emerged, 96.5% were solved by the departmental IT-group (82.6% within the time limit), with high solution rates for breakdowns of the clinical information systems (81.4%), standard hard- (84.1%), and software (including RIS, 91.9%) and acceptable solution rate for PACS (78.0%) and imaging devices (58.7%). 1073 cases (7.3%) required a troubleshooting within 2h (40.6% solved within 30 min by departmental IT-group). In 6.7% of the cases manufacturer's support was indispensable. Over time the total amount of IT-problems decreased by up to 73.2% for emergency and very urgent problems but increased for problems of lower urgency. The implementation of new RIS/PACS led to a short increase in the total number of IT-problems though those problems mostly were of low priority.

Conclusion: A departmental IT-group provides fast troubleshooting, solving a considerable proportion of occurring and even new IT-problems, necessitating manufacturer's support only in a small number of cases.

B-1015 15:12

Itemised or prose radiology reports? A survey of hospital clinicians and radiologists' preferences

L.W. Goh, H.S. Teh; *Singapore/SG* (LinWah.Goh@mohh.com.sg)

Purpose: To determine clinicians' and radiologists' preferences regarding the format of the radiology report and contents.

Methods and Materials: Questionnaires were sent out to all clinicians from various departments and radiologists practicing within Khoo Teck Puat Hospital, Singapore. The participants were invited to rank a variety of hypothetical ultrasound and computed tomography scan reports according to their level of satisfaction and provided reasons for their choices. Demographic information regarding the participants was obtained in the questionnaire.

Results: A total of 30 radiologists and 92 clinicians responded. 75% of clinicians vs 50% of radiologists were satisfied with the itemised report for an abnormal ultrasound scan ($p < 0.05$). 80% of radiologists vs 58% of clinicians were satisfied with the prose report for an abnormal ultrasound scan ($p < 0.05$). In general, most radiologists still preferred the prose reporting style, citing familiarity with this style of reporting. Most clinicians preferred itemised radiology reports as they felt that these reports were clearer and easier to comprehend.

Conclusion: Itemised reports are more popular with referring clinicians due to their clarity. Prose reports foster a lack of standardisation of content among different radiologists. A shift in paradigm to itemised reporting will make for faster, more consistent radiology reports that facilitate complete documentation of information and measurements. Changing the way radiology reports are structured requires adaptation among radiologists. Improved training in reporting during the radiology residency is de rigueur to familiarise radiologists with a new style of reporting.

B-1016 15:21

A web-based documentation system with exchange of DICOM RT data for multicenter clinical studies in particle therapy

K.A. Kessel¹, N. Bougatt¹, C. Bohn², D. Oetzel¹, U. Engelmann², R. Bendl³, J. Debus¹, S.E. Combs¹; ¹Heidelberg/DE, ²Dossenheim/DE, ³Heilbronn/DE (Kerstin.Kessel@med.uni-heidelberg.de)

Purpose: Conducting clinical studies is rather difficult because of the large variety of voluminous datasets, different documentation styles, and various information systems, especially in radiation oncology.

Methods and Materials: We developed a web-based documentation system for transnational and multicenter clinical studies in particle therapy. 550 patients

have been treated at the Heidelberg Ion Therapy (HIT) centre from November 2009 to August 2011. Protons, carbon ions or a combination of both, as well as a combination with photons were applied. To date, 12 studies have been initiated and more are in preparation.

Results: It is possible to immediately access all patient information and exchange, store, process, and visualise text data, any DICOM images and multimedia data. Accessing the system and submitting clinical data are possible for internal and external users. Security and privacy protection is ensured with the encrypted https protocol, client certificates, and an application gateway. Furthermore, all data can be pseudonymised. Integrated into the hospital environment, data are imported via interfaces over HL7-messages and DICOM. Several further features replace manual input and ensure data quality and entirety. Studies can be individually designed to fit specific needs. By including all treated patients (also non-study patients), we gain the possibility for overall large-scale, retrospective analyses.

Conclusion: Having recently begun documentation of our first 300 patients in six clinical studies, it has become apparent that the benefits lie in the simplification of research work, better study analyses quality and ultimately, the improvement of treatment concepts by evaluating the effectiveness of particle therapy.